

# Dissertation

---

## Light Actuation: From Synthesis to Material

---

A Thesis submitted Towards the Academic Degree

Doctor Rerum Naturalium

- Dr. rer. nat. -

Department of Biology and Chemistry  
of the University of Bremen

By

**Sven Schultze**

The work from this dissertation was conducted in the working group of Prof. Dr. Anne Staubitz at the Institute for Organic and Analytical Chemistry at the University of Bremen from November 2019 to February 2024.

Reviewer

Prof. Dr. Michael R. A. Giese

Prof. Dr. Matthias Lehmann

Prof. Dr. Anne Staubitz

Doctoral Colloquium: 02.04.24

*"At the start of my journey into the uncharted territory of synthetic molecular motors I consider it apt to emphasize the joy of discovery that I have experienced through synthetic chemistry. The molecular beauty, structural diversity and ingenious functions of the machinery of life, which evolved from a remarkably limited repertoire of building blocks, offers a tremendous source of inspiration to the synthetic chemist entering the field of dynamic molecular systems. However, far beyond Nature's designs, the creative power of synthetic chemistry provides unlimited opportunities to realize our own molecular world [...]."*

- Ben Feringa<sup>1</sup>

# Eidesstattliche Erklärung

Ich, Sven Schultzke (Adolf-Reichwein Str. 57, 28329 Bremen), versichere an Eides statt durch meine Unterschrift, dass ich die vorstehende Arbeit selbständig und ohne fremde Hilfe angefertigt und alle Stellen, die ich wörtlich dem Sinne nach aus Veröffentlichungen entnommen habe, als solche kenntlich gemacht habe und mich aus keiner anderen als der angegebenen Literatur oder sonstiger Hilfsmittel bedient habe.

Zusätzlich versichere ich, dass ich IT-gestützte oder auf künstlicher Intelligenz (KI) basierende Schreibwerkzeuge nur in Absprache mit der Betreuungsperson verwendet habe. Inhalte und Struktur des Textes sind vollständig meine eigene geistige Leistung; die KI Werkzeuge wurden lediglich zur sprachlichen Verfeinerung verwendet.

Ich versichere an Eides statt, dass ich die vorgenannten Angaben nach bestem Wissen und Gewissen gemacht habe und dass die Angaben der Wahrheit entsprechen und ich nichts verschwiegen habe.

Die Strafbarkeit einer falschen eidesstattlichen Versicherung ist mir bekannt, namentlich die Strafandrohung gemäß §156 StGB bis zu drei Jahren Freiheitsstrafe oder Geldstrafe bei vorsätzlicher Begehung der Tat bzw. gemäß §161 Abs. 1 StGB bis zu einem Jahr Freiheitsstrafe oder Geldstrafe bei fahrlässiger Begehung.

Bremen, April 9, 2024

---

(Sven Schultzke)

# Erklärung zur elektronischen Version und Überprüfung einer Dissertation

Hiermit erkläre ich gemäß §7 Abs. 7, Punkt 4, dass die zu Prüfungszwecken beigelegte elektronische Version meiner Dissertation identisch ist mit der abgegebenen gedruckten Version.

Ich bin mit der Überprüfung meiner Dissertation gemäß §6 Abs. 2, Punkt 5 mit qualifizierter Software im Rahmen der Untersuchung von Plagiatsvorwürfen einverstanden.

Bremen, April 9, 2024

---

(Sven Schultzke)

## Hinweis zur Überarbeitung

In dieser überarbeiteten Fassung wurde das Kapitel "Publication V" (Hidden Forces: Activation of Photobending in a Liquid Crystalline Elastomer by Mesogen Alignment with the Help of Thermoplastic Particles) als "Submitted Manuscript (V)" betitelt. Es wurde folgerichtig in der Aufzählung der Publikationen ausgenommen und in der Kurzzusammenfassung, sowie im Anhang angepasst.

Es wurde zudem das Scheme 7 im Kapitel 4.2 (Unpublished Work III) korrigiert.

# Danksagung

An dieser Stelle möchte ich mich bei allen bedanken, die mich auf dem Weg zur Fertigstellung dieser Arbeit begleitet und geholfen haben.

Dabei gebührt ein ganz großer Dank Prof. Dr. Anne Staubitz, die mir immer den richtigen Antrieb gegeben hat, um sich weiter zu verbessern. Zugleich gab sie mir aber auch den nötigen Freiraum, ohne den ich nicht mit meiner wissenschaftlichen Neugier die meisten Projekte in dieser Thesis hätte ausprobieren und vollenden können. Vielen Dank!

Außerdem möchte ich mich bei Prof. Dr. Matthias Lehmann und Prof. Michael R. A. Giese für die Begutachtung dieser Arbeit bedanken.

Besonderer Dank gilt auch meinen Kooperationspartnern, ohne die so manches Projekt nicht vorstellbar gewesen wäre. Die Woche in Würzburg bei der Gruppe von Prof. Lehmann mit Nikolai Scheuring war sehr lehrreich und zugleich unterhaltsam. Ich bedanke mich bei Nina Sindersberger für ihre Kooperationsbereitschaft und die zielstrebige Ausarbeitung. Hier ist auch Dr. Pim Puylaert zu danken, der nicht nur mit der Vermessung von Kristallstrukturen, sondern auch mit seiner wissenschaftlichen Expertise und den Feierabendgesprächen immer unterstützend war. Einen großen Dank gebührt auch Dr. Melanie Walther für unser Kooperationsprojekt, die Korrekturlesung dieser Arbeit und noch wichtiger für die unzähligen wissenschaftlichen Diskussionen und die Gespräche abseits der Arbeit.

Bedanken möchte ich mich auch bei Dr. Yannik Appiarius, Jan Thayssen, Jonas Gerken, Oliver Thüringer, Dr. Jonas Hoffmann, Phil Gliese und Jasmin Richter für das Arbeitsklima, die gemeinsame Laborarbeit und die Freizeitaktivitäten. Danke auch für die Unterstützung im Labor von Noah Wolf und Luca Schlautmann. Außerdem, bedanke ich mich auch bei unserer guten Seele Petra Grundmann, die mir organisatorisch immer aushelfen konnte. Danke an Dorit Kemken und Thomas Dülcks für die Vielzahl an gemessenen Massenspektren, sowie an Johannes Stelten und Dr. Wieland Wilker für die Bereitstellung der NMR-Geräte.

Dann möchte ich mich meiner indirekten Unterstützung zuwenden, da ich hier in der Stadt Bremen einen neuen Freundeskreis finden konnte, der immer für mich da ist. Diesen Rückhalt weiß ich sehr zu schätzen.

Den Rückhalt habe ich aber nicht nur durch Freunde genossen, sondern ich konnte meine Freude auch mit meiner Familie teilen. Vielen Dank, dass ihr mir das Studium ermöglicht habt, sodass ich heute diesen Satz in dieser Arbeit schreiben kann.

Der größte Dank geht aber an meine Frau, Isabell, deren Einfluss ich hier in diesen Sätzen nicht gerecht werden kann. Vom wissenschaftlichen Input bis zu den Abenteuern, die wir bestritten haben, bist du immer dabei gewesen, und ich bin unglaublich glücklich, dass wir die Reise nach Bremen angetreten haben und gemeinsam in den nächsten Abschnitt ziehen werden.

Vielen Dank.

# Publications

The work presented here was carried out under the supervision of Prof. Dr. Anne Staubitz during the period of November 2019 to February 2024. The thesis is being composed in a cumulative manner and developed in the framework of the DFG priority program SPP 2100 "Soft Materials Robotics Systems". The following 4 publications and a submitted manuscript were taken into account:

## Publication I

### **Modification of Azobenzenes by Cross-Coupling Reactions**

M. Walther, W. Kipke, S. Schultzke, S. Ghosh, A. Staubitz, *Synthesis*, **2021**, *53*, 1213-1228.

## Publication II

### **Active Ester Functionalized Azobenzenes as Versatile Building Blocks**

S. Schultzke, M. Walther, A. Staubitz, *Molecules*, **2021**, *26*, 3916.

## Publication III

### **Centennial Isomers: A Unique Fluorinated Azobenzene Macrocyclus with Dual Stability Over 120 Years**

S. Schultzke, P. Puylaert, H. Wang, I. Schultzke, J. Gerken, A. Staubitz, *Adv. Funct. Mater.* **2024**, 2313268.

## Publication IV

### **A Photomechanical Film in which Liquid Crystal Design Shifts the Absorption into the Visible Light Range**

S. Schultzke, N. Scheuring, P. Puylaert, M. Lehmann, A. Staubitz, *Adv. Sci.*, **2023**, *10*, 2302692.

## Submitted Manuscript (V)

### **Hidden Forces: Activation of Photobending in a Liquid Crystalline Elastomer by Mesogen Alignment with the Help of Thermoplastic Particles**

S. Schultzke, P. Schadte, N. Sindesberger, J. Gerken, L. Siebert, A. Staubitz, submitted at *Mater. Horiz.*, **2024**.

The work is based on collaborations with several scientists. Therefore, my contribution in % of the total workload to these publications is detailed as follows. All information is approximate and provided with the best intention to be as accurate as possible.



## **Publication I**

### **Modification of Azobenzenes by Cross-Coupling Reactions**

<u>Category</u>	<u>Contribution [in %]</u>
Concept and design of the manuscript	10%
Acquisition and structure of references	5%
Preparation of figures and tables	10%
Drafting of the manuscript	10%

## **Publication II**

### **Active Ester Functionalized Azobenzenes as Versatile Building Blocks**

<u>Category</u>	<u>Contribution [in %]</u>
Experimental concept and design	60%
Experimental work and/or acquisition of (experimental) data	50%
Data analysis and interpretation	50%
Preparation of figures and tables	50%
Drafting of the manuscript	40%

## **Publication III**

### **Centennial Isomers: A Unique Fluorinated Azobenzene Macrocyclus with Dual Stability Over 120 Years**

<u>Category</u>	<u>Contribution [in %]</u>
Experimental concept and design	95%
Experimental work and/or acquisition of (experimental) data	85%
Data analysis and interpretation	90%
Preparation of figures and tables	100%
Drafting of the manuscript	80%

## Publication IV

### **A Photomechanical Film in which Liquid Crystal Design Shifts the Absorption into the Visible Light Range**

Category	Contribution [in %]
Experimental concept and design	90%
Experimental work and/or acquisition of (experimental) data	95%
Data analysis and interpretation	85%
Preparation of figures, tables and videos	95%
Drafting of the manuscript	80%

## Submitted Manuscript (V)

### **Hidden Forces: Activation of Photobending in a Liquid Crystalline Elastomer by Mesogen Alignment with the Help of Thermoplastic Particles**

Category	Contribution [in %]
Experimental concept and design	95%
Experimental work and/or acquisition of (experimental) data	95%
Data analysis and interpretation	95%
Preparation of figures and tables	100%
Drafting of the manuscript	80%

Bremen, April 9, 2024

---

(Sven Schultzke)

# Abstract

This thesis explores the innovative manipulation and application of azobenzene based materials, with a particular emphasis on their functionalization for optical data storage and the development of responsive liquid crystalline polymer (LCP). Although azobenzenes have long been recognized as perhaps the most suitable photoswitch for applications due to their high photostability and thermal stability, tailored functionalization is always necessary to fulfill any significant role and meet specific application needs. Cross-coupling reactions are presented as an effective strategy for late-stage modifications of azobenzene and its derivatives, offering insights into recent advancements in this area. Current knowledge on this is summarized in Chapter 2.1. As an original research contribution to this field, in this thesis, a novel high-yielding palladium-catalyzed method is introduced for the selective functionalization of azobenzenes, demonstrating significant potential in biological systems and material science due to the efficient introduction of N-hydroxysuccinimide esters.

The second part of this thesis focuses on applications and deals with the question of how azobenzenes can be specifically functionalized to achieve selected goals. The first project in this regard had the aim to achieve high half-life times for an azobenzene with a view of applications in optical data storage. Rational design led to a uniquely stable macrocyclic azobenzene derivative, which showcases exceptional thermal stability of its metastable *Z*-isomer (120 years), while still switchable with visible light. This stability is attributed to strategic fluorination.

The second project led to the solution of the problem of preparing a photobendable polymer film that could be switched with visible rather than UV-light. The development of such liquid crystal networks (LCNs) is discussed. In this process, through molecular design, liquid crystallinity of an *ortho*-fluorinated azobenzene, known for its switching capabilities in visible light, could be designed, although this had been deemed not possible in the literature. This breakthrough addresses the limitations imposed by UV-light's harmful effects, offering a scalable solution for the synthesis of polymerizable azobenzene compounds with potential applications in soft robotics and biology.

The third project was the introduction of an innovative technique for manufacturing advanced soft shape-memory materials. By integrating azobenzene into main-chain liquid crystal elastomers (MC-LCEs) and blending them with thermoplastic polycaprolactone (PCL) particles, a composite material was developed. This material not only responds to light stimuli in thick configurations but also exhibits remarkable stretchability and high programmability, demonstrating its utility across various applications due to its excellent reusability and versatile actuation capabilities.

This thesis highlights the diverse applications of azobenzene derivatives in the development of sophisticated materials for emerging technologies.

# Kurzzusammenfassung

Diese Dissertation erforscht die innovative Manipulation und Anwendung von auf Azobenzol basierenden Materialien, mit besonderem Schwerpunkt auf deren Funktionalisierung für optische Datenspeicherung und die Entwicklung von responsiven flüssigkristallinen Polymeren (LCP). Obwohl Azobenzole schon lange als vielleicht am besten geeignete Fotoschalter für Anwendungen erkannt wurden, aufgrund ihrer hohen Fotostabilität und thermischen Stabilität, ist für eine signifikante Rolle immer eine maßgeschneiderte Funktionalisierung notwendig, um spezifischen Anwendungen gerecht zu werden. Kreuzkupplungsreaktionen werden als effektive Strategie für späte Modifikationen von Azobenzol und seinen Derivaten vorgestellt, die Einblicke in jüngste Fortschritte in diesem Bereich bieten. Der aktuelle Wissensstand dazu wird in Kapitel 2.1 zusammengefasst. Als originärer Forschungsbeitrag in diesem Feld wird in dieser Dissertation eine neue, hoch ergebnisreiche palladiumkatalysierte Methode für die selektive Funktionalisierung von Azobenzol vorgestellt, die aufgrund der effizienten Einführung von N-Hydroxysuccinimidestern erhebliches Potenzial in biologischen Systemen und der Materialwissenschaft zeigt.

Der zweite Teil dieser Dissertation konzentriert sich auf Anwendungen und behandelt die Frage, wie Azobenzole spezifisch funktionalisiert werden können, um ausgewählte Ziele zu erreichen. Das erste Projekt in dieser Hinsicht hatte das Ziel, hohe Halbwertszeiten für ein Azobenzol zu erreichen, mit Blick auf Anwendungen in der optischen Datenspeicherung. Ein rationales Design führte zu einem einzigartig stabilen makrozyklischen Azobenzol-Derivat, das eine außergewöhnliche thermische Stabilität seines metastabilen *Z*-Isomers (120 Jahre) aufweist, während es immer noch mit sichtbarem Licht schaltbar ist. Diese Stabilität wird einer strategischen Fluorierung zugeschrieben. Das zweite Projekt führte zur Lösung des Problems bei der Herstellung eines fotobiegbaren Polymerfilms, der mit sichtbarem statt UV-Licht geschaltet werden konnte. Die Entwicklung solcher flüssigkristallinen Netzwerke (LCNs) wird diskutiert. In diesem Prozess konnte durch molekulares Design die Flüssigkristallinität eines *ortho*-fluorierten Azobenzols, bekannt für seine Schaltfähigkeiten im sichtbaren Licht, entworfen werden, obwohl dies in der Literatur als nicht möglich angesehen wurde. Dieser Durchbruch adressiert die Einschränkungen an, die durch die schädlichen Effekte von UV-Licht auferlegt werden, und bietet eine skalierbare Lösung für die Synthese polymerisierbarer Azobenzolverbindungen mit potenziellen Anwendungen in der weichen Robotik und Biologie.

Das dritte Projekt war die Einführung einer innovativen Technik zur Herstellung fortschrittlicher weicher Formgedächtnismaterialien. Durch die Integration von Azobenzol in Hauptkettenflüssigkristalline Elastomere (MC-LCEs) und deren Mischung mit thermoplastischen Polycaprolacton (PCL)-Partikeln wurde ein Verbundmaterial entwickelt. Dieses Material reagiert nicht nur auf Lichtstimuli bei großen Proben, sondern weist auch eine bemerkenswerte Dehnbarkeit und hohe Programmierbarkeit auf, was seine Nützlichkeit in verschiedenen Anwendungen aufgrund seiner ausgezeichneten Wiederverwendbarkeit und vielseitigen Aktionsfähigkeiten demonstriert.

Diese Dissertation hebt die vielfältigen Anwendungen von Azobenzol-Derivaten bei der Entwicklung anspruchsvoller Materialien für aufkommende Technologien hervor.

# Contents

<b>Eigenständigkeitserklärung</b>	<b>ii</b>
<b>Erklärung zur elektronischen Version und Überprüfung einer Dissertation</b>	<b>iii</b>
<b>Hinweis zur Überarbeitung</b>	<b>iv</b>
<b>Danksagung</b>	<b>v</b>
<b>List of Publications</b>	<b>vi</b>
<b>Abstract</b>	<b>ix</b>
<b>Kurzzusammenfassung</b>	<b>x</b>
<b>1 Introduction Part I</b>	<b>1</b>
1.1 Molecular Switches . . . . .	2
1.2 Azobenzene . . . . .	5
1.2.1 Mechanistic Insight into the Isomerization of Azobenzene . . . . .	6
1.2.2 Addressability and Efficiency of Azobenzene . . . . .	11
1.2.3 Thermal Half-Life Time of the Metastable Azobenzene Isomer . . . . .	15
1.2.4 Synthesis of Tetra- <i>Ortho</i> -Substituted Azobenzenes . . . . .	16
1.2.5 Macrocyclic <i>Ortho</i> -Azobenzenes . . . . .	17
<b>2 Publication I</b>	<b>21</b>
2.1 Modification of Azobenzene by Cross-Coupling Reactions . . . . .	21
<b>3 Publication II</b>	<b>39</b>
3.1 Active Ester Functionalized Azobenzenes as Versatile Building Blocks . . . . .	39
<b>4 Publication III</b>	<b>55</b>
4.1 Centennial Isomers: A Unique Fluorinated Azobenzene Macrocyclus with Dual Stability Over 120 Years . . . . .	55
4.2 Unpublished Work III . . . . .	68
<b>5 Introduction Part II</b>	<b>73</b>
5.1 Liquid Crystallinity . . . . .	73
5.1.1 The Nature of Liquid Crystals . . . . .	73
5.1.2 External Director . . . . .	76
5.2 Liquid Crystalline Polymers . . . . .	78
5.2.1 Actuation of Liquid Crystalline Polymers . . . . .	80

<b>6</b>	<b>Publication IV</b>	<b>87</b>
6.1	A Photomechanical Film in which Liquid Crystal Design Shifts the Absorption into the Visible Light Range . . . . .	87
<b>7</b>	<b>Submitted Manuscript (V)</b>	<b>105</b>
7.1	Activation of Hidden Forces: Reshaping a Liquid Crystal Elastomer into a Monodomain with the Help of Thermoplastic Particles . . . . .	105
<b>8</b>	<b>Conclusion and Outlook</b>	<b>115</b>
	<b>Bibliography</b>	<b>115</b>
	<b>Abbreviation</b>	<b>127</b>
<b>9</b>	<b>Appendix</b>	<b>135</b>
9.1	Appendix Publication II . . . . .	135
9.2	Appendix Publication III . . . . .	249
9.3	Appendix Publication IV . . . . .	315
9.4	Appendix Submitted Manuscript (V) . . . . .	373
9.5	Appendix Unpublished Work . . . . .	389
9.6	Appendix Permissions to Reprint . . . . .	429

## Introduction Part I

In today's rapidly changing times, an increasing number of tasks is being taken over by robots of various kinds, especially with enhanced accessibility of artificial intelligence.<sup>2-5</sup> As AI advances to make robots more life-like, it necessitates the development of materials that can mimic the flexibility, durability, and sensitivity of biological tissues, thereby ensuring robots can emulate functions more authentically.<sup>5-8</sup> For many applications, the ideal solution lies in soft robotics.<sup>9,10</sup> In contrast to their hard, inflexible counterparts, soft robots are composed of deformable, lightweight components that are still robust.<sup>11</sup> Particularly in the fields of medical,<sup>12</sup> human-robot interaction<sup>13</sup> and mimicking human interaction with their environments,<sup>7,14,15</sup> soft robots have long been desirable (Figure 1.1).<sup>16-18</sup> While many existing approaches to soft robotics rely on material softness and are driven by means such as pneumatics<sup>19-22</sup> or dielectrics,<sup>23-25</sup> actuation can also be based on (untethered) interaction at the molecular level.<sup>26-32</sup>

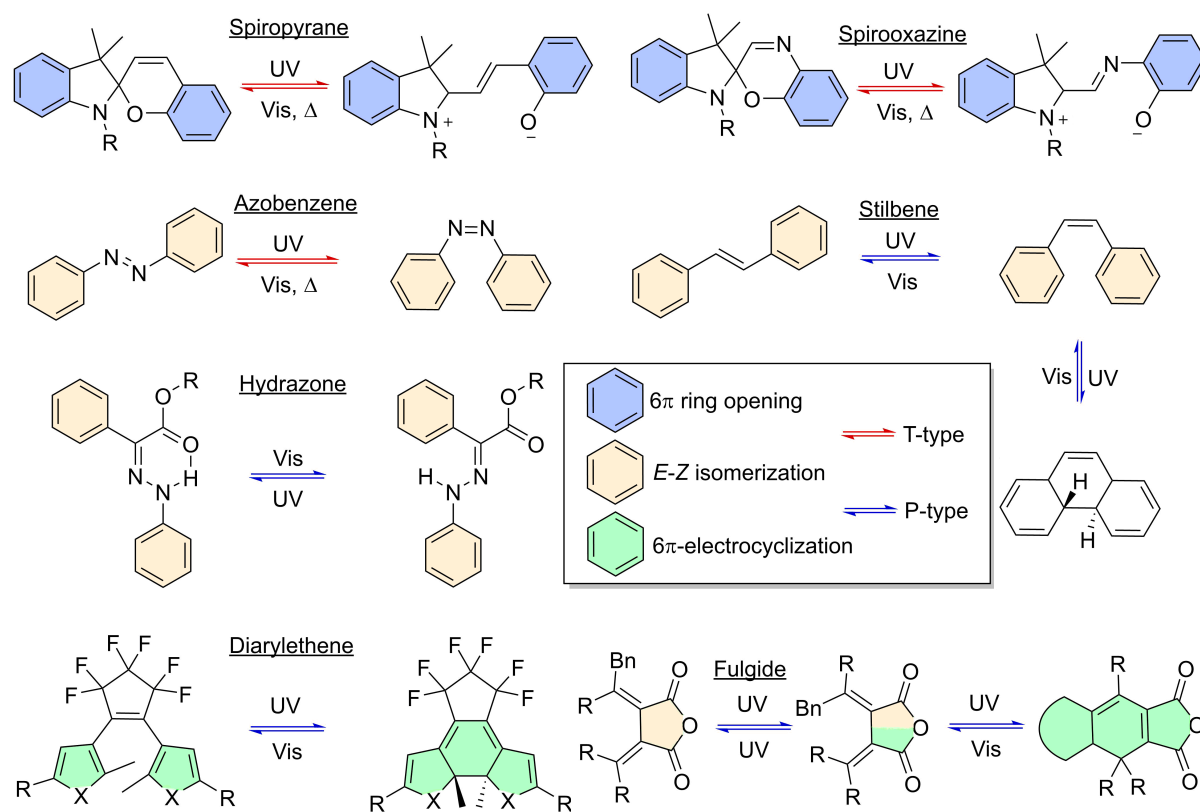


**Figure 1.1:** The handover of an object from a soft robot to the trunk of an elephant. The organic flexibility of the elephant's trunk serves as an excellent example of a versatile actuator and has been taken as a model in this context. Reprinted with permission. © 2024 Festo SE & Co. KG.

Molecular switches, known for their nanometer-scale motion, are particularly noteworthy in this context.<sup>33,34</sup> Molecular switches can change between two or more states in response to an external stimulus, altering their molecular geometry and, consequently, many of their properties.<sup>35-42</sup> This transformation can be harnessed to develop numerous actuators.<sup>43,44</sup> The introduction guides in its first part through the topic molecular switches, specifically azobenzene, and its properties. Current synthetic challenges are explained as well as strategies for their tailor-made properties to obtain specific functions. In the second part external stimulus actuation is explained and the background of liquid crystal elastomer actuators is introduced.

## 1.1 Molecular Switches

A molecular switch is characterized by the reversible switching between two or more states.<sup>35</sup> This switching is induced by external stimuli. The most frequent stimuli in this context are temperature, light, pH value, humidity, or even mechanical force.<sup>36,42,44–50</sup> Geometric alterations in molecular switches typically result in changed chemical properties. This change renders each molecular switch unique in its potential applications.<sup>35</sup> An ideal switch should exhibit at least two stable states that can each be attained in high yields through the respective stimulus. Furthermore, both states should exhibit distinguishable properties.<sup>51</sup> Among external stimuli, light is particularly noteworthy as modern light sources and optical setups enable precise control over its application, including adjustments to wavelength, polarization and intensity.<sup>33</sup> Additionally, the process of irradiation by an external source can occur through space and matter (until complete absorption). Some of the most studied and significant contributors are spiropyrans,<sup>52</sup> spirooxazines,<sup>53</sup> azobenzenes,<sup>54</sup> stilbenes,<sup>55</sup> diarylethenes,<sup>41</sup> fulgides<sup>56</sup> and hydrazones<sup>57</sup> (Scheme 1). These molecular actuators are pivotal for their ability to undergo structural transformations upon light activation, classified broadly into three main mechanisms: ring-opening and -closing reaction, *E-Z*-isomerization and electrocyclicization.<sup>41,51,58</sup> Furthermore, photochromic switches are classified into two types: T-type and P-type, depending on whether their back-isomerization is induced thermally or not, respectively. Molecular switches that undergo *E-Z*-isomerization or ring-opening and -closing reaction upon irradiation are mostly considered T-types. Representatives for T-types are azobenzene, spiropyrane and spirooxazine.<sup>59–62</sup>



**Scheme 1:** Chemical structure and isomerization of spiropyrans,<sup>52</sup> spirooxazines,<sup>53</sup> azobenzenes,<sup>54</sup> stilbenes,<sup>55</sup> diarylethenes,<sup>41</sup> fulgides<sup>56</sup> and hydrazones.<sup>57</sup>



**Spiropyrans** respond to various stimuli, including light, heat, protonation, metal ions, and solvent polarity.<sup>52</sup> This results in ring-opening- and -closing isomerization, significantly altering their dipole moment, dielectric constants, geometric motion, and optical properties.<sup>40,52</sup> Spiropyranes exhibit relatively low fatigue resistance and are unstable in the presence of environmental factors like oxygen.<sup>40,63</sup> Classified as mechanophores, their unique feature is used in sensors and mechanoresponsive polymers.<sup>52</sup> **Spirooxazines** as an analogue of the spiropyrane in which the carbon in the chromene unit is exchanged by a nitrogen atom, are distinguished by its exceptional fatigue resistance in comparison to spiropyrane.<sup>64,65</sup> They have found its niche primarily in chromophoric lenses and sunglasses.<sup>66</sup> Not many applications include spirooxazines as the thermal stability of the metastable ring-opened merocyanine form is lower and the synthesis remains challenging.<sup>65</sup>

**Azobenzenes** undergo isomerization upon irradiation with UV-light. The isomerization can be reverted thermally in the darkness or by irradiation with blue light.<sup>67</sup> During isomerization, the geometry changes from a planar, elongated (*E*-isomer) to a bent structure (*Z*-isomer), where the azobenzene rings are slightly twisted to each other. This reduces the distance between the hydrogen atoms in *para*-position from 9 Å to 5.5 Å, reflecting the enormous spatial movement at the molecular level.<sup>67,68</sup> Additionally, the dipole moment changes from almost 0 D to 3 D in its nonplanar *Z*-isomer.<sup>67</sup>

In recent years, further development has led to improvements in azobenzene. These advancements resulted in a switch operable with purely visible light and enhanced thermal stability. The following chapters will explore this development and address whether azobenzene qualifies as a P-type switch. To facilitate classification as a P-type switch, the switches fulgides, diarylethenes, hydrazones and (stiff-)stilbenes<sup>69</sup> will be introduced.

**Fulgides** combine a *E-Z*-photoisomerization and an additional  $6\pi$ -electrocyclization. The electrocyclization is thermally irreversible. Unfortunately, the electrocyclization can only occur in the *E*-isomer, thus limiting the efficiency by the competing *E*- and *Z*-isomerization.<sup>34,56</sup>

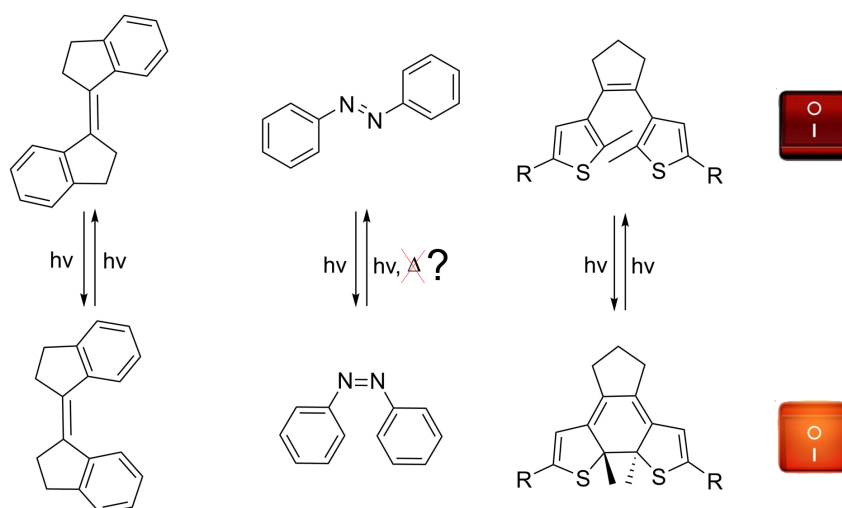
**Hydrazones** undergo upon exposure to light *E-Z*-isomerization around the C=N bond. Remarkably, certain hydrazone photoswitches exhibit exceptional qualities, including robust photoconversion efficiency, adjustable absorption wavelengths, resistance to degradation over repeated use and long thermal stability of the metastable *E*-isomer in the range of 1-1000 years.<sup>70</sup> Following their initial creation in 2017,<sup>70</sup> these hydrazone photoswitches quickly found applications across a range of adaptive materials.<sup>57,71,72</sup>

**Diarylethenes** on the other hand, have been recognized since 1988<sup>73</sup> for their reversible photo-switching capabilities, contributing significantly to the development of memory devices and smart receptors.<sup>41,74</sup> They are thermally stable, but have only minor dipole and geometrical changes after the  $6\pi$ -electrocyclization, thus their use in applications where large movements are required is limited.<sup>22,33</sup>

**Stilbenes** are the carbon analogon of azobenzene and therefore, their photochemistry has certain similarities, which was investigated in 1940 by G. Lewis.<sup>75</sup> When *E*-stilbene is excited with UV-light, it transforms into *Z*-stilbene. However, rather than only converting back from *Z*- to *E*-isomer through photoisomerization, *Z*-stilbene can also engage in a photocyclization process to form dihydrophenanthrene, with a yield greater than 10%.<sup>76</sup> This intermediate can

then be readily oxidized to phenanthrene.<sup>55,76</sup> The occurrence of this electrocyclization, along with other potential pathways for photooxidation and photocyclization, has greatly limited the use of stilbene as a molecular photoswitch. A 5-membered fused ring variant of stilbene, known as stiff-stilbene,<sup>69</sup> exhibits in comparison significantly enhanced stability, achieving clean photoisomerization upon UV-light exposure.<sup>77</sup> Stiff-stilbene is notable for its exceptionally high quantum yield for photoisomerization and large molecular motion upon switching. However, the change in the dipole moment is rather negligible.<sup>22,77</sup> Despite these beneficial characteristics and its long-standing recognition, it is only in recent times that applications of stiff-stilbene have started to emerge in the scientific literature.<sup>69</sup>

In the context of this work, the focus is on the deliberate switching between two long-lived, stable states, as this allows for high controllability, while inducing a large motion in the applied system. In the manner of a light switch (*on* vs. *off*) or a data point (*1* vs. *0*), switches at the molecular level are intended to carry new properties and information. The parent azobenzene cannot fulfill these properties, but the developments of the last few years might provide a solution in terms of thermal stability of the metastable isomer and addressability without UV-light for both isomerization (Scheme 2).<sup>54,78</sup>



**Scheme 2:** Example of a (stiff-)stilbene (P-type, left) and azobenzene (T-type, middle) with their respective *E*- and *Z*-isomerization. The diarylethene (P-type, right) exhibits an open/closed ring isomerization. All of them represent the switching of an *on/off* state on a molecular level.

To reduce the complexity of molecular switches and explain the phenomena in detail, the following discussion will specifically address azobenzene. Given the extensive body of research, azobenzene is a suitable candidate for integration into smart materials due to its robust chemical, thermal, and photobleaching resistance.<sup>67,78</sup> This choice necessitates a fundamental understanding of the molecular switch.

## 1.2 Azobenzene

First synthesized in 1834 by E. Mitscherlich,<sup>79</sup> azobenzene based compounds have gained significance as dyes due to their vivid coloration.<sup>80</sup> In contemporary research, azobenzenes have found applications as photomolecular switches: The discovery of the *Z*-isomer of azobenzene in 1937 marked the inception of a novel scientific domain.<sup>81</sup> The *E*-isomer of azobenzene exhibits a thermal stability that is approximately 50 kJ mol<sup>-1</sup> higher than its *Z*-isomer, thereby establishing a significant thermal energy difference between these two states.<sup>82</sup> Both the *E*- and the *Z*-isomer have a  $\pi\text{-}\pi^*$  transition and an  $n\text{-}\pi^*$  transition (Figure 1.2).

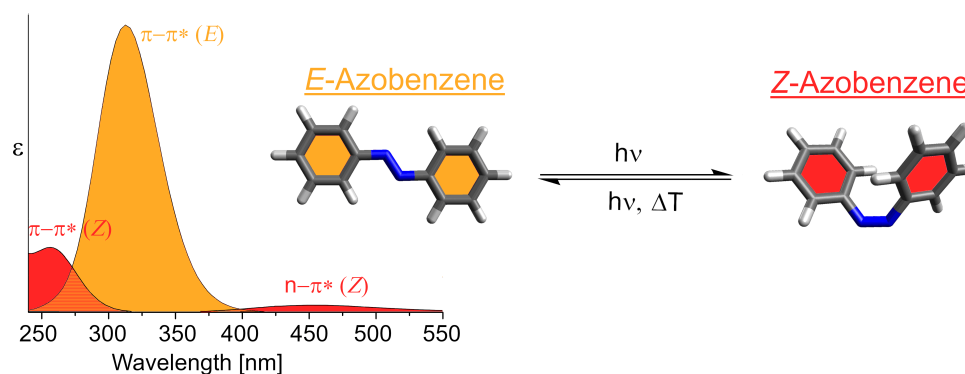
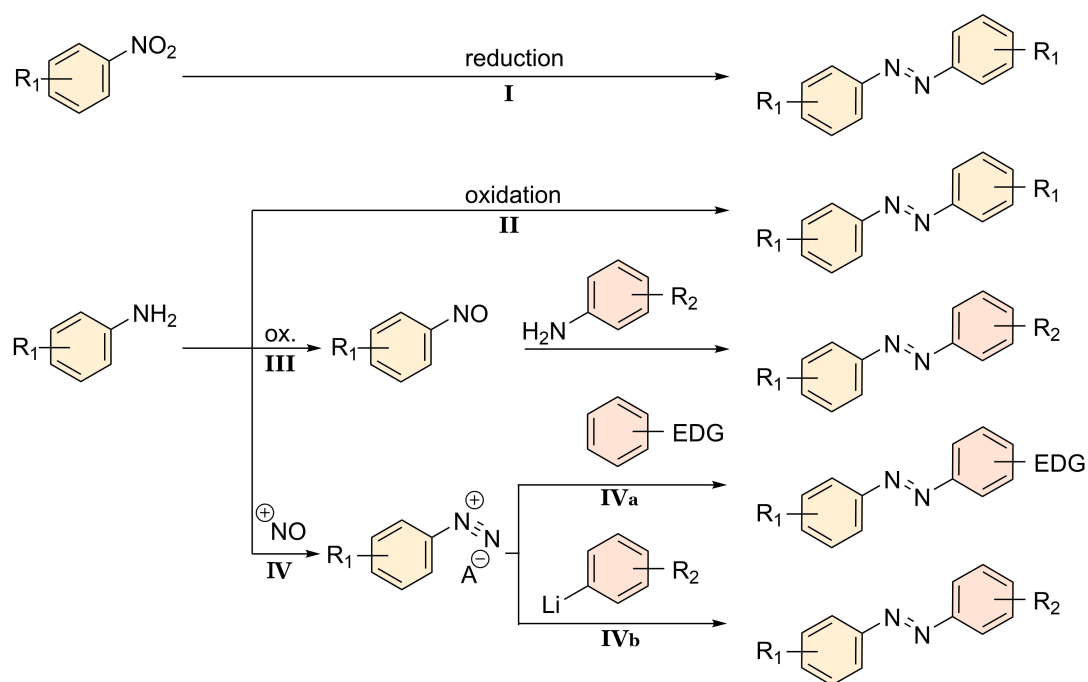


**Figure 1.2:** Calculated UV-vis spectrum of azobenzene in the gas phase for the *E*- and *Z*-isomer with their respective geometrical structures.

Computational studies show that the *E*-azobenzene tends to prefer a planar shape, both in the gas state and in solution.<sup>67</sup> Consequently, due to the  $C_{2h}$  symmetry  $\pi\text{-}\pi^*$  is symmetrical allowed and  $n\text{-}\pi^*$  absorption is forbidden.<sup>67</sup> It still occurs experimentally and is reasoned by vibrational movements in the molecules electronic structure.<sup>67,83</sup> Therefore, the *E*-isomer has an experimentally detected absorption in solution at 320 nm ( $\pi\text{-}\pi^*$ ) and a minor absorption at 420 nm ( $n\text{-}\pi^*$ ),<sup>67,84</sup> whereas the *Z*-isomer absorbs at 280 nm and 250 nm ( $\pi\text{-}\pi^*$ ) and 440 nm ( $n\text{-}\pi^*$ ).<sup>85</sup> Overall, it is possible to address these isomers separately with different wavelengths: To switch from *E* to *Z*, typically 320-360 nm (UV-light) are used, and for the reverse, >450 nm (blue light) is used.<sup>67</sup> Upon sufficient irradiation times, a photothermal equilibrium between the two forms can be reached (photostationary state, PSS), which is wavelength dependent.<sup>82</sup>

The methodologies to synthesize azobenzenes are versatile and continuously evolving (Scheme 3). For symmetric azobenzenes, reduction or oxidation methods are commonly used.<sup>86</sup> For the reduction (Scheme 3, **I**), a nitrobenzene is employed as the starting material, and the reductive coupling is achieved with reducing agents such as  $\text{NaBH}_4$ ,<sup>87</sup>  $\text{LiAlH}_4$ ,<sup>88</sup>  $\text{Zn}/\text{NaOH}$ ,<sup>89</sup> or glucose/ $\text{NaOH}$ .<sup>90</sup> Oxidative couplings (Scheme 3, **II**) are carried out starting from aniline with oxidizing agents like  $\text{Cu(I)}/\text{O}_2$ ,<sup>91</sup>  $\text{Pb(OAc)}_4$ ,<sup>92</sup> PIDA,<sup>93</sup>  $\text{MnO}_2$ ,<sup>94-96</sup> or  $\text{AgO}$ .<sup>97</sup> For asymmetric azobenzenes, the Mills reaction (Scheme 3, **III**) is a suitable method.<sup>98</sup> The synthesis starts from aniline using a mild oxidation to produce nitrosobenzene. This can then be converted with a second aniline under acidic conditions into an azobenzene in a condensation reaction. There is also the option of using the nitrosyl cation (Scheme 3, **IV**), generated *in situ* from sodium nitrite in acid, to synthesize a diazonium salt from aniline. The stability of the diazonium salt is



**Scheme 3:** Selection of synthetic pathways for the formation of azobenzene. **I)** The reductive coupling of two nitrobenzenes. **II)** The oxidative coupling of two anilines. Syntheses **I** and **II** are predominantly utilized in the synthesis of symmetric azobenzenes. **III)** Mills reaction via nitrosobenzene, which undergoes a condensation reaction with a second aniline. **IV)** Diazotization reaction of aniline with nitrosyl cation to form the diazonium ion. This can react with an aromatic electrophile (an activated aromatic (**IVa**) or lithiated aromatic (**IVb**)) to form the azobenzene. Reactions **III**) and **IV**) are preferred for the synthesis of asymmetric azobenzenes.<sup>86</sup>

influenced by the counterion. With a strong nucleophilic (**IVa**) or an organometallic aromatic species (**IVb**),<sup>99,100</sup> the azobenzene can be synthesized.

### 1.2.1 Mechanistic Insight into the Isomerization of Azobenzene

Based on the transition state theory (TST),<sup>101,102</sup> the isomerization of azobenzenes proceeds through a transition state.<sup>103</sup> These transition states involve a geometric change around the azo bridge, and the known transition states to date are: rotation,<sup>104</sup> inversion,<sup>104</sup> inversion-assisted rotation,<sup>104</sup> and concerted inversion<sup>105</sup> and concerted inversion<sup>106</sup> (Figure 1.3).<sup>51,103,107,108</sup>

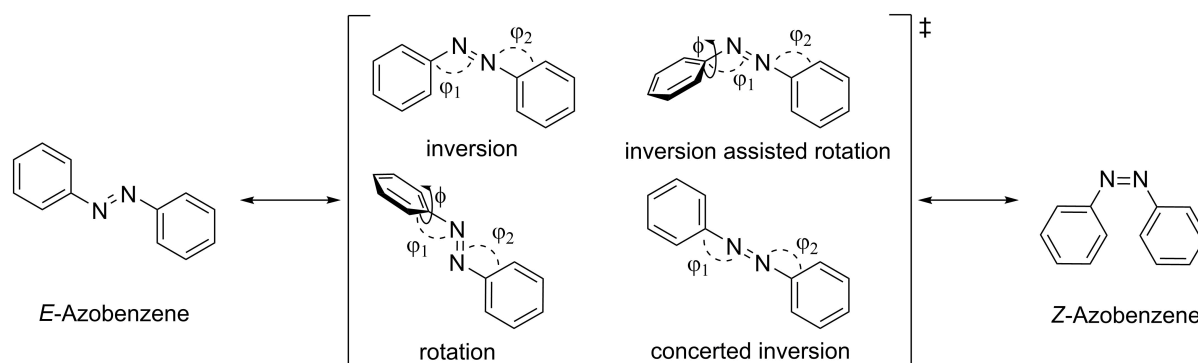


**Figure 1.3:** Theoretical transition states during the conversion of the azobenzene at thermal- and photoisomerization.

In a rotation, the double bond at the N=N azo bridge is formally broken to enable movement of the phenyl ring.<sup>104</sup> In an inversion, a linearization occurs at the N=N'-C angle, resulting in a hybridization of the nitrogen N' from  $sp^2$  to  $sp^1$ .<sup>104</sup> It is irrelevant for the existence of these transition states whether the isomerization is thermal or photochemical.<sup>51,103,107,109,110</sup> Typically for azobenzene, several transition states are possible for an isomerization.<sup>111</sup> However, there is a preferred transition state for each type of azobenzene and isomerization. This means that for an azobenzene the thermal and photochemical reactions from  $E$  to  $Z$  and  $Z$  to  $E$  do not have to be the same, which is indicated by the different quantum yields for the photoisomerizations ( $\Phi_{QY,E \rightarrow Z,\pi-\pi^*} = 0.11$  vs.  $\Phi_{QY,Z \rightarrow E,\pi-\pi^*} = 0.44$ ).<sup>111-113</sup> Although there is a continuous debate about the nature of the mechanism of thermal or photochemical switching, consistent tendencies are emerging, which will be detailed in the following.<sup>51,103,107,109,110</sup> For the photochemical isomerization there are two absorption bands to transition from the ground state ( $S_0$ ) to an excited state ( $S_1$  or  $S_2$ )(Figure 1.4).

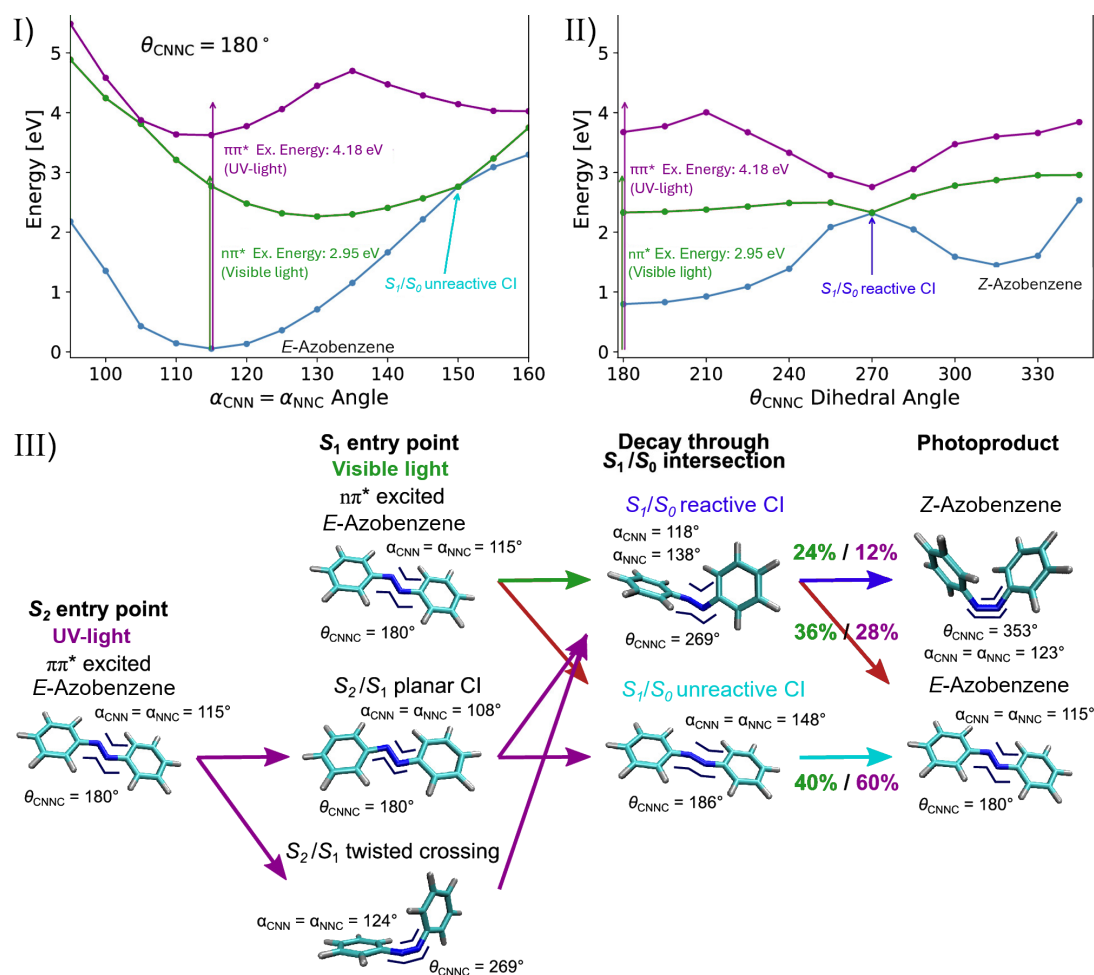


**Figure 1.4:** I) Potential energy surface (PES) scans along fixed values of the symmetric C-N=N angle bending coordinate. II) PES scans along fixed values of the C-N=N-C torsion coordinate. III) Graphical representation of the wavelength-dependent photochemistry of azobenzene. Adapted with permission from Yu *et al.*<sup>110</sup> © 2020 American Chemical Society.

Excitation of the  $\pi-\pi^*$  absorption band reaches the  $S_2$  state, while the  $n-\pi^*$  absorption band leads to the  $S_1$  state.<sup>104</sup> The quantum yield ( $\Phi_{QY}$ ) for the  $n-\pi^*$  excitation is known to be higher as experimental studies show ( $\Phi_{QY,E \rightarrow Z,\pi-\pi^*} = 0.11$  vs.  $\Phi_{QY,E \rightarrow Z,n-\pi^*} = 0.25$ ).<sup>112</sup> Theoretical

studies provide a better understanding of this process with data close to the values experimentally measured (Figure 1.3, III).<sup>110</sup> A potential energy surface (PES) is created for each state ( $S_0$ ,  $S_1$  and  $S_2$ ) based on the most important changes during isomerization. These are considered to be the C–N=N–C dihedral angle ( $\Phi$ ) and the C–N=N angle ( $\Psi$ ).<sup>110</sup> Due to the nature of those PSSs, conical intersections (CI) can be determined at contact points of the PESs. Starting at the  $S_2$  state, there is no efficient direct pathway for isomerization.<sup>110,111</sup> Instead, the  $S_1$  state is populated through a fast decay (<100 fs) in at least two different geometries. Reaching the  $S_1$  state by decay of the  $S_2$  state, different geometries are obtained in comparison to direct excitation through n- $\pi^*$  absorption.<sup>110</sup> At the  $S_1$  state, two competing conical intersections (CI) are present. One is a reactive CI resulting partially in the isomerization to the *Z*-azobenzene. The geometry at the reactive intersection is remarkably by its high C–N=N–C changes indicating an inversion assisted rotation (Figure 1.3).<sup>110</sup> However, the other unreactive CI results in the starting *E*-isomer. Overall, compared to the  $S_1$  excitation, the  $S_2$  excitation decreases the  $\Phi_{QY}$  by different starting geometries reaching the  $S_1$  state, which slightly prefers a decay through the unreactive CI.<sup>109,110,114</sup>

In contrast, for thermal relaxation, the rotation mechanism has been favored by theoretical studies for some time, but there was a discrepancy between theoretical and experimental activation energy values.<sup>115</sup> Usually, no excited states are involved here.<sup>103</sup> However, recent theoretical calculations suggest that a triplet-assisted rotational mechanism may be possible; for the transition entropies, and enthalpies, there is a higher agreement with the experiment. Transitioning between the ground state ( $S_0$ ) and the triplet state ( $T_1$ ) reduces the energy barrier for the rotational pathway.<sup>103,107,116,117</sup> Experimentally, prolonged thermal stability could be achieved by adding the heavy atom iodine. This induces a heavy atom effect, which lowered the probability for the triplet-state assistance during thermal isomerization and resulted in closer values to calculations not considering the triplet-assistance.<sup>103</sup>



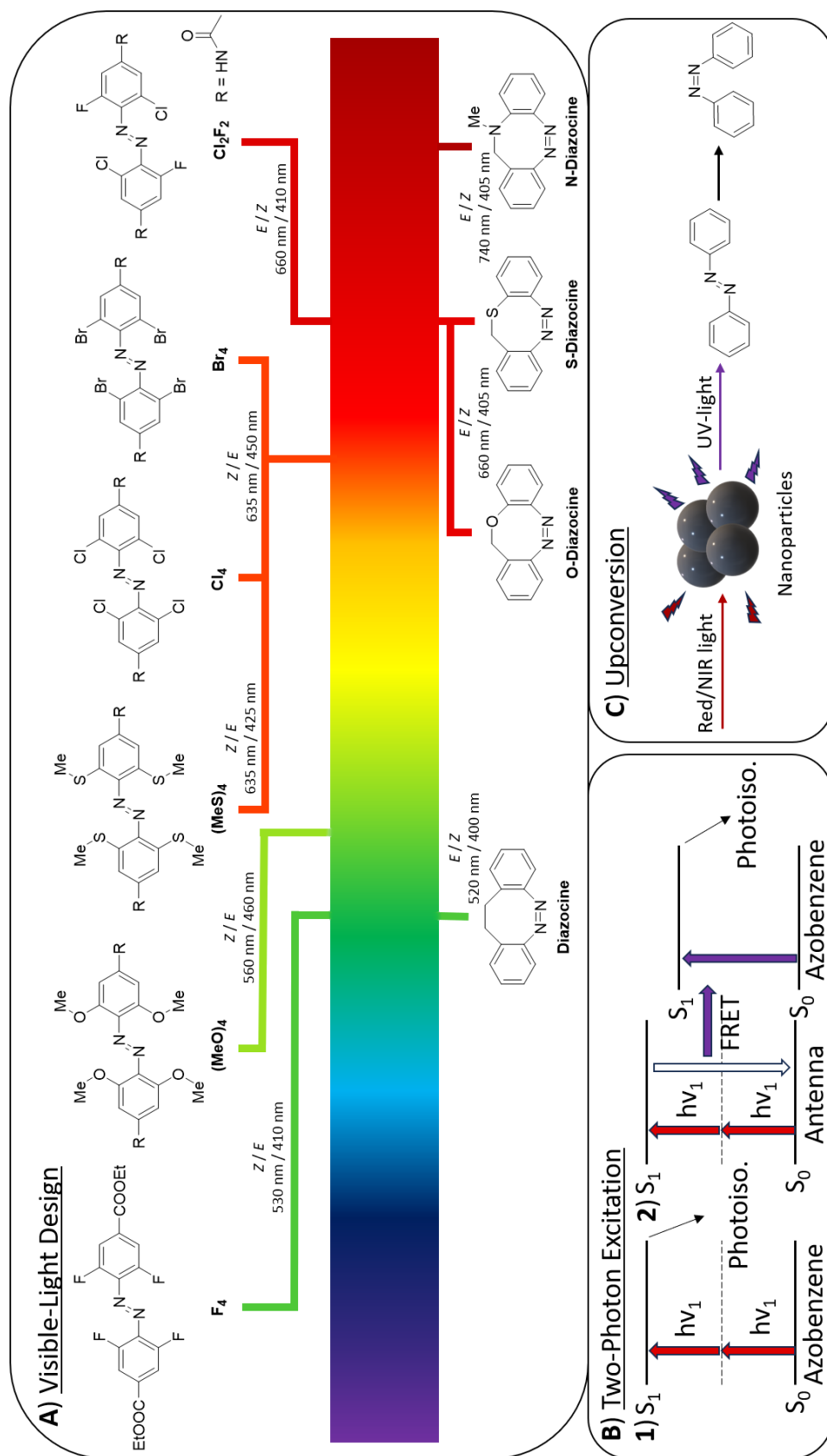


**Figure 1.5:** Three different concepts to photoisomerize azobenzene by visible light. **A)** The rational design of azobenzenes by different substitutions. The range of excitation wavelengths ranges from 530 (green) up to 740 nm (red/IR).<sup>118–126</sup> **B)** Excitation via two-photon absorption (TPA) of azobenzene directly (**B1**) or through fluorescence resonance energy transfer (FRET) of an antenna molecule to the azobenzene (**B2**). **C)** Photoisomerization of azobenzene induced through upconversion of higher wavelengths to shorter wavelengths by nanoparticles.



### 1.2.2 Addressability and Efficiency of Azobenzene

Switching with visible light is of increasing interest due its safe use of azobenzene in biological and medical sectors, as well as in close proximity to humans. This advancement permits significant applications previously considered unattainable.<sup>78,127</sup> The phototoxicity of UV-light is harmful for cells in general and the retina in particular.<sup>128,129</sup> To avoid UV-light irradiation, various modifications to azobenzene have already been introduced.<sup>54,130</sup> A well-known approach is the extension of the  $\pi$ - $\pi$  system through a push-pull effect of substituents on the azobenzene (pseudo-stilbene azobenzene).<sup>67,111</sup> Unfortunately, this not only leads to a red shift, but also to extremely short thermal half-life times, which is to be avoided in all applications considered in this thesis.<sup>67,111,131</sup> Recent development explored the topics of new rational design of azobenzene, two-photon excitation and upconversion to enable switching with visible light (Figure 1.5).<sup>54</sup>

#### Visible-Light Switching by Two Way $n$ - $\pi^*$ Excitation

The diazocine<sup>124</sup> published by Siewertsen *et al.* in 2009 is an ethylene bridged diazocine and is among the first compounds that photoisomerize around the visible range ( $>400$  nm) for both isomerizations.<sup>124,132</sup> Particularly notable about this molecule is not just its novel structure but also the fact that the angled *Z*-isomer is thermally favored (Figure 1.5).<sup>124,132</sup> These structural changes have paved the way for new applications benefiting from its unique shape.<sup>133–136</sup> Further modifications in recent years have led to switching processes at higher wavelengths by replacing the carbon in the ethylene bridge with heteroatoms, such as oxygen,<sup>137</sup> nitrogen,<sup>126</sup> or sulfur.<sup>137</sup>

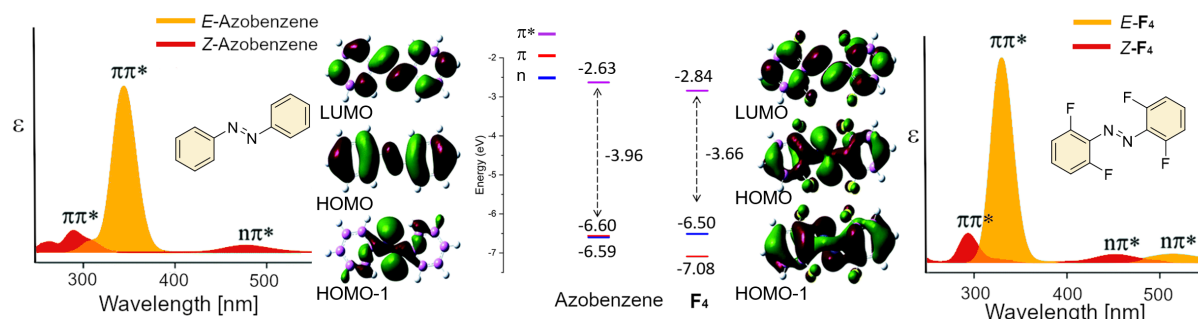


**Figure 1.6:** Vertical electronic absorption spectra, molecular orbital profiles for the *E*-isomer and frontier molecular orbital energy levels of the *E*-isomers of azobenzene and  $\mathbf{F}_4$ . The energy difference is reduced to -3.66 eV for the  $n$ - $\pi^*$  absorption in *E*- $\mathbf{F}_4$ , which results in an additional transition around 450 nm. Adapted with permission from Liu *et al.*<sup>138</sup>

Another class of switches in the visible range are the tetra-*ortho*-substituted azobenzene.<sup>a</sup> Initiated in 2011 by the Woolley group with tetra-*ortho*-methoxy substituted azobenzenes ( $(\mathbf{MeO})_4$ ),<sup>119</sup> switching with blue and green light became possible.<sup>54,119</sup> Since then, the publication of *ortho*-substituted azobenzenes has rapidly increased, and new systems have been developed.<sup>122,130,139</sup> Subsequently, tetra-*ortho*-fluoro azobenzenes ( $\mathbf{F}_4$ )<sup>118</sup> and tetra-*ortho*-chloro azobenzenes ( $\mathbf{Cl}_4$ )<sup>121</sup> were published. Later, this area was evolved by including chloro/fluoro hybrids ( $\mathbf{F}_2\mathbf{Cl}_2$ ),<sup>122</sup> tetra-*ortho*-bromo ( $\mathbf{Br}_4$ )<sup>123</sup> or tetra-*ortho*-thioether ( $(\mathbf{SEt})_4$ )<sup>120</sup> (Wavelength

<sup>a</sup>The notation for tetra-*ortho*-substituted azobenzene is  $\mathbf{R}_4$  and includes all azobenzenes with this motif. R stands for the substituted group.

for switching shown in Figure 1.5). Research to find a substitution pattern resulting in an even better switching in terms of red-shifted absorption and longer half-life times is still ongoing.<sup>122,123,140–142</sup>

However, all presented systems are based on pronouncing the  $n\text{-}\pi^*$  absorption in the  $E$ -isomer, which is almost absent in an unsubstituted azobenzene. The steric and electronic interaction of the lone pair of the nitrogen caused by the *ortho*-substitution enables the  $n\text{-}\pi^*$  absorption in the  $E$ -isomer and the separation to the  $Z$ -isomer  $n\text{-}\pi^*$  absorption.<sup>138,143</sup> It was observed that the  $\pi^*$  orbitals in  $E$ - and  $Z\text{-F}_4$  are stabilized, causing a hypsochromic (red-shift) in the  $n \rightarrow \pi^*$  band of  $E\text{-F}_4$  and a bathochromic shift (blue-shift) in the  $n \rightarrow \pi^*$  transition of  $Z\text{-F}_4$ .<sup>138</sup> As a result, unlike in many azobenzene derivatives where the  $n \rightarrow \pi^*$  band overlaps significantly with the  $\pi \rightarrow \pi^*$  transition these two bands are distinctly separated in  $\mathbf{F}_4$  (Figure 1.6).<sup>118,143</sup> In contrast to the significant twisting around the  $\text{N}=\text{N}$  double bond found in  $(\text{MeO})_4$ <sup>119</sup> and diazocines,<sup>132</sup>  $\mathbf{F}_4$  maintain a nearly flat structure.<sup>144</sup> This flatness is particularly relevant for certain uses that require efficient conjugation along the  $\pi$ -system, or for applications involving assemblies based on  $\pi\text{-}\pi$  stacking.<sup>138,142–144</sup>

The separation of the absorption bands of the  $E$ - and  $Z$ -isomer determines the switching efficiency measured by the photostationary state (PSS) and  $\Phi_{\text{QY}}$ . Due the overlap of absorption bands of the  $E$ - and  $Z$ -isomer, back-isomerisation occurs. The PSS is the established equilibrium of both isomers at a certain wavelength after irradiation.<sup>54,78,122,123,127</sup>  $\Phi_{\text{QY}}$  determines the successful isomerizations considering the absorbed photons. As mentioned before (Section 1.2.1), not every absorbed photon leads to the desired photoproduct. This phenomenon is respected in the  $\Phi_{\text{QY}}$  and is a value to determine the efficiency of a switching system. A value of  $\Phi_{\text{QY}} = 1$  is considered to be a perfect switch as each absorbed photon results in the desired isomerization product.<sup>132,145</sup>

## Two-Photon-Excitation

In two-photon absorption (TPA), the molecule is excited to a higher energy state by the simultaneous incidence of two photons. This nonlinear optical (NLO) phenomenon requires high light intensity for reliable activation. Typically, this intensity is achieved by strongly focusing a laser.<sup>146,147</sup> However, this approach not only allows for excitation of molecules through direct short-wavelength light but also enables the use of long-wavelength light for molecular excitation. This can trigger effects such as isomerization or fluorescence.<sup>147,148</sup> To use this effect for the photo-isomerization of azobenzene, there are two approaches: The first is to directly excite the azobenzene system through TPA (Figure 1.4, **B1**).<sup>149,150</sup> Altering the electron-donating groups (EDG) and electron-withdrawing groups (EWG) on azobenzene molecules led to improved nonlinear optical (NLO) properties.<sup>150,151</sup> The increase was especially notable when the molecules were modified to include both donor and acceptor substituents. Notably, alterations that enhance two-photon absorption (TPA) by boosting the probability of photon absorption considerably reduce the thermal half-life time.<sup>54,152,153</sup> Recent publications, however, show the potential for direct TPA of azobenzene with longer half-life times.<sup>154</sup> A  $\mathbf{F}_4$  derivative showed a cross-section

for two-photo-excitation in their given setup of  $\sigma^2 = 7 \text{ GM}^b$  in comparison to  $\sigma^2 = 1 \text{ GM}$  for the parent azobenzene.<sup>154</sup>

The second method is based on the incorporation of molecular motifs known to effectively undergo TPA.<sup>155</sup> These are called antenna and they are excited to a higher state. Typical antenna motifs are naphthalene,<sup>156</sup> anthracene<sup>157</sup> or triphenylamine<sup>154</sup> derivatives. Subsequently, they can initiate the photoisomerization of azobenzene through a resonance energy transfer to the azobenzene (Figure 1.4, **B2**).<sup>147,156–159</sup> Both variants have the advantage of using light with long wavelengths, thereby avoiding damage to photosensitive material and achieving increased light penetration.<sup>147,160–162</sup> These properties are particularly important for biological and optical data storage applications, owing to the deep penetration of various mediums by long wavelengths and the precise spatial three-dimensional addressability.<sup>156–158,163</sup>

### Upconversion

In the process of upconversion, nanoparticles convert long-wavelength, low-energy light into short-wavelength, high-energy light.<sup>160</sup> These upconverting nanoparticles (UCNPs) are doped with lanthanides, elements chosen for their unique electronic configurations that facilitate efficient energy transfer, enabling the upconversion process.<sup>164</sup> The emitted high-energy light from UCNPs can stimulate the photoisomerization of azobenzene when in close spatial proximity, a phenomenon depicted in Figure 1.5.<sup>165</sup> This capability of photosensitizing for visible light, although straightforward, is effective only at close ranges to the azobenzene molecules, highlighting a limitation in spatial application. The upconversion efficiency of these nanoparticles, quantified by quantum yields ( $\Phi_{\text{QY}}$ ), ranges from 1% to 13%, varying with particle size.<sup>166,167</sup> This relatively low quantum yield points to one of the significant challenges in the field, necessitating ongoing research to optimize the efficiency of upconversion through nanoparticle engineering.<sup>54,160,168</sup>

---

<sup>b</sup> $\sigma$  describes the cross-section and is a measure of the probability of an interaction between an incoming wave radiation;  $1 \text{ GM} = 10^{-50} \text{ cm}^4 \text{ s photon}^{-1} \text{ molecule}^{-1}$

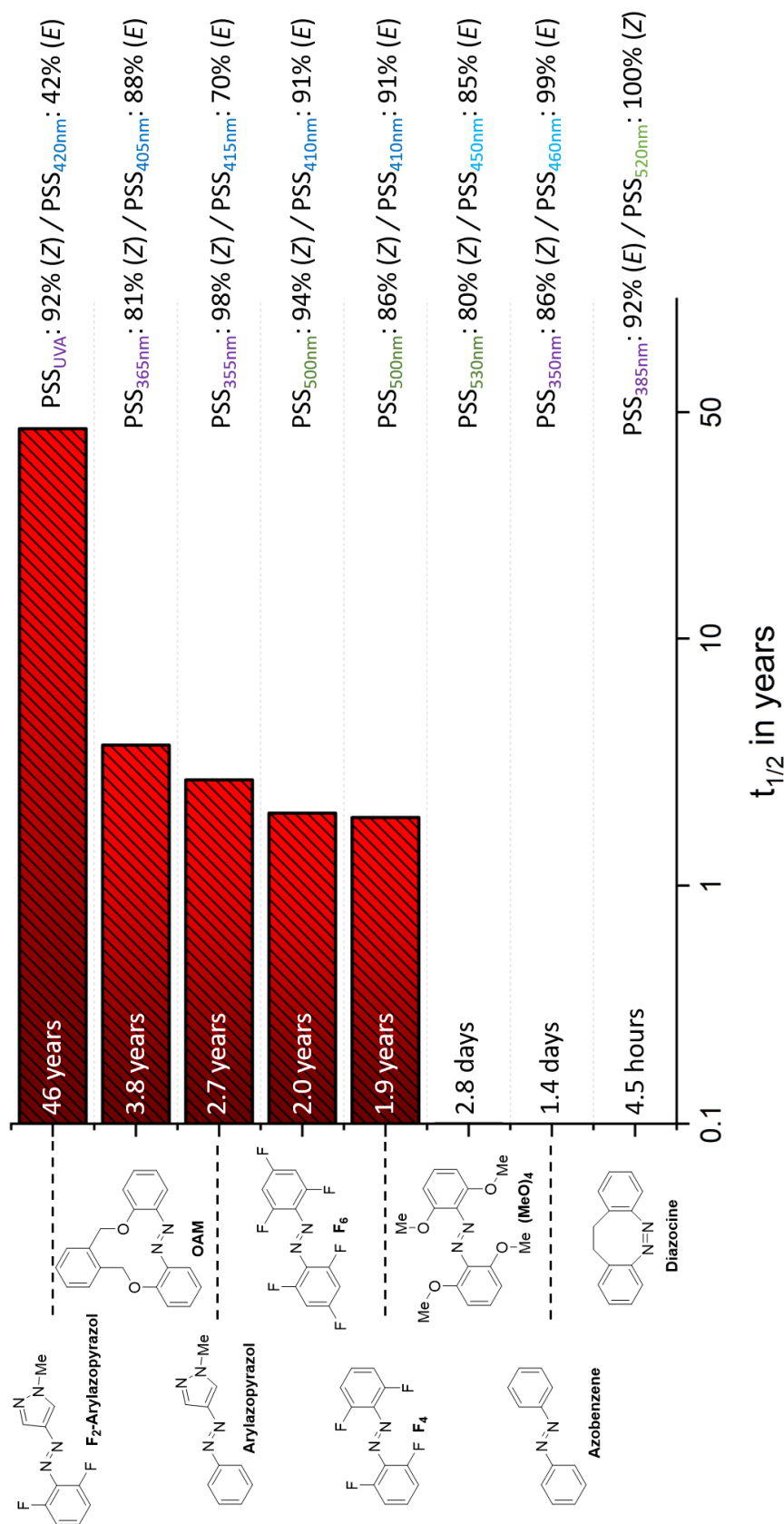


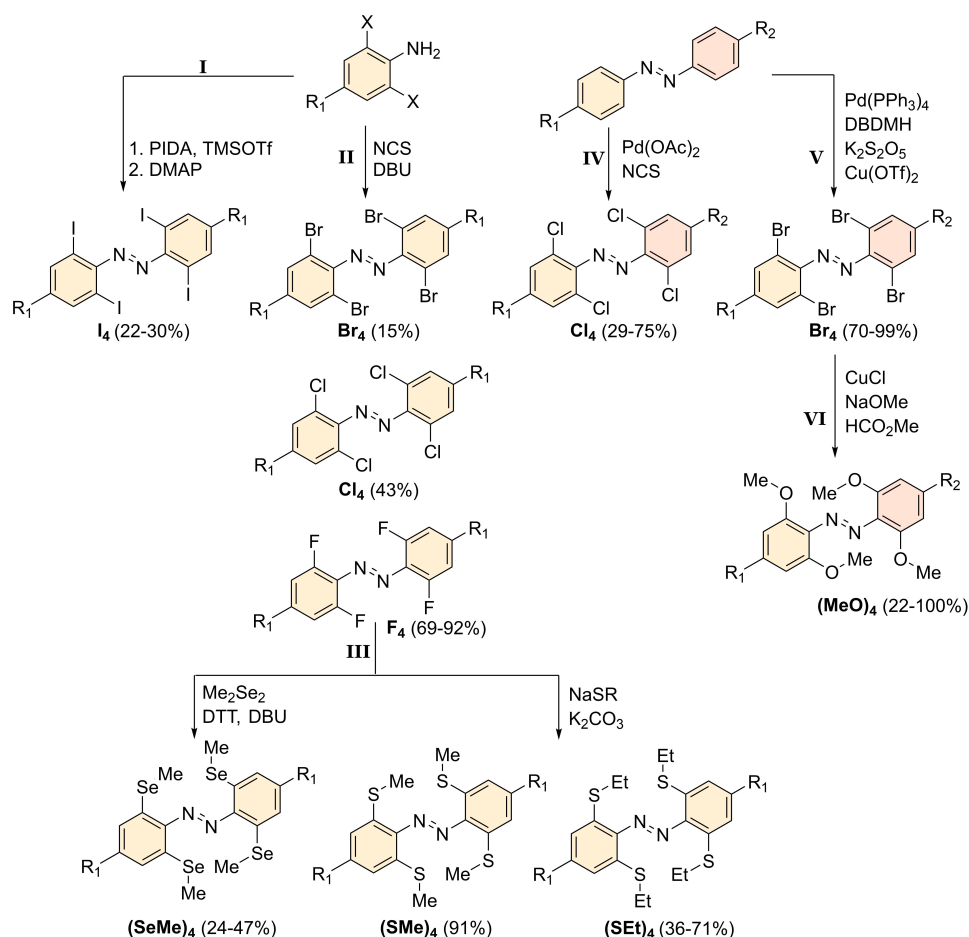
**Figure 1.7:** Comparison of the reported half-life time for different azo-type compounds and their given photoconversion at a certain wavelength (PSS). Solvent and minor temperature differences were not taken into account.<sup>118,124,143,169-172</sup> The half-life time ( $t_{1/2}$ ) for **azobenzene** is given at 35 °C and the value for **OAM** at 25 °C was determined during this thesis.

### 1.2.3 Thermal Half-Life Time of the Metastable Azobenzene Isomer

In the thermal relaxation of azobenzene from the metastable isomer to the thermally stable isomer, the thermal half-life time ( $t_{1/2}$ ) is the key parameter to consider. It describes the time taken for half of the azobenzene molecules in its metastable state to revert to the thermally stable isomer at a certain temperature. The isomerization rate is first order and the half-life time is influenced by several factors. Naturally, temperature is the most critical factor, as higher temperatures, like in many chemical reactions, increase the isomerization rate.<sup>173–175</sup> Then, the environment in which the azobenzene is embedded plays an important role. In solution, the polarity of the solvent can affect the stability of the metastable isomer. Similarly, in a densely packed polymer matrix, the surrounding environment can either stabilize or destabilize it.<sup>176,177</sup> Other factors relate to modifications of the azobenzene itself. Depending on their position, EDGs can stabilize the *Z*-isomer, while EWGs can have a destabilizing effect. The steric hindrance and molecular rigidity has a large influence on the thermal  $t_{1/2}$ . The introduction of bulky groups or ring-strain through a cyclization can also stabilize the *Z*-form.<sup>108,172,178–180</sup> The pure azobenzene possesses a  $t_{1/2}$  of 1.4 d in benzene at 35 °C (Figure 1.7).<sup>169</sup> In contrast, diazocine exhibits a reduced  $t_{1/2(25^\circ\text{C})}$  of just 4.5 h.<sup>124</sup> Only the tetra-*ortho*-substitution succeeded in significantly extending the  $t_{1/2}$  while maintaining the parent azobenzene motif. Whereas methoxy groups ((**MeO**)<sub>4</sub>) have a minor influence with  $t_{1/2(25^\circ\text{C})} = 2.8$  d,<sup>119</sup> fluorine (**F**<sub>4</sub>) substitution increased the  $t_{1/2(25^\circ\text{C})}$  to an impressive 1.9 years.<sup>118</sup> The notably long  $t_{1/2}$  and the high  $\text{PSS}_{530\text{nm},Z} = 86\%$  in the visible range contribute to the attractiveness of **F**<sub>4</sub> azobenzene. Further substitution in the *para*-position (**F**<sub>6</sub>) could extend the  $t_{1/2(25^\circ\text{C})}$  to 2 years.<sup>143</sup> It is noteworthy that a substitution in the *meta*-position with fluorine did not improve the half-life time or switchability.<sup>143</sup> Replacing the fluorine group with heavier halogens reduced the  $t_{1/2(25^\circ\text{C})}$  from days (**Cl**<sub>4</sub>) to hours (**Br**<sub>4</sub>) to minutes (**I**<sub>4</sub>).<sup>123</sup> It was only with the introduction of heterocycles by the Fuchter group that these half-life times were surpassed, exhibiting a stability ranging from 10 to 1000 d (3.8 years) for arylazopyrazole.<sup>170</sup> However, this class of azobenzene cannot be switched with visible light and exhibits less switching efficiency.<sup>170</sup> Combination of arylazopyrazoles with the **F**<sub>2</sub> substitution increased the  $t_{1/2(25^\circ\text{C})}$  to remarkable 46 years. Yet, the ability to switch fully with visible light remained elusive.<sup>171</sup> Another approach to modify the properties of azobenzene is cyclization.<sup>181–183</sup> For diazocine, a very short ethylene bridge was used to strain the azo linkage, leading to the thermodynamically stable *Z*-isomer. A more relaxed oxygen-linked azobenzene macrocyclic motif (**OAM**) was demonstrated by the Staubitz group, showing long half-life times of  $t_{1/2(70^\circ\text{C})} = 36.4$  h and a good switching efficiency in the UV range ( $\text{PSS}_{355\text{nm},Z} = 81\%$ ,  $\text{PSS}_{405\text{nm},E} = 88\%$ ).<sup>172</sup> Unfortunately, further optimization of this motif by replacing the oxygen atoms with carbon atoms resulted in a significant reduction in half-life times.<sup>184,185</sup>

1.2.4 Synthesis of Tetra-*Ortho*-Substituted Azobenzenes

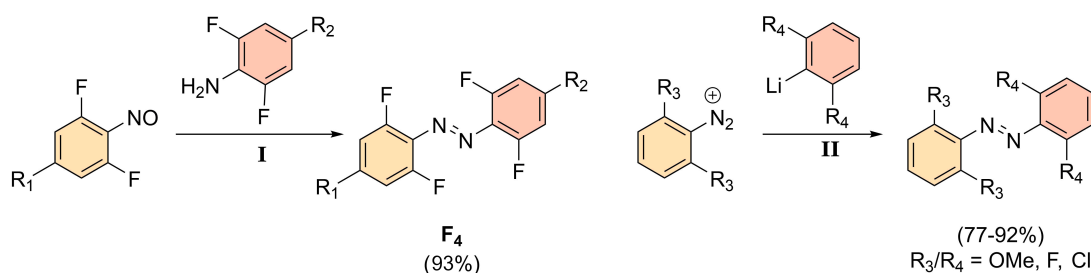
The initial syntheses of  $(\text{MeO})_4$ <sup>119</sup> and  $\text{F}_4$ <sup>118</sup> were documented with modest yields of 16%-24%. A common strategy in these procedures is the oxidation of aniline to azobenzene.<sup>118,119</sup> To achieve this, a diverse array of oxidizing agents has been evaluated over time: The Weiss reagent was used as an oxidant to create the first tetra-*ortho*-iodo azobenzene ( $\text{I}_4$ ) in a yield of 13-30% (Scheme 4, **I**).<sup>123</sup> The most common synthesis for  $\text{F}_4$  derivatives is an oxidation with N-chlorosuccinimide (NCS) and the base 1,8-diazabicyclo[5.4.0]undec-7-en (DBU) at -78 °C, resulting the corresponding azobenzene within 15 min (Scheme 4, **II**).<sup>186</sup> A nucleophilic aromatic substitution ( $\text{S}_{\text{N}}\text{Ar}$ ) of  $\text{F}_4$  yields the thio-ether  $(\text{SMe})_4$ ,  $(\text{SEt})_4$  and even  $(\text{SeMe})_4$  in moderate yields between 24% to 71% (Scheme 4, **III**).<sup>117,123</sup> Other approaches are based on the late-stage functionalization of azobenzenes. These methods rely on the *ortho*-directing effect of the azo group regarding a palladium catalyst, thus enabling C–H activation.<sup>189</sup> The major advantage for this synthetic strategy is the large access of published azobenzenes, which can be further functionalized.<sup>121</sup> The first reported C–H activation for the synthesis of tetra-*ortho*-substituted azobenzenes was reported by the group of Trauner.<sup>121</sup> By late-stage functionalization



**Scheme 4:** The overview was simplified by giving a selection of a few synthetic procedures. These are either high yielding or give access to new tetra-*ortho*-substituted azobenzenes.<sup>123</sup> **I**) Oxidation of aniline with Weiss reagent towards  $\text{I}_4$ . **II**) NCS and DBU oxidize the aniline to the azobenzenes  $\text{F}_4$ ,  $\text{Cl}_4$  and  $\text{Br}_4$ .<sup>186</sup> **III**) Aromatic  $\text{S}_{\text{N}}\text{Ar}$  substitution of  $\text{F}_4$  to convert to  $(\text{SeMe})_4$ ,  $(\text{SMe})_4$  and  $(\text{SEt})_4$ .<sup>117,123</sup> **IV**) Late-Stage chlorination of azobenzene by palladium catalyzed C–H activation to yield  $\text{Cl}_4$ .<sup>121</sup> **V**) Late-Stage bromination of azobenzene by palladium catalyzed C–H activation to yield  $\text{Br}_4$ .<sup>187</sup> **VI**) Copper catalyzed methoxylation of  $\text{Br}_4$  to obtain  $(\text{MeO})_4$ .<sup>188</sup>  $\text{R}_1$  and  $\text{R}_2$  are undefined and only symbolize symmetrical and asymmetrical compounds.

to azobenzene with palladium acetate and NCS as a chlorinating agent,  $\text{Cl}_4$  derivatives were obtained in moderate to good yields (Scheme 4, **IV**).<sup>121</sup> This procedure was optimized by Liu *et al.* with tetrakis(triphenylphosphine)palladium(0) as catalyst and  $\text{K}_2\text{S}_2\text{O}_5$  in combination with trichloro isocyanuric acid (TCCA) to produce chlorine radicals.<sup>187</sup> By only exchanging the TCCA with 1,3-dibromo-5,5-dimethylhydantoin (DBDMH), bromine radicals were produced and  $\text{Br}_4$  was obtained in high yields (70-99%, Scheme 4, **V**).<sup>187,188</sup> Recently, an even further functionalization of the  $\text{Br}_4$  to  $(\text{MeO})_4$  by a copper catalyzed methoxylation was published (Scheme 4, **VI**).<sup>188</sup> The reaction yielded  $(\text{MeO})_4$  in overall good yields (22-100%) in comparison to the direct methoxylation of azobenzenes by C-H activation, which resulted in low yields of 6-38% by the group of Thorn-Seshold.<sup>190</sup>

The classical approach for asymmetrical synthesis of tetra-*ortho*-substituted azobenzene is so far only reported for the synthesis of  $\text{F}_4$  derivatives. The Mills reaction was optimized by using a solvent mixture for the condensation reaction of the nitrosobenzene with the aniline. The solvent mixture contains the strong acidic trifluoroacetic acid (TFA) in combination with acetic acid and toluene (3:3:1). This mixture and prolonged reaction times gave asymmetrical  $\text{F}_4$  derivatives in high yields up to 93% (Scheme 5, **I**).<sup>127,154</sup> The azo coupling of the diazonium salt with an activated aromatic compound, was also conducted for different asymmetrical  $\text{R}_4$  ( $\text{R} = \text{F}, \text{Cl}, (\text{OMe})$ ) derivatives with yields ranging between 26 to 58%.<sup>191-194</sup> The diazonium-salts were also coupled with lithiated aromatics to yield different  $\text{R}_4$  azobenzenes in good yields (Scheme 5, **II**, 77-92%). However, further functionalization of these compounds were restricted.<sup>100</sup>



**Scheme 5:** Overview of synthetic procedures to obtain asymmetrical tetra-*ortho*-substituted azobenzenes. **I**) Mills reaction to obtain asymmetrical  $\text{F}_4$ .<sup>127,154</sup> **II**) Azo coupling of diazonium salts with aromatic organolithium derivatives resulting in different *ortho*-substituted azobenzenes and asymmetrical hybrids such as  $\text{MeO}_2\text{F}_2$ .<sup>100</sup>

For the formation of a tetra-*ortho*-substituted azobenzene, the desired substituent was mostly introduced by pre-functionalization of the corresponding aniline prior to the azo coupling.<sup>118</sup> Functionalization after the formation of the azobenzene moiety mostly included fundamental reactions like etherfication,<sup>195</sup> esterification<sup>192</sup> or amidiation.<sup>196</sup> Access to a variety of cross-coupling synthesis protocols for unsubstituted azobenzenes could also be applied to the functionalization of tetra-*ortho*-substituted azobenzenes.<sup>154,191,195,197-199</sup> Therefore, the published cross-coupling possibilities have been summarized in a review (Chapter 2.1).

### 1.2.5 Macrocyclic *Ortho*-Azobenzenes

Macrocycles are widely employed for the selective encapsulation of ions, exemplified by crown ethers, and serve as integral components in molecular machinery, notably in rotaxanes, where they function as shuttles.<sup>200</sup> This capability was further augmented by the integration of an

azobenzene unit, enabling the switchable control of the ion-binding affinity of the crown ether.<sup>200</sup> Additionally, the incorporation of azobenzenes allows for modulation of the cavity size in calixarenes, demonstrating the versatility of azobenzene in tuning molecular interactions.<sup>201</sup> After introducing already to diazocine and **OAM** as representatives for *ortho*-substituted cyclic azobenzenes, the selection was expanded to further systems.<sup>c</sup> Special attention is given to the ring size and elemental composition. While a 12-membered macrocycle (**OAM**) was described with an extended half-life time and a thermally stable *E*-isomer, the *Z*-isomer was observed as the thermally stable one in an 8-membered ring (diazocine, Figure 1.8).<sup>124</sup> No photoisomerization was observed in a 12-membered ring made of three azo units (**M1**).<sup>202</sup> Reducing the ring size to a 6-membered ring (**M2**), again no photoisomerization could be achieved.<sup>203</sup> Hence, not only the ring size but also the integrated atoms in the macrocyclic lasso have to be taken into consideration.

In order to approximately evaluate the influence of cyclization on the switching properties, the following selection discusses *ortho*-macrocyclic azobenzene with information on successful photoisomerization (Figure 1.9). Comparing the overall yields, moderate to low values were reported with an exception of the 12-membered rings **OAM** and **M3**. The 12-membered ring **OAM** possesses great PSS conversions for both photoisomerizations ( $\text{PSS}_{365\text{nm},Z} = 81\%$ ,  $\text{PSS}_{405\text{nm},E} = 88\%$ ) and high thermal stability for the metastable *Z*-isomer at 70 °C ( $t_{1/2(70^\circ\text{C})} = 36.4$  h). However, an expansion of the  $\pi$ -system by cross-coupling reactions in *para*- or *meta*-position significantly reduced the half-life time ( $t_{1/2(70^\circ\text{C})} = 0.8$  h up to 7.3 h).<sup>185</sup> Recently, the oxygen atom was exchanged with a carbon atom in the flexible linker (**M3**) by the group of Krbek<sup>184</sup> resulting in a reduction of  $t_{1/2(25^\circ\text{C})}$  to 16 d. Additionally, the PSS of **M3** ( $\text{PSS}_{365\text{nm},Z} = 53\%$ ) is lower in comparison to **OAM** ( $\text{PSS}_{365\text{nm},Z} = 81\%$ ). However, a full conversion back to the thermal stable *E*-isomer by irradiation with ambient light was achieved. They also conducted further late-stage modifications by C–H activation and obtained a di-*ortho*-methoxy substituted derivative (**(MeO)<sub>2</sub>M3**). Notably, **(MeO)<sub>2</sub>M3** could not be photoisomerized, which might be reminded in hindsight to the results of Publication III. Other *ortho*-substitution patterns and further *para*-substitution did not yield any improvements in terms of half-life time and PSS conversions.<sup>184</sup> The odd numbered 17-membered ring **M4** was bridged by a sugar. Although the rigid benzene is missing, the conformational barrier of the sugar led to a prolonged  $t_{1/2(25^\circ\text{C})}$  of 51 d and a good PSS for the *Z*-isomer ( $\text{PSS}_{365\text{nm},Z} = 95\%$ ). However, the back-isomerization was not sufficient with  $\text{PSS}_{435\text{nm},E} = 53\%$ .<sup>204</sup> The photoisomerization of the 16-membered rings **M5** and **M6** was reported to photoisomerize, but no exact values were

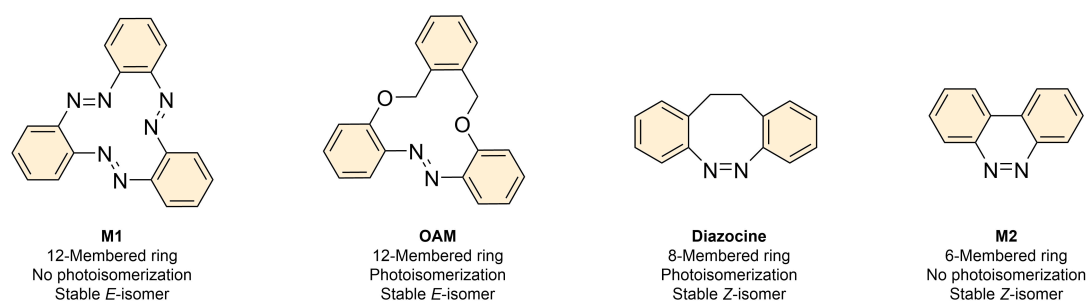


**Figure 1.8:** Influence of ring size and linker composition on photoisomerization and the thermal stable isomer.

<sup>c</sup>In this chapter, macrocyclic compounds that form the macrocycle via *meta*- or *para*-position are not considered.



determined.<sup>205,206</sup> The pyridine bridged 15-membered rings **M7** and **M8** were synthesized to bind metal cations. The thermal relaxation was measured to be  $t_{1/2}(25^\circ\text{C}) = 92$  d for the oxygen derivative **M7** and  $t_{1/2}(25^\circ\text{C}) = 118$  d for the sulfur derivative, respectively. Interestingly, in the presence of  $\text{Cu}^{2+}$  cations, the formed complex spontaneously relaxed to the *E*-isomer.<sup>207,208</sup> The binaphthol bridged azobenzenes **M9**, **M10**, **M11**, **M12** and **M13** are used as a chiroptical switch. Regardless of the different chain lengths, the reported PSS for both photoisomerizations are in a similar range of 58% to 68% to the *E*-isomer and 56% to 88% to the *Z*-isomer (Exact values given in Figure 1.9). Notably, the 14-membered ring **M10** resulted in a thermally stable *Z*-isomer, caused by the binaphthyl framework.<sup>209–212</sup> Photoisomerization was observed for compound **M14** with its two azo groups.<sup>213</sup> Additional long chain extensions at **M14** in its *para*-position led to a switchable liquid crystallinity. For the xanthene-based azobenzene dimer **M15**,<sup>182</sup> long thermal relaxation from the *Z,Z*-isomer to *E,Z*-isomer was reported with  $t_{1/2}(30^\circ\text{C})_{Z,Z} = 1600$  d. After the initial relaxation of the first azo group, the second one relaxed in a cascade effect, occurring significantly faster ( $t_{1/2}(30^\circ\text{C})_{E,Z} = 1.3$  min). Despite the constraints around the azo group in **M15**, good PSSs were obtained for both photoisomerizations (PSS<sub>405nm,E</sub> = 68%, PSS<sub>365nm,Z</sub> = 88%).<sup>182</sup>

In summary, rigidity and strain needs to be balanced out. Rigidity can be tuned by aromatic units in the linker, while the strain can be adjusted by the chain length and its incorporated atoms.

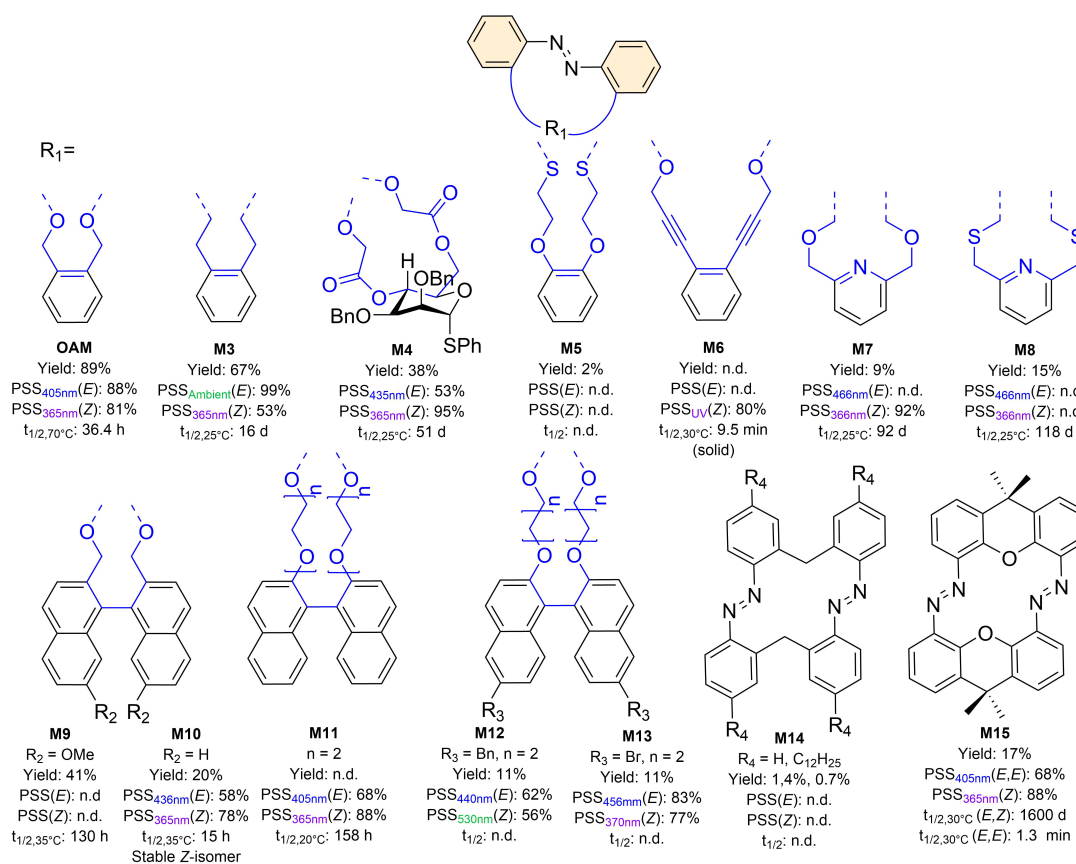


**Figure 1.9:** Overview of published *ortho*-macrocylic azobenzenes ranging from 12- up to 21-membered ring systems and their PSS as well as thermal half-life time. Note: n.d. = not determined in the publication.



# Publication I

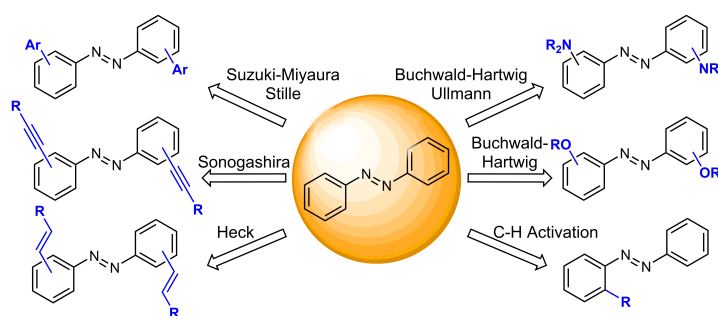
## 2.1 Modification of Azobenzene by Cross-Coupling Reactions

Title of Publication:

### Modification of Azobenzenes by Cross-Coupling Reactions

M. Walther, W. Kipke, S. Schultzke, S. Ghosh, A. Staubitz, *Synthesis*, **2021**, *53*, 1213-1228.

Permission to reprint in Appendix 9.6.



**Abstract:**

Azobenzenes are among the most extensively used molecular switches for many different applications. The need to tailor them to the required task often requires further functionalization. Cross-coupling reactions are ideally suited for late-stage modifications. This review provides an overview of recent developments in the modification of azobenzene and its derivatives by cross-coupling reactions.

**Abstract (deutsch):**

Azobenzole gehören zu den meist genutzten molekularen Schaltern für verschiedene Anwendungsbereiche. Die Anpassung der Azobenzole für die jeweilige Anwendung, benötigt weitere Funktionalisierung des Azobenzols. Kreuz-Kupplungen sind ideal geeignet, um eine funktionalisierende Modifikation auch im späten Stadium durchzuführen. Diese Review gibt eine Übersicht an derzeitigen Entwicklungen im Bereich der Modifikationen von Azobenzol und seine Derivate durch Kreuz-Kupplungsreaktionen.

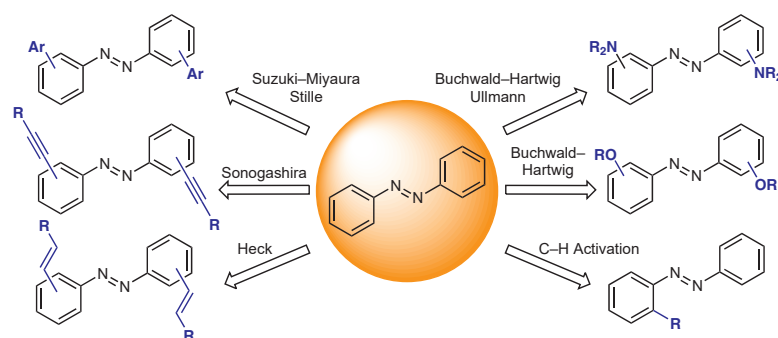
**Author Contribution to this Publication:** For this review article, I (Sven Schultzke) conducted in collaboration with the other authors the scientific research in the chapter of palladium catalyst with emphasize on and draft of the Suzuki-Miyaura cross-coupling reaction.

# Modification of Azobenzenes by Cross-Coupling Reactions

Melanie Walther<sup>a,b</sup> Waldemar Kipke<sup>a,b</sup> Sven Schultzke<sup>a,b</sup> Souvik Ghosh<sup>a,b</sup> Anne Staubitz<sup>\*a,b</sup>

<sup>a</sup> University of Bremen, Institute for Analytical and Organic Chemistry, Leobener Straße 7, 28359 Bremen, Germany  
staubitz@uni-bremen.de

<sup>b</sup> MAPEX Center for Materials and Processes, Bibliothekstraße 1, 28359 Bremen, Germany



Received: 07.10.2020

Accepted after revision: 19.11.2020

Published online: 28.01.2021

DOI: 10.1055/s-0040-1705999; Art ID: ss-2020-z0528-sr

License terms:

© 2021. The Author(s). This is an open access article published by Thieme under the terms of the Creative Commons Attribution License, permitting unrestricted use, distribution and reproduction, so long as the original work is properly cited. (<https://creativecommons.org/licenses/by/4.0/>)

**Abstract** Azobenzenes are among the most extensively used molecular switches for many different applications. The need to tailor them to the required task often requires further functionalization. Cross-coupling reactions are ideally suited for late-stage modifications. This review provides an overview of recent developments in the modification of azobenzene and its derivatives by cross-coupling reactions.

- 1 Introduction
- 2 Azobenzenes as Formally Electrophilic Components
  - 2.1 Palladium Catalysis
  - 2.2 Nickel Catalysis
  - 2.3 Copper Catalysis
  - 2.4 Cobalt Catalysis
- 3 Azobenzenes as Formally Nucleophilic Components
  - 3.1 Palladium Catalysis
  - 3.2 Copper Catalysis
  - 3.3 C–H Activation Reactions
- 4 Azobenzenes as Ligands in Catalysts
- 5 Diazocines
  - 5.1 Synthesis
  - 5.2 Cross-Coupling Reactions
- 6 Conclusion

**Key words** azobenzene, diazocine, molecular switches, cross-coupling reactions, C–H activation, metal-catalyzed

## 1 Introduction

Azobenzene and its derivatives are among the most investigated molecular switches.<sup>1</sup> They can interconvert photochemically and thermally between their metastable (*E*)- and (*Z*)-isomers (Figure 1).<sup>2</sup>

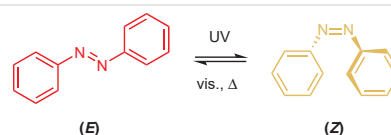


**Figure 1** Reversible isomerization of azobenzene<sup>2</sup>

Several physicochemical characteristics are affected by this photoisomerization, e.g. geometry and end-to-end distance,<sup>3</sup> electronic properties,<sup>4</sup> and polarity.<sup>2</sup> Whereas (*E*)-azobenzene is planar<sup>3a</sup> and without a dipole moment,<sup>4</sup> (*Z*)-azobenzene shows a non-planar geometry<sup>3b</sup> and a dipole moment of 3.0 D.<sup>4</sup> Consequently, azobenzene derivatives have gained great interest, for example for applications in data storage materials,<sup>5</sup> dynamic molecular devices,<sup>1</sup> or in photonics.<sup>6</sup>

Thus, manifold synthetic procedures have been developed for the preparation of azobenzene derivatives,<sup>7</sup> most with the formation of the diazenyl group as the key step. Methods to obtain symmetric azobenzenes range from reductive coupling of nitrobenzenes<sup>8</sup> or oxidative coupling of anilines.<sup>9</sup> The Mills reaction<sup>10</sup> or azo-coupling reactions<sup>11</sup> can be used to prepare asymmetric azobenzene derivatives. However, functionalized azobenzenes obtained in this way usually require prefunctionalized starting materials<sup>7</sup> which limits the synthetic modification possibilities. An additional problem is the susceptibility of the diazenyl group towards oxidizing<sup>11b,12</sup> and reducing<sup>13</sup> agents. Therefore, late-stage modification through cross-coupling reactions provides a valuable alternative to access a wider variety of azobenzene derivatives. This short review aims to give a broad, but not exhaustive, overview of the synthetic possibilities offered by cross-coupling reactions on azobenzenes and diazocines. In this short review, we distinguish between azobenzenes as formally electrophilic and formally nucleo-



(from left to right) **Melanie Walther** studied chemistry and business administration at the University of Kiel. After research stays at Cardiff University as well as at Stockholm University, she joined the Staubitz group for her master's thesis, dealing with photoswitchable polysiloxanes. During her following doctoral study at the University of Bremen she wants to expand the synthetic scope of molecular switches and their application into materials.

**Waldemar Kipke** studied biochemistry at Leibniz University in Hannover and obtained his bachelor's degree in 2016. He wrote his master's thesis about new ethylene-bridged molecular switches and obtained his master's degree in October 2018. During his Ph.D., he continues to work on molecular switches and new heterocycles containing B, Zr, and Sn.

**Sven Schultzke** studied chemistry at the University of Kiel and joined the Staubitz group for his bachelor's thesis about organogold(I) cross-coupling reactions. His upcoming research has been based on photoswitchable molecules, starting with a research exchange to the University of British Columbia in Vancouver for his master thesis and now his doctoral study, where he designs smart materials for 'soft grippers'.

**Souvik Ghosh** completed his M.Sc. from SVNIT, India. During his studies, he was a DAAD scholar at KIT, Germany and a OIST research scholar at OIST, Japan. In 2018, he joined the Staubitz group as Ph.D. student focusing on the synthesis of novel switchable molecules and their application in materials and polymer sciences.

**Anne Staubitz** was an assistant professor at the University of Kiel, before moving to the University of Bremen in 2015, where she has a full professorship for organic functional materials. Her main interests are light and force sensitive materials. The primary research focus is on their syntheses and properties, as well as applications. The second large research area in the group is comprised of compounds and materials that contain unusual combinations of main group elements and heavier elements.

philic components because of the different requirements and the corresponding difficulties in the synthesis of the azobenzene precursors, especially for nucleophilic derivatives.

## 2 Azobenzenes as Formally Electrophilic Components

(Pseudo)halogenated azobenzenes are used as an electrophilic component in cross-coupling reactions with a large variety of organometallic (nucleophilic) coupling partners. These (pseudo)halogenated species are usually obtained by employing prefunctionalized building blocks.<sup>7</sup> There are very few reported examples of the direct halogenation of azobenzene derivatives.<sup>14</sup> The relatively low reactivity of azobenzenes towards electrophilic halogenation reactions results from the electronic properties of the diazenyl group, which can form adducts with halogen halides leading to low yields.<sup>14a,b</sup> The use of elemental halogens often results in inseparable mixtures of mono-, di-, tri-, and tetrahalogenated products.<sup>14a,c,d</sup> Due to the lone-electron pairs on the nitrogen atoms, the diazenyl group can coordinate to metal catalysts facilitating substitution in the *ortho*-position.<sup>14e</sup> *ortho*-Halogenation is thus possible via metal-catalyzed C–H activation.<sup>14c,e,f</sup> However, different coordination patterns of the metal catalyst on the azobenzene moiety have been detected.<sup>14d</sup> Thus, selective halogenation remains challenging.<sup>14e</sup>

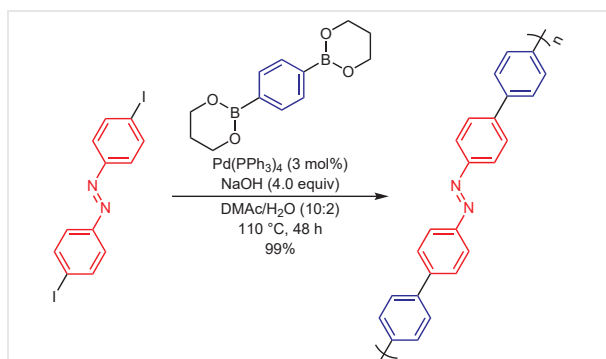
## 2.1 Palladium Catalysis

Palladium catalysts are the most frequently used catalysts in cross-coupling reactions. Therefore, the high number of palladium-catalyzed cross-coupling reactions of azobenzene derivatives that serve as a formally electrophilic component is no surprise.

### 2.1.1 Suzuki–Miyaura Cross-Coupling Reactions

The Suzuki–Miyaura cross-coupling reaction of (pseudo)halogenated azobenzenes with boronic acids or esters is one of the most frequently used cross-coupling reactions for the modification of azobenzenes. Due to its convenience, reliability, and high yields, it is often used as the final synthetic step to combine large building blocks.<sup>15</sup> Of the many available examples, in this review we place a certain focus on polymers or molecules that self-assemble: such larger molecules are often not easy to prepare and this is where the benefits of the Suzuki–Miyaura cross-coupling are most relevant. Consequently, the Suzuki–Miyaura cross-coupling reaction gives access to many azobenzene derivatives with new applications in self-assembled materials<sup>15a</sup> or many liquid crystals,<sup>15b–d,16</sup> compounds that show tunable fluorescence,<sup>17</sup> photoswitchable porphyrin systems,<sup>15e–g</sup> dendrimers,<sup>15h</sup> polymers,<sup>15i–o</sup> metal-organic frameworks (MOFs),<sup>15p</sup> as well as molecular machines such as rotaxanes.<sup>15q,r</sup>

The first successful Suzuki–Miyaura cross-coupling reaction of an azobenzene derivative was described in a polymerization reaction (Scheme 1);<sup>15i</sup> different conjugated polymers were synthesized with molecular weights up to  $M_n = 9700$  (in yields of 80–99%).



**Scheme 1** Suzuki–Miyaura cross-coupling reaction for polymerization of an azobenzene derivative<sup>15i</sup>

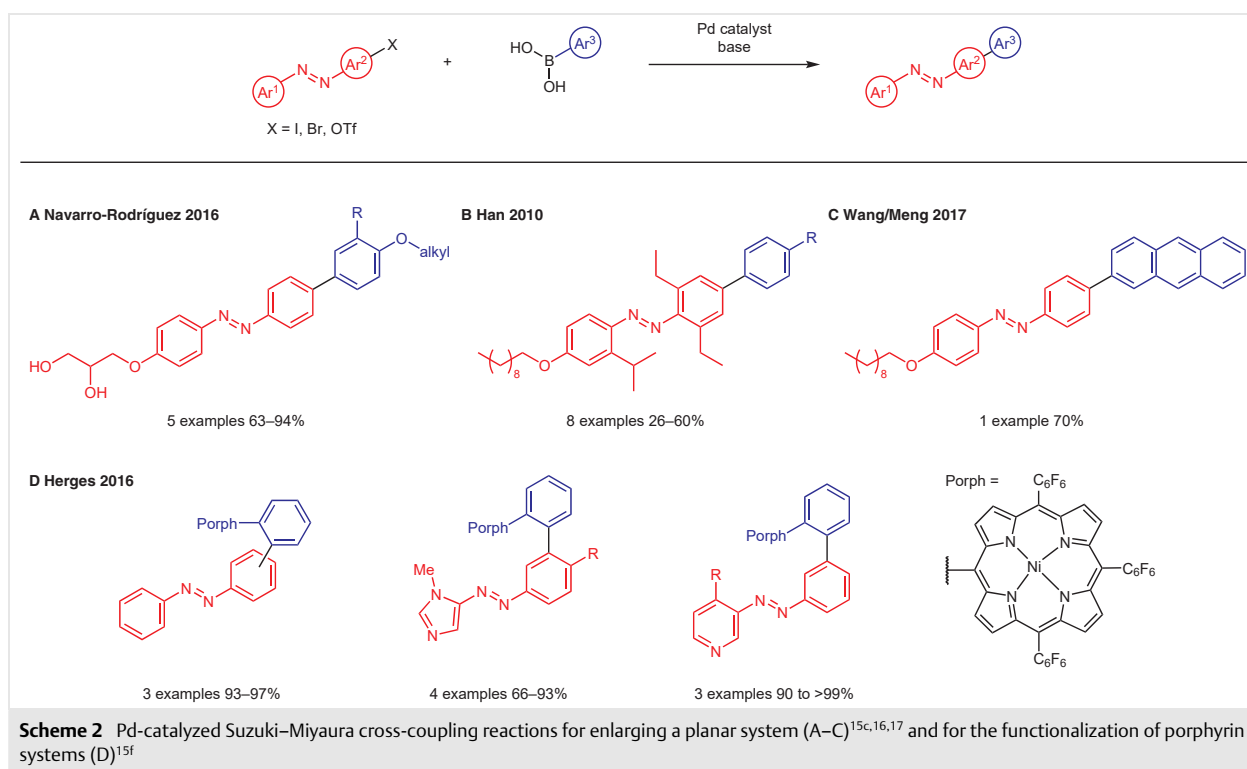
Besides a benzene ring,<sup>15i</sup> more complex motifs such as a fluorene ring<sup>15j,l,n,o</sup> or a carbazole ring<sup>15l,m,o</sup> were successfully integrated in the conjugated main chain.

For the synthesis of rotaxanes, azobenzene derivatives were connected with two  $\alpha$ -cyclodextrin units resulting in a [3]-rotaxane,<sup>18</sup> and later on a [1]-rotaxane.<sup>15q,r</sup> The azo-

benzene motif was either trapped in or bonded directly to the  $\alpha$ -cyclodextrin units and subsequently capped by benzo[de]isoquinoline derivatives via cross-coupling.<sup>15q,r,18</sup>

Further possibilities are demonstrated by the implementation of two consecutive Suzuki cross-coupling reactions. Starting from a 4,4'-diiodoazobenzene, initial coupling with 4-bromophenylboronic acid gave a 4,4'-bis(4-bromophenyl)azobenzene that underwent a second cross-coupling reaction with a 4-substituted phenylboronic acid to give an azoterphenyl derivative (37–54% over 2 steps).<sup>19</sup>

Since 2016, several cross-coupling reactions have been performed using asymmetric azobenzene derivatives; in this way, molecules capable of precise self-assembly with additional non-covalent interactions were prepared in yields ranging from 26% to 94% (Scheme 2, A–C).<sup>15c,16,17</sup> Suzuki–Miyaura cross-coupling was also applied to functionalize nickel porphyrin systems with azobenzene moieties in excellent overall yields (Scheme 2, D).<sup>15f</sup> Pd(PPh<sub>3</sub>)<sub>4</sub> served as Pd(0) catalyst with K<sub>2</sub>CO<sub>3</sub> as base and the reaction was carried out in a toluene/EtOH/water mixture at 90 °C leading to good and sometimes excellent yields. The coupling was even successful with an azopyridine and with adjusted conditions for an azoimidazole unit. For the latter, the free amine of the imidazole was N-methylated to prevent a possible side reaction with PdCl<sub>2</sub>(dppf) as the Pd(II) catalyst.<sup>15f</sup>



**Scheme 2** Pd-catalyzed Suzuki–Miyaura cross-coupling reactions for enlarging a planar system (A–C)<sup>15c,16,17</sup> and for the functionalization of porphyrin systems (D)<sup>15f</sup>

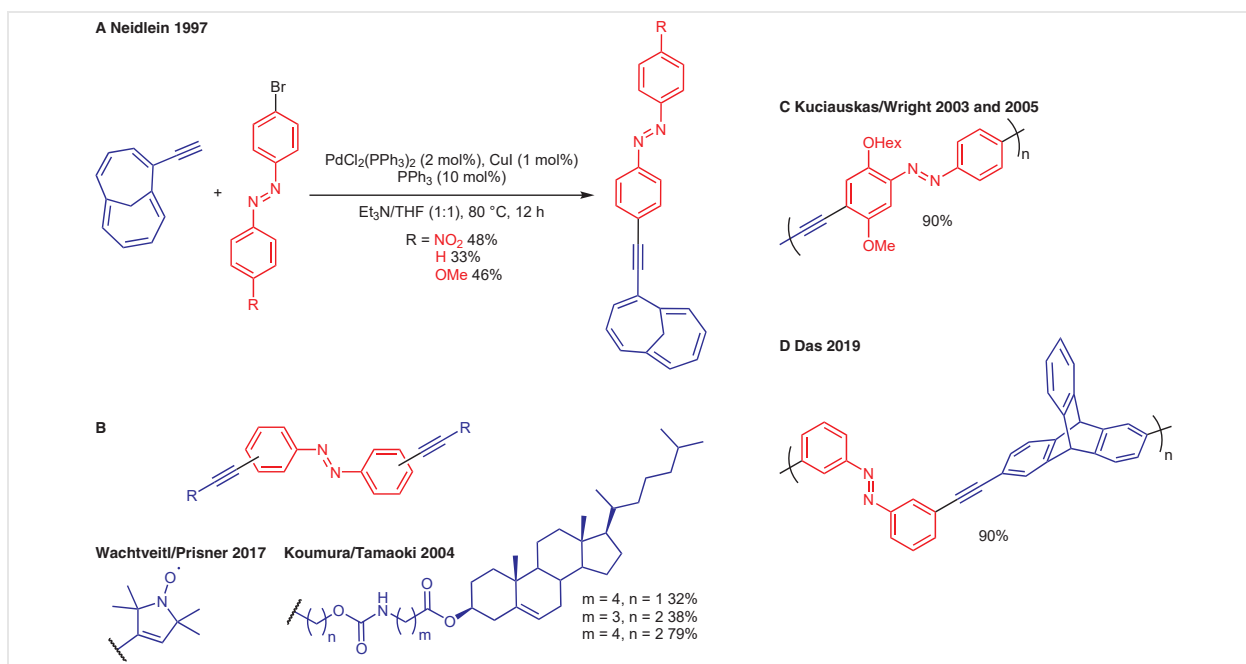
### 2.1.2 Sonogashira Cross-Coupling Reactions

The palladium-catalyzed cross-coupling reaction of a terminal alkyne with halogenated azobenzenes represents another widely used functionalization possibility. In this way, an azobenzene unit can be connected with relatively long, rigid, and  $\pi$ -conjugated linkers in good to excellent yields.<sup>20</sup> The incorporated linkers then serve a specific function in the molecule: For example, the functionalization of ethynyl-1,6-methano[10]annulenes with azobenzene demonstrated the synthesis of electron-donor/acceptor systems that are suitable substrates for nonlinear optics or liquid crystals (Scheme 3, A).<sup>20a</sup> In different azobenzene systems for the synthesis of photochromic self-assembled monolayers, the rigid linker ensures sufficient control over the distance from the headgroup to the surface and features a cooperative switching behavior of the azobenzene units.<sup>20b-d</sup>

Hydrophobic fluorescent azobenzenes were transformed into water-soluble fluorescent 2-borylazobenzenes by incorporating ionic functional groups via Sonogashira coupling.<sup>20e</sup> Employing 4,4'-diiodoazobenzene as the starting material enabled a double cross-coupling; in this way, an azobenzene moiety containing two paramagnetic nitroxide spin labels was synthesized in which the ethynyl groups supported the formation of spin exchange coupling (Scheme 3, B left).<sup>20f</sup> Low-molecular organogelators were obtained by double cross-coupling of 3,3'-diiodoazoben-

zene with acetylene derivatives (Scheme 3, B right).<sup>20g</sup> The two urethane moieties were required for strong hydrogen bonding, whereas the two cholesterol units led to relatively weak van der Waals interactions.<sup>20g</sup> Moreover, an azobenzene bisporphyrin system<sup>20d</sup> as well as different *para*-alkynylazobenzene ligands and their corresponding organometallic cobalt complexes were obtained.<sup>20h</sup> As azotolanes usually show liquid crystallinity as well as highly birefringent features, this method was utilized for the synthesis of several azotolane monomers<sup>20i,j</sup> or polymers with azobenzene in the side chain<sup>20k</sup> or main chain<sup>20l-n</sup> (Scheme 3, C), respectively. Additionally, photoresponsive and fluorescent co-polymers (Scheme 3, D),<sup>20o</sup> polyamide-phenyleneethynyls<sup>20p</sup> or a semiconducting colloidal porous organic polymer<sup>20q</sup> were obtained. The scope of electrophilic azobenzene cross-coupling partners was successfully broadened to bistriflates for the synthesis of rigid dendrimers in an acceptable yield.<sup>20s,t</sup>

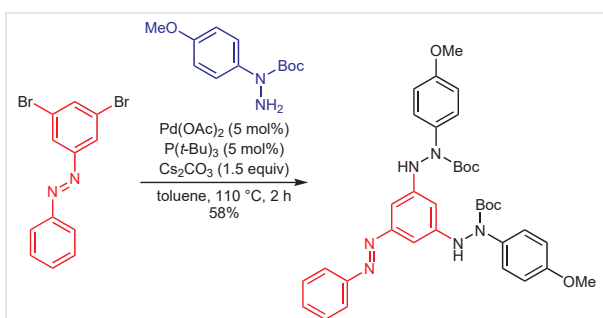
2-Iodoazobenzene reacted with (trimethylsilyl)acetylene under Sonogashira conditions, but even after optimization of the reaction conditions the yield of 2-[(trimethylsilyl)ethynyl]azobenzene remained 50%.<sup>21</sup> Additionally, the product decomposed during workup because of the lability of the protecting group and the instability of the deprotected diazene. Coupling with more robust (triisopropylsilyl)- and (triethylsilyl)acetylene solved both problems and the product 2-[(trialkylsilyl)ethynyl]azobenzenes were obtained in 97% and 87% yield, respectively.<sup>21</sup>



**Scheme 3** Pd-catalyzed Sonogashira cross-coupling reactions of halogenated azobenzenes<sup>20a,f,g,l,m,o</sup>

### 2.1.3 Buchwald–Hartwig Cross-Coupling Reactions

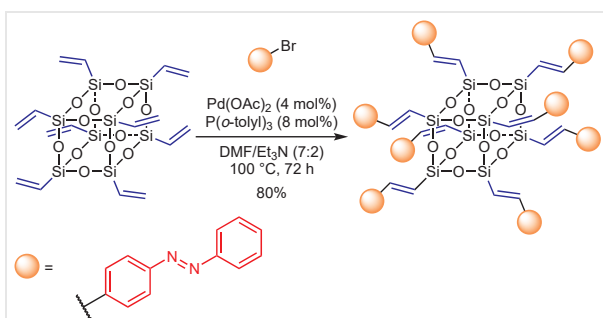
This type of cross-coupling reaction is used to form C–N bonds. In 2020, the coupling of 3,5-dibromoazobenzene with *N*-Boc-*N*-(4-methoxyphenyl)hydrazide to give 3,5-bis[*N*'-Boc-*N*'-(4-methoxyphenyl)hydrazino]azobenzene in 58% yield was reported (Scheme 4).<sup>22</sup> The obtained product was then oxidized to yield a C<sub>2</sub>-symmetric 3,5-bis(4-methoxyphenylazo)azobenzene. Unsymmetric tris(arylazo)-benzenes were accessible by sequential coupling.<sup>22</sup>



**Scheme 4** Pd-catalyzed Buchwald–Hartwig cross-coupling reaction of 3,5-dibromoazobenzene<sup>22</sup>

### 2.1.4 Heck Reactions

The Heck reaction can be employed in order to preserve double bonds within the starting material for later functionalization. As with the Suzuki–Miyaura cross-coupling, we mainly discuss reports of larger functional polymers and assemblies. One interesting example is the functionalization of cage silsesquioxanes with azobenzene units via the Heck reaction (Scheme 5).<sup>23</sup> The synthesis of new azobenzene-doped hybrid porous polymers was thus possible.<sup>24</sup>



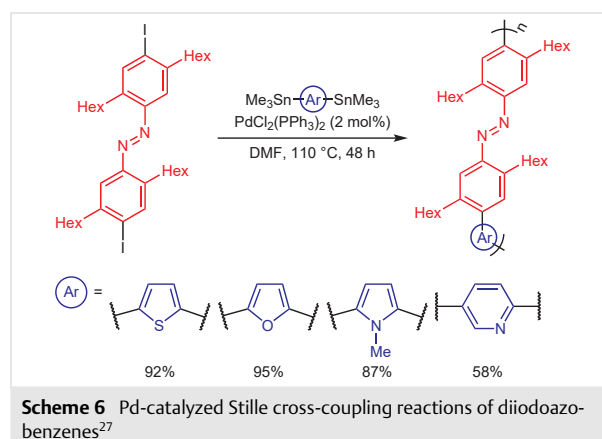
**Scheme 5** Pd-catalyzed Heck reaction of 4-bromoazobenzene<sup>23</sup>

Poly(phenylenevinylene)-based conjugated polymers with azobenzene derivatives incorporated directly in the  $\pi$ -conjugative building units were prepared in quantitative yield and with a high molecular weight ( $M_n > 10000$ ) by coupling polymerization of divinylbenzenes with 4,4'-di-

haloazobenzenes.<sup>25</sup> The Heck reaction of nipecotic acid (piperidine-3-carboxylic acid) derivatives with azobenzene triflates and iodides yielded vinyl ethers in good yields. However, the coupling was not possible for *ortho*-substituted azobenzenes. In this case, the Heck reaction needed to be performed with 1-iodo-2-nitrobenzene with the formation of the azobenzene by an azo coupling in a later step.<sup>26</sup>

### 2.1.5 Stille Reactions

In a Stille cross-coupling reaction, an organotin compound is reacted with a halide. Organostannanes are easy accessible and stable in air and moisture so that a broad range of functional groups can be used under mild conditions.<sup>20,25,27</sup> In this way, 4,4'-dibromoazobenzene was coupled with tributylvinylnit to yield 4,4'-divinylazobenzene in 70% yield.<sup>25</sup> It was also possible to introduce heteroaromatic compounds into a polymer backbone via a Stille cross-coupling: The monomer 4,4'-diiodoazobenzene was reacted with four different bis(trimethylstannyl)-substituted heteroaromatic compounds to give poly(phenylene)based-polymers that were soluble in common organic solvents in moderate to excellent yields (Scheme 6).<sup>27</sup> Due to the extended main-chain conjugation, the thiophene-, furan-, and *N*-methylpyrrole-containing poly(phenylenes) showed strongly red-shifted absorptions in the visible region. Only the pyridine-containing poly(phenylene) had a low degree of main-chain conjugation, but contrary to other examples, it showed in solution reversible photoisomerization of azobenzene units with an accompanied change of the electrochemical properties. The (*Z*)-enhanced polymer was less susceptible to oxidation.<sup>27</sup>



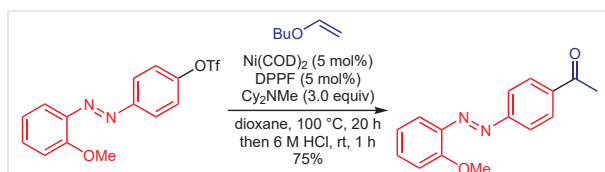
**Scheme 6** Pd-catalyzed Stille cross-coupling reactions of diiodoazobenzenes<sup>27</sup>

## 2.2 Nickel Catalysis

Although palladium complexes are the most common catalysts in cross-coupling reactions, attempts have been made to replace palladium by less expensive metals such as nickel. For example, a nickel-catalyzed Heck reaction of aryl



triflates with vinyl ethers proceeded under mild reaction conditions, using a catalytic system consisting of bis(cyclooctadiene)nickel(0), 1,1'-bis(diphenylphosphino)ferrocene (DPPF), and tertiary amine  $\text{Cy}_2\text{NMe}$ , followed by hydrolysis to give the corresponding acetyl-substituted products with good functional group tolerance. It was also possible to incorporate a photoswitchable unit by the olefination of an azobenzene triflate followed by hydrolysis to give the corresponding acetyl derivative (Scheme 7).<sup>28</sup>



**Scheme 7** Ni-catalyzed Heck reaction of an azobenzene triflate derivative<sup>28</sup>

## 2.3 Copper Catalysis

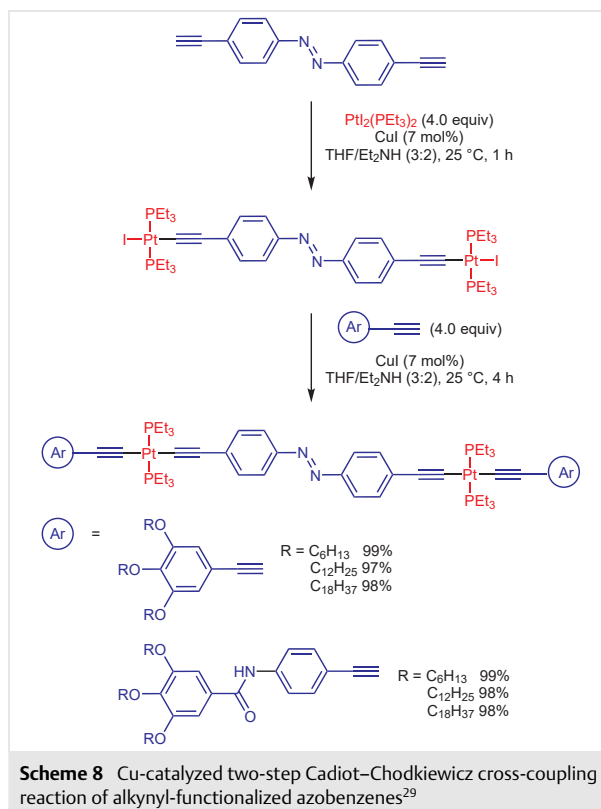
Copper catalysts are another alternative to palladium catalysts in cross-coupling reactions to obtain substrates otherwise not accessible.

### 2.3.1 Cadiot–Chodkiewicz Reactions

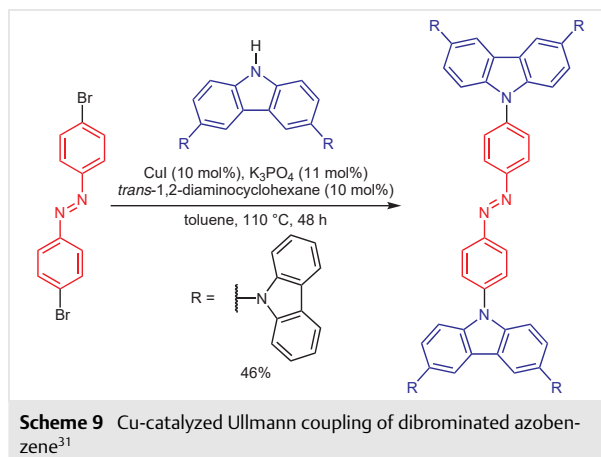
The copper-catalyzed Cadiot–Chodkiewicz reaction enables the formation of conjugated dienes. A synthetic route towards large-scale highly ordered porous structures from organometallic precursors via spontaneous self-assembly was established by using a two-step Cadiot–Chodkiewicz cross-coupling. Several neutral platinum–acetylide complexes with azobenzene groups in the center and long alkyl chains on both ends of the molecule were obtained in excellent to quantitative yields (Scheme 8).<sup>29</sup> In a similar fashion, poly(platinaynes) were synthesized with both *meta*- or *para*-substituted azobenzene spacers to compare their optoelectronic properties. In these complexes, the acetylide-functionalized azobenzene ligands could still undergo photoisomerization reversibly, although the switching process appeared to be more facile for *para*-substituted systems and with lower photoisomerization in solution in comparison to smaller systems.<sup>30</sup>

### 2.3.2 Ullmann Reactions

The Ullmann reaction is a powerful tool for C–N bond formation. The Ullmann coupling of 4,4'-dibromoazobenzene with 3,6-bis(9*H*-carbazol-9-yl)-9*H*-carbazole gave a bis(tercarbazole)azobenzene derivative in 46% yield that was used as a precursor for the fabrication of photoresponsive microporous films (Scheme 9).<sup>31</sup>



**Scheme 8** Cu-catalyzed two-step Cadiot–Chodkiewicz cross-coupling reaction of alkynyl-functionalized azobenzenes<sup>29</sup>

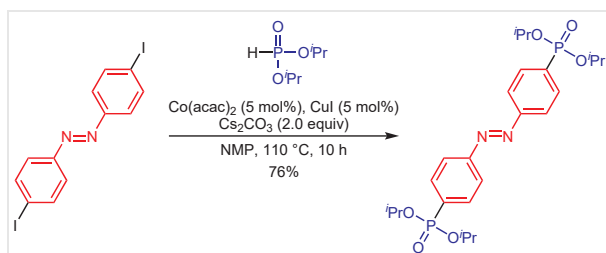


**Scheme 9** Cu-catalyzed Ullmann coupling of dibrominated azobenzene<sup>31</sup>

## 2.4 Cobalt Catalysis

Another alternative to palladium catalysis is the use of cobalt as an inexpensive metal. For example, the  $\text{C}(\text{sp}^2)\text{-P}$  cross-coupling of vinyl, styryl, and aryl halides with diphenyl phosphine oxide and dialkyl phosphinate using a unique Co/Cu catalytic system gave the corresponding

phosphoryl-substituted products. This protocol showed robust functional group tolerance that enabled the coupling of 4,4'-diiodoazobenzene with diisopropyl phosphite to give 4,4'-bis(diisopropoxyphosphoryl)azobenzene in 76% yield (Scheme 10).<sup>32</sup>



**Scheme 10** Co/Cu-catalyzed C(sp<sup>2</sup>)-P cross-coupling reaction of 4,4'-diiodoazobenzene<sup>32</sup>

### 3 Azobenzenes as Formally Nucleophilic Components

In cross-coupling reactions, the formal nucleophile is an (organo)metallic species. Organometallic, nucleophilic azobenzene derivatives can be obtained either by halogen-metal exchange of the (pseudo)halogenated azobenzene or by applying an appropriate cross-coupling reaction with a dimetallic reagent (Scheme 11, A) (see later for C-H activation).<sup>7b,33</sup> However, in the case of azobenzenes, halogen-metal exchange can lead to the reduction of the azo group as a dominating side reaction (Scheme 11, B).<sup>34</sup> From the perspective of the formally nucleophilic azobenzene, the main limitation is access to the azobenzene starting material. There has been very little research performed in this area in terms of systematic investigations and thus, it is difficult to distill common principles or indeed select the most seminal papers.

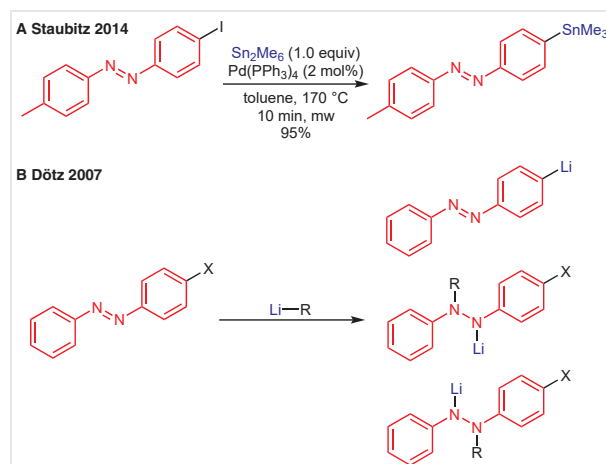
#### 3.1 Palladium Catalysis

Palladium catalysts are also most commonly used in cross-coupling reactions involving azobenzene derivatives as the formally nucleophilic component. In terms of the obtained product structure, the same criteria apply for the selection of the specific cross-coupling reaction as are utilized for electrophilic azobenzene derivatives. However, a key consideration is the availability of the metalated azobenzene.

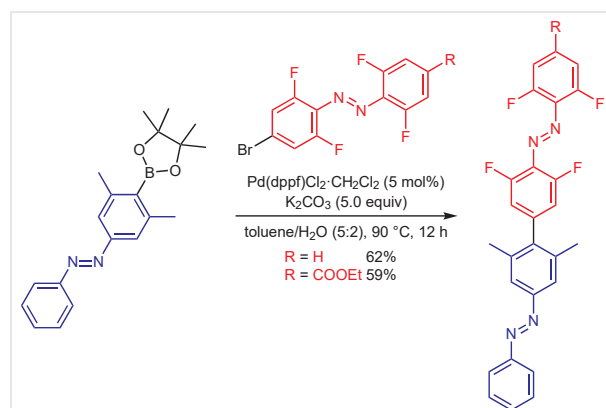
##### 3.1.1 Suzuki–Miyaura Cross-Coupling Reactions

The first use of an azobenzene derivative as a nucleophile in a Suzuki–Miyaura cross-coupling reaction was reported in 2007;<sup>36</sup> the coupling of a boronic acid pinacol ester functionalized azobenzene with diverse iodoarenes gave arylate azobenzenes in 41–72% yields.<sup>36</sup> While the

cross-coupling reactions themselves are relatively unremarkable, the importance is in the synthesis of the starting material by cross-coupling of a (pseudo)halogenated azobenzene with the boronic ester.<sup>36,37</sup> A second approach is the condensation of a nitrosobenzene and aniline boronic acid ester; the boronic acid ester is unaffected by the condensation reaction.<sup>36</sup> Due to the efficiency of this method, a number of synthetic targets<sup>38</sup> were assessed. Moreover, an azobenzene-4-boronic acid pinacol ester derivative was used as the nucleophile and 4-bromo-2,2,2',2'-tetrafluoroazobenzene derivatives as the electrophile, which enabled the use of azobenzene as both cross-coupling components. The resulting product undergoes orthogonal switching, where the azobenzene units are switched separately to give 4 different isomers by green, blue, or ultraviolet light or electrocatalytic isomerization (Scheme 12).<sup>37</sup>



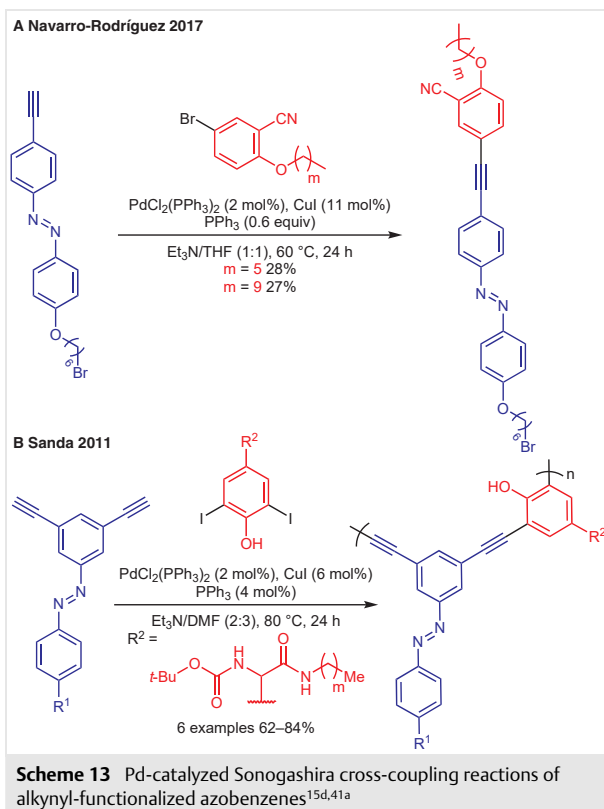
**Scheme 11** (A) Stille–Kelly cross-coupling reaction of 4-iodo-4'-methylazobenzene with hexamethyldistannane;<sup>33</sup> (B) halogen–metal exchange of a halogenated azobenzene with the possible reduction of the di-azeryl group<sup>35</sup>



**Scheme 12** Pd-catalyzed Suzuki–Miyaura cross-coupling reaction of an azobenzene-4-boronic acid pinacol ester and 4-bromo-2,2,2',2'-tetrafluoroazobenzene derivatives<sup>37</sup>

## 3.1.2 Sonogashira Cross-Coupling Reactions

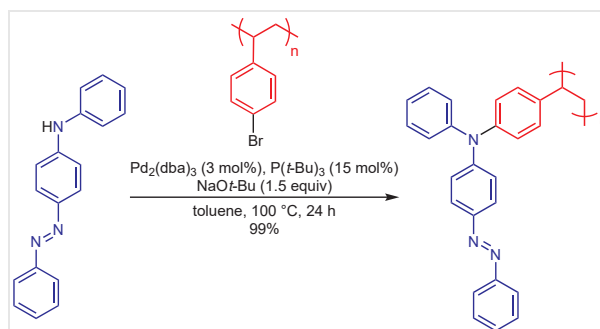
In 2014, the preparation of an azobenzene liquid crystal was reported by the Sonogashira cross-coupling reaction of an ethynyl-substituted azobenzene with 1-bromooctane.<sup>39</sup> This protocol was utilized in 2017 for the coupling of an azobenzene derivative with aryl bromides (Scheme 13, A).<sup>15d</sup> The Sonogashira cross-coupling reaction has also been used for the synthesis of artificial helical oligomers<sup>40</sup> or polymers<sup>41</sup> in which the photoisomerization of the azobenzene moieties triggers a geometric change. Novel azobenzene-containing hydroxyphenylglycine-derived poly(*m*-phenyleneethynylene)s were synthesized by polymerization through the Sonogashira couplings (thus formally a polycondensation) of 3,5-diethynylazobenzenes with various diiodinated amides (Scheme 13, B).<sup>41a</sup>



Furthermore, the Sonogashira reaction was used to prepare a hairy-rod like  $\pi$ -conjugated polymer with a fluorene unit in the backbone.<sup>42</sup> The late-stage functionalization of poly(aryl ethers) with azobenzene moieties was feasible, in which polymer bromo side groups react with 4-(dimethylamino)-3'-ethynylazobenzene.<sup>43</sup>

## 3.1.3 Buchwald–Hartwig Cross-Coupling Reactions

The Buchwald–Hartwig cross-coupling reaction can be used to form C–N bonds. The Buchwald–Hartwig amination of various polystyrene and poly(iminoarylene) derivatives was reported to give the corresponding products with aminoazobenzene groups in the side chain (Scheme 14).<sup>44</sup> The absence of characteristic stretching vibrations of the starting materials in the IR spectrum indicated a full loading of the obtained polymer.<sup>44</sup>



**Scheme 14** Pd-catalyzed Buchwald–Hartwig amination of 4-(phenylamino)azobenzene<sup>44</sup>

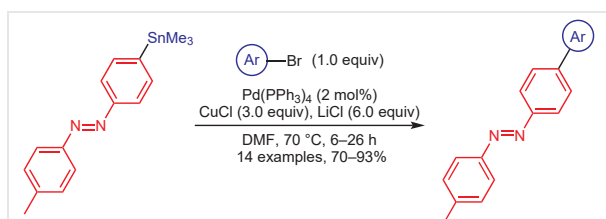
This methodology was applied to the synthesis of amorphous materials such as branched triarylamine derivatives,<sup>45</sup> a spiro-linked bifluorene<sup>46</sup> as well as a perfluorocyclobutane (PFCB) aryl ether polymer<sup>47</sup> or a poly(arylimino) derivative.<sup>48</sup> It was even possible to prepare ferrocenophanes with azobenzene derivatives in the ligand and to use them as a redox-active and chromophore site showing potential as electron- or acid-responsive organic materials.<sup>49</sup>

## 3.1.4 Heck Reactions

The Heck reaction of dihaloazobenzenes with divinylarenes as well as the reverse case, the coupling of 4,4'-divinylazobenzene with dihaloarenes, to produce photoresponsive poly(phenylenevinylene)s was investigated. However, the obtained polymers were largely insoluble in common organic solvents, hence this route was discarded.<sup>25</sup>

## 3.1.5 Stille Reactions

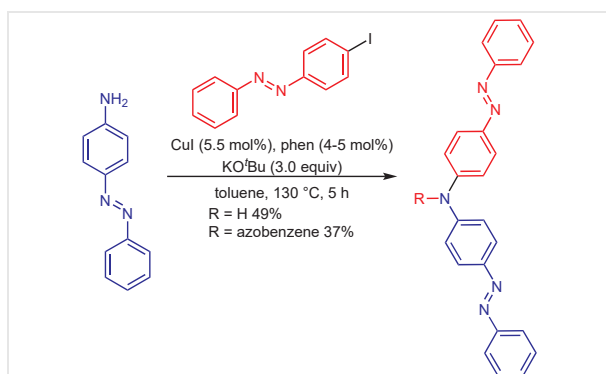
An efficient microwave-assisted method to prepare stannylated azobenzenes was developed to circumvent the possible reduction of the diazenyl group during halogen-metal exchange. These organostannyl-substituted azobenzenes subsequently served as nucleophiles in high-yielding Stille cross-coupling reactions (Scheme 15).<sup>33</sup>



**Scheme 15** Pd-catalyzed Stille cross-coupling reaction using stannylated azobenzene as nucleophile<sup>33</sup>

### 3.2 Copper Catalysis

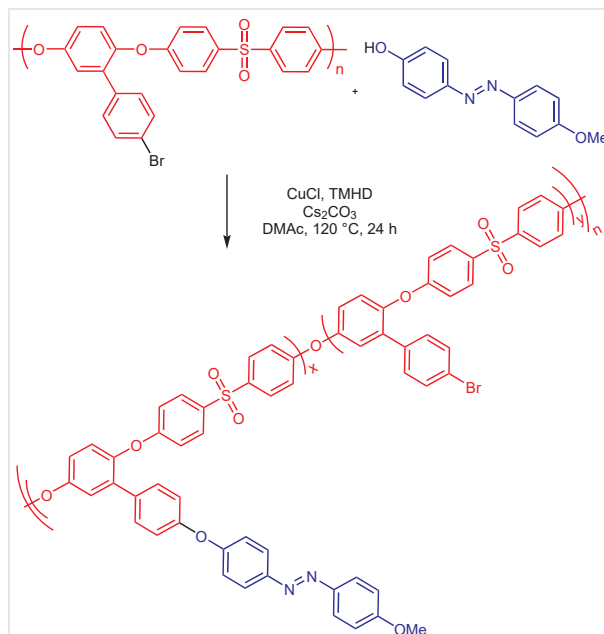
A copper-catalyzed Ullmann cross-coupling reaction was the method of choice for the synthesis of bis[4-(phenyldiazenyl)phenyl]amine and tris[4-(phenyldiazenyl)phenyl]amine by varying the stoichiometric quantities of the electrophilic component (Scheme 16).<sup>50</sup>



**Scheme 16** Cu-catalyzed Ullmann cross-coupling reaction of 4-iodoazobenzene with aminoazobenzene<sup>50</sup>

The Ullmann cross-coupling reaction is also useful for generating phenol ethers through C–O bond formation. In this way, a series of azobenzene-functionalized poly(ether sulfone)s were prepared, using a catalyst system of CuI and 2,2,6,6-tetramethylheptane-3,5-dione (TMHD), that had high glass transition temperatures ( $T_g > 199$  °C) (Scheme 17).<sup>51</sup> Irradiation and writing/erasing experiments indicated a large photoinduced birefringence and good stability of the photoinduced orientation of the polymers. This makes them interesting for applications in reversible optical storage.<sup>51</sup>

This synthetic procedure was expanded to the synthesis of an azobenzene-containing poly(aryl ether) with carboxyl side groups capable of coordination to rare earth complexes.<sup>43</sup>



**Scheme 17** Cu-catalyzed Ullmann cross-coupling reaction of poly(ether sulfone)s with bromine side groups and 4-[(4-methoxyphenyl)diazenyl]phenol with different functionalization degrees ( $x = 20, 45, 100$ )<sup>51</sup>

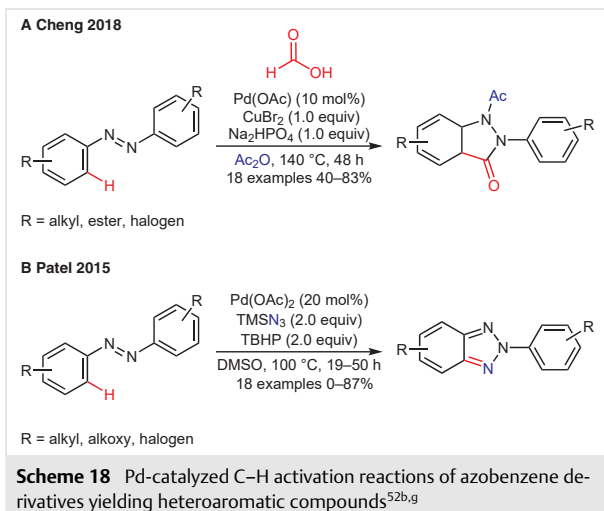
### 3.3 C–H Activation Reactions

C–H Activation reactions catalyzed by different transition metals have played an important role especially in the functionalization of azobenzene derivatives in the *ortho*-position.

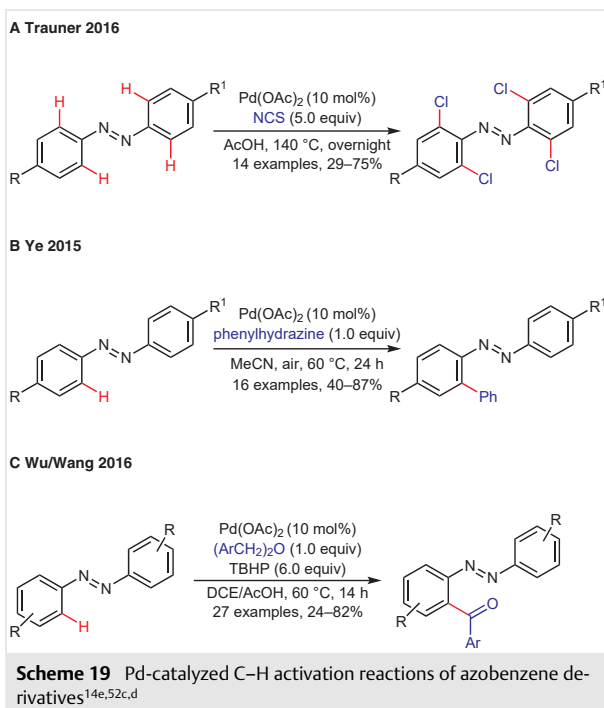
#### 3.3.1 Palladium-Catalyzed C–H Activation Reactions

The *ortho*-directing property of the azo group has been exploited in palladium-catalyzed C–H activation reactions.<sup>14e,52</sup> In many such reactions, the azobenzene is transformed by reaction with the diazenyl group. For example, azobenzenes were used for the synthesis of indazole backbones through palladium-catalyzed C–H functionalization and subsequent intramolecular cyclization.<sup>52a</sup> In a similar approach, 3*H*-indazol-3-ones were prepared from azobenzene derivatives using formic acid as carbon monoxide source (Scheme 18, A).<sup>52g</sup> *ortho*-C–H Amination of azoarenes with trimethylsilyl azide yielded 2-aryl-2*H*-benzotriazoles (Scheme 18, B).<sup>52b</sup> In this reaction, electron-donating substituents (alkyl, alkoxy) give higher product yields (58–87%) than electron-withdrawing groups, such as CF<sub>3</sub> (8%).

Late-stage functionalization of azobenzenes in the *ortho*-position was reported by the Trauner group (Scheme 19, A).<sup>14e</sup> These tetra-*ortho*-chlorinated azobenzenes are of



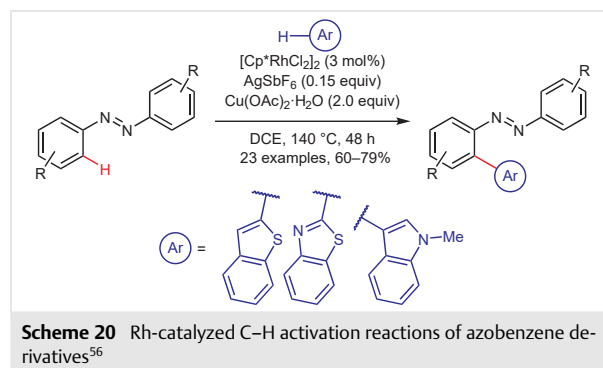
special interest because of their redshifted isomerization to *cis* at  $\lambda \approx 560$  nm. Azoarenes were functionalized with phenylhydrazine using a Pd(II) catalyst with atmospheric oxygen as the oxidant (Scheme 19, B).<sup>52c</sup> Wu, Wang, and co-workers reported the acylation of azobenzene derivatives with benzylic ethers (Scheme 19, C).<sup>52d</sup>



### 3.3.2 Rhodium-Catalyzed C–H Activation Reactions

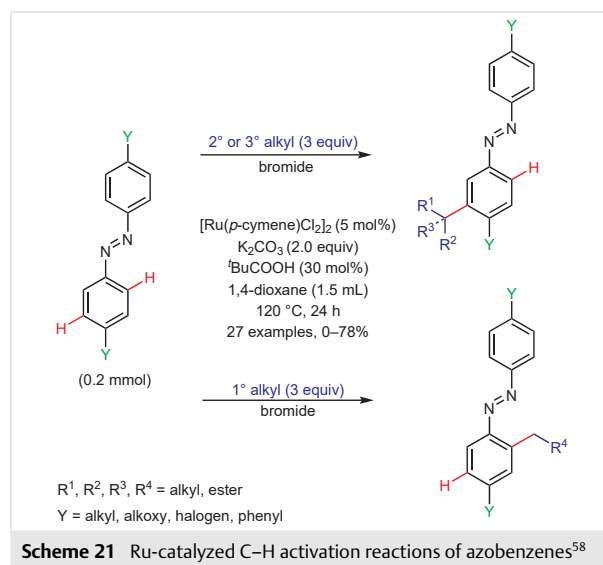
Rhodium has been shown to be a potent *ortho* C–H activator of azobenzene derivatives. There are several reported examples of the formation of C–N bonds,<sup>53</sup> 2-aryl-2H-ben-

zotriazoles,<sup>54</sup> and indazoles and indoles<sup>55</sup> similar in yields to the palladium-catalyzed reactions. A very useful reaction is the *ortho*-heteroarylation of azobenzenes by rhodium-catalyzed cross-dehydrogenative coupling (Scheme 20).<sup>56</sup> Such conjugated biaryls might be of special interest for luminous materials.



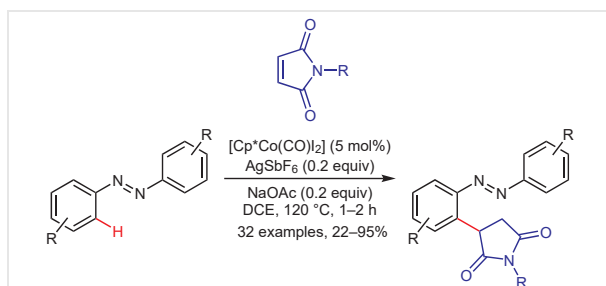
### 3.3.3 Ruthenium-Catalyzed C–H Activation Reactions

Ruthenium-catalyzed C–H activation reactions of azobenzene derivatives have been reported.<sup>57</sup> Of particular interest is the *meta/ortho*-selective C–H alkylation of azoarenes. Using a carboxylic acid promoted Ru(II)-catalyzed C<sub>Ar</sub>–H alkylation reaction of 4,4'-substituted azobenzenes with secondary and tertiary alkyl bromides gave selectively the *meta*-product (Scheme 21),<sup>58</sup> while under the same reaction conditions, primary alkyl groups gave the *ortho*-product. To our knowledge this is the only reported reaction so far which allows C–H activation in the *meta* position. Coupling with alkyl chlorides was unsuccessful. Furthermore, bulky groups, such as *tert*-butyl (Y = *t*-Bu), on the azobenzene, prevented the reaction.<sup>58</sup>



### 3.3.4 Cobalt-Catalyzed C–H Activation Reactions

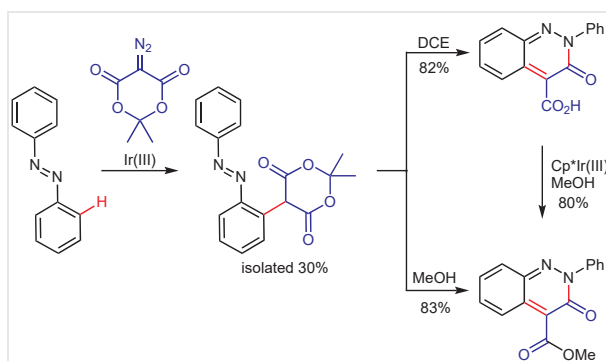
Cobalt-catalyzed C–H activation reactions are largely unknown on azobenzene derivatives and only a few examples exist.<sup>59</sup> A synthetic procedure for the azo-directed selective 1,4-addition of maleimides by Co(III)-catalyzed C–H activation was reported (Scheme 22).<sup>59c</sup> Worth noting is the use of low amounts of additives, as well as the fact that it does not require the use of a copper source.<sup>59c</sup>



**Scheme 22** Co-catalyzed C–H activation reactions of azobenzene derivatives<sup>59c</sup>

### 3.3.5 Iridium-Catalyzed C–H Activation Reactions

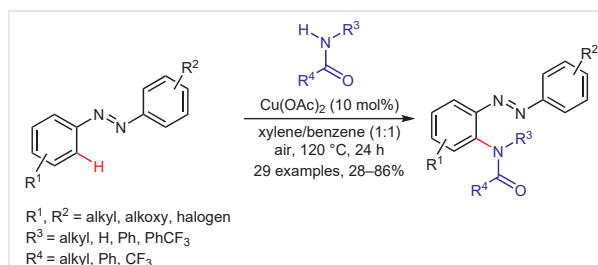
The Ir(III)-catalyzed [4+2] cyclization of azobenzenes with diazotized Meldrum's acid via a two-step reaction with an initial C–H alkylation, followed by intramolecular annulation gave 3-oxo-2,3-dihydrocinnoline-4-carboxylic acids or esters depending on the solvent used (Scheme 23).<sup>60</sup>



**Scheme 23** Ir-catalyzed C–H activation reaction of azobenzene<sup>60</sup>

### 3.3.6 Copper-Catalyzed C–H Activation Reactions

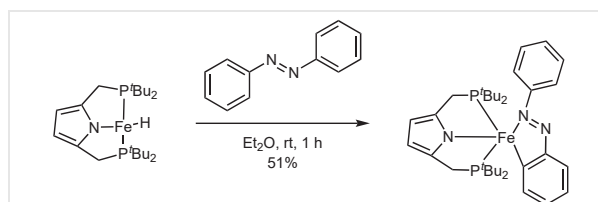
Azobenzenes can be functionalized by a Cu(II)-catalyzed aerobic oxidative amidation with amides yielding the corresponding 2-(acylamino)azobenzenes in moderate to excellent yields (Scheme 24).<sup>61</sup>



**Scheme 24** Cu-catalyzed C–H activation reactions of azobenzene derivatives<sup>61</sup>

### 3.3.7 Iron-Catalyzed C–H Activation Reactions

To date only one example of an iron-catalyzed C–H activation reaction has been reported. An iron hydride complex bearing a 2,5-bis(di-*tert*-butylphosphinomethyl)pyrrolide ligand reacted with azobenzene. However, further functionalization was unsuccessful since the pentacoordinated aryl–iron complex was inert toward various reagents (Scheme 25).<sup>62</sup>



**Scheme 25** Fe-catalyzed C–H activation of azobenzene<sup>62</sup>

## 4 Azobenzenes as Ligands in Catalysts

In addition to their use as a reactant in cross-coupling reactions, azobenzene derivatives can be also employed as ligands for catalysts in cross-coupling reactions.<sup>63</sup> Here, the N-donor capability of the diazenyl group (due to the lone electron pair on the nitrogen atoms) is used to form transition metal complexes. The incorporation of azo chromophores has enabled the synthesis of complexes with interesting physicochemical properties such as photoluminescence. Complexes with multidentate azoaromatic ligands are significantly stabilized because of the enhanced  $\pi$ -acceptor behavior compared to monocyclopalladated azobenzenes.<sup>63e</sup> Although the synthesis of azo-containing phosphine Pd(II) and Pt(II) complexes was reported in 1999, and the first results of their catalytic use were demonstrated in Heck reactions,<sup>64</sup> it took a further decade before this possibility was explored in more detail.<sup>63</sup>

In 2010, the synthesis of a polystyrene-anchored Pd(II) azo complex (Figure 2, A) and its application in the Suzuki–Miyaura as well as Sonogashira cross-coupling reactions was reported; various aryl halides were reacted with phen-

ylboronic acids or terminal alkynes in excellent yields (68–100% yield, 27 examples) under phosphine-free and aerobic reaction conditions in aqueous medium.<sup>63b</sup> A similar catalytic system showed comparable recyclability, but, in addition, it could even be employed in Heck reactions (89–96% yield, 5 examples).<sup>63d</sup>

A single core palladacyclic azobenzene catalyst with CNCN chelation was successfully synthesized (Figure 2, B) and used successfully in Suzuki–Miyaura and Heck reactions. However, it was only moderately active (27–70% yield, 4 examples) and required high temperatures that led to decomposition of the catalyst.<sup>63c</sup>

A symmetric bisazobenzene derivative was used as chelating ligand to obtain unsymmetric CNN pincer palladacycles (Figure 2, C) that showed high turnover numbers (TONs) even under the harsh conditions of the Heck reaction (60–93% yield, 9 examples, TONs up to 93000).<sup>63e</sup>

Phosphine-free Pd(II) complexes with 2,2'-bis(alkylamino)-azobenzene ligands were obtained in good yields by reaction of the ligands with sodium tetrachloropalladate. In this work, the benzyl derivative (Figure 2, D) showed high catalytic activity in Suzuki–Miyaura and Heck reactions under mild conditions in the presence of air and moisture (65–93% yield, 22 examples).<sup>63f</sup>

It should be noted that the photoswitchability of the azobenzenes in Figure 2 was not exploited.

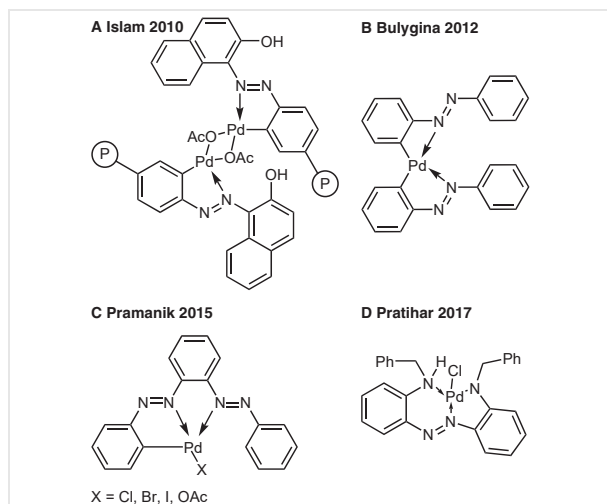


**Figure 2** Evolution of palladium azo catalysts used in different cross-coupling reactions<sup>63b,c,e,f</sup>

## 5 Diazocines

(*Z*)-11,12-Dihydrodibenzo[*c,g*][1,2]diazocines (diazocines) are ethylene-bridged azobenzenes that can be switched from their thermodynamic stable (*Z*)- to the metastable (*E*)-isomer by using blue light at  $\lambda \approx 370$ –400

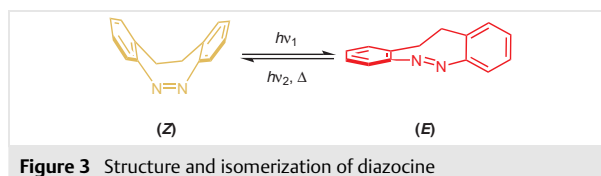


**Figure 3** Structure and isomerization of diazocine

nm and back from the (*E*)- to the (*Z*)-isomer by green light at  $\lambda \approx 480$ –550 nm (Figure 3).<sup>65</sup>

The switching properties of unsubstituted diazocines are different to unsubstituted azobenzenes. Diazocines show better resolution of absorption bands between the two isomeric states and switching is possible with light in the visible range.<sup>65</sup> However, the substituents have a great impact on the switching properties of both azobenzenes and diazocines. For example, tetra-*ortho*-chlorinated azobenzenes can be switched to (*Z*) at  $\lambda \approx 560$  nm, which exceeds the redshift of regular azobenzenes. Amino substituents on diazocines have also been shown to reduce the separation of the absorption bands yielding low amounts of (*E*)-isomers (25–30%).<sup>66</sup> The synthesis of diazocines is more demanding compared to azobenzenes, which is why only few applications have been reported to date.<sup>65,67</sup>

### 5.1 Synthesis

The key step in any diazocine synthesis is the cyclization to form the diazene moiety. This has been performed by reduction of 2,2'-dinitrobenzyls,<sup>65,67,68</sup> or the oxidation of 2,2'-ethylenedianilines (Figure 4).<sup>69</sup>

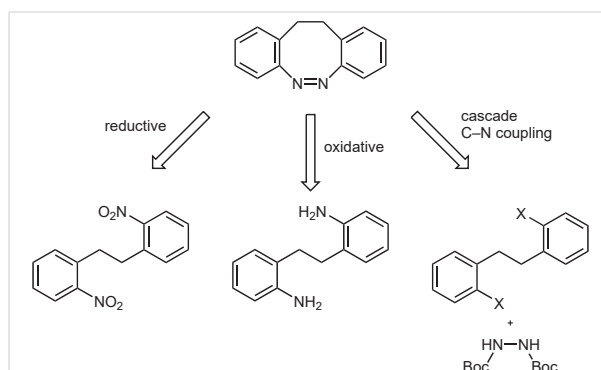
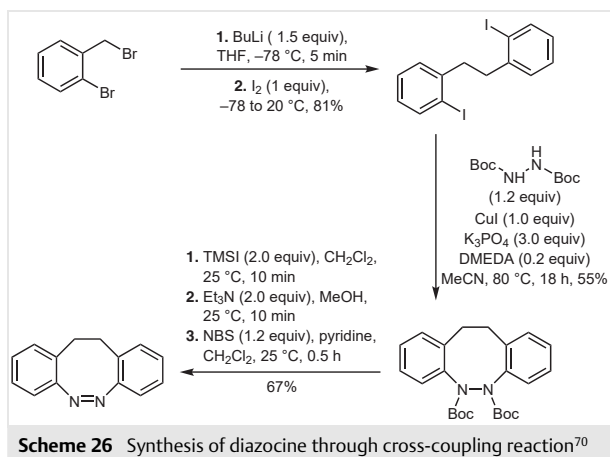


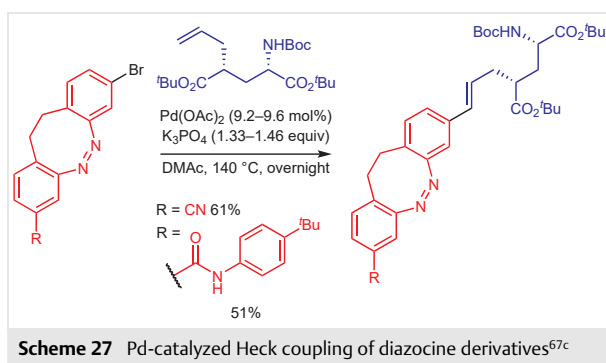
**Figure 4** Retrosynthetic approach towards diazocines<sup>65,67–70</sup>

A novel route involving a cross-coupling reaction has been introduced by connecting the C–N bond instead of the N–N bond (Scheme 26).<sup>70</sup> The diazocine ring in this route is formed via consecutive cross-coupling reactions between a 2,2'-dihaloethylbenzyl and di-*tert*-butyl hydrazodicarboxylate.<sup>70</sup>

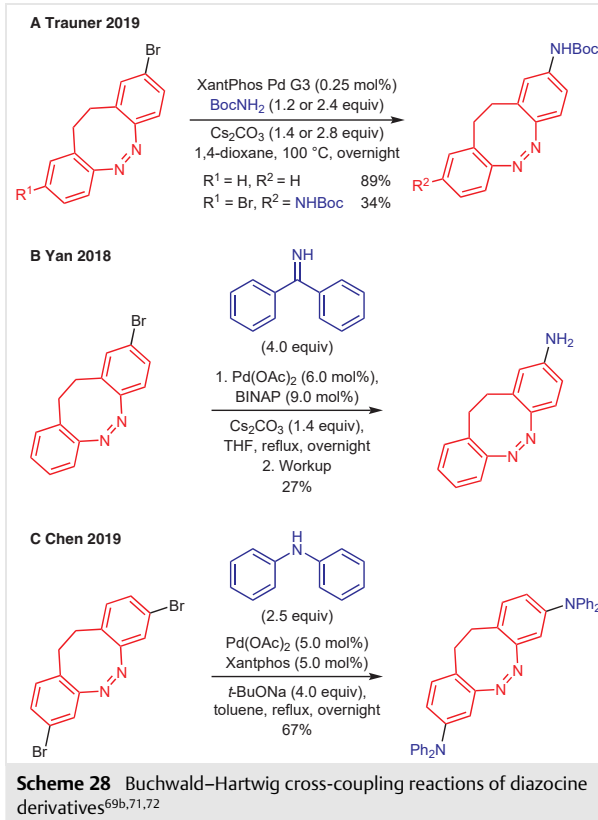


## 5.2 Cross-Coupling Reactions

To date there are only a few reports of palladium-catalyzed cross-coupling reactions of diazocines. Therefore, a comparison with cross-coupling reactions of azobenzenes is, at present, of little informative value. Due to the different electronic and geometric structures of azobenzenes and diazocines, a different reactivity can be expected (as the lone pairs in diazocine are not aligned with the  $\pi$ -systems of the aromatic rings). At first glance the yields seem to be lower for cross-coupling reactions on diazocines, but this might be misleading since it is unknown if the reaction conditions were optimized. The Heck reaction of an 8-substituted 3-bromodiazocine with a glutamate derivative yielded diazocine ligands capable of light-controlling neural receptors (Scheme 27).<sup>67c</sup>



A Buchwald–Hartwig coupling on 3-bromodiazocines with *tert*-butyl carbamates was successfully performed (Scheme 28, A).<sup>69b</sup> Furthermore, the coupling of benzophenone imine with bromodiazocines was reported (Scheme 28, B).<sup>71</sup> The synthesis of a diazocine with turn-on fluorescence was achieved by the coupling of 3,8-dibromodiazocine with diphenylamine (Scheme 28, C).<sup>72</sup>

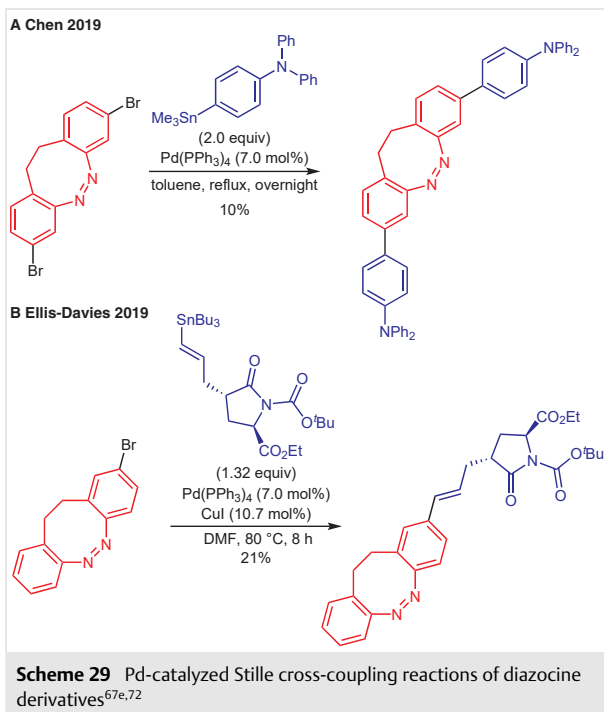


Turn-on fluorescence diazocines were prepared by a Stille cross-coupling reaction (Scheme 29, A).<sup>72</sup> Furthermore, it was possible to obtain a pyroglutamate diazocine derivative via the Stille cross-coupling reaction (Scheme 29, B).<sup>67e</sup>

## 6 Conclusion

Cross-coupling reactions have proved to be a powerful tool for the late-stage modification of both electrophilic and nucleophilic azobenzene derivatives, with palladium catalysis being most prevalent. The Suzuki–Miyaura and Sonogashira cross-coupling reactions are the most widely used. First examples of cross-coupling reactions catalyzed by other transition metals than palladium, such as nickel or cobalt, have been published thus broadening the scope of cross-coupling reactions towards new bond formations that are not possible with palladium catalysts. At present, the number of examples of the use of azobenzenes as formally electrophilic reactants is much greater than that for their use as formally nucleophilic reactants. Most likely, this does not reflect intrinsic problems with nucleophilic azobenzenes, but rather that their accessibility is limited at present





and requires more research. The reported yields do not significantly differ for cross-coupling reactions with azobenzene as formally the electrophilic or as nucleophilic component. However, due to the difficulties in the synthesis of nucleophilic azobenzene derivatives, cross-coupling reactions involving formally electrophilic azobenzene derivatives are favored. Normally, cross-coupling reactions with formally nucleophilic azobenzene derivatives are only used if the as nucleophilic coupling partner in the reaction of electrophilic azobenzene derivative cannot be synthesized. Most reported examples of cross-coupling reactions involving azobenzene derivatives employ the *para*-isomer; there are few examples of the use of the *meta*- or even the *ortho*-isomer. In fact, some groups specifically pointed out that cross-coupling reactions on *ortho*-azobenzene derivatives were unsuccessful. So cross-coupling reactions in the *ortho*-position of azobenzenes are almost, but not completely, unknown. The different reaction behavior of *ortho*-azobenzene derivatives in comparison to their corresponding *meta*- and *para*-isomers can be attributed to the nature of the diazenyl group; due to the adjacent lone electron pair on the nitrogen atoms, the diazenyl group can interact with substituents in the *ortho*-position. For example, *ortho*-halogenated precursors that are easily accessible can be directly lithiated because the *ortho*-lithiated species is significant stabilized by N→Li coordination. Although the diazenyl group has this directing and stabilizing effect also for transition metal insertions, only very few examples of metalated *ortho*-azobenzenes exist. C–H Activation is, therefore, a valuable al-

ternative especially for the modification of *ortho*-azobenzenes. In almost all examples of C–H activation on azobenzenes, the *ortho*-position was functionalized. Here, the use of palladium complexes as catalysts was not as dominant as for the cross-coupling reactions. Another promising field is the use of complexed azobenzene derivatives acting as ligands or promoters for catalysts. New synthetic procedures for the preparation of diazocines means that they are accessible in good yields. Therefore, further functionalization possibilities through cross-coupling reactions can now be explored.

### Funding Information

A.S. and S.S. thank the German Research Foundation (DFG) for the financial support within the priority program SPP 2100 'Soft Material Robotic Systems', Subproject STA1195/5-1, 'Insect feet inspired concepts soft touch grippers with dynamically adjustable grip strength'.

### Acknowledgment

The authors would like to thank Dr. Anne Heitmann for proofreading.

### References

- (1) Merino, E.; Ribagorda, M. *Beilstein J. Org. Chem.* **2012**, *8*, 1071.
- (2) Hartley, G. S. *Nature* **1937**, *140*, 281.
- (3) (a) Brown, C. J. *Acta Crystallogr.* **1966**, *21*, 146. (b) Mostad, A.; Rømming, C. *Acta Chem. Scand.* **1971**, *25*, 3561.
- (4) Hartley, G. S.; Le Fèvre, R. J. W. *J. Chem. Soc.* **1939**, 531.
- (5) Åstrand, P.-O.; Ramanujam, P. S.; Hvilsted, S.; Bak, K. L.; Sauer, S. P. A. *J. Am. Chem. Soc.* **2000**, *122*, 3482.
- (6) (a) Cheben, P.; del Monte, F.; Worsfold, D. J.; Carlsson, D. J.; Grover, C. P.; Mackenzie, J. D. *Nature* **2000**, *408*, 64. (b) Ikeda, T.; Sasaki, T.; Ichimura, K. *Nature* **1993**, *361*, 428.
- (7) (a) Merino, E. *Chem. Soc. Rev.* **2011**, *40*, 3835. (b) Léonard, E.; Mangin, F.; Villette, C.; Billamboz, M.; Len, C. *Catal. Sci. Technol.* **2016**, *6*, 379.
- (8) (a) Nystrom, R. F.; Brown, W. G. *J. Am. Chem. Soc.* **1948**, *70*, 3738. (b) Khan, A.; Hecht, S. *Chem. Commun.* **2006**, 4764.
- (9) (a) Pausacker, K. H. *J. Chem. Soc.* **1953**, 1989. (b) Lu, W.; Xi, C. *Tetrahedron Lett.* **2008**, *49*, 4011. (c) Ma, H.; Li, W.; Wang, J.; Xiao, G.; Gong, Y.; Qi, C.; Feng, Y.; Li, X.; Bao, Z.; Cao, W.; Sun, Q.; Veaceslav, C.; Wang, F.; Lei, Z. *Tetrahedron* **2012**, *68*, 8358. (d) Zhang, C.; Jiao, N. *Angew. Chem. Int. Ed.* **2010**, *49*, 6174.
- (10) (a) Ibne-Rasa, K. M.; Lauro, C. G.; Edwards, J. O. *J. Am. Chem. Soc.* **1963**, *85*, 1165. (b) Davey, M. H.; Lee, V. Y.; Miller, R. D.; Marks, T. J. *J. Org. Chem.* **1999**, *64*, 4976.
- (11) (a) Cohen, T.; Lewarchik, R. J.; Tarino, J. Z. *J. Am. Chem. Soc.* **1974**, *96*, 7753. (b) Shine, H. J.; Zmuda, H.; Kwart, H.; Horgan, A. G.; Brechbiel, M. *J. Am. Chem. Soc.* **1982**, *104*, 5181.
- (12) Matsui, M.; Iwata, Y.; Kato, T.; Shibata, K. *Dyes Pigm.* **1988**, *9*, 109.
- (13) (a) Katritzky, A. R.; Wu, J.; Verin, S. V. *Synthesis* **1995**, 651. (b) Farhadi, S.; Sepahvand, S. *J. Mol. Catal. A: Chem.* **2010**, *318*, 75. (c) Alberti, A.; Bedogni, N.; Benaglia, M.; Leardini, R.; Nanni, D.; Pedulli, G. F.; Tundo, A.; Zanardi, G. *J. Org. Chem.* **1992**, *57*, 607.

- (14) (a) Burns, J.; McCombie, H.; Scarborough, H. A. *J. Chem. Soc.* **1928**, 2928. (b) Robertson, P. W.; Hitchings, T. R.; Will, G. M. *J. Chem. Soc.* **1950**, 808. (c) Fahey, D. R. *J. Organomet. Chem.* **1971**, 27, 283. (d) Fahey, D. R. *J. Chem. Soc. D* **1970**, 417. (e) Konrad, D. B.; Frank, J. A.; Trauner, D. *Chem. Eur. J.* **2016**, 22, 4364. (f) Li, J.; Cong, W.; Gao, Z.; Zhang, J.; Yang, H.; Jiang, G. *Org. Biomol. Chem.* **2018**, 16, 3479.
- (15) (a) Han, M. R.; Hashizume, D.; Hara, M. *Acta Crystallogr., Sect. E* **2006**, 62, o3001. (b) Bléger, D.; Ciesielski, A.; Samorì, P.; Hecht, S. *Chem. Eur. J.* **2010**, 16, 14256. (c) De Jesús, M.; Larios-López, L.; Rodríguez-González, R. J.; Navarro-Rodríguez, D. *J. Mol. Liq.* **2016**, 222, 1031. (d) Torres-Rocha, O. L.; Larios-López, L.; Rodríguez-González, R. J.; Felix-Serrano, I.; Navarro-Rodríguez, D. *J. Mol. Liq.* **2017**, 225, 251. (e) Huang, W.; Lee, S.-K.; Sung, Y. M.; Peng, F.; Yin, B.; Ma, M.; Chen, B.; Liu, S.; Kirk, S. R.; Kim, D.; Song, J. *Chem. Eur. J.* **2015**, 21, 15328. (f) Heitmann, G.; Dommaschk, M.; Löw, R.; Herges, R. *Org. Lett.* **2016**, 18, 5228. (g) Yin, B.; Kim, T.; Zhou, M.; Huang, W.; Kim, D.; Song, J. *Org. Lett.* **2017**, 19, 2654. (h) Nguyen, T.-T.; Turp, D.; Wang, D.; Nolscher, B.; Laquai, F.; Mullen, K. J. *Am. Chem. Soc.* **2011**, 133, 11194. (i) Izumi, A.; Teraguchi, M.; Nomura, R.; Masuda, T. *Macromolecules* **2000**, 33, 5347. (j) Li, L.; He, F.; Wang, X.; Ma, N.; Li, L. *ACS Appl. Mater. Interfaces* **2012**, 4, 4927. (k) Cheng, H. L.; Tang, M. T.; Tuchinda, W.; Enomoto, K.; Chiba, A.; Saito, Y.; Kamiya, T.; Sugimoto, M.; Saeki, A.; Sakurai, T.; Omichi, M.; Sakamaki, D.; Seki, S. *Adv. Mater. Interfaces* **2015**, 2, 1400450. (l) Zhao, R.; Zhan, X.; Yao, L.; Chen, Q.; Xie, Z.; Ma, Y. *Macromol. Rapid Commun.* **2016**, 37, 610. (m) Huang, C.-W.; Ji, W.-Y.; Kuo, S.-W. *Polym. Chem.* **2018**, 9, 2813. (n) Wang, K.; Yin, L.; Miu, T.; Liu, M.; Zhao, Y.; Chen, Y.; Zhou, N.; Zhang, W.; Zhu, X. *Mater. Chem. Front.* **2018**, 2, 1112. (o) Otaki, M.; Kumai, R.; Goto, H. *J. Polym. Sci., Part A: Polym. Chem.* **2019**, 57, 1756. (p) Wang, Z.; Müller, K.; Valášek, M.; Grosjean, S.; Bräse, S.; Wöll, C.; Mayor, M.; Heinke, L. *J. Phys. Chem. C* **2018**, 122, 19044. (q) Ma, X.; Qu, D.; Ji, F.; Wang, Q.; Zhu, L.; Xu, Y.; Tian, H. *Chem. Commun.* **2007**, 1409. (r) Ma, X.; Wang, Q.; Tian, H. *Tetrahedron Lett.* **2007**, 48, 7112. (s) Reuter, R.; Wegner, H. A. *Beilstein J. Org. Chem.* **2012**, 8, 877.
- (16) Chen, Y.; Li, C.; Xu, X.; Liu, M.; He, Y.; Murtaza, I.; Zhang, D.; Yao, C.; Wang, Y.; Meng, H. *ACS Appl. Mater. Interfaces* **2017**, 9, 7305.
- (17) Han, M.; Norikane, Y.; Onda, K.; Matsuzawa, Y.; Yoshida, M.; Hara, M. *New J. Chem.* **2010**, 34, 2892.
- (18) Qu, D. H.; Wang, Q. C.; Ma, X.; Tian, H. *Chem. Eur. J.* **2005**, 11, 5929.
- (19) Köhl, I.; Lüning, U. *Synthesis* **2014**, 46, 2376.
- (20) (a) Bryant-Friedrich, A. C.; Neidlein, R. *Helv. Chim. Acta* **1997**, 80, 1639. (b) Yu, B.-C.; Shirai, Y.; Tour, J. M. *Tetrahedron* **2006**, 62, 10303. (c) Zarwell, S.; Rück-Braun, K. *Tetrahedron Lett.* **2008**, 49, 4020. (d) Zeitouny, J.; Aurisicchio, C.; Bonifazi, D.; De Zorzi, R.; Geremia, S.; Bonini, M.; Palma, C. A.; Samorì, P.; Listorti, A.; Belbakra, A.; Armaroli, N. *J. Mater. Chem.* **2009**, 19, 4715. (e) Itoi, H.; Kambe, T.; Kano, N.; Kawashima, T. *Inorg. Chim. Acta* **2012**, 381, 117. (f) Jaumann, E. A.; Steinwand, S.; Klenik, S.; Plackmeyer, J.; Bats, J. W.; Wachtveitl, J.; Prisner, T. F. *Phys. Chem. Chem. Phys.* **2017**, 19, 17263. (g) Koumura, N.; Kudo, M.; Tamaoki, N. *Langmuir* **2004**, 20, 9897. (h) Moreno, C.; Arnanz, A.; Medina, R.-M.; Macazaga, M.-J.; Pascual, M.; García-Frutos, E. M.; Martínez-Gimeno, E.; Marcos, M.-L. *Organometallics* **2015**, 34, 2971. (i) Zhao, Y.; Li, K.; Zhang, Y.; Zhao, Y.; Miao, Z. *Mol. Cryst. Liq. Cryst.* **2017**, 650, 7. (j) Huo, X.; Xu, Q. P.; Miao, Z. *Appl. Mech. Mater.* **2014**, 584-586, 1705. (k) Okano, K.; Tsutsumi, O.; Shishido, A.; Ikeda, T. *J. Am. Chem. Soc.* **2006**, 128, 15368. (l) Kuciauskas, D.; Porsch, M. J.; Pakalnis, S.; Lott, K. M.; Wright, M. E. *J. Phys. Chem. B* **2003**, 107, 1559. (m) Humphrey, J. L.; Lott, K. M.; Wright, M. E.; Kuciauskas, D. *J. Phys. Chem. B* **2005**, 109, 21496. (n) Shen, D.; Pan, Z.; Xu, H.; Cheng, S.; Zhu, X.; Fan, L. *Chin. J. Chem.* **2010**, 28, 1279. (o) Ansari, M.; Bera, R.; Mondal, S.; Das, N. *ACS Omega* **2019**, 4, 9383. (p) Iba, S.; Ishida, T.; Sanda, F. *Polym. Bull.* **2020**, 77, 1121. (q) Nath, I.; Chakraborty, J.; Khan, A.; Arshad, M. N.; Azum, N.; Rab, M. A.; Asiri, A. M.; Alamry, K. A.; Verpoort, F. *J. Catal.* **2019**, 377, 183. (r) Mohamed Ahmed, M. S.; Mori, A. *Tetrahedron* **2004**, 60, 9977. (s) Liao, L.-X.; Stellacci, F.; McGrath, D. V. *J. Am. Chem. Soc.* **2004**, 126, 2181. (t) Casas-Solvas, J. M.; Vargas-Berenguel, A. *Tetrahedron Lett.* **2008**, 49, 6778.
- (21) Shirtcliff, L. D.; Weakley, T. J. R.; Haley, M. M.; Köhler, F.; Herges, R. *J. Org. Chem.* **2004**, 69, 6979.
- (22) Heindl, A. H.; Wegner, H. A. *Beilstein J. Org. Chem.* **2020**, 16, 22.
- (23) Liu, Y.; Yang, W.; Liu, H. *Chem. Eur. J.* **2015**, 21, 4731.
- (24) Jiang, C.; Yang, W.; Liu, H. *Russ. Chem. Bull.* **2016**, 65, 1076.
- (25) Izumi, A.; Teraguchi, M.; Nomura, R.; Masuda, T. *J. Polym. Sci., Part A: Polym. Chem.* **2000**, 38, 1057.
- (26) Quandt, G.; Höfner, G.; Pabel, J.; Dine, J.; Eder, M.; Wanner, K. T. *J. Med. Chem.* **2014**, 57, 6809.
- (27) Izumi, A.; Nomura, R.; Masuda, T. *Macromolecules* **2001**, 34, 4342.
- (28) Gøsgis, T. M.; Kleimark, J.; Nilsson Lill, S. O.; Korsager, S.; Lindhardt, A. T.; Norrby, P. O.; Skrydstrup, T. *J. Am. Chem. Soc.* **2012**, 134, 443.
- (29) Xu, X.-D.; Zhang, J.; Chen, L.-J.; Zhao, X.-L.; Wang, D.-X.; Yang, H.-B. *Chem. Eur. J.* **2012**, 18, 1659.
- (30) Al-Balushi, R. A.; Haque, A.; Jayapal, M.; Al-Suti, M. K.; Husband, J.; Khan, M. S.; Skelton, J. M.; Molloy, K. C.; Raithby, P. R. *Inorg. Chem.* **2016**, 55, 10955.
- (31) Zhao, R.; Han, J.; Huang, M.; Liu, F.; Wang, L.; Ma, Y. *Macromol. Rapid Commun.* **2017**, 38, 1700274.
- (32) Ghosh, T.; Maity, P.; Kundu, D.; Ranu, B. C. *New J. Chem.* **2016**, 40, 9556.
- (33) Strueben, J.; Gates, P. J.; Staubitz, A. *J. Org. Chem.* **2014**, 79, 1719.
- (34) Strueben, J.; Lipfert, M.; Springer, J.-O.; Gould, C. A.; Gates, P. J.; Sönnichsen, F. D.; Staubitz, A. *Chem. Eur. J.* **2015**, 21, 11165.
- (35) Garlich-Zschoche, F. A.; Dötz, K. H. *Organometallics* **2007**, 26, 4535.
- (36) Harvey, J. H.; Butler, B. K.; Trauner, D. *Tetrahedron Lett.* **2007**, 48, 1661.
- (37) Zhao, F.; Grubert, L.; Hecht, S.; Bléger, D. *Chem. Commun.* **2017**, 53, 3323.
- (38) (a) Hansen, M. J.; Lerch, M. M.; Szymanski, W.; Feringa, B. L. *Angew. Chem. Int. Ed.* **2016**, 55, 13514. (b) Hierrezuelo, J.; Rico, R.; Valpuesta, M.; Díaz, A.; López-Romero, J. M.; Rutkis, M.; Kreigberga, J.; Kampars, V.; Algarra, M. *Tetrahedron* **2013**, 69, 3465.
- (39) Miao, Z.; Li, Y.; Zhang, X. *Appl. Mech. Mater.* **2014**, 584-586, 1673.
- (40) (a) Yu, Z.; Hecht, S. *Angew. Chem. Int. Ed.* **2011**, 50, 1640. (b) Yu, Z.; Hecht, S. *Chem. Eur. J.* **2012**, 18, 10519.
- (41) (a) Sogawa, H.; Shiotsuki, M.; Matsuoka, H.; Sanda, F. *Macromolecules* **2011**, 44, 3338. (b) Sogawa, H.; Shiotsuki, M.; Sanda, F. *Macromolecules* **2013**, 46, 4378. (c) Okano, K.; Shishido, A.; Ikeda, T. *Adv. Mater.* **2006**, 18, 523.
- (42) Gerstel, P.; Klumpp, S.; Hennrich, F.; Poschlad, A.; Meded, V.; Blasco, E.; Wenzel, W.; Kappes, M. M.; Barner-Kowollik, C. *ACS Macro Lett.* **2014**, 3, 10.
- (43) Zhang, Y.; Chen, S. *RSC Adv.* **2018**, 8, 37348.
- (44) Kanbara, T.; Oshima, M.; Imayasu, T.; Hasegawa, K. *Macromolecules* **1998**, 31, 8725.

- (45) Honma, A.; Kanbara, T.; Hasegawa, K. *Mol. Cryst. Liq. Cryst.* **2000**, *345*, 125.
- (46) Chun, C.; Kim, M.-J.; Vak, D.; Kim, D. Y. *J. Mater. Chem.* **2003**, *13*, 2904.
- (47) Chun, C.; Ghim, J.; Kim, M.-J.; Kim, D. Y. *J. Polym. Sci., Part A: Polym. Chem.* **2005**, *43*, 3525.
- (48) Chen, X.; Chang, G. *Chin. J. Chem.* **2009**, *27*, 2093.
- (49) Sakano, T.; Horie, M.; Osakada, K.; Nakao, H. *Eur. J. Inorg. Chem.* **2005**, 644.
- (50) Bahrenburg, J.; Sievers, C. M.; Schönborn, J. B.; Hartke, B.; Renth, F.; Temps, F.; Näther, C.; Sönnichsen, F. D. *Photochem. Photobiol. Sci.* **2013**, *12*, 511.
- (51) Zhang, Y.; Zhang, Q.; Pei, S.; Wang, Y.; Zhang, H.; Jiang, Z. *High Perform. Polym.* **2014**, *26*, 946.
- (52) (a) Li, H.; Li, P.; Wang, L. *Org. Lett.* **2013**, *15*, 620. (b) Khatun, N.; Modi, A.; Ali, W.; Patel, B. K. *J. Org. Chem.* **2015**, *80*, 9662. (c) Li, M.; Ye, Y. *ChemCatChem* **2015**, *7*, 4137. (d) Hong, G.; Aruma, A. N.; Zhu, X.; Wu, S.; Wang, L. *Synthesis* **2016**, *48*, 1147. (e) Yong, W. S.; Park, S.; Yun, H.; Lee, P. H. *Adv. Synth. Catal.* **2016**, *358*, 1958. (f) Fu, X.; Wei, Z.; Xia, C.; Shen, C.; Xu, J.; Yang, Y.; Wang, K.; Zhang, P. *Catal. Lett.* **2017**, *147*, 400. (g) Gu, N.; Sun, S.; Cheng, J. *Tetrahedron Lett.* **2018**, *59*, 1069.
- (53) (a) Wang, H.; Yu, Y.; Hong, X.; Tan, Q.; Xu, B. *J. Org. Chem.* **2014**, *79*, 3279. (b) Fu, T.; Yang, J.; Sun, H.; Zhang, C.; Xiang, H.; Zhou, X. *Asian J. Org. Chem.* **2018**, *7*, 1844.
- (54) Li, J.; Zhou, H.; Zhang, J.; Yang, H.; Jiang, G. *Chem. Commun.* **2016**, *52*, 9589.
- (55) (a) Cai, S.; Lin, S.; Yi, X.; Xi, C. *J. Org. Chem.* **2017**, *82*, 512. (b) Oh, Y.; Han, S. H.; Mishra, N. K.; De, U.; Lee, J.; Kim, H. S.; Jung, Y. H.; Kim, I. S. *Eur. J. Org. Chem.* **2017**, 6265. (c) Zhu, J.; Sun, S.; Cheng, J. *Tetrahedron Lett.* **2018**, *59*, 2284.
- (56) Deng, H.; Li, H.; Wang, L. *Org. Lett.* **2016**, *18*, 3110.
- (57) Bruce, M. I.; Iqbal, M. Z.; Stone, F. G. A. *Chem. Commun.* **1970**, 1325.
- (58) Li, G.; Ma, X.; Jia, C.; Han, Q.; Wang, Y.; Wang, J.; Yu, L.; Yang, S. *Chem. Commun.* **2017**, *53*, 1261.
- (59) (a) Borah, G.; Borah, P.; Patel, P. *Org. Biomol. Chem.* **2017**, *15*, 3854. (b) Hande, A. E.; Muniraj, N.; Prabhu, K. R. *ChemistrySelect* **2017**, *2*, 5965. (c) Muniraj, N.; Prabhu, K. R. *J. Org. Chem.* **2017**, *82*, 6913.
- (60) Borah, G.; Patel, P. *Org. Biomol. Chem.* **2019**, *17*, 2554.
- (61) Li, G.; Chen, X.; Lv, X.; Jia, C.; Gao, P.; Wang, Y.; Yang, S. *Sci. China: Chem.* **2018**, *61*, 660.
- (62) Kato, T.; Kuriyama, S.; Nakajima, K.; Nishibayashi, Y. *Chem. Asian J.* **2019**, *14*, 2097.
- (63) (a) Lee, K.-E.; Jeon, H.-T.; Han, S.-Y.; Ham, J.; Kim, Y.-J.; Lee, S. W. *Dalton Trans.* **2009**, 6578. (b) Islam, S. M.; Mondal, P.; Roy, A. S.; Mondal, S.; Hossain, D. *Tetrahedron Lett.* **2010**, *51*, 2067. (c) Bulygina, L. A.; Khrushcheva, N. S.; Peregudova, S. M.; Sokolov, V. I. *Russ. Chem. Bull.* **2012**, *61*, 1998. (d) Priyadarshani, N.; Suriboot, J.; Bergbreiter, D. E. *Green Chem.* **2013**, *15*, 1361. (e) Roy, S.; Pramanik, S.; Ghorui, T.; Pramanik, K. *RSC Adv.* **2015**, *5*, 22544. (f) Pratihari, J. L.; Mandal, P.; Lin, C.-H.; Lai, C. K.; Mal, D. *Polyhedron* **2017**, *135*, 224.
- (64) Alder, M. J.; Cross, W. I.; Flower, K. R.; Pritchard, R. G. *J. Organomet. Chem.* **1999**, 590, 123.
- (65) Siewertsen, R.; Neumann, H.; Buchheim-Stehn, B.; Herges, R.; Näther, C.; Renth, F.; Temps, F. *J. Am. Chem. Soc.* **2009**, *131*, 15594.
- (66) Moormann, W.; Langbehn, D.; Herges, R. *Beilstein J. Org. Chem.* **2019**, *15*, 727.
- (67) (a) Joshi, D. K.; Mitchell, M. J.; Bruce, D.; Lough, A. J.; Yan, H. *Tetrahedron* **2012**, *68*, 8670. (b) Eljabu, F.; Dhruval, J.; Yan, H. *Bioorg. Med. Chem. Lett.* **2015**, *25*, 5594. (c) Cabré, G.; Garrido-Charles, A.; González-Lafont, À.; Moormann, W.; Langbehn, D.; Egea, D.; Lluch, J. M.; Herges, R.; Alibés, R.; Busqué, F.; Gorostiza, P.; Hernando, J. *Org. Lett.* **2019**, *21*, 3780. (d) Trads, J. B.; Hüll, K.; Matsuura, B. S.; Laprell, L.; Fehrentz, T.; Gördlt, N.; Kozek, K. A.; Weaver, C. D.; Klöcker, N.; Barber, D. M.; Trauner, D. *Angew. Chem. Int. Ed.* **2019**, *58*, 15421. (e) Thapaliya, E. R.; Zhao, J.; Ellis-Davies, G. C. R. *ACS Chem. Neurosci.* **2019**, *10*, 2481.
- (68) (a) Tellkamp, T.; Shen, J.; Okamoto, Y.; Herges, R. *Eur. J. Org. Chem.* **2014**, 5456. (b) Moormann, W.; Langbehn, D.; Herges, R. *Synthesis* **2017**, *49*, 3471. (c) Samanta, S.; Qin, C.; Lough, A. J.; Woolley, G. A. *Angew. Chem. Int. Ed.* **2012**, *51*, 6452. (d) Li, S.; Han, G.; Zhang, W. *Macromolecules* **2018**, *51*, 4290. (e) Deo, C.; Bogliotti, N.; Métivier, R.; Retailleau, P.; Xie, J. *Chem. Eur. J.* **2016**, *22*, 9092.
- (69) (a) Wang, J.; He, J.; Zhi, C.; Luo, B.; Li, X.; Pan, Y.; Cao, X.; Gu, H. *RSC Adv.* **2014**, *4*, 16607. (b) Maier, M. S.; Hüll, K.; Reynders, M.; Matsuura, B. S.; Leippe, P.; Ko, T.; Schäffer, L.; Trauner, D. *J. Am. Chem. Soc.* **2019**, *141*, 17295.
- (70) Li, S.; Eleya, N.; Staubitz, A. *Org. Lett.* **2020**, *22*, 1624.
- (71) Jun, M.; Joshi, D. K.; Yalagala, R. S.; Vanloon, J.; Simionescu, R.; Lough, A. J.; Gordon, H. L.; Yan, H. *ChemistrySelect* **2018**, *3*, 2697.
- (72) Zhu, Q.; Wang, S.; Chen, P. *Org. Lett.* **2019**, *21*, 4025.



## Publication II

### 3.1 Active Ester Functionalized Azobenzenes as Versatile Building Blocks

#### Aim:

Initially, we sought a chemical interface for the integration of azobenzenes into biological systems to activate and deactivate proteins. The priority was on compatibility with new azobenzene switches that demonstrate improved properties through visible switching and half-life times. Avoiding UV-light was intended to prevent damage to the protein, and longer half-life times were aimed to enhance controllability. The published reactions for these new switching classes were limited.

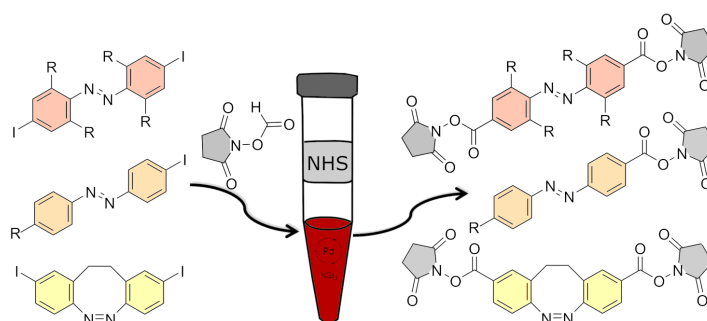
A new synthetic strategy was considered, and NHS ester was selected as a suitable interface. This active ester reacts selectively with primary amines under mild conditions. Nonetheless, this group can be isolated and exhibits stability under ambient conditions. A palladium-catalyzed reaction starting from readily available halogenated compounds was used as the synthesis route. Due to the high yield, the scope was expanded to offer azobenzenes also for material applications. A wide range of examples demonstrated the excellent conversion of iodinated compounds to active esters. Furthermore, the reaction of NHS esters with amines was demonstrated two examples in high yields to show the potential in biological application.

#### Title of Publication:

#### Active Ester Functionalized Azobenzenes as Versatile Building Blocks

S. Schultzke, M. Walther, A. Staubitz, *Molecules*, **2021**, *26*, 3916.

Permission to reprint in Appendix 9.6.



**Abstract:**

Azobenzenes are important molecular switches that can still be difficult to functionalize selectively. A high yielding Pd-catalyzed cross-coupling method under mild conditions for the introduction of NHS esters to azobenzenes and diazocines has been established. Yields were consistently high with very few exceptions. The NHS functionalized azobenzenes react with primary amines quantitatively. These amines are ubiquitous in biological systems and in material science.

**Abstract (deutsch):**

Azobenzole sind gefragte molekulare Schalter, die trotzdem noch schwierig selektiv funktionalisierbar sind. Eine Pd-katalysierte Kreuzkupplungsmethode unter milden Bedingungen für die Einführung von NHS-Estern in Azobenzole und Diazozine wurde etabliert. Dabei ergaben sich durchweg mit wenigen Ausnahmen hohe Ausbeuten. Die erhaltenen NHS-funktionalisierten Azobenzole reagieren quantitativ mit primären Aminen, die häufig in biologischen Systemen und in der Materialwissenschaft verwendet werden.

**Author Contribution to this Publication:**

Initiated by me (Sven Schultze, AG Staubitz, University of Bremen), I established the initial design of the photoswitches. The first synthetic implementation and examples were synthesized by me. Then, the synthesis was optimized in collaboration with M. Walther and the scope expanded (23 compounds by me, 18 compounds by M. Walther). The supporting information was written collaboratively for the respective compounds. The manuscript was conceived and written in collaboration with M. Walther and Prof. A. Staubitz. The table of content (ToC) image was designed by me. Both authors contributed equally.



Article

---

# Active Ester Functionalized Azobenzenes as Versatile Building Blocks

---

Sven Schultze, Melanie Walther and Anne Staubitz

Special Issue

Azobenzene and Applications: From Catalysis to Biology

Edited by

Dr. Estelle Léonard and Dr. Muriel Billamboz



<https://doi.org/10.3390/molecules26133916>

Article

# Active Ester Functionalized Azobenzenes as Versatile Building Blocks

Sven Schultze <sup>1,2,†</sup> , Melanie Walther <sup>1,2,†</sup>  and Anne Staubitz <sup>1,2,\*</sup> 

- <sup>1</sup> Institute for Analytical and Organic Chemistry, University of Bremen, Leobener Straße 7, D-28359 Bremen, Germany; schultzke@uni-bremen.de (S.S.); melanie.walther@uni-bremen.de (M.W.)
- <sup>2</sup> MAPEX Center for Materials and Processes, University of Bremen, Bibliothekstraße 1, D-28359 Bremen, Germany
- \* Correspondence: staubitz@uni-bremen.de; Tel.: +49-421-218-63210
- † These authors contributed equally to this work.

**Abstract:** Azobenzenes are important molecular switches that can still be difficult to functionalize selectively. A high yielding Pd-catalyzed cross-coupling method under mild conditions for the introduction of NHS esters to azobenzenes and diazocines has been established. Yields were consistently high with very few exceptions. The NHS functionalized azobenzenes react with primary amines quantitatively. These amines are ubiquitous in biological systems and in material science.

**Keywords:** azobenzene; diazocine; molecular switches; palladium-catalyzed carbonylation; photo-switchable NHS ester; *N*-hydroxysuccinimide; chemical biology



check for updates

**Citation:** Schultze, S.; Walther, M.; Staubitz, A. Active Ester Functionalized Azobenzenes as Versatile Building Blocks. *Molecules* **2021**, *26*, 3916. <https://doi.org/10.3390/molecules26133916>

Academic Editors: Estelle Léonard and Muriel Billamboz

Received: 31 May 2021  
Accepted: 23 June 2021  
Published: 26 June 2021

**Publisher's Note:** MDPI stays neutral with regard to jurisdictional claims in published maps and institutional affiliations.



**Copyright:** © 2021 by the authors. Licensee MDPI, Basel, Switzerland. This article is an open access article distributed under the terms and conditions of the Creative Commons Attribution (CC BY) license (<https://creativecommons.org/licenses/by/4.0/>).

## 1. Introduction

Photoswitchable molecules add photoresponsiveness to diverse materials such as polymers [1–6], dendrimers [7,8] or biomolecules [9–23]. By precise adjustment of the synthetic strategy the switch can be incorporated into the target material and its switching properties can be utilized. However, in many cases, it is exactly this tailored functionalization of the photoswitch that is the major challenge and the bottleneck in a successful project.

Due to its fast and efficient photoswitching characteristics, as well as its high fatigue-resistance [24], azobenzene is widely used in versatile applications such as molecular machines [3,25–28], data storage materials [29–32], or photopharmacology [9–23]. Upon irradiation with UV-light, typical azobenzenes undergo isomerization from the thermodynamically favored (*E*)-isomer to the less stable (*Z*)-isomer (Figure 1, left). The re-isomerization can occur either by irradiation with light or by thermal relaxation [24,33]. The half-lives of the latter strongly depend on the azobenzenes' substitution pattern and are therefore tunable for the specific application [34]. The isomerization is accompanied by a change of several physicochemical characteristics: the geometry [35,36], the end-to-end-distance [35,36], and the electronic properties [37] (e.g., absorption and dipole moment). The thermodynamically favored (*E*)-form is planar [35] and without a dipole moment [37]. The (*Z*)-isomer on the other hand has a bent geometry where the phenyl rings are twisted ~55° out of plane to the azo group [36]. Moreover, the (*Z*)-isomer shows a dipole moment of 3.0 Debye [37]. The end-to-end distance of the (*E*)- and (*Z*)-isomer differs by ~3.5 Å [35,36]. In biological systems, azobenzenes bind typically in an elongated confirmation; its biological activity is controllable via the switching process [9]. The isomerization to the (*Z*)-isomer occurs by irradiation with UV-light, which might harm cells and tissues [38–40]. Therefore, a red-shifting of the absorption wavelength is desirable and in biological applications may be even necessary [9]. In addition, a separation of the absorption spectra of both isomers is important to avoid mixtures of isomers. Starting from 2009, *ortho*-substituted azobenzenes [41–50] and ethylene-bridged azobenzenes, the so-called diazocines [51,52], have been discovered to be promising candidates to overcome the two limitations of a typical



azobenzene. Depending on the substituents in *ortho*-position, not only the absorption is shifted towards longer wavelength but also the thermal half-life may be drastically extended due to steric and electronic interactions [48]. Diazocines are also a particularly important class of azobenzenes, because the bent (*Z*)-isomer is thermodynamically favored due to the ring strain of the eight-membered ring (Figure 1, right). The isomerization of diazocines is in both directions possible using visible light; the isomerization to the elongated (*E*)-form occurs upon irradiation with light in the range of 400 nm, the re-isomerization to (*Z*) with 530 nm [51].

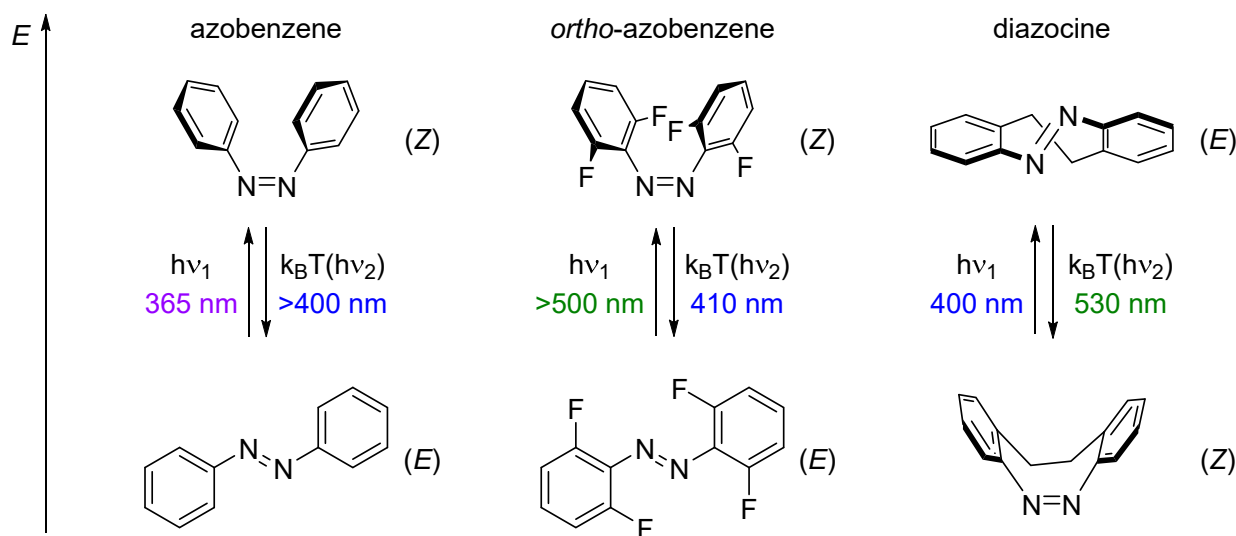
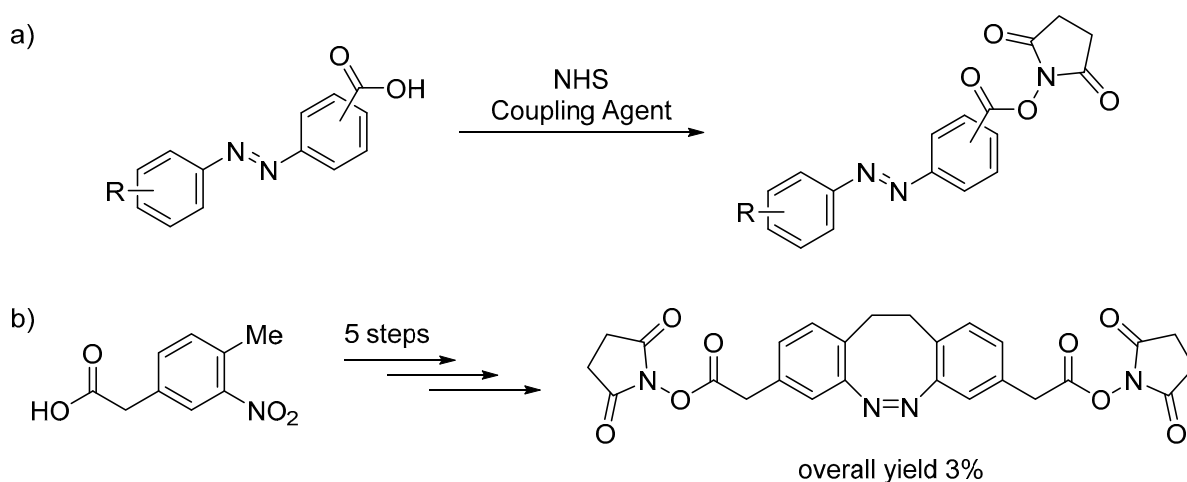


**Figure 1.** Isomerization of azobenzene [24], tetra-*ortho*-fluorinated azobenzene [48] and diazocine [51].

To incorporate such azobenzenes into a larger system, a suitable functional group is necessary that reacts selectively with the specific target position of the material. *N*-Hydroxysuccinimide (NHS) esters react selectively under mild conditions with primary amines, which can be found for example in commercially available polymers but of course also in all proteins and peptides as well as in nucleic acids. Due to the ubiquity of primary amines, NHS esters are versatile building blocks for instance in peptide synthesis [53–55], bioconjugate chemistry [56–60] as well as functionalized materials and polymers [61–71]. The use of NHS esters for the formation of amides has several advantages: NHS esters are comparatively easy to prepare. They are the only active esters that can be isolated [72]. In comparison to the coupling reaction of a primary amine with a carboxylic acid using a carbodiimide coupling agent such as *N,N'*-dicyclohexylcarbodiimide (DCC), NHS esters are less toxic. They can be used under physiologic or slightly basic conditions [72]. Moreover, the products of their transformations are easier to purify as water-soluble NHS is released during the amide formation [53].

Traditionally, NHS esters are synthesized by a coupling reaction of the carboxylic acid with NHS in the presence of a carbodiimide coupling agent [73,74], which is known to have an allergenic potential and to form urea as byproduct. Thus, the product purification might be challenging [72]. The carboxylic acid can also be activated by using anhydrides and their analogues for example *N,N'*-disuccinimidyl carbonate (DSC) [75]. More recently, coupling reactions of alcohols [76] and aldehydes [77] with NHS under oxidizing conditions have been investigated. Carbonylative cross-coupling reactions represents another synthetic strategy towards NHS esters [78,79]. Until recently, a carbon monoxide atmosphere was needed for this type of reaction prohibiting a safe and easy-to-handle implementation of the reaction. By using NHS formate as CO surrogate this drawback could be avoided and an efficient protocol on Pd-catalyzed carbonylation reactions under mild conditions developed [78].

The synthesis of NHS functionalized azobenzenes has been, so far, mainly performed via the traditional coupling approach of the corresponding carboxylic acid with NHS and a carbodiimide coupling agent [80–84] (Scheme 1a). Unsymmetric azobenzenes with a carboxylic acid moiety can be obtained via Mills reaction [85,86] or azo coupling [68,81–84], symmetric ones via a reductive coupling of nitrobenzoic acid [70,84,87–89]. Only a few examples exist with the NHS ester in *meta*-position and even fewer are reported for the *ortho*-position [80]. However, NHS functionalized azobenzenes with other *ortho*-substituents that shift the absorption wavelength in the region of visible light have not been reported so far. In case of the diazocines, their incorporation into materials is often performed via peptide coupling of an amine functionalized diazocine [90–92]. Only one example of a diazocine with an NHS ester in *meta*-position to the azo group has been reported (Scheme 1b) [93]. Here, the final diazocine was obtained in an overall yield of 3% after five steps. The carbonyl function was connected to the phenyl rings of the diazocine with a methylene bridge allowing more rotational degrees of freedom compared to a direct linkage [93].



**Scheme 1.** Synthetic approach towards NHS functionalized azobenzenes [80] (a) and diazocine [93] (b).

We could recently show that cross-coupling reactions are a versatile tool for late-stage functionalization of *para*-substituted azobenzene derivatives [94]. For diazocines, only few examples on cross-coupling reactions with differing yields have been reported, mainly Buchwald-Hartwig cross-coupling [95] or Stille reactions [11,96].

We report an efficient Pd-catalyzed carbonylation protocol, based on previously work of Barré et al. [78], to transform iodinated azobenzenes into the corresponding active NHS ester under mild conditions with NHS formate as CO surrogate. The iodinated precursors are easily accessible and a high tolerance of functional groups was achieved, including other halogen substituents. The usefulness of the obtained NHS functionalized azobenzenes was demonstrated in two examples by coupling the NHS esters with an amino acid.

## 2. Results

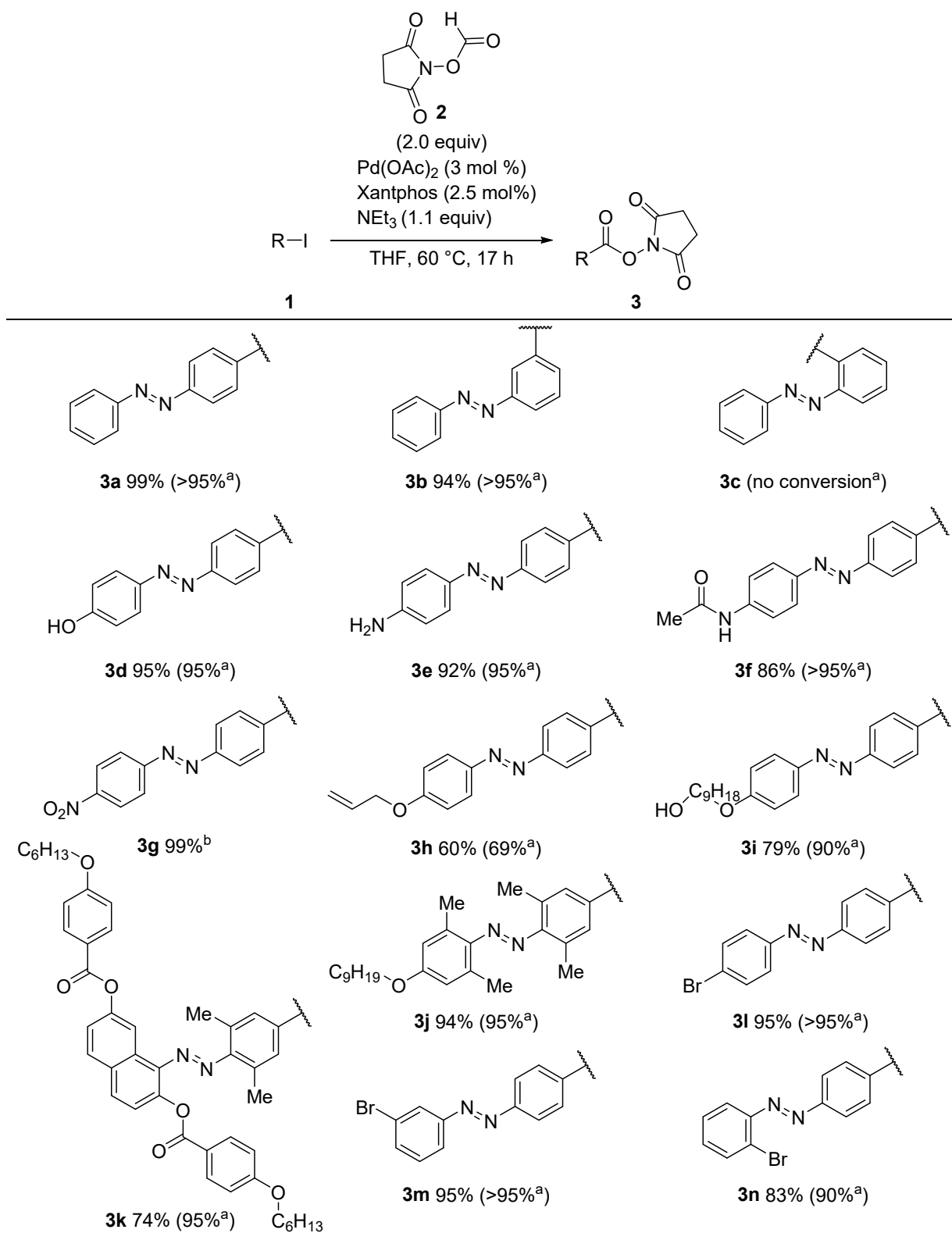
The combination of palladium acetate as catalyst and Xantphos as ligand was demonstrated to be a high yielding synthetic method in the literature for Pd-catalyzed carbonylation reactions [78,79]. Therefore, we started our investigation with this catalytic system for the functionalization of mono-iodinated azobenzenes **1** (Scheme 2). Although other possible ligands were screened, the combination of palladium acetate with Xantphos was shown to be the best condition for the catalytic carbonylation of iodinated azobenzenes. In this way, mono-iodinated azobenzenes, at first without further substituents were reacted with NHS formate (**2**). <sup>1</sup>H NMR analysis with an internal reference revealed a quantitative conversion to the desired *para*- **3a** and *meta*-derivative **3b**. Unfortunately, no conversion

to the *ortho*-functionalized azobenzene **3c** was detected; and the starting material was completely recovered. It is very common that the functionalization of azobenzenes by cross-coupling is low yielding or entirely unsuccessful. It also aligns with our own findings that cross-coupling reactions at *ortho*-position of azobenzenes are rarely possible [94]. Next, azobenzene derivatives with further substitutions were tested (**3d–3n**). A wide range of functional groups was tolerated: Starting with a hydroxy group in *para*-position, **3d** was obtained in an isolated yield of 95%. Also, an amine function on the azobenzene did not cause problems even though it might have been possible that the formed NHS ester directly reacts with this aromatic primary amine; **3e** could be isolated in 92%. The acetamide functionalized azobenzene **3f** was isolated in a yield of 86%. However, the conversion was determined by <sup>1</sup>H NMR analysis to be over 95%. Moreover, azobenzene derivatives containing an electron withdrawing group, such as 4-nitro-4'-iodoazobenzene (**1g**), were converted to the corresponding NHS ester in quantitative yield. Even the vinylated species **1h** was successfully transformed to **3h** and isolated in a yield of 60%. Moreover, the functionalization of three additional azobenzene derivatives proves the versatility of the demonstrated reaction: In particular, an azobenzene with both an ether and a primary hydroxyl group (**3i**, 79%), an alkoxyated tetra-*ortho*-azobenzene (**3j**, 94%) and a unique sterically hindered azobenzene with a naphthalene motif (**3k**, 74%) were all successfully synthesized.

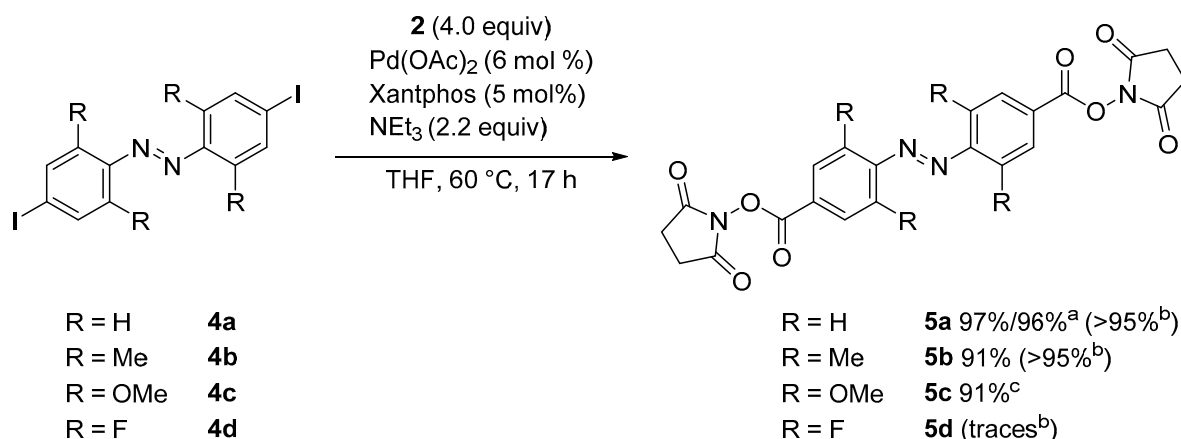
The coupling reaction proceeded chemo-selectively in excellent yields when azobenzene derivatives were used that had both, an iodine and a bromine substituent. Thus, the obtained NHS functionalized azobenzene derivatives **3l–n** enable potential further functionalization reactions by cross-coupling strategies.

Considering the latest research trends to use azobenzene derivatives that can be switched with visible light and to incorporate these into different types of applications, we were interested to transfer our results for mono-iodinated azobenzenes to di-iodinated azobenzenes (Scheme 3). This posed no problems for **5a** and **5b** (Scheme 3), which were synthesized in excellent yields. The synthesis of **5a** was additionally performed on a 2.00 mmol scale leading to a comparable yield as the 100 μmol batch (96%). Here, the reaction setup was slightly modified: A pressure tube was used as a reaction vessel which was closed quickly after the addition of triethylamine. However, difficulties occurred for **5c** and **5d**. For **5c**, we initially observed that the reaction was incomplete. A mixture of mono-substituted NHS ester-azobenzene and di-substituted NHS ester-azobenzene was detected. We hypothesized that the solubility of the iodinated azobenzene **4c** might be too low. Therefore, we changed the solvent to the more polar DMF, as this solvent was reported to lead to comparable yields as THF [78]. However, DMF is slightly basic [97] and thus initializes the decomposition of the NHS formate (**2**). Traces of dimethylamine, a common impurity in DMF [98], can enhance this decomposition. The concomitant release of carbon dioxide increased the pressure inside the vial so much that a subsequent addition of triethyl amine via syringe was difficult. Without the additional base, however, the decomposition of **2** was not sufficient for a full conversion. Changing the solvent to DMSO instead, resolved this problem. The conversion of **4c** increased drastically for the tetra-*ortho*-methoxylated-azobenzene; **5c** was synthesized in a yield of 91%.

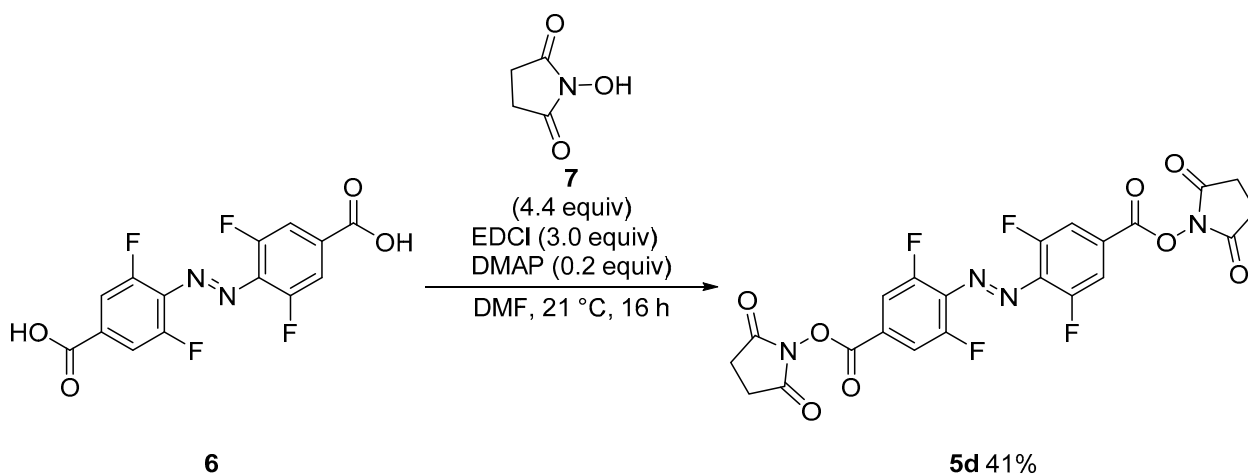
Unfortunately, the tetra-*ortho*-fluorinated azobenzene **4d** was only converted in traces to **5d** as detected by <sup>1</sup>H NMR analysis. Even the change to a more polar solvent did not increase the yield. Instead, there were so many reaction products that they could not be further analyzed. In these rare cases, in which the cross-coupling approach fails, alternative strategies need to be developed. In this instance, we were able to synthesize the fluorinated target molecule **5d** by the coupling of the carboxylic acid **6** with NHS (**7**) using 1-ethyl-3-(3-dimethylaminopropyl)carbodiimide (EDCI) and 4-dimethylaminopyridine (DMAP) as coupling agent (Scheme 4). The yield could not be improved by using other coupling agents such as DCC, HATU, HSPyU, 1,1'-carbonyldiimidazol (CDI) or 2,4,6-trichlorobenzoic acid (TCBC).



**Scheme 2.** Scope of the Pd-catalyzed NHS functionalization of mono-iodinated azobenzenes. <sup>a</sup> Yields in brackets were determined by using 1,3,5-trimethoxybenzene as internal reference for <sup>1</sup>H NMR analysis; all other yields are isolated yields. <sup>b</sup> In DMSO.



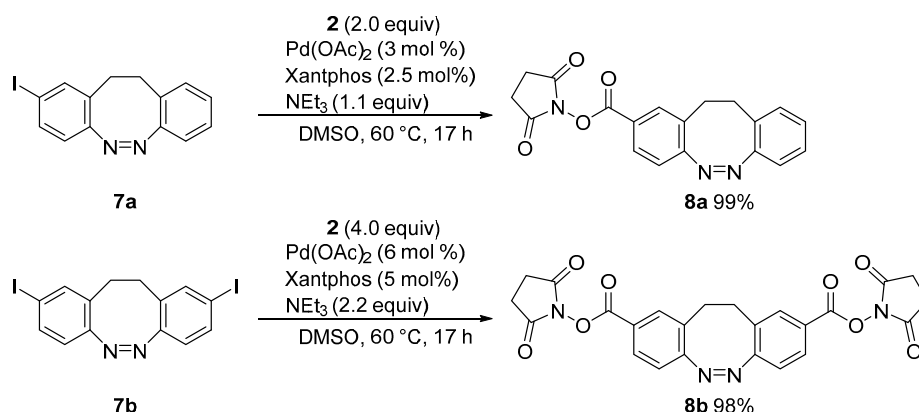
**Scheme 3.** Scope of the Pd-catalyzed NHS functionalization of di-iodinated azobenzenes. <sup>a</sup> 2.00 mmol scale. <sup>b</sup> Yields in brackets were determined by using 1,3,5-trimethoxybenzene as internal reference for <sup>1</sup>H NMR analysis; all other yields are isolated yields. <sup>c</sup> In DMSO.



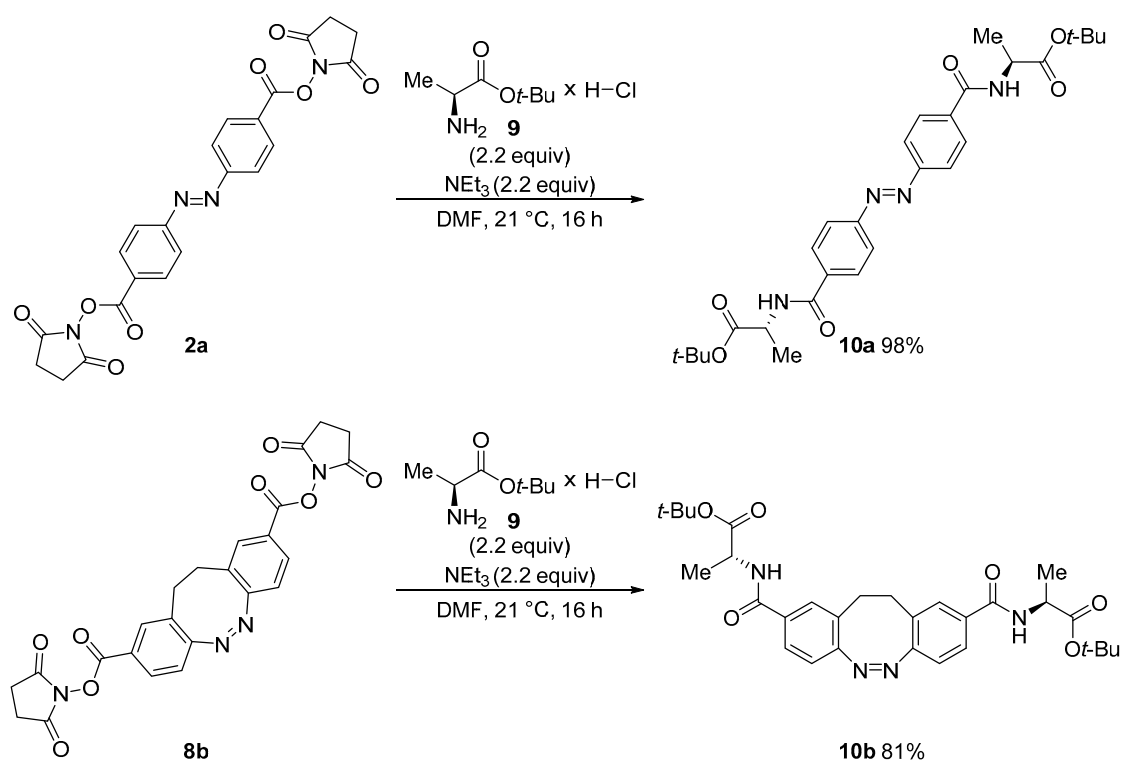
**Scheme 4.** Alternative synthetic route to obtain the NHS functionalized tetra-*ortho*-fluorinated azobenzene.

In contrast to typical azobenzenes, the (*Z*)-isomer is thermodynamically favored in diazocines making them a desirable molecule for applications. Moreover, the switching is possible with visible light. Diazocines bearing a carboxyl group are demanding to synthesize with moderate overall yields [99,100]. As iodinated diazocines can be easily obtained [95], we were interested to transfer our method to diazocines. Analogously to the difficulties for di-iodinated azobenzenes, the use of THF as solvent led only to a partial conversion; in case of the di-iodinated diazocine, a mixture of mono- and di-functionalized derivatives was obtained. Again, these problems were resolved by using DMSO as solvent and diazocines **6a** and **6b** were obtained in near-quantitative yields (Scheme 5).

To demonstrate the usefulness of the obtained NHS ester derivatives for reactions with a primary amine, azobenzene **2a** and diazocine **8b** were reacted with *L*-alanine *tert*-butyl ester hydrochloride under slightly basic conditions yielding the corresponding amino acid derivatives **9a** and **9b** in excellent to quantitative yield (Scheme 6).



Scheme 5. Pd-catalyzed NHS functionalization of iodinated diazocines.

Scheme 6. Condensation reaction of NHS derivatives with L-alanine *tert*-butyl ester hydrochloride.

### 3. Discussion

This robust and high-yielding protocol enables new possibilities for the molecular design of azobenzene and diazocine derivatives. A large scope of 14 mono-functionalized and 5 di-functionalized azobenzenes and diazocines were prepared in high to excellent yields. Iodinated azobenzenes are fairly easy to synthesize and a vast number of protocols are available. In contrast to this, the traditional synthetic route requires a carboxyl group on the azobenzene for the esterification to yield the NHS functionality. This is a severe synthetic limitation. Indeed, the carboxylated analogous of **3g**, **3k–l** have not been reported, but the corresponding NHS derivatives can now be synthesized via our synthetic approach. These advantages are even more important considering that the solubility of di-carboxylated azobenzenes in organic solvents is low. Furthermore, the synthesis of more complex azobenzenes with a carboxyl-functionality requires many synthetic steps or are

unknown until today. The practicality of the approach was shown by the condensation of two di-functionalized NHS esters with a protected amino acid.

#### 4. Materials and Methods

All synthetic procedures and characterization data for all compounds and precursors can be found in the supporting information.

##### 4.1. General Information

For reactions under inert conditions, a nitrogen filled glovebox (Pure Lab<sup>HE</sup> from Inert, Amesbury, MA USA) and standard Schlenk techniques were used (Supplementary Materials). All carbonylation reactions were performed in microwave reaction vials sealed with a septum cap from Biotage (Biotage, Uppsala, Sweden). All glassware was dried in an oven at 200 °C for several hours prior to use. NMR tubes were dried in an oven at 110 °C for several hours prior to use. NMR spectra were recorded on a Bruker Avance Neo 600 (Bruker BioSpin, Rheinstetten, Germany) (600 MHz (<sup>1</sup>H), 151 MHz (<sup>13</sup>C{<sup>1</sup>H})), 565 MHz (<sup>19</sup>F) at 298 K. All <sup>1</sup>H NMR and <sup>13</sup>C{<sup>1</sup>H} NMR spectra were referenced to the residual proton signals of the solvent (<sup>1</sup>H) or the solvent itself (<sup>13</sup>C{<sup>1</sup>H}). <sup>19</sup>F NMR spectra were referenced internally against trichlorofluoromethane. The exact assignment of the peaks was performed by two-dimensional NMR spectroscopy such as <sup>1</sup>H COSY, <sup>13</sup>C{<sup>1</sup>H} HSQC and <sup>1</sup>H/<sup>13</sup>C{<sup>1</sup>H} HMBC when possible. High-resolution EI mass spectra were recorded on a MAT 95XL double-focusing mass spectrometer from Finnigan MAT (Thermo Fisher Scientific, Waltham, MA, USA) at an ionization energy of 70 eV. Samples were measured by a direct or indirect inlet method with a source temperature of 200 °C. High-resolution ESI and APCI mass spectra were measured by a direct inlet method on an Impact II mass spectrometer from Bruker Daltonics (Bruker Daltonics, Bremen, Germany). ESI mass spectra were recorded in the positive ion collection mode.

IR spectra were recorded on a Nicolet i510 FT-IR spectrometer from Thermo Fisher Scientific (Thermo Fisher Scientific, Waltham, MA, USA) with a diamond window in an area from 500–4000 cm<sup>-1</sup> with a resolution of 4 cm<sup>-1</sup>. All samples were measured 16 times against a background scan. Melting points were recorded on a Büchi Melting Point M-560 (Büchi, Essen, Germany) and are reported corrected. Thin layer chromatography (TLC) was performed using TLC Silica gel 60 F<sub>254</sub> from Merck (Merck, Darmstadt, Germany) and compounds were visualized by exposure to UV light at a wavelength of 254 nm. Column chromatography was performed either manually using silica gel 60 (0.015–0.040 mm) from Merck (Merck, Darmstadt, Germany) or by using a PuriFlash 4250 column machine (Interchim, Mannheim, Germany). Silica gel columns of the type CHROMABOND Flash RS 15 SPHERE SiOH 15 µm (Macherey-Nagel, Düren, Germany) were used. The sample was applied via dry load with Celite<sup>®</sup> 503 (Macherey-Nagel, Düren, Germany) as column material. If stated, Celite<sup>®</sup> 503 (Macherey-Nagel, Düren, Germany) was used as filtration aid. The use of abbreviations follows the conventions from the ACS Style guide [101].

##### 4.2. General Procedures

###### 4.2.1. General Procedure 1 Carbonylation

###### (a) Mono-iodinated molecular switch

Under inert conditions, the corresponding mono-iodinated molecular switch (200 µmol, 2.00 equiv), Pd(OAc)<sub>2</sub> (1.35 mg, 6.00 µmol, 3 mol%), Xantphos (2.89 mg, 5.00 µmol, 2.5 mol%) and 2,5-dioxopyrrolidin-1-yl formate (57.2 mg, 400 µmol, 4.00 equiv) were dissolved in dry THF (3 mL) in a pressure reaction vial. A solution of 1,3,5-trimethoxybenzene (16.8 mg, 100 µmol) as an internal standard in dry THF (1 mL) was added. The vial was sealed and heated to 60 °C. A solution of triethyl amine (22.2 mg, 220 µmol, 2.20 equiv) in dry THF (1 mL) was quickly added. Fast gas evolution was observed and the reaction was stirred for 17 h at 60 °C. After cooling to 21 °C, the solvent was removed under reduced pressure. The residue was re-dissolved in DCM (10 mL), filtered through Celite<sup>®</sup> and the solvent removed under reduced pressure.

#### (b) Di-iodinated molecular switch

Under inert conditions, the corresponding di-iodinated molecular switch (100  $\mu\text{mol}$ , 1.00 equiv), Pd(OAc)<sub>2</sub> (1.35 mg, 6.00  $\mu\text{mol}$ , 6 mol%), Xantphos (2.89 mg, 5.00  $\mu\text{mol}$ , 5 mol%) and 2,5-dioxopyrrolidin-1-yl formate (57.2 mg, 400  $\mu\text{mol}$ , 4.00 equiv) were dissolved in dry THF (3 mL) in a pressure reaction vial. A solution of 1,3,5-trimethoxybenzene (16.8 mg, 100  $\mu\text{mol}$ ) as an internal standard in dry THF (1 mL) was added. The vial was sealed and heated to 60 °C. A solution of triethyl amine (22.2 mg, 220  $\mu\text{mol}$ , 2.20 equiv) in dry THF (1 mL) was quickly added. Fast gas evolution was observed and the reaction was stirred for 17 h at 60 °C. After cooling to 21 °C, the solvent was removed under reduced pressure. The residue was re-dissolved in DCM (10 mL), filtered through Celite® and the solvent removed under reduced pressure.

#### 4.2.2. General Procedure 2 Carbonylation

##### (a) Mono-iodinated molecular switch

Under inert conditions, the corresponding mono-iodinated switch (200  $\mu\text{mol}$ , 2.00 equiv), Pd(OAc)<sub>2</sub> (1.35 mg, 6.00  $\mu\text{mol}$ , 3 mol%), Xantphos (2.89 mg, 5.00  $\mu\text{mol}$ , 2.5 mol%) and 2,5-dioxopyrrolidin-1-yl formate (57.2 mg, 400  $\mu\text{mol}$ , 4.00 equiv) were dissolved in dry THF (4 mL) in a pressure reaction vial. The vial was sealed and heated to 60 °C. A solution of triethyl amine (22.2 mg, 220  $\mu\text{mol}$ , 2.20 equiv) in dry THF (1 mL) was quickly added. Fast gas evolution was observed and the reaction was stirred for 17 h at 60 °C. After cooling to 21 °C, the solvent was removed under reduced pressure. The residue was re-dissolved in DCM (10 mL) and extracted with water (20 mL) and brine (20 mL). The combined organic layers were dried over magnesium sulfate, filtered and the solvent removed under reduced pressure.

##### (b) Di-iodinated molecular switch

Under inert conditions, the corresponding di-iodinated switch (100  $\mu\text{mol}$ , 1.00 equiv), Pd(OAc)<sub>2</sub> (1.35 mg, 6.00  $\mu\text{mol}$ , 6 mol%), Xantphos (2.89 mg, 5.00  $\mu\text{mol}$ , 5 mol%) and 2,5-dioxopyrrolidin-1-yl formate (57.2 mg, 400  $\mu\text{mol}$ , 4.00 equiv) were dissolved in dry THF (4 mL) in a pressure reaction vial. The vial was sealed and heated to 60 °C. A solution of triethyl amine (22.2 mg, 220  $\mu\text{mol}$ , 2.20 equiv) in dry THF (1 mL) was quickly added. Fast gas evolution was observed and the reaction was stirred for 17 h at 60 °C. After cooling to 21 °C, the solvent was removed under reduced pressure. The residue was re-dissolved in DCM (10 mL) and extracted with water (20 mL) and brine (20 mL). The combined organic layers were dried over magnesium sulfate, filtered and the solvent removed under reduced pressure.

#### 4.2.3. General Procedure Condensation Reaction

Triethyl amine (2.20 equiv) was added to a solution of L-alanine *tert*-butyl ester hydrochloride (2.20 equiv) in dry DMF. A solution of the corresponding di-NHS functionalized molecular switch (1.00 equiv) in dry DMF was added and the resulting mixture was stirred at 21 °C for 16 h. Water and ethyl acetate were added, and the mixture was washed with brine (3 $\times$ ). The combined organic phases were dried over magnesium sulfate, filtered and the solvent removed under reduced pressure yielding the product.

**Supplementary Materials:** The following are available online: general information, a list of all reagents and solvents, experimental procedures and analytical data, determination of <sup>1</sup>H NMR yield, images of all NMR spectra.

**Author Contributions:** Conceptualization, S.S. and M.W.; methodology, S.S. and M.W.; validation, S.S., M.W. and A.S.; formal analysis, S.S. and M.W.; investigation, S.S., M.W. and A.S.; resources, A.S.; data curation, S.S. and M.W.; writing—original draft preparation, S.S., M.W. and A.S.; writing—review and editing, S.S., M.W. and A.S.; visualization, S.S. and M.W.; supervision, A.S.; project administration, A.S.; funding acquisition, A.S. All authors have read and agreed to the published version of the manuscript.



**Funding:** This research was funded by the GERMAN RESEARCH FOUNDATION (DFG) within the priority program SPP 2100 “Soft Material Robotic Systems”, Subproject STA1195/5-1, “Insect feet inspired concepts soft touch grippers with dynamically adjustable grip strength”.

**Institutional Review Board Statement:** The data presented in this study are openly available in the supporting information.

**Conflicts of Interest:** The authors declare no conflict of interest.

**Sample Availability:** Samples of the compounds may be available from the authors. Please contact the authors for further details.

## References

- Zhou, H.; Xue, C.; Weis, P.; Suzuki, Y.; Huang, S.; Koynov, K.; Auernhammer, G.K.; Berger, R.; Butt, H.-J.; Wu, S. Photoswitching of Glass Transition Temperatures of Azobenzene-Containing Polymers Induces Reversible Solid-to-Liquid Transitions. *Nat. Chem.* **2017**, *9*, 145–151. [[CrossRef](#)] [[PubMed](#)]
- Ikeda, T.; Sasaki, T.; Ichimura, K. Photochemical switching of polarization in ferroelectric liquid-crystal films. *Nature* **1993**, *361*, 428–430. [[CrossRef](#)]
- Yamada, M.; Kondo, M.; Mamiya, J.-I.; Yu, Y.; Kinoshita, M.; Barrett, C.J.; Ikeda, T. Photomobile Polymer Materials: Towards Light-Driven Plastic Motors. *Angew. Chem. Int. Ed.* **2008**, *47*, 4986–4988. [[CrossRef](#)] [[PubMed](#)]
- Kizilkan, E.; Strueben, J.; Jin, X.; Schaber, C.F.; Adelung, R.; Staubitz, A.; Gorb, S.N. Influence of the Porosity on the Photoresponse of a Liquid Crystal Elastomer. *R. Soc. Open. Sci.* **2016**, *3*, 150700. [[CrossRef](#)] [[PubMed](#)]
- Kizilkan, E.; Strueben, J.; Staubitz, A.; Gorb, S.N. Bioinspired Photocontrollable Microstructured Transport Device. *Sci. Robot.* **2017**, *2*, eaak9454. [[CrossRef](#)]
- Dowds, M.; Bank, D.; Strueben, J.; Soto, D.P.; Sönnichsen, F.D.; Renth, F.; Temps, F.; Staubitz, A. Efficient Reversible Photoisomerisation with Large Solvodynamic Size-Switching of a Main Chain poly(azobenzene-alt-trisiloxane). *J. Mater. Chem. C* **2020**, *8*, 1835–1845. [[CrossRef](#)]
- Archut, A.; Vögtle, F.; De Cola, L.; Azzelini, G.C.; Balzani, V.; Ramanujam, P.S.; Berg, R.H. Azobenzene-Functionalized Cascade Molecules: Photoswitchable Supramolecular Systems. *Chem. Eur. J.* **1998**, *4*, 699–706. [[CrossRef](#)]
- Pötschke, D.; Ballauff, M.; Lindner, P.; Fischer, M.; Vögtle, F. Analysis of the Structure of Dendrimers in Solution by Small-Angle Neutron Scattering Including Contrast Variation. *Macromolecules* **1999**, *32*, 4079–4087. [[CrossRef](#)]
- Beharry, A.A.; Woolley, G.A. Azobenzene Photoswitches for Biomolecules. *Chem. Soc. Rev.* **2011**, *40*, 4422–4437. [[CrossRef](#)]
- Schehr, M.; Ianes, C.; Weisner, J.; Heintze, L.; Müller, M.P.; Pichlo, C.; Charl, J.; Brunstein, E.; Ewert, J.; Lehr, M.; et al. 2-Azo-, 2-Diazocine-thiazols and 2-Azo-imidazoles as Photoswitchable Kinase Inhibitors: Limitations and Pitfalls of the Photoswitchable Inhibitor Approach. *Photochem. Photobiol. Sci.* **2019**, *18*, 1398–1407. [[CrossRef](#)] [[PubMed](#)]
- Heintze, L.; Schmidt, D.; Rodat, T.; Witt, L.; Ewert, J.; Kriegs, M.; Herges, R.; Peifer, C. Photoswitchable Azo- and Diazocine-Functionalized Derivatives of the VEGFR-2 Inhibitor Axitinib. *Int. J. Mol. Sci.* **2020**, *21*, 8961. [[CrossRef](#)]
- Wegener, M.; Hansen, M.J.; Driessen, A.J.M.; Szymanski, W.; Feringa, B.L. Photocontrol of Antibacterial Activity: Shifting from UV to Red Light Activation. *J. Am. Chem. Soc.* **2017**, *139*, 17979–17986. [[CrossRef](#)]
- Hoorens, M.W.H.; Ourailidou, M.E.; Rodat, T.; van der Wouden, P.E.; Kobauri, P.; Kriegs, M.; Peifer, C.; Feringa, B.L.; Dekker, F.J.; Szymanski, W. Light-Controlled Inhibition of BRAFV600E Kinase. *Eur. J. Med. Chem.* **2019**, *179*, 133–146. [[CrossRef](#)] [[PubMed](#)]
- Hull, K.; Morstein, J.; Trauner, D. In Vivo Photopharmacology. *Chem. Rev.* **2018**, *118*, 10710–10747. [[CrossRef](#)]
- Stein, M.; Middendorp, S.J.; Carta, V.; Pejo, E.; Raines, D.E.; Forman, S.A.; Sigel, E.; Trauner, D. Azo-Propofols: Photochromic Potentiators of GABA(A) Receptors. *Angew. Chem. Int. Ed.* **2012**, *51*, 10500–10504. [[CrossRef](#)] [[PubMed](#)]
- Velema, W.A.; Szymanski, W.; Feringa, B.L. Photopharmacology: Beyond Proof of Principle. *J. Am. Chem. Soc.* **2014**, *136*, 2178–2191. [[CrossRef](#)] [[PubMed](#)]
- Arkipova, V.; Fu, H.; Hoorens, M.W.H.; Trinco, G.; Lameijer, L.N.; Marin, E.; Feringa, B.L.; Poelarends, G.J.; Szymanski, W.; Slotboom, D.J.; et al. Structural Aspects of Photopharmacology: Insight into the Binding of Photoswitchable and Photocaged Inhibitors to the Glutamate Transporter Homologue. *J. Am. Chem. Soc.* **2021**, *143*, 1513–1520. [[CrossRef](#)] [[PubMed](#)]
- Kolarski, D.; Miller, S.; Oshima, T.; Nagai, Y.; Aoki, Y.; Kobauri, P.; Srivastava, A.; Sugiyama, A.; Amai, K.; Sato, A.; et al. Photopharmacological Manipulation of Mammalian CRY1 for Regulation of the Circadian Clock. *J. Am. Chem. Soc.* **2021**, *143*, 2078–2087. [[CrossRef](#)]
- Hansen, M.J.; Hille, J.I.C.; Szymanski, W.; Driessen, A.J.M.; Feringa, B.L. Easily Accessible, Highly Potent, Photocontrolled Modulators of Bacterial Communication. *Chem* **2019**, *5*, 1293–1301. [[CrossRef](#)]
- Volgraf, M.; Gorostiza, P.; Numano, R.; Kramer, R.H.; Isacoff, E.Y.; Trauner, D. Allosteric Control of an Ionotropic Glutamate Receptor with an Optical Switch. *Nat. Chem. Biol.* **2006**, *2*, 47–52. [[CrossRef](#)]
- Banghart, M.; Borges, K.; Isacoff, E.; Trauner, D.; Kramer, R.H. Light-Activated Ion Channels for Remote Control of Neuronal Firing. *Nat. Neurosci.* **2004**, *7*, 1381–1386. [[CrossRef](#)] [[PubMed](#)]
- Velema, W.A.; van der Berg, J.P.; Hansen, M.J.; Szymanski, W.; Driessen, A.J.; Feringa, B.L. Optical Control of Antibacterial Activity. *Nat. Chem.* **2013**, *5*, 924–928. [[CrossRef](#)]

23. Zhang, Y.; Erdmann, F.; Fischer, G. Augmented Photoswitching Modulates Immune Signaling. *Nat. Chem. Biol.* **2009**, *5*, 724–726. [[CrossRef](#)] [[PubMed](#)]
24. Yager, K.G.; Barrett, C.J. Novel Photo-Switching using Azobenzene Functional Materials. *J. Photochem. Photobiol. A* **2006**, *182*, 250–261. [[CrossRef](#)]
25. Lancia, F.; Ryabchun, A.; Katsonis, N. Life-Like Motion Driven by Artificial Molecular Machines. *Nat. Rev. Chem.* **2019**, *3*, 536–551. [[CrossRef](#)]
26. Iamsaard, S.; Asshoff, S.J.; Matt, B.; Kudernac, T.; Cornelissen, J.J.; Fletcher, S.P.; Katsonis, N. Conversion of Light into Macroscopic Helical Motion. *Nat. Chem.* **2014**, *6*, 229–235. [[CrossRef](#)] [[PubMed](#)]
27. Koshima, H.; Ojima, N.; Uchimoto, H. Mechanical Motion of Azobenzene Crystals upon Photoirradiation. *J. Am. Chem. Soc.* **2009**, *131*, 6890–6891. [[CrossRef](#)]
28. Gelebart, A.H.; Mulder, D.J.; Varga, M.; Konya, A.; Vantomme, G.; Meijer, E.W.; Selinger, R.L.B.; Broer, D.J. Making Waves in a Photoactive Polymer Film. *Nature* **2017**, *546*, 632–636. [[CrossRef](#)]
29. Ikeda, T.; Tsutsumi, O. Optical Switching and Image Storage by Means of Azobenzene Liquid-Crystal Films. *Science* **1995**, *268*. [[CrossRef](#)] [[PubMed](#)]
30. Liu, Z.F.; Hashimoto, K.; Fujishima, A. Photoelectrochemical Information Storage Using an Azobenzene Derivative. *Nature* **1990**, *347*, 658–660. [[CrossRef](#)]
31. Yamamoto, T.; Hasegawa, M.; Kanazawa, A.; Sihiono, T.; Ikeda, T. Holographic Gratings and Holographic Image Storage via Photochemical Phase Transitions of Polymer Azobenzene Liquid-Crystal Films. *J. Mater. Chem.* **2000**, *10*, 337–342. [[CrossRef](#)]
32. Åstrand, P.-O.; Ramanujam, P.S.; Hvilsted, S.; Bak, K.L.; Sauer, S.P.A. Ab Initio Calculation of the Electronic Spectrum of Azobenzene Dyes and Its Impact on the Design of Optical Data Storage Materials. *J. Am. Chem. Soc.* **2000**, *122*, 3482–3487. [[CrossRef](#)]
33. Hartley, G.S. The Cis-form of Azobenzene. *Nature* **1937**, *140*, 281. [[CrossRef](#)]
34. Bandara, H.M.; Burdette, S.C. Photoisomerization in Different Classes of Azobenzene. *Chem. Soc. Rev.* **2012**, *41*, 1809–1825. [[CrossRef](#)] [[PubMed](#)]
35. Brown, C.J. A Refinement of the Crystal Structure of Azobenzene. *Acta Cryst.* **1966**, *21*, 146–152. [[CrossRef](#)]
36. Mostad, A.; Rømming, C. A Refinement of the Crystal Structure of cis-Azobenzene. *Acta Chem. Scand.* **1971**, *25*, 3561–3568. [[CrossRef](#)]
37. Monti, S.; Orlandi, G.; Palmieri, P. Features of the Photochemically Active State Surfaces of Azobenzenes. *Chem. Phys.* **1982**, *71*, 87–99. [[CrossRef](#)]
38. Brash, D.E.; Rudolph, J.A.; Simon, J.A.; Lin, A.; McKenna, G.J.; Baden, H.P.; Halperin, A.J.; Pontén, J. A role for sunlight in skin cancer: UV-induced p53 mutations in squamous cell carcinoma. *Proc. Natl. Acad. Sci. USA* **1991**, *88*, 10124–10128. [[CrossRef](#)] [[PubMed](#)]
39. Forman, J.; Dietrich, M.; Todd Monroe, W. Photobiological and Thermal Effects of Photoactivating UVA Light Doses on Cell Cultures. *Photochem. Photobiol. Sci.* **2007**, *6*, 649–658. [[CrossRef](#)]
40. Dong, Q.; Svoboda, K.; Tiersch, T.R.; Todd Monroe, W. Photobiological effects of UVA and UVB light in zebrafish embryos: Evidence for a competent photorepair system. *J. Photochem. Photobiol. B* **2007**, *88*, 137–146. [[CrossRef](#)]
41. Beharry, A.A.; Sadovskii, O.; Woolley, G.A. Azobenzene Photoswitching without Ultraviolet Light. *J. Am. Chem. Soc.* **2011**, *133*, 19684–19687. [[CrossRef](#)] [[PubMed](#)]
42. Samanta, S.; McCormick, T.M.; Schmidt, S.K.; Seferos, D.S.; Woolley, G.A. Robust visible light photoswitching with ortho-thiol substituted azobenzenes. *Chem. Commun.* **2013**, *49*, 10314–10316. [[CrossRef](#)] [[PubMed](#)]
43. Samanta, S.; Beharry, A.A.; Sadovskii, O.; McCormick, T.M.; Babalhavaeji, A.; Tropepe, V.; Woolley, G.A. Photoswitching Azo Compounds in Vivo with Red Light. *J. Am. Chem. Soc.* **2013**, *135*, 9777–9784. [[CrossRef](#)]
44. Rullo, A.; Reiner, A.; Reiter, A.; Trauner, D.; Isacoff, E.Y.; Woolley, G.A. Long wavelength optical control of glutamate receptor ion channels using a tetra-ortho-substituted azobenzene derivative. *Chem. Commun.* **2014**, *50*, 14613–14615. [[CrossRef](#)]
45. Konrad, D.B.; Frank, J.A.; Trauner, D. Synthesis of Redshifted Azobenzene Photoswitches by Late-Stage Functionalization. *Chem. Eur. J.* **2016**, *22*, 4364–4368. [[CrossRef](#)]
46. Hansen, M.J.; Lerch, M.M.; Szymanski, W.; Feringa, B.L. Direct and Versatile Synthesis of Red-Shifted Azobenzenes. *Angew. Chem. Int. Ed.* **2016**, *55*, 13514–13518. [[CrossRef](#)]
47. Dong, M.; Babalhavaeji, A.; Collins, C.V.; Jarrah, K.; Sadovskii, O.; Dai, Q.; Woolley, G.A. Near-Infrared Photoswitching of Azobenzenes under Physiological Conditions. *J. Am. Chem. Soc.* **2017**, *139*, 13483–13486. [[CrossRef](#)] [[PubMed](#)]
48. Bléger, D.; Schwarz, J.; Brouwer, A.M.; Hecht, S. o-Fluoroazobenzenes as Readily Synthesized Photoswitches Offering Nearly Quantitative Two-Way Isomerization with Visible Light. *J. Am. Chem. Soc.* **2012**, *134*, 20597–20600. [[CrossRef](#)] [[PubMed](#)]
49. Lameijer, L.N.; Budzak, S.; Simeth, N.A.; Hansen, M.J.; Feringa, B.L.; Jacquemin, D.; Szymanski, W. General Principles for the Design of Visible-Light-Responsive Photoswitches: Tetra-ortho-Chloro-Azobenzenes. *Angew. Chem. Int. Ed.* **2020**, *59*, 21663–21670. [[CrossRef](#)]
50. Yang, Y.; Hughes, R.P.; Aprahamian, I. Near-Infrared Light Activated Azo-BF<sub>2</sub> Switches. *J. Am. Chem. Soc.* **2014**, *136*, 13190–13193. [[CrossRef](#)]

51. Siewertsen, R.; Neumann, H.; Buchheim-Stehn, B.; Herges, R.; Näther, C.; Renth, F.; Temps, F. Highly Efficient Reversible Z-E Photoisomerization of a Bridged Azobenzene with Visible Light through Resolved S1( $n\pi^*$ ) Absorption Bands. *J. Am. Chem. Soc.* **2009**, *131*, 15594–15595. [[CrossRef](#)]
52. Lentes, P.; Stadler, E.; Röhricht, F.; Brahms, A.; Gröbner, J.; Sönnichsen, F.D.; Gescheidt, G.; Herges, R. Nitrogen Bridged Diazocines: Photochromes Switching within the Near-Infrared Region with High Quantum Yields in Organic Solvents and in Water. *J. Am. Chem. Soc.* **2019**, *141*, 13592–13600. [[CrossRef](#)]
53. Anderson, G.W.; Zimmerman, J.E.; Callahan, F.M. N-Hydroxysuccinimide Esters in Peptide Synthesis. *J. Am. Chem. Soc.* **1963**, *85*, 3039. [[CrossRef](#)]
54. Anderson, G.W.; Zimmerman, J.E.; Callahan, F.M. The Use of Esters of N-Hydroxysuccinimide in Peptide Synthesis. *J. Am. Chem. Soc.* **1964**, *86*, 1839–1842. [[CrossRef](#)]
55. Anderson, G.W.; Callahan, F.M.; Zimmerman, J.E. Synthesis of N-Hydroxysuccinimide Esters of Acyl Peptides by the Mixed Anhydride Method. *J. Am. Chem. Soc.* **1967**, *89*, 178. [[CrossRef](#)] [[PubMed](#)]
56. Nicolas, J.; Khoshdel, E.; Haddleton, D.M. Bioconjugation onto Biological Surfaces with Fluorescently Labeled Polymers. *Chem. Commun.* **2007**, 1722–1724. [[CrossRef](#)]
57. Koniev, O.; Wagner, A. Developments and Recent Advancements in the Field of Endogenous Amino Acid Selective Bond Forming Reactions for Bioconjugation. *Chem. Soc. Rev.* **2015**, *44*, 5495–5551. [[CrossRef](#)]
58. A, S.; Xu, Q.; Zhou, D.; Gao, Y.; Vasquez, J.M.; Greiser, U.; Wang, W.; Liu, W.; Wang, W. Hyperbranched PEG-Based Multi-NHS Polymer and Bioconjugation with BSA. *Polym. Chem.* **2017**, *8*, 1283–1287. [[CrossRef](#)]
59. Stephanopoulos, N.; Francis, M.B. Choosing an Effective Protein Bioconjugation Strategy. *Nat. Chem. Biol.* **2011**, *7*, 876–884. [[CrossRef](#)]
60. Luo, Y.; Prestwich, G.D. Hyaluronic Acid-N-hydroxysuccinimide: A Useful Intermediate for Bioconjugation. *Bioconjugate Chem.* **2001**, *12*, 1085–1088. [[CrossRef](#)]
61. Fissi, A.; Ciardelli, F. Photoresponsive Polymers: Azobenzene-Containing Poly-(L-Lysine). *Biopolymers* **1987**, *26*, 1993–2007. [[CrossRef](#)]
62. Fang, L.; Han, G.; Zhang, J.; Zhang, H.; Zhang, H. Synthesis of Well-Defined Easily Crosslinkable Azobenzene Side-Chain Liquid Crystalline Polymers via Reversible Addition–Fragmentation Chain Transfer Polymerization and Photomechanical Properties of their Post-Crosslinked Fibers. *Eur. Polym. J.* **2015**, *69*, 592–604. [[CrossRef](#)]
63. Gallot, B.; Fafiotte, M. Poly(L-lysine) Containing Azobenzene Units in the Side Chains: Influence of the Degree of Substitution on Liquid Crystalline Structure and Thermotropic Behaviour. *Liq. Cryst.* **1997**, *23*, 137–146. [[CrossRef](#)]
64. Guo, C.; Gao, J.; Ma, S.; Zhang, H. Efficient Preparation of Chemically Crosslinked Recyclable Photodeformable Azobenzene Polymer Fibers with High Processability and Reconstruction Ability via a Facile Post-Crosslinking Method. *Eur. Polym. J.* **2020**, *139*, 109998. [[CrossRef](#)]
65. Han, G.; Zhang, H.; Chen, J.; Sun, Q.; Zhang, Y.; Zhang, H. Easily Crosslinkable Side-Chain Azobenzene Polymers for Fast and Persistent Fixation of Surface Relief Gratings. *New J. Chem.* **2015**, *39*, 1410–1420. [[CrossRef](#)]
66. Li, X.; Gao, Y.; Kuang, Y.; Xu, B. Enzymatic Formation of a Photoresponsive Supramolecular Hydrogel. *Chem. Commun.* **2010**, *46*, 5364–5366. [[CrossRef](#)]
67. Li, X.; Wen, R.; Zhang, Y.; Zhu, L.; Zhang, B.; Zhang, H. Photoresponsive Side-Chain Liquid Crystalline Polymers with an Easily Cross-Linkable Azobenzene Mesogen. *J. Mater. Chem.* **2009**, *19*, 236–245. [[CrossRef](#)]
68. Lv, J.-a.; Wang, W.; Wu, W.; Yu, Y. A Reactive Azobenzene Liquid-Crystalline Block Copolymer as a Promising Material for Practical Application of Light-Driven Soft Actuators. *J. Mater. Chem. C* **2015**, *3*, 6621–6626. [[CrossRef](#)]
69. Pang, X.; Xu, B.; Qing, X.; Wei, J.; Yu, Y. Photo-Induced Bending Behavior of Post-Crosslinked Liquid Crystalline Polymer/Polyurethane Blend Films. *Macromol. Rapid. Commun.* **2018**, *39*, 1700237. [[CrossRef](#)]
70. Rastogi, S.K.; Anderson, H.E.; Lamas, J.; Barret, S.; Cantu, T.; Zauscher, S.; Brittain, W.J.; Betancourt, T. Enhanced Release of Molecules upon Ultraviolet (UV) Light Irradiation from Photoresponsive Hydrogels Prepared from Bifunctional Azobenzene and Four-Arm Poly(ethylene glycol). *ACS Appl. Mater. Interfaces* **2018**, *10*, 30071–30080. [[CrossRef](#)]
71. Wang, C.; Fadeev, M.; Zhang, J.; Vazquez-Gonzalez, M.; Davidson-Rozenfeld, G.; Tian, H.; Willner, I. Shape-Memory and Self-Healing Functions of DNA-Based Carboxymethyl Cellulose Hydrogels Driven by Chemical or Light Triggers. *Chem. Sci.* **2018**, *9*, 7145–7152. [[CrossRef](#)] [[PubMed](#)]
72. Barré, A.; Țințaș, M.-L.; Levacher, V.; Papamicaël, C.; Gembus, V. An Overview of the Synthesis of Highly Versatile N-Hydroxysuccinimide Esters. *Synthesis* **2016**, *49*, 472–483. [[CrossRef](#)]
73. Patel, N.; Davies, M.C.; Hartshorne, M.; Heaton, R.J.; Roberts, C.J.; Tendler, S.J.B.; Williams, P.M. Immobilization of Protein Molecules onto Homogeneous and Mixed Carboxylate-Terminated Self-Assembled Monolayers. *Langmuir* **1997**, *13*, 6485–6490. [[CrossRef](#)]
74. Zhan, N.; Palui, G.; Merkl, J.-P.; Mattoussi, H. Bio-Orthogonal Coupling as a Means of Quantifying the Ligand Density on Hydrophilic Quantum Dots. *J. Am. Chem. Soc.* **2016**, *138*, 3190–3201. [[CrossRef](#)]
75. Ghosh, A.K.; Doung, T.T.; McKee, S.P.; Thompson, W.J. N,N'-Dissuccinimidyl Carbonate: A Useful Reagent for Alkoxy-carbonylation of Amines. *Tetrahedron Lett.* **1992**, *33*, 2781–2784. [[CrossRef](#)]
76. Schulze, A.; Giannis, A. IBX-Mediated Conversion of Primary Alcohols and Aldehydes to N-Hydroxysuccinimide Esters. *Adv. Synth. Catal.* **2004**, *346*, 252–256. [[CrossRef](#)]

77. Tan, B.; Toda, N.; Barbas, C.F., 3rd. Organocatalytic Amidation and Esterification of Aldehydes with Activating Reagents by a Cross-Coupling Strategy. *Angew. Chem. Int. Ed.* **2012**, *51*, 12538–12541. [[CrossRef](#)]
78. Barré, A.; Tîntaş, M.-L.; Alix, F.; Gembus, V.; Papamicaël, C.; Levacher, V. Palladium-Catalyzed Carbonylation of (Hetero)Aryl, Alkenyl and Allyl Halides by Means of N-Hydroxysuccinimidyl Formate as CO Surrogate. *J. Org. Chem.* **2015**, *80*, 6537–6544. [[CrossRef](#)]
79. Ueda, T.; Konishi, H.; Manabe, K. Trichlorophenyl Formate: Highly Reactive and Easily Accessible Crystalline CO Surrogate for Palladium-Catalyzed Carbonylation of Aryl/Alkenyl Halides and Triflates. *Org. Lett.* **2012**, *14*, 5370–5373. [[CrossRef](#)]
80. Keiper, S.; Vyle, J.S. Reversible Photocontrol of Deoxyribozyme-Catalyzed RNA Cleavage under Multiple-Turnover Conditions. *Angew. Chem. Int. Ed.* **2006**, *45*, 3306–3309. [[CrossRef](#)]
81. Zhou, M.; Haldar, S.; Franses, J.; Kim, J.-M.; Thompson, D.H. Synthesis and Self-assembly Properties of Acylated Cyclodextrins and Nitrilotriacetic Acid (NTA)-modified Inclusion Ligands for Interfacial Protein Crystallization. *Supramol. Chem.* **2006**, *17*, 101–111. [[CrossRef](#)]
82. Hu, M.; Li, L.; Wu, H.; Su, Y.; Yang, P.Y.; Uttamchandani, M.; Xu, Q.H.; Yao, S.Q. Multicolor, one- and two-photon imaging of enzymatic activities in live cells with fluorescently Quenched Activity-Based Probes (qABPs). *J. Am. Chem. Soc.* **2011**, *133*, 12009–12020. [[CrossRef](#)]
83. Tuuttila, T.; Lipsonen, J.; Huuskonen, J.; Rissanen, K. Chiral Donor- $\pi$ -Acceptor Azobenzene Dyes. *Dyes Pigm.* **2009**, *80*, 34–40. [[CrossRef](#)]
84. Zhao, D.; Ouyang, D.; Jiang, M.; Liao, Y.; Peng, H.; Xie, X. Photomodulated Electro-optical Response in Self-Supporting Liquid Crystalline Physical Gels. *Langmuir* **2018**, *34*, 7519–7526. [[CrossRef](#)] [[PubMed](#)]
85. Fatas, P.; Longo, E.; Rastrelli, F.; Crisma, M.; Toniolo, C.; Jimenez, A.I.; Cativiela, C.; Moretto, A. Bis(azobenzene)-Based Photoswitchable, Prochiral, Alpha-Tetrasubstituted Alpha-Amino Acids for Nanomaterials Applications. *Chem. Eur. J.* **2011**, *17*, 12606–12611. [[CrossRef](#)] [[PubMed](#)]
86. Velema, W.A.; Hansen, M.J.; Lerch, M.M.; Driessen, A.J.; Szymanski, W.; Feringa, B.L. Ciprofloxacin-Photoswitch Conjugates: A Facile Strategy for Photopharmacology. *Bioconjug. Chem.* **2015**, *26*, 2592–2597. [[CrossRef](#)] [[PubMed](#)]
87. Liu, D.; Xie, Y.; Shao, H.; Jiang, X. Using Azobenzene-Embedded Self-Assembled Monolayers to Photochemically Control Cell Adhesion Reversibly. *Angew. Chem. Int. Ed.* **2009**, *48*, 4406–4408. [[CrossRef](#)] [[PubMed](#)]
88. Tarn, D.; Ferris, D.P.; Barnes, J.C.; Ambrogio, M.W.; Stoddart, J.F.; Zink, J.I. A reversible light-operated nanovalve on mesoporous silica nanoparticles. *Nanoscale* **2014**, *6*, 3335–3343. [[CrossRef](#)]
89. Hamon, F.; Blaszkiewicz, C.; Buchotte, M.; Banaszak-Léonard, E.; Bricout, H.; Tilloy, S.; Monflier, E.; Cézard, C.; Bouteiller, L.; Len, C.; et al. Synthesis and characterization of a new photoinduced switchable beta-cyclodextrin dimer. *Beilstein J. Org. Chem.* **2014**, *10*, 2874–2885. [[CrossRef](#)]
90. Samanta, S.; Qin, C.; Lough, A.J.; Woolley, G.A. Bidirectional Photocontrol of Peptide Conformation with a Bridged Azobenzene Derivative. *Angew. Chem. Int. Ed.* **2012**, *51*, 6452–6455. [[CrossRef](#)] [[PubMed](#)]
91. Trads, J.B.; Hull, K.; Matsuura, B.S.; Laprell, L.; Fehrentz, T.; Gorldt, N.; Kozek, K.A.; Weaver, C.D.; Klocker, N.; Barber, D.M.; et al. Sign Inversion in Photopharmacology: Incorporation of Cyclic Azobenzenes in Photoswitchable Potassium Channel Blockers and Openers. *Angew. Chem. Int. Ed.* **2019**, *58*, 15421–15428. [[CrossRef](#)]
92. Reynders, M.; Matsuura, B.S.; Bérouti, M.; Simoneschi, D.; Marzio, A.; Pagano, M.; Trauner, D. PHOTACs Enable Optical Control of Protein Degradation. *Sci. Adv.* **2020**, *6*, eaay5064. [[CrossRef](#)] [[PubMed](#)]
93. Preußke, N.; Moormann, W.; Bamberg, K.; Lipfert, M.; Herges, R.; Sönnichsen, F.D. Visible-Light-Driven Photocontrol of the Trp-Cage Protein Fold by a Diazocine Cross-Linker. *Org. Biomol. Chem.* **2020**, *18*, 2650–2660. [[CrossRef](#)] [[PubMed](#)]
94. Walther, M.; Kipke, W.; Schultzke, S.; Ghosh, S.; Staubitz, A. Modification of Azobenzenes by Cross-Coupling Reactions. *Synthesis* **2021**, *53*, 1213–1228. [[CrossRef](#)]
95. Maier, M.S.; Hüll, K.; Reynders, M.; Matsuura, B.S.; Leippe, P.; Ko, T.; Schäffer, L.; Trauner, D. Oxidative Approach Enables Efficient Access to Cyclic Azobenzenes. *J. Am. Chem. Soc.* **2019**, *141*, 17295–17304. [[CrossRef](#)] [[PubMed](#)]
96. Thapaliya, E.R.; Zhao, J.; Ellis-Davies, G.C.R. Locked-Azobenzene: Testing the Scope of a Unique Photoswitchable Scaffold for Cell Physiology. *ACS Chem. Neurosci.* **2019**, *10*, 2481–2488. [[CrossRef](#)]
97. Fawcett, W.R. Acidity and Basicity Scales for Polar Solvents. *J. Phys. Chem.* **1993**, *97*, 9540–9546. [[CrossRef](#)]
98. Magtaan, J.K.; Devocelle, M.; Kelleher, F. Regeneration of Aged DMF for Use in Solid-Phase Peptide Synthesis. *J. Pep. Sci.* **2019**, *25*, e3139. [[CrossRef](#)] [[PubMed](#)]
99. Li, S.; Eleya, N.; Staubitz, A. Cross-coupling strategy for the synthesis of diazocines. *Org. Lett.* **2020**, *22*, 1624–1627. [[CrossRef](#)] [[PubMed](#)]
100. Joshi, D.K.; Mitchell, M.J.; Bruce, D.; Lough, A.J.; Yan, H. Synthesis of cyclic azobenzene analogues. *Tetrahedron* **2012**, *68*, 8670–8676. [[CrossRef](#)]
101. A.M.; Garson, L.R. (Eds.) *The ACS Style Guide: Effective Communication of Scientific Information*, 3rd ed.; Coghil, American Chemical Society: Washington, DC, USA, 2006.

## Publication III

### 4.1 Centennial Isomers: A Unique Fluorinated Azobenzene Macrocyclus with Dual Stability Over 120 Years

#### Aim:

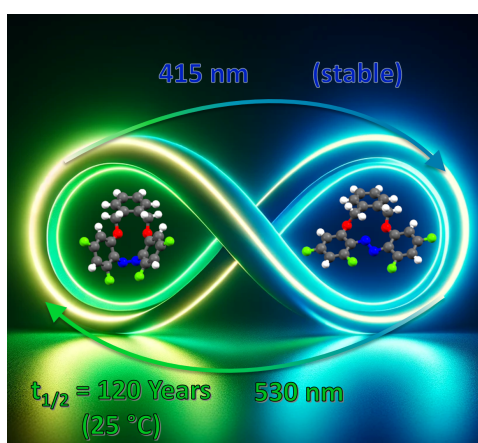
Driven by the continuous improvements in photoswitches in terms of switching efficiency, longer wavelengths for switching, and thermal stability, a combinatorial approach was used to enhance the properties of the previously macrocyclic ring established in the Staubitz group. Based on calculations, a cyclic azobenzene was equipped with fluorine atoms in the *ortho*-position. A comparative study with similar, synthesized azobenzenes should provide a better understanding beyond calculations for the origin of the outstanding properties.

#### Title of Publication:

#### Centennial Isomers: A Unique Fluorinated Azobenzene Macrocyclus with Dual Stability Over 120 Years

S. Schultzke, P. Puylaert, H. Wang, I. Schultzke, J. Gerken, A. Staubitz, Centennial Isomers: A Unique Fluorinated Azobenzene Macrocyclus with Dual Stability Over 120 Years. *Adv. Funct. Mater.* **2024**, 2313268.

Permission to reprint in Appendix 9.6.



### Abstract:

A macrocyclic azobenzene with unique thermal stability, demonstrating potential for use in optical data storage material is presented: The *Z*-isomer of this novel photoswitch exhibits unparalleled thermal stability, with a thermal half-life time surpassing 120 years at 25 °C. This stability is attributed to the strategic fluorination at two *ortho*- and both *para*-positions. Comparative analyses involving its non-fluorinated counterpart, *ortho*-only-fluorinated variant, and open chain analog were performed. Employing NMR and UV-vis spectroscopy, X-ray diffraction, alongside Arrhenius, Eyring, and DFT calculations, revealed insights into its extraordinary stability. Furthermore, when incorporated into poly(methylmethacrylate) (PMMA), this material showcased efficient switching with visible light in the solid state, emphasizing its potential for optical data storage applications.

### Abstract (deutsch):

Ein makrozyklisches Azobenzol mit einzigartiger thermischer Stabilität wird vorgestellt. Dieses zeigt Potenzial für den Einsatz in optischen Datenspeichermaterialien. Das *Z*-Isomer dieses neuartigen Fotoschalters weist eine beispiellose thermische Stabilität auf, mit einer thermischen Halbwertszeit von über 120 Jahren bei 25 °C. Diese Stabilität wird der strategischen Fluorierung an zwei *ortho*- und beiden *para*-Positionen zugeschrieben. Vergleichsanalysen mit dem nicht fluorierten Gegenstück, der nur *ortho*-fluorierten Variante und dem offenkettigen Analogon wurden durchgeführt. Mit Hilfe von NMR- und UV-Vis-Spektroskopie, Röntgenbeugung sowie Arrhenius-, Eyring- und DFT-Berechnungen wurden Erkenntnisse zu den Ursachen seiner außergewöhnlichen Stabilität gewonnen. Darüber hinaus zeigte dieses Material, wenn es in Poly(methylmethacrylat) (PMMA) dispergiert wurde, einen effizienten Schaltvorgang mit sichtbarem Licht im festen Zustand, was sein Potenzial für Anwendungen in der optischen Datenspeicherung hervorhebt.

### Author Contribution to this Publication:

For this research article, I conducted the initial concept and the molecular design. I and H. Wang performed the synthesis. Calculation and characterization were performed by me. P. Puylaert performed the X-ray diffraction analysis and refinements. I. Schultzke evaluated the crystal properties and J. Gerken was involved in the UV-vis switching experiments. The supporting information and the manuscript was written by me with additional input by Prof. A. Staubitz in the introduction. Additional video material was produced by me. The ToC image was designed by me. A. Staubitz, P. Puylaert and I. Schultzke contributed in the reviewing process of the manuscript.



## RESEARCH ARTICLE

ADVANCED  
FUNCTIONAL  
MATERIALS

www.afm-journal.de

# Centennial Isomers: A Unique Fluorinated Azobenzene Macrocyclus with Dual Stability Over 120 Years

Sven Schultze, Pim Puylaert, Henry Wang, Isabell Schultze, Jonas Gerken, and Anne Staubitz\*

A macrocyclic azobenzene with unique thermal stability, demonstrating potential for use in optical data storage material is presented: The Z-isomer of this novel photoswitch exhibits unparalleled thermal stability, with a thermal half-life surpassing 120 years at 25 °C. This stability is attributed to the strategic fluorination at two *ortho*- and both *para*-positions. Comparative analyses involving its non-fluorinated counterpart, *ortho*-only-fluorinated variant, and open-chain analog are performed. Employing NMR and UV–vis spectroscopy, X-ray diffraction, alongside Arrhenius, Eyring, and DFT calculations, revealed insights into its extraordinary stability. Furthermore, when incorporated into poly(methylmethacrylate), this material showcase efficient switching with visible light in the solid state, emphasizing its potential for optical data storage applications.

artificial intelligence (AI), underscores the formidable challenge of data management and preservation. The administration of vast digital repositories transcends logistics, representing a pivotal issue resonating across sectors. Proficient data storage significantly impacts businesses, research, and socio-economic structures, underscoring the imperative of data integrity, accessibility, and sustainability.<sup>[3]</sup>

Traditional data storage modalities, such as magnetic hard drives<sup>[4]</sup> and solid-state drives (SSD),<sup>[5]</sup> have commendably served the purposes of data storage. Magnetic storage, with its long-established reliability and high capacity, coexists with the newer, nimble SSDs, which excel in speed

and energy efficiency. However, neither is impervious to drawbacks. Magnetic storage may succumb to data degradation over time, and SSDs have finite lifespans defined by write-cycle limitations.

This confluence of data growth and the intrinsic limitations of existing storage technologies has rekindled interest in optical data storage, reviving its potential to address the data storage predicament effectively. Optical data storage (ODS), leveraging the unique properties of light, offers distinctive advantages over traditional methods. It exhibits inherent resilience to magnetic interference and holds the promise of ultra-high storage densities. For example, a study demonstrated up to 0.2 terabytes (TB) of storage capacity by employing up to 20 layers of embedded data, showcasing the potential for ultrahigh-density ODS.<sup>[6]</sup> Another perspective notes that the theoretical maximum storage density for an aberration-free objective with a high numerical aperture (NA) of 1.4 is on the order of TB per disc, indicating substantial storage potential.<sup>[7]</sup> An impressive improvement in this respect was reported using a thermally very stable dipentaerythritol pentaacrylate based monomer with up to 10 TB of data on a DVD sized disk with a record storage time of 250 years at 27 °C.<sup>[8]</sup>

These are important advances in the field, especially if one considers that most data stored is archived data that does not need erasing and re-writing. A multitude of mainly inorganic nanomaterials has emerged, which are being developed to serve this purpose.<sup>[1a]</sup> However, with few exceptions<sup>[9]</sup> these are not rewritable. In order to achieve this, organic molecular switches have been used:<sup>[10]</sup> In the realm of data storage, the simplest unit of information, the “bit,” operates on a binary principle, embodying two distinct values: 0 and 1. This binary foundation, which is ingrained in the digital landscape, also finds its echo in the

## 1. Introduction

In the contemporary digital era, the significance of electronic data storage cannot be overstated. At the time of writing, the global digital data sphere has reached a staggering magnitude, estimated at over 44 to 59 zettabytes (ZB) in 2020,<sup>[1]</sup> with projections indicating a doubling every two years<sup>[2]</sup> – a phenomenon colloquially referred to as the “data deluge”. This exponential growth, fueled by many sources, including the proliferation of internet-connected devices, cloud computing, and the advent of

S. Schultze, H. Wang, J. Gerken, A. Staubitz  
Institute for Organic and Analytical Chemistry  
University of Bremen  
Leobener Straße 7, D-28359 Bremen, Germany  
E-mail: [staubitz@uni-bremen.de](mailto:staubitz@uni-bremen.de)

S. Schultze, J. Gerken, A. Staubitz  
MAPEX Center for Materials and Processes  
University of Bremen  
Bibliothekstraße 1, D-28359 Bremen, Germany

P. Puylaert, I. Schultze  
Institute for Inorganic Chemistry and Crystallography  
University of Bremen  
Leobener Straße 7, D-28359 Bremen, Germany

The ORCID identification number(s) for the author(s) of this article can be found under <https://doi.org/10.1002/adfm.202313268>

© 2024 The Authors. Advanced Functional Materials published by Wiley-VCH GmbH. This is an open access article under the terms of the [Creative Commons Attribution](#) License, which permits use, distribution and reproduction in any medium, provided the original work is properly cited.

DOI: 10.1002/adfm.202313268

molecular world, particularly within the context of molecular switches. Molecular switches are intricate compounds capable of transitioning between distinct structural states in response to external stimuli. Much like the binary 0 and 1 representation in classical computing, molecular switches toggle between two metastable states.

Several types of molecular switches,<sup>[11]</sup> such as spiropyrans,<sup>[12]</sup> stilbenes,<sup>[13]</sup> stiffstilbenes,<sup>[14]</sup> or diarylethenes,<sup>[15]</sup> are well-documented in the literature. While spiropyrans offer a large spectral change upon switching, they suffer from photodegradation, which is the loss of chemical properties by extended or repeated exposure to light, and thermal instability. Therefore, they are insufficient as candidates for long-term optical storage. Much better suited are the diarylethenes: Due to the pericyclic nature of the switching mechanism, the isomers are thermally independent. Moreover, switching by visible light has become possible in some cases<sup>[16]</sup> and the first applications in the realm of data storage have been reported.<sup>[17]</sup> Another promising candidate is the “stiff-stilbene” with an astonishing half-life time of  $\approx 1\,000$  years at room temperature.<sup>[14,18]</sup> However, both isomers can only be activated by UV light and have the added complication of racemization in both the *E*- and *Z*-isomer to two possible enantiomers with a small energy barrier at room temperature.<sup>[18a]</sup> This is a problem for the optical read-out and also for the alignment of such molecular switches as they stay in motion and are not locked into position. Additionally, optical storage technologies at the present time are based on lasers with wavelengths of 405 nm (blue, “Blu-Ray”) up to 780 nm (red, “CD”); but it also has to be said that the write-read-delete-rewrite technology may well evolve to accommodate these photoswitches as well.

In contrast, azobenzene and many azobenzene-based materials are resistant to photobleaching; in one example over 20 000 switching cycles were reported.<sup>[19]</sup> In azobenzenes, typically, the more thermally stable isomer is in the *E* (*trans*) configuration, whereas the less stable isomer is in the *Z* (*cis*) configuration.<sup>[20]</sup> These two species are typically sufficiently distinct that these molecular transitions can form the basis for encoding data, at the molecular scale. The technologies typically used are holographic, which uses the different birefringence of the two species and a change in the liquid crystal properties of certain azobenzenes.<sup>[10a,b,21]</sup> Although most reports concern 2D or 3D ODS with azobenzenes, indeed, azobenzenes have been used in 4D ODS in combination with nanocrystal quantum rods in poly(methylmethacrylate).<sup>[22]</sup> Here, the writing and read-out process was based on polarization transfer from the two-photon absorbing nanocrystal quantum rod to the azodyes only in the correct orientation, but not another. Therefore, if a technology based on the reorientation of azobenzenes by repeated light absorption is required, longevity of the less stable isomer is not required per se;<sup>[23]</sup> however, as not all light that is absorbed will lead to isomerization and much energy is lost as heat, these materials warm up. The storage time in these cases is dependent on the molecular environment. This issue has been discussed in previous publications: for example, in a case with azo-SAMs (self-assembled monolayers), data storage for 4 years has been reported; the mechanism in this case was based on liquid crystalline azobenzene materials.<sup>[21a]</sup> However, azobenzenes have never been considered as direct data storage molecules, because their thermal half-life time is prohibitively low.<sup>[24]</sup>

For an optical molecular switch to serve directly as a viable candidate for data storage, i.e., without the detour of supramolecular ordering, it must fulfill a set of critical attributes: The paramount requirement, in this case, is an extended thermal half-life, ensuring the stability of the metastable isomer (most often the *Z*-isomer) over extended periods of time.<sup>[25]</sup> This thermal stability is necessary to safeguard against data loss due to thermal relaxation—a fundamental concern in data storage. Additionally, an optical switch must exhibit well-separated UV–vis absorption spectra for its isomeric states. This spectral differentiation is instrumental in facilitating precise data readout and writing, reducing the risk of information crossover. Photostability, though not the primary focus, remains significant, especially when considering the longevity of data storage devices and their resilience to repeated read-write cycles. Furthermore, practical data storage demands compatibility with solid matrices and switchability in the solid state. Many researchers have sought to solve this issue by incorporating azobenzenes into polymers or dendrimers, which aids the controlled dilution of the dye and thus increases the penetration depth of light. The ability to function as an optical switch in a solid matrix is essential, ensuring seamless integration into storage devices while retaining its switching capability.

The issue of preparing azobenzenes with long thermal half-life times and separating the  $n-\pi^*$  absorption bands for the *E* and *Z* isomer, which should enable switching with visible light, has been addressed by a number of strategies. For example, the ethylene bridged azobenzene (diazocine) is a cyclic azobenzene, which can be switched with visible light.<sup>[26]</sup> The strain of the 8-membered ring, in which the azo group is incorporated, unusually results in a thermally stable *Z*-isomer. More importantly, the  $n-\pi^*$  absorption maxima of both isomers are well separated. However, the half-life times are low with 4.5 h at 28.5 °C and could not significantly increased in recent years.<sup>[27]</sup> Later, the tetra-*ortho*-methoxy-substituted azobenzene was introduced, which allowed switching with visible light by also separating the  $n-\pi^*$  absorption maxima of both isomers, but in this case the *E*-isomer is the thermally stable one.<sup>[24c]</sup> The half-life time remained low at 2.4 days in an aqueous solution. The first azobenzene type molecule achieving a longer half-life time as well as switching with visible light, was reported by Hecht and coworkers, who noted that a tetra-*ortho*-fluoro-azobenzene had a thermal half-life of 2 years in acetonitrile.<sup>[28]</sup> While the tetra-*ortho*-fluorinated azobenzene paved the way toward high thermal stability (92 h at 60 °C, 2 years at 25 °C), the longest half-life time reported was 95 h at 60 °C in acetonitrile for a di-*para*-tetra-*ortho*-fluorinated azobenzene.<sup>[28–29]</sup> Other approaches included azobenzene derivatives, in which one of the benzene rings was replaced by pyrazoles.<sup>[30]</sup> For one compound, a half-life time of ca. 2.7 years at 25 °C was reported with excellent photostability and selectivity for the respective photostationary states (PSS). The record for such molecules is currently an azopyrazole with a *Z*-isomer thermal half-life of  $\approx 46$  years in DMSO- $d_6$ .<sup>[31]</sup>

We recently reported an azobenzene macrocycle (HOAM) with a half-life time of 36.4 h at 70 °C in acetonitrile (Figure 1),<sup>[32]</sup> but early attempts to improve the thermal stability of the *Z*-isomer by substitution did not extend the half-life, but rather shortened it.<sup>[33]</sup> That this macrocycle cannot easily be adapted to a system with higher half-life times was also found by K. S. von Krbeck and



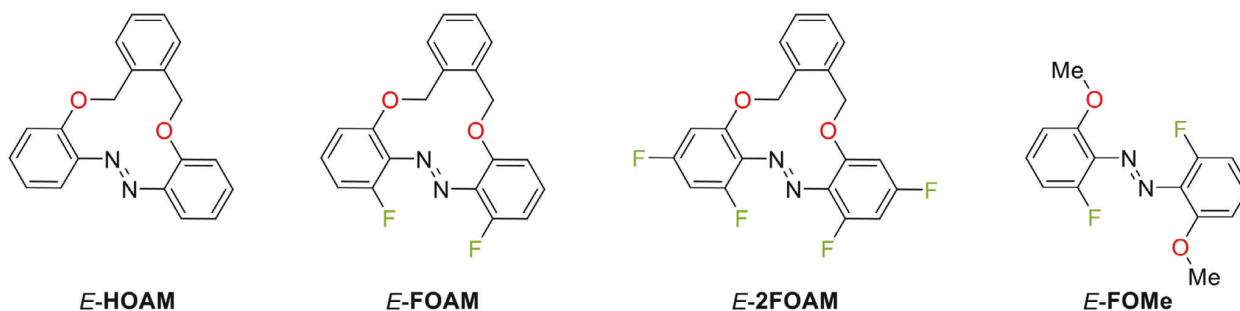


**Figure 1.** Overview of the synthesized cyclic azobenzene compounds. **FOMe** serves as an open-chain analogue, to gauge the influence of ring strain on the system.

coworkers who replaced the oxygen atoms by methylene groups; this gave a half-life time of 19 h at 45 °C in DMF.<sup>[34]</sup>

Based on studies demonstrating extended half-life times of *Z*-azobenzenes with fluorine substituents,<sup>[28,35]</sup> our objective was to systematically introduce fluorine atoms into the **HOAM** ring. This approach aimed to combine the influence of the fluorine atoms with the inherent ring strain to develop molecular switches exhibiting prolonged half-lives. Through strategic fluorine substitutions at both the *ortho* and *para* positions of the **HOAM** macrocycle, can now report thermal half-lives of up to 120 years at 25 °C and  $\approx 14\,370$  years at 0 °C. Such longevity positions these azobenzenes as pioneering candidates for direct long-term data storage. Furthermore, we have optimized the synthetic procedures to ensure high yield and efficacy. Notably, the switchability has been confirmed not only in solution but also when embedded in a poly(methylmethacrylate) (PMMA) film, a fundamental criterion for potential data storage applications.<sup>[6,20d,36]</sup>

## 2. Results and Discussion

### 2.1. Synthesis

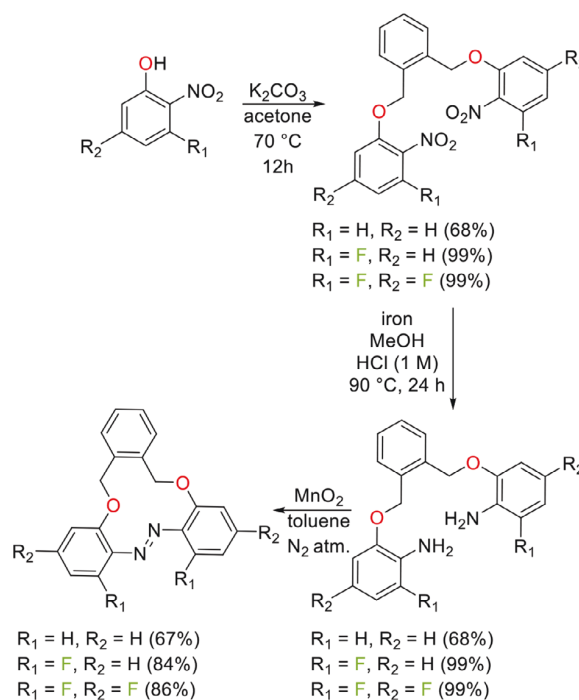
All three cyclic azobenzenes **HOAM**,<sup>[32]</sup> **FOAM**, and **2FOAM** were obtained in three synthetic steps based on the respective 2-nitrophenol derivative (**Scheme 1**) after an initial Williamson ether synthesis<sup>[37]</sup> to introduce the *ortho*-dibenzyl ether bridge, the nitro groups were subsequently reduced with elemental iron particles under mild conditions (Bechamp reduction).<sup>[38]</sup> The resulting anilines were subjected to oxidative coupling on the surface of  $\text{MnO}_2$  to form the azobenzene compounds under oxygen-free conditions.<sup>[39]</sup> The overall yields were 37% (**HOAM**), 82% (**FOAM**), and 84% (**2FOAM**). **2-FOMe**,<sup>[40]</sup> which was prepared as a reference compound to assess the impact of the macrocyclic architecture, was synthesized starting from 2-fluoro-4-methoxyaniline through oxidative coupling with  $\text{MnO}_2$  under oxygen-free conditions with a yield of 72% (For further details see the Supporting Information).

### 2.2. Crystal Structures

The synthesized compounds could be crystallized by solvent evaporation ( $\text{Et}_2\text{O}$  or DCM / hexane) and characterized by X-ray

single crystal diffraction (XRD). To obtain the *Z*-isomers, the solution was irradiated with 530 nm for 1 h before crystallization (for the photochemistry of these compounds see below).

When examining the crystal structures (**Table 1**), it becomes clear that the ring structure in the macrocyclic molecules forces the two fluorine atoms in *ortho*-position to the azobridge onto the same side, irrespective of electronic or steric repulsion. This is not the case for the acyclic reference molecule **FOMe**: here, the fluorine atoms can avoid each other's proximity both in the *E*- and the *Z*-isomers by positioning themselves on opposite sides of the azobridge. Furthermore, the cyclic *ortho*-dibenzylether bridge in the *E*-isomers shows different inclinations toward the azobenzene. In **E-HOAM**, the plane of the aromatic ring in the bridge is oriented perpendicular to the plane of the azobenzene,<sup>[41]</sup> but the **E-FOAM** shows a tilt, whereas the **E-2FOAM** bridge exhibits



**Scheme 1.** Synthesis of the cyclic azobenzene **HOAM**, **FOAM** and **2FOAM**.

**Table 1.** Crystal structure of compounds **HOAM**, **FOAM**, **2FOAM**, and **FOMe** in their *E*/*Z*-isomers characterized by XRD.

	<i>E</i> / <i>Z</i> -HOAM	<i>E</i> / <i>Z</i> -FOAM	<i>E</i> / <i>Z</i> -2FOAM	<i>E</i> <sup>a</sup> / <i>Z</i> -FOMe
N01 = N02	1.258(3)/1.246(1)	1.257(2)/1.244(2)	1.23(1)/1.247(1)	1.260(2)/1.263(3)
N01–C01	1.423(3)/1.456(1)	1.425(2)/1.453(2)	1.42(1)/1.450(1)	1.425(1)/1.434(3)
N02–C20	1.433(3)/1.453(3)	1.420(2)/1.451(3)	1.461(8)/1.448(1)	–/1.424(3)
C01–N01 = N02–C20 ( $\Psi$ )	172.5(2)/2.1(1)	–178.9(1)/6.9(2)	178.9(5)/7.0(2)	180.0(8)/7.2(3)
C15–C20–N02 = N01	40.8(4)/95.1(1)	153.0(1)/73.5(2)	–152.5(6)/78.0(1)	$\pm$ 145.2(9)/–137.3(2)
C06–C01–N01 = N02	164.6(2)/–98.3(1)	36.2(2)/–115.3(2)	–35.2(9)/–112.4(1)	–/–136.3(2)
Azo-Phenyl-Twist	24.9°/74.9°	5.3°/66.1°	4.1°/76.7°	0.0°/63.4°

<sup>a</sup>) The atom numbering for this molecule differs from that of the cycles as it is symmetrical in the *E*-form. However, it is unsymmetrical for the *Z*-form and to avoid confusion when comparing the bond lengths and angles, the numbers have been adjusted for the molecule; Therefore, the numbers here differ from those in the CIF-file.

a more planar orientation with respect to the azobenzene. The inclination is evident in the dihedral angle labeled “C<sub>01</sub>–N<sub>01</sub> = N<sub>02</sub>–C<sub>20</sub>” ( $\Psi$ ) and the twist angle of the azobenzene aromatic rings. The twist is measured by the angle between the two layers, which is determined by the positions of the atoms in the azobenzene’s phenyl ring. (Graphical visualization see Supporting Information) **E-2FOAM** exhibits an arrangement of the azobenzene motif that is the closest to the planar parent molecule azobenzene (180°). The measured dihedral angles C<sub>01</sub>–N<sub>01</sub> = N<sub>02</sub>–C<sub>20</sub> ( $\Psi$ ) are 175.5° (**E-HOAM**) < 178.9° (**E-FOAM**) = 178.9° (**E-2FOAM**) < 180° (**E-FOMe**) and the twist angles of the azobenzene aromatic rings are 24.9° (**E-HOAM**) > 5.3° (**E-FOAM**) > 4.1° (**E-2FOAM**).

In general, the crystal structure of the macrocyclic *Z*-isomers **HOAM**, **FOAM**, and **2FOAM** appear more similar to one another. However, the dihedral angle “C<sub>01</sub>–N<sub>01</sub> = N<sub>02</sub>–C<sub>20</sub>” follows the trend of 2.1° (**Z-HOAM**) < 6.9° (**Z-FOAM**) < 7.0° (**Z-2FOAM**) < 7.2° (**Z-FOMe**). This can be interpreted as increased ring strain for the *Z*-isomers with an additional fluorine atom in *ortho*-position next to the azo-bridge. This observation holds apparently irrespective of whether the switching unit is incorporated into a macrocycle or not. However, the relative change of the dihedral angles upon switching is very similar for all compounds (6.6° **HOAM**, 8.0° **FOAM**, 8.1° **2FOAM**, 7.2° **FOMe**).

### 2.3. Photoswitching, Photostability, and Thermal Stability of the *Z*-Isomers

The photoswitching properties were characterized by UV–vis spectroscopy and NMR spectroscopy. DMSO was chosen as a solvent for all measurements to enable thermal relaxation experi-

ments at elevated temperatures and ensure the comparability between all measurements. All the molecules in this study exhibited photoswitching behavior upon exposure to visible light. In particular, upon exposure to green light (530 nm, 100 mW cm<sup>–2</sup>, 5 min), the respective *Z*-isomers were generated, (**Figure 2A**, **Table 1**) yielding PSS<sub>530nm</sub> values ranging from 91% (**Z-FOMe**) to 97% (**Z-2FOAM**), with the open chain reference molecule giving 83%. Reverting the switches to the *E*-isomers was achieved by irradiating them with blue light (415 nm, 80 mW cm<sup>–2</sup>, 5 min), resulting in the conversion of the respective *E*-isomers with PSS<sub>415nm</sub> values ranging from 74% (**E-HOAM**) to 93% (**E-2FOAM**). This results in a remarkably high switching efficiency of  $\approx$ 90% for **2FOAM** (77% for tetra-*ortho*-fluoro-azobenzene (F<sub>4</sub>)).<sup>[28]</sup> The UV–vis spectra for **HOAM** and **FOMe** have been discussed elsewhere;<sup>[32,40]</sup> **FOAM** and **2FOAM** are very similar and therefore, only **2FOAM** is discussed here in details (see the Supporting Information for a collection of all spectra). The UV–vis spectrum (**Figure 2B**) for **E-2FOAM** exhibited the characteristic azobenzene  $\pi$ – $\pi^*$  absorption band<sup>[42]</sup> at 325 nm (**E-HOAM**: 290 nm, **E-FOAM**: 300 nm, **E-FOMe**: 300 nm, F<sub>4</sub>:<sup>[29]</sup> 305 nm) with an emission coefficient of  $\epsilon_{325nm} = 8\,871\text{ M}^{-1}\text{cm}^{-1}$  (**E-FOAM**  $\epsilon_{300nm} = 10\,604\text{ M}^{-1}\text{cm}^{-1}$ ), which is significantly lower in comparison to F<sub>4</sub> ( $\epsilon_{305nm} = 18\,000\text{ M}^{-1}\text{cm}^{-1}$ ).<sup>[29]</sup> Furthermore, a secondary absorption band, corresponding to the *n*– $\pi^*$  transition was observed at  $\approx$ 415 nm for **Z-2FOAM** and 465 nm for **E2FOAM**, characteristic of *ortho*-substituted azobenzenes (*Z*-F<sub>4</sub>: 414 nm, *E*-F<sub>4</sub>: 456 nm).<sup>[29]</sup> These *n*– $\pi^*$  bands are very well separated from each other, with a difference of their maxima of  $\Delta$ 50 nm (F<sub>4</sub>:  $\Delta = 42$  nm).<sup>[29]</sup> This feature not only enables photoswitching using visible light through the *n*– $\pi^*$  absorption band, but it also makes the two isomers discernible with the naked eye

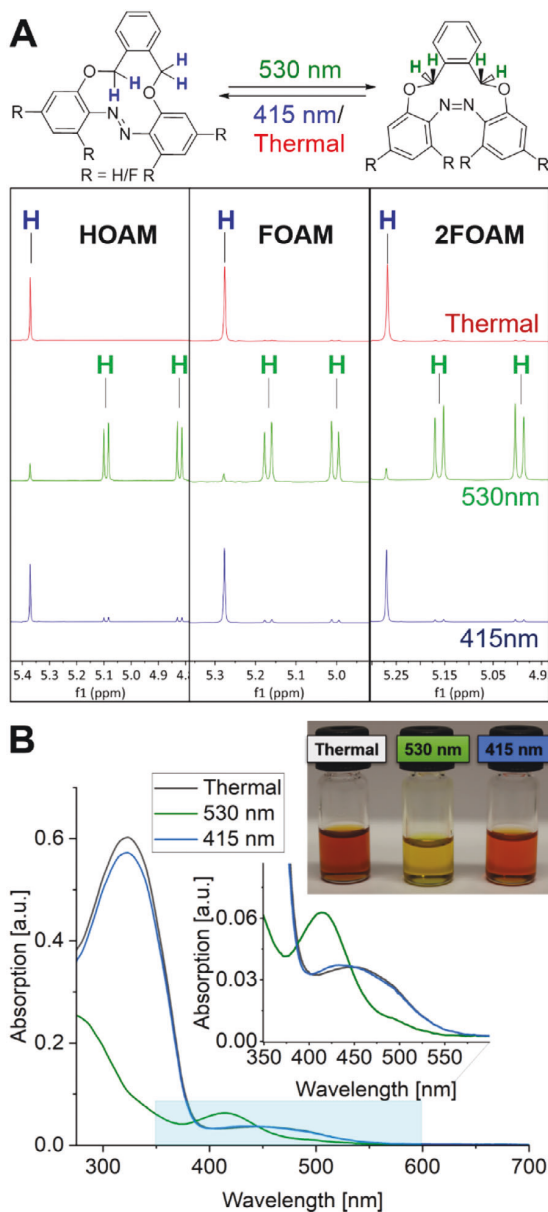


**Figure 2.** A) NMR spectroscopic study of the irradiation of **HOAM**, **FOAM** and **2FOAM** (for the data for **FOMe** see the Supporting Information) in  $\text{DMSO-}d_6$  after thermal treatment (red spectrum), after irradiation with green light (525 nm) and violet light (420 nm) ( $\text{conc}_{\text{HOAM}} = 6.20 \mu\text{mol mL}^{-1}$ ,  $\text{conc}_{\text{FOAM}} = 6.24 \mu\text{mol mL}^{-1}$ ,  $\text{conc}_{\text{2FOAM}} = 5.67 \mu\text{mol mL}^{-1}$ ). Values are given in Table 1. B) UV-vis spectrum for **2FOAM** ( $\text{conc} = 0.317 \mu\text{mol mL}^{-1}$ ) as an example; for **FOAM**, **2FOAM**, and **FOMe** see the Supporting Information). The photograph shows the optically visible color change of the **2FOAM** in solution.

(Figure 1B). Because the photostability is a vital process parameter for potential ODS materials, the photostability was tested with over 35 successive irradiation cycles between both isomers (irradiation wavelengths of 530 and 415 nm). With a concentration of  $0.0936 \mu\text{mol mL}^{-1}$  and using LEDs with the power of  $50 \text{ mW cm}^{-2}$

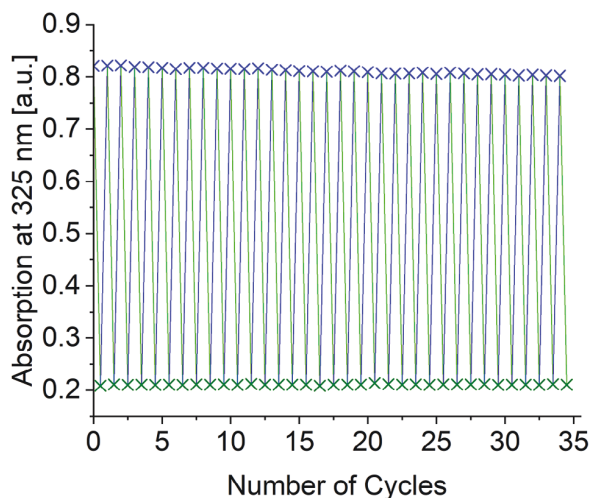


**Figure 3.** Cycle stability for the isomerization of **2FOAM** after irradiation with 530 nm (green cross) and 415 nm (blue cross) over 35 cycles. ( $\text{conc} = 0.0936 \mu\text{mol mL}^{-1}$ ).

(530 nm) and  $30 \text{ mW cm}^{-2}$  (415 nm), only minor photodegradation was observed with a relative change of 0.5% for green irradiation and 1% for blue irradiation (Figure 3B).

#### 2.4. The Increased Longevity of Z-OAMs

Based on the long thermal half-life times ( $t_{1/2}$ ) of the **Z-HOAM**, we hypothesized that for the fluorinated macrocycles, the half-life times for the Z-isomers might be even longer. In order to ensure complete comparability between the thermal half-life times of **Z-FOMe**, **Z-HOAM**, **Z-FOAM**, and **Z-2FOAM**, all measurements were performed in  $\text{DMSO}$  as the solvent, with five measurements of the  $t_{1/2}$  at elevated temperatures between  $90 \text{ }^\circ\text{C}$  and  $110 \text{ }^\circ\text{C}$  (Figure 4).

The temperature of  $25 \text{ }^\circ\text{C}$  ("room temperature") is particularly relevant in terms of the material's applicability. Ideally, an ODS device should be able to operate at this temperature. In addition, half-life times of thermally long-lived switches are provided at many different temperatures in the literature, but this temperature is often the point of reference. Therefore, the half-life time for this temperature was extrapolated with the aid of the Arrhenius Equation (1) (Figure 4A).

$$k = A e^{-\frac{E_a}{RT}} \quad (1)$$

Where  $k$  is the rate constant,  $A$  the Arrhenius factor,  $E_a$  the activation energy,  $R$  the universal gas constant and  $T$  the Temperature.

For instance, the macrocyclic compound **Z-HOAM** had a thermal half-life  $t_{1/2(25^\circ\text{C})} = 3.8$  years. In contrast, introducing fluorine atoms in the *ortho*-position (**Z-FOAM**) increased the value to  $t_{1/2(25^\circ\text{C})} = 106$  years. By introducing two additional fluorine atoms in the *para*-position, the thermal half-life time further increased to  $t_{1/2(25^\circ\text{C})} = 120$  years for **Z-2FOAM** – a value unprecedented in the literature. The confinement of the azobenzene moiety in a macrocycle appeared to be the most relevant structural feature: Without it, the half-life decreased dramatically by a factor of ca.

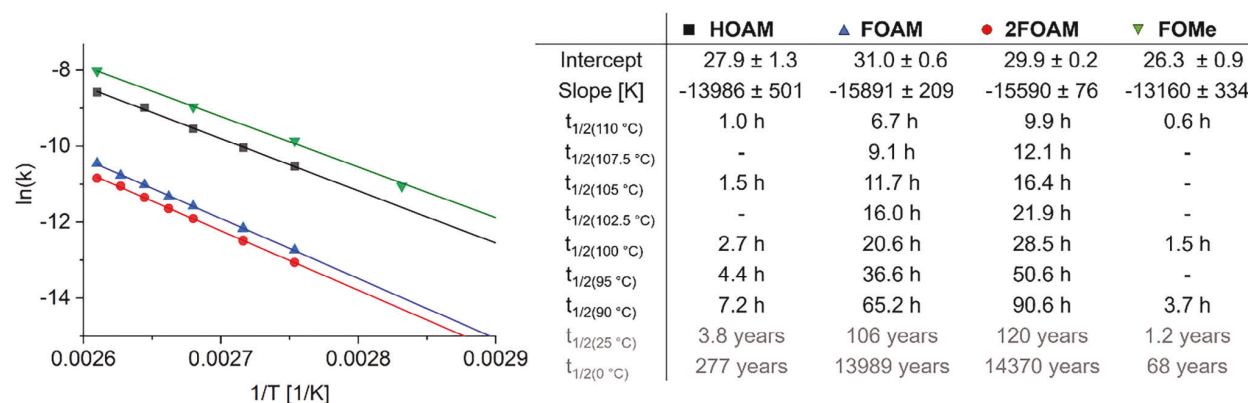


**Figure 4.** Direct comparison of the Arrhenius-plots of **HOAM**, **FOAM**, **2FOAM** and **FOMe** in DMSO and their  $t_{1/2}$  at the given temperature (Note:  $t_{1/2}(110\text{ °C})$  -  $t_{1/2}(90\text{ °C})$  are experimental data points,  $t_{1/2}(25\text{ °C})$  and  $t_{1/2}(0\text{ °C})$  are extrapolated values.

50 ( $t_{1/2}(25\text{ °C}) = 1.2$  years for **Z-FOMe**, compared to **Z-FOAM**). The Eyring Equation (2) and the plots derived from it contain additional and mechanistically relevant information (Table 2).

$$k = \frac{\kappa k_B T}{h} e^{-\frac{\Delta G^\ddagger}{RT}} \quad (2)$$

Where  $\kappa$  is the transmission coefficient,  $k_B$  the Boltzmann constant,  $T$  the temperature,  $h$  the Planck's constant,  $\Delta G^\ddagger$  the Gibbs energy of activation.

The Eyring equation allows to assess the contribution of the enthalpy, entropy, and Gibbs free energy of the transition states. In the case of azobenzenes, these are indicative of the isomerization mechanism: Azobenzene can undergo thermal- and photoisomerization through various mechanisms. Commonly proposed mechanisms for thermal isomerization include rotational, inversion, inversion-assisted rotation, and concerted inversion (Figure 5).<sup>[29,40,43]</sup> Inversion mechanisms have a characteristic angle inversion angle (C–N=N,  $\varphi$ )  $\varphi_1 \approx 120^\circ$  and  $\varphi_2 \approx 180^\circ$  and a dihedral angle (C–N=N–C,  $\phi$ ) of  $\phi \approx 180^\circ$  (in plane), while inversion-assisted rotation has additional rotation around the dihedral angle  $\phi \approx 90^\circ$  (out of plane). Concerted inversion has an angle of  $\varphi_1 \approx \varphi_2 \approx 180^\circ$  and for the rotation mechanism a change in the dihedral angle  $\phi \approx 90^\circ$ , while  $\varphi_1 \approx \varphi_2 \approx 120^\circ$  is expected.<sup>[43g]</sup>

The path for photoisomerization depends on the exploration of the  $S_2$  or  $S_1$  potential energy surface (PES) after excitation, depending on whether the excitation occurs via the  $\pi$ - $\pi^*$  transition or the  $n$ - $\pi^*$  transition.<sup>[24b]</sup> In contrast, thermal relaxation does not involve excitation and takes place in the ground state

$S_0$  PES. This process requires overcoming a transition state (TS). Currently, for the parent azobenzene the rotational pathway is considered to be the preferred one.<sup>[44]</sup> However, in macrocyclic compounds, this pathway might be sterically less accessible, and the inversion pathway is favored as described by Rau et al.<sup>[45]</sup> To better understand the prolonged half-life observed in **FOAM** and **2FOAM**, we conducted a DFT calculation using B3LYP/cc-pVDZ level of theory (Table 3).<sup>[46]</sup> We simulated the solvent DMSO (consistent with the experiment) using the solvation model based on density (SMD) in a self-consistent reaction field (SCRFF) and applied Grimme D3-correction<sup>[47]</sup> to include dispersion effects. For the ground state, only positive frequencies were obtained, and for the TS, only one imaginary frequency. For the cyclic compounds, a TS was found, which lies in between the inversion-assisted rotation (IAR) mechanism and the inversion mechanism. For **TS-2FOAM** the C–N=N angle was  $\varphi_1 = 178^\circ$ ,  $\varphi_2 = 120^\circ$ , while the dihedral angle (C–N=N–C) was  $\phi = 123^\circ$ . This dihedral angle lies between the values for a clear inversion mechanism ( $\phi = 180^\circ$ ), and a clear inversion-assisted rotation ( $\phi = 90^\circ$ ). This observation can be made for all OAM's. The imaginary frequency of each TS was in the range of  $-500$  to  $-250\text{ cm}^{-1}$  which is similar to the inversion mechanism as observed by Lopez et al.<sup>[43a]</sup> It is important to note that the calculated values closely match the experimental values for the thermal relaxation for **2FOAM** ( $\Delta G^\ddagger_{\text{calc,IAR}} = 126.0\text{ kJ mol}^{-1}$ ,  $\Delta G^\ddagger_{\text{exp}} = 127.4\text{ kJ mol}^{-1}$ ), **FOAM** ( $\Delta G^\ddagger_{\text{calc,IAR}} = 123.7\text{ kJ mol}^{-1}$ ,  $\Delta G^\ddagger_{\text{exp}} = 128.2\text{ kJ mol}^{-1}$ ), although somewhat less so for **HOAM** ( $\Delta G^\ddagger_{\text{calc,IAR}} = 113.4\text{ kJ mol}^{-1}$ ,  $\Delta G^\ddagger_{\text{exp}} = 119.5\text{ kJ mol}^{-1}$ ). This gives us confidence that the calculated mechanisms are correct. While the energy

**Table 2.** Summary of  $^1\text{H-NMR}$  spectroscopic studies of the irradiation of **HOAM**, **FOAM**, **2FOAM**, and **FOMe**, after irradiation with 530 nm and 415 nm in the solvent DMSO- $d_6$ . The % values for the E- and Z-isomer were obtained by the integration of the  $\text{CH}_2$ -proton signals of the ether bridge (conc =  $7.55\text{ }\mu\text{mol mL}^{-1}$ ).

	HOAM		FOAM		2FOAM		FOMe	
	E	Z	E	Z	E	Z	E	Z
Thermal	100%	0%	99%	1%	99%	1%	100%	0%
415 nm	74%	26%	85%	15%	93%	7%	78%	22%
530 nm	9%	91%	5%	95%	3%	97%	17%	83%

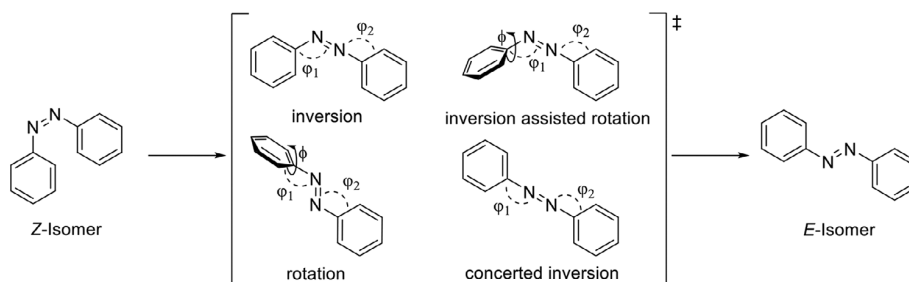


**Figure 5.** Graphical visualization of the possible mechanisms for the thermal relaxation with remarked changes in angles during the back-isomerization for the inversion, inversion assisted rotation, rotation, and concerted inversion mechanism.

level of the *E*- and the *Z*-isomer are closer together for the FOAM's (2FOAM:  $\Delta G_{Z-2FOAM}^\ddagger - \Delta G_{E-2FOAM}^\ddagger = 22.4 \text{ kJ mol}^{-1}$  versus HOAM:  $\Delta G_{Z-HOAM}^\ddagger - \Delta G_{E-HOAM}^\ddagger = 36.2 \text{ kJ mol}^{-1}$ ), the barrier toward the TS is higher for FOAMs, leading to a much longer half-life for the FOAMs. The thermal isomerization of the linear compound Z-FOMe can also be described by an IAR mechanism with a dihedral angle  $\phi = 123^\circ$  for TS-FOMe. ( $\Delta G_{\text{calc,IAR}}^\ddagger = 117.4 \text{ kJ mol}^{-1}$ ,  $\Delta G_{\text{exp}}^\ddagger = 120.3 \text{ kJ mol}^{-1}$ ).

Based on these calculations and together with the observation that the relative change in the dihedral angles from *Z* to *E* is almost the same for all four compounds, we hypothesize that a change in ring strain does not play a major role for the different half-life times. Rather, a high dihedral angle in the *Z*-isomer in the macrocycles is blocking the rotational movement, which in turn leads to higher energy TSs and longer half-life times. At the same time, the energies of the *Z*-ground states of the FOAMs are relatively decreased (compared to Z-HOAM).

In summary, the calculations support our hypothesis regarding the increased stability of the Z-FOAM's, emphasizing the importance of the fluorination in *ortho*-position and the macrocyclic structure for the long-lived *Z*-isomer (Table 4).

## 2.5. Switching in the Solid State

The new azobenzene macrocycles have very promising properties for ODS. However, for this to be realized, it has to be demonstrated that the molecules can be dispersed in a suitable polymer and still switch to the solid state.<sup>[6,20d,36]</sup> This was showcased by dispersing the molecule 2FOAM, as the most promising candidate into PMMA (polymethyl methacrylate)

(Figure 7). To achieve this, PMMA (500 mg) and 2FOAM (50 mg) were dissolved in toluene, filtered through a syringe filter, and then cast into a petri dish, allowing the solvent to slowly evaporate under ambient conditions. The resultant PMMA-2FOAM composite, now tinged orange due to the presence of 2FOAM, remained optically clear (Figure 6). The thickness of the film was measured using an electronic caliper and was  $100 \pm 15 \mu\text{m}$ . This polymer film was subjected to multiple cycles of irradiation with blue (415 nm, 20 mW cm<sup>-2</sup>) and green light (530 nm, 25 mW cm<sup>-2</sup>), enabling the writing and erasing of "data" on the polymer. As an illustrative example, we utilized light to create the well-known motif of the "Bremer Stadtmusikanten" (the "town musicians of Bremen")<sup>[49]</sup> in the polymer film by using a mask when irradiating the film. To demonstrate the efficacy of the approach, samples with lower concentrations 2FOAM (2 mg and 5 mg) in a PMMA matrix (500 mg) were also prepared, highlighting the pronounced switchability and thermal relaxation characteristics of 2FOAM within the solid PMMA matrix, as demonstrated by UV-vis spectroscopy (Figure 7). The thermal half-life of 2FOAM in the PMMA composition was determined at 90 °C by the lowest concentrated sample (2 mg in 500 mg PMMA) after irradiation with green light. The polymer was glued inside a cuvette with glycerin (non-solvent) and heated to 90 °C (below the glass transition temperature ( $T_g$ ) of PMMA) for 4 days. The thermal half-life was determined to be  $t_{1/2, \text{PMMA}, 90^\circ\text{C}} = 69 \text{ h}$  (Figure S15, Supporting Information), which is faster than in the solvent DMSO  $t_{1/2, \text{PMMA}, 90^\circ\text{C}} = 91 \text{ h}$  and contrary to the belief that the half-life time in a polymer matrix below the  $T_g$  is prolonged.<sup>[50]</sup> However, covalently bonded 2FOAM to the PMMA matrix, higher concentrations, and different polymer blends need to be further studied to fully understand the behavior of 2FOAM in polymer blends.

**Table 3.** Calculated results of HOAM, FOAM, 2FOAM, and FOMe for the rate constant (*k*), the Arrhenius factor (*A*), the activation energy ( $E_a$ ), Enthalpy ( $\Delta H^\ddagger$ ), Entropy ( $\Delta S^\ddagger$ ), Gibbs-Energy ( $\Delta G^\ddagger$ ) and the half-life times for the isomerization of the respective *Z*-isomers at room temperature ( $t_{1/2}$  (25 °C)).

	$k_{(25^\circ\text{C})}$ [s <sup>-1</sup> ]	<i>A</i> [s <sup>-1</sup> ]	$E_a$ [kJ mol <sup>-1</sup> ]	$\Delta H^\ddagger$ [kJ mol <sup>-1</sup> ]	$\Delta S^\ddagger$ [J K <sup>-1</sup> mol <sup>-1</sup> ]	$\Delta G^\ddagger$ [25 °C] [kJ mol <sup>-1</sup> ]	$t_{1/2}$ [25 °C] [Years]
HOAM	$5.81 \times 10^{-9}$	$1.37 \times 10^{12}$	116	113.1	-22.9	120.0	3.8
FOAM	$2.06 \times 10^{-10}$	$2.90 \times 10^{13}$	132	128.3	0.8	128.1	106
2FOAM	$1.83 \times 10^{-10}$	$9.38 \times 10^{13}$	130	127.0	-5.4	128.6	120
FOMe	$1.83 \times 10^{-8}$	$2.71 \times 10^{11}$	109	107.5	-33.2	117.4	1.2

**Table 4.** Results of the DFT calculations with B3LYP/cc-pVTZ level of theory and Grimme D3-dispersion correction in the gas phase and in solution (DMSO). For the solvent simulation, a self-consistent reaction field (SCRF) with the SMD model for the solvent DMSO, the B3LYP/cc-pVDZ level of theory, and Grimme D3-dispersion correction were used.<sup>[48]</sup> The calculated TS shows an IAR mechanism. The given energy values are the difference to the respective Z-isomer.

	$\Delta G_{\text{SMD}}^{\ddagger}$ [kJ mol <sup>-1</sup> ]	$\mu_{\text{SMD}}$ [D]	$\Delta G_{\text{gas}}^{\ddagger}$ [kJ mol <sup>-1</sup> ]	$\mu_{\text{gas}}$ [D]
Z-HOAM	0.00	6.6	0.00	4.5
Z-FOAM	0.00	9.8	0.00	6.7
Z-2FOAM	0.00	8.3	0.00	5.7
Z-FOMe	0.00	5.0	0.00	3.4
TS <sub>IAR</sub> -HOAM	113.4	7.0	109.1	4.7
TS <sub>IAR</sub> -FOAM	123.7	9.8	116.3	6.6
TS <sub>IAR</sub> - 2FOAM	126.0	8.6	119.9	6.1
TS <sub>IAR</sub> -FOMe	120.3	5.7	111.9	4.5
E-HOAM	-36.2	2.6	-42.0	1.6
E-FOAM	-20.1	3.4	-29.8	1.7
E-2FOAM	-22.4	3.5	-31.6	2.7
E-FOMe	-20.5	0.2	-20.7	0.0

Furthermore, based on the ability to switch 2FOAM in PMMA, studies can be undertaken to investigate the quantum yield,<sup>[51]</sup> optical response time, the change in refractive index,<sup>[52]</sup> and holographic gratings,<sup>[36g]</sup> in order to fully assess the potential of this switch as an ODS device.<sup>[36e,53]</sup>

### 3. Conclusion

Optical data storage that can be written, read, erased and re-written is likely to impact heavily on data storage technologies. One approach is using molecular switches, but for the development of a direct writing – erasing – re-writing

system, light should be the only stimulus. Azobenzenes, although very photostable, suffer from too short of thermal half-life times. Here, the synthesis of an extremely thermally stable macrocyclic azobenzene compound is reported: The extrapolated half-life values span the range of a human life-time and even exceed it when cooled (Z-2FOAM:  $t_{1/2}$ , 0 °C  $\approx$ 14 370 years). This is unprecedented in the literature. Through comprehensive analysis encompassing NMR, UV-vis, and XRD studies on four distinct azobenzenes in both isomeric forms, we have established that the combined influence of the macrocyclic structure and *ortho*-fluoro-substitution is crucial for achieving such exceptional stability. Further fluorination in the *para*-position leads to even higher half-life times. A key mechanistic feature is the difficulty in accessing the TS for a thermal relaxation due to geometric constraints. This prolonged half-life time, coupled with efficient and safe photoconversion using visible light, underscores the effectiveness of our molecule as a highly viable switch. This bi-stability holds potential for versatile I/O switching applications in data storage, but it may also become useful biological, physical, and materials science as a form of information storage.

### 4. Experimental Section

Only the key equipment, methods, and experimental procedures are listed. For more details see the Supporting Information.

**Equipment for the Irradiation Experiments:** A UPLED power supply powered the high-power LED modules from Thorlabs (US, NJ): M365L3 (365 nm), M415L4 (415 nm), M530L4 (530 nm), M590L4 (590 nm). A collimator was used to focus the light beam. The light intensity was measured using an ILT2400 hand-held light meter manufactured by International Light Technologies, Inc., (Peabody, USA). Additionally, a 420 nm (1.0 W) and a 525 nm LED (1.0 W) from EPILED were built in laboratories.

UV-vis spectra were recorded with a resolution of 0.5–0.1 nm on a UV-2700 spectrometer from Shimadzu (Shimadzu, Kyoto, Japan) with a double monochromator. In all cases, DMSO (spectroscopy grade) was used as

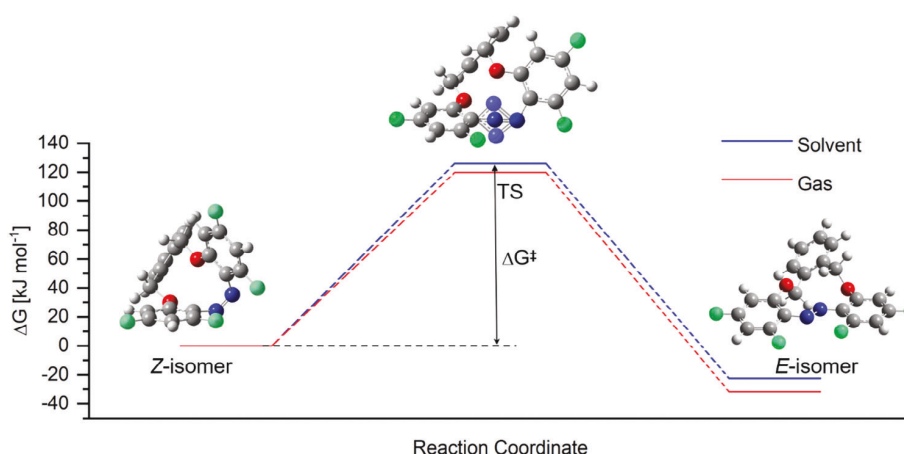


**Figure 6.** Thermal relaxation of Z-2FOAM. The computational method was B3LYP/cc-pVTZ level of theory including the Grimme D3<sup>[47]</sup> correction for the gas phase. B3LYP/cc-pVTZ level of theory and SCRF with SMD correction for the solvent DMSO and Grimme D3<sup>[47]</sup> correction was used for the solvent calculation. The data is referenced on the Z-isomer. Shown is the IAR pathway for Z-2FOAM toward E-2FOAM via the TS. In the TS, the vibronic frequency is shown shaded.

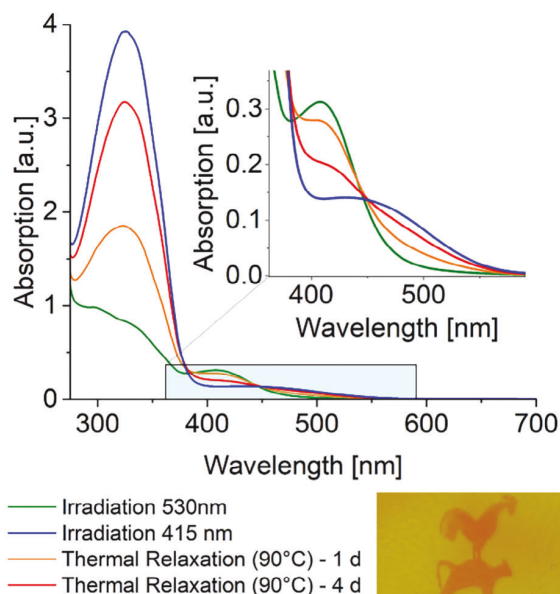
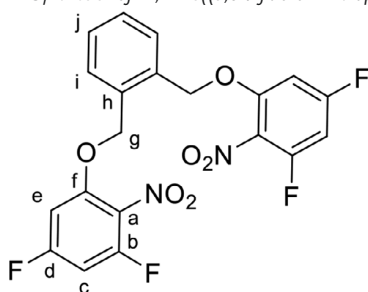


**Figure 7.** UV–vis spectra of **2FOAM** immersed in PMMA (conc. 5 mg in 500 mg PMMA) after irradiation with blue light (415 nm), green light (530 nm), and thermal treatment of the Z-isomer at 90 °C for 1 day and 4 days. An image of the “Bremer Stadtmusikanten” was produced by irradiation on a **2FOAM**/PMMA polymer mixture (conc. 50 mg in 500 mg PMMA) with green light using a mask. The picture can be erased by blue light and the composite irradiates with green light again to program a new picture.

a solvent. The controlled heating was made possible by the qx2/Shimadzu inlet from Quantum Northwest (WA, USA). Additionally, a Cary 3500 Multicell UV–vis Spectrophotometer from Agilent (CA, USA) was used for UV–vis thermal measurements.

For the sake of brevity, only the synthesis of **2FOAM** is presented here. For all other compounds see the Supporting Information.

Synthesis of 1,2-Bis((3,5-difluoro-2-nitrophenoxy)methyl)benzene (**S5**):



1,2-Bis(bromomethyl)benzene (1.68 g, 6.36 mmol, 0.500 equiv.) was added over a period of 10 min to a solution of 3,5-difluoro-2-nitrophenol (2.22 g, 12.7 mmol,

1.00 equiv.) and potassium carbonate (2.64 g, 69.0 mmol, 1.50 equiv.) in acetone (50 mL) and the mixture was heated to reflux at 65 °C for 12 h. The mixture was cooled to 25 °C and DCM (400 mL) was added. The organic phase was washed with water (2 × 200 mL) and brine (150 mL) and dried over MgSO<sub>4</sub>. The solvent was evaporated *in vacuo*. Purification of the residue by column chromatography (gradient: *n*-hexane → DCM), gave the product as a colorless solid (2.85 g, 6.30 mmol, 99%).

<sup>1</sup>H NMR (600 MHz, CDCl<sub>3</sub>) δ = 7.47–7.42 (m, 4H, H-i, H-j), 6.75 (dd, <sup>3</sup>J = 10.0, <sup>5</sup>J = 2.2 Hz, 2H, H-c), 6.63–6.58 (m, 2H, H-e), 5.28 (s, 4H, H-g) ppm.

<sup>13</sup>C{<sup>1</sup>H} NMR (151 MHz, CDCl<sub>3</sub>) δ = 163.94 (d, <sup>1</sup>J = 255.3 Hz, <sup>3</sup>J = 15.0 Hz, C-b), 155.66 (d, <sup>1</sup>J = 258.9 Hz, <sup>3</sup>J = 15.0 Hz, C-d), 152.85–152.74 (m, 2C, C-f, C-a), 132.99 (C-h) 129.80 (C-i), 129.69 (C-j), 98.30–97.77 (m, C-c), 97.82 (d, <sup>2</sup>J = 50.8 Hz, C-e), 70.68 (C-g) ppm.

<sup>19</sup>F NMR (565 MHz, CDCl<sub>3</sub>) δ = –100.56 (ddd, <sup>3</sup>J = 9.2 Hz, F-d), –117.84 (dd, <sup>3</sup>J = 9.2 Hz, F-b) ppm.

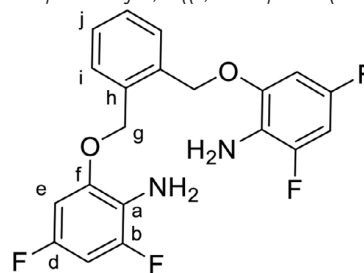
IR (ATR):  $\bar{\nu}$  = 1662 (s), 198 (m), 1527 (s), 1497 (w), 1446 (m), 1368 (m), 1338 (m), 1304 (w), 1199 (m), 1137 (s), 1121 (m), 1088 (s), 1007 (m), 942 (w), 844 (m), 830 (m), 773 (m) cm<sup>–1</sup>.

HRMS (ESI) *m/z* (%): [M+Na]<sup>+</sup> calcd for [C<sub>20</sub>H<sub>12</sub>N<sub>2</sub>O<sub>6</sub>F<sub>4</sub>Na]<sup>+</sup> 475.05237, found 475.05163.

Mp: 157 °C.

R<sub>f</sub>: 0.80 (chloroform).

Synthesis of 2,2'-((1,2-Phenylenebis(methylene))bis(oxy))dianiline (**S6**):



Iron powder (4.41 g, 78.9 mmol, 10.0 equiv.) was added portion-wise to a solution of **S5** (3.57 g, 7.89 mmol, 1.00 equiv.) in MeOH (100 mL). Subsequently, HCl (1 M, 5 mL) was slowly added to the reaction. The reaction mixture was heated to 90 °C for 70 min. After cooling down the mixture, it was filtered. The solid residue was washed with ethyl acetate (100 mL). The combined organic layers were washed with water (3 × 200 mL) and brine (1 × 100 mL). The organic layer was dried over MgSO<sub>4</sub> and concentrated under reduced pressure. The crude product was purified by column chromatography (ethyl acetate : *n*-hexane, 2 : 1) to obtain the product as a white solid, which was not stable under ambient conditions and should be used immediately or stored under nitrogen in the dark (3.08 g, 7.85 mmol, 99%).

<sup>1</sup>H NMR (600 MHz, CDCl<sub>3</sub>) δ = 7.50 (dd, <sup>3</sup>J = 5.6 Hz, <sup>4</sup>J = 3.5 Hz, 2H, H-i), 7.42 (dd, <sup>3</sup>J = 5.6 Hz, <sup>3</sup>J = 3.5 Hz, 2H, H-i), 6.50–6.46 (m, 4H, H-c, H-e), 5.16 (s, 4H, H-g), 3.56 (s, 4H, NH-a) ppm.

<sup>13</sup>C{<sup>1</sup>H} NMR (151 MHz, CDCl<sub>3</sub>) δ = 154.81 (d, <sup>1</sup>J = 237.2 Hz, <sup>3</sup>J = 14.9 Hz, C-b), 151.06 (d, <sup>1</sup>J = 238.3 Hz, <sup>3</sup>J = 14.9 Hz, C-d), 147.42 (dd, <sup>3</sup>J = 11.6 Hz, <sup>3</sup>J = 9.5 Hz, C-f), 134.60 (C-h), 129.70 (C-i), 129.19 (C-j), 121.27 (dd, <sup>2</sup>J = 15.5 Hz, <sup>4</sup>J = 4.0 Hz, C-a), 96.89–96.44 (m, C-c), 96.84 (d, <sup>2</sup>J = 50.1 Hz, C-e), 69.14 (C-g) ppm.

<sup>19</sup>F NMR (565 MHz, CDCl<sub>3</sub>) δ = –131.73 (dd, <sup>3</sup>J = 11.1 Hz, <sup>5</sup>J = 2.5 Hz F-b), –123.86 (dd, <sup>3</sup>J = 9.4 Hz, F-d) ppm.

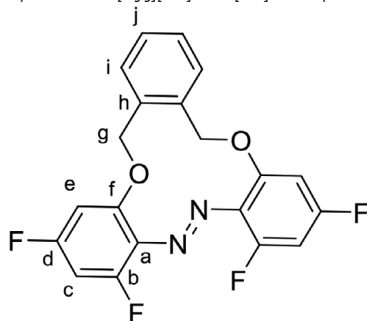
HRMS (EI, 70 eV) *m/z* (%): [M]<sup>+</sup> calcd for [C<sub>20</sub>H<sub>16</sub>N<sub>2</sub>O<sub>2</sub>F<sub>4</sub>]<sup>+</sup> 392.11424, found 392.11484 (20), [C<sub>14</sub>H<sub>12</sub>F<sub>2</sub>NO]<sup>+</sup> 248 (100).

IR (ATR):  $\bar{\nu}$  = 3452 (w), 3365 (w), 1629 (m), 1608 (m), 1588 (m), 1509 (s), 1477 (s), 1446 (s), 1388 (w), 1360 (w), 1325 (w), 1245 (w), 1192 (w), 1151 (s), 1110 (s), 1034 (s), 997 (s), 813 (s), 767 (s) cm<sup>–1</sup>.

Mp: 112 °C.

R<sub>f</sub>: 0.35 (chloroform)

Synthesis of (E)-12,17-Dihydrotribenzo[b,f,j][1,8]dioxo[4,5]diazacyclo-



decine (2FOAM) **56**:

(734 mg, 1.87 mmol, 1.00 equiv.) was dissolved in toluene (30 mL). A stream of nitrogen was passed through the solution for 1 h. MnO<sub>2</sub> (1.30 g, 15.0 mmol, 8.00 equiv.) was added and the suspension was heated to 110 °C for 48 h. The hot reaction mixture was filtered through celite and the celite rinsed with chloroform (2 x 30 mL). The filtrate was evaporated to dryness under reduced pressure, and the residue was purified by column chromatography (DCM/*n*-hexane, 2:1) to obtain final compound (625 mg, 1.61 mmol, 86%) as a yellow solid.

<sup>1</sup>H NMR (600 MHz, CDCl<sub>3</sub>) δ = 7.49–7.42 (m, 4H, H-i, H-j), 7.49–7.45 (m, 2H, H-i), 6.91 (dd, <sup>3</sup>J = 9.0 Hz, <sup>4</sup>J = 2.4 Hz, 2H, H-e), 6.82 (ddd, <sup>3</sup>J = 11.0 Hz, <sup>3</sup>J = 9.0 Hz, <sup>4</sup>J = 2.4 Hz, 2H, H-c), 5.31 (s, 4H, H-g) ppm.

<sup>13</sup>C{<sup>1</sup>H} NMR (151 MHz, CDCl<sub>3</sub>) δ = 163.27 (d, <sup>1</sup>J = 256 Hz, <sup>3</sup>J = 15.2 Hz, C-b), 156.36 (d, <sup>1</sup>J = 256 Hz, <sup>3</sup>J = 15.2 Hz, C-d), 154.11 (dd, <sup>3</sup>J = 13.3 Hz, <sup>5</sup>J = 4.6 Hz, C-f), 135.59 (C-h), 133.37 (dd, <sup>3</sup>J = 8.0 Hz, <sup>3</sup>J = 4.6 Hz, C-a), 131.56 (C-i), 129.39 (C-j), 106.75 (dd, <sup>2</sup>J = 24.2 Hz, <sup>4</sup>J = 3.8 Hz, C-e), 101.28 (t, <sup>2</sup>J = 24.2 Hz, C-c), 76.51 (C-g) ppm.

<sup>19</sup>F NMR (565 MHz, CDCl<sub>3</sub>) δ = -105.01 (ddd, <sup>3</sup>J = 9.0 Hz, F-b), -117.17 (dd, <sup>3</sup>J = 9.0 Hz, F-d) ppm.

IR (ATR):  $\bar{\nu}$  = 1589 (s), 1443 (s), 1380 (m), 1338 (w), 1214 (w), 1177 (m), 1087 (s), 1063 (s), 1004 (m), 958 (m), 932 (m), 854 (m), 837 (m), 825 (m), 781 (m), 763 (s) cm<sup>-1</sup>.

HRMS (ESI) *m/z* (%): [M+Na]<sup>+</sup> calcd for [C<sub>20</sub>H<sub>12</sub>N<sub>2</sub>O<sub>4</sub>F<sub>4</sub>Na]<sup>+</sup> 411.07271, found 411.07189.

Mp: 178 °C.

R<sub>f</sub>: 0.80 (chloroform).

[CCDC 2 289 033, 2 289 034, 2 289 035, 2 289 036, 2 289 037, 2 290 135] contain the supplementary crystallographic data for this paper. These data can be obtained free of charge from The Cambridge Crystallographic Data Centre via [www.ccdc.cam.ac.uk/data\\_request/cif](http://www.ccdc.cam.ac.uk/data_request/cif).

## Supporting Information

Supporting Information is available from the Wiley Online Library or from the author.

## Acknowledgements

This research was funded by the GERMAN RESEARCH FOUNDATION (DFG) within the priority program SPP 2100 “Soft Material Robotic Systems”, Subproject STA1195/5-1, “Insect feet inspired concepts soft touch grippers with dynamically adjustable grip strength”.

Open access funding enabled and organized by Projekt DEAL.

## Conflict of Interest

The authors declare no conflict of interest.

## Data Availability Statement

The data that support the findings of this study are available in the supplementary material of this article.

## Keywords

azobenzene, long half-life time, macrocycle, optical data storage, visible light

Received: October 25, 2023

Revised: December 22, 2023

Published online:

- [1] a) M. Gu, Q. Zhang, S. Lamon, *Nat. Rev. Mater.* **2016**, *1*, 16070; b) M. Völske, J. Bevendorff, J. Kiesel, B. Stein, M. Fröbe, M. Hagen, M. Potthast, **2021**, 61.
- [2] D. Al Kez, A. M. Foley, D. Laverty, D. F. Del Rio, B. Sovacool, *J. Cleaner Prod.* **2022**, *371*, 133633.
- [3] J. M. Cavanillas, E. Curry, W. Wahlster, *New Horizons for a Data-Driven Economy*, Springer, Berlin, **2016**.
- [4] D. D. Tang, C.-F. Pai, *Magnetic Memory Technology: Spin-transfer torque Mram and Beyond*, John Wiley & Sons, New Jersey, US **2020**.
- [5] R. Micheloni, A. Marelli, K. Eshghi, *Inside Solid State Drives (SSDs)*, 2nd ed Springer, Berlin **2018**.
- [6] D. L. N. Kallepalli, A. M. Alshehri, D. T. Marquez, L. Andrzejewski, J. C. Scaiano, R. Bhardwaj, *Sci. Rep.* **2016**, *6*, 26163.
- [7] M. Gu, X. Li, Y. Cao, *Light: Sci. Appl.* **2014**, *3*, e177.
- [8] L. Gao, Q. Zhang, R. A. Evans, M. Gu, *Adv. Opt. Mater.* **2021**, *9*, 2100487.
- [9] C. Lee, E. Z. Xu, K. W. C. Kwock, A. Teitelboim, Y. Liu, H. S. Park, B. Ursprung, M. E. Ziffer, Y. Karube, N. Fardian-Melamed, C. C. S. Pedroso, J. Kim, S. D. Pritzl, S. H. Nam, T. Lohmueller, J. S. Owen, P. Ercius, Y. D. Suh, B. E. Cohen, E. M. Chan, P. J. Schuck, *Nature* **2023**, *618*, 951.
- [10] a) E. Blasco, M. Piñol, C. Berges, C. Sánchez-Somolinos, L. Oriol, in *Smart Polymers and their Applications*, (Eds: M. R. Aguilar, J. San Román), Woodhead Publishing, Sawston, Cambridge **2014**; b) S. Kawata, Y. Kawata, *Chem. Rev.* **2000**, *100*, 1777; c) H. Wang, H. K. Bisoyi, X. Zhang, F. Hassan, Q. Li, *Chemistry* **2022**, *28*, 202103906; d) Y. Zhuang, R. Xiuli, C. Xueting, S. Liu, W. Huang, Q. Zhao, *Advanced Photonics* **2020**, *3*, 014001.
- [11] a) M.-M. Russew, S. Hecht, *Adv. Mater.* **2010**, *22*, 3348; b) D. Cameron, S. Eisler, *J. Phys. Org. Chem.* **2018**, *31*, e3858.
- [12] a) L. Kortekaas, W. R. Browne, *Chem. Soc. Rev.* **2019**, *48*, 3406; b) R. Klajn, *Chem. Soc. Rev.* **2014**, *43*, 148.
- [13] V. Papper, G. I. Likhtenshtein, *J. Photochem Photobiol A Chem* **2001**, *140*, 39.
- [14] D. Villarón, S. J. Wezenberg, *Angew. Chem., Int. Ed.* **2020**, *59*, 13192.
- [15] a) M. Irie, *Chem. Rev.* **2000**, *100*, 1685; b) M. Irie, T. Fukaminato, K. Matsuda, S. Kobatake, *Chem. Rev.* **2014**, *114*, 12174; c) J. Zhang, H. Tian, *Adv. Opt. Mater.* **2018**, *6*, 1701278.
- [16] a) Z. Zhang, W. Wang, P. Jin, J. Xue, L. Sun, J. Huang, J. Zhang, H. Tian, *Nat. Commun.* **2019**, *10*, 4232; b) Z. Li, C. He, Z. Lu, P. Li, Y.-P. Zhu, *Dyes Pigment.* **2020**, *182*, 108623; c) I. Ikariko, S. Kim, Y. Hiroyasu, K. Higashiguchi, K. Matsuda, T. Hirose, H. Sotome, H. Miyasaka, S. Yokojima, M. Irie, S. Kurihara, T. Fukaminato, *J. Phys. Chem. Lett.* **2022**, *13*, 7429.
- [17] Y.-Y. Tang, Y.-L. Zeng, R.-G. Xiong, *J. Am. Chem. Soc.* **2022**, *144*, 8633.
- [18] a) K. Imato, A. Sasaki, A. Ishii, T. Hino, N. Kaneda, K. Ohira, I. Imae, Y. Ooyama, *J. Org. Chem.* **2022**, *87*, 15762; b) K. Imato, A. Ishii, N. Kaneda, T. Hidaka, A. Sasaki, I. Imae, Y. Ooyama, *JACS Au* **2023**, *3*, 2458.
- [19] M. Poutanen, Z. Ahmed, L. Rautkari, O. Ikkala, A. Priimagi, *ACS Macro Lett.* **2018**, *7*, 381.
- [20] a) H. M. D. Bandara, S. C. Burdette, *Chem. Soc. Rev.* **2012**, *41*, 1809; b) D. Blegler, S. Hecht, *Angew. Chem., Int. Ed.* **2015**, *54*, 11338; c) F.

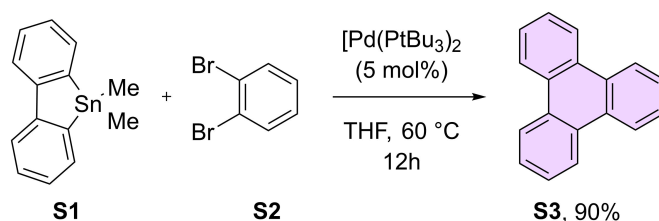


- A. Jerca, V. V. Jerca, R. Hoogenboom, *Nat Rev Chem* **2021**, 6, 51; d) S. De Martino, F. Mauro, P. A. Netti, *La Rivista del Nuovo Cimento* **2020**, 43, 599.
- [21] a) G. Fang, Y. Shi, J. E. MacLennan, N. A. Clark, M. J. Farrow, D. M. Walba, *Langmuir* **2010**, 26, 17482; b) C. Hahn, Y. Choi, J. W. Yoon, S. H. Song, C. H. Oh, P. Berini, *Nat. Commun.* **2016**, 7, 12201.
- [22] X. Li, J. W. Chon, R. A. Evans, M. Gu, *Opt. Express* **2009**, 17, 2954.
- [23] A. S. Matharu, S. Jeeva, P. S. Ramanujam, *Chem. Soc. Rev.* **2007**, 36, 1868.
- [24] a) M. Gao, D. Kwaria, Y. Norikane, Y. Yue, *Natural Sciences* **2023**, 3, 220020; b) F. A. Jerca, V. V. Jerca, R. Hoogenboom, *Nat Rev Chem* **2022**, 6, 51; c) A. A. Beharry, G. A. Woolley, *Chem. Soc. Rev.* **2011**, 40, 4422.
- [25] X. Li, J. Cui, W. Zhang, J. Huang, W. Li, C. Lin, Y. Jiang, Y. Zhang, G. Li, *J. Mater. Chem.* **2011**, 21, 17953.
- [26] R. Siewertsen, H. Neumann, B. Buchheim-Stehn, R. Herges, C. Näther, F. Renth, F. Temps, *J. Am. Chem. Soc.* **2009**, 131, 15594.
- [27] a) F. Klockmann, C. Fangmann, E. Zender, T. Schanz, C. Catapano, A. Terfort, *ACS Omega* **2021**, 6, 18434; b) H. Sell, C. Näther, R. Herges, *Beilstein J. Org. Chem.* **2013**, 9, 1; c) W. Moormann, D. Langbehm, R. Herges, *Beilstein J. Org. Chem.* **2019**, 15, 727; d) S. Li, K. Bamberg, Y. Lu, F. D. Sönnichsen, A. Staubitz, *Polymers* **2023**, 15, 1306; e) M. Schehr, D. Hugenbusch, T. Moje, C. Näther, R. Herges, *Beilstein J. Org. Chem.* **2018**, 14, 2799.
- [28] D. Bléger, J. Schwarz, A. M. Brouwer, S. Hecht, *J. Am. Chem. Soc.* **2012**, 134, 20597.
- [29] C. Knie, M. Utecht, F. Zhao, H. Kulla, S. Kovalenko, A. M. Brouwer, P. Saalfrank, S. Hecht, D. Bléger, *Chemistry* **2014**, 20, 16492.
- [30] C. E. Weston, R. D. Richardson, P. R. Haycock, A. J. P. White, M. J. Fuchter, *J. Am. Chem. Soc.* **2014**, 136, 11878.
- [31] J. Calbo, A. R. Thawani, R. S. L. Gibson, A. J. P. White, M. J. Fuchter, *Beilstein J. Org. Chem.* **2019**, 15, 2753.
- [32] N. Eleya, S. Ghosh, E. Lork, A. Staubitz, *J. Mater. Chem. C* **2021**, 9, 82.
- [33] S. Ghosh, C. Eschen, N. Eleya, A. Staubitz, *J. Org. Chem.* **2023**, 88, 3372.
- [34] R. Falkenburg, M. J. Notheis, G. Schnakenburg, L. K. S. Von Krbeek, *Org. Biomol. Chem.* **2023**, 21, 4993.
- [35] a) A. L. Leistner, S. Kirchner, J. Karcher, T. Bantle, M. L. Schulte, P. Gödtel, C. Fengler, Z. L. Pianowski, *Chemistry* **2021**, 27, 8094; b) D. B. Konrad, G. Savasci, L. Allmendinger, D. Trauner, C. Ochsenfeld, A. M. Ali, *J. Am. Chem. Soc.* **2020**, 142, 6538; c) S. Schultze, N. Scheuring, P. Puylaert, M. Lehmann, A. Staubitz, *Adv. Sci.* **2023**, 10, 2302692.
- [36] a) L. M. Silva, D. L. Silva, M. V. Boas, Y. Bretonniere, C. Andraud, M. G. Vivas, *RSC Adv.* **2020**, 10, 40806; b) F. Pirani, A. Angelini, F. Frascella, R. Rizzo, S. Ricciardi, E. Descrovi, *Sci. Rep.* **2016**, 6, 31702; c) A. Szukalski, K. Haupa, A. Miniewicz, J. Mysliwiec, *J. Phys. Chem. C* **2015**, 119, 10007; d) S. Hvilsted, C. Sánchez, R. Alcalá, *J. Mater. Chem.* **2009**, 19, 6641; e) H. Ono, N. Kowatari, N. Kawatsuki, *Optical Materials* **2001**, 17, 387; f) Y. Zhai, L. Cao, Y. Liu, X. Tan, *Materials* **2020**, 13, 5562; g) S. Bian, M. G. Kuzyk, *Opt. Lett.* **2002**, 27, 1761.
- [37] A. Williamson, *Journal of Science* **1850**, 37, 350.
- [38] a) A. J. Bechamp, *Ann. Chim. Phys.* **1854**, 42, 186; b) S. Yuan, X. Ye, J. Cai, Z. Song, Y. Tan, Y. Peng, Q. Ding, *J. Org. Chem.* **2022**, 87, 1485.
- [39] O. H. Wheeler, D. Gonzalez, *Tetrahedron* **1964**, 20, 189.
- [40] A. Müller-Deku, O. Thorn-Seshold, *J. Org. Chem.* **2022**, 87, 16526.
- [41] This observation is made in a qualitative manner, because the azobenzenes are not entirely planar as in the parent compound. The deviations are not large, but defining which is the plane to be referred to would be arbitrary.
- [42] L. u. Vetráková, V. Ladányi, J. Al Anshori, P. Dvořák, J. Wirz, D. Heger, *Photochem. Photobiol. Sci.* **2017**, 16, 1749.
- [43] a) D. M. Adrion, D. S. Kaliakin, P. Neal, S. A. Lopez, *J Phys Chem A* **2021**, 125, 6474; b) S. Axelrod, E. Shakhnovich, R. Gómez-Bombarelli, *ACS Cent. Sci.* **2023**, 9, 166; c) D. L. Isac, A. Airinei, M. Homocianu, N. Fifere, C. Cojocaru, C. Hulubei, *J. Photochem. Photobiol., A* **2020**, 390, 112300; d) H. J. Hofmann, R. Cimiriaglia, J. Tomasi, *J Mol Struct* **1987**, 152, 19; e) T. Asano, T. Okada, *J. Org. Chem.* **1984**, 49, 4387; f) D. M. Shin, D. G. Whitten, *J. Am. Chem. Soc.* **1988**, 110, 5206; g) J. Dokić, M. Gothe, J. Wirth, M. V. Peters, J. Schwarz, S. Hecht, P. Saalfrank, *J Phys Chem A* **2009**, 113, 6763; h) I. Conti, M. Garavelli, G. Orlandi, *J. Am. Chem. Soc.* **2008**, 130, 5216.
- [44] M. Reimann, E. Teichmann, S. Hecht, M. Kaupp, *J. Phys. Chem. Lett.* **2022**, 13, 10882.
- [45] a) H. Rau, I. Waldner, *Phys. Chem. Chem. Phys.* **2002**, 4, 1776; b) H. Rau, E. Lueddecke, *J. Am. Chem. Soc.* **1982**, 104, 1616.
- [46] M. J. Frisch, G. W. Trucks, H. B. Schlegel, G. E. Scuseria, M. A. Robb, J. R. Cheeseman, G. Scalmani, V. Barone, B. Mennucci, G. A. Petersson, H. Nakatsuji, M. Caricato, X. Li, H. P. Hratchian, A. F. Izmaylov, J. Bloino, G. Zheng, J. L. Sonnenberg, M. Hada, M. Ehara, K. Toyota, R. Fukuda, J. Hasegawa, M. Ishida, T. Nakajima, Y. Honda, O. Kitao, H. Nakai, T. Vreven, J. A. Montgomery, et al., **2009**.
- [47] S. Grimme, J. Antony, S. Ehrlich, H. Krieg, *J. Chem. Phys.* **2010**, 132, 154104.
- [48] For the solvent simulation, only a double zeta potential could be used due to computational cost.
- [49] a) J. Grimm, W. Grimm, *Kinder- und Haus-Märchen*, Vol. 1, Reimer, Berlin, Germany **1819**; b) B. Grimm, A. Smet, *The Bremen Town Musicians*, Atlântico Press, Lisboa, Portugal **2019**.
- [50] a) C. D. Eisenbach, *Die Makromolekulare Chemie* **1978**, 179, 2489; b) U. Georgi, P. Reichenbach, U. Oertel, L. M. Eng, B. Voit, *React. Funct. Polym.* **2012**, 72, 242.
- [51] K. Stranius, K. Börjesson, *Sci. Rep.* **2017**, 7, 41145.
- [52] A. A. A. Hameed, T. Osama, *Journal of Optics A: Pure and Applied Optics* **2003**, 5, S487.
- [53] a) S. Luo, K. Chen, L. Cao, G. Liu, Q. He, G. Jin, D. Zeng, Y. Chen, *Opt. Express* **2005**, 13, 3123; b) A. Yavrian, T. V. Galstian, M. Piché, *Optical Materials* **2004**, 26, 261; c) N. H. Nataj, E. Mohajerani, H. Nemati, A. Moheghi, M. R. Yazdanbakhsh, M. Goli, A. Mohammadi, *J. Appl. Polym. Sci.* **2013**, 127, 456; d) E. Blasco, M. Piñol, C. Berges, C. Sánchez-Somolinos, L. Oriol, in *Smart Polymers and their Applications*, 2nd ed, (Eds: M. R. Aguilar, J. San Román), Woodhead Publishing, Sawston, Cambridge **2019**; e) C. C. Corredor, Z.-L. Huang, K. D. Belfield, A. R. Morales, M. V. Bondar, *Chem. Mater.* **2007**, 19, 5165; f) C. O. Yanez, C. D. Andrade, S. Yao, G. Luchita, M. V. Bondar, K. D. Belfield, *ACS Appl. Mater. Interfaces* **2009**, 1, 2219; g) P. Wei, B. Li, A. de Leon, E. Pentzer, *J. Mater. Chem. C* **2017**, 5, 5780; h) J. Bahrenburg, F. Renth, F. Temps, F. Plamper, W. Richtering, *Phys. Chem. Chem. Phys.* **2014**, 16, 11549.

## 4.2 Unpublished Work III

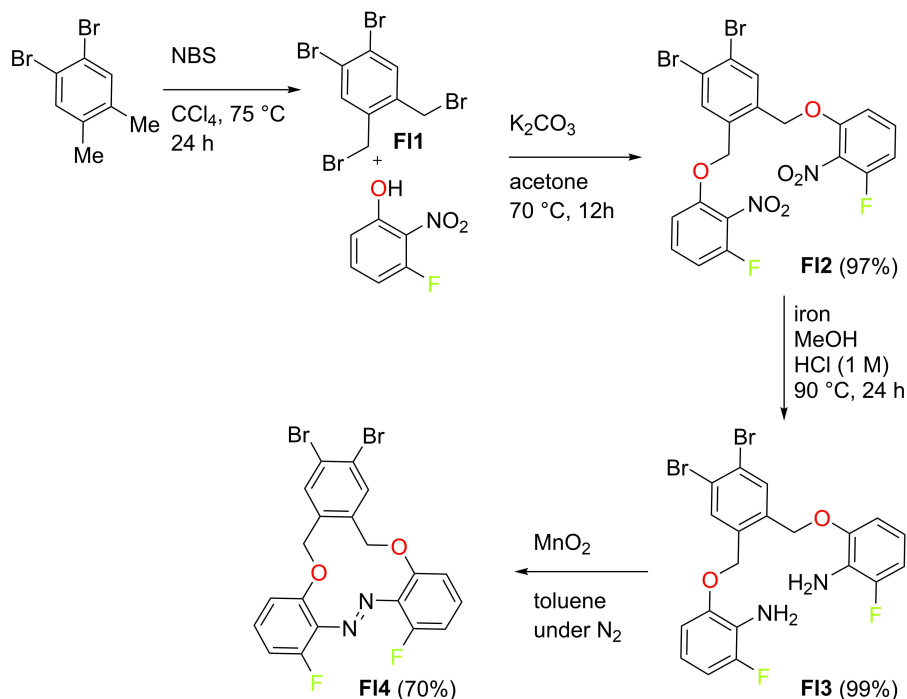
Encouraged by the favorable properties of the **FOAM** system with regard to long thermal half-life times (presented in S. Schultze *et al.*, *Adv. Funct. Mater.*, **2024**, 2313268),<sup>214</sup> we aimed to develop a molecular scaffold capable of not only transitioning into a kinetically highly stable state but also of providing a measurable response. The writing potential (in the context of optical data storage) of **FOAM** was demonstrated in our previously published work. However, for 3D optical storage, it is essential not only to write information but also to read it out to access the stored data.<sup>74,215,216</sup> To this end, various approaches have been explored that incorporate molecular switches. These include altering the refractive index,<sup>217</sup> manipulating the orientation of molecules,<sup>218</sup> tuning fluorophores,<sup>219</sup> or employing a chiroptical<sup>38</sup> molecular switch.<sup>38,217,220</sup>

For our newly designed molecular switch, we intended that this response should occur through different emission properties of the two isomers. This was achieved by an expansion of the aromatic system of the benzene unit in the linker bridge. This position was chosen, because it was expected to have only a minor influence on the switching properties in comparison to the direct extension at the aromatic core around the azo bridge, regarding PSS conversions and lowering half-life time. A synthetic approach to achieve our objective was to expand the aromatic ring to a polycyclic aromatic hydrocarbons (PAHs) through cross-coupling with stannoles. PAHs, are known fluorophores, emitting blue light. In the literature, an elegant method for preparing these compounds has been demonstrated, which was amenable to our system (Scheme 6).<sup>221</sup> A dibromobenzene derivative can be reacted with a reactive cyclic stannylated compound, stannafluorene. This annulation was reported to give good to high yields (71%-99%) for symmetrical and asymmetrical products.



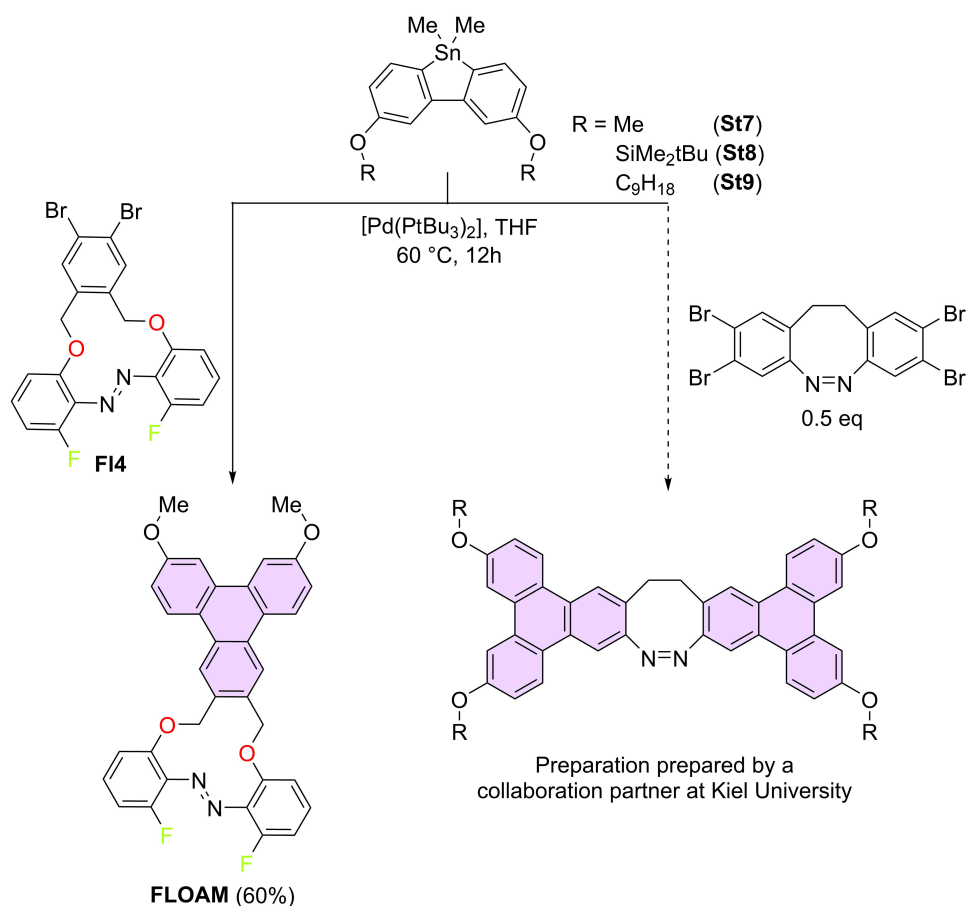
**Scheme 6:** Synthesis of PAHs by a palladium catalyzed double cross-coupling reaction.

To obtain the stannylated precursor (**S1**), a dihalogenated biphenyl in *ortho*-position needs to be lithiated and exchanged with Me<sub>2</sub>SnCl<sub>2</sub>. The second reactant is an aromatic system with two bromine or iodine atoms in *ortho*-position (**S2**). An approach to synthesize stannole motif **S1** within the **FOAM** framework was unsuitable. Lithiation in the presence of the azobenzene can reduce the azo groups.<sup>222</sup> It is only possible for highly optimized conditions and remains difficult.<sup>223</sup> Therefore, the integration of **S2** in **FOAM** was chosen for the realization of the emitting **FOAM** derivative. Therefore, to the scaffold from the previous publication (S. Schultze *et al.*, *Adv. Funct. Mater.*, **2024**, 2313268) two additional brominated sites (**F14**) for further functionalization through cross-coupling were added. The synthesis procedures to obtain **F14** was similar to **FOAM** with an additional step towards the precursor (Scheme 7).



**Scheme 7:** General synthesis overview for the FLOAM precursors.

Starting from 1,2-dibromo-4,5-dimethylbenzene a Wohl-Ziegler bromination<sup>224</sup> was conducted on both methyl groups. A mixture of starting material, mono brominated and double brominated (**F11**, 70% purity) product was obtained and used without further purification in a Williamson-Ether<sup>225</sup> synthesis with 3-fluoro-2-nitrophenol to obtain **F12** in 97% yield. Under mild conditions the nitro-groups of **F12** were reduced to amines in a Bechamp reaction<sup>226</sup> (99% yield). The macrocyclic ring was closed by the oxidation with MnO<sub>2</sub> to obtain the azobenzene **F14**. Overall, a yield of 55% was achieved for **F14**. The synthesis of the stannoles was performed according to the published procedure<sup>221</sup> and can be found in the supporting information of this thesis (Appendix Unpublished Work 9.5).



**Scheme 8:** Synthesis of the aromatic expansion via palladium catalyzed cross-coupling with stannoles of the FOAM and diazocine for emitting photoswitches.

In a palladium-catalyzed reaction, the precursor **F14** was cross-coupled with **St7** to obtain the fluorescence FOAM (**FLOAM**) in 60% yield (Scheme 8). The methoxy group in **FLOAM** was incorporated to increase solubility. Additionally, in collaboration with the Herges group (University of Kiel), additional stannoles were prepared in our lab as cross-coupling partner with diazocines, which is not part of this thesis.

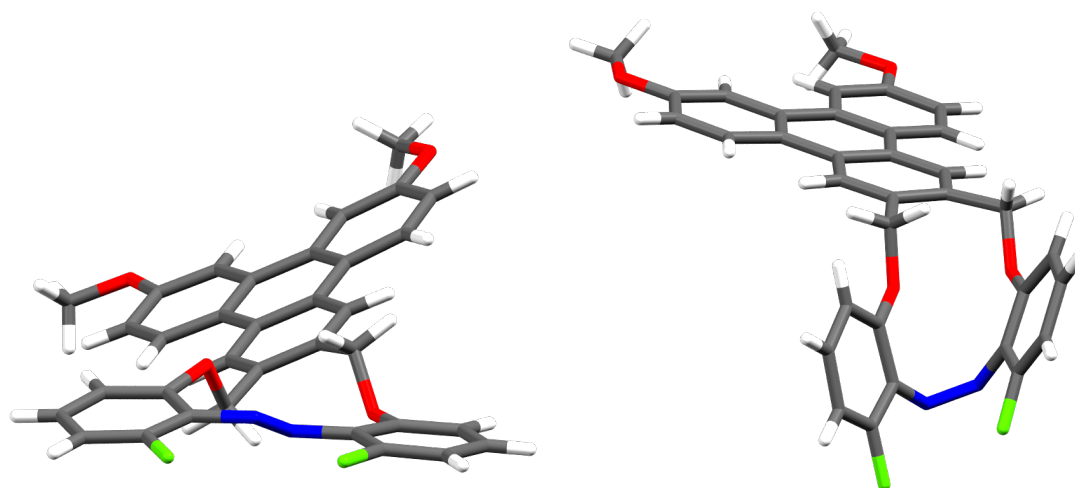


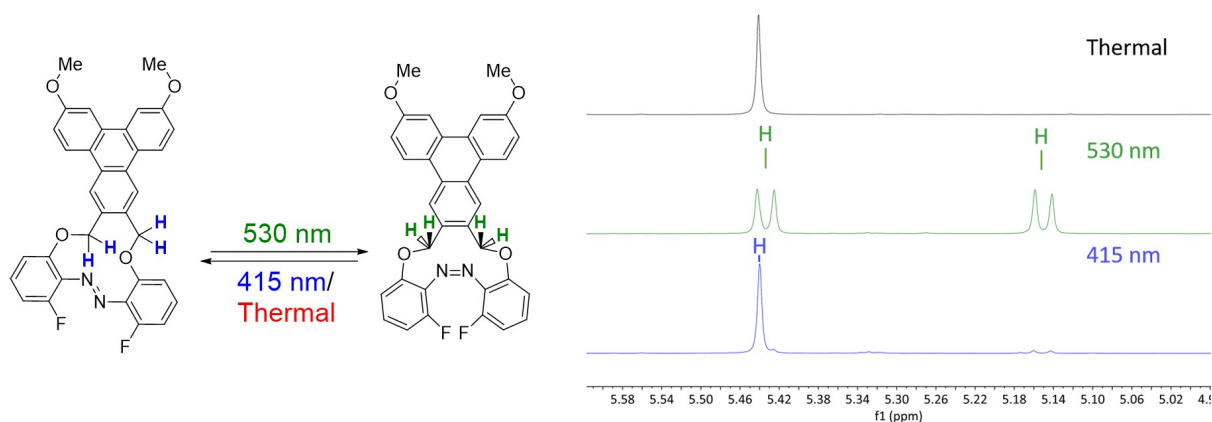
**Figure 4.1:** Crystal structure of **FLOAM** in its *E*- (left) and *Z*-isomer (right) characterized by XRD.

**Table 4.1:** Specific bond length, angles and dihedral angles of the crystal Structures of **FOAM**, **2FOAM** and **FLOAM**.

	<b>FOAM</b>		<b>2FOAM</b>		<b>FLOAM</b>	
	<i>E</i>	<i>Z</i>	<i>E</i>	<i>Z</i>	<i>E</i>	<i>Z</i>
N01=N02 (Å)	1.26	1.24	1.23	1.25	1.26	1.25
N01-C01 (Å)	1.43	1.45	1.42	1.45	1.42	1.45
N02=N01-C01	1.42°	1.45°	1.46°	1.45°	1.42°	1.45°
C01-N01=N02-C20 ( $\Phi$ )	178.9°	6.9°	178.9°	7.0°	179.4°	6.1°
C15-C20-N02=N01	153.0°	73.5°	152.5°	78.0°	141.4°	63.2°
C06-C01-N01=N02	143.8°	64.7°	144.9°	67.6°	157.2°	59.3°
Azo-Phenyl-Twist	5.3°	66.1°	4.1°	76.7°	12.3°	55.6°

Single crystal structures of *E*-**FLOAM** could be obtained by slow evaporation from a saturated Et<sub>2</sub>O solution. One sample was irradiated with green light (525 nm) for 15 minutes; from this solution, the slightly yellow crystals of *Z*-**FLOAM** were obtained. Both were analyzed by X-Ray diffraction (XRD) (Figure 4.1) and their geometrical structure compared with **FOAM** and **2FOAM** (Table 4.1). **FLOAM** shows very similar bond lengths and angles around the azo unit in comparison to **FOAM** and **2FOAM** for both isomers. A difference can be noted in the dihedral angle C01-N01=N02-C20 ( $\Phi$ ) with  $\Phi_{\mathbf{FLOAM},E} = 179.4^\circ$  ( $\Phi_{\mathbf{FOAM},E} = 178.9^\circ$ ). Although the  $\Phi$  is close to the dihedral angle of azobenzene ( $\Phi = 180^\circ$ ), **FLOAM** is less planar. This can be seen by the phenyl-twist (definition given in Publication III), which is 12.3° for **FLOAM** and 5.3° for **FOAM**. A similar tendency can be observed for the *Z*-isomer. The dihedral angle  $\Phi$  is with  $\Phi_{\mathbf{FLOAM},Z} = 6.1^\circ$  is the between the values of  $\Phi_{\mathbf{FOAM},Z} = 6.9^\circ$  and  $\Phi_{\mathbf{HOAM},Z} = 2.1^\circ$ . Notably, the azo-phenyl-twist is the sharpest of all **OAMs** with an angle of 55.6°, thus indicating a higher strain in the 12-membered ring in *Z*-**FLOAM**.<sup>a</sup>

The photoswitching properties were analyzed by UV-vis spectroscopy and <sup>1</sup>H NMR spectroscopy. The switching of **FLOAM** shifts all proton signals highfield. However, because of many signals in the aromatic region, there are a number of multiplets and overlap between the signals. Therefore, the bridging CH<sub>2</sub> groups were used to analyze the switching quantitatively (Figure 4.2).

**Figure 4.2:** NMR spectroscopic study of the irradiation of **FLOAM** in DMSO-*d*<sub>6</sub> after thermal treatment (the solid was heated at 105 °C for 72 h before dissolution, black spectrum), after irradiation with green light (525 nm) and blue light (420 nm) (conc<sub>**FLOAM**</sub> = 7.11 μmol mL<sup>-1</sup>).<sup>a</sup>Strain-calculations are necessary for further evaluation.

**FLOAM** showed very good switching efficiency in DMSO-*db* (PSS<sub>415nm,E</sub>: 85% (**FOAM**) vs. 86% (**FLOAM**)) and in the PSS<sub>530nm,Z</sub>: 95% (**FOAM**) vs. 96% (**FLOAM**)). In the UV-vis spectrum a clear separation of the  $n-\pi^*$  (400-550 nm) of *E*-**FLOAM** and *Z*-**FLOAM** can be observed. The strong absorption of the PAHs motif conceals the change of the absorption of the isomers in the UV area (300-400 nm). However, a reduced absorption was observed here, which indicates the lower absorption of the  $\pi \rightarrow \pi^*$  band in the *Z*-**FLOAM**. Furthermore, the half-life time has been measured in DMSO with  $t_{1/2}(100^\circ\text{C}) = 57.3$  h (**FOAM**  $t_{1/2}(100^\circ\text{C}) = 20.6$  h). This is an almost threefold increase of the half-life time of **FLOAM** in comparison to the previously very high half-life time of **FOAM** (Appendix Unpublished Work 9.5). The large PAHs motif seems to have a stabilizing effect on the thermal stability of the *Z*-isomer.<sup>b</sup>

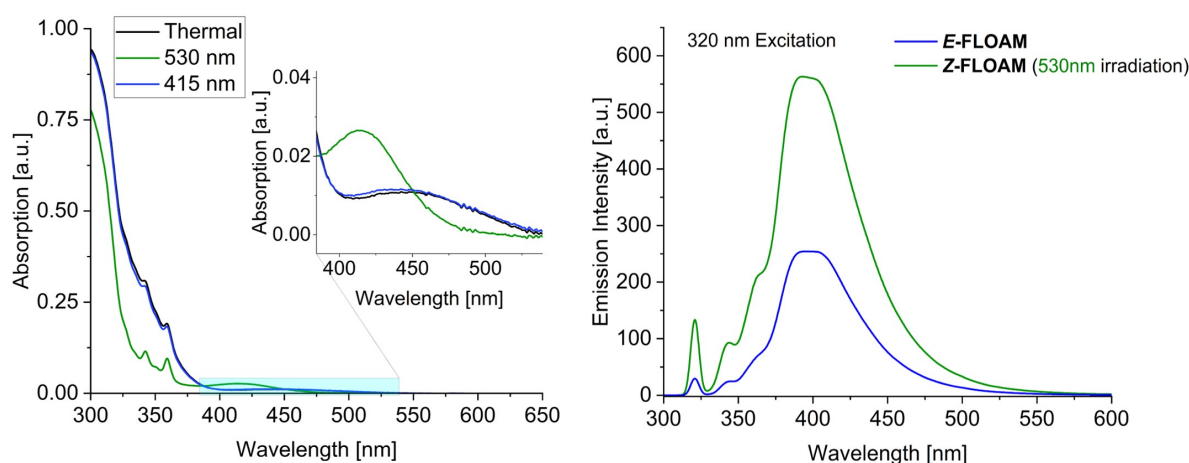


**Figure 4.3:** UV-vis spectrum of **FLOAM** in DMSO after thermal treatment (black, 140 °C, 4 h) and irradiation with green (530 nm) and violet light (415 nm) respectively (conc<sub>**FLOAM**</sub> = 0.0133  $\mu\text{mol mL}^{-1}$ ) and the fluorescence spectrum of **FLOAM** after excitation with 320 nm in dichloromethane of *E*-**FLOAM** (blue) and after excitation with 320 nm of the same sample after irradiation with green light (530 nm).

The resulting triphenyl framework emits light upon UV-light excitation. This allows the switching of the azo motif in the visible range (420 nm and 530 nm) independently, while the excitation operates in the UV range.

**FLOAM** emits with excitation wavelengths of 320 nm, 330 nm, and 350 nm a blue light in a broad spectrum of 350-500 nm (Figure 4.3, right)(Appendix Unpublished Work 9.5 for the emission spectrum with 330 nm and 350 nm). The quantum yield for the fluorescence of *E*-**FLOAM** was determined to be  $\Phi_F = 6\%$  and is in a typical range for PAHs.<sup>227</sup> A solid-state emission for *E*-**FLOAM** was not observed.

However, the different emission at the same irradiation intensity is remarkable. This is significantly higher for the switched *Z*-**FLOAM** than for *E*-**FLOAM**. We suspect that the lower absorption of the azo unit in *Z*-**FLOAM** allows more photons to pass through to the triphenyl unit. Due to this phenomenon, **FLOAM** can be irradiated with a defined portion of light, and the intensity of the emitted response indicating the isomer present. Thus, a large area can be read out within a short time by CCD cameras, which enables high read-out up to hundredths GB/s.<sup>220</sup>

<sup>b</sup>However, it should be noted that only a complete Arrhenius plot can accurately determine the thermal stability at room temperature as the slope is crucial.

## Introduction Part II

### 5.1 Liquid Crystallinity

#### 5.1.1 The Nature of Liquid Crystals

The liquid crystalline phase, in addition to the three states of solid, liquid, and gaseous, positions itself as the fourth state of matter. More precisely, it is situated between the highly ordered crystalline phase (solid) and the disordered isotropic phase (liquid) (Figure 5.1).<sup>228,229</sup>

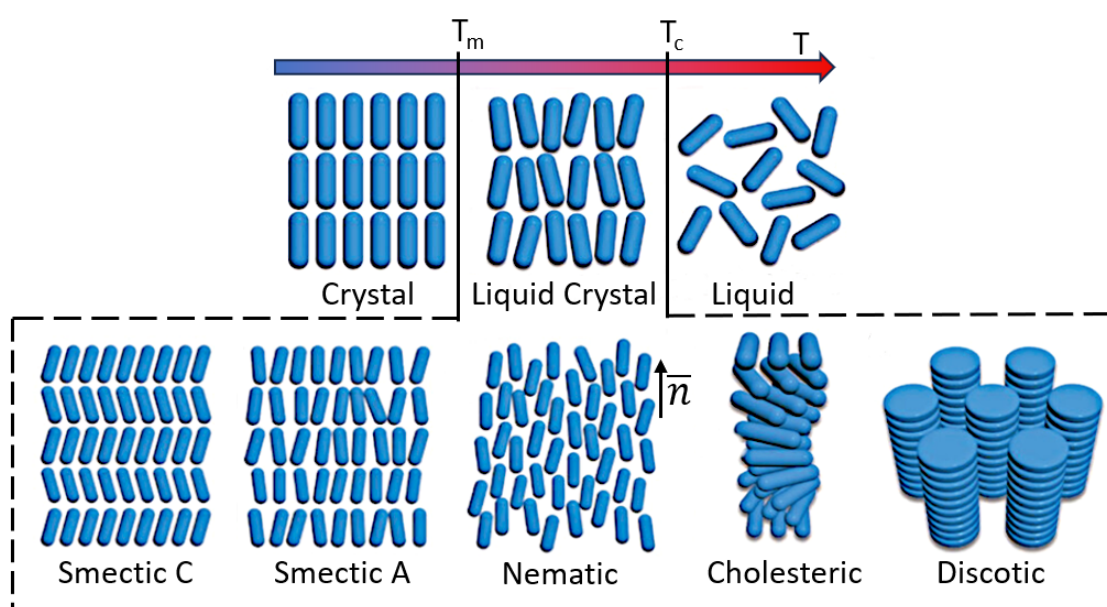


**Figure 5.1:** Schematic view of the liquid crystalline state between the solid (crystalline) and liquid (isotropic) phase. The subclassification of liquid crystal are shown below and depend on shape of the mesogen. Adapted with permission.<sup>230</sup> © 2023 Wiley-VCH GmbH

Characterized by their short-range order and alignment, they combine the strong interaction of crystallinity with the flexibility of liquids. Molecules that exhibit such properties are called mesogens. The corresponding liquid crystalline phase is known as the mesophase. The formation of a mesophase occurs within a specific temperature range and is characterized by anisotropy.<sup>229</sup> The direction of the order is given by the director vector  $\bar{n}$ . The degree of order can be described by  $S$  and is given as:

$$S = \frac{1}{2}(3 \langle \cos^2 \Theta - 1 \rangle) \quad (5.1)$$

with  $\Theta$  being the angle between the director  $\bar{n}$  and the long direction of each molecule.<sup>231,232</sup> The average of all molecules in a sample is given through the notation in brackets. An ideal alignment is described by  $S = 1$ , while  $S = 0$  represents a loss of order, which is equivalent to an

isotropic phase. Typically  $S$  ranges from 0.3 to 0.9 for a liquid crystal, and higher temperatures decrease the order parameter.

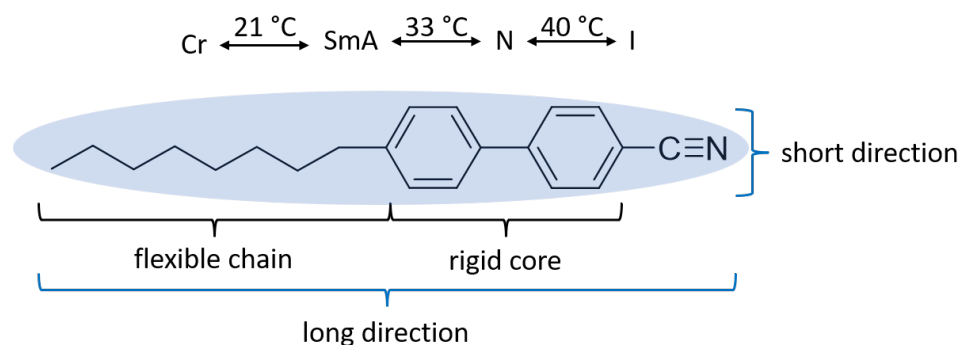


**Figure 5.2:** Presentation and analysis of a calamitic, rod-shaped molecule that exhibits a smectic A phase between 21 and 33 °C and a nematic phase between 33 and 40 °C.<sup>233</sup>

To ensure mobility in thermotropic liquid crystals, flexible structural elements must be utilized. Traditional mesogens consist of a rigid, predominantly aromatic core with a highly anisotropic shape and high polarizability, along with terminal chains (Figure 5.2). These are flexible side groups usually consisting of long-chain carbon compounds such as alkyl, alkoxy, or alkenyl groups. The length of the side chain can dramatically determine the liquid crystalline properties of a rigid core motif. The most well-known are calamitic (rod-like, Figure 5.2) and discotic (disc-shaped) mesogens.<sup>234,235</sup>

The self-organization of these anisometric molecules primarily relies on the anisotropy of intermolecular interactions, especially steric and dispersion interactions, leading to the formation of liquid crystalline phases. The analysis of a liquid crystalline phase can be conducted through the distances between molecules in X-ray diffraction,<sup>238</sup> and through the absorption as well as release of heat during the phase transition by dynamical scanning calorimetry (DSC).<sup>228</sup> Due to the specific light refraction induced by the anisotropic arrangement, liquid crystals can also be particularly well observed under a polarizing optical microscope (POM, Figure 5.3), often revealing spectacular images. Anisotropic crystals and liquid crystals both exhibit distinctive light refraction resulting in birefringence.<sup>236</sup> In liquid crystals, incident light is refracted by varying degrees depending on the direction of the mesogen and the polarization of the incident beam. This is caused by the asymmetric molecular structure, resulting in two different refractive indices, the ordinary and extraordinary refractive indices.<sup>229,239–242</sup>

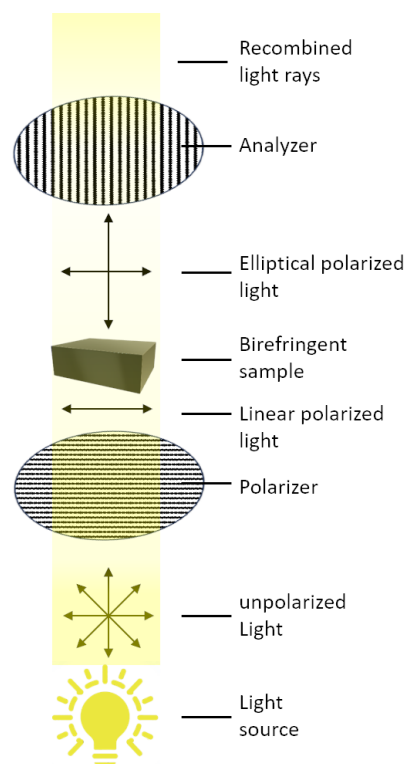


**Figure 5.3:** The working principle of a POM observing a birefringent sample.<sup>236,237</sup>



The working principle of a POM is as follows: When linearly polarized light (LPL) penetrates the anisotropic and birefringent mesophase, it divides into two rays - ordinary and extraordinary - which possess polarizations perpendicular to each other. These rays progress through the birefringent liquid crystal at distinct velocities, creating a phase shift. This shift leads to the emergence of elliptically polarized light. As this elliptically polarized light traverses through the second polarizer, it generates interference colors, yielding a texture that is characteristic to a particular liquid crystal phase (Figure 5.4).<sup>229,236,239–242</sup> Since the birefringence depends on the orientation and layer thickness of the sample, the textures can exhibit various colors.<sup>236,237,243</sup> A sample in its isotropic state causes no birefringence and the polarized light is blocked by a second polarizer, which is perpendicular to the polarized light, thus no light reaches the microscope and a dark image is observed.<sup>236</sup> In the case of homeotropic alignment of mesogens, a dark image can also be observed under POM.<sup>236</sup> For example, with calamitic mesogens, the long molecular axis and the higher refractive index are oriented along the path of the light beam. If a homeotropic sample is present, its optical character can also be determined using conoscopic analysis.<sup>236,237</sup> During conoscopic observation in a POM, a Bertrand lens is added to the optical path. This lens focuses the light rays onto a focal plane behind the specimen, creating not an enlarged image of the sample but an interference pattern, which appears as an Maltese cross.<sup>236,237</sup> Each Maltese cross corresponds to a different angle at which the LPL passes through the sample. The optical character of the sample can be determined using a  $\lambda$  plate (gypsum plate).<sup>237</sup> For optically negative materials, the high refractive indices of the sample and the  $\lambda$  retardation plate subtract in quadrants I and III and add in quadrants II and IV. Conversely, for optically positive phases, the color sequence is reversed.<sup>237</sup> Alternatively, the sample can be mechanically sheared to force the mesogens out of their homeotropic orientation.<sup>240</sup>

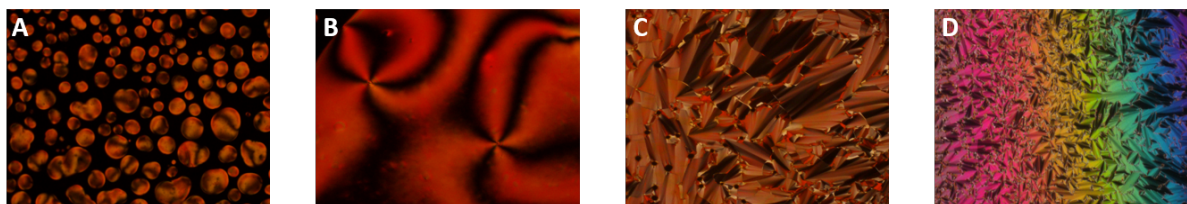


**Figure 5.4:** **A)** Formation of droplets at the phase transition from isotropic state to the nematic phase. **B)** *Schlieren* texture in the nematic phase with four-brush disclinations. **C)** Smectic phase with the striking fan-shaped structures. **D)** Same smectic phase with colourful birefringence caused by a thickness gradient at the outer sample edge. All pictures were taken during this thesis under cross-polarizer at a POM.<sup>243</sup>

## Nematic Phase

Liquid crystals share the characteristic of aligning in a common axis, known as the director. This is the least order of all liquid crystalline phases. Long, rod-like molecules align preferred along their molecular axis, the director  $\bar{n}$ , resulting in long-range orientational order. However, there is no long-range positional order of the molecular centroids in nematic phases, resulting in a characteristic higher molecular mobility and a slightly viscous phase. Under POM it exhibits *schlieren* or marble texture and *schlieren* defects can be observed (Figure 5.4, **B**). These are 2- or 4-point defects with black lines emerging from it.<sup>241,243–247</sup>

### Smectic Phase

In contrast, the smectic phase is much more densely packed and has a stronger interaction among the molecules. It adopts an one-dimensional long-range positional order in addition to the orientational order. These consist of layered structures, in which the incompatible molecular segments are segregated. The formation of nematic phases is exclusively attributed to the anisometric shape of mesogens, whereas smectic phases organization predominantly depends on nanoscale segregation of cores and chains, leading to the creation of distinct compartments at the nanometer scale. These can be observed as focal-conic or fan-shaped texture under the POM (Figure 5.4, **C** and **D**). Additionally, this leads to a higher viscosity, almost solid-like behavior of the smectic phase. Within the smectic phase, there are further subdivisions, such as smectic A, B, and C. In a smectic A phase (SmA), the long molecular axes are oriented on average orthogonal to the layer planes, whereas in a smectic C phase (SmC), the director  $\bar{n}$  is slightly inclined to the layers.<sup>240,243,248</sup>

### Cholesteric Phase

The incorporation of a chiral center into the mesogen can induce the formation of a cholesteric phase. This phase is distinguished by in-plane alignment and distinct orientations across planes that are rotationally displaced relative to each other. The term "cholesteric" originates from cholesterol, as its derivative was the first compound to exhibit liquid crystalline behavior, identified through the discovery of an intermediate phase between the solid state and the transparent liquid state by F. Reinitzer.<sup>249</sup> This intermediate phase, which appeared optically cloudy, prompted further investigation by O. Lehmann, leading to the coining and development of the concept of liquid crystals.<sup>250–252</sup>

### Discotic Phase

Another class, formed by disc-shaped molecules, is the discotic nematic mesophase. The discotic nematic phase, where the average orientation direction of the short molecular axes of discotic mesogens is reflected by the director  $\bar{n}$ , and the long axes are oriented parallel to a plane on average. In discotic liquid crystals, a high level of organization among the liquid crystal units can lead to the formation of ordered columnar mesophases, which display semiconducting characteristics suitable for optical applications.<sup>240,243,253–255</sup>

## 5.1.2 External Director

The natural alignment and orientation of liquid crystals in their respective liquid crystalline phase can also be induced and influenced by external factors. These external factors include mechanical force, shear force, field-assistance (magnetic and electrical), surface- and photoalignment (Figure 5.5).<sup>236,240,256</sup> After ordering the mesogens, the alignment can be frozen by additional bonding through functional groups.

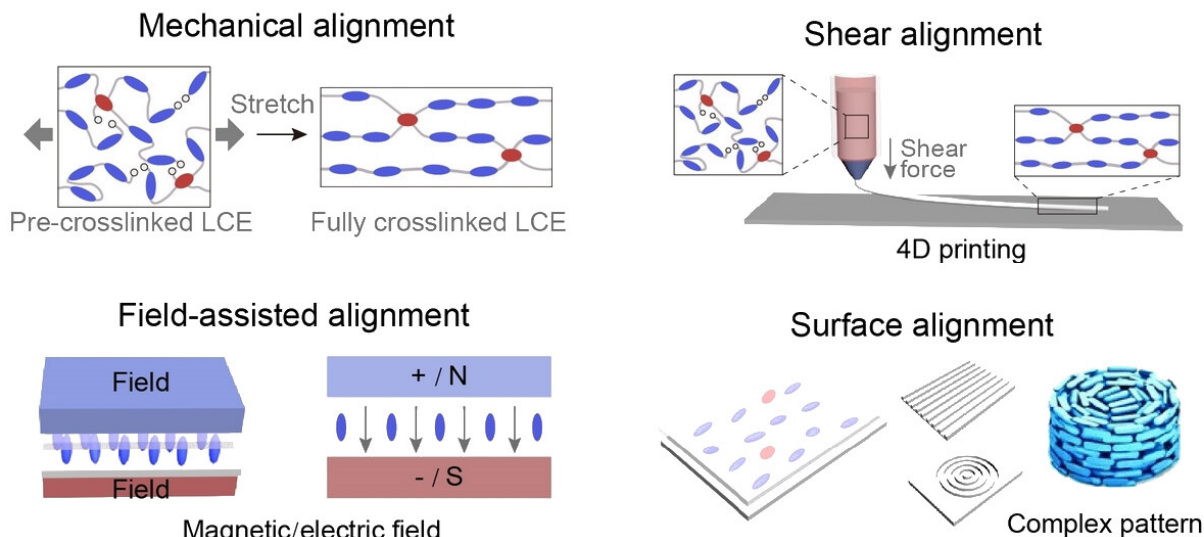


**Figure 5.5:** Schematic overview of regularly used external directors to align liquid crystal monomer and polymer. Reprinted with permission.<sup>257</sup> © 2023 Wiley-VCH GmbH

### Mechanical and Shear Alignment

Mechanical stress induced alignment can be achieved through stretching or shear forces on a group of mesogens. Reported methods include tensile, compressive and shear stress. The latter is primarily found in 4D printing and microfluidics. However, the alignment in both methods is only temporary during the application of force. To be permanent, the aligned mesogens must be fixed in place.<sup>258</sup>

### Electric and Magnetic Field Alignment

Due to their dipole moment, liquid crystals can also be aligned in an electric or magnetic field. Known from liquid crystal display (LCD) technology, liquid crystals can be quickly aligned along the electric field when voltage is applied, simplified either blocking or transmitting the light beam of the light source underneath.<sup>259,260</sup>

### Surface Alignment

When liquid crystals come into contact with specific surfaces, an alignment can be induced. There are two different concepts of surface effects. In one method, channels are mechanically created in the surface at nano to micro scales. Long, rod-like liquid crystals align themselves along the longitudinal axis of these channels, inducing a preferred direction for all subsequent molecules. Another method is based on the intermolecular interactions between the surface and the liquid crystal with its dipole moment. For surface alignment, a thin layer of e.g. polyimide, polyvinylamide, lecithin, or epoxy resin is applied by spin-coating or doctor blade method.<sup>261</sup>

### Photoalignment of Liquid Crystals

A very important method in the context of azobenzenes, is light-induced alignment. For example, azobenzene, when irradiated with light that triggers both *E*- and *Z*-isomerization, can switch rapidly between these two states. During these isomerizations, the molecule rotates on its own

axis. However, azobenzene only absorbs light that enters parallel to the longitudinal axis of the molecule. When linearly polarized light (LPL) is used, only azobenzene molecules that are not yet orthogonally aligned to the LPL can isomerize (Figure 5.6). This results in the accumulation of azobenzene molecules orthogonal to the LPL. This effect is called the Weigert effect.<sup>262–264</sup> When photoactive substances like azobenzene are mixed with other mesogens, a cooperative effect occurs, and the non-photoactive mesogens also align orthogonally to the LPL.<sup>265–267</sup>

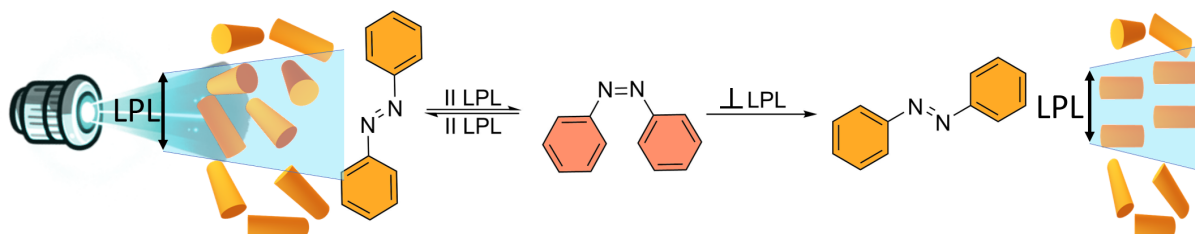


**Figure 5.6:** Schematic explanation of the Weigert effect utilized for photoalignment. The azobenzene is irradiated by linear polarized light (LPL) orthogonally to the desired final orientation. An LPL source that activates both isomerization (left) leads to the accumulation of the oriented azobenzene, which does not interfere with the LPL (right).

## 5.2 Liquid Crystalline Polymers

Liquid crystalline polymers (LCP) are liquid crystals that have been polymerized through functional groups. The glass transition determines whether it is a Liquid Crystal Network (LCN) or a Liquid Crystal Elastomer (LCE): If the glass transition temperature is above room temperature, the LCP is described as LCN. The glass transition temperature depends on a variety of factors, such as the degree of crosslinking, intermolecular interactions (like hydrogen bonding), and properties of the main chain. A typically less crosslinked liquid crystal polymer with a more flexible main chain can have a glass transition temperature below room temperature and is referred to as an LCE.<sup>268</sup>

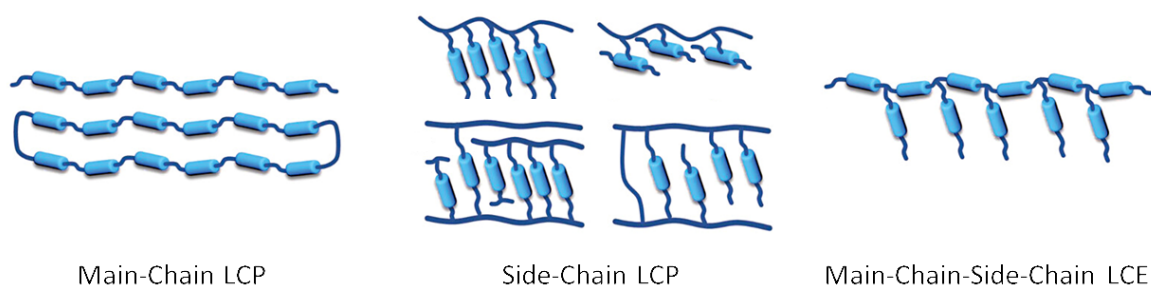


**Figure 5.7:** Visualization of the classification of the different LCP regarding their mesogen position when incorporated into a polymer. Adapted with permission.<sup>230</sup> © 2023 Wiley-VCH GmbH

LCPs are further divided into two additional groups that describe the position of the mesogens within the polymer. The first group is the main-chain LCP (MC-LCP), where the mesogens represent the main-chain backbone of the polymer and are first oligomerized through chain extenders and achieve in a second reaction step their functional strength through slight crosslinking (Figure 5.7). Most common reactions in the MC-LCP category involve the click reaction of

Aza-Michael and Thiol-Michael reaction (Figure 5.8), which are characterized by mild reaction conditions and high-conversion rates. The second group is the side-chain LCP (SC-LCP), which is further subdivided into end-on and side-on SC-LCP (Figure 5.7). This categorization considers the orientation of the mesogens in relation to the main chain. The most well-known reaction types are the polymerization of acrylates via radical initiators and the hydrosilylation of a polymethylhydrosiloxane with vinyl-functionalized liquid crystal using a Pt-catalyst (Figure 5.8). Notably, the main chain in the polymer dictates the final properties, even after the incorporation of mesogens into the side chain.<sup>269</sup>

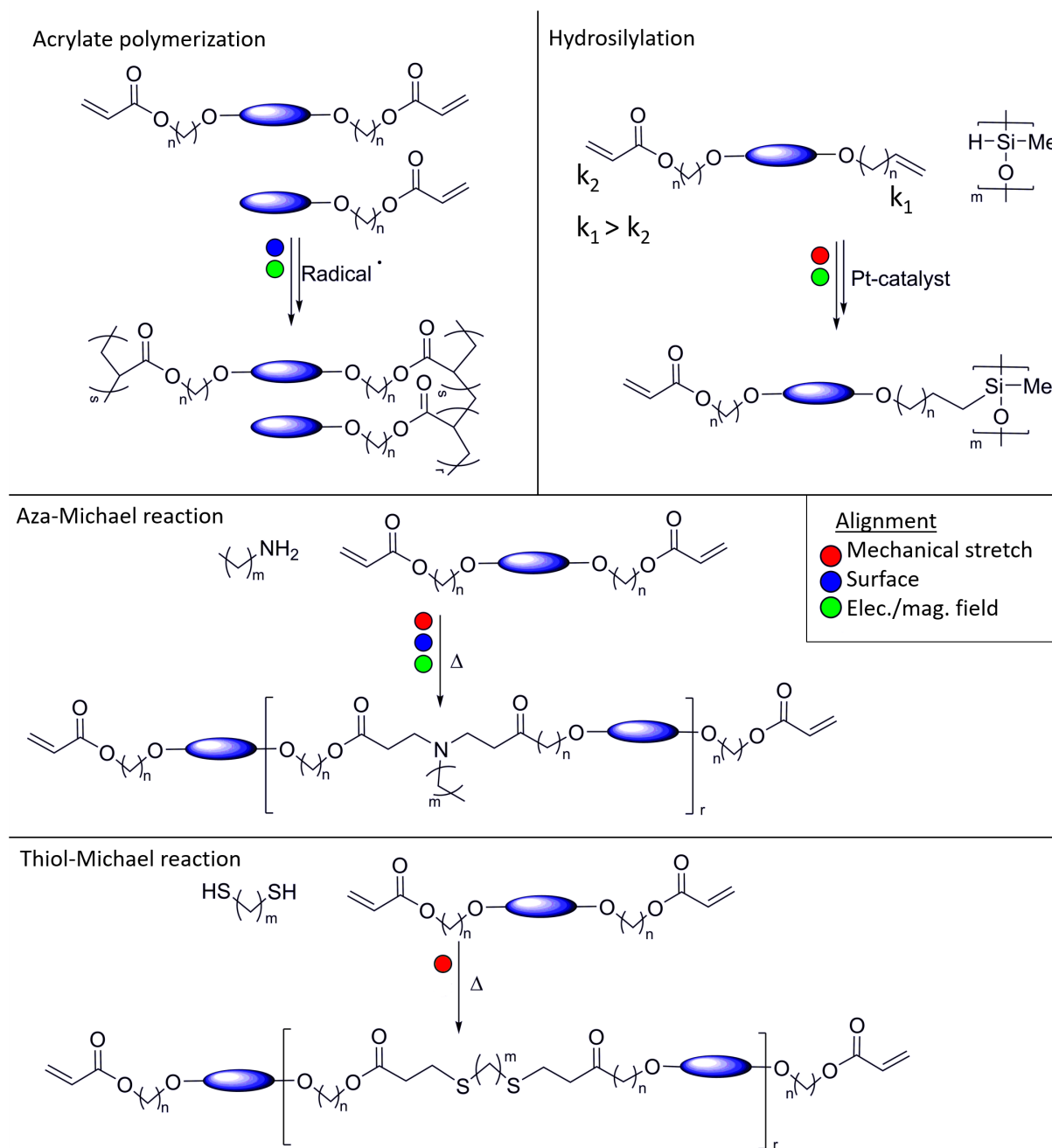


**Figure 5.8:** Schematic overview of regularly used polymerization reactions to produce LCP.<sup>257</sup>

### 5.2.1 Actuation of Liquid Crystalline Polymers

Some LCP are classified as a stimuli-responsive material or smart material. By applying a stimulus, the LCP undergoes changes on molecular level, which can be translated to macroscopic motion. If this motion is repeatable and controllable, we consider it an actuator. For the better utilization of LCP as an actuator, the mesogens need to be aligned to achieve a high degree of order. A fitting combination of external director for arranging the desired alignment and chemistry for keeping the induced alignment is necessary to obtain a liquid crystalline polymer actuator. There are two different approaches to fulfill this task. The first one is a complete polymerization after alignment and can be performed by surface and field assisted alignment, mostly with the acrylate based polymerization.<sup>270</sup> The second approach is based on a two-step system, where oligomerization leads to a still formable pre-polymer. This oligomer is aligned by mechanical or shear force and the final alignment fixed by a second functional group. Hydrosilylation, Aza-Michael and Thiol-Michael reactions are the most common examples for these methods, whereas an excess of acrylate groups fixes the stretched, aligned state by photopolymerization.<sup>257,271,272</sup> This approach is also known as the "Finkelmann Method".<sup>273,274</sup>

#### Thermoresponsive LCP

In a heat-mediated actuation, a shortening of the material is produced through the phase transition from the liquid crystalline phase to the isotropic phase (transparent) (Figure 5.9).

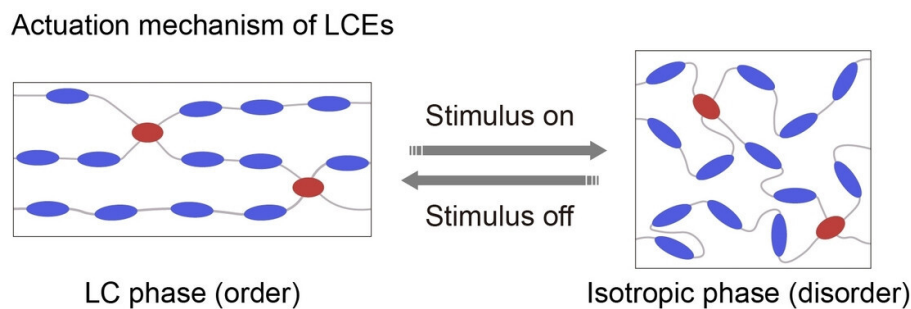


**Figure 5.9:** Schematic representation of the contraction through disorder of an LCE by the phase transition to the isotropic phase upon application of a stimulus. Reprinted with permission.<sup>257</sup> © 2023 Wiley-VCH GmbH

The entropy-driven motion arises from the disorder and entanglement of the mesogens. Upon cooling, the restoring force of the elastomer and the natural alignment of the mesogens in the liquid crystalline phase cause the material to expand and return to its original length. This process is reversible and allows for a change in length of up to a factor of four.<sup>269,275</sup> Since external heat supply is oftentimes impractical and imprecise in practice, many publications focus on internal heat sources. These range from graphene/LCE composites<sup>276,277</sup> and infrared receptors<sup>278,279</sup> to the extremely rapid isomerization of azobenzene to produce heat, but this is a fairly uncontrolled process.<sup>62</sup>

### Photoresponsive LCP

In a photoresponsive LCP, molecular switches that are also liquid crystals are either added or make up the material. The first successful combination was demonstrated in 2003 by T. Ikeda (Figure 5.10).<sup>43</sup> An azobenzene with long alkyloxy chains and acryl functionality was synthesized. It shows liquid crystallinity and was polymerized through the functional acryl group. The polydomain thin film bends upon irradiation with polarized UV-light and its straightening with green light, while heated up to 85 °C. Without polarized light all azobenzene molecules within the film isomerize and thus cancel out their macroscopic bending. This was the first time it was possible to induce a mechanical, macroscopic movement at the molecular level using light.<sup>43,280</sup>

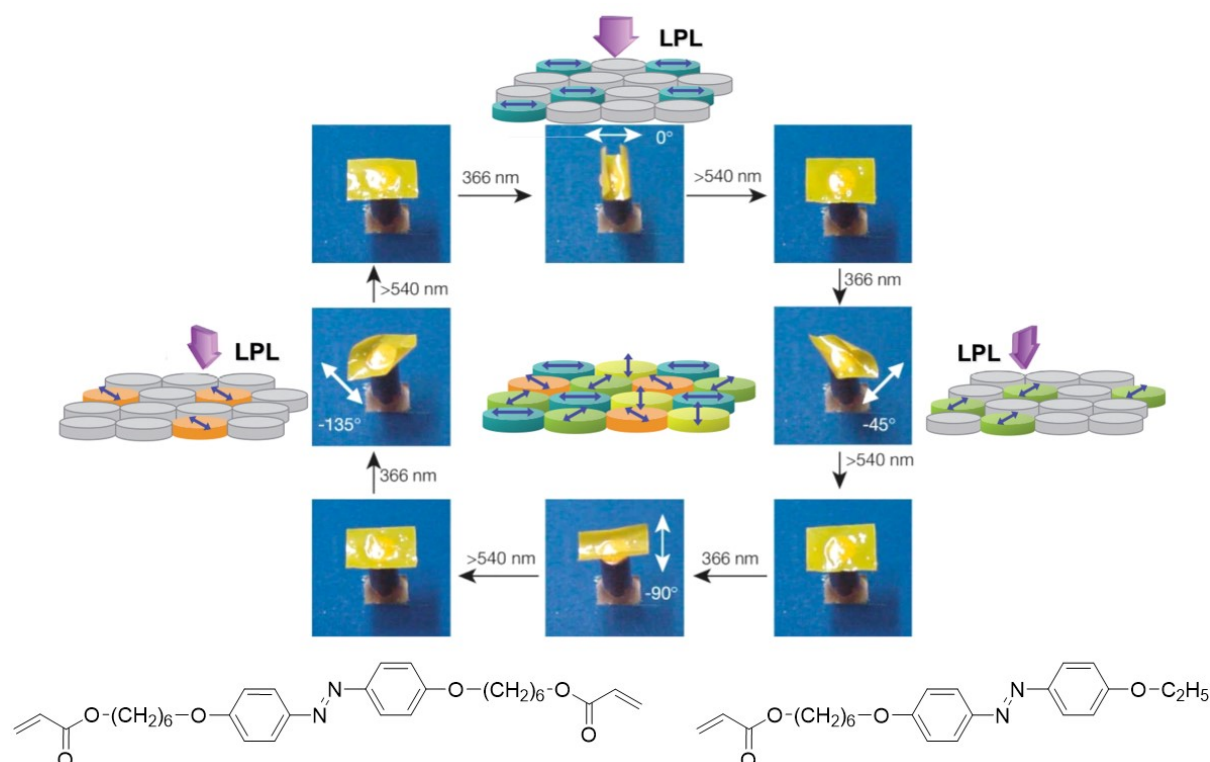


**Figure 5.10:** Polarized light induced bending based on polydomain azobenzene LCP with the azobenzene units used shown on the bottom. The illustration shows that only a fraction of the azobenzene in the polydomain LCP is addressed by the polarized light (compare Figure 5.6) to generate an aligned force. Adapted with permission from Y. Yu *et al.* and T. Ikeda *et al.*<sup>43,281</sup> © 2003 Springer-Nature and © 2011 Elsevier Ltd.

A stronger photomechanical bending without polarized light and at room temperature can be induced with aligned photoresponsive mesogens within the LCP. In this case all photomotifs can be addressed at the surface; the depth profile is dependent on the penetration of light. To achieve bending, the azobenzenes on the surface are isomerized ( $E \rightarrow Z$ ). Depending on the orientation of the mesogens, this leads to disorder and either contraction or expansion of the surface (Figure 5.11). A planar (horizontal) alignment results in contraction, while a homeotropic (vertical) alignment causes expansion. Since the molecules on the backside remain unaffected by the light, a bending of the material can be observed. This photochemical actuation is durable and can be maintained for the duration of the isomerization.<sup>267,282</sup>

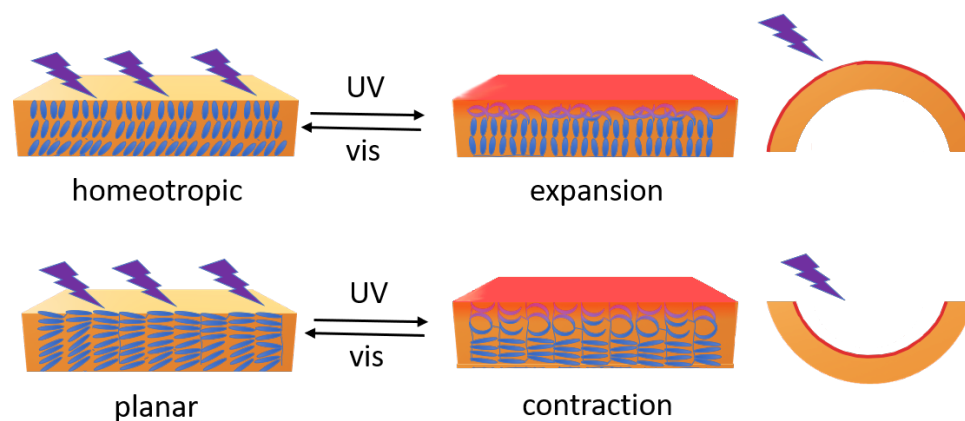


**Figure 5.11:** Photoinduced bending of a film in a homeotropic aligned (top) and a planar aligned film (bottom), while UV-light irradiates for the isomerization from the top. Triggered by the isomerization the irradiated surface expands or contracts depending on the previous programmed alignment.

In conclusion, if a photoresponsive LCP actuator is to be designed, the following parameters need to be considered:

- **Alignment:** Mesogen alignment determines the strength and the direction of the motion. Besides the homeotropic and planar orientation (see Figure 5.11), hybrid alignments such as hybrid aligned nematic (HAN) or twisted nematic (TN) are possible.<sup>283</sup>
- **Cross-linking density:** A higher cross-linking density can lead to a stronger actuation, but also increase stiffness, brittleness and higher glass transition temperature.<sup>284</sup>
- **Chemical composition:** The mixture of different ingredients in the monomer solution produces new liquid crystalline phases or even quenches them. The main-chain chemistry predominantly determines the glass transition of the resulting LCP.<sup>268,269</sup> Incorporation of chiral motifs induces bending out of plane.<sup>285</sup>
- **Photocatalyzed polymerization:** To prevent azobenzene isomerization during polymerization, careful selection of the photocatalyst is essential. Alternatively, a thermal radical initiator may be employed, though this approach may complicate alignment, typically achieved by cooling from the isotropic to the liquid crystalline phase. Such a strategy can significantly decrease the thermal half-life, potentially initiating polymerization prematurely.

The increasing number of new switchable molecules (see Introduction I) led scientists to transfer these new properties, such as long half-life or visible switching, to applications in LCP. For example, the  $\pi$ -system of azobenzene was expanded in an azotolane to enable switching with visible light.<sup>286</sup> Chiral centers were incorporated into the mesogens to induce a twisting motion during bending.<sup>195,285,287</sup> Furthermore, new molecular systems like diarylethene or hydrazone were designed as liquid crystals and successfully used in an LCE actuator.<sup>288–290</sup> These UV-light-driven actuators were highly stable in its bending due to the long half-life times. While *ortho*-fluorinated azobenzenes without liquid crystalline properties were copolymerized with commercial liquid crystals to generate oscillations with visible light,<sup>291</sup> another study observed a delayed bending that was highly stable (>8 d) but only actuated with UV-light.<sup>195</sup> In addition to the chemist's intuitive solution of adapting the molecule to its application, creative approaches for visible switching were pursued, using upconversion of light. With an additional layer of molecules



that upconvert long-wavelength light into short-wavelength light or incorporating upconverting nanoparticles (see Introduction I), the necessary UV-light for switching the molecules in the underlying material layer could be generated *in situ*, thus creating a bending.<sup>292,293</sup>

### Applications of Light-Driven LCP

The photomechanical bending in photoresponsive LCP can be used to design small actuators and small scaled robots for different applications in biological and medical sector in mind. There are examples for gripper, crawler and swimmer robots and artificial muscles or light driven motors. However, the examples remain in small-scale as the chemicals mostly needs to be synthesized and the manufacturing of LCP limits scaling. Furthermore, only photoreactive molecules on the surface are capable of absorbing short-wavelength UV-light, as the materials thickness absorbs the light, leading to bending rather than contraction of the material. This, however, limits the maximum thickness and generated force of a light-based actuator. However, these light-driven actuators justify their existence as the light can be induced in an untethered manner. With creative solutions and biological mimicry, as well as through the combination of various actuators, several applications have been demonstrated, four of them will be briefly presented.

**I)** A polymer nanocomposite was developed that reacts to both near-infrared (NIR) and UV-light by incorporating gold nanorods into a liquid-crystal polymer network.<sup>294</sup> This material can bend or stretch in response to light, thanks to two effects: A photochemical change of azobenzenes in the polymer and a heating effect from incorporated gold rods (Figure 5.12, **I**). This feature was used to create a polymer "crane" capable of complex, light-controlled movements like grasping and moving objects, showcasing the potential for advanced robotic motions.

**II)** In another demonstrator, a way to move small amounts of liquid using light was developed, which is useful in areas like biomedical devices (Figure 5.12, **II**).<sup>295</sup> This method overcomes previous challenges where liquid movement was hindered by the liquid sticking to surfaces. By photoresponsive compression of the shape of tiny tube-like actuators, forces were created that move the liquid. These actuators can be made in various shapes and can control the movement of different liquids over distances, with adjustable speed and direction, even causing liquids to mix or move uphill.

**III)** Utilizing a ribbon coated with LCE, Ikeda's research team successfully engineered a photomechanical motor (Figure 5.12, **III**).<sup>296</sup> This device employs a belt configuration encircling two pulleys of disparate diameters. Differential exposure to UV-light on one flank and visible light on the opposite induces sequential contraction and extension along the respective sides, thereby generating rotational motion in the pulley system.

**IV)** Inspired by the complex movements of living organisms, a synthetic soft robot capable of multidirectional movement and cargo handling under blue light illumination has been developed (Figure 5.12, **IV**).<sup>297</sup> This robot utilizes light-responsive liquid crystalline polymers, enabling precise control over its movements to perform advanced tasks in dry environments. Its legs (yellow, photochemical actuation) can achieves strides over 4 mm in any direction and navigating around obstacles, while its arms (red, photothermal actuation) facilitate untethered cargo pickup and release. This approach showcases the potential of combining actuator assemblies for complex, nature-inspired functionalities.

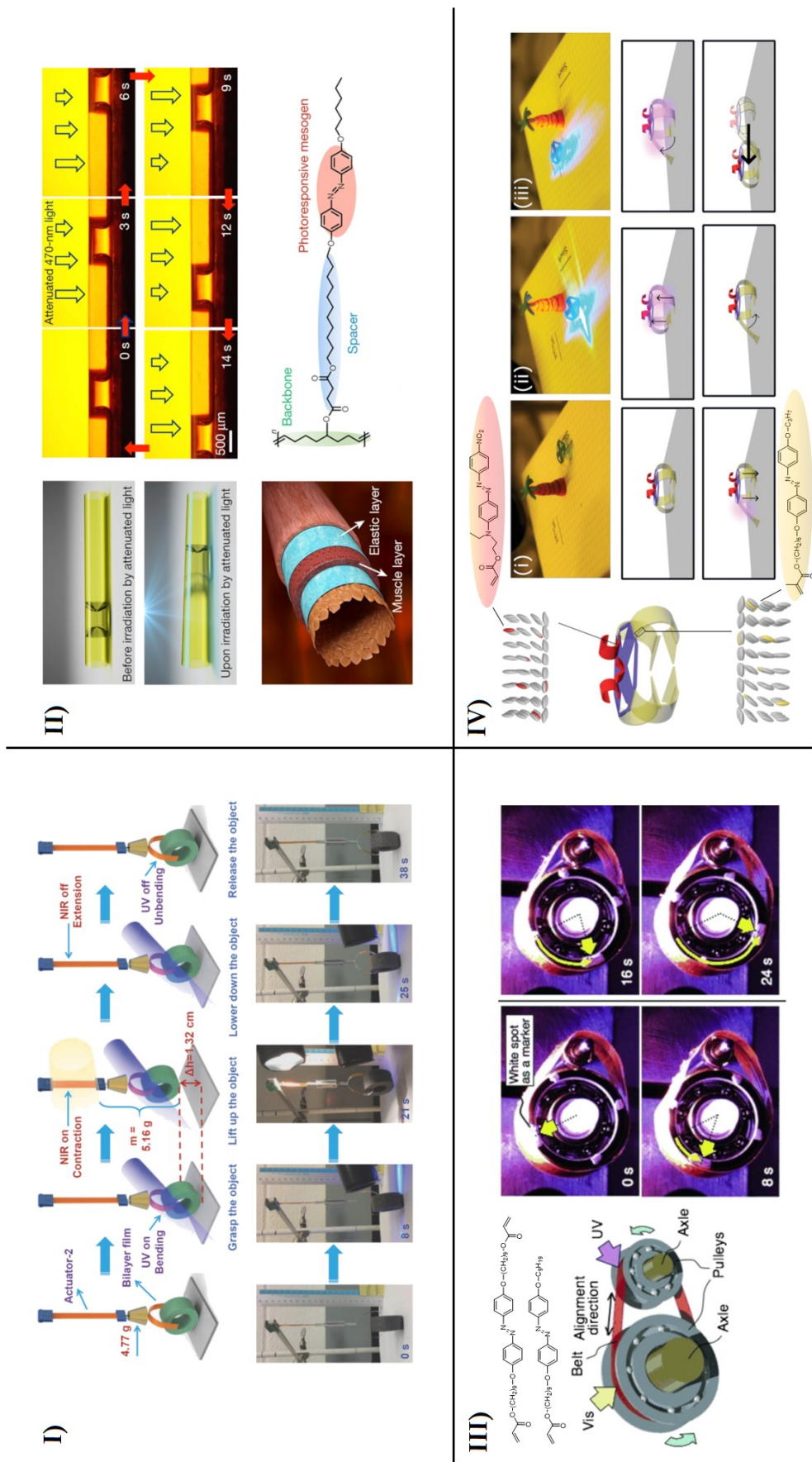


**Figure 5.12:** I) Photothermal and photochemical LCE actuator combined in a gripper robot to grasp and pull objects. Reprinted with permission from X. Lu *et al.*<sup>294</sup> © 2018 Wiley-VCH GmbH II) Photocontrolled artificial muscle by LCP microactuation. Reprinted with permission from J. Lv *et al.*<sup>295</sup> © 2016 Macmillan Publishers Limited, part of Springer Nature III) Light-driven motor based on azobenzene liquid crystal actuation. Adapted with permission from M. Yamada *et al.*<sup>296</sup> © 2008 Wiley-VCH GmbH IV) Dimodular light-driven soft transporter robot. The assembly and movement is based on four legs made of photobendable LCE actuators. Adapted with permission from P. Cunha *et al.*<sup>297</sup> © 2020 Wiley-VCH GmbH.



## Publication IV

### 6.1 A Photomechanical Film in which Liquid Crystal Design Shifts the Absorption into the Visible Light Range

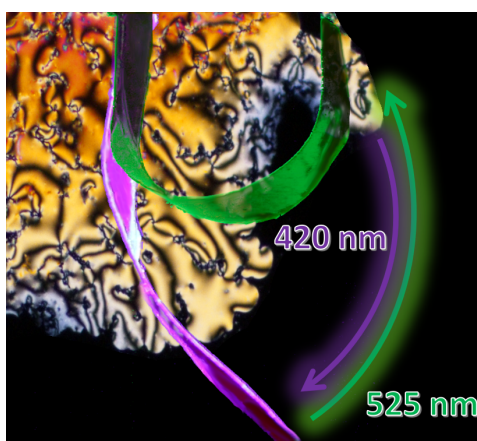
#### Aim:

To avoid the use of UV-light in the application of photochemical actuators, we turned to the repertoire of tetra-*ortho* substituted azobenzenes to shift the switching into the visible region of the absorption spectrum. However, with the tetra-*ortho*-fluorine substitution on azobenzene, the molecule lost its liquid crystalline properties when following the classic design. Therefore, a new synthetic and conceptual method was developed to regain the liquid crystallinity, which we considered essential for successful actuation in an LCP. Crucial to the strategy for this project was not only the switchability and prolonged half-life of the new molecule, but also overcoming the synthetic challenges involved in producing the monomer at scales suitable for polymers. We demonstrated that the use of different molecular switches, after adaptation to the molecular structure, is feasible and that liquid crystallinity is indispensable even in photoactive switching.

#### Title of Publication:

#### A Photomechanical Film in which Liquid Crystal Design Shifts the Absorption into the Visible Light Range

S. Schultze, N. Scheuring, P. Puylaert, M. Lehmann, A. Staubitz, *Adv. Sci.* **2023**, *10*, 2302692.  
Permission to reprint in Appendix 9.6.



**Abstract:**

Liquid crystalline polymer networks (LCN) with azobenzene monomers bend reversibly when irradiated with UV-light, combining photomechanical and photothermal effects. However, the harmful nature of UV-light limits their use in biology and soft robotics. Although visible light-absorbing tetra-*ortho*-fluoro-substituted azobenzenes exist, liquid crystalline monomers could never be prepared. Previously, azobenzenes were added as photoactive additives (up to 10%) to otherwise passive liquid crystalline polymer networks. We present a novel molecular design enabling synthesis of a polymerizable azobenzene compound with a liquid crystalline (nematic) phase and visible light absorption. Polymerization results in a smectic C phase, enabling visible light-induced film actuation. The films consist solely of the monomer without additional liquid crystalline components. Bending experiments in air and underwater differentiate photomechanical and photothermal effects. Remarkably, a 60  $\mu\text{m}$  splay aligned film maintains stable bending for hours, slowly reverting over days. Monomer liquid crystallinity was characterized using differential scanning calorimetry (DSC), wide-angle X-ray scattering (WAXS), and polarized optical microscopy (POM); polymer films were analyzed using WAXS and DSC on a homogeneously aligned film. The synthetic procedure yields high azobenzene monomer quantities; polymer film fabrication is scalable, which enables the use of safe and efficient photomechanical LCNs in soft robotics, engineering and biology.

**Abstract (deutsch):**

Flüssigkristalline Polymer-Netzwerke mit Azobenzol-Monomeren biegen sich reversibel, wenn sie mit UV-Licht bestrahlt werden, wobei sie photomechanische und photothermische Effekte kombinieren. Die schädliche Natur des UV-Lichts begrenzt jedoch ihren Einsatz in Biologie und weicher Robotik. Obwohl tetra-*ortho*-fluorsubstituierte Azobenzole, die sichtbares Licht absorbieren, existieren, konnten flüssigkristalline Monomere noch nicht hergestellt werden. Zuvor wurden Azobenzole als fotoaktive Zusätze (bis zu 10%) zu ansonsten passiven flüssigkristallinen Polymer-Netzwerken hinzugefügt. Wir präsentieren ein neues molekulares Design, das die Synthese einer polymerisierbaren Azobenzol-Verbindung mit einer flüssigkristallinen (nematischen) Phase und der Absorption von sichtbarem Licht realisiert. Die Polymerisation führt zu einer smektischen C-Phase, die eine Aktuierung des Films durch sichtbares Licht ermöglicht. Die Filme bestehen ausschließlich aus dem Monomer ohne zusätzliche flüssigkristalline Komponenten. Biege-Experimente in Luft und unter Wasser differenzieren photomechanische und photothermische Effekte. Bemerkenswert ist, dass ein 60  $\mu\text{m}$  dicker, splay-ausgerichteter Film für Stunden stabiles Biegen aufrechterhält und langsam über Tage relaxiert. Die Flüssigkristallinität des Monomers wurde mit Differentialkalorimetrie (DSC), Weitwinkel-Röntgenstreuung (WAXS) und polarisierter optischer Mikroskopie (POM) charakterisiert; Polymerfilme wurden mit WAXS und DSC an einem homogen ausgerichteten Film analysiert. Das synthetische Verfahren liefert hohe Mengen an Azobenzol-Monomeren; die Herstellung von Polymerfilmen ist skalierbar, was den Einsatz von sicheren und effizienten photomechanischen flüssigkristallinen Polymer-Netzwerken in der weichen Robotik, im Ingenieurwesen und in der Biologie ermöglicht.

**Author Contribution to this Publication:**

In this research article, I designed under initial project idea of A. Staubitz the new liquid crystal monomer. The syntheses, analysis, characteristics were performed and evaluated by me. POM analysis were performed by me under the guidance of N. Scheuring and M. Lehmann (University of Würzburg). WAXS measurements of the monomer and polymer were conducted and evaluated from N. Scheuring and M. Lehmann. P. Puylaert performed the X-Ray diffraction and refinement of the crystal structure. The supporting information and manuscript was written by me. Additional input in the manuscript was given in the subject of X-Ray analysis of liquid crystals by Lehmann. The ToC image was designed by me. All authors contributed in the reviewing process.

Supporting Information Videos can be accessed under: <https://doi.org/10.1002/advs.202302692>

# A Photomechanical Film in which Liquid Crystal Design Shifts the Absorption into the Visible Light Range

Sven Schultzke, Nikolai Scheuring, Pim Puylaert, Matthias Lehmann, and Anne Staubitz\*

Liquid crystalline polymer networks (LCN) with azobenzene monomers bend reversibly under UV-light irradiation, combining photomechanical and photothermal effects. However, the harmful nature of UV-light limits their use in biology and soft robotics. Although visible light-absorbing tetra-*ortho*-fluoro-substituted azobenzenes exist, liquid crystalline monomers have never been prepared. Previously, such azobenzenes were added as photoactive additives (up to 10%) to otherwise passive liquid crystalline polymer networks. In this work, a molecular design of a liquid crystalline, polymerizable azobenzene switchable by visible light is presented. The monomer assembles in a highly fluid nematic phase, but polymerizes in a layered smectic C phase. The films are produced solely from the monomer without additional liquid crystalline components and are actuated with visible light. Bending experiments in air and under water differentiate photomechanical and photothermal effects. Remarkably, a 60  $\mu\text{m}$  splay aligned film maintains its deformation for hours, slowly reverting over days. Monomer liquid crystallinity is characterized using differential scanning calorimetry (DSC), wide-angle X-ray scattering (WAXS), and polarized optical microscopy (POM); polymer films are analyzed using WAXS and DSC on a homogeneously aligned film. The synthetic procedure is high yielding and polymer film fabrication is scalable, which enables the use of safe and efficient photomechanical LCNs in soft robotics, engineering and biology.

performed with conventional rigid-bodied robots. Soft robots can often imitate the complex natural movements better<sup>[2]</sup> and may be superior in the context of our human environment,<sup>[3]</sup> providing gripping,<sup>[4]</sup> locomotion,<sup>[5]</sup> artificial muscles,<sup>[1]</sup> or oscillation.<sup>[6]</sup>

To achieve this ambitious goal, at present the most often used actuation design is using soft, but non-functional materials, which are then moved pneumatically or hydraulically.<sup>[7]</sup> Such solutions typically require that the robot is tethered to an air or liquid supply. A more intuitive approach is using an intrinsically functional movable material, for which bioinspired designs are becoming increasingly attractive.<sup>[8]</sup> Such stimuli-responsive materials can be actuated by changes in their environment.<sup>[9]</sup> A specific subgroup of these materials comprises photoresponsive polymer films, which incorporate light-sensitive molecules into their structure. When illuminated, these films undergo a noticeable macroscopic deformation.<sup>[10]</sup> However, the reverse movement can be difficult to control. This controlled reversibility is crucial for maintaining precise control over an

actuation that enables repetitive movements or movements that are controlled in their direction and amplitude as would be required for a robot. This means that the desideratum for a photoreponsive film is that actuation in both directions is controlled by defined wavelengths of illumination and little uncontrolled thermal actuation.

## 1. Introduction


In soft robotics, soft materials are used, which allow for new actuation principles, or different types of grippers or movement compared to those that can be achieved with hard components only.<sup>[1]</sup> This greatly expands the number of tasks that can be

S. Schultzke, A. Staubitz  
 University of Bremen  
 Institute for Analytical and Organic Chemistry  
 Leobener Straße 7, D-28359 Bremen, Germany  
 E-mail: staubitz@uni-bremen.de

S. Schultzke, A. Staubitz  
 University of Bremen  
 MAPEX Center for Materials and Processes  
 Bibliothekstraße 1, D-28359 Bremen, Germany

N. Scheuring, M. Lehmann  
 University of Würzburg  
 Institute of Organic Chemistry  
 Am Hubland  
 D-97074 Würzburg, Germany

P. Puylaert  
 University of Bremen  
 Institute for Inorganic Chemistry and Crystallography  
 Leobener Straße 7, D-28359- Bremen, Germany

 The ORCID identification number(s) for the author(s) of this article can be found under <https://doi.org/10.1002/advs.202302692>

© 2023 The Authors. Advanced Science published by Wiley-VCH GmbH. This is an open access article under the terms of the Creative Commons Attribution License, which permits use, distribution and reproduction in any medium, provided the original work is properly cited.

DOI: 10.1002/advs.202302692



For such a reversible photo response, the most investigated molecular switch is azobenzene and its derivatives.<sup>[11]</sup> Upon irradiation with light, azobenzene undergoes a *E*- to *Z*-isomerization resulting in a geometrical change: The distance between the carbon atoms at the *para*-position is 9 Å in the planar, thermally stable *E*-isomer and is reduced to 5.5 Å in its non-planar, metastable *Z*-isomer.<sup>[12]</sup> By incorporating azobenzenes as mesogens of liquid crystals and attaching polymerizable, flexible linkers, it is possible to prepare light-switchable liquid crystalline elastomers or the more densely cross-linked liquid crystalline polymer networks (LCNs) from these monomers.<sup>[13]</sup>

In photoswitchable LCNs, combination of light-induced processes leads to a macroscopically observable bending effect, although the precise underlying mechanisms are still a subject of debate:

All mechanisms are based on the fact that the polymer films are highly anisotropic in their morphology, irrespective of which alignment of the mesogens is present. In addition, they all take into account that the light illuminates the film from one side and that the extent of the photoreaction of the azobenzenes depends on a) their alignment with respect to the incident light; b) the penetration depth of the light, i.e., into what depth of the film does isomerization take place. However, the matter is complicated by the fact that the illumination of azobenzenes may lead to a substantial heating of the polymer film, because first, not all azobenzene molecules isomerize, but some will merely follow a vibrational relaxation and second, even the azobenzenes that do isomerize can thermally relax to the *E*-isomer. Furthermore, as there are no azobenzene monomers LCs, in which the spectra of the *E* and *Z* isomers are fully separated, in all cases under constant illumination, a photostationary state (PSS) will be reached that continues to produce heat. Heating polymers leads to changes in volume and modulus (among other parameters) and thus separating different effects is not always possible.

The first and most simple mechanism considers the substantial geometry change of the azobenzenes upon photoisomerization.<sup>[14]</sup> If the azobenzenes are parallel to the plane of the film (homogeneous alignment), then the isomerization of the first few layers of azobenzene will give rise to a shortening and thickening of these layers, causing overall contraction and bending toward the light source. Conversely, in azobenzenes arranged perpendicularly to the plane of the film (homeotropic), the isomerization will cause a sidewise expansion, leading to a bending away from the light. In this way, a molecular movement is translated to a macroscopically observable movement.

However, later experiments suggested that the mechanism might be more complex:<sup>[15]</sup> the basic hypothesis that the geometrical change leads to a change in volume (or density) in the illuminated layers still holds. However, not only is the *E* to *Z* isomerization thought to increase the volume, but also the reverse, *Z* to *E* isomerization. This takes into account that not only do the isomers themselves have different spatial requirements (a thermodynamic point), but also the molecular movement itself requires space (a kinetic point). This work argues that the thermal expansion (a photothermal effect) as a result of heating by the thermal relaxation of the *Z*-isomer would be insufficient to explain their results. This is also borne out by earlier work,<sup>[16]</sup> in which the thermal expansion for thin (15 μm) azobenzene doped films (2–20%) was measured by conventional heating rather than pho-

tothermal heating and comparing the obtained values. Although the polymer did heat up to ca. 60 °C, (with a very high illumination power (1 W cm<sup>-2</sup>)), thermal expansion alone could not explain the results.

An ingenious setup to separate the two effects (photothermal and photomechanical) was proposed by Finkelmann and co-workers.<sup>[17]</sup> They used a set-up to measure the mechanical stress as a function of irradiation or non-irradiation (i. e. darkness) for samples in which the azobenzene was part of the cross-linker and for others, in which it was pendant. By using an IR filter to remove any irradiative thermal heating they could quantify and separate a quite substantial thermal contribution to the stress in the film. Moreover, they concluded that the most relevant parameter for strong actuation is cross-linking the azobenzene into the LCN rather than using it as a side chain, which led to less actuation.

Another technique that is often used to separate the photothermal from the photomechanical effect is to perform the bending experiments under water, because water can serve as a heat sink. However, the interactions between water and LCNs are complex and because not all reports include these measurements under consideration of all potential experimental parameters, our understanding of the detailed effects of water or other media is still only rudimentary.<sup>[18]</sup> In this context, the emergence of photo-switchable liquid crystalline hydrogels is worth mentioning, which are materials specifically adapted to underwater actuation with soft materials.<sup>[19]</sup>

Irrespective of whether a photomechanical and / or photothermal effect is the most important for a light-bendable polymer film, an intriguing question remained of how this macroscopic movement of azobenzene LCNs could occur below the glass transition temperature. This was addressed by an IR spectroscopic study that was able to prove that on the molecular level that the effective temperature could reach well beyond 200 °C, while the material in bulk stayed much cooler.<sup>[20]</sup> This heating was highly heterogeneous and led to the postulate that essentially, this local photothermal effect may be disguised as an order-disorder effect or geometrical effect in experiments that observe purely macroscopical parameters. Photosoftening that is not merely a simple thermal effect was also experimentally shown by nanoindentation experiments.<sup>[21]</sup> Importantly, whatever the mechanisms in the particular examples are, the materials bend upon irradiation with light.<sup>[22]</sup>

In addition to these different mechanisms, there is substantial variety in film fabrication, leading to different geometries, in particular film thicknesses and different morphologies. In general, twisted nematic (TN) or splay arrangements have been shown to generate the highest bending effect.<sup>[23]</sup> Film thicknesses vary greatly between 2<sup>[24]</sup> and 48 μm,<sup>[25]</sup> but thicknesses ≈20 to 30 μm are most common.<sup>[26]</sup> This is a limitation, because although thinner films bend more easily, they are more fragile and less useful in actuators.

For photomechanical polymers, certain basic robotic movements have been described.<sup>[26a,27]</sup> However, the photo sensitive molecules used in this first generation of smart material require harmful UV-light or blue light (blue light can also be harmful for organisms. See for example ref. [28, 29]) for their activation (360 – 440 nm).<sup>[30]</sup> Avoiding the necessity of UV-light for actuation is a required step if one wishes to use this material for a broader

range of applications especially at the interface of robots and living beings. In addition, two technical aspects favor visible light as a desirable stimulus: First, the depth of penetration for longer wavelengths is significantly larger: This parameter is influenced by the absorption coefficient and the scattering of the light. In general, for shorter wavelengths, more scattering occurs compared to Vis or NIR light, resulting in less penetration depth.<sup>[31]</sup> Second, linearly polarized light (LPL) can be generated by using linear polarizer, which is more accessible in the visible range<sup>[32,33]</sup> and enables photoalignment (Weigert effect).<sup>[34]</sup> In combination with the deeper penetration depth of visible light, higher photomechanical and photoalignment effects might be observed. Despite these compelling advantages and recent reports<sup>[32c-f]</sup> of photoactive molecules that do switch with visible light, the number of photomechanical materials based on such compounds is low: One attempt was to use tetra-*ortho*-fluorinated azobenzene derivatives, which are known for their absorbance in the visible range.<sup>[32c,35]</sup> However, upon incorporation of these molecules into a polymer, the photomechanical effect vanished.<sup>[36]</sup> The problem was the loss of liquid-crystallinity in the solid. A way to circumvent this problem has been to use tetra-*ortho*-fluorinated azobenzenes merely as co-monomers with loadings of up to 10%.<sup>[36,37]</sup> In this way, the liquid crystallinity of the LCN is imparted by a conventional LCN mixture, whereas the photoactivity in the visible range can be attributed to photoswitching of the azobenzene. Other successful attempts to move the absorption of switchable LCNs into the visible range have been described. A thin film of a thickness of 12  $\mu\text{m}$  with incorporated azotolane moieties was also switchable with visible light. While the bending motion (436 nm) was achieved within a few seconds, the unbending motion with light  $>577$  nm was only after a few minutes without being able to fix the geometry for a longer time.<sup>[38]</sup> Further work in this area led to bending with even longer wavelengths using upconversion.<sup>[26c,39]</sup> However, this approach necessitated a bilayer configuration, in which the controlled unbending had to be sacrificed.

In this work, we present a significant advancement by introducing a novel approach to the design of visible light switchable monomers for photomechanical liquid crystalline networks (LCNs). Our innovation lies in the reintroduction of liquid crystallinity to a tetra-*ortho*-fluorinated azobenzene monomer. Unlike previous methods, our newly designed molecule possesses both liquid crystalline properties and the ability to undergo switching with visible light. Notably, this monomer can be polymerized within a liquid crystal cell (LC) without the need for passive liquid crystalline phase forming co-monomers, which typically limit azobenzene concentrations below 10%. The resulting films exhibit a remarkable reversible bending movement on a macroscopic scale. Because of the actuation wavelength of 425 nm, absorption and scattering of this light in water is low and thus, underwater actuation is also possible.

## 2. Liquid Crystal Design of *Ortho*-Fluorinated Azobenzene

In order to create an intrinsically liquid crystalline monomer capable of absorbing within the visible range of the spectrum, several design principles were taken into account for this study.

First, it was crucial to ensure a high selectivity for each photostationary state by maximizing the separation of the absorption bands ( $\pi \rightarrow \pi^*$  and/or  $n \rightarrow \pi^*$ -absorption) of the two isomers.

Second, the metastable isomer's half-life time needed to be as long as possible to ensure reliable actuation without the occurrence of uncontrollable thermal relaxation reactions. Ideally, all actuation should be photomechanical rather than photothermal. Before polymerization, the monomers were to be aligned in a hybrid aligned nematic (HAN) cell to enable a subsequent anisotropic bending.<sup>[40]</sup>

Therefore, the design of a photomechanical LCN requires a molecule, which is reversibly switchable with visible light; which has a long thermal half-life time; which is a liquid crystal, and which also contains polymerizable units. This has been attempted previously using monomers based on the tetra-*ortho*-fluorinated azobenzene, no formation of LC phases with the pure monomer were reported<sup>[37a,c]</sup>

Previous investigations on fluorinated terphenyl systems with similar structural characteristics to our target molecule have demonstrated the presence of nematic phases.<sup>[41]</sup> The elongation of the azobenzene core with a benzoic acid ester motif has also been used before in an LC monomer designed for polymerization.<sup>[42]</sup> Because of the lack of fluorine atoms, this LC does not switch with visible light, but with 365 nm. This monomer mixture shows a smectic C' ( $\text{SmC}'$ ) and SmC phase, which can be polymerized into a  $\text{SmC}'$  or rectangular columnal phases.

These reports encouraged us to combine tetra-*ortho*-fluorinated azobenzenes with a benzoic acid ester motif, reintroducing liquid crystallinity by expanding the rigid core along with a polymerizable acrylate linked by a long aliphatic spacer (**Figure 1**).

### 2.1. Synthetic Strategy

The synthesis process (**Scheme 1**) followed a highly efficient convergent strategy utilizing two large fragments (**2** and **4**). Building block **2** was easily obtained with an overall yield of 54% through standard transformations (for detailed information, see Supporting Information). Initially, the coupling fragment containing the azobenzene was envisioned as a di-carboxylic acid. However, a conventional Steglich esterification yielded the target molecule **5** with only a 20% yield. Consequently, we synthesized the more reactive di-acyl chloride azobenzene derivative. The crucial convergent step involved joining both fragments through an esterification reaction, resulting in the formation of monomer **5** with a yield of 77%.

### 2.2. Switching Properties

The switching properties were analyzed using UV-analysis in combination with NMR spectroscopy to quantify the *E* / *Z* ratios of the photostationary states (PSS). Compound **5** was irradiated with different wavelengths (420 nm (33 mW  $\text{cm}^{-2}$ ), 490 nm (28 mW  $\text{cm}^{-2}$ ), 525 nm (20 mW  $\text{cm}^{-2}$ ), 565 nm (21 mW  $\text{cm}^{-2}$ ) for one minute for the UV-vis spectroscopic study and five minutes for the NMR spectroscopic study (**Figure 2**, further information in the Supporting Information).

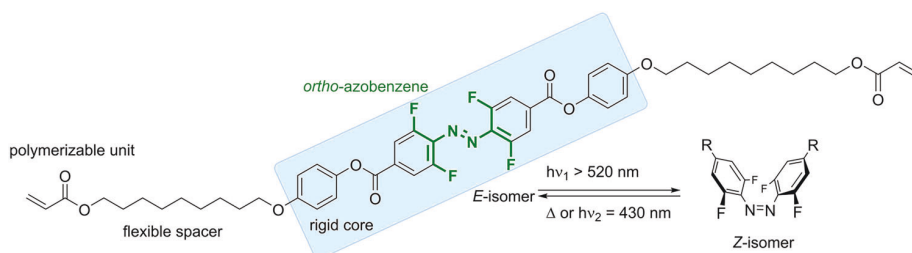


**Figure 1.** Design of an azobenzene switchable with visible light and being a liquid crystal.

The required irradiation times for achieving the respective (PSS) were dependent on the sample concentration and the intensity of irradiation. The UV spectra exhibited well-separated  $n \rightarrow \pi^*$  absorption bands ( $\Delta = 49$  nm) due to the combined influence of fluorine atoms and the electron-withdrawing effect of the *para*-positioned phenyl benzoate motif.<sup>[32c]</sup> The  $\pi \rightarrow \pi^*$  transition of the Z-isomer was observed at a wavelength of 316 nm in cyclohexane (315 nm in chloroform), while the  $n \rightarrow \pi^*$  transition reached a maximum of 471 nm in cyclohexane (482 nm in chloroform). Regarding the Z-isomer, the  $n \rightarrow \pi^*$  transition took place at 422 nm in cyclohexane (421 nm in chloroform), but the  $\pi \rightarrow \pi^*$  transition overlapped with that of the E-isomer. The E-isomer's  $n \rightarrow \pi^*$  transition could be induced using green light ( $< 525$  nm) to isomerize the tetra-*ortho*-fluorinated azobenzene monomer **5** into its Z-isomer (70% yield, maximum  $n \rightarrow \pi^*$  absorption at 421 nm). Subsequently, violet light (420 nm) facilitated the transformation of the molecules back to the E-isomer (93% yield, maximum  $n \rightarrow \pi^*$  absorption at 470 nm).

The *E/Z* ratios of the photostationary states in  $\text{CDCl}_3$  and benzene- $d_6$  were determined through complementary NMR spectroscopic analysis (see **Table 1**, Figure 2). Upon irradiation with green light, the proton signals of the aromatic ring (designated as  $H_1$ ,  $H_2$ , and  $H_3$ ) exhibited highfield shifts, indicating the formation of the metastable Z-isomer of compound **5**. Green light irradiation at a wavelength of 525 nm resulted in the highest enrichment of the Z-isomer (70%), whereas violet light at 420 nm led to the highest enrichment of the E-isomer (93%). The *E/Z* ratio and the UV-vis spectra were largely independent of the solvent.

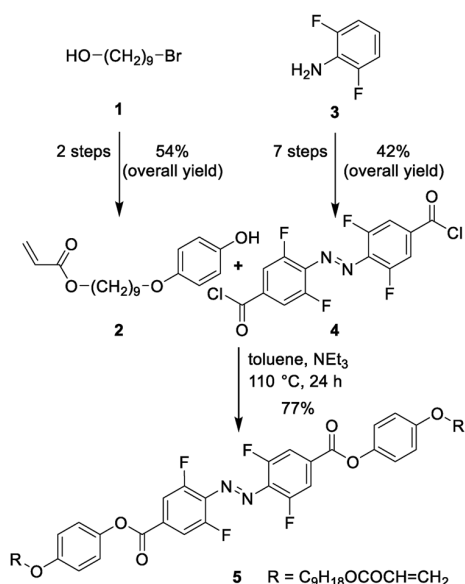
The thermal half-life time ( $t_{1/2}$ ) of Z-**5** was determined by UV-vis spectroscopy to be 49 d (25 °C, toluene). This value is in accordance with a similar azobenzene in the literature: (diethyl 4,4'-(diazene-1,2-diyl)-bis(3,5-difluorobenzoate):  $t_{1/2}$  (60 °C, MeCN): 14 h, **5**:  $t_{1/2}$  (60 °C, toluene) = 12 h. (Figure S3, Supporting Information).<sup>[35]</sup>

### 2.3. Liquid Crystal Analysis

The thermotropic properties of **5** were studied by means of polarization optical microscopy (POM), differential scanning calorimetry (DSC) and a wide-angle X-ray scattering (WAXS). The DSC heating scan of **5**, in the range of  $-20$  °C to  $170$  °C at a scan rate of  $5$  K  $\text{min}^{-1}$ , showed a large endothermic phase transition at  $119.8$  °C with a large transition enthalpy of  $99.1$  kJ  $\text{mol}^{-1}$ , which can be attributed to the melting of the material (**Figure 3A**). At  $152.3$  °C a second phase transition occurred with a transition enthalpy of only  $0.1$  kJ  $\text{mol}^{-1}$ . This indicates the existence of a liquid-crystalline phase of low positional order. The cooling scan revealed a similar phase transition at  $152.5$  °C, i.e., no hysteresis was observed. The liquid crystal can be subsequently supercooled and recrystallized at  $100.9$  °C. Thus, a typical hysteresis of  $\approx 20$  °C is determined for the melting.

The POM analysis yielded further insight into the nature of the liquid-crystalline phase. Compound **5** reveals a highly fluid phase with a characteristic Schlieren texture. This points to a nematic order in the LC phase (**Figure 3A**).

To achieve a uniform self-assembly of the mesogens, the sample was allowed to equilibrate at  $130$  °C in the dark for 60 min. This treatment resulted in a homeotropic alignment. Subsequent conoscopy confirmed the uniaxial, optically positive nature of the nematic liquid crystal (**Figure 4B**). Mechanical shearing of the homeotropic texture caused strong birefringence originating from the induced planar alignment of the molecules (**Figure 3B**). However, the homeotropic alignment was rapidly



**Scheme 1.** Key steps of the synthesis of (*E*)-4,4'-(diazene-1,2-diyl)bis(3,5-difluorobenzoic acid) (**5**) via the di-acyl chloride as reactive intermediate. Compound **4** was synthesized in 7 steps starting with 2,6-difluoroaniline (**3**). The second building block **2** was prepared over two steps from 9-bromonan-1-ol (**1**). Details see Supporting Information.

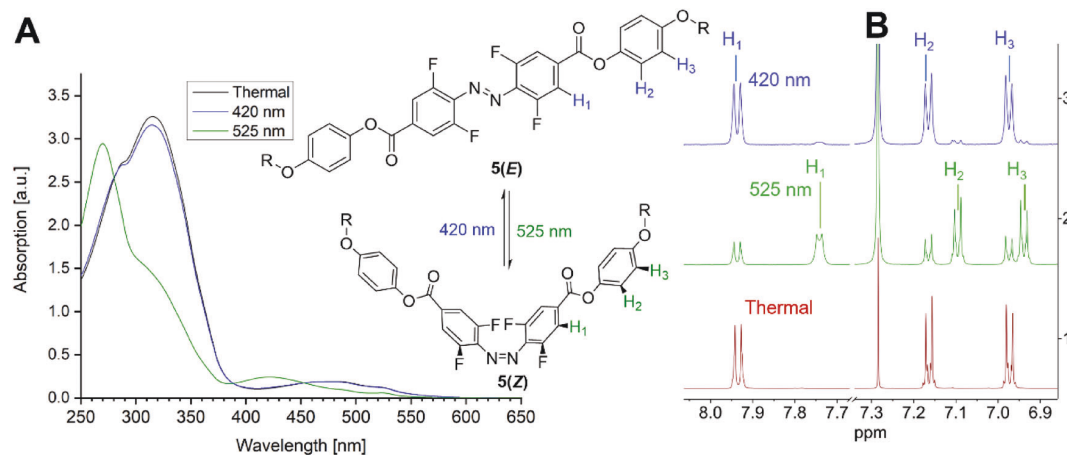


**Figure 2.** A) Switching properties of **5** determined by UV-vis spectroscopy in  $\text{CHCl}_3$  (conc. =  $0.16 \mu\text{L mol}^{-1}$ ). B) The quantification of the switching determined via  $^1\text{H}$  NMR spectroscopy in  $\text{CDCl}_3$  (conc. =  $0.28 \mu\text{L mol}^{-1}$ ).

**Table 1.** Amount of *E* and *Z* isomers in the PSS determined by NMR spectroscopy after irradiation of *E*-**5** with different wavelengths in the solvents chloroform-*d* (conc. =  $0.28 \mu\text{L mol}^{-1}$ ) and benzene-*d*<sub>6</sub> (conc. =  $0.26 \mu\text{L mol}^{-1}$ ).

	Chloroform- <i>d</i>		Benzene- <i>d</i> <sub>6</sub>	
	<i>E</i> - <b>5</b>	<i>Z</i> - <b>5</b>	<i>E</i> - <b>5</b>	<i>Z</i> - <b>5</b>
Thermal	100%	0%	100%	0%
420 nm	93%	7%	92%	8%
490 nm	53%	47%	57%	43%
525 nm	30%	70%	30%	70%
565 nm	39%	61%	35%	65%

restored (Figure 3C). In an indium tin oxide (ITO) coated cell with planar alignment layers, a planar alignment of **5** could be enforced. Rotating the sample out of the plane ( $45^\circ$ ) of the crossed analyzer/polarizer position, resulted in the highest birefringence (Figure 4C).

WAXS studies were performed in the liquid crystal phase at  $148^\circ\text{C}$  using ring magnets (1 Tesla) to induce uniform alignment (Figure 5). Only two broad signals could be observed at small and wide angles respectively, which correspond to distances of

$50.3$  and  $4.5 \text{ \AA}$ . The pattern showed that the molecular long axes are aligned with the magnetic field, which is reasonable since the diamagnetic ring current of the aromatic rings are turned out of the field, minimizing the energy of the system. The correlation lengths were calculated by the Scherer formula<sup>[43]</sup> based on the full-width-at-half-maximum of the X-ray signals and amount to  $2.8$  molecular lengths for the small angle and  $6.5$  for the wide angle signal. These values are indicative of a short range positional order like in a nematic phase. Consequently, along the director, the material has a liquid like correlation, which increases slightly in the transverse assembly. The XRS distance can be attributed to the molecular length, which is  $53.5 \text{ \AA}$  for a model of a fully extended calamitic mesogen **5** and  $4.5 \text{ \AA}$  for the average molecular breadth. Thus, the data are in full agreement with an optically positive nematic phase.

The wide-angle X-ray scattering (WAXS) data may also indicate the possibility of a SmA (smectic A) phase. The SmA phase is the second lowest ordered liquid crystal (LC) phase following the nematic phase. Optically, the SmA phase exhibits positive birefringence for rod-shaped mesogens, resulting in conoscopic images similar to those observed in a homeotropically aligned nematic phase. It is expected to align in a magnetic field in a manner identical to the nematic phase. The transition enthalpy associated with the SmA phase is also very small. However, it is worth

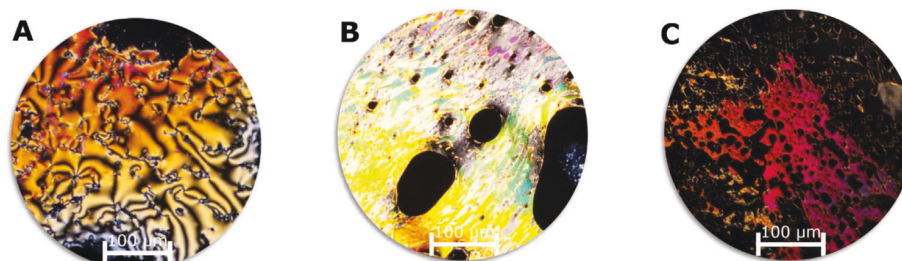


**Figure 3.** A) POM image of **5** at  $130^\circ\text{C}$  between two glass slides showing nematic Schlieren textures. B) Strong birefringence of **5** after mechanical shearing of the homeotropic aligned phase (completely black domain; not shown) C) After the mechanical shearing the homeotropic alignment restores within a few seconds. The image shows the fading out of the strong birefringence. All images were taken through crossed polarizer.

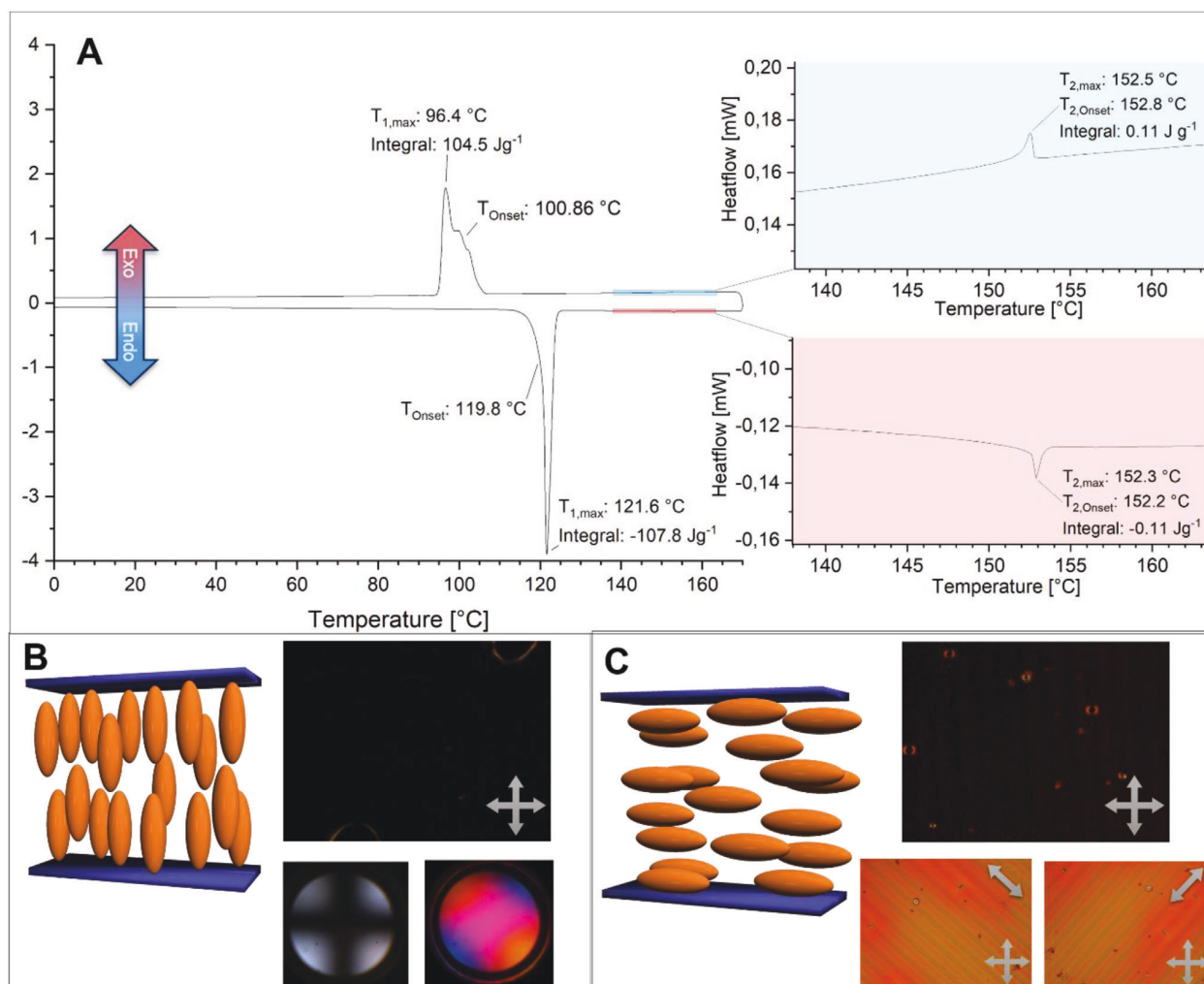


**Figure 4.** A) The DSC shows the first cycle ( $5 \text{ K min}^{-1}$ ,  $6.0481 \text{ mg}$ ) in the temperature range  $-40 \text{ }^{\circ}\text{C}$  to  $170 \text{ }^{\circ}\text{C}$  after annealing the sample at  $120 \text{ }^{\circ}\text{C}$  for one hour in an isothermal program to ensure full *E*-isomerization. B) The image is taken from the POM at  $130 \text{ }^{\circ}\text{C}$  after annealing the sample without light irradiation. The molecule showed a spontaneous homeotropic alignment between two glass slides. Consocopy confirmed the uniaxial, optically positive nature of the phase. C) Between an ITO coated glass slide with planar alignment layers, a planar alignment could be enforced. The sample was turned by  $45^{\circ}$  relative to the polarizers to show the highest birefringence and thus the alignment of the nematic director.

noting that Schlieren texture, a characteristic feature, is not reported for SmA phases; instead, it is observed in SmC phases or nematic phases. Considering the WAXS data and the uniaxial nature of the phase, which is inconsistent with a SmC phase, the most plausible option is a nematic phase. Furthermore, the relatively large full-width-at-half-maximum indicates a very small correlation length, resembling that of a liquid. In particular, for this molecule, the correlation length associated with its long axis is short.

When the nematic phase at  $130 \text{ }^{\circ}\text{C}$  was irradiated with light of  $525 \text{ nm}$  under the POM, to switch the molecule into the *Z*-isomer, the birefringence was lost; the *Z*-enriched sample was isotropic at this temperature. After turning off the light source, colorful sparkles appeared, which we assign to events of thermal relaxation of the *Z*-isomer to the *E*-isomer leading to the immediate reorientation of **5** (Figure 6).

#### 2.4. Single Crystal X-Ray Diffraction

In addition to the liquid crystalline properties of **5**, it was desirable to understand the structure in the crystal on a molecular level. Unfortunately, it was impossible to grow single crystals of **5**; therefore, a structurally similar molecule, **6**, was prepared. In this molecule, the flexible chain length was shortened which facilitated the growth of single crystals and no acrylate groups were present (For the synthetic details see the Supporting Information). This derivative **6** proved to be liquid-crystalline as well with similar properties to **5** (melting transition at  $99 \text{ }^{\circ}\text{C}$ , nematic to isotropic transition at  $240 \text{ }^{\circ}\text{C}$ , for details see the Supporting Information). Given that the rigid part of compound **6** is identical to that of compound **5**, the crystal structure of compound **6** serves as a suitable model for assessing the intermolecular interactions of monomer **5**.

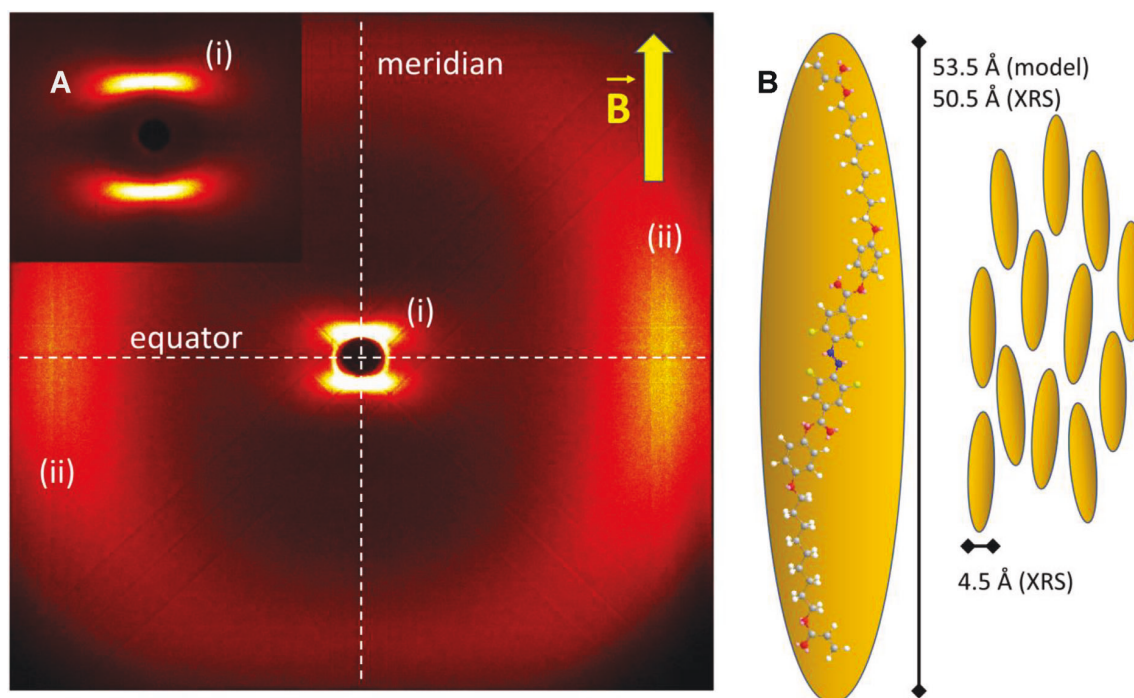


**Figure 5.** A) WAXS pattern recorded in the liquid crystal phase of compound **5** at 148 °C. The liquid crystal was aligned in the magnetic field (yellow arrow). The small angle signals i) are aligned with the meridian and the wide-angle signals ii) with the equator. Inset: Signals at small angles recorded at a larger sample-detector distance in order to avoid the influence of the beam stop. This demonstrates the quality of the alignment. B) The molecular long axis is aligned parallel with the magnetic field. The XRS length is in good agreement with the length of the fully extended mesogen.

The geometry for the parent azobenzene is planar with a N=N bond length of 1.242 Å, a N=N bond geometry of 180° (C-N=N-C  $\Psi$  dihedral angle), a C-N=N angle of 114.1 (2x) and a C-C-N=N dihedral angle  $\Phi$  of 0°.<sup>[12]</sup> The tetra-*ortho* fluorination of azobenzene changes the geometry of the C-N=N angle (124.6° and 125.3°) and the dihedral angle  $\Phi$  (40.5°), but only slightly the  $\Psi$  dihedral angle (179.2°). This results in the phenyl-rings remaining parallel to each other.<sup>[44]</sup> Larger substituents in the *ortho*-position are reported to change both dihedral angles.<sup>[45]</sup>

Surprisingly, the tetra-*ortho*-fluorinated azobenzene **6** shows changes in both  $\Phi$  and  $\Psi$  dihedral angles: The  $\Psi$  dihedral angle was 170.2° and the  $\Phi$  dihedral angle was uncommonly high with 59.8°. This is very unusual for a tetra-*ortho*-fluorinated azobenzene and results in highly twisted phenyl-rings (60.5°, measured

by the angle of planes through the phenyl-rings.) around the azo-bridge. The N=N bond is elongated to 1.255 Å and a C-N=N angle of 112.2° and 112.7° has been observed.

Within the crystal structure, the aligned molecules are packed densely within one layer (colored in blue, **Figure 7**). The interaction between the layers is different to the interaction within the layer. Between the layers, an azo-group stacks on top of an ester-group leading to a stair-wise stacking (Figure 4). While it is difficult to transfer specific features within the crystal packaging to the mesogen order and alignment in the liquid crystal phase, these observations in the crystal are similar to the tilt of mesogens in SmC phases, which were reported also for the fluorine substituted terphenyl as the low temperature phase below their nematic temperature interval.<sup>[41]</sup> The tilt angle in the crystal of **6**

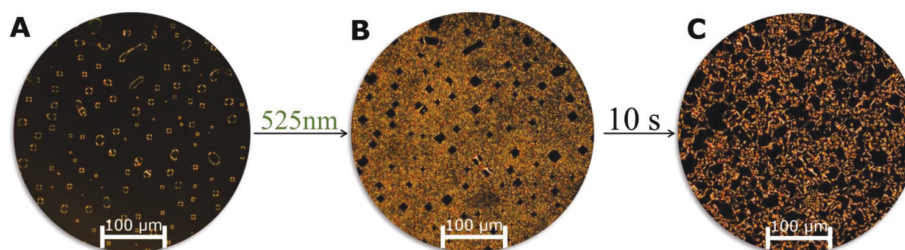


**Figure 6.** A) POM Image of **5** at 130 °C at the homeotropically state between two glass slides. B) The sample was irradiated with green light (525 nm) for 20 s, during which time yellow-orange sparkles appeared. C) The transition of **5** without irradiation by thermal relaxation toward its original state. All images were taking through crossed polarizer.

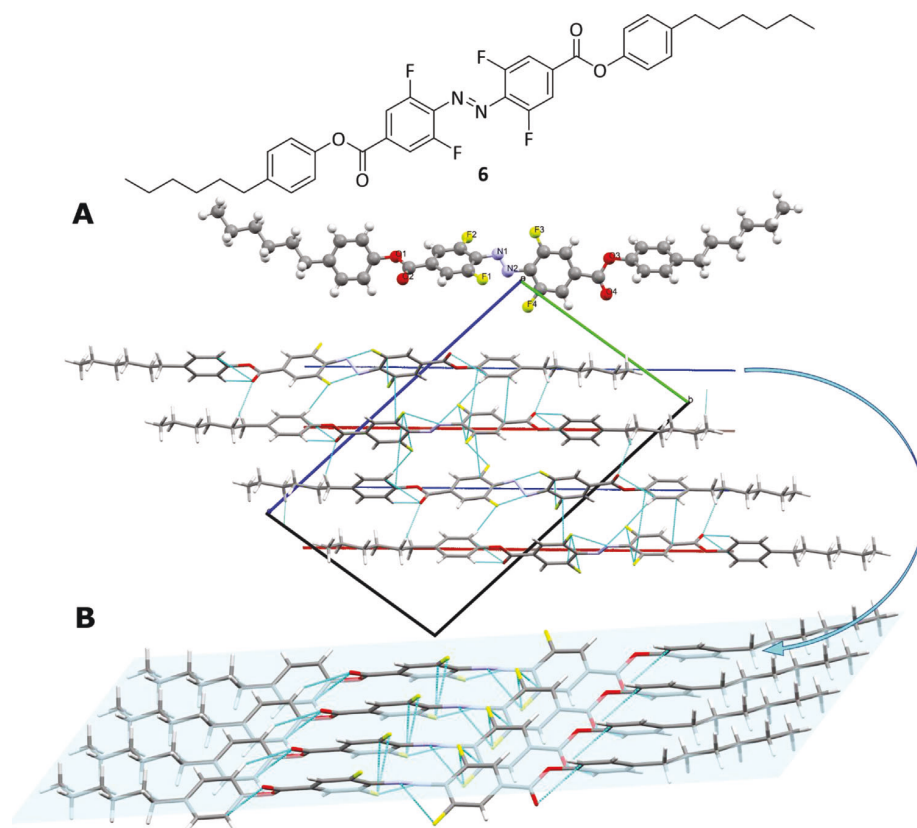


**Figure 7.** Molecular structure of derivative **6** with its in-plane A) and out-of-plane B) inter-molecular interaction.

was measured at ca.  $35^\circ$  (see Supporting Information for details, and see below for the morphology of the polymer film measured by WAXS). Moreover, the crystal structure confirms that a complete parallel packing with the cores at the same lateral position is sterically impossible, but it allows the formation of a high temperature nematic phase with a wide temperature interval of such compounds. Therefore, it becomes clear that the preferred alignment of such mesogens is parallel to the molecular long axes, as expected for such calamitic mesogens.

### 3. Liquid-Crystalline Polymer

#### 3.1. Preparation of the Thin Film

There are several types of LC cells that can be used for the alignment of LC monomers: Both top and bottom can be homeotropically or homogeneously aligned. Alternatively, a hybrid aligned nematic (HAN) type LC-cell can be used, which leads to a splay alignment or a twisted nematic (TN) morphology can be used. For optimal bending results, a splay alignment or twisted nematic alignment is best, because it has been shown that the mechanical work in such morphologies is much increased compared to purely homogeneously aligned films.<sup>[46]</sup> In addition, splay or TN alignments have the advantage that the film can bend both toward the light, but also away from it:<sup>[47]</sup> The planar alignment (Side PI) of the mesogens leads to a contraction of the meso-

gen upon irradiation resulting in a bending toward the light source.<sup>[46,47]</sup> On the other side of the polymer, the mesogens are aligned homotropically (Side Ho) resulting in an expansion upon isomerization and a bending away from the light source.<sup>[46,47]</sup> The overall splay-bend alignment within the cell also increases the anisotropic bending effect.<sup>[40,46]</sup>

In addition, a splay alignment leads to better control of the bending motion than other twisted nematic and uniform director distribution arrangements,<sup>[23]</sup> because of the suppression of saddle inducing deformations and giving higher bending angles.

However, for the optical and structural analysis of the film, the additional dimension of depth anisotropy introduced into the film by a splay alignment adds much complexity and a homogeneous arrangement was produced as a simplified model of the film.

For the hybrid aligned nematic (HAN) type LC-cells, two polyimide spin-coated glass substrates were used; one of them was rubbed over a velvet cloth for planar alignment, whereas the second one was left untreated. For the homogeneous alignment, both were rubbed over the velvet cloth. The two glass substrates were spaced by thin films of PTFE stripes of different thicknesses. Subsequently, the glass substrates were glued together with UV-acrylate adhesive Norland 65. A mixture prepared of **5** and the photoinitiator (phenyl-bis-(2,4,6-trimethylbenzoyl)-phosphine oxide (BAPO), 3 mol%) were dissolved in DCM and the solvent subsequently removed in vacuo. The cell was placed

on a heating stage; the dried mixture was melted (isotropic phase at 155 °C) and allowed to be sucked into the LC cell by capillary forces in the dark. Then, the cell was slowly cooled (0.5 °C min<sup>-1</sup>) to 130 °C to reach the nematic phase. Subsequently, polymerization was initiated by using linearly polarized 420 nm light from an LED source, with the polarizer orthogonal to the planar alignment of the LC cell. In addition, a PMMA slide was used as a filter so that the photocatalyst could be activated, while avoiding photoisomerization.<sup>[1]</sup> After 24 h the cell was opened and the film was extracted by sliding a razor blade underneath, which had been rinsed with hot water to reduce friction between the blade and the polymer during extraction (for further details see the Supporting Information).

The films were dried and their thickness was measured using an electronic cantilever. The splay aligned films had thicknesses of 40 μm (denoted  $P_{\text{planar},40}$ ), 60 μm (denoted  $P_{\text{planar},60}$ ), and 105 μm (denoted  $P_{\text{planar},105}$ ) and for the homogenous alignment, films with the thicknesses of 31 μm ( $P_{\text{planar},31}$ ), 49 μm ( $P_{\text{planar},49}$ ), and 80 μm ( $P_{\text{planar},80}$ ) were produced.

### 3.2. Structural and Optical Characterizations of the Polymer Films

The planar homogeneously aligned films served as models that would allow the morphological assessment of the new LCN films, now entirely composed of the azobenzene. The films ( $P_{\text{planar},31}$ ), ( $P_{\text{planar},49}$ ), and ( $P_{\text{planar},80}$ ) were analyzed using wide-angle X-ray scattering (WAXS) measurements (Figure 8). The obtained patterns stem from distinct synclinc SmC phases that manifest in varying domains within the films to different extents. Consequently, it is not uncommon for the intensities of the left and right signals to exhibit disparities. Within the SmC phases, the aromatic rings exhibit enhanced packing efficiency, giving rise to a subtle  $\pi$ - $\pi$  signal. Remarkably, the WAXS signal aligns precisely along the bisecting line, orthogonal to the rubbing direction, offering a plausible explanation for its well-defined position.

Whereas the LC phase of the monomer was nematic, the polymerization process significantly augmented the level of order within the film; it is now smectic C. It is reasonable to presume that the molecular structure closely resembles that of the crystalline state of the model compound **6**; in this crystal structure, a tilt angle of ca. 35° was found which is very close to the tilt angle of ca. 32° found in the polymer prepared from **5**. The layer thickness for this LC morphology was now 46 Å and the correlation length 366 Å corresponding to 7.9 molecular units compared to 2.8 units in the monomer. Measurements at higher temperatures (93 °C) did not significantly change the WAXS pattern; the correlation length dropped only slightly to 7.7 molecular units (see Supporting Information for the diffraction pattern). Therefore, it can be concluded that the smectic C phase is preserved even at higher temperatures.

To understand the thermal properties of the polymer, a differential scanning calorimetry (DSC) measurement was performed on the  $P_{\text{splay},105}$  film, because it was the thickest and thus gave the best signal to noise ratio. The measurement used a heating rate of 10 K/min for the temperature range -40 °C to 170 °C. We observed a glass transition temperature with an onset temperature

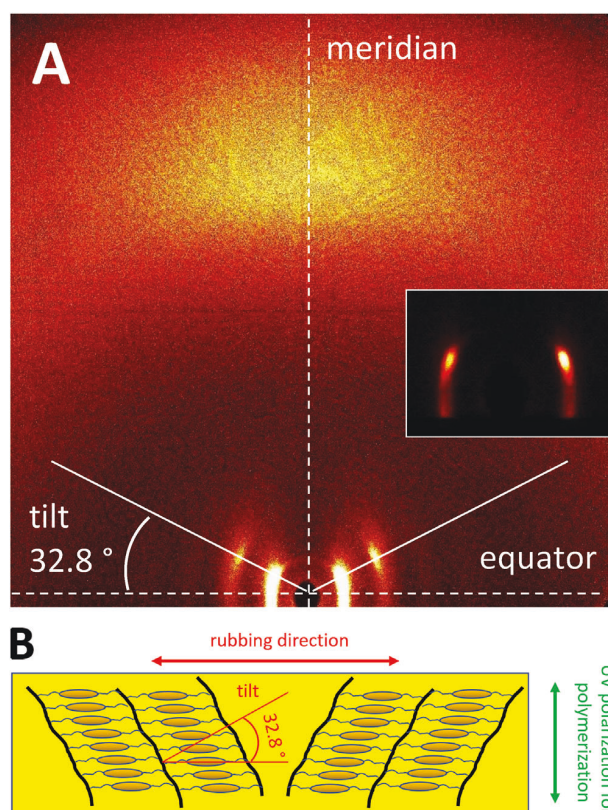


**Figure 8.** A) WAXS diffraction pattern of a 49 μm thick film ( $P_{\text{planar},49}$ )<sup>[1]</sup> at 25 °C. Inset: The intensities of the small angle reflections at the left and right are different since they originate from different domains of synclinc SmC phases. B) Schematic for the film orientation for the WAXS experiment, rubbing and alignment direction as well as the direction of the polarized UV light used for the polymerization. The red lines show the tilt of the mesogens versus the layer normal. <sup>1)</sup> The other planar aligned films showed the same pattern.

of 60 °C, with some amount of enthalpy relaxation (see Supporting Information<sup>[48]</sup>).

### 3.3. Photochemical Bending

For the photochemical bending experiments, a polymer film,  $P_{\text{splay},60}$ , was employed. The film was precisely cut into a piece measuring 1.5 cm x 0.2 cm x 60 μm. The piece was then vertically fixed, ensuring the side with homogeneous alignment faced the light source. The use of relatively large films was preferred for two reasons: first, the ability to easily bend thick films is uncommon (as discussed in the introduction), and second, for potential applications in soft robotics, a minimum size requirement is necessary. To facilitate underwater actuation, the same experimental setup was utilized, with the polymer immersed in a quartz cuvette filled with water (measuring 5 cm x 5 cm x 10 cm). Two light sources were utilized for the experiments: an LED emitting green light at 525 nm and another emitting blue light at 420 nm. These LEDs were focused on the polymer strip to induce bending. The intensity of light reaching the polymer could



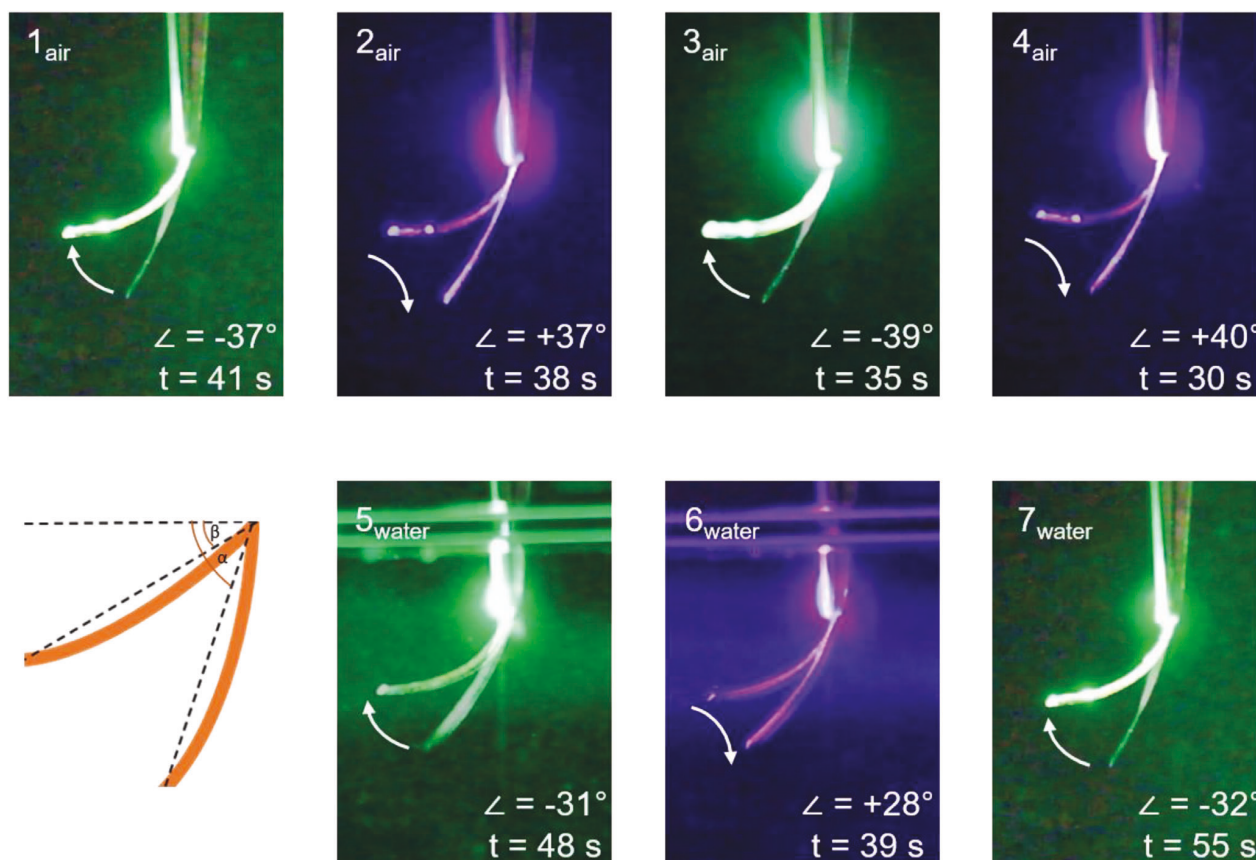


**Figure 9.** Analysis of the bending angles of the  $P_{\text{splay},60}$  film in air (top row) and in water (bottom row) depending on the illumination wavelength (525 or 420 nm). The images are overlaid stills from the video Video S3 (Supporting Information). The angle given in the images are the amplitude change between both angles ( $\Delta =$  starting angle – ending angle; see schematic for its definition) and the sign indicated the change upon illumination; the time indicates the duration of illumination required to reach this stage.

be adjusted between 40 and 200  $\text{mW cm}^{-2}$ , depending on the collimator's focus. This range was a compromise between exposure strength and area since the LED beams were not wide enough to fully irradiate the sample with both optimal focus and intensity.

### 3.4. Photochemical Bending in Air

Exposure of the  $P_{\text{splay},60}$  film to green light (525 nm) caused bending in air, resulting in a final bending angle amplitude of  $40^\circ$  at a rate of  $1^\circ\text{s}^{-1}$  (see Figure 9). The ultimate bending angle was primarily influenced by the geometry and intensity of irradiation. By adjusting the lamp's position during the film bending process, even a U-shaped configuration could be achieved (Figure S18, Supporting Information). Importantly, the bending behavior, driven by the *E-Z* isomerization of the tetra-*ortho*-fluorinated azobenzene monomer, could be completely reversed by illuminating the film with blue light (420 nm). However, if the bent film was left in the dark at  $23^\circ\text{C}$ , its shape only relaxed by  $25^\circ$  within 3 days. This characteristic is particularly advantageous for applications requiring precise control over movement solely through light ma-

nipulation, as it circumvents the largely uncontrollable thermal relaxation that occurs as a background reaction. In contrast, most azobenzene-based liquid crystal networks (LCN) and liquid crystal elastomers (LCE) fully relax within 24 h. The polymer film  $P_{\text{splay},105}$  showed only a slow bending motion with a small amplitude, which is presumably due to the relatively low illumination power in combination with the film thickness.<sup>[49]</sup> The temperature change caused by the illumination was measured using an IR camera (see Supporting Information). Illumination with 525 nm led to a temperature increase to  $40^\circ\text{C}$ , and 420 nm caused heating to  $33^\circ\text{C}$ . Some heat development during illumination is to be expected due to thermal relaxation (see introduction), and molecular local heat may be higher,<sup>[20]</sup> but at least macroscopically, this points to a relatively small photothermal effect.

### 3.5. Bending under Water

Water exerts a profound influence on the behavior of light passing through. In particular, higher energy radiation experiences scattering<sup>[50]</sup> and backscattering<sup>[51]</sup> phenomena, which

diminish as the wavelength increases. However, at  $\approx 600$  nm and beyond, absorption by water significantly intensifies.<sup>[52]</sup> These contrasting tendencies establish a distinct optical window for water, spanning roughly 400 to 500 nm. Consequently, photoswitches reliant on shorter ultraviolet (UV) wavelengths are less suitable for underwater switching. However, the actuation wavelength of the new polymer aligns perfectly with this window. An additional noteworthy characteristic of water is its cooling effect, whereby its natural heat convection transfer coefficient surpasses that of air by a factor of 100 to 200.<sup>[53]</sup> Consequently, it is reasonable to anticipate isothermal conditions in an underwater environment. This supposition finds support in the analyses conducted by Schenning and colleagues,<sup>[54]</sup> who investigated the bending of photomechanical liquid crystal networks in both air and water. Their findings confirm the presence of photomechanical rather than photothermal effects when actuation occurs underwater. To explore underwater switching, a polymer film with a thickness of 60  $\mu\text{m}$  and splay alignment was immersed in water at 21 °C within an elongated glass cuvette, with the homogeneous side facing the respective light sources (see Figure 9 and Video S1–S33, Supporting Information). Illumination with collimated 525 nm light, propagating through water for a distance of  $\approx 3$  cm, induced bending toward the light at a rate of  $0.65^\circ \text{ s}^{-1}$ . The final bending angle reached  $32^\circ$ , which slightly falls short of the bending rate and angle observed in air (as described above). The bent shape of the polymer film remained intact until illuminated with 420 nm light (collimated source, 40 (low focused beam) up to 200  $\text{mW cm}^{-2}$  (high focused beam) (intensity measured max. 120  $\text{mW cm}^{-2}$  for 420 nm and max. 140  $\text{mW cm}^{-2}$  for 525 nm, traversing water for  $\approx 3$  cm). Upon exposure to this light, the polymer film returned to its original shape, demonstrating complete reversibility.

However, when subjected to UV light, no discernible bending occurred. This underpins the importance of the wavelength dependent depth of penetration in different media.

Furthermore, a large bending motion was also observed by irradiation with orange light (590 nm). These experiments underscore the remarkable utility of tetrafluorinated LC photoswitches in the film for underwater actuation and provide evidence for a genuinely photomechanical and non-photothermal effect in water, with only a minor contribution from photothermal effects in air.

It is known that the macroscopically observed relaxation of an azobenzene containing LCN can be very different from the actual half-life time of the azobenzenes.<sup>[15]</sup> Therefore, the thermal relaxation of the Z-tetrafluoroazobenzene in the polymer film  $\text{P}_{\text{planar},31}$  was measured by UV-vis spectroscopy (For the spectra see the Supporting Information). Because the films consist solely of the azobenzene monomer, they are highly absorbing and only the thinnest film could be measured (for photographic images of the films, as well as the effect of a polarizer see Supporting Information). In addition, only a homogenous alignment was possible, because of the intransparency of the splay aligned films. Because the amount of switched monomer will be a function of the penetration depth of light, the local dielectric constant in the polymer film will have a depth profile. Also, the stiffness of the polymer will have a depth profile. Therefore, the thermal decay of the monomer is unlikely to follow a first-order kinetic

and a thermal half-life cannot be given with any precision. From the decay profile, we can merely estimate that the half-time is roughly 17 h.

In this respect, this new LCN is unusual: It has been reported that the thermal Z to E isomerization is much slower than the mechanical deformation (hours vs seconds).<sup>[15]</sup> However, in our case, thermal relaxation appears to be somewhat faster, although not by orders of magnitude. It also has to be considered that the macroscopic relaxation was observed with the  $\text{P}_{\text{splay},60}$  film, whereas the UV-vis measurement was performed with the  $\text{P}_{\text{planar},31}$  film.

The splay LCN films reported in this work  $\text{P}_{\text{splay},60}$  and  $\text{P}_{\text{splay},105}$  are thicker in comparison to the UV-light actuated analogs. This limitation of thickness is a direct function of the wavelength penetration depth of light in matter. This is a function of absorbance, but also scattering. In azobenzene, isomerization to the Z-isomer is typically affected by irradiating in the UV range, exciting the allowed  $\pi$ - $\pi^*$  transition which has a large extinction coefficient ( $2.6 \times 10^4 \text{ M}^{-1} \text{ cm}^{-1}$ ). Due to this and the fact that light with shorter wavelengths scatters more, it was postulated that in azobenzene containing thin polymer films, most photons are absorbed within a thickness of  $>1 \mu\text{m}$  for UV-light irradiation.<sup>[26b]</sup> However, in tetra-ortho fluorinated azobenzene, the longer wavelength n- $\pi^*$  transitions are well separated and have a higher absorption coefficient so that they can be used instead for the isomerization. The longer wavelength combined with the lower extinction coefficient for the n- $\pi$  absorbance ( $1 \text{ M}^{-1} \text{ cm}^{-1}$ ),<sup>[32c]</sup> may lead to a deeper penetration depth of the green light, which may enable bending the motion in thicker samples. Indeed, the UV-vis spectra for the polymer film  $\text{P}_{\text{planar},31}$  showed that the film was intransparent in the UV-region, but spectra were observable in the range from 400–700 nm (see Supporting Information).

Because this work eventually aims at introducing visible light switchable LCNs to the area of soft robotics, in addition to the narrow polymer film strips, a larger piece of a splay aligned polymer film  $\text{P}_{\text{splay},40}$  with dimensions of 2.5 cm  $\times$  1.5 cm 40  $\mu\text{m}$  was prepared. This film could be bent within 7 s to an angle of  $90^\circ$  with a remarkably low light intensity of 10  $\text{mW cm}^{-2}$  (Figure 10, Video S4, Supporting Information). During illumination with green light for 30 s, the temperature in the film, observed with an IR camera, increased to 37.4 °C and cooled down within seconds after illumination (see Supporting Information).

#### 4. Conclusion

A novel synthetic design for the first tetra-ortho-fluorinated liquid crystal azobenzene monomer capable of reversible switching solely with visible light in both directions has been introduced. This was made possible through the tetra-ortho fluorination of the azobenzene combined with the expansion of the rigid core of the mesogen. The monomer exhibits a nematic phase over a wide temperature range (32 K), as confirmed by comprehensive studies employing DSC, POM, and WAXS techniques. The monomer was polymerized in a hybrid nematic aligned liquid crystal cell, resulting in films with splay alignment and thicknesses of 40, 60, and 105  $\mu\text{m}$ . These films exhibit a glass transition temperature of 60 °C. WAXS measurements

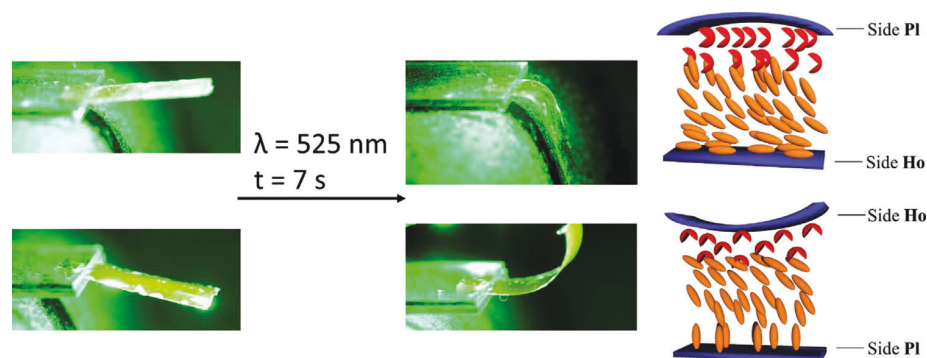


**Figure 10.** Photobending of  $P_{\text{Splay},40}$  in air. The polymer stripe was clamped between two microscope slides. Pictures taken from the video after 7 s of irradiation with the schematic representation of the actuation within the material on the right. For a video of the switching process see supporting video Video S4 (Supporting Information).

performed on a model film with homogeneous planar alignment revealed that polymerization increased the molecular order, transitioning to a smectic C phase. The splay aligned film with a thickness of 60  $\mu\text{m}$  demonstrated reversible photomechanical actuation when irradiated alternately with violet and green light. Remarkably, despite the film's significant thickness and the relatively low irradiation power ranging from 40 to 200  $\text{mW cm}^{-2}$ , the bending occurred with substantial changes in angle ( $40^\circ$ ) and at high speed ( $1^\circ \text{s}^{-1}$ ). This can be attributed to the longer wavelengths of the light sources penetrating deeply into the film, the high monomer concentration (100%), and the dense cross-linking. Additionally, the bent shape exhibited a thermal shape stability over several days. Underwater conditions only slightly affected the bending angle and rate, suggesting that for a thickness of 60  $\mu\text{m}$ , the photothermal effect is minimal, and the bending process is primarily driven by photomechanical mechanisms.

To summarize, this study presents a robust photomechanical liquid crystal network (LCN) capable of actuation with green light, avoiding the use of potentially harmful UV light. This material holds significant potential for applications in biosafe soft robotics that require precise control. Moreover, the synthesis process offers high yields, while film preparation is straightforward, ensuring the accessibility of this material.

## 5. Experimental Section

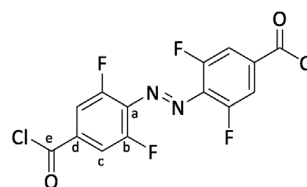
**General Synthetic and Analytical Methods:** For all equipment, syntheses, fabrication processes, images and spectra see the Supporting Information.

**Preparation of the LCN:** In a glass vial, **5** and the photocatalyst (3 wt.%) were dissolved in DCM. The solvent was removed in vacuo. The polymerizations were performed on a Linkam LTS-420 heating stage in between PI coated glass slides. The glass slides were spin-coated with a 5 wt.% PI (P84, Elsinger) solution in NMP and dried for 1 h at  $100^\circ\text{C}$  and another 24 h at  $200^\circ\text{C}$  in a drying oven. One of the glass slides were rubbed with a velvet cloth along one axis before use. A stripe of a 10, 30, or 50  $\mu\text{m}$  thin PTFE film was used as a spacer to form the LC cell. The LC cell was glued together by the UV-curing acrylate adhesive NOA61 from Norland Optical Adhesive. The monomer mixture was inserted into the LC by capillary force at  $155^\circ\text{C}$  (isotropic phase). Subsequently, the tem-

perature was slowly lowered ( $0.5 \text{ K min}^{-1}$ ) to the nematic phase ( $130^\circ\text{C}$ ). This temperature was held for 30 min. Afterward, a LED with a wavelength of 420 nm was used to irradiate the LC cell through a linear polarizer orthogonally to the planar alignment of the LC cell for 12 h to activate the photocatalyst without switching the azobenzene. Additionally, a PMMA slide was placed between the light source and the LC cell to block irradiation in the UV-range. Then, the temperature was raised to  $155^\circ\text{C}$  again and hold for 15 min. The lamp was turned off and the temperature hold for another 15 min, before cooling down to room temperature and carefully opening the LC cell using a razor blade. To facilitate the extraction of the thin film, the razor blade and the LC cell were periodically immersed in hot water. The final thickness of the films was measured using a digital caliper

Further information can be found in the supporting information: equipment, syntheses, spectra, crystallographic data, further images.

(E)-4,4'-(Diazene-1,2-diyl)bis(3,5-difluorobenzoyl chloride) (**4**)



This reaction was performed under inert conditions.

In an oven dried flask, (E)-4,4'-(diazene-1,2-diyl)bis(3,5-difluorobenzoic acid) (**5**) (1.03 g, 3.00 mmol, 1.00 equiv.) was dissolved in excess  $\text{SOCl}_2$  (5 mL). Then, a single drop of dry DMF was added and the reaction mixture heated up to  $80^\circ\text{C}$  for 17 h. Afterward, the solvent was removed in vacuo by adding a cooling trap to the apparatus. The crude product was transferred to the glovebox and crystallized in dry toluene at  $-20^\circ\text{C}$ . After filtration, the dark red product **4** was obtained in 96% (1.09 g, 2.88 mmol, 96%) yield.

$^1\text{H NMR}$  (600 MHz,  $\text{CDCl}_3$ )  $\delta = 7.86$  (d,  $^3J = 8.4$  Hz, 4H, H-c) ppm.

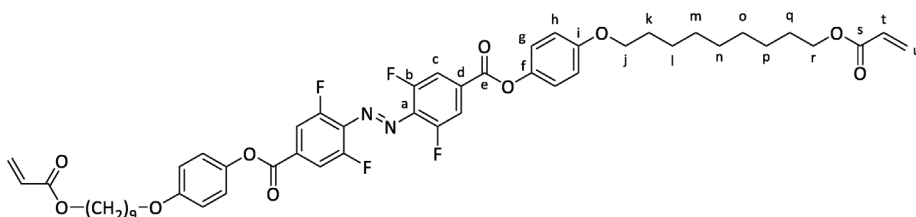
$^{13}\text{C}\{^1\text{H}\}$  NMR (151 MHz,  $\text{CDCl}_3$ )  $\delta = 165.92$  (C-e), 155.06 (dd,  $^2J = 265.0$ ,  $^4J = 3.8$  Hz, C-b), 136.05 (t,  $^4J = 9.1$  Hz, C-d), 135.54 (t,  $^3J = 10.4$  Hz, C-a), 115.68 (dd,  $^2J = 22.1$ ,  $^4J = 4.4$  Hz, C-c).

$^{19}\text{F NMR}$  (565 MHz,  $\text{CDCl}_3$ )  $\delta = -117.46$  (d,  $^3J = 8.4$  Hz, F-b) ppm.

HRMS (EI, 70 eV)  $m/z$  (%):  $[\text{M}]^+$  calcd for  $[\text{C}_{14}\text{H}_4\text{N}_2\text{O}_4\text{F}_4]^+$  377.95801; found 377.95805 (10), 86.1 (100).

IR (ATR):  $\tilde{\nu} = 1746$  (m), 1698 (m), 1684 (w), 1576 (s), 1558 (m), 1540 (w), 1473 (w), 1431 (m), 1418 (m), 1396 (w), 1328 (w), 1260 (w), 1123 (m), 1054 (s), 1004 (s), 891 (m), 878 (w), 807 (m), 772 (w), 701 (m)  $\text{cm}^{-1}$ .

(E)-4,4'-(Diazene-1,2-diyl)bis(3,5-difluorobenzoic acid) (5)



This reaction was performed under inert conditions.

In a glovebox, (E)-4,4'-(diazene-1,2-diyl)bis(3,5-difluorobenzoyl chloride) (**4**) (342 mg, 1 mmol, 1 equiv.) and 9-(4-hydroxyphenoxy)nonyl acrylate (**2**) (674 mg, 2.20 mmol, 2.20 equiv.) and triethylamine (1.0 mL) were dissolved in toluene (30 mL). The reaction was heated to 110 °C for 24 h. Then, the solvent was removed in vacuo and the crude product was directly purified by column chromatography (eluent gradient: Hexane → DCM) to afford **5** as an orange solid. (707 mg, 0.769 mmol, 77%)

<sup>1</sup>H NMR (600 MHz, CDCl<sub>3</sub>) δ = 7.91 (d, <sup>3</sup>J = 9.3 Hz, 4H, H-c), 7.14 (d, <sup>3</sup>J = 9.0 Hz, 4H, H-g), 6.95 (d, <sup>3</sup>J = 9.0 Hz, 4H, H-h), 6.40 (dd, <sup>2</sup>J = 17.4, <sup>4</sup>J = 1.5 Hz, 2H, H-u), 6.13 (dd, <sup>3</sup>J = 17.4, <sup>3</sup>J = 10.4 Hz, 2H, H-t), 5.82 (dd, <sup>3</sup>J = 10.4, <sup>4</sup>J = 1.5 Hz, 2H, H-u), 4.16 (t, <sup>3</sup>J = 6.7 Hz, 4H, H-j), 3.97 (t, <sup>3</sup>J = 6.5 Hz, 4H, H-r), 1.83–1.77 (m, 4H, H-q), 1.71–1.65 (m, 4H, H-k), 1.48–1.46 (m, 4H, H-p), 1.37 (s, 16H, H-l,m,n,o).

<sup>13</sup>C{<sup>1</sup>H} NMR (151 MHz, CDCl<sub>3</sub>) δ = 166.51 (C-s), 162.84 (C-e), 157.43 (C-f), 155.24 (d, <sup>1</sup>J = 263.4 Hz, C-b), 143.88 (C-i), 134.71 (t, <sup>2</sup>J = 10.0 Hz, C-a), 133.13 (t, <sup>3</sup>J = 9.5 Hz, C-d), 130.61 (C-u), 128.80 (C-t), 122.21 (C-g), 115.36 (C-h), 114.65 (dd, <sup>2</sup>J = 21.7, <sup>4</sup>J = 4.0 Hz, C-c), 68.56 (C-r), 64.83 (C-j), 29.57 (C-q), 29.43 (C-l,m,n,o), 29.37 (C-k), 29.32 (C-l,m,n,o), 28.75 (C-l,m,n,o), 26.16 (C-l,m,n,o), 26.05 (C-p).

<sup>19</sup>F NMR (565 MHz, CDCl<sub>3</sub>) δ = -118.92 (d, <sup>3</sup>J = 9.3 Hz, F-b).

HRMS (ESI) m/z (%): [M+Na]<sup>+</sup> calcd for [C<sub>50</sub>H<sub>54</sub>F<sub>4</sub>N<sub>2</sub>NaO<sub>10</sub>]<sup>+</sup> 941.36068; found 941.36095.

IR (ATR): ν̄ = 2923 (w), 1710 (m), 1575 (w), 1501 (w), 1473 (m), 1434 (w), 1336 (m), 1295 (m), 1204 (s), 1184 (s), 1110 (m), 1048 (m), 1017 (m), 988 (m), 968 (m), 958 (m), 912 (w), 898 (w), 827 (m), 812 (s), 773 (m), 886 (m), 752 (m), 725 (w) cm<sup>-1</sup>.

Mp: Cr120N1531

Rf: 0.5 (n-hexane:DCM, 1:1).

[CCDC 2 224 454 contains the supplementary crystallographic data for this paper. These data can be obtained free of charge from The Cambridge Crystallographic Data Centre via www.ccdc.cam.ac.uk/data\_request/cif.]

## Supporting Information

Supporting Information is available from the Wiley Online Library or from the author.

## Acknowledgements

This research was funded by the German Research Foundation (DFG) within the priority program SPP 2100 “Soft Material Robotic Systems”, Subproject STA1195/5-1, “Insect feet inspired concepts soft touch grippers with dynamically adjustable grip strength.”

Open access funding enabled and organized by Projekt DEAL.

## Conflict of Interest

The authors declare no conflict of interest.

## Data Availability Statement

The data that support the findings of this study are available in the supplementary material of this article.

## Keywords

actuator, azo compounds, fluorinated azobenzene, liquid crystalline polymer network, liquid crystals, photomechanical effect, visible light actuation

Received: April 27, 2023

Revised: July 28, 2023

Published online:

- [1] J. Wang, D. Gao, P. S. Lee, *Adv. Mater.* **2021**, *33*, 2003088.
- [2] P. Won, K. K. Kim, H. Kim, J. J. Park, I. Ha, J. Shin, J. Jung, H. Cho, J. Kwon, H. Lee, S. H. Ko, *Adv. Mater.* **2021**, *33*, 2170147.
- [3] J. Xiong, J. Chen, P. S. Lee, *Adv. Mater.* **2021**, *33*, 2002640.
- [4] J. Shintake, V. Cacucciolo, D. Floreano, H. Shea, *Adv. Mater.* **2018**, *30*, 1707035.
- [5] C. S. X. Ng, M. W. M. Tan, C. Xu, Z. Yang, P. S. Lee, G. Z. Lum, *Adv. Mater.* **2021**, *33*, 2003558.
- [6] J. Li, L. Mou, Z. Liu, X. Zhou, Y. Chen, *Nat. Commun.* **2022**, *13*, 5621.
- [7] C. Majidi, *Soft Rob.* **2013**, *1*, 5.
- [8] N. El-Atab, R. B. Mishra, F. Al-Modaf, L. Joharji, A. A. Alsharif, H. Alamoudi, M. Diaz, N. Qaiser, M. M. Hussain, *Adv. Intel. Syst.* **2020**, *2*, 2000128.
- [9] K. Wang, K. Amin, Z. An, Z. Cai, H. Chen, H. Chen, Y. Dong, X. Feng, W. Fu, J. Gu, Y. Han, D. Hu, R. Hu, D. Huang, F. Huang, F. Huang, Y. Huang, J. Jin, X. Jin, Q. Li, T. Li, Z. Li, Z. Li, J. Liu, J. Liu, S. Liu, H. Peng, A. Qin, X. Qing, Y. Shen, et al., *Mater. Chem. Front.* **2020**, *4*, 1803.
- [10] T. J. White, D. J. Broer, *Nat. Mater.* **2015**, *14*, 1087.
- [11] Z. Mahimwalla, K. G. Yager, J.-I. Mamiya, A. Shishido, A. Priimagi, C. J. Barrett, *Polym. Bull.* **2012**, *69*, 967.
- [12] J. J. De Lange, J. M. Robertson, I. Woodward, *Proc. R. Soc. London, Ser. A* **1939**, *171*, 398.
- [13] Y. Yu, T. Ikeda, *J. Photochem. Photobiol., C* **2004**, *5*, 247.
- [14] M. Kondo, Y. Yu, T. Ikeda, *Angew. Chem., Int. Ed.* **2006**, *45*, 1378.
- [15] D. Liu, D. J. Broer, *Nat. Commun.* **2015**, *6*, 8334.
- [16] K. D. Harris, R. Cuypers, P. Scheibe, C. L. van Oosten, C. W. M. Bastiaansen, J. Lub, D. J. Broer, *J. Mater. Chem.* **2005**, *15*, 5043.
- [17] A. Sánchez-Ferrer, A. Merekalov, H. Finkelmann, *Macromol. Rapid Commun.* **2011**, *32*, 671.
- [18] N. P. Pinchin, H. Guo, H. Meteling, Z. Deng, A. Priimagi, H. Shahsavan, *Adv. Mater.* **2023**, 2303740.
- [19] H. Shahsavan, A. Aghakhani, H. Zeng, Y. Guo, Z. S. Davidson, A. Priimagi, M. Sitti, *Proc. Natl. Acad. Sci. USA* **2020**, *117*, 5125.
- [20] J. Vapaavuori, A. Laventure, C. G. Bazuin, O. Lebel, C. Pellerin, *J. Am. Chem. Soc.* **2015**, *137*, 13510.
- [21] J. M. Harrison, D. Goldbaum, T. C. Corkery, C. J. Barrett, R. R. Chromik, *J. Mater. Chem. C* **2015**, *3*, 995.
- [22] C. J. Barrett, J.-I. Mamiya, K. G. Yager, T. Ikeda, *Soft Matter* **2007**, *3*, 1249.
- [23] K. Mehta, A. R. Peeketi, L. Liu, D. Broer, P. Onck, R. K. Annabattula, *Appl. Phys. Rev.* **2020**, *7*.

- [24] Y. Yu, M. Nakano, A. Shishido, T. Shiono, T. Ikeda, *Chem. Mater.* **2004**, *16*, 1637.
- [25] S. Iamsaard, S. J. Aßhoff, B. Matt, T. Kudernak, J. J. L. M. Cornelissen, S. P. Fletcher, N. Katsonis, *Nat. Chem.* **2014**, *6*, 229.
- [26] a) M. Pilz da Cunha, S. Ambergen, M. G. Debije, E. F. G. A. Homburg, J. M. J. den Toonder, A. P. H. J. Schenning, *Adv. Sci.* **2020**, *7*, 1902842; b) T. Ikeda, M. Nakano, Y. Yu, O. Tsutsumi, A. Kanazawa, *Adv. Mater.* **2003**, *15*, 201; c) W. Wu, L. Yao, T. Yang, R. Yin, F. Li, Y. Yu, *J. Am. Chem. Soc.* **2011**, *133*, 15810; d) S. Fredrich, T. Engels, A. P. H. J. Schenning, *ACS Appl. Polym. Mater.* **2022**, *4*, 7751.
- [27] a) M. Pilz da Cunha, M. G. Debije, A. P. H. J. Schenning, *Chem. Soc. Rev.* **2020**, *49*, 6568; b) E. Kizilkhan, J. Strubeen, A. Staubit, S. N. Gorb, *Sci. Robot.* **2017**, *2*, eaak9454.
- [28] C. Opländer, S. Hidding, F. B. Werners, M. Born, N. Pallua, C. V. Suschek, *J. Photochem. Photobiol., B* **2011**, *103*, 118.
- [29] G. Tosini, I. Ferguson, K. Tsubota, *Mol. Vis.* **2016**, *22*, 61.
- [30] T. Ikeda, J.-i. Mamiya, Y. Yu, *Angew. Chem., Int. Ed.* **2007**, *46*, 506.
- [31] a) S. K. Choi, in *Photonanotechnology for Therapeutics and Imaging*, (Ed: S. k. Choi), Elsevier, Amsterdam, New York, **2020**; b) S. Pearson, J. Feng, A. del Campo, *Adv. Funct. Mater.* **2021**, *31*, 2105989; c) A. N. Bashkatov, E. A. Genina, V. I. Kochubey, V. V. Tuchin, *J. Phys. D: Appl. Phys.* **2005**, *38*, 2543.
- [32] a) A.-L. Leistner, Z. L. Pianowski, *Eur. J. Org. Chem.* **2022**, *2022*, e202101271; b) H. Wang, H. K. Bisoyi, X. Zhang, F. Hassan, Q. Li, *Chemistry* **2022**, *28*, e202103906; c) D. Bleger, J. Schwarz, A. M. Brouwer, S. Hecht, *J. Am. Chem. Soc.* **2012**, *134*, 20597; d) R. Siewertsen, H. Neumann, B. Buchheim-Stehn, R. Herges, C. Näther, F. Renth, F. Temps, *J. Am. Chem. Soc.* **2009**, *131*, 15594; e) S. Samanta, A. A. Beharry, O. Sadovski, T. M. McCormick, A. Babalhaveji, V. Tropepe, G. A. Woolley, *J. Am. Chem. Soc.* **2013**, *135*, 9777; f) D. B. Konrad, J. A. Frank, D. Trauner, *Chemistry* **2016**, *22*.
- [33] There are polarizers for UV-light, but they rely on a different fabrication principle. Polarizers for visible light are based on stretched polymers (often PVA). These often age and decompose over time when exposed to UV light.
- [34] T. Kondo, *Z. Wissenschaft. Photogr. Photophys. Photochem.* **1932**, *31*, 153.
- [35] C. Knie, M. Utecht, F. Zhao, H. Kulla, S. Kovalenko, A. M. Brouwer, P. Saalfrank, S. Hecht, D. Bléger, *Chemistry* **2014**, *20*, 16492.
- [36] S. Iamsaard, E. Anger, S. J. Aßhoff, A. Depauw, S. P. Fletcher, N. Katsonis, *Angew. Chem., Int. Ed.* **2016**, *55*, 9908.
- [37] a) K. Kumar, C. Knie, D. Bléger, M. A. Peletier, H. Friedrich, S. Hecht, D. J. Broer, M. G. Debije, A. P. H. J. Schenning, *Nat. Commun.* **2016**, *7*, 11975; b) M. Hendrikx, J. ter Schiphorst, E. P. A. van Heeswijk, G. Koçer, C. Knie, D. Bléger, S. Hecht, P. Jonkheijm, D. J. Broer, A. P. H. J. Schenning, *Small* **2018**, *14*, 1803274; c) D. Ditter, L. B. Braun, R. Zentel, *Macromol. Chem. Phys.* **2019**, *221*, 1900256.
- [38] R. Yin, W. Xu, M. Kondo, C.-C. Yen, J.-i. Mamiya, T. Ikeda, Y. Yu, *J. Mater. Chem.* **2009**, *19*, 3141.
- [39] Z. Jiang, M. Xu, F. Li, Y. Yu, *J. Am. Chem. Soc.* **2013**, *135*, 16446.
- [40] G. Vantomme, A. H. Gelebart, D. J. Broer, E. W. Meijer, *J. Polym. Sci., Part A: Polym. Chem.* **2018**, *56*, 1331.
- [41] G. W. Gray, M. Hird, D. Lacey, K. J. Toyne, *J. Chem. Soc. Perkin Trans.* **1989**, *2*, 2041.
- [42] H. Sakaino, D. J. Broer, S. C. J. Meskers, E. W. Meijer, G. Vantomme, *Angew. Chem., Int. Ed.* **2022**, *61*, e202200839.
- [43] P. Scherrer, *Nachr. Ges. Wiss. Goettingen Math.-Phys. Kl.* **1918**, *2*, 98.
- [44] D. Hermann, H. A. Schwartz, U. Ruschewitz, *ChemistrySelect* **2017**, *2*, 11846.
- [45] D. B. Konrad, G. Savasci, L. Allmendinger, D. Trauner, C. Ochsenfeld, A. M. Ali, *J. Am. Chem. Soc.* **2020**, *142*, 6538.
- [46] C. L. van Oosten, K. D. Harris, C. W. M. Bastiaansen, D. J. Broer, *Eur. Phys. J. Spec. Top.* **2007**, *23*, 329.
- [47] M. Kondo, Y. Yu, T. Ikeda, *Angew. Chem. Int. Ed. Engl.* **2006**, *45*, 1378.
- [48] It is notable that in some films, quite pronounced endothermal peaks may occur between 30 and 40 °C; depending on the polymerization conditions. We assume that these are due to incomplete polymerization, because using modulated DSC (TOPEM method), they solely manifested in the non-reversing heat flow, indicating a kinetic contribution. During the cooling phase, the peaks were absent. The bending behavior of these films (see below) was not remarkably different to the fully polymerized films, but because in some instances remaining monomer does seem to change the properties substantially, it is recommended to analyze films with respect to this feature. See: S. Fredrich, T. Engels, A. P. H. J. Schenning, *ACS Appl. Polym. Mater.* **2022**, *4*, 7751.
- [49] In an example of an LCN with an azobenzene comonomer, an oscillator was realized, in which the bending angle was highly dependent on the illumination strength. The film had a thickness of only 15 µm, but 1 W cm<sup>-2</sup> was necessary to produce only a 20° bending angle: K. M. Lee, M. L. Smith, H. Koerner, N. Tabiryan, R. A. Vaia, T. J. Bunning, T. J. White, *Adv. Funct. Mater.* **2011**, *21*, 2913.
- [50] A. Metallo, *Scientia* **1975**, *69*, 276.
- [51] A. Morel, B. Gentili, H. Claustre, M. Babin, A. Bricaud, J. Ras, F. Tièche, *Limnol. Oceanogr.* **2007**, *52*, 217.
- [52] R. M. Pope, E. S. Fry, *Appl. Opt.* **1997**, *36*, 8710.
- [53] M. Xiao, L. Tang, X. Zhang, I. Y. F. Lun, Y. Yuan, *Energies* **2018**, *11*, 3416.
- [54] M. Pilz da Cunha, E. A. J. van Thoor, M. G. Debije, D. J. Broer, A. P. H. J. Schenning, *J. Mater. Chem. C* **2019**, *7*, 13502.



## 7.1 Activation of Hidden Forces: Reshaping a Liquid Crystal Elastomer into a Monodomain with the Help of Thermoplastic Particles

### Aim:

The complex fabrication of liquid crystalline actuators is a barrier to the accessibility of these materials for material scientists and engineers to incorporate the actuators into their systems. By combining particles with LCP in a composite, we enable a straightforward representation of the actuators, where alignment of the mesogens occurs after polymerization. Inspired by the work of my co-authoring colleague Nina Sindersberger from the joint DFG SPP 2100 program, the idea of a shape-memory effect through thermoplastic particles was applied to solidify and reorganize the alignment of the mesogens in the LCP. This led to an actuator that can be manufactured on a larger scale, and tailored and shaped according to specific needs. The potential combination of LCP with additional thermoplastic particles opens a wide range of new composites that can be tested for their liquid crystalline actuation without undergoing difficult manufacturing processes.

### Title of Manuscript:

**Hidden Forces: Activation of Photobending in a Liquid Crystalline Elastomer by Mesogen Alignment with the Help of Thermoplastic Particles.**

S. Schultzke, P. Schadte, N. Sindersberger, J. Gerken, L. Siebert, A. Staubitz, *Mater. Horiz.*, **2024**, *submitted*.

Permission to reprint in Appendix 9.6.



**Abstract:**

In this research, we introduce an innovative technique for developing advanced soft shape-memory materials, with a particular emphasis on enhancing the capabilities of main-chain liquid crystal elastomers (MC-LCEs). Our novel composite, comprising an azobenzene incorporated MC-LCE blended with thermoplastic polycaprolactone (PCL) particles, exhibits remarkable properties. It shows responsive actuation to light stimuli in configurations thicker than 1 mm and boasts an impressive stretchability of up to 190%, assuming multiple shapes with high programmability. This versatility stems from the unique interaction between the low-temperature melting and subsequent solidification of the PCL inclusions, which effectively retain various deformations. Upon thermal activation, the composite reliably returns to its original shape, demonstrating excellent reusability and potential for diverse applications.

**Abstract (deutsch):**

In dieser Forschungsarbeit stellen wir eine innovative Technik zur Entwicklung fortschrittlicher weicher Formgedächtnismaterialien vor, mit besonderem Schwerpunkt auf der Verbesserung der Fähigkeiten von Hauptketten-Flüssigkristall-Elastomeren (MC-LCEs). Unser neuartiges Verbundmaterial, bestehend aus einem in MC-LCE eingebetteten Azobenzol, das mit thermoplastischen Polycaprolacton (PCL)-Partikeln vermischt ist, weist bemerkenswerte Eigenschaften auf. Es zeigt eine reaktive Aktuierung auf Lichtreize in Konfigurationen, die dicker als 1 mm sind, und verfügt über eine beeindruckende Dehnbarkeit von bis zu 190%, wobei es mehrere Formen mit hoher Programmierbarkeit annimmt. Diese Vielseitigkeit resultiert aus der einzigartigen Wechselwirkung zwischen dem niedrigtemperaturigen Schmelzen und der anschließenden Verfestigung der PCL-Einschlüsse, welche effektiv verschiedene Deformationen beibehalten. Bei thermischer Aktivierung kehrt das Verbundmaterial zuverlässig in seine ursprüngliche Form zurück und zeigt ausgezeichnete Wiederverwendbarkeit und Potenzial für vielfältige Anwendungen.

**Author Contribution to this Manuscript:**

In this research article, based on the presented idea from N. Sindorsberger, I initiated a cooperation project. The particles and know-how were provided by N. Sindorsberger. I and J. Gerken optimized the material composition, reaction conditions and the final assembly of the polymer. The final composite was analysed and characterized by me. The DMA measurement was performed by P. Schadte and L. Siebert. The supporting information and manuscript was written by me with help in the introduction part by A. Staubitz. All authors contributed in the reviewing process.



## Hidden Forces: Activation of Photobending in a Liquid Crystalline Elastomer by Mesogen Alignment with the Help of Thermoplastic Particles.

Received 00th January 20xx,  
Accepted 00th January 20xx

DOI: 10.1039/x0xx00000x

Sven Schultze<sup>1,2</sup>, Philipp Schadt<sup>3</sup>, Nina Sindersberger<sup>4</sup>, Jonas Gerken<sup>1,2</sup>, Leonard Siebert,<sup>3</sup> and Anne Staubitz<sup>1,2,5\*</sup>

Azobenzene containing main-chain liquid crystal elastomers (MC-LCEs) can reversibly bend under illumination. A prerequisite for this functionality is the alignment of the azobenzene mesogens, but the common fabrication techniques severely limit film thickness. In this research, we introduce a novel composite, comprising an azobenzene incorporated in a MC-LCE that is blended with thermoplastic polycaprolactone (PCL) particles. Above their melting point, this allows alignment by stretching under heat and remain oriented upon subsequent cooling. The composite shows reversible photo actuation with unprecedented film thicknesses (> 1 mm) and boasts a stretchability of up to 190%, assuming multiple shapes with high programmability (shape-memory effect). This versatility stems from the unique interaction between the low-temperature melting PCL inclusions, which efficiently retain various deformations states. Upon thermal activation, the composite reliably returns to its original shape, demonstrating excellent reusability and potential for diverse applications.

### Introduction

Soft robotics<sup>1</sup> is a transformative approach in the field of automation. It diverges from traditional robotics by emphasizing compliance, adaptability, and a closer imitation of the functionality of biological systems.<sup>2, 3</sup> The field has gained significant momentum because it has the potential to revolutionize applications, ranging from small scale medical devices,<sup>4, 5</sup> to search and rescue operations.<sup>6</sup> To a much higher extent than hard robots, soft robots can interact safely with humans<sup>7-9</sup> and other delicate environments.<sup>10</sup> Although initially, passive, soft materials, were used that were actuated, e.g. with pneumatics of hydraulics,<sup>11, 12</sup> the advent of active functional materials enables smart robotics, which is based on the

### New concepts

The research field of light-actuated materials in soft robotics is of high relevance, because it enables precise and non-invasive control of soft robotic structures. Light offers a versatile and remote means to manipulate these materials, allowing for applications in minimally invasive medical procedures, delicate object handling, and adaptable soft robotic devices for various industries. However, several limiting challenges remain: Previous light-responsive materials used in soft robotics were mainly limited to thin polymer films, below 100 µm and few centimetres in length and width at most. This affects their mechanical strength and durability. Finding ways to enhance the mechanical properties of these materials while maintaining their responsiveness to light is a critical challenge. Additionally, these materials were produced in one shape only and changing the shape and reuse for other purposes was impossible. The new composite material, with thermoplastic particles blended with a polydomain main-chain liquid crystal elastomer (MC-LCE), overcomes these previous limitations associated with the fabrication of macro-sized, solid three-dimensional objects. Our approach enables the effortless molding of these composites into arbitrary shapes or sizes. Upon melting the thermoplastic particles, free volume is generated to align the mesogen within liquid crystal elastomer. After solidification of the particles, it efficiently locks in any deformations introduced mechanically. The oriented mesogen (monodomain) are now capable of anisotropic actuation. When thermally reset, the composite is capable of reverting to its initial form and structure, making it ready for subsequent shape programming, by stretching in another direction. These features may inspire applications in soft grippers and manipulators, adaptive prosthetics and biomedical devices, which may be scaled up to larger devices than previously possible due to the mechanical robustness of the composite. Moreover, because of the reprogrammability of the shape, recyclability is possible, which might lead to more sustainable developments in the field.

materials themselves rather than electronic controls.<sup>13</sup> These materials, capable of responding to environmental stimuli with changes in shape, stiffness, or motion, offer unparalleled advantages in creating more autonomous, adaptable, and intelligent robotic systems. Advancements in soft active functional materials, include for example, shape memory polymers<sup>14</sup>, dielectric elastomers,<sup>15, 16</sup> and stimuli-responsive hydrogels.<sup>17, 18</sup>

A very attractive stimulus is light because of the high spatial resolution and the easily controllable intensity and wavelength of the beam. The first break-through in this area was achieved by Ikeda and co-workers, who demonstrated the first

<sup>1</sup> University of Bremen, Institute for Organic and Analytical Chemistry, Leobener Straße 7, D-28359 Bremen, Germany

<sup>2</sup> University of Bremen, MAPEX Center for Materials and Processes, Bibliothekstraße 1, D-28359 Bremen, Germany

<sup>3</sup> Kiel University, Department of Materials Science, Kaiserstraße 2, D-24143 Kiel, Germany

<sup>4</sup> Technical University of Ilmenau, Faculty of Mechanical Engineering, Max-Planck Ring 12, D-98684 Ilmenau, Germany

<sup>5</sup> University of Kiel, Otto-Diels Institute for Organic Chemistry, Otto-Hahn Platz 4, D-24118 Kiel, Germany

E-mail: staubitz@uni-bremen.de

Electronic Supplementary Information (ESI) available: See DOI: 10.1039/x0xx00000x

photomechanical polymer, initially at relatively high temperatures ( $> 85\text{ }^{\circ}\text{C}$ ),<sup>19</sup> which could later be adapted to room temperature.<sup>19, 20</sup> Even a photo driven motor was built.<sup>21</sup> Since then, a large body of work has appeared in this area.<sup>22-30</sup> While the majority of these function with UV light or blue light,<sup>31-36</sup> now there are even photobendable polymers that can operate with much safer visible light and even under water.<sup>37-41</sup>

The physical processes that allow photobendable materials to change their shape are complex: On a molecular basis, they depend on molecular photoswitches. It is either their change in geometry upon photoisomerization (photomechanical effect) or the heat transfer to the material caused by thermal relaxation (photothermal effect) or a mixture of the two.<sup>42</sup> As a consequence, on a supramolecular level, there are also several different mechanisms and oftentimes, it is unknown which is operational. For an in-depth discussion of these, we refer to recent reviews and papers,<sup>42, 43</sup> but for the purpose of this work, the focus is on azobenzene photoswitches in liquid crystalline polymers: Azobenzene is one of the best researched molecular switches. In its *E*-isomer, it is long and rigid, with a distance of  $9\text{ \AA}$  between the most peripheral carbon atoms.<sup>44</sup> Its photoisomer, the *Z*-form, however, is bent and the carbon atoms move much closer to each other with a distance of  $5.5\text{ \AA}$ . The *E*-isomer has a predominant  $\pi\pi^*$  transition, which occur at  $320\text{ nm}$  ( $\pi\pi^*$ ), whereas for the *Z*-isomer is addressed by the  $n\pi^*$  transition at  $440\text{ nm}$ .<sup>45</sup> To switch from *E* to *Z*, typically  $360\text{ nm}$  are used, and for the reverse,  $450\text{ nm}$  is used. Upon sufficient irradiation times, a photothermal equilibrium between the two forms can be reached (photostationary state, PSS),<sup>46, [1]</sup> which is wavelength dependent. Because of the rigid nature of the *E*-azobenzene, it can be used as a mesogens in liquid crystalline materials if flexible side groups are attached. These can be functionalized with polymerizable groups, and when these are polymerized when the mesogens form a liquid crystalline phase, liquid crystalline polymers (LCPs) may be obtained.<sup>47</sup> Liquid crystalline networks (LCNs) are highly cross-linked LCPs with fixed orientations. Liquid crystalline elastomers (LCEs) are lightly cross-linked, with a glass transition below room temperature.<sup>25</sup> However, recently even a non-cross-linked LCP film has been reported.<sup>48</sup>

The photobending effect in liquid crystal elastomer (LCEs) films originates from the *E*- to *Z*-isomerization of the azobenzene component, but it also requires the alignment of liquid crystal mesogens. This alignment can be induced for example through surface effects, photoalignment, electrical, or mechanical forces. In LCEs,<sup>23</sup> achieving a permanent monodomain requires fixing this alignment, commonly by polymerization. Hence, in photomechanical LCEs, monomers are aligned and polymerized in this state. This means that once the polymer has been formed, it is entirely fixed in this state and shape.<sup>25, 49</sup> Shape-memory deformations are therefore entirely incompatible with this form of processing the polymer.

The predominant alignment techniques used for photobendable LCEs<sup>23</sup> are through surface patterning or photoalignment, which, due to the limited photopermeability of the materials can also be considered a surface dependent patterning technique. Mechanical forces can be applied, for example, by extrusion through a nozzle,<sup>50</sup> but also here, the force can only be applied to the surfaces because this processing step occurs before stabilizing the LCE by cross-linking. Because the molecules align based on self-assembly starting from the surface, the long-range order decreases with increasing distance from the surface.<sup>49</sup> This limits film thickness. However, for alignment using electrical forces, the case is different, because the field permeates the sample. However, even with this technique, the film thickness is limited as it is inversely proportional to the threshold field strength that must be surpassed for alignment.<sup>51, 52</sup>

At the time of writing, to our knowledge, the maximal film thickness of a photobendable film is  $450\text{ }\mu\text{m}$  as a bilayer construction. In this case, this was possible, because a two-step processing procedure was used: In the first step, the linear polymer precursor was formed with a polydomain morphology. This was then stretched to achieve the alignment of the mesogens (monodomain morphology), followed by photo cross-linking.<sup>53</sup> This work is remarkable in that a covalent adaptable network was used, in which bond exchange reactions were used that allow reprogramming, reprocessed, and self-healing.

Inspired by the results of the group of Odenbach, who showed a shape-memory effect by incorporating poly(caprolactone) (PCL) particles in PDMS,<sup>54</sup> we wished to transfer this methodology to affect shape-memory properties in an LCE. In contrast to a PDMS rubber, an LCE poses the additional challenge of the alignment of the mesogens. Because one alignment method is unidirectional stretching, we hoped to achieve this concomitantly with the shape memory programming by stretching the material at a temperature when the thermoplastic particles are molten. Moreover, we desired this LCE to be light-switchable, which meant that a certain amount to the mesogens had to be molecular switches.

The classic fabrication of LCEs consists of pre-polymerization, followed by the alignment of mesogens, and subsequent chemical fixation of the mesogens through a second reaction, which is a hurdle for the widespread application of LCEs. The described shape-memory effect should not only enable a new form of the LCE but primarily undertake the fixation of the aligned mesogens. This would render a second reaction redundant and allow for simpler fabrication.

## Results and discussion

The composite used consisted of a MC-LCE cross-linked polymer blend with the thermoplastic PCL particles. Using thermoplastic

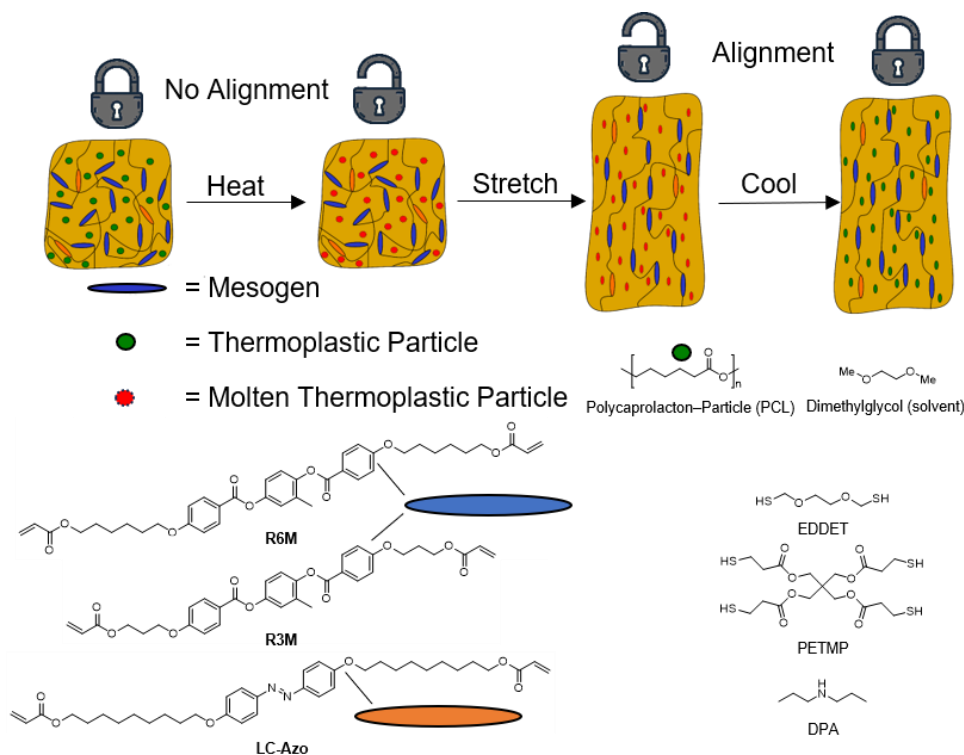


Fig. 1 Top: Concept for aligning the mesogens in the composite and fixing it: The composite with the thermoplastic particles and unaligned mesogens is heated to melt the particles. This allows for the material to be stretched, thus aligning the mesogens. The alignment is fixed by cooling and thus “freezing” the thermoplastic particles again. The alignment allows to address them to move synergistically with light (see below). Bottom: monomer mesogens, cross-linkers, solvent and catalyst (DPA) used in the thiol-michael-reaction to form the polymer-particle composition.

particles both leads to a shape memory function and provide a stable alignment of the mesogens. Two samples were prepared: **LCE<sub>Azo</sub>**, without the particles, and **LCE<sub>Azo/PCL</sub>** with the particles to demonstrate the principle. For further sample compositions testing the necessity of each component see the ESI. The mixture contained several components (Fig 1): The core functionality of liquid crystallinity was conferred by two passive, polymerizable mesogens, **R6M** ( $T_{CN} = 84\text{ }^{\circ}\text{C}$ ,  $T_{NI} = 117\text{ }^{\circ}\text{C}$ ) and **R3M** ( $T_{CN} = 65\text{ }^{\circ}\text{C}$ ,  $T_{NI} = 124\text{ }^{\circ}\text{C}$ ),<sup>55</sup> which are known for producing stable LC phases ( $T_{CN}$  = temperature of crystallization / melting;  $T_{NI}$  = temperature of the phase change nematic / isotropic).<sup>56-60</sup> As the photoactive mesogen monomer, **LC-Azo** ( $T_{CSm} = 78\text{ }^{\circ}\text{C}$ ,  $T_{Sml} = 91\text{ }^{\circ}\text{C}$ )<sup>61</sup> was prepared in three steps in an overall yield of 36% (see ESI). The three components were used in a ratio of 0.45 : 0.45 : 0.1. This particular ratio was used to achieve a low melting point of this mixture ( $T_{m(\text{mesogen-mix})} \approx 43\text{ }^{\circ}\text{C}$ ) below the melting point of the particles ( $T_{m(\text{PCL})} = 53\text{ }^{\circ}\text{C}$ ). This is important for the second composite, **LCE<sub>Azo/PCL</sub>**, see below. The individual melting points were: **R6M** ( $T_m \approx 84\text{ }^{\circ}\text{C}$ ), **R3M** ( $T_m \approx 65\text{ }^{\circ}\text{C}$ ) and **LC-Azo** ( $T_m \approx 78\text{ }^{\circ}\text{C}$ ). The incorporation of the azobenzene was designed to allow actuation with light after alignment of the mesogen in one predominant direction (monodomain). A melting of the particles would dissolve the particles in the monomer mixture and had to be avoided. The addition of dimethylglycol (**DME**) and the thiols even further stabilized the liquidity of the monomer mixture, ensuring complete

polymerization without dissolving PCL. However, this effect could not be measured, because of the starting polymerization process after mixing. These mesogens with the acrylates as reactive groups were polymerized in a thiol-Michael reaction<sup>56, 62</sup> with thiols in ratio of 1:1 (acrylate functional groups: thiol functional groups). 2,2'-(ethylenedioxy)diethanthiol (**EDDET**) was used as a chain-extender to increase flexibility, while pentaerythritol-tetrakis(3-mercaptopropionate) (**PETMP**) served as a cross-linking agent. After the addition of the catalyst diisopropylamine (**DPA**) diluted in **DME** (1:20 wt%), the mixture was polymerized to give the covalently bonded copolymer in which the mesogens were yet unaligned (polydomain) MC-LCE (**LCE<sub>Azo</sub>**). Thus, an ideal monomer composition comprised the acrylates, **R6M**, **R3M** and **LC-Azo** (0.45:0.45:0.10 eq.), the thiols **EDDET** (0.80 eq.) and **PETMP** (0.10 eq.), (**DPA**) as a catalyst (0.9 wt%) and **DME** as solvent (0.17 wt%), and additional 20 wt% PCL particles (100-600  $\mu\text{m}$ ). Thermal analysis using dynamic scanning calorimetry (DSC) showed that this polymer blend **LCE<sub>Azo</sub>** had a glass transition temperature ( $T_g$ ) of  $-19\text{ }^{\circ}\text{C}$  and showed a broad liquid crystalline phase between  $26\text{ }^{\circ}\text{C}$  and  $73\text{ }^{\circ}\text{C}$  (see SI for details).

The second composite, **LCE<sub>Azo/PCL</sub>**, was prepared in the same way, but PCL particles were added to the monomer mixture (20 wt%). These had a diameter between  $100\text{ }\mu\text{m}$  -  $600\text{ }\mu\text{m}$ , and a melting point of  $T_m \approx 53\text{ }^{\circ}\text{C}$ , as confirmed by dynamic scanning

calorimetry (DSC) (see ESI). This composite  $\text{LCE}_{\text{Azo/PCL}}$  had a similar glass transition at  $-17\text{ }^{\circ}\text{C}$  and a nematic phase ranging from  $29\text{ }^{\circ}\text{C}$  to  $65\text{ }^{\circ}\text{C}$ , but the melting of PCL could clearly be discerned as an endothermic peak with an onset of  $53\text{ }^{\circ}\text{C}$ .

For the preparation of the functional composite, the components were mixed in the desired mold. The reaction temperature was maintained at  $40\text{ }^{\circ}\text{C}$  for 2 h. This allowed the thiol-Michael polymerization reaction to proceed to form a cross-linked LCE which included the spherical thermoplastic PCL particles, but did not react with them or melt or dissolve them. This procedure yielded a relatively stiff polymer  $\text{LCE}_{\text{Azo/PCL}}$ . After the polymerization, the composite could be heated to  $70\text{ }^{\circ}\text{C}$ , at which temperature the PCL particles were entirely melted. This decreases the stiffness in composites.<sup>54</sup> Therefore, at this temperature, the composite was easily stretched to an elongation of 150%. The successful post-alignment and actuation, crucially relying on the shape-memory effect, is contingent upon particle incorporation. For instance, stretching a polydomain stripe (dimensions  $5.0\text{ cm} \times 1.0\text{ cm} \times 2.0\text{ mm}$ ) clamped in a bench vice by 135% at  $70\text{ }^{\circ}\text{C}$  (Fig. 2) and then cooling it results in the solidification the particles, effectively locking the mesogens' alignment. This process was efficient up to 195% elongation before reaching the breaking point (Fig. 3). A tensile test was conducted under thermal treatment for both  $\text{LCE}_{\text{Azo}}$  and  $\text{LCE}_{\text{Azo/PCL}}$  under thermal heating. A stress of 50 kPa was applied to the sample, and the elongation was measured with a temperature program ramp of 5 K/min. The resulting curve represent the state after full force application and the polymer creep did not change.  $\text{LCE}_{\text{Azo}}$  (indicated by the red curve) exhibited significant elongation amplitude upon heating, which initiated at the phase transition to the nematic phase ( $T_{\text{Ni}}(\text{LCE}_{\text{Azo}}) = 28\text{ }^{\circ}\text{C}$ ). Post this transition, the mesogens gained increased freedom and volume, enhancing the elasticity. Around  $58\text{ }^{\circ}\text{C}$ , a peak at 431% elongation was observed. The extreme stretch aligns the mesogens without the necessity of the molten particles, but at this point, the induced anisotropic alignment strengthens the material, which counteracts the applied force of the clamps.

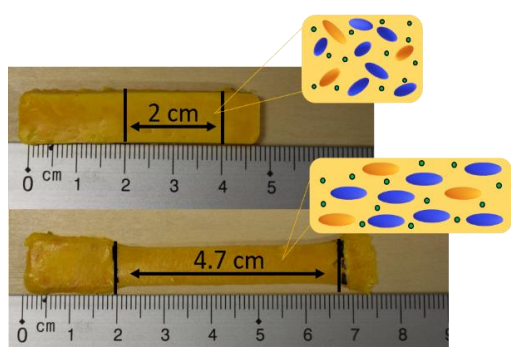


Fig. 2 Top: Photograph of  $\text{LCE}_{\text{Azo/PCL}}$  before the stretching process. Bottom: Photograph of the same sample after stretching and cooling (bottom). The sample was clamped on the outer edges in a bench vice. Upon heating  $\text{LCE}_{\text{Azo/PCL}}$  to  $70\text{ }^{\circ}\text{C}$ , the marked area (2 cm) was stretched (4.7 cm, 135% elongation). Cooling down to  $25\text{ }^{\circ}\text{C}$  froze the elongated shape. The drawings show the change in the molecular arrangement within the polymer during this process.

Therefore, the  $\text{LCE}_{\text{Azo}}$  contracted, surpassing the 50 kPa applied force at temperatures between  $58\text{ }^{\circ}\text{C}$  to  $73\text{ }^{\circ}\text{C}$ . Near the second phase transition to the isotropic phase ( $T_{\text{Iso}}(\text{LCE}_{\text{Azo}}) = 73\text{ }^{\circ}\text{C}$ ), the contraction further increased with the temperature. On the other hand,  $\text{LCE}_{\text{Azo/PCL}}$  elongated only an additional 50% under an applied force of 100 kPa within the  $25\text{ }^{\circ}\text{C}$  to  $60\text{ }^{\circ}\text{C}$  temperature range. No noticeable change was observed upon passing the nematic phase transition ( $T_{\text{Ni}}(\text{LCE}_{\text{Azo/PCL}}) = 29\text{ }^{\circ}\text{C}$ ). This highlights the effectiveness of the incorporated particles in increasing the stiffness of the polymer holding the force of 100 kPa. As the PCL particles completely melted, which was delayed compared to the melting point of PCL due to sample thickness, elasticity markedly increased.  $\text{LCE}_{\text{Azo/PCL}}$  stretched up to 195% before reaching its breaking point. Once the particles have melted, the polymer matrix is subjected to increased stress in proportion to the volume previously occupied by the particle (i.e., the filler content or cross-sectional area). This implies that the stress acting on the LCE is increased by the factor of the volume fraction (volume of LCE / volume of LCE + PCL). As a result, the tensile strength of the LCE is achieved, leading to the subsequent failure of the matrix.

The particle size and shape within the mixture varied randomly, with a size limit of  $100\text{--}600\text{ }\mu\text{m}$ , achieved through sieving. These particles are distributed evenly throughout the polymer and their presence on the surface is visibly noticeable on both sides (see Fig. 4). However, excessive addition of the solvent (DME) can lower the viscosity of the monomer mixture leading to density-based separation of the particles. A microscopic image at 5x magnification reveals the variation in particle sizes within  $\text{LCE}_{\text{Azo/PCL}}$ , noticeable by the darker areas. Following three cycles of programming and deprogramming, the particles on the surface remain in their original positions, indicating the composite's durability. To demonstrate the composite's programmability, we created three distinct shapes. In addition to the previously demonstrated stretching, we introduced also helical stretching,

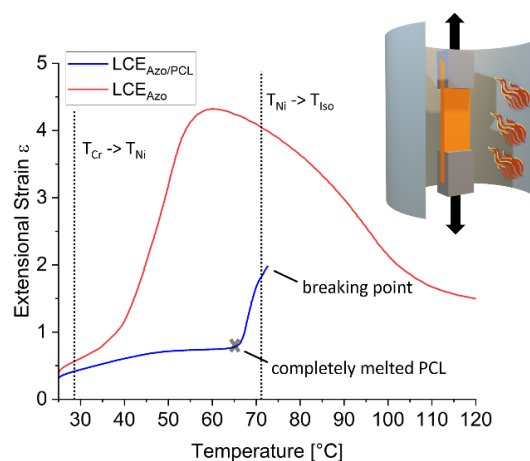


Fig. 3 Tensile curve of  $\text{LCE}_{\text{Azo}}$  and  $\text{LCE}_{\text{Azo/PCL}}$  during a temperature program with a heating rate of 5 K/min. The sample was clamped in the device and a force of 50 kPa ( $\text{LCE}_{\text{Azo}}$ ) and 100 kPa ( $\text{LCE}_{\text{Azo/PCL}}$ ) was applied.

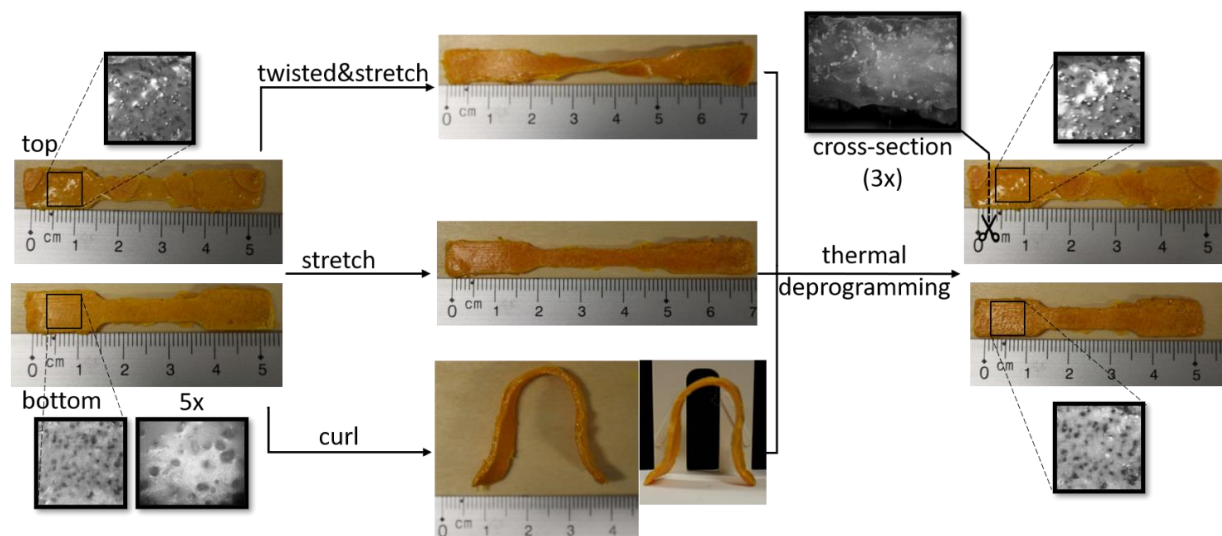


Fig. 4(left) Sample of LCE<sub>Azo</sub>/PCL from top and bottom view. Additionally, a zoomed in area is shown to see the distribution of the particles on both surfaces and their shape still intact after polymerization. The particle size varies and is not homogenous, but smaller than 600  $\mu\text{m}$  when deployed in the reaction mixture. The brightness and contrast of the zoomed inlet was increased and the colour removed for clarification. LCE<sub>Azo</sub>/PCL can be programmed in different shapes during heating at 70  $^{\circ}\text{C}$ , for example twisted&stretched, stretched or curled. (middle). On the right the thermal deprogramming of LCE<sub>Azo</sub>/PCL is shown, which occurs at heating up the sample without any force. The picture shows the polymer in its almost original shape after three programming/deprogramming cycles. A cross-section was cut out of the polymer and taken under the microscope. The lighter spots indicate the holes, where the particles were.

generating a twisted shape. The third shape was a curled U-shape LCE<sub>Azo</sub>/PCL, serving as a bent actuator that can initiate an unbending motion upon receiving an external stimulus. Regardless of the specific shape, thermal deprogramming consistently restored the original shape, down to the smallest details. To assess the particle distribution within the sample LCE<sub>Azo</sub>/PCL, a cross-section was cut out of the polymer and a microscopical image was obtained with a 5x magnification. During the cutting process, PCL particles fell out of the blend and holes, seen as white spots, were left throughout the sample. This shows clearly that there is no chemical interaction between the LCE and the PCL. This image revealed that the particles are not only distributed on the outer surfaces of the polymer, but also evenly distributed throughout the sample.

**Light-induced bending of the polymer composite.** To assess whether the alignment process together with the shape memory properties would still allow photobending of the composite, a sample, measuring 9.5 cm x 1 cm x 1.2 mm and stretched by 95%, was clamped and suspended vertically. (see Figure 5) When exposed to UV-light (65  $\text{mW cm}^{-2}$ ), during an irradiation time of 60 seconds, the irradiated surface changed from yellow to orange and eventually to red. This color change indicates the switching of *E*-azobenzene to *Z*-azobenzene under light exposure.<sup>[2]</sup> The unexposed side of the polymer, which was opposite to the light source, remained yellow. This is because the UV light does not completely penetrate the material. During this irradiation, a large bending motion was observed, with a bending angle of 36 $^{\circ}$  (Fig. 5). This can be attributed to a contraction of the surface by the switching of the azobenzene moieties close to the irradiated surface, while the rest of the LCE remained unaffected. Therefore, the bending

motion is based on a bimaterial-strip principle, like a bimetallic strip. Compared to previously reported film thicknesses of 300  $\mu\text{m}$ ,<sup>41, 53</sup> the polymer composite here is four times as thick. A shape reversal towards the original state could be induced by green light irradiation (530 nm, 50  $\text{mW/cm}^2$ ) for only 30 seconds: A color change back to yellow was observed, indicative of switching the azobenzene back to the *E*-isomer and leading to the relaxation of the surface. From the photochemical assessment of the monomer, Due In chloroform, with a concentration of  $\text{conc}_{\text{LCAzo}} = 6.60 \mu\text{mol mL}^{-1}$ , under irradiation of UV-light (365 nm, 5 min, 55  $\text{mW cm}^{-2}$ ) a PSS of 5%/95% (*E*-/*Z*-isomer) was reached. Under green light irradiation (530 nm, 5 min, 70  $\text{mW/cm}^2$ ) the isomerization was reverted and a PSS of 92%/8% (*E*-/*Z*-isomer) was obtained. Although the PSS is dependent on the medium to some extent, it is likely that in the case of the azobenzene embedded in the LCE, switching will also be to some extent incomplete. Therefore, due to the attainment of photostationary state, a minor fraction of the azobenzene remained in the *Z*-isomer form. This accounts for the incomplete unbending motion (37 $^{\circ}$  vs 30 $^{\circ}$ ). Additionally, LCE<sub>Azo</sub>/PCL can be thermally actuated. However, this effect was constrained to temperatures below 55  $^{\circ}\text{C}$ , the melting point of PCL. We placed the stretched LCE<sub>Azo</sub>/PCL in a heated water bath (50  $^{\circ}\text{C}$ ). Upon contact with the hot water, the LCE<sub>Azo</sub>/PCL shrunk and curled. Removing the LCE<sub>Azo</sub>/PCL from the hot water resulted in the original flat geometry. (see ESI) The curling effect was unexpected and it is possible that an uneven distribution of the particles within LCE<sub>Azo</sub>/PCL is the cause. Therefore, the contraction effect from the disorder mesogen is stronger on one surface, resulting in a similar bilayer bending actuation (see above).

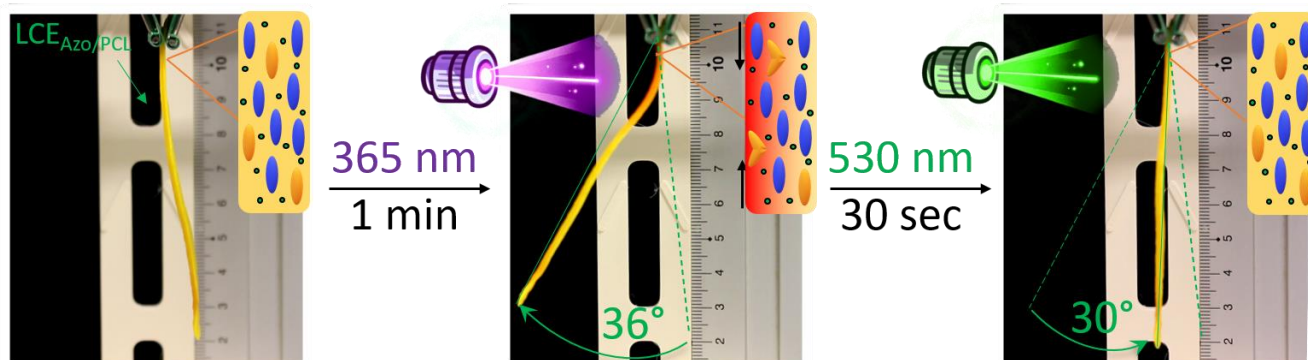


Fig. 5 Light induced bending of the monodomain  $\text{LCE}_{\text{Azo/PCL}}$  (95% stretched) LCE (9.5 cm x 1 cm x 1.2 mm). A bending motion of 37° was observed for UV-light (365 nm, 65 mW/cm<sup>2</sup>, 60 s) irradiation of the left surface, which showed an orange coloration.(middle) On the left, the bending motion is reverted up to 30° with green light (530 nm, 50 mW/cm<sup>2</sup>, 30 s) accompanied by discoloration back to yellow.(right)

## Conclusions

In summary, this study introduces an innovative approach for aligning mesogens using thermoplastic particles in a liquid crystal elastomer. In their solid state, these particles enhance the elastomer's stiffness, but when molten, they enable stretching of the polymer. Thereby, temperature can be used as a parameter that combined with mechanical force effectively programmes the composite's shape and also alignment of the mesogens.

The photobending of the azobenzene containing LCE part of the composite is very fast, efficient, and reversible. Taken together, the composite is therefore re-usable in two dimensions: First, the alignment direction can be set, erased and set again, and second, the bending can be directed with UV-light in one direction and visible light in the opposite direction. This provides a versatile, mechanically robust new material for the soft robotics community. Additionally, it is a first step towards more sustainable reusable materials, which has become one of the "new frontiers in soft robotics".<sup>63</sup>

## Experimental Section and Methods

### Bulk Polymerization of Polydomain-LCE

For the preparation of the polydomain LCE, the mesogen **R6M** (303 mg, 0.450 eq., 31 wt%), **R3M** (265 mg, 0.450 eq., 27 wt%) and **LC-Azo** (60.7 mg, 0.100 eq., 6.0 wt%) were added in a vial and melt mixed. The mesogen mixture was cast in a PTFE mold and kept at 50 °C. Then, a solution of **EDDET** (0.800 eq.) and **PETMP** (0.100 eq.) was prepared. Via a syringe, 195 mg (**EDDET**: 146 mg, 0.800 eq., 15 wt%, **PETMP**: 49.0 mg, 0.100 eq., 5.0 wt%) of the stock solution was taken. A second freshly prepared stock solution of DME and **DPA** (20:1 wt%) was prepared and 165 mg (17 wt%, **DPA**: 8.25 mg, 0.008 eq., 0.90 wt%) taken from it. Both liquids were added to the PTFE mold (5 cm x 1 cm or dogbone type), the temperature lowered to 40 °C and the liquid manually stirred. After 1 min, polycaprolactone (PCL) particles (100-600 μm, 197 mg, additional 20 wt%) were added and dispersed and well mixed in the polymer mixture. The composite was left in the oven for 2 h

at 40 °C for the first curing, then 2 h at 50 °C and 16 h at 60 °C to avoid the dissolving of the particles, but ensure a complete polymerization.

For the sample without particles, the particles were not added and the polymer directly cured at 60 °C.

### Programming of Polydomain-LCE to Monodomain-LCE

A polydomain-LCE stripe was clamped in a bench vice (pictures in supporting information). The bench vice was placed in the oven and heat to 70 °C. The polymer was drawn to the desired length up to 190% inside the oven at 70 °C. Then the apparatus was taken out of the oven and cooled down in a stretched state.

### Methods

Dynamic mechanical analysis (DMA) was conducted on a MCR 702e Multidrive (Anton Paar, Austria). A tensile test during a heating curve was run. The sample was clamped inside the oven and a force of 50 kPa or 100 kPa was applied on the sample. Upon reaching the full applied force, a temperature program (5 K/min) was run. The elongation during the change of temperature was measured.

Equipment for the irradiation experiments: A UPLED power supply powered the high-power LED modules from Thorlabs (US, NJ): M365L3 (365 nm), M415L4 (415 nm), M530L4 (530 nm). A collimator was used to focus the light beam. The light intensity was measured using an ILT2400 hand-held light meter manufactured by International Light Technologies, Inc., (Peabody, USA).

UV-vis spectra were recorded with a resolution of 0.5 nm on a Cary 3500 Multicell UV-Vis Spectrophotometer from Agilent (CA, USA). Chloroform (spectroscopy grade) was used as a solvent.

### Supporting Information

Supporting Information is available from the Wiley Online Library or from the author.

## ORCID-Numbers of the Authors

Sven Schultzke: <https://orcid.org/0000-0002-4975-6218>  
Philipp Schadte: <https://orcid.org/0009-0006-9908-4815>  
Nina Sindesberger: <https://orcid.org/0000-0001-9438-9536>  
Jonas Gerken: <https://orcid.org/0009-0005-5527-3828>  
Leonard Siebert: <https://orcid.org/0000-0001-5316-7240>  
Anne Staubitz: <https://orcid.org/0000-0002-9040-3297>

## Author contributions

A.S. supervised the project; S.S. conceived the idea and designed the idea in collaboration with N.S.; S.S. and J.G. performed the experiments; general measurements were conducted from S.S. with support from P.S. and L.S.; data analysis was carried out from S.S. with support from A.S. and L.S.; S.S. wrote the manuscript with input from L. S. and A.S.; All authors discussed the results and contributed in the reviewing of the manuscript.

## Conflicts of interest

There are no conflicts to declare.

## Acknowledgements

This research was funded by the GERMAN RESEARCH FOUNDATION (DFG) within the priority program SPP 2100 "Soft Material Robotic Systems", Subproject STA1195/5-1, "Insect feet inspired concepts soft touch grippers with dynamically adjustable grip strength", and Subproject "ZIM 540/20-1".

## Notes and references

<sup>[1]</sup>In the literature, this is most often referred to as PSS, but in azobenzenes, there is always a thermal relaxation process, which, for short half-live times, cannot be ignored.

<sup>[2]</sup>This color change is typical for azobenzenes and was also observed when the switching properties of the monomer were measured (see supporting information).

- G. M. Whitesides, *Angewandte Chemie International Edition*, 2018, **57**, 4258-4273.
- M. Cianchetti, C. Laschi, A. Menciassi and P. Dario, *Nature Reviews Materials*, 2018, **3**, 143-153.
- C. Appiah, C. Arndt, K. Siemsen, A. Heitmann, A. Staubitz and C. Selhuber-Unkel, *Advanced Materials*, 2019, **31**, 1807747.
- U. Georgi, P. Reichenbach, U. Oertel, L. M. Eng and B. Voit, *Reactive and Functional Polymers*, 2012, **72**, 242-251.
- L. Blanc, A. Delchambre and P. Lambert, *Actuators*, 2017, **6**, 23.
- P. A. d. Maur, B. Djambazi, Y. Haberthür, P. Hörmann, A. Kübler, M. Lustenberger, S. Sigrist, O. Vigen, J. Förster, F. Achermann, E. Hampf, R. K. Katzschmann and R. Siegwart, 2021.
- S. Puhlmann, J. Harris and O. Brock, *IEEE Transactions on Robotics*, 2022, **38**, 3434-3449.
- P. Polygerinos, N. Correll, S. A. Morin, B. Mosadegh, C. D. Onal, K. Petersen, M. Cianchetti, M. T. Tolley and R. F. Shepherd, *Advanced Engineering Materials*, 2017, **19**, 1700016.
- E. Q. Yumbla, Z. Qiao, W. Tao and W. Zhang, *Current Robotics Reports*, 2021, **2**, 399-413.
- D. F. Gruber and R. J. Wood, *Sci. Robot.*, 2022, **7**, eabm6807.
- J. Walker, T. Zidek, C. Harbel, S. Yoon, F. S. Strickland, S. Kumar and M. Shin, *Actuators*, 2020, **9**, 3.
- P. Boyraz, G. Runge and A. Raatz, *Actuators*, 2018, **7**, 48.
- Z. Shen, F. Chen, X. Zhu, K.-T. Yong and G. Gu, *Journal of Materials Chemistry B*, 2020, **8**, 8972-8991.
- G. Scalet, *Actuators*, 2020, **9**, 10.
- J. Wang, D. Gao and P. S. Lee, *Advanced Materials*, 2021, **33**, 2003088.
- Y. Guo, L. Liu, Y. Liu and J. Leng, *Advanced Intelligent Systems*, 2021, **3**, 2000282.
- Y. Zhao, C. Xuan, X. Qian, Y. Alsaïd, M. Hua, L. Jin and X. He, *Sci. Robot.*, 2019, **4**, eaax7112.
- Z. Jiang, M. L. Tan, M. Taheri, Q. Yan, T. Tsuzuki, M. G. Gardiner, B. Diggie and L. A. Connal, *Angewandte Chemie International Edition*, 2020, **59**, 7049-7056.
- Y. Yu, M. Nakano and T. Ikeda, *Nature*, 2003, **425**, 145.
- T. Ikeda, J.-i. Mamiya and Y. Yu, *Angewandte Chemie International Edition*, 2007, **46**, 506-528.
- M. Yamada, M. Kondo, J.-i. Mamiya, Y. Yu, M. Kinoshita, C. J. Barrett and T. Ikeda, *Angewandte Chemie International Edition*, 2008, **47**, 4986-4988.
- X. Pang, J.-a. Lv, C. Zhu, L. Qin and Y. Yu, *Advanced Materials*, 2019, **31**, 1904224.
- K. M. Herbert, H. E. Fowler, J. M. McCracken, K. R. Schlafmann, J. A. Koch and T. J. White, *Nature Reviews Materials*, 2022, **7**, 23-38.
- F. A. Jerca, V. V. Jerca and R. Hoogenboom, *Nature Reviews Chemistry*, 2022, **6**, 51-69.
- T. J. White and D. J. Broer, *Nature Materials*, 2015, **14**, 1087-1098.
- T. Ikeda and T. Ube, *Materials Today*, 2011, **14**, 480-487.
- X. Qing, L. Qin, W. Gu and Y. Yu, *Journal*, 2016, **43**, 2114-2135.
- F. Cheng, R. Yin, Y. Zhang, C.-C. Yen and Y. Yu, *Soft Matter*, 2010, **6**, 3447-3449.
- M. Pilz da Cunha, M. G. Debije and A. P. H. J. Schenning, *Chemical Society Reviews*, 2020, **49**, 6568-6578.
- M. R. A. Bhatti, A. Kernin, M. Tausif, H. Zhang, D. Papageorgiou, E. Bilotti, T. Peijs and C. W. M. Bastiaansen, *Advanced Optical Materials*, 2022, **10**, 2102186.
- E. Kizilkan, J. Strueben, A. Staubitz and S. N. Gorb, *Sci. Robot.*, 2017, **2**, eaak9454.
- Y. Li, Y. Liu and D. Luo, *Advanced Optical Materials*, 2021, **9**, 2001861.
- Q. Liu, Y. Liu, J.-a. Lv, E. Chen and Y. Yu, *Advanced Intelligent Systems*, 2019, **1**, 1900060.
- Y. Li, O. Rios, J. K. Keum, J. Chen and M. R. Kessler, *ACS Applied Materials & Interfaces*, 2016, **8**, 15750-15757.
- T. S. Hebner, M. Podgórski, S. Mavila, T. J. White and C. N. Bowman, *Angewandte Chemie International Edition*, 2022, **61**, e202116522.
- S. Fredrich, T. Engels and A. P. H. J. Schenning, *ACS Applied Polymer Materials*, 2022, **4**, 7751-7758.
- Z. Jiang, M. Xu, F. Li and Y. Yu, *Journal*, 2013, **135**, 16446-16453.

38. S. Sasaki, T. Ube, K. Katayama, M. Muramatsu, H. Miyasaka and T. Ikeda, *Journal*, 2018, **662**, 53-60.
39. Z. Jiang, M. Xu, F. Li and Y. Yu, *Journal of the American Chemical Society*, 2013, **135**, 16446-16453.
40. K. Kumar, C. Knie, D. Bléger, M. A. Peletier, H. Friedrich, S. Hecht, D. J. Broer, M. G. Debije and A. P. H. J. Schenning, *Nature Communications*, 2016, **7**, 11975.
41. S. Schultzke, N. Scheuring, P. Puylaert, M. Lehmann and A. Staubitz, *Advanced Science*, 2023, **10**, 2302692.
42. M. Pilz da Cunha, E. A. J. van Thoor, M. G. Debije, D. J. Broer and A. P. H. J. Schenning, *Journal of Materials Chemistry C*, 2019, **7**, 13502-13509.
43. K. M. Lee and T. J. White, *Macromolecules*, 2012, **45**, 7163-7170.
44. S. Monti, G. Orlandi and P. Palmieri, *Journal*, 1982, **71**, 87-99.
45. A. R. Dias, M. E. Minas Da Piedade, J. A. Martinho Simões, J. A. Simoni, C. Teixeira, H. P. Diogo, Y. Meng-Yan and G. Pilcher, *The Journal of Chemical Thermodynamics*, 1992, **24**, 439-447.
46. K. Stranius and K. Börjesson, *Scientific Reports*, 2017, **7**, 41145.
47. A. S. Angeloni, D. Caretti, C. Carlini, E. Chiellini, G. Galli, A. Altomare, R. Solaro and M. Laus, *Journal*, 1989, **4**, 513-527.
48. Z. Yang and L. Zhang, *Macromolecules*, 2023, **56**, 7551-7560.
49. Z.-Z. Nie, M. Wang and H. Yang, *Chemistry – A European Journal*, 2023, **29**, e202301027.
50. L. Ceamanos, Z. Kahveci, M. López-Valdeolivas, D. Liu, D. J. Broer and C. Sánchez-Somolinos, *ACS Applied Materials & Interfaces*, 2020, **12**, 44195-44204.
51. V. Fréedericksz and A. Repiewa, *Zeitschrift für Physik*, 1927, **42**, 532-546.
52. V. Fréedericksz and V. Zolina, *Transactions of the Faraday Society*, 1933, **29**, 919-930.
53. Y.-J. Jeong and S.-Y. Park, *ACS Applied Materials & Interfaces*, 2024, DOI: 10.1021/acsami.3c17068.
54. N. Prem, F. Schale, K. Zimmermann, D. K. Gowda and S. Odenbach, *Journal of Applied Polymer Science*, 2021, **138**, 51296.
55. J. M. McCracken, B. R. Donovan, K. M. Lynch and T. J. White, *Advanced Functional Materials*, 2021, **31**, 2100564.
56. C. M. Yakacki, M. Saed, D. P. Nair, T. Gong, S. M. Reed and C. N. Bowman, *RSC Advances*, 2015, **5**, 18997-19001.
57. M. O. Saed, R. H. Volpe, N. A. Traugutt, R. Visvanathan, N. A. Clark and C. M. Yakacki, *Soft Matter*, 2017, **13**, 7537-7547.
58. T. Ohzono, K. Katoh, H. Minamikawa, M. O. Saed and E. M. Terentjev, *Nature Communications*, 2021, **12**, 787.
59. S. Li, H. Bai, Z. Liu, X. Zhang, C. Huang, L. W. Wiesner, M. Silberstein and R. F. Shepherd, *Science Advances*, 2021, **7**, eabg3677.
60. H. Tokumoto, H. Zhou, A. Takebe, K. Kamitani, K. Kojio, A. Takahara, K. Bhattacharya and K. Urayama, *Science Advances*, 2021, **7**, eabe9495.
61. E. Kizilkan, J. Strueben, X. Jin, C. F. Schaber, R. Adelung, A. Staubitz and S. N. Gorb, *Royal Society Open Science*, 2016, **3**.
62. G. E. Bauman, J. M. McCracken and T. J. White, *Angewandte Chemie International Edition*, 2022, **61**, e202202577.
63. F. Hartmann, M. Baumgartner and M. Kaltenbrunner, *Advanced Materials*, 2021, **33**, 2004413.



## Conclusion and Outlook

This thesis focused on advancing visible switching for applications, delving into synthesis, molecular properties, and their effects on material characteristics, alongside the preparation methods for liquid crystalline actuators. Significant advancements were achieved across these areas:

**1. Synthesis and Optimization:** New methods for synthesis were developed, enhancing synthetic yields and scaling up production for material-focused tasks. The combination of macrocyclic elements with *ortho*-fluoro substitution increased the thermal half-life time, setting a record for the longest half-life of an azobenzene derivative while maintaining the ability for visible light switching. These enhancements are pivotal for optical data storage applications.

**2. Emissive Azobenzene Research (FOAM):** Our investigations into **FOAM**, particularly its long half-life times and temperature-dependent stability, aim to further understand its application in optical data storage. Key to this is differentiating the emissive properties of *E-FLOAM* and *Z-FLOAM*. Further investigations in the subject of emission and two-photon absorption might result in an optimized candidate for optical data storage.

**3. Liquid Crystalline Actuators:** Adjustments in molecular design recovered liquid crystalline properties lost to *ortho*-fluoro substitution, crucial for photoswitchable actuators functionality. These actuators have demonstrated effective bending in response to visible light. The streamlined synthesis process allows for the creation of diverse liquid crystal fluorinated azobenzenes, facilitating the exploration of different core groups and chain lengths for optimal phase behavior and actuator performance. Modifications, such as the use of vinyl groups and the reduction of aromatic cores, offer pathways to new liquid crystalline polymers (LCP) with improved characteristics.

**4. Manufacturing LCE:** Innovations in the composition of LCEs and a simplified method for aligning liquid crystals within polymers have broadened the accessibility of liquid crystalline actuators. By integrating thermoplastic particles with liquid crystalline polymers, we have developed a composite that simplifies the alignment process, allowing for the use of a variety of particles and liquid crystal formulations. This opens up new possibilities for material design and application, making these advanced materials more accessible to a wider audience.

In conclusion, this thesis has laid the groundwork for significant improvements in visible switching technologies and liquid crystalline actuators, with broad implications for optical data storage and beyond. Future work will continue to explore the potential of these materials, focusing on enhancing their properties and applications.



# Bibliography

- (1) Feringa, B. L. *Angew. Chem. Int. Ed.* **2017**, *56* (37), 11060–11078.
- (2) Soori, M.; Arezoo, B.; Dastres, R. *Cognitive Robotics* **2023**, *3*, 54–70.
- (3) Maslej, N.; Fattorini, L.; Brynjolfsson, E.; Etchemendy, J.; Ligett, K.; Lyons, T.; Manyika, J.; Ngo, H.; Niebles, J. C.; Parli, V.; Shoham, Y.; Wald, R.; Clark, J.; Perrault, R. *Artificial Intelligence Index Report 2023*; tech. rep.; Stanford University, Stanford, CA: Institute for Human-Centered AI, **2023**.
- (4) Roy, N.; Posner, I.; Barfoot, T.; Beaudoin, P.; Bengio, Y.; Bohg, J.; Brock, O.; Depatie, I.; Fox, D.; Koditschek, D.; Lozano-Perez, T.; Mansinghka, V.; Pal, C.; Richards, B.; Sadigh, D.; Schaal, S.; Sukhatme, G.; Therien, D.; Toussaint, M.; Van de Panne, M. From Machine Learning to Robotics: Challenges and Opportunities for Embodied Intelligence, **2021**.
- (5) Zhou, Y.; Li, H. *Front. Robot. AI* **2022**, *9* (68682).
- (6) Sündenhauf, N.; Brock, O.; Scheirer, W.; Hadsell, R.; Fox, D.; Leitner, J.; Upcroft, B.; Abbeel, P.; Burgard, W.; Milford, M.; Corke, P. *The International Journal of Robotics Research* **2018**, *37* (4-5), 405–420.
- (7) Wang, Z.; Hirai, S.; Kawamura, S. *Front. Robot. AI* **2022**, *8* (789107).
- (8) Majidi, C. *Soft Robotics* **2014**, *1* (1), 5–11.
- (9) Tauber, F.; Desmulliez, M.; Piccin, O.; Stokes, A. A. *Bioinspir. Biomim.* **2023**, *18* (3), 035001.
- (10) Yasa, O.; Toshimitsu, Y.; Michelis, M. Y.; Jones, L. S.; Filippi, M.; Buchner, T.; Katzschmann, R. K. *Annual Review of Control, Robotics, and Autonomous Systems* **2023**, *6* (1), 1–29.
- (11) Schmitt, F.; Piccin, O.; Barbé, L.; Bayle, B. *Front. Robot. AI* **2018**, *5* (84).
- (12) Runciman, M.; Darzi, A.; Mylonas, G. P. *Soft Robotics* **2019**, *6*, 4, 423–443.
- (13) Hughes, J.; Culha, U.; Giardina, F.; Guenther, F.; Rosendo, A.; Iida, F. *Front. Robot. AI* **2016**, *3* (69).
- (14) Puhlmann, S.; Harris, J.; Brock, O. *IEEE Trans. Rob.* **2022**, *38* (6), 3434–3449.
- (15) Knoop, E.; Bächer, M.; Wall, V.; Deimel, R.; Brock, O.; Beardsley, P. In *IEEE/RSJ International Conference on Intelligent Robots and Systems (IROS)*, **2017**, pp 4982–4989.
- (16) Paternò, L.; Lorenzon, L. *Front. Robot. AI* **2023**, *10*.
- (17) Murphy, R. R. *Science Robotics* **2022**, *7* (70), eade5835.
- (18) Garcia, L.; Kerns, G.; O'Reilley, K.; Okesanjo, O.; Lozano, J.; Narendran, J.; Broeking, C.; Ma, X.; Thompson, H.; Njapa Njeuha, P.; Sikligar, D.; Brockstein, R.; Golecki, H. M. *Micromachines* **2022**, *13* (1), 28.
- (19) Su, H.; Hou, X.; Zhang, X.; Qi, W.; Cai, S.; Xiong, X.; Guo, J. *Actuators* **2022**, *11* (3), 92.
- (20) Xavier, M. S.; Tawk, C. D.; Zolfagharian, A.; Pinski, J.; Howard, D.; Young, T.; Lai, J.; Harrison, S. M.; Yong, Y. K.; Bodaghi, M.; Fleming, A. J. *IEEE Access* **2022**, *10*, 59442–59485.
- (21) Nguyen, P. H.; Zhang, W. *Sci Rep* **2020**, *10* (9638).

- (22) Imato, K.; Ishii, A.; Kaneda, N.; Hidaka, T.; Sasaki, A.; Imae, I.; Ooyama, Y. *JACS Au* **2023**, *3* (9), 2458–2466.
- (23) Lu, J.; Miao, Z.; Wang, Z.; Liu, Y.; Zhu, D.; Yin, J.; Tang, F.; Wang, X.; Ding, W.; Zhang, M. *Nano Res.* **2023**, *16* (4), 4970–4979.
- (24) Chen, E.; Yang, Y.; Li, M.; Li, B.; Liu, G.; Mu, W.; Yin, R. *Adv. Sci.* **2023**, *10* (20), 2300673.
- (25) Rothmund, P.; Kellaris, N.; Mitchell, S. K.; Acome, E.; Keplinger, C. *Adv. Mater.* **2021**, *33* (19), 2003375.
- (26) Zhang, L.; Zhang, J.; Xia, N.; Dong, Y., *Untethered Miniature Soft Robots: Materials, Fabrications, and Applications*; Wiley-VCH GmbH: **2023**.
- (27) Rich, S. I.; Wood, R. J.; Majidi, C. *Nat Electron* **2018**, *1* (2), 102–112.
- (28) Dicker, M. P. M.; Baker, A. B.; Iredale, R. J.; Naficy, S.; Bond, I. P.; Faul, C. F. J.; Rossiter, J. M.; Spinks, G. M.; Weaver, P. M. *Sci Rep* **2017**, *7* (9197).
- (29) Lancia, F.; Ryabchun, A.; Nguindjel, A.-D.; Kwangmettatam, S.; Katsonis, N. *Nat. Commun.* **2019**, *10* (4819).
- (30) Li, W.; Hu, D.; Yang, L. *Appl. Sci.* **2023**, *13* (16), 9255.
- (31) Li, M.; Pal, A.; Aghakhani, A.; Pena-Francesch, A.; Sitti, M. *Nat. Rev. Mater.* **2022**, *7*, 235–249.
- (32) Pilz da Cunha, M.; Debije, M. G.; Schenning, A. P. H. J. *Chem. Soc. Rev.* **2020**, *49*, 6568–6578.
- (33) Boelke, J.; Hecht, S. *Adv. Opt. Mater.* **2019**, *7* (16), 1900404.
- (34) Dattler, D.; Fuks, G.; Heiser, J.; Moulin, E.; Perrot, A.; Yao, X.; Giuseppone, N. *Chem. Rev.* **2020**, *120* (1), 310–433.
- (35) Feringa, B.; Browne, W., *Molecular Switches*; Wiley-VCH: **2011**.
- (36) Briek, C.; Rohrbach, F.; Gottschalk, A.; Mayer, G.; Heckel, A. *Angew. Chem. Int. Ed.* **2012**, *51* (34), 8446–8476.
- (37) Russev, M.-M.; Hecht, S. *Adv. Mater.* **2010**, *22* (31), 3348–3360.
- (38) Feringa, B. L.; van Delden, R. A.; Koumura, N.; Geertsema, E. M. *Chem. Rev.* **2000**, *100* (5), 1789–1816.
- (39) Tian, H.; Yang, S. *Chem. Soc. Rev.* **2004**, *33*, 85–97.
- (40) Klajn, R. *Chem. Soc. Rev.* **2014**, *43*, 148–184.
- (41) Irie, M.; Fukaminato, T.; Matsuda, K.; Kobatake, S. *Chem. Rev.* **2014**, *114* (24), 12174–12277.
- (42) Abendroth, J. M.; Bushuyev, O. S.; Weiss, P. S.; Barrett, C. J. *ACS Nano* **2015**, *9* (8), 7746–7768.
- (43) Yu, Y.; Nakano, M.; Ikeda, T. *Nature* **2003**, *425* (6954), 145–145.
- (44) Kondo, M. *Polym. J.* **2020**, *52* (9), 1027–1034.
- (45) Shafraneck, R. T.; Millik, S. C.; Smith, P. T.; Lee, C.-U.; Boydston, A. J.; Nelson, A. *Prog. Polym. Sci.* **2019**, *93*, 36–67.
- (46) Jeong, M.; Park, J.; Kwon, S. *Eur. J. Org. Chem.* **2020**, *2020* (47), 7254–7283.
- (47) Goulet-Hanssens, A.; Utecht, M.; Mutruc, D.; Titov, E.; Schwarz, J.; Grubert, L.; Bléger, D.; Saalfrank, P.; Hecht, S. *J. Am. Chem. Soc.* **2017**, *139* (1), 335–341.
- (48) Raithel, A. L.; Meador, W. E.; Kim, T.-Y.; Staples, R. J.; Delcamp, J. H.; Hamann, T. W. *J. Am. Chem. Soc.* **2023**, *145* (2), 1367–1377.
- (49) Martínez, R.; Ratera, I.; Tárraga, A.; Molina, P.; Veciana, J. *Chem. Commun.* **2006**, 3809–3811.

- (50) Gallardo, I.; Guirado, G.; Moreno, M.; Prats, G.; Takeshita, M. *Chem. Eur. J.* **2012**, *18* (32), 9807–9812.
- (51) Giles, L. W.; Faul, C. F. J.; Tabor, R. F. *Mater. Adv.* **2021**, *2*, 4152–4164.
- (52) Keyvan Rad, J.; Balzade, Z.; Mahdavian, A. R. *J. Photochem. Photobiol., C* **2022**, *51*, 100487.
- (53) Berkovic, G.; Krongauz, V.; Weiss, V. *Chem. Rev.* **2000**, *100* (5), 1741–1754.
- (54) Jerca, F. A.; Jerca, V. V.; Hoogenboom, R. *Nat. Rev. Chem.* **2022**, *6* (1), 51–69.
- (55) Waldeck, D. H. *Chem. Rev.* **1991**, *91* (3), 415–436.
- (56) Yokoyama, Y. *Chem. Rev.* **2000**, *100* (5), 1717–1740.
- (57) Shao, B.; Qian, H.; Li, Q.; Aprahamian, I. *J. Am. Chem. Soc.* **2019**, *141* (20), 8364–8371.
- (58) Schultz, T.; Quenneville, J.; Levine, B.; Toniolo, A.; Martínez, T. J.; Lochbrunner, S.; Schmitt, M.; Shaffer, J. P.; Zgierski, M. Z.; Stolow, A. *J. Am. Chem. Soc.* **2003**, *125* (27), 8098–8099.
- (59) Garcia-Amorós, J.; Díaz-Lobo, M.; Nonell, S.; Velasco, D. *Angew. Chem. Int. Ed.* **2012**, *51* (51), 12820–12823.
- (60) Höglspenger, F.; Vos, B. E.; Hofemeier, A. D.; Seyfried, M. D.; Stövesand, B.; Alavizargar, A.; Topp, L.; Heuer, A.; Betz, T.; Ravoo, B. J. *Nat. Commun.* **2023**, *14* (3760).
- (61) Ayala-Orozco, C.; Galvez-Aranda, D.; Corona, A.; Seminario, J. M.; Rangel, R.; Myers, J. N.; Tour, J. M. *Nat. Chem.* **2023**.
- (62) Shahsavan, H.; Aghakhani, A.; Zeng, H.; Guo, Y.; Davidson, Z. S.; Priimagi, A.; Sitti, M. *PNAS* **2020**, *117* (10), 5125–5133.
- (63) Sakuragi, M.; Aoki, K.; Tamaki, T.; Ichimura, K. *Bull. Chem. Soc. Jpn.* **1990**, *63* (1), 74–79.
- (64) Kong, L.; Wong, H.-L.; Tam, A. Y.-Y.; Lam, W. H.; Wu, L.; Yam, V. W.-W. *ACS Appl. Mater. Interfaces* **2014**, *6* (3), 1550–1562.
- (65) Xia, H.; Xie, K.; Zou, G. *Molecules* **2017**, *22* (12), 2236.
- (66) Towns, A. *Physical Sciences Reviews* **2020**, *5* (6), 20200013.
- (67) Rau, H. In *Photoreactive Organic Thin Films*, Sekkat, Z., Knoll, W., Eds.; Academic Press: San Diego, **2002**, pp 3–47.
- (68) Merino, E.; Ribagorda, M. *Beilstein J. Org. Chem.* **2012**, *8*, 1071–1090.
- (69) Villarón, D.; Wezenberg, S. J. *Angew. Chem. Int. Ed.* **2020**, *59* (32), 13192–13202.
- (70) Qian, H.; Pramanik, S.; Aprahamian, I. *J. Am. Chem. Soc.* **2017**, *139* (27), 9140–9143.
- (71) Shao, B.; Baroncini, M.; Qian, H.; Bussotti, L.; Di Donato, M.; Credi, A.; Aprahamian, I. *J. Am. Chem. Soc.* **2018**, *140* (39), 12323–12327.
- (72) Jeong, M.; Park, J.; Seo, Y.; Lee, K.; Pramanik, S.; Ahn, S.; Kwon, S. *Chem. Eur. J.* **2022**, *28* (11), e202103972.
- (73) Irie, M.; Mohri, M. *J. Org. Chem.* **1988**, *53* (4), 803–808.
- (74) Dai, D.; Zhang, Y.; Yang, S.; Kong, W.; Yang, J.; Zhang, J. *Molecules* **2024**, *29* (1), 254.
- (75) Lewis, G. N.; Magel, T. T.; Lipkin, D. *J. Am. Chem. Soc.* **1940**, *62* (11), 2973–2980.
- (76) Muszkat, K. A.; Fischer, E. *J. Chem. Soc.* **1967**, 662–678.
- (77) Imato, K.; Sasaki, A.; Ishii, A.; Hino, T.; Kaneda, N.; Ohira, K.; Imae, I.; Ooyama, Y. *J. Org. Chem.* **2022**, *87* (23), 15762–15770.
- (78) Gao, M.; Kwaria, D.; Norikane, Y.; Yue, Y. *Nat. Sci.* **2023**, *3* (1), e220020.

## Bibliography

- (79) Mitscherlich, E. *Annalen der Pharmacie* **1834**, *12* (2-3), 305–311.
- (80) Dawson, J. F. *J. Soc. Dyers Colour.* **1991**, *107* (11), 395–400.
- (81) Hartley, G. S. *Nature* **1937**, *140* (3537), 281–281.
- (82) Monti, S.; Orlandi, G.; Palmieri, P. *Chem. Phys.* **1982**, *71* (1), 87–99.
- (83) Cusati, T.; Granucci, G.; Persico, M.; Spighi, G. *J. Chem. Phys.* **2008**, *128* (19), 194312.
- (84) Rau, H. *Angew. Chem. Int. Ed. Engl.* **1973**, *12* (3), 224–235.
- (85) Vetráková, L.; Ladányi, V.; Al Anshori, J.; Dvořák, P.; Wirz, J.; Heger, D. *Photochem. Photobiol. Sci.* **2017**, *16*, 1749–1756.
- (86) Merino, E. *Chem. Soc. Rev.* **2011**, *40*, 3835–3853.
- (87) Hutchins, R. O.; Lamson, D. W.; Rua, L.; Milewski, C.; Maryanoff, B. *J. Org. Chem.* **1971**, *36* (6), 803–806.
- (88) Nystrom, R. F.; Brown, W. G. *J. Am. Chem. Soc.* **1948**, *70* (11), 3738–3740.
- (89) Khan, A.; Hecht, S. *Chem. Eur. J.* **2006**, *12* (18), 4764–4774.
- (90) Ameerunisha, S.; Zacharias, P. S. *J. Chem. Soc., Perkin Trans. 2* **1995**, 1679–1682.
- (91) Kinoshita, K. *Bull. Chem. Soc. Jpn.* **1959**, *32* (8), 777–780.
- (92) Baer, E.; Tosoni, A. L. *J. Am. Chem. Soc.* **1956**, *78* (12), 2857–2858.
- (93) Pausacker, K. H. *J. Chem. Soc.* **1953**, 1989–1990.
- (94) Hombrecher, H. K.; Lüdtke, K. *Tetrahedron* **1993**, *49* (42), 9489–9494.
- (95) Takahashi, H.; Ishioka, T.; Koiso, Y.; Sodeoka, M.; Hshimoto, Y. *Biol. Pharm. Bull.* **2000**, *23* (11), 1387–1390.
- (96) Wang, M.; Ma, J.; Yu, M.; Zhang, Z.; Wang, F. *Catal. Sci. Technol.* **2016**, *6*, 1940–1945.
- (97) Ortiz, B.; Villanueva, P.; Walls, F. *J. Org. Chem.* **1972**, *37* (17), 2748–2750.
- (98) Davey, M. H.; Lee, V. Y.; Miller, R. D.; Marks, T. J. *J. Org. Chem.* **1999**, *64* (13), 4976–4979.
- (99) Barbero, M.; Degani, I.; Dughera, S.; Fochi, R.; Perracino, P. *Synthesis* **1998**, *1998* (9), 1235–1237.
- (100) Hansen, M. J.; Lerch, M. M.; Szymanski, W.; Feringa, B. L. *Angew. Chem. Int. Ed.* **2016**, *55* (43), 13514–13518.
- (101) Roussel, M. R., *Transition-state theory*; 2053-2563; IOP Publishing: **2023**; Chapter 7, pp 1–33.
- (102) Laidler, K. J.; King, M. C. *J. Phys. Chem.* **1983**, *87* (15), 2657–2664.
- (103) Reimann, M.; Teichmann, E.; Hecht, S.; Kaupp, M. *J. Phys. Chem. Lett.* **2022**, *13* (46), 10882–10888.
- (104) Crecca, C. R.; Roitberg, A. E. *J. Phys. Chem. A* **2006**, *110* (26), 8188–8203.
- (105) Aleotti, F.; Soprani, L.; Nenov, A.; Berardi, R.; Arcioni, A.; Zannoni, C.; Garavelli, M. *J. Chem. Theory Comput.* **2019**, *15* (12), 6813–6823.
- (106) Bandara, H. M. D.; Friss, T. R.; Enriquez, M. M.; Isley, W.; Incarvito, C.; Frank, H. A.; Gascon, J.; Burdette, S. C. *J. Org. Chem.* **2010**, *75* (14), 4817–4827.
- (107) Axelrod, S.; Shakhnovich, E.; Gómez-Bombarelli, R. *ACS Cent. Sci.* **2023**, *9* (2), 166–176.
- (108) Dokić, J.; Gothe, M.; Wirth, J.; Peters, M. V.; Schwarz, J.; Hecht, S.; Saalfrank, P. *J. Phys. Chem. A* **2009**, *113* (24), 6763–6773.
- (109) Conti, I.; Garavelli, M.; Orlandi, G. *J. Am. Chem. Soc.* **2008**, *130* (15), 5216–5230.

- (110) Yu, J. K.; Bannwarth, C.; Liang, R.; Hohenstein, E. G.; Martínez, T. J. *J. Am. Chem. Soc.* **2020**, *142* (49), 20680–20690.
- (111) Bandara, H. M. D.; Burdette, S. C. *Chem. Soc. Rev.* **2012**, *41*, 1809–1825.
- (112) Bortolus, P.; Monti, S. *J. Phys. Chem.* **1979**, *83* (6), 648–652.
- (113) Siampiringue, N.; Guyot, G.; Monti, S.; Bortolus, P. *J. Photochem.* **1987**, *37* (1), 185–188.
- (114) Cembran, A.; Bernardi, F.; Garavelli, M.; Gagliardi, L.; Orlandi, G. *J. Am. Chem. Soc.* **2004**, *126* (10), 3234–3243.
- (115) Rietze, C.; Titov, E.; Lindner, S.; Saalfrank, P. *J. Phys.: Condens. Matter* **2017**, *29* (31), 314002.
- (116) Heindl, A. H.; Wegner, H. A. *Chem. Eur. J.* **2020**, *26* (60), 13730–13737.
- (117) Kuntze, K.; Viljakka, J.; Titov, E.; Ahmed, Z.; Kalenius, E.; Saalfrank, P.; Priimagi, A. *Photochem. Photobiol. Sci.* **2022**, *21* (2), 159–173.
- (118) Bléger, D.; Schwarz, J.; Brouwer, A. M.; Hecht, S. *J. Am. Chem. Soc.* **2012**, *134* (51), 20597–20600.
- (119) Beharry, A. A.; Sadvoski, O.; Woolley, G. A. *J. Am. Chem. Soc.* **2011**, *133* (49), 19684–19687.
- (120) Samanta, S.; McCormick, T. M.; Schmidt, S. K.; Seferos, D. S.; Woolley, G. A. *Chem. Commun.* **2013**, *49*, 10314–10316.
- (121) Konrad, D. B.; Frank, J. A.; Trauner, D. *Chem. Eur. J.* **2016**, *22* (13), 4364–4368.
- (122) Konrad, D. B.; Savasci, G.; Allmendinger, L.; Trauner, D.; Ochsenfeld, C.; Ali, A. M. *J. Am. Chem. Soc.* **2020**, *142* (14), 6538–6547.
- (123) Kerckhoffs, A.; Christensen, K. E.; Langton, M. J. *Chem. Sci.* **2022**, *13*, 11551–11559.
- (124) Siewertsen, R.; Neumann, H.; Buchheim-Stehn, B.; Herges, R.; Näther, C.; Renth, F.; Temps, F. *J. Am. Chem. Soc.* **2009**, *131* (43), 15594–15595.
- (125) Schehr, M.; Hugenbusch, D.; Moje, T.; Näther, C.; Herges, R. *Beilstein J. Org. Chem.* **2018**, *14*, 2799–2804.
- (126) Lentès, P.; Stadler, E.; Röhricht, F.; Brahms, A.; Gröbner, J.; Sönnichsen, F. D.; Gescheidt, G.; Herges, R. *J. Am. Chem. Soc.* **2019**, *141* (34), 13592–13600.
- (127) Volarić, J.; Buter, J.; Schulte, A. M.; van den Berg, K.-O.; Santamaría-Aranda, E.; Szymanski, W.; Feringa, B. L. *J. Org. Chem.* **2022**, *87* (21), 14319–14333.
- (128) Kim, K.; Park, H.; Lim, K.-M. *Toxicol. Res.* **2015**, *31* (2), 97–104.
- (129) Glickman, R. D. *Eye & Contact Lens: Science & Clinical Practice* **2011**, *37* (4), 196–205.
- (130) Dong, M.; Babalhavaeji, A.; Samanta, S.; Beharry, A. A.; Woolley, G. A. *Acc. Chem. Res.* **2015**, *48* (10), 2662–2670.
- (131) Goulet-Hanssens, A.; Barrett, C. J. *J. Polym. Sci., Part A: Polym. Chem.* **2013**, *51* (14), 3058–3070.
- (132) Siewertsen, R.; Schönborn, J. B.; Hartke, B.; Renth, F.; Temps, F. *Phys. Chem. Chem. Phys.* **2011**, *13*, 1054–1063.
- (133) Wang, Y.; Li, M.; Yan, C.; Ma, N.; Chen, Y. *CCS Chemistry* **2022**, *4* (2), 704–712.
- (134) Zhu, Q.; Wang, S.; Chen, P. *Org. Lett.* **2019**, *21* (11), 4025–4029.
- (135) Hugenbusch, D.; Lehr, M.; von Glasenapp, J.-S.; McConnell, A. J.; Herges, R. *Angew. Chem. Int. Ed.* **2023**, *62* (1), e202212571.

- (136) Ewert, J.; Heintze, L.; Jordà-Redondo, M.; von Glasenapp, J.-S.; Nonell, S.; Bucher, G.; Peifer, C.; Herges, R. *J. Am. Chem. Soc.* **2022**, *144* (33), 15059–15071.
- (137) Hammerich, M.; Schütt, C.; Stähler, C.; Lentès, P.; Röhricht, F.; Höppner, R.; Herges, R. *J. Am. Chem. Soc.* **2016**, *138* (40), 13111–13114.
- (138) Liu, X.-M.; Jin, X.-Y.; Zhang, Z.-X.; Wang, J.; Bai, F.-Q. *RSC Adv.* **2018**, *8*, 11580–11588.
- (139) Wang, H.; Bisoyi, H. K.; Zhang, X.; Hassan, F.; Li, Q. *Chem. Eur. J.* **2022**, *28* (18), e202103906.
- (140) Gelabert, R.; Moreno, M.; Lluch, J. M. *Int. J. Mol. Sci.* **2023**, *24* (1).
- (141) Lameijer, L. N.; Budzak, S.; Simeth, N. A.; Hansen, M. J.; Feringa, B. L.; Jacquemin, D.; Szymanski, W. *Angew. Chem. Int. Ed.* **2020**, *59* (48), 21663–21670.
- (142) Leistner, A.-L.; Kirchner, S.; Karcher, J.; Bantle, T.; Schulte, M. L.; Gödtel, P.; Fengler, C.; Pianowski, Z. L. *Chem. Eur. J.* **2021**, *27* (31), 8094–8099.
- (143) Knie, C.; Utecht, M.; Zhao, F.; Kulla, H.; Kovalenko, S.; Brouwer, A. M.; Saalfrank, P.; Hecht, S.; Bléger, D. *Chem. Eur. J.* **2014**, *20* (50), 16492–16501.
- (144) Hermann, D.; Schwartz, H. A.; Ruschewitz, U. *ChemistrySelect* **2017**, *2* (35), 11846–11852.
- (145) Rau, H.; Greiner, G.; Gauglitz, G.; Meier, H. *J. Phys. Chem.* **1990**, *94* (17), 6523–6524.
- (146) Rumi, M.; Perry, J. W. *Adv. Opt. Photon.* **2010**, *2* (4), 451–518.
- (147) Dudek, M.; Tarnowicz-Staniak, N.; Deiana, M.; Pokładek, Z.; Samoć, M.; Matczyszyn, K. *RSC Adv.* **2020**, *10*, 40489–40507.
- (148) Gu, B.; Keefer, D.; Aleotti, F.; Nenov, A.; Garavelli, M.; Mukamel, S. *Proc. Natl. Acad. Sci.* **2021**, *118* (47), e2116868118.
- (149) Mendonça, C.; dos Santos, D.; De Boni, L.; Oliveira, O.; Zilio, S. *Synth. Met.* **2001**, *121* (1), 1489–1490.
- (150) De Boni, L.; Rodrigues, J.; dos Santos, D.; Silva, C.; Balogh, D.; Oliveira, O.; Zilio, S.; Misoguti, L.; Mendonça, C. *Chem. Phys. Lett.* **2002**, *361* (3), 209–213.
- (151) Derkowska-Zielinska, B.; Matczyszyn, K.; Dudek, M.; Samoc, M.; Czaplicki, R.; Kaczmarek-Kedziera, A.; Smokal, V.; Biitseva, A.; Krupka, O. *J. Phys. Chem. C* **2019**, *123* (1), 725–734.
- (152) Breukers, R.; Janssens, S.; Raymond, S.; Bhuiyan, M.; Kay, A. *Dyes Pigment.* **2015**, *112*, 17–23.
- (153) Magennis, S. W.; Mackay, F. S.; Jones, A. C.; Tait, K. M.; Sadler, P. J. *Chem. Mater.* **2005**, *17* (8), 2059–2062.
- (154) Moreno, J.; Gerecke, M.; Grubert, L.; Kovalenko, S. A.; Hecht, S. *Angew. Chem. Int. Ed.* **2016**, *55* (4), 1544–1547.
- (155) Bléger, D.; Hecht, S. *Angew. Chem. Int. Ed.* **2015**, *54* (39), 11338–11349.
- (156) Izquierdo-Serra, M.; Gascón-Moya, M.; Hirtz, J. J.; Pittolo, S.; Poskanzer, K. E.; Ferrer, È.; Alibés, R.; Busqué, F.; Yuste, R.; Hernando, J.; Gorostiza, P. *J. Am. Chem. Soc.* **2014**, *136* (24), 8693–8701.
- (157) Gascón-Moya, M.; Pejoan, A.; Izquierdo-Serra, M.; Pittolo, S.; Cabré, G.; Hernando, J.; Alibés, R.; Gorostiza, P.; Busqué, F. *J. Org. Chem.* **2015**, *80* (20), 9915–9925.
- (158) Cabré, G.; Garrido-Charles, A.; Moreno, M.; Bosch, M.; Porta-de-la-Riva, M.; Krieg, M.; Gascón-Moya, M.; Camarero, N.; Gelabert, R.; Lluch, J. M.; Busqué, F.; Hernando, J.; Gorostiza, P.; Alibés, R. *Nat. Commun.* **2019**, *10* (1).



- (159) Moreno, J.; Gerecke, M.; Dobryakov, A. L.; Ioffe, I. N.; Granovsky, A. A.; Bléger, D.; Hecht, S.; Kovalenko, S. A. *J. Phys. Chem.* **2015**, *119* (37), 12281–12288.
- (160) Wu, S.; Blinco, J. P.; Barner-Kowollik, C. *Chem. Eur. J.* **2017**, *23* (35), 8325–8332.
- (161) Ash, C.; Dubec, M.; Donne, K.; Bashford, T. *Laser. Med. Sci.* **2017**, *32* (8), 1909–1918.
- (162) Marc Clement, G. D.; Trelles, M. *J. Cosmet. Laser Ther.* **2005**, *7* (3-4), 177–189.
- (163) Pu, S.; Tang, H.; Chen, B.; Xu, J.; Huang, W. *Mater. Lett.* **2006**, *60* (29), 3553–3557.
- (164) Haase, M.; Schäfer, H. *Angew. Chem. Int. Ed.* **2011**, *50* (26), 5808–5829.
- (165) Carling, C.-J.; Boyer, J.-C.; Branda, N. R. *J. Am. Chem. Soc.* **2009**, *131* (31), 10838–10839.
- (166) Boyer, J.-C.; van Veggel, F. C. J. M. *Nanoscale* **2010**, *2*, 1417–1419.
- (167) Faulkner, D. O.; Petrov, S.; Perovic, D. D.; Kherani, N. P.; Ozin, G. A. *J. Mater. Chem.* **2012**, *22*, 24330–24334.
- (168) Jalani, G.; Tam, V.; Vetrone, F.; Cerruti, M. *J. Am. Chem. Soc.* **2018**, *140* (35), 10923–10931.
- (169) Talaty, E. R.; Fargo, J. C. *Chem. Commun.* **1967**, 65–66.
- (170) Weston, C. E.; Richardson, R. D.; Haycock, P. R.; White, A. J. P.; Fuchter, M. J. *J. Am. Chem. Soc.* **2014**, *136* (34), 11878–11881.
- (171) Calbo, J.; Thawani, A. R.; Gibson, R. S. L.; White, A. J. P.; Fuchter, M. J. *Beilstein J. Org. Chem.* **2019**, *15*, 2753–2764.
- (172) Eleya, N.; Ghosh, S.; Lork, E.; Staubitz, A. *J. Mater. Chem. C* **2021**, *9*, 82–87.
- (173) Andersson, J.-Å. *J. Photochem.* **1983**, *22* (3), 255–261.
- (174) Pezzo, R. D.; Bandeira, N. A.; Trojanowska, A.; Prieto, S. F.; Underiner, T.; Giamberini, M.; Tytkowski, B. *Pure Appl. Chem.* **2019**, *91* (9), 1533–1546.
- (175) Whitten, D. G.; Wildes, P. D.; Pacifici, J. G.; Irick, G. J. *J. Am. Chem. Soc.* **1971**, *93* (8), 2004–2008.
- (176) Angelini, G.; Canilho, N.; Emo, M.; Kingsley, M.; Gasbarri, C. *J. Org. Chem.* **2015**, *80* (15), 7430–7434.
- (177) Janus, K.; Koshets, I. A.; Sworakowski, J.; Nešpůrek, S. *J. Mater. Chem.* **2002**, *12*, 1657–1663.
- (178) Strauss, M. A.; Wegner, H. A. *Angew. Chem. Int. Ed.* **2019**, *58* (51), 18552–18556.
- (179) Mehrparvar, S.; Scheller, Z. N.; Wölper, C.; Haberhauer, G. *J. Am. Chem. Soc.* **2021**, *143* (47), 19856–19864.
- (180) Shin, D. M.; Whitten, D. G. *J. Am. Chem. Soc.* **1988**, *110* (15), 5206–5208.
- (181) Shinkai, S.; Minami, T.; Kusano, Y.; Manabe, O. *J. Am. Chem. Soc.* **1983**, *105* (7), 1851–1856.
- (182) Nagamani, S. A.; Norikane, Y.; Tamaoki, N. *J. Org. Chem.* **2005**, *70* (23), 9304–9313.
- (183) Luboch, E.; Wagner-Wysiecka, E.; Poleska-Muchlado, Z.; Kravtsov, V. C. *Tetrahedron* **2005**, *61* (45), 10738–10747.
- (184) Falkenburg, R.; Notheis, M. J.; Schnakenburg, G.; von Krbek, L. K. S. *Org. Biomol. Chem.* **2023**, *21*, 4993–4998.
- (185) Ghosh, S.; Eschen, C.; Eleya, N.; Staubitz, A. *J. Org. Chem.* **2023**, *88* (6), 3372–3377.
- (186) Antoine John, A.; Lin, Q. *J. Org. Chem.* **2017**, *82* (18), 9873–9876.
- (187) Liu, Q.; Luo, X.; Wei, S.; Wang, Y.; Zhu, J.; Liu, Y.; Quan, F.; Zhang, M.; Xia, C. *Tetrahedron Lett.* **2019**, *60* (26), 1715–1719.

## Bibliography

- (188) Ruiz-Soriano, A.; Lamelza, L.; Pizzamiglio, E.; Just-Baringo, X. **2023**, working paper.
- (189) Lyons, T. W.; Sanford, M. S. *Chem. Rev.* **2010**, *110* (2), 1147–1169.
- (190) Müller-Deku, A.; Thorn-Seshold, O. *J. Org. Chem.* **2022**, *87* (24), 16526–16531.
- (191) Wang, H.; Bisoyi, H. K.; Urbas, A. M.; Bunning, T. J.; Li, Q. *J. Am. Chem. Soc.* **2019**, *141* (20), 8078–8082.
- (192) Shi, Y.; Gerkman, M. A.; Qiu, Q.; Zhang, S.; Han, G. G. D. *J. Mater. Chem. A* **2021**, *9*, 9798–9808.
- (193) Josa-Culleré, L.; Llebaria, A. *J. Med. Chem.* **2023**, *66* (3), 1909–1927.
- (194) Zheng, M.; Ye, Q.; Chen, X.; Zeng, M.; Song, G.; Zhang, J.; Yuan, J. *Chem. Commun.* **2022**, *58*, 6922–6925.
- (195) Iamsaard, S.; Anger, E.; Asshoff, S. J.; Depauw, A.; Fletcher, S. P.; Katsonis, N. *Angew. Chem. Int. Ed.* **2016**, *55* (34), 9908–9912.
- (196) Heinrich, B.; Bouazoune, K.; Wojcik, M.; Bakowsky, U.; Vázquez, O. *Org. Biomol. Chem.* **2019**, *17*, 1827–1833.
- (197) Okumura, S.; Lin, C.-H.; Takeda, Y.; Minakata, S. *J. Org. Chem.* **2013**, *78* (23), 12090–12105.
- (198) Liu, Q.; Dong, H.; Li, Y.; Li, H.; Chen, D.; Wang, L.; Xu, Q.; Lu, J. *Chem. Asian. J.* **2016**, *11* (4), 512–519.
- (199) Kennedy, A. D. W.; DiNardi, R. G.; Fillbrook, L. L.; Donald, W. A.; Beves, J. E. *Chem. Eur. J.* **2022**, *28* (16), e202104461.
- (200) He, L.; Zhang, T.; Zhu, C.; Yan, T.; Liu, J. *Chem. Eur. J.* **2023**, *29* (25), e202300044.
- (201) Rojanathanes, R.; Pipoosananakaton, B.; Tuntulani, T.; Bhanthumnavin, W.; Orton, J. B.; Cole, S. J.; Hursthouse, M. B.; Grossel, M. C.; Sukwattanasinitt, M. *Tetrahedron* **2005**, *61* (5), 1317–1324.
- (202) Reuter, R.; Hostettler, N.; Neuburger, M.; Wegner, H. A. *Chimia* **2010**, *64* (3), 180.
- (203) Takeda, Y.; Okazaki, M.; Maruoka, Y.; Minakata, S. *Beilstein J. Org. Chem.* **2015**, *11*, 9–15.
- (204) Lin, C.; Maisonneuve, S.; Métivier, R.; Xie, J. *Chem. Eur. J.* **2017**, *23* (60), 14996–15001.
- (205) Kertmen, A.; Szczygelska-Tao, J.; Chojnacki, J. *Tetrahedron* **2013**, *69* (49), 10662–10668.
- (206) Kar, M.; Basak, A.; Bhattacharjee, M. *Bioorg. Med. Chem. Lett.* **2005**, *15* (24), 5392–5396.
- (207) Hossain, M. S.; Rahaman, S. A.; Hatai, J.; Saha, M.; Bandyopadhyay, S. *Chem. Commun.* **2020**, *56*, 4172–4175.
- (208) Hossain, M. S.; Bandyopadhyay, S. *J. Org. Chem.* **2021**, *86* (9), 6314–6321.
- (209) Wang, H.; Tang, Y.; Krishna Bisoyi, H.; Li, Q. *Angew. Chem. Int. Ed.* **2023**, *62* (8), e202216600.
- (210) Kondo, M.; Nakamura, K.; Krishnan, C. G.; Takizawa, S.; Abe, T.; Sasai, H. *ACS Catal.* **2021**, *11* (3), 1863–1867.
- (211) Sahoo, D.; Majeed, M. A.; Lathwal, A.; De, S. *Chem. Eur. J.* **2023**, *29* (28), e202300092.
- (212) Takaishi, K.; Kawamoto, M.; Tsubaki, K.; Wada, T. *J. Org. Chem.* **2009**, *74* (15), 5723–5726.
- (213) Norikane, Y.; Hirai, Y.; Yoshida, M. *Chem. Commun.* **2011**, *47*, 1770–1772.
- (214) Schultzke, S.; Puylaert, P.; Wang, H.; Schultzke, I.; Gerken, J.; Staubitz, A. *Adv. Funct. Mater.* **2024**, 2313268.

- (215) Kariduraganavar, M. Y.; Doddamani, R. V.; Waddar, B.; Parne, S. R. In *Nonlinear Optics : From Solitons to Similaritons*, Bakırtaş, İ., Antar, N., Eds.; IntechOpen: Rijeka, **2021**; Chapter 9.
- (216) Hong, P.; Liu, J.; Qin, K.-X.; Tian, R.; Peng, L.-Y.; Su, Y.-S.; Gan, Z.; Yu, X.-X.; Ye, L.; Zhu, M.-Q.; Li, C. *Angew. Chem. Int. Ed.*, e202316706.
- (217) Kawata, S.; Kawata, Y. *Chem. Rev.* **2000**, *100* (5), 1777–1788.
- (218) Gindre, D.; Boeglin, A.; Fort, A.; Mager, L.; Dorkenoo, K. D. *Opt. Express* **2006**, *14* (21), 9896–9901.
- (219) Zhang, C.; Zhou, H.-P.; Liao, L.-Y.; Feng, W.; Sun, W.; Li, Z.-X.; Xu, C.-H.; Fang, C.-J.; Sun, L.-D.; Zhang, Y.-W.; Yan, C.-H. *Adv. Mater.* **2010**, *22* (5), 633–637.
- (220) Goradia, I.; Doshi, J.; Deulkar, K. *International Journal of Current Engineering and Technology* **2014**, *4* (3), 2933–2936.
- (221) Nagao, I.; Shimizu, M.; Hiyama, T. *Angew. Chem. Int. Ed.* **2009**, *48* (41), 7573–7576.
- (222) Katritzky, A. R.; Wu, J.; Verin, S. V. *Synthesis* **1995**, *1995* (06), 651–653.
- (223) Strueben, J.; Lipfert, M.; Springer, J.-O.; Gould, C. A.; Gates, P. J.; Sönnichsen, F. D.; Staubitz, A. *Chem. Eur. J.* **2015**, *21* (31), 11165–11173.
- (224) Djerassi, C. *Chem. Rev.* **1948**, *43* (2), 271–317.
- (225) Williamson, A. *The London, Edinburgh, and Dublin Philosophical Magazine and Journal of Science* **1850**, *37* (251), 350–356.
- (226) Béchamp, A. *Ann. Chim. Phys* **1854**, *3* (42), 186–196.
- (227) Levell, J. W.; Ruseckas, A.; Henry, J. B.; Wang, Y.; Stretton, A. D.; Mount, A. R.; Galow, T. H.; Samuel, I. D. W. *J. Phys. Chem. A* **2010**, *114* (51), 13291–13295.
- (228) Goodby, J. W. In *Handbook of Liquid Crystals*; Wiley-VCH: **2014**; Chapter 3, pp 1–18.
- (229) Andrienko, D. *J. Mol. Liq.* **2018**, *267*, 520–541.
- (230) Zhang, Z.; Yang, X.; Zhao, Y.; Ye, F.; Shang, L. *Adv. Mater.* **2023**, *35* (36), 2300220.
- (231) Kuczyński, W.; Żywucki, B.; Małecki, J. *Mol. Cryst. Liq. Cryst.* **2002**, *381* (1), 1–19.
- (232) Dunmur, D.; Luckhurst, G. In *Handbook of Liquid Crystals*; Wiley-VCH: **2014**; Chapter 1, pp 1–39.
- (233) Coles, H. J.; Strazielle, C. *Mol. Cryst. Liq. Cryst.* **1979**, *55* (1), 237–250.
- (234) Mandle, R. J.; Goodby, J. W. In *Handbook of Liquid Crystals*; Wiley-VCH: **2014**; Chapter 6, pp 1–27.
- (235) Goodby, J. W.; Davis, E. J.; Mandle, R. J.; Cowling, S. J. In *Handbook of Liquid Crystals*; Wiley-VCH: **2014**; Chapter 8, pp 1–30.
- (236) Miller, D. S.; Carlton, R. J.; Mushenheim, P. C.; Abbott, N. L. *Langmuir* **2013**, *29* (10), 3154–3169.
- (237) Dierking, I. In *Textures of Liquid Crystals*; Wiley-VCH: **2003**; Chapter 3, pp 33–42.
- (238) Agra-Kooijman, D. M.; Kumar, S. In *Handbook of Liquid Crystals*; Wiley-VCH: **2014**; Chapter 10, pp 1–38.
- (239) Dunmur, D. In *Handbook of Liquid Crystals*; Wiley-VCH: **2014**; Chapter 3, pp 1–26.
- (240) Cowling, S. J. In *Handbook of Liquid Crystals*; Wiley-VCH: **2014**; Chapter 9, pp 1–38.
- (241) Gleeson, H. F. In *Handbook of Liquid Crystals*; Wiley-VCH: **2014**; Chapter 15, pp 1–27.

- (242) De Jeu, W. H.; Ostrovskii, I., B. In *Liquid Crystal Elastomers: Materials and Applications*, de Jeu, W. H., Ed.; Springer Berlin Heidelberg: Berlin, Heidelberg, **2012**, pp 187–234.
- (243) Dierking, I. In *Textures of Liquid Crystals*; Wiley-VCH: **2003**, pp 167–212.
- (244) Toyne, K. J. In *Handbook of Liquid Crystals Set*; Wiley-VCH: **1998**; Chapter 1, pp 47–59.
- (245) Pelzl, G. In *Handbook of Liquid Crystals Set*; Wiley-VCH: **1998**; Chapter 2.4, pp 128–141.
- (246) Osipov, M. In *Handbook of Liquid Crystals*; Wiley-VCH: **2014**; Chapter 5, pp 1–54.
- (247) Dierking, I. In *Textures of Liquid Crystals*; Wiley-VCH: **2003**; Chapter 5, pp 51–74.
- (248) Dierking, I. In *Textures of Liquid Crystals*; Wiley-VCH: **2003**; Chapter 7, pp 91–122.
- (249) Reinitzer, F. *Monatshefte für Chemie - Chemical Monthly* **1888**, *9* (1), 421–441.
- (250) Lehmann, O. *Zeitschrift für Physikalische Chemie* **1890**, *5U* (1), 427–435.
- (251) Lehmann, O. *Ann. Phys.* **1890**, *276* (7), 401–423.
- (252) Lehmann, O. *Ann. Phys.* **1900**, *307* (8), 649–705.
- (253) Demus, D. In *Handbook of Liquid Crystals Set*; Wiley-VCH: **1998**; Chapter 6, pp 133–187.
- (254) Chandrasekhar, S. In *Handbook of Liquid Crystals Set*; Wiley-VCH: **1998**; Chapter 8, pp 749–780.
- (255) Dierking, I. In *Textures of Liquid Crystals*; Wiley-VCH: **2003**; Chapter 11, pp 145–153.
- (256) Dierking, I. In *Textures of Liquid Crystals*; Wiley-VCH: **2003**; Chapter 2, pp 21–32.
- (257) Nie, Z.-Z.; Wang, M.; Yang, H. *Chem. Eur. J.* **2023**, *29* (38), e202301027.
- (258) Knepe, H.; Schneider, F. In *Handbook of Liquid Crystals*; Wiley-VCH: **2014**; Chapter 7, pp 1–37.
- (259) Dunmur, D.; Kaczmarek, M.; Sluckin, T. In *Handbook of Liquid Crystals*; Wiley-VCH: **2014**; Chapter 2, pp 1–32.
- (260) Blinov, L. M. In *Handbook of Liquid Crystals*; Wiley-VCH: **2014**; Chapter 8, pp 1–27.
- (261) Broughton, B. In *Handbook of Liquid Crystals*; Wiley-VCH: **2014**; Chapter 9, pp 1–22.
- (262) Kondo, T. *Z. Wissenschaft. Photogr. Photophys. Photochem.* **1932**, *31* (6), 153.
- (263) Ebralidze, T. D.; Ebralidze, N. A.; Bazadze, M. A. *Appl. Opt.* **2002**, *41* (1), 78–79.
- (264) Eggert, J. *Berichte der Bunsengesellschaft für physikalische Chemie* **1971**, *75* (8), 725–728.
- (265) Jánossy, I. In *Handbook of Liquid Crystals*; Wiley-VCH: **2014**; Chapter 10, pp 1–26.
- (266) De Martino, S.; Mauro, F.; Netti, P. A. *Riv. Nuovo Cimento (3)* **2020**, *43* (12), 599–629.
- (267) Pang, X.; Lv, J.-a.; Zhu, C.; Qin, L.; Yu, Y. *Adv. Mater.* **2019**, *31* (52), 1904224.
- (268) White, T. J.; Broer, D. J. *Nat. Mater.* **2015**, *14* (11), 1087–1098.
- (269) Herbert, K. M.; Fowler, H. E.; McCracken, J. M.; Schlafmann, K. R.; Koch, J. A.; White, T. J. *Nat. Rev. Mater.* **2022**, *7* (1), 23–38.
- (270) Talroze, R.; Zubarev, E.; Kuptsov, S.; Merekalov, A.; Yuranova, T.; Plate', N.; Finkelmann, H. *React. Funct. Polym.* **1999**, *41* (1), 1–11.
- (271) Roach, D. J.; Kuang, X.; Yuan, C.; Chen, K.; Qi, H. J. *Smart. Mater. Struct.* **2018**, *27* (12), 125011.
- (272) Kotikian, A.; Truby, R. L.; Boley, J. W.; White, T. J.; Lewis, J. A. *Adv. Mater.* **2018**, *30* (10), 1706164.
- (273) Donnio, B.; Wermter, H.; Finkelmann, H. *Macromolecules* **2000**, *33* (21), 7724–7729.
- (274) Küpfer, J.; Finkelmann, H. *Makromol. Chem. Rapid Commun.* **1991**, *12* (12), 717–726.

- (275) Lall, J.; Zappe, H. *Macromol. Mater. Eng.* **2023**, *308* (5), 2300063.
- (276) Liu, J.; Gao, Y.; Wang, H.; Poling-Skutvik, R.; Osuji, C. O.; Yang, S. *Adv. Intell. Syst.* **2020**, *2* (6), 1900163.
- (277) Mirvakili, S. M.; Hunter, I. W. *Adv. Mater.* **2018**, *30* (6), 1704407.
- (278) Guo, Y.; Liu, N.; Cao, Q.; Cheng, X.; Zhang, P.; Guan, Q.; Zheng, W.; He, G.; Chen, J. *ACS Appl. Polym. Mater.* **2022**, *4* (8), 6202–6210.
- (279) Liu, W.; Guo, L.-X.; Lin, B.-P.; Zhang, X.-Q.; Sun, Y.; Yang, H. *Macromolecules* **2016**, *49* (11), 4023–4030.
- (280) Ikeda, T.; Mamiya, J.-i.; Yu, Y. *Angew. Chem. Int. Ed.* **2007**, *46* (4), 506–528.
- (281) Ikeda, T.; Ube, T. *Mater. Today* **2011**, *14* (10), 480–487.
- (282) Pilz da Cunha, M.; van Thoor, E. A. J.; Debije, M. G.; Broer, D. J.; Schenning, A. P. H. J. *J. Mater. Chem. C* **2019**, *7*, 13502–13509.
- (283) Jones, L. P. In *Handbook of Visual Display Technology*, Chen, J., Cranton, W., Fihn, M., Eds.; Springer Berlin Heidelberg: Berlin, Heidelberg, **2012**, pp 1387–1402.
- (284) Yu, Y.; Nakano, M.; Shishido, A.; Shiono, T.; Ikeda, T. *Chem. Mater.* **2004**, *16* (9), 1637–1643.
- (285) Iamsaard, S.; Asshoff, S. J.; Matt, B.; Kudernac, T.; Cornelissen, J. J. L. M.; Fletcher, S. P.; Katsonis, N. *Nat. Chem.* **2014**, *6* (3), 229–235.
- (286) Yin, R.; Xu, W.; Kondo, M.; Yen, C.-C.; Mamiya, J.-i.; Ikeda, T.; Yu, Y. *J. Mater. Chem.* **2009**, *19*, 3141–3143.
- (287) Iamsaard, S.; Villemin, E.; Lancia, F.; Asshoff, S.-J.; Fletcher, S. P.; Katsonis, N. *Nat. Protoc.* **2016**, *11* (10), 1788–1797.
- (288) Lahikainen, M.; Kuntze, K.; Zeng, H.; Helantera, S.; Hecht, S.; Priimagi, A. *ACS Appl. Mater. Interfaces* **2020**, *12* (42), 47939–47947.
- (289) Hebner, T. S.; Podgórski, M.; Mavila, S.; White, T. J.; Bowman, C. N. *Angew. Chem. Int. Ed.* **2022**, *61* (11), e202116522.
- (290) Ryabchun, A.; Li, Q.; Lancia, F.; Aprahamian, I.; Katsonis, N. *J. Am. Chem. Soc.* **2019**, *141* (3), 1196–1200.
- (291) Kumar, K.; Knie, C.; Bléger, D.; Peletier, M. A.; Friedrich, H.; Hecht, S.; Broer, D. J.; Debije, M. G.; Schenning, A. P. H. J. *Nat. Commun.* **2016**, *7* (11975).
- (292) Jiang, Z.; Xu, M.; Li, F.; Yu, Y. *J. Am. Chem. Soc.* **2013**, *135* (44), 16446–16453.
- (293) Wu, W.; Yao, L.; Yang, T.; Yin, R.; Li, F.; Yu, Y. *J. Am. Chem. Soc.* **2011**, *133* (40), 15810–15813.
- (294) Lu, X.; Zhang, H.; Fei, G.; Yu, B.; Tong, X.; Xia, H.; Zhao, Y. *Adv. Mater.* **2018**, *30* (14), 1706597.
- (295) Lv, J.-a.; Liu, Y.; Wei, J.; Chen, E.; Qin, L.; Yu, Y. *Nature* **2016**, *537* (7619), 179–184.
- (296) Yamada, M.; Kondo, M.; Mamiya, J.-i.; Yu, Y.; Kinoshita, M.; Barrett, C. J.; Ikeda, T. *Angew. Chem. Int. Ed.* **2008**, *47* (27), 4986–4988.
- (297) Pilz da Cunha, M.; Ambergen, S.; Debije, M. G.; Homburg, E. F. G. A.; den Toonder, J. M. J.; Schenning, A. P. H. J. *Adv. Sci.* **2020**, *7* (5), 1902842.



# Abbreviations

a.u.	Atomic units
acac	Acetylacetonate ligand
AcOH	Acetic acid
AI	Artificial intelligence
APCI	Atmospheric-pressure chemical ionization
Ar	Aryl
ATR	Attenuated total reflection
BAPO	Phenyl-bis-(2,4,6-trimethylbenzoyl)-phosphine oxide
BINAP	2,2'-Bis(diphenylphosphino)-1,1'-binaphthyl ligand
Boc	<i>tert</i> -Butyloxycarbonyl group
Br <sub>4</sub>	Tetra- <i>ortho</i> -bromo-substituted
Bu	Butyl group
calc; calcd	Calculated
CCD camera	Charge-coupled device camera
CCDC	Cambridge crystallographic data centre
CD	Compact disc
CDI	1,1'-Carbonyldiimidazol
CI	Conical intersection
CIF	Crystallographic information files
Cl <sub>4</sub>	Tetra- <i>ortho</i> -chloro-substituted
COD	Cyclooctadiene group
conc	Concentration
COSY	Correlation spectroscopy
Cp*	1,2,3,4,5-Pentamethylcyclopentadiene
Cy	Cyclohexane group
D	Dimension; 2D,3D,4D
d	Day
d	Doublet (NMR)
dba	Dibenzylideneacetone
DBDMH	1,3-Dibromo-5,5-dimethylhydantoin
DBU	1,8-Diazabicyclo[5.4.0]undec-7-en
DCC	<i>N,N'</i> -Dicyclohexylcarbodiimide
DCE	1,2-Dichlorethane
DCM	Dichloromethane
dd	Double doublet (NMR)
DEPT	Distortionless enhancement by polarization transfer

## Abbreviations

DFT	Density functional theorem
DMA	Dynamic mechanical analysis
DMAc	Dimethylacetamide
DMAP	4- <i>N,N</i> -Dimethylaminopyridin
DME	Dimethylglycol
DMEDA	1,2-Dimethylethylenediamine
DMF	<i>N,N</i> -Dimethylformamid
DMSO	Dimethyl sulfoxide
DPA	Diisopropylamine
dppf, DPPF	1,1'-Bis(diphenylphosphino)ferrocene
DSC	Differential scanning calorimetry
DSC; chemical	<i>N,N</i> -Disuccinimidyl carbonate
DTT	Dithiothreitol
DVD	Digital versatile disc
e.g.	Exempli gratia; for example
EDCI	1-Ethyl-3-(3-dimethylaminopropyl)carbodiimide
EDDET	2,2'-(Ethylendioxy)diethanthiol
EDG	Electron-donating group
EI	Electron ionisation
Elec.	Electronic
eq., equiv.	Equivalent
ESI	Electron spray ionization; electronic supporting information
Et	Ethyl group
Et <sub>2</sub> O	Diethyl ether
EtOAc	Ethyl acetate
EWG	Electron-withdrawing group
F <sub>4</sub>	Tetra <i>ortho</i> -fluoro-substituted
FRET	Fluorescence resonance energy transfer
FT-IR	Fourier transformation- infrared spectroscopy
GB	Gigabyte
h	Hour
HAN	Hybrid aligned
HATU	O-(7-Azabenzotriazol-1-yl)- <i>N,N,N',N'</i> -Tetramethyluronium-hexafluorophosphat
HMBC	Heteronuclear multiple-bond correlation spectroscopy
HRMS	High resolution mass spectrometry
HSPyU	O-( <i>N</i> -Succinimidyl)- <i>N,N,N',N'</i> -bis(tetramethylene)uronium hexafluorophosphate
HSQC	Heteronuclear single-quantum correlation spectroscopy
i.e.	It est; that is
IAR	Inversion-assisted rotation
IR	Infrared
ITO	Indium tin oxide



J	Coupling constant (NMR)
LC	Liquid crystal (cell)
LCD	Liquid crystal display
LCE	Liquid crystal elastomer
LCN	Liquid crystal network
LCP	Liquid crystal polymer
LED	Light-emitting diode
LPL	Linearly polarized light
m	Medium (IR)
m	Multiplet (NMR)
M <sub>p</sub>	Melting point
mag.	Magnetic
MC-LCE	Main-chain liquid crystal elastomer
MC-LCP	Main-chain liquid crystal polymers
Me	Methyl group
Me <sub>4</sub>	Tetra- <i>ortho</i> -methyl-substituted
MeCN	Acetonitrile
MeO <sub>4</sub>	Tetra- <i>ortho</i> -methoxy-substituted
MeOH	Methanol
min	Minute
MOF	Metal-organic framework
MS	Mass spectrometry
mw	Microwave
n.d.	Not determined
NA	Numerical aperture
NBS	<i>N</i> -Bromosuccinimide
NCS	<i>N</i> -Chlorosuccinimide
NHS	<i>N</i> -Hydroxysuccinimide
NIR	Near IR
NLO	Nonlinear optical
NMP	<i>N</i> -Methyl-2-pyrrolidone
NMR	Nuclear magnetic resonance spectroscopy
<i>o</i> -tolyl	<i>Ortho</i> -toluene substituted group
OAc	Acetate
OAM	Oxygen-linked azobenzene macrocycle
ODS	Optical data storage
OTf	Triflate
ox.	Oxidation
p	Pentet (NMR)
PAH	Polycyclic aromatic hydrocarbon
PCL	Polycaprolactone
PDMS	Polydimethylsiloxane

## Abbreviations

PES	Potential energy surface
PETMP	Pentaerythritol-tetrakis(3-mercaptopropionate)
PFCB	Perfluorocyclobutane
Ph	Phenyl group
pH	Potential concentration of protons
Photoiso.	Photoisomerization
PI coated glass slides	Polyimide coated glass slides
PIDA	(Diacetoxyiodo)benzene
PMMA	Poly(methylmethacrylate)
POM	Polarizing optical microscope
ppm	Parts per million
PSS	Photostationary state
PTFE	Polytetrafluoroethylene
R <sub>f</sub>	Retention factor
Red	Reduction
rt	Room temperature
s	Singlet (NMR)
s	Strong (IR)
S <sub>N</sub> Ar	Nucleophilic aromatic substitution
SAM	Self-assembled monolayer
SC-LCP	Side-chain liquid crystal polymers
SCRF	Self-consistent reaction field
SmA	Smectic phase A
SmC	Smectic phase C
SMD	Solvation model based on density
SSD	Solid-state drives
t	Triplet (NMR)
t <sub>1/2</sub>	Half-life time
T <sub>g</sub>	Glass transition temperature
t-Bu, <i>t</i> -Bu	<i>Tert</i> -butyl group
TB	Terabytes
TBHP	<i>Tert</i> -butyl hydroperoxide
TCBC	2,4,6-Trichlorobenzoic acid
TCCA	Trichloro isocyanuric acid
TFA	Trifluoroacetic acid
THF	Tetrahydrofuran
TLC	Thin layer chromatography
TMHD	2,2,6,6-Tetramethylheptane-3,5-dione
TMS	Tetramethylsilane
TN	Twisted nematic
TON	Turnover number
TPA	Two-photon absorption

TST	Transition state theory
UCNP	Upconverting nanoparticle
UV	Ultra violet
vis	Visible
w	Weak (IR)
WAXS	Wide-angle X-ray scattering
X-ray	X-radiation, high-energy electromagnetic radiation
Xantphos	(9,9-Dimethyl-9H-xanthene-4,5-diyl)bis(diphenylphosphane)
XRD	X-ray diffraction
XRS	X-Ray Spectroscopy
ZB	Zettabytes



# Appendix

Supporting Information

## 9.1 Appendix Publication II Active Ester Functionalized Azobenzenes as Versatile Building Blocks

Sven Schultzke <sup>1,2,†</sup>, Melanie Walther <sup>1,2,†</sup> and Anne Staubitz <sup>1,2,\*</sup>

<sup>1</sup> University of Bremen, Institute for Analytical and Organic Chemistry, Leobener Straße 7, D-28359 Bremen, Germany

<sup>2</sup> University of Bremen, MAPEX Center for Materials and Processes, Bibliothekstraße 1, D-28359 Bremen, Germany

\* Correspondence: [staubitz@uni-bremen.de](mailto:staubitz@uni-bremen.de); Tel.: +49421/21863210

† Both authors contributed equally to this work.

### Table of Contents

General Information.....	3
Reagents.....	4
Solvents.....	5
Syntheses.....	6
General procedure 1.....	6
General procedure 2.....	6
2,5-Dioxopyrrolidin-1-yl ( <i>E</i> )-4-(phenyldiazenyl)benzoate[2] ( <b>3a</b> ).....	7
2,5-Dioxopyrrolidin-1-yl ( <i>E</i> )-3-(phenyldiazenyl)benzoate[2] ( <b>3b</b> ).....	7
2,5-Dioxopyrrolidin-1-yl ( <i>E</i> )-4-((4-hydroxyphenyl)diazenyl)benzoate[3] ( <b>3d</b> ).....	8
2,5-Dioxopyrrolidin-1-yl ( <i>E</i> )-4-((4-aminophenyl)diazenyl)benzoate ( <b>3e</b> ).....	8
2,5-Dioxopyrrolidin-1-yl ( <i>E</i> )-4-((4-acetamidophenyl)diazenyl)benzoate ( <b>3f</b> ).....	9
2,5-Dioxopyrrolidin-1-yl ( <i>E</i> )-4-((4-nitrophenyl)diazenyl)benzoate ( <b>3g</b> ).....	9
2,5-Dioxopyrrolidin-1-yl ( <i>E</i> )-4-((4-(allyloxy)phenyl)diazenyl)benzoate ( <b>3h</b> ).....	10
2,5-Dioxopyrrolidin-1-yl ( <i>E</i> )-4-((4-((9-hydroxynonyl)oxy)phenyl)diazenyl)benzoate ( <b>3i</b> ).....	10
2,5-Dioxopyrrolidin-1-yl ( <i>E</i> )-4-((2,6-dimethyl-4-(nonyloxy)phenyl)diazenyl)-3,5-dimethylbenzoate ( <b>3j</b> ).....	11

2,5-Dioxopyrrolidin-1-yl ( <i>E</i> )-4-((2,7-bis(4-(hexyloxy)phenoxy)naphthalen-1-yl)diazenyl)-3,5-dimethylbenzoate ( <b>3k</b> ) .....	12
2,5-Dioxopyrrolidin-1-yl ( <i>E</i> )-4-((4-bromophenyl)diazenyl)benzoate ( <b>3l</b> ) .....	12
2,5-Dioxopyrrolidin-1-yl ( <i>E</i> )-4-((3-bromophenyl)diazenyl)benzoate ( <b>3m</b> ) .....	13
2,5-Dioxopyrrolidin-1-yl ( <i>E</i> )-4-((2-bromophenyl)diazenyl)benzoate ( <b>3n</b> ) .....	13
Bis(2,5-dioxopyrrolidin-1-yl)4,4'-(diazene-1,2-diyl)( <i>E</i> )-dibenzoate[5] ( <b>5a</b> ) .....	14
Bis(2,5-dioxopyrrolidin-1-yl) 4,4'-(diazene-1,2-diyl)( <i>E</i> )-bis(3,5-dimethoxybenzoate) ( <b>5b</b> ) .....	14
Bis(2,5-dioxopyrrolidin-1-yl) 4,4'-(diazene-1,2-diyl)( <i>E</i> )-bis(3,5-dimethylbenzoate) ( <b>5c</b> ) .....	15
Bis(2,5-dioxopyrrolidin-1-yl) 4,4'-(diazene-1,2-diyl)( <i>E</i> )-bis(3,5-difluorobenzoate) ( <b>5d</b> ) .....	15
2,5-Dioxopyrrolidin-1-yl ( <i>Z</i> )-11,12-dihydrodibenzo[ <i>c,g</i> ][1,2]diazocine-2-carboxylate ( <b>8a</b> ) .....	16
Bis(2,5-dioxopyrrolidin-1-yl) ( <i>Z</i> )-11,12-dihydrodibenzo[ <i>c,g</i> ][1,2]diazocine-2,9-dicarboxylate ( <b>8b</b> ) .....	17
Di- <i>tert</i> -butyl 2,2'-((4,4'-(diazene-1,2-diyl)bis(benzoyl))bis(azanediy))( <i>E</i> )-dipropionate ( <b>10a</b> ) .....	17
Di- <i>tert</i> -butyl 2,2'-((11,12-dihydrodibenzo[ <i>c,g</i> ][1,2]diazocine-2,9-dicarbonyl)bis(azane-diyl))( <i>Z</i> )-dipropionate ( <b>10b</b> ) .....	18
Determination of the <sup>1</sup> H NMR Yields .....	19
<i>N</i> -Hydroxysuccinimidyl formate[5] ( <b>2</b> ) .....	21
( <i>E</i> )-1-(4-Iodophenyl)-2-phenyldiazene[6] ( <b>1a</b> ) .....	21
( <i>E</i> )-1-(3-Iodophenyl)-2-phenyldiazene[6] ( <b>1b</b> ) .....	22
( <i>E</i> )-1-(2-Iodophenyl)-2-phenyldiazene[6] ( <b>1c</b> ) .....	22
( <i>E</i> )-4-((4-Iodophenyl)diazenyl)phenol[7] ( <b>1d</b> ) .....	23
( <i>E</i> )-4-((4-Iodophenyl)diazenyl)aniline ( <b>1e</b> ) .....	23
( <i>E</i> )- <i>N</i> -4-((4-Iodophenyl)diazenyl)phenylacetamide ( <b>1f</b> ) .....	24
( <i>E</i> )-1-(4-Iodophenyl)-2-(4-nitrophenyl)diazene[8] ( <b>1g</b> ) .....	24
( <i>E</i> )-1-(4-(Allyloxy)phenyl)-2-(4-iodophenyl)diazene[9] ( <b>1h</b> ) .....	25
( <i>E</i> )-9-(4-((4-Iodophenyl)diazenyl)phenoxy)nonan-1-ol ( <b>1i</b> ) .....	26
( <i>E</i> )-4-((4-Iodo-2,6-dimethylphenyl)diazenyl)-3,5-dimethylphenol ( <b>S1</b> ) .....	26
( <i>E</i> )-1-(2,6-Dimethyl-4-(nonyloxy)phenyl)-2-(4-iodo-2,6-dimethylphenyl)diazene ( <b>1j</b> ) .....	27
( <i>E</i> )-1-((4-Iodo-2,6-dimethylphenyl)diazenyl)naphthalene-2,7-diol ( <b>S2</b> ) .....	27
( <i>E</i> )-1-((4-Iodo-2,6-dimethylphenyl)diazenyl)naphthalene-2,7-diyl bis(4-(hexyloxy)benzoate) ( <b>1k</b> ) .....	28
( <i>E</i> )-1-(4-Bromophenyl)-2-(4-iodophenyl)diazene[10] ( <b>1l</b> ) .....	29
( <i>E</i> )-1-(3-Bromophenyl)-2-(4-iodophenyl)diazene ( <b>1m</b> ) .....	29
( <i>E</i> )-1-(2-Bromophenyl)-2-(4-iodophenyl)diazene ( <b>1n</b> ) .....	30
( <i>E</i> )-1,2-Bis(4-iodophenyl)diazene[11] ( <b>4a</b> ) .....	31
4-Iodo-2,6-dimethylaniline[12] ( <b>S3</b> ) .....	31
( <i>E</i> )-1,2-Bis(4-iodo-2,6-dimethylphenyl)diazene[13] ( <b>4b</b> ) .....	32
4-Bromo-2,6-dimethoxyaniline[14] ( <b>S4</b> ) .....	32
( <i>E</i> )-1,2-Bis(4-bromo-2,6-dimethoxyphenyl)diazene[15] ( <b>S5</b> ) .....	33

( <i>E</i> )-1,2-Bis(4-iodo-2,6-dimethoxyphenyl)diazene ( <b>4c</b> ) .....	33
4-Iodo-2,6-difluoro-aniline[16] ( <b>S6</b> ) .....	34
( <i>E</i> )-1,2-bis(2,6-difluoro-4-iodophenyl)diazene[17] ( <b>4d</b> ) .....	34
4-Bromo-2,6-difluoroaniline[18] ( <b>S7</b> ) .....	35
4-Amino-3,5-difluorobenzonitrile[19] ( <b>S8</b> ) .....	35
4-Amino-3,5-difluorobenzoic acid[20] ( <b>S9</b> ) .....	36
Ethyl 4-amino-3,5-difluorobenzoate[20] ( <b>S10</b> ) .....	36
( <i>E</i> )-4,4'-(Diazene-1,2-diyl)bis(3,5-difluorobenzoic acid)[17] ( <b>S11</b> ) .....	37
( <i>E</i> )-4,4'-(Diazene-1,2-diyl)bis(3,5-difluorobenzoic acid)[20] ( <b>6</b> ) .....	37
2-(2-(2-Aminophenethyl)phenyl)isoindoline-1,3-dione[21] ( <b>S12</b> ) .....	38
2-(2-Aminophenethyl)-4-iodoaniline[21] ( <b>S13</b> ) .....	39
( <i>Z</i> )-2-Iodo-11,12-dihydrodibenzo[ <i>c,g</i> ][1,2]diazocine[21] ( <b>7a</b> ) .....	39
2,2'-(Ethane-1,2-diyl)bis(4-iodoaniline)[21] ( <b>S14</b> ) .....	40
( <i>Z</i> )-2,9-Diiodo-11,12-dihydrodibenzo[ <i>c,g</i> ][1,2]diazocine[21] ( <b>7b</b> ) .....	40
References .....	41
<sup>1</sup> H, <sup>13</sup> C{ <sup>1</sup> H} and <sup>19</sup> F NMR Spectra of the Purified Compounds .....	43
<sup>1</sup> H NMR Spectra for the Determination of the <sup>1</sup> H NMR Yield .....	105

## General Information

For reactions under inert conditions, a nitrogen filled glovebox (Pure Lab<sup>HE</sup> from Inert, Amesbury, MA USA) and standard Schlenk techniques were used.

All carbonylation reactions were performed in microwave reaction vials sealed with a septum cap from Biotage (Biotage, Uppsala, Sweden).

All glassware was dried in an oven at 200 °C for several hours prior to use. NMR tubes were dried in an oven at 110 °C for several hours prior to use.

NMR spectra were recorded on a Bruker Avance Neo 600 (Bruker BioSpin, Rheinstetten, Germany) (600 MHz (<sup>1</sup>H), 151 MHz (<sup>13</sup>C{<sup>1</sup>H}), 565 MHz (<sup>19</sup>F)) at 298 K. All <sup>1</sup>H NMR and <sup>13</sup>C{<sup>1</sup>H} NMR spectra were referenced to the residual proton signals of the solvent (<sup>1</sup>H) or the solvent itself (<sup>13</sup>C{<sup>1</sup>H}). <sup>19</sup>F NMR spectra were referenced internally against trichlorofluoromethane. The exact assignment of the peaks was performed by two-dimensional NMR spectroscopy such as <sup>1</sup>H COSY, <sup>13</sup>C{<sup>1</sup>H} HSQC and <sup>1</sup>H/<sup>13</sup>C{<sup>1</sup>H} HMBC when possible.

High-resolution EI mass spectra were recorded on a MAT 95XL double-focusing mass spectrometer from Finnigan MAT (Thermo Fisher Scientific, Waltham, MA, USA) at an ionization energy of 70 eV. Samples were measured by a direct or indirect inlet method with a source temperature of 200 °C. High-resolution ESI and APCI mass spectra were measured by a direct inlet method on an Impact II mass spectrometer from Bruker Daltonics (Bruker Daltonics, Bremen, Germany). ESI mass spectra were recorded in the positive ion collection mode.

IR spectra were recorded on a Nicolet i510 FT-IR spectrometer from Thermo Fisher Scientific (Thermo Fisher Scientific, Waltham, MA, USA) with a diamond window in an area from 500 – 4000  $\text{cm}^{-1}$  with a resolution of 4  $\text{cm}^{-1}$ . All samples were measured 16 times against a background scan.

Melting points were recorded on a Büchi Melting Point M-560 (Büchi, Essen, Germany) and are reported corrected.

Thin layer chromatography (TLC) was performed using TLC Silica gel 60 F<sub>254</sub> from Merck (Merck, Darmstadt, Germany) and compounds were visualized by exposure to UV light at a wavelength of 254 nm. Column chromatography was performed either manually using silica gel 60 (0.015-0.040 mm) from Merck (Merck, Darmstadt, Germany) or by using a PuriFlash 4250 column machine (Interchim, Mannheim, Germany). Silica gel columns of the type CHROMABOND Flash RS 15 SPHERE SiOH 15  $\mu\text{m}$  (Macherey-Nagel, Düren, Germany) were used. The sample was applied via dry load with Celite® 503 (Macherey-Nagel, Düren, Germany) as column material. If stated, Celite® 503 (Macherey-Nagel, Düren, Germany) was used as filtration aid.

The use of abbreviations follows the conventions from the ACS Style guide[1].

#### Reagents

All chemicals were commercially available and used without purification unless stated otherwise.

**Table S1.** List of supplier and purity of used chemicals.

Reagent	Supplier	Purity	Comments
L-Alanine <i>tert</i> -butyl ester hydrochloride	Apollo Scientific		stored in a fridge in a glovebox
4-Aminoacetanilide	TCI	>98%	
2-Bromoaniline	Fluorochem	97%	
3-Bromoaniline	TCI	>98.0%	
4-Bromoaniline	Sigma Aldrich	97%	
9-Bromo-1-nonanol	Sigma Aldrich	95%	
<i>N</i> -Bromosuccinimide	Sigma Aldrich	98%	
1,8-Diazabicyclo[5.4.0]-undec-7-ene	Apollo	99.6%	
2,6-Difluoroanilin	chemPur	97%	
2,7-Dihydroxynapthalene	TCI	99%	
2,6-Dimethoxyanilin	BLDPharm	97%	
2,6-Dimethylaniline	TCI	99%	
3,5-Dimethylphenol	Sigma Aldrich	98%	
2,2'-Ethylenedianiline	TCI	>98%	
Hydrazine monohydrate	abcr	98%	
Hydrochloric acid	Sigma Aldrich		fuming, $\geq 37\%$
<i>N</i> -Hydroxysuccinimide	Apollo Scientific	>97%	
Iodine	abcr	99%	
4-Iodoaniline	Sigma Aldrich	98%	
<i>N</i> -Iodosuccinimide	Apollo Scientific	98%	
Magnesium sulfate	VWR		dried
Manganese dioxide	Merck		(precipitated active) for synthesis



<i>meta</i> -Chloroperoxybenzoic acid	Acros	70 – 75% <sup>1</sup>	
Nitrosobenzene	TCI	>98.0%	stored in a fridge
Oxone®	abcr		monopersulfate
Palladium acetate	Carbolution	98%	
Phenol	Sigma Aldrich	99%	
Phthalic anhydride	Acros	99%	
Potassium iodide	abcr	99%	
Sodium carbonate	Org Laborchemie	99.9%	
Sodium chloride	Th. Geyer	min 99.0%	
Sodium hydrogen carbonate	VWR	ACS, Reag. Ph. Eur.	
Sodium hydroxide	VWR	98%	
Sodium nitrite	Sigma Aldrich	97%	
Triethyl amine	Fluorochem	anhydrous	degassed, stored in a glovebox
1,3,5-Trimethoxybenzene	Sigma Aldrich	≥99%	
Xantphos	BLD Pharm	98%	

## Solvents

All solvents for purification and extraction were used as received. All solvents used for synthesis under inert conditions were dried by a solvent purification system (SPS) from Inert Technologies.

**Table S2.** List of supplier and purity of used solvents.

Solvent	Supplier	Purity	Comments
Acetic Acid	Merck	≥99.8%	
Acetone	Sigma Aldrich	>99.5%	
Acetonitrile	Fisher Scientific	≥99.5%	
Cyclohexane	Merck	≥99.5%	
Chloroform	Sigma Aldrich	>99%	
Chloroform- <i>d</i> <sub>1</sub>	Euroisotop	99.8%	
DCM	Merck	≥99.9%	
DMF	Acros Organics	99.8%	Extra dry, AcroSeal™
DMSO	VWR	technical grade	
DMSO	Acros Organics	99.7%	Extra dry, AcroSeal™
DMSO- <i>d</i> <sub>6</sub>		>99.00%	
Ethanol	VWR	≥99.8%	absolute
Ethyl acetate	Merck	≥99.5%	
Formic acid	Sigma Aldrich	97%	
Methanol	VWR	≥99.8%	
1-Methyl-2-pyrrolidone	TCI	>99%	Low water content
Tetrahydrofuran	VWR	HPLC grade	anhydrous from SPS, stored in a glovebox
Tetrahydrofuran	Fisher Scientific	≥99.8%	
Toluene	Merck	≥99.7%	
Water		deionized	

<sup>1</sup> The exact concentration was determined by iodometric titration against sodium thiosulfate.

## Syntheses

### General procedure 1

#### a) Mono-iodinated molecular switch

Under inert conditions, the corresponding mono-iodinated switch (200  $\mu\text{mol}$ , 2.00 equiv),  $\text{Pd}(\text{OAc})_2$  (1.35 mg, 6.00  $\mu\text{mol}$ , 3 mol%), Xantphos (2.89 mg, 5.00  $\mu\text{mol}$ , 2.5 mol%) and 2,5-dioxopyrrolidin-1-yl formate (**2**) (57.2 mg, 400  $\mu\text{mol}$ , 4.00 equiv) were dissolved in dry THF (3 mL) in a pressure reaction vial. A solution of 1,3,5-trimethoxybenzene (16.8 mg, 100  $\mu\text{mol}$ ) as an internal standard in dry THF (1 mL) was added. The vial was sealed and heated to 60 °C. A solution of triethyl amine (22.2 mg, 220  $\mu\text{mol}$ , 2.20 equiv) in dry THF (1 mL) was quickly added. Fast gas evolution was observed and the reaction was stirred for 17 h at 60 °C. After cooling to 21 °C, the solvent was removed under reduced pressure. The residue was re-dissolved in DCM (10 mL), filtered through Celite® and the solvent removed under reduced pressure.

#### b) Di-iodinated molecular switch

Under inert conditions, the corresponding di-iodinated molecular switch (100  $\mu\text{mol}$ , 1.00 equiv),  $\text{Pd}(\text{OAc})_2$  (1.35 mg, 6.00  $\mu\text{mol}$ , 6 mol%), Xantphos (2.89 mg, 5.00  $\mu\text{mol}$ , 5 mol%) and 2,5-dioxopyrrolidin-1-yl formate (**2**) (57.2 mg, 400  $\mu\text{mol}$ , 4.00 equiv) were dissolved in dry THF (3 mL) in a pressure reaction vial. A solution of 1,3,5-trimethoxybenzene (16.8 mg, 100  $\mu\text{mol}$ ) as an internal standard in dry THF (1 mL) was added. The vial was sealed and heated to 60 °C. A solution of triethyl amine (22.2 mg, 220  $\mu\text{mol}$ , 2.20 equiv) in dry THF (1 mL) was quickly added. Fast gas evolution was observed and the reaction was stirred for 17 h at 60 °C. After cooling to 21 °C, the solvent was removed under reduced pressure. The residue was re-dissolved in DCM (10 mL), filtered through Celite® and the solvent removed under reduced pressure.

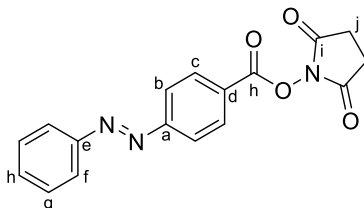
### General procedure 2

#### a) Mono-iodinated molecular switch

Under inert conditions, the corresponding mono-iodinated switch (200  $\mu\text{mol}$ , 2.00 equiv),  $\text{Pd}(\text{OAc})_2$  (1.35 mg, 6.00  $\mu\text{mol}$ , 3 mol%), Xantphos (2.89 mg, 5.00  $\mu\text{mol}$ , 2.5 mol%) and 2,5-dioxopyrrolidin-1-yl formate (**2**) (57.2 mg, 400  $\mu\text{mol}$ , 4.00 equiv) were dissolved in dry THF (4 mL) in a pressure reaction vial. The vial was sealed and heated to 60 °C. A solution of triethyl amine (22.2 mg, 220  $\mu\text{mol}$ , 2.20 equiv) in dry THF (1 mL) was quickly added. Fast gas evolution was observed and the reaction was stirred for 17 h at 60 °C. After cooling to 21 °C, the solvent was removed under reduced pressure. The residue was re-dissolved in DCM (10 mL) and extracted with water (20 mL) and brine (20 mL). The combined organic layers were dried over  $\text{MgSO}_4$ , filtered and the solvent removed under reduced pressure.

#### b) Di-iodinated molecular switch

Under inert conditions, the corresponding di-iodinated switch (100  $\mu\text{mol}$ , 1.00 equiv),  $\text{Pd}(\text{OAc})_2$  (1.35 mg, 6.00  $\mu\text{mol}$ , 6 mol%), Xantphos (2.89 mg, 5.00  $\mu\text{mol}$ , 5 mol%) and 2,5-dioxopyrrolidin-1-yl formate (**2**) (57.2 mg, 400  $\mu\text{mol}$ , 4.00 equiv) were dissolved in dry THF (4 mL) in a pressure reaction vial. The vial was sealed and heated to 60 °C. A solution of triethyl amine (22.2 mg, 220  $\mu\text{mol}$ , 2.20 equiv) in dry THF (1 mL) was quickly added. Fast gas evolution was observed and the reaction was stirred for 17 h at 60 °C. After cooling to 21 °C, the solvent was removed under reduced pressure. The residue was re-dissolved in DCM (10 mL) and extracted with water (20 mL) and brine (20 mL). The combined organic layers were dried over  $\text{MgSO}_4$ , filtered and the solvent removed under reduced pressure.

2,5-Dioxopyrrolidin-1-yl (*E*)-4-(phenyldiazenyl)benzoate<sup>[2]</sup> (**3a**)

Compound **3a** was synthesized according to general procedure 2a from (*E*)-1-(4-iodophenyl)-2-phenyldiazene (**1a**) (61.6 mg, 200  $\mu$ mol, 2.00 equiv). The product **3b** was obtained after crystallization from *n*-hexane/DCM (3:1) at -21  $^{\circ}$ C as a red solid (64.1 mg, 198  $\mu$ mol, 99%, Lit.:<sup>[2]</sup> 84%<sup>2</sup>).

<sup>1</sup>H NMR (600 MHz, CDCl<sub>3</sub>)  $\delta$  = 8.30 (d, <sup>3</sup>J = 8.5 Hz, 2H, *H*-c), 8.02 (d, <sup>3</sup>J = 8.5 Hz, 2H, *H*-b), 7.99 – 7.96 (m, 2H, *H*-f), 7.57 – 7.52 (m, 3H, *H*-g/h), 2.94 (s, br, 4H, *H*-j) ppm.

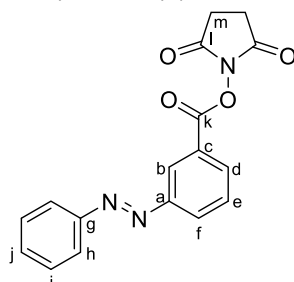
<sup>13</sup>C{<sup>1</sup>H} NMR (151 MHz, CDCl<sub>3</sub>)  $\delta$  = 169.3 (C-i), 161.6 (C-h), 156.3 (C-a), 152.6 (C-e), 132.3 (C-h), 131.9 (C-c), 129.4 (C-g), 126.7 (C-d), 123.5 (C-f), 123.2 (C-b), 25.9 (C-j) ppm.

IR (ATR):  $\tilde{\nu}$  = 2999 (w), 2359 (w), 1790 (s), 1726 (s), 1600 (m), 1496 (w), 1427 (m), 1408 (m), 1366 (m), 1306 (w), 1256 (w), 1204 (s), 1151 (m), 1070 (s), 1019 (m), 999 (s), 928 (m), 867 (s), 849 (m), 812 (m), 771 (s) cm<sup>-1</sup>.

HRMS (EI, 70 eV) *m/z* (%): [M]<sup>+</sup> calcd for [C<sub>17</sub>H<sub>13</sub>N<sub>3</sub>O<sub>4</sub>]<sup>+</sup> 323.09006; found 323.09003 (10), 209.2 (100).

**Mp**: 226  $^{\circ}$ C.

**R<sub>f</sub>**: 0.65 (*n*-hexane/DCM 1:1).

2,5-Dioxopyrrolidin-1-yl (*E*)-3-(phenyldiazenyl)benzoate<sup>[2]</sup> (**3b**)

Compound **3b** was synthesized according to general procedure 1a from (*E*)-1-(4-iodophenyl)-2-phenyldiazene (**1b**) (61.6 mg, 200  $\mu$ mol, 2.00 equiv). The compound was purified by column chromatography on silica (eluent: gradient *n*-hexane/ethyl acetate 1:0  $\rightarrow$  0:1) yielding **3b** as an orange solid (60.5 mg, 188  $\mu$ mol, 94%, Lit.:<sup>[2]</sup> 95%<sup>3</sup>).

<sup>1</sup>H NMR (600 MHz, CDCl<sub>3</sub>)  $\delta$  = 8.68 (at, <sup>4</sup>J = 1.9 Hz, 1H, *H*-b), 8.25 – 8.22 (m, 2H, *H*-d/f), 7.97 – 7.94 (m, 2H, *H*-h), 7.69 (t, <sup>3</sup>J = 7.8 Hz, 1H, *H*-e), 7.57 – 7.50 (m, 3H, *H*-i/j), 2.94 (s, br, 4H, *H*-m) ppm.

<sup>13</sup>C{<sup>1</sup>H} NMR (151 MHz, CDCl<sub>3</sub>)  $\delta$  = 169.2 (C-l), 161.6 (C-k), 152.8 (C-a), 152.5 (C-g), 132.5 (C-d), 131.9 (C-j), 129.9 (C-e), 129.4 (C-i), 129.1 (C-f), 126.4 (C-d), 125.0 (C-b), 123.3 (C-h), 25.9 (C-m) ppm.

IR (ATR):  $\tilde{\nu}$  = 2921 (w), 2359 (w), 1766 (m), 1727 (s), 1431 (m), 1371 (m), 1287 (w), 1257 (m), 1203 (s), 1149 (m), 1135 (m), 1070 (s), 1038 (m), 1014 (m), 923 (m), 867 (m), 812 (m), 765 (s), 740 (s) cm<sup>-1</sup>.

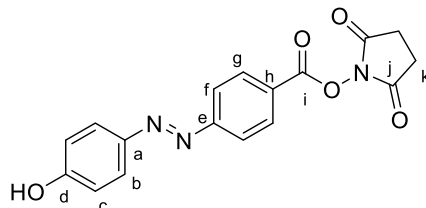
HRMS (EI, 70 eV) *m/z* (%): [M]<sup>+</sup> calcd for [C<sub>17</sub>H<sub>13</sub>N<sub>3</sub>O<sub>4</sub>]<sup>+</sup> 323.09006; found 323.09006 (7), 77.0 (100).

**Mp**: 151  $^{\circ}$ C.

**R<sub>f</sub>**: 0.59 (*n*-hexane/DCM 1:1).

<sup>2</sup> In this report, the product was prepared by coupling of the corresponding carboxylic acid with NHS using DCC.

<sup>3</sup> In this report, the product was prepared by coupling of the corresponding carboxylic acid with NHS using DCC.

2,5-Dioxopyrrolidin-1-yl (*E*)-4-((4-hydroxyphenyl)diazenyl)benzoate<sup>[3]</sup> (**3d**)

Compound **3d** was synthesized according to general procedure 1a from (*E*)-4-((4-iodophenyl)diazenyl)phenol (**1d**) (64.8 mg, 200  $\mu$ mol, 2.00 equiv). The compound was purified by column chromatography on silica (eluent: gradient *n*-hexane/ethyl acetate 1:0  $\rightarrow$  0:1) yielding **3d** as an orange powder (64.5 mg, 190  $\mu$ mol, 95%, Lit.:<sup>[3]</sup> 90%<sup>4</sup>).

<sup>1</sup>H NMR (600 MHz, DMSO-*d*<sub>6</sub>)  $\delta$  = 10.60 (s, 1H, OH-d), 8.27 (d, <sup>3</sup>*J* = 8.2 Hz, 2H, H-g), 8.01 (d, <sup>3</sup>*J* = 8.2 Hz, 2H, H-f), 7.89 (d, <sup>3</sup>*J* = 8.4 Hz, 2H, H-b), 6.99 (d, <sup>3</sup>*J* = 8.4 Hz, 2H, H-c), 2.92 (s, 4H, H-k) ppm.

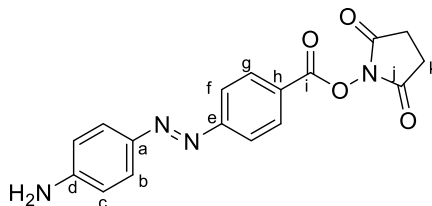
<sup>13</sup>C{<sup>1</sup>H} NMR (151 MHz, DMSO-*d*<sub>6</sub>)  $\delta$  = 170.79 (C-j), 162.66 (C-a), 161.82 (C-i), 156.45 (C-e), 145.85 (C-d), 132.01 (C-g), 126.20 (C-b), 125.62 (C-h), 123.33 (C-f), 116.68 (C-c), 26.03 (C-k).

IR (ATR):  $\tilde{\nu}$  = 3487 (w), 1764 (m), 1719 (s), 1601 (m), 1591 (w), 1431 (m), 1405 (m), 1275 (m), 1206 (s), 1156 (m), 1098 (m), 1015 (m), 1005 (s), 991 (m), 859 (w), 841 (s), 738 (m), 723 (m), 690 (m), 661 (m) cm<sup>-1</sup>.

HRMS (EI, 70 eV) *m/z* (%): [M]<sup>+</sup> calcd for [C<sub>17</sub>H<sub>13</sub>N<sub>3</sub>O<sub>5</sub>]<sup>+</sup> 339.08497; found 339.08536 (15), 93.0 (100).

Mp: 241 °C.

R<sub>f</sub>: 0.25 (*n*-hexane/ethyl acetate 1:1).

2,5-Dioxopyrrolidin-1-yl (*E*)-4-((4-aminophenyl)diazenyl)benzoate (**3e**)

Compound **3e** was synthesized according to general procedure 1a from (*E*)-4-((4-iodophenyl)diazenyl)aniline (**1e**) (64.8 mg, 200  $\mu$ mol, 2.00 equiv). The solid was dissolved in ethyl acetate, washed with water (2  $\times$  20 mL) and brine (20 mL). The combined organic phases were dried over MgSO<sub>4</sub>, filtered and the solvent removed under reduced pressure. The crude product was crystallized from *n*-hexane/DCM (3:1) to obtain **3e** as an orange solid (65.6 mg, 172  $\mu$ mol, 86%).

<sup>1</sup>H NMR (600 MHz, DMSO-*d*<sub>6</sub>)  $\delta$  = 8.22 (d, <sup>3</sup>*J* = 8.6 Hz, 2H, H-g), 7.93 (d, <sup>3</sup>*J* = 8.6 Hz, 2H, H-f), 7.75 (d, <sup>3</sup>*J* = 8.9 Hz, 2H, H-b), 6.71 (d, <sup>3</sup>*J* = 8.9 Hz, 2H, H-c), 6.47 (s, 2H, NH<sub>2</sub>-d) 2.91 (s, br, 4H, H-k) ppm.

<sup>13</sup>C{<sup>1</sup>H} NMR (151 MHz, DMSO-*d*<sub>6</sub>)  $\delta$  = 170.37 (C-j), 161.43 (C-i), 156.65 (C-e), 154.35 (C-a), 143.04 (C-d), 131.46 (C-g), 126.37 (C-b), 123.82 (C-h), 122.37 (C-f), 113.54 (C-c), 25.57 (C-k) ppm.

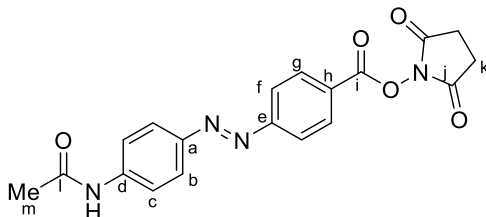
IR (ATR):  $\tilde{\nu}$  = 3451 (w), 3366 (w), 1761 (s), 1725 (s), 1597 (m), 1456 (s), 1427 (m), 1401 (w), 1320 (w), 1255 (w), 1231 (w), 1205 (s), 1076 (m), 1046 (w), 1014 (m), 1014 (m), 861 (m), 835 (s), 726 (w), 690 (w) cm<sup>-1</sup>.

HRMS (EI, 70 eV) *m/z* (%): [M]<sup>+</sup> calcd for [C<sub>17</sub>H<sub>14</sub>N<sub>4</sub>O<sub>4</sub>]<sup>+</sup> 338.10096; found 338.10115 (10), 92.1 (100).

Mp: 218 °C.

R<sub>f</sub>: 0.25 (*n*-hexane/ethyl acetate 1:1).

<sup>4</sup> In this report, the product was prepared by coupling of the corresponding carboxylic acid with NHS using DCC.

2,5-Dioxopyrrolidin-1-yl (*E*)-4-((4-acetamidophenyl)diazenyl)benzoate (**3f**)

Compound **3f** was synthesized according to general procedure 1a from (*E*)-*N*-(4-((4-iodophenyl)diazenyl)phenyl)acetamide (**1f**) (64.8 mg, 200  $\mu$ mol, 2.00 equiv). The solid was dissolved in ethyl acetate, washed with water (2  $\times$  20 mL) and brine (20 mL). The combined organic phases were dried over MgSO<sub>4</sub>, filtered and the solvent removed under reduced pressure. The crude product was crystallized from *n*-hexane/DCM (3:1) to obtain **3f** as an orange solid (65.6 mg, 172  $\mu$ mol, 86%).

<sup>1</sup>H NMR (600 MHz, DMSO- *d*<sub>6</sub>)  $\delta$  = 10.40 (s, 1H, NH-d) 8.29 (d, <sup>3</sup>*J* = 8.5 Hz, 2H, *H*-g), 8.05 (d, <sup>3</sup>*J* = 8.5 Hz, 2H, *H*-f), 7.97 (d, <sup>3</sup>*J* = 8.9 Hz, 2H, *H*-c), 7.85 (d, <sup>3</sup>*J* = 8.9 Hz, 2H, *H*-b), 2.92 (s, br, 4H, *H*-k), 2.12 (s, 3H, *H*-m) ppm.

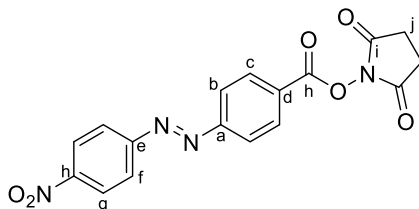
<sup>13</sup>C{<sup>1</sup>H} NMR (151 MHz, DMSO- *d*<sub>6</sub>)  $\delta$  = 170.31 (C-j), 169.05 (C-l), 161.33 (C-i), 155.84 (C-a), 147.44 (C-d), 143.57 (C-a), 131.59 (C-g), 125.63 (C-h), 124.50 (C-c), 123.08 (C-f), 119.15 (C-b), 25.59 (C-k), 24.25 (C-m) ppm.

IR (ATR):  $\tilde{\nu}$  = 3559 (w), 1757 (m), 1732 (m), 1688 (m), 1529 (s), 1446 (m), 1311 (m), 1300 (m), 1235 (m), 1208 (s), 998.3 (m), 861 (s), 848 (m), 739 (m) cm<sup>-1</sup>.

HRMS (EI, 70 eV) *m/z* (%): [M]<sup>+</sup> calcd for [C<sub>19</sub>H<sub>16</sub>N<sub>4</sub>O<sub>5</sub>]<sup>+</sup> 380.11152; found 380.11201 (15), 134.2 (100).

Mp: 274 °C.

R<sub>f</sub>: 0.15 (*n*-hexane/ethyl acetate 1:1).

2,5-Dioxopyrrolidin-1-yl (*E*)-4-((4-nitrophenyl)diazenyl)benzoate (**3g**)

Compound **3c** was synthesized according to general procedure 2a from (*E*)-1-(4-nitrophenyl)-2-(4-iodophenyl)diazene (**1g**) (77.4 mg, 200  $\mu$ mol, 2.00 equiv). The product **3g** was obtained after crystallization from *n*-hexane/DCM (3:1) at -21 °C as an orange solid (73.1 mg, 198  $\mu$ mol, 99%).

<sup>1</sup>H NMR (600 MHz, CDCl<sub>3</sub>)  $\delta$  = 8.42 (d, <sup>3</sup>*J* = 8.5 Hz, 2H, *H*-g), 8.33 (d, <sup>3</sup>*J* = 8.1 Hz, 2H, *H*-c), 8.11 (d, <sup>3</sup>*J* = 8.5 Hz, 2H, *H*-f), 8.08 (d, <sup>3</sup>*J* = 8.1 Hz, 2H, *H*-b), 2.95 (s, br, 4H, *H*-j) ppm.

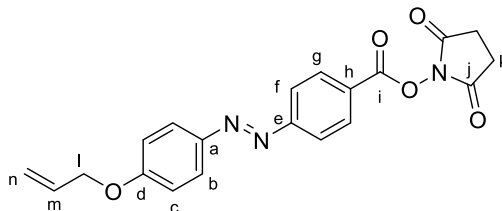
<sup>13</sup>C{<sup>1</sup>H} NMR (151 MHz, CDCl<sub>3</sub>)  $\delta$  = 169.2 (C-i), 161.3 (C-h), 155.7 (C-a), 155.4 (C-e), 149.5 (C-h), 132.0 (C-c), 128.0 (C-d), 125.0 (C-g), 124.1 (C-f), 123.7 (C-b), 25.9 (C-j) ppm.

IR (ATR):  $\tilde{\nu}$  = 3080 (w), 1767 (m), 1761 (s), 1606 (m), 1530 (s), 1431 (m), 1407(m), 1346 (s), 1322 (m), 1259 (m), 1237 (m), 1199 (s), 1110 (m), 1076 (s), 1023 (m), 1007 (s), 870 (s), 854 (m), 816 (m), 764 (m), 752 (m) cm<sup>-1</sup>.

HRMS (EI, 70 eV) *m/z* (%): [M]<sup>+</sup> calcd for [C<sub>17</sub>H<sub>12</sub>N<sub>4</sub>O<sub>6</sub>]<sup>+</sup> 368.07514; found 368.07562 (4), 254.2 (100).

Mp: 245 °C.

R<sub>f</sub>: 0.59 (*n*-hexane/DCM 1:1).

2,5-Dioxopyrrolidin-1-yl (*E*)-4-((4-(allyloxy)phenyl)diazenyl)benzoate (**3h**)

Compound **3h** was synthesized according to general procedure 1a from (*E*)-1-(4-(allyloxy)phenyl)-2-(4-iodophenyl)diazene (**1h**) (72.8 mg, 200  $\mu$ mol, 2.00 equiv). The compound was purified by column chromatography on silica (eluent: gradient *n*-hexane/ethyl acetate 1:0  $\rightarrow$  0:1) yielding **3h** as an orange powder (45.3 mg, 119  $\mu$ mol, 60%).

$^1\text{H NMR}$  (600 MHz,  $\text{CDCl}_3$ )  $\delta$  = 8.27 (d,  $^3J$  = 8.6 Hz, 2H, *H-g*), 7.97 (d,  $^3J$  = 8.6 Hz, 4H, *H-f/b*), 7.05 (d,  $^3J$  = 8.9 Hz, 2H, *H-c*), 6.09 (m, 1H, *H-m*), 5.46 (d,  $^2J$  = 10.5 Hz, 1H, *H-n*), 5.35 (d,  $^2J$  = 10.5 Hz, 1H, *H-n*), 4.65 (d,  $^3J$  = 5.0 Hz, 2H, *H-l*), 2.93 (s, 4H, *H-k*) ppm.

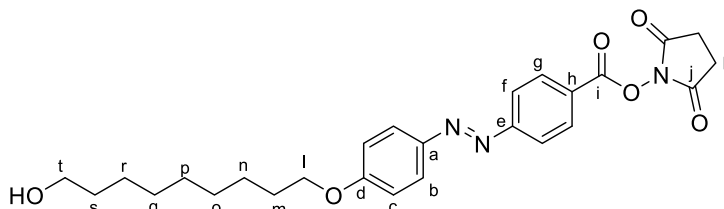
$^{13}\text{C}\{^1\text{H}\}$  NMR (151 MHz,  $\text{CDCl}_3$ )  $\delta$  = 169.32 (*C-j*), 162.17 (*C-d*), 161.62 (*C-i*), 157.04 (*C-e*), 148.03 (*C-a*), 132.69 (*C-m*), 131.87 (*C-g*), 126.02 (*C-h*), 125.60 (*C-f/b*), 122.92 (*C-f/b*), 118.41 (*C-n*), 115.27 (*C-c*), 69.26 (*C-l*), 24.35 (*C-k*).

IR (ATR):  $\tilde{\nu}$  = 2921 (w), 2851 (w), 1768 (w), 1731 (m), 1600 (m), 1499 (m), 1371 (w), 1204 (s), 1070 (s), 1016 (m), 992 (s), 861 (m), 812 (w), 760 (w), 723 (w), 687 (w)  $\text{cm}^{-1}$ .

HRMS (EI, 70 eV)  $m/z$  (%):  $[\text{M}]^+$  calcd for  $[\text{C}_{20}\text{H}_{17}\text{N}_3\text{O}_5]^+$  379.11627; found 379.11643 (20), 133.1 (100)

**Mp**: - (decomposition).

**R<sub>f</sub>**: 0.35 (*n*-hexane/ethyl acetate 1:1).

2,5-Dioxopyrrolidin-1-yl (*E*)-4-((4-((9-hydroxynonyl)oxy)phenyl)diazenyl)benzoate (**3i**)

Compound **3i** was synthesized according to general procedure 1a from (*E*)-9-(4-((4-iodophenyl)diazenyl)phenoxy)nonan-1-ol (**1i**) (93.2 mg, 200  $\mu$ mol, 2.00 equiv). The compound was purified by column chromatography on silica (eluent: gradient *n*-hexane/ethyl acetate 1:0  $\rightarrow$  0:1) yielding **3i** as a yellow solid (76.3 mg, 158  $\mu$ mol, 79%).

$^1\text{H NMR}$  (600 MHz,  $\text{CDCl}_3$ )  $\delta$  = 8.27 (d,  $^3J$  = 6.6 Hz, 2H, *H-g*), 7.96 (dd,  $^3J$  = 8.9, 6.6 Hz, 4H, *H-f/b*), 7.02 (d,  $^3J$  = 8.9 Hz, 2H, *H-c*), 4.06 (t,  $^3J$  = 6.5 Hz, 2H, *H-l*), 3.65 (t,  $^3J$  = 6.6 Hz, 2H, *H-t*), 2.93 (s, 4H, *H-k*), 1.87 – 1.79 (m, 2H, *H-m*), 1.60 – 1.52 (m, 2H, *H-s*), 1.51 – 1.48 (m, 2H, *H-n*), 1.41 – 1.30 (m, 8H, *H-o/p/r/q*), 1.23 (s, 1H, *OH-t*) ppm.

$^{13}\text{C}\{^1\text{H}\}$  NMR (151 MHz,  $\text{CDCl}_3$ )  $\delta$  = 169.12 (*C-j*), 162.63 (*C-d*), 161.42 (*C-i*), 156.42 (*C-e*), 146.77 (*C-a*), 131.65 (*C-g*), 125.72 (*C-h*), 125.42 (*C-f/b*), 122.68 (*C-f/b*), 115.65 (*C-c*), 68.38 (*C-l*), 63.00 (*C-t*), 32.71 (*C-s*), 29.43 (*C-o/p/r/q*), 29.28 (*C-o/p/r/q*), 29.22 (*C-o/p/r/q*), 29.07 (*C-m*), 25.92 (*C-o/p/r/q*), 25.66 (*C-n*), 25.64 (*C-k*) ppm.

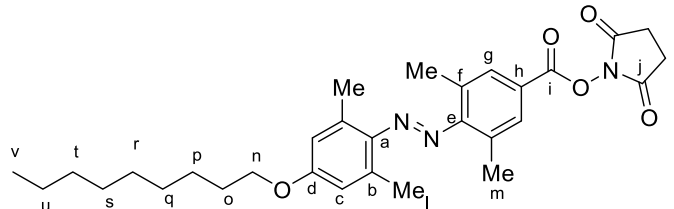
IR (ATR):  $\tilde{\nu}$  = 3523 (w), 2921 (w), 2850 (w), 1797 (m), 1773 (s), 1715 (s), 1600 (w), 1500 (m), 1381 (w), 1296 (m), 1255 (m), 1210 (s), 1138 (m), 1107 (m), 1075 (s), 1050 (s), 1016 (s), 988 (s), 863 (m), 843 (s), 814 (m), 723 (m), 688 (w)  $\text{cm}^{-1}$ .

**HRMS** (EI, 70 eV)  $m/z$  (%):  $[M]^+$  calcd for  $[C_{26}H_{31}N_3O_6]^+$  481.22074; found 481.22050 (5), 55.1 (100).

**Mp**: 156 °C.

**R<sub>f</sub>**: 0.15 (*n*-hexane/ethyl acetate 1:1).

2,5-Dioxopyrrolidin-1-yl (*E*)-4-((2,6-dimethyl-4-(nonyloxy)phenyl)diazenyl)-3,5-dimethylbenzoate (**3j**)



Compound **3j** was synthesized according to general procedure 2a from (*E*)-1-(2,6-dimethyl-4-(nonyloxy)phenyl)-2-(4-iodo-2,6-dimethylphenyl)diazene (**1j**) (92.8 mg, 200 μmol, 2.00 equiv). The compound was purified by column chromatography on silica (eluent: gradient *n*-hexane/ethyl acetate 1:0 → 0:1) yielding **3j** as a red powder (97.0 mg, 186 μmol, 94%).

The NMR yield was obtained according to general procedure 1a with the difference that **1j** (46.4 mg, 100 μmol, 1.00 equiv), Pd(OAc)<sub>2</sub> (675 μg, 3.00 μmol, 3 mol%), Xantphos (1.45 mg, 2.50 μmol, 2.5 mol%), 2,5-dioxopyrrolidin-1-yl formate (**2**) (28.6 mg, 200 μmol, 2.00 equiv), 1,3,5-trimethoxybenzene (16.8 mg, 100 μmol) and triethyl amine (22.2 mg, 220 μmol, 1.10 equiv) were used.

**<sup>1</sup>H NMR** (600 MHz, CDCl<sub>3</sub>) δ = 7.91 (s, 2H, *H*-g), 6.70 (s, 2H, *H*-c), 4.03 (t, <sup>3</sup>*J* = 6.5 Hz, 2H, *H*-n), 2.92 (s, 4H, *H*-k), 2.55 (s, 6H, *H*-l), 2.34 (s, 6H, *H*-m), 1.85 – 1.77 (m, 2H, *H*-o), 1.53 – 1.43 (m, 2H, *H*-p), 1.40 – 1.25 (m, 10H, *H*-q,r,s,t,u), 0.92 – 0.86 (m, 3H, *H*-v).

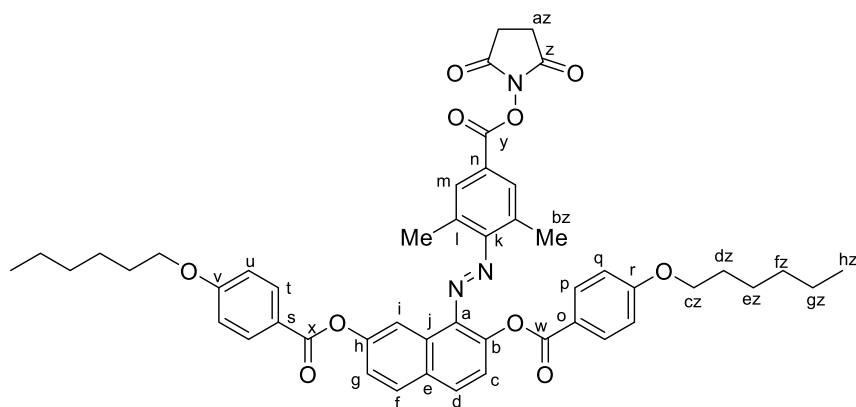
**<sup>13</sup>C{<sup>1</sup>H} NMR** (151 MHz, CDCl<sub>3</sub>) δ = 169.32 (*C*-j), 161.72 (*C*-i), 160.34 (*C*-d), 157.55 (*C*-e), 143.83 (*C*-a), 136.72 (*C*-b), 131.32 (*C*-g), 130.41 (*C*-f), 122.77 (*C*-h), 115.31 (*C*-c), 68.13 (*C*-n), 31.90 (*C*-q,r,s,t,u), 29.55 (*C*-q,r,s,t,u), 29.38 (*C*-q,r,s,t,u), 29.28 (*C*-q,r,s,t,u), 29.21 (*C*-o), 26.02 (*C*-p), 25.71 (*C*-k), 22.69 (*C*-q,r,s,t,u), 21.38 (*C*-m), 19.09 (*C*-l), 14.13 (*C*-v).

**IR** (ATR):  $\tilde{\nu}$  = 2922 (m), 2848 (m), 1761 (s), 1732(s), 1599 (m), 1489 (w), 1465 (w), 1431 (w), 1356 (w), 1313 (m), 1297 (m), 1248 (m), 1187 (s), 1161 (s), 1139 (s), 1077 (s), 1058 (s), 1044 (m), 994 (w), 911 (s), 903(s), 868 (m), 854 (m), 827 (w), 806 (w), 689 (w) cm<sup>-1</sup>.

**HRMS** (EI, 70 eV)  $m/z$  (%):  $[M]^+$  calcd for  $[C_{30}H_{39}N_3O_5]^+$  521.28842; found 521.28660 (10), 69.1 (100).

**Mp**: 78 °C.

**R<sub>f</sub>**: 0.45 (*n*-hexane/ethyl acetate 1:1).

2,5-Dioxopyrrolidin-1-yl (*E*)-4-((2,7-bis(4-(hexyloxy)phenoxy)naphthalen-1-yl)diazenyl)-3,5-dimethylbenzoate (**3k**)

Compound **3k** was synthesized according to general procedure 1a from (*E*)-1-(2,7-bis(4-(hexyloxy)phenoxy)naphthalen-1-yl)-2-(4-iodo-2,6-dimethylphenyl)diazene (**1k**) (154 mg, 200  $\mu$ mol, 2.00 equiv). The compound was purified by column chromatography on silica (eluent: gradient *n*-hexane/ethyl acetate 1:0  $\rightarrow$  0:1) yielding **3k** as a red powder (125 mg, 148  $\mu$ mol, 74%).

<sup>1</sup>H NMR (600 MHz, CDCl<sub>3</sub>)  $\delta$  = 8.53 (d, <sup>4</sup>*J* = 2.3 Hz, 1H, *H*-i), 8.16 (d, <sup>3</sup>*J* = 8.8 Hz, 2H, *H*-t), 8.06 – 8.03 (m, 3H, *H*-p/c), 8.01 (d, <sup>3</sup>*J* = 8.9 Hz, 1H, *H*-g), 7.81 (s, 2H, *H*-m), 7.49 (dd, <sup>3</sup>*J* = 8.9, <sup>4</sup>*J* = 2.3 Hz, 1H, *H*-f), 7.44 (d, <sup>3</sup>*J* = 8.8 Hz, 1H, *H*-d), 6.97 (d, <sup>3</sup>*J* = 8.8 Hz, 2H, *H*-u), 6.91 (d, <sup>3</sup>*J* = 8.8 Hz, 2H, *H*-q), 4.03 (dt, <sup>2</sup>*J* = 13.3, <sup>3</sup>*J* = 6.7 Hz, 4H, *H*-cz), 2.90 (s, 4H, *H*-az), 2.24 (s, 6H, *H*-bz), 1.80 (dt, <sup>2</sup>*J* = 13.3, <sup>3</sup>*J* = 6.7 Hz, 4H, *H*-dz), 1.55 – 1.44 (m, 4H, *H*-ez), 1.38 - 1.32 (m, 8H, *H*-fz/gz), 0.93 – 0.90 (m, 6H, *H*-hz) ppm.

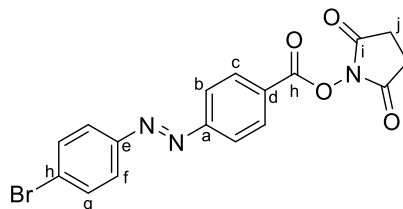
<sup>13</sup>C{<sup>1</sup>H} NMR (151 MHz, CDCl<sub>3</sub>)  $\delta$  = 169.35 (C-z), 165.11 (C-x), 165.08 (C-w), 163.81 (C-s), 163.75 (C-o), 161.68 (C-y), 157.03 (C-k), 151.06 (C-b), 140.03 (C-e), 137.81 (C-j), 132.53 (C-t), 132.45 (C-p), 131.33 (C-m), 131.20 (C-f), 131.01 (C-a), 130.53 (C-h), 129.67 (C-g), 123.74 (C-c), 123.03 (C-d), 122.40 (C-n), 121.40 (C-v), 121.17 (C-r), 115.84 (C-i), 114.47 (C-u/q), 68.48 (C-cz), 68.45 (C-cz), 31.71 (C-fz/gz), 31.69 (C-fz/gz), 29.22 (C-dz), 29.20 (C-dz), 25.80 (C-az, C-ez), 22.73 (C-fz/gz), 18.74 (C-bz), 14.17 (C-hz) ppm.

IR (ATR):  $\tilde{\nu}$  = 2929 (w), 1774 (w), 1735 (s), 1604 (m), 1577 (w), 1511 (w), 1456 (w), 1420 (w), 1367 (w), 1293 (w), 1247 (s), 1202 (s), 1161 (s), 1063 (s), 1017 (s), 1007 (m), 995 (w), 919 (w), 890 (m), 874 (w), 846 (m), 759 (w), 749 (w), 689 (w) cm<sup>-1</sup>.

HRMS (ESI): *m/z* = [M + Na]<sup>+</sup> calcd for [C<sub>49</sub>H<sub>51</sub>N<sub>3</sub>O<sub>10</sub> + Na]<sup>+</sup> 864.34619, found 864.34667.

Mp: 80 °C.

R<sub>f</sub>: 0.45 (*n*-hexane/ethyl acetate 1:1).

2,5-Dioxopyrrolidin-1-yl (*E*)-4-((4-bromophenyl)diazenyl)benzoate (**3l**)

Compound **3l** was synthesized according to general procedure 2a from (*E*)-1-(4-bromophenyl)-2-(4-iodophenyl)diazene (**1l**) (77.4 mg, 200  $\mu$ mol, 2.00 equiv). The product was obtained after crystallization from *n*-hexane/DCM (3:1) at -21 °C as an orange solid (76.3 mg, 190  $\mu$ mol, 95%).



**<sup>1</sup>H NMR** (600 MHz, CDCl<sub>3</sub>) δ = 8.30 (d, <sup>3</sup>J = 8.3 Hz, 2H, H-c), 8.01 (d, <sup>3</sup>J = 8.3 Hz, 2H, H-b), 7.85 (d, <sup>3</sup>J = 8.8 Hz, 2H, H-f), 7.69 (d, <sup>3</sup>J = 8.8 Hz, 2H, H-g), 2.94 (s, br, 4H, H-j) ppm.

**<sup>13</sup>C{<sup>1</sup>H} NMR** (151 MHz, CDCl<sub>3</sub>) δ = 169.3 (C-i), 161.5 (C-h), 156.1 (C-a), 151.3 (C-e), 132.7 (C-g), 131.9 (C-c), 127.0 (C-d), 126.9 (C-h), 124.9 (C-f), 123.3 (C-b), 25.9 (C-j) ppm.

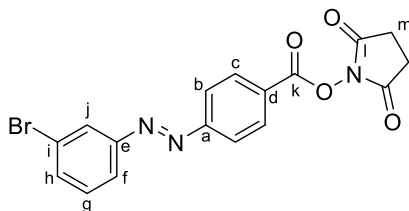
**IR** (ATR):  $\tilde{\nu}$  = 2987 (w), 2359 (w), 1790 (w), 1770 (m), 1722 (s), 1601 (m), 1571 (m), 1478 (m), 1426 (m), 1368 (m), 1260 (m), 1231 (m), 1206 (s), 1144 (m), 1074 (s), 1016 (m), 995 (s), 859 (m), 838 (m), 819 (m), 759 (m), 706 (m) cm<sup>-1</sup>.

**HRMS** (EI, 70 eV) *m/z* (%): [M]<sup>+</sup> calcd for [C<sub>17</sub>H<sub>12</sub>BrN<sub>3</sub>O<sub>4</sub>]<sup>+</sup> 401.00057; found 401.00131 (7), 76.1 (100).

**Mp**: 285 °C.

**R<sub>f</sub>**: 0.65 (*n*-hexane/DCM 1:1).

2,5-Dioxopyrrolidin-1-yl (*E*)-4-((3-bromophenyl)diazenyl)benzoate (**3m**)



Compound **3m** was synthesized according to general procedure 2a from (*E*)-1-(3-bromophenyl)-2-(4-iodophenyl)diazene (**1m**) (77.4 mg, 200 μmol, 2.00 equiv). The product was obtained after crystallization from *n*-hexane/DCM (3:1) at -21 °C as an orange solid (76.9 mg, 198 μmol, 99%).

**<sup>1</sup>H NMR** (600 MHz, CDCl<sub>3</sub>) δ = 8.31 (d, <sup>3</sup>J = 8.5 Hz, 2H, H-c), 8.11 (at, <sup>4</sup>J = 1.9 Hz, 1H, H-j), 8.02 (d, <sup>3</sup>J = 8.5 Hz, 2H, H-b), 7.94 (ddt, <sup>3</sup>J = 7.9 Hz, <sup>4</sup>J = 1.9 Hz, <sup>4</sup>J = 0.9 Hz, 1H, H-f/h), 7.66 (ddt, <sup>3</sup>J = 7.9 Hz, <sup>4</sup>J = 1.9 Hz, <sup>4</sup>J = 0.9 Hz, 1H, H-f/h), 7.44 (t, <sup>3</sup>J = 7.9 Hz, 1H, H-g), 2.94 (s, br, 4H, H-m) ppm.

**<sup>13</sup>C{<sup>1</sup>H} NMR** (151 MHz, CDCl<sub>3</sub>) δ = 169.2 (C-l), 161.5 (C-k), 155.9 (C-a), 153.4 (C-e), 134.8 (C-h), 131.9 (C-c), 130.8 (C-g), 127.2 (C-d), 125.1 (C-j), 123.7 (C-f), 123.4 (C-i), 123.4 (C-b), 25.9 (C-m) ppm.

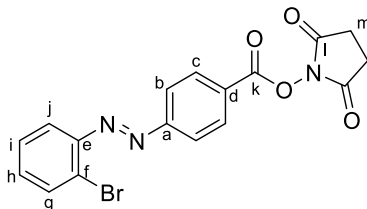
**IR** (ATR):  $\tilde{\nu}$  = 2937 (w), 1769 (m), 1729 (s), 1598 (m), 1568 (m), 1455 (w), 1435 (m), 1409 (m), 1353 (m), 1257 (m), 1237 (m), 1196 (s), 1143 (m), 1071 (s), 1017 (m), 994 (s), 892 (m), 862 (s), 853 (s), 808 (m), 796 (s), 760 (m), 742 (m) cm<sup>-1</sup>.

**HRMS** (EI, 70 eV) *m/z* (%): [M]<sup>+</sup> calcd for [C<sub>17</sub>H<sub>12</sub>BrN<sub>3</sub>O<sub>4</sub>]<sup>+</sup> 401.00057; found 401.00120 (7), 76.1 (100).

**Mp**: 192 °C.

**R<sub>f</sub>**: 0.65 (*n*-hexane/DCM 1:1).

2,5-Dioxopyrrolidin-1-yl (*E*)-4-((2-bromophenyl)diazenyl)benzoate (**3n**)



Compound **3n** was synthesized according to general procedure 2a from (*E*)-1-(2-bromophenyl)-2-(4-iodophenyl)diazene (**1n**) (77.4 mg, 200 μmol, 2.00 equiv). The product was obtained after crystallization from *n*-hexane/DCM (3:1) at -21 °C as a red solid (71.6 mg, 178 μmol, 89%).

**<sup>1</sup>H NMR** (600 MHz, CDCl<sub>3</sub>) δ = 8.31 (d, <sup>3</sup>J = 8.5 Hz, 2H, H-c), 8.07 (d, <sup>3</sup>J = 8.5 Hz, 2H, H-b), 7.80 (dd, <sup>3</sup>J = 7.9 Hz, <sup>4</sup>J = 1.7 Hz, 1H, H-g), 7.73 (dd, <sup>3</sup>J = 7.9 Hz, <sup>4</sup>J = 1.7 Hz, 1H, H-j), 7.42 (td, <sup>3</sup>J = 7.9 Hz, <sup>4</sup>J = 1.7 Hz, 1H, H-i), 7.38 (td, <sup>3</sup>J = 7.9 Hz, <sup>4</sup>J = 1.7 Hz, 1H, H-h), 2.94 (s, br, 4H, H-m) ppm.

$^{13}\text{C}\{^1\text{H}\}$  NMR (151 MHz,  $\text{CDCl}_3$ )  $\delta$  = 169.2 (C-l), 161.5 (C-k), 156.1 (C-a), 149.6 (C-e), 134.2 (C-g), 133.2 (C-h), 131.9 (C-c), 128.2 (C-i), 127.2 (C-d), 127.1 (C-f), 123.7 (C-b), 117.8 (C-j), 25.9 (C-m) ppm.

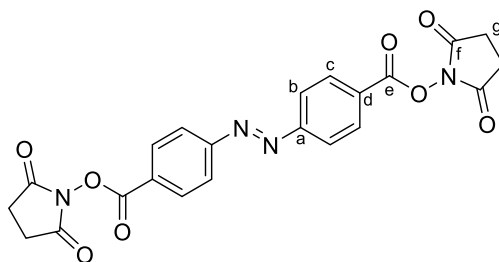
IR (ATR):  $\tilde{\nu}$  = 2957 (w), 2359 (w), 1769 (m), 1731 (s), 1600 (m), 1458 (w), 1422 (m), 1407 (m), 1359 (m), 1255 (m), 1235 (m), 1199 (s), 1066 (s), 1045 (m), 997 (s), 859 (m), 849 (m), 807 (m), 780 (m), 761 (m), 716 (m)  $\text{cm}^{-1}$ .

HRMS (EI, 70 eV)  $m/z$  (%):  $[\text{M}]^+$  calcd for  $[\text{C}_{17}\text{H}_{12}\text{BrN}_3\text{O}_4]^+$  401.00057; found 401.00125 (9), 76.1 (100).

Mp: 173 °C.

R<sub>f</sub>: 0.65 (*n*-hexane/DCM 1:1).

Bis(2,5-dioxopyrrolidin-1-yl)4,4'-(diazene-1,2-diyl)(*E*)-dibenzoate[5](5a)



Compound **5a** was synthesized according to general procedure 2b from (*E*)-1,2-bis(4-iodophenyl)diazene (**4a**) (43.4 mg, 200  $\mu\text{mol}$ ). The product was obtained after crystallization from *n*-hexane/DCM (3:1) as a red solid (42.0 mg, 194  $\mu\text{mol}$ , 97%, Lit.:<sup>[4]</sup> 94%<sup>4</sup>).

$^1\text{H}$  NMR (600 MHz,  $\text{CDCl}_3$ )  $\delta$  = 8.33 (d,  $^3J$  = 8.5 Hz, 2H, *H*-c), 8.08 (d,  $^3J$  = 8.1 Hz, 2H, *H*-b), 2.94 (s, br, 4H, *H*-g) ppm.

$^{13}\text{C}\{^1\text{H}\}$  NMR (151 MHz,  $\text{CDCl}_3$ )  $\delta$  = 169.2 (C-f), 161.4 (C-e), 155.9 (C-a), 132.0 (C-c), 127.7 (C-d), 123.6 (C-b), 25.9 (C-g) ppm.

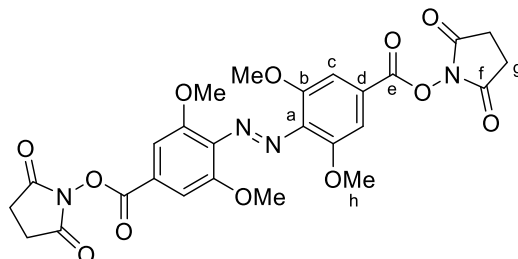
IR (ATR):  $\tilde{\nu}$  = 2923 (w), 1770 (m), 1732 (s), 1600 (m), 1426 (w), 1414 (m), 1365 (m), 1310 (m), 1256 (m), 1236 (m), 1201 (s), 1066 (s), 1046 (m), 1015 (m), 987 (s), 977 (s), 873 (s), 843 (m), 809 (m), 767 (m), 727 (m)  $\text{cm}^{-1}$ .

HRMS (EI, 70 eV)  $m/z$  (%):  $[\text{M}]^+$  calcd for  $[\text{C}_{22}\text{H}_{16}\text{N}_4\text{O}_8]^+$  464.09626; found 464.09599 (9), 349.9 (100).

Mp: 276 °C Lit.:<sup>[4]</sup> >250 °C).

R<sub>f</sub> = 0.65 (*n*-hexane/DCM 1:1).

Bis(2,5-dioxopyrrolidin-1-yl) 4,4'-(diazene-1,2-diyl)(*E*)-bis(3,5-dimethoxybenzoate) (**5b**)



Compound **5b** was synthesized according to general procedure 1b from (*E*)-1,2-bis(4-iodo-2,6-dimethoxyphenyl)diazene<sup>5</sup> (**4b**) (54.4 mg, 100  $\mu\text{mol}$ , 1.00 equiv). The compound was purified by column chromatography on silica (eluent: gradient *n*-hexane/ethyl acetate 1:0  $\rightarrow$  0:1) yielding **5b** as a red powder (47.1 mg, 90.5  $\mu\text{mol}$ , 91%).

<sup>4</sup> In this report, the product was prepared by coupling of the corresponding carboxylic acid with NHS using EDC and DMAP.

<sup>5</sup> 90% purity

$^1\text{H NMR}$  (600 MHz,  $\text{DMSO-}d_6$ )  $\delta$  = 7.45 (s, 4H, *H-c*), 3.93 (s, 12H, *H-h*), 2.94 (s, 4H, *H-g*) ppm.

$^{13}\text{C}\{^1\text{H}\}$  NMR (151 MHz,  $\text{DMSO-}d_6$ )  $\delta$  = 169.2 (*C-f*), 161.5 (*C-e*), 151.9 (*C-a*), 138.3 (*C-b*), 125.7 (*C-d*), 107.4 (*C-c*), 57.0 (*C-h*), 25.9 (*C-g*) ppm.

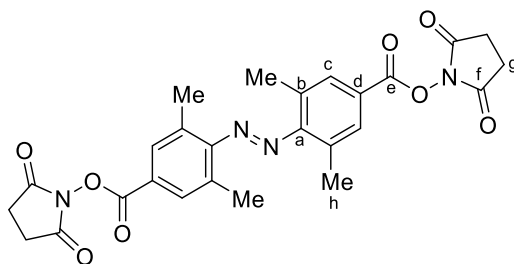
IR (ATR):  $\tilde{\nu}$  = 2956 (w), 1732 (s), 1574 (m), 1455 (m), 1408 (m), 1360 (m), 1325 (m), 1231 (m), 1195 (m), 1120 (s), 1071 (s), 1016 (m), 993 (w), 894 (m), 853 (m), 833 (w), 808 (w), 771 (w), 741 (w)  $\text{cm}^{-1}$ .

HRMS (EI, 70 eV)  $m/z$  (%):  $[\text{M}]^+$  calcd for  $[\text{C}_{26}\text{H}_{24}\text{N}_4\text{O}_{12}]^+$  584.13852; found 584.13941 (13), 149.1 (100).

**Mp:** 212 °C.

**R<sub>f</sub>:** 0.50 (ethyl acetate).

Bis(2,5-dioxopyrrolidin-1-yl) 4,4'-(diazene-1,2-diyl)(*E*)-bis(3,5-dimethylbenzoate) (**5c**)



Compound **5c** was synthesized according to general procedure 1b from (*E*)-1,2-bis(4-iodo-2,6-dimethylphenyl)diazene (**4c**) (49.0 mg, 100  $\mu\text{mol}$ , 1.00 equiv). The compound was purified by column chromatography on silica (eluent: gradient *n*-hexane/ethyl acetate 1:0  $\rightarrow$  0:1) yielding **5c** as a red powder (47.1 mg, 90.5  $\mu\text{mol}$ , 91%).

$^1\text{H NMR}$  (600 MHz,  $\text{CDCl}_3$ )  $\delta$  = 7.98 (s, 4 H, *H-c*), 2.95 (s, 8 H, *H-g*), 2.46 (s, 12 H, *H-h*) ppm.

$^{13}\text{C}\{^1\text{H}\}$  NMR (151 MHz,  $\text{CDCl}_3$ )  $\delta$  = 169.3 (*C-f*), 161.6 (*C-e*), 155.7 (*C-a*), 131.8 (*C-c*), 131.7 (*C-b*), 124.8 (*C-d*), 25.7 (*C-g*), 19.4 (*C-h*) ppm.

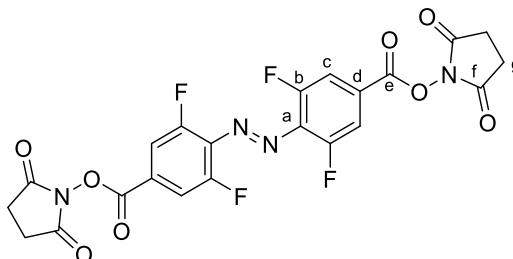
IR (ATR):  $\tilde{\nu}$  = 3429 (m), 3351 (m), 3078 (w), 2926 (w), 2863 (w), 1614 (s), 1567 (m), 1481 (s), 1404 (s), 1309 (s), 1290 (s), 1270 (s), 1191 (m), 1163 (m), 1121 (m), 1069 (m), 933 (m), 884 (m), 862 (m), 812 (s), 780 (m), 748 (m), 733 (m)  $\text{cm}^{-1}$ .

HRMS (APCI):  $m/z$  =  $[\text{M}+\text{H}]^+$  calcd for  $[\text{C}_{26}\text{H}_{24}\text{N}_4\text{O}_8 + \text{H}]^+$  521.166669; found 521.16629.

**Mp:** 175 °C.

**R<sub>f</sub>:** 0.30 (DCM/ethyl acetate 1:1).

Bis(2,5-dioxopyrrolidin-1-yl) 4,4'-(diazene-1,2-diyl)(*E*)-bis(3,5-difluorobenzoate) (**5d**)



(*E*)-1,2-Bis(2,6-difluoro-4-iodophenyl)diazene (**4d**) (171 mg, 0.500 mmol, 1.00 equiv), *N*-hydroxy-succinimide (**7**) (253 mg, 2.20 mmol, 4.40 equiv) and 4-dimethylaminopyridine (DMAP) (12.5 mg, 100  $\mu\text{mol}$ , 0.20 equiv) were dissolved in DMF (10 mL) at 21 °C. After 10 min of stirring, 1-ethyl-3-(3-dimethylaminopropyl)carbodiimide (EDCI) (310 mg, 11.1 mmol, 3.00 equiv) was added and the solution was stirred at 21 °C for 16 h under a nitrogen atmosphere. The mixture was diluted with DCM (100 mL) and washed with hydrochloric acid (0.1 M, 100 mL). The aqueous phase was extracted DCM (2  $\times$  50 mL). The combined organic phases were dried over sodium sulphate and purified by column

chromatography on silica (eluent: gradient *n*-hexane/ethyl acetate 0:1 → 1:1). **5d** was obtained as an orange solid after crystallisation from THF/*n*-hexane (110 mg, 205 μmol, 41%).

<sup>1</sup>H NMR (600 MHz, DMSO-*d*<sub>6</sub>) δ = 8.11 (d, <sup>3</sup>J = 8.6 Hz, 4H, *H*-c), 2.93 (s, 8H, *H*-g) ppm.

<sup>13</sup>C{<sup>1</sup>H} NMR (151 MHz, DMSO-*d*<sub>6</sub>) δ = 172.25 (C-e), 170.4 (C-f), 155.00 (d, <sup>1</sup>J = 264.3 Hz, C-b), 134.9 (C-a), 128.6 (C-d), 115.9 (d, <sup>2</sup>J = 24 Hz, C-c), 25.59 (C-g) ppm.

<sup>19</sup>F NMR (565 MHz, DMSO-*d*<sub>6</sub>) δ = -118.20 (s, *F*-b)

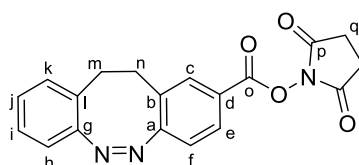
IR (ATR):  $\tilde{\nu}$  = 3092 (w), 1804 (w), 1774 (w), 1731 (s), 1580 (m), 1431 (m), 1327 (m), 1200 (s), 1165 (s), 1072 (s), 1038 (s), 904 (m), 826 (w), 764 (w), 741 (s) cm<sup>-1</sup>.

HRMS (EI, 70 eV) *m/z* (%): [M]<sup>+</sup> calcd for [C<sub>22</sub>H<sub>12</sub>F<sub>4</sub>N<sub>4</sub>O<sub>8</sub>]<sup>+</sup> 536.05858; found 536.05884 (16), 140.1 (100).

Mp: 296 °C.

R<sub>f</sub>: 0.60 (ethyl acetate).

2,5-Dioxopyrrolidin-1-yl (*Z*)-11,12-dihydrodibenzo[*c,g*][1,2]diazocine-2-carboxylate (**8a**)



Compound **8a** was synthesized according to general procedure 2a from (*Z*)-2-iodo-11,12-dihydrodibenzo[*c,g*][1,2]diazocine (**7a**) (43.4 mg, 200 μmol) in dry DMSO. The product was obtained after crystallization from *n*-hexane/DCM (3:1) as a yellow solid (69.9 mg, 198 μmol, 99%).

<sup>1</sup>H NMR (600 MHz, CDCl<sub>3</sub>) δ = 7.89 (dd, <sup>3</sup>J = 8.2 Hz, <sup>4</sup>J = 1.8 Hz, 1H, *H*-e), 7.78 (d, <sup>4</sup>J = 1.8 Hz, 1H, *H*-c), 7.17 (t, <sup>3</sup>J = 7.5 Hz, 1H, *H*-i), 7.06 (t, <sup>3</sup>J = 7.5 Hz, 1H, *H*-j), 6.99 (d, <sup>3</sup>J = 7.5 Hz, 1H, *H*-k), 6.93 (d, <sup>3</sup>J = 8.2 Hz, 1H, *H*-f), 6.85 (d, <sup>3</sup>J = 7.5 Hz, 1H, *H*-h), 3.07 – 2.77 (m, 8H, *H*-m/n/q) ppm.

<sup>13</sup>C{<sup>1</sup>H} NMR (151 MHz, CDCl<sub>3</sub>) δ = 169.3 (C-p), 161.2 (C-o), 160.8 (C-a), 155.5 (C-g), 132.4 (C-c), 130.2 (C-k), 129.7 (C-b), 129.5 (C-e), 128.0 (C-j), 127.3 (C-l), 127.2 (C-i), 123.6 (C-d), 119.3 (C-f), 118.7 (C-h), 31.6 (C-n), 31.5 (C-m), 25.8 (C-q) ppm.

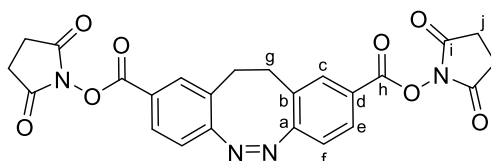
IR (ATR):  $\tilde{\nu}$  = 2921 (w), 2851 (w), 2359 (w), 1769 (m), 1733 (s), 1601 (w), 1417 (m), 1358 (m), 1282 (m), 1236 (m), 1196 (s), 1064 (s), 1036 (m), 914 (m), 874 (m), 765 (m), 742 (s) cm<sup>-1</sup>.

HRMS (EI, 70 eV) *m/z* (%): [M]<sup>+</sup> calcd for [C<sub>19</sub>H<sub>15</sub>N<sub>3</sub>O<sub>4</sub>]<sup>+</sup> 349.10571; found 349.10536 (7), 178.1 (100).

Mp: 207 °C.

R<sub>f</sub>: 0.46 (*n*-hexane/DCM 1:1).

Bis(2,5-dioxopyrrolidin-1-yl) (Z)-11,12-dihydrodibenzo[c,g][1,2]diazocine-2,9-dicarboxylate (**8b**)



Compound **8b** was synthesized according to general procedure 2b from (Z)-2,9-diiodo-11,12-dihydrodibenzo[c,g][1,2]diazocine (**7b**) (43.4 mg, 200  $\mu$ mol) in dry DMSO. The product was obtained after crystallization from *n*-hexane/DCM (3:1) as a yellow solid (47.8 mg, 196  $\mu$ mol, 98%).

$^1\text{H NMR}$  (600 MHz,  $\text{CDCl}_3$ )  $\delta$  = 7.95 (d,  $^3J$  = 8.2 Hz, 2H, *H-e*), 7.82 (s, 2H, *H-c*), 7.00 (d,  $^3J$  = 8.2 Hz, 2H, *H-f*), 3.12 – 2.91 (m, 4H, *H-g*), 2.88 (s, br, 8H, *H-j*) ppm.

$^{13}\text{C}\{^1\text{H}\}$  NMR (151 MHz,  $\text{CDCl}_3$ )  $\delta$  = 169.1 (*C-i*), 161.0 (*C-h*), 160.1 (*C-a*), 132.8 (*C-c*), 129.9 (*C-e*), 128.5 (*C-b*), 124.5 (*C-d*), 119.4 (*C-f*), 31.4 (*C-g*), 25.8 (*C-j*) ppm.

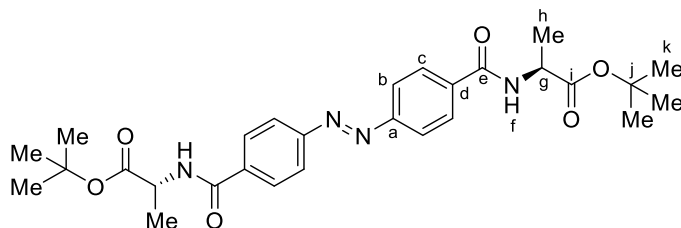
IR (ATR):  $\tilde{\nu}$  = 2990 (w), 2359 (w), 1769 (m), 1732 (s), 1602 (m), 1482 (w), 1425 (m), 1366 (m), 1202 (s), 1069 (s), 1029 (m), 986 (m), 911 (m), 813 (m), 740 (s)  $\text{cm}^{-1}$ .

HRMS (ESI)  $m/z$ :  $[\text{M} + \text{Na}]^+$  calcd for  $[\text{C}_{24}\text{H}_{18}\text{N}_4\text{O}_8 + \text{Na}]^+$  513.10168; found 513.10105.

Mp: 187 °C.

$R_f$ : 0.61 (ethyl acetate).

Di-*tert*-butyl 2,2'-((4,4'-(diazene-1,2-diyl)bis(benzoyl))bis(azanediy))(*E*)-dipropionate (**10a**)



Triethyl amine (153  $\mu$ L, 1.10 mmol, 2.20 equiv) was added to a solution of L-alanine *tert*-butyl ester hydrochloride (**9**) (200 mg, 1.10 mmol, 2.20 equiv) in dry DMF (10 mL). A solution of bis(2,5-dioxopyrrolidin-1-yl) 4,4'-(diazene-1,2-diyl)(*E*)-dibenzoate (**5a**) (232 mg, 500  $\mu$ mol, 1.00 equiv) in dry DMF (7 mL) was added and the resulting mixture was stirred at 21 °C for 16 h. Water (100 mL) and ethyl acetate (15 mL) were added and the mixture was washed with brine (3  $\times$  50 mL). The combined organic phases were dried over  $\text{MgSO}_4$ , filtered and the solvent removed under reduced pressure yielding the product as an orange-red solid (257 mg, 490  $\mu$ mol, 98%).

$^1\text{H NMR}$  (600 MHz,  $\text{CDCl}_3$ )  $\delta$  = 8.01 – 7.95 (m, 8H, *H-b/c*), 6.89 (d,  $^3J$  = 7.1 Hz, 2H, *H-f*), 4.70 (p,  $^3J$  = 7.1 Hz, 2H, *H-g*), 1.52 (d,  $^3J$  = 7.1 Hz, 6H, *H-h*), 1.51 (s, 18H, *H-k*) ppm.

$^{13}\text{C}\{^1\text{H}\}$  NMR (151 MHz,  $\text{CDCl}_3$ )  $\delta$  = 172.6 (*C-i*), 166.0 (*C-e*), 154.3 (*C-a*), 136.5 (*C-d*), 128.2 (*C-c*), 123.3 (*C-b*), 82.6 (*C-j*), 49.4 (*C-g*), 28.2 (*C-k*), 19.0 (*C-h*) ppm.

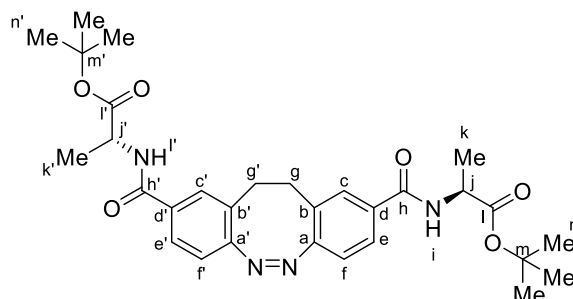
IR (ATR):  $\tilde{\nu}$  = 3320 (br), 2979 (w), 2359 (w), 1731 (m), 1634 (s), 1529 (s), 1490 (m), 1454 (m), 1368 (m), 1343 (m), 1306 (m), 1271 (m), 1335 (m), 1153 (s), 1046 (m), 1012 (m), 942 (w), 893 (w), 861 (s), 848 (m), 779 (m), 737 (m), 708 (m)  $\text{cm}^{-1}$ .

HRMS (ESI)  $m/z$ :  $[\text{M} + \text{Na}]^+$  calcd for  $[\text{C}_{28}\text{H}_{36}\text{N}_4\text{O}_6 + \text{Na}]^+$  547.25271; found 547.25271.

Mp: 187 °C.

$R_f$  = 0.70 (*n*-hexane/DCM 1:1).

Di-*tert*-butyl 2,2'-((11,12-dihydrodibenzo[*c,g*][1,2]diazocine-2,9-dicarbonyl)bis(azane-diyl))(*Z*)-dipropionate (**10b**)



Triethyl amine (22.9  $\mu\text{L}$ , 164  $\mu\text{mol}$ , 2.20 equiv) was added to a solution of L-alanine *tert*-butyl ester hydrochloride (**9**) (29.8 mg, 164  $\mu\text{mol}$ , 2.20 equiv) in dry DMF (2 mL). A solution of bis(2,5-dioxopyrrolidin-1-yl) 4,4'-(diazene-1,2-diyl)(*E*)-dibenzoate (**8b**) (36.5 mg, 74.4  $\mu\text{mol}$ , 1.00 equiv) in dry DMF (1 mL) was added and the resulting mixture was stirred at 21  $^{\circ}\text{C}$  for 16 h. Water (30 mL) and ethyl acetate (15 mL) were added and the mixture was washed with brine (3  $\times$  50 mL). The combined organic phases were dried over  $\text{MgSO}_4$ , filtered and the solvent removed under reduced pressure yielding the product as a yellow solid (33.2 mg, 60.2  $\mu\text{mol}$ , 81%).

**$^1\text{H}$  NMR** (600 MHz,  $\text{CDCl}_3$ )  $\delta$  = 7.55 (dd,  $^3J$  = 8.2 Hz,  $^4J$  = 1.8 Hz, 1H, *H-e*), 7.48 (dd,  $^3J$  = 8.2 Hz,  $^4J$  = 1.8 Hz, 1H, *H-e'*), 7.44 (ad,  $^4J$  = 1.8 Hz, 1H, *H-c*), 7.38 (ad,  $^4J$  = 1.8 Hz, 1H, *H-c'*), 6.87 (d,  $^3J$  = 8.2 Hz, 1H, *H-f*), 6.84 (d,  $^3J$  = 8.2 Hz, 1H, *H-f'*), 4.57 (dp,  $^3J$  = 19.0 Hz, 7.1 Hz, 2H, *H-j/j'*), 3.04 – 2.73 (m, 4H, *H-g/g'*), 1.48 (s, 9H, *H-n*), 1.47 (s, 9H, *H-n'*) 1.43 (d,  $^3J$  = 7.1 Hz, 3H, *H-k*), 1.38 (d,  $^3J$  = 7.1 Hz, 3H, *H-k'*) ppm.

3.04 – 2.73 (m, 4H, *H-g/g'*), 3.63 (s, br, 4H, *H-h*), 2.69 (s, 4H, *H-g*) ppm.

**$^{13}\text{C}\{^1\text{H}\}$  NMR** (151 MHz,  $\text{CDCl}_3$ )  $\delta$  = 172.8 (*C-l*), 172.6 (*C-l'*), 165.8 (*C-h*), 165.8 (*C-h'*), 157.8 (*C-a*), 157.8 (*C-a'*), 133.3 (*C-b*), 133.0 (*C-b'*), 129.2 (*C-c*), 129.2 (*C-c'*), 128.4 (*C-d*), 128.4 (*C-d'*), 126.1 (*C-e*), 125.8 (*C-e'*), 119.0 (*C-f*), 118.9 (*C-f'*), 82.5 (*C-m*), 82.4 (*C-m'*), 49.2 (*C-j*), 49.2 (*C-j'*), 31.6 (*C-g*), 31.4 (*C-g'*), 28.1 (*C-n*), 28.0 (*C-n'*), 18.8 (*C-k*), 18.7 (*C-k'*) ppm.

**IR** (ATR):  $\tilde{\nu}$  = 3306 (br), 2978 (w), 2359 (w), 1722 (m), 1641 (s), 1530 (s), 1480 (m), 1451 (m), 1368 (m), 1347 (m), 1227 (m), 1147 (s), 908 (m), 847 (m), 728 (m)  $\text{cm}^{-1}$ .

**HRMS** (ESI)  $m/z$ :  $[\text{M} + \text{Na}]^+$  calcd for  $[\text{C}_{30}\text{H}_{38}\text{N}_4\text{O}_6 + \text{Na}]^+$  573.26836; found 573.26779.

**Mp**: 115  $^{\circ}\text{C}$ .

**R<sub>f</sub>** = 0.49 (*n*-hexane/DCM 1:1).

Determination of the  $^1\text{H}$  NMR Yields

Reaction controls by  $^1\text{H}$  NMR spectroscopy were performed using 1,3,5-trimethoxybenzene as internal standard. The molar amount of the corresponding product was calculated according to equation (1).

$$n_{\text{P}} = n_{\text{IS}} \times r_{\text{P/IS}} = n_{\text{IS}} \times \frac{\text{integral}_{\text{P}}/N_{\text{P}}}{\text{integral}_{\text{IS}}/N_{\text{IS}}} \quad (1)$$

In each reaction, 100  $\mu\text{mol}$  of the standard was used and the integral of the three aromatic protons of the internal standard at 6.09 ppm was assigned to a value of one.

If DMSO was used as a solvent, no internal standard was used as DMSO could not be removed without an aqueous workup. If an internal standard was used, this would lead to a larger error in the procedure.

**Table S3.** Determination of the  $^1\text{H}$  NMR Yield.

Product	Peak <sub>P</sub> [ppm]	Integral <sub>P</sub> /N <sub>P</sub>	n <sub>P</sub> [ $\mu\text{mol}$ ]	Yield [%]
2,5-Dioxopyrrolidin-1-yl ( <i>E</i> )-4-(phenyldiazenyl)benzoate ( <b>3a</b> )	8.29	1.33/2	200	>95
2,5-Dioxopyrrolidin-1-yl ( <i>E</i> )-3-(phenyldiazenyl)benzoate ( <b>3b</b> )	8.23	1.31/2	197	>95
2,5-Dioxopyrrolidin-1-yl ( <i>E</i> )-2-(phenyldiazenyl)benzoate ( <b>3c</b> )	No conversion visible			
2,5-Dioxopyrrolidin-1-yl ( <i>E</i> )-4-((4-hydroxyphenyl)diazenyl)benzoate ( <b>3d</b> )	6.99	1.26/2	189	95
2,5-Dioxopyrrolidin-1-yl ( <i>E</i> )-4-((4-aminophenyl)diazenyl)benzoate ( <b>3e</b> )	6.71	1.26/2	189	95
2,5-Dioxopyrrolidin-1-yl ( <i>E</i> )-4-((4-acetamidophenyl)diazenyl)benzoate ( <b>3f</b> )	8.31	1.27/2	191	>95
2,5-Dioxopyrrolidin-1-yl ( <i>E</i> )-4-((4-allyloxy)phenyl)diazenyl)benzoate ( <b>3h</b> )	8.26	0.91/2	137	69
2,5-Dioxopyrrolidin-1-yl ( <i>E</i> )-4-((4-(9-hydroxynonyl)oxy)phenyl)diazenyl)benzoate ( <b>3i</b> )	8.27	1.20/2	180	90
2,5-Dioxopyrrolidin-1-yl ( <i>E</i> )-4-((2,6-dimethyl-4-(nonyloxy)phenyl)diazenyl)-3,5-dimethylbenzoate ( <b>3j</b> )	7.90	0.63/4	95	95
2,5-Dioxopyrrolidin-1-yl ( <i>E</i> )-4-((2,7-bis(4-(hexyloxy)phenoxy)naphthalen-1-yl)diazenyl)-3,5-dimethylbenzoate ( <b>3k</b> )	7.80	1.26/4	189	95
2,5-Dioxopyrrolidin-1-yl ( <i>E</i> )-4-((4-bromophenyl)diazenyl)benzoate ( <b>3l</b> )	8.30	1.32/2	198	>95
2,5-Dioxopyrrolidin-1-yl ( <i>E</i> )-4-((3-bromophenyl)diazenyl)benzoate ( <b>3m</b> )	8.31	1.32/2	198	>95
2,5-Dioxopyrrolidin-1-yl ( <i>E</i> )-4-((2-bromophenyl)diazenyl)benzoate ( <b>3n</b> )	8.31	1.20/2	180	90
Bis(2,5-dioxopyrrolidin-1-yl) 4,4'-(diazene-1,2-diyl)( <i>E</i> )-dibenzoate ( <b>5a</b> )	8.07	1.30/4	97.5	>95
Bis(2,5-dioxopyrrolidin-1-yl) 4,4'-(diazene-1,2-diyl)( <i>E</i> )-bis(3,5-dimethylbenzoate) ( <b>5b</b> )	8.00	1.35/4	101	>95

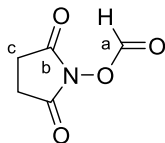
The influence of the ligand was investigated using bis(2,5-dioxopyrrolidin-1-yl) 4,4'-(diazene-1,2-diyl)(*E*)-dibenzoate (**5a**) as model reaction.

**Table S4:** Screening of ligands.

Ligand	Peak [ppm]	integral <sub>P</sub> /N <sub>P</sub>	n <sub>P</sub> [μmol]	Yield [%]
1,1'-Bis(diphenylphosphino)ferrocene	8.07	0.06/4	4.50	5
2,2'-Bis(diphenylphosphino)-1,1'-binaphthyl	8.07	0.02/4	1.50	2
Di-(1-adamantyl)- <i>n</i> -butylphosphine	8.07	0.10/4	7.5	8
Tri- <i>tert</i> -butylphosphine	8.07	0.03/4	2.25	2
Xantphos	8.07	1.30/4	97.5	>95



*N*-Hydroxysuccinimidyl formate<sup>[5]</sup> (**2**)



This reaction was not performed under inert conditions.

Acetic anhydride (77.0 mL, 800  $\mu$ mol, 8.00 equiv) was cooled to 0 °C. Formic acid (38.0 mL, 1.00 mol, 10.0 equiv) was added over the course of 10 min and the solution was stirred at 23 °C for 2 h. 1-Hydroxypyrrolidine-2,5-dione (11.7 g, 100  $\mu$ mol, 1.00 equiv) was added and the reaction mixture was stirred for further 14 h. Afterwards, the solvent was removed *in vacuo* and the resulting solid dried under reduced pressure at  $8 \times 10^{-3}$  mbar several hours to afford **2**<sup>6</sup> as a colorless solid (14.4 g, 1.00 mol, 100%, Lit.:<sup>[5]</sup> 99%).

<sup>1</sup>H NMR (600 MHz, CDCl<sub>3</sub>)  $\delta$  = 8.18 (s, 1H, *H*-a), 2.86 (s, 4H, *H*-c) ppm.

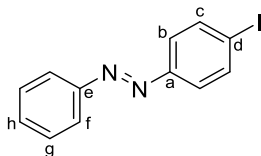
<sup>13</sup>C{<sup>1</sup>H} NMR (151 MHz, CDCl<sub>3</sub>)  $\delta$  = 168.6 (*C*-a), 155.1 (*C*-b), 25.7 (*C*-c) ppm.

HRMS (ESI) *m/z*: [M + Na]<sup>+</sup> calcd for [C<sub>5</sub>H<sub>5</sub>NO<sub>4</sub> + Na]<sup>+</sup> 166.01108; found 166.01100.

IR (ATR):  $\tilde{\nu}$  = 3002 (m), 2956 (w), 1698 (s), 1209 (m), 646 (m) cm<sup>-1</sup>.

Mp: 177 °C.

(*E*)-1-(4-Iodophenyl)-2-phenyldiazene<sup>[6]</sup> (**1a**)



This reaction was not performed under inert conditions.

A solution of 4-iodoaniline (1.10 g, 5.00 mmol, 1.00 equiv) and nitrosobenzene (696 mg, 6.50 mmol, 1.30 equiv) in acetic acid (25 mL) was stirred for 16 h at 25 °C. The solvent was evaporated yielding **1a** as an orange solid (1.54 g, 5.00 mmol, >99%, Lit.:<sup>[6]</sup> 91%).

<sup>1</sup>H NMR (600 MHz, CDCl<sub>3</sub>)  $\delta$  = 7.92 (d, <sup>3</sup>*J* = 7.1 Hz, 2H, *H*-f), 7.87 (d, <sup>3</sup>*J* = 8.4 Hz, 2H, *H*-c), 7.66 (d, <sup>3</sup>*J* = 8.4 Hz, 2H, *H*-b), 7.54 – 7.48 (m, 3H, *H*-g/h) ppm.

<sup>13</sup>C{<sup>1</sup>H} NMR (151 MHz, CDCl<sub>3</sub>)  $\delta$  = 152.6 (*C*-e), 152.1 (*C*-a), 138.5 (*C*-c), 131.5 (*C*-h), 129.3 (*C*-g), 124.6 (*C*-b), 123.1 (*C*-f), 97.8 (*C*-d) ppm.

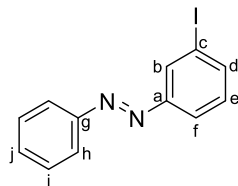
IR (ATR):  $\tilde{\nu}$  = 3038 (br), 2357 (w), 2107 (w), 1809 (br), 1668 (w), 1563 (m), 1473 (s), 1438 (m), 1391 (m), 1293 (m), 1100 (m), 1049 (m), 998 (s), 915 (m), 838 (s), 768 (s), 701 (m) cm<sup>-1</sup>.

HRMS (EI, 70 eV) *m/z* (%): [M]<sup>+</sup> calcd for [C<sub>12</sub>H<sub>9</sub>N<sub>2</sub>I]<sup>+</sup> 307.98050; found 307.98043 (56), 77.0 (100).

Mp: 105 °C (Lit.:<sup>[6]</sup> 105 °C).

R<sub>f</sub> = 0.75 (*n*-hexane/DCM 3:1).

<sup>6</sup> The product was stored under dry conditions and a nitrogen atmosphere.

*(E)*-1-(3-Iodophenyl)-2-phenyldiazene[6] (**1b**)

This reaction was not performed under inert conditions.

A solution of 3-iodoaniline (5.48 g, 25.0 mmol, 1.00 equiv) and nitrosobenzene (3.48 g, 32.5 mmol, 1.30 equiv) in acetic acid (150 mL) was stirred for 16 h at 25 °C. The solvent was evaporated yielding **1b** as an orange solid (7.47 g, 24.2 mmol, 97%, Lit.:<sup>[6]</sup> 96%).

<sup>1</sup>H NMR (600 MHz, CDCl<sub>3</sub>) δ = 8.25 (at, <sup>4</sup>J = 1.8 Hz, 1H, *H*-b), 7.94 – 7.90 (m, 3H, *H*-f/h), 7.80 (ddd, <sup>3</sup>J = 7.9 Hz, <sup>4</sup>J = 1.4 Hz, 1.0 Hz, 1H, *H*-d), 7.55 – 7.48 (m, 3H, *H*-i/j), 7.27 (t, <sup>3</sup>J = 7.9 Hz, 1H, *H*-e) ppm.

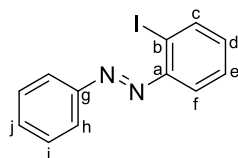
<sup>13</sup>C{<sup>1</sup>H} NMR (151 MHz, CDCl<sub>3</sub>) δ = 153.5 (C-a), 152.5 (C-g), 140.0 (C-d), 131.6 (C-j), 130.8 (C-e), 130.7 (C-b), 129.3 (C-i), 123.7 (C-f), 123.2 (C-h), 94.7 (C-c) ppm.

IR (ATR):  $\tilde{\nu}$  = 3056 (w), 1828 (br), 1560 (w), 1451 (m), 1403 (m), 1302 (w), 1203 (m), 1148 (m), 1086 (w), 1070 (w), 1051 (w), 1018 (m), 992 (w), 914 (m), 880 (m), 833 (w), 792 (s), 761 (s) cm<sup>-1</sup>.

HRMS (EI, 70 eV) *m/z* (%): [M]<sup>+</sup> calcd for [C<sub>12</sub>H<sub>9</sub>N<sub>2</sub>]<sup>+</sup> 307.98050; found 307.98052 (57), 77.0 (100).

**Mp**: 71 °C (Lit.:<sup>[6]</sup> 67 °C).

**R<sub>f</sub>**: 0.75 (*n*-hexane/DCM 3:1).

*(E)*-1-(2-Iodophenyl)-2-phenyldiazene[6] (**1c**)

This reaction was not performed under inert conditions.

A solution of 2-iodoaniline (14.2 g, 65.0 mmol, 1.00 equiv) and nitrosobenzene (9.05 g, 84.5 mmol, 1.30 equiv) in acetic acid (400 mL) was stirred for 16 h at 40 °C. The solvent was removed under reduced pressure and the residue crystallized from methanol at -21 °C yielding **1c** as an orange solid (7.47 g, 24.2 mmol, 28%, Lit.:<sup>[6]</sup> 25%).

<sup>1</sup>H NMR (600 MHz, CDCl<sub>3</sub>) δ = 8.04 (dd, <sup>3</sup>J = 7.9 Hz, <sup>4</sup>J = 1.3 Hz, 1H, *H*-c), 8.01 (d, <sup>3</sup>J = 8.2 Hz, 2H, *H*-h), 7.64 (dd, <sup>3</sup>J = 8.0 Hz, <sup>4</sup>J = 1.6 Hz, 1H, *H*-f), 7.57 – 7.49 (m, 3H, *H*-i/j), 7.43 (ddd, <sup>3</sup>J = 7.9 Hz, 7.2 Hz, <sup>4</sup>J = 1.3 Hz, 1H, *H*-e), 7.17 (ddd, <sup>3</sup>J = 7.9 Hz, 7.2 Hz, <sup>4</sup>J = 1.6 Hz, 1H, *H*-d) ppm.

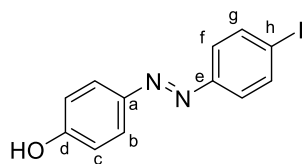
<sup>13</sup>C{<sup>1</sup>H} NMR (151 MHz, CDCl<sub>3</sub>) δ = 152.5 (C-g), 151.5 (C-a), 140.0 (C-c), 132.3 (C-d), 131.7 (C-j), 129.3 (C-i), 129.1 (C-e), 123.7 (C-h), 117.5 (C-f), 102.6 (C-b) ppm.

IR (ATR):  $\tilde{\nu}$  = 3055 (w), 1887 (br), 1572 (w), 1562 (m), 1489 (w), 1446 (m), 1419 (w), 1303 (w), 1249 (w), 1220 (w), 1142 (m), 1015 (s), 999 (w), 948 (w), 920 (w), 771 (s), 708 (s) cm<sup>-1</sup>.

HRMS (EI, 70 eV) *m/z* (%): [M]<sup>+</sup> calcd for [C<sub>12</sub>H<sub>9</sub>N<sub>2</sub>]<sup>+</sup> 307.98050; found 307.98052 (72), 77.0 (100).

**Mp**: 61 °C (Lit.:<sup>[6]</sup> 59 °C).

**R<sub>f</sub>**: 0.70 (*n*-hexane/DCM 3:1).

*(E)*-4-((4-Iodophenyl)diazenyl)phenol[7] (**1d**)

This reaction was not performed under inert conditions.

4-Iodoaniline (2.00 g, 9.13 mmol, 1.20 equiv) was dissolved in a mixture of acetone:water (1:1, 25 mL) and cooled to 0 °C. Subsequently, conc. HCl (1.15 mL, 1.50 equiv) was slowly added to the solution over the course of 10 min and left to stir for another 10 min. Sodium nitrite (735 mg, 10.6 mmol, 1.40 equiv) dissolved in water (6 mL) was added slowly over the course of 3 min and the reaction mixture was stirred for 30 min. Meanwhile, a second mixture with phenol (716 mg, 7.61 mmol, 1.00 equiv), Na<sub>2</sub>CO<sub>3</sub> (1.61 g, 15.2 mmol, 2.00 equiv) and NaOH (1.22 g, 30.4 mmol, 4.00 equiv) dissolved in acetone/water (1:1, 25 mL) was cooled to 0 °C. The first prepared solution was slowly added to the solution containing the phenol over the course of 5 min. The resulting mixture was stirred for 12 h while slowly warmed to 21 °C. Subsequently, the mixture was diluted with a HCl solution (1 M, 30 mL). The precipitate that formed was removed by filtration and washed with water (2 × 10 mL). The precipitate was crystallized from MeOH at -21 °C to give **1d** as a yellow solid (2.39 g, 7.38 mmol, 97%, Lit.: [7]81%).

<sup>1</sup>H NMR (600 MHz, CDCl<sub>3</sub>) δ = 7.87 (d, <sup>3</sup>J = 8.9 Hz, 2H, *H*-g), 7.84 (d, <sup>3</sup>J = 8.7 Hz, 2H, *H*-c), 7.61 (d, <sup>3</sup>J = 8.7 Hz, 2H, *H*-b), 6.94 (d, <sup>3</sup>J = 8.9 Hz, 2H, *H*-f), 5.11 (s, 1H, *OH*-d) ppm.

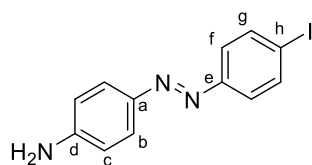
<sup>13</sup>C{<sup>1</sup>H} NMR (125 MHz, CDCl<sub>3</sub>) δ = 158.41 (*C*-d), 151.99 (*C*-e), 147.06 (*C*-a), 138.27 (*C*-g), 125.16 (*C*-c), 124.24 (*C*-b), 115.86 (*C*-f), 96.82 (*C*-h) ppm.

HRMS (EI, 70 eV) *m/z* (%): [M]<sup>+</sup> calcd for [C<sub>12</sub>H<sub>9</sub>IN<sub>2</sub>O]<sup>+</sup> 323.97541; found 323.97570 (45), 93.0 (100).

IR:  $\tilde{\nu}$  = 3024 (b), 1590 (s), 1562 (w), 1466 (s), 1438 (m), 1298 (s), 1240 (m), 1152 (s), 1140 (s), 1101 (m), 1051 (w), 1002 (w), 829 (s), 724 (s), 704 (m) cm<sup>-1</sup>.

Mp: 168 °C.

R<sub>f</sub>: 0.50 (*n*-hexane/ethyl acetate 4:1).

*(E)*-*N*-4-((4-Iodophenyl)diazenyl)aniline (**1e**)

To *(E)*-*N*-4-((4-Iodophenyl)diazenyl)phenylacetamide (365 mg, 1.00 mmol, 1.00 equiv.) was added MeOH (15 mL) and HCl (3 M, 75 mL). The suspension was stirred for 18 h at 85 °C, resulting in a clear red solution. The mixture was neutralized with a saturated aqueous NaHCO<sub>3</sub> solution and the precipitate was filtered. The precipitate was washed with water (2 × 20 mL) and the product was crystallized from EtOH at -21 °C to obtain **1e** as a red solid (280 mg, 0.866 mmol, 87%).

<sup>1</sup>H NMR (600 MHz, DMSO-*d*<sub>6</sub>) δ = 7.87 (d, <sup>3</sup>J = 8.2 Hz, 2H, *H*-g), 7.67 (d, <sup>3</sup>J = 8.4 Hz, 2H, *H*-c), 7.53 (d, <sup>3</sup>J = 8.2 Hz, 2H, *H*-f), 6.67 (d, <sup>3</sup>J = 8.4 Hz, 2H, *H*-b), 6.20 (s, 2H, NH<sub>2</sub>-d) ppm.

<sup>13</sup>C{<sup>1</sup>H} NMR (151 MHz, DMSO-*d*<sub>6</sub>) δ = 153.74 (*C*-a/e), 152.32 (*C*-a/e), 143.13 (*C*-d), 138.54 (*C*-g), 125.94 (*C*-c), 124.15 (*C*-f), 113.8 (*C*-b), 96.20 (*C*-h) ppm.

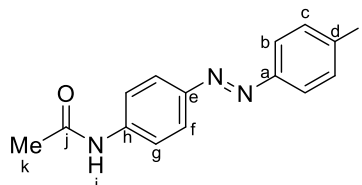
**IR** (ATR):  $\tilde{\nu}$  = 3446 (m), 3319 (m), 3205 (m), 2667 (w), 1893 (w), 1628 (m), 1593 (s), 1504 (m), 1473 (w), 1416 (m), 1385 (s), 1304 (s), 1230 (w), 1186 (m), 1153 (m), 1138 (s), 1119 (s), 1094 (w), 1004 (w), 943 (w), 829 (s), 722 (s), 699 (w)  $\text{cm}^{-1}$ .

**HRMS** (EI, 70 eV)  $m/z$  (%):  $[M]^+$  calcd for  $[\text{C}_{12}\text{H}_{10}\text{IN}_3]^+$  322.99140; found 322.99152 (10), 92.1 (100).

**Mp**: 162 °C.

**R<sub>f</sub>**: 0.40 (*n*-hexane/ethyl acetate 1:1).

(*E*)-*N*-(4-((4-Iodophenyl)diazenyl)phenyl)acetamide (**1f**)



4-Aminoacetanilide (2.40 g, 16.0 mmol, 1.00 equiv) was dissolved in water (200 mL). Oxone® (19.7 g, 32 mmol, 2.00 equiv) was dissolved in water (100 mL) and added to the solution. The mixture was stirred for five minutes, while a green solid precipitated. The precipitate was filtered and the filter cake was extracted with ethyl acetate. The organic phase was dried over  $\text{MgSO}_4$  and filtered. The solvent was removed and NMR analysis revealed that the nitroso compound was obtained in a high purity and a yield of 850 mg (5.18 mmol, 32%).

This product was used without further purification. 4-Nitrosoacetaniliden (820 mg, 5.00 mmol, 1.00 equiv) was dissolved in acetic acid (100 mL). To this solution, 4-iodoaniline (1.10 g, 5.00 mmol, 1.00 equiv) was added and the mixture was stirred for 1 d at 22 °C. The solvent was removed *in vacuo* and the crude product filtered through a short plug of silica (eluent: DCM). The solvent was removed and the crude product was crystallized in MeOH at -21 °C to yield **1f** as an orange solid (1.25 g, 3.42 mmol, 68%).

**<sup>1</sup>H NMR** (600 MHz,  $\text{DMSO}-d_6$ )  $\delta$  = 10.32 (s, 1H, NH-j), 7.95 (d,  $^3J$  = 8.4 Hz, 2H, H-g), 7.88 (d,  $^3J$  = 8.4 Hz, 2H, H-f), 7.80 (d,  $^3J$  = 8.7 Hz, 2H, H-b), 7.63 (d,  $^3J$  = 8.7 Hz, 2H, H-c), 2.10 (s, 3H, H-k) ppm.

**<sup>13</sup>C{<sup>1</sup>H} NMR** (151 MHz,  $\text{DMSO}-d_6$ )  $\delta$  = 168.9 (C-j), 151.4 (C-h), 147.3 (C-e), 142.8 (C-a), 138.4 (C-g), 124.2 (C-f), 123.9 (C-b), 119.1 (C-c), 98.2 (C-d), 24.2 (C-k) ppm.

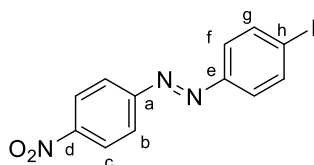
**IR** (ATR):  $\tilde{\nu}$  = 3247 (w), 1658 (m), 1589 (m), 1520 (m), 1495 (m), 1473 (m), 1403 (w), 1367 (m), 1298 (m), 1264 (m), 1156 (w), 1142 (w), 1097 (w), 1037 (w), 1013 (w), 1001 (m), 835 (s), 728 (s), 701 (w)  $\text{cm}^{-1}$ .

**HRMS** (EI, 70 eV)  $m/z$  (%):  $[M]^+$  calcd for  $[\text{C}_{14}\text{H}_{12}\text{IN}_3\text{O}]^+$  365.00196; found 365.00248 (25), 134.2 (100).

**Mp**: 230 °C.

**R<sub>f</sub>**: 0.15 (*n*-hexane/ethyl acetate 1:1).

(*E*)-1-(4-Iodophenyl)-2-(4-nitrophenyl)diazene[8] (**1g**)



This reaction was not performed under inert conditions.

4-Amino-nitrophenol (20.0 g, 145 mmol, 1.00 equiv) was dissolved in DCM (60 mL). Oxone® (178 g, 190 mmol, 2.00 equiv) was dissolved in water (750 mL) and added to the solution. The biphasic mixture was stirred vigorously for 12 h. The phases were separated and the organic phase was dried over

MgSO<sub>4</sub> and filtered to yield 16.8 g crude product with a 60% conversion to the desired nitroso compound. This product was used without further purification.

4-Nitro-nitrosophenol (telescoped from the above reaction, 10.1 g, 66.1 mmol, 1.00 equiv) was dissolved in acetic acid (200 mL). To this solution, 4-iodoaniline (15.9 g, 72.7 mmol, 1.10 equiv) was added and the mixture was stirred for 3 d at 85 °C. The solvent was removed *in vacuo* and the crude product was crystallized two times from MeOH at -21 °C to yield **1g** 15.8 g (44.7 mmol, 68%, Lit.:<sup>[8]</sup> 51%).

<sup>1</sup>H NMR (600 MHz, CDCl<sub>3</sub>) δ = 8.39 (d, <sup>3</sup>J = 9.1 Hz, 2H, H-g), 8.04 (d, <sup>3</sup>J = 9.1 Hz, 2H, H-f), 7.92 (d, <sup>3</sup>J = 8.7 Hz, 2H, H-c), 7.70 (d, <sup>3</sup>J = 8.7 Hz, 2H, H-b) ppm.

<sup>13</sup>C{<sup>1</sup>H} NMR (125 MHz, CDCl<sub>3</sub>) δ = 155.46 (C-h), 151.63 (C-e), 148.89 (C-a), 138.65 (C-c), 124.85 (C-b), 124.78 (C-g), 123.55 (C-h), 99.68 (C-d) ppm.

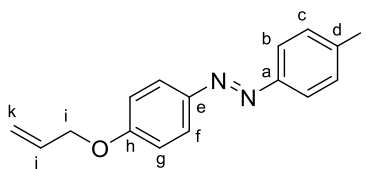
IR:  $\tilde{\nu}$  = 1604 (m), 1514 (s), 1451 (m), 1338 (s), 1324 (m), 1139 (m), 1104 (w), 1048 (m), 1004 (m), 856 (s), 830 (s), 818 (m), 751 (s), 704 (s), 682 (m) cm<sup>-1</sup>.

HRMS (EI, 70 eV) *m/z* (%): [M]<sup>+</sup> calcd for [C<sub>12</sub>H<sub>8</sub>IN<sub>3</sub>O<sub>2</sub>]<sup>+</sup> 352.96558; found 352.96538 (40, 76.0 (100)).

Mp: 240 °C.

R<sub>f</sub>: 0.40 (*n*-hexane/ethyl acetate 1:1).

(*E*)-1-(4-(Allyloxy)phenyl)-2-(4-iodophenyl)diazene<sup>[9]</sup> (**1h**)



**1d** (1.62 g, 5.00 mmol, 1.00 equiv) and potassium carbonate (829 mg, 6.00 mmol, 1.10 equiv) were dissolved in anhydrous DMF (20 mL) under nitrogen. The solution was heated to 50 °C. Allyl bromide (1.21 g, 10.0 mmol, 2.00 equiv) in 20 mL DMF were added dropwise. The mixture was stirred at 50 °C for 17 h. After adding ethyl acetate (100 mL), the solution was washed with water (100 mL), brine (100 mL) and dried over MgSO<sub>4</sub>. After filtration, the solvent was removed by evaporation under reduced pressure. The crude product was filtered through a short plug of silica and further purified by crystallization in methanol to give **1h** as a yellow solid (1.29 g, 3.55 mmol, 71% Lit.:<sup>[9]</sup> 88%).

<sup>1</sup>H NMR (600 MHz, CDCl<sub>3</sub>) δ = 7.90 (d, *J* = 8.9 Hz, 2H, H-g), 7.84 (d, *J* = 8.7 Hz, 2H, H-b), 7.61 (d, *J* = 8.7 Hz, 2H, H-c), 7.02 (d, *J* = 8.9 Hz, 2H, H-f), 6.12 – 6.04 (m, 1H, H-j), 5.45 (d, *J* = 17.3 Hz, 1H, H-k), 5.33 (d, *J* = 10.5 Hz, 1H, H-k), 4.63 (d, *J* = 6.6 Hz, 2H, H-i).

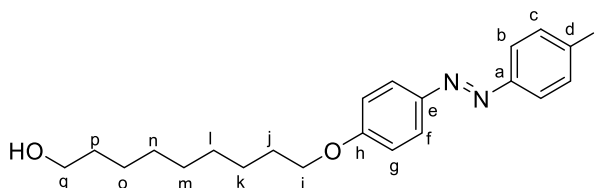
<sup>13</sup>C{<sup>1</sup>H} NMR (151 MHz, CDCl<sub>3</sub>) δ 161.50 (C-h), 152.23 (C-a), 147.04 (C-e), 138.41 (C-b), 132.81 (C-j), 125.05 (C-g), 124.39 (C-c), 118.30 (C-k), 115.17 (C-f), 96.87 (C-d), 69.21 (C-i).

IR:  $\tilde{\nu}$  = 1600 (s), 1579 (m), 1563 (m), 1492 (m), 1473 (w), 1426 (w), 1391 (w), 1362 (w), 1296 (w), 1239 (m), 1152 (m), 1141 (m), 1016 (m), 1016 (m), 993 (s), 930 (m), 838 (s), 826 (s), 727 (m), 705 (m) cm<sup>-1</sup>.

HRMS (EI, 70 eV) *m/z* (%): [M]<sup>+</sup> calcd for [C<sub>15</sub>H<sub>13</sub>N<sub>2</sub>O]<sup>+</sup> 364.00671; found 364.00660 (60), 133.1 (100).

Mp: 148 °C.

R<sub>f</sub>: 0.65 (*n*-hexane/ethyl acetate 1:1).

*(E)*-9-(4-((4-Iodophenyl)diazenyl)phenoxy)nonan-1-ol (**1i**)

This reaction was not performed under inert conditions.

A mixture of **1d** (6.00 g, 18.5 mmol, 1.00 equiv) and 9-bromo-1-nonanol (4.95 g, 22.2 mmol, 1.20 equiv) was dissolved in acetone (100 mL). Potassium iodide (100 mg, 602  $\mu$ mol, 3 mol%) and potassium carbonate (5.11 g, 37.0 mmol, 2.00 equiv) was added to the solution. The resulting solution was heated to reflux at 60 °C for 5 h. After the reaction mixture was cooled to 24 °C, water (300 mL) was added to the mixture. A precipitate was formed, which was collected by filtration. The aqueous solution was extracted with DCM (3  $\times$  20 mL). Both the precipitate and the extract were combined and dried *in vacuo*. The resulting crude product was purified by column chromatography (gradient *n*-pentane  $\rightarrow$  DCM) to give **1i** as a yellow solid (3.40 g, 7.29 mmol, 57%).

<sup>1</sup>H NMR (600 MHz, CDCl<sub>3</sub>)  $\delta$  = 7.90 (d, <sup>3</sup>J = 9.0 Hz, 2H, H-g), 7.83 (d, <sup>3</sup>J = 8.7 Hz, 2H, H-c), 7.61 (d, <sup>3</sup>J = 8.7 Hz, 2H, H-b), 6.99 (d, <sup>3</sup>J = 9.0 Hz, 2H, H-f), 4.04 (t, <sup>3</sup>J = 6.5 Hz, 2H, H-i), 3.65 (t, <sup>3</sup>J = 6.6 Hz, 2H, H-q), 1.86-1.77 (m, 2H, H-j), 1.58 (p, <sup>3</sup>J = 6.6 Hz, 2H, H-p), 1.48 (m, 2H, C2-H-k), 1.35 (m, 8H, H-l,m,n,o) ppm.

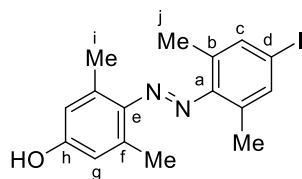
<sup>13</sup>C{<sup>1</sup>H} NMR (125 MHz, CDCl<sub>3</sub>)  $\delta$  = 162.00 (C-h), 152.10 (C-e), 146.67 (C-d)), 138.23 (C-c), 124.92 (C-g), 124.20 (C-b), 114.76 (C-f), 96.59 (C-d), 68.37 (C-i), 63.07 (C-q), 32.78 (C-p), 29.50 (C-m), 29.34 (C-n), 29.29 (C-j), 29.16 (C-l), 25.99 (C-k), 25.72 (C-o) ppm.

IR:  $\tilde{\nu}$  = 3298 (b), 2917 (m), 2849 (m), 1602 (s), 1582 (m), 1500 (w), 1471 (w), 1297 (s), 1251 (m), 1143 (s), 1107 (m), 1020 (m), 843 (s), 829 (s), 721 (m), 705 (w) cm<sup>-1</sup>.

HRMS (EI, 70 eV) *m/z* (%): [M]<sup>+</sup> calcd for [C<sub>21</sub>H<sub>27</sub>IN<sub>2</sub>O<sub>2</sub>]<sup>+</sup> 466.11118; found 466.11064 (10), 55.0 (100).

Mp: 133 °C.

R<sub>f</sub>: 0.50 (*n*-pentane: DCM 1:1).

*(E)*-4-((4-Iodo-2,6-dimethylphenyl)diazenyl)-3,5-dimethylphenol (**S1**)

This reaction was not performed under inert conditions.

2,6-Dimethyl-4-nitroaniline (500 mg, 3.01 mmol, 1.00 equiv) and K<sub>2</sub>CO<sub>3</sub> (410 mg, 3.01 mmol, 1.00 equiv) were dissolved in water (10 mL). NaNO<sub>2</sub> (205 mg, 3.01 mmol, 1.00 equiv) dissolved in water (10 mL) was added dropwise over the course of 1 min. The mixture was cooled to 0 °C and HCl (4 M, 10 mL) was slowly added dropwise over the course of 10 min forming white crystals. The dispersion was stirred for 1 h at 0 °C. The mixture was slowly added dropwise over the course of 10 min to a second solution of 3,5-dimethylphenol (400 mg, 3.27 mmol, 1.08 eq) and NaOH (5 wt%, 10 mL), which was cooled to 0 °C in beforehand. The resulting dispersion was stirred for another 21 h while warming up to 23 °C. The mixture was diluted with HCl (1 M, 20 mL). The precipitate was removed by filtration and washed with water (2  $\times$  10 mL). The residue was crystallized in MeOH at -20 °C to yield **S1** as a dark red solid. (410 mg, 1.34 mmol, 45%).

**<sup>1</sup>H NMR** (600 MHz, CDCl<sub>3</sub>)  $\delta$  = 7.52 (s, 2 H, *H-c*), 6.65 (s, 2 H, *OH-g*), 2.50 (s, 6 H, *H-i*), 2.35 (s, 6 H, *H-j*) ppm.

**<sup>13</sup>C{<sup>1</sup>H} NMR** (151 MHz, CDCl<sub>3</sub>)  $\delta$  = 156.2 (*C-h*), 151.5 (*C-a*), 144.6 (*C-e*), 137.9 (*C-c*), 136.0 (*C-b*), 132.9 (*C-f*), 116.1 (*C-g*), 93.1 (*C-d*), 21.0 (*C-i*), 19.4 (*C-j*) ppm.

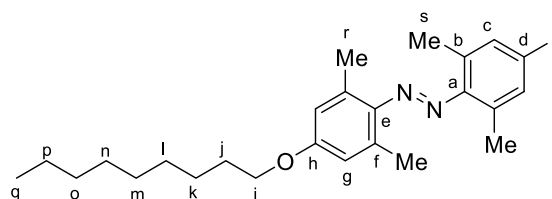
**IR:**  $\tilde{\nu}$  = 3418 (m) 2956 (w), 1609 (m), 1507 (s), 1466 (m), 1376 (s), 1337 (s), 1302 (s), 1217 (m), 1148 (s), 1099 (w), 941 (m), 895 (m), 800 (w), 746 (s) cm<sup>-1</sup>.

**HRMS** (ESI):  $m/z$  = [M + Na]<sup>+</sup> calcd for [C<sub>16</sub>H<sub>17</sub>N<sub>3</sub>O<sub>3</sub> + Na]<sup>+</sup> 322.11621, found 322.11633.

**Mp:** 190 °C.

**R<sub>f</sub>:** 0.70 (*n*-hexane/ethyl acetate 4:1).

(*E*)-1-(2,6-Dimethyl-4-(nonyloxy)phenyl)-2-(4-iodo-2,6-dimethylphenyl)diazene (**1j**)



This reaction was not performed under inert conditions.

A mixture of **S1** (1.30 g, 3.42 mmol, 1.00 equiv), K<sub>2</sub>CO<sub>3</sub> (886 mg, 6.40 mmol) and 1-bromohexane (2.30 mL, 4.65 mmol, 1.36 equiv) in acetonitrile (20 mL) was stirred at 80 °C. After stirring for 24 h, the solvent was removed. DCM was added and washed with HCl (1 M, 20 mL), water (20 mL), sat. NaHCO<sub>3</sub> (20 mL) and brine (20 mL). The organic phase was dried over MgSO<sub>4</sub> and filtered. The solvent was removed in vacuo and the residue was purified by column chromatography to afford **1j** as a red oil, which solidified after several hours. (1.02 g, 2.13 mmol, 62%).

**<sup>1</sup>H NMR** (600 MHz, CDCl<sub>3</sub>)  $\delta$  = 7.49 (s, 2H, *H-c*), 6.68 (s, 2H, *H-g*), 4.01 (t, <sup>3</sup>*J* = 6.6 Hz, 2H *H-i*), 2.50 (s, 6H, *H-r*), 2.33 (s, 6H, *H-s*), 1.83 – 1.78 (m, 2H, *H-j*), 1.47 (p, <sup>3</sup>*J* = 7.5, 7.1 Hz, 2H, *H-k*), 1.39 – 1.25 (m, 12H, *H-l-p*), 0.90 (d, <sup>3</sup>*J* = 7.2 Hz, 3H, *H-q*) ppm.

**<sup>13</sup>C{<sup>1</sup>H} NMR** (151 MHz, CDCl<sub>3</sub>)  $\delta$  = 159.79 (*C-h*), 151.73 (*C-a*), 144.41 (*C-e*), 138.00 (*C-c*), 135.88 (*C-f*), 133.02 (*C-b*), 115.33 (*C-g*), 93.11 (*C-d*), 68.21 (*C-i*), 32.03 (*C-l-p*), 29.69 (*C-l-p*), 29.53 (*C-l-p*), 29.42 (*C-l-p*), 29.38 (*C-j*), 26.17 (*C-k*), 22.83 (*C-l-p*), 21.39 (*C-r*), 19.47 (*C-s*), 14.27 (*C-q*) ppm

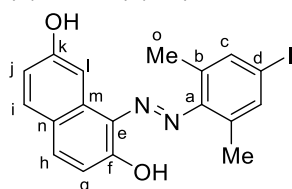
**IR** (ATR):  $\tilde{\nu}$  = 2966 (s), 2935 (s), 2921 (m), 2850 (w), 1599 (m), 1588 (w), 1487 (w), 1487 (m), 1462 (m), 1454 (s), 1375 (w), 1311 (s), 1245 (w), 1168 (m), 1147 (s), 1127 (m), 1064 (s), 1036 (m), 877 (m), 863 (s), 854 (s), 825 (m), 779 (w), 747 (m), 730 (w) cm<sup>-1</sup>.

**HRMS** (EI, 70 eV)  $m/z$  (%): [M]<sup>+</sup> calcd for [C<sub>25</sub>H<sub>35</sub>N<sub>2</sub>OI]<sup>+</sup> 506.17886; found 506.17900 (10), 43.1 (100).

**Mp:** 66 °C.

**R<sub>f</sub>:** 0.70 (*n*-hexane/ethyl acetate 1:1).

(*E*)-1-((4-iodo-2,6-dimethylphenyl)diazenyl)naphthalene-2,7-diol (**S2**)



This reaction was not performed under inert conditions.

4-iodo-2,5-dimethylanilin (2.47 g, 10 mmol, 1.00 equiv) and K<sub>2</sub>CO<sub>3</sub> (1.26 g, 10.00 mmol, 1.00 equiv) were dissolved in water (10 mL). NaNO<sub>2</sub> (680 mg, 10.0 mmol, 1.00 equiv) dissolved in water (10 mL)

27

was added dropwise. The mixture was cooled to 0 °C under constant stirring and HCl (4 M, 10 mL) was added dropwise. The mixture was stirred for 1h and was then added dropwise to a mixture of 2,7-dihydroxynaphthalene (1.60 g, 10.0 mmol, 1.00 equiv) and 15 wt% NaOH solution (10 mL). The reaction was stirred for a further 3 h while warming up to 21 °C. The mixture was diluted with HCl (1 M, 50 mL). The precipitate was removed by filtration and washed with water (2 × 10 mL). The residue was crystallized from ethanol/water (5:1) at -21 °C to yield **S2** as a dark red solid (3.49 g, 8.70 mmol, 87%).

**<sup>1</sup>H NMR** (600 MHz, DMSO-*d*<sub>6</sub>) δ = 10.14 (s, 2H, OH-f/k), 7.83 (d, <sup>3</sup>J = 9.3 Hz, 1H, H-j), 7.66 (s, 2H, H-c), 7.66 (s, 1H, H-l), 7.63 (d, 1H, <sup>3</sup>J = 8.5 Hz, H-g), 6.91 (dd, <sup>3</sup>J = 8.5, <sup>4</sup>J = 2.4 Hz, 1H, H-h), 6.67 (d, <sup>3</sup>J = 9.3 Hz, 1H, H-i), 2.51 (s, 9H, H-o) ppm.

**<sup>13</sup>C{<sup>1</sup>H} NMR** (151 MHz, DMSO-*d*<sub>6</sub>) δ = 169.88 (C-k), 158.80 (C-f), 141.20 (C-a), 140.27 (C-j), 138.09 (C-c), 135.18 (C-e), 132.01 (C-b), 130.98 (C-g), 130.03 (C-m), 121.33 (C-n), 120.12 (C-i), 115.71 (C-h), 105.15 (C-l), 92.64 (C-d), 19.47 (C-o) ppm.

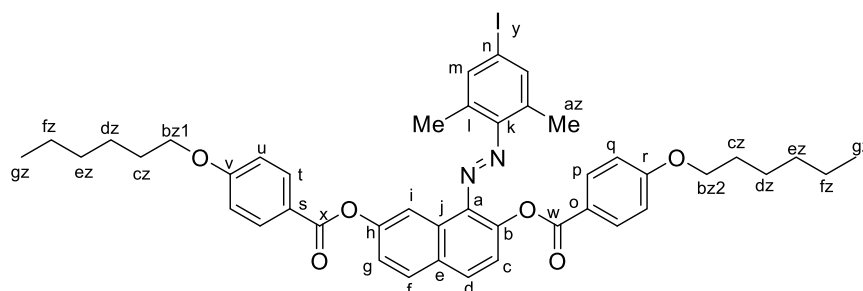
**IR** (ATR):  $\tilde{\nu}$  = 3137 (br), 1621 (m), 1548 (m), 1506 (s), 1479 (s), 1460 (s), 1418 (m), 1356 (w), 1331 (s), 1271 (m), 1242 (m), 1216 (m), 1198 (m), 1163 (m), 1141 (w), 1019 (w), 946 (w), 888 (m), 875 (m), 833 (s), 813 (m) cm<sup>-1</sup>.

**HRMS** (EI): *m/z* = [M]<sup>+</sup> calcd for [C<sub>18</sub>H<sub>15</sub>N<sub>2</sub>O<sub>2</sub>]<sup>+</sup> 418.01728, found 418.01727 (30), 159.1 (100).

**Mp**: 232 °C.

**R<sub>f</sub>**: 0.50 (*n*-hexane/ethyl acetate 1:1).

(*E*)-1-((4-Iodo-2,6-dimethylphenyl)diazenyl)naphthalene-2,7-diyl bis(4-(hexyloxy)benzoate) (**1k**)



4-Hexyloxybenzoic acid (571 mg, 3.00 mmol, 3.00 equiv), **S2** (418 mg, 1.00 mmol, 1.00 equiv) and DMAP (122 mg, 1.00 mmol, 1.00 equiv) were dissolved in dry DCM (15 mL). Afterwards DCC (1.03 g, 5.00 mmol, 5.00 equiv) was added portion-wise. The mixture was stirred for 16 h. The resulting suspension was filtered, washed with a saturated NaHCO<sub>3</sub> solution (30 mL), water (30 mL), brine (30 mL). The organic phase was dried over MgSO<sub>4</sub>, filtered and the solvent was removed under reduced pressure. The product was purified by column chromatography (eluent: DCM/*n*-hexane 1:1) to yield **1k** as a red solid (637 mg, 720 μmol, 72%).

**<sup>1</sup>H NMR** (600 MHz, CDCl<sub>3</sub>) δ = 8.46 (d, <sup>4</sup>J = 2.3 Hz, 1H, H-i), 8.16 (d, <sup>3</sup>J = 8.9 Hz, 2H, H-t), 8.04 (d, <sup>3</sup>J = 8.9 Hz, 2H, H-p), 7.99 (t, <sup>3</sup>J = 8.8 Hz, 2H, H-f/d), 7.46 (dd, <sup>3</sup>J = 8.8, 2.3 Hz, 1H, H-g), 7.41 (d, <sup>3</sup>J = 8.8 Hz, 1H, H-c), 7.39 (s, 2H, H-m), 6.07 (d, <sup>3</sup>J = 8.9 Hz, 2H, H-u), 6.90 (d, <sup>3</sup>J = 8.9 Hz, 2H, H-q), 4.05 (t, <sup>3</sup>J = 6.5 Hz, 2H, H-bz1), 4.02 (t, <sup>3</sup>J = 6.6 Hz, 2H, H-bz2), 2.22 (s, 6H, H-az), 1.82 (dd, <sup>2</sup>J = 14.8, <sup>3</sup>J = 6.6 Hz, 4H, H-cz), 1.52-1.43 (m, 4H, H-dz), 1.40-1.31 (m, 8H, H-ez/fz), 0.94 – 0.90 (m, 6H, H-gz) ppm.

**<sup>13</sup>C{<sup>1</sup>H} NMR** (151 MHz, CDCl<sub>3</sub>) δ = 165.13 (C-x), 165.09 (C-w), 163.78 (C-s), 163.65 (C-o), 151.40 (C-k), 150.80 (C-b), 139.82 (C-e), 138.49 (C-j), 138.02 (C-m), 133.79 (C-l), 132.50 (C-p+t), 131.40 (C-f), 130.62 (C-d), 130.54 (C-h), 129.58 (C-a), 123.01 (C-c), 122.19 (C-g), 121.48 (C-v), 121.38 (C-r), 115.97 (C-i), 114.47 (C-u), 114.39 (C-q), 94.85 (C-n), 68.49 (C-bz1), 68.45 (C-bz2), 31.70 (C-fz/ez), 29.21 (C-cz), 25.81 (C-dz), 24.85 (C-ez), 22.74 (C-fz/ez), 19.10 (C-az), 14.18 (C-gz) ppm.



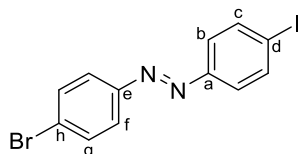
**IR** (ATR):  $\tilde{\nu}$  = 2924 (m), 1721 (s), 1604 (s), 1563 (m), 1512 (m), 1469 (m), 1421 (w), 1249 (s), 1201 (s), 1217 (s), 1201 (m), 1162 (s), 1067 (s), 1006 (m), 934 (m), 916 (m), 899 (w), 875 (m), 848 (w), 759 (s), 690 (m)  $\text{cm}^{-1}$ .

**HRMS** (ESI):  $m/z$  =  $[M+Na]^+$  calcd for  $[C_{44}H_{47}IN_2O_6+Na]^+$  849.23669, found 849.23711.

**Mp**: 232 °C.

**R<sub>f</sub>**: 0.50 (*n*-hexane/ethyl acetate 1:1).

(*E*)-1-(4-Bromophenyl)-2-(4-iodophenyl)diazene<sup>[10]</sup> (**1l**)



This reaction was not performed under inert conditions.

4-Bromoaniline (3.70 g, 21.5 mmol, 1.00 equiv) was dissolved in DCM (75 mL). To this solution, Oxone<sup>®</sup> (26.4 g, 43.0 mmol, 2.00 equiv) dissolved in water (300 mL) was added. The solution was stirred under a nitrogen atmosphere at 25 °C for 2 h. The color of the solution turned to green as the corresponding nitrosoarene formed. The layers were separated and the aqueous layer was extracted with DCM (3 × 100 mL). The combined organic layers were washed with HCl (1 M, 150 mL), saturated sodium hydrogen carbonate solution (150 mL), water (150 mL) and brine (150 mL). The organic phase was dried over MgSO<sub>4</sub> and filtered. The solvent was removed under reduced pressure. The obtained crude 1-bromo-4-nitrosobenzene (4.00 g, 21.5 mmol, 1.00 equiv) was dissolved in acetic acid (100 mL) and 4-iodoaniline was added (4.71 g, 21.5 mmol, 1.00 equiv). The resulting mixture was stirred at 25 °C for 14 h. The precipitate was separated by filtration and washed with acetic acid (100 mL). The residue was crystallized from methanol at -21 °C yielding **1l** as an orange solid (6.63 g, 17.1 mmol, 80%, Lit.:<sup>[10]</sup> 86%).

**<sup>1</sup>H NMR** (600 MHz, CDCl<sub>3</sub>)  $\delta$  = 7.87 (d, <sup>3</sup>J = 8.6 Hz, 2H, *H*-c), 7.79 (d, <sup>3</sup>J = 8.7 Hz, 2H, *H*-f), 7.65 (d, <sup>3</sup>J = 8.7 Hz, 2H, *H*-g), 7.64 (d, <sup>3</sup>J = 8.6 Hz, 2H, *H*-b) ppm.

**<sup>13</sup>C{<sup>1</sup>H} NMR** (151 MHz, CDCl<sub>3</sub>)  $\delta$  = 151.9 (*C*-a), 151.3 (*C*-e), 138.6 (*C*-c), 132.6 (*C*-b), 126.0 (*C*-h), 124.7 (*C*-g), 124.6 (*C*-f), 98.3 (*C*-d) ppm.

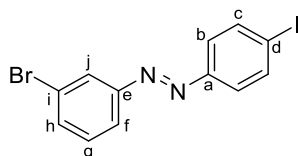
**IR** (ATR):  $\tilde{\nu}$  = 2355 (w), 2093 (br), 1904 (w), 1652 (w), 1563 (m), 1470 (m), 1395 (m), 1280 (w), 1222 (w), 1143 (w), 1095 (m), 1061 (m), 1001 (s), 831 (s), 773 (s), 709 (s)  $\text{cm}^{-1}$ .

**HRMS** (EI, 70 eV)  $m/z$  (%):  $[M]^+$  calcd for  $[C_{12}H_8BrIN_2]^+$  385.89101; found 385.89136 (45), 76.0 (100).

**Mp**: 205 °C (Lit.:<sup>[6]</sup> 201 °C).

**R<sub>f</sub>**: 0.75 (*n*-hexane/DCM 3:1).

(*E*)-1-(3-Bromophenyl)-2-(4-iodophenyl)diazene (**1m**)



This reaction was not performed under inert conditions.

3-Bromoaniline (6.00 g, 35.0 mmol, 1.00 equiv) was dissolved in DCM (75 mL). To this solution, Oxone<sup>®</sup> (43.1 g, 75.0 mmol, 2.00 equiv) dissolved in water (300 mL) was added. The solution was stirred under a nitrogen atmosphere at 25 °C for 6 h. The color of the solution turned to green as the corresponding nitrosoarene formed. The layers were separated and the aqueous layer was extracted with DCM (3 ×

29

100 mL). The combined organic layers were washed with HCl (1 M, 150 mL), saturated sodium hydrogen carbonate solution (150 mL), water (150 mL) and brine (150 mL). The organic phase was dried over MgSO<sub>4</sub> and filtered. The solvent was removed under reduced pressure. The obtained crude 1-bromo-3-nitrosobenzene (6.51 g, 35.0 mmol, 1.00 equiv) was dissolved in acetic acid (100 mL) and 4-iodoaniline was added (7.67 g, 35.0 mmol, 1.00 equiv). The resulting mixture was stirred at 25 °C for 16 h. The precipitate was separated by filtration and washed with acetic acid (100 mL). The residue was crystallized from methanol at -21 °C yielding **1m** as an orange solid (9.65 g, 24.9 mmol, 72%).

<sup>1</sup>H NMR (600 MHz, CDCl<sub>3</sub>) δ = 8.05 (at, <sup>4</sup>J = 1.9 Hz, 1H, H-j), 7.88 – 7.86 (m, 3H, H-c/h), 7.65 (d, <sup>3</sup>J = 8.6 Hz, 2H, H-b), 7.61 (ddd, <sup>3</sup>J = 7.9 Hz, <sup>4</sup>J = 1.9 Hz, 1.0 Hz, 1H, H-f), 7.41 (t, <sup>3</sup>J = 7.9 Hz, 1H, H-g) ppm.

<sup>13</sup>C{<sup>1</sup>H} NMR (151 MHz, CDCl<sub>3</sub>) δ = 153.5 (C-e), 151.8 (C-a), 138.6 (C-c), 134.1 (C-f), 130.7 (C-g), 124.8 (C-j), 124.8 (C-b), 123.3 (C-h), 123.3 (C-i), 98.6 (C-d) ppm.

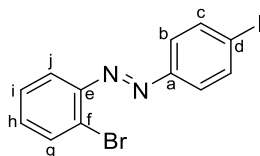
IR (ATR):  $\tilde{\nu}$  = 2990 (w), 2356 (w), 2120 (w), 1893 (w), 1652 (w), 1563 (m), 1465 (m), 1446 (m), 1409 (m), 1387 (m), 1297 (m), 1209 (w), 1170 (m), 1147 (m), 1089 (m), 1050 (m), 1000 (s), 921 (m), 879 (m), 833 (s), 819 (s), 790 (s), 775 (m), 710 (s), 703 (s) cm<sup>-1</sup>.

HRMS (EI, 70 eV) *m/z* (%): [M]<sup>+</sup> calcd for [C<sub>12</sub>H<sub>8</sub>BrIN<sub>2</sub>]<sup>+</sup> 385.89101; found 385.89122 (14), 76.0 (100).

Mp: 129 °C.

R<sub>f</sub>: 0.75 (*n*-hexane/DCM 3:1).

(*E*)-1-(2-Bromophenyl)-2-(4-iodophenyl)diazene (**1n**)



This reaction was not performed under inert conditions.

2-Bromoaniline (12.0 g, 70.0 mmol, 1.00 equiv) was dissolved in DCM (150 mL). To this solution, Oxone® (86.1 g, 140 mmol, 2.00 equiv) dissolved in water (300 mL) was added. The solution was stirred under a nitrogen atmosphere at 25 °C for 24 h. The color of the solution turned to green as the corresponding nitrosoarene formed. The layers were separated and the aqueous layer was extracted with DCM (3 × 100 mL). The combined organic layers were washed with HCl (1 M, 150 mL), saturated sodium hydrogen carbonate solution (150 mL), water (150 mL) and brine (150 mL). The organic phase was dried over MgSO<sub>4</sub> and filtered. The solvent was removed under reduced pressure. The obtained crude 1-bromo-2-nitrosobenzene (13.0 g, 70.0 mmol, 1.00 equiv) was dissolved in acetic acid (200 mL) and 4-iodoaniline was added (15.3 g, 70.0 mmol, 1.00 equiv). The resulting mixture was stirred at 25 °C for 16 h. The precipitate was separated by filtration and washed with acetic acid (100 mL). The residue was crystallized from methanol at -21 °C yielding **1n** as an orange solid (19.6 g, 50.6 mmol, 72%).

<sup>1</sup>H NMR (600 MHz, CDCl<sub>3</sub>) δ = 7.88 (d, <sup>3</sup>J = 8.6 Hz, 2H, H-c), 7.76 (dd, <sup>3</sup>J = 7.9 Hz, <sup>4</sup>J = 1.4 Hz, 1H, H-g), 7.70 (d, <sup>3</sup>J = 8.6 Hz, 2H, H-b), 7.68 (dd, <sup>3</sup>J = 7.9 Hz, <sup>4</sup>J = 1.7 Hz, 1H, H-j), 7.39 (td, <sup>3</sup>J = 7.2 Hz, <sup>4</sup>J = 1.4 Hz, 1H, H-i), 7.33 (td, <sup>3</sup>J = 7.2 Hz, <sup>4</sup>J = 1.7 Hz, 1H, H-h) ppm.

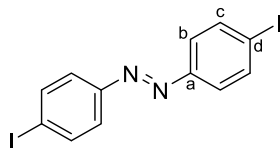
<sup>13</sup>C{<sup>1</sup>H} NMR (151 MHz, CDCl<sub>3</sub>) δ = 152.1 (C-a), 149.6 (C-e), 138.6 (C-c), 134.0 (C-g), 132.4 (C-h), 128.2 (C-i), 126.2 (C-f), 125.1 (C-b), 117.9 (C-j), 98.7 (C-d) ppm.

IR (ATR):  $\tilde{\nu}$  = 2356 (w), 2121 (w), 1821 (w), 1660 (w), 1576 (w), 1564 (m), 1475 (w), 1456 (m), 1422 (m), 1392 (w), 1225 (w), 1044 (m), 1024 (s), 1003 (s), 953 (m), 831 (s), 759 (s), 717 (s), 702 (m) cm<sup>-1</sup>.

HRMS (EI, 70 eV) *m/z* (%): [M]<sup>+</sup> calcd for [C<sub>12</sub>H<sub>8</sub>BrIN<sub>2</sub>]<sup>+</sup> 385.89101; found 385.89146 (36), 76.0 (100).

Mp: 93 °C.

R<sub>f</sub>: 0.75 (*n*-hexane/DCM 3:1).

*(E)*-1,2-Bis(4-iodophenyl)diazene<sup>[11]</sup> (**4a**)

This reaction was not performed under inert conditions.

A solution of 4-iodoaniline (10.0 g, 45.7 mmol, 1.00 equiv) and manganese dioxide (70.0 g, 805 mmol, 17.6 equiv) in toluene (700 mL) was stirred for 3 h at 120 °C. The warm reaction mixture was filtered through a short plug of silica and washed with toluene (400 mL). The solvent was removed under reduced pressure yielding **4a** as a red solid (9.43 g, 21.7 mmol, %, Lit.:<sup>[11]</sup> 61%<sup>7</sup>).

<sup>1</sup>H NMR (600 MHz, CDCl<sub>3</sub>) δ = 7.87 (d, <sup>3</sup>J = 8.7 Hz, 4H, *H*-c), 7.64 (d, <sup>3</sup>J = 8.7 Hz, 4H, *H*-b) ppm.

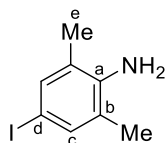
<sup>13</sup>C{<sup>1</sup>H} NMR (151 MHz, CDCl<sub>3</sub>) δ = 151.8 (*C*-a), 138.6 (*C*-c), 124.7 (*C*-b), 98.3 (*C*-d) ppm.

IR (ATR):  $\tilde{\nu}$  = 3067 (w), 2359 (w), 2111 (w), 1640 (w), 1574 (m), 1560 (m), 1470 (m), 1393 (m), 1296 (m), 1279 (m), 1096 (m), 1051 (m), 1002 (m), 834 (s), 810 (s), 774 (m), 713 (s) cm<sup>-1</sup>.

HRMS (APCI) *m/z*: [M + H]<sup>+</sup> calcd for [C<sub>12</sub>H<sub>8</sub>N<sub>2</sub>I<sub>2</sub> + H]<sup>+</sup> 434.88497; found 434.88462.

**Mp**: 244 °C (Lit.:<sup>[11]</sup> 210 °C).

**R<sub>f</sub>** = 0.75 (*n*-hexane/DCM 3:1).

4-Iodo-2,6-dimethylaniline<sup>[12]</sup> (**S3**)

This reaction was not performed under inert conditions.

2,6-Dimethylaniline (31.5 mL, 31.0 g, 212 mmol, 1.00 equiv) was added to diethyl ether (200 mL). Iodine (59.2 g, 233 mmol, 1.10 equiv) and a sat. NaHCO<sub>3</sub> solution (600 mL) were added. The resulting biphasic mixture was stirred vigorously. After 5 h, the reaction mixture was diluted with a saturated sodium thiosulfate solution (300 mL). The phases were separated and the aqueous phase was extracted with diethyl ether (2 × 100 mL). The combined organic phases were washed with water (200 mL), dried over MgSO<sub>4</sub> and filtered. The solvent was evaporated yielding **S3** as a brown oil, which solidified upon standing at 20 °C (49.7 g, 201 mmol, 95%, Lit.:<sup>[12]</sup> 99%).

<sup>1</sup>H NMR (600 MHz, CDCl<sub>3</sub>) δ = 7.24 (s, 2 H, *H*-c), 3.58 (s, 2 H, NH<sub>2</sub>-a), 2.13 (s, 6 H, *H*-e) ppm.

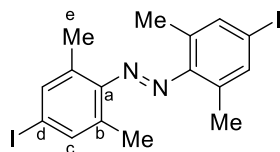
<sup>13</sup>C{<sup>1</sup>H} NMR (151 MHz, CDCl<sub>3</sub>) δ = 142.6 (*C*-a), 136.5 (*C*-c), 124.1 (*C*-b), 79.1 (*C*-d), 17.3 (*C*-e) ppm.

IR:  $\tilde{\nu}$  = 3402 (m), 3199 (m), 1625 (m), 1582 (s), 1270 (m), 1222 (w), 1034 (w), 857 (s), 730 (s) cm<sup>-1</sup>.

HRMS (EI, 70 eV) *m/z* (%): [M]<sup>+</sup> calcd for [C<sub>8</sub>H<sub>10</sub>I]<sup>+</sup> 246.98525; found 246.98532 (100).

**Mp**: 48 °C.

<sup>7</sup> In this report, the product was obtained by oxidation using copper chloride.

*(E)*-1,2-Bis(4-iodo-2,6-dimethylphenyl)diazene<sup>[13]</sup> (**4b**)

This reaction was not performed under inert conditions.

4-Iodo-2,6-dimethylaniline (**S3**) (3.00 g, 12.1 mmol, 1.00 equiv) was dissolved in toluene (300 mL).  $\text{MnO}_2$  (26.3 g, 302 mmol, 25.0 equiv) was added and the solution was heated up to 130 °C for 3 h while vigorously stirring. After allowing the solution to cool to ambient temperature, it was filtered through a pad consisting of a layer of Celite<sup>®</sup> followed by silica. This assembly was washed with HCl (1 M, 20 mL), sat. sodium hydrogen carbonate (100 mL) and brine (100 mL). The organic phase was dried over  $\text{MgSO}_4$ , filtered and the solvent was evaporated. The crude product was purified by column chromatography (eluent: cyclohexane) yielding **4b** as an orange solid (593 mg, 1.21 mmol, 22%, Lit.:<sup>[13]</sup> 20%).

<sup>1</sup>H NMR (500 MHz,  $\text{CDCl}_3$ )  $\delta$  = 7.52 (s, 4 H, *H*-c), 2.36 (s, 12 H, *H*-e) ppm.

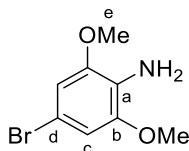
<sup>13</sup>C{<sup>1</sup>H} NMR (151 MHz,  $\text{CDCl}_3$ )  $\delta$  = 150.6 (*C*-a), 138.2 (*C*-b), 133.6 (*C*-c), 94.7 (*C*-d), 19.5 (*C*-e) ppm.

IR:  $\tilde{\nu}$  = 2964 (w), 1616 (w), 1553 (m), 1435 (m), 1398 (w), 1244 (m), 1184 (w), 1033 (w), 880 (s), 864 (s), 843 (s)  $\text{cm}^{-1}$ .

HRMS (APCI):  $m/z$  =  $[M + H]^+$  calcd for  $[\text{C}_{16}\text{H}_{16}\text{I}_2\text{N}_2 + \text{H}]^+$  490.94757, found 490.94704.

Mp: 130 °C.

R<sub>f</sub>: 0.40 (cyclohexane).

4-Bromo-2,6-dimethoxyaniline<sup>[14]</sup> (**S4**)

This reaction was not performed under inert conditions.

A solution of bromine (1.00 mL, 3.12 g, 1.95 mmol, 1.00 equiv) in chloroform (50 mL) was added to a solution of 2,6-dimethoxyaniline (3.06 g, 2.00 mmol, 1.03 equiv) in chloroform (50 mL) at 0 °C over the course of 1 h. Afterwards, the solution was warmed up to 21 °C and stirred for additional 14 h. Then, NaOH (2 M) was added to adjust the pH to 11. The water phase was extracted with ethyl acetate (3 × 100 mL). The combined organic phases were washed with water (100 mL), brine (100 mL), dried over  $\text{MgSO}_4$  and filtered. The crude product was purified by column chromatography (eluent: *n*-hexane/DCM 95:5) to yield **S4** as a colorless solid (3.66 g, 1.58 mmol, 79%, Lit.:<sup>[14]</sup> 77%)

<sup>1</sup>H NMR (600 MHz,  $\text{CDCl}_3$ )  $\delta$  = 6.65 (s, 2H, *H*-c), 3.83 (s, 6H, *H*-e), 3.77 (s, 2H,  $\text{NH}_2$ -a) ppm.

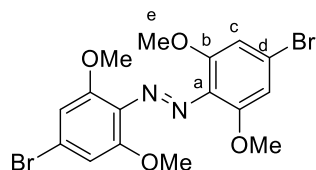
<sup>13</sup>C{<sup>1</sup>H} NMR (151 MHz,  $\text{CDCl}_3$ )  $\delta$  = 147.8 (*C*-a), 124.7 (*C*-b), 108.8 (*C*-d), 107.8 (*C*-c), 56.2 (*C*-e) ppm.

IR (ATR):  $\tilde{\nu}$  = 3369 (w), 2926 (w), 1732 (w), 1604 (m), 1503 (m), 1450 (s), 1375 (m), 1297 (s), 1202 (m), 1184 (m), 1155 (s), 1054 (s), 848 (s), 811 (m), 797 (w)  $\text{cm}^{-1}$ .

HRMS (EI, 70 eV)  $m/z$  (%):  $[M]^+$  calcd for  $[\text{C}_8\text{H}_{10}\text{NO}_2\text{Br}]^+$  230.98894; found 230.98907 (95), 233.0 (100).

Mp: 74 °C (Lit: <sup>[14]</sup> 75-76 °C).

R<sub>f</sub> = 0.45 (*n*-hexane: ethyl acetate 1:1).

*(E)*-1,2-Bis(4-bromo-2,6-dimethoxyphenyl)diazene<sup>[15]</sup> (**S5**)

This reaction was not performed under inert conditions.

4-Bromo-2,6-dimethoxyaniline (**S4**) (2.32 g, 10.0 mmol, 1.00 equiv) was dissolved in toluene (100 mL).  $\text{MnO}_2$  (10.9 g, 125 mmol, 12.0 equiv) was added and the solution was heated up to 130 °C for 3 h while vigorously stirring. After allowing the solution to cool to ambient temperature, it was filtered through a pad consisting of a layer of Celite<sup>®</sup> followed by silica. This assembly was washed with HCl (1 M, 20 mL), sat. sodium hydrogen carbonate (20 mL) and brine (20 mL). The organic phase was dried over  $\text{MgSO}_4$ , filtered and the solvent was evaporated. The crude product was purified by column chromatography (eluent: DCM) to obtain **S5** as an orange solid (1.20 g, 2.61 mmol, 52%, Lit.:<sup>[15]</sup> 20%).

<sup>1</sup>H NMR (600 MHz,  $\text{CDCl}_3$ )  $\delta$  = 6.82 (s, 4H, *H*-c), 3.84 (s, 12H, *H*-e); *Z*-Isomer: 6.60 (s, 4H, *H*-c), 3.66 (s, 12H, *H*-e) ppm.

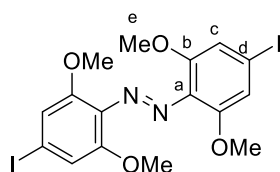
<sup>13</sup>C{<sup>1</sup>H} NMR (151 MHz,  $\text{CDCl}_3$ )  $\delta$  = 152.90 (*C*-a), 133.22 (*C*-b), 123.05 (*C*-c), 109.00 (*C*-c), 56.94 (*C*-e) ppm.

IR (ATR):  $\tilde{\nu}$  = 2924 (w), 1731 (w), 1603 (s), 1564 (m), 1514 (w), 1471 (m), 1450 (m), 1398 (m), 1230 (s), 1157 (w), 1117 (s), 1015 (w), 848 (m), 830 (m), 801 (m), 757 (m).  $\text{cm}^{-1}$ .

HRMS (EI, 70 eV)  $m/z$  (%):  $[\text{M}]^+$  calcd for  $[\text{C}_{16}\text{H}_{16}\text{N}_2\text{O}_4\text{Br}_2]^+$  457.94713; found 457.94716 (20), 243.0 (100).

**Mp**: 211 °C.

**R<sub>f</sub>** = 0.50 (*n*-hexane/ethyl acetate 1:1).

*(E)*-1,2-Bis(4-iodo-2,6-dimethoxyphenyl)diazene (**4c**)

A vial was charged with 4,4'-dibromo-2,2',6,6'-tetrakis(methoxy)-azobenzene (**S5**) (230 mg, 500  $\mu\text{mol}$ , 2.00 equiv), copper iodide (9.52 mg, 50.0  $\mu\text{mol}$ , 5.00 mol%) and sodium iodide (300 mg, 2.00 mmol, 4.00 equiv). *N,N'*-dimethylethylenediamine (10.8  $\mu\text{L}$ , 0.100 mmol, 10.0 mol%) and dry dioxane (6 mL) were added. The reaction mixture was stirred at 110 °C for 48 h. After cooling down to 21 °C, the suspension was diluted with an aqueous sodium hydrogen carbonate solution (2 M, 50 mL), poured into water (200 mL), and extracted with DCM (3  $\times$  150 mL). The combined organic phases were washed with hydrochloric acid (1 M, 100 mL) and brine (100 mL). After drying over  $\text{MgSO}_4$  and filtration, the solvent was removed under reduced pressure. The product **4c** was obtained in 90% purity with 10% mono-brominated species left. (260 mg, 469  $\mu\text{mol}$ , 94%).

<sup>1</sup>H NMR (600 MHz,  $\text{CDCl}_3$ )  $\delta$  = 7.00 (s, 4H, *H*-c), 3.83 (s, 12H, *H*-e) ppm.

<sup>13</sup>C{<sup>1</sup>H} NMR (151 MHz,  $\text{CDCl}_3$ )  $\delta$  = 152.61 (*C*-a), 134.02 (*C*-b), 115.08 (*C*-c), 94.05 (*C*-d), 56.97 (*C*-e) ppm.

IR (ATR):  $\tilde{\nu}$  = 2933 (w), 1558 (s), 1449 (m), 1395 (s), 1230 (s), 1158 (w), 1115 (s), 1018 (w), 828 (s), 803 (m), 742 (w)  $\text{cm}^{-1}$ .

**HRMS** (EI, 70 eV)  $m/z$  (%):  $[M]^+$  calcd for  $[C_{16}H_{16}I_2N_2O_4]^+$  553.91940; found 553.91926 (25), 248.0 (100).

**Mp**: 265°C.

$R_f$  = 0.65 (*n*-hexane/ethyl acetate 1:1).

4-Iodo-2,6-difluoro-aniline<sup>[16]</sup> (**S6**)



This reaction was not performed under inert conditions.

A solution of *N*-iodosuccinimide (4.95 g, 22.0 mmol, 1.10 equiv) in DMF (25 mL) was added dropwise to a solution of 2,6-difluoroaniline (2.15 g, 20.0 mmol, 1.00 equiv) and *p*-toluenesulfonic acid (760 mg, 4.00 mmol, 20 mol%) in DMF (35 mL) at 5 °C. The mixture was stirred for 2.5 h at 21 °C, diluted with ethyl acetate (250 mL), and thoroughly washed with brine (4 × 150 mL). The phases were separated. The organic phase was dried over  $MgSO_4$ , filtered, and concentrated under reduced pressure to give **S6** as a light brown solid (5.10 g, 19.8 mmol, 99%, Lit.:<sup>[16]</sup> 99%).

**<sup>1</sup>H NMR** (600 MHz,  $CDCl_3$ )  $\delta$  = 7.46 (d,  $^3J$  = 8.0 Hz, 2H, *H*-c), 3.76 (s, 2H,  $NH_2$ -a) ppm.

**<sup>13</sup>C{<sup>1</sup>H} NMR** (151 MHz,  $CDCl_3$ )  $\delta$  = 151.92 (dd,  $^1J$  = 245.4 Hz,  $^4J$  = 8.1 Hz, *C*-b), 124.3 (t,  $^2J$  = 16.2 Hz, *C*-a), 120.5 – 120.0 (m, *C*-c), 74.28 (t,  $^3J$  = 10.0 Hz, *C*-d) ppm.

**<sup>19</sup>F NMR** (565 MHz,  $CDCl_3$ )  $\delta$  -119.4 (d,  $^3J$  = 9.2 Hz, *F*-b) ppm.

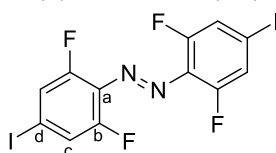
**IR** (ATR):  $\tilde{\nu}$  = 3458 (m), 3373 (m), 1631 (s), 1593 (m), 1578 (w), 1497 (s), 1416 (s), 1288 (s), 1202 (w), 1152 (s), 1123 (w), 984 (w), 951 (s), 860 (m), 836 (s), 746 (m)  $cm^{-1}$ .

**HRMS** (EI, 70 eV)  $m/z$  (%):  $[M]^+$  calcd for  $[C_6H_4IN_2F_2]^+$  254.93498; found 254.93498 (100), 128.1 (95).

**Mp**: 81°C.

$R_f$  = 0.70 (*n*-hexane/ethyl acetate 1:1).

(*E*)-1,2-bis(2,6-difluoro-4-iodophenyl)diazene<sup>[17]</sup> (**4d**)



This reaction was not performed under inert conditions.

To a solution of 4-iodo-2,6-difluoroaniline (**S6**) (637 mg, 2.50 mmol, 1.00 equiv) in DCM (40 mL) was added 1,8-diazabicyclo[5.4.0]undec-7-ene (761 mg, 5.00 mmol, 2.00 equiv). The solution was stirred at 21 °C for 5 min before being cooled down to -78 °C. *N*-Chlorosuccinimide (668 mg, 5.00 mmol, 2.00 equiv) was added to the reaction mixture. The orange solution was stirred for 30 min at -78 °C, and a saturated  $NaHCO_3$  solution (50 mL) was added. The layers were separated. The organic layer was washed with water (50 mL) and HCl (1 M, 50 mL). The combined organic layers were dried over  $MgSO_4$ , filtered and concentrated under reduced pressure. The residue was purified by silica gel flash chromatography (eluent: gradient *n*-hexane/ethyl acetate 1:0 → 1:1). **4d** was obtained as a red solid (474 mg, 937  $\mu$ mol, 75%, Lit.:<sup>[17]</sup> 63%).

**<sup>1</sup>H NMR** (600 MHz,  $CDCl_3$ )  $\delta$  = 7.46 (d,  $^3J$  = 8.0 Hz, 4H, *H*-c) ppm.

**<sup>13</sup>C{<sup>1</sup>H} NMR** (151 MHz,  $CDCl_3$ )  $\delta$  = 155.00 (dd,  $^1J$  = 267.2 Hz,  $^4J$  = 4.4 Hz, *C*-d), 131.5 (t,  $^2J$  = 9.3 Hz, *C*-a), 122.7 (dd,  $^2J$  = 22.6,  $^4J$  = 3.9 Hz, *C*-c), 94.9 (t,  $^3J$  = 10.4 Hz, *C*-d) ppm.

**<sup>19</sup>F NMR** (565 MHz,  $CDCl_3$ )  $\delta$  = -119.44 (d,  $^4J$  = 9.2 Hz, *F*-b) ppm.

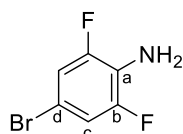
**IR** (ATR):  $\tilde{\nu}$  = 1595 (s), 1566 (s), 1445 (w), 1412 (s), 1289 (w), 1203 (m), 1046 (s), 866 (m), 855 (m), 838 (s), 747 (m)  $\text{cm}^{-1}$ .

**HRMS** (EI, 70 eV)  $m/z$  (%):  $[M]^+$  calcd for  $[\text{C}_{12}\text{H}_4\text{F}_4\text{I}_2\text{N}_2]^+$  505.83946; found 505.83960 (12), 112.1 (100).

**Mp**: 201 °C.

**R<sub>f</sub>** = 0.50 (*n*-hexane/ethyl acetate 1:1).

4-Bromo-2,6-difluoroaniline[18] (**S7**)



This reaction was not performed under inert conditions.

To a solution of 2,6-difluoroaniline (12.9 g, 100 mmol, 1.00 equiv) in acetonitrile (200 mL) was added a solution of *N*-bromosuccinimide (17.8 g, 100 mmol, 1.00 equiv) in acetonitrile (100 mL) at 0 °C dropwise over a duration of 1h. The mixture was stirred overnight while warming up to 21 °C, and then diluted with water (800 mL). The product was extracted with ethyl acetate (3 × 100 mL). The combined organic phases were dried over  $\text{MgSO}_4$ , filtered, and concentrated under reduced pressure. The crude residue was purified by column chromatography over silica gel (eluent: *n*-hexane/DCM, 4:1) to yield **S7** as a colorless solid (17.2 g, 99.0 mmol, 99%, Lit.: [18] 99%).

**<sup>1</sup>H NMR** (600 MHz,  $\text{CDCl}_3$ )  $\delta$  = 7.02 (d,  $^3J$  = 7.8 Hz, 2H, *H*-c), 3.73 (s, 2H,  $\text{NH}_2$ -a) ppm.

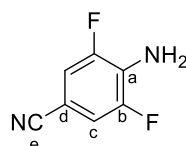
**<sup>13</sup>C{<sup>1</sup>H} NMR** (151 MHz,  $\text{CDCl}_3$ )  $\delta$  = 151.76 (dd,  $^1J$  = 244.2,  $^4J$  = 8.7 Hz, *C*-b), 123.52 (t,  $^2J$  = 16.1 Hz, *C*-a), 115.17 – 114.21 (m, *C*-c), 107.09 (t,  $^3J$  = 11.6 Hz, *C*-d) ppm.

**<sup>19</sup>F NMR** (565 MHz,  $\text{CDCl}_3$ )  $\delta$  -130.69 (d,  $^4J$  = 6.3 Hz, *F*-b) ppm.

**Mp**: 66 °C.

**R<sub>f</sub>**: 0.42 (*n*-hexane/DCM 4:1).

4-Amino-3,5-difluorobenzonitrile[19] (**S8**)



A mixture of copper(I) cyanide (29.3 g, 325 mmol, 1.70 equiv) and 4-bromo-2,6-difluoroaniline (**S7**) (39.5 g, 190 mmol, 1.00 equiv) in *N*-methyl-2-pyrrolidone (120 mL) was stirred under a nitrogen atmosphere at 204 °C for 4 h. After cooling to 30 °C, the resulting mixture was poured into aqueous ammonia until a white precipitate was formed. The suspension was extracted with toluene (5 × 100 mL). The combined organic phases were washed with water (100 mL), brine (100 mL), dried over  $\text{MgSO}_4$  and filtered. The solvent was removed *in vacuo*. The crude product was dissolved in DCM and purified by column chromatography (eluent: DCM/hexane 1:1). **S8** was obtained as a colorless solid (20.5 g, 133 mmol, 70%, Lit.: [19] 87%).

**<sup>1</sup>H NMR** (600 MHz,  $\text{CDCl}_3$ )  $\delta$  = 7.14 (dd,  $^3J$  = 6.0,  $^4J$  = 2.3 Hz, 2H, *H*-c), 4.27 (s, 2H,  $\text{NH}_2$ -a) ppm.

**<sup>13</sup>C{<sup>1</sup>H} NMR** (151 MHz,  $\text{CDCl}_3$ )  $\delta$  = 150.66 (dd,  $^1J$  = 243.5 Hz,  $^4J$  = 9.1 Hz, *C*-b), 129.75 (t,  $^2J$  = 15.7 Hz, *C*-a), 118.05 (t,  $^5J$  = 3.4 Hz, *C*-e), 115.60 (dd,  $^2J$  = 17.5,  $^4J$  = 7.1 Hz, *C*-c), 98.47 (t,  $^3J$  = 11.1 Hz, *C*-d) ppm.

**<sup>19</sup>F NMR** (565 MHz,  $\text{CDCl}_3$ )  $\delta$  = -130.76 (dd,  $^4J$  = 6.1 Hz,  $^6J$  = 2.2 Hz, *F*-b) ppm.

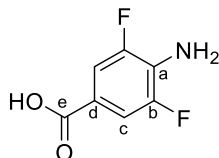
**IR** (ATR):  $\tilde{\nu}$  = 3376 (w), 3313 (w), 2224 (m), 1650 (w), 1608 (w), 1587 (m), 1523 (m), 1443 (s), 1338 (m), 1163 (s), 977 (s), 875 (s), 862 (m), 727 (s)  $\text{cm}^{-1}$ .

**HRMS** (EI, 70 eV)  $m/z$  (%):  $[M]^+$  calcd for  $[\text{C}_7\text{H}_4\text{N}_2\text{F}_2]^+$  154.03371; found 154.03383 (100).

**Mp:** 112 °C.

**R<sub>f</sub>:** 0.40 (*n*-hexane/DCM 1:2).

4-Amino-3,5-difluorobenzoic acid[20] (**S9**)



This reaction was not performed under inert conditions.

A mixture of 4-amino-3,5-difluorobenzonitrile (**S8**) (5.00 g, 32,4 mmol, 1.00 equiv) was dissolved in a 25 wt% solution of KOH in water (100 mL). The mixture was heated up to 110 °C for 19 h. After cooling down to 21 °C, the aqueous phase was acidified to pH = 2 with HCl (2 M) and extracted with ethyl acetate (2 × 100 mL). The combined organic extracts were washed with water (75 mL), brine (75 mL), dried over MgSO<sub>4</sub> and filtered. The solvent was removed under reduced pressure to obtain **S9** as a slightly yellowish solid (4.99 g, 28.8 mmol, 89%, Lit.: [20] 87%).

<sup>1</sup>H NMR (600 MHz, DMSO-*d*<sub>6</sub>) δ = 7.39 (dd, <sup>3</sup>J = 7.2 Hz, <sup>4</sup>J = 2.4 Hz, 2H, *H*-c), 6.04 (s, 2H, NH<sub>2</sub>-a) ppm.

<sup>13</sup>C{<sup>1</sup>H} NMR (151 MHz, DMSO-*d*<sub>6</sub>) δ = 166.12 (C-e), 149.80 (dd, <sup>1</sup>J = 239.6, <sup>4</sup>J = 9.5 Hz, C-b), 130.61 (t, <sup>2</sup>J = 16.7 Hz, C-a), 112.31 (dd, <sup>2</sup>J = 15.8 Hz, <sup>4</sup>J = 5.9 Hz, C-c), 59.83 (C-d) ppm.

<sup>19</sup>F NMR (565 MHz, DMSO-*d*<sub>6</sub>) δ -131.62 (d, <sup>4</sup>J = 7.2 Hz, F-b) ppm.

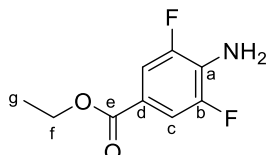
IR (ATR):  $\tilde{\nu}$  = 3397 (w), 1683 (m), 1628 (s), 1587 (m), 1538 (w), 1454 (m), 1422 (s), 1341 (s), 1277 (s), 1243 (m), 1145 (m), 1082 (w), 953 (m), 889 (m), 765 (s), 719 (s) cm<sup>-1</sup>.

HRMS (EI, 70 eV) *m/z* (%): [M]<sup>+</sup> calcd for [C<sub>7</sub>H<sub>5</sub>NO<sub>2</sub>F<sub>2</sub>]<sup>+</sup> 173.02829; found 173.02830 (75), 156.1 (100).

**Mp:** 171 °C.

**R<sub>f</sub>:** 0.90 (ethyl acetate).

Ethyl 4-amino-3,5-difluorobenzoate[20] (**S10**)



This reaction was not performed under inert conditions.

**S9** (2.42 g, 14.0 mmol) was dissolved in EtOH (50 mL) and H<sub>2</sub>SO<sub>4</sub> (1 mL), and refluxed for 5 h. The mixture was neutralized (pH = 7) with a saturated NaHCO<sub>3</sub> solution and extracted with DCM (3 × 50 mL). The combined organic phases were dried over MgSO<sub>4</sub>, filtered, and concentrated under reduced pressure to yield **S10** as a pale brown solid (2.74 g, 13.6 mmol, 97%, Lit.: [20] 94%).

<sup>1</sup>H NMR (600 MHz, CDCl<sub>3</sub>) δ = 7.53 (dd, *J* = 7.1, 2.2 Hz, 2H, *H*-c), 4.33 (q, <sup>3</sup>J = 7.1 Hz, 2H, *H*-f), 4.13 (s, 2H, NH<sub>2</sub>-a), 1.36 (t, <sup>3</sup>J = 7.1 Hz, 3H, *H*-g) ppm.

<sup>13</sup>C{<sup>1</sup>H} NMR (151 MHz, CDCl<sub>3</sub>) δ = 165.30 (t, <sup>5</sup>J = 3.5 Hz, C-e), 150.80 (dd, <sup>1</sup>J = 240.8 Hz, <sup>4</sup>J = 7.9 Hz, C-b), 128.92 (t, <sup>3</sup>J = 16.1 Hz, C-a), 118.72 (t, <sup>4</sup>J = 8.2 Hz, C-d), 113.13 – 112.08 (m, C-c), 61.20 (C-f), 14.45 (C-g) ppm.

<sup>19</sup>F NMR (565 MHz, CDCl<sub>3</sub>) δ -132.93 (dd, <sup>4</sup>J = 7.2 Hz, <sup>6</sup>J = 2.3 Hz, F-b) ppm.

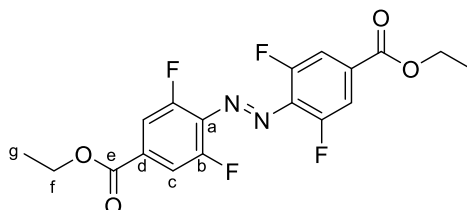
IR (ATR):  $\tilde{\nu}$  = 3505 (w), 3368 (m), 1697 (s), 1629 (s), 1585 (m), 1531 (m), 1477 (w), 1444 (m), 1397 (m), 1370 (m), 1339 (s), 1270 (s), 1222 (s), 1133 (m), 1089 (s), 1027 (s), 946 (s), 881 (m), 760 (m) cm<sup>-1</sup>.

HRMS (EI, 70 eV) *m/z* (%): [M]<sup>+</sup> calcd for [C<sub>9</sub>H<sub>9</sub>NO<sub>2</sub>F<sub>2</sub>]<sup>+</sup> 201.0599; found 201.05932 (15), 156.1 (100).

**R<sub>f</sub>:** 0.30 (*n*-hexane/DCM 1:1).



(*E*)-4,4'-(Diazene-1,2-diyl)bis(3,5-difluorobenzoic acid)<sup>[17]</sup> (**S11**)



This reaction was not performed under inert conditions.

To a solution of 4-iodo-2,6-difluoroaniline (**S10**) (637 mg, 2.50 mmol, 1.00 equiv) in DCM (40 mL) was added 1,8-diazabicyclo[5.4.0]undec-7-ene (761 mg, 5.00 mmol, 2.00 equiv). The solution was stirred at 21 °C for 5 min before being cooled down to -78 °C. *N*-Chlorosuccinimide (668 mg, 5.00 mmol, 2.00 equiv) was added to the reaction mixture. The orange solution was stirred for 30 min at -78 °C, and a saturated NaHCO<sub>3</sub> solution (50 mL) was added. The layers were separated. The organic layer was washed with water (50 mL) and HCl (1 M, 50 mL). The combined organic layers were dried over MgSO<sub>4</sub>, filtered and concentrated under reduced pressure. The residue was purified by silica gel flash chromatography (eluent: gradient *n*-hexane/DCM 1:0 → 1:1) to obtain **S11** as a red solid (402 mg, 1.01 mmol, 81%, Lit.:<sup>[17]</sup> 62%).

<sup>1</sup>H NMR (600 MHz, CDCl<sub>3</sub>) δ = 7.75 (d, <sup>3</sup>J = 8.9 Hz, 4H, *H*-c), 4.43 (q, <sup>3</sup>J = 7.1 Hz, 4H, *H*-f), 1.43 (t, <sup>3</sup>J = 7.1 Hz, 6H, *H*-g) ppm.

<sup>13</sup>C{<sup>1</sup>H} NMR (151 MHz, CDCl<sub>3</sub>) δ = 163.84 (*C*-e), 155.17 (dd, <sup>1</sup>J = 262.6 Hz, <sup>4</sup>J = 3.8 Hz, *C*-b), 134.31 (t, <sup>3</sup>J = 10.1 Hz, *C*-a), 133.89 (t, <sup>4</sup>J = 9.2 Hz, *C*-d), 114.07 (dd, <sup>2</sup>J = 21.7, <sup>4</sup>J = 3.9 Hz, *C*-c), 62.34 (*C*-f), 14.36 (*C*-g) ppm.

<sup>19</sup>F NMR (565 MHz, CDCl<sub>3</sub>) δ = -120.06 (d, <sup>4</sup>J = 10.4 Hz, *F*-b) ppm.

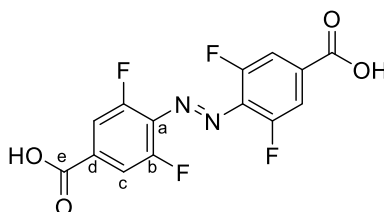
IR (ATR):  $\tilde{\nu}$  = 1721 (m), 1573 (m), 1434 (m), 1369 (s), 1330 (m), 1238 (m), 1192 (m), 1089 (w), 1052 (s), 1017 (s), 886 (s), 767 (s), 752 (s) cm<sup>-1</sup>.

HRMS (EI, 70 eV) *m/z* (%): [M]<sup>+</sup> calcd for [C<sub>18</sub>H<sub>14</sub>N<sub>2</sub>O<sub>4</sub>F<sub>2</sub>]<sup>+</sup> 398.08842; found 398.08876 (15), 101.1 (100).

Mp: 147°C.

R<sub>f</sub>: 0.35 (*n*-hexane/DCM 1:1).

(*E*)-4,4'-(Diazene-1,2-diyl)bis(3,5-difluorobenzoic acid)<sup>[20]</sup> (**6**)



This reaction was not performed under inert conditions.

Diethyl 4,4'-(diazene-1,2-diyl)-bis(3,5-difluorobenzoate) (**S11**) (1.19 g, 3.00 mmol, 1.00 equiv) was dissolved in THF (40 mL) and KOH (673 mg, 12.0 mmol, 4.00 equiv) dissolved in H<sub>2</sub>O (40 mL) was added. The reaction mixture was stirred for 1 h at 21 °C and acidified with HCl (1 M) until a precipitate formed. The precipitate was filtered and dried in a vacuum oven at 50°C to yield the desired product **6** (924 mg, 2.70 mmol, 90 %, Lit.:<sup>[20]</sup> 94%) as a pink solid.

<sup>1</sup>H NMR (600 MHz, DMSO-*d*<sub>6</sub>) δ = 7.80 (d, <sup>3</sup>J = 9.3 Hz, 4H, *H*-c) ppm.

<sup>13</sup>C{<sup>1</sup>H} NMR (151 MHz, DMSO-*d*<sub>6</sub>) δ = 164.64 (*C*-e), 154.35 (dd, <sup>1</sup>J = 260.9 Hz, <sup>4</sup>J = 3.8 Hz, *C*-b), 135.46 (t, <sup>3</sup>J = 9.3 Hz, *C*-d), 133.00 (t, <sup>2</sup>J = 10.3 Hz, *C*-a), 113.97 (dd, <sup>2</sup>J = 21.3 Hz, <sup>4</sup>J = 3.6 Hz, *C*-c) ppm.

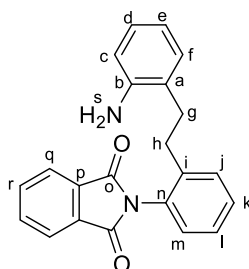
<sup>19</sup>F NMR (565 MHz, DMSO-*d*<sub>6</sub>)  $\delta$  = -120.06 (d, <sup>4</sup>*J* = 10.4 Hz, *F*-b) ppm.

IR (ATR):  $\tilde{\nu}$  = 2871 (br), 1693 (s), 1577 (s), 1481 (m), 1436 (m), 1414 (m), 1259 (s), 1195 (m), 1054 (s), 893 (s), 879 (m), 773 (s), 729 (m) cm<sup>-1</sup>.

HRMS (EI, 70 eV) *m/z* (%): [M]<sup>+</sup> calcd for [C<sub>14</sub>H<sub>6</sub>N<sub>2</sub>O<sub>4</sub>F<sub>4</sub>]<sup>+</sup> 342.02582; found 342.02604 (5), 101.1 (100).

Mp: >300 °C.

2-(2-(2-Aminophenethyl)phenyl)isoindoline-1,3-dione[21] (**S12**)



This reaction was not performed under inert conditions.

Phthalic anhydride (2.22 g, 15.0 mmol, 1.00 equiv) and 2,2'-ethylenedianiline (3.18 g, 15.0 mmol, 1.00 equiv) were dissolved in acetic acid (60 mL). The mixture was vigorously stirred for 3 h at 118 °C. After cooling down to 25 °C, water (40 mL) was added and the formed precipitate was filtered. The precipitate was recrystallized from ethanol at 78 °C. The solids were discarded and the filtrate was concentrated. The residue was re-dissolved in DCM (20 mL) and washed with water (20 mL). The aqueous phase was extracted with DCM (3 × 20 mL). Hydrogen chloride (1 M, 20 mL) was added to the combined organic layers. The obtained thick slurry was stirred for 1 h at 0 °C. The precipitate was filtered, washed with water (20 mL) and suspended in DCM (20 mL). An aqueous solution of sodium carbonate was added (2 M, 20 mL). The mixture was stirred for 1 h at 25 °C, until everything was fully dissolved. An aqueous solution of sodium hydroxide (2 M, 20 mL) was added and the phases were separated. The organic phase was dried over MgSO<sub>4</sub>, filtered and concentrated yielding the product **S12** as yellow solid (1.40 g, 4.09 mmol, 41%, Lit.: [21] 52%).

<sup>1</sup>H NMR (600 MHz, CDCl<sub>3</sub>)  $\delta$  = 7.99 – 7.92 (m, 2H, *H*-q), 7.84 – 7.78 (m, 2H, *H*-r), 7.46 – 7.33 (m, 3H, *H*-k/l/m), 7.21 (dd, <sup>3</sup>*J* = 7.5 Hz, <sup>4</sup>*J* = 1.7 Hz, 1H, *H*-j), 6.98 (ddt, <sup>3</sup>*J* = 8.2 Hz, <sup>4</sup>*J* = 4.2 Hz, 1.7 Hz, 2H, *H*-d/f), 6.66 (td (<sup>3</sup>*J* = 7.5 Hz, <sup>4</sup>*J* = 1.2 Hz, 1H, *H*-e), 6.56 (dd, <sup>3</sup>*J* = 8.2 Hz, <sup>4</sup>*J* = 1.2 Hz, 1H, *H*-c), 3.54 (s, br, 2H, *H*-s), 2.84 – 2.72 (m, 4H, *H*-g/h) ppm.

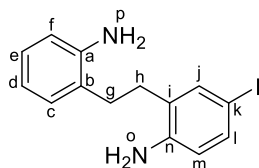
<sup>13</sup>C{<sup>1</sup>H} NMR (151 MHz, CDCl<sub>3</sub>)  $\delta$  = 168.1 (*C*-o), 144.5 (*C*-b), 140.4 (*C*-n), 134.6 (*C*-r), 132.1 (*C*-p), 130.5 (*C*-l), 129.8 (*C*-i), 129.7 (*C*-k), 129.4 (*C*-f), 127.5 (*C*-m), 127.4 (*C*-d), 125.5 (*C*-l), 124.1 (*C*-a), 124.0 (*C*-q), 118.8 (*C*-e), 115.7 (*C*-c), 32.3 (*C*-g), 31.2 (*C*-h) ppm.

IR (ATR):  $\tilde{\nu}$  = 3346 (w, br), 2937 (w), 2359 (w), 1708 (s), 1605 (m), 1492 (m), 1466 (m), 1454 (m), 1378 (s), 1220 (m), 1161 (m), 1109 (m), 1082 (m), 1003 (m), 888 (m), 765 (s), 724 (s) cm<sup>-1</sup>.

HRMS (EI, 70 eV) *m/z* (%): [M]<sup>+</sup> calcd for [C<sub>22</sub>H<sub>18</sub>N<sub>2</sub>O<sub>2</sub>]<sup>+</sup> 342.13628; found 342.13649 (6), 106.1 (100).

Mp: 134 °C.

R<sub>f</sub> = 0.70 (*n*-hexane/DCM 1:1).

2-(2-Aminophenethyl)-4-iodoaniline[21] (**S13**)

This reaction was not performed under inert conditions.

*N*-Iodosuccinimide (1.11 g, 7.46 mmol, 1.00 equiv) was added in one portion to a solution of 2-(2-(2-aminophenethyl)phenyl)isoindoline-1,3-dione (**S12**) (2.55 g, 7.46 mmol, 1.00 equiv) in DMSO (50 mL). After stirring the mixture for 3 h at 23 °C, brine (50 mL) was added and the mixture was extracted with DCM (3 × 30 mL). The combined organic layers were washed with water (50 mL) and brine (3 × 50 mL). The solution was filtered over a short plug of silica and the solvent removed under reduced pressure. The crude iodination product (2.61 g, 5.57 mmol) was dissolved in THF (30 mL) and hydrazine monohydrate (1.67 mL, 33.4 mmol, 6.00 equiv) was added. The mixture was stirred at 64 °C for 2 h. After cooling to 23 °C, the mixture was filtered. The solids were washed with THF (60 mL) and discarded. Water (30 mL) was added to the filtrate. The THF was removed under reduced pressure and the residue was extracted with diethyl ether (3 × 30 mL). The combined organic layers were washed with brine (30 mL), dried over MgSO<sub>4</sub> and filtered. The solvent was removed under reduced pressure. The residue was dissolved in DCM (5 mL) and precipitated with *n*-hexane (5 mL) yielding **S13** as a brownish-yellow solid (1.51 g, 4.47 mmol, 60%, Lit.: [21] 93%).

<sup>1</sup>H NMR (600 MHz, CDCl<sub>3</sub>) δ = 7.36 (ad, <sup>4</sup>J = 2.1 Hz, 1H, *H*-j), 7.30 (dd, <sup>3</sup>J = 8.3 Hz, <sup>4</sup>J = 2.1 Hz, 1H, *H*-l), 7.10 – 7.01 (m, 2H, *H*-c/e), 6.75 (td, <sup>3</sup>J = 7.4 Hz, <sup>4</sup>J = 1.2 Hz, 1H, *H*-d), 6.69 (dd, <sup>3</sup>J = 7.9 Hz, <sup>4</sup>J = 1.2 Hz, 1H, *H*-f), 6.44 (d, <sup>3</sup>J = 8.3 Hz, 1H, *H*-m), 3.60 (s, br, 4H, *H*-o/p), 2.80 – 2.70 (m, 4H, *H*-g/h) ppm.

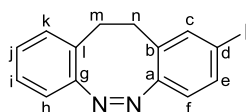
<sup>13</sup>C{<sup>1</sup>H} NMR (151 MHz, CDCl<sub>3</sub>) δ = 144.3 (*C*-a), 144.3 (*C*-n), 138.0 (*C*-j), 136.0 (*C*-l), 129.7 (*C*-c), 129.1 (*C*-i), 127.6 (*C*-e), 126.0 (*C*-b), 119.3 (*C*-d), 118.0 (*C*-m), 116.1 (*C*-f), 80.2 (*C*-k), 31.1 (*C*-g), 30.7 (*C*-h) ppm.

IR (ATR):  $\tilde{\nu}$  = 3353 (w, br), 3021 (w), 2927 (w), 2867 (w), 1715 (m), 1616 (s), 1494 (s), 1448 (s), 1368 (m), 1263 (s), 1159 (m), 1055 (m), 858 (m), 749 (s) cm<sup>-1</sup>.

HRMS (ESI) *m/z*: [M + H]<sup>+</sup> calcd for [C<sub>14</sub>H<sub>15</sub>IN<sub>2</sub> + H]<sup>+</sup> 339.03527; found 339.03462.

Mp: 131 °C.

R<sub>f</sub> = 0.57 (*n*-hexane/DCM 1:1).

*Z*-2-Iodo-11,12-dihydrodibenzo[*c,g*][1,2]diazocine[21] (**7a**)

This reaction was not performed under inert conditions.

A freshly prepared solution of *meta*-chloroperoxybenzoic acid (1.44 g, 8.34 mmol, 70%, 2.00 equiv) in acetic acid (50 mL) was added over the course of 2 h under rapid stirring to a solution of 2,2'-(ethane-1,2-diyl)bis(4-iodoaniline) (**S13**) (988 mg, 2.92 mmol, 1.00 equiv) in acetic acid (100 mL) and DCM (300 mL). After the complete addition, the mixture was stirred for a further 1 h at 25 °C. The solvent was removed under reduced pressure. The crude product was purified by column chromatography on silica gel (eluent: cyclohexane) to afford **7a** as a yellow solid (680 mg, 2.04 mmol, 70%, Lit.: [21] 75%).

<sup>1</sup>H NMR (600 MHz, CDCl<sub>3</sub>) δ = 7.44 (dd, <sup>3</sup>J = 8.3 Hz, <sup>4</sup>J = 1.8 Hz, 1H, *H*-e), 7.34 (d, <sup>4</sup>J = 1.8 Hz, 1H, *H*-c), 7.16 (dd, <sup>3</sup>J = 7.6 Hz, <sup>4</sup>J = 1.4 Hz, 1H, *H*-i), 7.05 (dd, <sup>3</sup>J = 7.6 Hz, <sup>4</sup>J = 1.4 Hz, 1H, *H*-j), 7.00 (dd, <sup>3</sup>J = 7.6 Hz,

$^4J = 1.4$  Hz, 1H, *H-k*), 6.83 (dd,  $^3J = 7.6$  Hz,  $^4J = 1.4$  Hz, 1H, *H-h*), 6.58 (d,  $^3J = 8.3$  Hz, 1H, *H-f*), 3.06 – 2.62 (m, 4H, *H-m/n*) ppm.

$^{13}\text{C}\{^1\text{H}\}$  NMR (151 MHz,  $\text{CDCl}_3$ )  $\delta = 155.5$  (C-g), 155.0 (C-a), 138.4 (C-c), 135.8 (C-e), 130.7 (C-b), 129.9 (C-k), 127.6 (C-l), 127.5 (C-j), 127.1 (C-i), 120.9 (C-f), 118.9 (C-h), 91.9 (C-d), 31.6 (C-m), 31.5 (C-n) ppm.

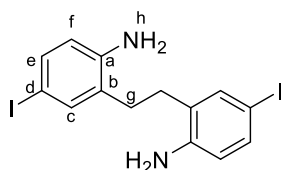
IR (ATR):  $\tilde{\nu} = 2923$  (w, br), 2359 (w), 1737 (s), 1605 (m), 1511 (m), 1453 (w), 1248 (s), 1200 (s), 1163 (s), 1062 (s), 891 (m), 848 (m), 760 (m), 751 (m)  $\text{cm}^{-1}$ .

HRMS (EI, 70 eV)  $m/z$  (%):  $[\text{M}]^+$  calcd for  $[\text{C}_{14}\text{H}_{11}\text{IN}_2]^+$  333.99615; found 333.99606 (7), 178.1 (100).

**Mp:** 131 °C.

**R<sub>f</sub>** = 0.60 (*n*-hexane/DCM 3:1).

#### 2,2'-(Ethane-1,2-diyl)bis(4-iodoaniline)[21] (**S14**)



This reaction was not performed under inert conditions.

*N*-Iodosuccinimide (21.7 g, 96.6 mmol, 2.05 equiv) was added in three portions over 10 min to a solution of 2,2'-ethylenedianiline (10.0 g, 47.1 mmol, 1.00 equiv) in DMSO (125 mL) at 25 °C. After stirring the mixture for 23 h at 25 °C, DCM (100 mL) and water (100 mL) were added. The phases were separated, and the organic layer was washed with an aqueous solution of sodium hydrogen carbonate (2 M, 2 × 100 mL), water (100 mL) and brine (100 mL). The organic phase was dried over  $\text{MgSO}_4$ , filtered and the solvent removed under reduced pressure. **S14** was obtained as a red-brown solid (21.2 g, 45.7 mmol, 97%, Lit.: [21] 87%).

$^1\text{H}$  NMR (600 MHz,  $\text{CDCl}_3$ )  $\delta = 7.34$  – 7.30 (m, 4H, *H-e/f*), 6.48 – 6.44 (m, 2H, *H-c*), 3.64 (s, br, 4H, *H-h*), 2.69 (s, 4H, *H-g*) ppm.

$^{13}\text{C}\{^1\text{H}\}$  NMR (151 MHz,  $\text{CDCl}_3$ )  $\delta = 144.2$  (C-a), 138.0 (C-f), 136.2 (C-e), 128.6 (C-b), 118.1 (C-c), 80.3 (C-d), 30.6 (C-g) ppm.

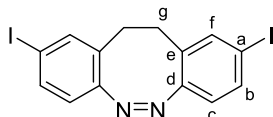
IR (ATR):  $\tilde{\nu} = 3397$  (m, br), 3317 (m), 3219 (w), 2882 (w), 2359 (w), 1626 (m), 1562 (w), 1486 (s), 1470 (m), 1436 (m), 1398 (m), 1297 (s), 1268 (s), 1142 (m), 1096 (m), 1052 (m), 1002 (m), 931 (m), 868 (m), 834 (m), 809 (s), 709 (s)  $\text{cm}^{-1}$ .

HRMS (EI, 70 eV)  $m/z$  (%):  $[\text{M}]^+$  calcd for  $[\text{C}_{14}\text{H}_{14}\text{I}_2\text{N}_2]^+$  463.92410; found 463.92397 (78), 232.0 (100).

**Mp:** 165 °C.

**R<sub>f</sub>** = 0.57 (*n*-hexane/DCM 1:1).

#### (*Z*)-2,9-Diiodo-11,12-dihydrodibenzo[*c,g*][1,2]diazocine[21] (**7b**)



This reaction was not performed under inert conditions.

A freshly prepared solution of *meta*-chloroperoxybenzoic acid (1.75 g, 10.1 mmol, 71%, 2.00 equiv) in acetic acid (125 mL) was added over the course of 3 h under rapid stirring to a solution of 2,2'-(ethane-1,2-diyl)bis(4-iodoaniline) (**S14**) (1.67 g, 3.60 mmol, 1.00 equiv) in acetic acid (100 mL) and DCM (300 mL). After the complete addition, the mixture was stirred for a further 1 h at 25 °C. The solvent was removed under reduced pressure. The crude product was purified by column chromatography on

40

silica gel (eluent: cyclohexane/DCM 1:4) to afford **7b** as a yellow solid (1.23 g, 2.66 mmol, 71%, Lit.: [21] 72%).

**<sup>1</sup>H NMR** (600 MHz, CDCl<sub>3</sub>)  $\delta$  = 7.48 (dd, <sup>3</sup>J = 8.3 Hz, <sup>4</sup>J = 1.8 Hz, 2H, H-b), 7.36 (d, <sup>4</sup>J = 1.8 Hz, 2H, H-f), 6.59 (d, <sup>3</sup>J = 8.3 Hz, 2H, H-c), 2.97 – 2.62 (m, 4H, H-g) ppm.

**<sup>13</sup>C{<sup>1</sup>H} NMR** (151 MHz, CDCl<sub>3</sub>)  $\delta$  = 154.9 (C-d), 138.6 (C-f), 136.1 (C-b), 130.1 (C-e), 120.9 (C-c), 92.4 (C-a), 31.3 (C-g) ppm.

**IR** (ATR):  $\tilde{\nu}$  = 2921 (w), 2358 (w), 1575 (m), 1533 (w), 1467 (m), 1383 (w), 1280 (w), 1156 (m), 1097 (m), 1052 (w), 1002 (m), 979 (w), 959 (w), 918 (w), 891 (m), 878 (m), 801 (s), 714 (m) cm<sup>-1</sup>.

**HRMS** (EI, 70 eV) *m/z* (%): [M]<sup>+</sup> calcd for [C<sub>14</sub>H<sub>10</sub>l<sub>2</sub>N<sub>2</sub>]<sup>+</sup> 459.89280; found 459.89287 (49), 178.1 (100).

**Mp**: 173 °C.

**R<sub>f</sub>** = 0.60 (*n*-hexane/DCM 3:1).

## References

1. *The ACS Style Guide: Effective Communication of Scientific Information*, 3rd ed.; Coghill, A.M., Garson, L.R., Eds.; American Chemical Society: Washington, DC, 2006.
2. Keiper, S.; Vyle, J.S. Reversible Photocontrol of Deoxyribozyme-Catalyzed RNA Cleavage under Multiple-Turnover Conditions. *Angew. Chem. Int. Ed.* **2006**, *45*, 3306-3309, doi:10.1002/anie.200600164.
3. Zhou, M.; Haldar, S.; Franses, J.; Kim, J.-M.; Thompson, D.H. Synthesis and Self-assembly Properties of Acylated Cyclodextrins and Nitrilotriacetic Acid (NTA)-modified Inclusion Ligands for Interfacial Protein Crystallization. *Supramol. Chem.* **2006**, *17*, 101-111, doi:10.1080/10610270412331329005.
4. Liu, D.; Xie, Y.; Shao, H.; Jiang, X. Using Azobenzene-Embedded Self-Assembled Monolayers to Photochemically Control Cell Adhesion Reversibly. *Angew. Chem. Int. Ed.* **2009**, *48*, 4406-4408, doi:10.1002/anie.200901130.
5. Barré, A.; Țințaș, M.-L.; Alix, F.; Gembus, V.; Papamicaël, C.; Levacher, V. Palladium-Catalyzed Carbonylation of (Hetero)Aryl, Alkenyl and Allyl Halides by Means of N-Hydroxysuccinimidyl Formate as CO Surrogate. *J. Org. Chem.* **2015**, *80*, 6537-6544, doi:10.1021/acs.joc.5b01119.
6. Strueben, J.; Lipfert, M.; Springer, J.O.; Gould, C.A.; Gates, P.J.; Sönnichsen, F.D.; Staubitz, A. High-Yield Lithiation of Azobenzenes by Tin-Lithium Exchange. *Chem. Eur. J.* **2015**, *21*, 11165-11173, doi:10.1002/chem.201500003.
7. Tiwari, V.K.; Kumar, A.; Schmidt, R.R. Disaccharide-Containing Macrocycles by Click Chemistry and Intramolecular Glycosylation. *Eur. J. Org. Chem.* **2012**, 2945-2956, doi:10.1002/ejoc.201101815.
8. Yu, B.-C.; Shirai, Y.; Tour, J.M. Syntheses of New Functionalized Azobenzenes for Potential Molecular Electronic Devices. *Tetrahedron* **2006**, *62*, 10303-10310, doi:10.1016/j.tet.2006.08.069.
9. Rasheed, O.K.; Raftery, J.; Quayle, P. A New Benzannulation Reaction of Azoaromatics. *Synlett* **2015**, *26*, 2806-2810.
10. Nguyen, T.-T.-T.; Turp, D.; Wang, D.; Nolscher, B.; Laquai, F.; Mullen, K. A Fluorescent, Shape-Persistent Dendritic Host with Photoswitchable Guest Encapsulation and Intramolecular Energy Transfer. *J. Am. Chem. Soc.* **2011**, *133*, 11194-11204, doi:10.1021/ja2022398.
11. Strueben, J.; Gates, P.J.; Staubitz, A. Tin-Functionalized Azobenzenes as Nucleophiles in Stille Cross-Coupling Reactions. *J. Org. Chem.* **2014**, *79*, 1719-1728, doi:10.1021/jo402598u.
12. Brown, D.G.; Schauer, P.A.; Borau-Garcia, J.; Fancy, B.R.; Berlinguette, C.P. Stabilization of Ruthenium Sensitizers to TiO<sub>2</sub> Surfaces through Cooperative Anchoring Groups. *J. Am. Chem. Soc.* **2013**, *135*, 1692-1695, doi:10.1021/ja310965h.
13. Abboud, M.; Sayari, A. Novel Family of Periodic Mesoporous Organosilicas Containing Azobenzene within the Pore Walls. *Microporous Mesoporous Mater.* **2017**, *249*, 157-164, doi:10.1016/j.micromeso.2017.04.061.

14. Broser, W.; Harrer, W. Synthesen, spektroskopische Charakterisierung, Gleichgewichts- und kinetische Messungen an m-methoxylierten Parafuchsinen. *Z. Naturforsch., B: J. Chem. Sci.* **1969**, *24*, 542-547, doi:doi:10.1515/znb-1969-0514.
15. Samanta, S.; Beharry, A.A.; Sadovski, O.; McCormick, T.M.; Babalhavaeji, A.; Tropepe, V.; Woolley, G.A. Photoswitching Azo Compounds in Vivo with Red Light. *J. Am. Chem. Soc.* **2013**, *135*, 9777-9784, doi:10.1021/ja402220t.
16. Bléger, D.; Schwarz, J.; Brouwer, A.M.; Hecht, S. o-Fluoroazobenzenes as Readily Synthesized Photoswitches Offering Nearly Quantitative Two-Way Isomerization with Visible Light. *J. Am. Chem. Soc.* **2012**, *134*, 20597-20600, doi:10.1021/ja310323y.
17. Antoine John, A.; Lin, Q. Synthesis of Azobenzenes Using N-Chlorosuccinimide and 1,8-Diazabicyclo[5.4.0]undec-7-ene (DBU). *J. Org. Chem.* **2017**, *82*, 9873-9876, doi:10.1021/acs.joc.7b01530.
18. Moreno, J.; Gerecke, M.; Grubert, L.; Kovalenko, S.A.; Hecht, S. Sensitized Two-NIR-Photon Z→E Isomerization of a Visible-Light-Addressable Bistable Azobenzene Derivative. *Angew. Chem. Int. Ed.* **2016**, *55*, 1544-1547, doi:10.1002/anie.201509111.
19. Cigl, M.; Bubnov, A.; Kašpar, M.; Hampl, F.; Hamplová, V.; Pacherová, O.; Svoboda, J. Photosensitive Chiral Self-Assembling Materials: Significant Effects of Small Lateral Substituents. *J. Mater. Chem. C* **2016**, *4*, 5326-5333, doi:10.1039/C6TC01103A.
20. Heinrich, B.; Bouazoune, K.; Wojcik, M.; Bakowsky, U.; Vázquez, O. ortho-Fluoroazobenzene Derivatives as DNA Intercalators for Photocontrol of DNA and Nucleosome Binding by Visible Light. *Org. Biomol. Chem.* **2019**, *17*, 1827-1833, doi:10.1039/C8OB02343C.
21. Maier, M.S.; Hüll, K.; Reynders, M.; Matsuura, B.S.; Leippe, P.; Ko, T.; Schäffer, L.; Trauner, D. Oxidative Approach Enables Efficient Access to Cyclic Azobenzenes. *J. Am. Chem. Soc.* **2019**, *141*, 17295-17304, doi:10.1021/jacs.9b08794.

$^1\text{H}$ ,  $^{13}\text{C}\{^1\text{H}\}$  and  $^{19}\text{F}$  NMR Spectra of the Purified Compounds  
2,5-Dioxopyrrolidin-1-yl (*E*)-4-(phenyldiazenyl)benzoate (**3a**)

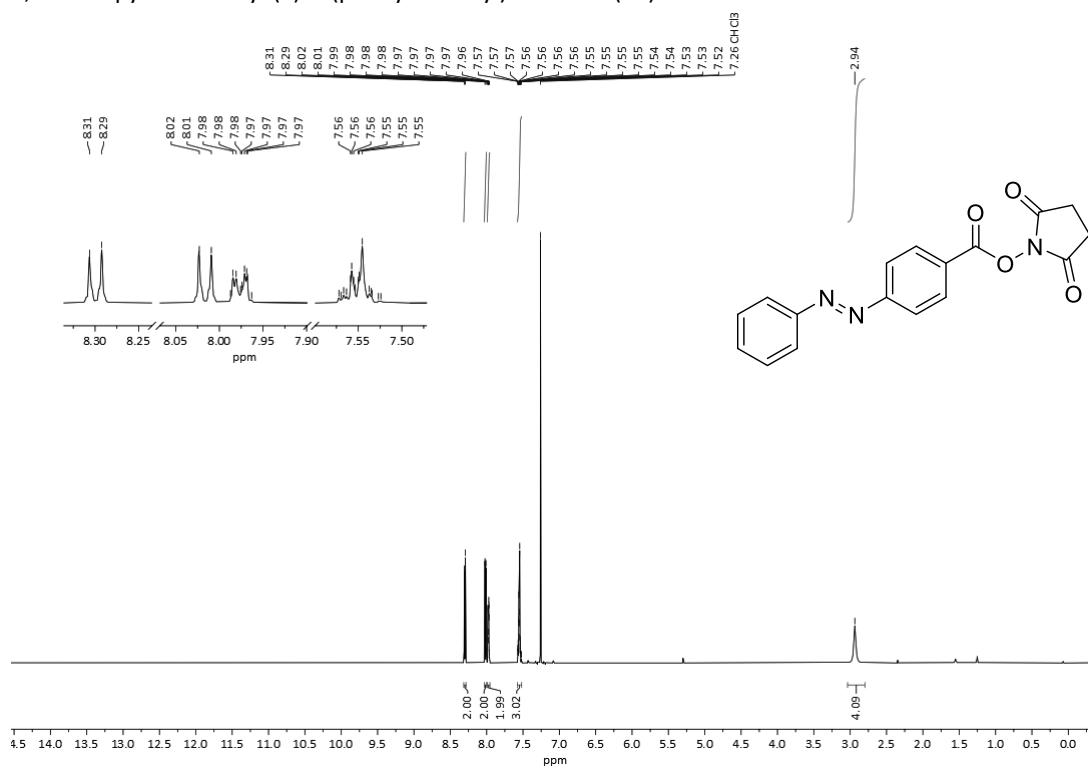


Figure S1:  $^1\text{H}$  NMR spectrum of **3a** in  $\text{CDCl}_3$ .

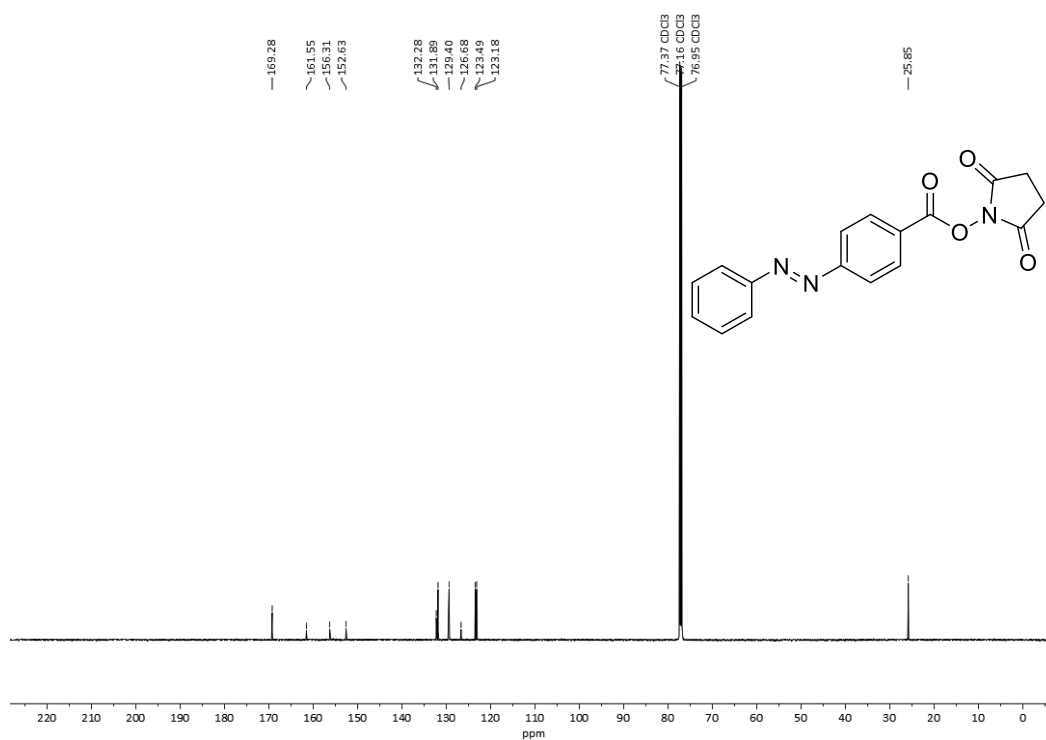
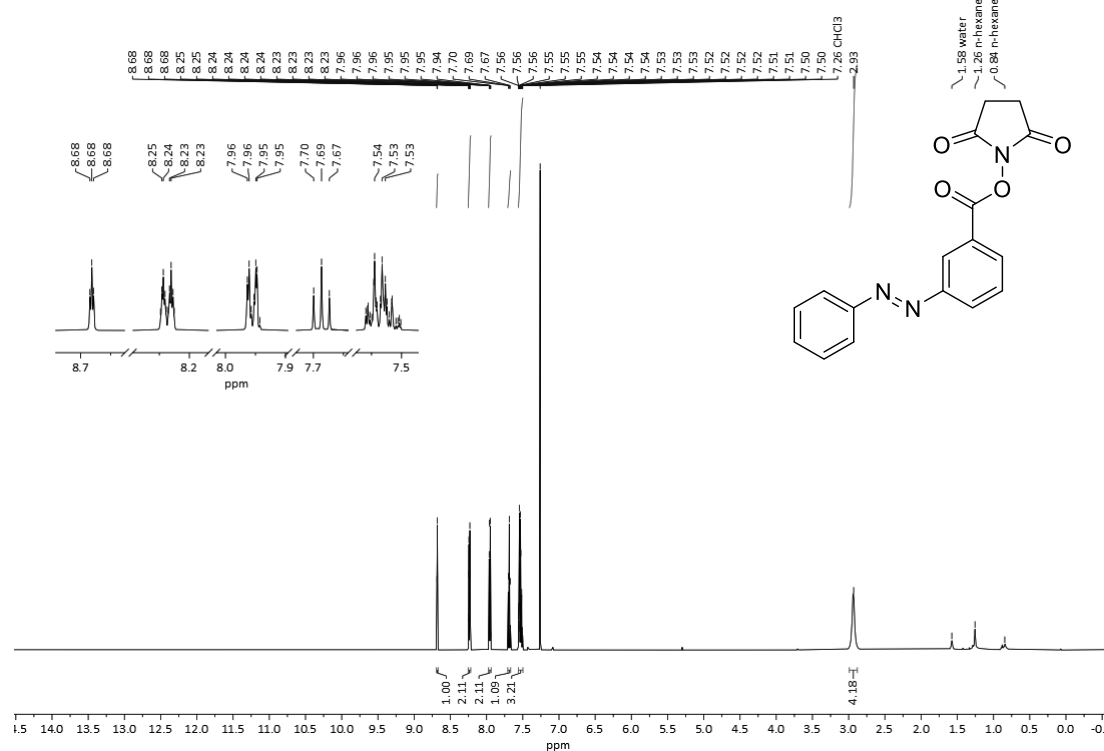
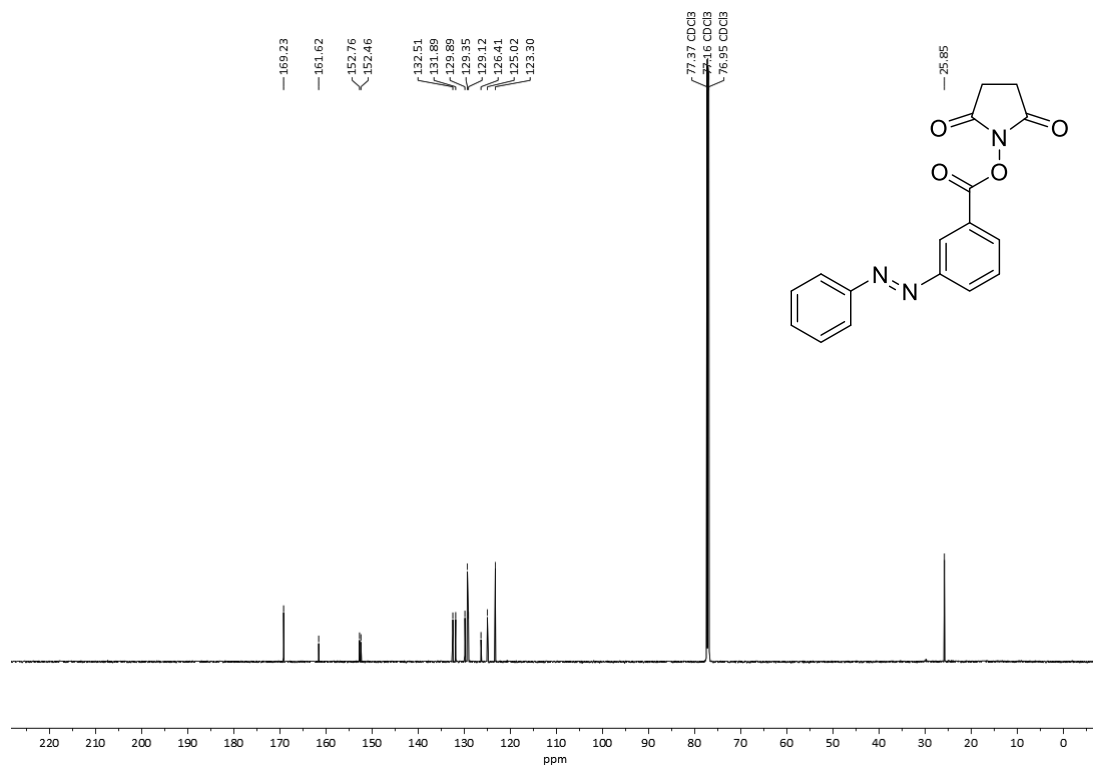
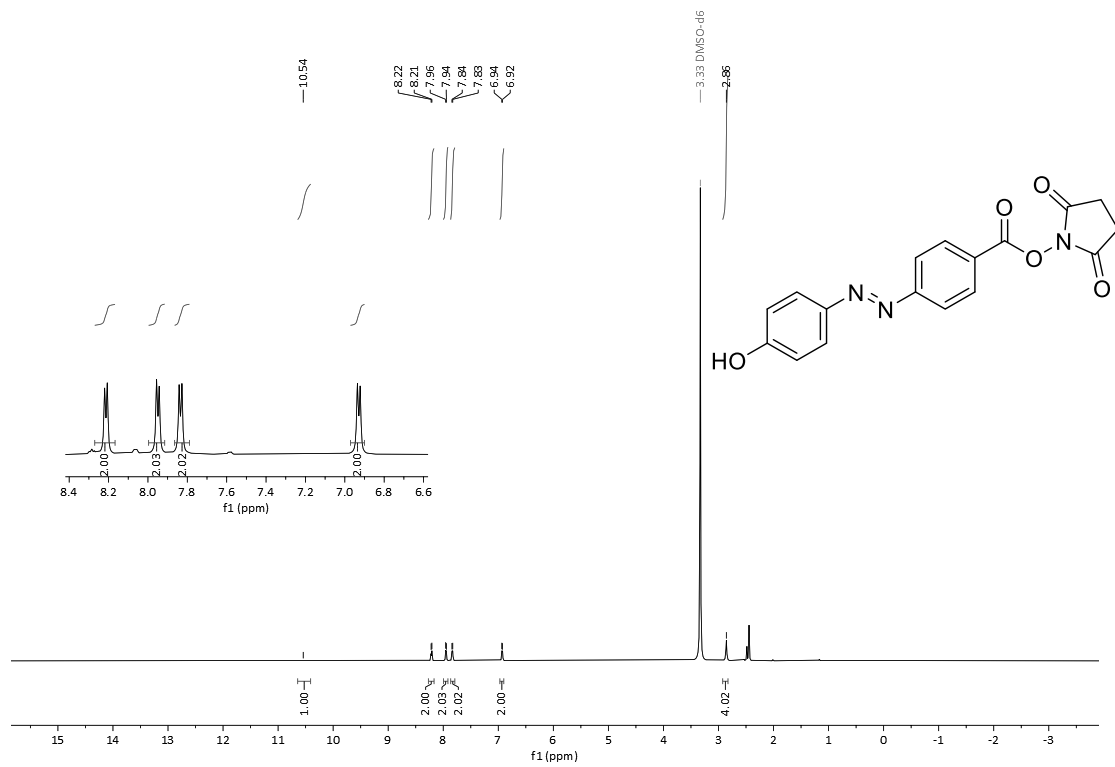
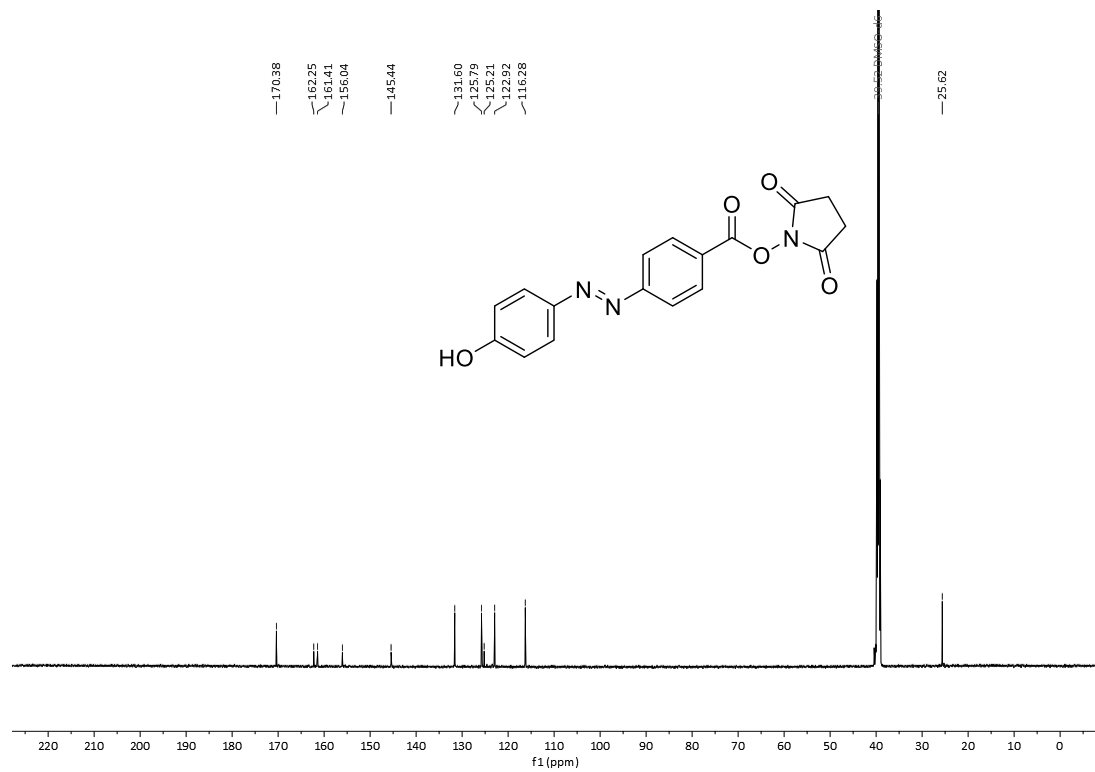
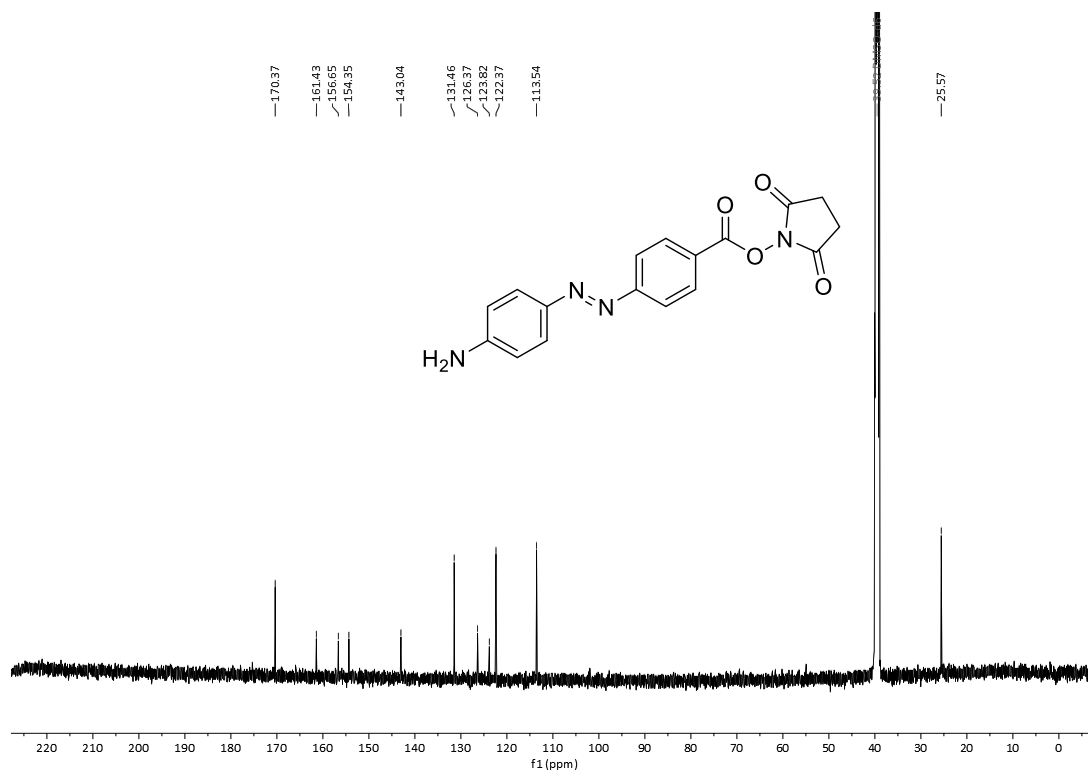


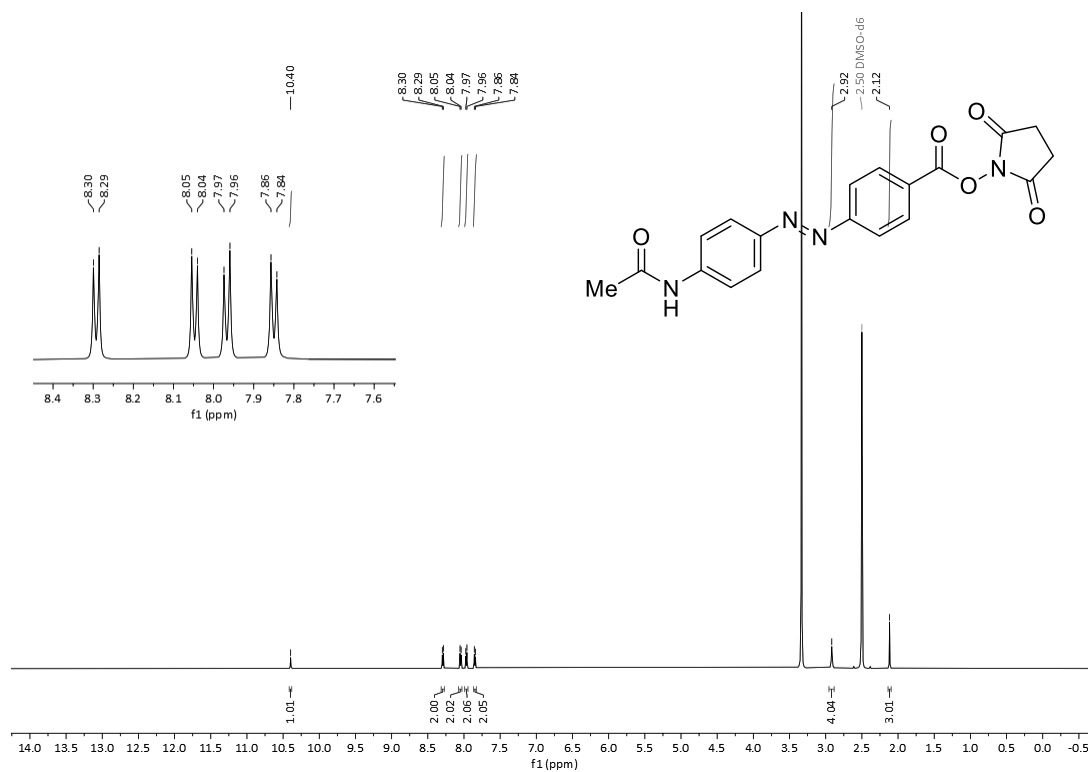
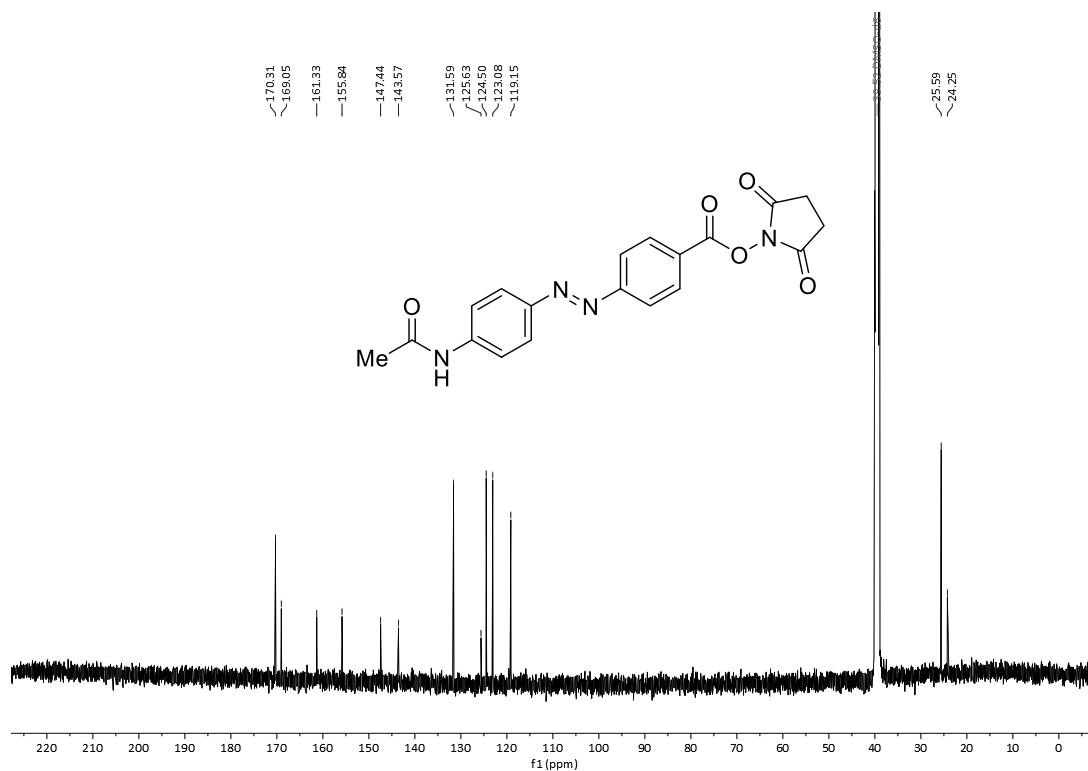
Figure S2:  $^{13}\text{C}\{^1\text{H}\}$  NMR spectrum of **3a** in  $\text{CDCl}_3$ .

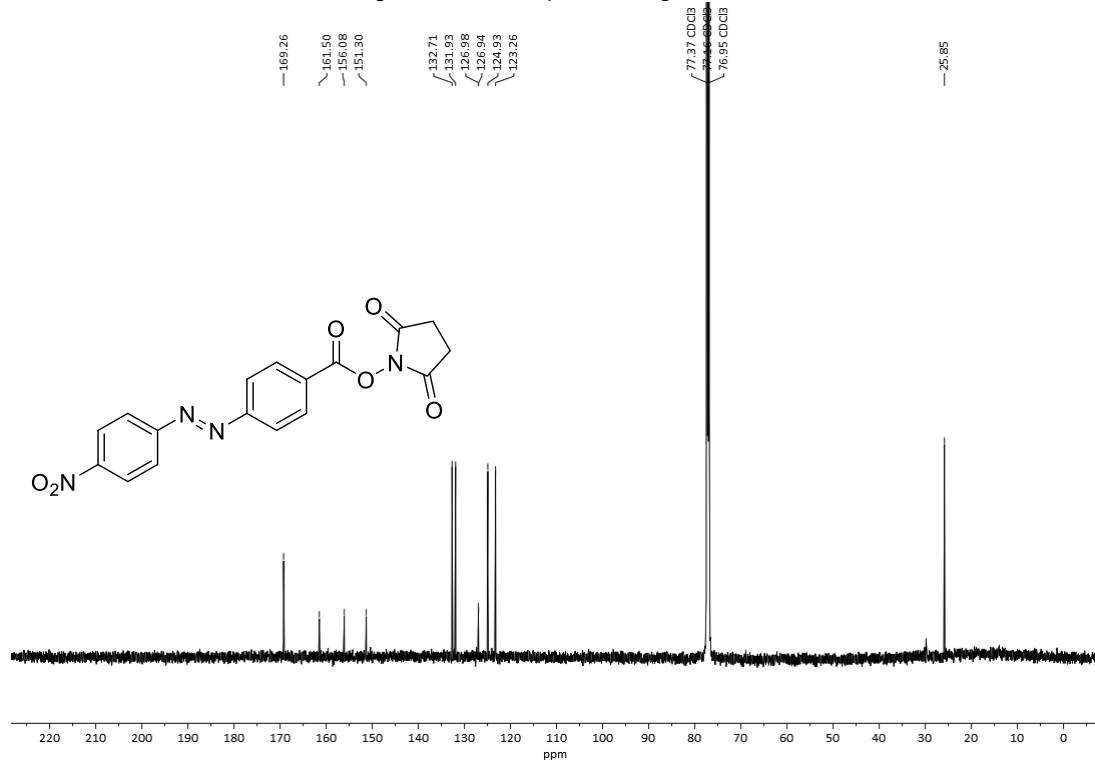
2,5-Dioxopyrrolidin-1-yl (*E*)-3-(phenyldiazenyl)benzoate (**3b**)Figure S3: <sup>1</sup>H NMR spectrum of **3b** in CDCl<sub>3</sub>.Figure S4: <sup>13</sup>C{<sup>1</sup>H} NMR spectrum of **3b** in CDCl<sub>3</sub>.

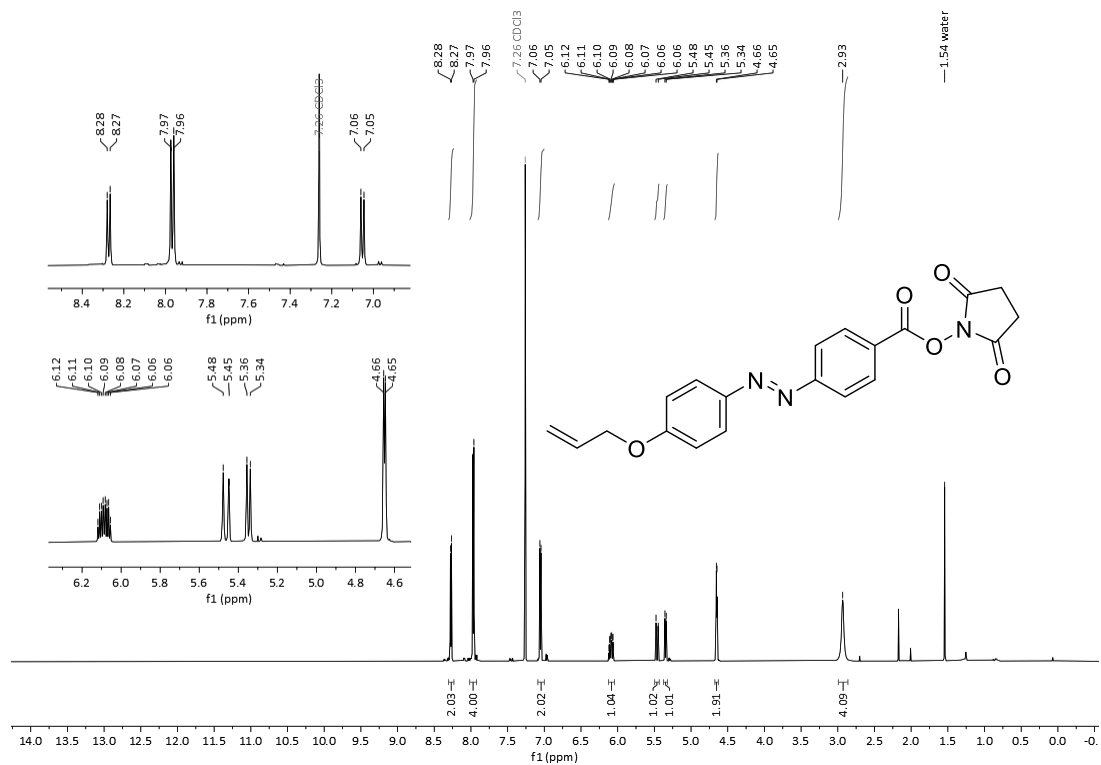
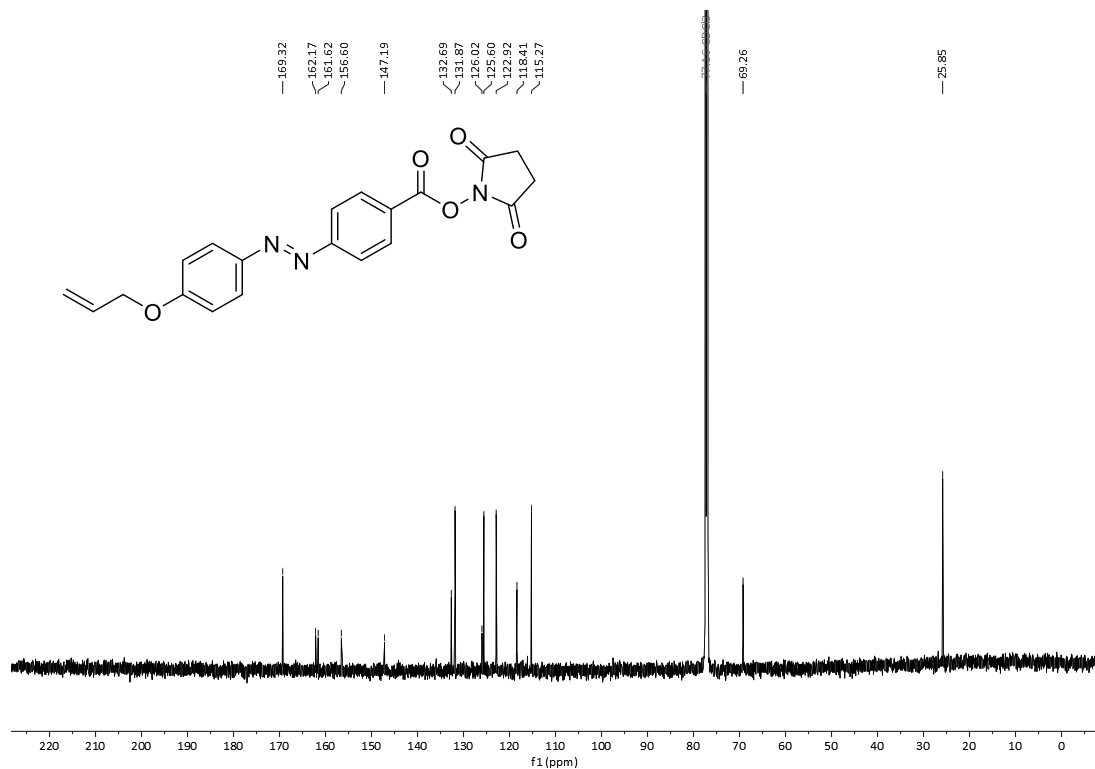


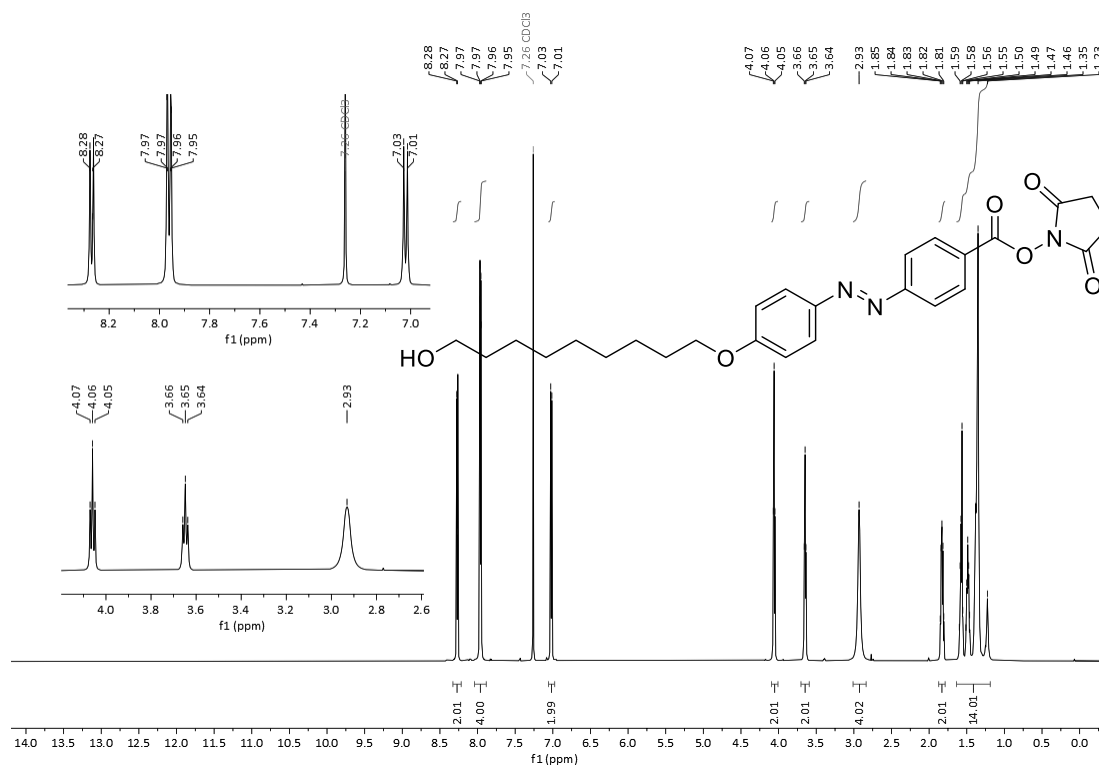
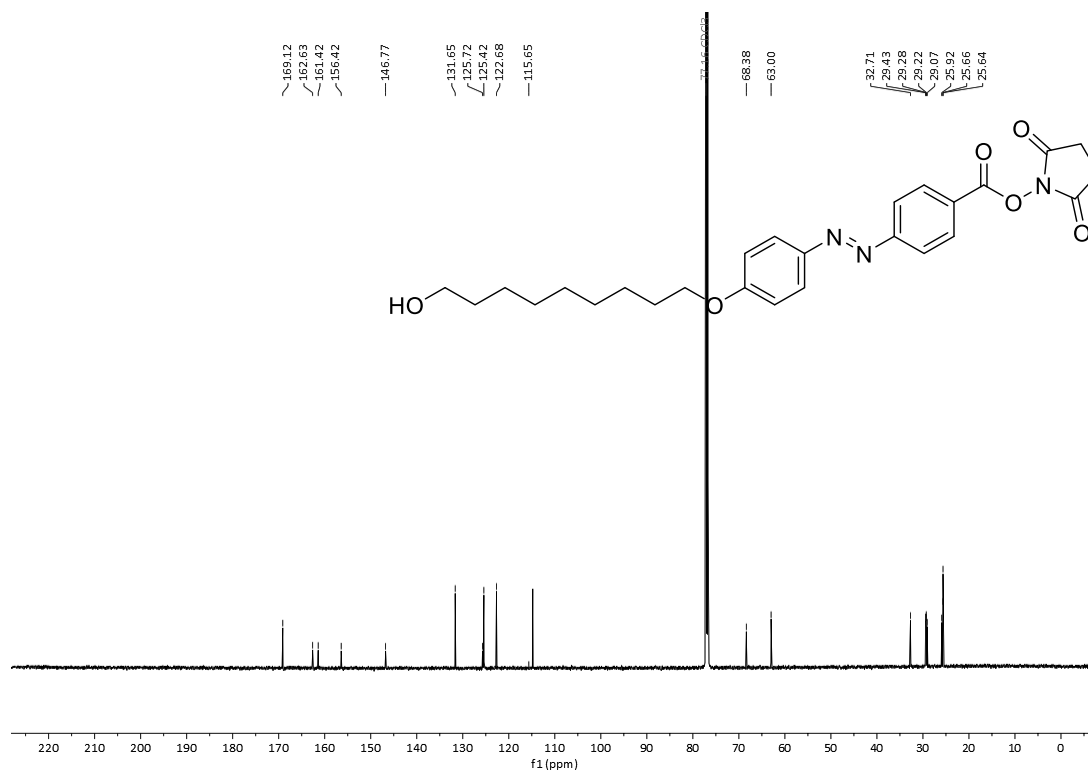
2,5-Dioxopyrrolidin-1-yl (*E*)-4-((4-hydroxyphenyl)diazenyl)benzoate (**3d**)Figure S5: <sup>1</sup>H NMR spectrum of **3d** in DMSO-*d*<sub>6</sub>.Figure S6: <sup>13</sup>C{<sup>1</sup>H} NMR spectrum of **3d** in DMSO-*d*<sub>6</sub>.

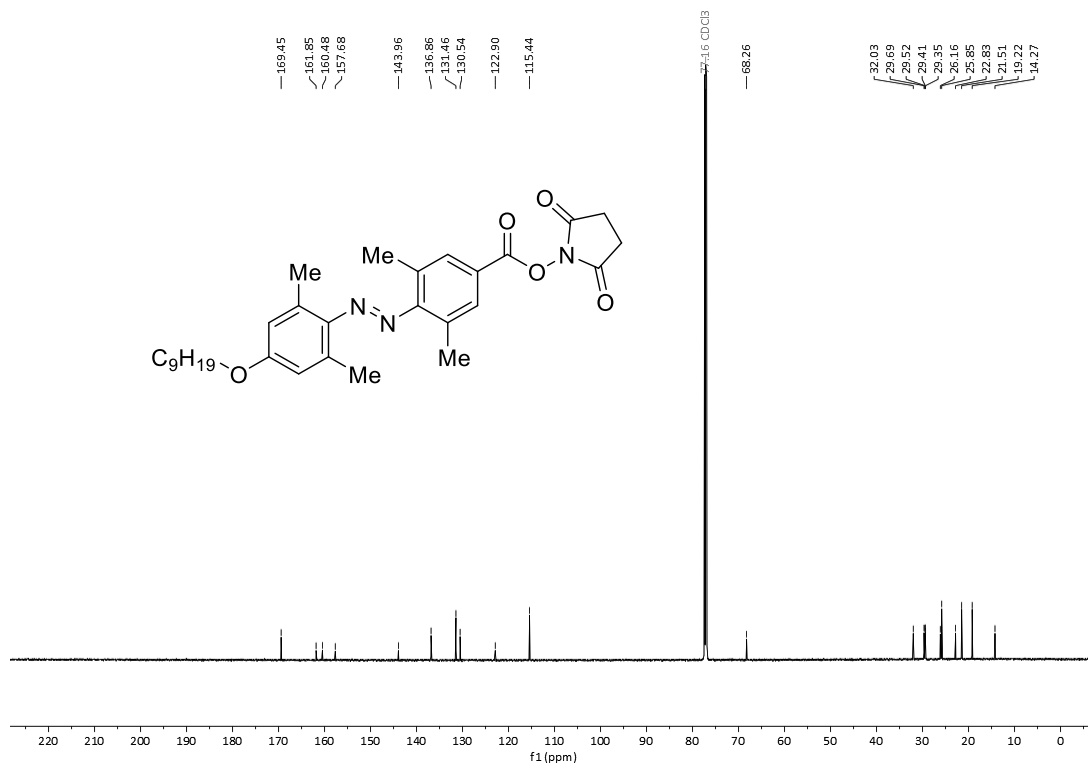
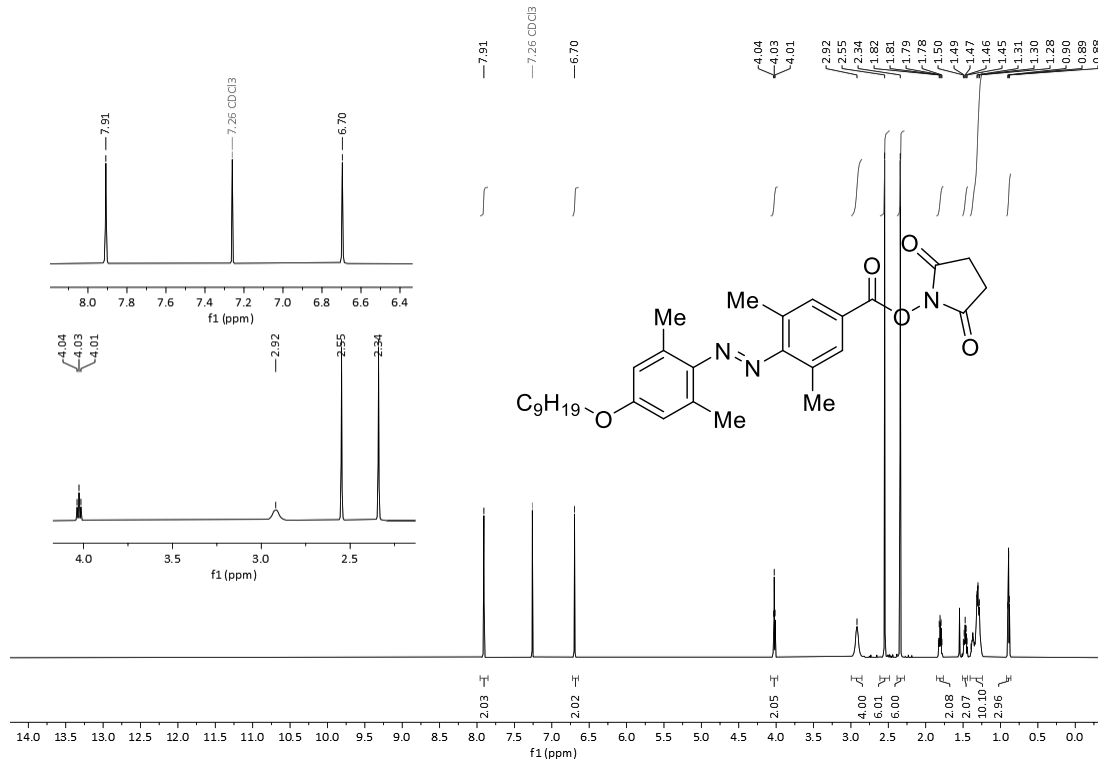
2,5-Dioxopyrrolidin-1-yl (*E*)-4-((4-aminophenyl)diazenyl)benzoate (**3e**)Figure S7: <sup>1</sup>H NMR spectrum of **3e** in DMSO-*d*<sub>6</sub>.Figure S8: <sup>13</sup>C{<sup>1</sup>H} NMR spectrum of **3e** in DMSO-*d*<sub>6</sub>.

2,5-Dioxopyrrolidin-1-yl (*E*)-4-((4-acetamidophenyl)diazenyl)benzoate (**3f**)Figure S9:  $^1\text{H}$  NMR spectrum of **3f** in  $\text{DMSO-}d_6$ .Figure S10:  $^{13}\text{C}$  NMR spectrum of **3f** in  $\text{DMSO-}d_6$ .

2,5-Dioxopyrrolidin-1-yl (*E*)-4-((4-nitrophenyl)diazenyl)benzoate (**3g**)Figure S11: <sup>1</sup>H NMR spectrum of **3g** in CDCl<sub>3</sub>.Figure S12: <sup>13</sup>C{<sup>1</sup>H} NMR spectrum of **3g** in CDCl<sub>3</sub>.

2,5-Dioxopyrrolidin-1-yl (*E*)-4-((4-allyloxy)phenyl)diazenyl)benzoate (**3h**)Figure S13: <sup>1</sup>H NMR spectrum of **3h** in CDCl<sub>3</sub>.Figure S14: <sup>13</sup>C{<sup>1</sup>H} NMR spectrum of **3h** in CDCl<sub>3</sub>.

2,5-Dioxopyrrolidin-1-yl (*E*)-4-((4-(9-hydroxynonyloxy)phenyl)diazenyl)benzoate (**3i**)Figure S15: <sup>1</sup>H NMR spectrum of **3i** in CDCl<sub>3</sub>.Figure S16: <sup>13</sup>C{<sup>1</sup>H} NMR spectrum of **3i** in CDCl<sub>3</sub>.

2,5-Dioxopyrrolidin-1-yl (E)-4-((2,6-dimethyl-4-(nonyloxy)phenyl)diazenyl)-3,5-dimethylbenzoate (**3j**)

2,5-Dioxopyrrolidin-1-yl (*E*)-4-((2,7-bis(4-(hexyloxy)phenoxy)naphthalen-1-yl)diazenyl)-3,5-dimethylbenzoate (**3k**)

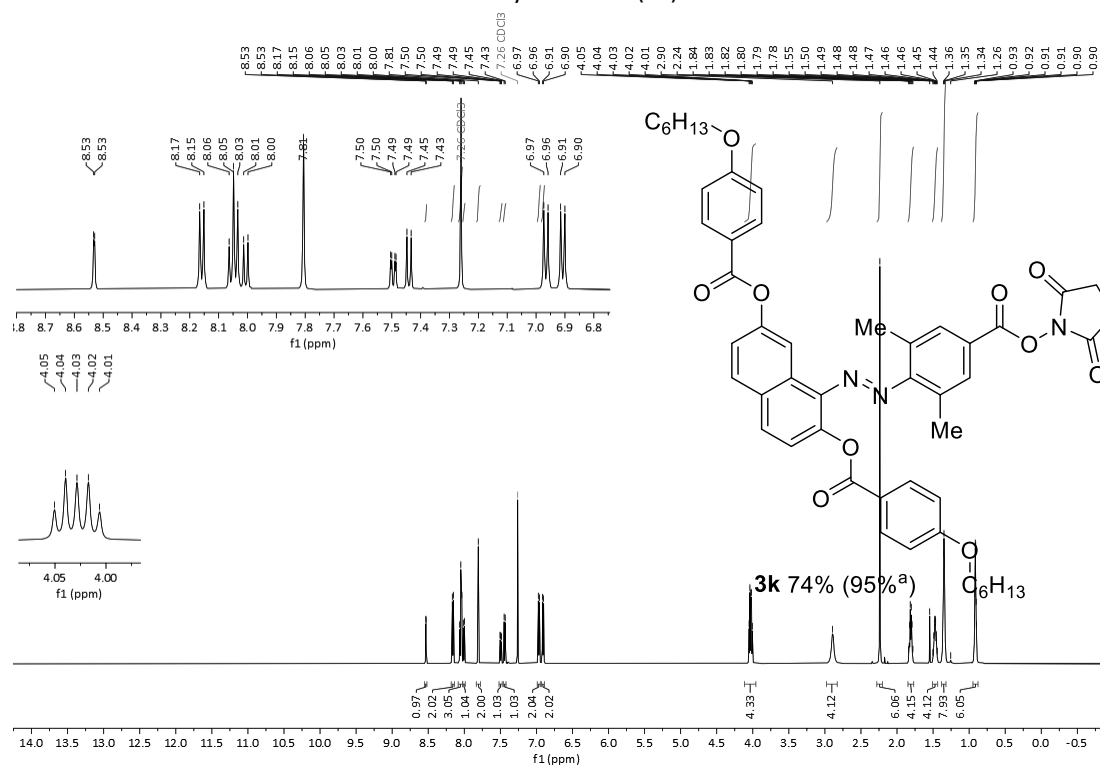


Figure S19: <sup>1</sup>H NMR spectrum of **3k** in CDCl<sub>3</sub>.

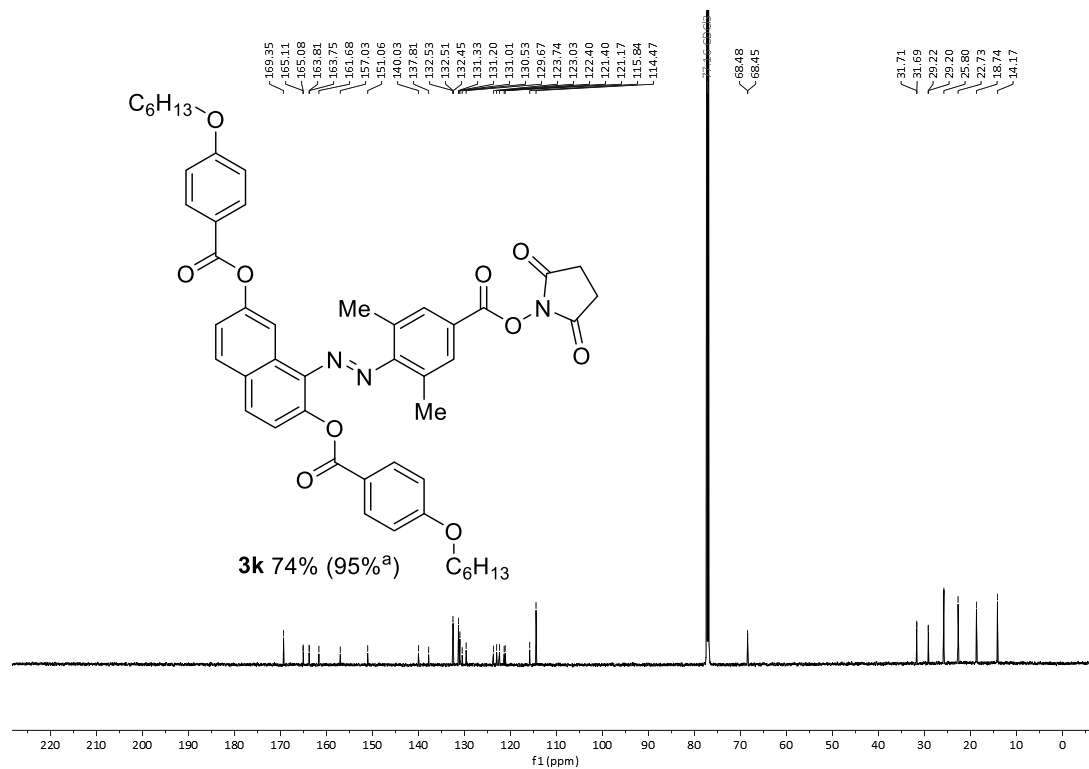
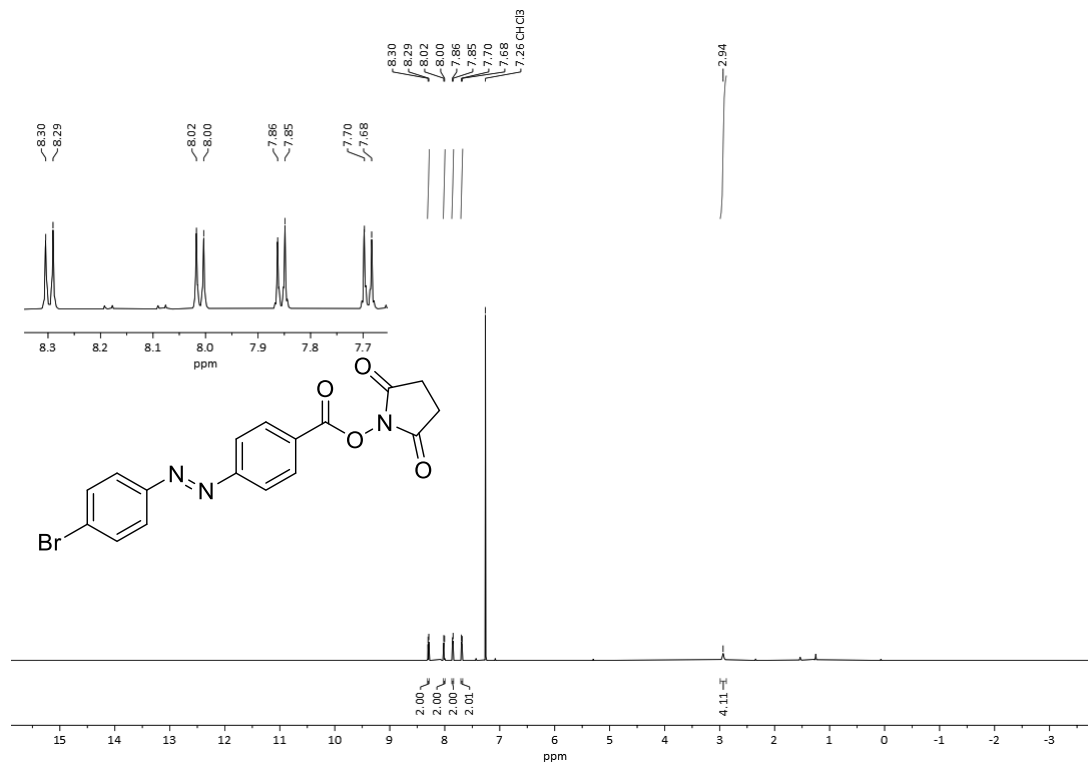
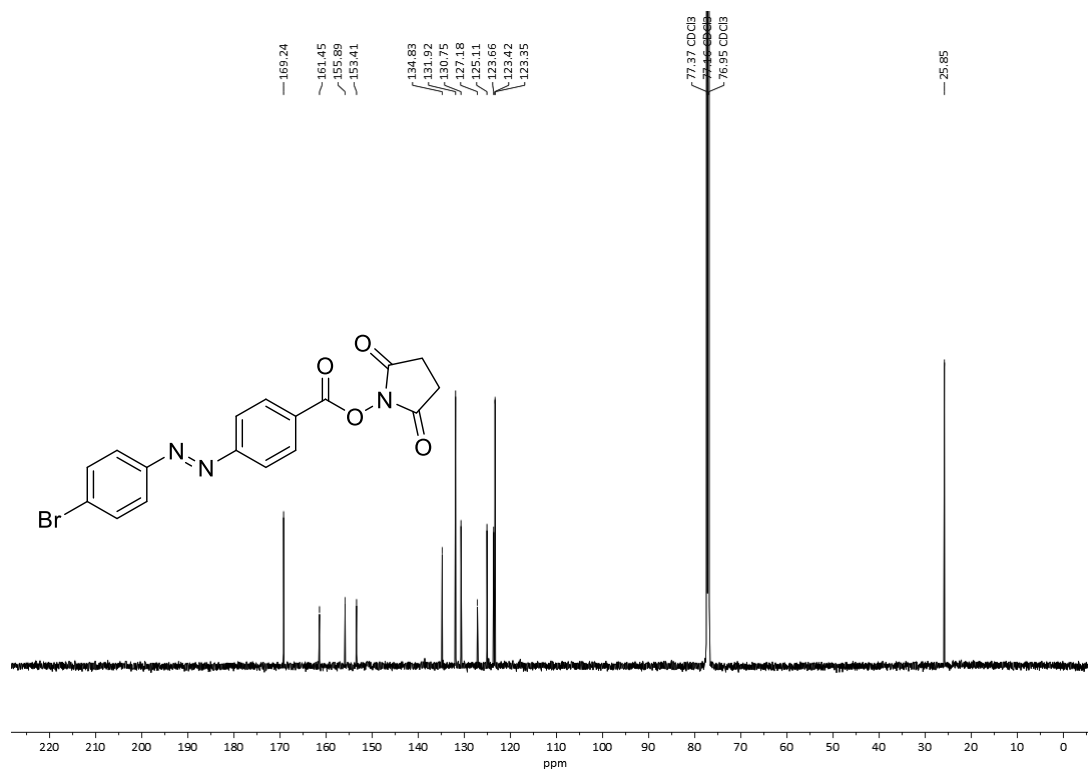
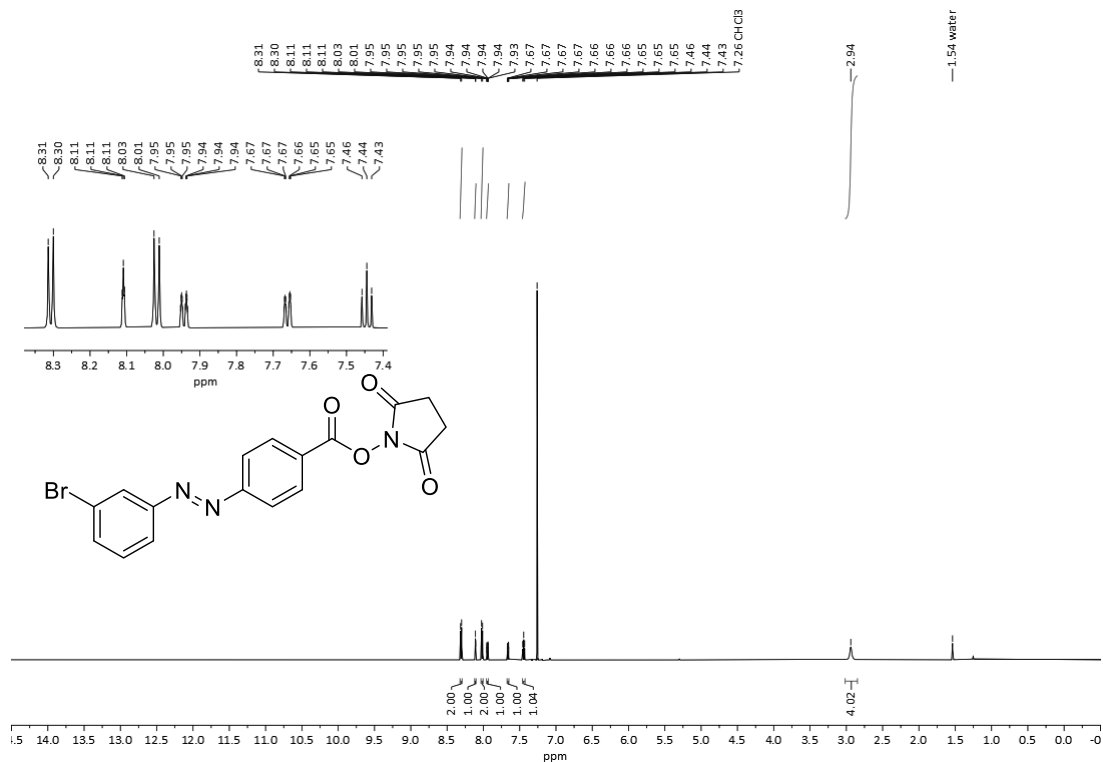
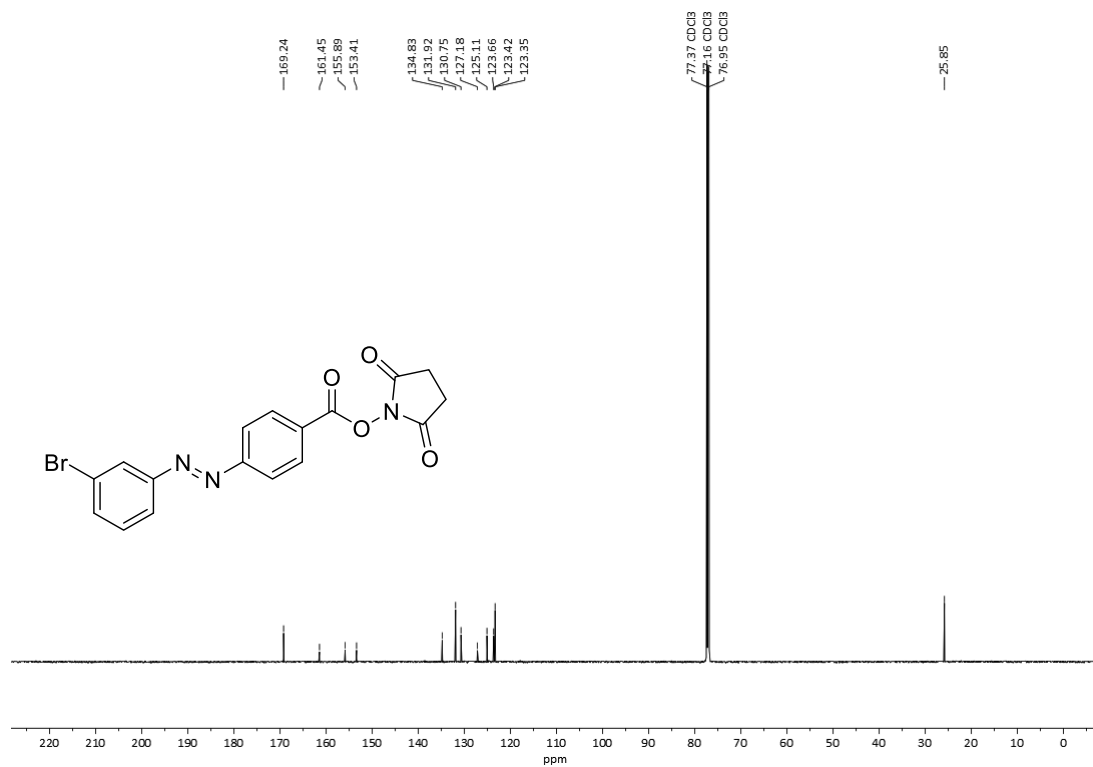
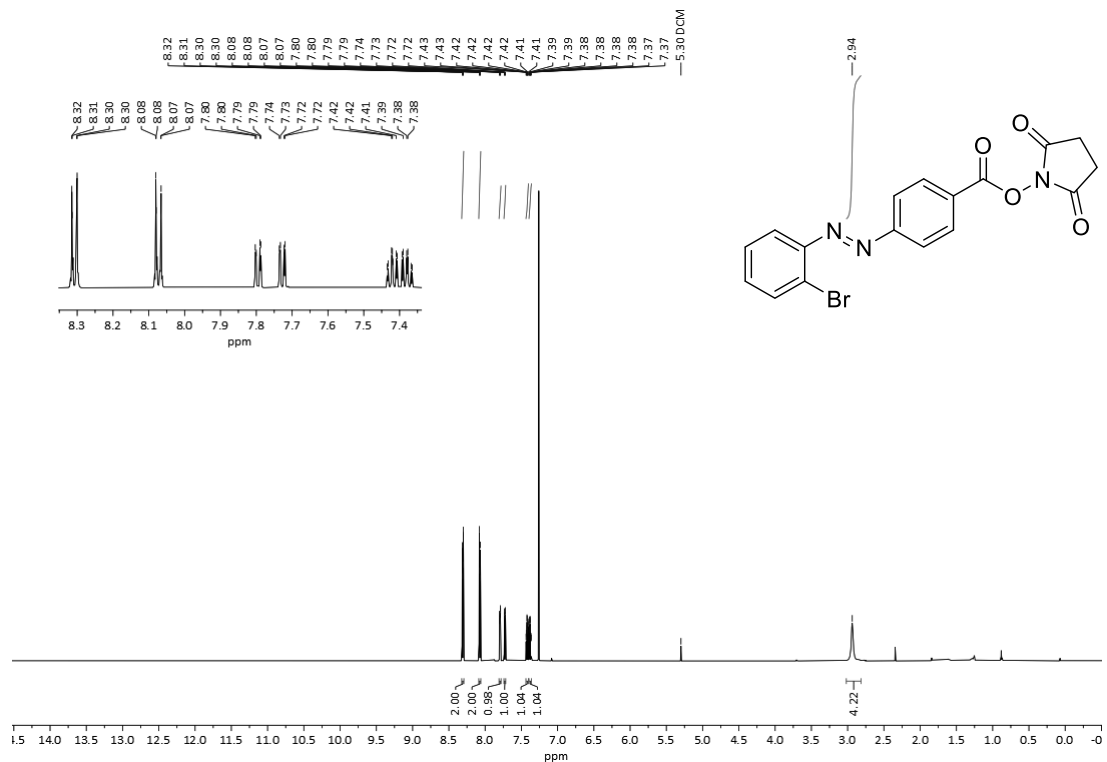
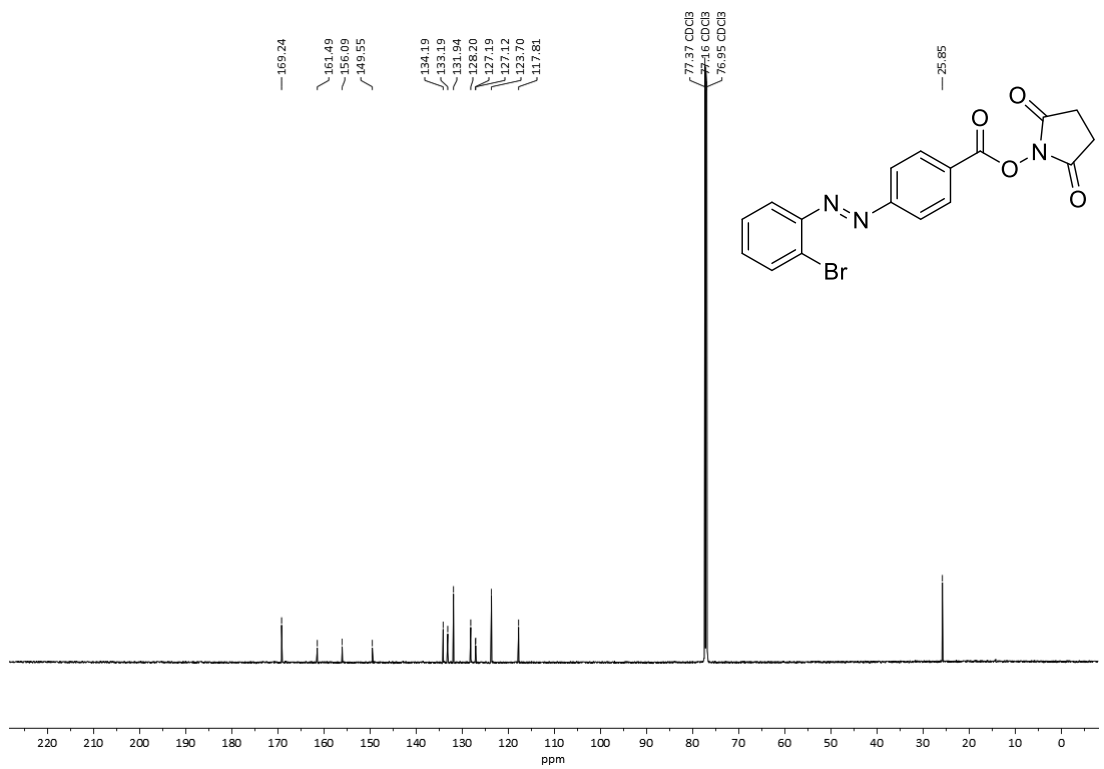


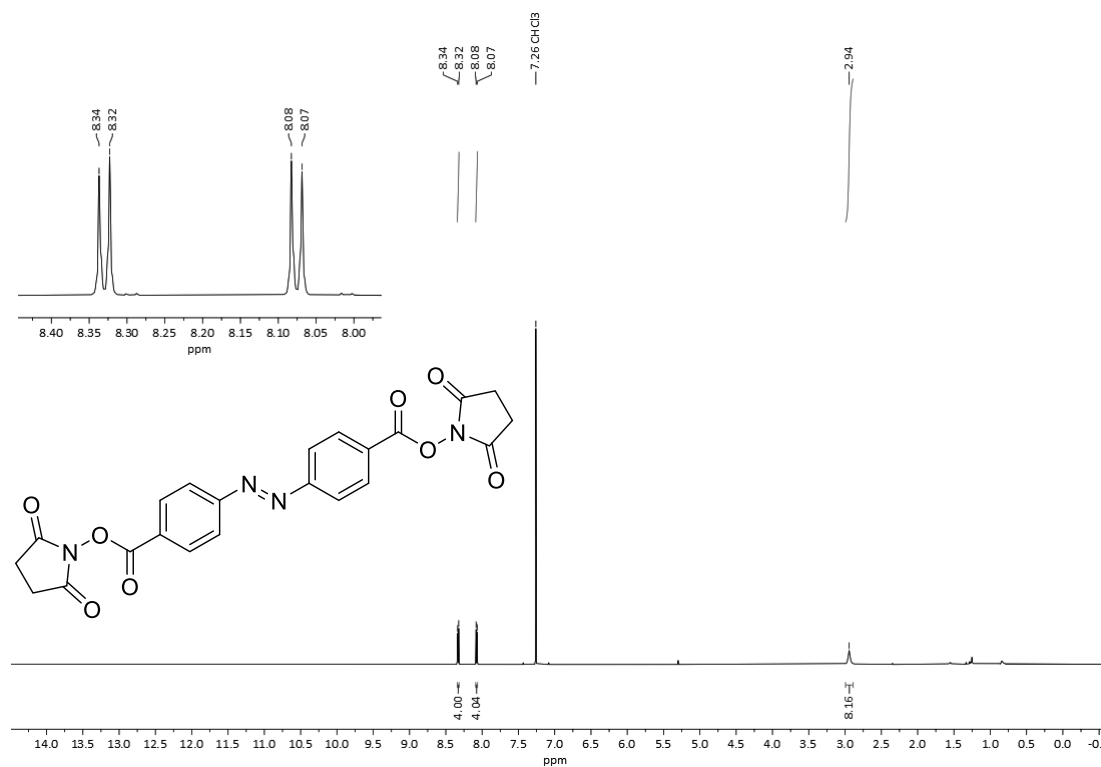
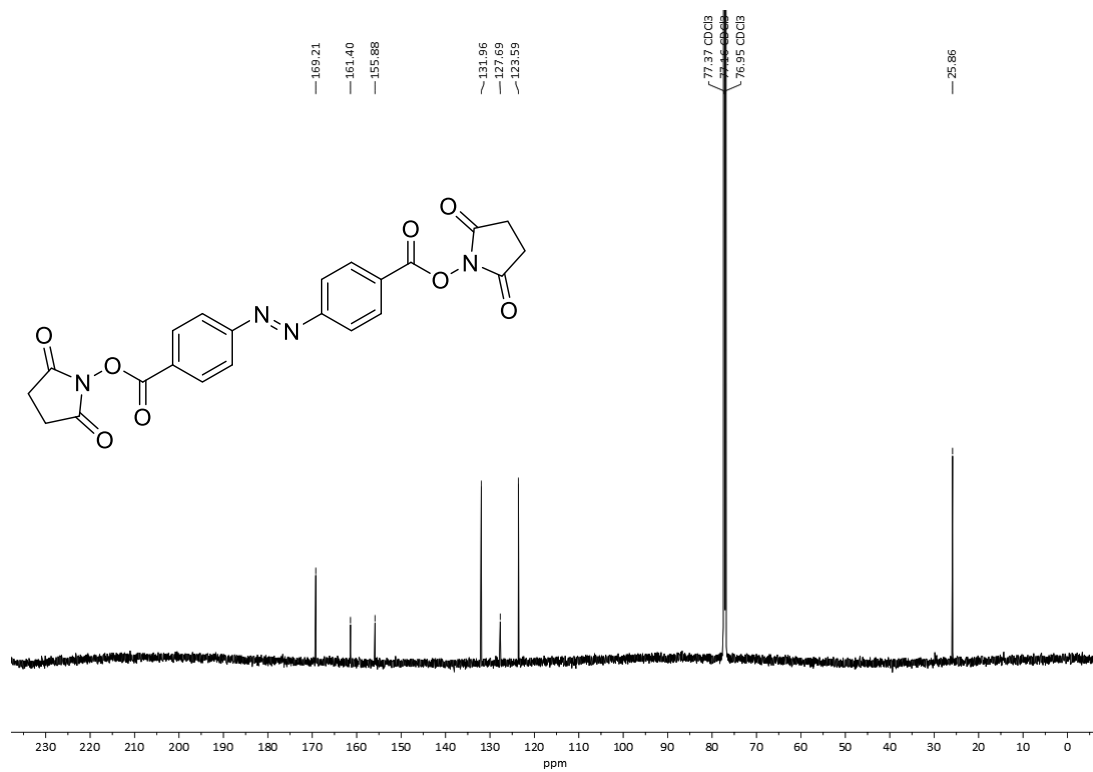
Figure S20: <sup>13</sup>C{<sup>1</sup>H} NMR spectrum of **3k** in CDCl<sub>3</sub>.

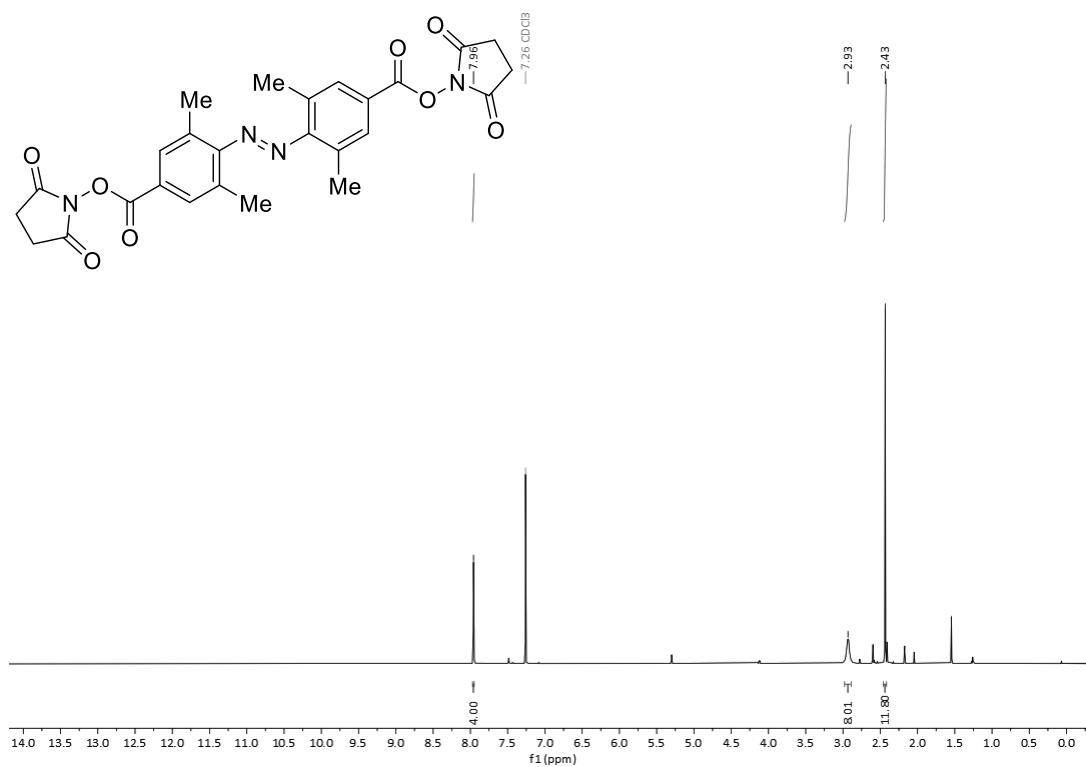
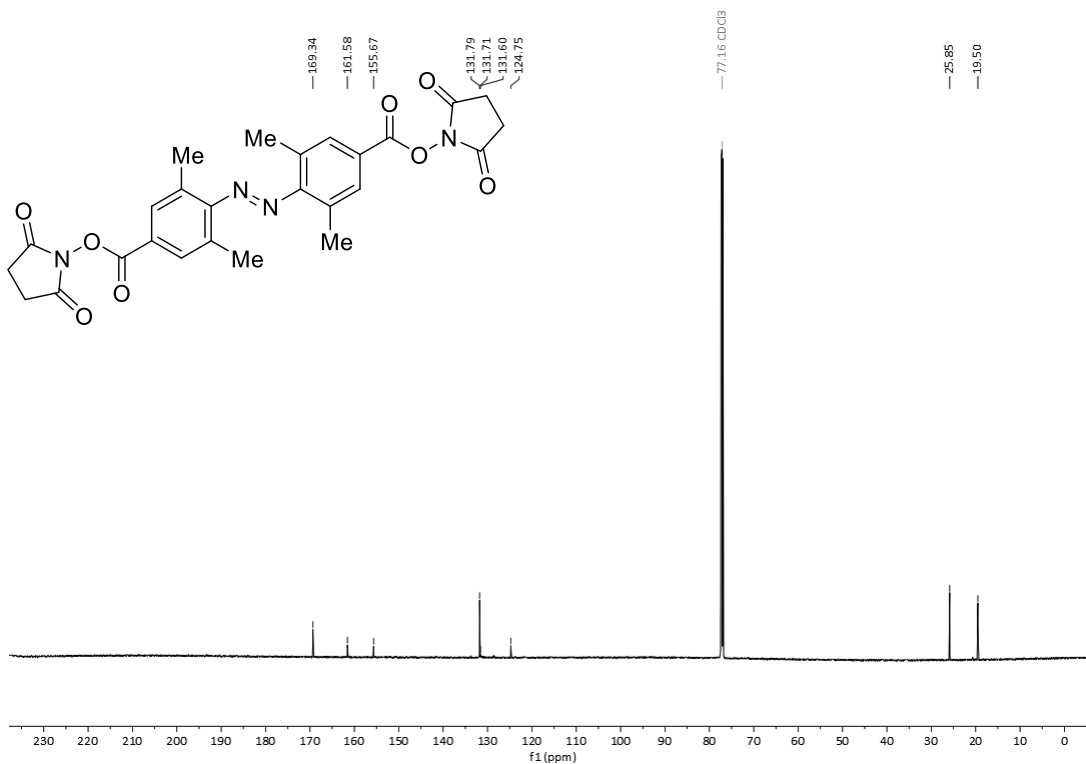


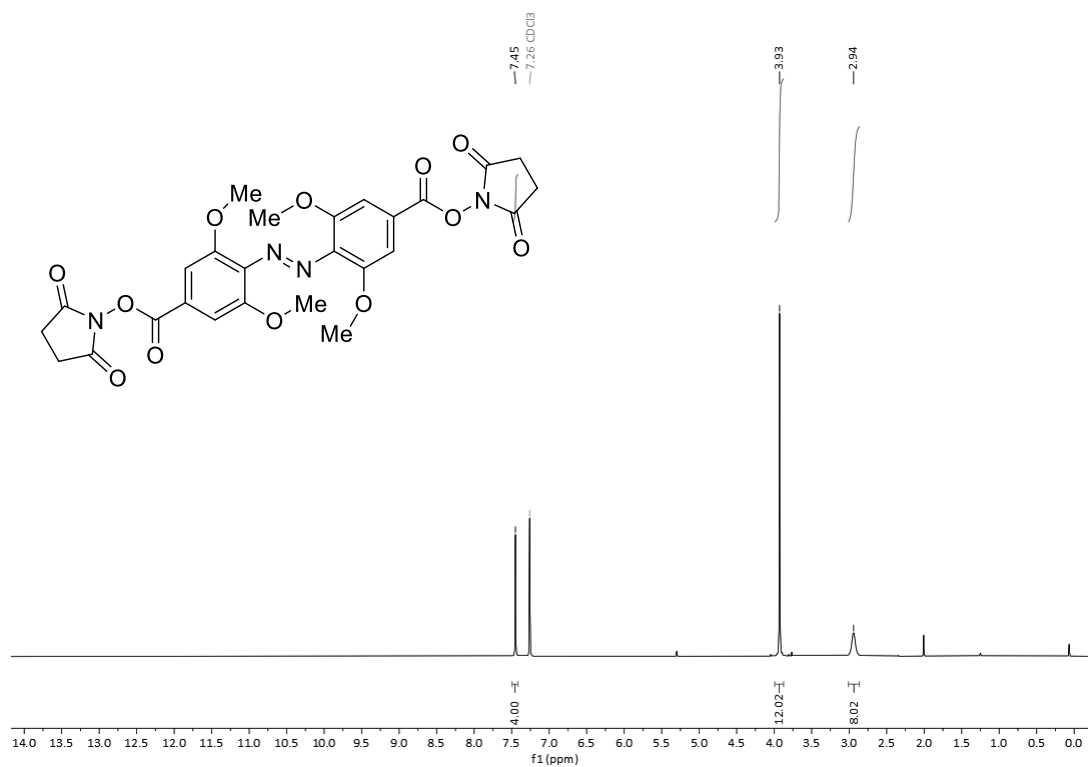
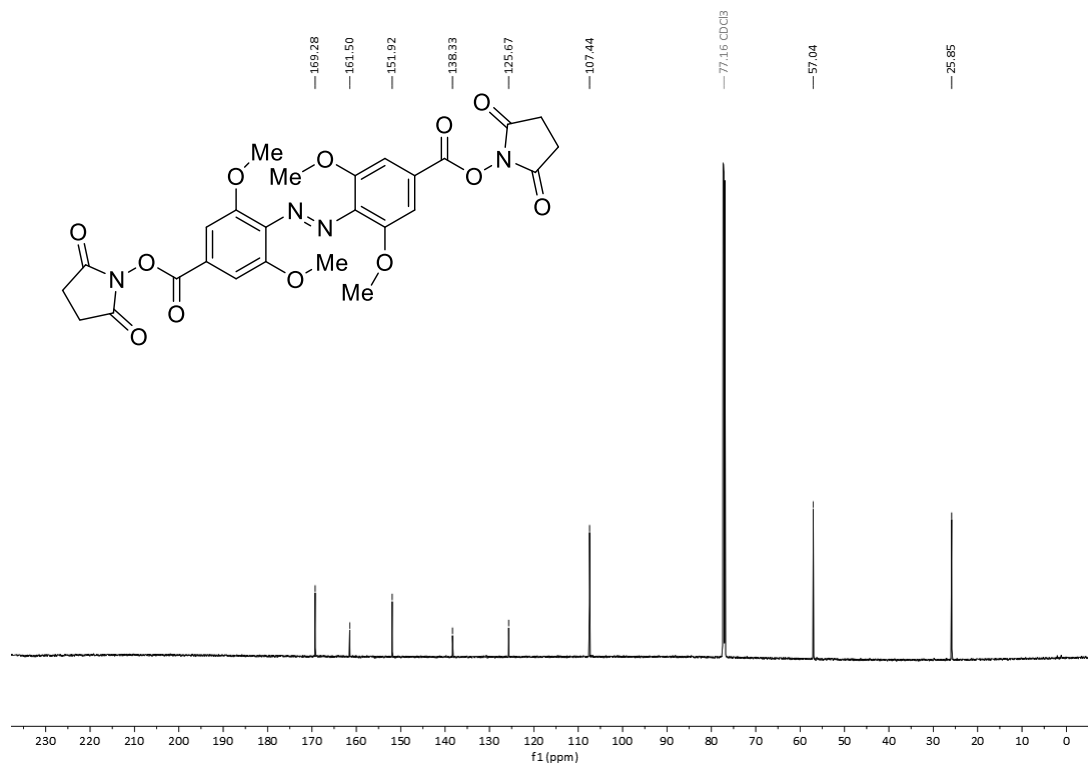
2,5-Dioxopyrrolidin-1-yl (*E*)-4-((4-bromophenyl)diazenyl)benzoate (**31**)Figure S21: <sup>1</sup>H NMR spectrum of **31** in CDCl<sub>3</sub>.Figure S22: <sup>13</sup>C{<sup>1</sup>H} NMR spectrum of **31** in CDCl<sub>3</sub>.

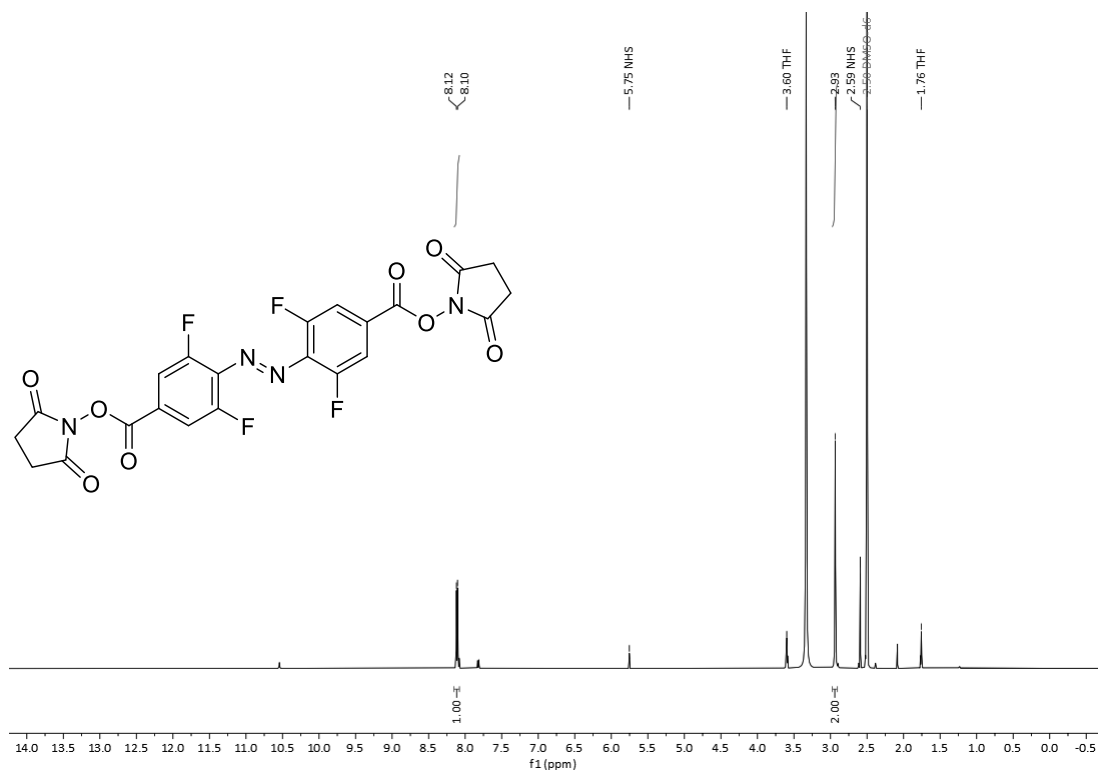
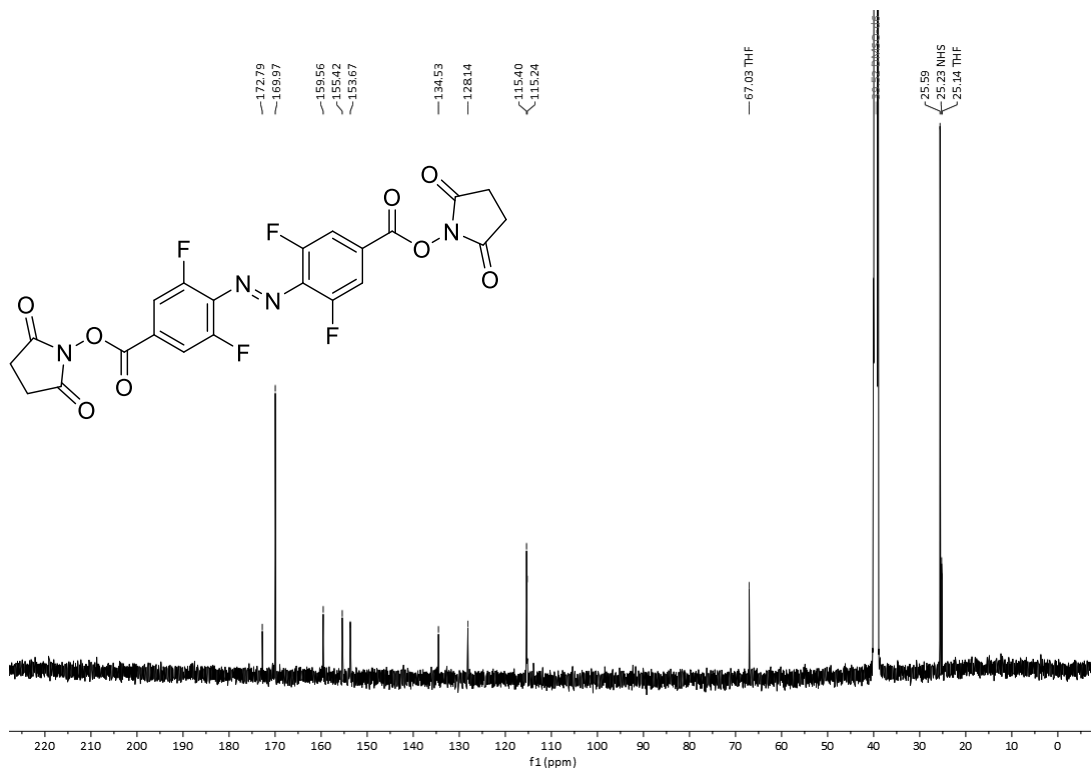
2,5-Dioxopyrrolidin-1-yl (*E*)-4-((3-bromophenyl)diazenyl)benzoate (**3m**)Figure S23: <sup>1</sup>H NMR spectrum of **3m** in CDCl<sub>3</sub>.Figure S24: <sup>13</sup>C{<sup>1</sup>H} NMR spectrum of **3m** in CDCl<sub>3</sub>.

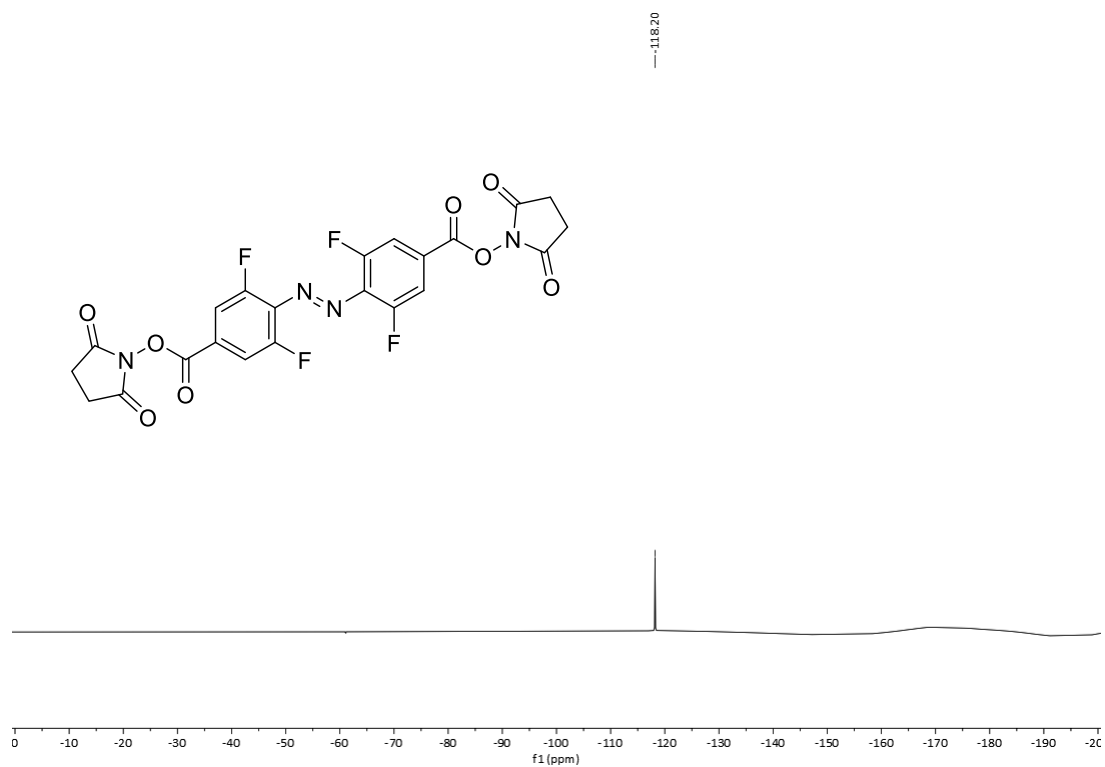
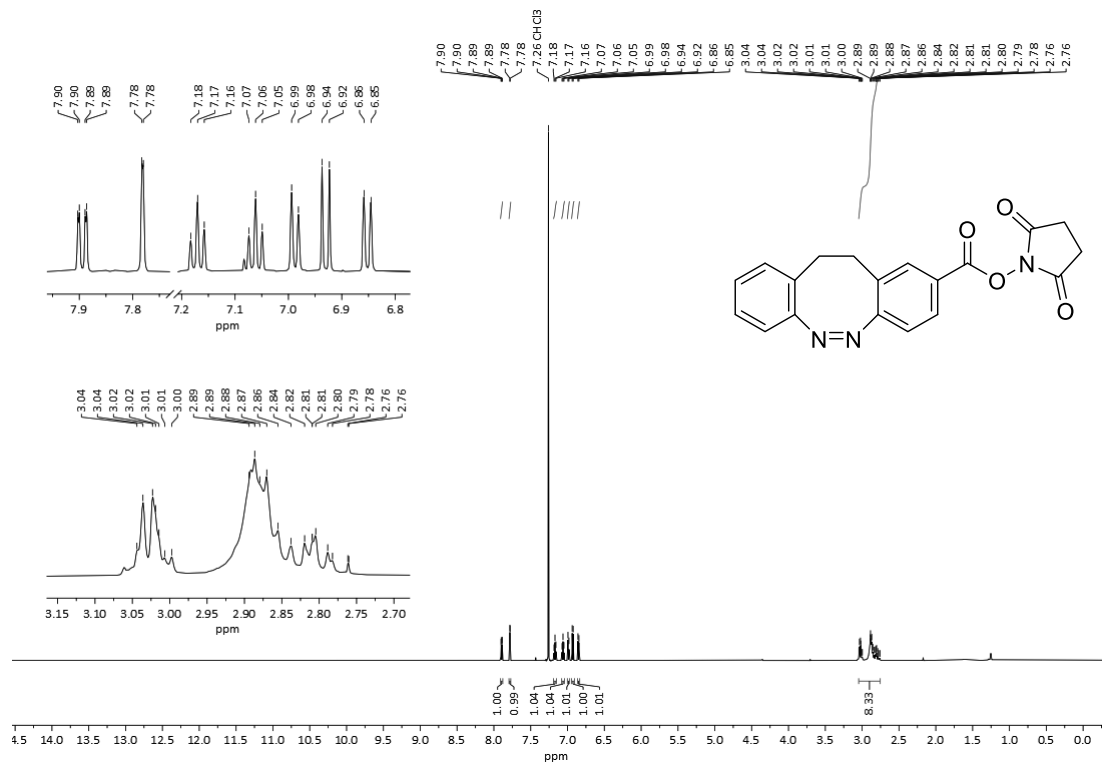
2,5-Dioxopyrrolidin-1-yl (*E*)-4-((2-bromophenyl)diazenyl)benzoate (**3n**)Figure S25: <sup>1</sup>H NMR spectrum of **3n** in CDCl<sub>3</sub>.Figure S26: <sup>13</sup>C NMR spectrum of **3n** in CDCl<sub>3</sub>.

Bis(2,5-dioxopyrrolidin-1-yl) 4,4'-(diazene-1,2-diyl)(*E*)-dibenzoate (**5a**)Figure S27: <sup>1</sup>H NMR spectrum of **5a** in CDCl<sub>3</sub>.Figure S28: <sup>13</sup>C{<sup>1</sup>H} NMR spectrum of **5a** in CDCl<sub>3</sub>.

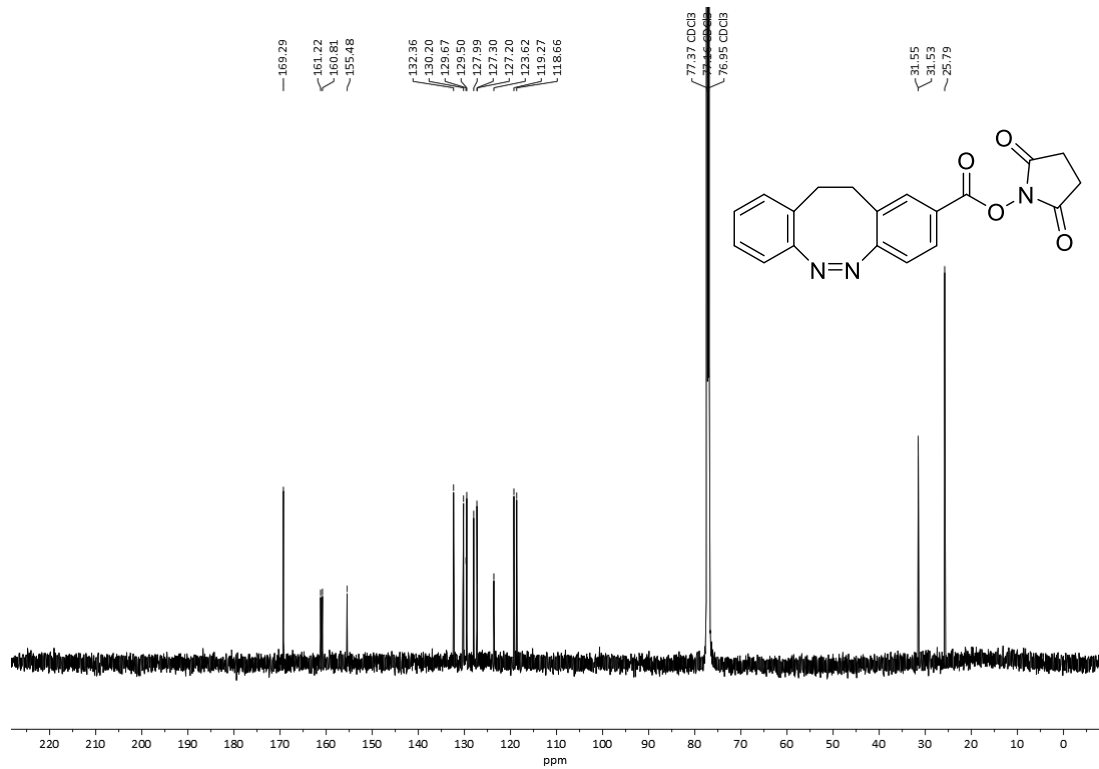
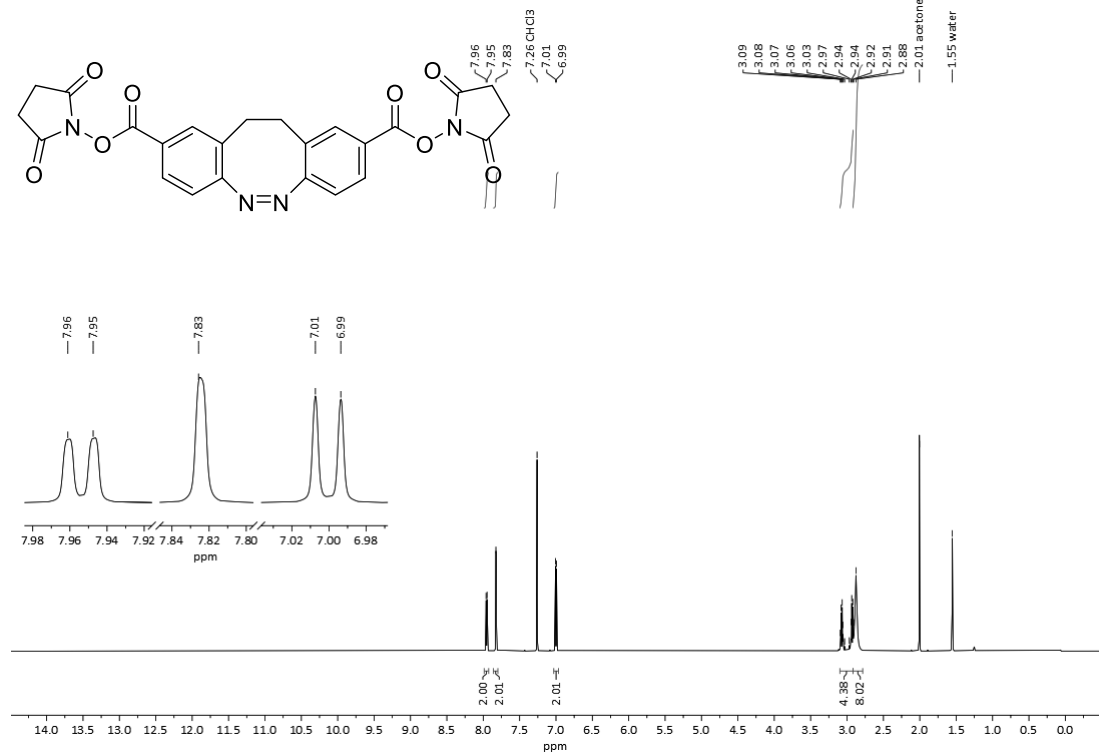
Bis(2,5-dioxopyrrolidin-1-yl) 4,4'-(diazene-1,2-diyl)(*E*)-bis(3,5-dimethylbenzoate) (**5b**)Figure S29:  $^1\text{H}$  NMR spectrum of **5b** in  $\text{CDCl}_3$ .Figure S30:  $^{13}\text{C}$  NMR spectrum of **5b** in  $\text{CDCl}_3$ .

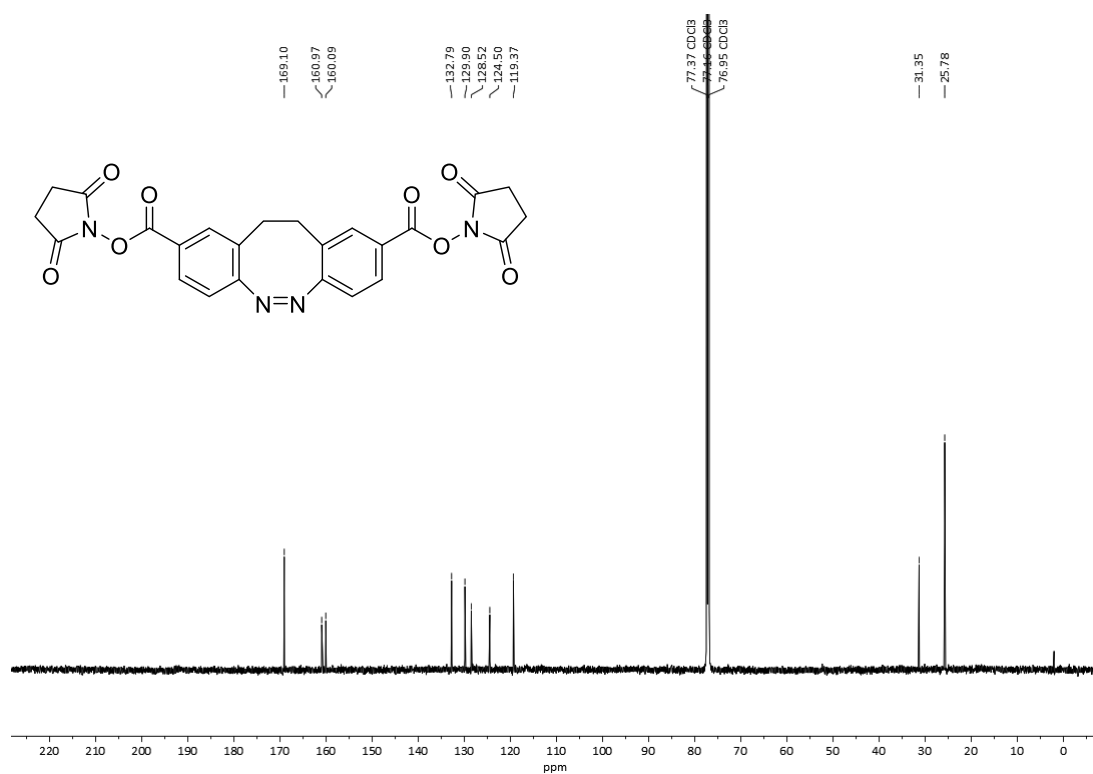
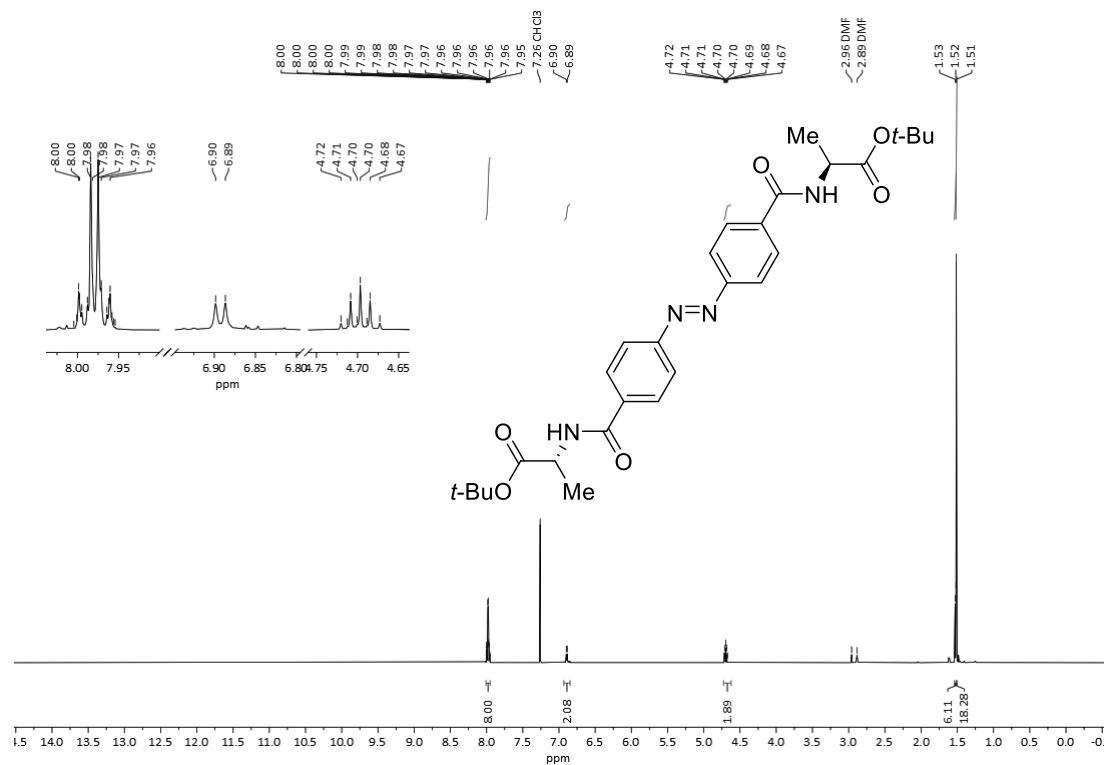
Bis(2,5-dioxopyrrolidin-1-yl) 4,4'-(diazene-1,2-diyl)(*E*)-bis(3,5-dimethoxybenzoate) (**5c**)Figure S31: <sup>1</sup>H NMR spectrum of **5c** in CDCl<sub>3</sub>.Figure S32: <sup>13</sup>C{<sup>1</sup>H} NMR spectrum of **5c** in CDCl<sub>3</sub>.

Bis(2,5-dioxopyrrolidin-1-yl) 4,4'-(diazene-1,2-diyl)(*E*)-bis(3,5-difluorobenzoate) (**5d**)Figure S33:  $^1\text{H}$  NMR spectrum of **5d** in  $\text{DMSO-}d_6$ .Figure S34:  $^{13}\text{C}\{^1\text{H}\}$  NMR spectrum of **5d** in  $\text{DMSO-}d_6$ .

Figure S35:  $^{19}\text{F}$  NMR spectrum of **5d** in  $\text{DMSO-}d_6$ .2,5-Dioxopyrrolidin-1-yl (Z)-11,12-dihydrodibenzo[*c,g*][1,2]diazocine-2-carboxylate (**8a**)Figure S36:  $^1\text{H}$  NMR spectrum of **8a** in  $\text{CDCl}_3$ .



Figure S37:  $^{13}\text{C}\{^1\text{H}\}$  NMR spectrum of **8a** in  $\text{CDCl}_3$ .Bis(2,5-dioxopyrrolidin-1-yl) (Z)-11,12-dihydrobenzo[*c,g*][1,2]diazocine-2,9-dicarboxylate (**8b**)Figure S38:  $^1\text{H}$  NMR spectrum of **8b** in  $\text{CDCl}_3$ .

Figure S39:  $^{13}\text{C}\{^1\text{H}\}$  NMR spectrum of **8b** in  $\text{CDCl}_3$ .Di-tert-butyl 2,2'-((4,4'-(diazene-1,2-diyl)bis(benzoyl))bis(azanediyloxy))(*E*)-dipropionate (**10a**)Figure S40:  $^1\text{H}$  NMR spectrum of **10a** in  $\text{CDCl}_3$ .

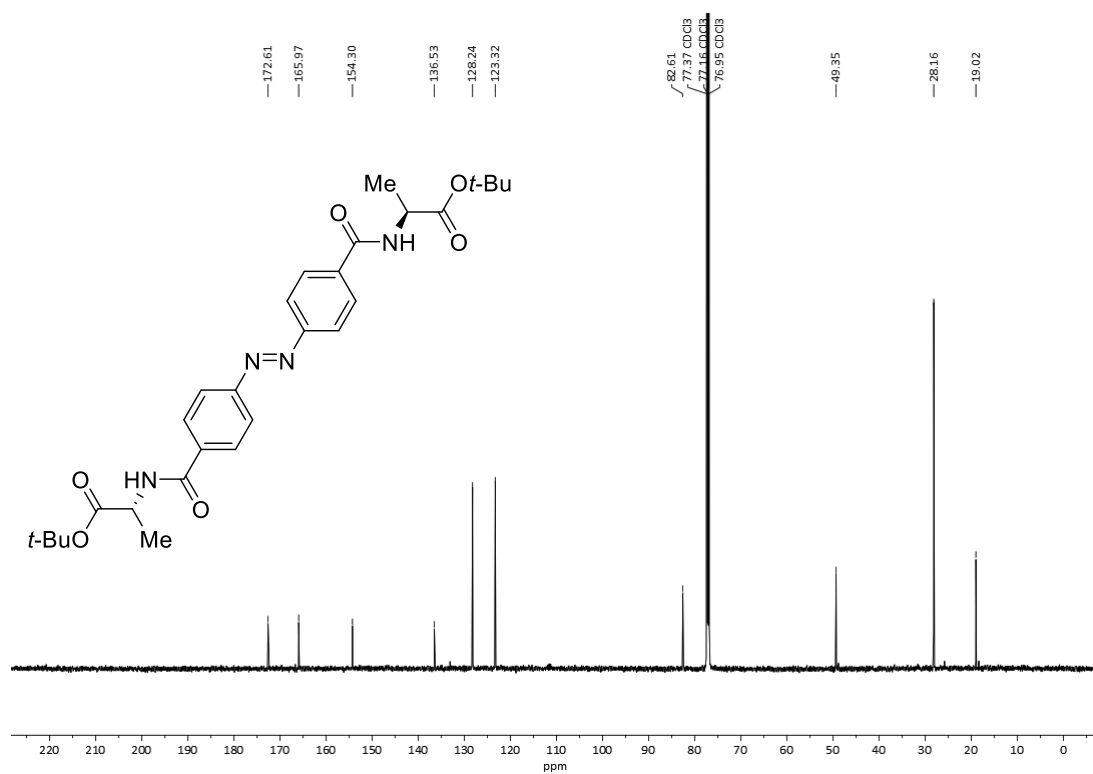
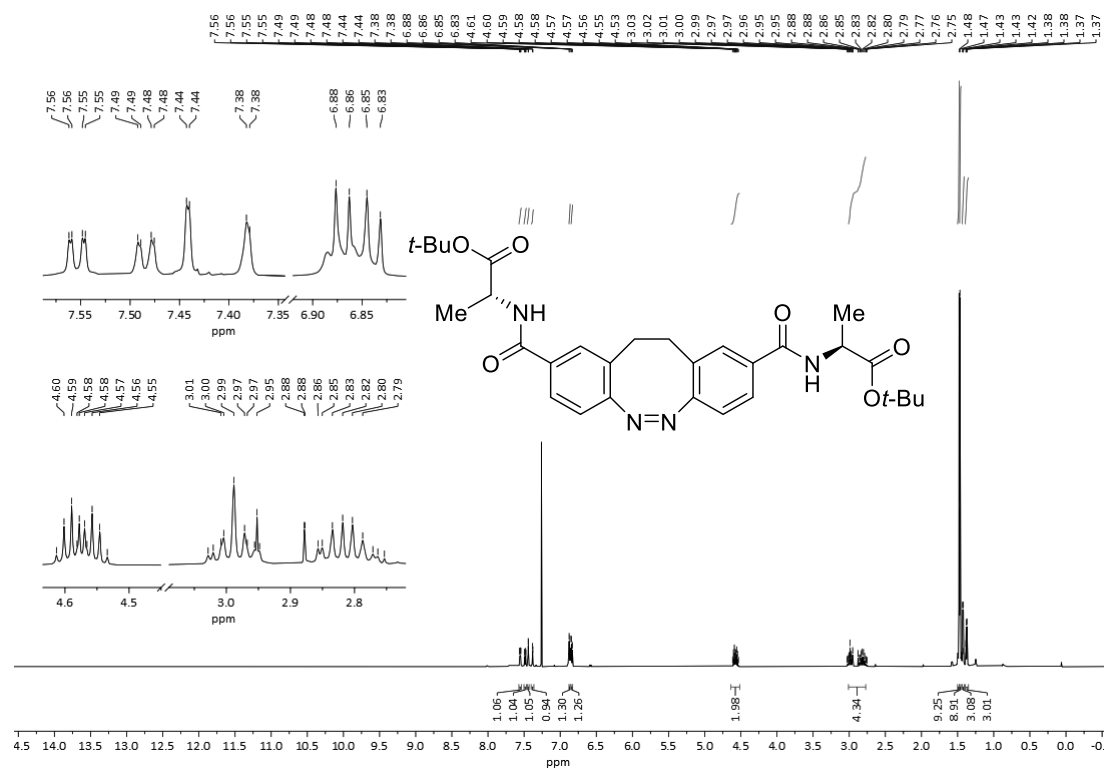
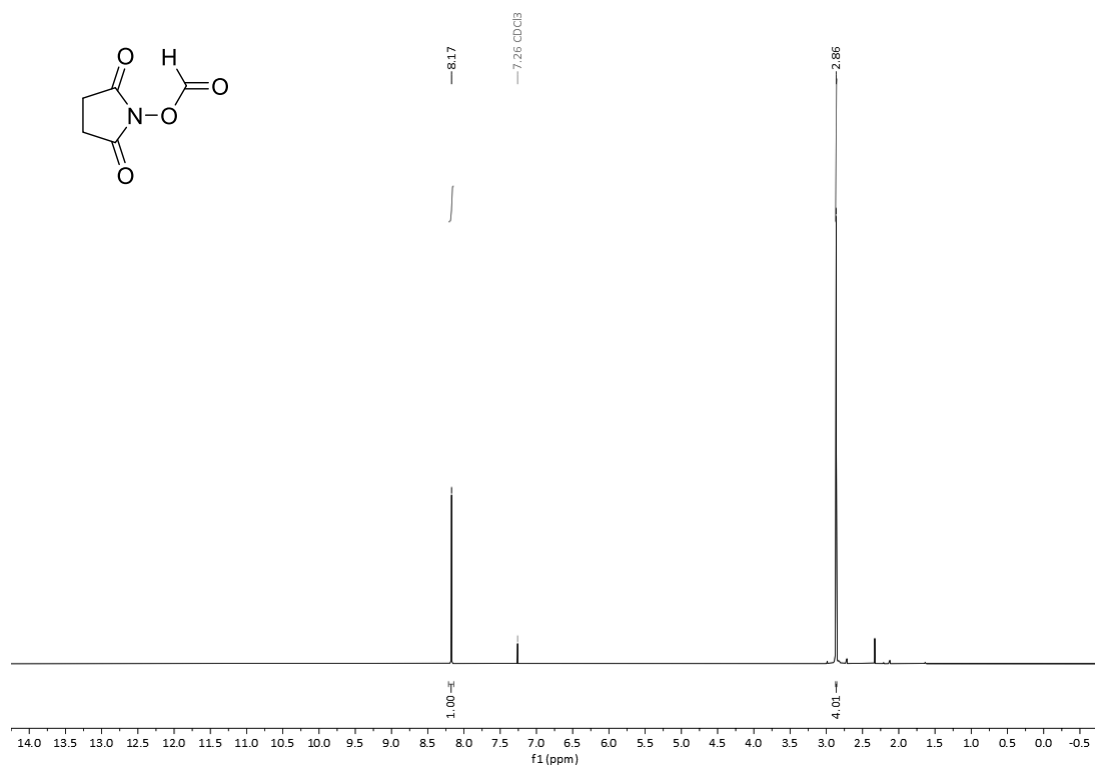
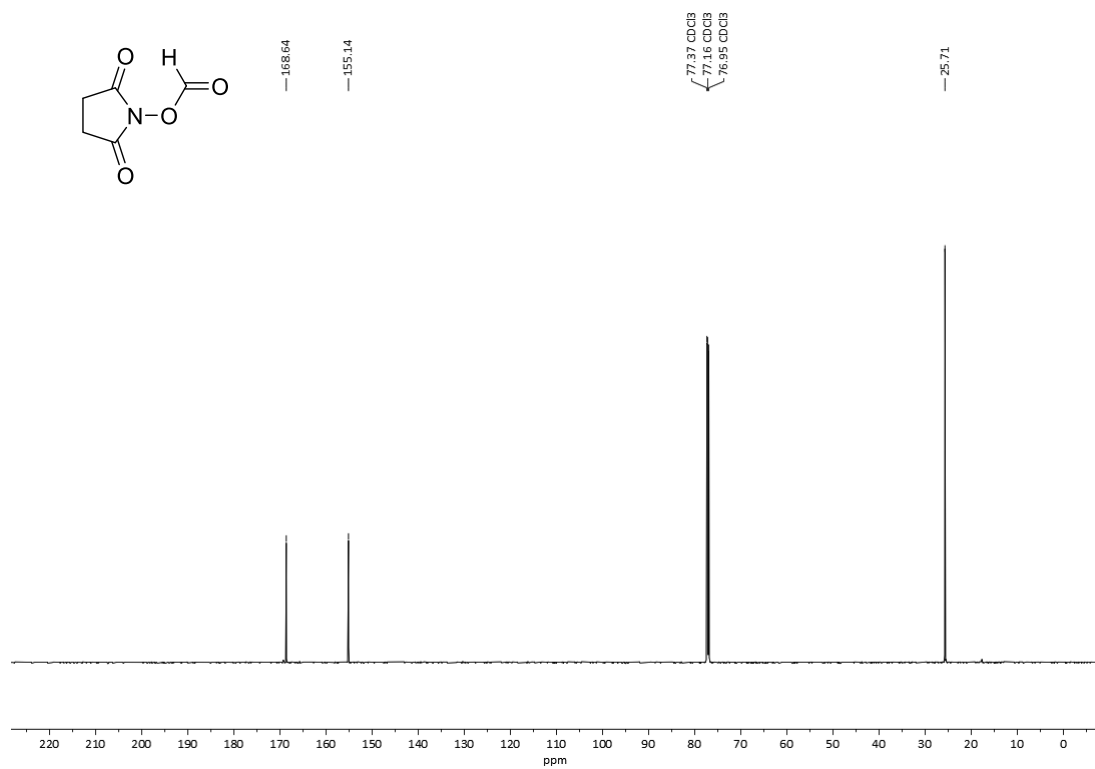
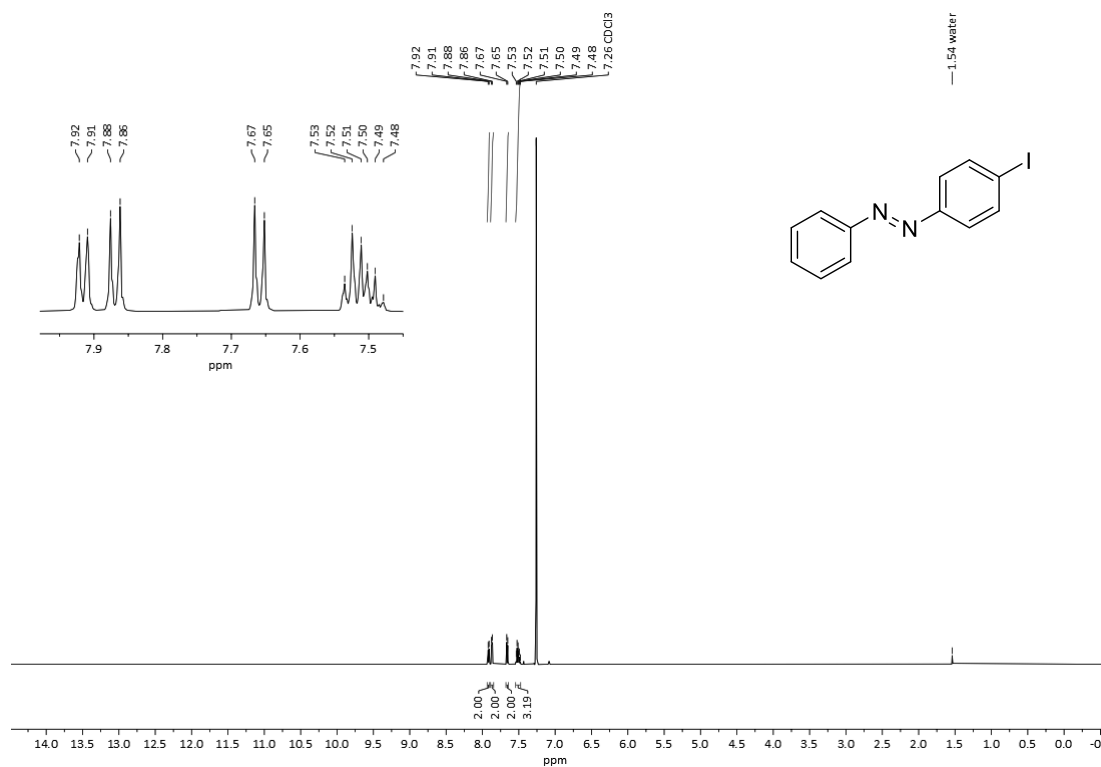
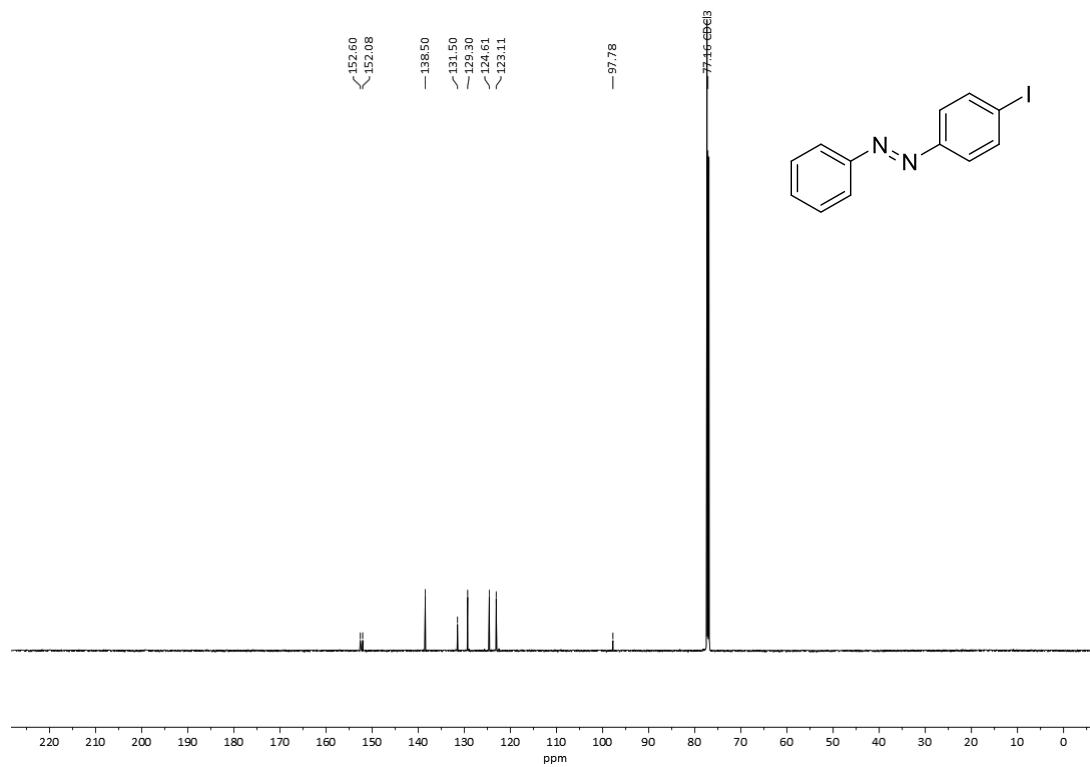


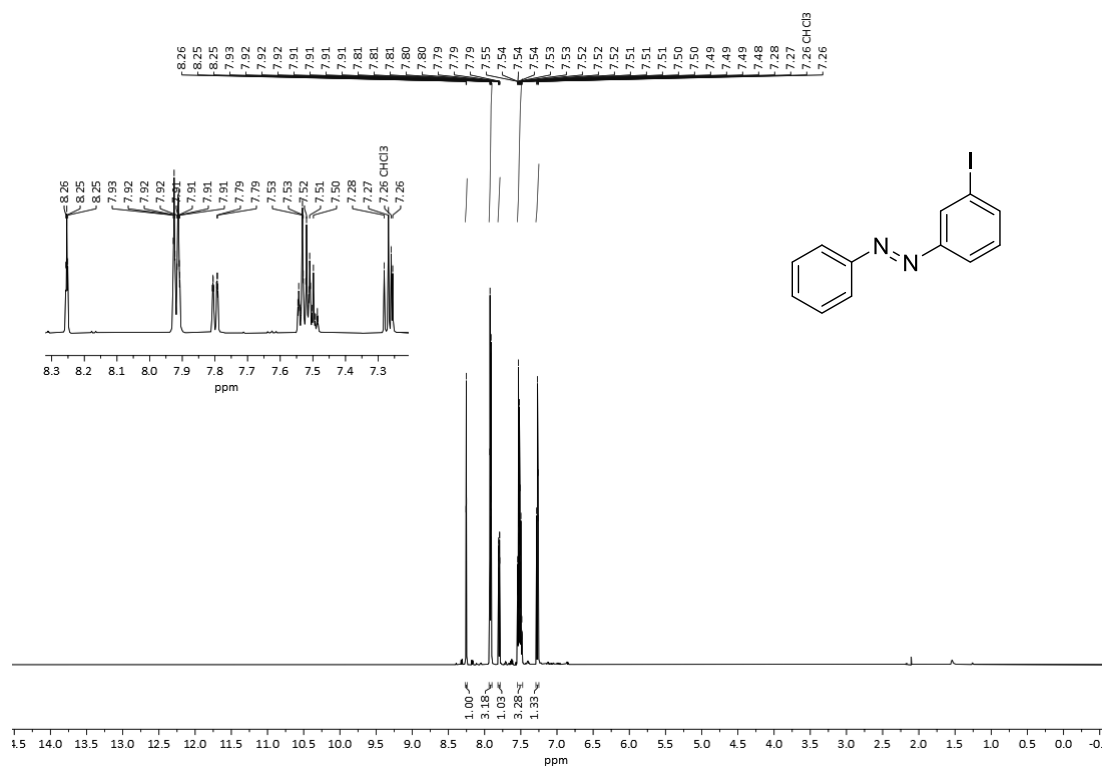
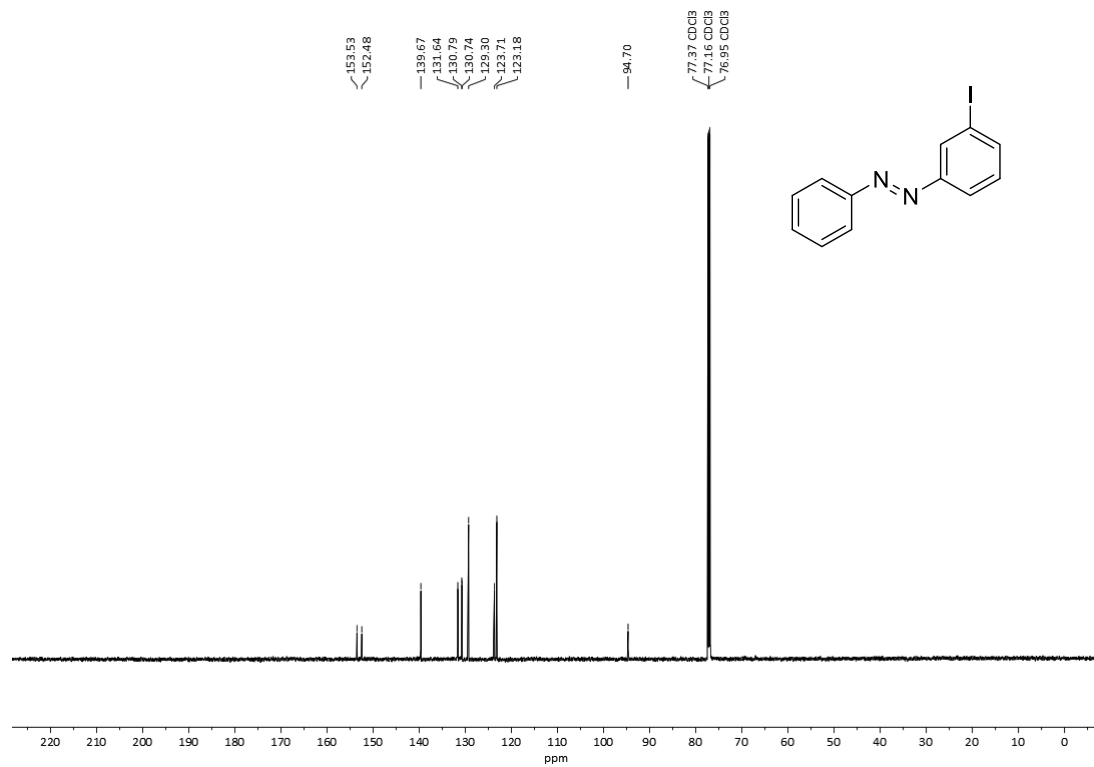
Figure S41:  $^{13}\text{C}\{^1\text{H}\}$  NMR spectrum of **10a** in  $\text{CDCl}_3$ .

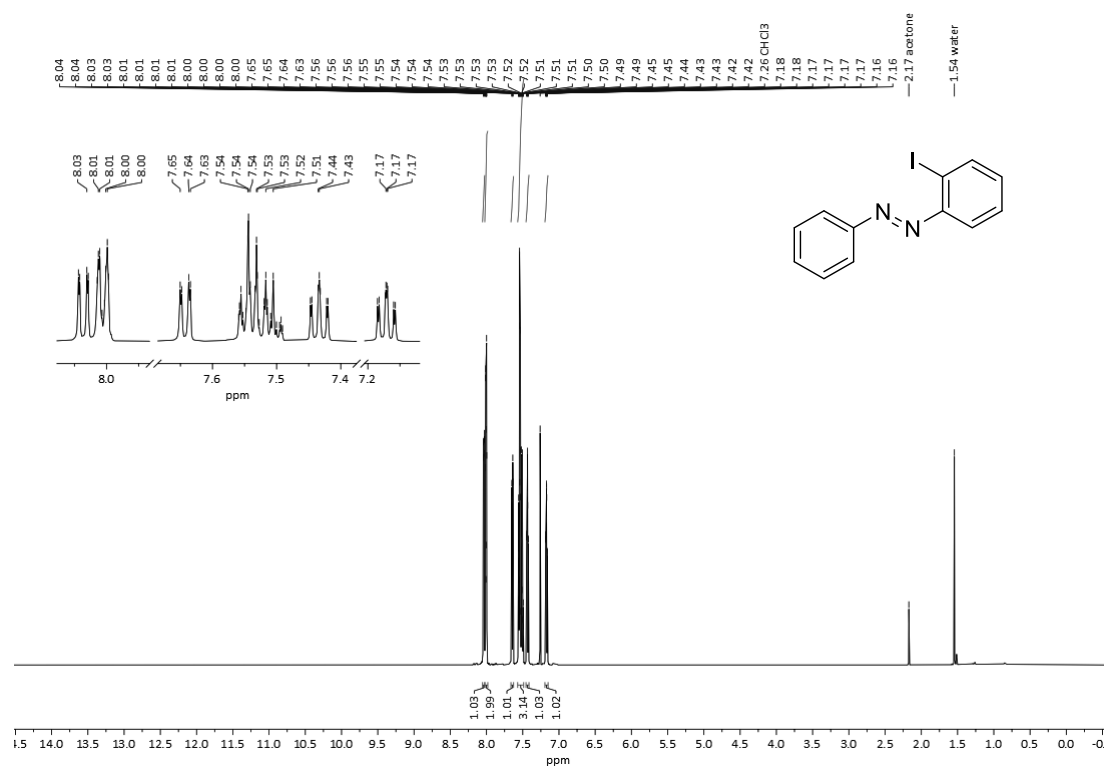
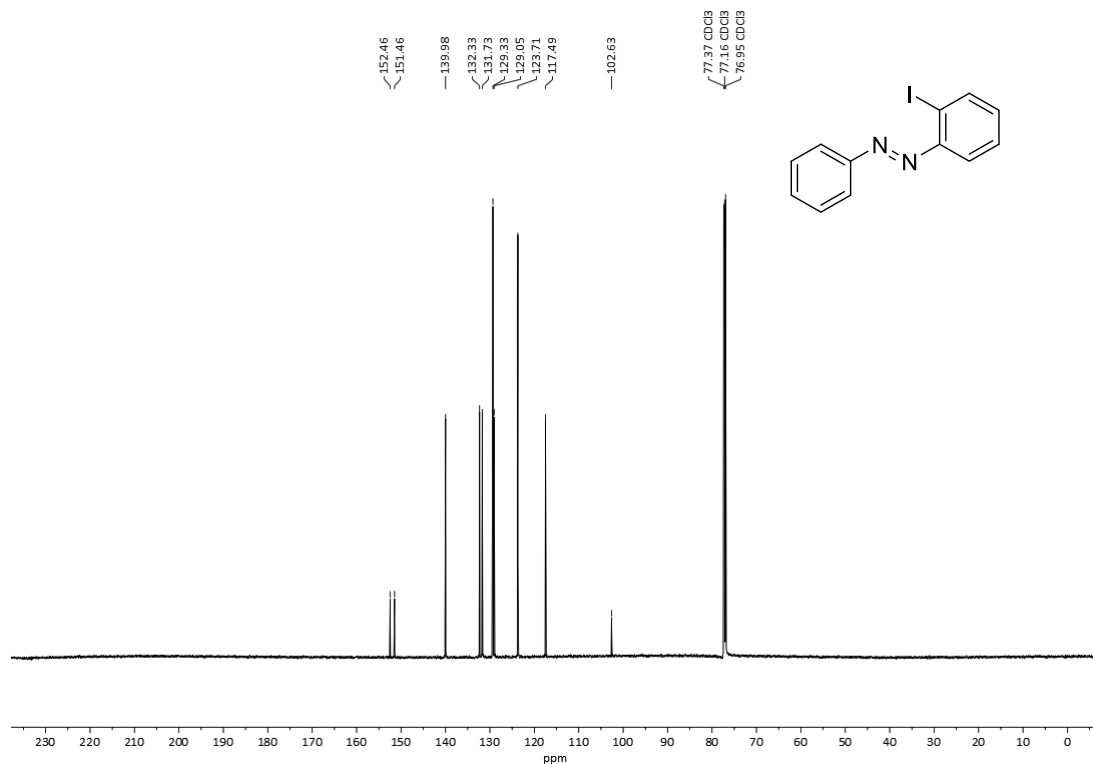
Di-tert-butyl 2,2'-((11,12-dihydrodibenzo[*c,g*][1,2]diazocine-2,9-dicarbonyl)bis(azane-diyl))(*Z*)-dipropionate (**10b**)

Figure S42:  $^1\text{H}$  NMR spectrum of **10b** in  $\text{CDCl}_3$ .Figure S43:  $^{13}\text{C}\{^1\text{H}\}$  NMR spectrum of **10b** in  $\text{CDCl}_3$ .

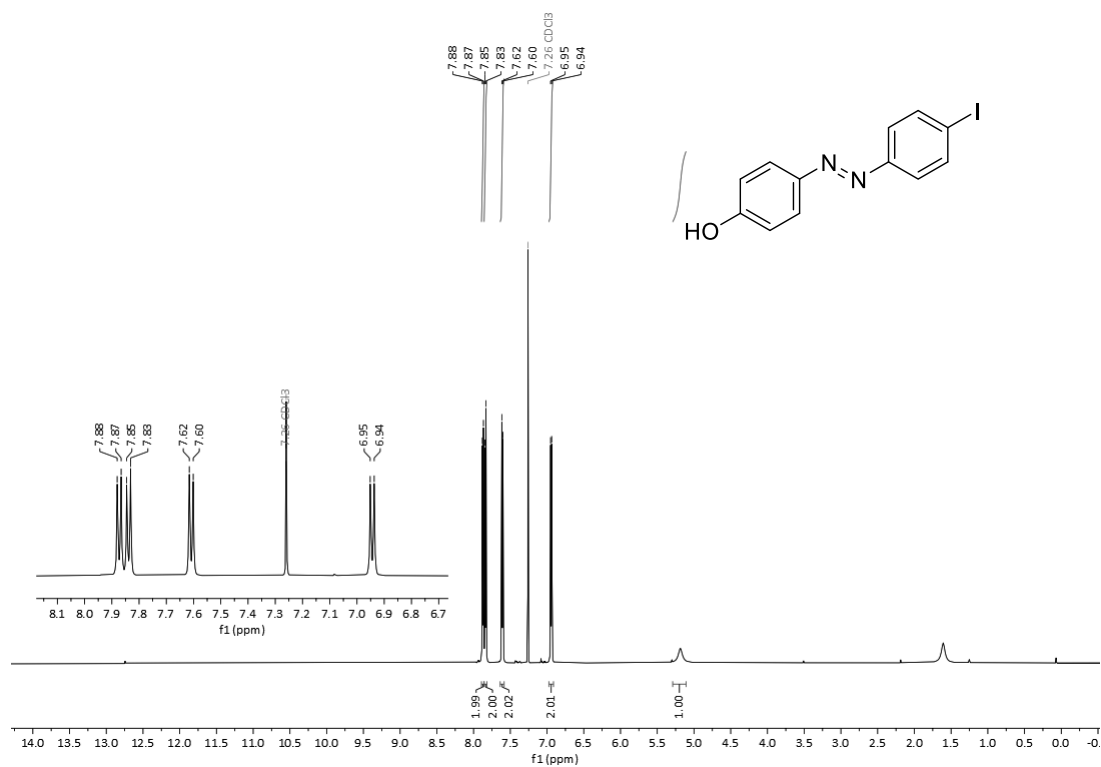
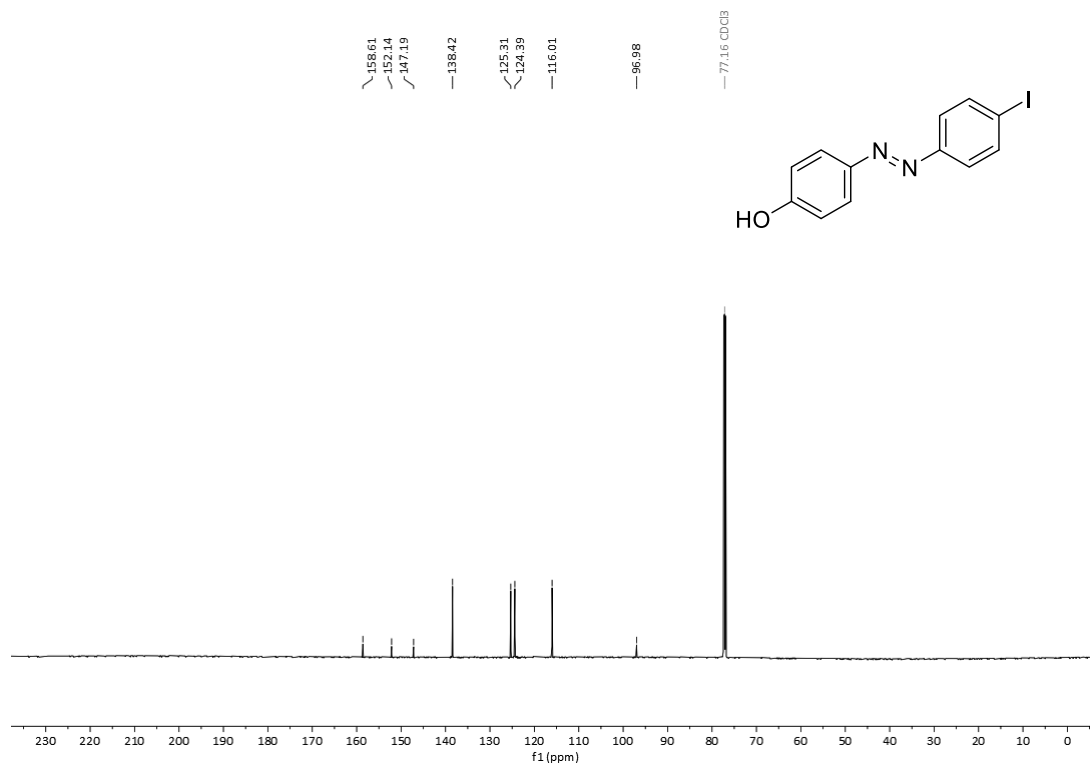
*N*-Hydroxysuccinimidyl formate (**2**)Figure S44: <sup>1</sup>H NMR spectrum of **2** in CDCl<sub>3</sub>.Figure S45: <sup>13</sup>C{<sup>1</sup>H} NMR spectrum of **2** in CDCl<sub>3</sub>.

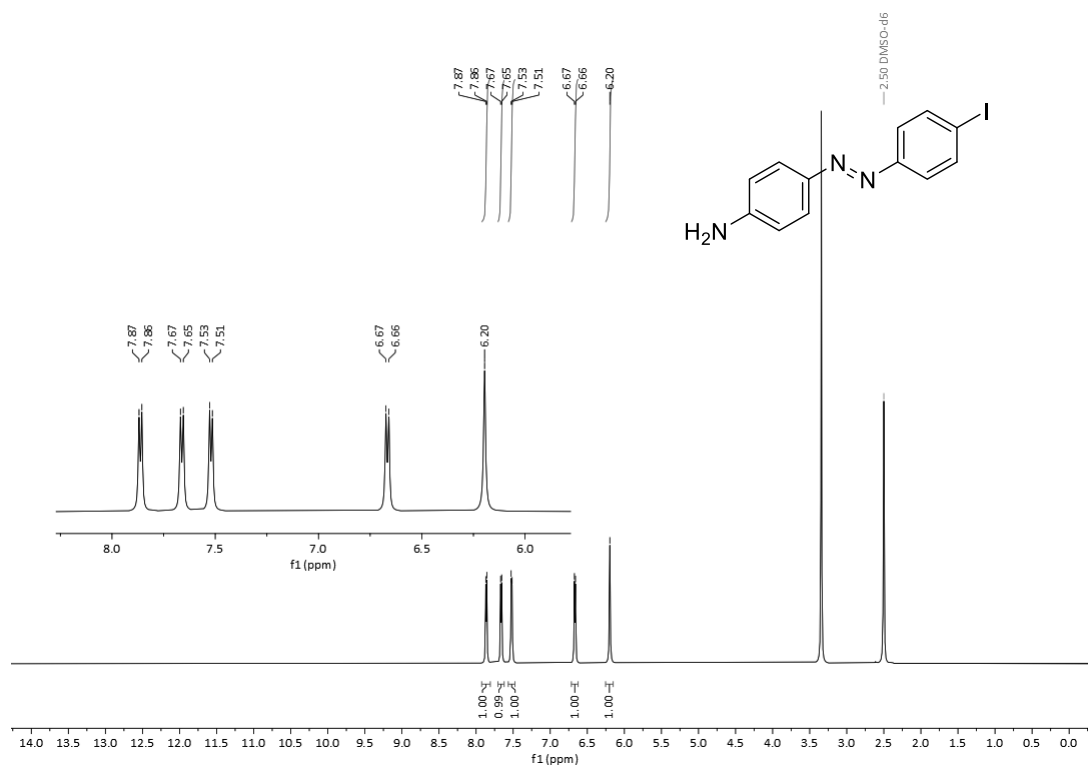
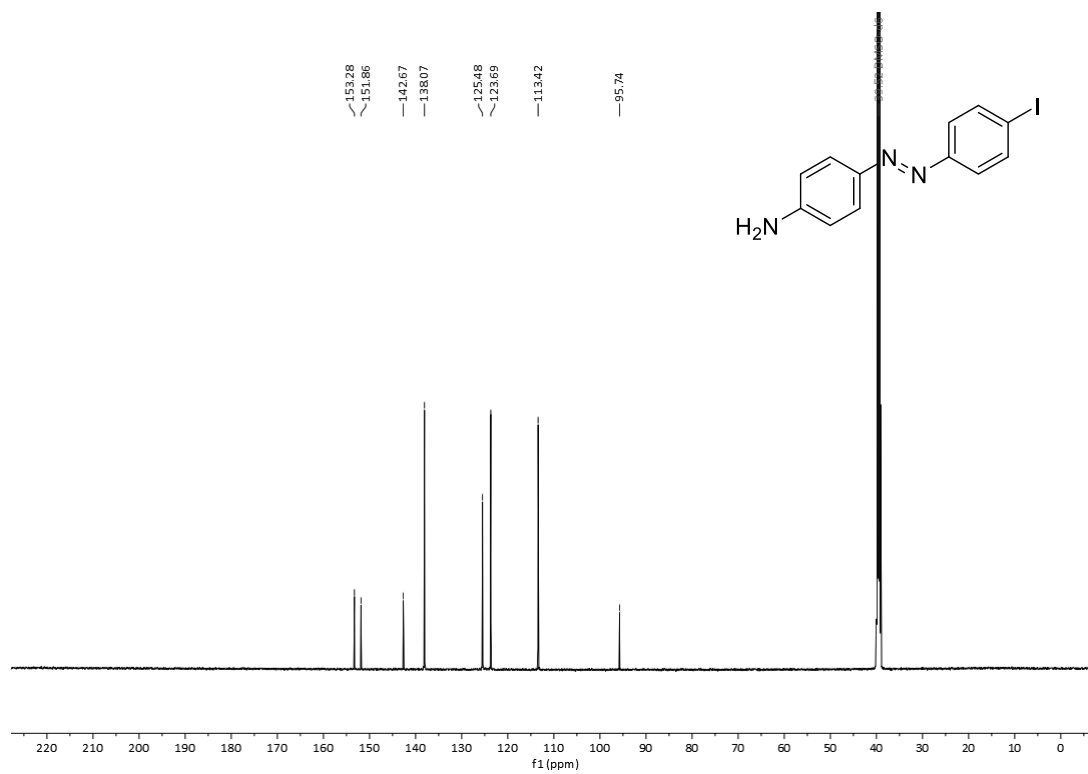
**(E)-1-(4-Iodophenyl)-2-phenyldiazene (1a)****Figure S46:  $^1\text{H}$  NMR spectrum of 1a in  $\text{CDCl}_3$ .****Figure S47:  $^{13}\text{C}$  NMR spectrum of 1a in  $\text{CDCl}_3$ .**

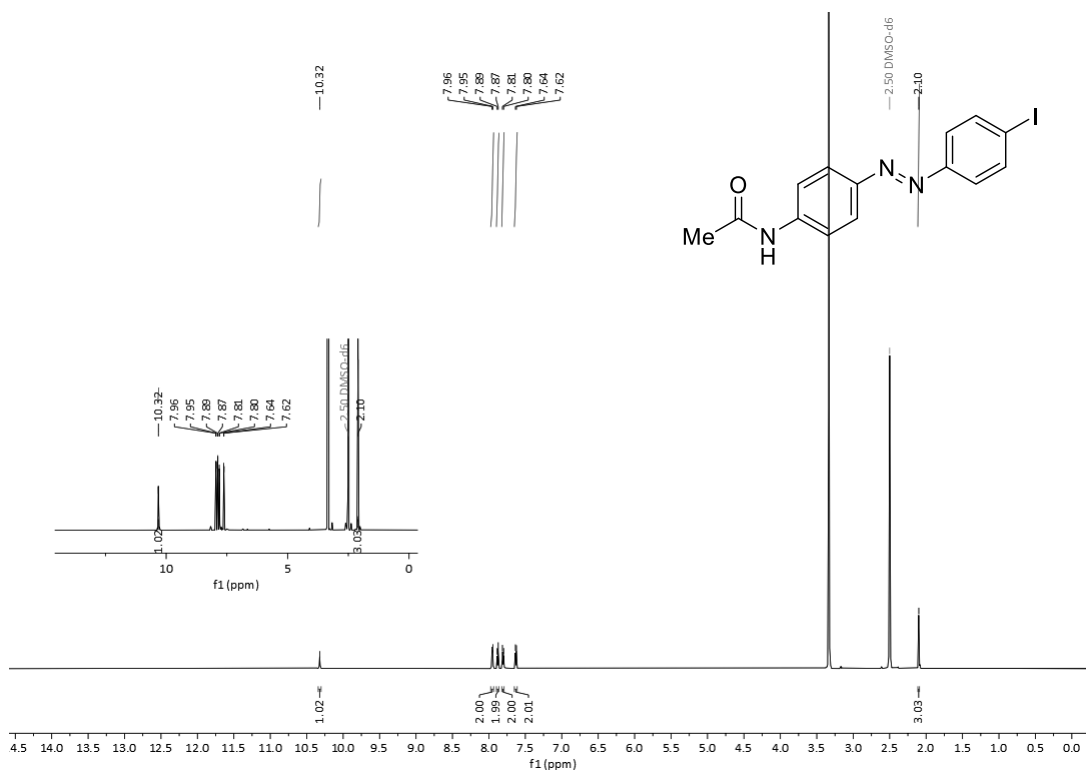
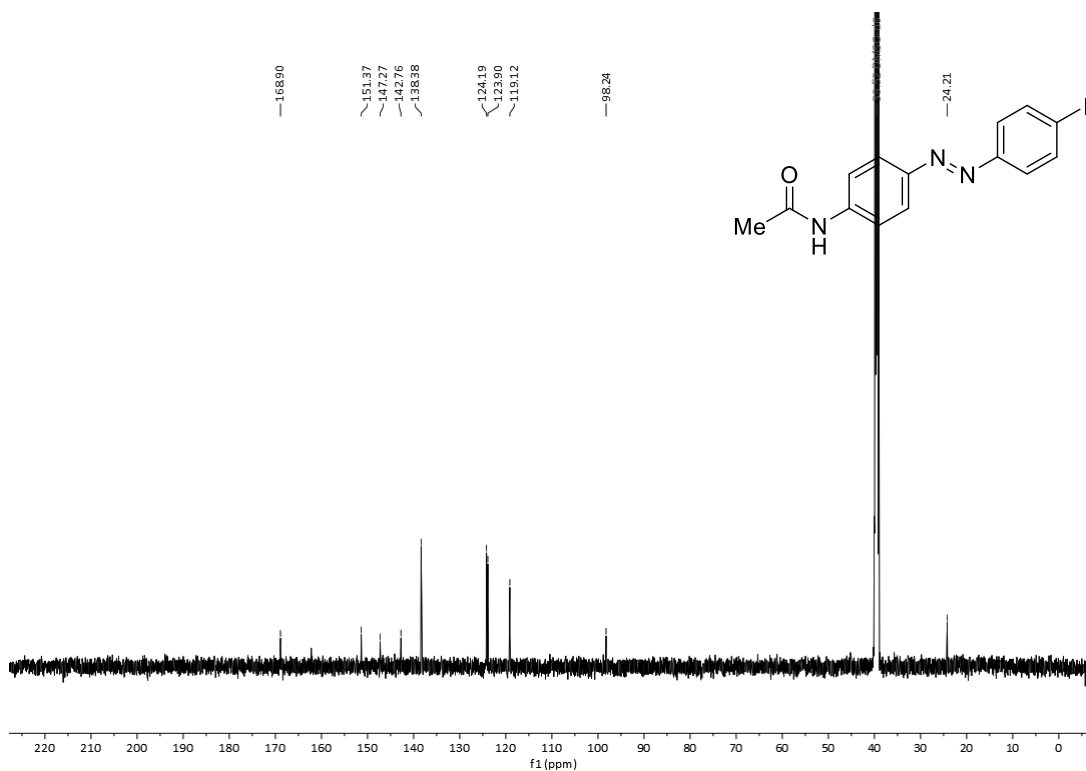
**(E)-1-(3-Iodophenyl)-2-phenyldiazene (1b)**Figure S48: <sup>1</sup>H NMR spectrum of 1b in CDCl<sub>3</sub>.Figure S49: <sup>13</sup>C{<sup>1</sup>H} NMR spectrum of 1b in CDCl<sub>3</sub>.

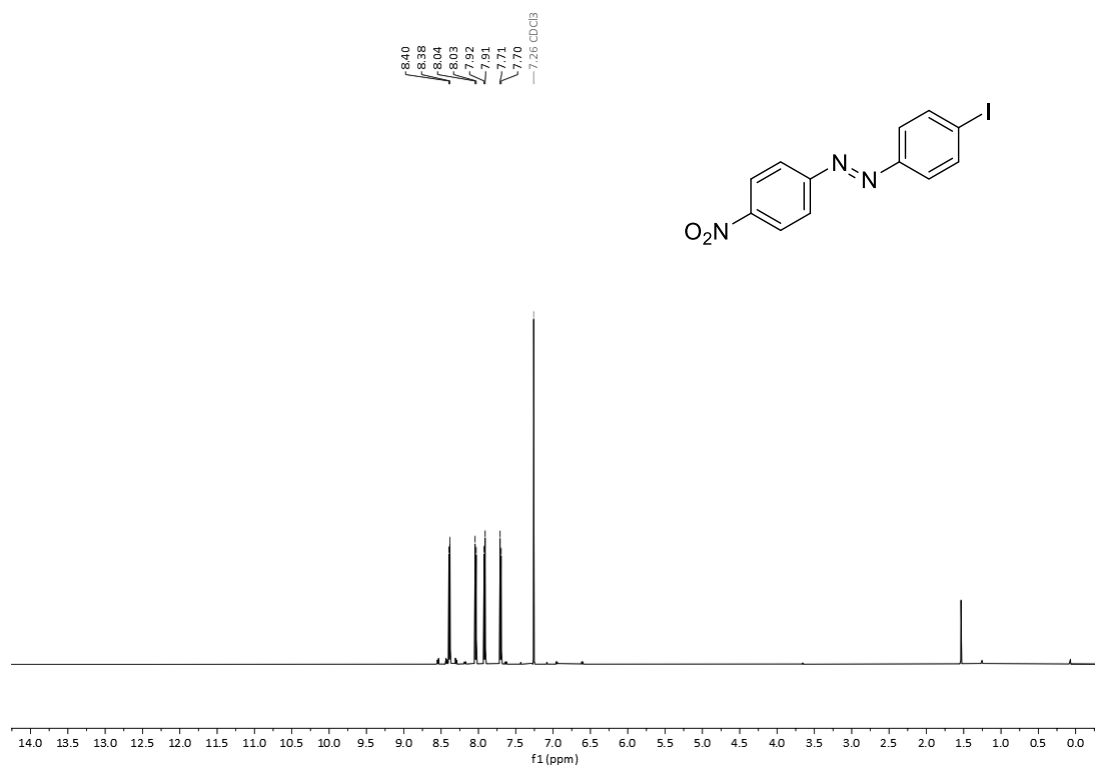
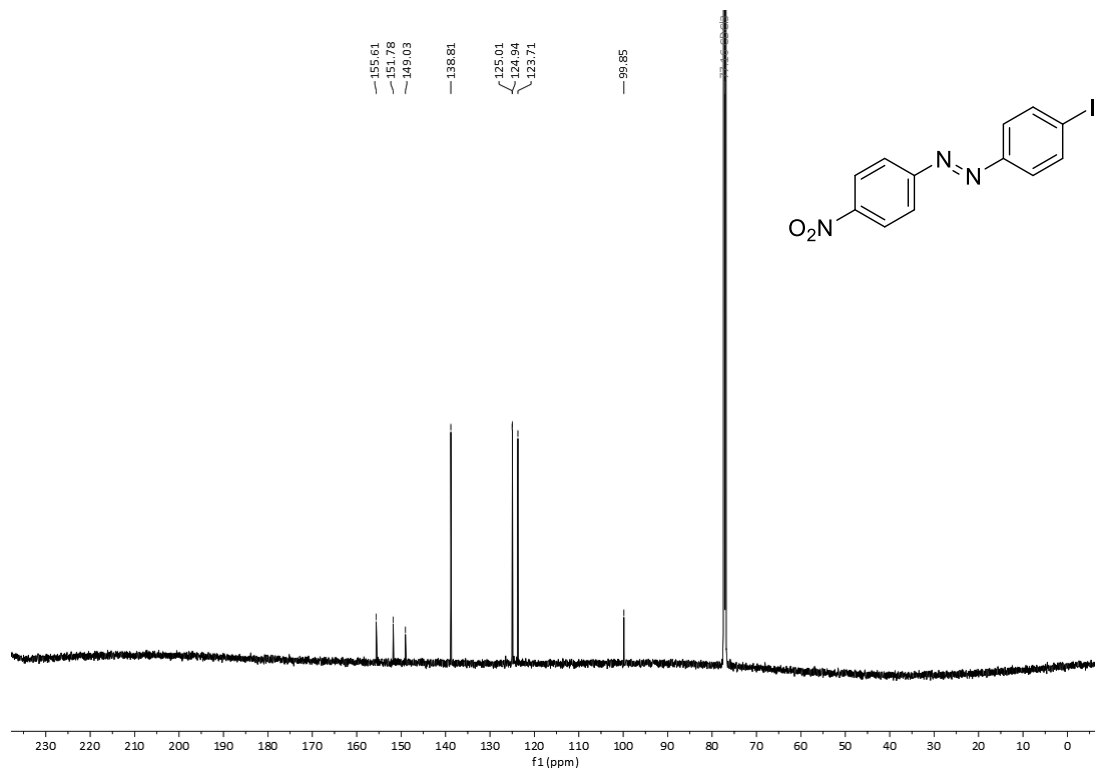
**(E)-1-(2-Iodophenyl)-2-phenyldiazene (1c)****Figure S50:  $^1\text{H}$  NMR spectrum of 1c in  $\text{CDCl}_3$ .****Figure S51:  $^{13}\text{C}\{^1\text{H}\}$  NMR spectrum of 1c in  $\text{CDCl}_3$ .**

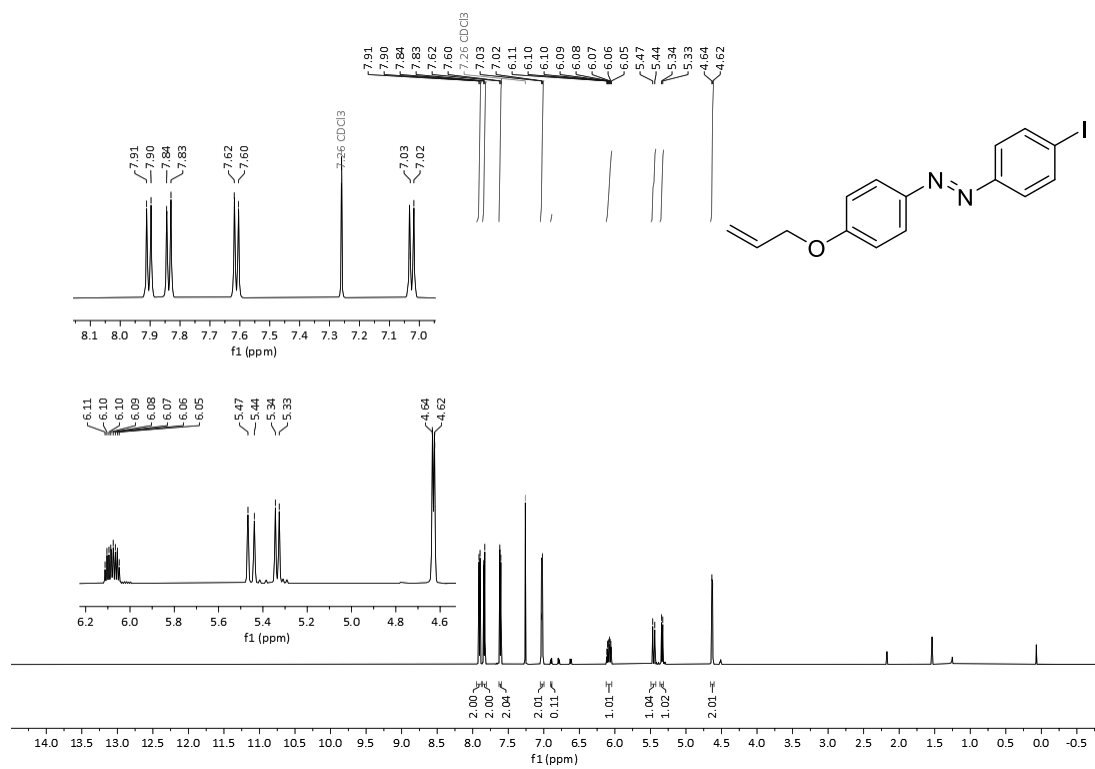
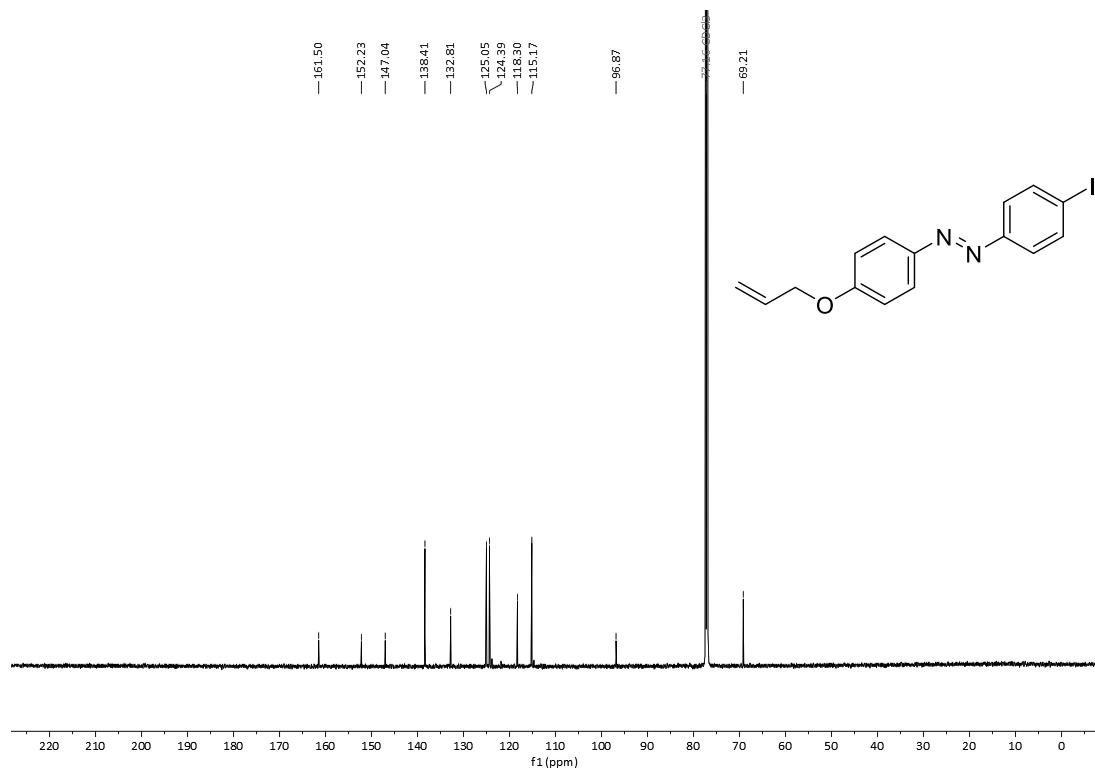


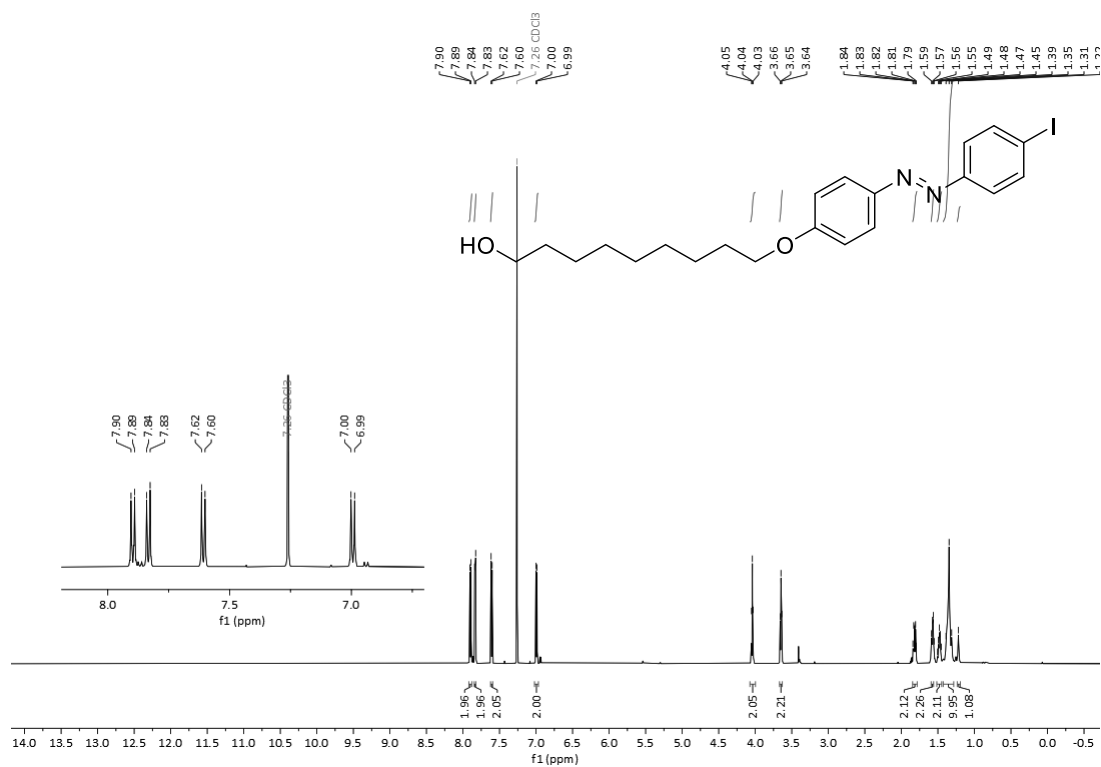
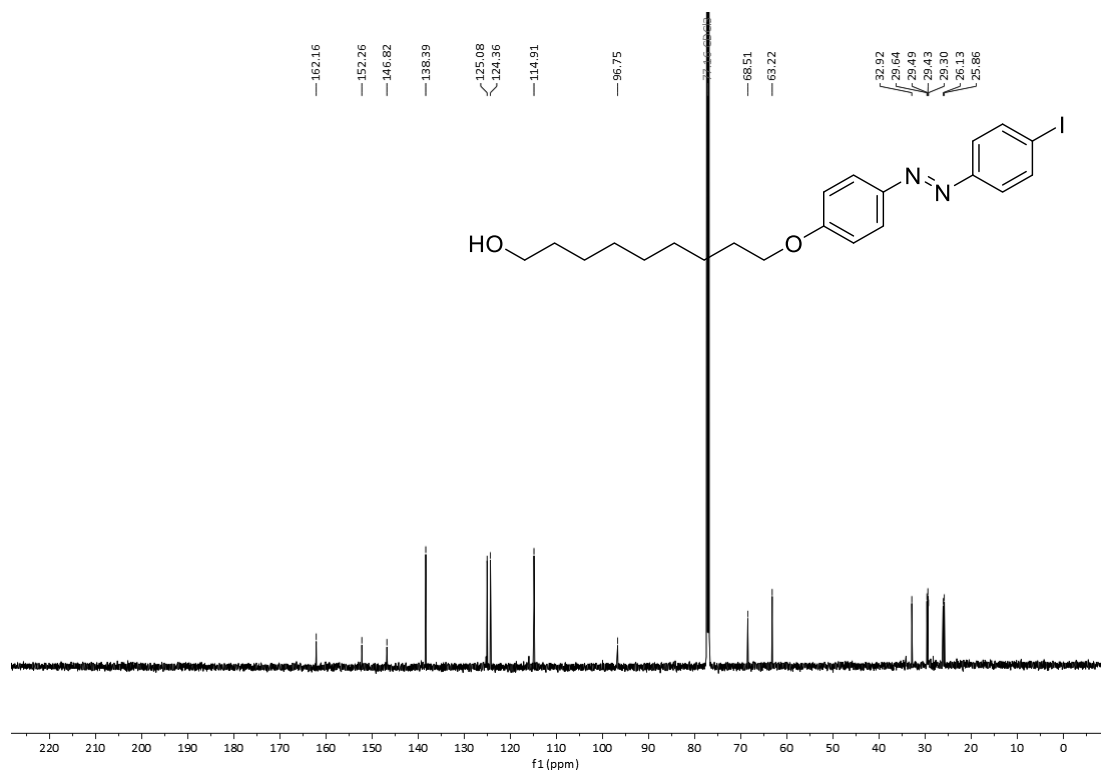
**(E)-4-((4-Iodophenyl)diazenyl)phenol (1d)****Figure S52:  $^1\text{H}$  NMR spectrum of 1d in  $\text{CDCl}_3$ .****Figure S53:  $^{13}\text{C}\{^1\text{H}\}$  NMR spectrum of 1d in  $\text{CDCl}_3$ .**

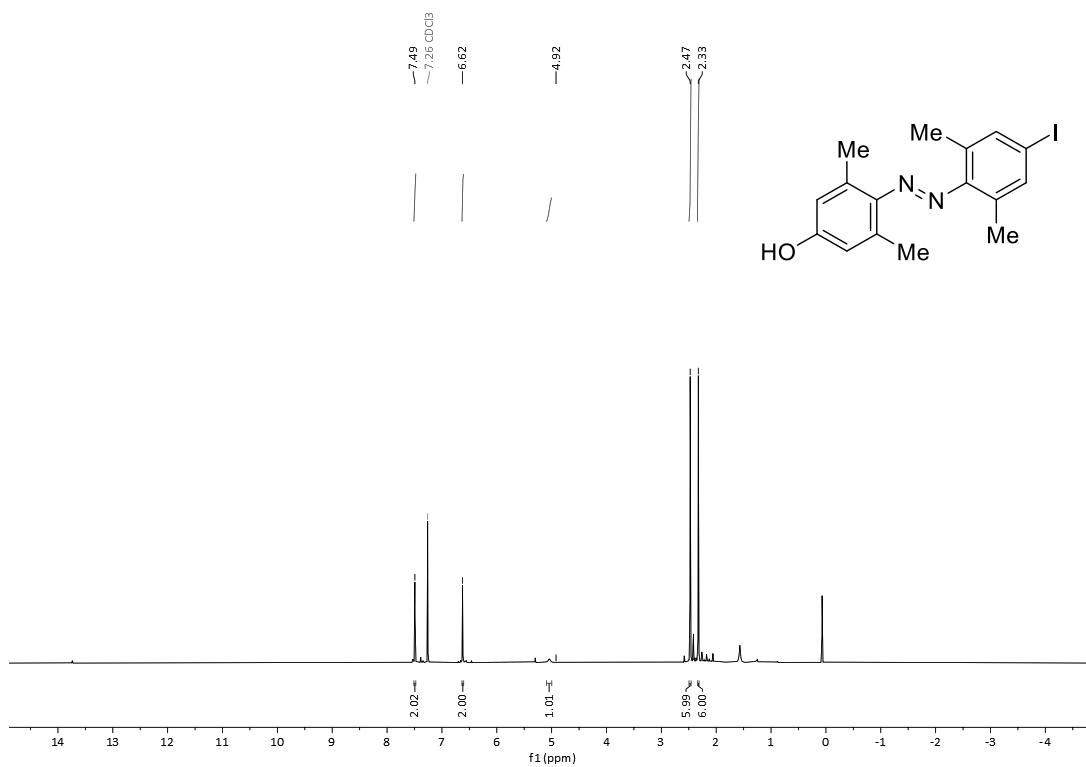
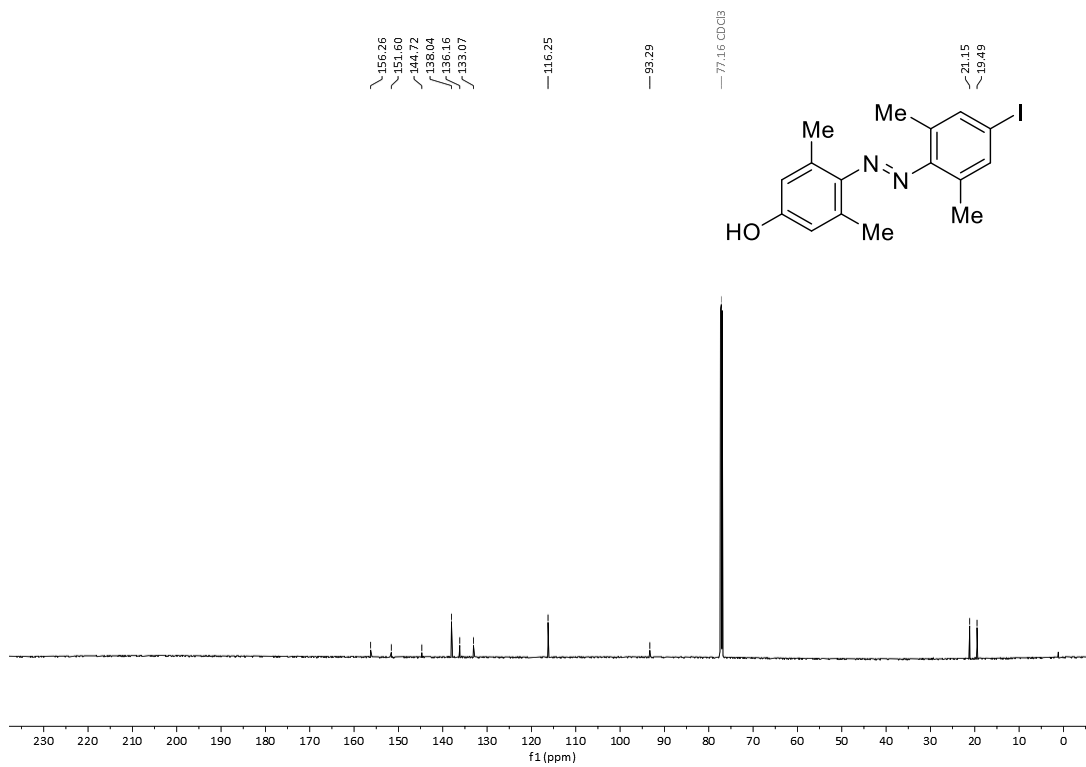
**(E)-4-((4-Iodophenyl)diazenyl)aniline (**1e**)****Figure S54:**  $^1\text{H}$  NMR spectrum of **1e** in  $\text{DMSO-}d_6$ .**Figure S55:**  $^{13}\text{C}\{^1\text{H}\}$  NMR spectrum of **1e** in  $\text{DMSO-}d_6$ .

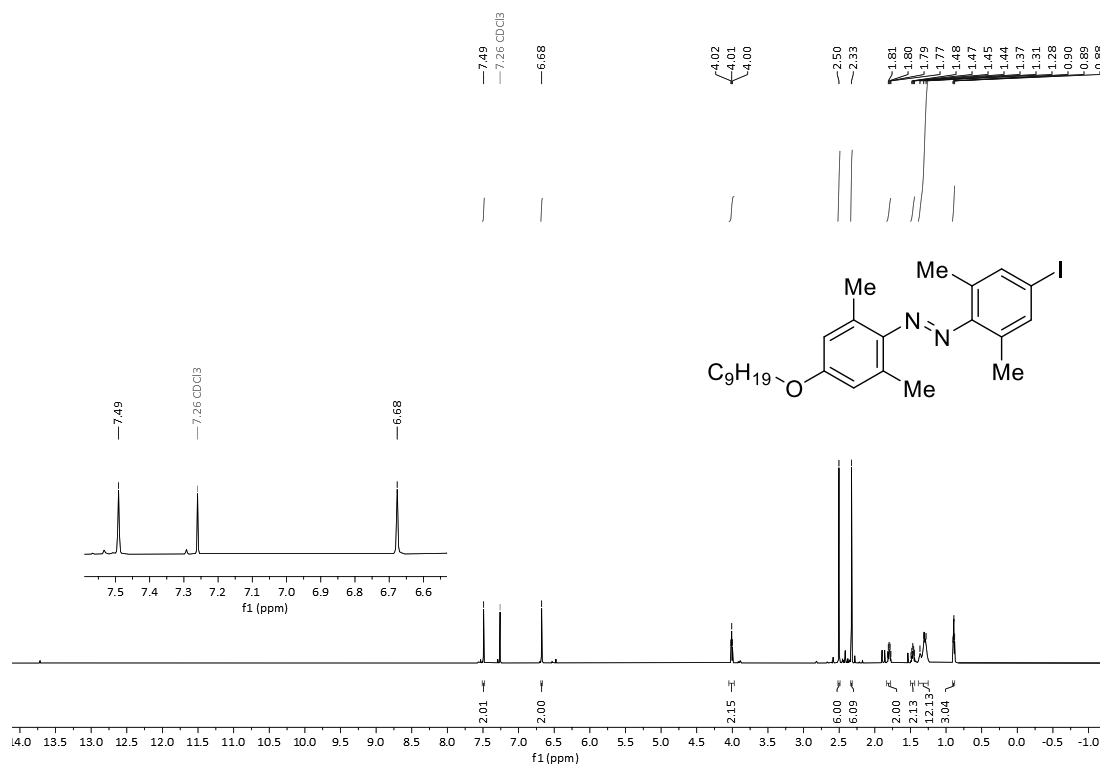
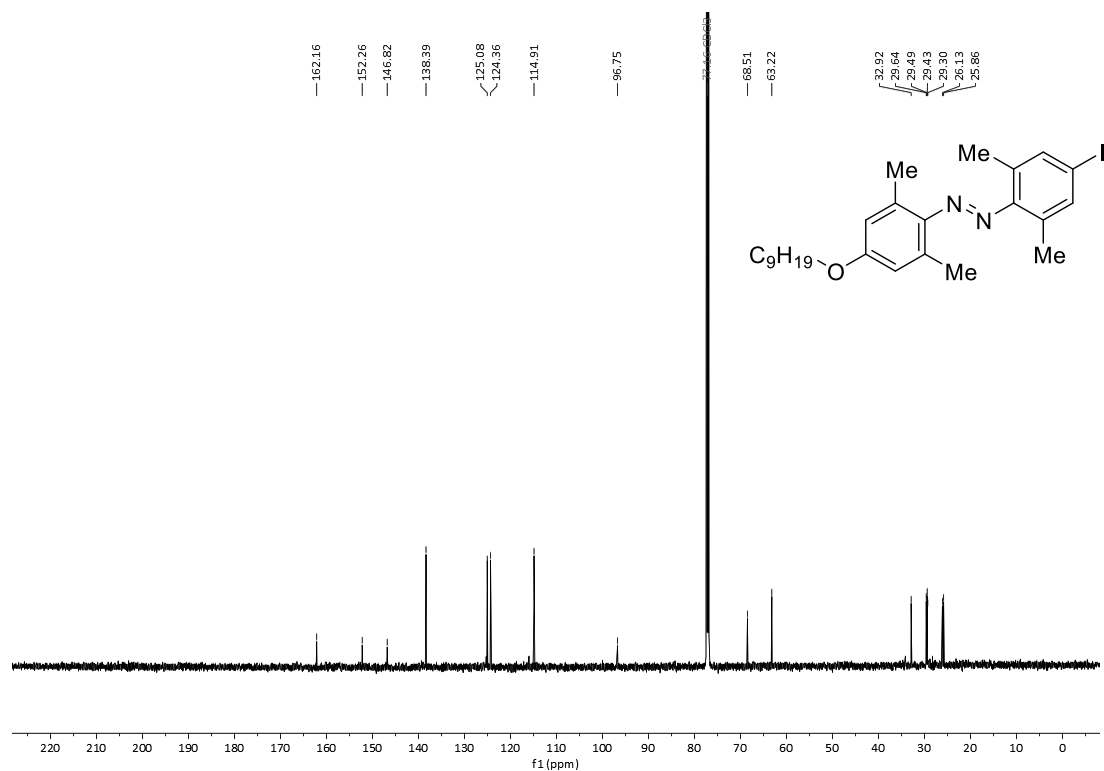
**(E)-N-(4-((4-iodophenyl)diazenyl)phenyl)acetamide (1f)****Figure S56:** <sup>1</sup>H NMR spectrum of **1f** in DMSO-*d*<sub>6</sub>.**Figure S57:** <sup>13</sup>C NMR spectrum of **1f** in DMSO-*d*<sub>6</sub>.

**(E)-1-(4-Iodophenyl)-2-(4-nitrophenyl)diazene (1g)**Figure S58: <sup>1</sup>H NMR spectrum of 1g in CDCl<sub>3</sub>.Figure S59: <sup>13</sup>C{<sup>1</sup>H} NMR spectrum of 1g in CDCl<sub>3</sub>.

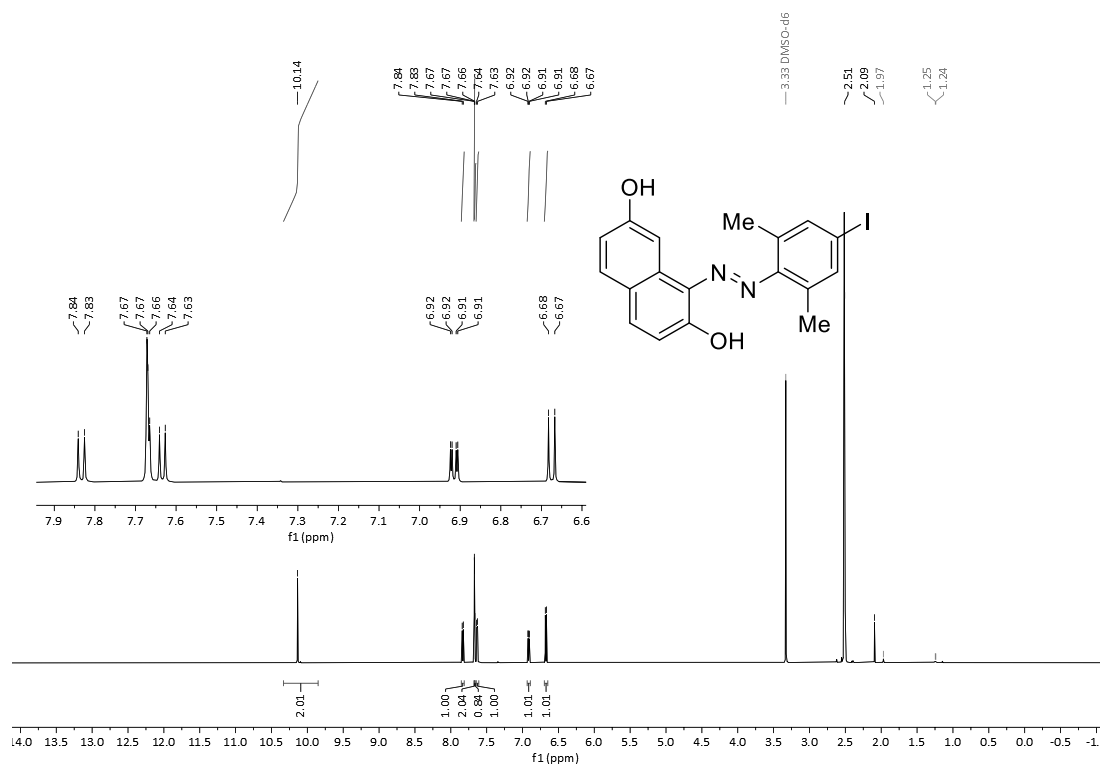
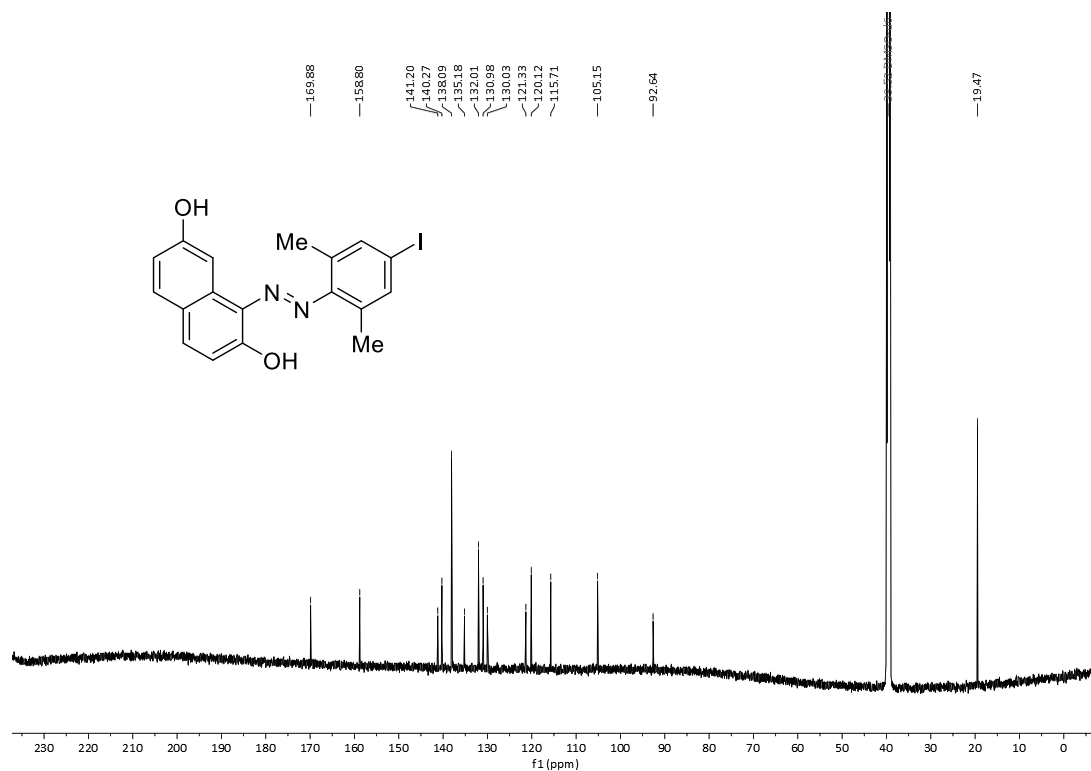
**(E)-1-(4-(Allyloxy)phenyl)-2-(4-iodophenyl)diazene (1h)****Figure S60:  $^1\text{H}$  NMR spectrum of 1h in  $\text{CDCl}_3$ .****Figure S61:  $^{13}\text{C}$  NMR spectrum of 1h in  $\text{CDCl}_3$ .**

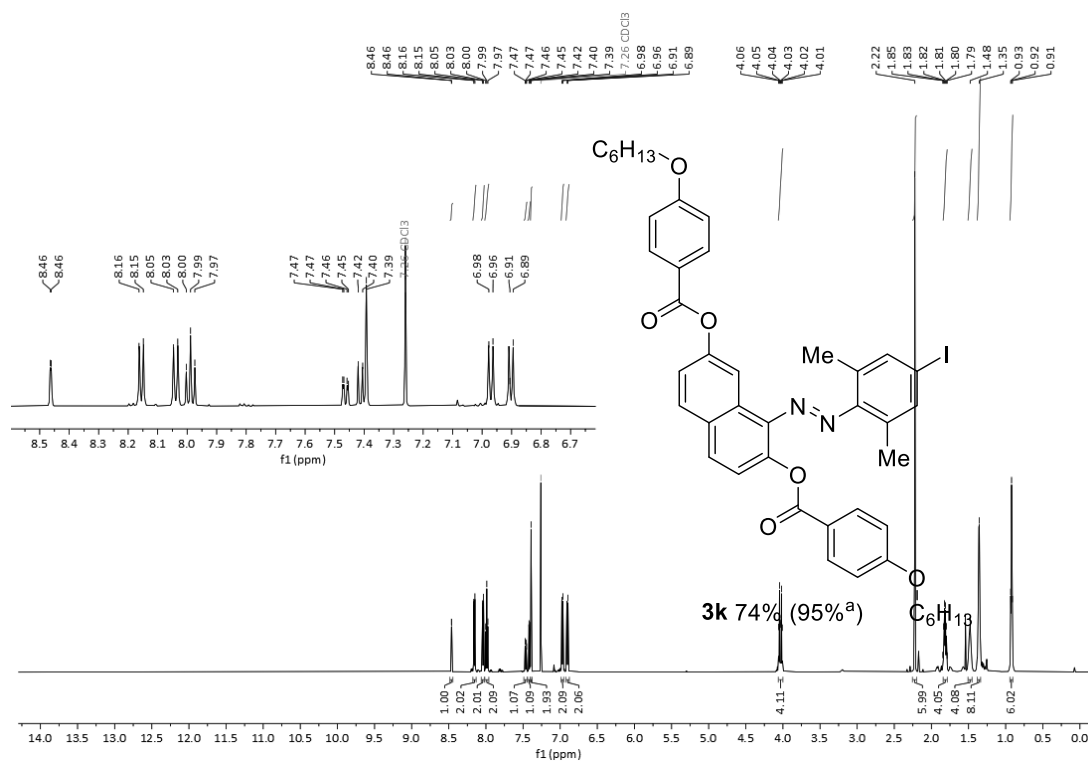
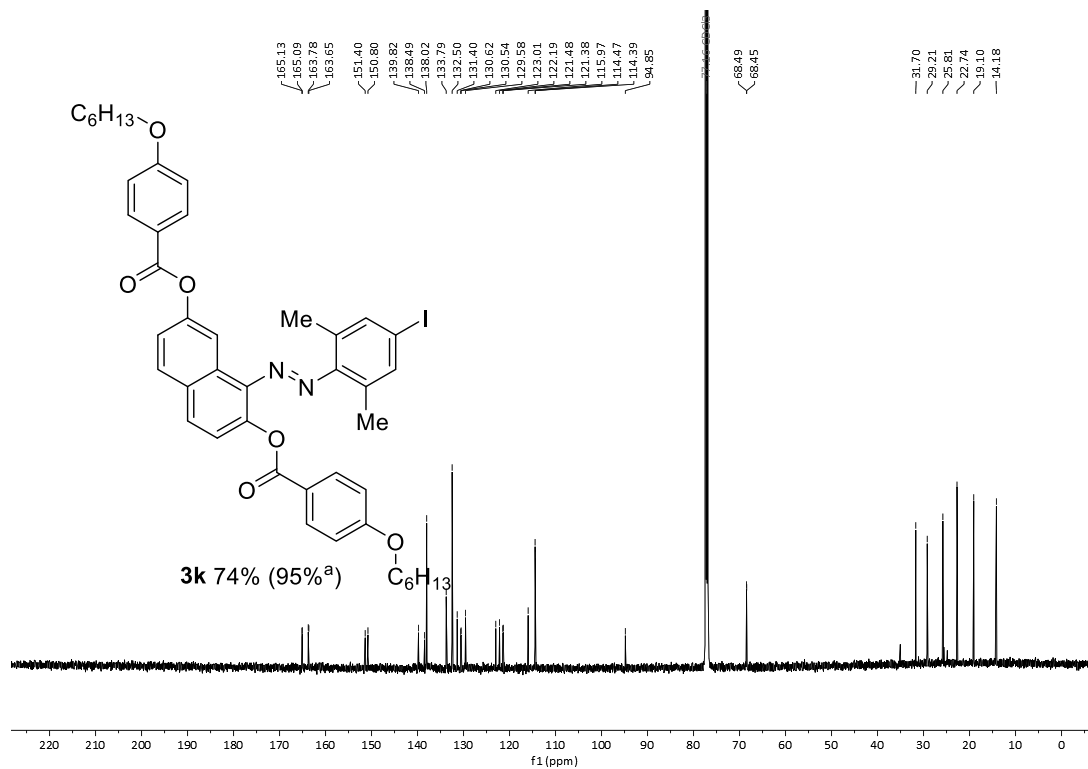
*(E)*-9-((4-(4-iodophenyl)diazenyl)phenoxy)nonan-1-ol (**1i**)**Figure S62:**  $^1\text{H}$  NMR spectrum of **1i** in  $\text{CDCl}_3$ .**Figure S63:**  $^{13}\text{C}$  NMR spectrum of **1i** in  $\text{CDCl}_3$ .

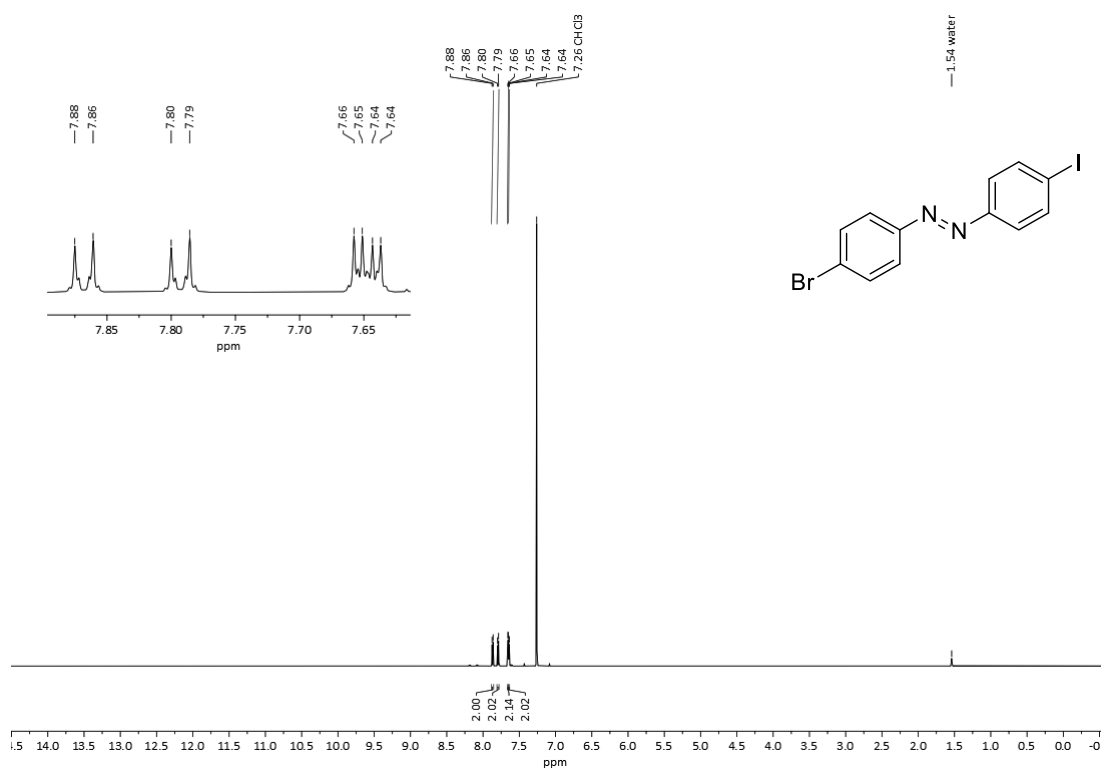
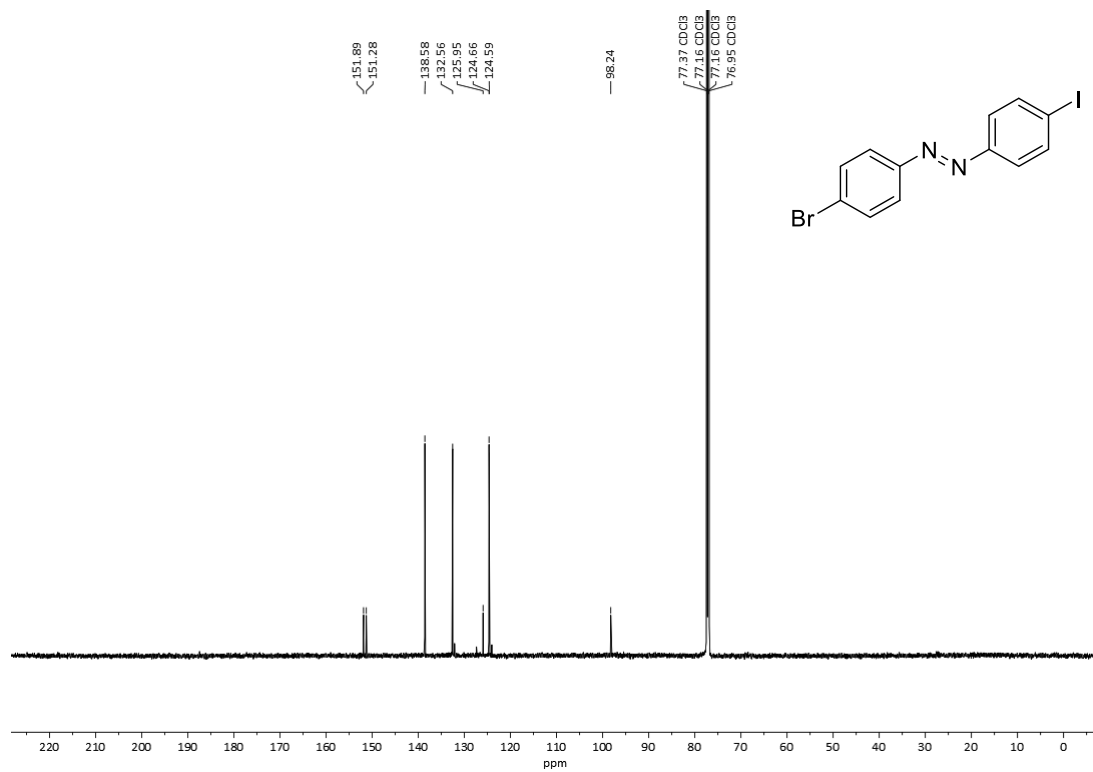
**(E)-4-((4-Iodo-2,6-dimethylphenyl)diazenyl)-3,5-dimethylphenol (S1)****Figure S64:** <sup>1</sup>H NMR spectrum of **S1** in CDCl<sub>3</sub>.**Figure S65:** <sup>13</sup>C{<sup>1</sup>H} NMR spectrum of **S1** in CDCl<sub>3</sub>.

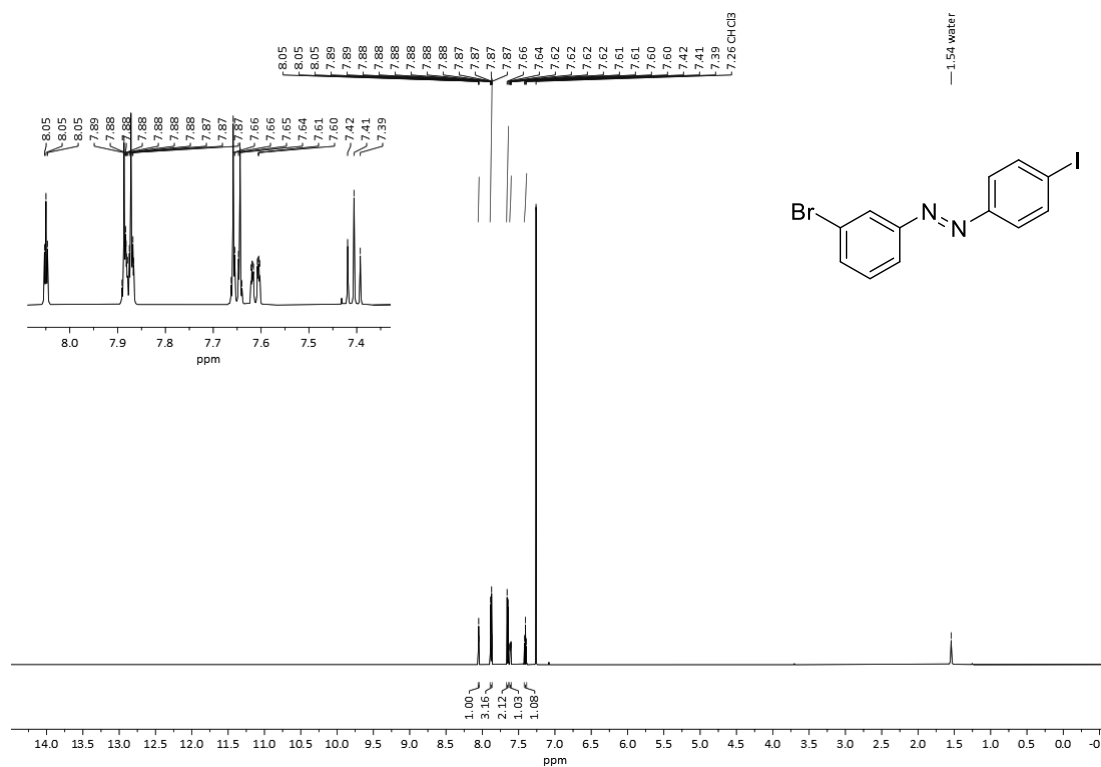
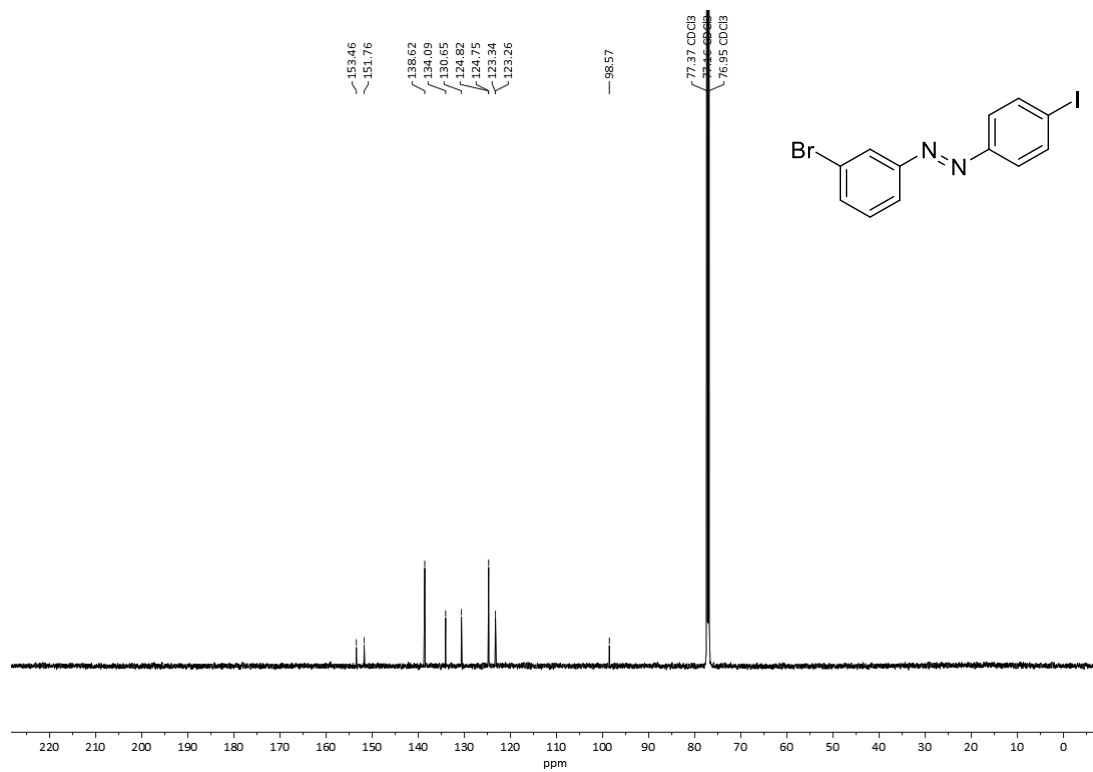
*(E)*-1-(2,6-Dimethyl-4-(nonyloxy)phenyl)-2-(4-iodo-2,6-dimethylphenyl)diazene (**1j**)Figure S66: <sup>1</sup>H NMR spectrum of **1j** in CDCl<sub>3</sub>.Figure S67: <sup>13</sup>C[<sup>1</sup>H] NMR spectrum of **1j** in CDCl<sub>3</sub>.

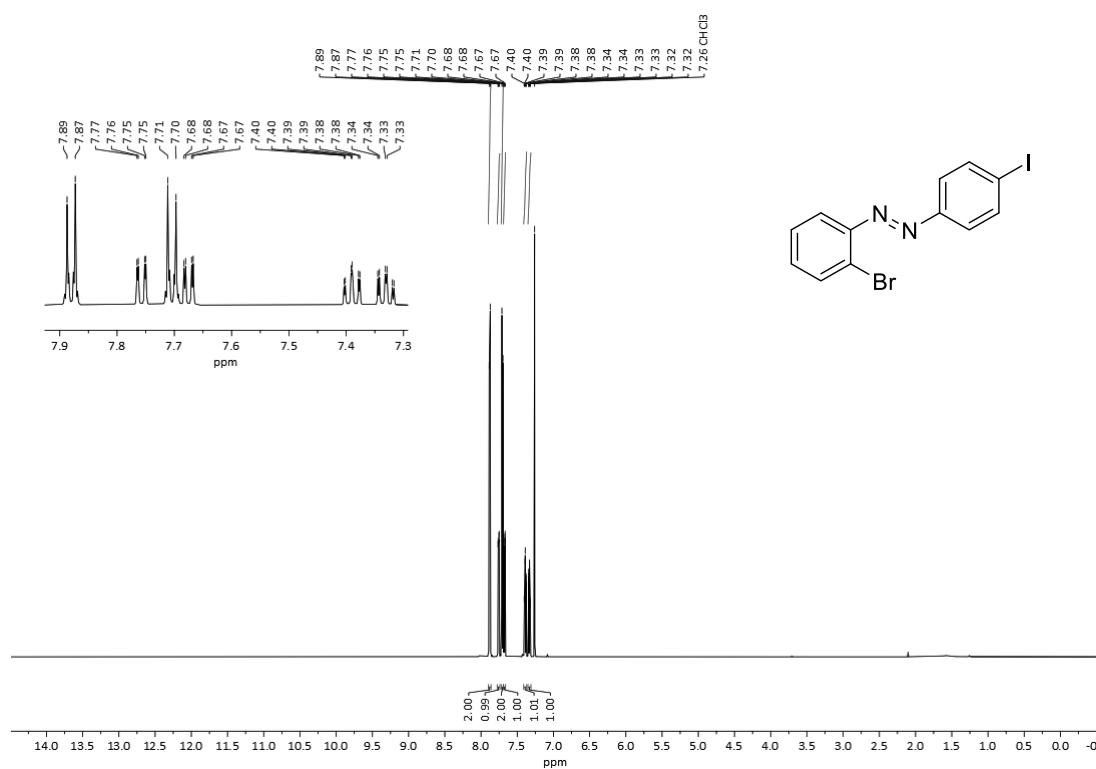
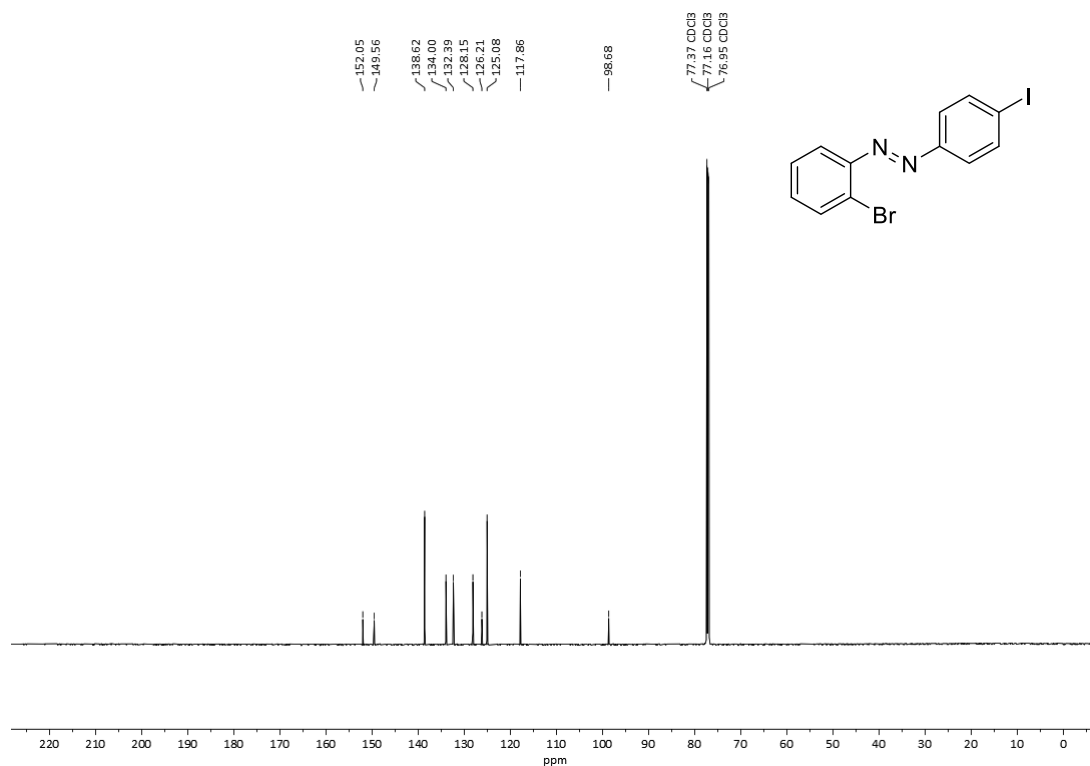


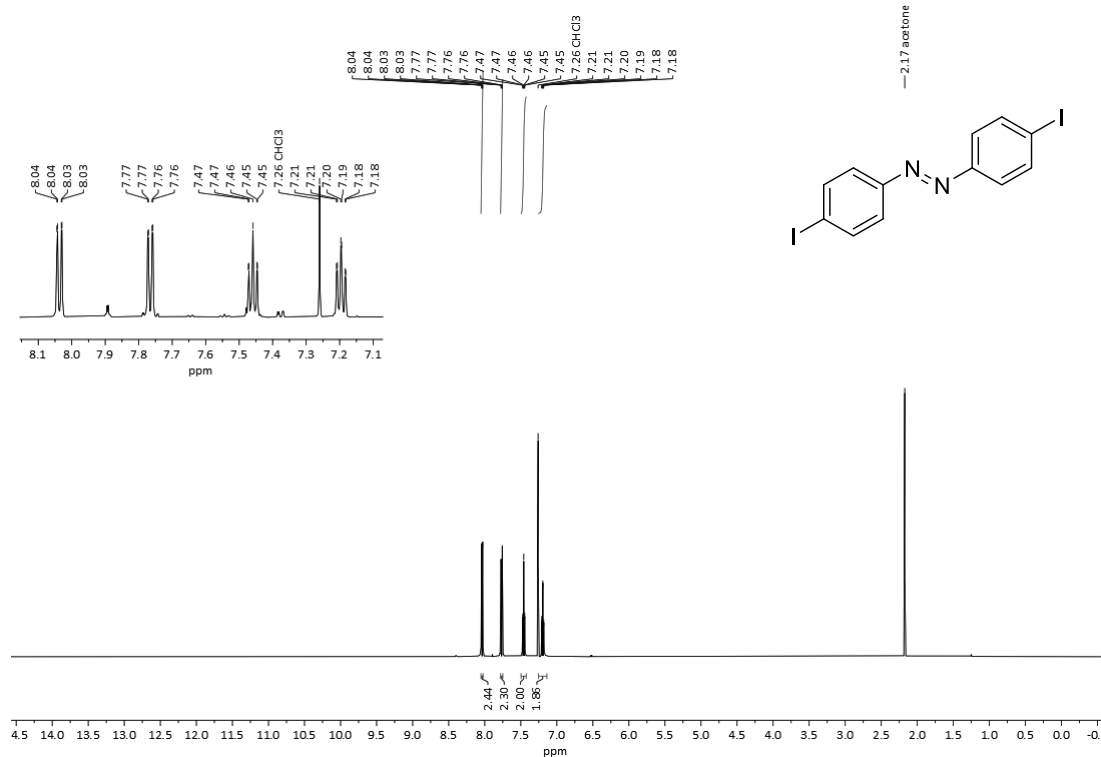
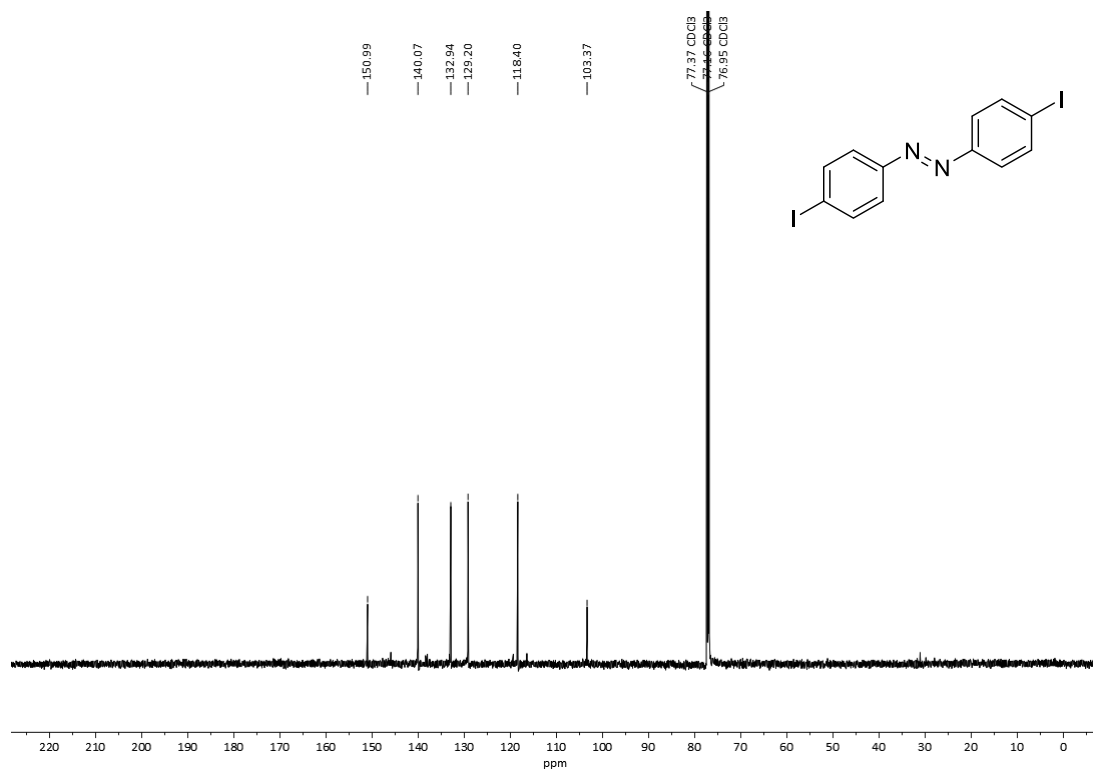
**(E)-1-((4-Iodo-2,6-dimethylphenyl)diazenyl)naphthalene-2,7-diol (S2)**Figure S68:  $^1\text{H}$  NMR spectrum of **S2** in  $\text{DMSO-}d_6$ .Figure S69:  $^{13}\text{C}$  NMR spectrum of **S2** in  $\text{DMSO-}d_6$ .

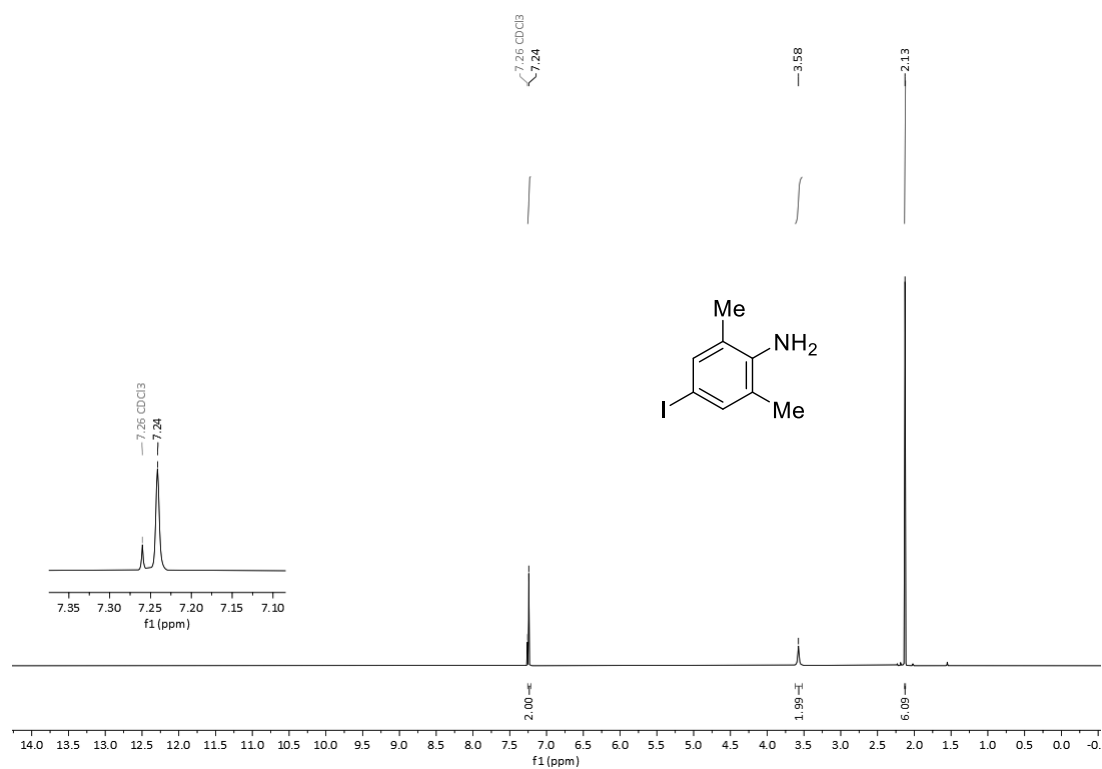
*(E)*-1-((4-Iodo-2,6-dimethylphenyl)diazenyl)naphthalene-2,7-diyl bis(4-(hexyloxy)benzoate) (**1k**)Figure S70: <sup>1</sup>H NMR spectrum of **1k** in CDCl<sub>3</sub>.Figure S71: <sup>13</sup>C{<sup>1</sup>H} NMR spectrum of **1k** in CDCl<sub>3</sub>.

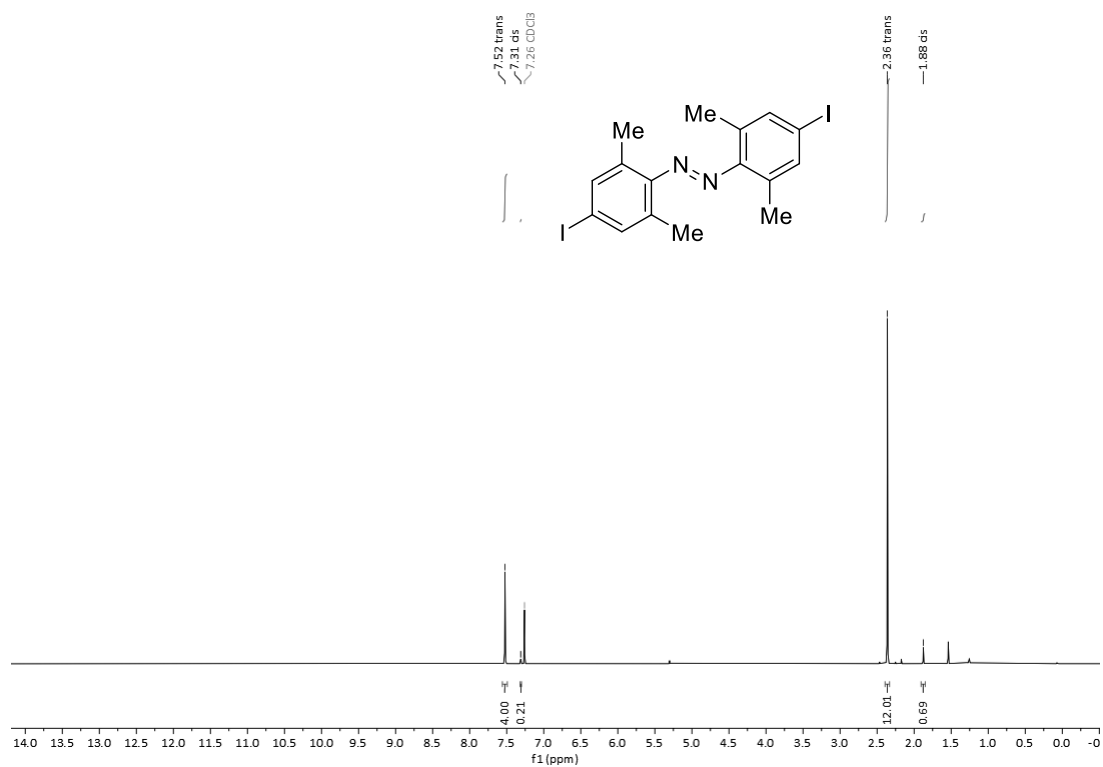
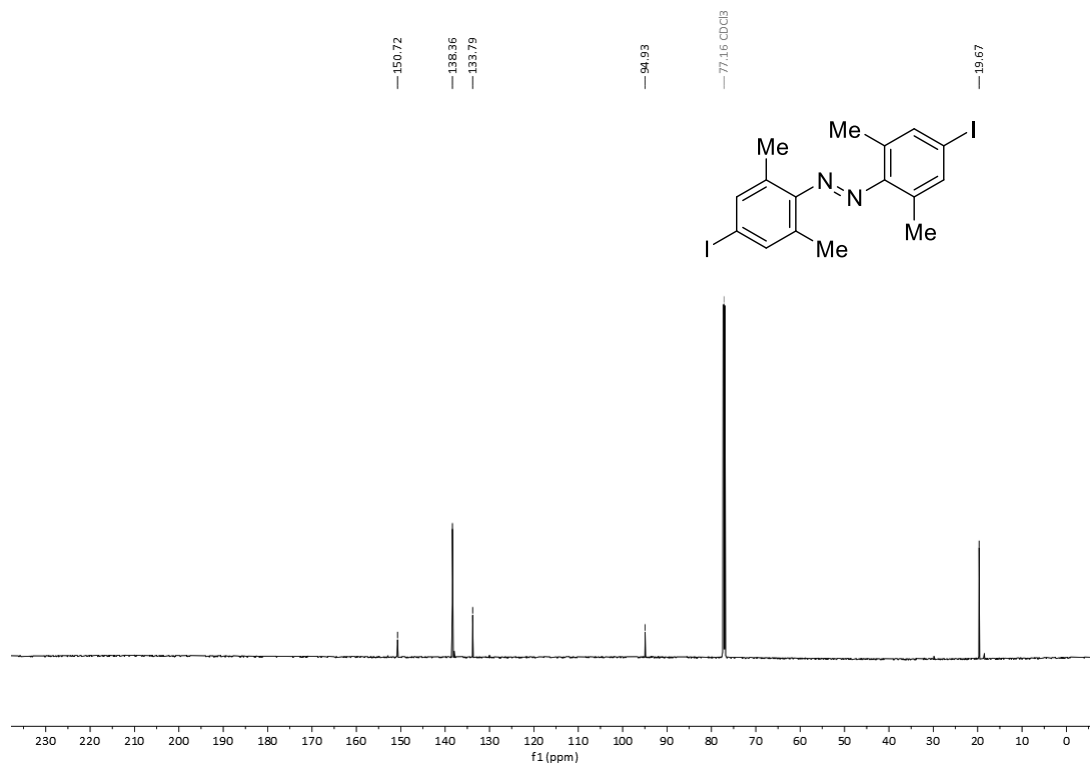
**(E)-1-(4-Bromophenyl)-2-(4-iodophenyl)diazene (11)****Figure S72:** <sup>1</sup>H NMR spectrum of **11** in CDCl<sub>3</sub>.**Figure S73:** <sup>13</sup>C(<sup>1</sup>H) NMR spectrum of **11** in CDCl<sub>3</sub>.

*(E)*-1-(3-Bromophenyl)-2-(4-iodophenyl)diazene (**1m**)Figure S74: <sup>1</sup>H NMR spectrum of **1m** in CDCl<sub>3</sub>.Figure S75: <sup>13</sup>C{<sup>1</sup>H} NMR spectrum of **1m** in CDCl<sub>3</sub>.

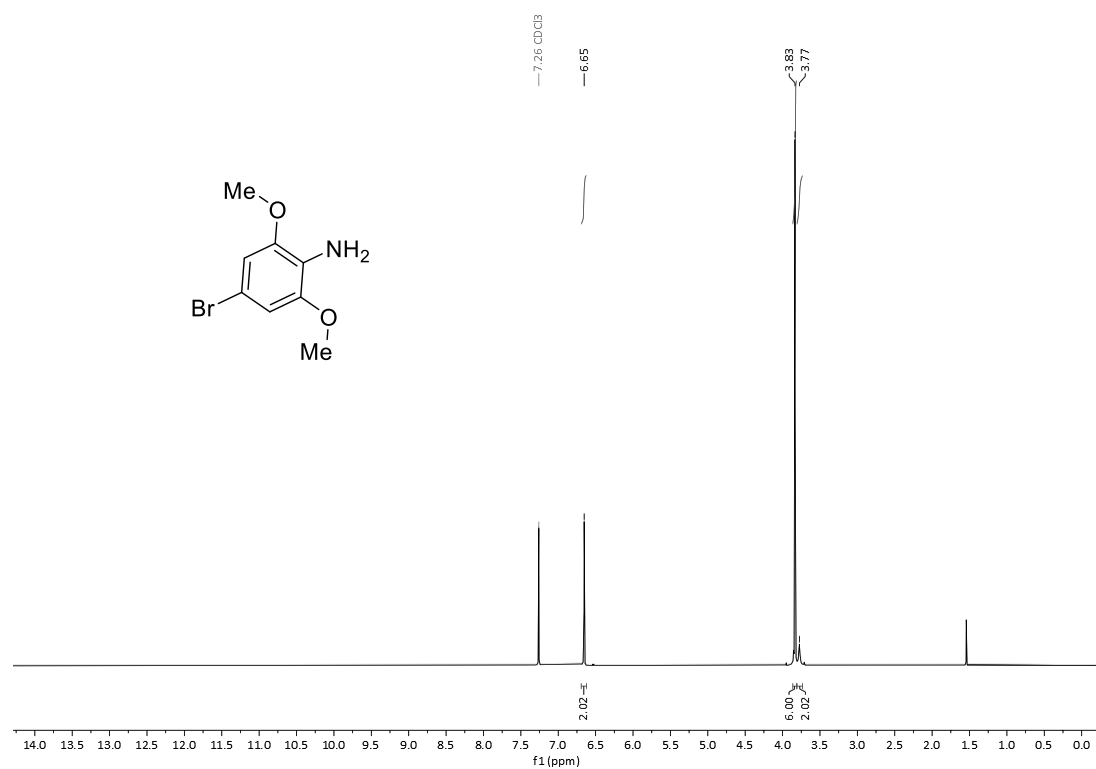
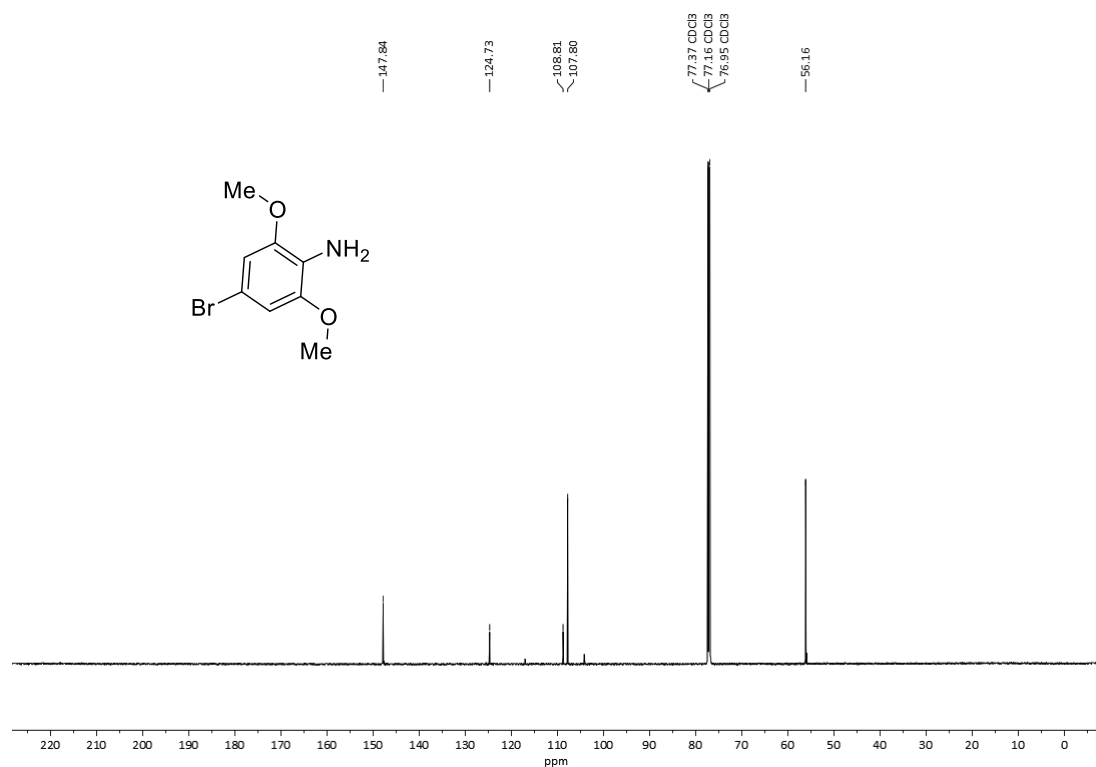
**(E)-1-(2-Bromophenyl)-2-(4-iodophenyl)diazene (1n)****Figure S76:** <sup>1</sup>H NMR spectrum of **1n** in CDCl<sub>3</sub>.**Figure S77:** <sup>13</sup>C{<sup>1</sup>H} NMR spectrum of **1n** in CDCl<sub>3</sub>.

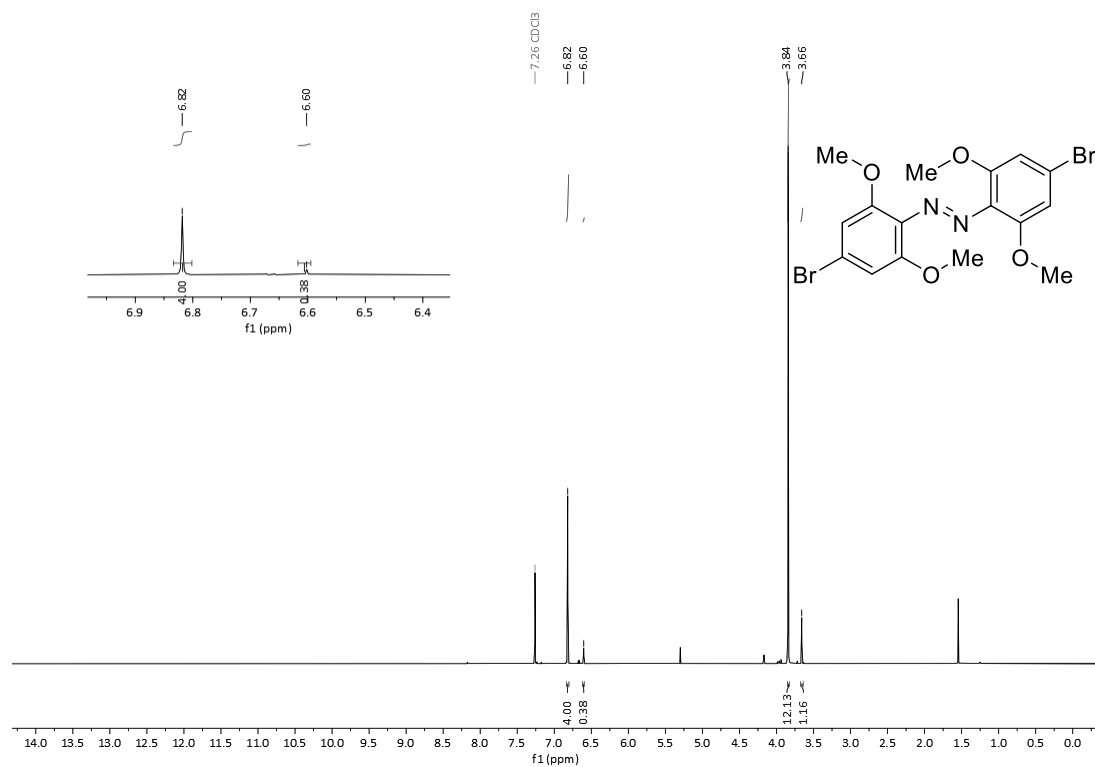
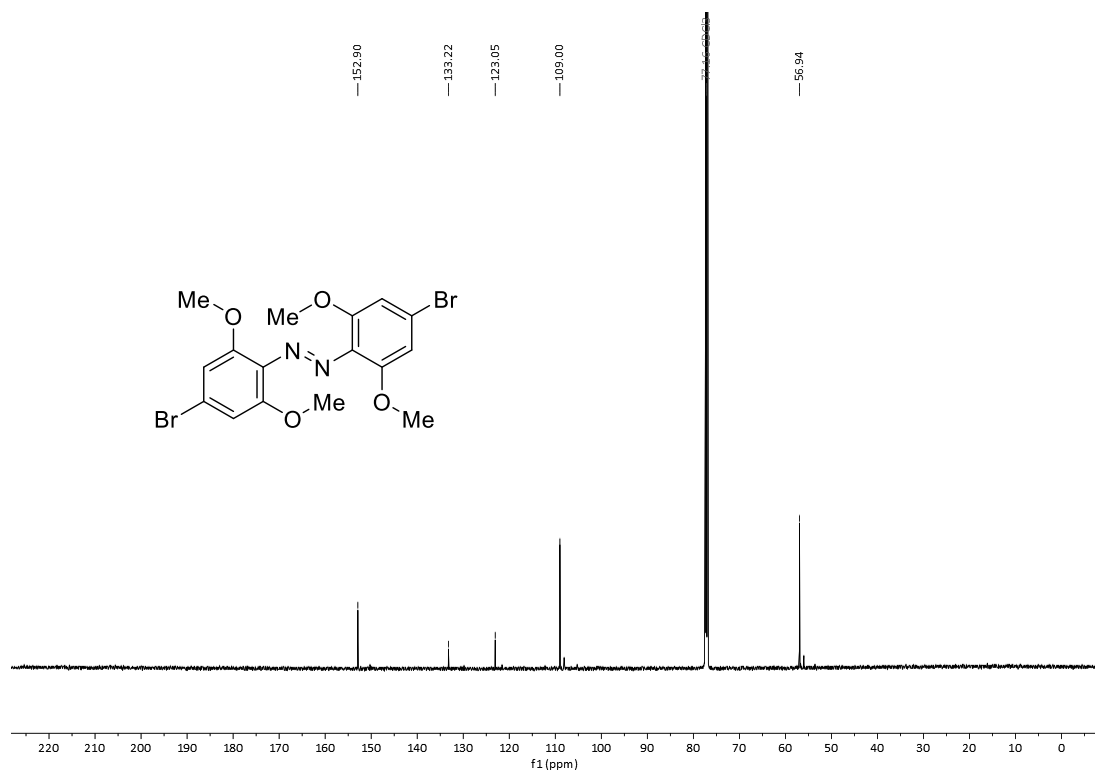
*(E)*-1,2-Bis(4-iodophenyl)diazene (**4a**)Figure S78: <sup>1</sup>H NMR spectrum of **4a** in CDCl<sub>3</sub>.Figure S79: <sup>13</sup>C{<sup>1</sup>H} NMR spectrum of **4a** in CDCl<sub>3</sub>.

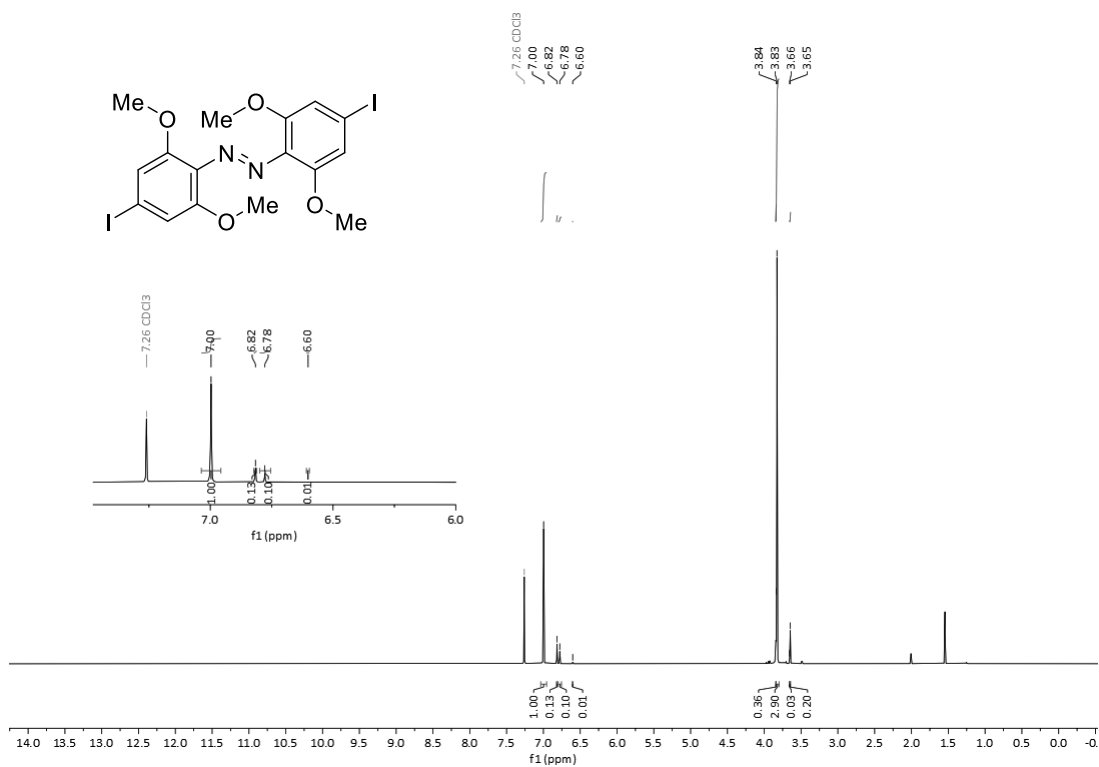
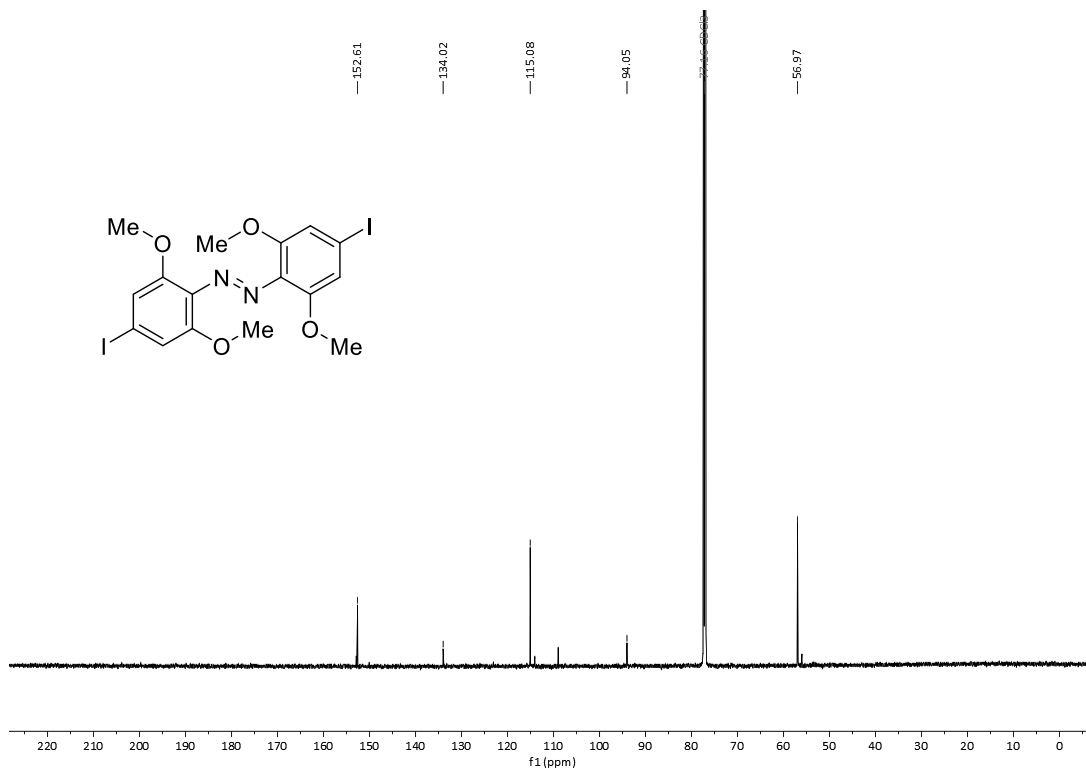
4-Iodo-2,6-dimethylaniline (**S3**)Figure S80:  $^1\text{H}$  NMR spectrum of **S3** in  $\text{CDCl}_3$ .Figure S81:  $^{13}\text{C}\{^1\text{H}\}$  NMR spectrum of **S3** in  $\text{CDCl}_3$ .

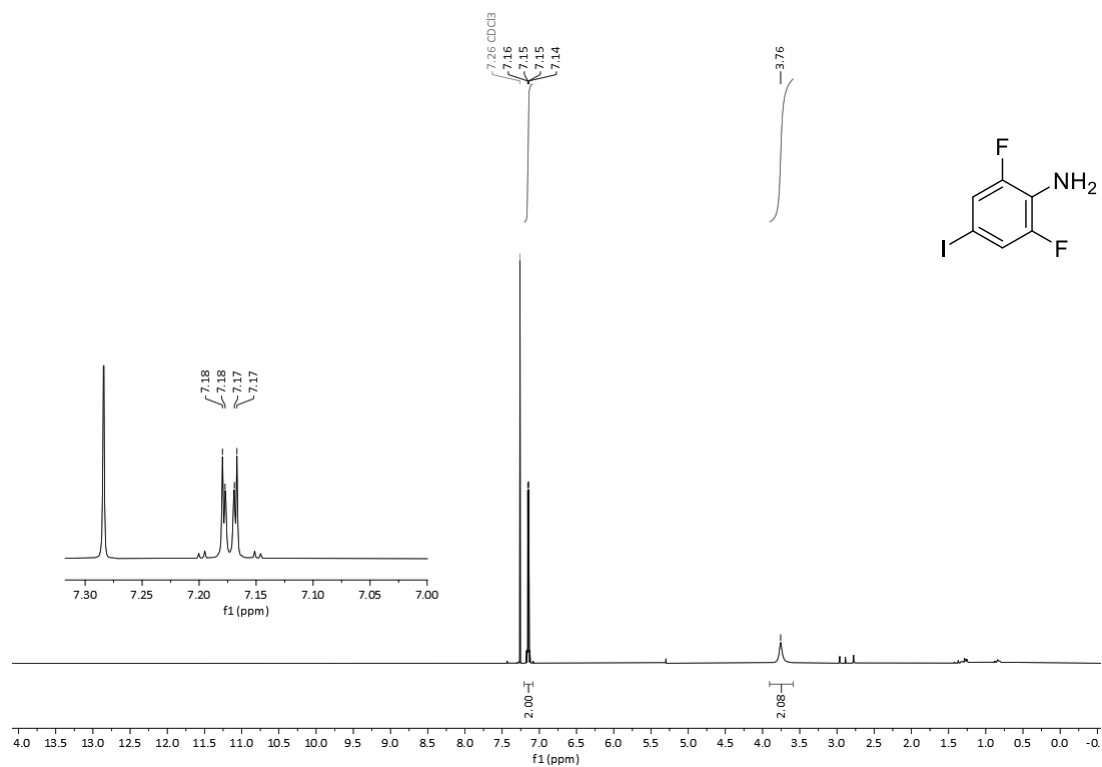
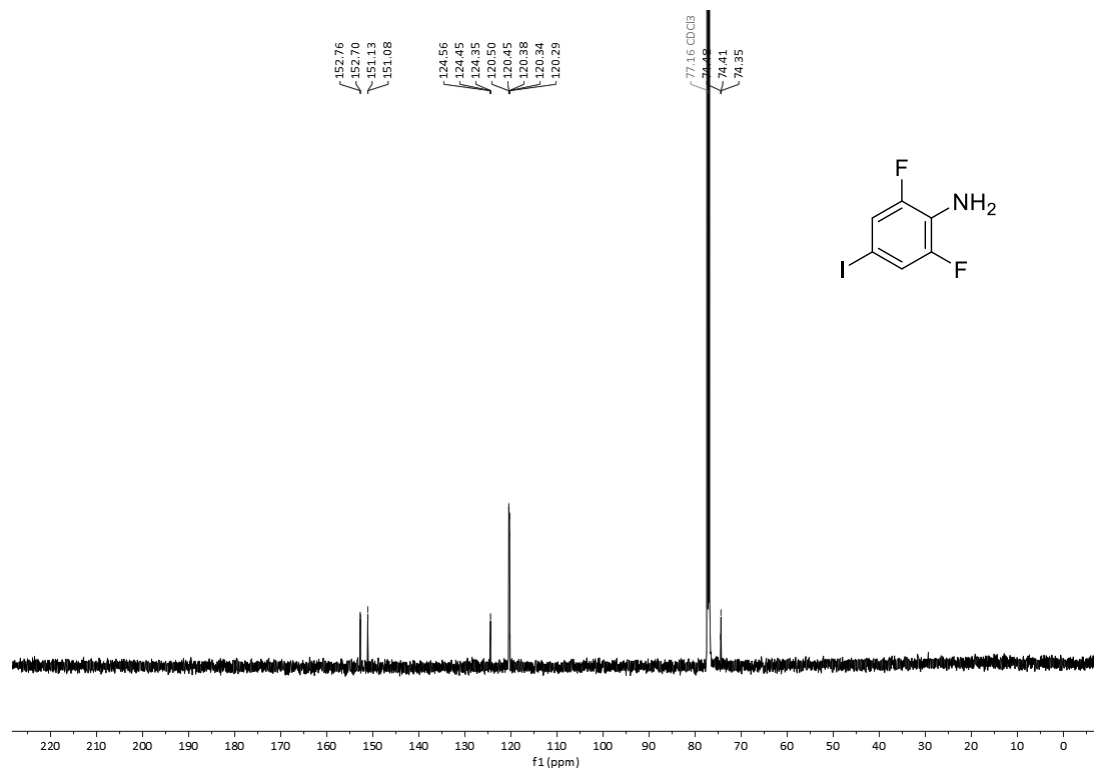
**(E)-1,2-Bis(4-iodo-2,6-dimethylphenyl)diazene (4b)****Figure S82:** <sup>1</sup>H NMR spectrum of **4b** in CDCl<sub>3</sub>.**Figure S83:** <sup>13</sup>C{<sup>1</sup>H} NMR spectrum of **4b** in CDCl<sub>3</sub>.

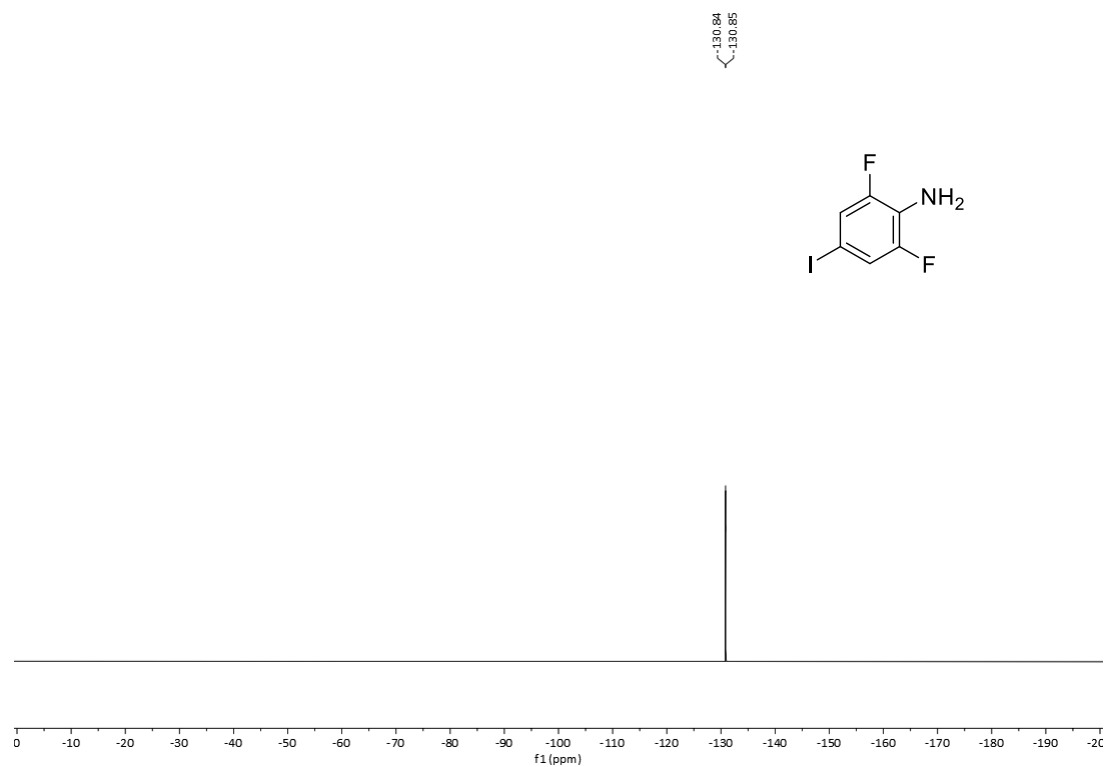


4-Bromo-2,6-dimethoxyaniline (**S4**)Figure S84:  $^1\text{H}$  NMR spectrum of **S4** in  $\text{CDCl}_3$ .Figure S85:  $^{13}\text{C}$  NMR spectrum of **S4** in  $\text{CDCl}_3$ .

*(E)*-1,2-Bis(4-bromo-2,6-dimethoxyphenyl)diazene (**S5**)Figure S86:  $^1\text{H}$  NMR spectrum of **S5** in  $\text{CDCl}_3$ .Figure S87:  $^{13}\text{C}\{^1\text{H}\}$  NMR spectrum of **S5** in  $\text{CDCl}_3$ .

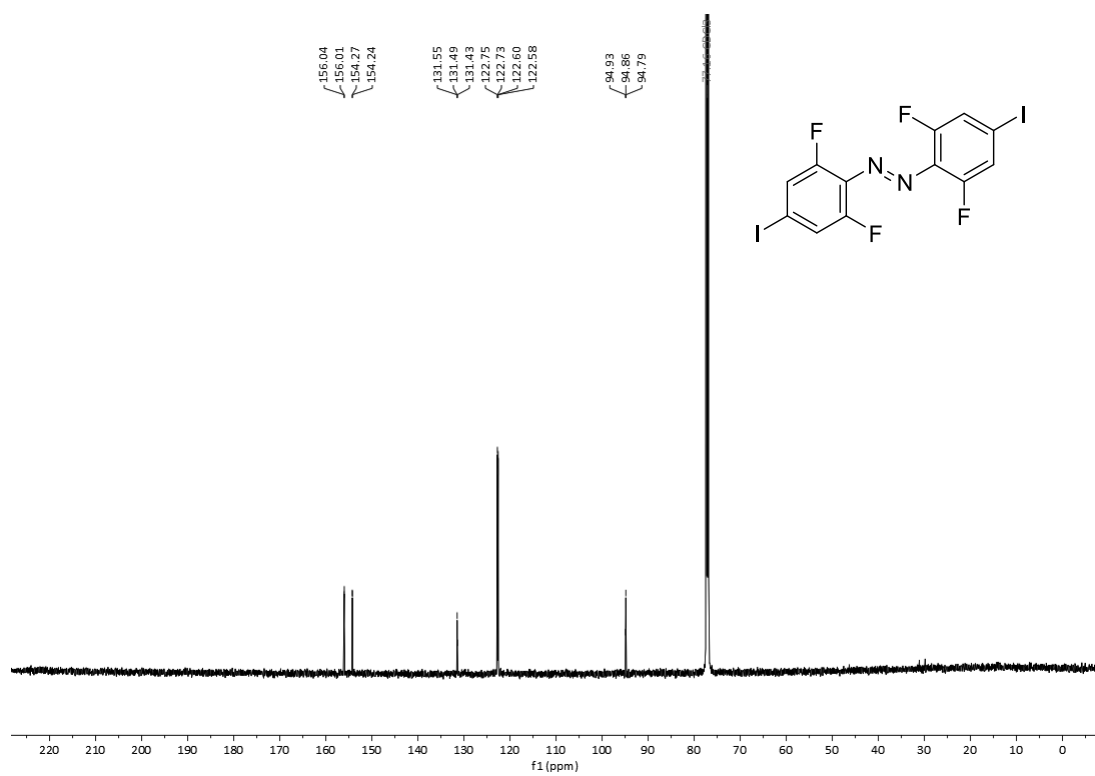
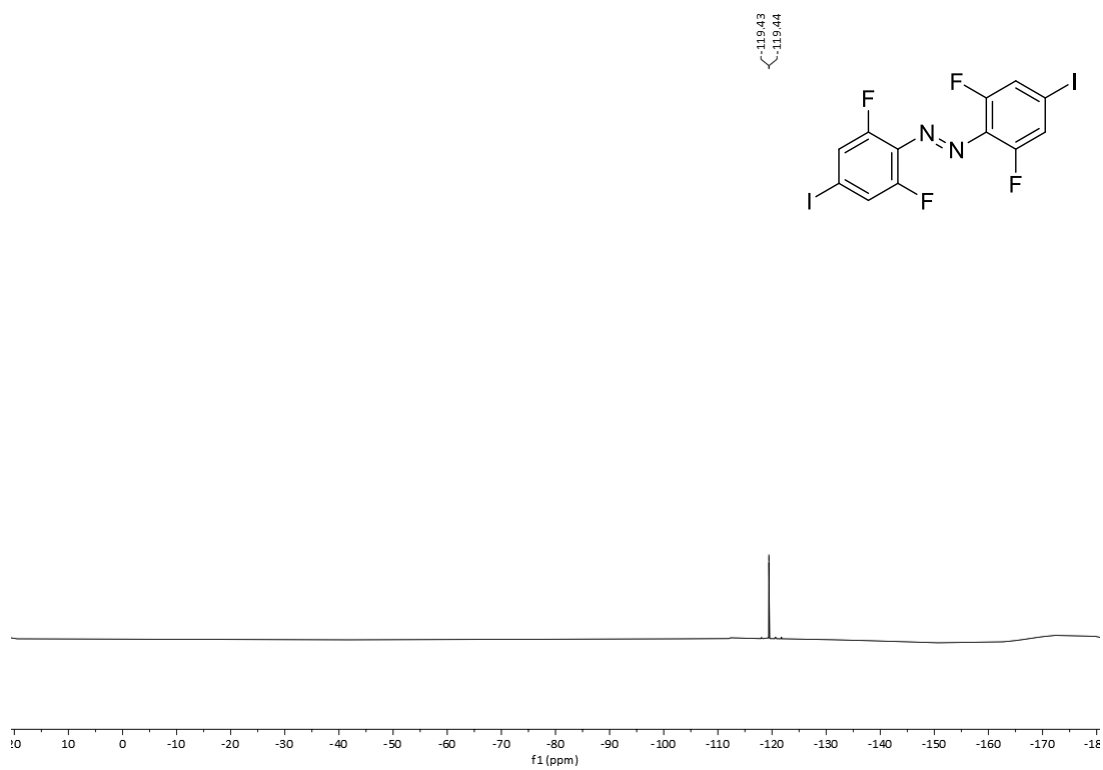
**(E)-1,2-Bis(4-iodo-2,6-dimethoxyphenyl)diazene (4c)****Figure S88:**  $^1\text{H}$  NMR spectrum of **4c** in  $\text{CDCl}_3$ .**Figure S89:**  $^{13}\text{C}$  NMR spectrum of **4c** in  $\text{CDCl}_3$ .

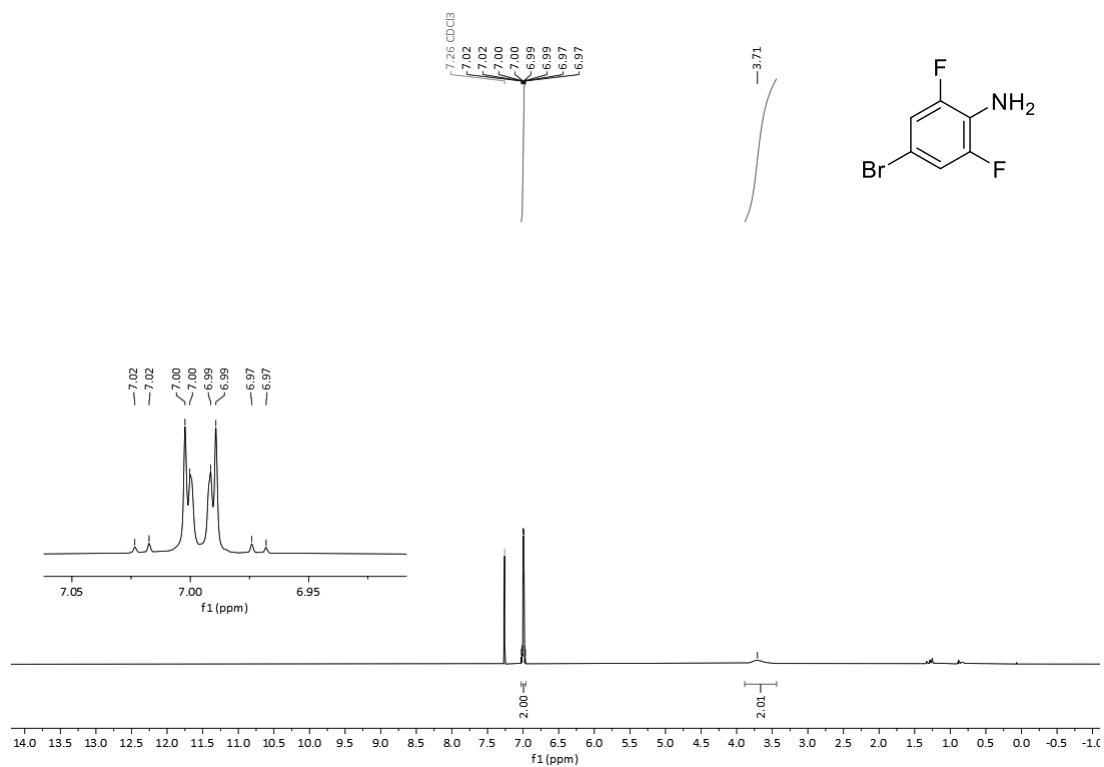
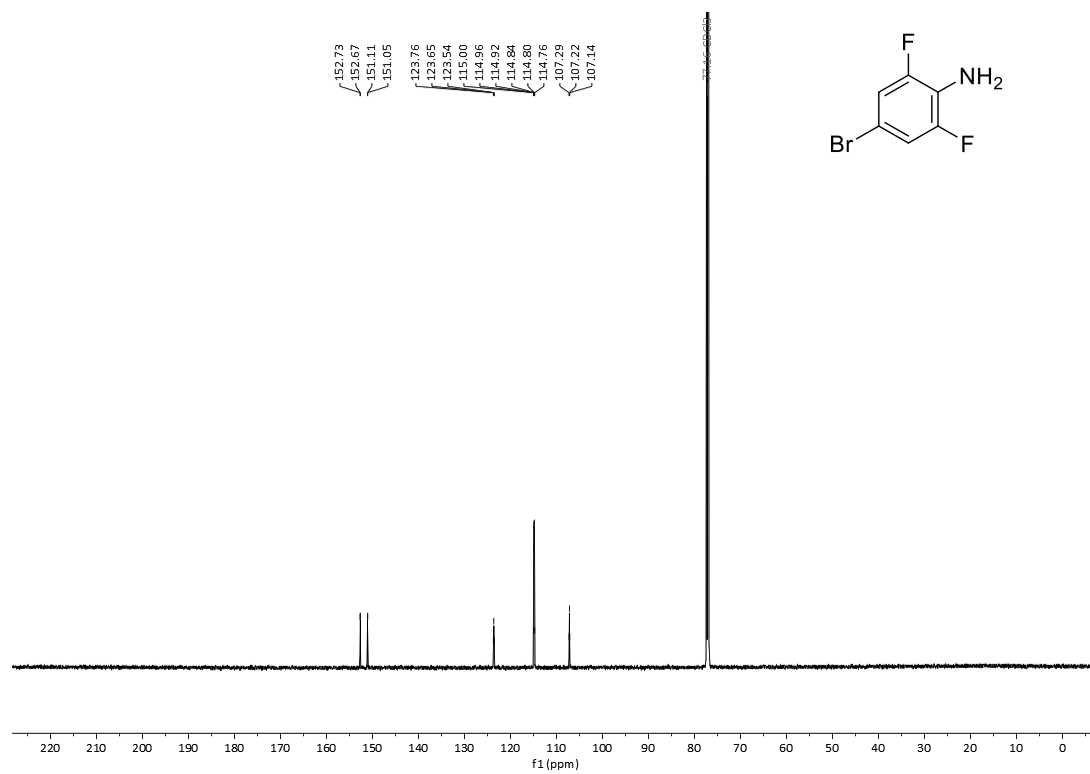
4-Iodo-2,6-difluoro-aniline (**S6**)**Figure S90:**  $^1\text{H}$  NMR spectrum of **S6** in  $\text{CDCl}_3$ .**Figure S91:**  $^{13}\text{C}$  NMR spectrum of **S6** in  $\text{CDCl}_3$ .

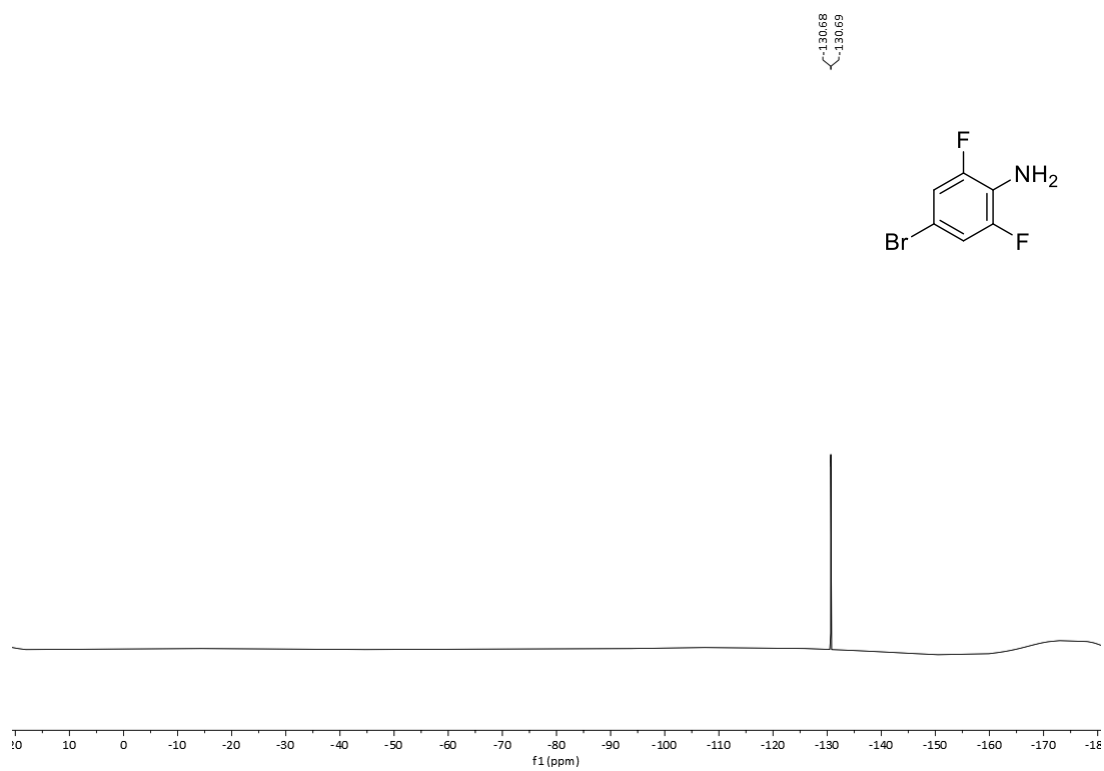
Figure S92:  $^{19}\text{F}$  NMR spectrum of **56** in  $\text{CDCl}_3$ .

(*E*)-1,2-bis(2,6-difluoro-4-iodophenyl)diazene (**4d**)

Figure S93:  $^1\text{H}$  NMR spectrum of **4d** in  $\text{CDCl}_3$ .

Figure S94:  $^{13}\text{C}\{^1\text{H}\}$  NMR spectrum of **4d** in  $\text{CDCl}_3$ .Figure S95:  $^{19}\text{F}$  NMR spectrum of **4d** in  $\text{CDCl}_3$ .

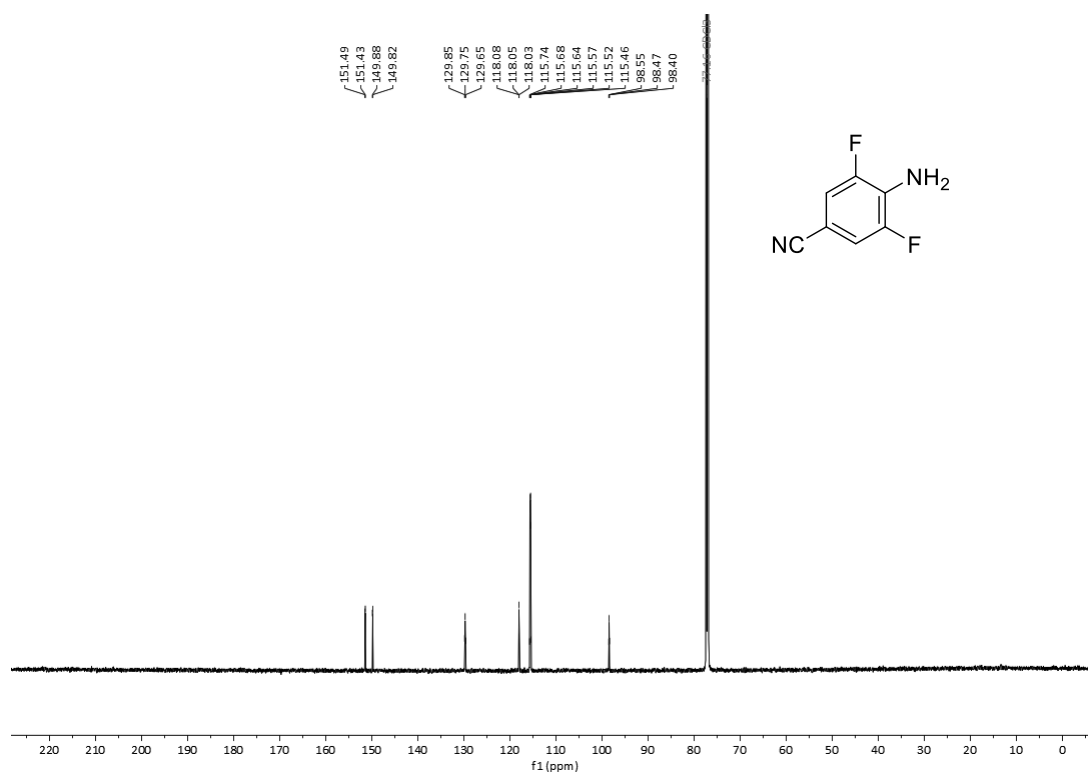
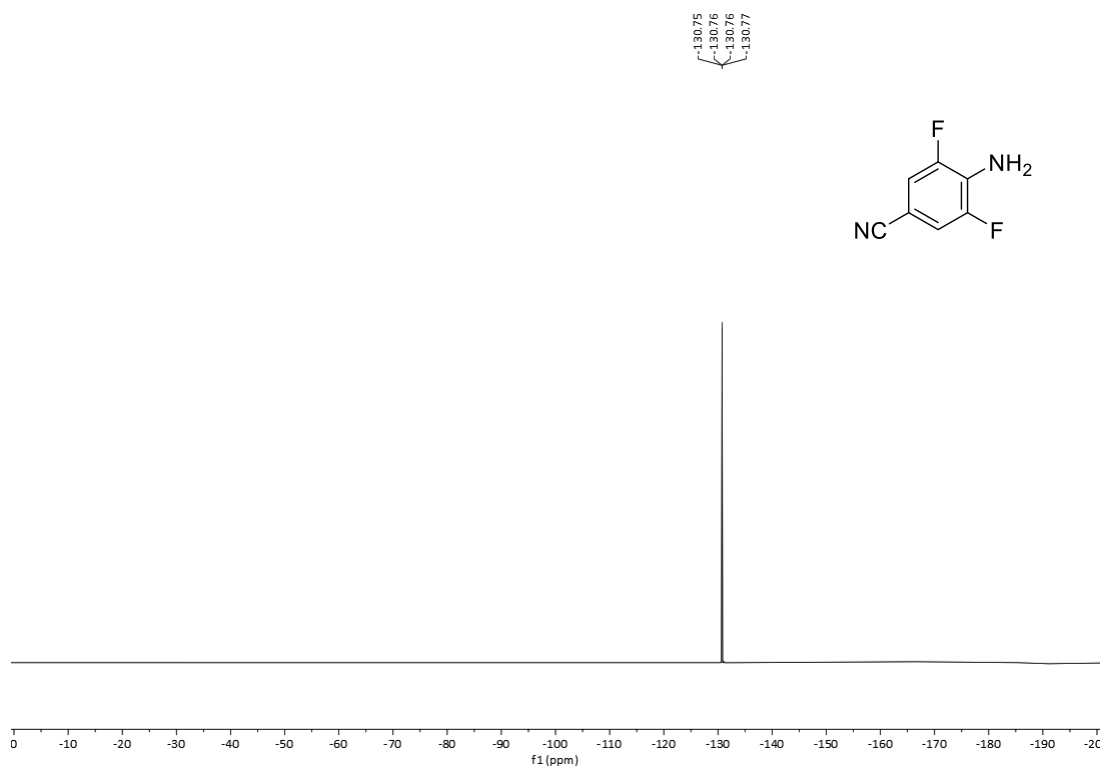
4-Bromo-2,6-difluoroaniline (**S7**)Figure S96: <sup>1</sup>H NMR spectrum of **S7** in CDCl<sub>3</sub>.Figure S97: <sup>13</sup>C NMR spectrum of **S7** in CDCl<sub>3</sub>.

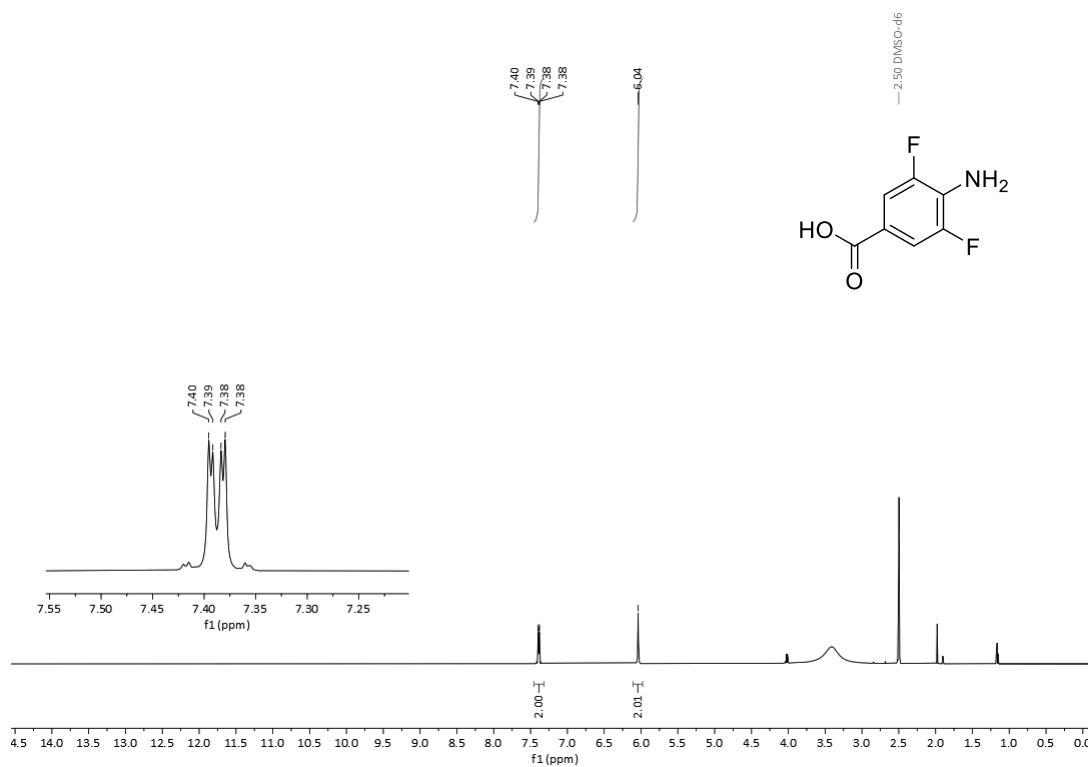
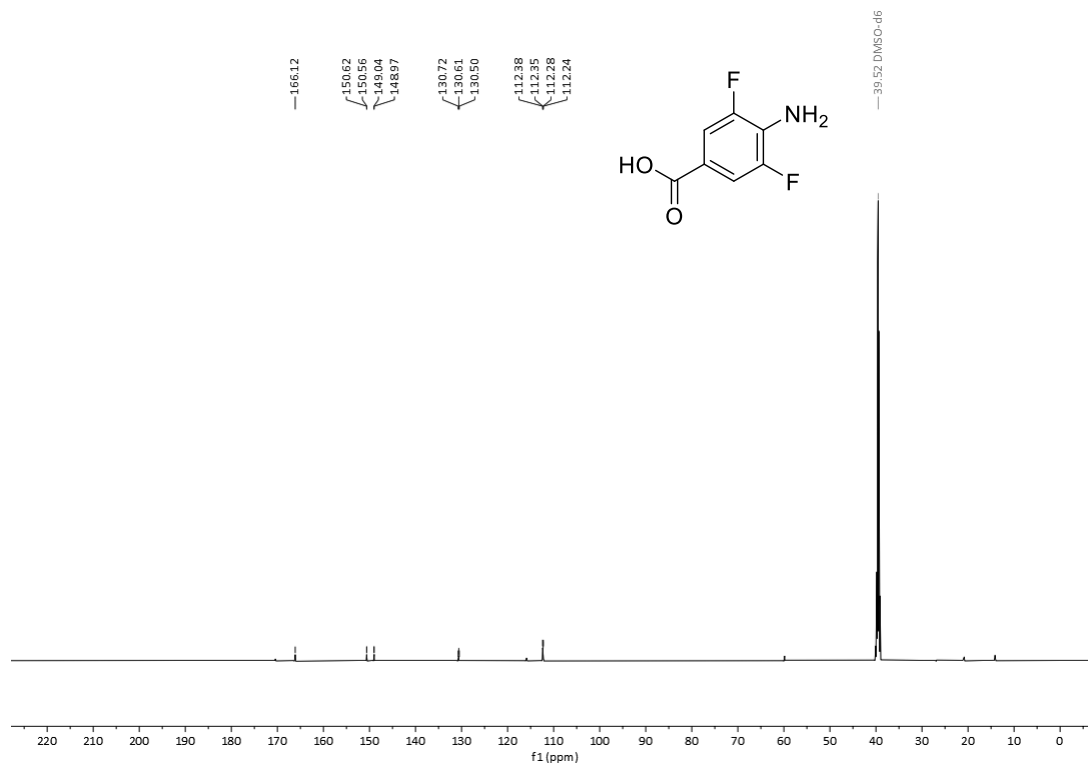
Figure S98:  $^{19}\text{F}$  NMR spectrum of S7 in  $\text{CDCl}_3$ .

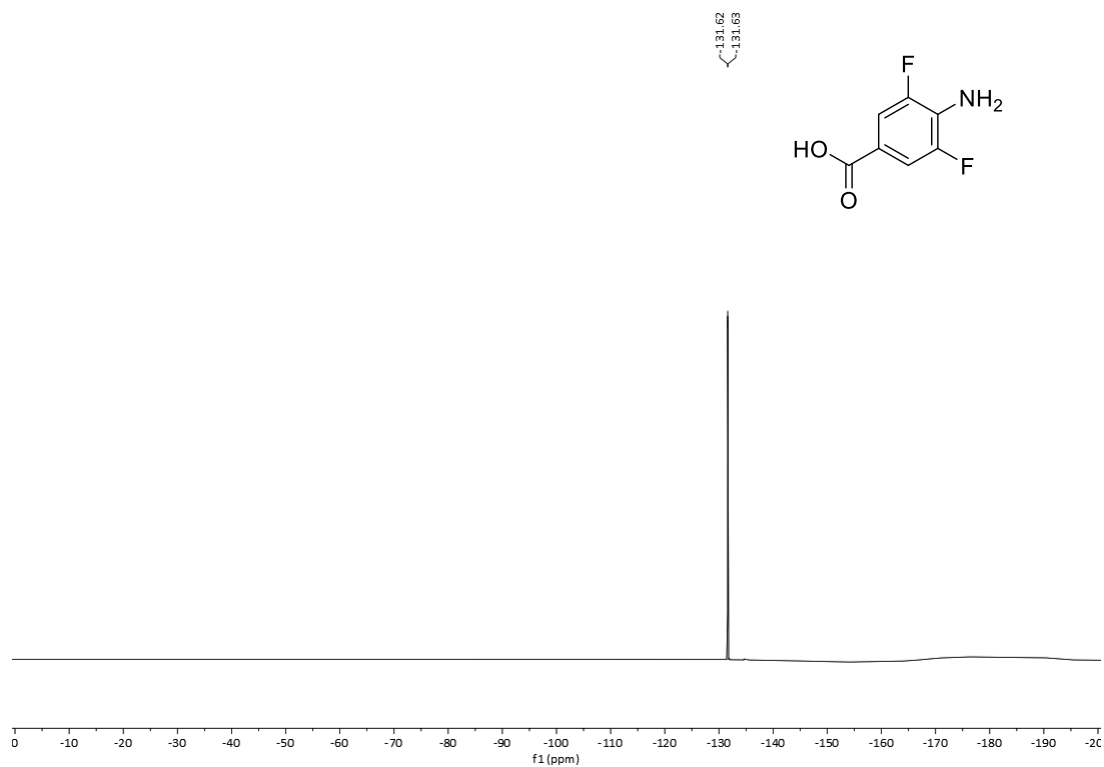
## 4-Amino-3,5-difluorobenzonitrile (S8)

Figure S99:  $^1\text{H}$  NMR spectrum of S8 in  $\text{CDCl}_3$ .

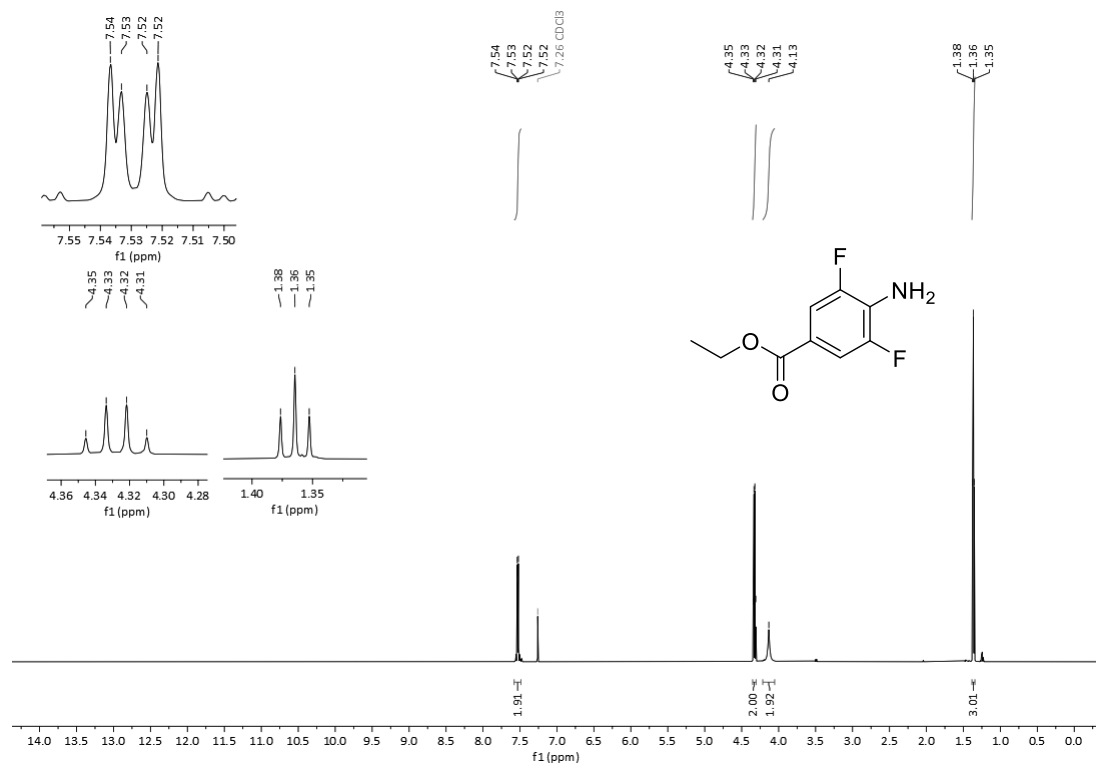


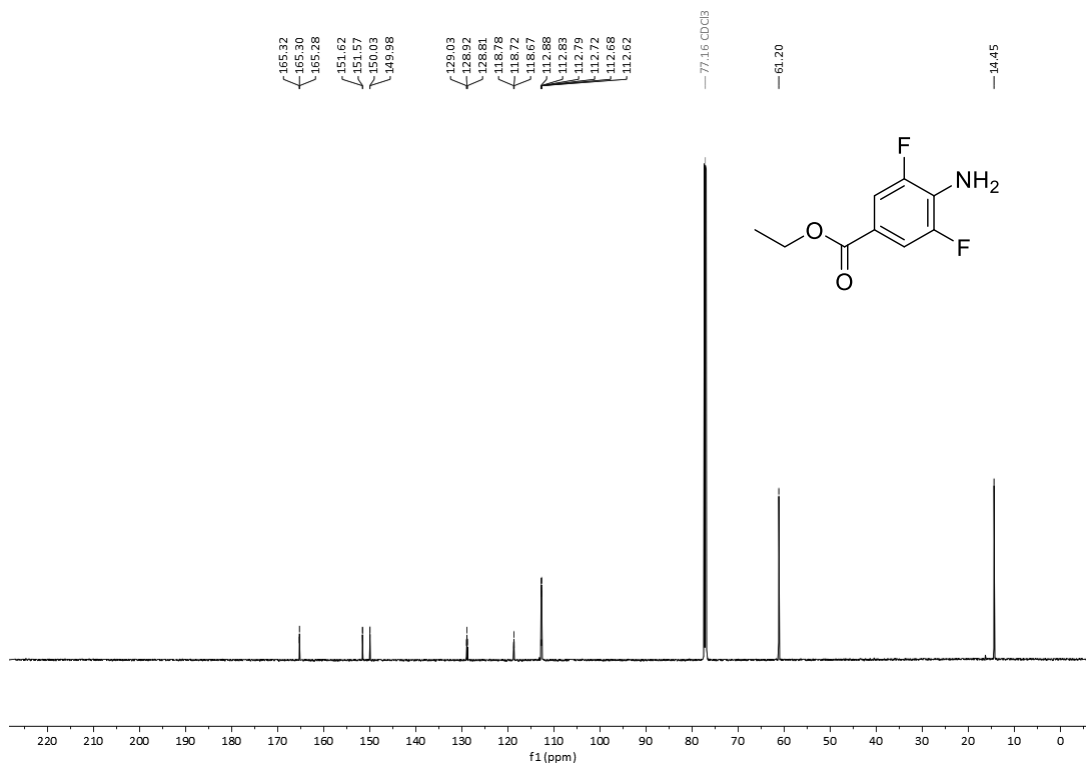
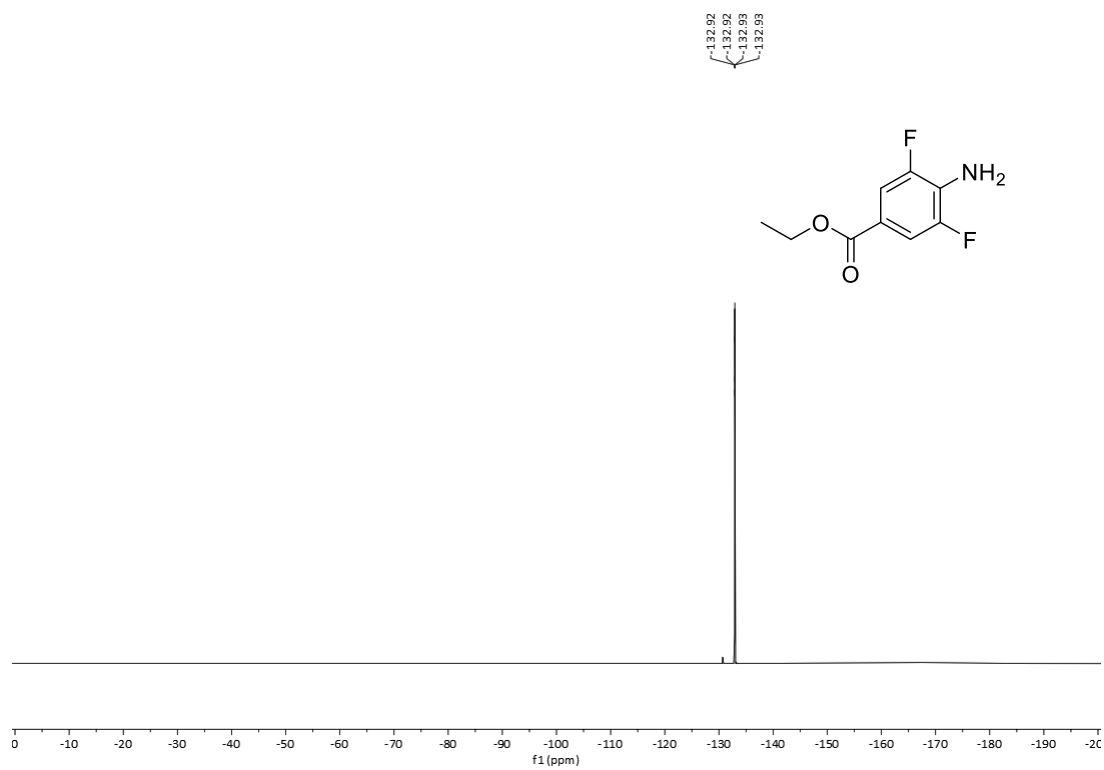
Figure S100:  $^{13}\text{C}\{^1\text{H}\}$  NMR spectrum of **S8** in  $\text{CDCl}_3$ .Figure S101:  $^{19}\text{F}$  NMR spectrum of **S8** in  $\text{CDCl}_3$ .

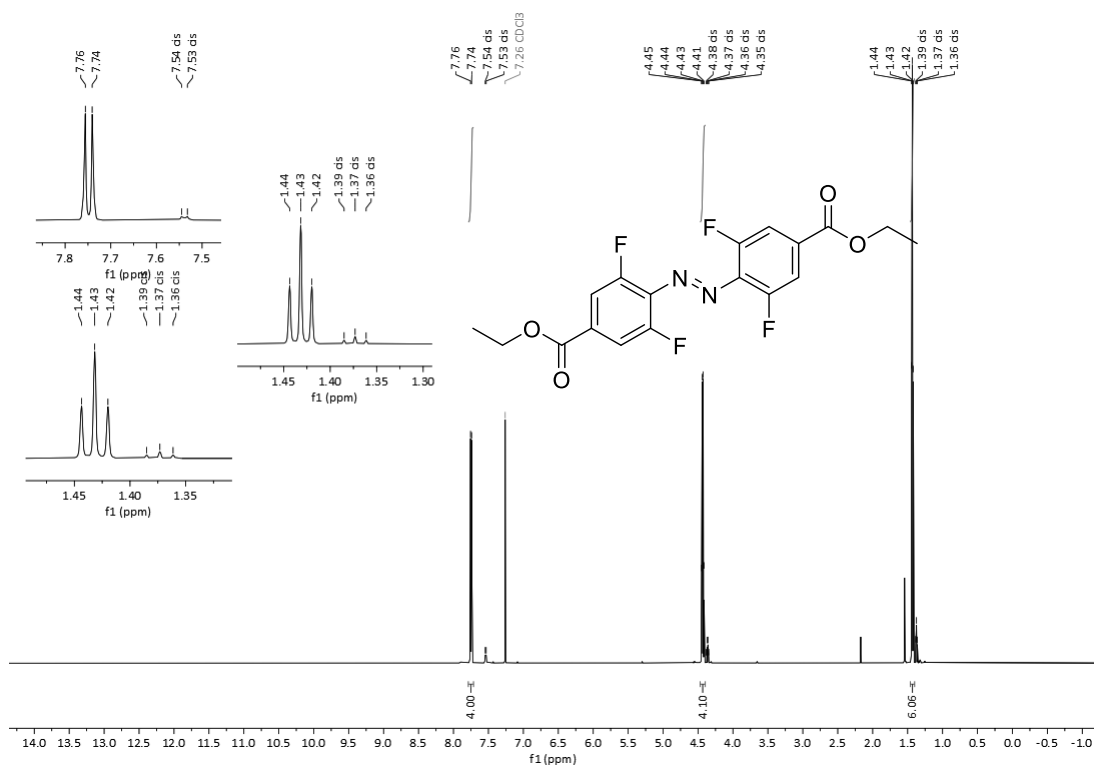
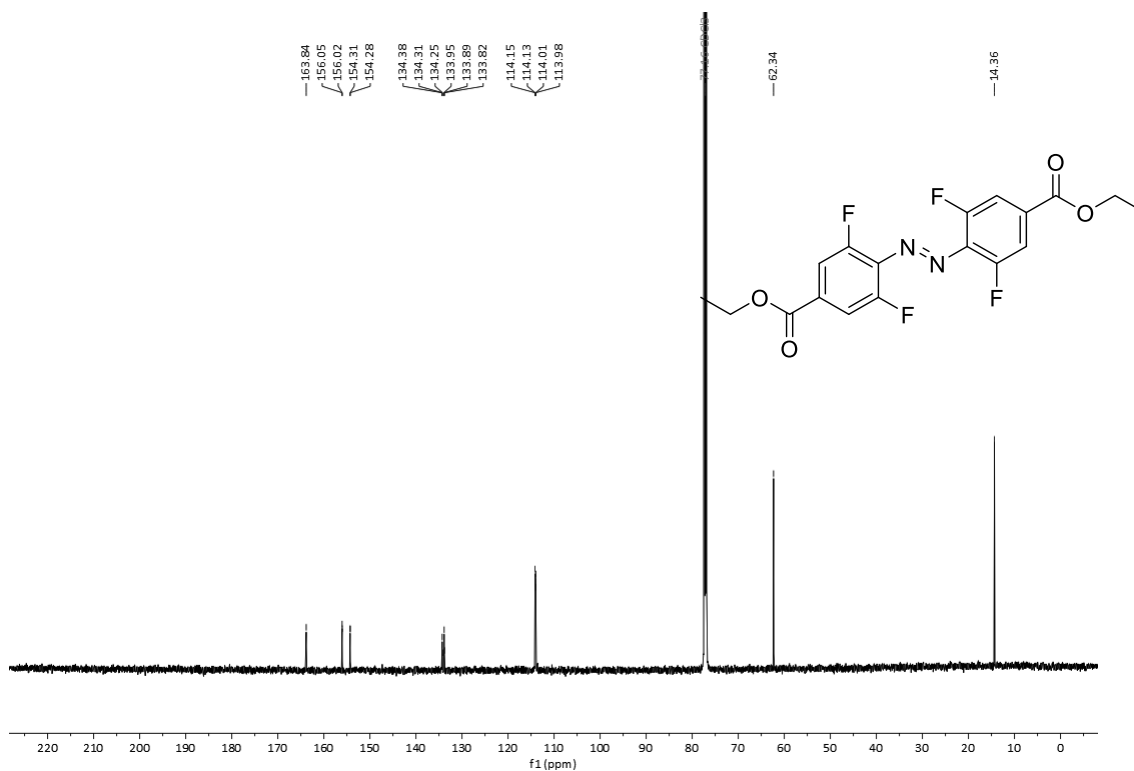
4-Amino-3,5-difluorobenzoic acid (**S9**)Figure S102:  $^1\text{H}$  NMR spectrum of **S9** in  $\text{DMSO-}d_6$ .Figure S103:  $^{13}\text{C}\{^1\text{H}\}$  NMR spectrum of **S9** in  $\text{DMSO-}d_6$ .

Figure S104:  $^{19}\text{F}$  NMR spectrum of S9 in  $\text{DMSO-}d_6$ .

## Ethyl 4-amino-3,5-difluorobenzoate (S10)

Figure S105:  $^1\text{H}$  NMR spectrum of S10 in  $\text{CDCl}_3$ .

Figure S106: <sup>13</sup>C{<sup>1</sup>H} NMR spectrum of S10 in CDCl<sub>3</sub>.Figure S107: <sup>19</sup>F NMR spectrum of S10 in CDCl<sub>3</sub>.

Diethyl 4,4'-(diazene-1,2-diyl)(E)-bis(3,5-difluorobenzoate) (**S11**)Figure S108:  $^1\text{H}$  NMR spectrum of **S11** in  $\text{CDCl}_3$ .Figure S109:  $^{13}\text{C}$  NMR spectrum of **S11** in  $\text{CDCl}_3$ .

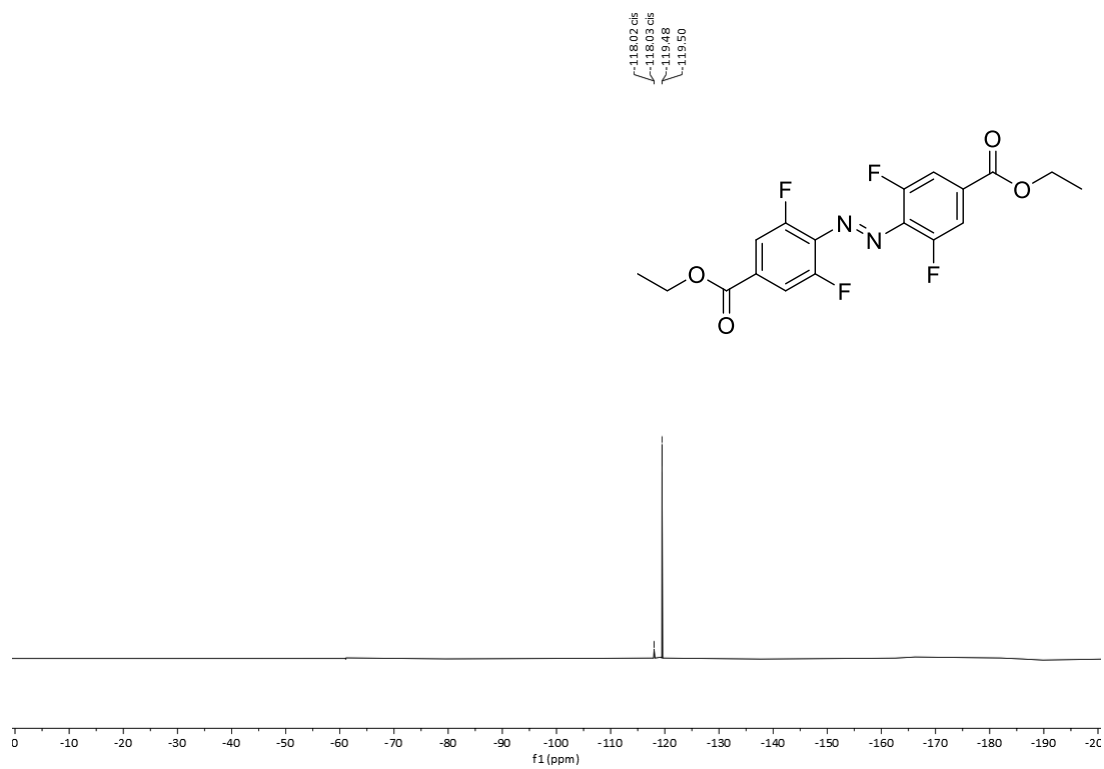


Figure S110:  $^{19}\text{F}$  NMR spectrum of **S11** in  $\text{CDCl}_3$ .

(*E*)-4,4'-(Diazene-1,2-diyl)bis(3,5-difluorobenzoic acid) (**6**)

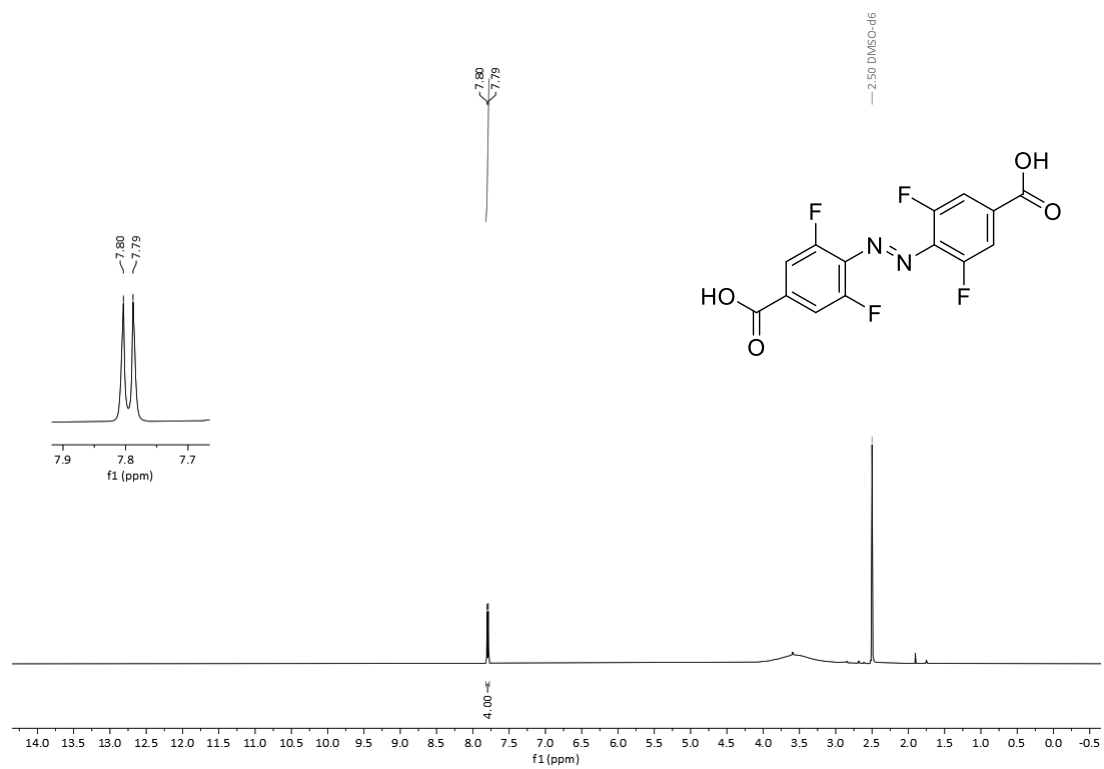
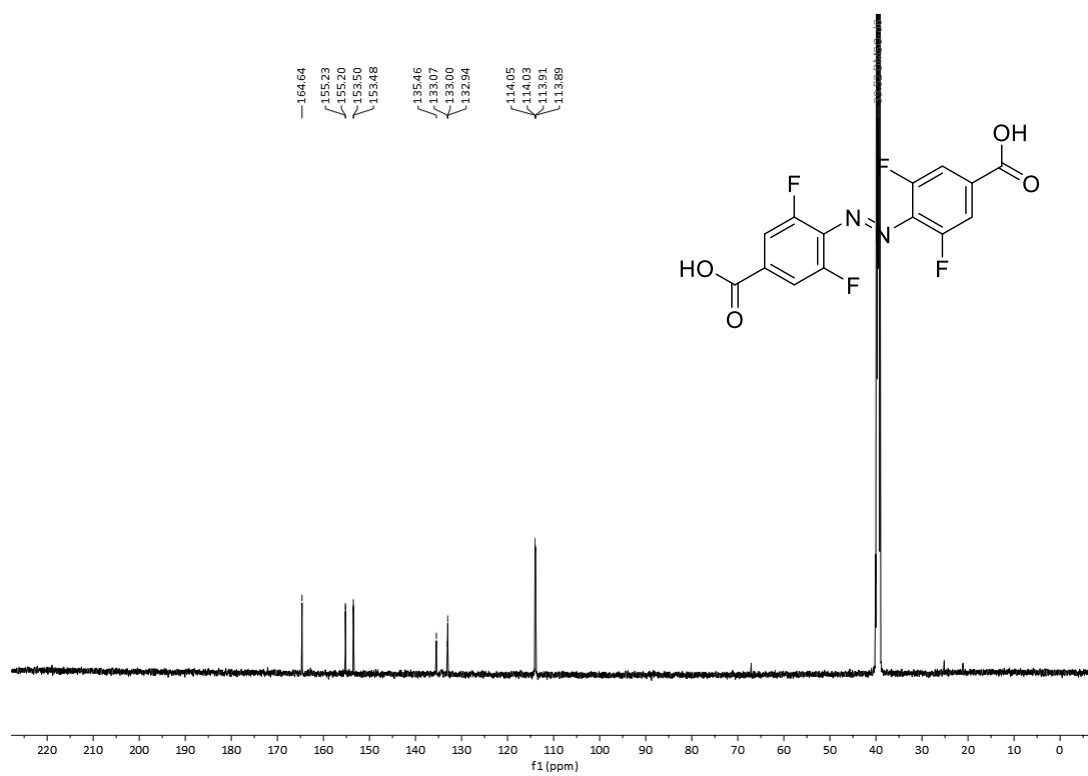
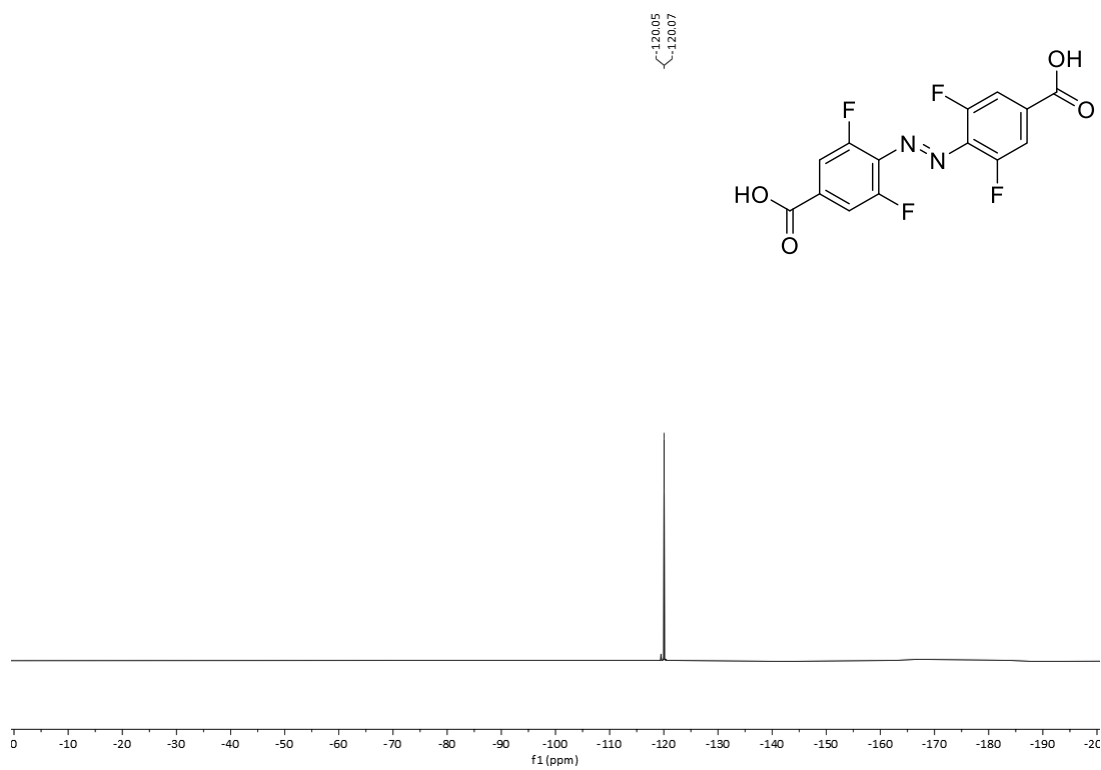
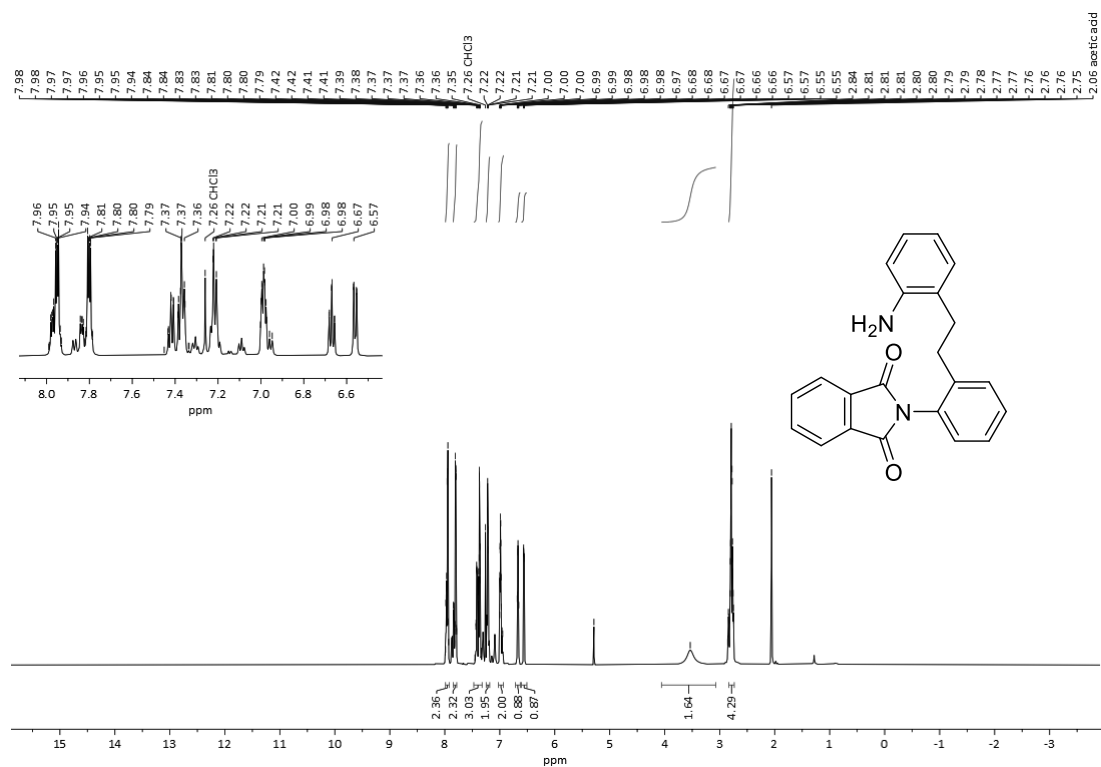
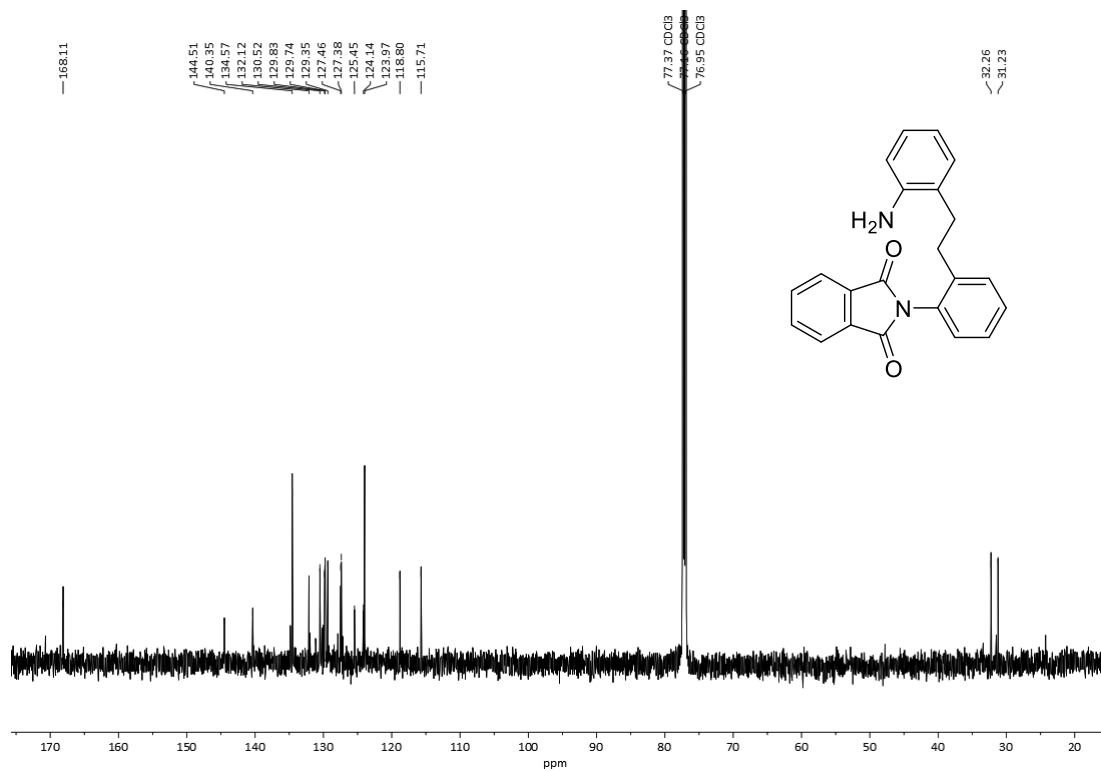
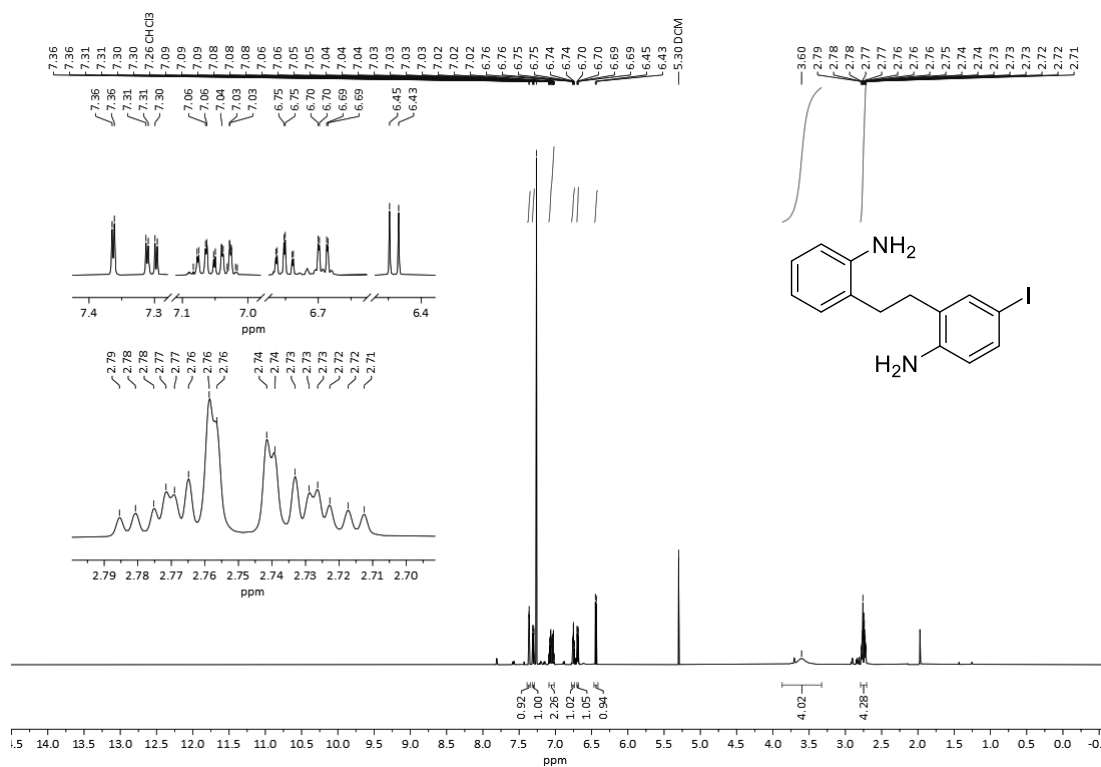
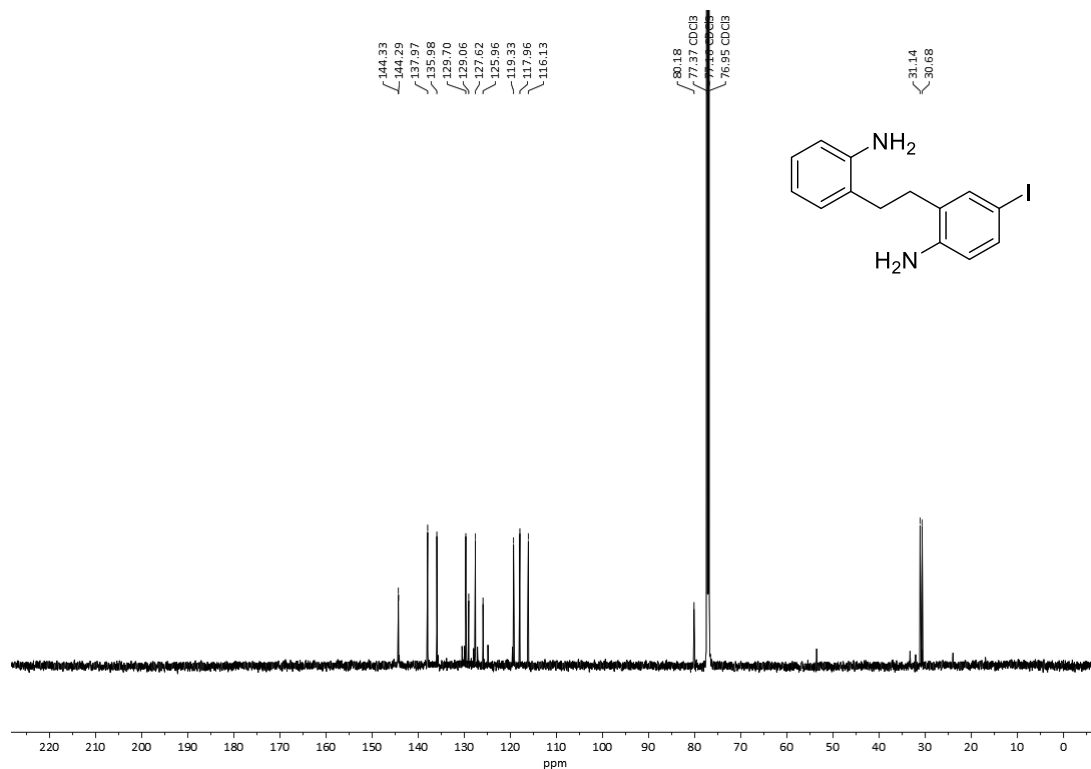


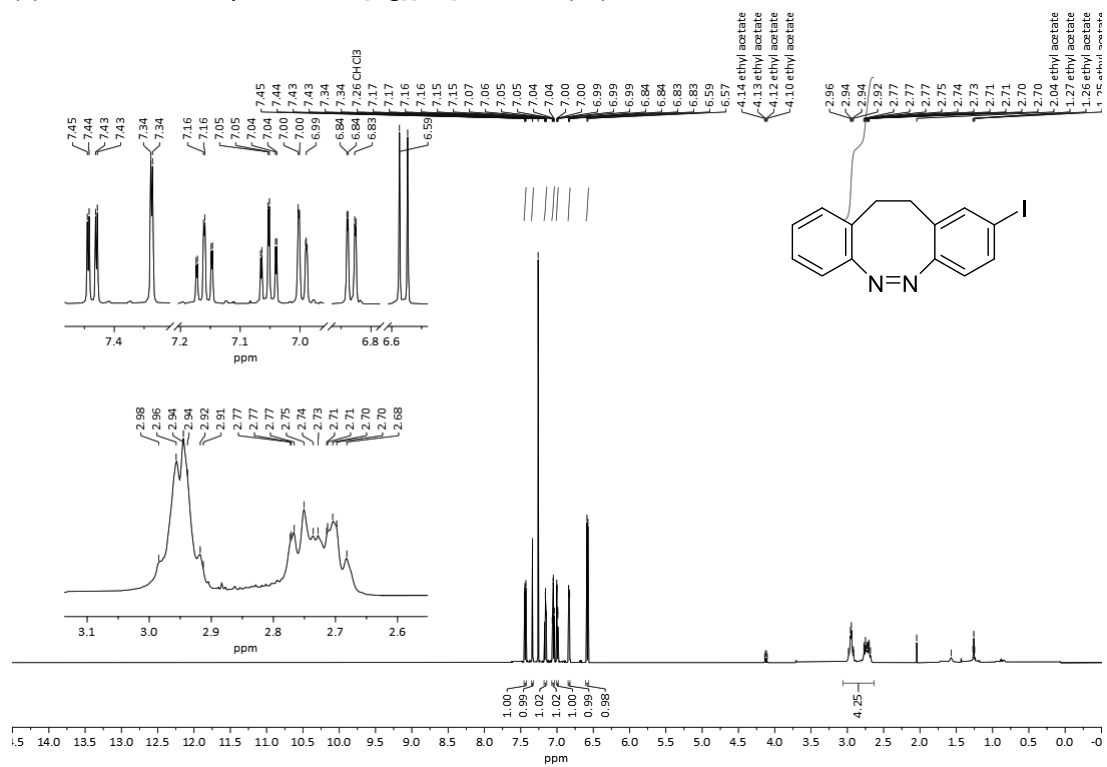
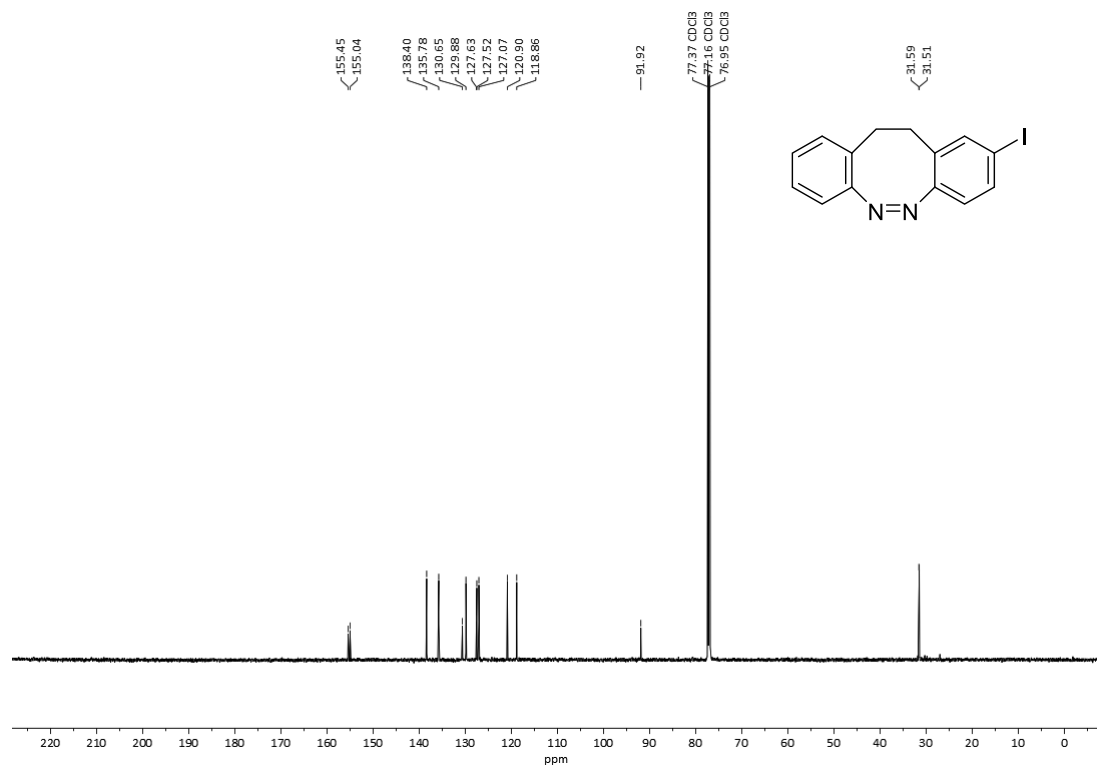
Figure S111:  $^1\text{H}$  NMR spectrum of **6** in  $\text{DMSO}-d_6$ .

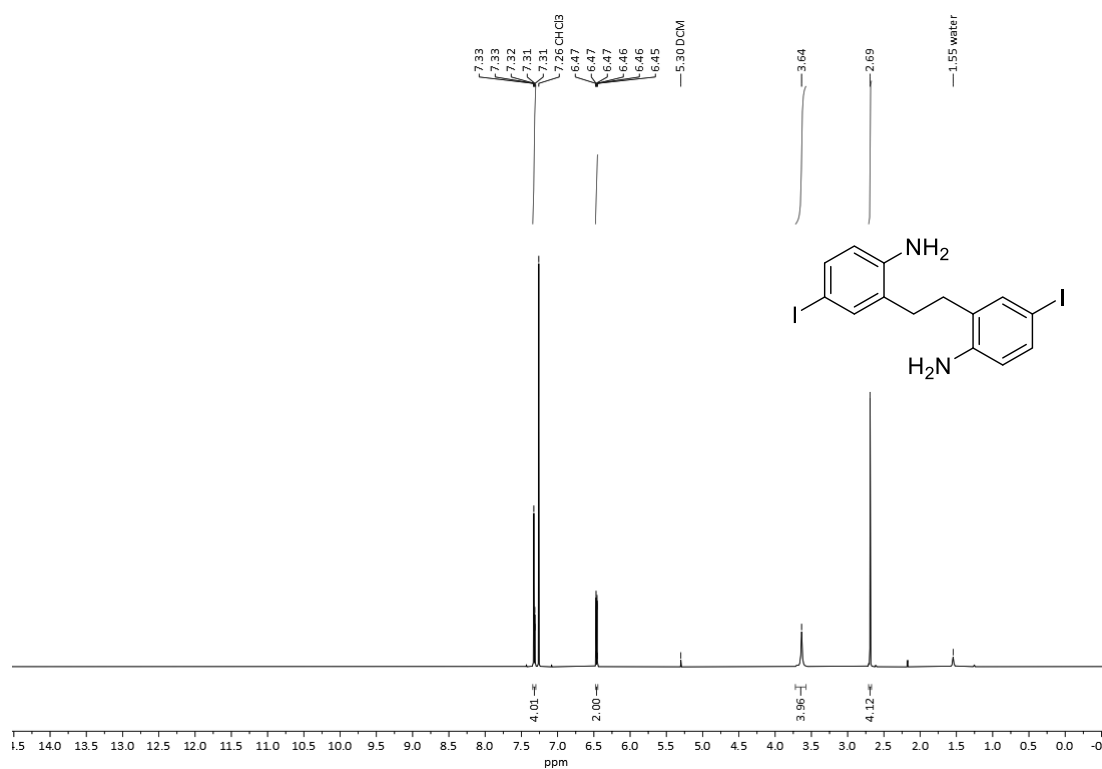
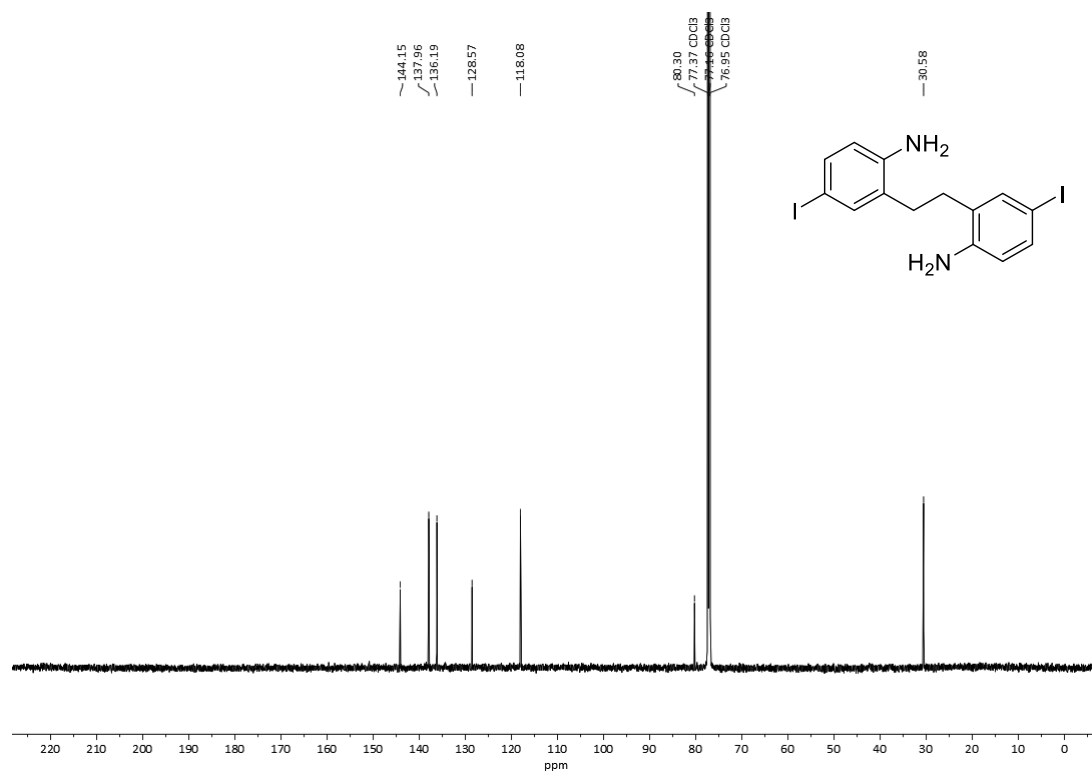
Figure S112:  $^{13}\text{C}\{^1\text{H}\}$  NMR spectrum of 6 in  $\text{DMSO-}d_6$ .Figure S113:  $^{19}\text{F}$  NMR spectrum of 6 in  $\text{DMSO-}d_6$ .

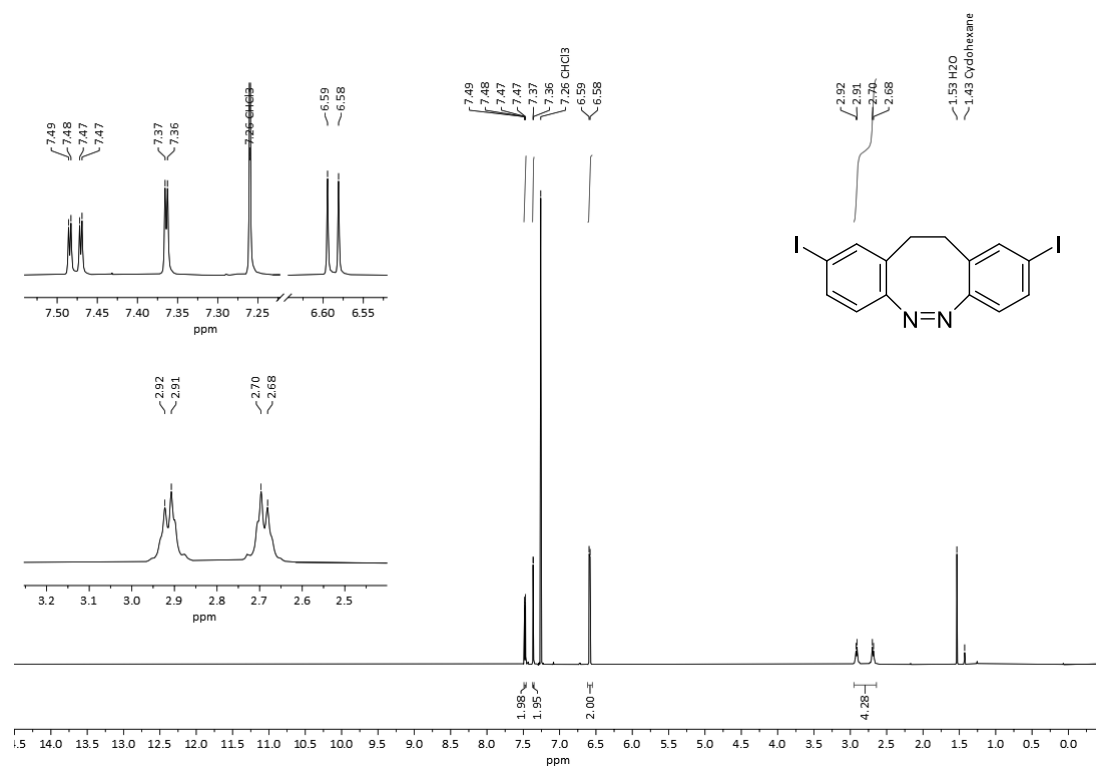
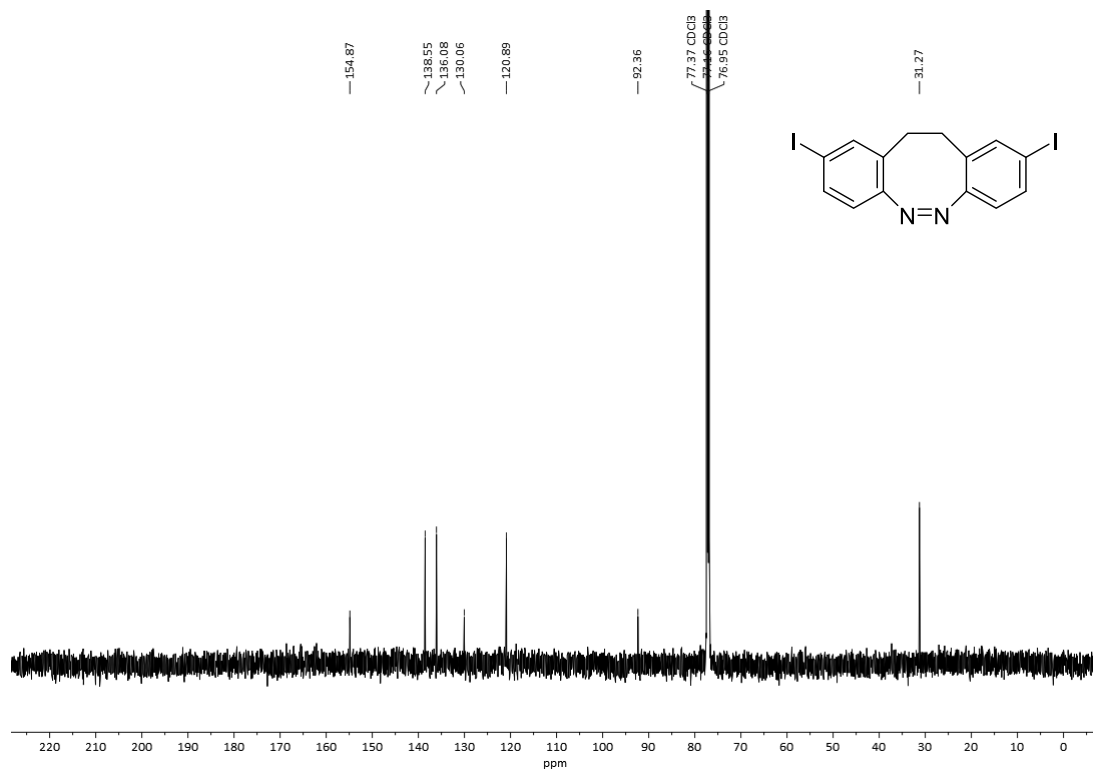
2-(2-(2-Aminophenethyl)phenyl)isoindoline-1,3-dione (**S12**)Figure S114:  $^1\text{H}$  NMR spectrum of **S12** in  $\text{CDCl}_3$ .Figure S115:  $^{13}\text{C}$  NMR spectrum of **S12** in  $\text{CDCl}_3$ .



2-(2-Aminophenethyl)-4-iodoaniline (**S13**)Figure S116:  $^1\text{H}$  NMR spectrum of **S13** in  $\text{CDCl}_3$ .Figure S117:  $^{13}\text{C}\{^1\text{H}\}$  NMR spectrum of **S13** in  $\text{CDCl}_3$ .

**(Z)-2-Iodo-11,12-dihydrodibenzo[c,g][1,2]diazocine (7a)**Figure S1218:  $^1\text{H}$  NMR spectrum of **7a** in  $\text{CDCl}_3$ .Figure S1219:  $^{13}\text{C}\{^1\text{H}\}$  NMR spectrum of **7a** in  $\text{CDCl}_3$ .

2,2'-(Ethane-1,2-diyl)bis(4-iodoaniline) (**S14**)Figure S120:  $^1\text{H}$  NMR spectrum of **S14** in  $\text{CDCl}_3$ .Figure S121:  $^{13}\text{C}\{^1\text{H}\}$  NMR spectrum of **S14** in  $\text{CDCl}_3$ .

**(Z)-2,9-Diiodo-11,12-dihydrodibenzo[c,g][1,2]diazocine (7b)**Figure S122: <sup>1</sup>H NMR spectrum of **7b** in CDCl<sub>3</sub>.Figure S123: <sup>13</sup>C{<sup>1</sup>H} NMR spectrum of **7b** in CDCl<sub>3</sub>.

$^1\text{H}$  NMR Spectra for the Determination of the  $^1\text{H}$  NMR Yield  
2,5-Dioxopyrrolidin-1-yl (*E*)-4-(phenyldiazenyl)benzoate (**3a**)

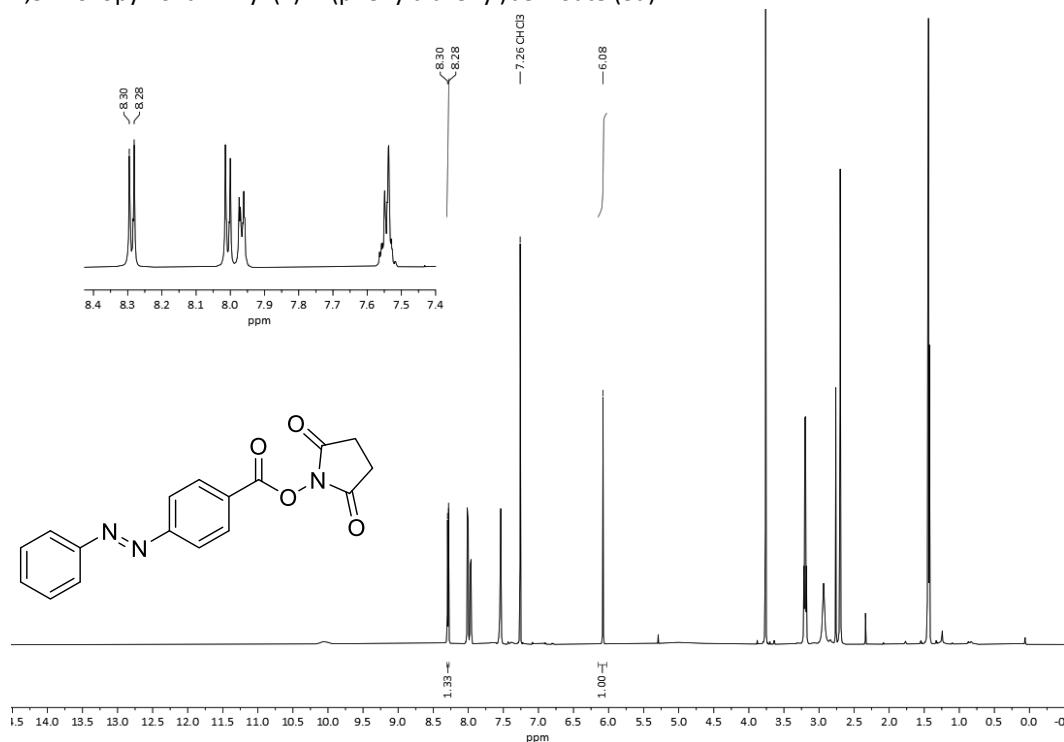


Figure S124: Crude  $^1\text{H}$  NMR spectrum of **3a** in  $\text{CDCl}_3$ .

2,5-Dioxopyrrolidin-1-yl (*E*)-3-(phenyldiazenyl)benzoate (**3b**)

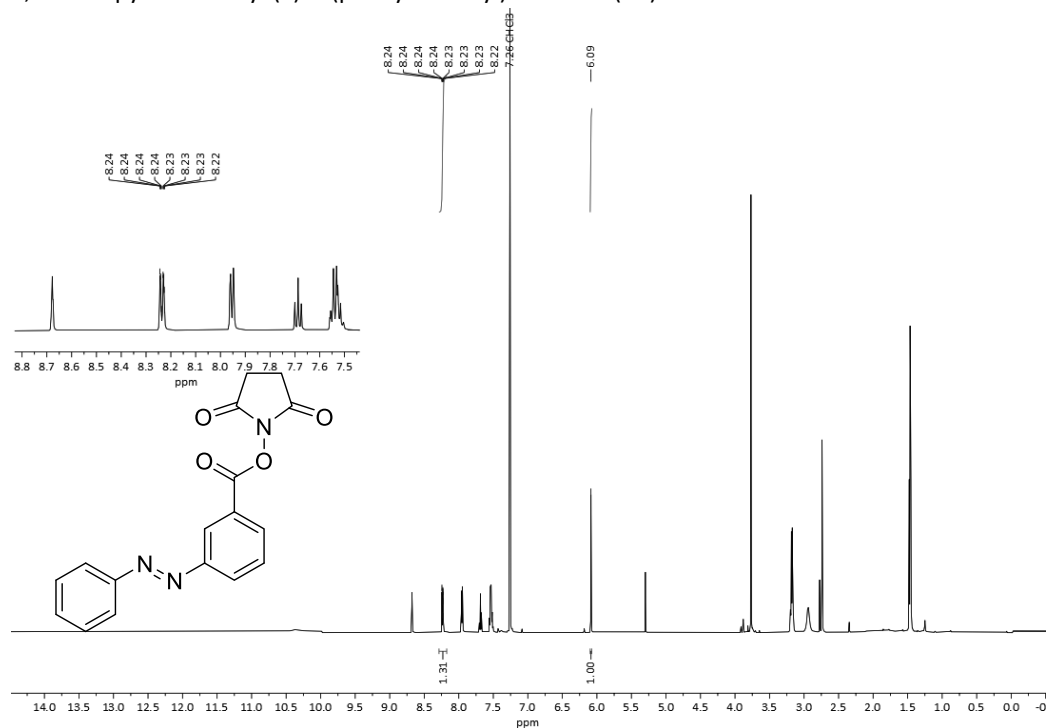
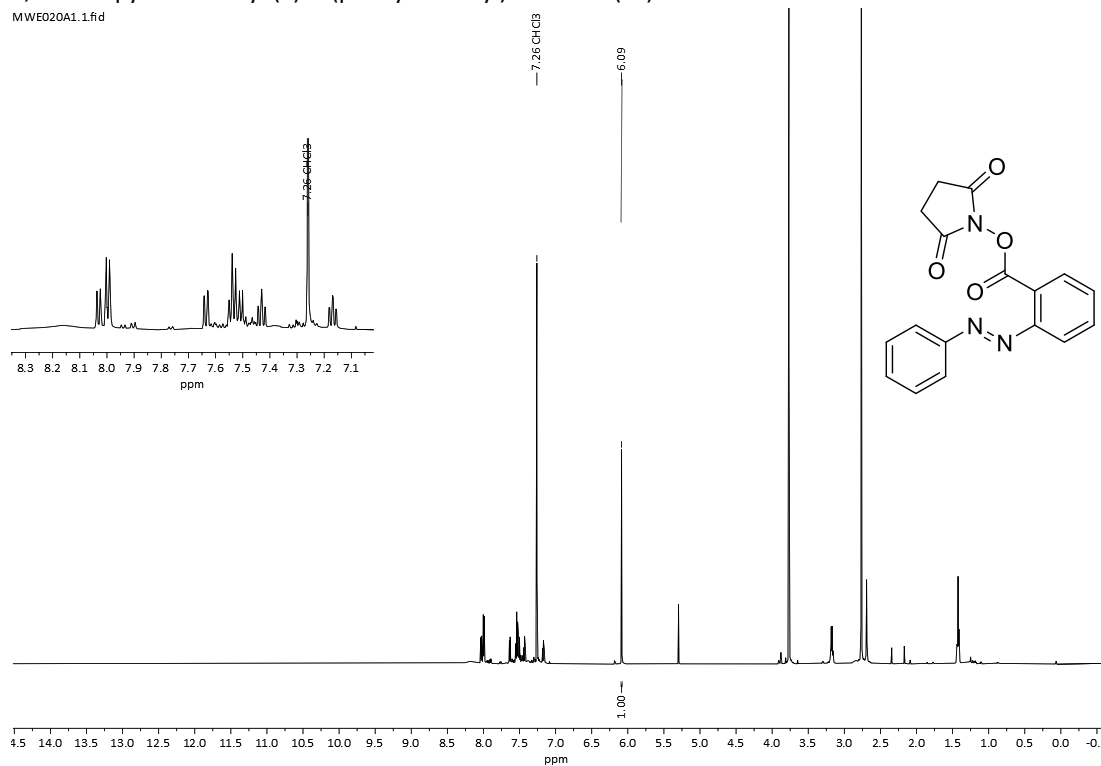
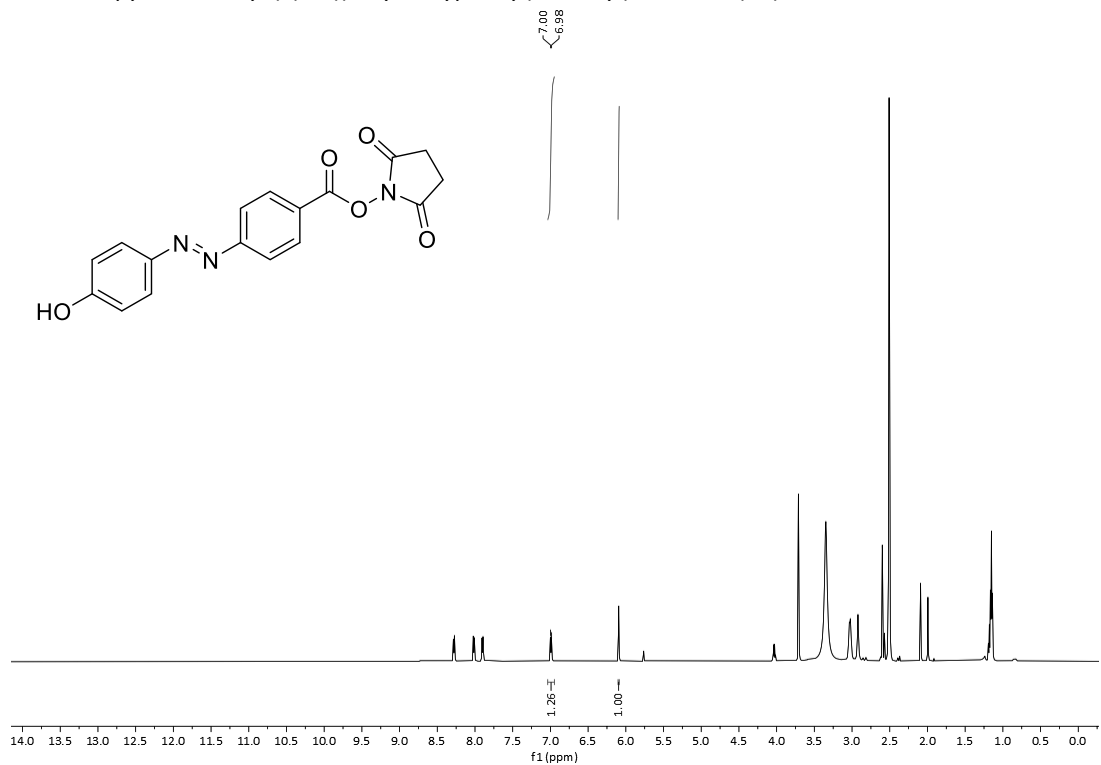
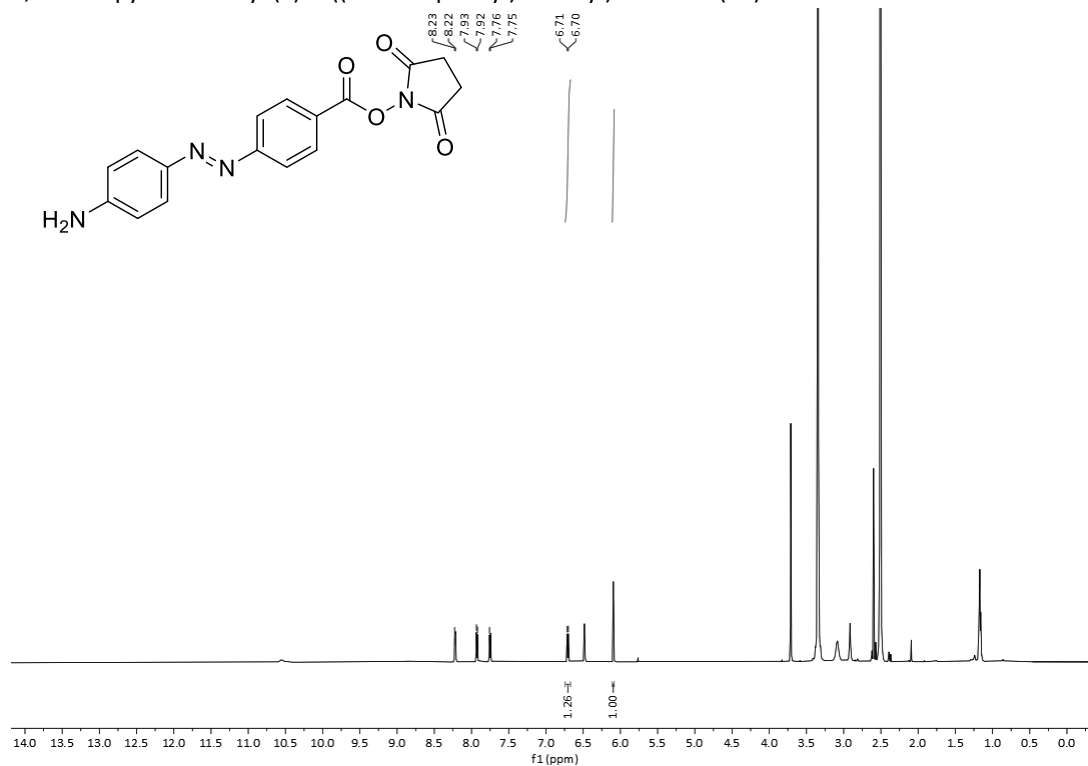
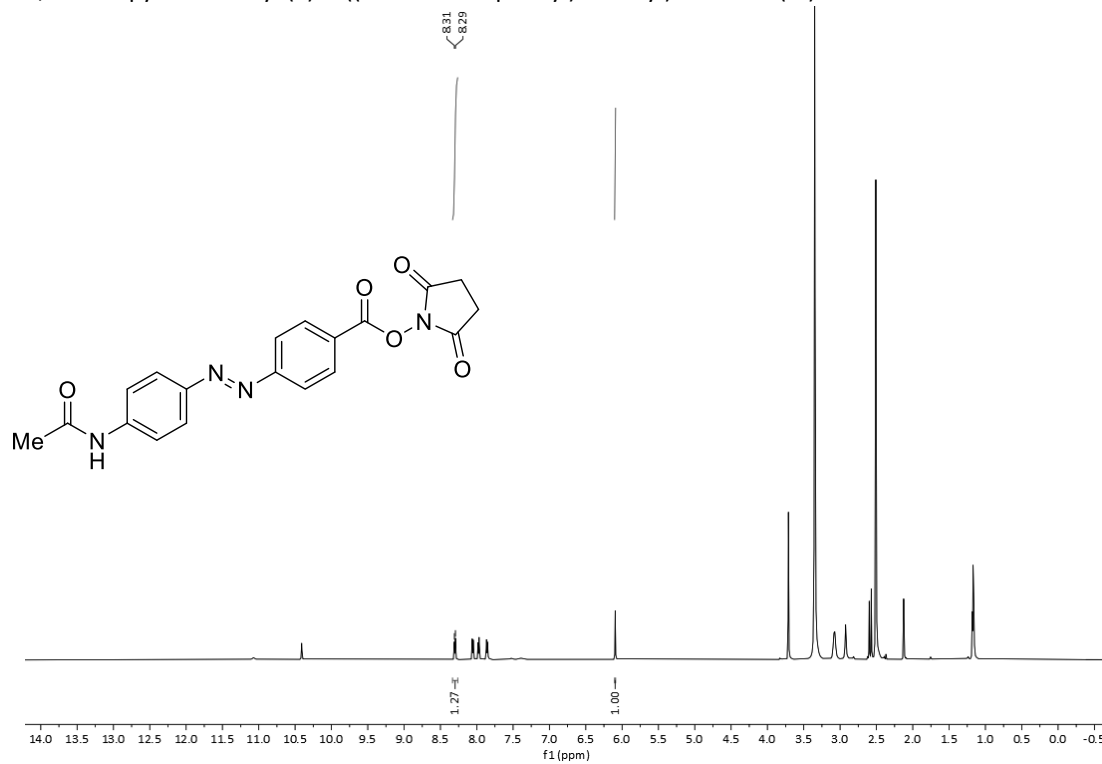


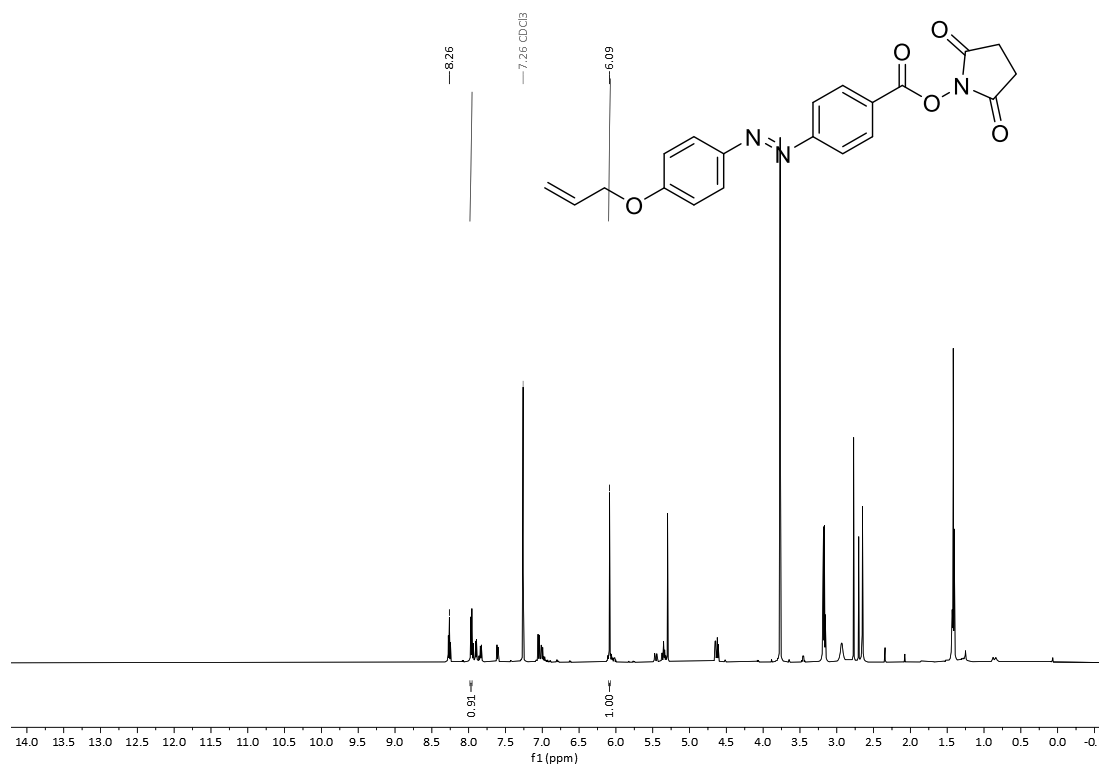
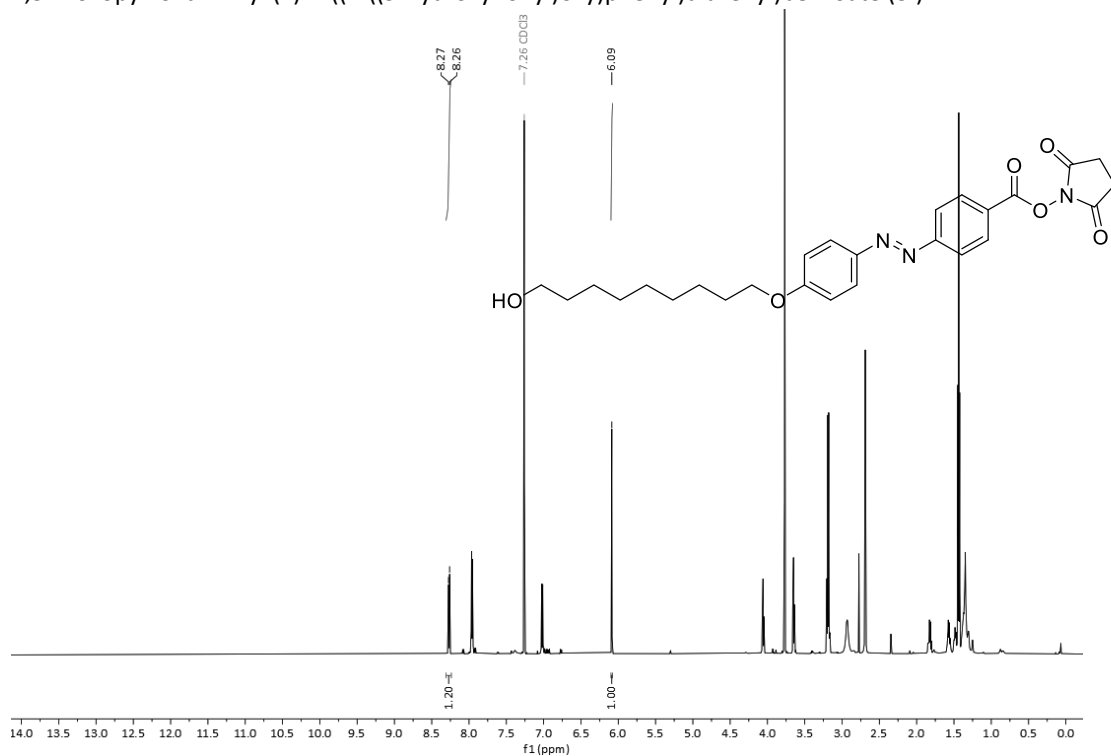
Figure S125: Crude  $^1\text{H}$  NMR spectrum of **3b** in  $\text{CDCl}_3$ .

2,5-Dioxopyrrolidin-1-yl (*E*)-2-(phenyldiazenyl)benzoate (**3c**)

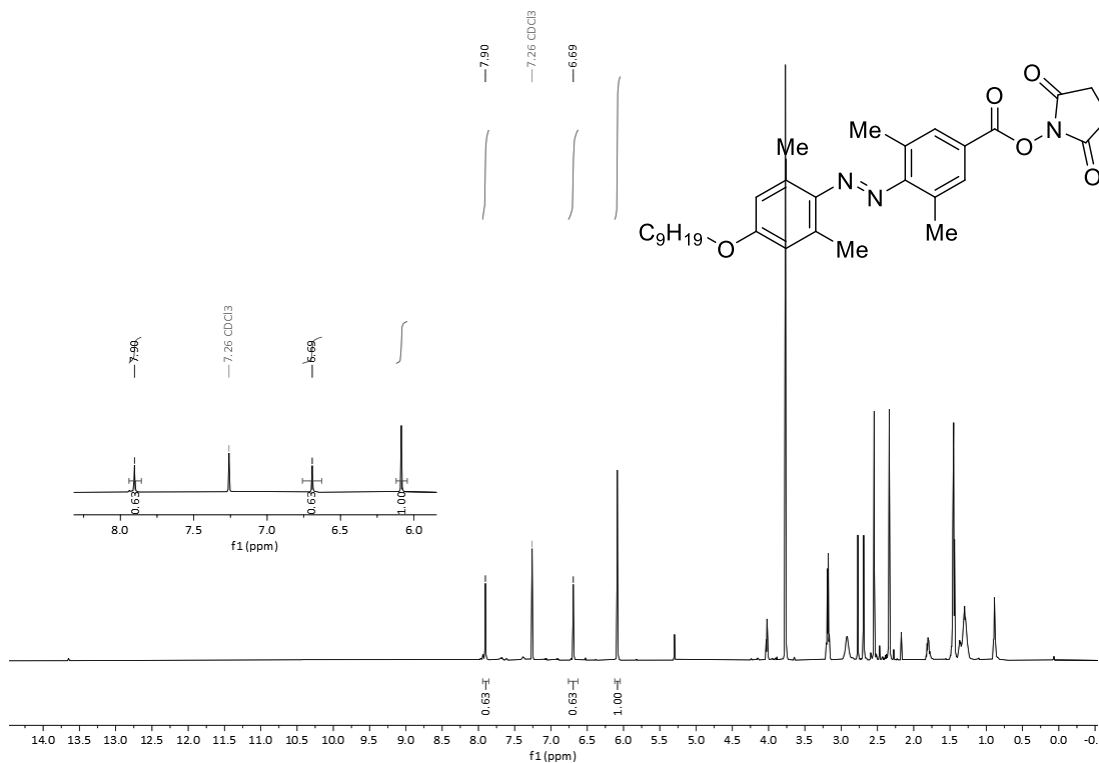
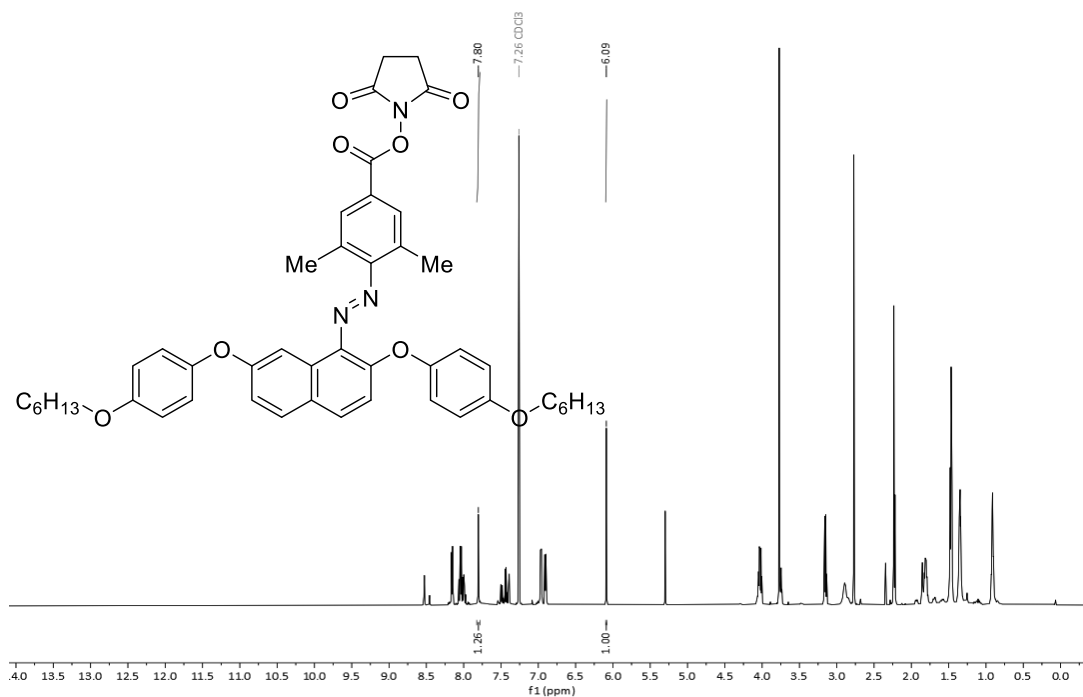
MWE020A1.1.fid

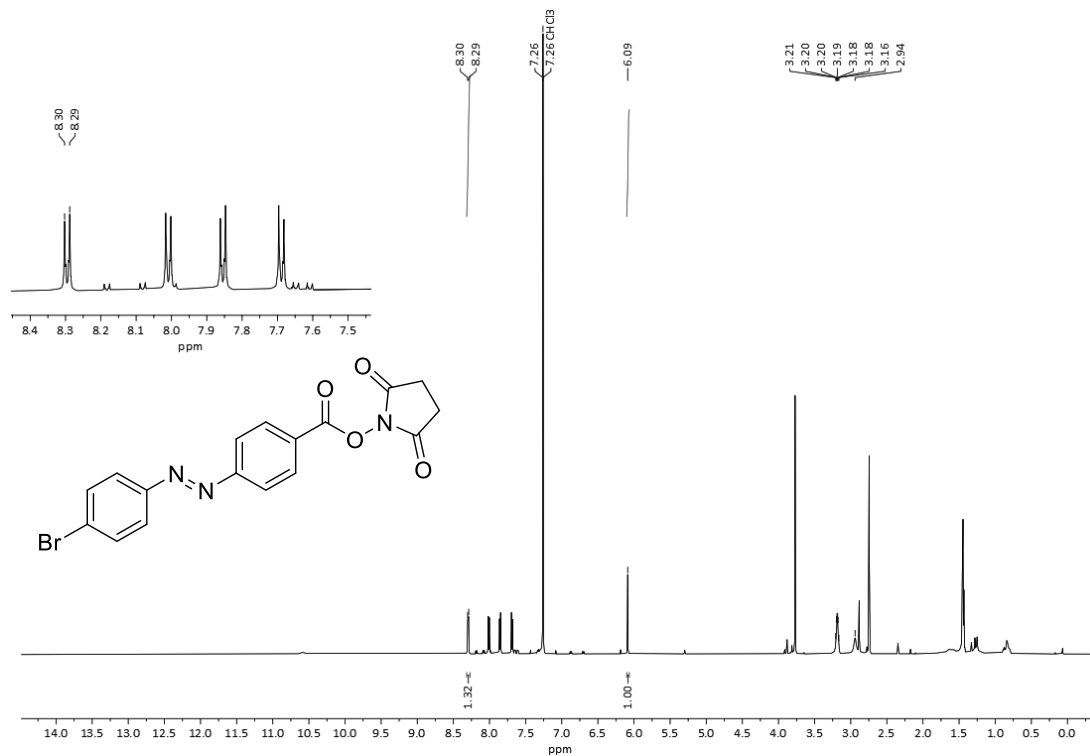
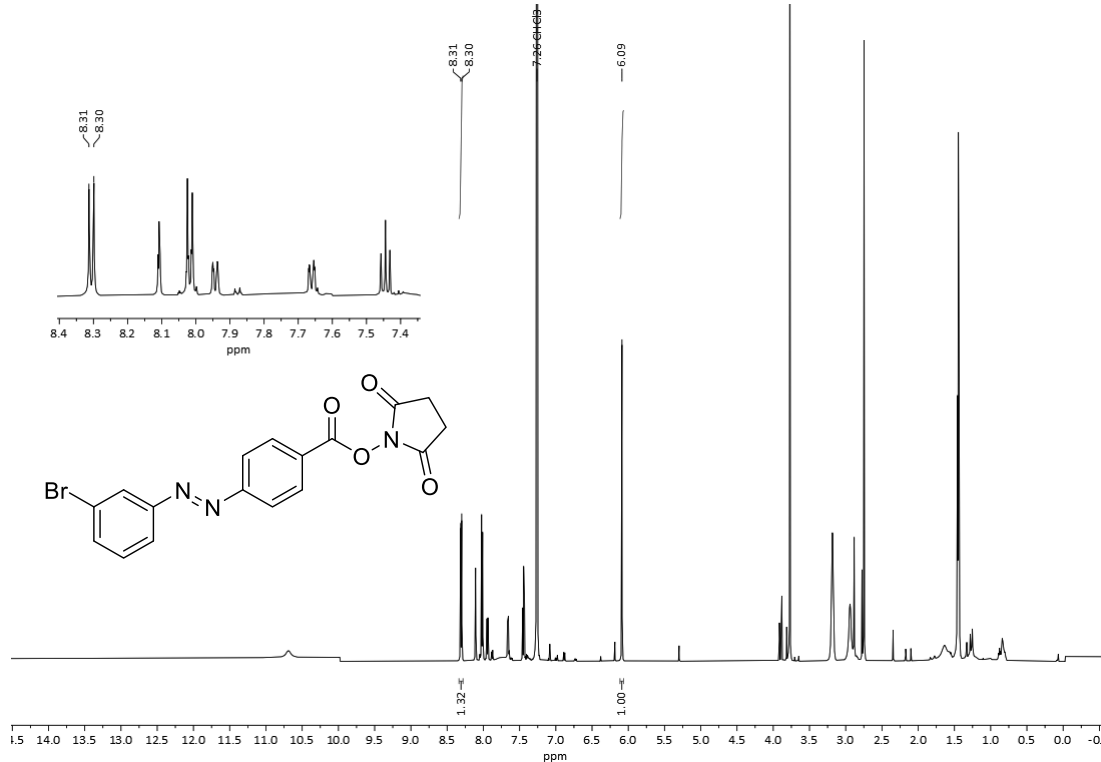
Figure S126: Crude  $^1\text{H}$  NMR spectrum of **3c** in  $\text{CDCl}_3$ .2,5-Dioxopyrrolidin-1-yl (*E*)-4-((4-hydroxyphenyl)diazenyl)benzoate (**3d**)Figure S127: Crude  $^1\text{H}$  NMR spectrum of **3d** in  $\text{DMSO}-d_6$ .

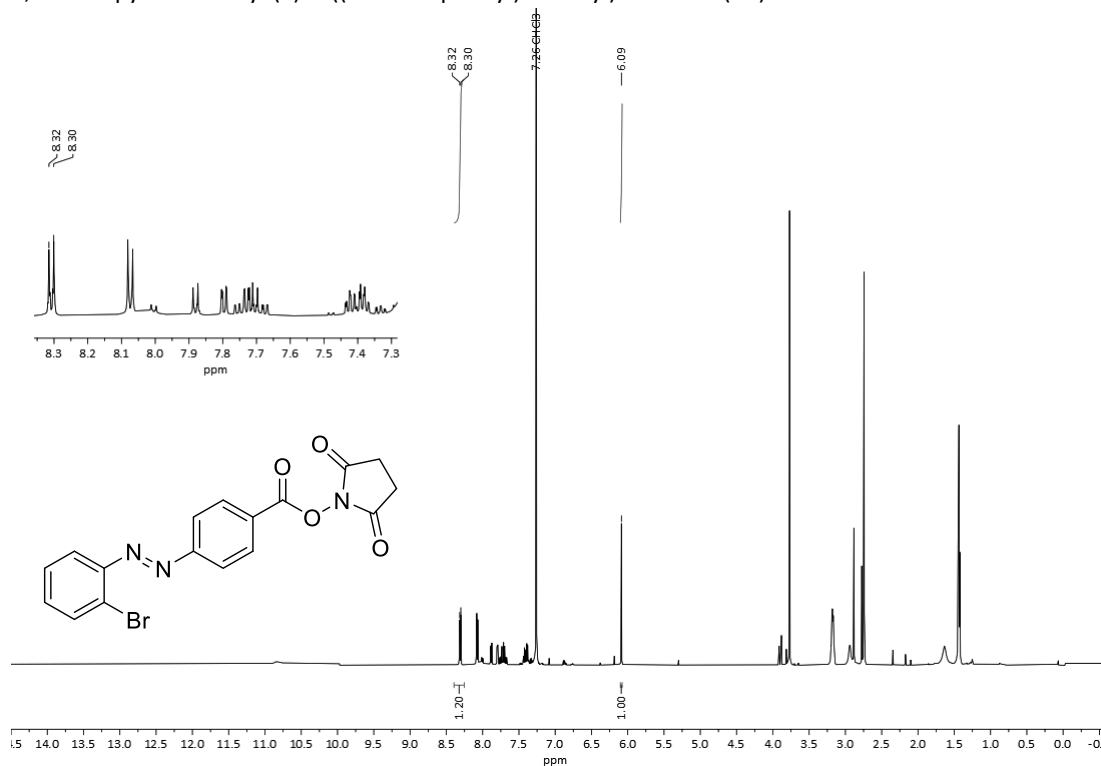
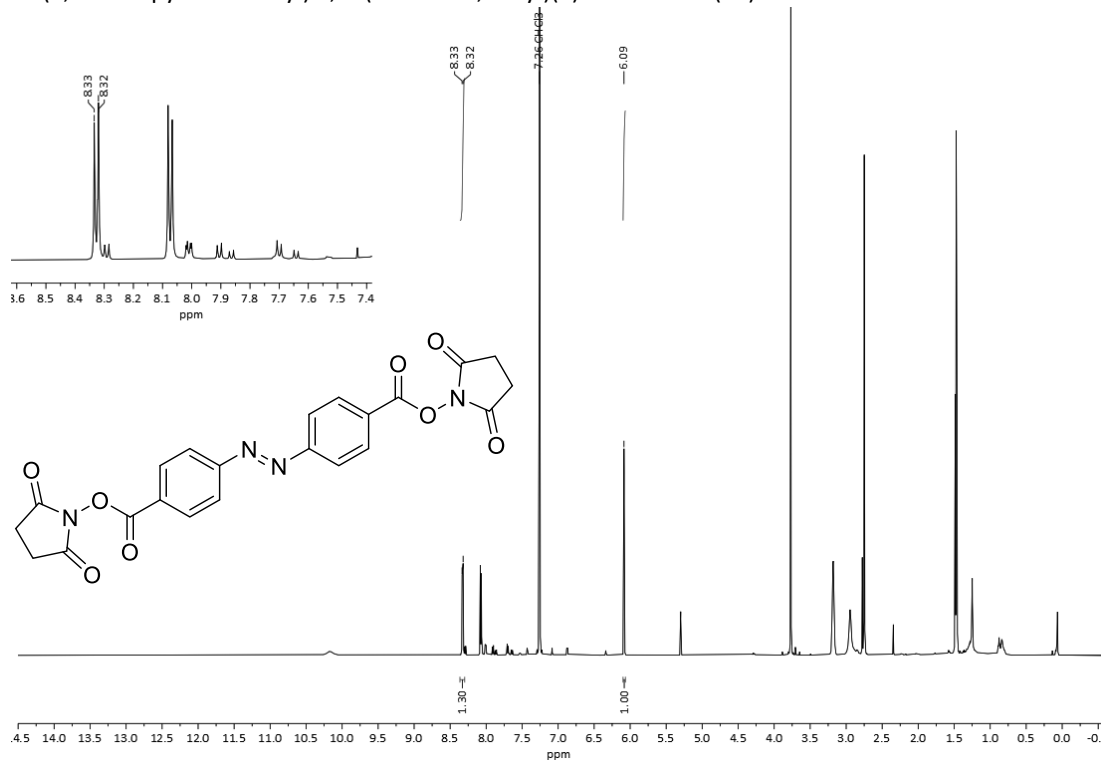
2,5-Dioxopyrrolidin-1-yl (*E*)-4-((4-aminophenyl)diazenyl)benzoate (**3e**)Figure S128: Crude <sup>1</sup>H NMR spectrum of **3e** in CDCl<sub>3</sub>.2,5-Dioxopyrrolidin-1-yl (*E*)-4-((4-acetamidophenyl)diazenyl)benzoate (**3f**)Figure S129: Crude <sup>1</sup>H NMR spectrum of **3f** in CDCl<sub>3</sub>.

2,5-Dioxopyrrolidin-1-yl (*E*)-4-((4-(allyloxy)phenyl)diazenyl)benzoate (**3h**)Figure S130: Crude <sup>1</sup>H NMR spectrum of **3h** in CDCl<sub>3</sub>.2,5-Dioxopyrrolidin-1-yl (*E*)-4-((9-(hydroxynonyl)oxy)phenyl)diazenyl)benzoate (**3i**)Figure S131: Crude <sup>1</sup>H NMR spectrum of **3i** in CDCl<sub>3</sub>.



2,5-Dioxopyrrolidin-1-yl (*E*)-4-((2,6-dimethyl-4-(nonyloxy)phenyl)diazenyl)-3,5-dimethylbenzoate (**3j**)Figure S132: Crude <sup>1</sup>H NMR spectrum of **3j** in CDCl<sub>3</sub>.2,5-Dioxopyrrolidin-1-yl (*E*)-4-((2,7-bis(4-(hexyloxy)phenoxy)naphthalen-1-yl)diazenyl)-3,5-dimethylbenzoate (**3k**)Figure S133: Crude <sup>1</sup>H NMR spectrum of **3k** in CDCl<sub>3</sub>.

2,5-Dioxopyrrolidin-1-yl (*E*)-4-((4-bromophenyl)diazenyl)benzoate (**3l**)Figure S134: Crude  $^1\text{H}$  NMR spectrum of **3l** in  $\text{CDCl}_3$ .2,5-Dioxopyrrolidin-1-yl (*E*)-4-((3-bromophenyl)diazenyl)benzoate (**3m**)Figure S135: Crude  $^1\text{H}$  NMR spectrum of **3m** in  $\text{CDCl}_3$ .

2,5-Dioxopyrrolidin-1-yl (*E*)-4-((4-bromophenyl)diazenyl)benzoate (**3n**)Figure S136: Crude <sup>1</sup>H NMR spectrum of **3n** in CDCl<sub>3</sub>.Bis(2,5-dioxopyrrolidin-1-yl) 4,4'-(diazene-1,2-diyl)(*E*)-dibenzoate (**5a**)Figure S137: Crude <sup>1</sup>H NMR spectrum of **5a** in CDCl<sub>3</sub>.

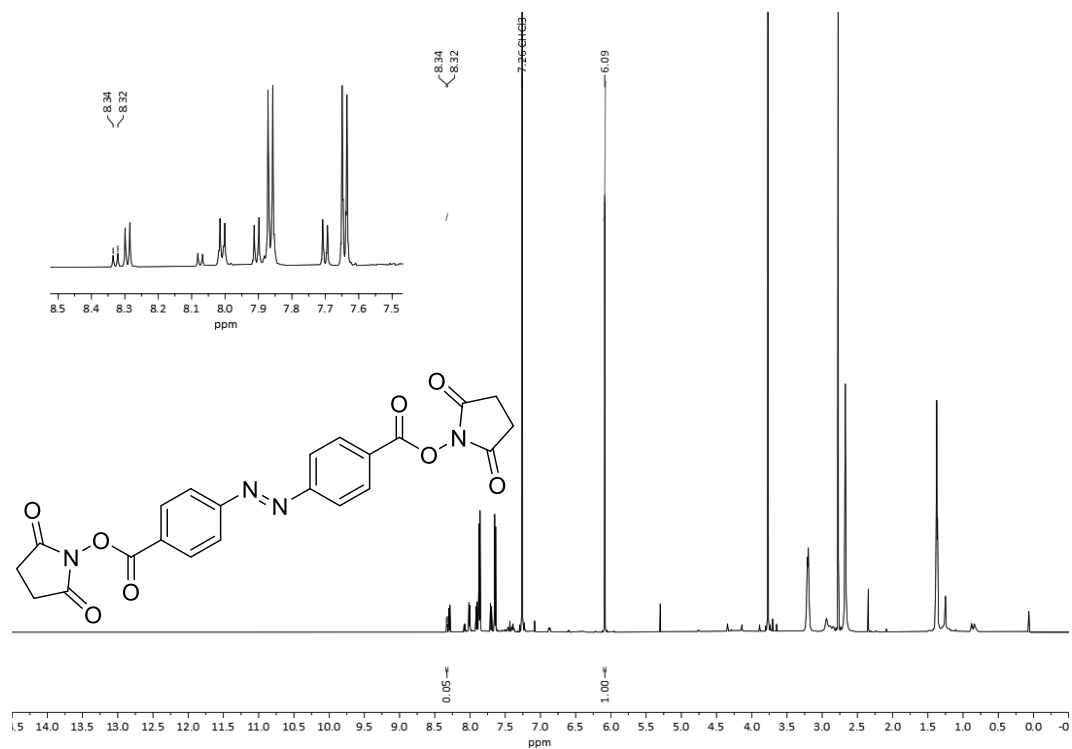


Figure S138: Crude <sup>1</sup>H NMR spectrum of 5a in CDCl<sub>3</sub> using 1,1'-bis(diphenylphosphino)ferrocene as ligand.

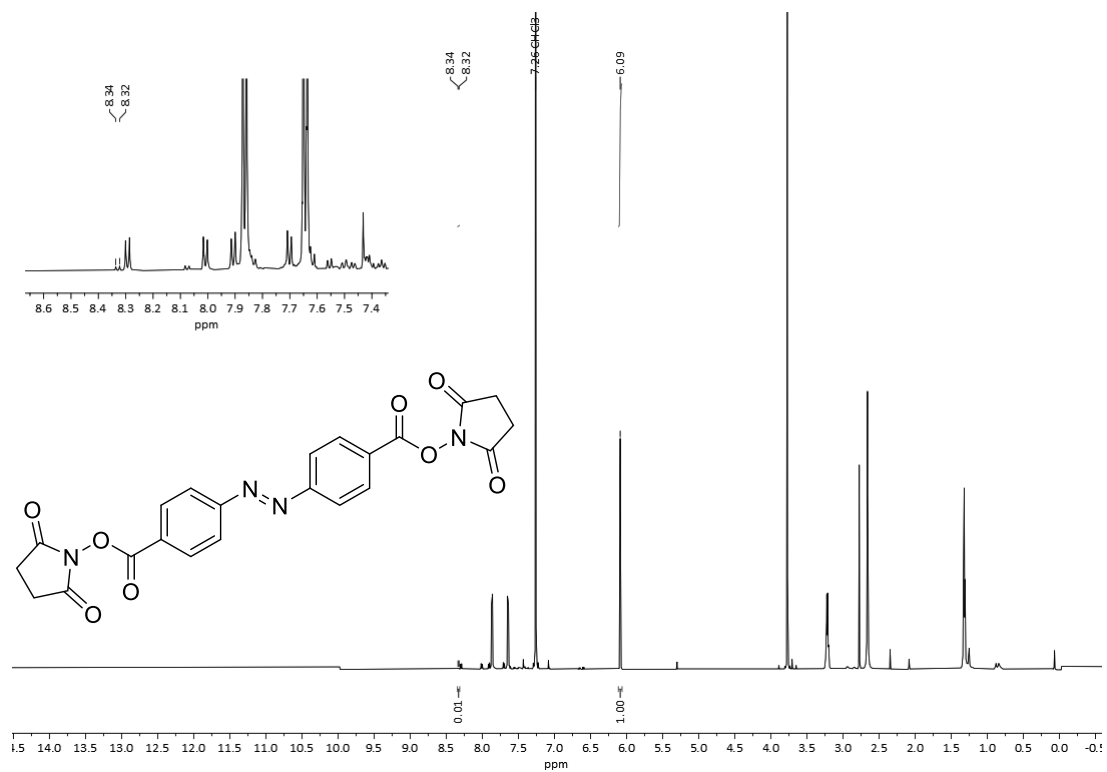


Figure S139: Crude <sup>1</sup>H NMR spectrum of 5a in CDCl<sub>3</sub> using 2,2'-bis(diphenylphosphino)-1,1'-binaphthyl as ligand.

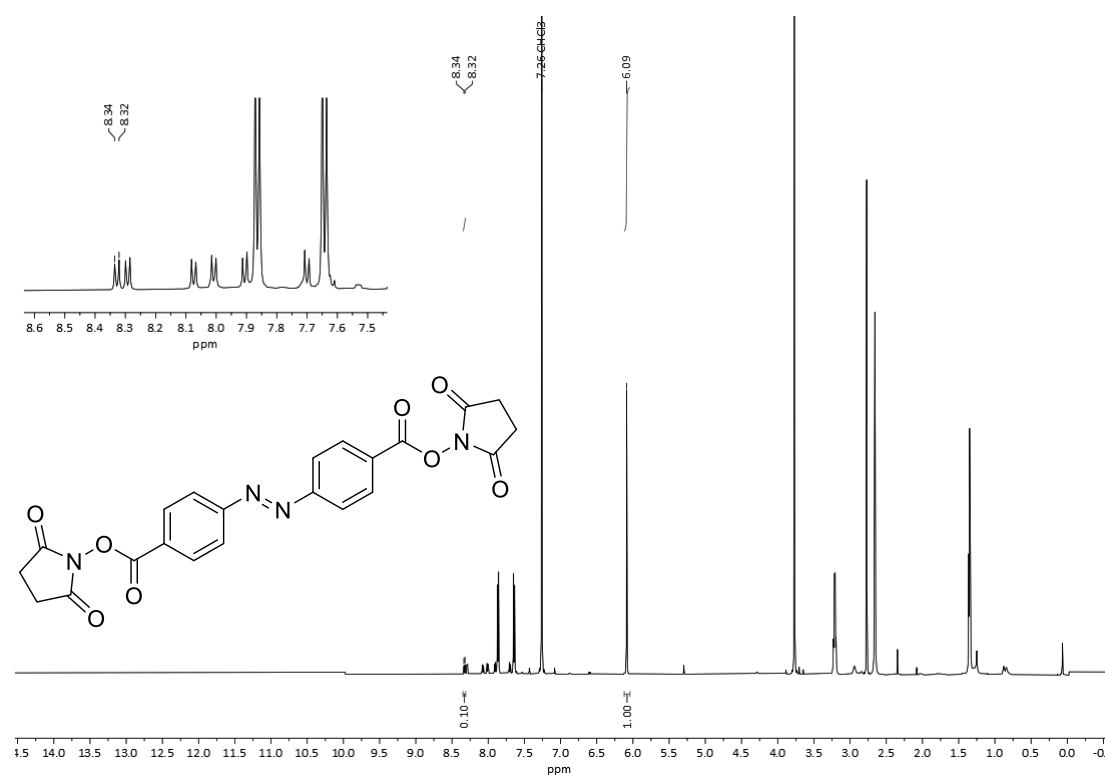


Figure S140: Crude <sup>1</sup>H NMR spectrum of 5a in CDCl<sub>3</sub> using di-(1-adamantyl)-*n*-butylphosphine as ligand.

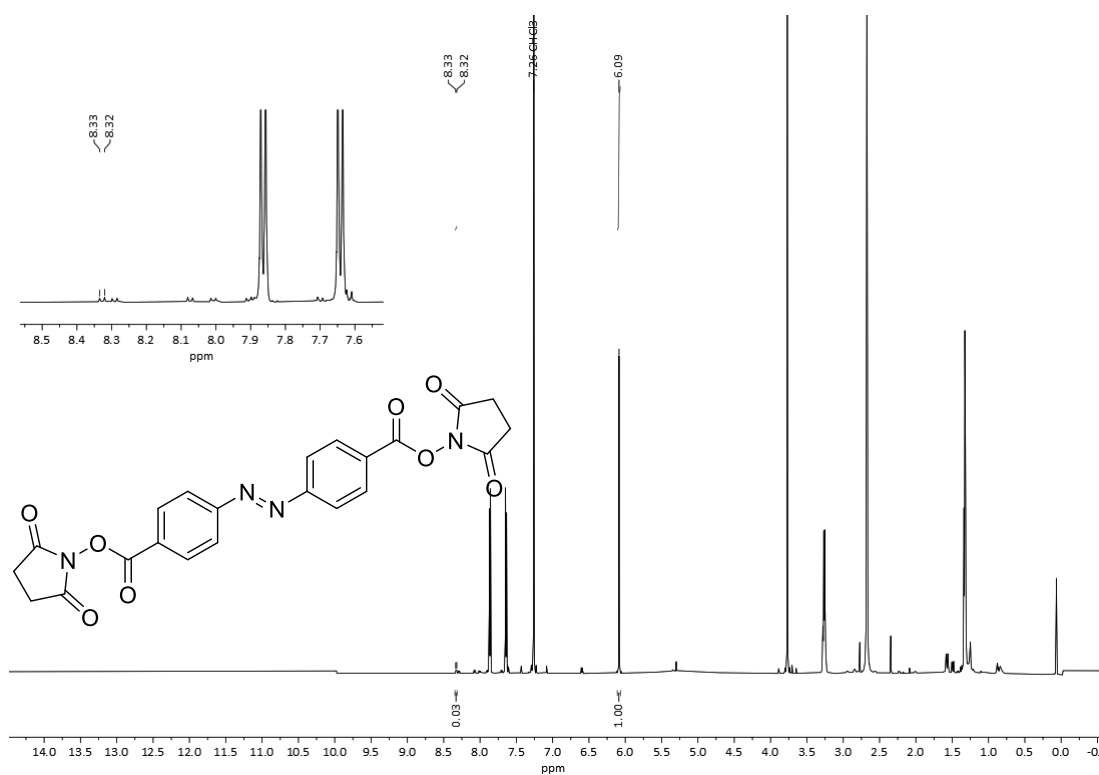
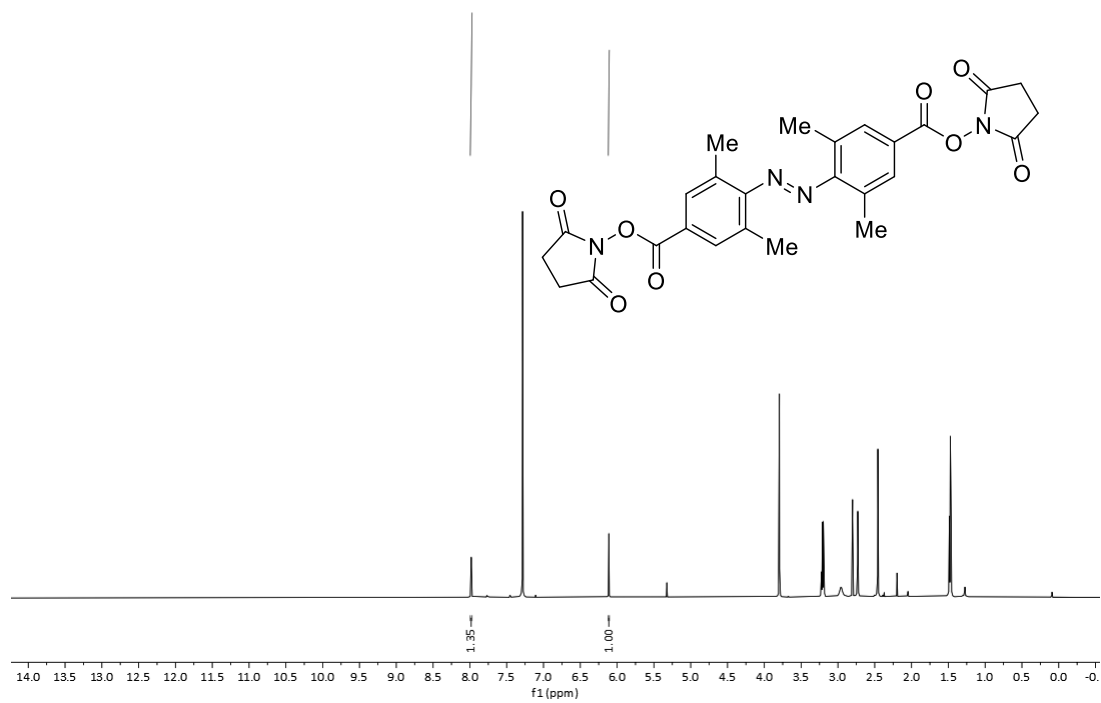


Figure S141: Crude <sup>1</sup>H NMR spectrum of 5a in CDCl<sub>3</sub> using tri-*tert*-butylphosphine as ligand.

Bis(2,5-dioxopyrrolidin-1-yl) 4,4'-(diazene-1,2-diyl)(*E*)-bis(3,5-dimethylbenzoate) (**5b**)Figure S142: Crude <sup>1</sup>H NMR spectrum of **5b** in CDCl<sub>3</sub>.

## 9.2 Appendix Publication III

### *Supporting Information*

#### **Centennial Isomers: A Unique Fluorinated Azobenzene Macrocyclus with Dual Stability over 120 years.**

*Sven Schultzke*<sup>1,2</sup>, *Pim Puylaert*<sup>3</sup>, *Henry Wang*<sup>1</sup>, *Isabell Schultzke*<sup>3</sup>, *Jonas Gerken*<sup>1,2</sup>

*Anne Staubitz*<sup>1,2,\*</sup>

M. Sc. Sven Schultzke, M. Sc. Henry Wang, Jonas Gerken, Prof. Dr. Anne Staubitz

<sup>1</sup> University of Bremen, Institute for Organic and Analytical Chemistry,

Leobener Straße 7, D-28359 Bremen, Germany

<sup>2</sup> University of Bremen, MAPEX Center for Materials and Processes,

Bibliothekstraße 1, D-28359 Bremen, Germany

Dr. Pim Puylaert, M. Sc. Isabell Schultzke

<sup>3</sup> University of Bremen, Institute for Inorganic Chemistry and Crystallography,

Leobener Straße 7, D-28359-Bremen, Germany

E-mail: [staubitz@uni-bremen.de](mailto:staubitz@uni-bremen.de)

\* Correspondence: [staubitz@uni-bremen.de](mailto:staubitz@uni-bremen.de)

## Contents

1 General Information.....	3
1.1 Reagents.....	4
1.2 Solvents.....	4
2 Analytical Data.....	6
2.1 Switching Properties of <b>OAM</b> 's and <b>FOMe</b> .....	6
2.1.1 UV-Vis Analysis: Switching Behavior of <b>FOAM</b> .....	6
2.1.2 UV-Vis Analysis: Qualitative Switching Behavior of <b>2FOAM</b> .....	9
2.1.3 UV-Vis Analysis: Qualitative Switching Behavior of <b>FOMe</b> .....	13
2.1.4 Half-Life Time of <b>HOAM</b> .....	14
2.1.5 Half-Life Time of <b>FOAM</b> .....	17
2.1.6 Half-Life Time of <b>2FOAM</b> .....	21
2.1.7 Half-Life Time of <b>FOMe</b> .....	26
2.1.9 Cycle Stability of <b>FOAM</b> and <b>2FOAM</b> .....	29
2.1.9 NMR Analysis: Quantitative Switching Behavior of <b>HOAM</b> , <b>FOAM</b> , <b>2FOAM</b> and <b>FOMe</b> .....	30
3 Crystal Structure Analysis of <b>HOAM</b> , <b>FOAM</b> , <b>2FOAM</b> .....	32
4 DFT Calculations of <b>HOAM</b> , <b>FOAM</b> , <b>2FOAM</b> .....	37
5 Syntheses.....	38
5.1 1,2-Bis((2-nitrophenoxy)methyl)benzene ( <b>S1</b> ) <sup>[8]</sup> .....	39
5.2 2,2'-((1,2-Phenylenebis(methylene))bis(oxy))dianiline ( <b>S2</b> ) <sup>[8]</sup> .....	39
5.3 ( <i>E</i> )-12,17-Dihydrotribenzo[b,f,j][1,8]dioxo[4,5]diazacyclododecine ( <b>HOAM</b> ) <sup>[9]</sup> .....	40
5.4 1,2-Bis((3-fluoro-2-nitrophenoxy)methyl)benzene ( <b>S3</b> ).....	40
5.5 ( <i>E</i> )-4,7-Difluoro-12,17-dihydrotribenzo[b,f,j][1,8]dioxo[4,5]diazacyclododecine ( <b>S4</b> ).....	41
5.6 Ethyl 4-amino-3,5-difluorobenzoate ( <b>FOAM</b> ).....	42
5.7 1,2-bis((3,5-difluoro-2-nitrophenoxy)methyl)benzene ( <b>S5</b> ).....	42
5.8 2,2'-((1,2-Phenylenebis(methylene))bis(oxy))dianiline ( <b>S6</b> ).....	43
5.9 ( <i>E</i> )-12,17-Dihydrotribenzo[b,f,j][1,8]dioxo[4,5]diazacyclododecine ( <b>2FOAM</b> ).....	44
5.10 ( <i>E</i> )-1,2-Bis(2-fluoro-6-methoxyphenyl)diazene ( <b>FOMe</b> ) <sup>[10]</sup> .....	45
5 References.....	45
6 <sup>1</sup> H, <sup>13</sup> C{ <sup>1</sup> H} and <sup>19</sup> F NMR Spectra of the Purified Compounds.....	47
7 Emission spectra of the LED's.....	61
8. Crystallographic Analysis.....	64



## 1 General Information

For reactions under inert conditions, a nitrogen filled glovebox (Pure Lab<sup>HE</sup> from Inert, Amesbury, MA USA) and standard Schlenk techniques were used.

All glassware was dried in an oven at 200 °C for several hours prior to use. NMR tubes were dried in an oven at 110 °C for several hours prior to use.

NMR spectra were recorded on a Bruker Avance Neo 600 (Bruker BioSpin, Rheinstetten, Germany) (600 MHz (<sup>1</sup>H), 151 MHz (<sup>13</sup>C<sup>[1]</sup>), 565 MHz (<sup>19</sup>F) at 298 K. All <sup>1</sup>H NMR and <sup>13</sup>C{<sup>1</sup>H} NMR spectra were referenced to the residual proton signals of the solvent (<sup>1</sup>H) or the solvent itself (<sup>13</sup>C{<sup>1</sup>H}). <sup>19</sup>F NMR spectra were referenced internally against trichlorofluoromethane. The exact assignment of the peaks was performed by two-dimensional NMR spectroscopy such as <sup>1</sup>H COSY, <sup>13</sup>C{<sup>1</sup>H} HSQC and <sup>1</sup>H/<sup>13</sup>C{<sup>1</sup>H} HMBC when possible.

High-resolution EI mass spectra were recorded on a MAT 95XL double-focusing mass spectrometer from Finnigan MAT (Thermo Fisher Scientific, Waltham, MA, USA) at an ionization energy of 70 eV. Samples were measured by a direct or indirect inlet method with a source temperature of 200 °C. High-resolution ESI and APCI mass spectra were measured by a direct inlet method on an Impact II mass spectrometer from Bruker Daltonics (Bruker Daltonics, Bremen, Germany).

IR spectra were recorded on a Nicolet i510 FT-IR spectrometer from Thermo Fisher Scientific (Thermo Fisher Scientific, Waltham, MA, USA) with a diamond window in an area from 500 – 4 000 cm<sup>-1</sup> with a resolution of 4 cm<sup>-1</sup>. All samples were measured 16 times against a background scan.

Melting points were recorded on a Büchi Melting Point M-560 (Büchi, Essen, Germany) and are reported corrected.

UV-vis spectra were recorded with a resolution of 0.5-0.1 nm on a UV-2700 spectrometer from Shimadzu (Shimadzu, Kyoto, Japan) with a double monochromator. In all cases, DMSO (spectroscopy grade) was used as a solvent. The controlled heating was made possible by the qx2/Shimadzu inlet from Quantum Northwest (WA, USA). A Cary 3500 Multicell UV-Vis Spectrophotometer from Agilent (CA, USA) was used additionally for UV-vis measurements at elevated temperatures.

For the irradiation experiments: A UPLED power supply powered the high-power LED modules: M365L3 (365 nm), M415L4 (415 nm), M530L4 (530 nm), M590L4 (590 nm). A collimator was used to focus the light beam. The light intensity was measured using an ILT2400 hand-held light meter manufactured by International Light Technologies, Inc., (Peabody, USA). Additionally, a 420 nm (1.0 W) and a 525 nm LED (1.0 W) from EPILED was built in our laboratories.

Single crystal X-ray diffraction data were collected at 100 K using an open flow nitrogen stream on a Bruker Venture D8 diffractometer (Bruker, Karlsruhe, Germany) with a Photon 100 detector in shutterless mode with Mo-K $\alpha$  (0.7107 Å) radiation. All structures were solved by intrinsic phasing and refined based on F<sup>2</sup> by use of the SHELX program package, as implemented in OLEX2<sup>[2]</sup> All non-hydrogen atoms were refined using anisotropic displacement parameters. Hydrogen atoms attached to carbon atoms were included in geometrically calculated positions using a riding model. The crystal was obtained by slow evaporation of an *n*-hexane/dichloromethane mixture at 20 °C. For the Z-Isomer the *n*-hexane/dichloromethane solution was irradiated for 2 h with green light (525nm). The crystals were then grown by slow evaporation in the dark. Evaluation of angles and bond lengths were performed with the software Diamond (version 4.6.8) and the visualization was made with the software Mercury (version 4.1.0).

Crystals of **Z-FOMe** were obtained as clear yellow plates by slow evaporation of a concentrated solution in Et<sub>2</sub>O. Various crystals invariably showed non-merohedral twinning, as determined by the TwinRotMat functionality in PLATON.<sup>[3]</sup> For the selected crystal, implementing the suggested twin

matrix (-1 0 0, 0 -1 0, 0.006 0 1) significantly improved the refinement (from  $R1$  12.60%,  $wR2$  29.28% to 4.70% and 13.74%, respectively).

Optimized geometries were calculated based on the crystal structure with Gaussian 09, revision D.01<sup>[4]</sup> quantum package for a single molecule in the gas phase using B3LYP/cc-pVTZ level of theory including the Grimme D3<sup>[5]</sup> correction. Additionally, for solvent simulation the self-consistent reaction field (SCRF) with the solvation model based on density (SMD) for the solvent DMSO on a B3LYP/cc-pVDZ level of theory including the Grimme D3<sup>[5]</sup> correction was used.

Thin layer chromatography (TLC) was performed using TLC Silica gel 60 F<sub>254</sub> from Merck (Merck, Darmstadt, Germany) and the compounds were visualized by exposure to UV light at a wavelength of 254 nm. Column chromatography was performed manually using silica gel 60 (0.015-0.040 mm) from Merck (Merck, Darmstadt, Germany). The samples were applied via dry load with Celite® 503 (Macherey-Nagel, Düren, Germany) as column material. If stated, Celite® 503 was used as filtration aid.

2FOAM (5mg or 2mg) blends in PMMA (500mg) were obtained by dissolving both compounds in Xylene/DMF (95:5, 6 mL) under stirring and heating. The solution was filtered through a syringe filter and casted in a petri dish. Over three days the solvent was removed by slow air evaporation. Afterwards, the solid PMMA blend was further dried in a dry oven at 60 °C for 24 h. The PMMA was removed from the petri dish with hot water (~50°C) and a razor blade.

The UV-Vis spectrum of the 2FOAM/PMMA (5 mg/500 mg) was taken by taping the polymer on a cuvette holder in air and placing the sample in the light path. The kinetic study of 2FOAM/PMMA (2 mg/500 mg) was taken by glueing a polymer stripe inside a quartz cuvette with an acrylate UV adhesive. The quartz cuvette was filled with the non-solvent glycerin for heat transfer.

The use of abbreviations follows the conventions from the ACS Style guide.<sup>[6]</sup>

## 1.1 Reagents

All chemicals were commercially available and used without purification unless stated otherwise.

**Table S1.** List of suppliers and purity of chemicals used.

Reagent	Supplier	Purity
1,2-Bromomethylbenzene	Apollo Scientific	99%
3,5-Difluoro-2-nitrophenol	BLD Pharm	97%
2-Fluoro-4-methoxyanilin	BLD Pharm	98%
3-Fluoro-2-nitrophenol	BLD Pharm	99.9%
Iron (10 µm)	Alfa Aesar	99.5%
K <sub>2</sub> CO <sub>3</sub>	Acros Organics	99%, anhydrous
2-Nitrophenol	Fisher Scientific	99%
Magnesium sulfate	VWR	99.2%
Manganese(IV)Oxide	Merck	~85%, precipitated active
Polymethylmethacrylate (PMMA)	Phywe	
Sodium carbonate	Chem Solute%	99.8%
Sodium chloride	CarlRoth	>99.5%
Sodium hydroxide	VWR	98.6%

## 1.2 Solvents

All solvents for purification and extraction were used as received. All solvents used for synthesis under inert conditions were dried by a solvent purification system (SPS) from Inert Technologies.

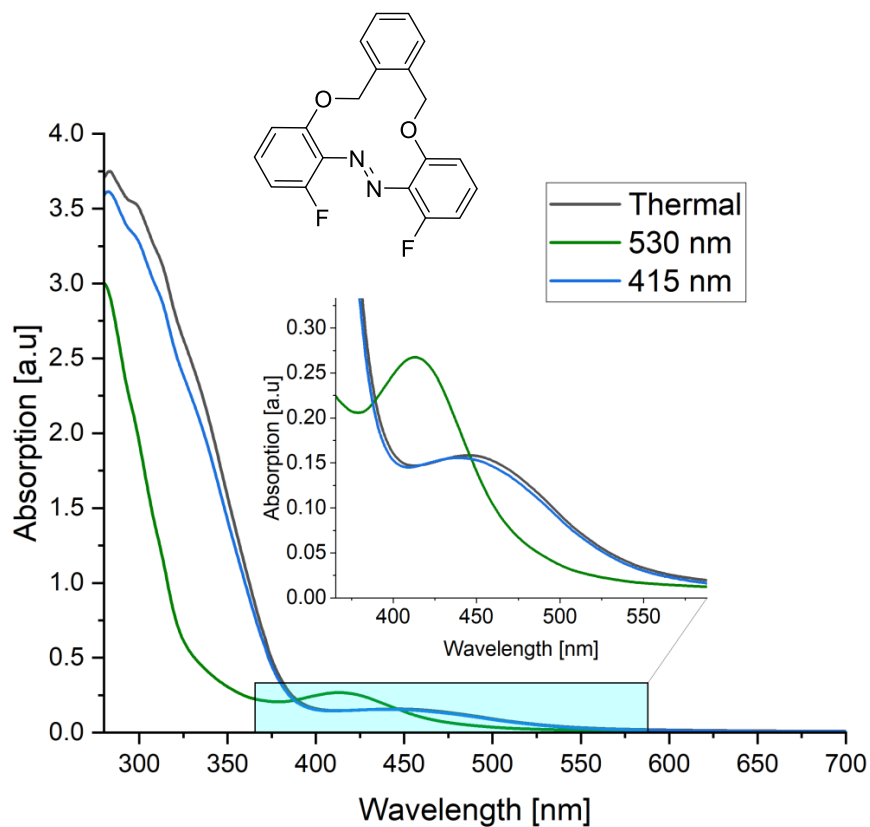
**Table S2.** List of supplier and purity of used solvents.

<b>Solvent</b>	<b>Supplier and Purity</b>	<b>Comments</b>
Acetic Acid	Merck $\geq 99.8\%$	
Acetone	Sigma Aldrich	
Acetonitrile	Fisher Scientific 99.5%	
Chloroform	VWR, 99.0% + 0.6 % EtOH (stab.)	
Chloroform- $d_1$	Euroisotop 99.8%	
Cyclohexane	Merck $\geq 99.5\%$ (GC)	
DCM	Merck $\geq 99.9\%$ (GC)	
DMSO	VWR technical grade	
DMSO- $d_6$	Sigma Aldrich, 99.9%	
Ethanol	VWR $\geq 99.8\%$	absolute
Ethyl acetate	Merck $> 99.5\%$ (GC)	
Hydrochloric acid (37%)	Merck, fuming $> 37.0\%$	
Methanol	VWR $> 99.8\%$ (GC)	
<i>n</i> -Hexane	Merck, $> 95\%$	
Toluene	Merck $> 99.7\%$ (GC)	
Water	deionized	

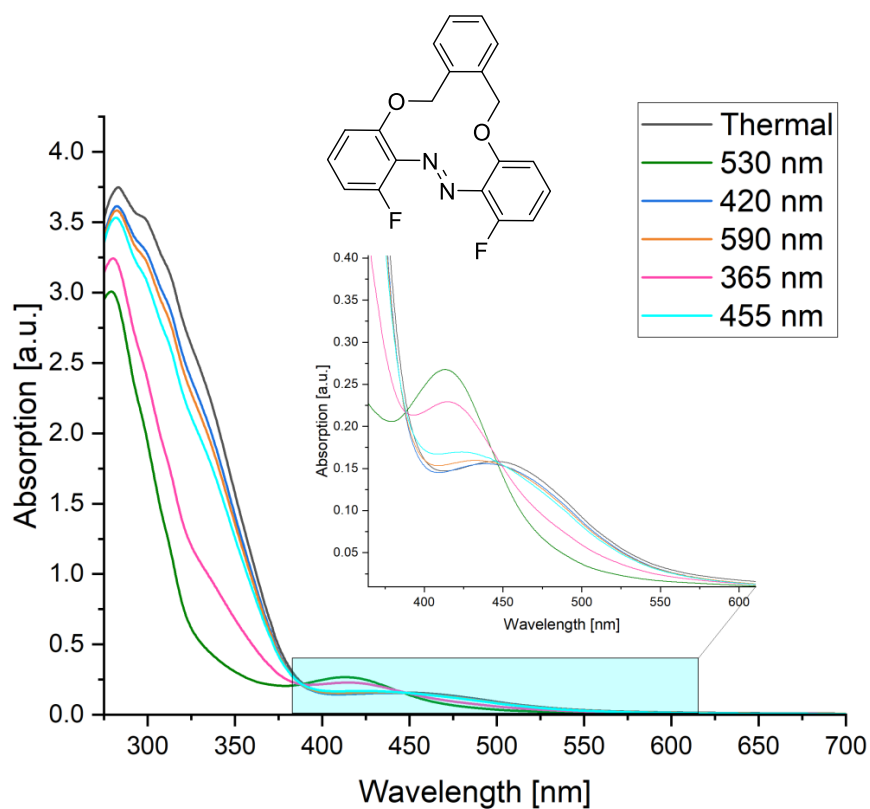
## 2 Analytical Data

### 2.1 Switching Properties of **OAM**'s and **FOMe**

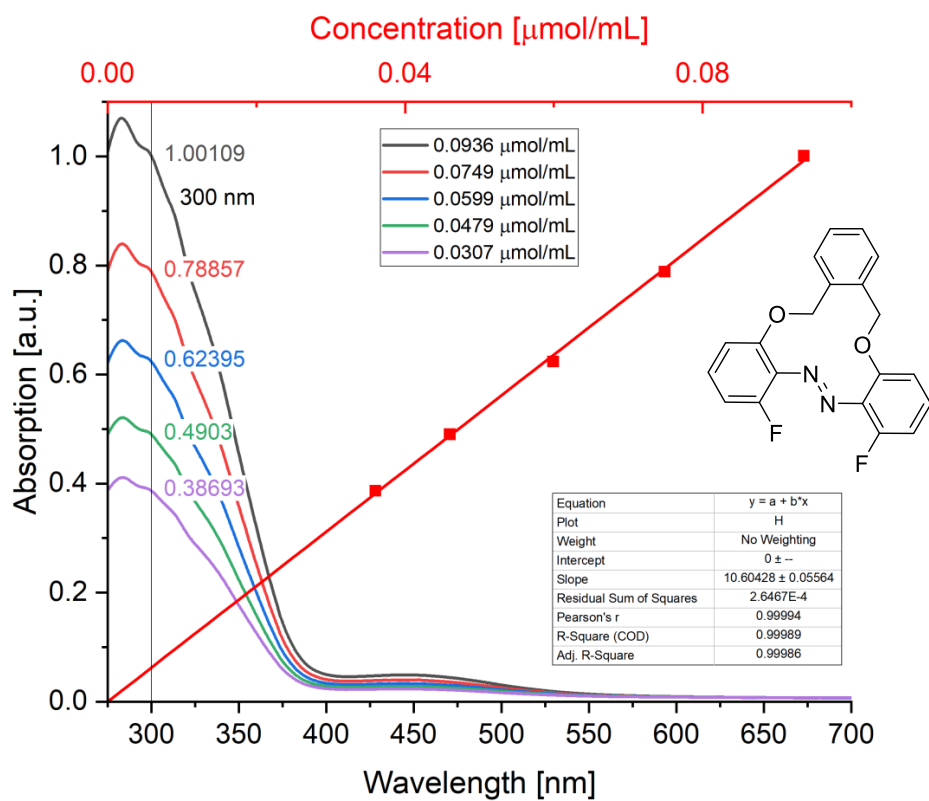
#### 2.1.1 UV-Vis Analysis: Switching Behavior of **FOAM**



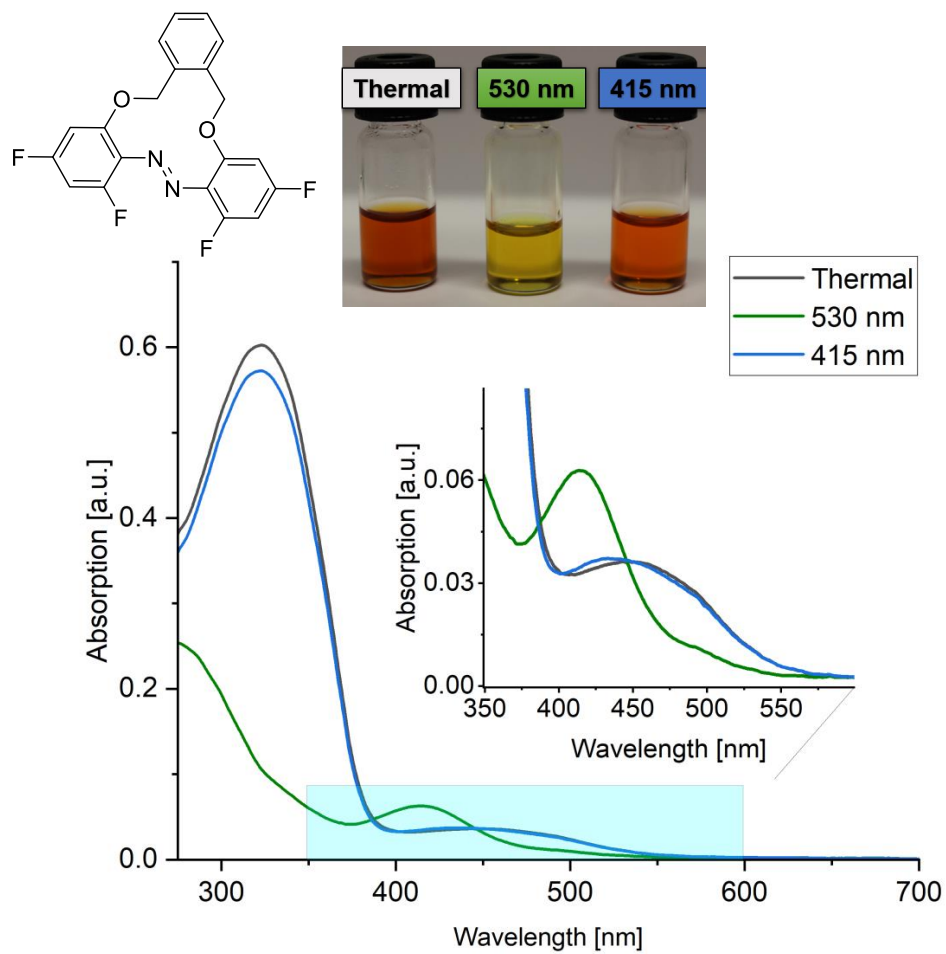
**Figure S1.** UV-vis spectrum of **FOAM** in DMSO after thermal treatment (140 °C, 4 h) and irradiation with green (530 nm) and violet light (415 nm) respectively (conc = 0.312  $\mu\text{mol mL}^{-1}$ ).



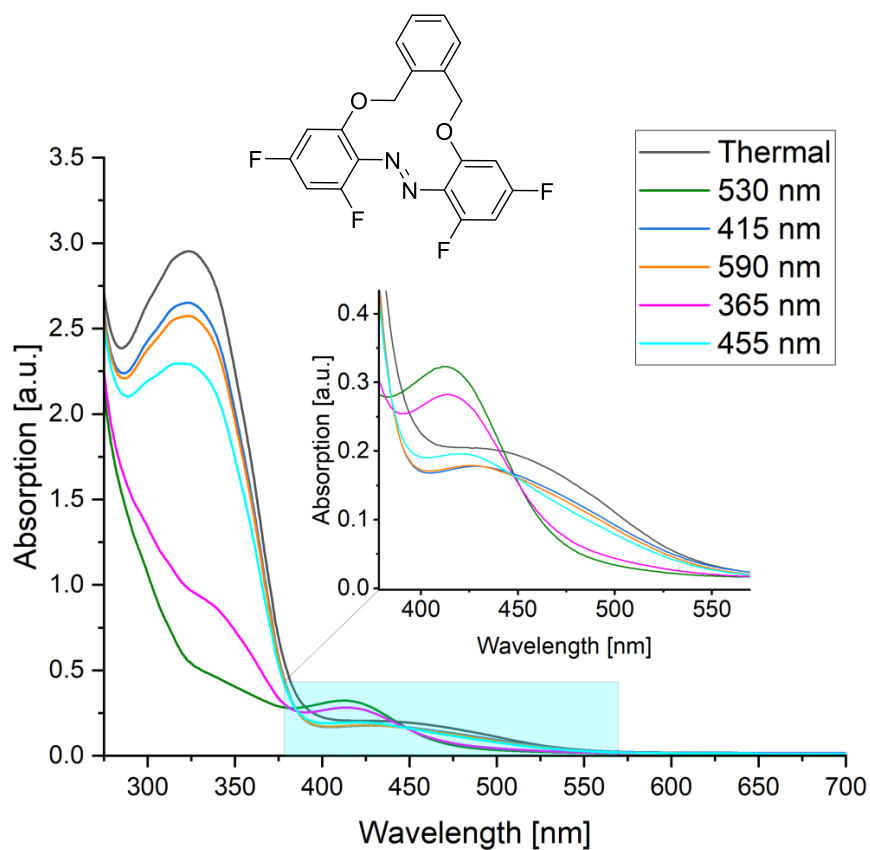
**Figure S2.** UV-vis spectrum of **FOAM** in DMSO after thermal treatment and irradiation with green (530 nm), violet (415 nm), orange (590 nm), UV (365 nm) and cyan (455 nm) light until the PSS was reached. After each irradiation the sample was reset by irradiation with 420 nm (conc = 0.312  $\mu\text{mol mL}^{-1}$ ).



**Figure S3.** UV-vis spectrum of FOAM after thermal treatment with different concentration to determine the extinction coefficient  $\epsilon$  at 300 nm in the solvent DMSO. The extinction coefficient was determined according to the Lambert-Beer-Law  $\epsilon_{300 \text{ nm}} = 10\,604 \text{ L/mol}\cdot\text{cm}$ .

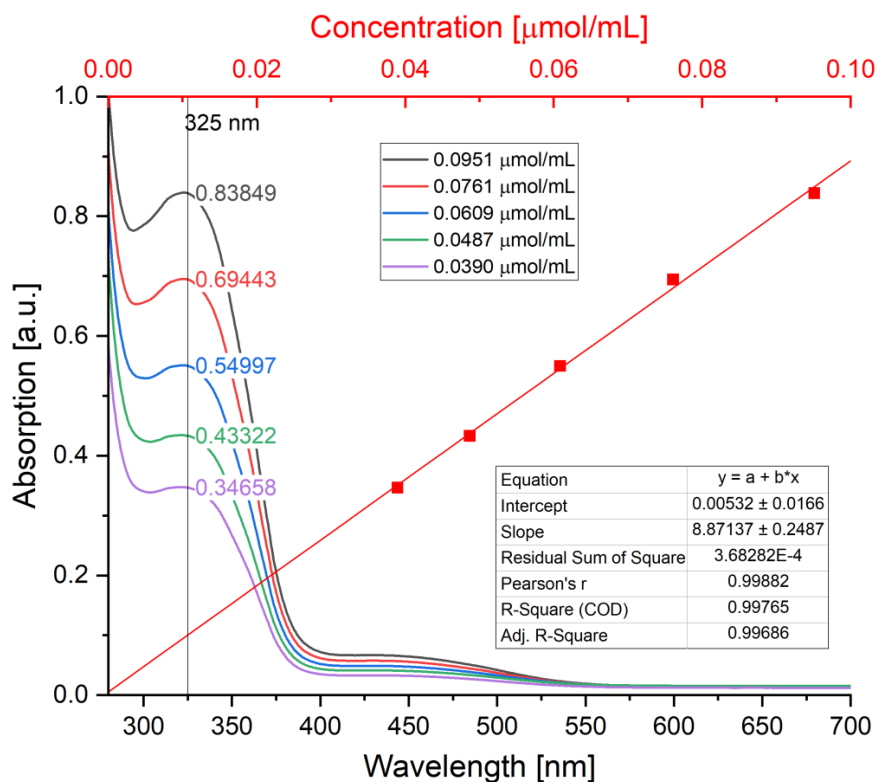
2.1.2 UV-Vis Analysis: Qualitative Switching Behavior of **2FOAM**

**Figure S4.** UV-vis spectrum of **FOAM** in DMSO after thermal treatment and irradiation with green (530 nm) and violet light (415 nm) respectively (conc = 0.0662  $\mu\text{mol mL}^{-1}$ ).

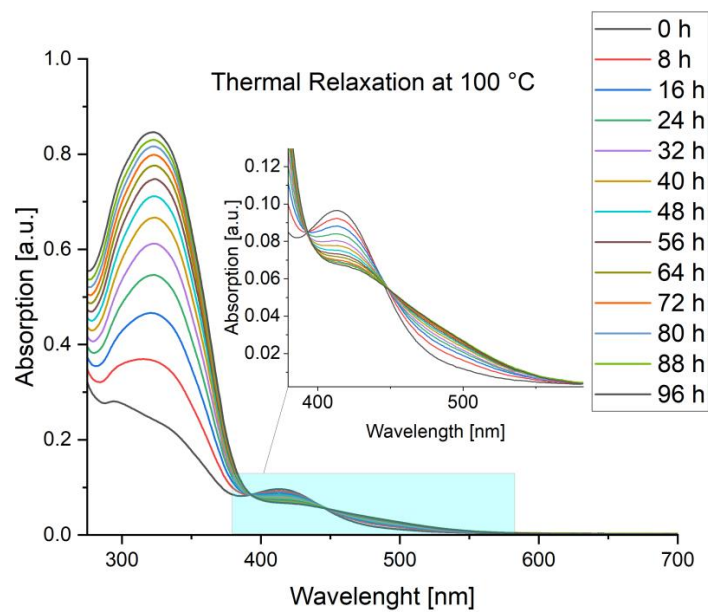


**Figure S5.** UV-vis spectrum of **2FOAM** in DMSO after thermal treatment and irradiation with green (530 nm), violet (415 nm), orange (590 nm), UV (365 nm) and cyan (455 nm) light until the PSS was reached. After each irradiation the sample was resettled by irradiation with 420 nm (conc = 0.317  $\mu\text{mol mL}^{-1}$ ).

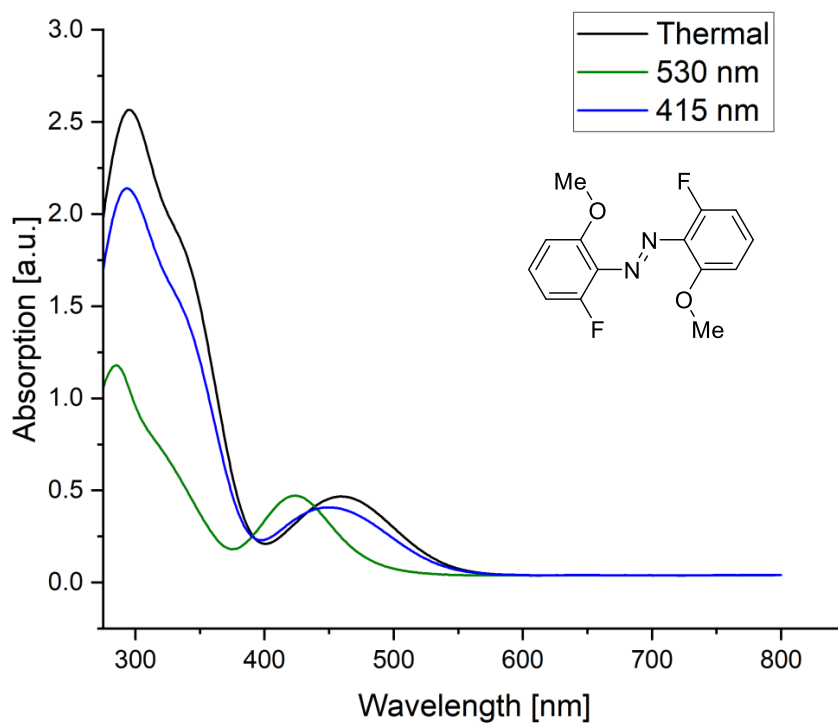




**Figure S6.** UV-vis spectrum of **2FOAM** after thermal treatment with different concentration to determine the extinction coefficient  $\epsilon$  at 325 nm in the solvent DMSO. The extinction coefficient was determined according to the Lambert-Beer-Law  $\epsilon_{325\text{nm}} = 8\,871 \text{ L/mol}\cdot\text{cm}$ .

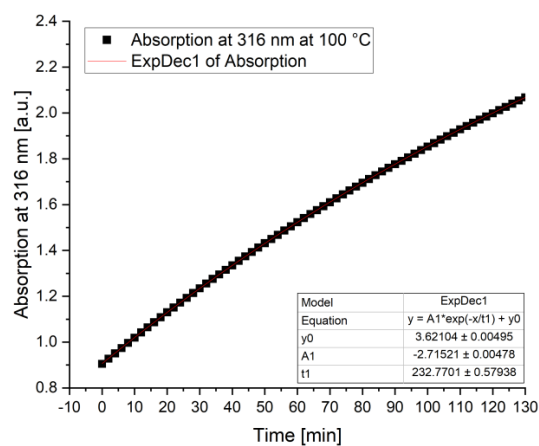
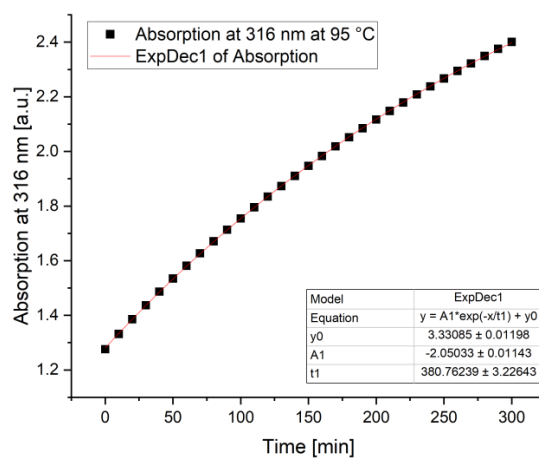
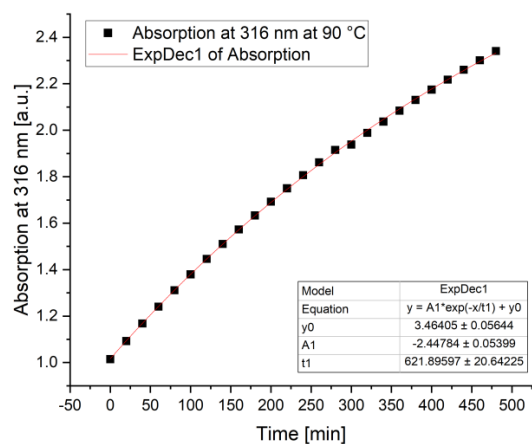


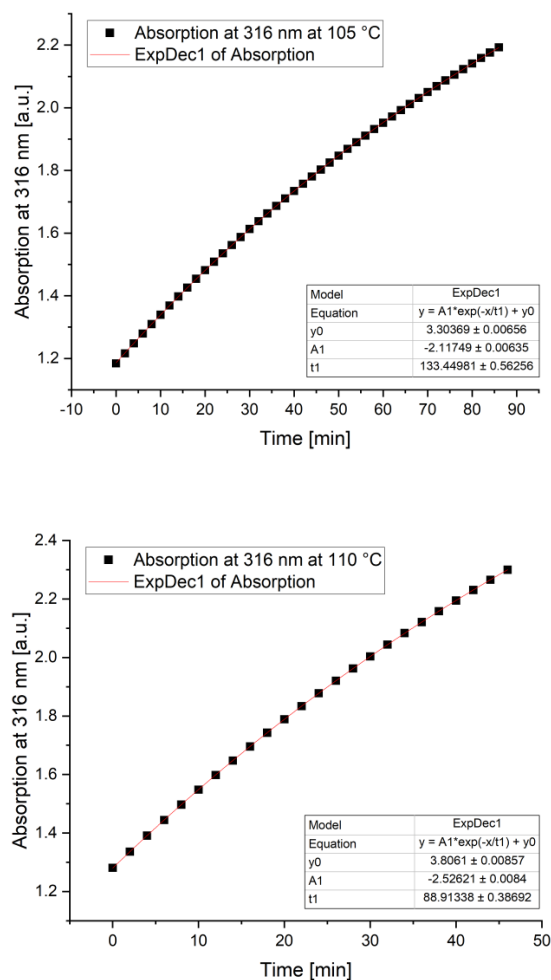
**Figure S7.** UV-vis spectrum of **2FOAM** in DMSO after irradiation with green light (530 nm) until the PSS was reached. Afterwards, the thermal relaxation was measured in 8 h intervals at 100 °C for the complete spectrum. This is only an example as the measurement of a whole spectrum for the kinetic measurements of the thermal relaxation was impracticable and disturbed the results by unnecessary irradiation.

2.1.3 UV-Vis Analysis: Qualitative Switching Behavior of **FOMe**

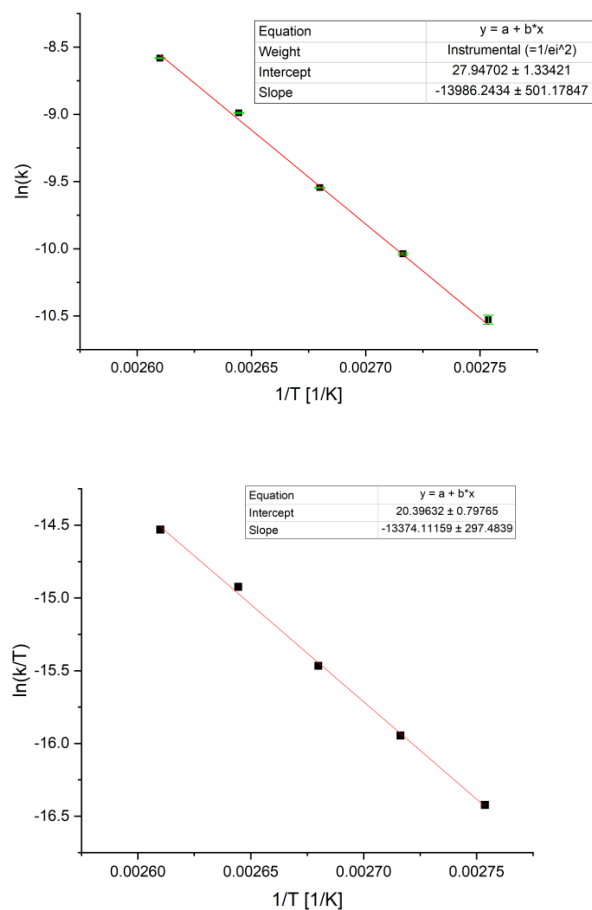
**Figure S8.** UV-vis spectrum of **FOMe** in DMSO after thermal treatment and irradiation with green (530 nm), violet (415 nm) light until the PSS was reached. After each irradiation the sample was resettled by irradiation with 420 nm (conc = 0.151  $\mu\text{mol mL}^{-1}$ ).

## 2.1.4 Half-Life Time of HOAM



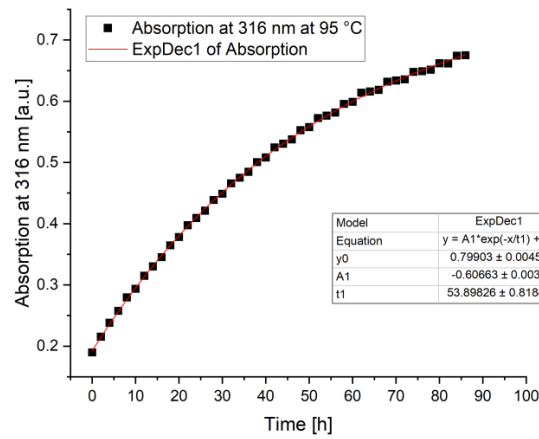
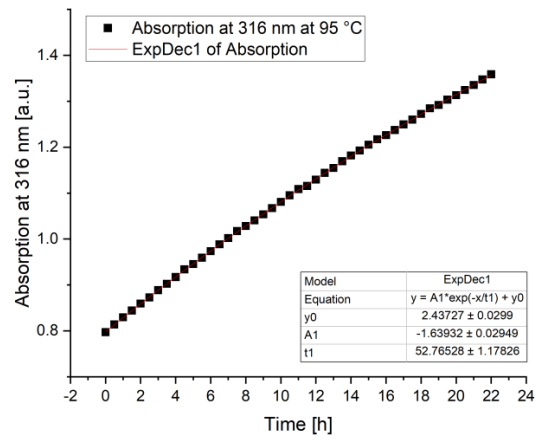
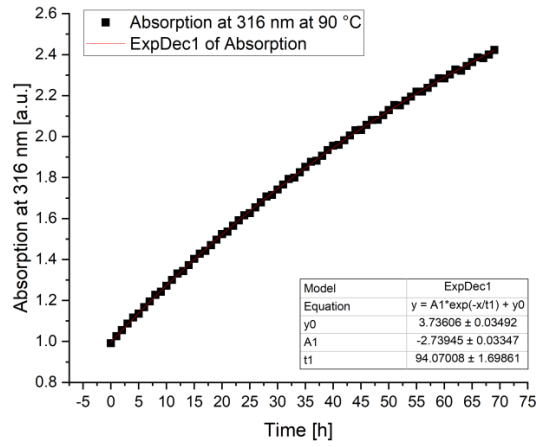


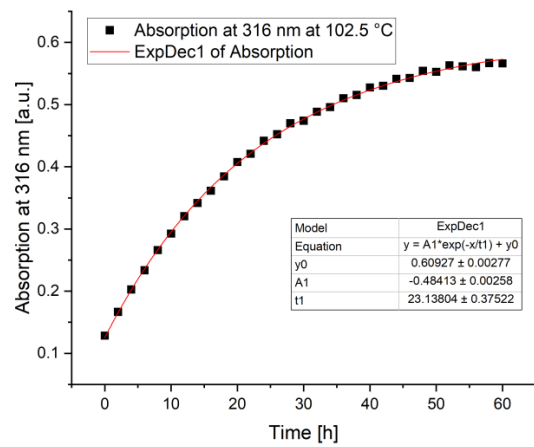
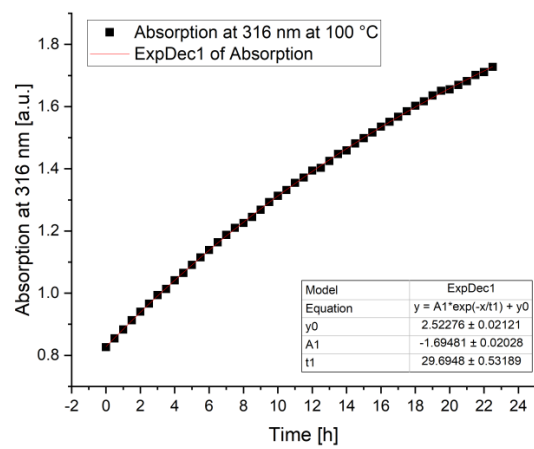
**Figure S9.** Kinetic measurements of HOAM in DMSO after irradiation with green light (530 nm) at the temperatures 90 °C, 95 °C, 100 °C, 105 °C and 110 °C. The first measurement points are not shown because the sample needed time to adapt to the temperature. An exponential decay fit was used to evaluate the data and determine  $t_{1/2}$  and  $k(T)$ . conc = 0.383  $\mu\text{mol mL}^{-1}$



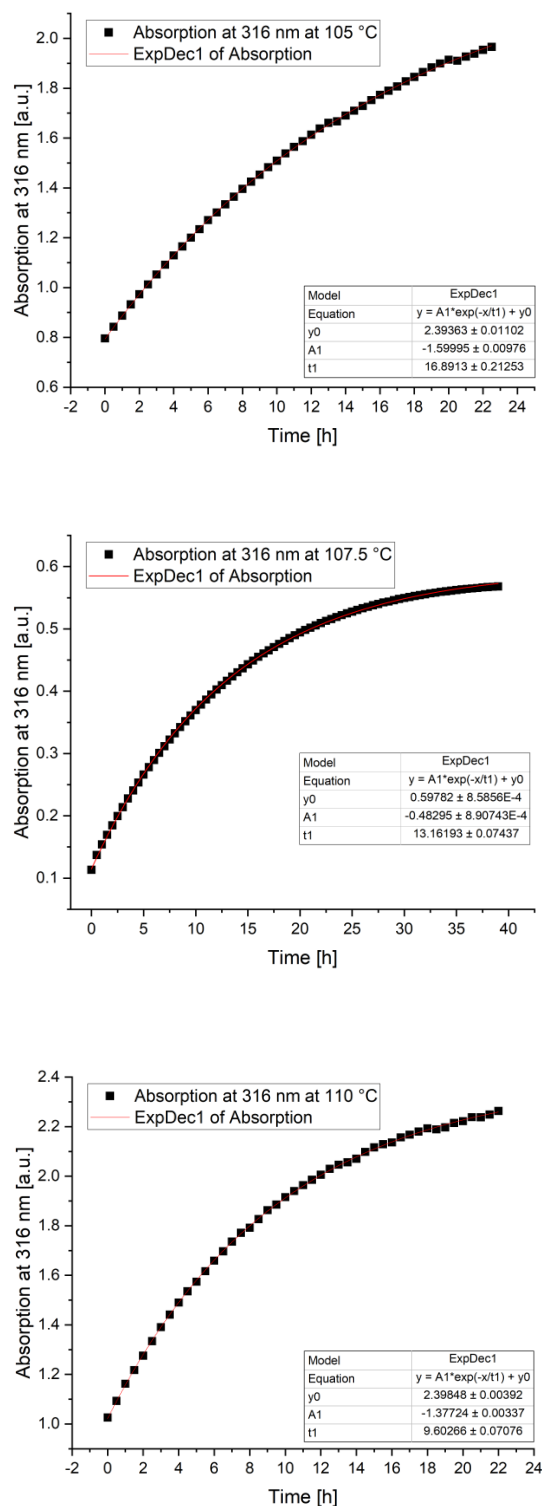
**Figure S10.** The Arrhenius-Plot with error propagation of  $\Delta t_1$  to  $\ln(k)$  and Eyring-Plot of HOAM. A linear fit was used to determine the values for  $k$ ,  $A$ ,  $E_a$ ,  $\Delta H$ ,  $\Delta S$ ,  $\Delta G$  and  $t_{1/2}(T)$ . The results are given in **Table S3**.

2.1.5 Half-Life Time of FOAM



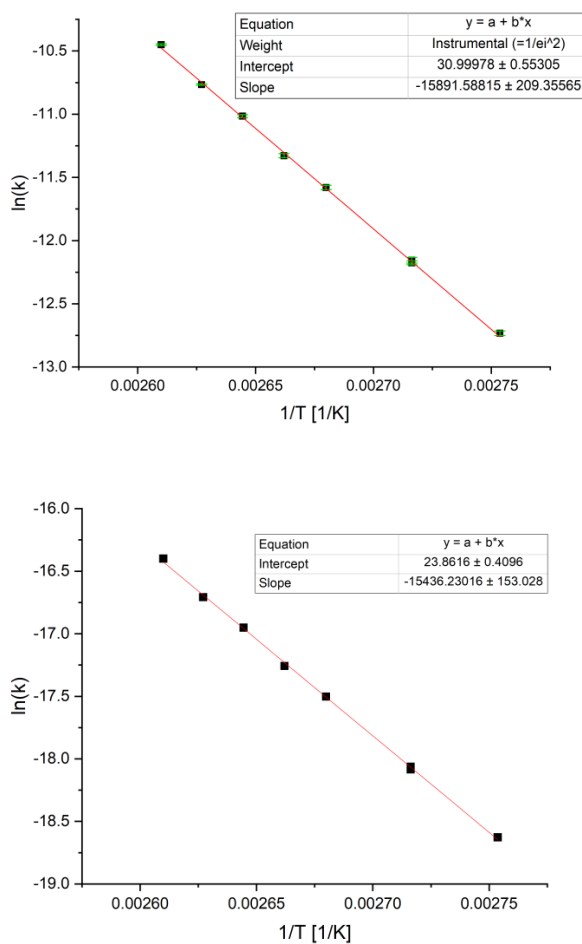






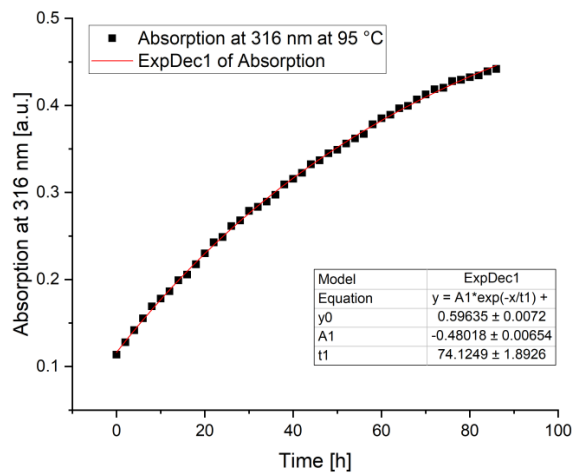
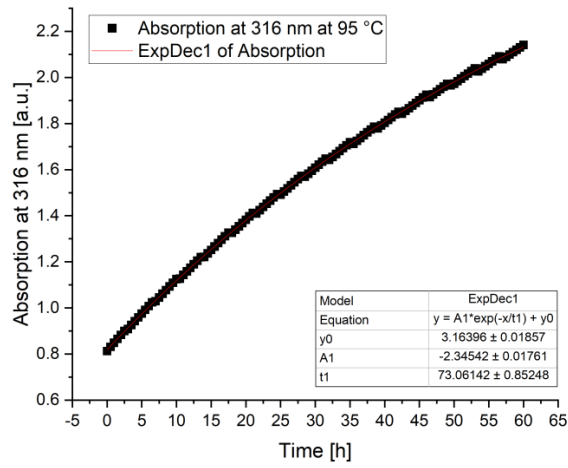
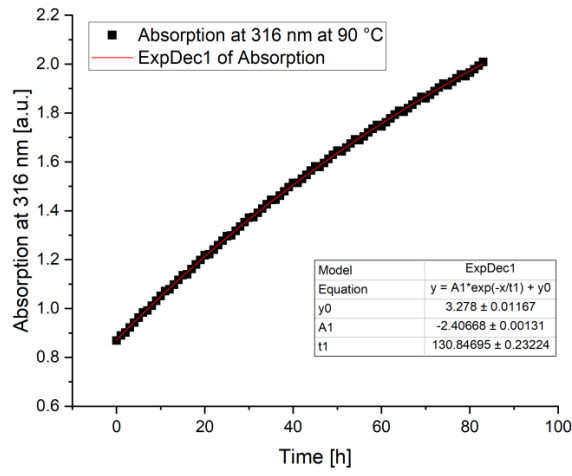
**Figure S11.** Kinetic measurements of **FOAM** in DMSO after irradiation with green light (530 nm) at the temperature 90 °C, 95 °C (2x), 100 °C, 102.5 °C, 105 °C, 107.5 °C and 110 °C respectively. The first

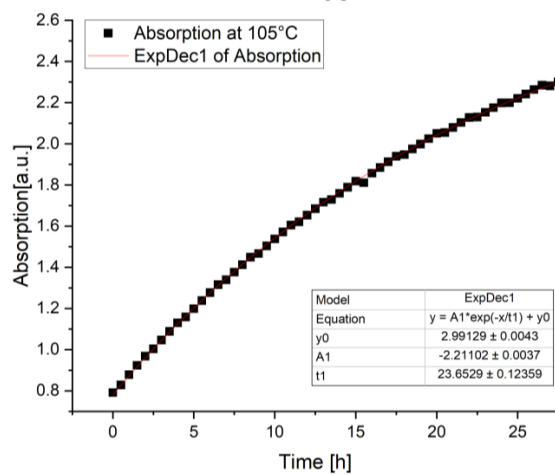
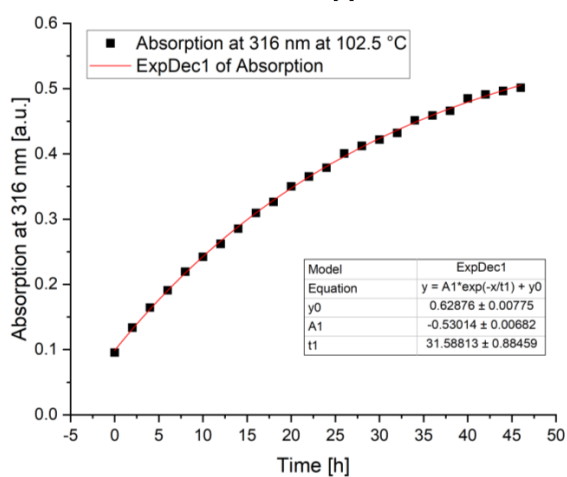
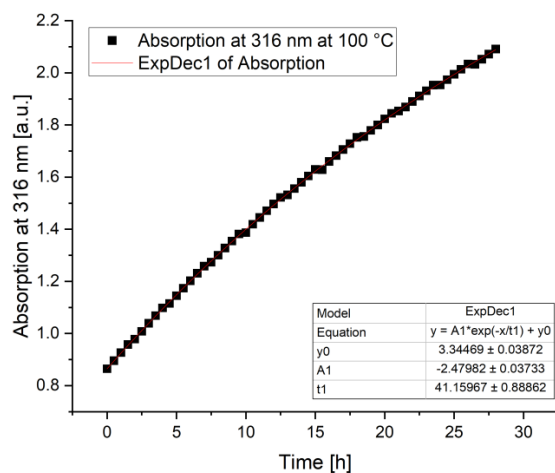
measurement points are not shown because the sample needed time to adapt to the temperature. An exponential decay fit was used to evaluate the data and determine  $t_{1/2}$  and  $k(T)$ .  
 conc =  $0.412 \mu\text{mol mL}^{-1}$  ( $90^\circ\text{C}$ ), conc =  $0.335 \mu\text{mol mL}^{-1}$  ( $95^\circ$ ,  $100^\circ\text{C}$ ,  $105^\circ\text{C}$ ,  $110^\circ\text{C}$ ), conc =  $0.113 \mu\text{mol mL}^{-1}$  ( $95^\circ\text{C}$ ,  $102.5^\circ\text{C}$ ,  $107.5^\circ\text{C}$ ).

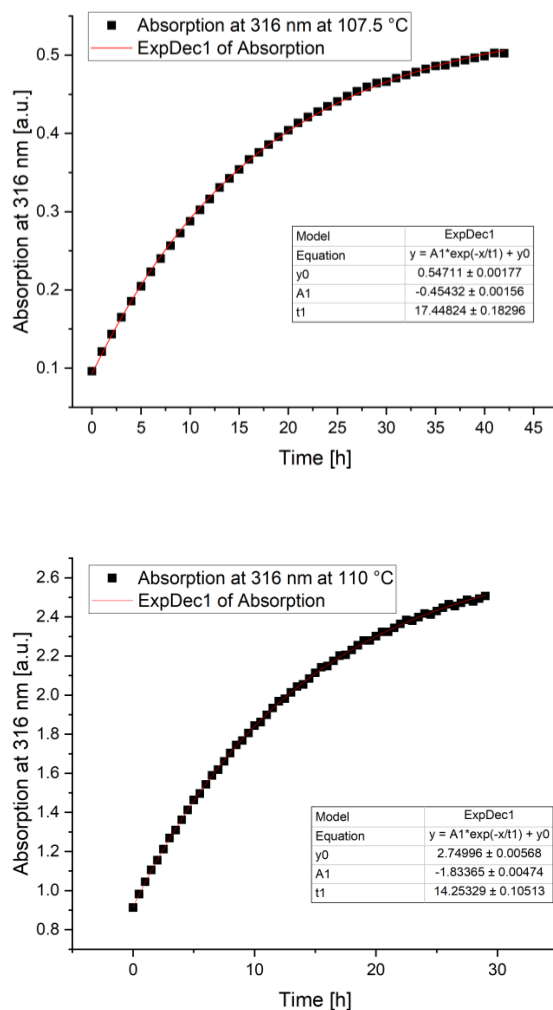


**Figure S12.** The Arrhenius-Plot with error propagation of  $\Delta t_1$  to  $\ln(k)$  and Eyring-Plot of **FOAM**. A linear fit was used to determine the values for  $k$ ,  $A$ ,  $E_a$ ,  $\Delta H$ ,  $\Delta S$ ,  $\Delta G$  and  $t_{1/2}(T)$ . The results are given in **Table S3**.

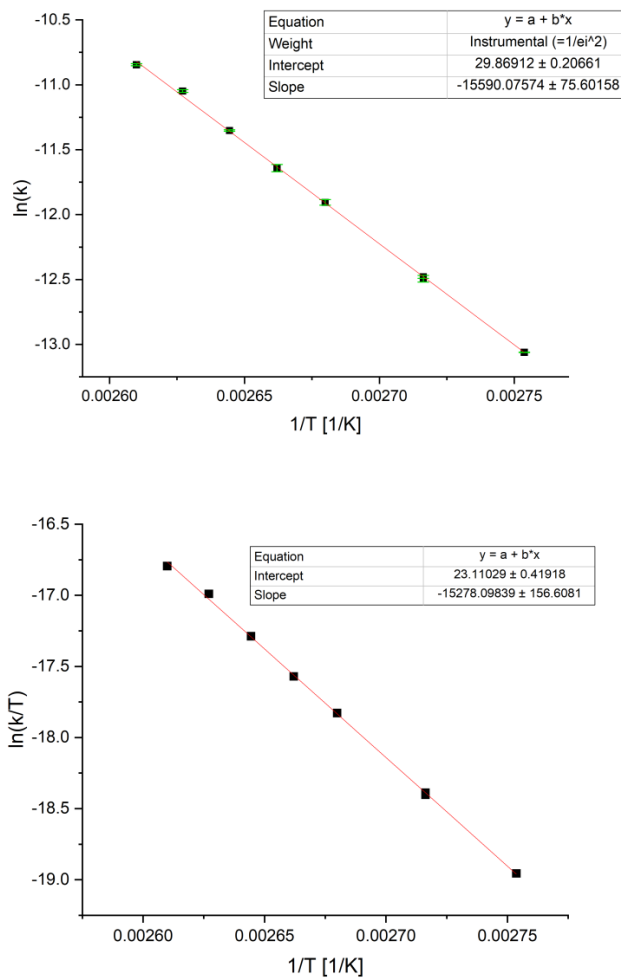
2.1.6 Half-Life Time of **2FOAM**



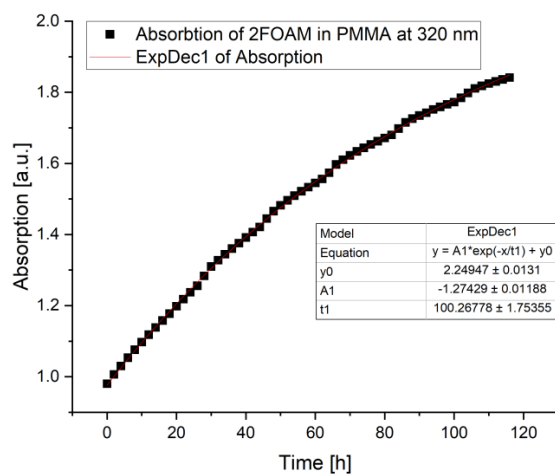




**Figure S13.** Kinetic measurements of **2FOAM** in DMSO after irradiation with green light (530 nm) at the temperature 90 °C, 95 °C (2x), 100 °C, 102.5 °C, 105 °C, 107.5 °C, 110 °C. The first measurement points are not shown because the sample needed time to adapt to the temperature. An exponential decay fit was used to evaluate the data and determine  $t_{1/2}$  and  $k(T)$ . conc =  $0.283 \mu\text{mol mL}^{-1}$  (90 °C, 95 °C, 100 °C, 105 °C, 110 °C), conc =  $0.0842 \mu\text{mol mL}^{-1}$  (95 °C, 102.5 °C, 107.5 °C)

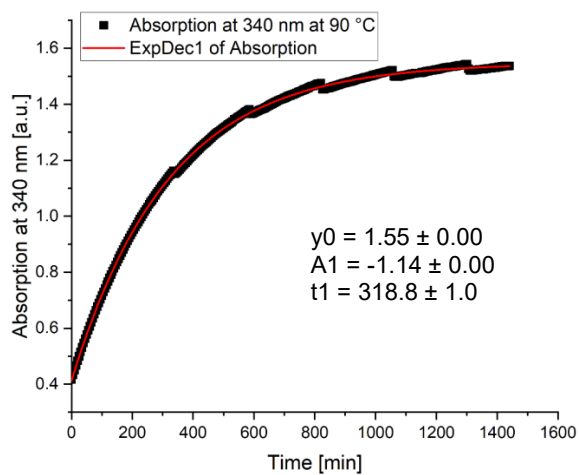
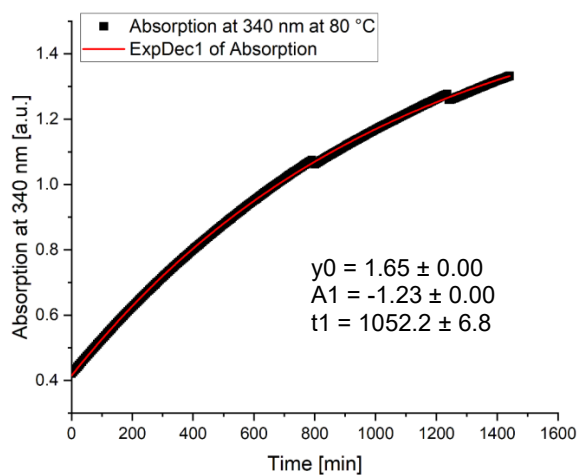
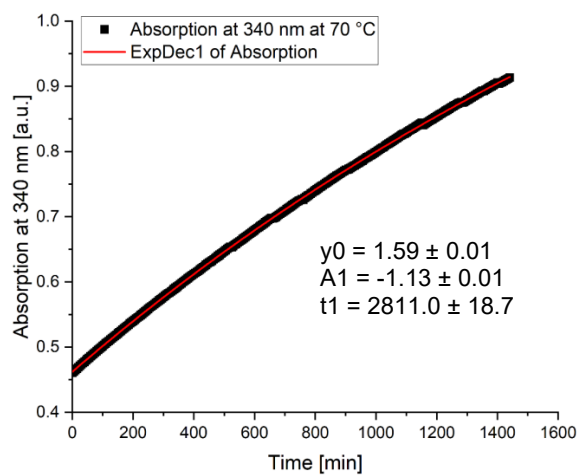


**Figure S14.** The Arrhenius-Plot with error propagation of  $\Delta t_1$  to  $\ln(k)$  and Eyring-Plot of **2FOAM**. A linear fit was used to determine the values for  $k$ ,  $A$ ,  $E_a$ ,  $\Delta H$ ,  $\Delta S$ ,  $\Delta G$  and  $t_{1/2}(T)$ . The results are given in **Table S3**.

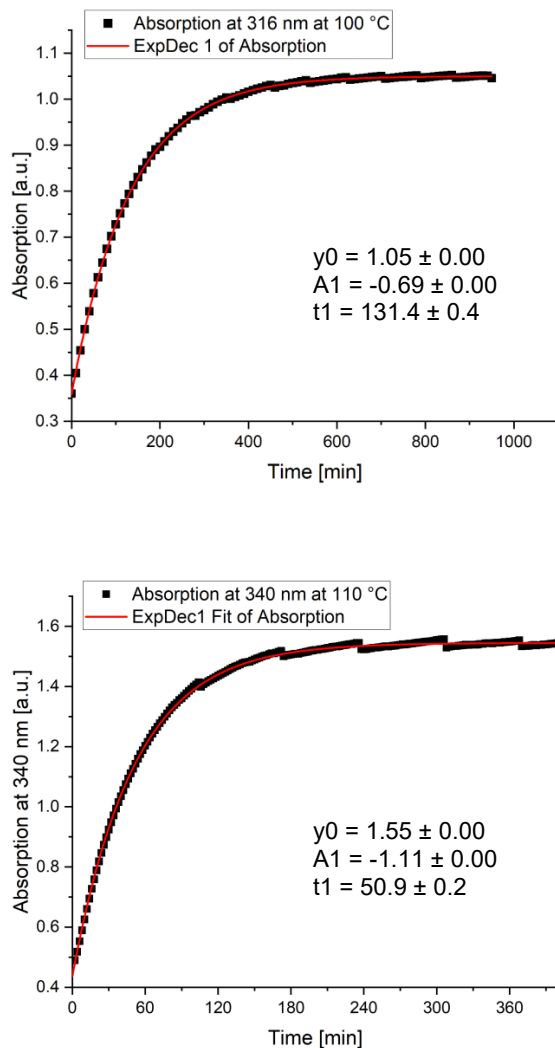


**Figure S15.** Kinetic measurements of **2FOAM** (2 mg) in PMMA (500 mg) after irradiation with green light (530 nm) at 90 °C. The first measurement points are not shown because the sample needed time to adapt to the temperature. An exponential decay fit was used to evaluate the data and determine  $t_{1/2}$  and  $k(T)$ . Note: Concentration does not correlate with the absorption because of the influence of the thickness of the sample.

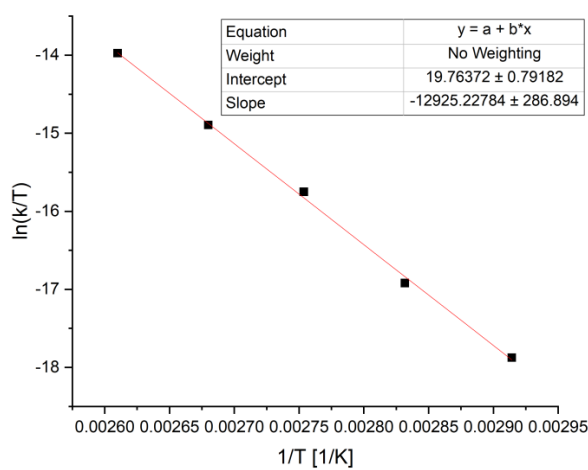
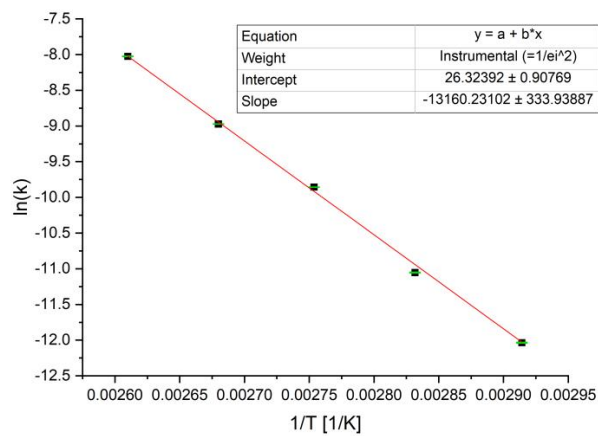
## 2.1.7 Half-Life Time of FOMe



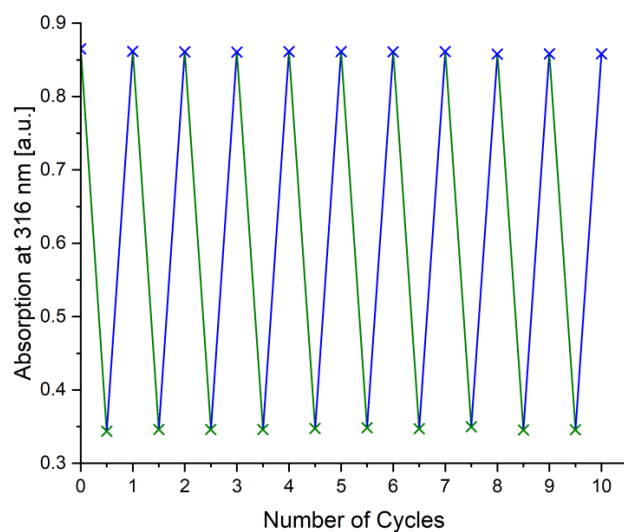




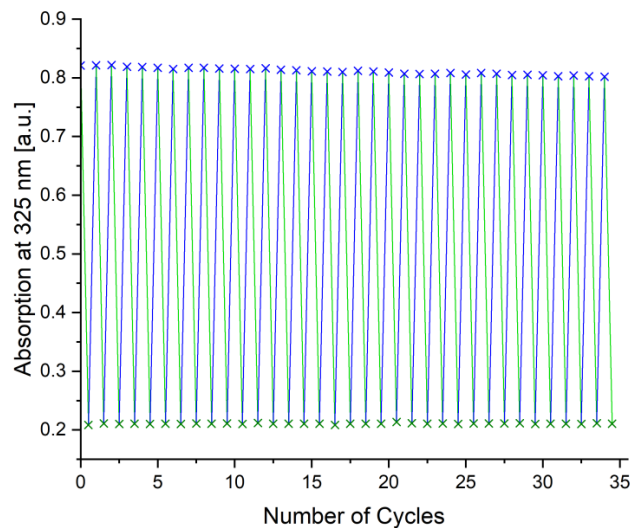
**Figure S16.** Kinetic measurements of **FOMe** in DMSO after irradiation with green light (530 nm) at the temperature 70 °C, 80 °C, 90 °C, 100 °C and 110 °C. The first measurement points are not shown because the sample needed time to adapt to the temperature. An exponential decay fit was used to evaluate the data and determine  $t_{1/2}$  and  $k(T)$ . conc = 0.151  $\mu\text{mol mL}^{-1}$  (70 °C, 80 °C, 90 °C, 110 °C), conc = 0.102  $\mu\text{mol mL}^{-1}$  (100 °C).



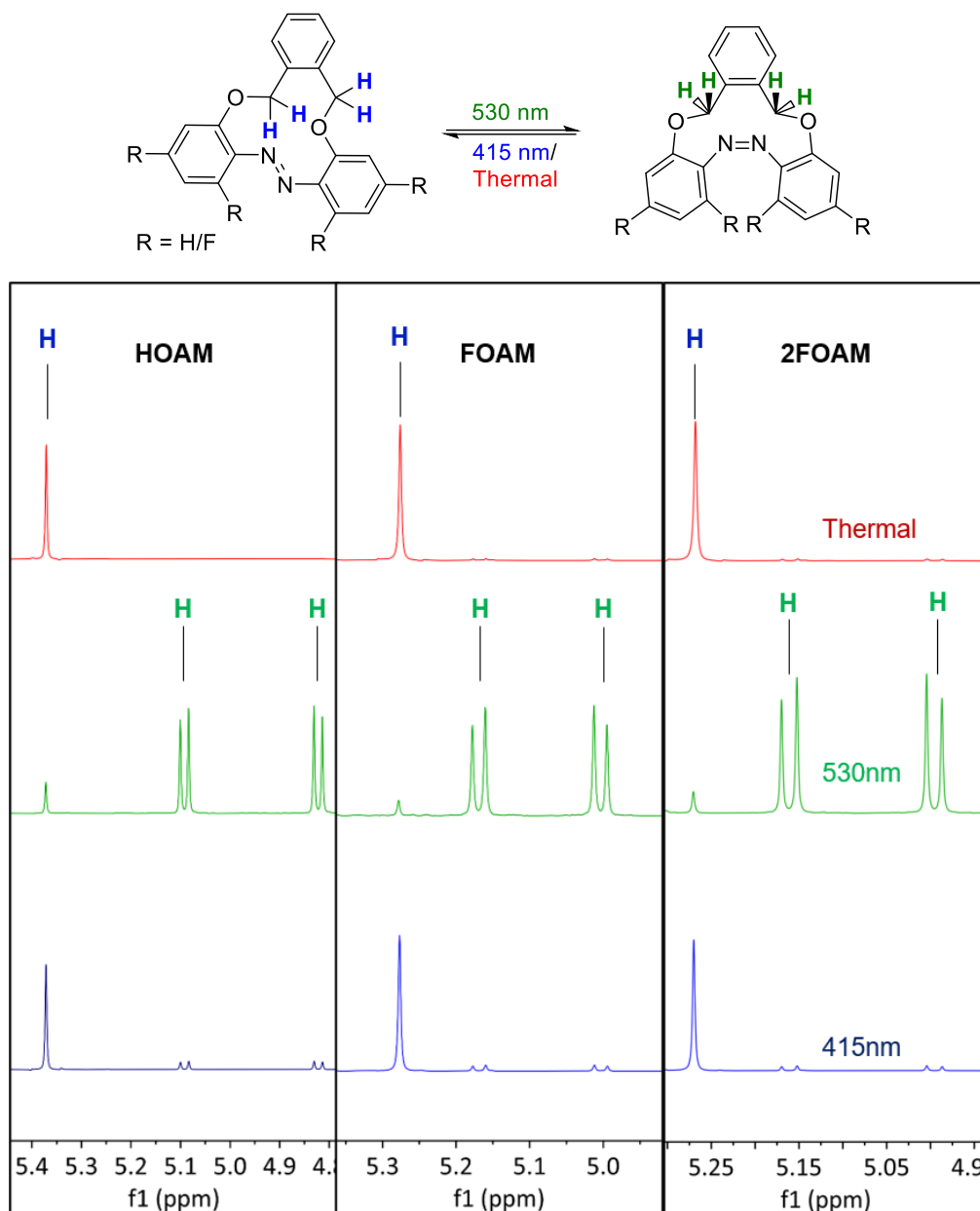
**Figure S17.** The Arrhenius-Plot with error propagation of  $\Delta t_1$  to  $\ln(k)$  and Eyring-Plot of **FOMe**. A linear fit was used to determine the values for  $k$ ,  $A$ ,  $E_a$ ,  $\Delta H$ ,  $\Delta S$ ,  $\Delta G$  and  $t_{1/2}(T)$ . The results are given in **Table S3**.

2.1.9 Cycle Stability of **FOAM** and **2FOAM**

**Figure S18.** Cycle stability for the isomerization of **FOAM** after irradiation with 530 nm (green cross) and 415 nm (blue cross) over 70 cycles. The concentration of the sample in DMSO was  $\text{conc} = 0.0936 \mu\text{mol ml}^{-1}$ .



**Figure S19.** Cycle stability for the isomerization of **2FOAM** after irradiation with 530 nm (green cross) and 415 nm (blue cross) over 35 cycles. The concentration of the sample in DMSO was  $\text{conc} = 0.0951 \mu\text{mol ml}^{-1}$ .

2.1.9 NMR Analysis: Quantitative Switching Behavior of **HOAM**, **FOAM**, **2FOAM** and **FOMe**

**Figure S20.** NMR spectroscopic study of the irradiation of **HOAM**, **FOAM** and **2FOAM** in DMSO- $d_6$  after thermal treatment\* (red spectrum), after irradiation with green light (525 nm) and violet light (420 nm) ( $\text{conc}_{\text{HOAM}} = 6.20 \mu\text{mol mL}^{-1}$ ,  $\text{conc}_{\text{FOAM}} = 6.24 \mu\text{mol mL}^{-1}$ ,  $\text{conc}_{\text{2FOAM}} = 5.67 \mu\text{mol mL}^{-1}$ ).

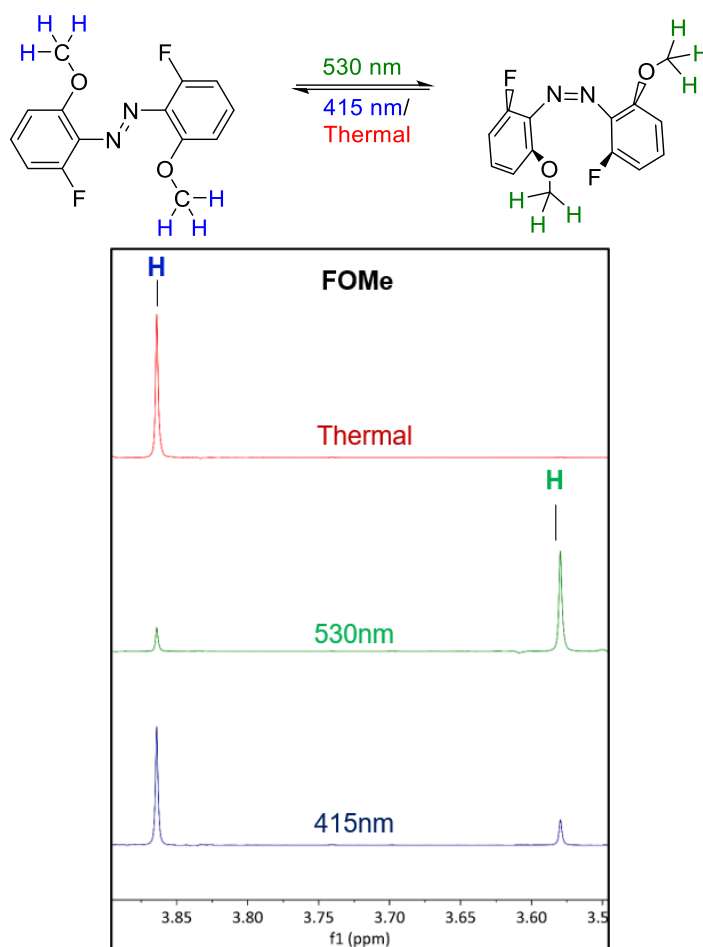


**Table S3.** Summary of NMR spectroscopic studies of the irradiation of **HOAM**, **FOAM**, **2FOAM** and **FOMe**, after irradiation with 530 nm and 415 nm in the solvents DMSO-*d*<sub>6</sub>. The % values for the *E* and *Z* isomer were obtained by the integration of the CH<sub>2</sub>-proton signals of the ether bridge. conc = 7.55 μmol mL<sup>-1</sup>

	<b>HOAM</b>		<b>FOAM</b>		<b>2FOAM</b>		<b>FOMe</b>	
	<i>E</i>	<i>Z</i>	<i>E</i>	<i>Z</i>	<i>E</i>	<i>Z</i>	<i>E</i>	<i>Z</i>
<b>Thermal</b>	100%	0%	99%	1%	99%	1%	100%	0%
<b>415 nm</b>	74%	26%	85%	15%	93%	7%	22%	78%
<b>530 nm</b>	9%	91%	5%	95%	3%	97%	17%	83%

\*Thermal treatment: Heating up the sample dissolved in DMSO to 140°C for 12 h before measurement

### 3 Crystal Structure Analysis of HOAM, FOAM, 2FOAM

The twist in the following graphic is measured by the angle of the two projected layer (visualized in green and red) based of the azobenzene aromatic-ring planarity.

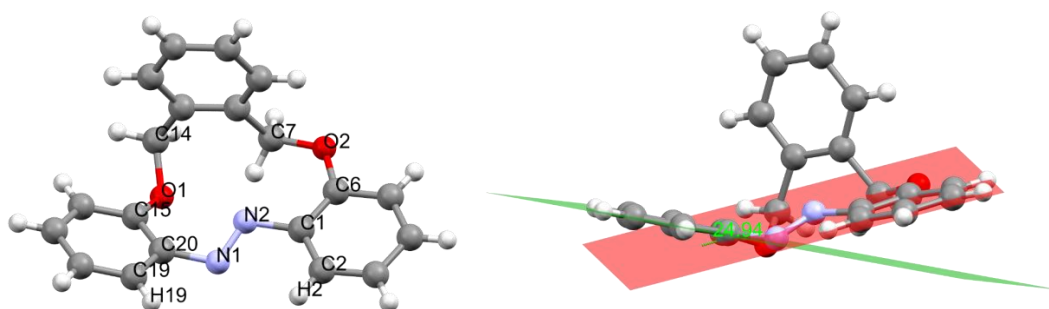


**Figure S21.** Crystal structure of *E*-HOAM (left) and its visualized plane twist of the phenyl rings (right).

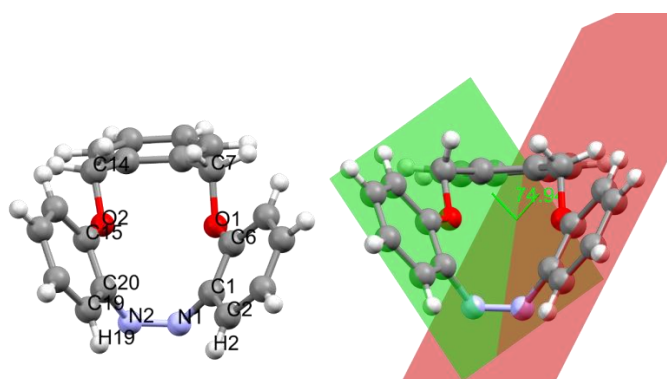


**Figure S22.** Crystal structure of *Z*-HOAM (left) and its visualized plane twist of the phenyl rings (right).

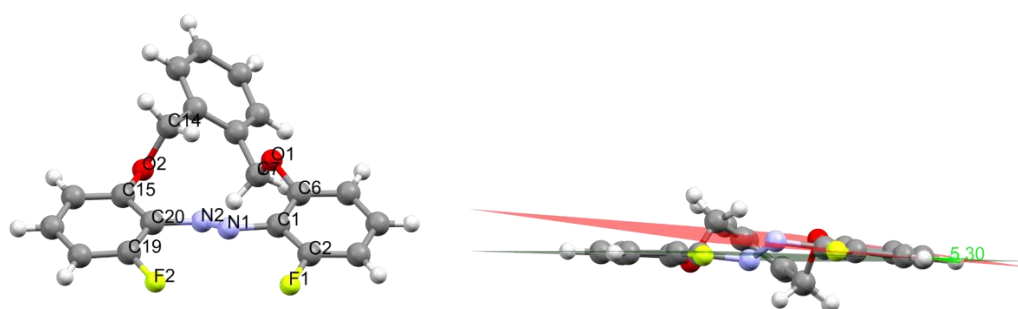


**Figure S23.** Crystal structure of *E*-FOAM (left) and its visualized plane twist of the phenyl rings (right).

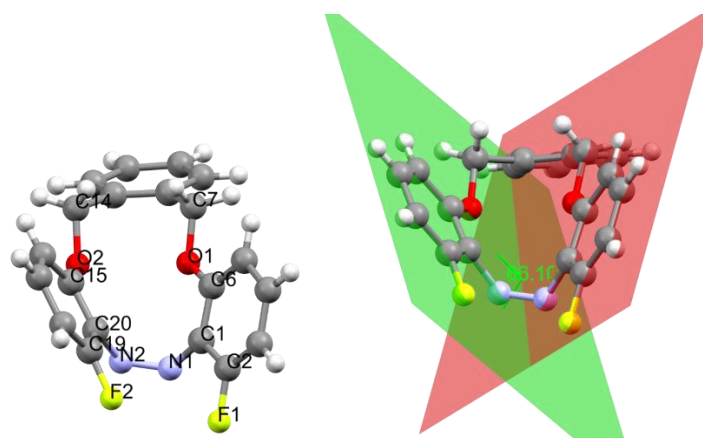


**Figure S24.** Crystal structure of **Z-FOAM** (left) and its visualized plane twist of the phenyl rings (right).

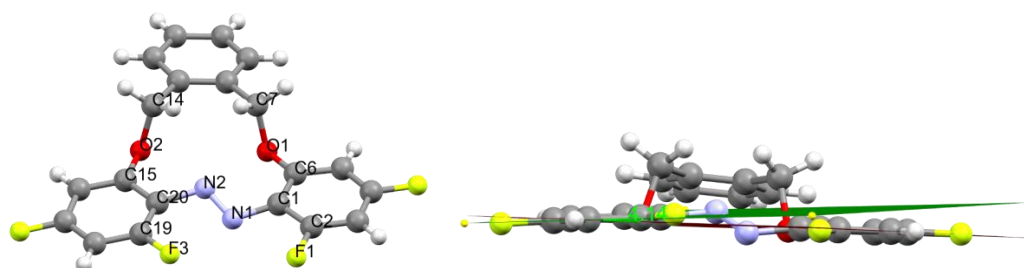


**Figure S25.** Crystal structure of **E-2FOAM** (left) and its visualized plane twist of the phenyl rings (right).

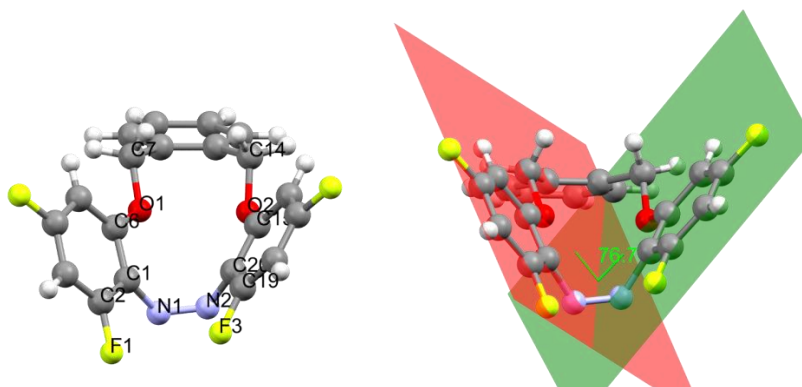


**Figure S26.** Crystal structure of **Z-2FOAM** (left) and its visualized plane twist of the phenyl rings (right).

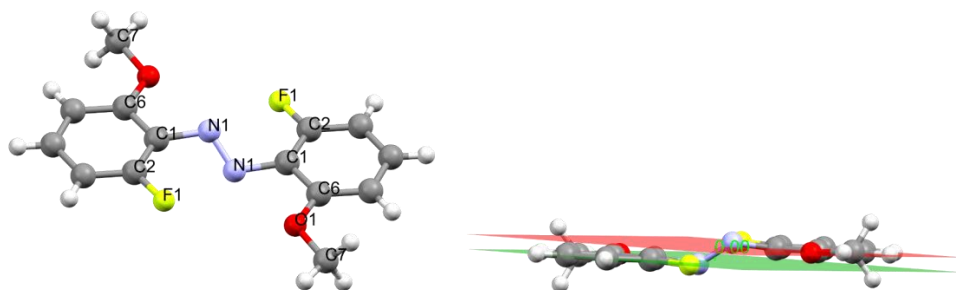


**Figure S27.** Crystal structure of *E*-FOMe (left) and its visualized plane twist of the phenyl rings (right).

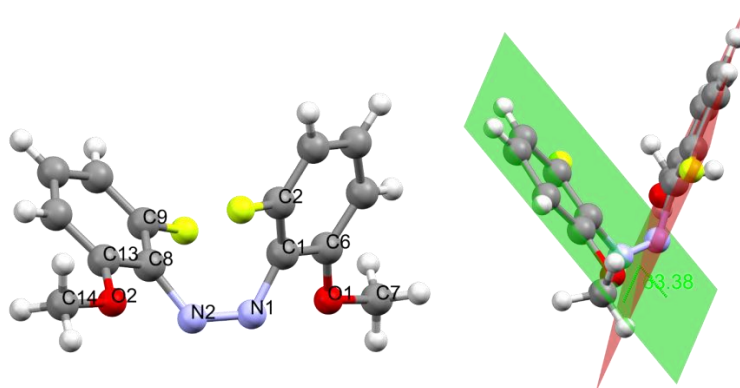
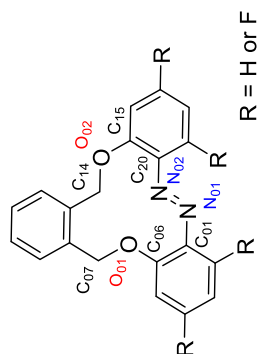


**Figure S28.** Crystal structure of *Z*-FOMe (left) and its visualized plane twist of the phenyl rings (right).



**Table S4:** Specific Bond Length of the Crystal Structures of **HOAM**, **FOAM**, **2FOAM** and **FOME**.

The evaluation of specific bond lengths and angles, torsion angles were performed with the software Diamond (version 4.6.8).<sup>[7]</sup>



	<b>E-HOAM</b>	<b>Z-HOAM</b>	<b>E-FOAM</b>	<b>Z-FOAM</b>	<b>E-2FOAM</b>	<b>Z-2FOAM</b>		<b>E-FOME</b>	<b>Z-FOME</b>
N01-N02	1.258(3)	1.2462(11)	1.2569(17)	1.244(2)	1.232(7)	1.2465(1)		1.2596(17)	1.263(3)
N01-C01	1.423(3)	1.4558(12)	1.4253(19)	1.453(2)	1.424(8)	1.4500(1)		1.4253(12)	1.434(3)
N02-C20	1.433(3)	1.4525(12)	1.4202(18)	1.451(3)	1.461(8)	1.4484(1)	N02-C08	-	1.424(3)
C01-C06	1.406(4)	1.4026(13)	1.407(2)	1.396(3)	1.415(7)	1.4014(1)		1.4095(14)	1.402(3)
C20-C15	1.400(4)	1.4012(12)	1.407(2)	1.405(3)	1.461(8)	1.4064(1)	C08-C13	-	1.404(3)
C06-O01	1.362(3)	1.3749(11)	1.3775(17)	1.362(2)	1.357(7)	1.3550(1)		1.3569(12)	1.358(3)
C15-O02	1.3545(13)	1.371(6)	1.361(2)	1.3764(17)	1.3681(11)	1.377(3)		1.351(3)	-
O01-C07	1.4442(13)	1.464(7)	1.438(2)	1.4543(17)	1.4358(11)	1.440(3)		1.425(3)	1.4346(13)
O02-C14	1.4405(13)	1.454(7)	1.436(2)	1.4543(17)	1.4257(11)	1.449(3)		1.433(3)	-

Table S5: Specific Bond Angles and Torsion Angles (C-N=N-C &amp; C-C-N=N) of HOAM, FOAM, ZFOAM and FOMe.

	E-HOAM	Z-HOAM	E-FOAM	Z-FOAM	E-ZFOAM	Z-ZFOAM		E-FOMe	Z-FOMe
N02-N01-C01	114.8(2)	120.31(8)	112.30(12)	119.21(15)	112.4(5)	120.06(9)		113.42(10)	122.2(2)
N01-N02-C20	112.8(2)	121.39(8)	115.38(12)	119.73(15)	113.4(5)	120.34(9)	N01-N02-C08	-	123.26(19)
N01-C01-C06	119.3(2)	119.65(8)	125.92(13)	120.66(15)	126.8(6)	120.72(9)		117.38(8)	117.6(2)
N02-C20-C15	125.4(2)	117.88(8)	116.15(13)	120.50(15)	116.0(5)	120.16(9)	N02-C08-C13	-	117.15(19)
C01-C06-O01	128.3(2)	116.20(8)	121.56(13)	115.53(15)	122.7(5)	116.05(9)		115.27(8)	114.8(2)
C20-C15-O02	118.4(2)	114.53(8)	120.37(13)	114.44(16)	119.4(5)	114.81(9)	C08-C13-O02	-	114.9(2)
C06-O01-C07	122.5(2)	116.64(7)	113.83(11)	117.38(14)	111.5(5)	116.59(8)		117.06(8)	116.5(2)
C15-O02-C14	116.5(2)	117.52(7)	115.74(11)	118.41(14)	114.0(4)	114.81(9)	C13-O02-C14	-	117.0(2)
C01-N01-N02-C20	172.468(213)	2.117(134)	-178.938(136)	6.9(2)	178.870(506)	6.972(151)	C01-N01-N02-C08	180.000(76)	7.223(347)
C15-C20-N02-N01	40.780(356)	95.11(10)	153.03(13)	73.464(236)	-152.5(6)	77.99(13)	C13-C08-N02-N01	±145.234(87)	-137.3(2)
C06-C01-N01-N02	164.6(2)	-98.25(11)	36.2(2)	-115.31(19)	-35.2(9)	-112.42(12)		-	-136.3(2)

#### 4 DFT Calculations of **HOAM**, **FOAM**, **2FOAM**

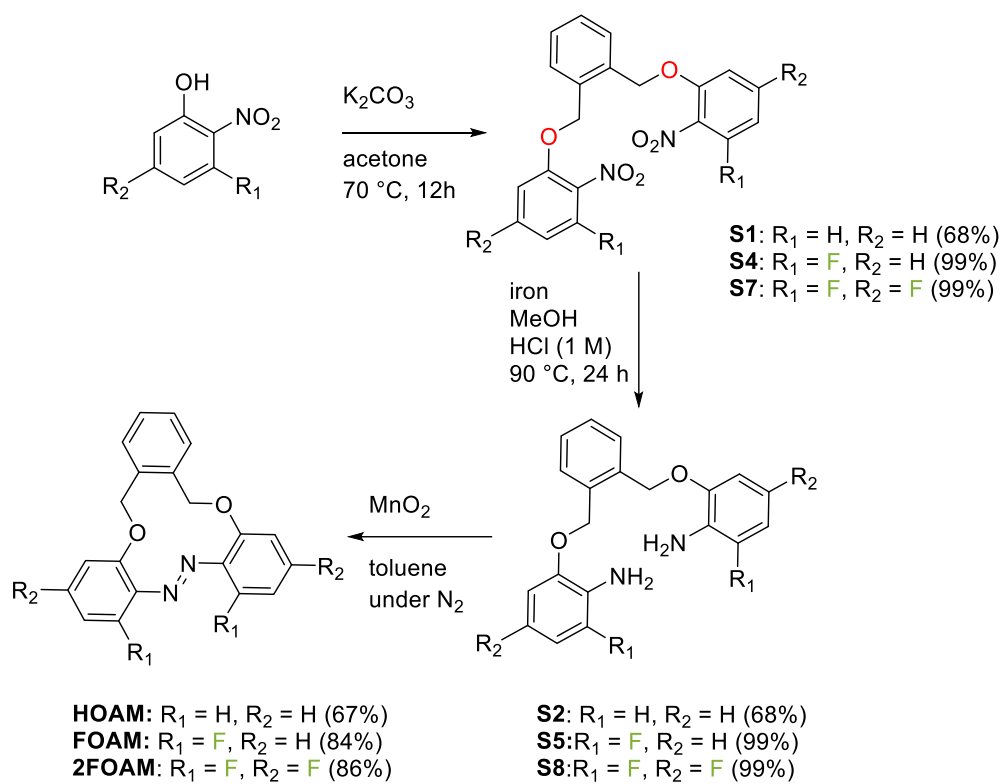
**Table S6:** Results of the gaussian DFT calculation with B3LYP/cc-pVDZ level of theory, self-consistent reaction field (SCRF) with the SMD model for the solvent DMSO and Grimme D3-Dispersion correction. All values are given as the difference to their respective Z-isomer. The experimental data is given in the table below for a direct comparison.

	$\Delta$ Electronic Energy [kJ/mol]	$\Delta H$ [kJ/mol]	$\Delta S$ kJ/mol (at 298.15 K)	$\Delta G$ (kJ/mol) (at 298.15 K)
<b>HOAM-Z</b>	0.00	0.00	0.00	0.00
<b>HOAM-TS</b>	116.29	111.22	-2.15	113.37
<b>HOAM-E</b>	-36.83	-36.46	-0.26	-36.20
<b>FOAM-Z</b>	0.00	0.00	0.00	0.00
<b>FOAM-TS</b>	128.06	122.76	-0.90	123.69
<b>FOAM-E</b>	-19.15	-19.76	0.36	-20.12
<b>2FOAM-Z</b>	0.00	0.00	0.00	0.00
<b>2FOAM-TS</b>	129.59	125.39	-0.57	125.96
<b>2FOAM-E</b>	-20.13	-20.57	1.82	-22.39
<b>FOMe-Z</b>	0.00	0.00	0.00	0.00
<b>FOMe-TS</b>	123.25	124.01	3.75	120.26
<b>FOMe-E</b>	15.83	-14.71	5.76	-20.48

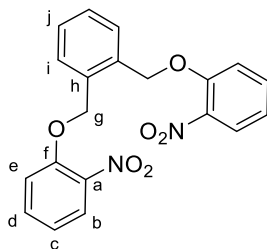
  

	$k_{(25^\circ\text{C})}$ [s <sup>-1</sup> ]	A [s <sup>-1</sup> ]	Ea [kJ/mol]	$\Delta H$ [kJ/mol]	$\Delta S$ [J/mol]	$\Delta G$ (25 °C) [kJ/mol]	$t_{1/2}$ (25°C) [Years]
<b>HOAM</b>	$6.91 \cdot 10^{-9}$	$7.31 \cdot 10^{11}$	114	111.2	-28.0	119.5	3.2
<b>FOAM</b>	$2.13 \cdot 10^{-10}$	$2.81 \cdot 10^{13}$	132	128.9	2.4	128.2	103
<b>2FOAM</b>	$1.97 \cdot 10^{-10}$	$6.86 \cdot 10^{12}$	129	120.6	-22.8	127.4	111
<b>FOMe</b>	$1.67 \cdot 10^{-8}$	$3.78 \cdot 10^{11}$	110	107.5	-33.2	117.4	1.3

## 5 Syntheses



Scheme 1: General Synthesis Overview

5.1 1,2-Bis((2-nitrophenoxy)methyl)benzene (**S1**)<sup>[8]</sup>

1,2-bis(bromomethyl)benzene (6.00 g, 22.7 mmol, 0.49 equiv.) was added over a period of 10 min to a solution of 2-nitrophenol (6.40 g, 46.0 mmol, 1.00 equiv.) and potassium carbonate (9.54 g, 69.0 mmol, 1.50 equiv.) in acetone (100 mL) at 50 °C, and the mixture was heated to reflux at 65 °C for 2 h. The mixture was cooled to 25 °C and 400 mL DCM was added. The organic phase was washed with water (2x200 mL) and brine (150 mL) and dried over MgSO<sub>4</sub>. The solvent was evaporated *in vacuo*. Purification of the residue by column chromatography (gradient: *n*-hexane → DCM), gave the product as a colorless solid (6.95 g, 18.3 mmol, 80%, Lit: <sup>[8]</sup> 62%).

<sup>1</sup>H NMR (601 MHz, CDCl<sub>3</sub>) δ = 7.82 (dd, <sup>3</sup>J=8.1 Hz, <sup>4</sup>J=1.7 Hz, 2H, *H*-b), 7.64-7.50 (m, 4H, *H*-i, *H*-d), 7.44-7.39 (m, 2H, *H*-j), 7.30-7.21 (m, 2H, *H*-e), 7.03 (ddd, <sup>3</sup>J=8.4 Hz, <sup>3</sup>J=7.5 Hz, <sup>4</sup>J=1.1 Hz, 2H, *H*-c), 5.43 (s, 4H, *H*-g) ppm.

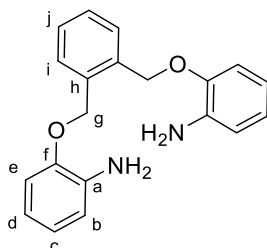
<sup>13</sup>C{<sup>1</sup>H} NMR (151 MHz, CDCl<sub>3</sub>) δ = 151.73 (*C*-f), 139.83 (*C*-a), 134.34 (*C*-d), 133.82 (*C*-h), 129.16 (*C*-i), 128.91 (*C*-j), 125.67 (*C*-b), 120.58 (*C*-c), 114.69 (*C*-e), 69.67 (*C*-g) ppm.

HRMS (ESI) *m/z* (%): [M+Na]<sup>+</sup> calcd for [C<sub>20</sub>H<sub>16</sub>N<sub>2</sub>O<sub>6</sub>+Na]<sup>+</sup> 403.09006, found 403.08969.

IR (ATR):  $\tilde{\nu}$  = 1609 (m), 1580 (w), 1518 (s), 1453 (w), 1390 (w), 1342 (m), 1315 (w), 1268 (m), 1253 (m), 1167 (w), 1152 (m), 1085 (w), 1046 (w), 1017 (m), 983 (m), 946 (w), 885 (w), 818 (w), 778 (w), 752 (m), 737 (s), 695 (m), 668 (m) cm<sup>-1</sup>.

Mp: 135 °C.

R<sub>f</sub>: 0.76 (DCM)

5.2 2,2'-((1,2-Phenylenebis(methylene))bis(oxy)dianiline (**S2**)<sup>[8]</sup>

Iron powder (4.41 g, 78.9 mmol, 10.0 equiv.) was added portionwise to a solution of **S1** (3.00 g, 7.89 mmol, 1.00 equiv.) in MeOH (100 mL). Afterwards, HCl (1 M, 5 mL) was slowly added to the reaction. The reaction mixture was heated to 90 °C for 70 min. After cooling down the mixture was filtered. The solid residue was washed with ethyl acetate (100 mL). The combined organic layers were washed with water (3x 200 mL) and brine (1x 100 mL). The organic layer was dried over MgSO<sub>4</sub> and concentrated under reduced pressure. The crude product was purified by column chromatography (ethyl acetate/*n*-hexane 2:1) to get the product as a off-white solid. The solid was crystallized in *n*-hexane/DCM (20 mL/5 mL) to get a colorless solid (1.74 g, 5.43 mmol, 68%, Lit:<sup>[8]</sup> 45%)

**<sup>1</sup>H NMR** (600 MHz, CDCl<sub>3</sub>)  $\delta$  = 6.755-7.51 (m, 2H, *H*-b), 7.42–7.38 (m, 2H, *H*-i), 6.87 (dd, <sup>3</sup>*J*=8.0 Hz, <sup>4</sup>*J*=1.3 Hz, 2H, *H*-d), 6.82 (td, <sup>3</sup>*J*=7.6 Hz, <sup>4</sup>*J*=1.3 Hz, 2H, *H*-j), 6.73 (dd, <sup>3</sup>*J*=7.7 Hz, <sup>4</sup>*J*=1.6 Hz, 2H, *H*-e), 6.70 (ddd, <sup>3</sup>*J*=8.0 Hz, <sup>3</sup>*J*=7.4 Hz, <sup>4</sup>*J*=1.6 Hz 2H, *H*-c), 5.20 (s, 4H, *H*-g), 3.80 (s, 4H, *NH*-a) ppm.

**<sup>13</sup>C{<sup>1</sup>H} NMR** (151 MHz, CDCl<sub>3</sub>)  $\delta$  = 146.21 (*C*-f), 136.56 (*C*-a), 135.36 (*C*-h), 129.17 (*C*-d), 128.45 (*C*-i), 121.66 (*C*-j), 118.33 (*C*-c), 115.20 (*C*-e), 112.21 (*C*-b), 68.26 (*C*-g) ppm.

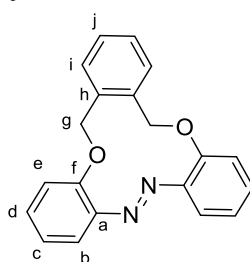
**HRMS** (EI, 70 eV) *m/z* (%): [M]<sup>+</sup> calcd for [C<sub>20</sub>H<sub>20</sub>N<sub>2</sub>O<sub>2</sub>]<sup>+</sup> 320.15193, found 320.15160 (7), [C<sub>5</sub>H<sub>6</sub>N]<sup>+</sup> 80.1 (100).

**IR** (ATR):  $\tilde{\nu}$  = 3470 (w), 3372 (m), 1612 (m), 1582 (w), 1504 (s), 1458 (m), 1373 (w), 1342 (w), 1281 (m), 1220 (m), 1204 (s), 1134 (m), 1065 (w), 1043 (m), 1026 (w), 1007 (m), 949 (w), 910 (w), 882 (w), 862 (w), 795 (w), 740 (s) cm<sup>-1</sup>.

**Rf**: 0.5 (ethyl acetate:*n*-hexane, 1:4).

**Mp**: 95 °C.

### 5.3 (*E*)-12,17-Dihydrotribenzo[*b*,*f*,*j*][1,8]dioxo[4,5]diazacyclododecine (**HOAM**)<sup>[9]</sup>



**S2** (600 mg, 1.87 mmol, 1.00 equiv.) was dissolved in toluene (30 mL). A stream of nitrogen was passed through the solution for 1 h. MnO<sub>2</sub> (1.30 g, 15.0 mmol, 8.00 equiv.) was added and the suspension was heated to 110 °C for 48 h. The hot reaction mixture was filtered through celite and the celite rinsed with chloroform (2x, 30 mL). The filtrate was evaporated to dryness under reduced pressure, and the residue was purified by column chromatography (DCM/*n*-hexane 2:1) to obtain final compound (402 mg, 1.25 mmol, 67%, Lit.:<sup>[9]</sup> 89%) as an orange solid.

**<sup>1</sup>H NMR** (600 MHz, CDCl<sub>3</sub>)  $\delta$  = 7.84 (dd, <sup>3</sup>*J*=7.9 Hz, 1.7 Hz, 2H, *H*-b), 7.49-7.45 (m, 2H, *H*-i), 7.42 (ddd, <sup>3</sup>*J*=8.0 Hz, <sup>3</sup>*J*=7.2 Hz, <sup>4</sup>*J*=1.7 Hz, 2H, *H*-d), 7.39-7.36 (m, 2H, *H*-j), 7.34 (dd, <sup>3</sup>*J*=8.0 Hz, <sup>4</sup>*J*=1.3 Hz, 2H, *H*-e), 7.31-7.25 (m, 2H, *H*-c), 5.40 (s, 4H, *H*-g) ppm.

**<sup>13</sup>C{<sup>1</sup>H} NMR** (151 MHz, CDCl<sub>3</sub>)  $\delta$  = 152.89 (*C*-f), 146.22 (*C*-a), 136.78 (*C*-h), 131.75 (*C*-d), 131.47 (*C*-i), 128.94 (*C*-j), 124.43 (*C*-c), 124.14 (*C*-e), 123.39 (*C*-b), 76.78 (*C*-g) ppm.

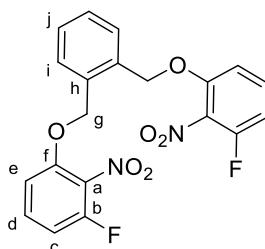
**IR** (ATR):  $\tilde{\nu}$  = 1590 (w), 1568 (w), 1466 (m), 1331 (m), 1263 (m), 1200 (m), 1149 (m), 1104 (m), 1043 (m), 1015 (w), 978 (m), 945 (m), 911 (w), 863 (w), 845 (w), 789 (s), 754 (s), 736 (s), 721 (s) cm<sup>-1</sup>.

**HRMS** (EI, 70 eV) *m/z* (%): [M]<sup>+</sup> calcd for [C<sub>20</sub>H<sub>16</sub>N<sub>2</sub>O<sub>2</sub>]<sup>+</sup> 316.12063, found 316.12073 (1), [C<sub>6</sub>H<sub>6</sub>]<sup>+</sup> 78.1 (100).

**Mp**: 135 °C.

**Rf**: 0.53 (*n*-hexane:DCM 1:2).

### 5.4 1,2-Bis((3-fluoro-2-nitrophenoxy)methyl)benzene (**S3**)



1,2-bis(bromomethyl)benzene (1.68 g, 6.36 mmol, 0.50 equiv.) was added over a period of 10 min to a solution of 3-fluoro-2-nitrophenol (2.00 g, 12.7 mmol, 1.00 equiv.) and potassium carbonate (2.64 g, 69.0 mmol, 1.50 equiv.) in acetone (50 mL) and the mixture was heated to reflux at 65 °C for 12 h. The mixture was cooled to 25 °C and 400 mL DCM was added. The organic phase was washed with water (2x200 mL) and brine (150 mL) and dried over MgSO<sub>4</sub>. The solvent was evaporated *in vacuo*. Purification of the residue by column chromatography (gradient: *n*-hexane → DCM), gave the product as a colorless solid (2.62 g, 6.30 mmol, 99%).

<sup>1</sup>H NMR (600 MHz, CDCl<sub>3</sub>) δ = 7.48-7.44 (m, 2H, H-i), 7.44 - 7.38 (m, 4H, H-d, H-j), 6.99 (d, <sup>3</sup>J=8.7 Hz, 2H, H-e), 6.84 (t, <sup>3</sup>J=8.7 Hz, 2H, H-c), 5.29 (s, 4H, H-g) ppm.

<sup>13</sup>C{<sup>1</sup>H} NMR (151 MHz, CDCl<sub>3</sub>) δ = 155.33 (d, <sup>1</sup>J=257.3 Hz, C-b), 151.27 (C-f), 133.38 (C-h), 132.11 (d, <sup>3</sup>J=9.8 Hz, C-d), 130.98 (C-a), 129.39 (C-i), 129.18 (C-j), 109.25 (d, <sup>4</sup>J=3.2 Hz, C-e), 108.98 (d, <sup>2</sup>J=19.0 Hz, C-c), 69.95 (C-g) ppm.

<sup>19</sup>F NMR (565 MHz, CDCl<sub>3</sub>) δ = -122.34 (dd, <sup>3</sup>J = 6.1 Hz, <sup>4</sup>J = 2.2 Hz, F-b) ppm.

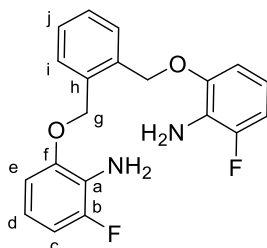
IR (ATR):  $\tilde{\nu}$  = 1615 (m), 1595 (m), 1525 (s), 1472 (m), 1446 (m), 1366 (s), 1295 (m), 1250 (s), 1179 (w), 1115 (m), 1084 (s), 1061 (s), 994 (w), 974 (w), 937 (w), 878 (w), 853 (m), 782 (s), 767 (w), 743 (s), 712 (m) cm<sup>-1</sup>.

HRMS (ESI) *m/z* (%): [M+Na]<sup>+</sup> calcd for [C<sub>20</sub>H<sub>14</sub>N<sub>2</sub>O<sub>6</sub>+Na]<sup>+</sup> 439.07121, found 439.07082.

Mp: 125 °C.

R<sub>f</sub>: 0.53 (DCM : cyclohexane, 1:1).

#### 5.5 (*E*)-4,7-Difluoro-12,17-dihydrotribenzo[*b,f,j*][1,8]dioxo[4,5]diazacyclododecine (**S4**)



Iron powder (4.41 g, 78.9 mmol, 10.00 equiv.) was added portion wise to a solution of **S3** (3.00 g, 7.89 mmol, 1.00 equiv.) in MeOH (100 mL). Afterwards, HCl (1 M, 5 mL) was slowly added to the reaction. The reaction mixture was heated to 90 °C for 70 min. After cooling down the mixture was filtered. The solid residue was washed with ethyl acetate (100 mL). The combined organic layers were washed with water (3x 200 mL) and brine (1x 100 mL). The organic layer was dried over MgSO<sub>4</sub> and concentrated under reduced pressure. The crude product was purified by column chromatography (ethyl acetate/*n*-hexane 2:1) to get the product as a white solid, which is not stable under ambient conditions and should be used immediately or stored under nitrogen in the dark. (2.80 g, 7.85 mmol, 99%)

<sup>1</sup>H NMR (600 MHz, CDCl<sub>3</sub>) δ = 7.53-7.49 (m, 2H, H-i), 7.44-7.39 (m, 2H-j), 6.74-6.65 (m, 4H, H-c, H-e), 6.61 (td, <sup>3</sup>J=8.2 Hz, <sup>3</sup>J=6.2 Hz, 2H, H-d), 5.20 (s, 4H, H-g), 3.76 (s, 4H, NH-a) ppm.

<sup>13</sup>C{<sup>1</sup>H} NMR (151 MHz, CDCl<sub>3</sub>) δ = 152.53 (d, <sup>1</sup>J=237.2 Hz, C-b), 147.47 (d, <sup>2</sup>J=7.6 Hz, C-f), 135.04 (C-h), 129.35 (C-i), 128.69 (C-j), 125.06 (d, <sup>2</sup>J=14.8 Hz, C-a), 116.72 (d, <sup>3</sup>J=9.2 Hz, C-d), 108.64 (d, <sup>2</sup>J=19.1 Hz, C-c), 107.77 (d, <sup>4</sup>J=2.6 Hz, C-e), 68.79 (C-g) ppm.

<sup>19</sup>F NMR (565 MHz, CDCl<sub>3</sub>) δ = -134.22 (dd, <sup>3</sup>J = 6.1 Hz, <sup>4</sup>J = 2.2 Hz, F-b) ppm.

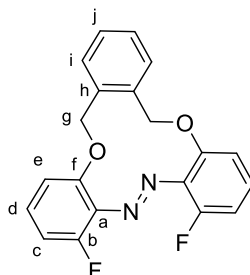
IR (ATR):  $\tilde{\nu}$  = 3460 (m), 3371 (m), 2887 (w), 1624 (m), 1599 (m), 1584 (m), 1507 (m), 1469 (s), 1394 (m), 1385 (m), 1291 (m), 1255 (m), 1232 (w), 1221 (w), 1197 (w), 1163 (m), 1137 (m), 1074 (w), 1036 (s), 997 (m), 968 (m), 925 (m), 880 (w), 848 (w), 774 (m), 752 (m), 729 (m), 707 (s) cm<sup>-1</sup>.

**HRMS** (EI, 70 eV)  $m/z$  (%):  $[M]^+$  calcd for  $[C_{20}H_{18}F_2N_2O_2]^+$  356.13309, found 356.13251 (8),  $[C_8H_8]^+$  104.1 (100).

**Mp**: 108 °C.

**R<sub>f</sub>**: 0.60 (ethyl acetate:cyclohexane, 1:2).

### 5.6 Ethyl 4-amino-3,5-difluorobenzoate (**FOAM**)



**S4** (600 mg, 1.87 mmol, 1.00 equiv.) was dissolved in toluene (30 mL). A stream of nitrogen was passed through the solution for 1 h.  $MnO_2$  (1.30 g, 15.0 mmol, 8.00 equiv.) was added and the suspension was heated to 110 °C for 48 h. The hot reaction mixture was filtered through celite and the celite rinsed with chloroform (2x, 30 mL). The filtrate was evaporated to dryness under reduced pressure, and the residue was purified by column chromatography (DCM/*n*-hexane 2:1) to obtain final compound (554 mg, 1.57 mmol, 84%) as a yellow solid.

**<sup>1</sup>H NMR** (600 MHz,  $CDCl_3$ )  $\delta$  = 7.48-7.44 (m, 2H, *H*-i), 7.41-7.39 (m, 2H, *H*-j), 7.35 (td,  $^3J=8.3$  Hz,  $^4J=6.0$  Hz, 2H, *H*-d), 7.15 (dt,  $^3J=8.3$  Hz,  $^4J=1.2$  Hz, 2H, *H*-e), 7.05 (ddd,  $^3J=10.1$  Hz,  $^3J=8.4$  Hz,  $^4J=1.2$  Hz, 2H, *H*-c), 5.26 (s, 4H, *H*-g) ppm.

**<sup>13</sup>C{<sup>1</sup>H} NMR** (151 MHz,  $CDCl_3$ )  $\delta$  = 156.17 (d,  $^1J=259.1$  Hz, *C*-b), 152.48 (*C*-f), 136.94 (d,  $^2J=8.4$  Hz, *C*-a) 136.00 (*C*-h), 131.65 (*C*-i), 130.91 (d,  $^3J=10.1$  Hz, *C*-d), 129.20 (*C*-j), 118.86 (d,  $^4J=3.3$  Hz, *C*-e), 112.62 (d,  $^2J=20.1$  Hz, *C*-c) 76.70 (*C*-g) ppm.

**<sup>19</sup>F NMR** (565 MHz,  $CDCl_3$ )  $\delta$  = -122.31 (dd,  $^3J=7.2$  Hz,  $^4J=2.3$  Hz, *F*-b) ppm.

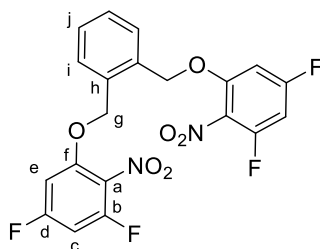
**IR** (ATR):  $\tilde{\nu}$  = 3505 (w), 3368 (m), 1697 (s), 1629 (s), 1585 (m), 1531 (m), 1477 (w), 1444 (m), 1397 (m), 1370 (m), 1339 (s), 1270 (s), 1222 (s), 1133 (m), 1089 (s), 1027 (s), 946 (s), 881 (m), 760 (m)  $cm^{-1}$ .

**HRMS** (EI, 70 eV)  $m/z$  (%):  $[M]^+$  calcd for  $[C_{20}H_{14}F_2N_2O_2]^+$  352.10179, found 352.10112 (5),  $[C_{14}H_{10}FNO]^+$  227.2 (100).

**Mp**: 158 °C.

**R<sub>f</sub>**: 0.68 (ethyl acetate/*n*-hexane, 1:2).

### 5.7 1,2-bis((3,5-difluoro-2-nitrophenoxy)methyl)benzene (**S5**)



1,2-Bis(bromomethyl)benzene (1.68 g, 6.36 mmol, 0.500 equiv.) was added over a period of 10 min to a solution of 3,5-difluoro-2-nitrophenol (2.22 g, 12.7 mmol, 1.00 equiv.) and potassium carbonate (2.64 g, 69.0 mmol, 1.50 equiv.) in acetone (50 mL) and the mixture was heated to reflux at 65 °C for 12 h. The mixture was cooled to 25 °C and DCM (400 mL) was added. The organic phase was washed with water (2x200 mL) and brine (150 mL) and dried over  $MgSO_4$ . The solvent was evaporated *in vacuo*.



Purification of the residue by column chromatography (gradient: *n*-hexane → DCM), gave the product as a colorless solid (2.85 g, 6.30 mmol, 99%).

**<sup>1</sup>H NMR** (600 MHz, CDCl<sub>3</sub>) δ = 7.47-7.42 (m, 4H, *H*-i, *H*-j), 6.75 (dd, <sup>3</sup>*J* = 10.0, <sup>5</sup>*J* = 2.2 Hz, 2H, *H*-c), 6.63-6.58 (m, 2H, *H*-e), 5.28 (s, 4H, *H*-g) ppm.

**<sup>13</sup>C{<sup>1</sup>H} NMR** (151 MHz, CDCl<sub>3</sub>) δ = 163.94 (d, <sup>1</sup>*J* = 255.3 Hz, <sup>3</sup>*J* = 15.0 Hz, *C*-b), 155.66 (d, <sup>1</sup>*J* = 258.9 Hz, <sup>3</sup>*J* = 15.0 Hz, *C*-d), 152.85-152.74 (m, 2C, *C*-f, *C*-a), 132.99 (*C*-h) 129.80 (*C*-i), 129.69 (*C*-j), 98.30-97.77 (m, *C*-c), 97.82 (d, <sup>2</sup>*J* = 50.8 Hz, *C*-e), 70.68 (*C*-g) ppm.

**<sup>19</sup>F NMR** (565 MHz, CDCl<sub>3</sub>) δ -100.56 (ddd, <sup>3</sup>*J* = 9.2 Hz, *F*-d), -117.84 (dd, <sup>3</sup>*J* = 9.2 Hz, *F*-b) ppm.

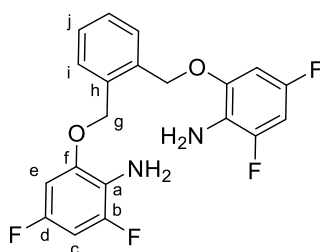
**IR** (ATR):  $\tilde{\nu}$  = 1662 (s), 198 (m), 1527 (s), 1497 (w), 1446 (m), 1368 (m), 1338 (m), 1304 (w), 1199 (m), 1137 (s), 1121 (m), 1088 (s), 1007 (m), 942 (w), 844 (m), 830 (m), 773 (m) cm<sup>-1</sup>.

**HRMS** (ESI) *m/z* (%): [M+Na]<sup>+</sup> calcd for [C<sub>20</sub>H<sub>12</sub>N<sub>2</sub>O<sub>6</sub>F<sub>4</sub>Na]<sup>+</sup> 475.05237, found 475.05163.

**Mp**: 157 °C.

**R<sub>f</sub>**: 0.80 (chloroform).

### 5.8 2,2'-((1,2-Phenylenebis(methylene))bis(oxy)dianiline (**S6**))



Iron powder (4.41 g, 78.9 mmol, 10.0 equiv.) was added portion wise to a solution of **S5** (3.57 g, 7.89 mmol, 1.00 equiv.) in MeOH (100 mL). Subsequently, HCl (1 M, 5 mL) was slowly added to the reaction. The reaction mixture was heated to 90 °C for 70 min. After cooling down the mixture, it was filtered. The solid residue was washed with ethyl acetate (100 mL). The combined organic layers were washed with water (3 x 200 mL) and brine (1 x 100 mL). The organic layer was dried over MgSO<sub>4</sub> and concentrated under reduced pressure. The crude product was purified by column chromatography (ethyl acetate : *n*-hexane 2 : 1) to obtain the product as a white solid, which was not stable under ambient conditions and should be used immediately or stored under nitrogen in the dark (3.08 g, 7.85 mmol, 99%).

**<sup>1</sup>H NMR** (600 MHz, CDCl<sub>3</sub>) δ = 7.50 (dd, <sup>3</sup>*J* = 5.6 Hz, <sup>4</sup>*J* = 3.5 Hz, 2H, *H*-i), 7.42 (dd, <sup>3</sup>*J* = 5.6 Hz, <sup>3</sup>*J* = 3.5 Hz, 2H, *H*-i), 6.50-6.46 (m, 2H, *H*-c, *H*-e), 5.16 (s, 2H, *H*-g), 3.56 (s, 4H, *NH*-a) ppm.

**<sup>13</sup>C{<sup>1</sup>H} NMR** (151 MHz, CDCl<sub>3</sub>) δ = 154.81 (d, <sup>1</sup>*J* = 237.2 Hz, <sup>3</sup>*J* = 14.9 Hz, *C*-b), 151.06 (d, <sup>1</sup>*J* = 238.3 Hz, <sup>3</sup>*J* = 14.9 Hz, *C*-d), 147.42 (dd, <sup>3</sup>*J* = 11.6 Hz, <sup>3</sup>*J* = 9.5 Hz, *C*-f), 134.60 (*C*-h), 129.70 (*C*-i), 129.19 (*C*-j), 121.27 (dd, <sup>2</sup>*J* = 15.5 Hz, <sup>4</sup>*J* = 4.0 Hz, *C*-a), 96.89-96.44 (m, *C*-c), 96.84 (d, <sup>2</sup>*J* = 50.1 Hz, *C*-e), 69.14 (*C*-g) ppm.

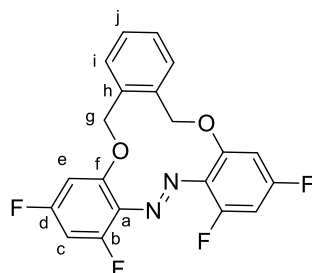
**<sup>19</sup>F NMR** (565 MHz, CDCl<sub>3</sub>) δ -131.73 (dd, <sup>3</sup>*J* = 11.1 Hz, <sup>5</sup>*J* = 2.5 Hz *F*-e), -123.86 (dd <sup>3</sup>*J* = 9.4 Hz, *F*-d) ppm.

**HRMS** (EI, 70 eV) *m/z* (%): [M]<sup>+</sup> calcd for [C<sub>20</sub>H<sub>16</sub>N<sub>2</sub>O<sub>2</sub>F<sub>4</sub>]<sup>+</sup> 392.11424, found 392.11484 (20), [C<sub>14</sub>H<sub>12</sub>F<sub>2</sub>NO]<sup>+</sup> 248 (100).

**IR** (ATR):  $\tilde{\nu}$  = 3452 (w), 3365 (w), 1629 (m), 1608 (m), 1588 (m), 1509 (s), 1477 (s), 1446 (s), 1388 (w), 1360 (w), 1325 (w), 1245 (w), 1192 (w), 1151 (s), 1110 (s), 1034 (s), 997 (s), 813 (s), 767 (s) cm<sup>-1</sup>.

**Mp**: 112 °C.

**R<sub>f</sub>**: 0.35 (chloroform)

5.9 (*E*)-12,17-Dihydrotribenzo[*b,f,j*][1,8]dioxo[4,5]diazacyclododecine (**2FOAM**)

**S7** (734 mg, 1.87 mmol, 1.00 equiv.) was dissolved in toluene (30 mL). A stream of nitrogen was passed through the solution for 1 h.  $\text{MnO}_2$  (1.30 g, 15.0 mmol, 8.00 equiv.) was added and the suspension was heated to 110 °C for 48 h. The hot reaction mixture was filtered through celite and the celite rinsed with chloroform (2x, 30 mL). The filtrate was evaporated to dryness under reduced pressure, and the residue was purified by column chromatography (DCM/*n*-hexane 2:1) to obtain final compound (625 mg, 1.61 mmol, 86%) as a yellow solid.

$^1\text{H NMR}$  (600 MHz,  $\text{CDCl}_3$ )  $\delta$  = 7.49-7.42 (m, 4H, *H*-i, *H*-j), 7.49-7.45 (m, 2H, *H*i), 6.91 (dd,  $^3J$  = 9.0 Hz,  $^4J$  = 2.4 Hz, 2H, *H*-e), 6.82 (ddd,  $^3J$  = 11.0 Hz,  $^3J$  = 9.0 Hz,  $^4J$  = 2.4 Hz, 2H, *H*-c), 5.31 (s, 4H, *H*-g) ppm.

$^{13}\text{C}\{^1\text{H}\}$  NMR (151 MHz,  $\text{CDCl}_3$ )  $\delta$  = 163.27 (d,  $^1J$  = 256 Hz,  $^3J$  = 15.2 Hz, *C*-b), 156.36 (d,  $^1J$  = 256 Hz,  $^3J$  = 15.2 Hz, *C*-d), 154.11 (dd,  $^3J$  = 13.3 Hz,  $^5J$  = 4.6 Hz, *C*-f), 135.59 (*C*-h), 133.37 (dd,  $^3J$  = 8.0,  $^3J$  = 4.6 Hz, *C*-a), 131.56 (*C*-i), 129.39 (*C*-j), 106.75 (dd,  $^2J$  = 24.2 Hz,  $^4J$  = 3.8 Hz, *C*-e), 101.28 (t,  $^2J$  = 24.2 Hz, *C*-c), 76.51 (*C*-g) ppm.

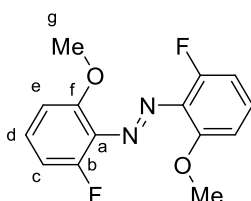
$^{19}\text{F NMR}$  (565 MHz,  $\text{CDCl}_3$ )  $\delta$  -105.01 (ddd,  $^3J$  = 9.0 Hz, *F*-b), -117.17 (dd,  $^3J$  = 9.0 Hz, *F*-d) ppm.

IR (ATR):  $\tilde{\nu}$  = 1589 (s), 1443 (s), 1380 (m), 1338 (w), 1214 (w), 1177 (m), 1087 (s), 1063 (s), 1004 (m), 958 (m), 932 (m), 854 (m), 837 (m), 825 (m), 781 (m), 763 (s)  $\text{cm}^{-1}$ .

HRMS (ESI)  $m/z$  (%):  $[\text{M}+\text{Na}]^+$  calcd for  $[\text{C}_{20}\text{H}_{12}\text{N}_2\text{O}_2\text{F}_4\text{Na}]^+$  411.07271, found 411.07189.

**Mp**: 178 °C.

**R<sub>f</sub>**: 0.80 (chloroform).

5.10 (*E*)-1,2-Bis(2-fluoro-6-methoxyphenyl)diazene (**FOMe**)<sup>[10]</sup>

2-Fluoro-4-methoxyanilin (264 mg, 1.87 mmol, 1.00 equiv.) was dissolved in toluene (30 mL). A stream of nitrogen was passed through the solution for 1 h. MnO<sub>2</sub> (1.30 g, 15.0 mmol, 8.00 equiv.) was added and the suspension was heated to 110 °C for 48 h. The hot reaction mixture was filtered through celite and the celite rinsed with chloroform (2x, 30 mL). The filtrate was evaporated to dryness under reduced pressure, and the residue was purified by column chromatography (DCM/*n*-hexane 2/1) to obtain final compound (117 mg, 421 μmol, 45%, Lit.<sup>[10]</sup> 5%) as an orange solid.

<sup>1</sup>H NMR (600 MHz, CDCl<sub>3</sub>) δ = δ 7.32 – 7.26 (m, 1H, *H*-d), 6.87 – 6.77 (m, 2H, *H*-c, *H*-e), 3.93 (s, 3H, *H*-g) ppm.

<sup>13</sup>C{<sup>1</sup>H} NMR (151 MHz, CDCl<sub>3</sub>) δ = 155.17 (d, <sup>3</sup>*J* = 4.5 Hz, C-f), 153.39 (d, <sup>1</sup>*J* = 257.0 Hz, C-b), 133.19 (d, <sup>2</sup>*J* = 9.1 Hz, C-a), 130.56 (d, <sup>3</sup>*J* = 10.8 Hz, C-d), 109.22 (d, <sup>2</sup>*J* = 20.7 Hz, C-c), 107.87 (d, <sup>4</sup>*J* = 3.2 Hz, C-e), 56.89 (C-g) ppm.

IR (ATR):  $\tilde{\nu}$  = 1602 (w), 1582 (m), 1475 (s), 1436 (m), 1299 (s), 1281 (m), 1244 (m), 1213 (w), 1186 (w), 1080 (s), 1069 (s), 944 (m), 784 (s), 739 (s) cm<sup>-1</sup>.

HRMS (EI, 70 eV) *m/z* (%): [M]<sup>+</sup> calcd for [C<sub>14</sub>H<sub>12</sub>N<sub>2</sub>O<sub>2</sub>F<sub>2</sub>]<sup>+</sup> 278.08620, found 278.08614 (25), [C<sub>14</sub>H<sub>12</sub>F<sub>2</sub>NO]<sup>+</sup> 153 (100).

Mp: 109 °C.

R<sub>f</sub>: 0.55 (chloroform).

## 5 References

- [1] J. Bahrenburg, C. M. Sievers, J. B. Schönborn, B. Hartke, F. Renth, F. Temps, C. Näther, F. D. Sönnichsen, *Photochemical and Photobiological Sciences* **2013**, 12, 511.
- [2] O. V. Dolomanov, Bourhis, L. J., Gildea, R. J., Howard, J. A. K., Puschmann, H., *J. Appl. Crystallogr.* **2009**, 42.
- [3] A. Spek, *Acta Crystallographica Section E* **2020**, 76, 1.
- [4] G. W. T. M. J. Frisch, H. B. Schlegel, G. E. Scuseria, J. R. C. M. A. Robb, G. Scalmani, V. Barone, B. Mennucci, H. N. G. A. Petersson, M. Caricato, X. Li, H. P. Hratchian, J. B. A. F. Izmaylov, G. Zheng, J. L. Sonnenberg, M. Hada, K. T. M. Ehara, R. Fukuda, J. Hasegawa, M. Ishida, T. Nakajima, O. K. Y. Honda, H. Nakai, T. Vreven, J. A. Montgomery, Jr., F. O. J. E. Peralta, M. Bearpark, J. J. Heyd, E. Brothers, V. N. S. K. N. Kudin, T. Keith, R. Kobayashi, J. Normand, A. R. K. Raghavachari, J. C. Burant, S. S. Iyengar, J. Tomasi, N. R. M. Cossi, J. M. Millam, M. Klene, J. E. Knox, J. B. Cross, C. A. V. Bakken, J. Jaramillo, R. Gomperts, R. E. Stratmann, A. J. A. O. Yazyev, R. Cammi, C. Pomelli, J. W. Ochterski, K. M. R. L. Martin, V. G. Zakrzewski, G. A. Voth, J. J. D. P. Salvador, S. Dapprich, A. D. Daniels, J. B. F. O. Farkas, J. V. Ortiz, J. Cioslowski, G. and D. J. Fox, Inc., Wallingford CT, 2013.
- [5] S. Grimme, J. Antony, S. Ehrlich, H. Krieg, *The Journal of Chemical Physics* **2010**, 132.
- [6] *The ACS Style Guide: Effective Communication of Scientific Information*, American Chemical Society, Washington, DC **2006**.
- [7] H. Putz, K. Brandenburg, *Diamond - Crystal and Molecular Structure Visualization*, Crystal Impact, <https://www.crystalimpact.de/diamond>.
- [8] D. E. Fenton, R. W. Matthews, M. McPartlin, B. P. Murphy, I. J. Scowen, P. A. Tasker, *Journal of the Chemical Society, Dalton Transactions* **1996**, 3421.

- [9] N. Eleya, S. Ghosh, E. Lork, A. Staubitz, *Journal of Materials Chemistry C* **2021**, 9, 82.
- [10] A. Müller-Deku, O. Thorn-Seshold, *The Journal of Organic Chemistry* **2022**, 87, 16526.

# $^1\text{H}$ , $^{13}\text{C}\{^1\text{H}\}$ and $^{19}\text{F}$ NMR Spectra of the Purified Compounds

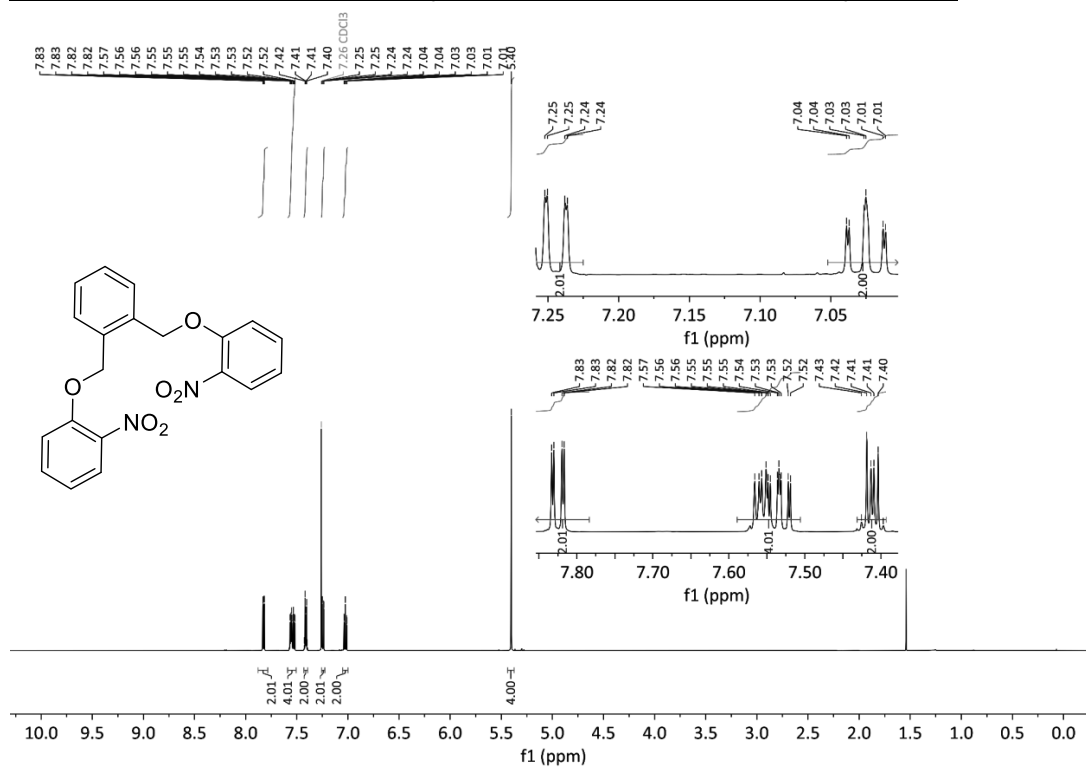


Figure S28:  $^1\text{H}$  NMR spectrum of **S1** in  $\text{CDCl}_3$ .

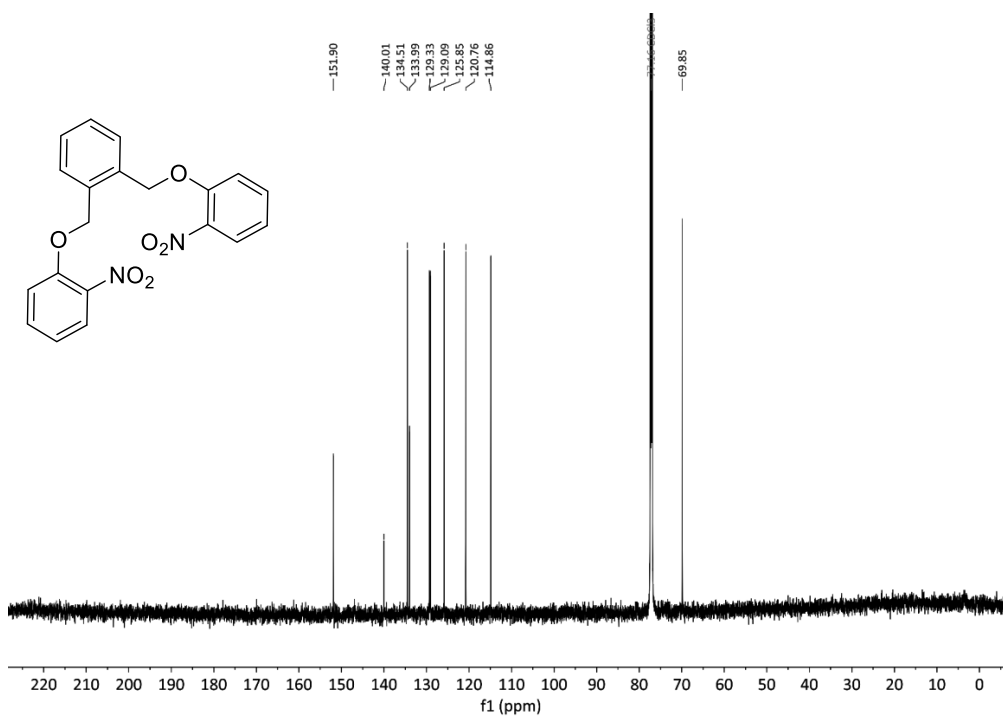
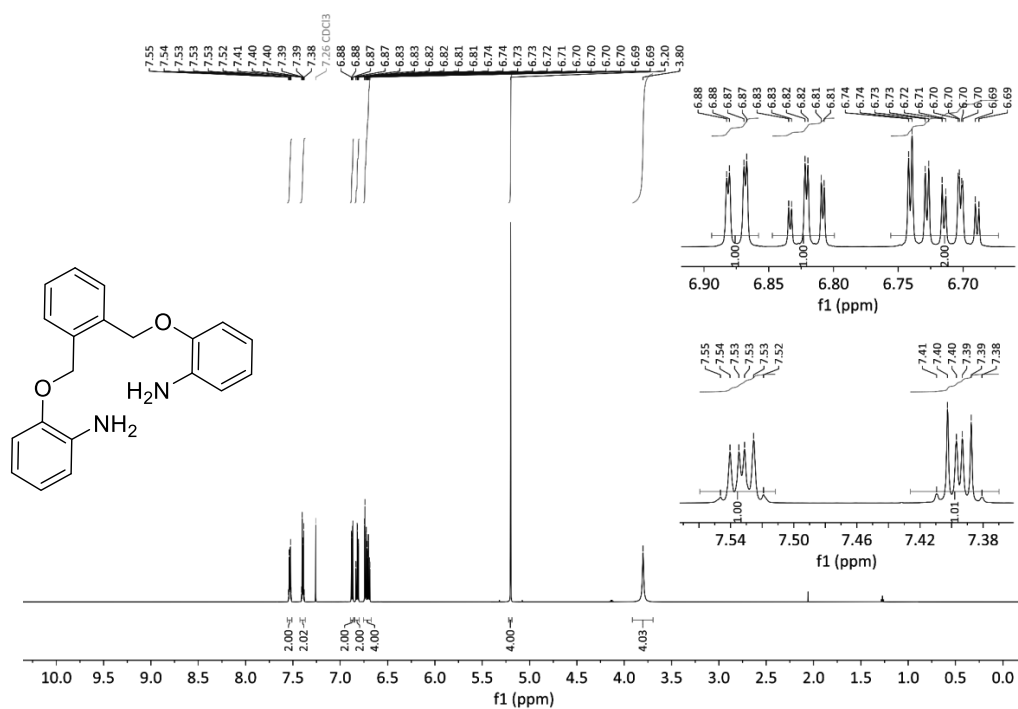
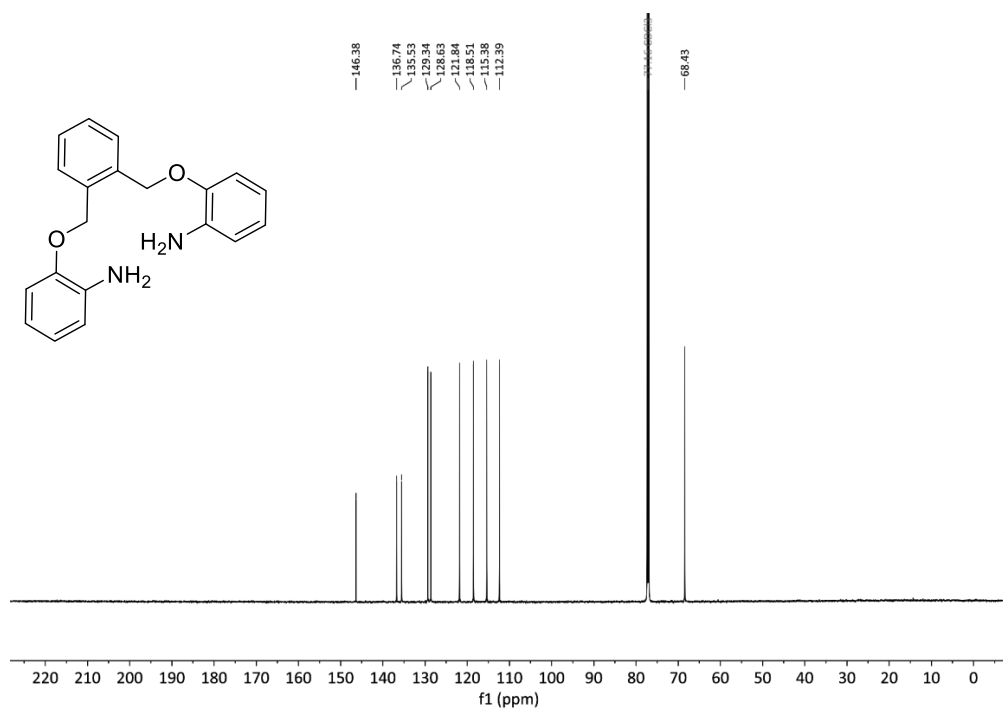
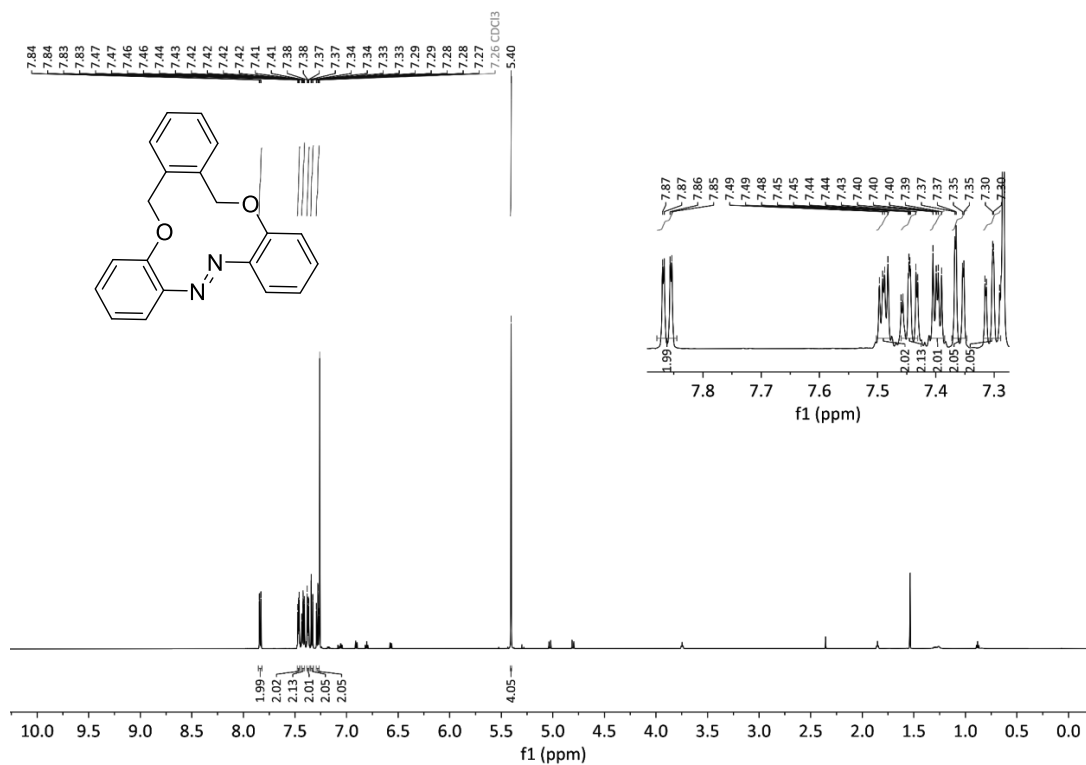
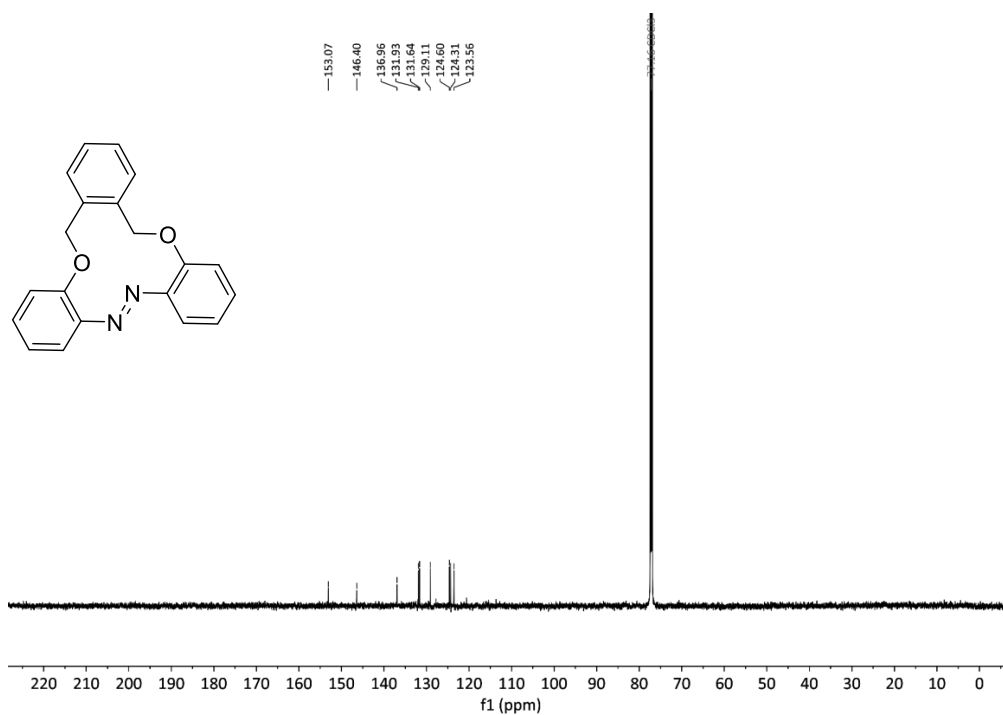


Figure S29:  $^{13}\text{C}\{^1\text{H}\}$  NMR spectrum of **S1** in  $\text{CDCl}_3$ .

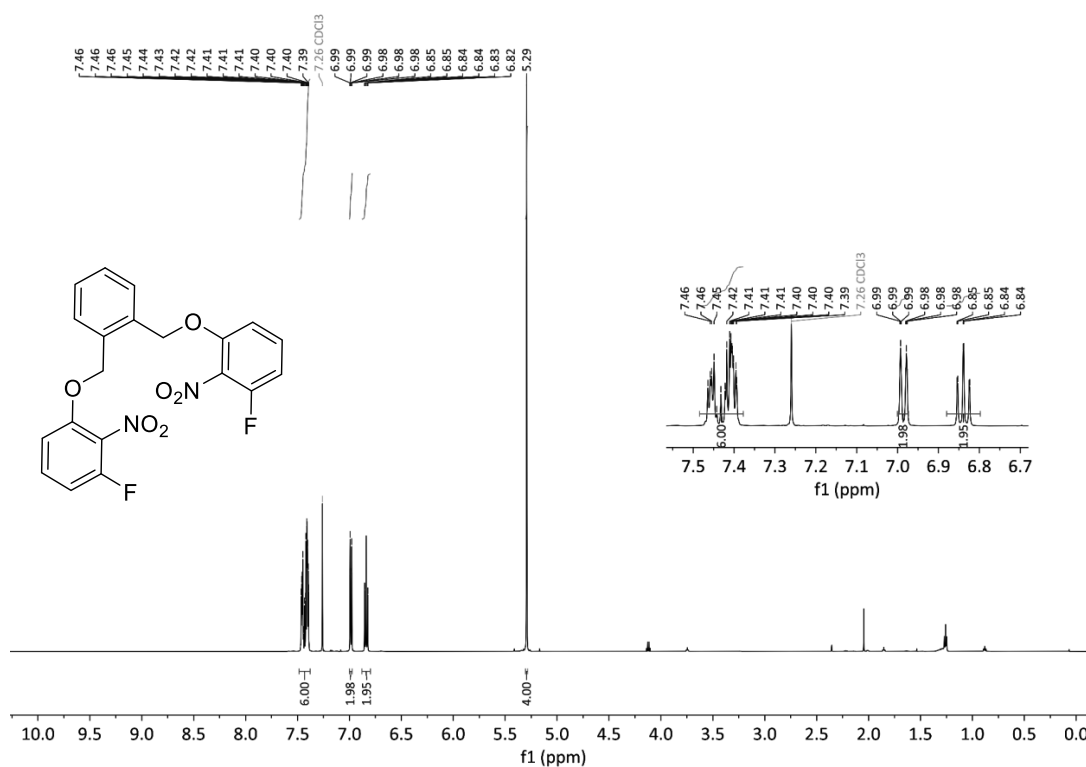
Figure S30:  $^1\text{H}$  NMR spectrum of S2 in  $\text{CDCl}_3$ .Figure S31:  $^{13}\text{C}\{^1\text{H}\}$  NMR spectrum of S2 in  $\text{CDCl}_3$ .



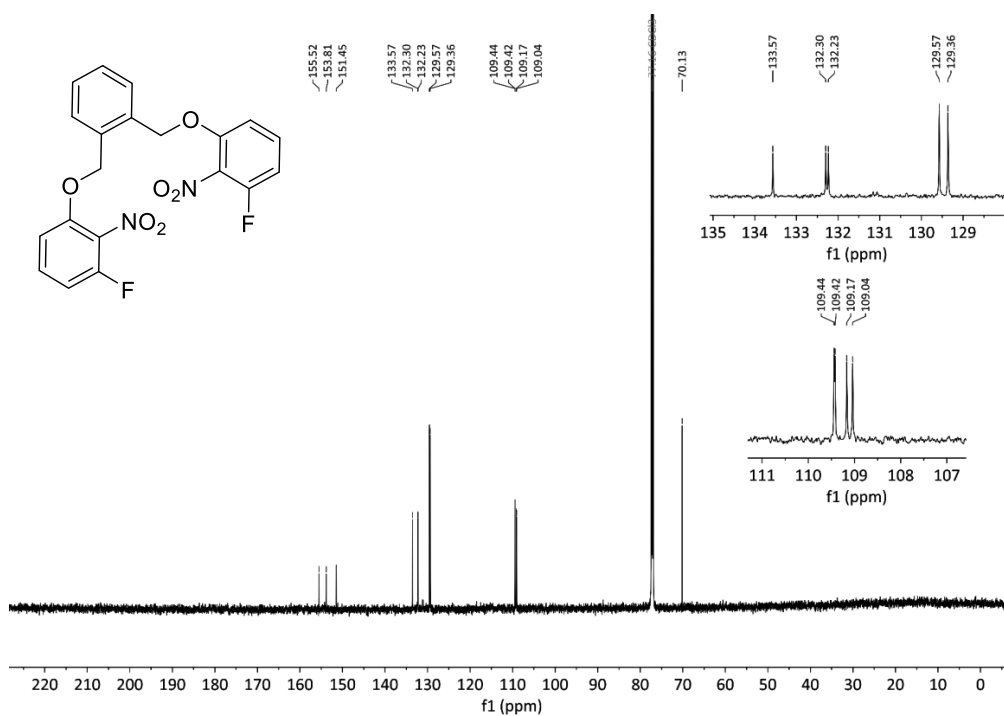
**Figure S32:**  $^1\text{H}$  NMR spectrum of **S3** in  $\text{CDCl}_3$ .



**Figure S33:**  $^{13}\text{C}\{^1\text{H}\}$  NMR spectrum of **S3** in  $\text{CDCl}_3$ .

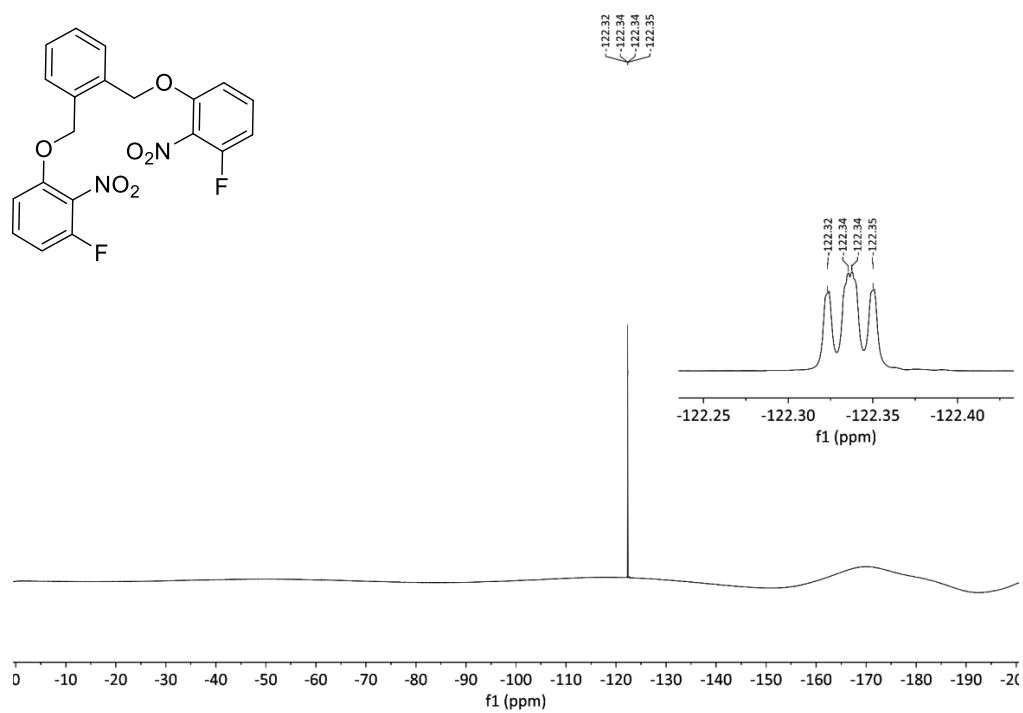


**Figure S34:**  $^1\text{H}$  NMR spectrum of **S4** in  $\text{CDCl}_3$ .

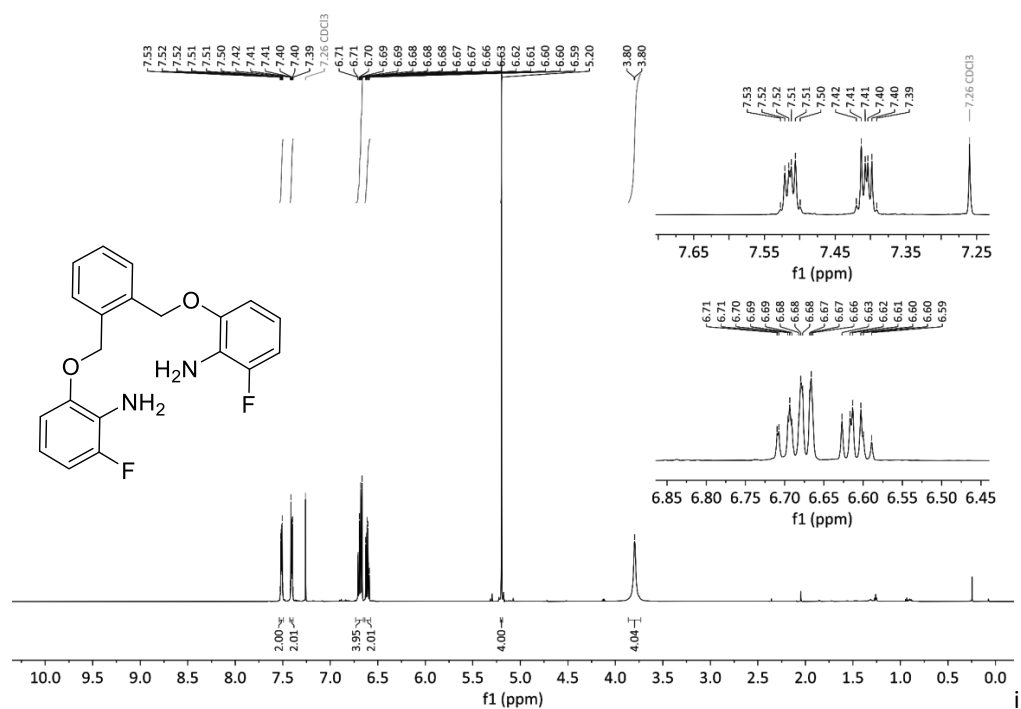
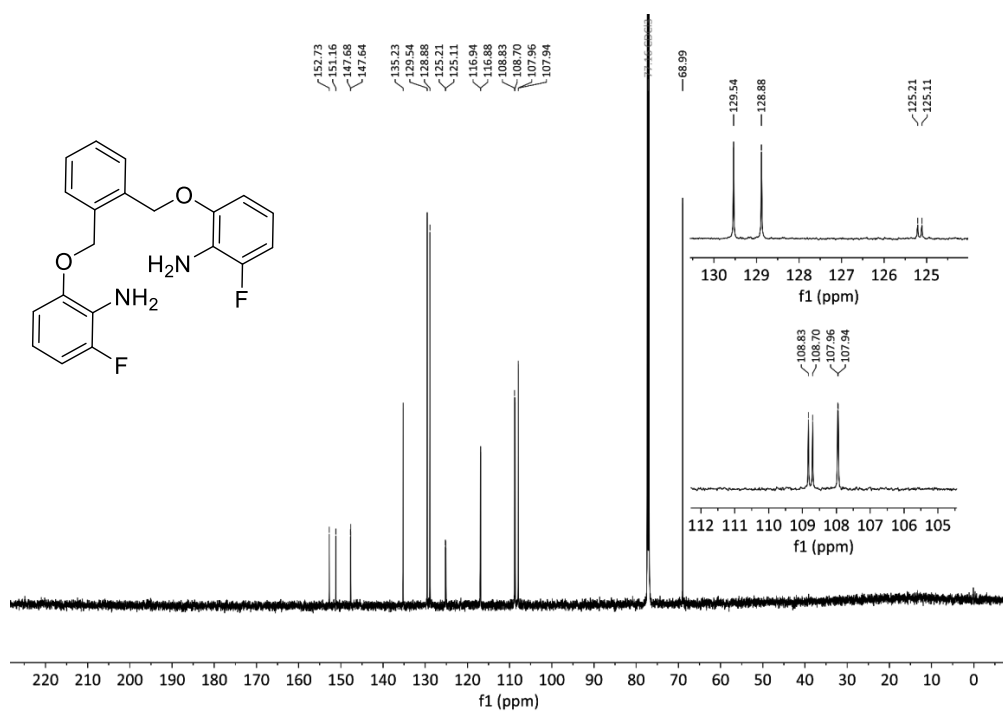


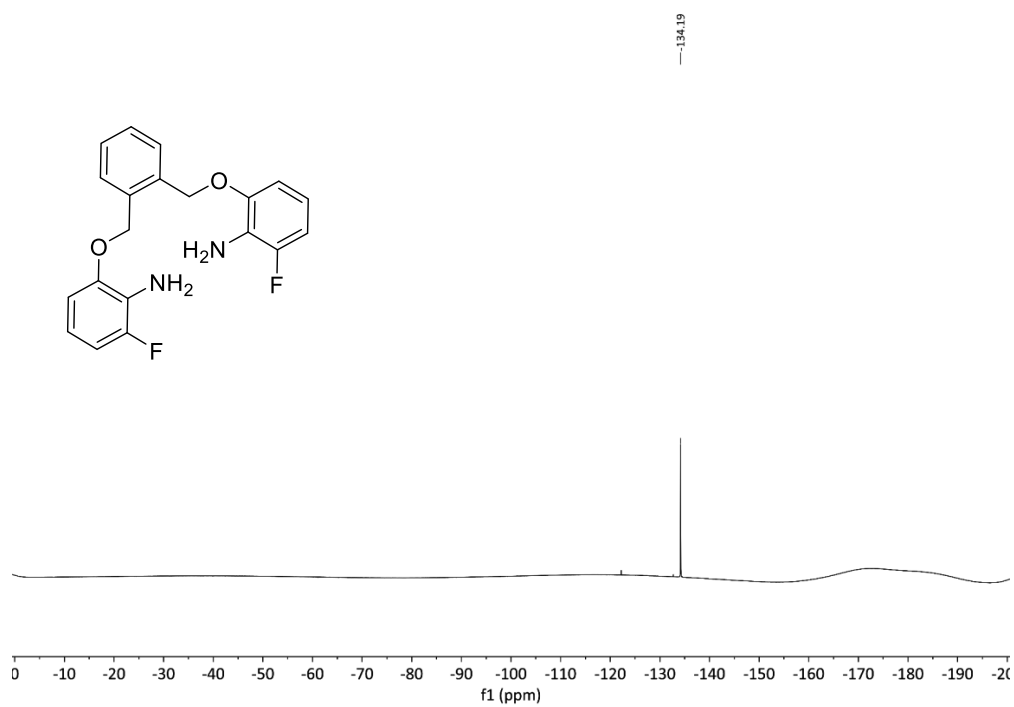
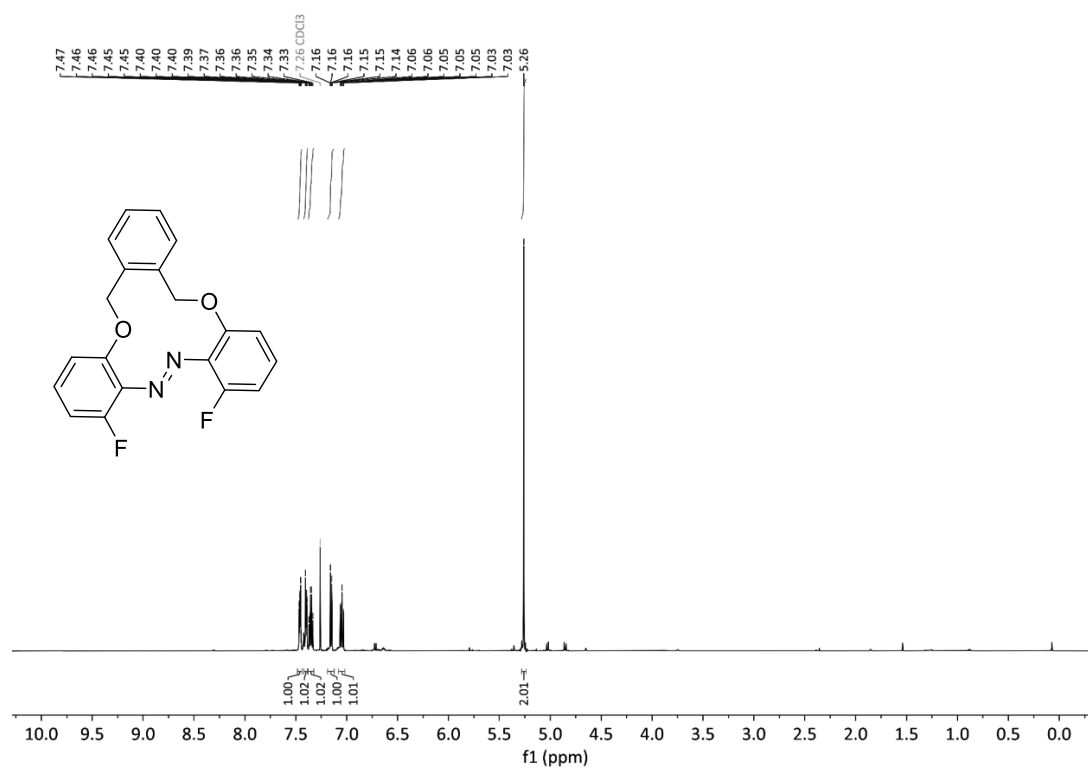
**Figure S35:**  $^{13}\text{C}\{^1\text{H}\}$  NMR spectrum of **S4** in  $\text{CDCl}_3$ .

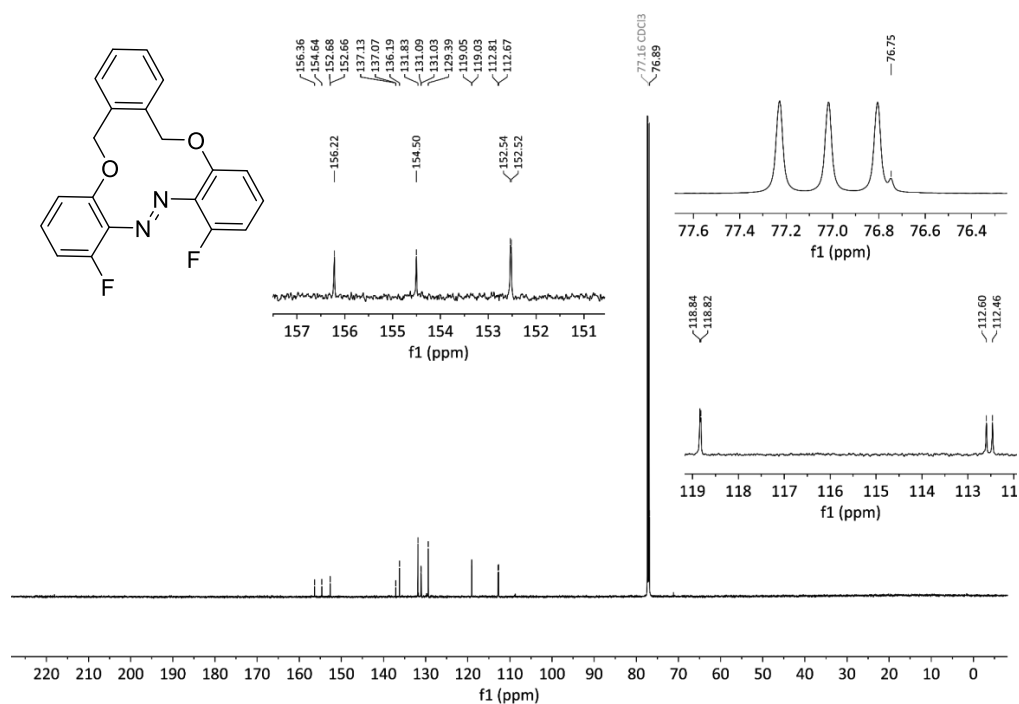
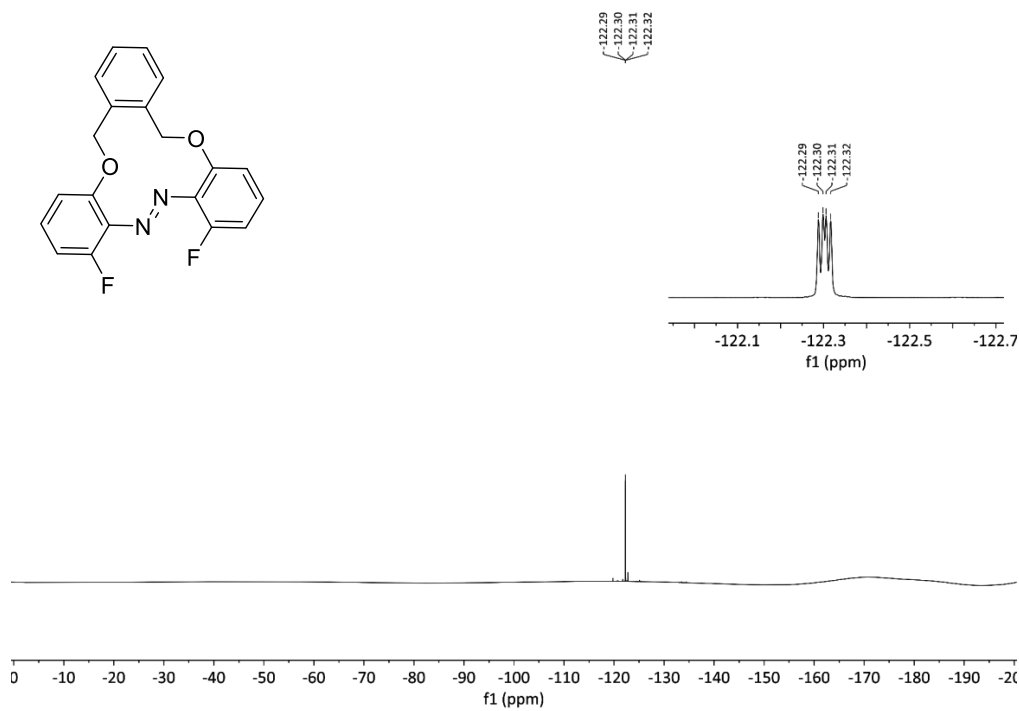


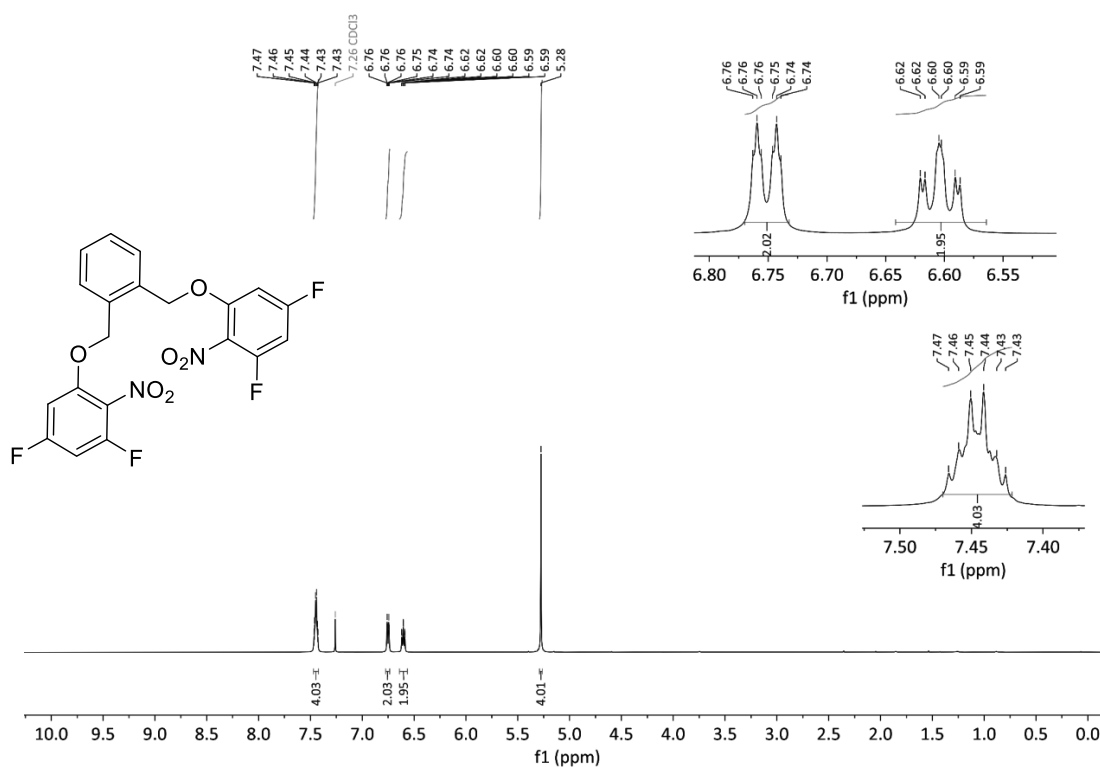


**Figure S36:**  $^{19}\text{F}$  NMR spectrum of **S4** in  $\text{CDCl}_3$ .

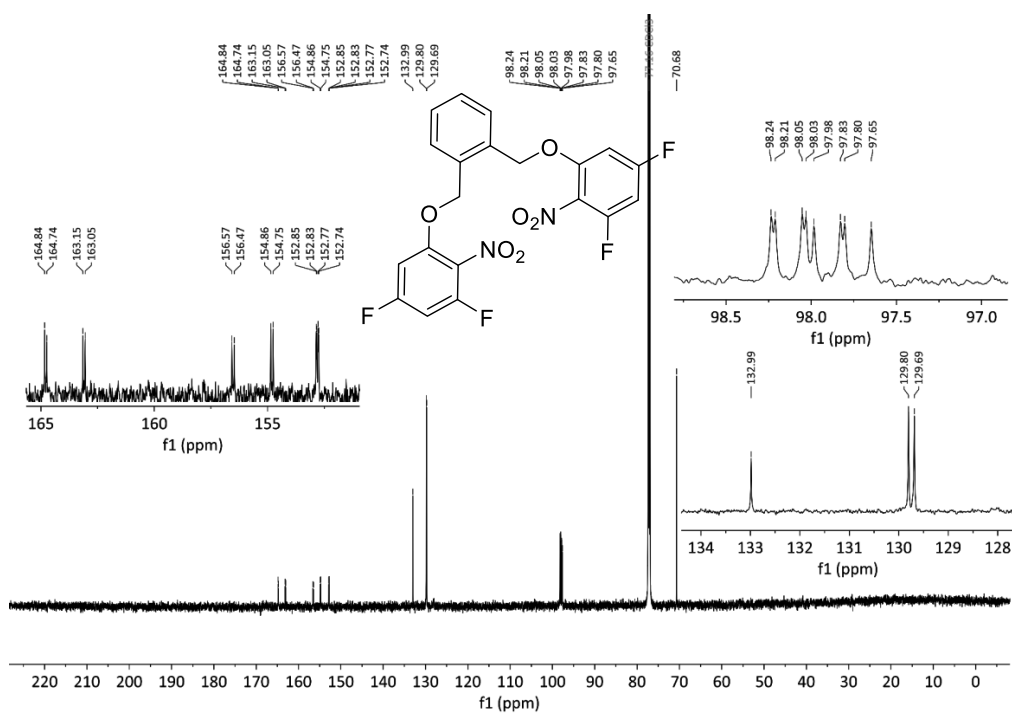
Figure S37:  $^1\text{H}$  NMR spectrum of S5 in  $\text{CDCl}_3$ .Figure S38:  $^{13}\text{C}\{^1\text{H}\}$  NMR spectrum of S5 in  $\text{CDCl}_3$ .

Figure S39:  $^{19}\text{F}$  NMR spectrum of S5 in  $\text{CDCl}_3$ .Figure S40:  $^1\text{H}$  NMR spectrum of S6 in  $\text{CDCl}_3$ .

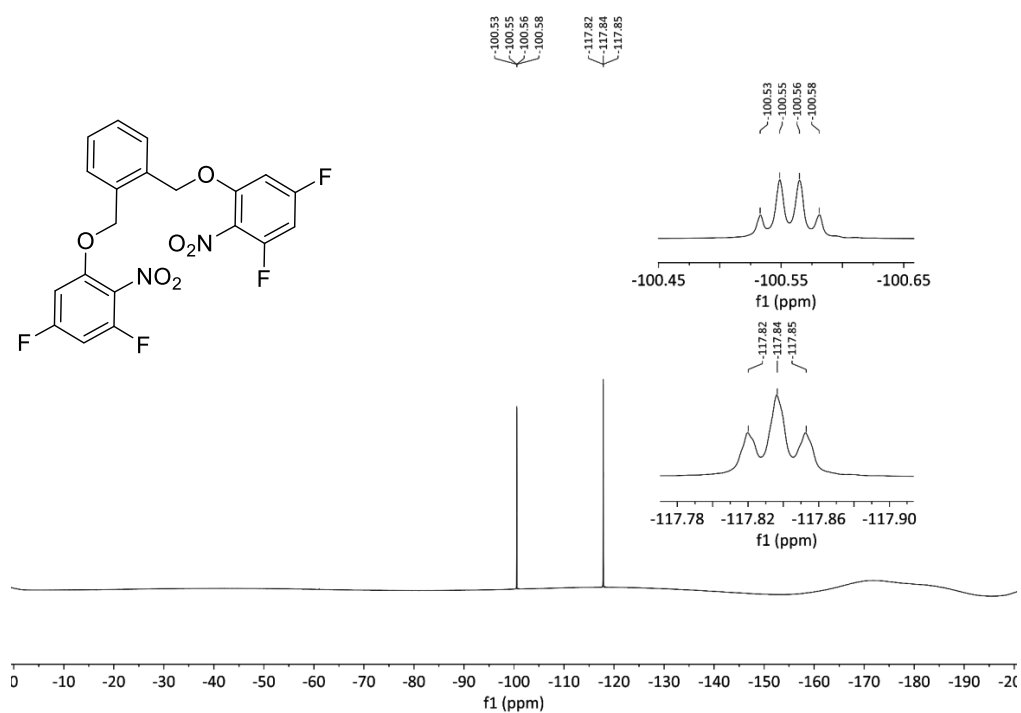
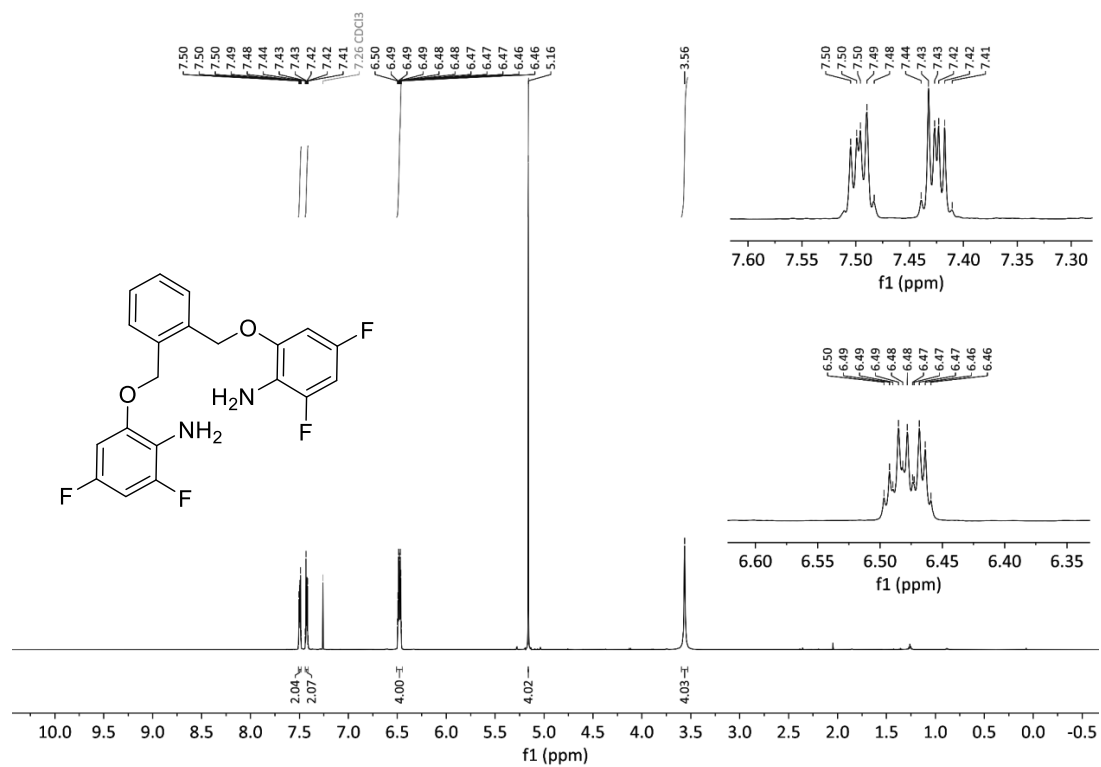
Figure S41:  $^{13}\text{C}\{^1\text{H}\}$  NMR spectrum of S6 in  $\text{CDCl}_3$ .Figure S42:  $^{13}\text{C}\{^1\text{H}\}$  NMR spectrum of S6 in  $\text{CDCl}_3$ .

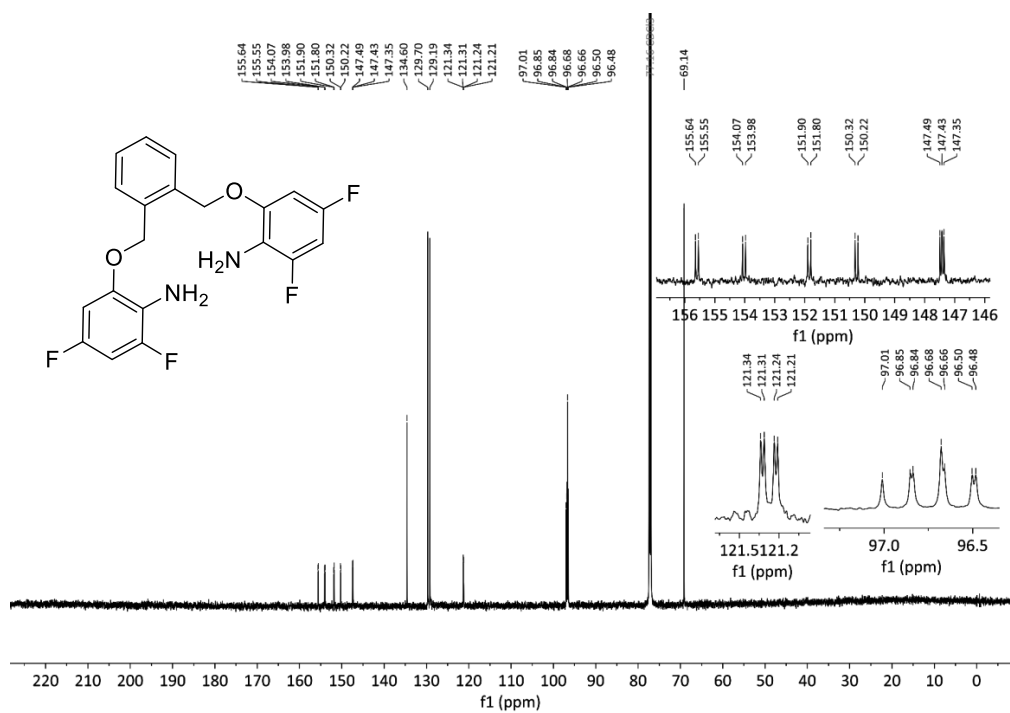
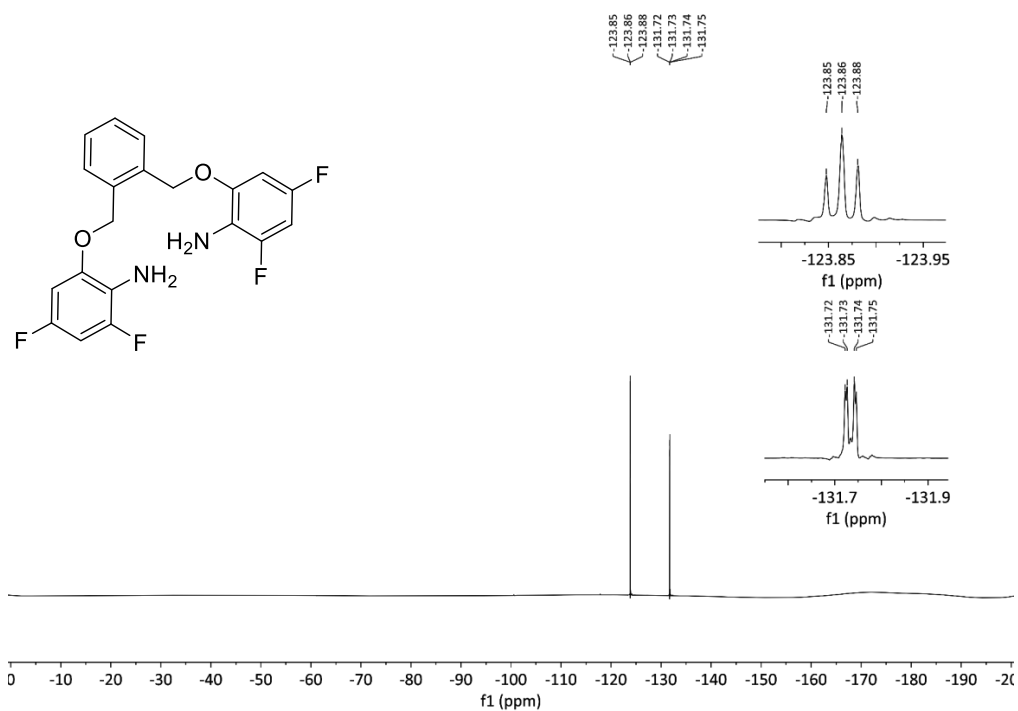


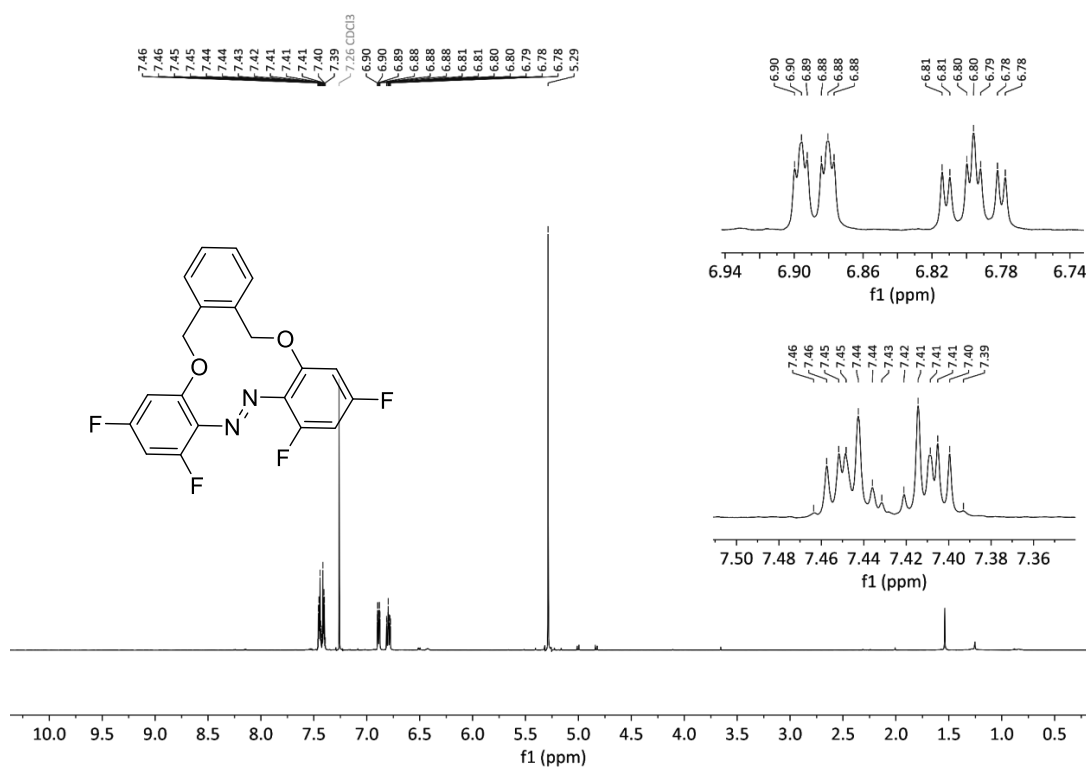
**Figure S43:**  $^1\text{H}$  NMR spectrum of **S7** in  $\text{CDCl}_3$ .



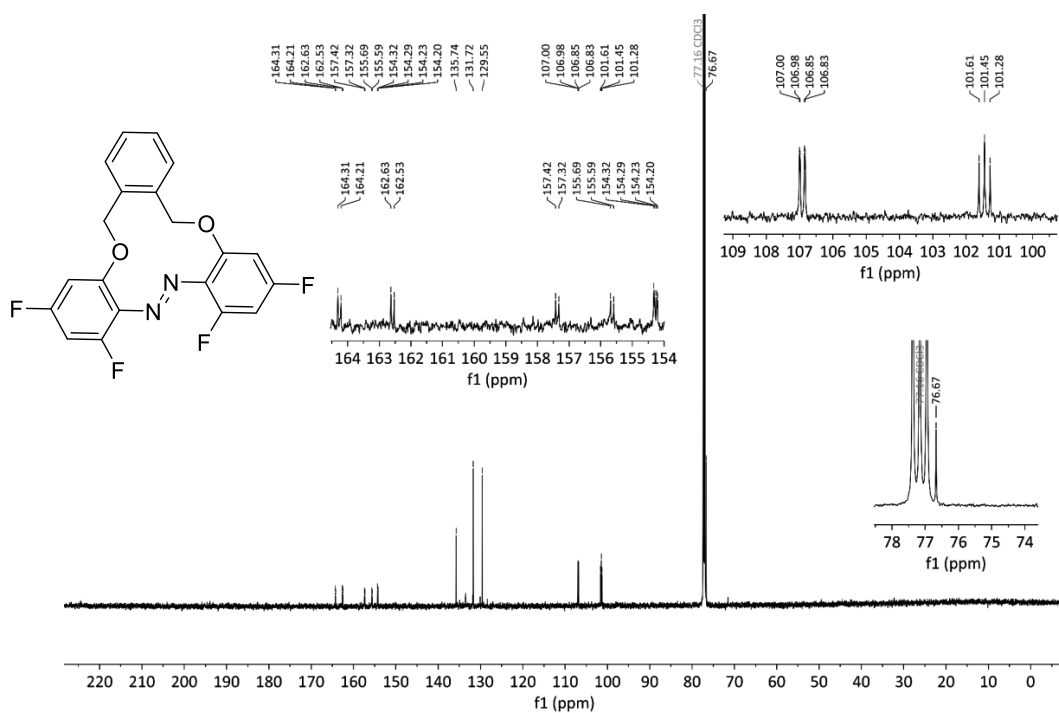
**Figure S44:**  $^{13}\text{C}\{^1\text{H}\}$  NMR spectrum of **S7** in  $\text{CDCl}_3$ .

Figure S45:  $^{19}\text{F}$  NMR spectrum of **S7** in  $\text{CDCl}_3$ .Figure S46:  $^1\text{H}$  NMR spectrum of **S8** in  $\text{CDCl}_3$ .

Figure S47:  $^{13}\text{C}\{^1\text{H}\}$  NMR spectrum of **S8** in  $\text{CDCl}_3$ .Figure S48:  $^{19}\text{F}$  NMR spectrum of **S8** in  $\text{CDCl}_3$ .

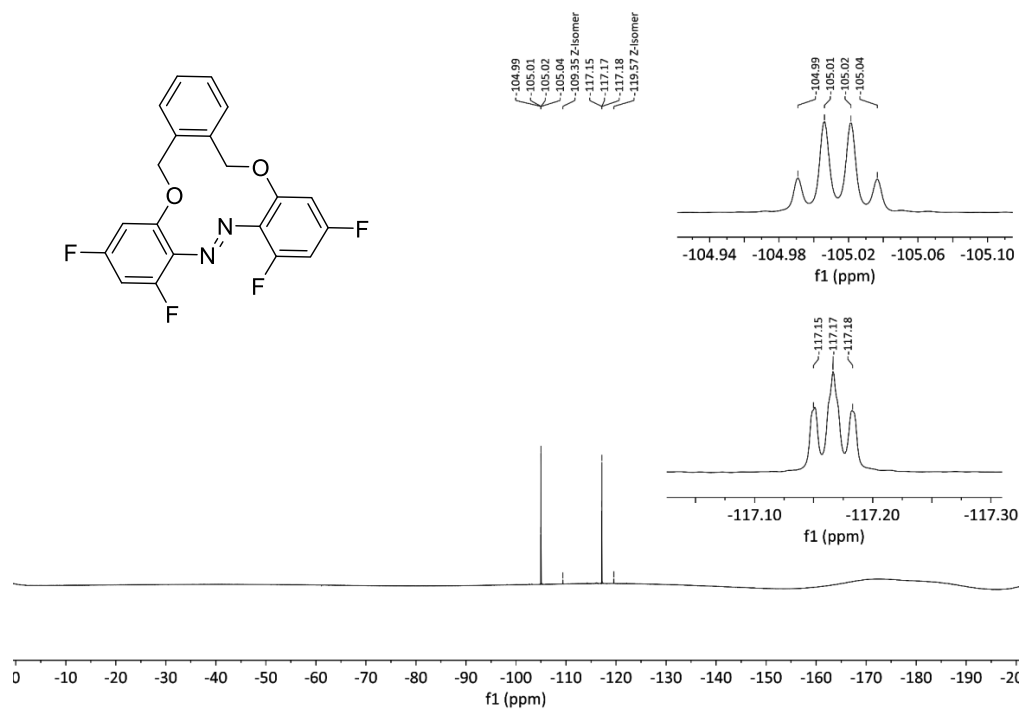
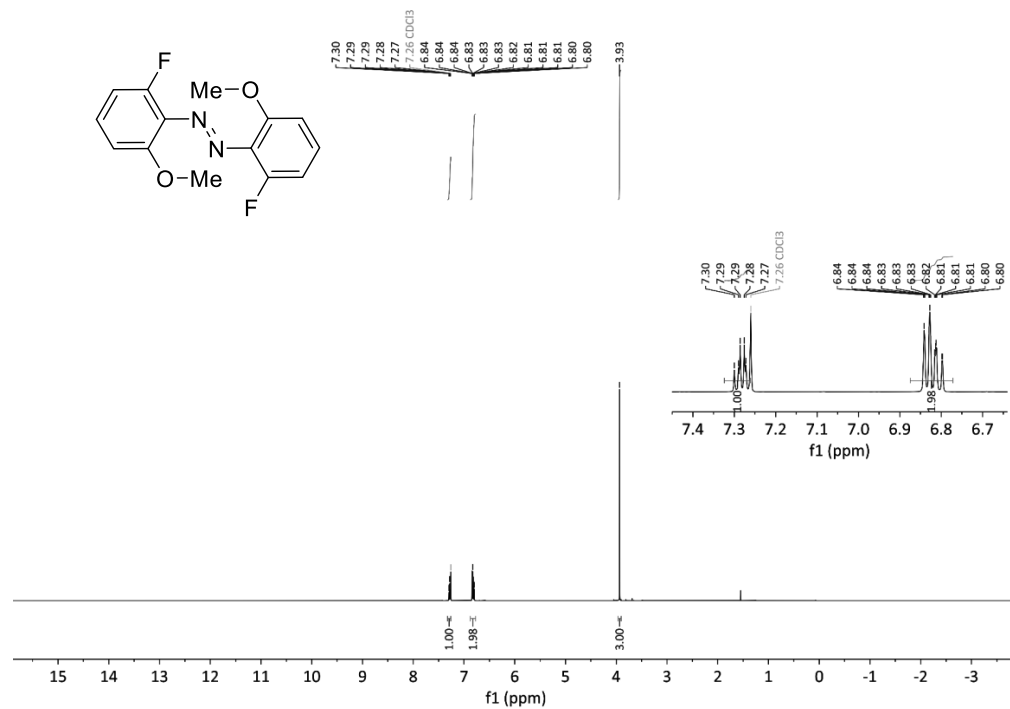


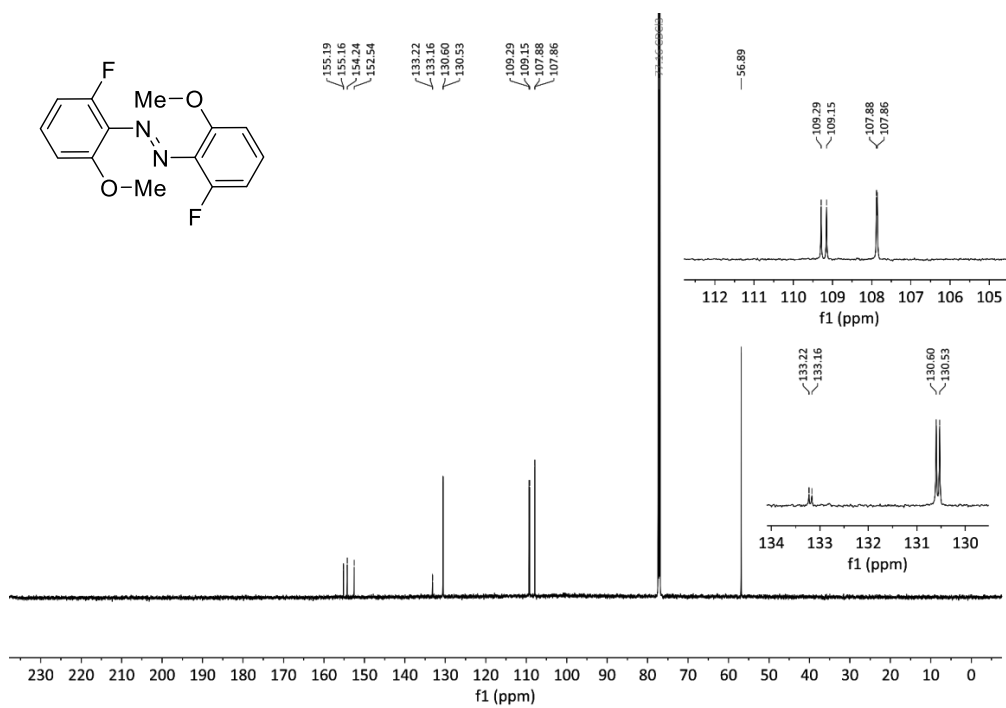
**Figure S49:**  $^1\text{H}$  NMR spectrum of **S9** in  $\text{CDCl}_3$ .



**Figure S50:**  $^{13}\text{C}\{^1\text{H}\}$  NMR spectrum of **S9** in  $\text{CDCl}_3$ .

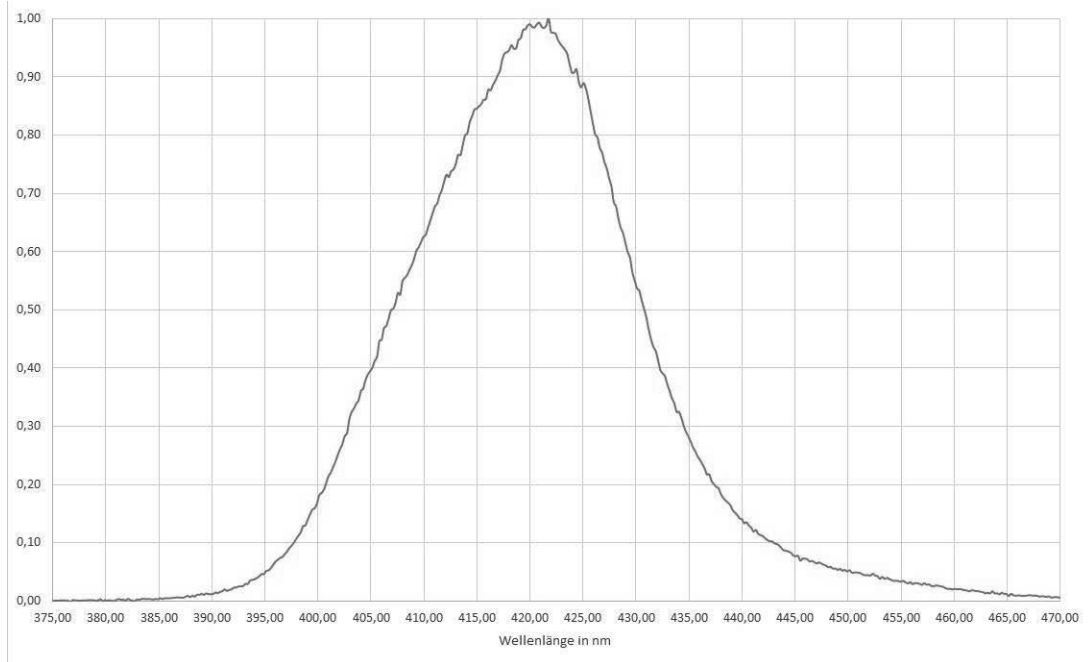


Figure S51:  $^{19}\text{F}$  NMR spectrum of **S9** in  $\text{CDCl}_3$ .Figure S52:  $^1\text{H}$  NMR spectrum of **S10** in  $\text{CDCl}_3$ .



**Figure S53:**  $^{13}\text{C}\{^1\text{H}\}$  NMR spectrum of **S10** in  $\text{CDCl}_3$ .

## 7 Emission spectra of the LED's



**Figure S54:** Spectral measurement of the 420 nm (violet) LED measured by Avonec. Reprinted with permission from Avonec.

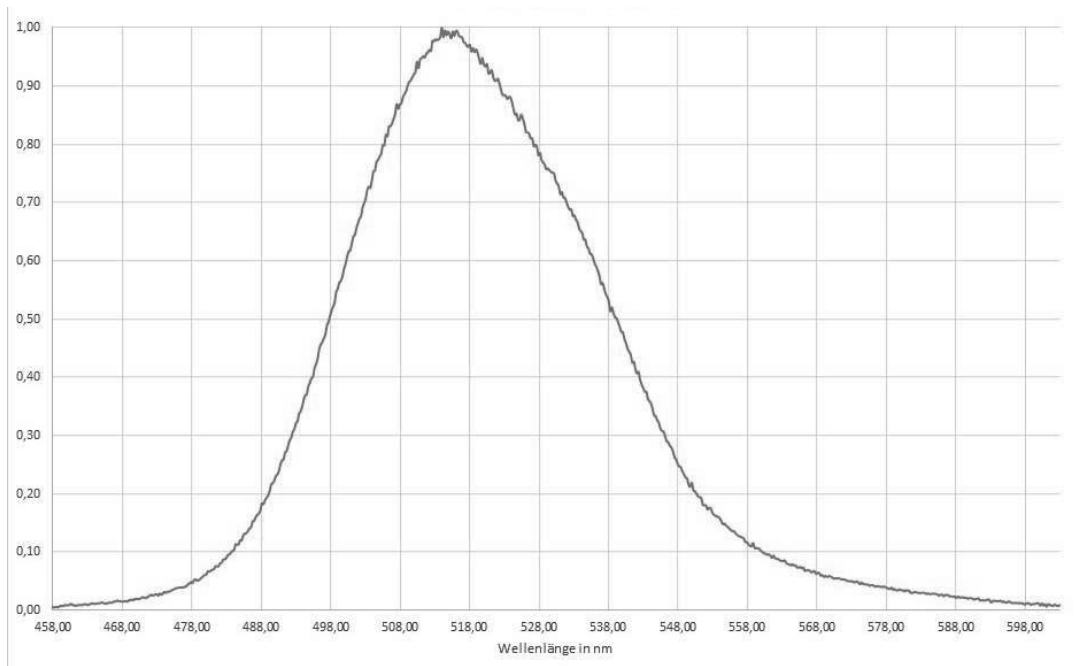


**Figure S55:** Spectral measurement of the 515 nm (green) LED measured by Avonec. Reprinted with permission from Avonec.

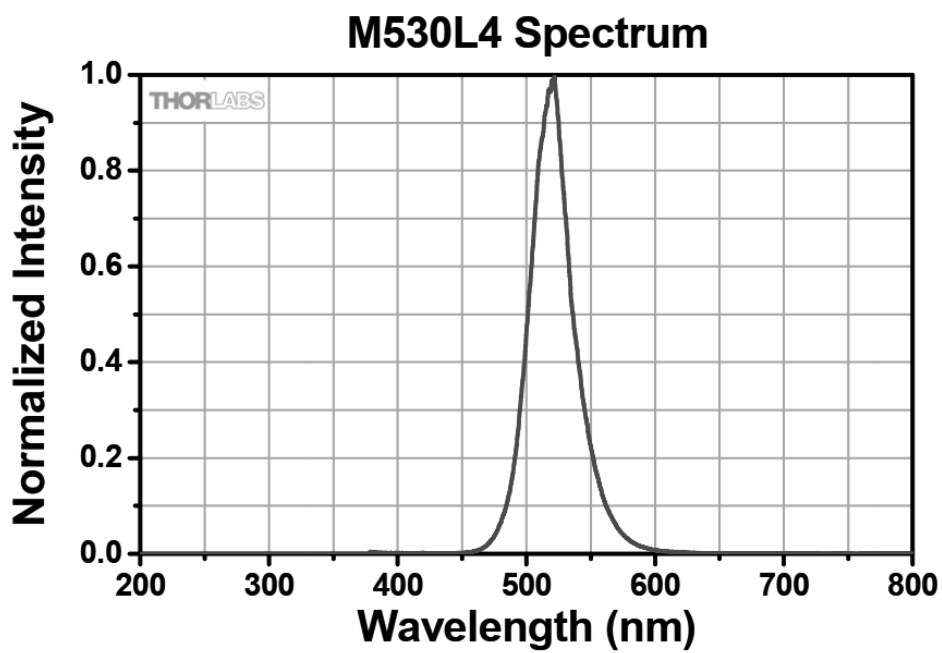


Figure S56: Spectral measurement of the 525 nm (green) LED measured by Thorlabs. Reprinted with permission from Thorlabs.

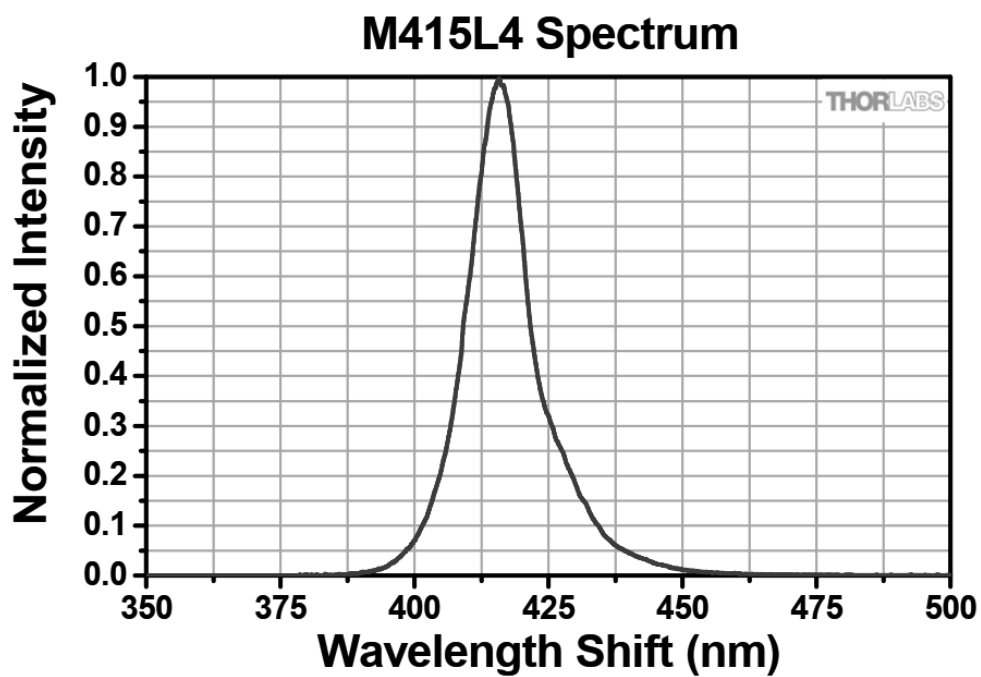


Figure S57: Spectral measurement of the 415 nm (purple) LED measured by Thorlabs. Reprinted with permission from Thorlabs.

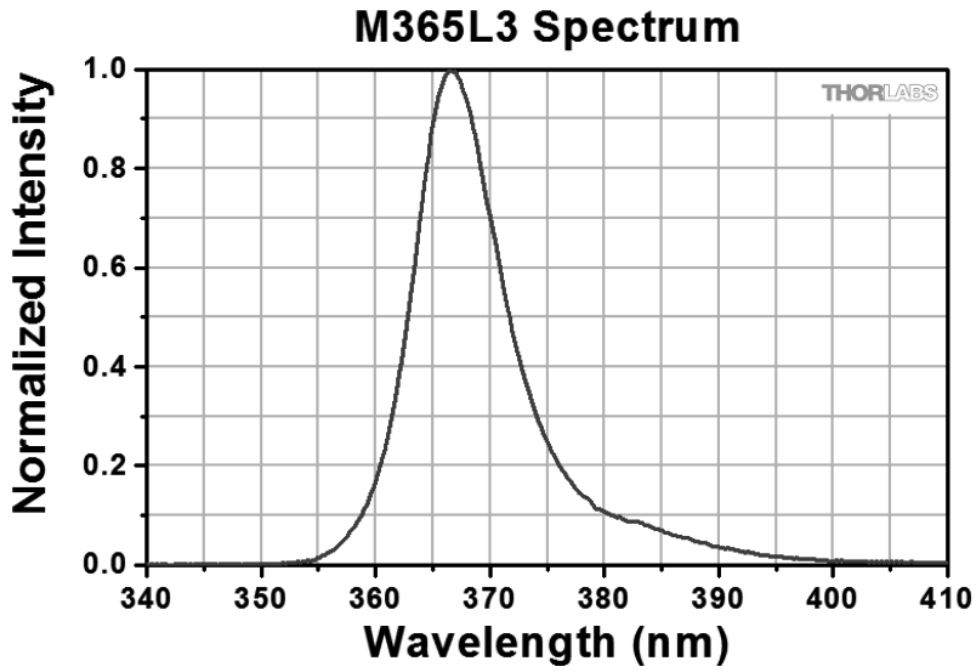


Figure S58: Spectral measurement of the 365 nm (UV) LED measured by Thorlabs. Reprinted with permission from Thorlabs.

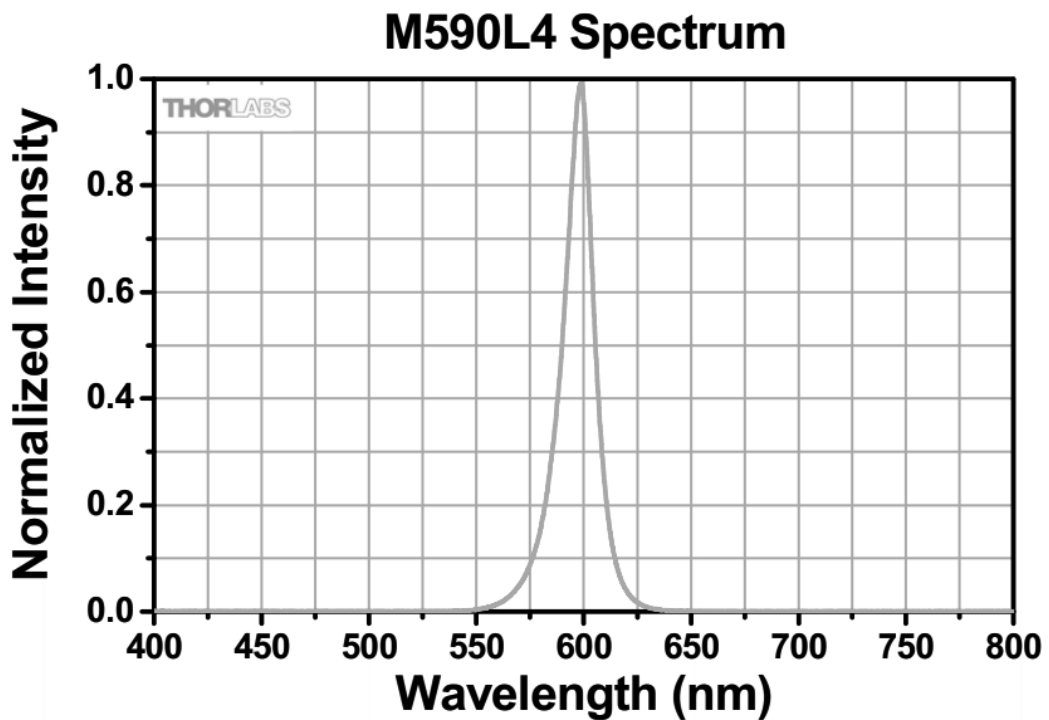


Figure S59: Spectral measurement of the 590 nm (orange) LED measured by Thorlabs. Reprinted with permission from Thorlabs.

## 8. Crystallographic Analysis

Table S7: Crystal data and structure refinement for HOAM, FOAM and 2FOAM and FOME.

	Z-2FOAM	E-2FOAM	Z-FOAM	E-FOAM	Z-HOAM	E-HOAM	Z-FOAM	E-FOME
Formula	C <sub>20</sub> H <sub>12</sub> F <sub>4</sub> N <sub>2</sub> O <sub>2</sub>	C <sub>20</sub> H <sub>12</sub> F <sub>4</sub> N <sub>2</sub> O <sub>2</sub>	C <sub>20</sub> H <sub>14</sub> F <sub>2</sub> N <sub>2</sub> O <sub>2</sub>	C <sub>20</sub> H <sub>14</sub> F <sub>2</sub> N <sub>2</sub> O <sub>2</sub>	C <sub>20</sub> H <sub>16</sub> N <sub>2</sub> O <sub>2</sub>	C <sub>20</sub> H <sub>16</sub> N <sub>2</sub> O <sub>2</sub>	C <sub>14</sub> H <sub>12</sub> F <sub>2</sub> N <sub>2</sub> O <sub>2</sub>	C <sub>14</sub> H <sub>12</sub> F <sub>2</sub> N <sub>2</sub> O <sub>2</sub>
Formula weight, g mol <sup>-1</sup>	388.32	388.32	352.33	352.33	316.35	316.35	278.26	278.26
Crystal system	monoclinic	monoclinic	triclinic	triclinic	triclinic	orthorhombic	monoclinic	orthorhombic
Crystal size, mm	0.485 × 0.336 × 0.196	0.22 × 0.05 × 0.05	0.222 × 0.301 × 0.58	0.3 × 0.2 × 0.05	0.8 × 0.6 × 0.3	0.3 × 0.2 × 0.05	0.31 × 0.18 × 0.07	0.42 × 0.32 × 0.1
Space group	P2 <sub>1</sub> /c	C2/c	P-1	P-1	P-1	P2 <sub>1</sub> 2 <sub>1</sub> 2 <sub>1</sub>	P2 <sub>1</sub> /n	P bca
a, Å	15.8432(7)	36.166(6)	7.5019(7)	9.5908(5)	11.2738(4)	5.230(2)	7.557(3)	7.3159(6)
b, Å	13.4863(6)	4.4672(8)	7.5368(7)	9.7196(5)	11.8460(5)	9.581(4)	13.329(5)	12.9678(13)
c, Å	7.6751(3)	40.429(7)	14.3061(13)	10.4649(6)	12.9378(6)	30.168(11)	12.731(6)	13.4347(12)
α, °	90	90	80.339(3)	115.427(2)	74.490(2)	90	90	90
β, °	100.906(2)	91.364(6)	89.093(3)	105.953(2)	71.876(2)	90	90.101(12)	90
γ, °	90	90	89.053(3)	99.175(2)	75.571(2)	90	90	90
V, Å <sup>3</sup>	1610.29(12)	6530(2)	797.22(13)	802.69(8)	1556.10(12)	1511.5(11)	1282.4(9)	1274.6(2)
Z	4	16	2	2	4	4	4	4
ρ <sub>calcd</sub> , g cm <sup>-3</sup>	1.602	1.580	1.468	1.458	1.350	1.390	1.441	1.450
μ (Mo Kα) (λ=0.71073), mm <sup>-1</sup>	0.136	0.134	0.112	0.111	0.088	0.091	0.117	0.118
F (000)	792.0	3168.0	364.0	364.0	664.0	664.0	576.0	576.0
T, K	100	100	100	100	100	100	100	100
2θ range, deg	6.042 to 61.12	4.506 to 52.74	5.432 to 56.638	4.67 to 54.966	3.866 to 61.166	4.46 to 56.998	4.424 to 53.458	6.066 to 61.022
Index ranges	-22 ≤ h ≤ 22 -19 ≤ k ≤ 19 -10 ≤ l ≤ 9	-44 ≤ h ≤ 44 -5 ≤ k ≤ 4 -49 ≤ l ≤ 50	-10 ≤ h ≤ 10 -10 ≤ k ≤ 10 -19 ≤ l ≤ 19	-12 ≤ h ≤ 12 -12 ≤ k ≤ 12 -13 ≤ l ≤ 13	-16 ≤ h ≤ 16 -16 ≤ k ≤ 16 -18 ≤ l ≤ 18	-6 ≤ h ≤ 6 -12 ≤ k ≤ 11 -38 ≤ l ≤ 34	-9 ≤ h ≤ 9 -16 ≤ k ≤ 16 -16 ≤ l ≤ 16	-10 ≤ h ≤ 10 -16 ≤ k ≤ 18 -19 ≤ l ≤ 17

No. of reflns collected	36741	22489	18773	23850	55343	23263	20997	14871
No. indep.reflins	4913	6558	3952	3686	9527	3206	2725	1943
Goof (F <sup>2</sup> )	[R <sub>int</sub> = 0.0587, R <sub>sigma</sub> = 0.0343]	[R <sub>int</sub> = 0.0659, R <sub>sigma</sub> = 0.0842]	[R <sub>int</sub> = 0.0349, R <sub>sigma</sub> = 0.0274]	[R <sub>int</sub> = 0.0443, R <sub>sigma</sub> = 0.0288]	[R <sub>int</sub> = 0.0294, R <sub>sigma</sub> = 0.0221]	[R <sub>int</sub> = 0.0860, R <sub>sigma</sub> = 0.0558]	[R <sub>int</sub> = 0.0782, R <sub>sigma</sub> = 0.0459]	[R <sub>int</sub> = 0.0404, R <sub>sigma</sub> = 0.0253]
R <sub>1</sub> (F) and wR <sub>2</sub> (F <sup>2</sup> ) ( <i>l</i> > 2σ( <i>l</i> ))	1.036 R <sub>1</sub> = 0.0390, wR <sub>2</sub> = 0.0970	1.111 R <sub>1</sub> = 0.1171, wR <sub>2</sub> = 0.2927	1.042 R <sub>1</sub> = 0.0554, wR <sub>2</sub> = 0.1353	1.012 R <sub>1</sub> = 0.0418, wR <sub>2</sub> = 0.0956	1.022 R <sub>1</sub> = 0.0402, wR <sub>2</sub> = 0.1037	1.093 R <sub>1</sub> = 0.0462, wR <sub>2</sub> = 0.0847	1.046 R <sub>1</sub> = 0.0470, wR <sub>2</sub> = 0.1263	1.068 R <sub>1</sub> = 0.0379, wR <sub>2</sub> = 0.0973
R <sub>1</sub> (F) and wR <sub>2</sub> (F <sup>2</sup> ) (all data)	R <sub>1</sub> = 0.0463, wR <sub>2</sub> = 0.1017	R <sub>1</sub> = 0.1529, wR <sub>2</sub> = 0.3123	R <sub>1</sub> = 0.0673, wR <sub>2</sub> = 0.1439	R <sub>1</sub> = 0.0601, wR <sub>2</sub> = 0.1036	R <sub>1</sub> = 0.0449, wR <sub>2</sub> = 0.1070	R <sub>1</sub> = 0.0682, wR <sub>2</sub> = 0.0912	R <sub>1</sub> = 0.0601, wR <sub>2</sub> = 0.1375	R <sub>1</sub> = 0.0495, wR <sub>2</sub> = 0.1042
Largest diff. peak/hole / e Å <sup>-3</sup>	0.47/-0.20	0.58/-0.38	1.39/-0.30	0.29/-0.30	0.42/-0.21	0.19/-0.25	0.34/-0.23	0.43/-0.24





## 9.3 Appendix Publication IV

### *Supporting Information*

#### **A Photomechanical Film in which Liquid Crystal Design Shifts the Absorption into the Visible Light Range**

*Sven Schultzke*<sup>1,2</sup>, *Nikolai Scheuring*<sup>3</sup>, *Dr. Pim Puylaert*<sup>4</sup>, *Prof. Matthias Lehmann*<sup>3</sup>,  
*Prof. Anne Staubitz*<sup>1,2,\*</sup>

Sven Schultzke, Prof. Anne Staubitz

<sup>1</sup> University of Bremen, Institute for Analytical and Organic Chemistry,  
Leobener Straße 7, D-28359 Bremen, Germany

<sup>2</sup> University of Bremen, MAPEX Center for Materials and Processes,  
Bibliothekstraße 1, D-28359 Bremen, Germany

<sup>3</sup> University of Würzburg, Institute of Organic Chemistry,  
Am Hubland, D-97074 Würzburg, Germany

<sup>4</sup> University of Bremen, Institute for Inorganic Chemistry and Crystallography,  
Leobener Straße 7, D-28359-Bremen, Germany

E-mail: staubitz@uni-bremen.de

\* Correspondence: staubitz@uni-bremen.de; Tel.: +49421/21863210

### Contents

1. General Information .....	2
1.2 Reagents .....	5
1.3 Solvents .....	5
2. Analytical Data .....	7
2.1 Switching Properties of <b>5</b> .....	7
2.1.1 UV-Vis Analysis: Qualitative Switching Behavior of <b>5</b> .....	7
2.1.2 Switching Properties of <b>5</b> .....	8
2.1.3 UV-Vis Spectra After the Irradiation of <b>5</b> with Different Wavelengths in Chloroform and Cyclohexane .....	9
2.1.4 NMR Analysis: Quantitative Switching Behavior of <b>5</b> .....	10
2.2 Liquid Crystal Analysis .....	11
2.2.1 DSC: Phase-Transitions of <b>5</b> up to 170 °C.....	11
2.2.2 TGA: Thermal Stability of <b>5</b> at the Polymerization Temperature (130 °C) .....	12

2.2.3 TGA: Thermal Stability and Decomposition of <b>5</b> .....	12
2.2.4 DSC: Phase-Transition of <b>S8</b> up to 200 °C.....	13
2.2.5 DSC: Phase-Transition of <b>6</b> up to 250 °C.....	14
2.2.6 Crystal Structure Analysis of <b>6</b> .....	15
2.3 Analysis of the Polymer .....	18
2.3.1 DSC: Phase-Transition of <b>P<sub>Splay,105</sub></b> up to 200 °C .....	18
2.3.2 WAXS Measurements of the Homogeneously Aligned Polymer Film <b>P<sub>Planar,49</sub></b> .....	19
2.3.3 UV-Vis Analysis with Different Wavelength Irradiation of <b>P<sub>Planar,31</sub></b> .....	20
2.3.4 Photochemical Bending of <b>P<sub>Splay,60</sub></b> by Irradiation.....	20
2.3.5 Bending of <b>P<sub>Splay,60</sub></b> and Relaxation in the Dark .....	22
2.3.6 UV-Vis Analysis: Relaxation of <b>P<sub>Planar,31</sub></b> after Irradiation with 525 nm .....	22
2.3.7 UV-Vis Analysis: Relaxation of <b>P<sub>Planar,31</sub></b> after Irradiation with 525 nm Determined at 440 nm. ..	23
2.3.8 IR-Analysis: Thermal Heating during Irradiation of <b>P<sub>Splay,40</sub></b> and <b>P<sub>Splay,60</sub></b> .....	24
3.1. Comparison of the Transparency Depending on the Alignment and Thickness. ....	26
4. Syntheses.....	28
4.1 9-Bromononyl acrylate ( <b>S1</b> ).....	28
4.2 9-(4-hydroxyphenoxy)nonyl acrylate ( <b>2</b> ).....	28
4.3 4-Bromo-2,6-difluoroaniline ( <b>S2</b> ) <sup>[5]</sup> .....	29
4.4 4-Amino-3,5-difluorobenzonitrile ( <b>S3</b> ) <sup>[6]</sup> .....	29
4.5 4-Amino-3,5-difluorobenzoic acid ( <b>S4</b> ) <sup>[6]</sup> .....	30
4.6 Ethyl 4-amino-3,5-difluorobenzoate ( <b>S5</b> ) <sup>[6]</sup> .....	30
4.7 ( <i>E</i> )-4,4'-(Diazene-1,2-diyl)bis(3,5-difluorobenzoic acid) ( <b>S6</b> ) <sup>[9]</sup> .....	31
4.8 ( <i>E</i> )-4,4'-(Diazene-1,2-diyl)bis(3,5-difluorobenzoic acid) ( <b>S7</b> ) <sup>[6]</sup> .....	32
4.9 ( <i>E</i> )-4,4'-(Diazene-1,2-diyl)bis(3,5-difluorobenzoyl chloride) ( <b>4</b> ).....	32
4.10 ( <i>E</i> )-4,4'-(Diazene-1,2-diyl)bis(3,5-difluorobenzoic acid) ( <b>5</b> ).....	33
4.11 Bis(9-(acryloyloxy)nonyl) 4,4'-(diazene-1,2-diyl)( <i>E</i> )-bis(3,5-difluorobenzoate) ( <b>S8</b> ).....	34
4.12 Bis(4-hexylphenyl) 4,4'-(diazene-1,2-diyl)( <i>E</i> )-bis(3,5-difluorobenzoate) ( <b>6</b> ).....	34
5. References.....	35
6. <sup>1</sup> H, <sup>13</sup> C{ <sup>1</sup> H} and <sup>19</sup> F NMR Spectra of the Purified Compounds.....	36
7. Emission spectra of the LED's.....	54
8. Crystallographic Analysis.....	58

## 1. General Information

For reactions under inert conditions, a nitrogen filled glovebox (Pure Lab<sup>HE</sup> from Inert, Amesbury, MA USA) and standard Schlenk techniques were used.

All glassware was dried in an oven at 200 °C for several hours prior to use. NMR tubes were dried in an oven at 110 °C for several hours prior to use.

NMR spectra were recorded on a Bruker Avance Neo 600 (Bruker BioSpin, Rheinstetten, Germany) (600 MHz ( $^1\text{H}$ ), 151 MHz ( $^{13}\text{C}\{^1\text{H}\}$ ), 565 MHz ( $^{19}\text{F}$ ) at 298 K. All  $^1\text{H}$  NMR and  $^{13}\text{C}\{^1\text{H}\}$  NMR spectra were referenced to the residual proton signals of the solvent ( $^1\text{H}$ ) or the solvent itself ( $^{13}\text{C}\{^1\text{H}\}$ ).  $^{19}\text{F}$  NMR spectra were referenced internally against trichlorofluoromethane. The exact assignment of the peaks was performed by two-dimensional NMR spectroscopy such as  $^1\text{H}$  COSY,  $^{13}\text{C}\{^1\text{H}\}$  HSQC and  $^1\text{H}/^{13}\text{C}\{^1\text{H}\}$  HMBC when possible.

High-resolution EI mass spectra were recorded on a MAT 95XL double-focusing mass spectrometer from Finnigan MAT (Thermo Fisher Scientific, Waltham, MA, USA) at an ionization energy of 70 eV. Samples were measured by a direct or indirect inlet method with a source temperature of 200 °C. High-resolution ESI and APCI mass spectra were measured by a direct inlet method on an Impact II mass spectrometer from Bruker Daltonics (Bruker Daltonics, Bremen, Germany).

IR spectra were recorded on a Nicolet i510 FT-IR spectrometer from Thermo Fisher Scientific (Thermo Fisher Scientific, Waltham, MA, USA) with a diamond window in an area from 500 – 4000  $\text{cm}^{-1}$  with a resolution of 4  $\text{cm}^{-1}$ . All samples were measured 16 times against a background scan.

Melting points were recorded on a Büchi Melting Point M-560 (Büchi, Essen, Germany) and are reported corrected.

UV-vis spectra were recorded with a resolution of 0.5-0.1 nm on a UV-2700 spectrometer from Shimadzu (Shimadzu, Kyoto, Japan) with a double monochromator. In all cases, chloroform (spectroscopy grade), toluene (spectroscopy grade) or cyclohexane (spectroscopy grade) were used as a solvent.

For the UV switching experiments LED lamps with 340 nm, 365 nm (Ocean Optics USB 4000, Sahlmann Photochemical Solutions, Bad Segeberg, Germany) full width at half maximum (FWHM) (10 nm, 1.0 W), 443 nm, 470 nm, 525 nm, 565 nm and 627 nm LED lamp (Ocean Optics USB 4000, Sahlmann Photochemical Solutions, Bad Segeberg, Germany, FWHM 19 nm, 0.9 W) were used, while a constant distance towards the cuvettes of 1 cm was ensured. The samples were measured immediately after irradiation. Additionally, a 420 nm (1.0 W) and a 525 nm LED (1.0 W) from EPILED was built in our laboratories. These additional LEDs were matching the absorbance of the azobenzene investigated in this paper and could be run for several hours for polymerization.

To facilitate the photochemical bending of the polymers, we employed LED modules provided by Thorlabs (Bergkirchen, Germany). These modules were powered by a UPLED power supply and focused using a collimator. The following high-power LED modules were utilized: M365L3 (365 nm), M415L4 (415 nm), M530L4 (530 nm), M590L4 (590 nm), and MWWHL4 (3000 K, "warm white"). The light intensity was measured using an ILT2400 hand-held light meter manufactured by International Light Technologies, Inc., (Peabody, USA). For linear polarization of the light, we used high contrast polarizing films (400-700 nm) obtained from Edmund Optics (York, UK). The polarization direction was determined using a polarization tester also provided by Edmund Optics.

Thermal analyses were performed on a standalone Mettler Toledo DSC 3+ STAR (Mettler-Toledo, Columbus, OH, USA) or a Mettler Toledo TGA/DSC 3+ System (Mettler-Toledo, Columbus, OH, USA), where 40  $\mu\text{L}$  aluminum crucibles were used. In DSC experiments, pierced lids were used. A standard measurement of an azobenzene derivative included an isothermal treatment at 100 °C for 60 min before running the thermal analysis. This ensured a full conversion to the Z-isomer of the azobenzene derivative. All analysis were run from -40 °C up to the desired temperature. Thermo analytical data were analyzed with the STARe software (Version 16.00, Mettler-Toledo, Columbus, OH, USA) by Mettler Toledo and further plotted with the Origin Pro software. IR measurements were realized and recorded with a FLIR ONE Pro infrared camera. (Teledyne FLIR Systems, OR, USA).

WAXS investigations were performed on a Bruker Nanostar (Detector Vantec2000, Microfocus copper anode X-ray tube Incoatec). The compound was transferred to Mark capillaries, which were sealed and glued into a metal sample holder, where the liquid crystal phase was uniform aligned using ring magnets (1 Tesla). The XRS data were evaluated using the program Datasqueeze<sup>[1]</sup> with silver behenate as a calibration standard. The correlation lengths were estimated using the Scherrer formula.<sup>[2]</sup> The studies of optical textures of the mesophases were realized with a Nikon Eclipse LV100Pol optical polarizing microscope equipped with a Linkam LTS420 heating stage and a Linkam T95-HS system controller. Single crystal X-ray diffraction data were collected at 100 K using an open flow nitrogen stream on a Bruker Venture D8 diffractometer (Bruker, Karlsruhe, Germany) with a Photon 100 detector in shutterless mode with Mo-K $\alpha$  (0.7107 Å) radiation. All structures were solved by intrinsic phasing and refined based on  $F^2$  by use of the SHELX program package, as implemented in OLEX2<sup>[3]</sup> All non-hydrogen atoms were refined using anisotropic displacement parameters. Hydrogen atoms attached to carbon atoms were included in geometrically calculated positions using a riding model. The crystal was obtained by slow evaporation of an *n*-hexane/dichloromethane mixture at 20 °C.

Polymerization was performed on a Linkam LTS-420 heating stage in between PI coated glass slides. The glass slides were spin-coated with a 5 wt% PI solution in NMP and dried for 1h at 100 °C and another 24 h at 200 °C in a dry oven.

For splay alignment: One of the glass slides was rubbed along a one axis using a velvet cloth before use.

For homogeneous alignment: Both glass slides were rubbed along an axis using a velvet cloth before use and placed in an antiparallel configuration to avoid disturbance due possible pre-tilts of the mesogen.

For homeotropic alignment: No rubbing was performed, or an untreated clean glass substrate could be used.

To form the LC cell, a stripe of a 10, 30, or 50  $\mu\text{m}$  thin PTFE film was used as a spacer. The LC cell was then glued together using the UV-curing acrylate adhesive NOA61 from Norland Optical Adhesive. The monomer mixture was introduced into the LC cell through capillary action in the isotropic phase (155 °C). Subsequently, the temperature was slowly decreased at a rate of 0.5 K/min until reaching the polymerization temperature (130 °C). This temperature was maintained for 30 minutes to allow mesogen alignment.

Afterwards, a LED with a wavelength of 420 nm was used to irradiate the LC cell through a linear polarizer that was orthogonal to the planar alignment. In this way, the photocatalyst could be activated without inducing azobenzene switching. Additionally, a PMMA slide was placed between the light source and the LC cell to block UV-range irradiation.

The final thickness of the films was measured using a digital caliper type 6012/1 (DIN 863,  $\pm 1 \mu\text{m}$ ) from Richter Messwerkzeuge (95469 Speichersdorf, Germany). The alignment direction was assessed using a linear polarizer.

Thin layer chromatography (TLC) was performed using TLC Silica gel 60 F<sub>254</sub> from Merck (Merck, Darmstadt, Germany) and the compounds were visualized by exposure to UV light at a wavelength of 254 nm. Column chromatography was performed manually using silica gel 60 (0.015-0.040 mm) from Merck (Merck, Darmstadt, Germany). The samples were applied via dry load with Celite® 503 (Macherey-Nagel, Düren, Germany) as column material. If stated, Celite® 503 was used as filtration aid.

The use of abbreviations follows the conventions from the ACS Style guide.<sup>[4]</sup>

## 1.2 Reagents

All chemicals were commercially available and used without purification unless stated otherwise.

**Table S1.** List of supplier and purity of used chemicals.

Reagent	Supplier, Purity	Comments
Acryloyl chloride	Acros Organics, 96%	stab. with 400 ppm phenothiazine
Bis[2,6-difluoro-3-(1-hydropyrrol-1-yl)phenyl]titanocene; 97%	Abcr, 97%	
9-Bromo-1-nonanol	Sigma-Aldrich, 95%	
<i>N</i> -Bromosuccinimide	Sigma Aldrich, 98%	
Copper (I) cyanide	TCI, >98.0%	
1,8-Diazabicyclo[5.4.0]undec-7-ene	Apollo Scientific, 99.7 (GC)	
4-Ethylaniline	Sigma-Aldrich, 98%	
<i>d</i> -Glucose	Sigma-Aldrich, 99.5%	
Hydroquinone	TCI, >99.0%	
<i>N,N'</i> -Dicyclohexycarbodiimide	Alfa Aesar, 99%	
4-Nitrobenzoic acid	Alfa Aesar, 99%	
Magnesium sulfate	VWR, 99.2%	
Oxone, monopersulfate	Abcr, -	
Potassium iodide	Abcr, 99.5%	
Polyimide Powder P84	Ensinger	Sample provided by Ensinger
Sodium carbonate	Chem Solute, 99.8%	
Sodium chloride	CarlRoth, >99.5%	
Sodium hydroxide	VWR, 98.6%	
Thionyl chloride	Acros Organics 99.7%	
Triethyl amine	Fluorochem, 99% (anhydrous)	degassed, stored in a glovebox

## 1.3 Solvents

All solvents for purification and extraction were used as received. All solvents used for synthesis under inert conditions were dried by a solvent purification system (SPS) from Inert Technologies.

**Table S2.** List of supplier and purity of used solvents.

Solvent	Supplier and Purity	Comments
Acetic Acid	Merck $\geq 99.8\%$	
Acetone	Sigma Aldrich	
Acetonitrile	Fisher Scientific 99.5%	
Aq. Ammonia (25%)	Merck, 25% aq. puriss. p.a.	
Benzene- <i>d</i> <sub>6</sub>	Eurisotop, 99.5%	
Chloroform	VWR, 99.0% + 0.6 % EtOH (stab.)	
Chloroform- <i>d</i> <sub>1</sub>	Euroisotop 99.8%	
Cyclohexane	Merck $\geq 99.5\%$ (GC)	
DCM	Merck $\geq 99.9\%$ (GC)	
DMF	Acros Organics 99.8%	Extra dry, AcroSeal™
DMSO	VWR technical grade	
DMSO- <i>d</i> <sub>6</sub>	Sigma Aldrich, 99.9%	

## 9 Appendix

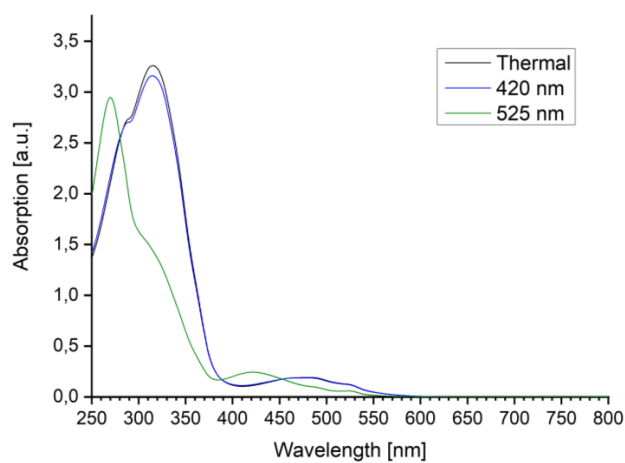
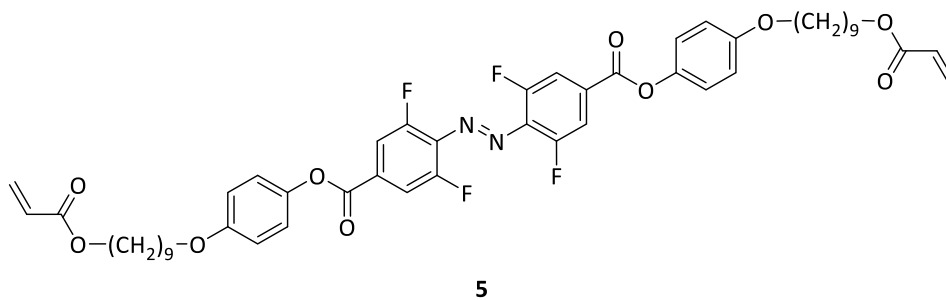
Ethanol	VWR $\geq 99.8\%$	absolute
Ethyl acetate	Merck $>99.5\%$ (GC)	
Hydrochloric acid (37%)	Merck, fuming $>37.0\%$	
Methanol	VWR $>99.8\%$ (GC)	
<i>n</i> -Hexane	Merck, $>95\%$	
<i>N</i> -Methyl-2-pyrrolidone	Fisher Scientific, $99.5\%$	Extra dry, AcroSeal™
Sulfuric acid	Merck $95\%$	
Tetrahydrofuran	VWR HPLC grade	anhydrous from SPS, stored in a glovebox
Tetrahydrofuran	Fisher Scientific $\geq 99.8\%$	
Toluene	Merck $>99.7\%$ (GC)	
Toluene	Merck $>99.7\%$ (GC)	anhydrous from SPS, stored in a glovebox
Water	deionized	

---

## 2. Analytical Data

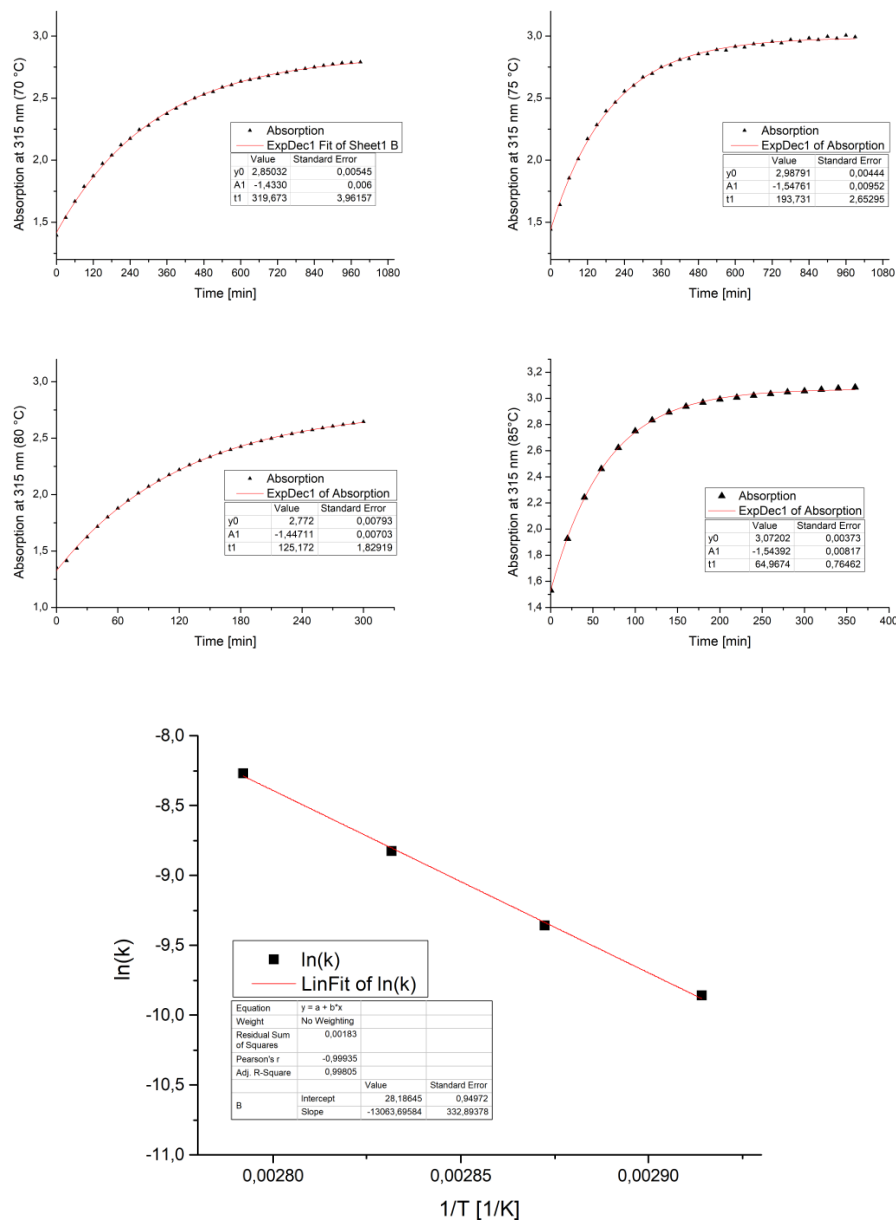
### 2.1 Switching Properties of **5**

#### 2.1.1 UV-Vis Analysis: Qualitative Switching Behavior of **5**



**Figure S1.** UV-vis spectrum of **5** in chloroform after thermal treatment and irradiation with green and violet light respectively.

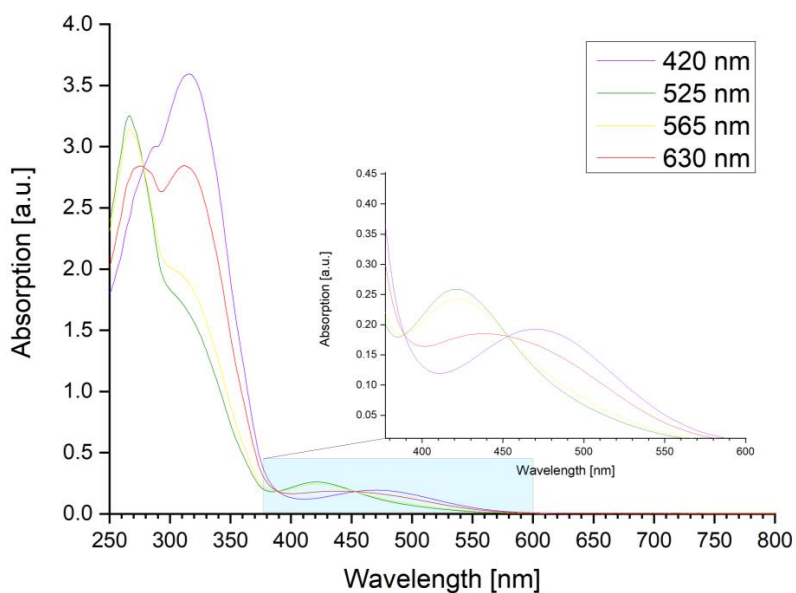
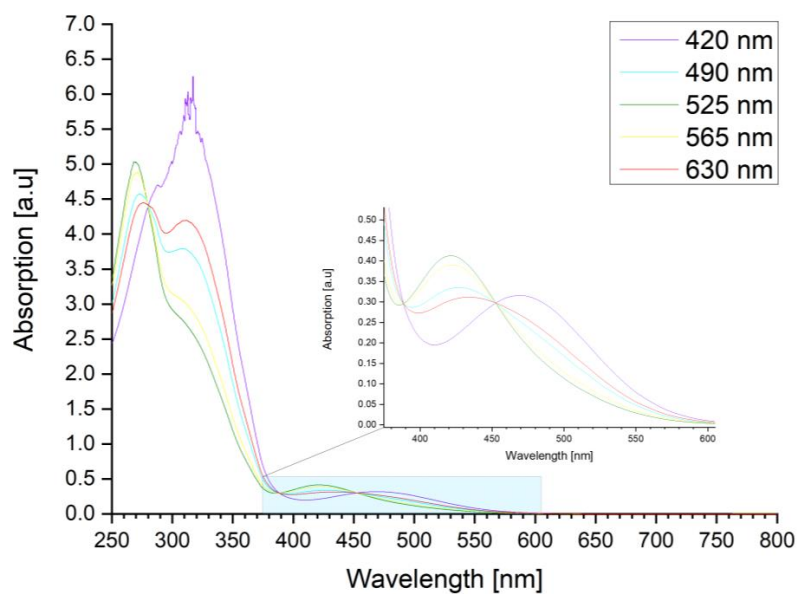
## 2.1.2 Switching Properties of 5



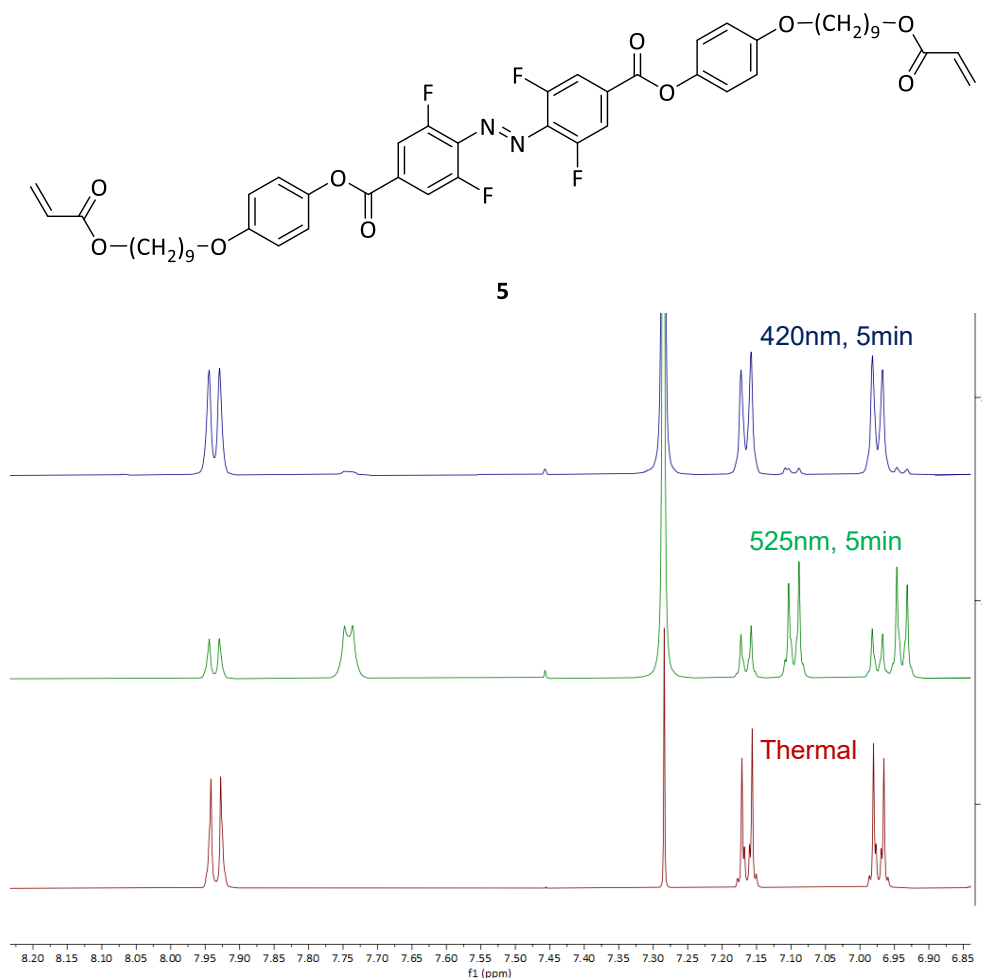
**Figure S2.** Half-life time measurement of **5** after irradiation with green light (525 nm) with a concentration of  $120 \mu\text{mol mL}^{-1}$  in toluene. The half-life time for the thermal relaxation was determined at 85 °C, 80 °C, 75 °C and 70 °C by an exponential fit for the absorption at 315 nm. The half-life time for **5** at 25 °C was then estimated by an Arrhenius-Plot based on the measurements at higher temperatures. The rate constant  $k$  was  $1.63 \cdot 10^{-7} \text{s}^{-1}$ , which translates to a half-life time  $t_{1/2}$  of 49 d at 25 °C.



### 2.1.3 UV-Vis Spectra After the Irradiation of 5 with Different Wavelengths in Chloroform and Cyclohexane



**Figure S3.** UV-vis spectrum of **5** in chloroform (top) and cyclohexane (bottom) after irradiation with different wavelengths for 1 min. Every illumination experiment was performed with a solution that had been brought into the PSS beforehand by illuminating it with 420 nm.

2.1.4 NMR Analysis: Quantitative Switching Behavior of **5**

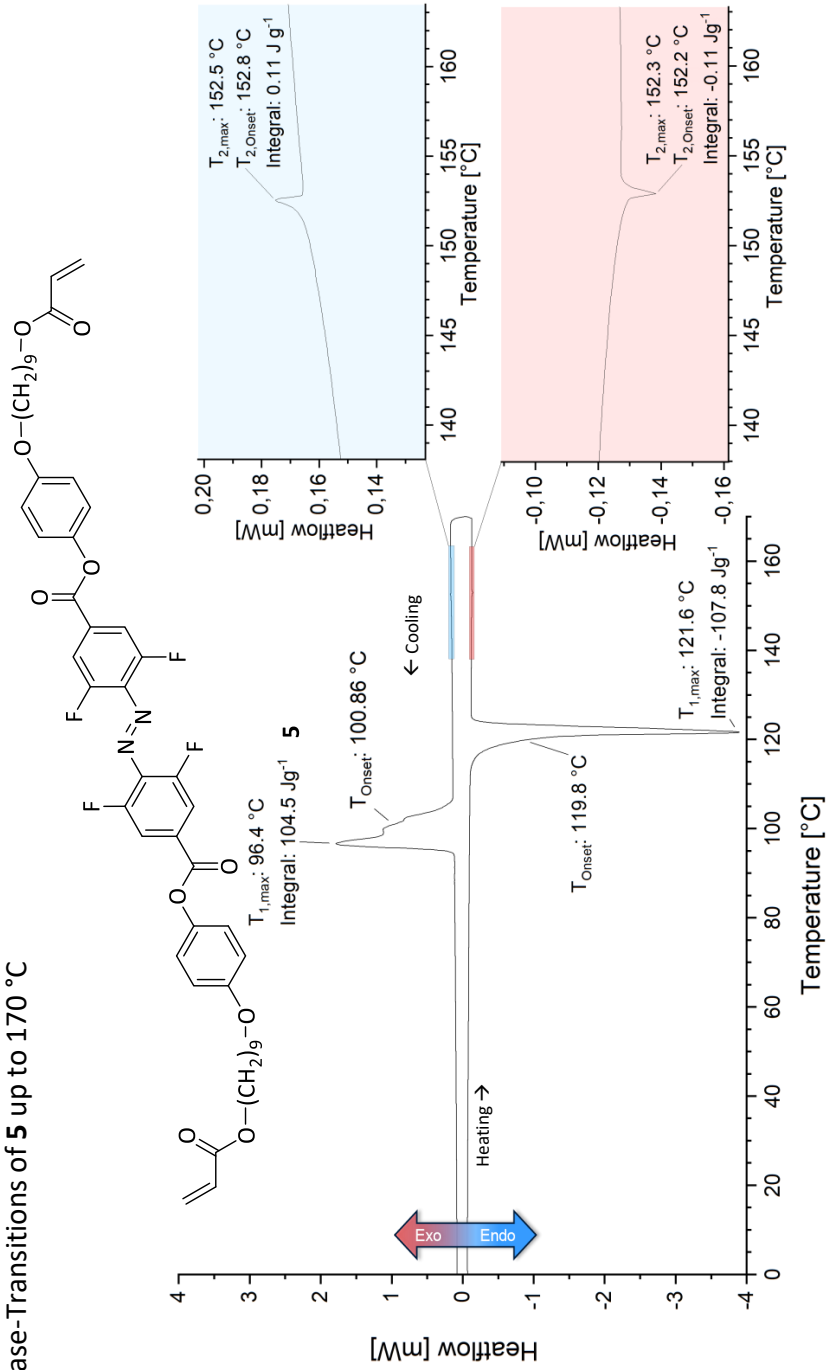
**Figure S4.** NMR spectroscopic study of the irradiation of **5** in  $\text{CDCl}_3$  after thermal treatment\* (red spectrum), after irradiation with green light (525 nm) and violet light (420 nm) for 5 min each.

**Table S3.** Summary of all NMR spectroscopic studies of the irradiation of **5**, after irradiation with different wavelengths in the solvents chloroform- $d$  and benzene- $d_6$ . The % values for the *E* and *Z* isomer were obtained by the integration of the aromatic proton signal.

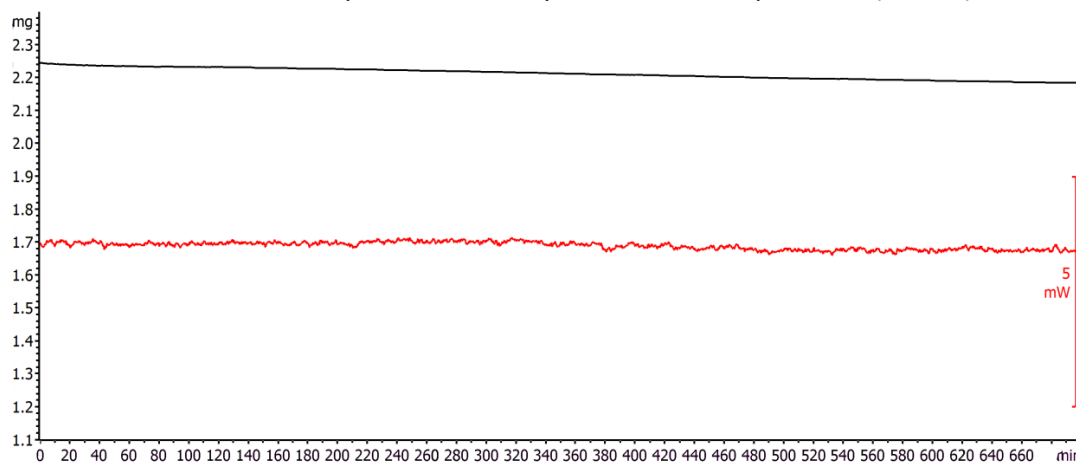
	Chloroform- $d$		Benzene- $d_6$	
	<i>E</i>	<i>Z</i>	<i>E</i>	<i>Z</i>
Thermal	100%	0%	100%	0%
420 nm	93%	7%	92%	8%
490 nm	53%	47%	57%	43%
525 nm	30%	70%	30%	70%
565 nm	39%	61%	35%	65%

\*Thermal treatment: Heating **5** up to 120°C for 24 h before dissolving the compound in the NMR solvent.

## 2.2 Liquid Crystal Analysis

2.2.1 DSC: Phase-Transitions of **5** up to 170 °C

**Figure S5.** DSC curve of **5** (6.0481 mg) with a heating rate of 5 K/min for the temperature range -40 °C to 170°C. Right: Zoomed in area of the nematic to isotropic phase transition.

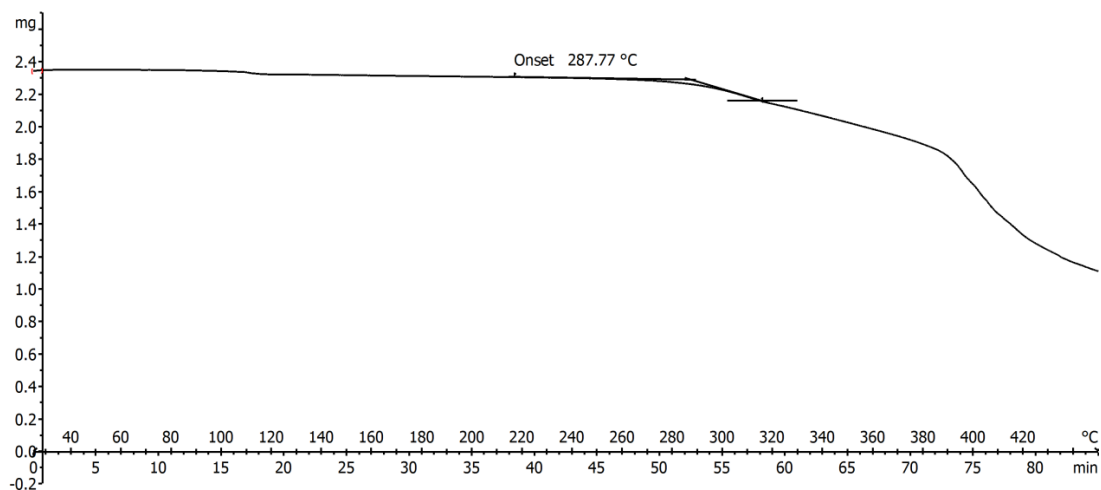
2.2.2 TGA: Thermal Stability of **5** at the Polymerization Temperature (130 °C)

**Figure S7.** Isothermal TGA at 130 °C of **5** (2.26709 mg) in a 40  $\mu$ L aluminum crucible under  $N_2$  (20 mL  $min^{-1}$ ) over 700 min.

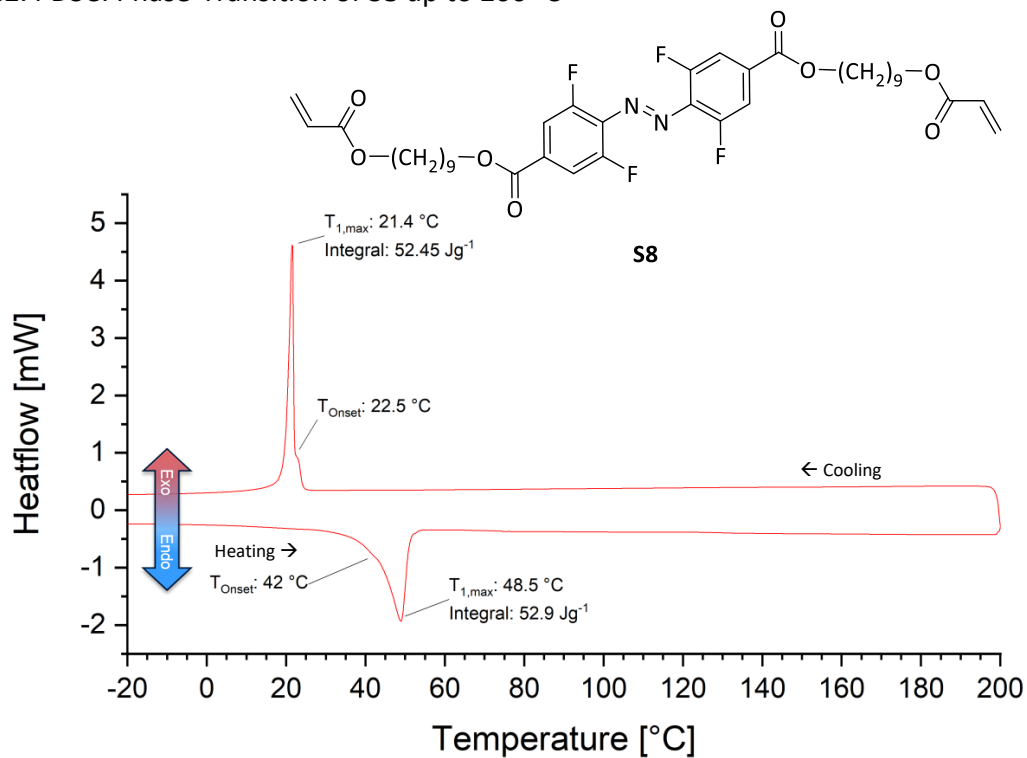
An isothermal TGA experiment combined with a DSC analysis of the monomer **5** was performed. Over a time of 700 mins with a T of 130 °C and a gas flow of  $N_2$  20 mL  $min^{-1}$  no appreciable weight loss occurred. Also, there was no significant change in the heat flow. From this, it can be concluded that the monomer **5** neither decomposes at this temperature nor that it polymerizes to any significant extent.

2.2.3 TGA: Thermal Stability and Decomposition of **5**

The monomer was thermally stable up to an onset temperature of 288 °C, at which temperature a weight loss step occurred, indicating decomposition of the sample.

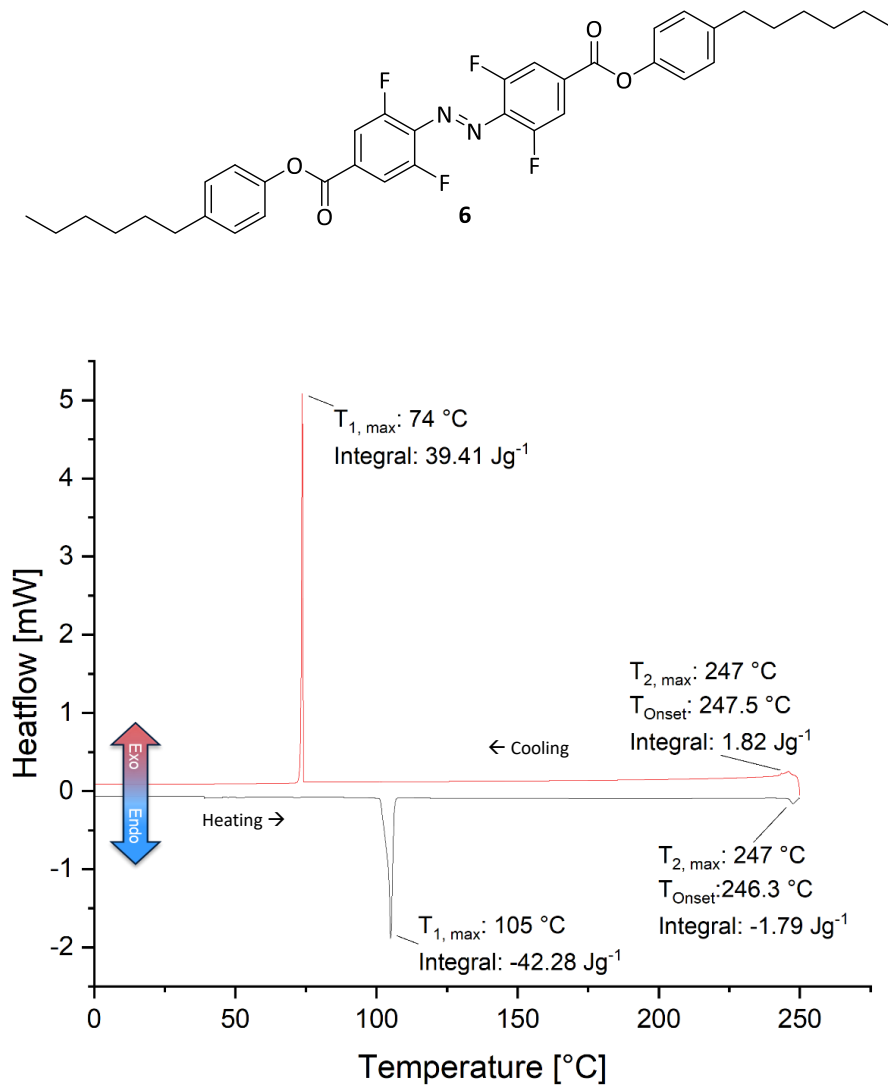


**Figure S8.** TGA Ramp with 5 K/min of **5** (2.34154 mg) in a 40  $\mu$ L aluminum crucible under  $N_2$  (20 mL/min) up to 450 °C.

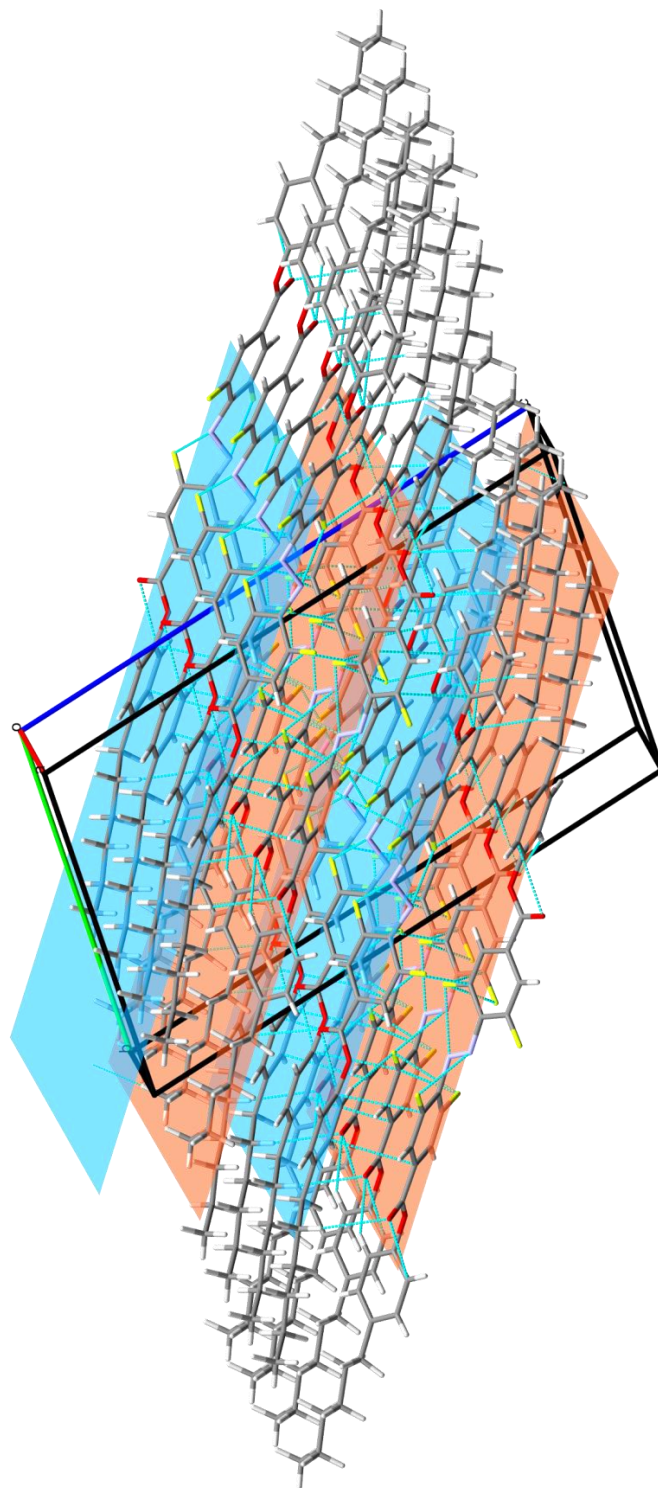
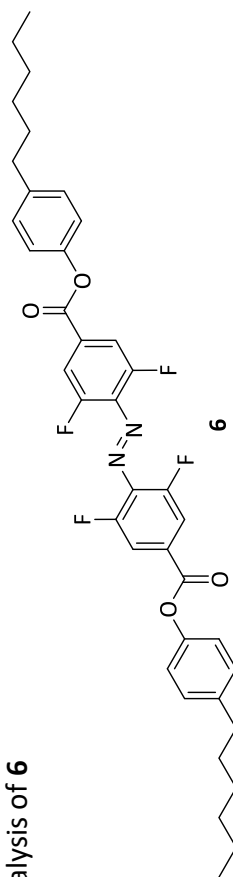
2.2.4 DSC: Phase-Transition of **S8** up to 200 °C

**Figure S9.** DSC curve of **S8** (3.5658 mg) with a heating rate of 5 K/min for the temperature range -40 °C to 200 °C.

The monomer **S8** without the extended core showed (in comparison to monomer **5**) no signs of liquid crystallinity in the DSC (Figure S8) and POM (not shown).

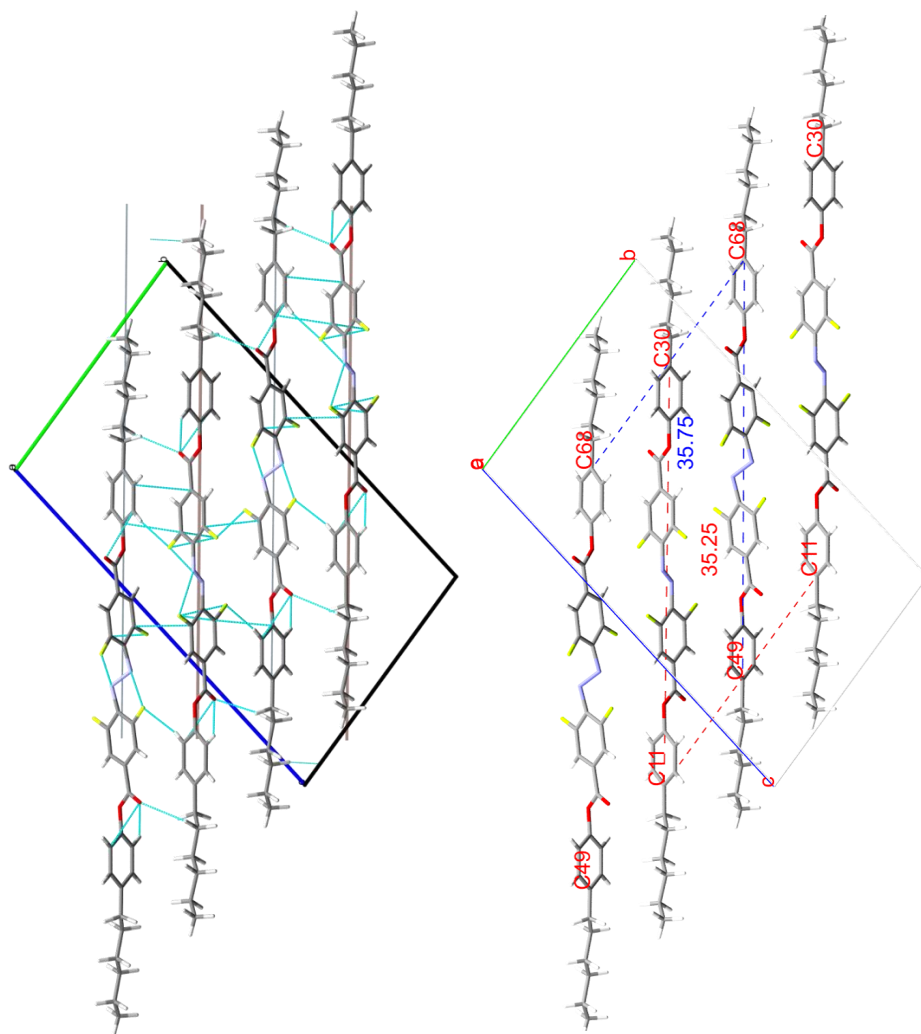
2.2.5 DSC: Phase-Transition of **6** up to 250 °C

**Figure S10.** DSC curve of **6** (3.9546 mg) with a heating rate of 5 K/min for the temperature range -20 °C to 250 °C for the second cycle.

2.2.6 Crystal Structure Analysis of **6**

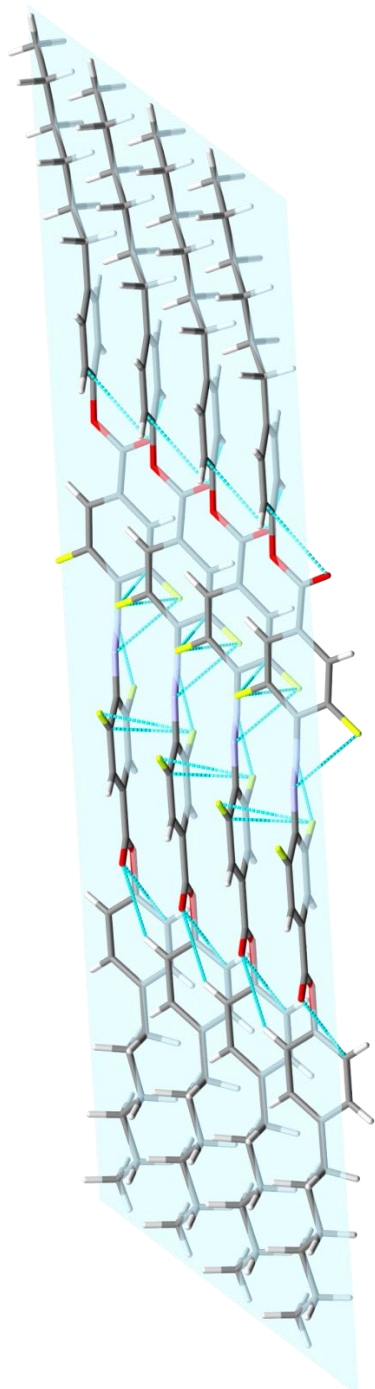
**Figure S11.** Crystal structure of **6** in its clustered alignment showing intermolecular interaction within the plane and between the levels marked in red and blue.

15



**Figure S12.** Crystal structure of **6** seen in the axis of the plane to distinguish the intermolecular forces between layers. (top) Tilt angle between the mesogens. As the mesogens show an internal torsion due to the fluorine atoms and thus is not entirely flat, the angle can only be defined between every second layer (marked in red and blue in **Figure S11**). As an approximation, the mesogen was modelled by a straight line from atom C30 to atom C49 and atom C11 to atom C68 respectively. (bottom)

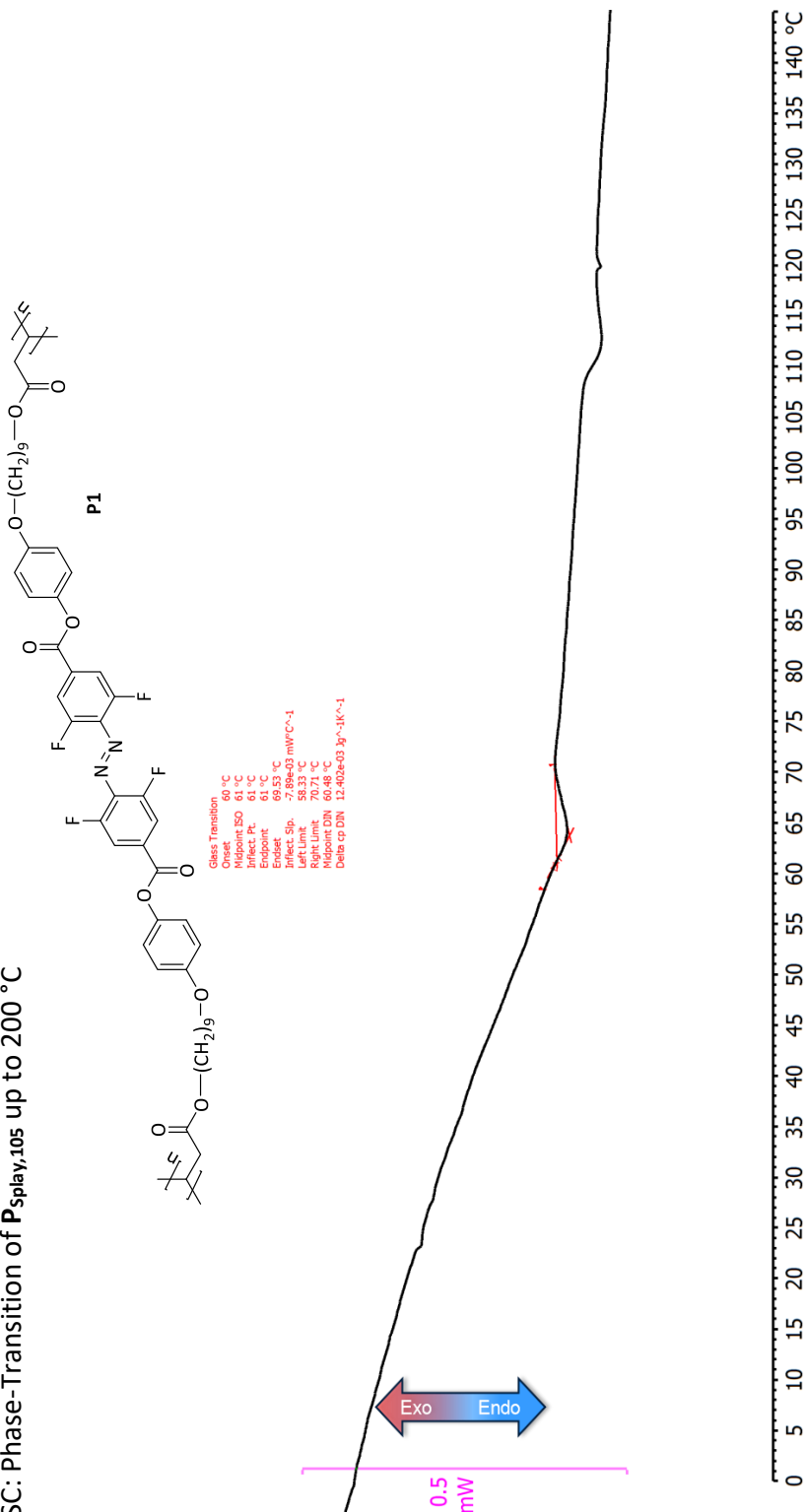




**Figure S13.** Crystal structure of **6** seen on top of a single plane to distinguish the intermolecular forces within the layer.

### 2.3 Analysis of the Polymer

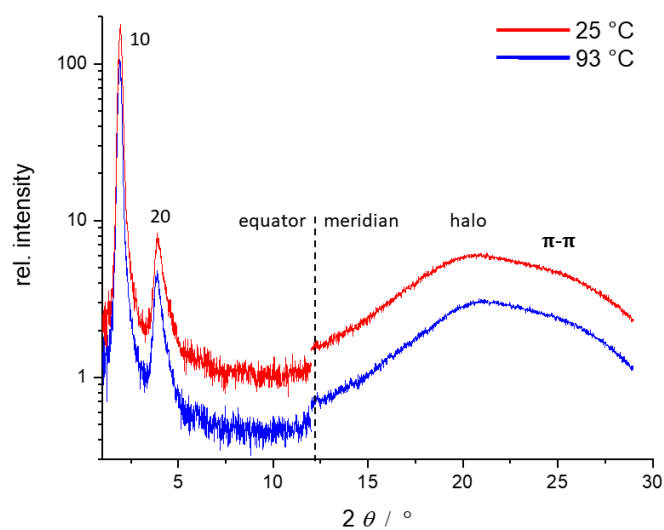
#### 2.3.1 DSC: Phase-Transition of P<sub>Splay,105</sub> up to 200 °C



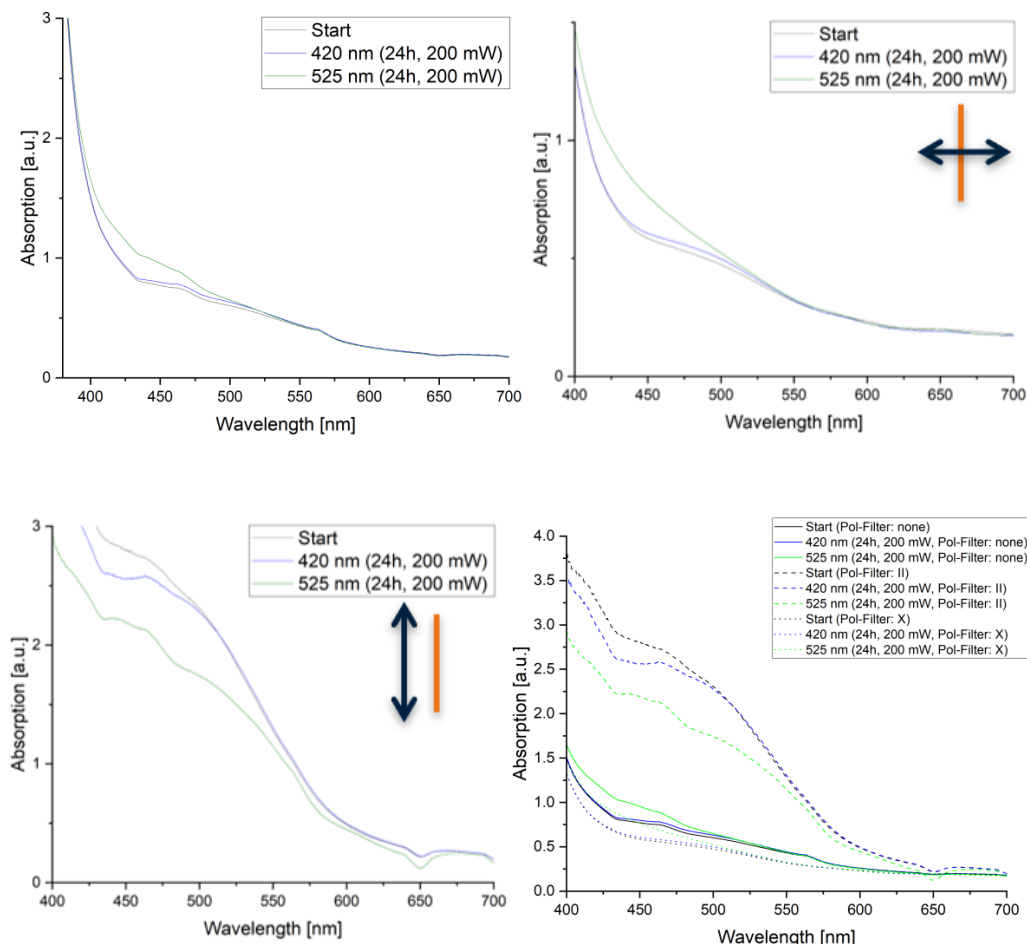
**Figure S14.** DSC curve of P<sub>Splay,105</sub> (3.3714 mg) with a heating rate of 10 K/min for the temperature range -40 °C to 170°C.

2.3.2 WAXS Measurements of the Homogeneously Aligned Polymer Film  $P_{\text{Planar},49}$ 

Temperature-dependent WAXS studies of the  $P_{\text{Planar},49}$  polymer film reveal that the synclitic SmC phase remains stable within the examined temperature range, up to 93 °C (**Figure S15**). As anticipated, the structure undergoes only very slight changes, characterized by a reduction in the lamellar distance and an increase in the intermolecular distances:  $c$  (25°C) = 46.0 Å;  $c$  (93 °C) = 45.5 Å;  $d_{\text{halo}}$  (25°C) = 4.2 Å;  $d_{\text{halo}}$  (93°C) = 4.3 Å;  $d_{\pi\pi}$  (25°C) = 3.4 Å;  $d_{\pi\pi}$  (93°C) = 3.5 Å. The results were also obtained for the polymer film  $P_{\text{Planar},31}$  and  $P_{\text{Planar},80}$ .



**Figure S15.** WAXS measurement of the polymer  $P_{\text{Planar},49}$  at 25 °C and 93 °C.

2.3.3 UV-Vis Analysis with Different Wavelength Irradiation of  $P_{\text{Planar},31}$ .

**Figure S16.** UV-vis spectra of the homogeneously aligned  $P_{\text{Planar},31}$  ( $2 \text{ cm} \times 1 \text{ cm} \times 40 \mu\text{m}$ ); after irradiation with green light ( $525 \text{ nm}$ ,  $200 \text{ mW cm}^{-2}$ ) for 24 h; and afterwards violet light ( $420 \text{ nm}$ ,  $200 \text{ mW cm}^{-2}$ ) irradiation for another 24 h. Each UV-Vis-spectrum was measured three times: With no polarization (top left), a linear polarization filter (400-700 nm) orthogonal (“X”, top right), and a linear polarization filter parallel to the orientation (“II”, bottom left) of the mesogen orientation. A combined UV-Vis spectrum is shown on the bottom right.

For the measurement, the  $P_{\text{Planar},31}$  was taped on a cuvette holder with Kapton tape. The tape was not placed in the pathway of the light beam. The linear polarization filter was taped in front of the light beam of the sample and the reference. A baseline was taken after the installment of the polarizer.

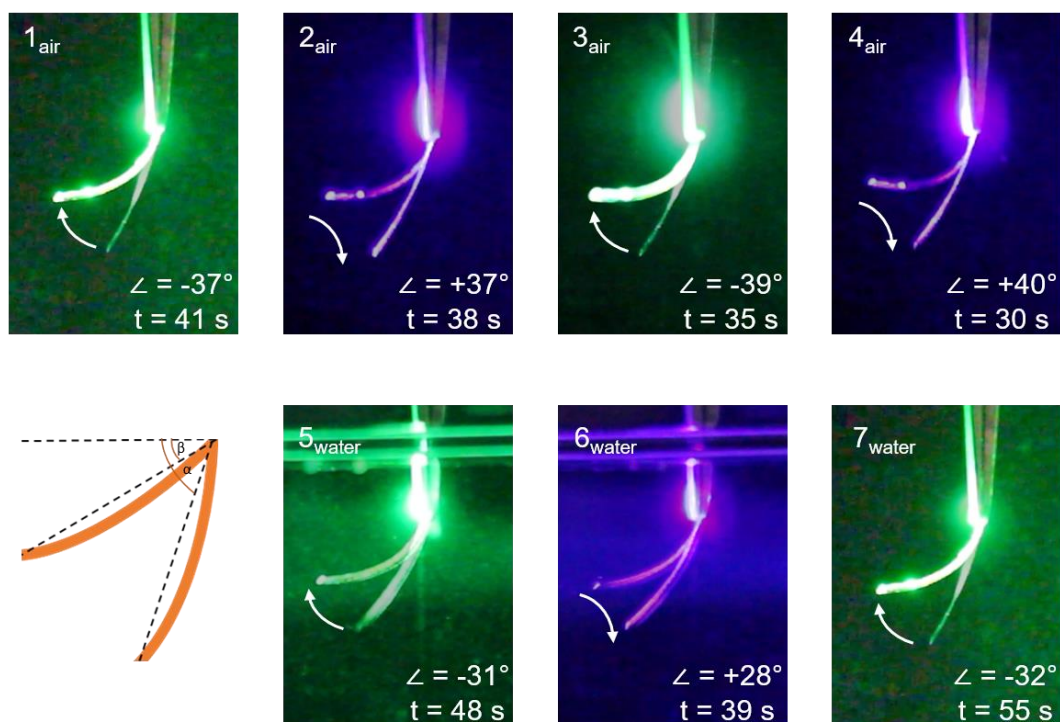
2.3.4 Photochemical Bending of  $P_{\text{Splay},60}$  by Irradiation

The polymer stripe  $P_{\text{Splay},60}$  ( $1.5 \text{ cm} \times 0.2 \text{ cm} \times 60 \mu\text{m}$ ) was irradiated with green light ( $525 \text{ nm}$ ) and violet light ( $420 \text{ nm}$ ) with an intensity of 40 up to  $200 \text{ mW cm}^{-2}$  to induce photochemical bending. The strength of the light power is a trade-off between irradiated surface area and intensity and could be varied by the focus of the collimator. This procedure was performed in air (top row) and under water (bottom row). For the underwater measurement, a cuvette ( $5 \text{ cm} \times 5 \text{ cm} \times 5 \text{ cm}$ ) filled with water was used to submerge the film. In all other respects, the experimental set-up was the same as for the bending in air. For the analysis of the final bending angles, captures from the supplementary

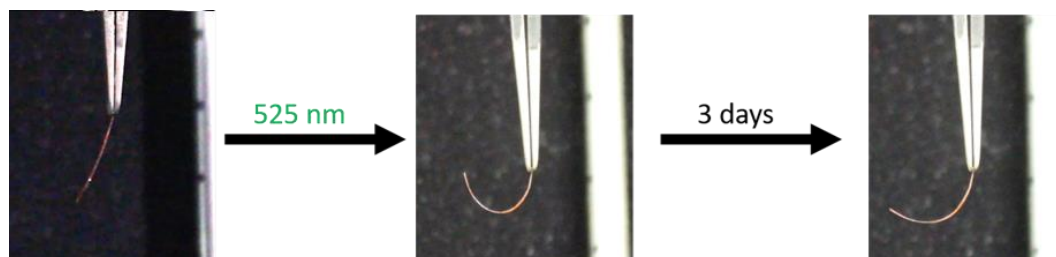
**Supplementary Video S1-2** were used, the respective time was from the tracked timeline in the video. The angles were measured with the program GIMP (**Table S4**).

**Table S4:** Measured Bending Angle after Irradiation

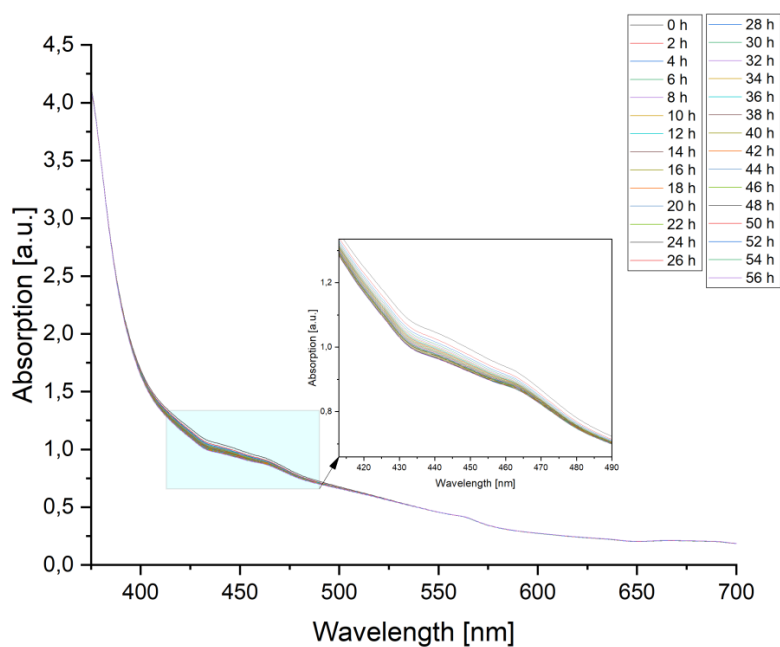
In Air	Angle Start	Angle End	Difference	Time
1 - 525 nm	68°	31°	37°	41s
2 - 420 nm	27°	64°	37°	38s
3 - 525 nm	64°	25°	39°	35s
4 - 420 nm	24°	64°	40°	30s
<b>In Water</b>				
5 - 525 nm	58°	27°	31°	48s
6 - 420 nm	30°	58°	28°	39s
7 - 525 nm	60°	28°	32°	55s



**Figure S17.** Bending of the polymer film  $P_{\text{Splay},60}$  in water and air under illumination with violet (420 nm) and green (525 nm) light. Images captured from the **Supplementary Video S1-2**.

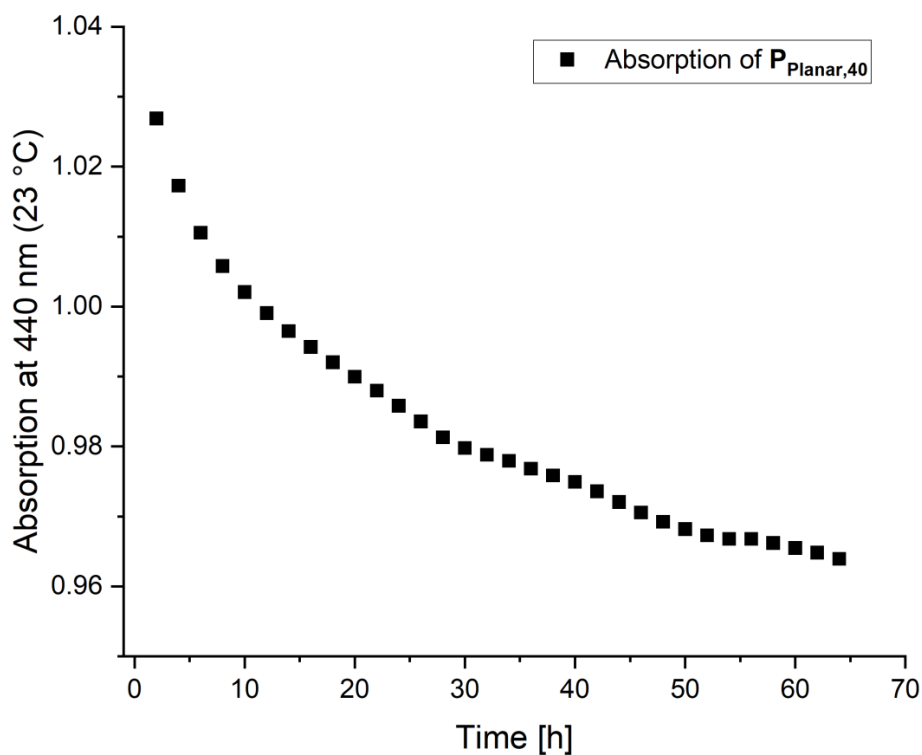
2.3.5 Bending of  $P_{\text{Splay},60}$  and Relaxation in the Dark.

**Figure S18.** Bending of  $P_{\text{Splay},60}$  (1.5 cm x 0.2 cm x 60  $\mu\text{m}$ ) before (left) and after (middle) irradiation with green light (525 nm) by light following the bending movement with the LED (tracking). Subsequently, the polymer was allowed to hang in darkness for 3 days to monitor the relaxation process (right). The marks on the metal rod to the right are spaced 1 cm apart.

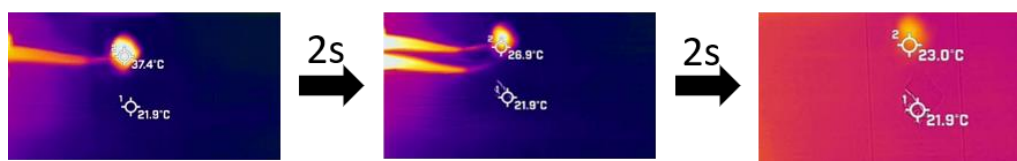
2.3.6 UV-Vis Analysis: Relaxation of  $P_{\text{Planar},31}$  after Irradiation with 525 nm.

**Figure S19.** Half-life time measurement of  $P_{\text{Planar},31}$  (2 cm x 1 cm x 39  $\mu\text{m}$ ) after irradiation with green light (525 nm) for 1 h. The half-life time for the thermal relaxation was determined at 23  $^{\circ}\text{C}$  under air every 2 h.

### 2.3.7 UV-Vis Analysis: Relaxation of $P_{\text{Planar},31}$ after Irradiation with 525 nm Determined at 440 nm.



**Figure S20.** Measurement of the decay of the absorption signal at 440 nm of  $P_{\text{Planar},31}$  (2 cm x 1 cm x 40  $\mu\text{m}$ ) after irradiation with green light (525 nm) for 1 h at 23 °C. Because of the constraints of the azobenzene in the polymer, it is unlikely that the relaxation follows a first order kinetic. Therefore, the curve was not fitted to such a function.

2.3.8 IR-Analysis: Thermal Heating during Irradiation of  $P_{\text{Splay},40}$  and  $P_{\text{Splay},60}$ .

**Figure S21.** Thermal images taken with an infrared camera of two pieces of  $P_{\text{Splay},40}$  ( $0.5 \text{ cm} \times 0.5 \text{ cm} \times 40 \mu\text{m}$ ). The first measurement point (bottom) was a sample without irradiation and the second measurement point (top) after irradiation with green light ( $20 \text{ mW cm}^{-2}$ ) for 30s. The cooling down process is shown without irradiation in 2 second intervals.

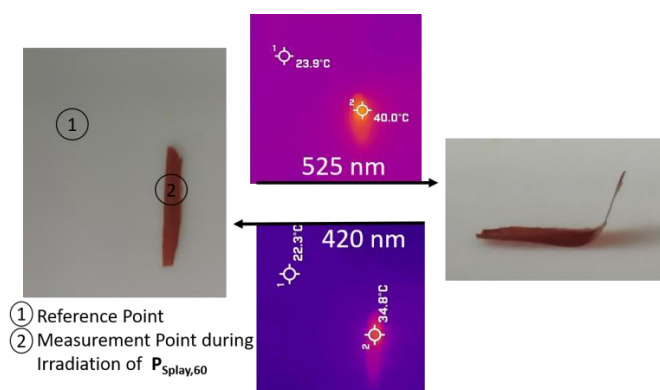


**Figure S22.** Thermal images taken with an infrared camera. The setup is shown on the left and the final bending angle on the right. An IR-video was taken during irradiation on  $P_{\text{Splay},60}$  ( $2 \text{ cm} \times 0.3 \text{ cm} \times 60 \mu\text{m}$ ). The highest peak temperature recorded is shown in the picture with  $40.0 \text{ }^\circ\text{C}$  for green light (525 nm) and  $34.8 \text{ }^\circ\text{C}$  for violet irradiation (420 nm). The average temperature was around  $33 \text{ }^\circ\text{C}$  for green light and  $30 \text{ }^\circ\text{C}$  for violet light.



### 3. Preparation of the LCE

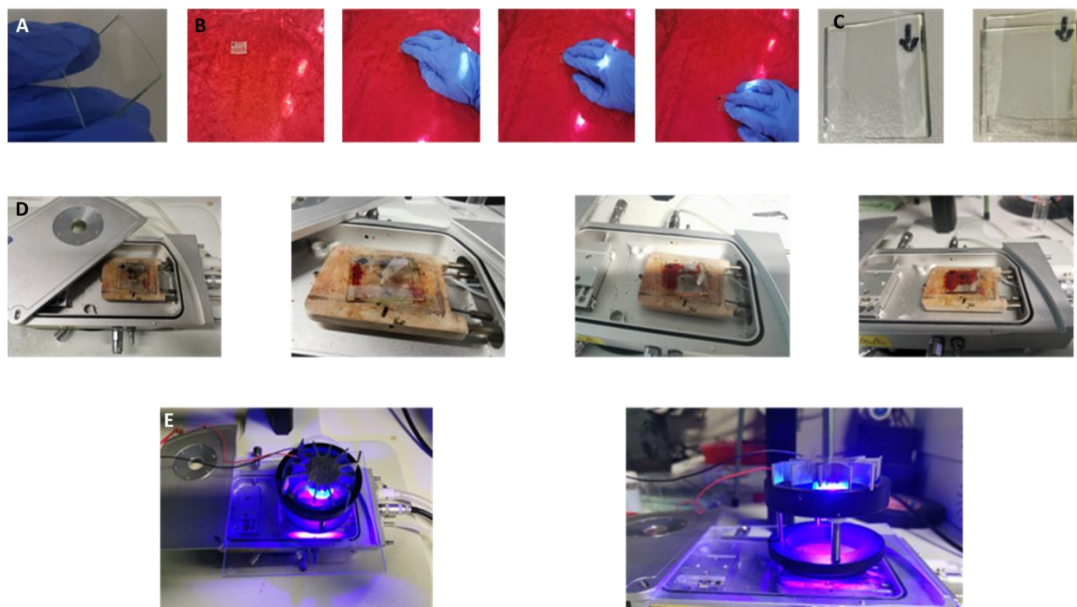


**Figure S23.** Visualization for the preparation of a photo bendable LCE within an LC cell. A) A glass substrate washed with hot water, EtOH, spin coated with an 5% wt PI solution and dried at 200 °C. B) Surface alignment by rubbing the glass substrate with gently pressure on a velvet cloth along one direction. C) A thin PTFE stripe of 10  $\mu\text{m}$ , 30  $\mu\text{m}$  ,or 50  $\mu\text{m}$  thickness was cut out of a PTFE sheet and used as a spacer. A second PI coated non-rubbed glass substrate was used to form the LC cell. Both glass substrates were glued together. D) The LC cell was heated on the Linkam eating stage LTS 420 to 160°C. At this temperature the LC cell was filled with the LC mixture by capillary force. Afterwards, the temperature was slowly lowered (0.5 °C min<sup>-1</sup>) to 130 °C. E)

Polymerization was initiated by employing a linearly polarized 420 nm light source from a 1 W LED, which was shone orthogonally to the planar alignment through a PMMA glass to activate the photocatalyst. This setup was maintained for a minimum of 5 hours. Afterwards, the temperature was raised to 155 °C again and hold for 15 min. The lamp was turned off and the temperature hold for another 15 min, before cooling down to room temperature and carefully opening the LC cell using a razor blade. To facilitate the extraction of the thin film, the razor blade and the LC cell were periodically immersed in hot water. The final thickness of the films was measured using a digital caliper.

## 3.1. Comparison of the Transparency Depending on the Alignment and Thickness.

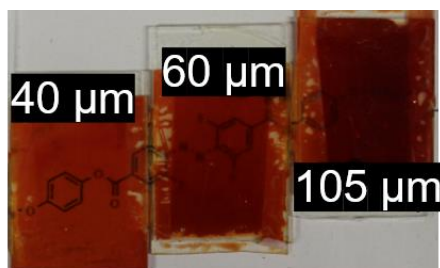
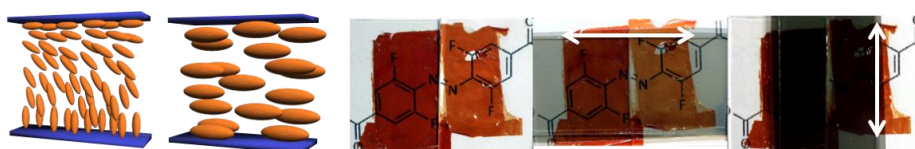


**Figure S24.** Photograph of the polymers (From left to right:  $P_{\text{Splay},40}$ ,  $P_{\text{Splay},60}$ ,  $P_{\text{Splay},105}$ ) still within the cell and their final thickness. It can be seen that this directly affects their transparency. The actual thickness of the films is higher than that of the spacer, because at the high polymerization temperature, the glue for the cell softens, widening the gap. The thicknesses of the films are uniform throughout.

Splay Alignment (40 μm), PlanarHomogenous Alignment (31 μm)



Splay Alignment (60 μm), Planar/Homogenous Alignment (49 μm)



Homeotropic Alignment – 49 μm

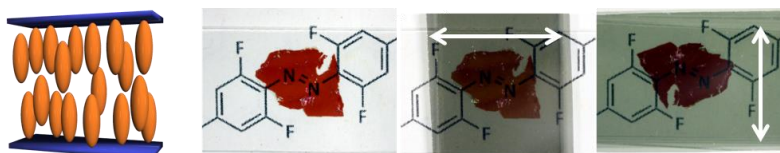
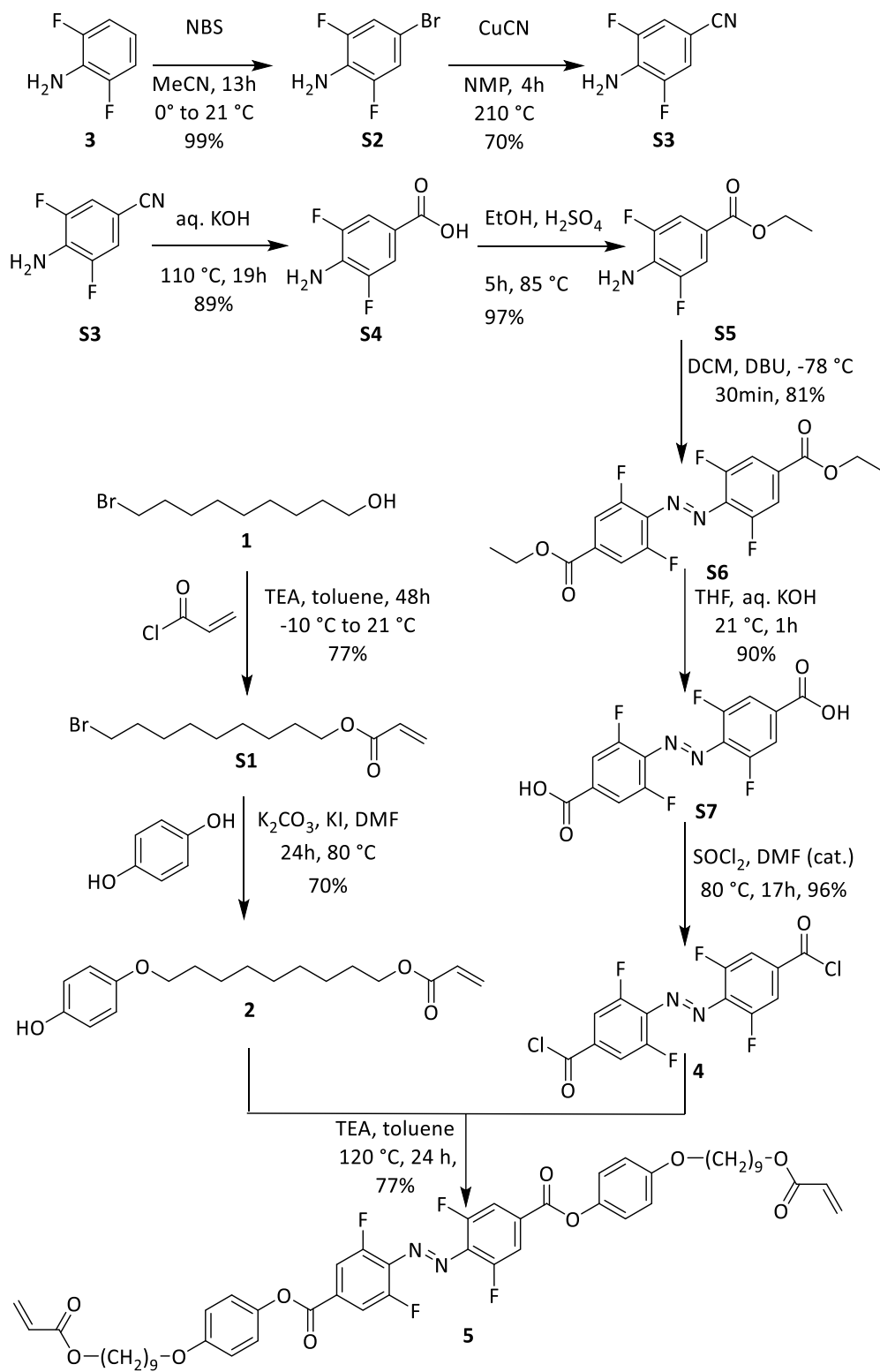


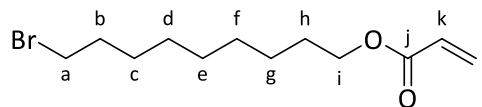
**Figure S25.** Test of the alignment by polarization filter. (Note: Azobenzene orientated along the polarization direction absorbs the light.) The splay and homogenous (planar) polymer side by side are photographed with no polarization filter (left), a polarizing filter orthogonal to the orientation of the mesogen (middle) and in plane with the mesogen (right) for the thickness of  $P_{\text{Splay},40}$  and  $P_{\text{Planar},31}$  (first row),  $P_{\text{Splay},60}$  and  $P_{\text{Planar},49}$  (middle row). The same procedure is shown in the last row for the homeotropic alignment of a  $P_{\text{Homeotropic},49}$  thick polymer film.

Scheme 1: Synthesis Overview



## 4. Syntheses

### 4.1 9-Bromononyl acrylate (**S1**)



This reaction was performed under inert conditions.

Triethylamine (9.12 g, 90.2 mmol, 1.09 equiv.) and 9-bromo-nonanol (18.5 g, 82.8 mmol, 1.00 equiv.) were dissolved in dry toluene (90 mL). The mixture was then cooled to  $-10\text{ }^{\circ}\text{C}$  *via* a salt and ice bath, and a solution of acryloyl chloride (8.16 g, 90.2 mmol, 1.09 equiv.) in dry toluene (30 mL) was added dropwise over the course of 30 min. The reaction was warmed to  $21\text{ }^{\circ}\text{C}$  and stirred for 48 h. The organic phase was subsequently washed with sat. solution of  $\text{Na}_2\text{CO}_3$  (100 mL), an aqueous hydrochloric acid solution (1 M, 2 x 100 mL) and with brine (50 mL). The organic phase was then dried over  $\text{MgSO}_4$ , filtered and the solvent removed *in vacuo* to obtain a slightly yellow oil. After filtration through a short plug of silica (eluent: DCM) the product **S1** was obtained as a colorless oil. (17.7 g, 63.9 mmol, 77%)

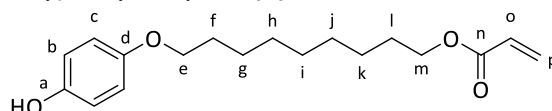
$^1\text{H NMR}$  (601 MHz,  $\text{CDCl}_3$ )  $\delta$  6.40 (dd,  $^3J = 17.4$ ,  $^4J = 1.5$  Hz, 1H, H-l), 6.12 (dd,  $^3J = 17.4$ ,  $^3J = 10.5$  Hz, 1H, H-k), 5.81 (dd,  $^3J = 10.5$ ,  $^4J = 1.5$  Hz, 1H, H-l), 4.15 (t,  $^3J = 6.8$  Hz, 2H, H-a), 3.41 (t,  $^3J = 6.8$  Hz, 2H, H-i), 1.85 (m, 2H, H-h), 1.69 – 1.64 (m, 2H, H-b), 1.31 (m, 10H, H-c,d,e,f,g).

$^{13}\text{C}\{^1\text{H}\}$  NMR (151 MHz,  $\text{CDCl}_3$ )  $\delta$  = 166.48 (C-l), 130.60 (C-j), 128.78, (C-k), 64.79 (C-a), 34.14 (C-i), 32.93 (C-h), 29.43 (C-b), 29.26 (C-c,d,e,f,g), 28.80 (C-c,d,e,f,g), 28.72 (C-c,d,e,f,g), 28.26 (C-c,d,e,f,g), 26.01 (C-c,d,e,f,g) ppm.

HRMS (ESI)  $m/z$  (%):  $[\text{M}+\text{Na}]^+$  calcd for  $[\text{C}_{12}\text{H}_{21}\text{Br}^{79}\text{NaO}_2]^+$  299.06171; found 299.06185.

IR (ATR):  $\tilde{\nu}$  = 2927 (m), 2854 (m), 1721 (s), 1636 (w), 1464 (w), 1406 (m), 1294 (w), 1269 (m), 1185 (s), 1085 (m), 983 (m), 965 (m), 809 (m), 722 (w)  $\text{cm}^{-1}$ .

### 4.2 9-(4-hydroxyphenoxy)nonyl acrylate (**2**)



Hydroquinone (24.8 g, 225 mmol, 5.00 equiv.), **S1** (13.8 g, 45.0 mmol, 1.00 equiv.),  $\text{K}_2\text{CO}_3$  (31.2 g, 225 mmol, 5.00 equiv.), a catalytic amount KI (100 mg) was dissolved in anhydrous DMF (150 mL). The solution was stirred for 24 h at  $80\text{ }^{\circ}\text{C}$ . Then, water (150 mL) was added and the mixture was placed in the fridge at  $6\text{ }^{\circ}\text{C}$  for 3 h. The precipitate was filtered and washed with water (3 x 100 mL). Afterwards, the filter cake was dissolved in ethyl acetate (200 mL). The organic layer was washed with water (3 x 150 mL), brine (3 x 150 mL) and dried over anhydrous  $\text{MgSO}_4$ . After filtration, the solvent was removed by evaporation under reduced pressure. The crude product was purified by silica gel column chromatography (ethyl acetate:hexane, 1:4) to obtain **2** as a pale-yellow solid (9.65 g, 31.5 mmol, 70%).

$^1\text{H NMR}$  (600 MHz,  $\text{CDCl}_3$ )  $\delta$  = 6.82 – 6.72 (m, 4H, H-b,c), 6.40 (dd,  $^3J = 17.4$ ,  $^4J = 1.4$  Hz, 1H, H-p), 6.12 (dd,  $^3J = 17.4$ ,  $^3J = 10.4$  Hz, 1H, H-o), 5.82 (dd,  $^3J = 10.5$ ,  $^4J = 1.4$  Hz, 1H, H-p), 4.54 (s, 1H, HO-a), 4.15 (t,  $^3J = 6.7$  Hz, 2H, H-e), 3.89 (t,  $^3J = 6.6$  Hz, 2H, H-m), 1.77 – 1.71 (m, 2H, H-l), 1.69 – 1.64 (m, 2H, H-f), 1.46 – 1.41 (m, 2H, H-k), 1.37 – 1.30 (m, 8H, H-g,h,i,j).

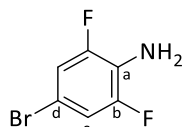
$^{13}\text{C}\{^1\text{H}\}$  NMR (151 MHz,  $\text{CDCl}_3$ )  $\delta$  = 166.58 (C-n), 153.45 (C-a), 149.49 (C-d), 130.67 (C-p), 128.76 (C-o), 116.12 (C-b,c), 115.74 (C-b,c), 68.79 (C-m), 64.87 (C-e), 29.54 (C-l), 29.48 (C-g,h,l,j), 29.42 (C-f), 29.29 (C-g,h,l,j), 28.73 (C-g,h,l,j), 26.14 (C-g,h,l,j), 26.03 (C-k).

HRMS (EI, 70 eV)  $m/z$  (%):  $[\text{M}]^+$  calcd for  $[\text{C}_{18}\text{H}_{26}\text{O}_4]^+$  306.18244; found 306.18256 (20), 110.1 (100).

IR (ATR):  $\tilde{\nu}$  = 3372 (br), 2918 (m), 2851 (w), 1696 (m), 1511 (s), 1473 (m), 1423 (m), 1392 (w), 1300 (w), 1256 (w), 1212 (s), 1024 (s), 983 (w), 827 (m), 809 (m), 766 (m), 751 (m)  $\text{cm}^{-1}$ .

R<sub>f</sub>: 0.5 (ethyl acetate:*n*-hexane, 1:4).

#### 4.3 4-Bromo-2,6-difluoroaniline (**S2**)<sup>[5]</sup>



To a solution of 2,6-difluoroaniline (12.9 g, 100 mmol, 1.00 equiv.) in acetonitrile (200 mL), *N*-bromosuccinimide (17.8 g, 100 mmol, 1.00 equiv) dissolved in acetonitrile (100 mL) was added dropwise at 0°C over the duration of 1 h. The mixture was stirred for 12 h while warming up to 21°C, and then diluted with water (800 mL). The product was extracted with ethyl acetate (3 × 100 mL). The organic phase was dried over  $\text{MgSO}_4$ , filtered, and concentrated under reduced pressure. The crude residue was purified by column chromatography over silica gel (eluent: *n*-hexane:DCM, 4:1) to give **S2** as a colorless solid (17.2 g, 99%, Lit.: 99%).<sup>[5]</sup>

$^1\text{H}$  NMR (600 MHz,  $\text{CDCl}_3$ )  $\delta$  6.99 (d,  $^3J$  = 7.8 Hz, 2H, *H*-c), 3.73 (s, 2H,  $\text{NH}_2$ -a) ppm.

$^{13}\text{C}\{^1\text{H}\}$  NMR (151 MHz,  $\text{CDCl}_3$ )  $\delta$  151.88 (dd,  $^1J$  = 244.1 Hz,  $^4J$  = 8.6 Hz, C-b), 123.64 (t,  $^2J$  = 16.2 Hz, C-a), 114.85 (dd,  $^2J$  = 18.5,  $^4J$  = 7.2 Hz, C-c), 107.20 (t,  $^3J$  = 11.6 Hz, C-d) ppm.

$^{19}\text{F}$  NMR (565 MHz,  $\text{CDCl}_3$ )  $\delta$  -130.69 (d,  $^3J$  = 6.3 Hz, F-b) ppm.

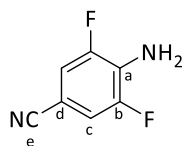
IR (ATR):  $\tilde{\nu}$  = 3421(m), 3328 (m), 1643 (w), 1605 (m), 1583 (m), 1497 (s), 1428 (s), 1299 (m), 1272 (m), 1199 (w), 1150 (s), 963 (s), 869 (m), 839 (m), 761 (w), 717 (s)  $^{-1}$ .

HRMS (EI, 70 eV)  $m/z$  (%): calcd for  $[\text{C}_6\text{H}_4\text{NBr}^{79}\text{F}_2]^+$  206.94921, found 206.94897(100).

Mp: 65 °C.

R<sub>f</sub>: 0.40 (*n*-hexane:DCM, 1:2).

#### 4.4 4-Amino-3,5-difluorobenzonitrile (**S3**)<sup>[6]</sup>



A mixture of copper(I) cyanide (29.3 g, 325 mmol, 1.70 equiv.) and 4-bromo-2,6-difluoroaniline (**S2**) (39.5 g, 190 mmol, 1.00 equiv.) in *N*-methyl-2-pyrrolidone (120 mL) was heated to 210 °C under anhydrous conditions for 4 h. After cooling to 30 °C the resulting mixture was poured into aqueous ammonia (conc. 30%) until a white precipitate was formed. The suspension was extracted with toluene (5 × 100 mL). The organic phase was washed with water (3 × 100 mL), brine (2 × 100 mL), dried over  $\text{MgSO}_4$  and filtered. The solvent was removed *in vacuo*. The crude product was dissolved in dichloromethane and purified by adsorption filtration through a large column of silica (eluent: DCM:hexane, 1:1). **S3** was obtained as a colorless solid (20.5 g, 133 mmol, 70%, Lit.: 87%).<sup>[7]</sup>

$^1\text{H}$  NMR (600 MHz,  $\text{CDCl}_3$ )  $\delta$  = 7.14 (dd,  $^3J$  = 6.1,  $^5J$  = 2.2 Hz, 2H, *H*-c), 4.27 (s, 2H,  $\text{NH}_2$ -a) ppm.

$^{13}\text{C}\{^1\text{H}\}$  NMR (151 MHz,  $\text{CDCl}_3$ )  $\delta$  150.66 (dd,  $^1J$  = 243.5 Hz,  $^4J$  = 9.1 Hz, C-b), 129.75 (t,  $^2J$  = 15.7 Hz, C-a), 118.05 (t,  $^5J$  = 3.4 Hz, C-e), 115.60 (dd,  $^2J$  = 17.5,  $^4J$  = 7.1 Hz, C-c), 98.47 (t,  $^3J$  = 11.1 Hz, C-d) ppm.

**<sup>19</sup>F NMR** (565 MHz, CDCl<sub>3</sub>)  $\delta$  = -130.76 (dd, <sup>3</sup>J = 6.1 Hz, <sup>5</sup>J = 2.2 Hz, F-b) ppm.

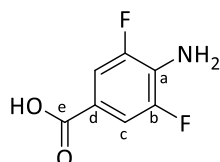
**IR** (ATR):  $\tilde{\nu}$  = 3376 (w), 3313 (w), 2224 (m), 1650 (w), 1608 (w), 1587 (m), 1523 (m), 1443 (s), 1338 (m), 1163 (s), 977 (s), 875 (s), 862 (m), 727 (s) cm<sup>-1</sup>.

**HRMS** (EI, 70 eV) *m/z* (%): [M]<sup>+</sup> calcd for [C<sub>7</sub>H<sub>4</sub>N<sub>2</sub>F<sub>2</sub>]<sup>+</sup> 154.03371; found 154.03383 (100).

**Mp**: 112 °C.

**R<sub>f</sub>**: 0.40 (*n*-hexane:DCM, 1:2).

#### 4.5 4-Amino-3,5-difluorobenzoic acid (**S4**)<sup>[6]</sup>



A mixture of 4-amino-3,5-difluorobenzonitrile (**S3**) (5.00 g, 32.4 mmol, 1.00 equiv.) was dissolved in aq. KOH (25 wt%, 100 mL). The mixture was heated to 110 °C for 19 h. After cooling down to 21 °C, the aqueous phase was acidified to pH = 2 with HCl (2 M) and extracted with ethyl acetate (2 × 100 mL). The combined organic extracts were washed with water (3 × 75 mL), brine (2 × 75 mL), dried over MgSO<sub>4</sub> and filtered. The solvent was removed *in vacuo* to obtain **S4** as a slightly yellowish solid (4.99 g, 28.8 mmol, 89%, Lit.: 89%).<sup>[8]</sup>

**<sup>1</sup>H NMR** (600 MHz, DMSO-*d*<sub>6</sub>)  $\delta$  = 7.39 (dd, <sup>3</sup>J = 7.2 Hz, <sup>5</sup>J = 2.4 Hz, 2H, H-c), 6.04 (s, 2H, NH<sub>2</sub>-a) ppm.

**<sup>13</sup>C{<sup>1</sup>H} NMR** (151 MHz, DMSO-*d*<sub>6</sub>)  $\delta$  = 166.12 (C-e), 149.80 (dd, <sup>1</sup>J = 239.6, <sup>4</sup>J = 9.5 Hz, C-b), 130.61 (t, <sup>2</sup>J = 16.7 Hz, C-a), 112.31 (dd, <sup>2</sup>J = 15.8 Hz, <sup>4</sup>J = 5.9 Hz, C-c), 59.83 (C-d) ppm.

**<sup>19</sup>F NMR** (565 MHz, DMSO-*d*<sub>6</sub>)  $\delta$  -131.62 (d, <sup>3</sup>J = 7.2 Hz, F-b) ppm.

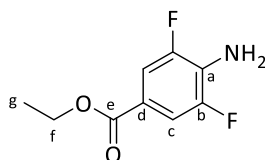
**IR** (ATR):  $\tilde{\nu}$  = 3397 (w), 1683 (m), 1628 (s), 1587 (m), 1538 (w), 1454 (m), 1422 (s), 1341 (s), 1277 (s), 1243 (m), 1145 (m), 1082 (w), 953 (m), 889 (m), 765 (s), 719 (s) cm<sup>-1</sup>.

**HRMS** (EI, 70 eV) *m/z* (%): [M]<sup>+</sup> calcd for [C<sub>7</sub>H<sub>5</sub>NO<sub>2</sub>F<sub>2</sub>]<sup>+</sup> 173.02829; found 173.02830 (75), 156.1 (100).

**Mp**: 171 °C.

**R<sub>f</sub>**: 0.90 (ethyl acetate).

#### 4.6 Ethyl 4-amino-3,5-difluorobenzoate (**S5**)<sup>[6]</sup>



**S4** (2.42 g, 14.0 mmol) was dissolved in EtOH (50 mL) and H<sub>2</sub>SO<sub>4</sub> (95%, 1 mL), and heated to 85 °C for 5 h. The mixture was neutralized (pH 7) with saturated NaHCO<sub>3</sub>, and extracted with DCM (3 × 50 mL). The organic phase was dried over MgSO<sub>4</sub>, filtered, and concentrated under reduced pressure to give **S5** as a pale brown solid (2.74 g, 13.6 mmol, 97%, Lit.: 97%).<sup>[8]</sup>

**<sup>1</sup>H NMR** (600 MHz, CDCl<sub>3</sub>)  $\delta$  = 7.53 (dd, <sup>3</sup>J = 7.1, <sup>5</sup>J = 2.2 Hz, 2H, H-c), 4.33 (q, <sup>3</sup>J = 7.1 Hz, 2H, H-f), 4.13 (s, 2H, NH<sub>2</sub>-a), 1.36 (t, <sup>3</sup>J = 7.1 Hz, 3H, H-g) ppm.

**<sup>13</sup>C{<sup>1</sup>H} NMR** (151 MHz, CDCl<sub>3</sub>)  $\delta$  = 165.30 (t, <sup>5</sup>J = 3.5 Hz, C-e), 150.80 (dd, <sup>1</sup>J = 240.8 Hz, <sup>4</sup>J = 7.9 Hz, C-b), 128.92 (t, <sup>3</sup>J = 16.1 Hz, C-a), 118.72 (t, <sup>4</sup>J = 8.2 Hz, C-d), 113.13 – 112.08 (m, C-c), 61.20 (C-f), 14.45 (C-g) ppm.

**<sup>19</sup>F NMR** (565 MHz, CDCl<sub>3</sub>)  $\delta$  -132.93 (dd, <sup>3</sup>J = 7.2 Hz, <sup>5</sup>J = 2.3 Hz, F-b) ppm.

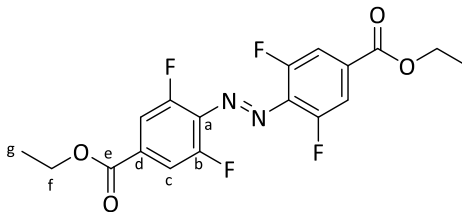
**IR** (ATR):  $\tilde{\nu}$  = 3505 (w), 3368 (m), 1697 (s), 1629 (s), 1585 (m), 1531 (m), 1477 (w), 1444 (m), 1397 (m), 1370 (m), 1339 (s), 1270 (s), 1222 (s), 1133 (m), 1089 (s), 1027 (s), 946 (s), 881 (m), 760 (m) cm<sup>-1</sup>.

**HRMS** (EI, 70 eV) *m/z* (%): [M]<sup>+</sup> calcd for [C<sub>9</sub>H<sub>9</sub>NO<sub>2</sub>F<sub>2</sub>]<sup>+</sup> 201.0599; found 201.05932 (15), 156.1 (100).

30

R<sub>f</sub>: 0.30 (*n*-hexane:DCM, 1:1).

4.7 (*E*)-4,4'-(Diazene-1,2-diyl)bis(3,5-difluorobenzoic acid) (**S6**)<sup>[9]</sup>



To a solution of **S5** (637 mg, 2.50 mmol, 1.00 equiv.) dissolved in DCM (40 mL) 1,8-diazabicyclo[5.4.0]undec-7-ene (761 mg, 5.00 mmol, 2.00 equiv.) was added. The solution was stirred at 21 °C for 5 min before being cooled down to -78 °C. *N*-Chlorosuccinimide (668 mg, 5.00 mmol, 2.00 equiv.) was added as a solid to the reaction mixture. The orange solution was stirred for 30 min at -78 °C, before quenching by addition of a saturated bicarbonate solution (50 mL). The organic layer was separated, washed sequentially with water (3 x 50 mL) and HCl (1 M, 50 mL), dried over MgSO<sub>4</sub>, filtered and concentrated *in vacuo*. The residue was purified by silica gel flash chromatography (eluent: gradient *n*-hexane:DCM, 1:0 → 1:1) to obtain **S6** as a red solid (402 mg, 1.01 mmol, 81%, Lit.: 81%)<sup>[8]</sup>.

<sup>1</sup>H NMR (600 MHz, CDCl<sub>3</sub>) δ = 7.75 (d, <sup>3</sup>J = 9.1 Hz, 4H, *H*-c), 4.43 (q, <sup>3</sup>J = 7.1 Hz, 4H, *H*-f), 1.43 (t, <sup>3</sup>J = 7.1 Hz, 6H, *H*-g) ppm.

<sup>13</sup>C{<sup>1</sup>H} NMR (151 MHz, CDCl<sub>3</sub>) δ = 163.84 (*C*-e), 155.17 (dd, <sup>1</sup>J = 262.6 Hz, <sup>4</sup>J = 3.8 Hz, *C*-b), 134.31 (t, <sup>3</sup>J = 10.1 Hz, *C*-a), 133.89 (t, <sup>4</sup>J = 9.2 Hz, *C*-d), 114.07 (dd, <sup>2</sup>J = 21.7, <sup>4</sup>J = 3.9 Hz, *C*-c), 62.34 (*C*-f), 14.36 (*C*-g) ppm.

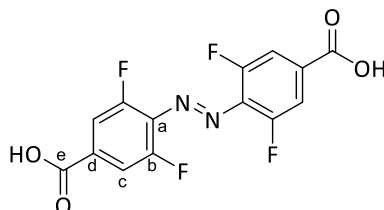
<sup>19</sup>F NMR (565 MHz, CDCl<sub>3</sub>) δ = -119.5 (d, <sup>3</sup>J = 9.1 Hz, *F*-b) ppm.

IR (ATR):  $\tilde{\nu}$  = 1721 (m), 1573 (m), 1434 (m), 1369 (s), 1330 (m), 1238 (m), 1192 (m), 1089 (w), 1052 (s), 1017 (s), 886 (s), 767 (s), 752 (s) cm<sup>-1</sup>.

HRMS (EI, 70 eV) *m/z* (%): [M]<sup>+</sup> calcd for [C<sub>18</sub>H<sub>14</sub>N<sub>2</sub>O<sub>4</sub>F<sub>4</sub>]<sup>+</sup> 398.08842; found 398.08876 (15), 101.1 (100).

Mp: 147°C.

R<sub>f</sub>: 0.35 (*n*-hexane:DCM, 1:1).

4.8 (*E*)-4,4'-(Diazene-1,2-diyl)bis(3,5-difluorobenzoic acid) (**S7**)<sup>[6]</sup>

Diethyl 4,4'-(diazene-1,2-diyl)-bis(3,5-difluorobenzoate) (**S6**) (1.19 g, 3.00 mmol, 1.00 equiv.) was dissolved in THF (40 mL). KOH (673 mg, 12.0 mmol, 4.00 equiv.) dissolved in H<sub>2</sub>O (40 mL) was added. The reaction mixture was stirred for 1 h and acidified with HCl (1 M) until a precipitate was formed. The precipitate was filtered and dried in a vacuum oven at 50 °C for 24 h to yield the desired product **S7** (924 mg, 2.70 mmol, 90 %, Lit.: 94%) as a pink solid.<sup>[6]</sup>

<sup>1</sup>H NMR (600 MHz, DMSO-*d*<sub>6</sub>) δ = 7.80 (d, <sup>3</sup>J = 9.5 Hz, 4H, *H*-c) ppm.

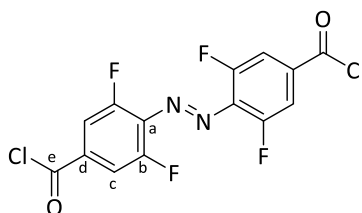
<sup>13</sup>C{<sup>1</sup>H} NMR (151 MHz, DMSO-*d*<sub>6</sub>) δ = 202.28 (C-e), 192.00 (dd, <sup>1</sup>J = 260.9, <sup>4</sup>J = 3.7 Hz, C-b), 173.11 (t, <sup>4</sup>J = 9.0 Hz, C-d), 170.65 (t, <sup>3</sup>J = 10.4 Hz, C-a), 151.61 (dd, <sup>2</sup>J = 21.3, <sup>4</sup>J = 3.7 Hz, C-c) ppm.

<sup>19</sup>F NMR (565 MHz, DMSO-*d*<sub>6</sub>) δ = -120.06 (d, <sup>3</sup>J = 9.5 Hz, F-b) ppm.

HRMS (ESI) *m/z* (%): [M-H]<sup>-</sup> calcd for [C<sub>14</sub>H<sub>5</sub>N<sub>2</sub>O<sub>4</sub>F<sub>4</sub>]<sup>-</sup> 341.01909; found 341.01902.

IR (ATR):  $\tilde{\nu}$  = 2871 (br), 1693 (s), 1577 (s), 1481 (m), 1436 (m), 1414 (m), 1259 (s), 1195 (m), 1054 (s), 893 (s), 879 (m), 773 (s), 729 (m) cm<sup>-1</sup>.

Mp: >300 °C.

4.9 (*E*)-4,4'-(Diazene-1,2-diyl)bis(3,5-difluorobenzoyl chloride) (**4**)

This reaction was performed under inert conditions.

In an oven dried flask, **S7** (1.03 g, 3.00 mmol, 1.00 equiv.) was dissolved in an excess of SOCl<sub>2</sub> (5 mL). Then, a single drop of dry DMF was added and the reaction mixture heated up to 80 °C for 17 h. Afterwards, the solvent was removed *in vacuo* by adding a cooling trap to the apparatus. The crude product was transferred to the glovebox and crystallized in dry toluene at -20 °C. After filtration, the dark red solid **4** was obtained in 96% (1.09 g, 2.88 mmol) yield.

<sup>1</sup>H NMR (600 MHz, CDCl<sub>3</sub>) δ = 7.86 (d, <sup>3</sup>J = 8.4 Hz, 4H, *H*-c) ppm.

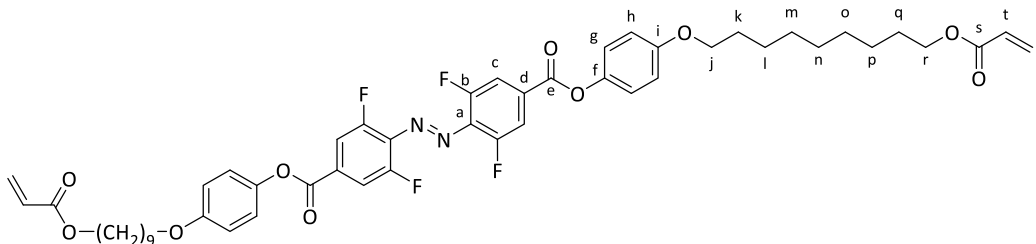
<sup>13</sup>C{<sup>1</sup>H} NMR (151 MHz, CDCl<sub>3</sub>) δ = 165.92 (C-e), 155.06 (dd, <sup>2</sup>J = 265.0, <sup>4</sup>J = 3.8 Hz, C-b), 136.05 (t, <sup>4</sup>J = 9.1 Hz, C-d), 135.54 (t, <sup>3</sup>J = 10.4 Hz, C-a), 115.68 (dd, <sup>2</sup>J = 22.1, <sup>4</sup>J = 4.4 Hz, C-c).

<sup>19</sup>F NMR (565 MHz, CDCl<sub>3</sub>) δ = -117.46 (d, <sup>3</sup>J = 8.4 Hz, F-b) ppm.

HRMS (EI, 70 eV) *m/z* (%): [M]<sup>+</sup> calcd for [C<sub>14</sub>H<sub>4</sub>N<sub>2</sub>O<sub>4</sub>F<sub>4</sub>]<sup>+</sup> 377.95801; found 377.95805 (10), 86.1 (100).

IR (ATR):  $\tilde{\nu}$  = 1746 (m), 1698 (m), 1684 (w), 1576 (s), 1558 (m), 1540 (w), 1473 (w), 1431 (m), 1418 (m), 1396 (w), 1328 (w), 1260 (w), 1123 (m), 1054 (s), 1004 (s), 891 (m), 878 (w), 807 (m), 772 (w), 701 (m) cm<sup>-1</sup>.



4.10 (*E*)-4,4'-(Diazene-1,2-diyl)bis(3,5-difluorobenzoic acid) (**5**)

This reaction was performed under inert conditions.

In a glovebox, **4** (342 mg, 1 mmol, 1 equiv.) and **2** (674 mg, 2.20 mmol, 2.20 equiv.) and triethylamine (1 mL) were dissolved in toluene (30 mL). The reaction was heated to 110 °C for 24 h. Then, the solvent was removed *in vacuo* and the crude product was directly purified by column chromatography (eluent gradient: Hexane → DCM) to afford **5** as an orange solid. (707 mg, 0.769 mmol, 77%)

**<sup>1</sup>H NMR** (600 MHz, CDCl<sub>3</sub>) δ = 7.91 (d, <sup>3</sup>J = 9.3 Hz, 4H, *H*-c), 7.14 (d, <sup>3</sup>J = 9.0 Hz, 4H, *H*-g), 6.95 (d, <sup>3</sup>J = 9.0 Hz, 4H, *H*-h), 6.40 (dd, <sup>2</sup>J = 17.4, <sup>4</sup>J = 1.5 Hz, 2H, *H*-u), 6.13 (dd, <sup>3</sup>J = 17.4, <sup>3</sup>J = 10.4 Hz, 2H, *H*-t), 5.82 (dd, <sup>3</sup>J = 10.4, <sup>4</sup>J = 1.5 Hz, 2H, *H*-u), 4.16 (t, <sup>3</sup>J = 6.7 Hz, 4H, *H*-j), 3.97 (t, <sup>3</sup>J = 6.5 Hz, 4H, *H*-r), 1.83 - 1.77 (m, 4H, *H*-q), 1.71 - 1.65 (m, 4H, *H*-k), 1.48-1.46 (m, 4H, *H*-p), 1.37 (s, 16H, *H*-l,m,n,o).

**<sup>13</sup>C{<sup>1</sup>H} NMR** (151 MHz, CDCl<sub>3</sub>) δ = 166.51 (*C*-s), 162.84 (*C*-e), 157.43 (*C*-f), 155.24 (d, <sup>1</sup>J = 263.4 Hz, *C*-b), 143.88 (*C*-i), 134.71 (t, <sup>2</sup>J = 10.0 Hz, *C*-a), 133.13 (t, <sup>3</sup>J = 9.5 Hz, *C*-d), 130.61 (*C*-u), 128.80 (*C*-t), 122.21 (*C*-g), 115.36 (*C*-h), 114.65 (dd, <sup>2</sup>J = 21.7, <sup>4</sup>J = 4.0 Hz, *C*-c), 68.56 (*C*-r), 64.83 (*C*-j), 29.57 (*C*-q), 29.43 (*C*-l,m,n,o), 29.37 (*C*-k), 29.32 (*C*-l,m,n,o), 28.75 (*C*-l,m,n,o), 26.16 (*C*-l,m,n,o), 26.05 (*C*-p).

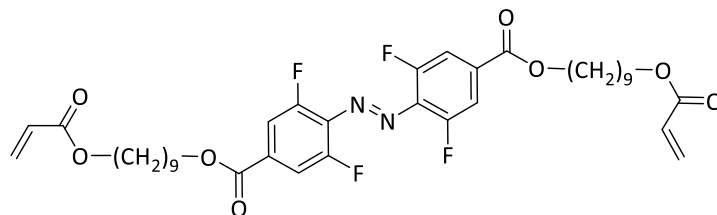
**<sup>19</sup>F NMR** (565 MHz, CDCl<sub>3</sub>) δ = -118.92 (d, <sup>3</sup>J = 9.3 Hz, *F*-b).

**HRMS** (ESI) *m/z* (%): [M+Na]<sup>+</sup> calcd for [C<sub>50</sub>H<sub>54</sub>F<sub>4</sub>N<sub>2</sub>NaO<sub>10</sub>]<sup>+</sup> 941.36068; found 941.36095.

**IR** (ATR):  $\tilde{\nu}$  = 2923 (w), 1710 (m), 1575 (w), 1501 (w), 1473 (m), 1434 (w), 1336 (m), 1295 (m), 1204 (s), 1184 (s), 1110 (m), 1048 (m), 1017 (m), 988 (m), 968 (m), 958 (m), 912 (w), 898 (w), 827 (m), 812 (s), 773 (m), 886 (m), 752 (m), 725 (w) cm<sup>-1</sup>.

**Mp**: Cr120N153I

**R<sub>f</sub>**: 0.5 (*n*-hexane:DCM, 1:1).

4.11 Bis(9-(acryloyloxy)nonyl) 4,4'-(diazene-1,2-diyl)(*E*)-bis(3,5-difluorobenzoate) (**S8**)

In a glovebox, **6** (342 mg, 1 mmol, 1 equiv.) and excess of nonane-1,9-diol (641 mg, 4.00 mmol, 4.00 equiv.) and triethylamine (1 mL) were dissolved in toluene (30 mL). The reaction was heated to 110 °C for 24h. Then, the solvent was removed in vacuo and the crude product was purified by column chromatography (cyclohexane: ethyl acetate, 2:1) to afford a crude product (532 mg), which was used without further purification.

Triethylamine (202 mg, 2.00 mmol, 2.00 equiv.) and the crude material (532 mg, 0.840 equiv.) were dissolved in dry THF (10 mL). The mixture was then cooled to -10 °C *via* a salt and ice bath, and a solution of acryloyl chloride (270 mg, 3.00 mmol, 3.00 equiv.) in dry THF (5 mL) was added dropwise. The reaction was warmed to 21°C and stirred for 18 h. DCM (25 mL) was added to the organic phase. The organic phase is subsequently washed with sat. solution of sodium carbonate (2 x 20 mL), an aqueous hydrochloric acid solution (1 M, 2 x 20 mL) and with brine (20 mL). The organic phase was then dried over MgSO<sub>4</sub>, filtered and the solvent removed *in vacuo*. The crude product was purified by column chromatography (eluent: DCM) and crystallized in acetonitrile to obtained **S8** as an orange solid. (360 mg, 490 μmol, 49%)

<sup>1</sup>H NMR (600 MHz, CDCl<sub>3</sub>) δ = 7.74 (d, *J* = 9.0 Hz, 4H), 6.40 (dd, *J* = 17.3, 1.5 Hz, 2H), 6.12 (dd, *J* = 17.4, 10.4 Hz, 2H), 5.81 (dd, *J* = 10.4, 1.5 Hz, 2H), 4.36 (t, *J* = 6.7 Hz, 4H), 4.15 (t, *J* = 6.7 Hz, 4H), 1.79 (dt, *J* = 14.6, 6.8 Hz, 4H), 1.71 – 1.64 (m, 4H), 1.47 – 1.33 (m, 21H).

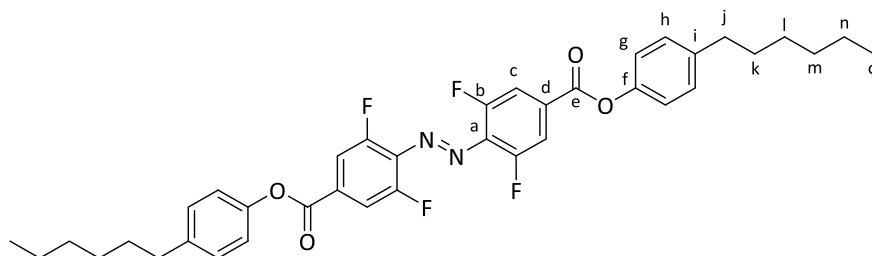
<sup>13</sup>C{<sup>1</sup>H} NMR (151 MHz, CDCl<sub>3</sub>) δ = 166.50, 156.04 (d, *J* = 3.1 Hz), 154.30 (d, *J* = 3.6 Hz), 130.62, 128.78, 114.13 (d, *J* = 2.8 Hz), 113.98 (d, *J* = 3.5 Hz), 66.45, 64.80, 29.51, 2x 29.31, 28.74, 28.71, 26.08, 26.04.

<sup>19</sup>F NMR (565 MHz, CDCl<sub>3</sub>) δ = -117.97 (d, *J* = 6.6 Hz, (*E*-isomer <5%), *F*-b), -119.45 (d, *J* = 9.0 Hz (*Z*-isomer), *F*-b).

HRMS (ESI) *m/z* (%): [M+Na]<sup>+</sup> calcd for [C<sub>38</sub>H<sub>46</sub>N<sub>2</sub>O<sub>8</sub>F<sub>4</sub>Na]<sup>+</sup> 757.30825; found 757.30683.

IR (ATR):  $\tilde{\nu}$  = 2928 (m), 2855 (m), 1716 (s), 1577 (m), 1474 (w), 1431 (m), 1336 (m), 1232 (s), 1192 (s), 1088 (w), 1049 (s), 1010 (m), 982 (m), 883 (m), 810 (w), 768 (m), 753 (m).

Mp: 53 °C

4.12 Bis(4-hexylphenyl) 4,4'-(diazene-1,2-diyl)(*E*)-bis(3,5-difluorobenzoate) (**6**)

This reaction was performed under inert conditions.

In a glovebox, **4** (342 mg, 1 mmol, 1 equiv.) and hexylphenol (392 mg, 2.20 mmol, 2.20 equiv.) and triethylamine (1 mL) were dissolved in toluene (30 mL). The reaction was heated to 110 °C for 24 h.

Then, the solvent was removed *in vacuo* and the crude product was directly purified by column chromatography (eluent gradient: Hexane → DCM) to afford **6** as an orange solid. (541 mg, 0.800 mmol, 80%)

**<sup>1</sup>H NMR** (600 MHz, CDCl<sub>3</sub>) δ = 7.93 (d, *J* = 8.5 Hz, 4H, *H*-c), 7.27-7.26 (m, 4H, *H*-g), 7.15 (d, *J* = 8.5 Hz, 4H, *H*-h), 2.68 – 2.63 (m, 4H, *H*-j), 1.65 (p, *J* = 7.7, 7.3 Hz, 4H, *H*-k), 1.38-1.31 (m, 12H, *H*-l,m,n), 0.94-0.91 (m, 6H, *H*-o) ppm.

**<sup>13</sup>C{<sup>1</sup>H} NMR** (151 MHz, CDCl<sub>3</sub>) δ = 162.64 (C-e), 155.24 (dd, <sup>1</sup>*J* = 263.2, <sup>4</sup>*J* = 3.7 Hz, (C-b)), 148.48 (C-f), 141.40 (C-i), 134.59 (t, <sup>2</sup>*J* = 10.2 Hz, (C-a)), 133.02 (t, <sup>4</sup>*J* = 9.4 Hz, (C-d)), 129.66 (C-g), 121.10 (C-h), 114.66 (dd, <sup>2</sup>*J* = 21.8, <sup>4</sup>*J* = 3.9 Hz, (C-d)), 35.54 (C-j), 31.85 (C-l,m,n), 31.56 (C-k), 29.10 (C-l,m,n), 22.76 (C-l,m,n), 14.25 (C-o) ppm.

**<sup>19</sup>F NMR** (565 MHz, CDCl<sub>3</sub>) δ = -118.90 (d, <sup>3</sup>*J* = 9.3 Hz, *F*-b) ppm.

**HRMS** (EI) *m/z* (%): [M+]<sup>+</sup> calcd for [C<sub>38</sub>H<sub>38</sub>F<sub>4</sub>N<sub>2</sub>O<sub>4</sub>]<sup>+</sup> 662.27564; found 662.27622.

**IR** (ATR):  $\tilde{\nu}$  = 2953 (w), 2930 (w), 2854 (w), 1727 (s), 1580 (m), 1510 (m), 1467 (w), 1429 (s), 1338 (s), 1216 (s), 1187 (s), 1096 (w), 1037 (s), 1020 (m), 971 (w), 954 (m), 876 (s), 852 (m), 803 (m), 783 (m), 724 (w) cm<sup>-1</sup>.

**Mp**: Cr91N247I

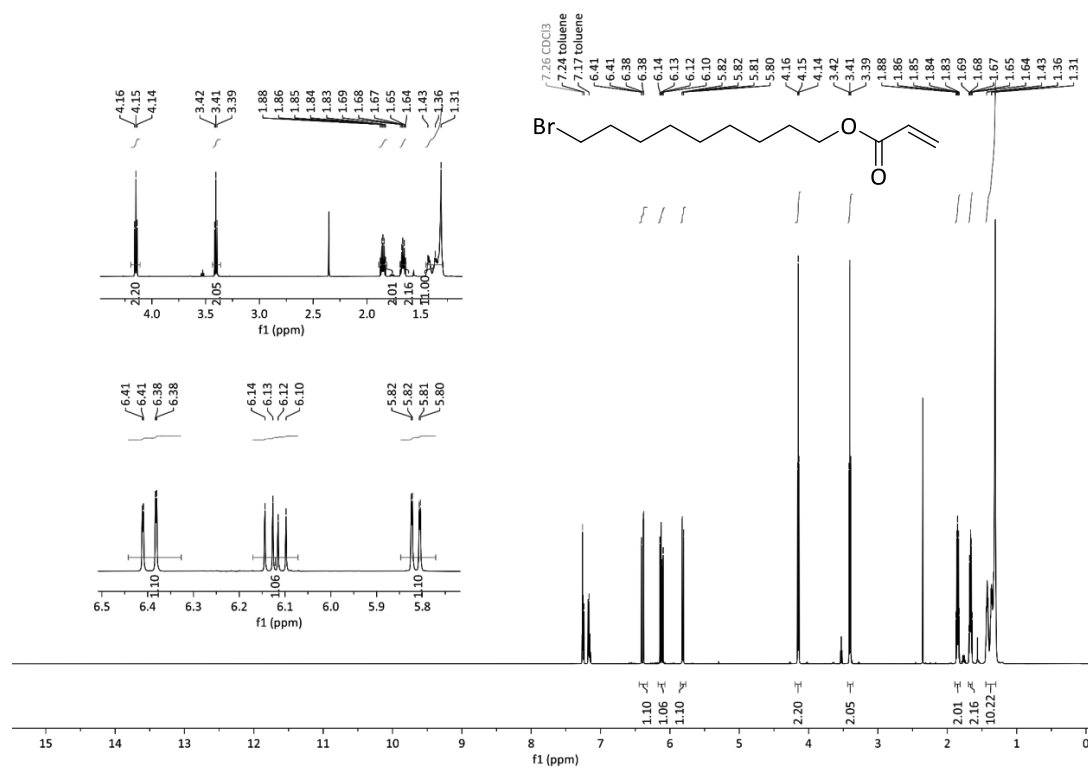
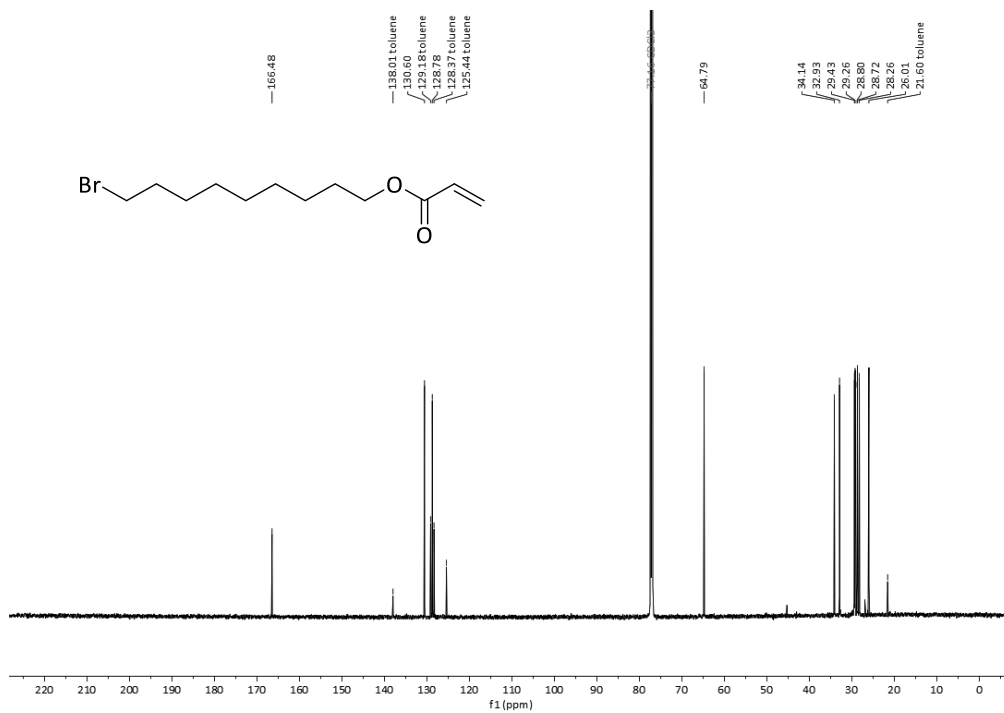
**Rf**: 0.6 (*n*-hexane:DCM, 1:1).

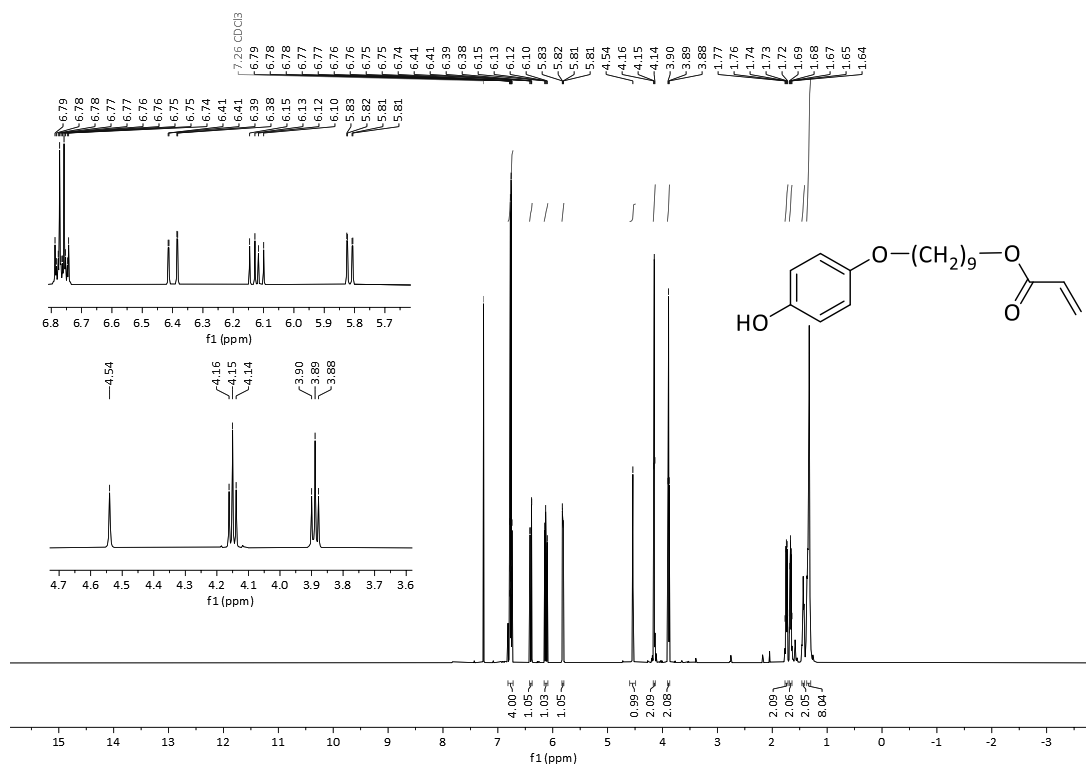
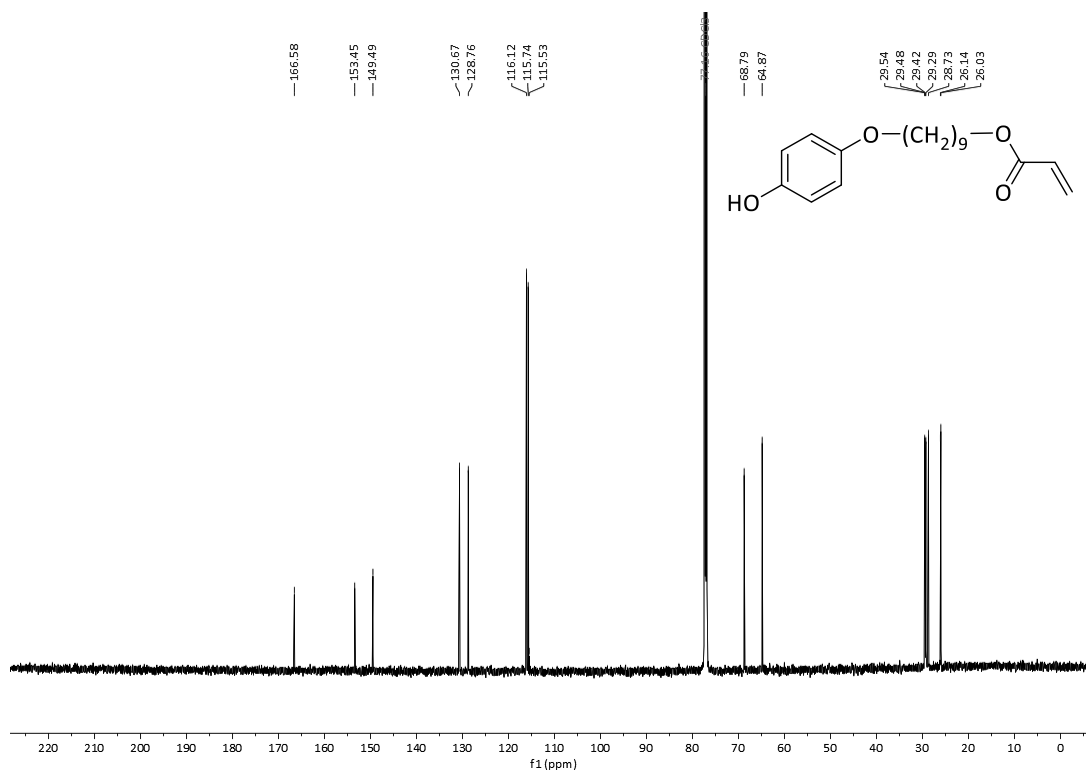
## 5. References

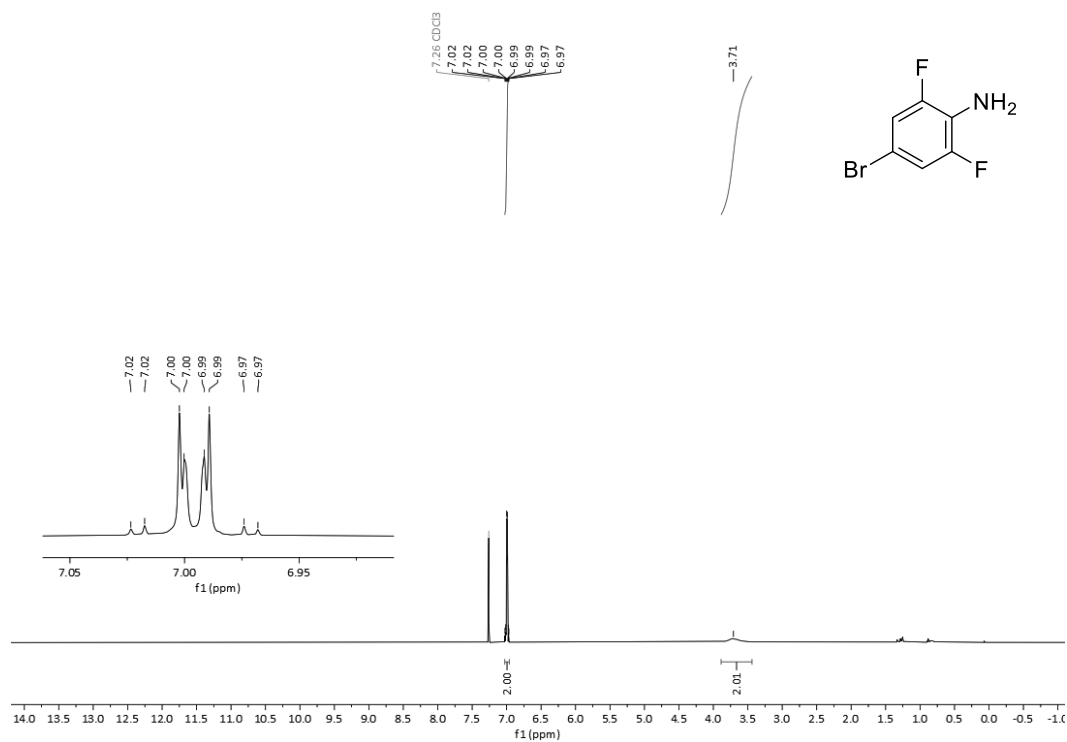
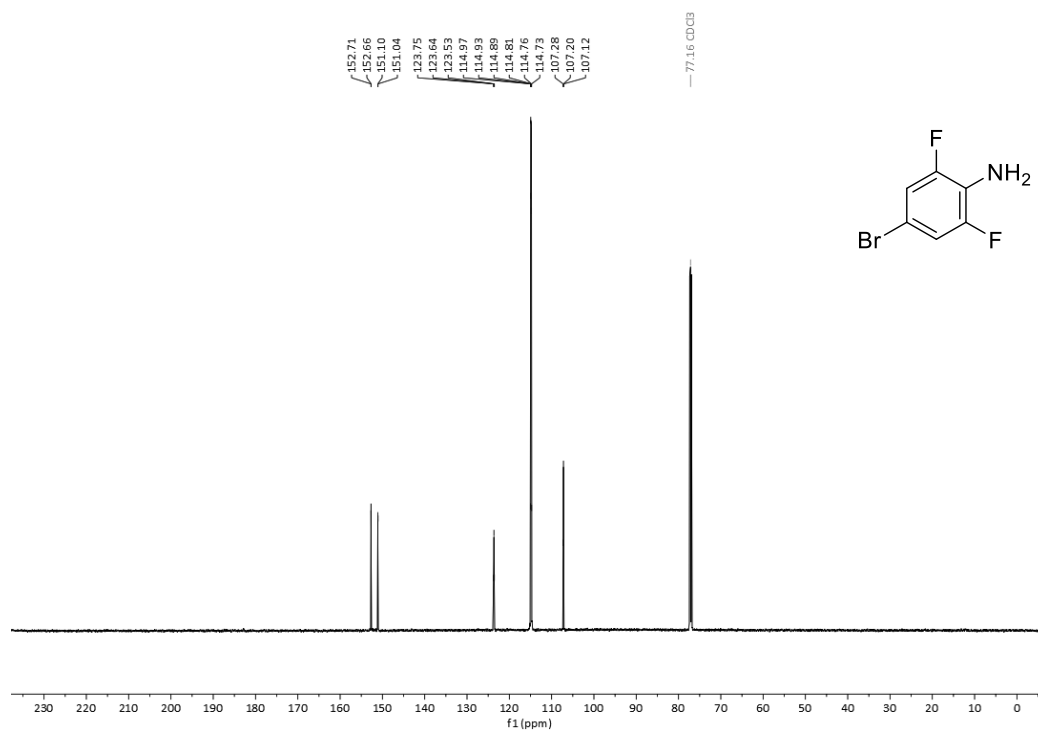
- [1] P. A. Heiney, <http://www.datasqueezesoftware.com>, 2006.
- [2] P. Scherrer, *Nachr. Ges. Wiss. Goettingen Math.-Phys. Kl.* **1918**, 2, 98.
- [3] O. V. Dolomanov, Bourhis, L. J., Gildea, R. J., Howard, J. A. K., Puschmann, H., *J. Appl. Crystallogr.* **2009**, 42.
- [4] *The ACS Style Guide: Effective Communication of Scientific Information*, American Chemical Society, Washington, DC **2006**.
- [5] J. Moreno, M. Gerecke, L. Grubert, S. A. Kovalenko, S. Hecht, *Angew. Chem. Int. Ed.* **2016**, 55, 1544.
- [6] B. Heinrich, K. Bouazoune, M. Wojcik, U. Bakowsky, O. Vázquez, *Org. Biomol. Chem.* **2019**, 17, 1827.
- [7] M. Cigl, A. Bubnov, M. Kašpar, F. Hampl, V. Hamplová, O. Pacherová, J. Svoboda, *J. Mater. Chem. C* **2016**, 4, 5326.
- [8] S. Schultzke, M. Walther, A. Staubitz, *Molecules* **2021**, 26, 3916.
- [9] A. Antoine John, Q. Lin, *J. Org. Chem.* **2017**, 82, 9873.

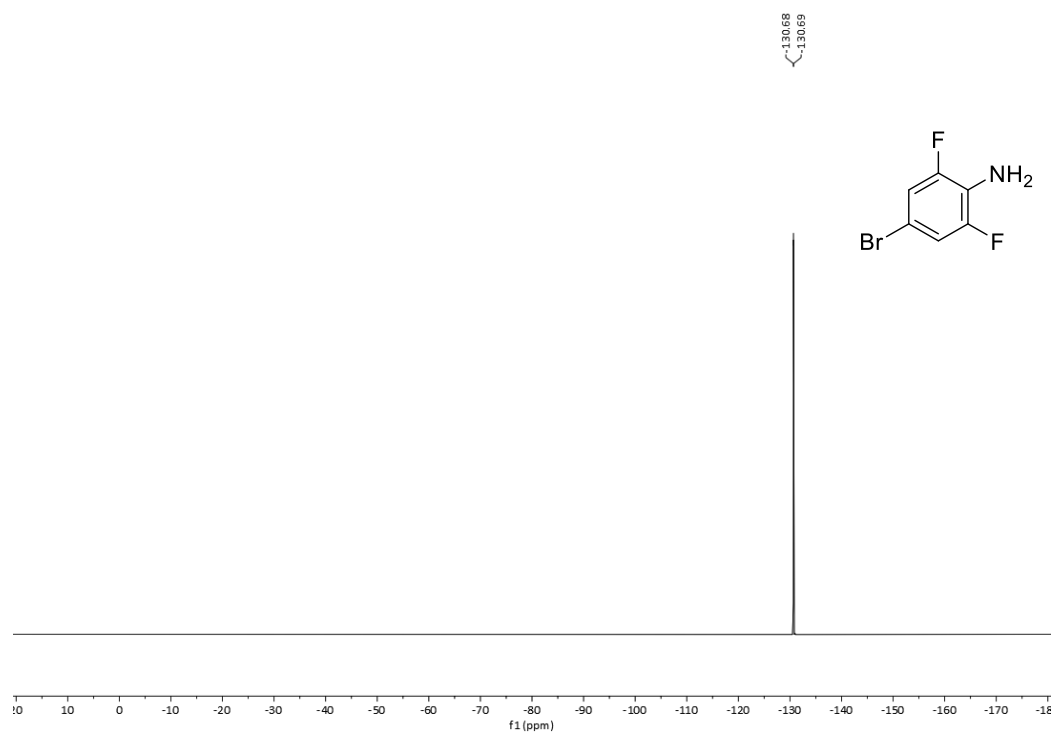
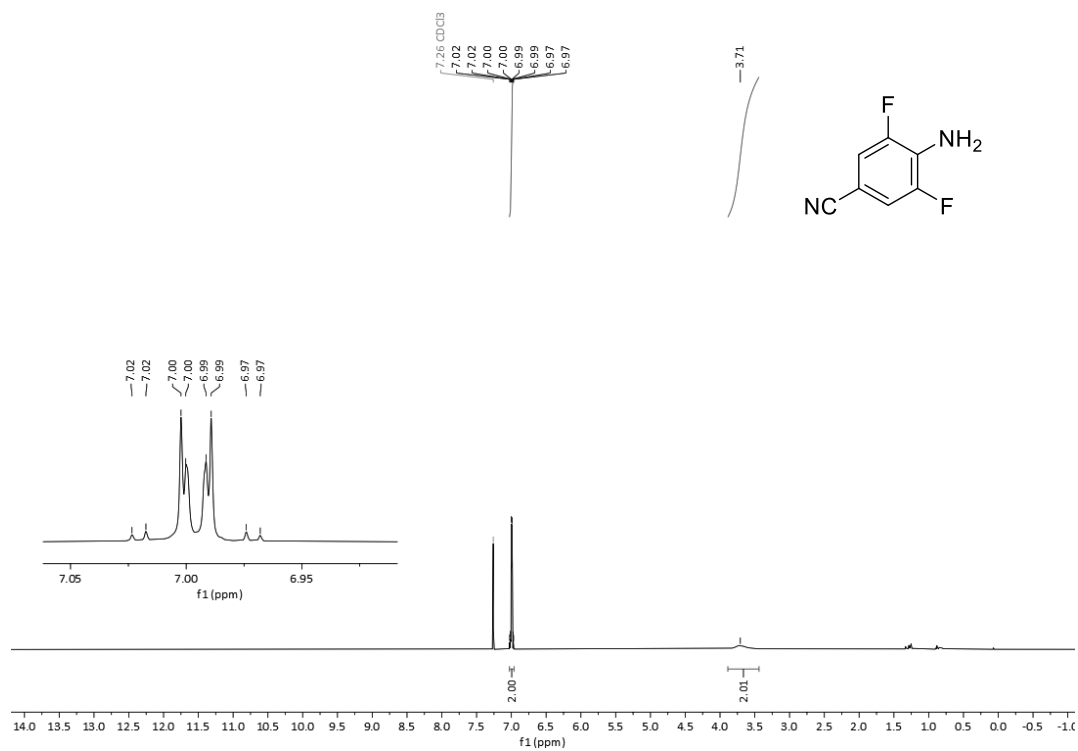
6.  $^1\text{H}$ ,  $^{13}\text{C}\{^1\text{H}\}$  and  $^{19}\text{F}$  NMR Spectra of the Purified Compounds

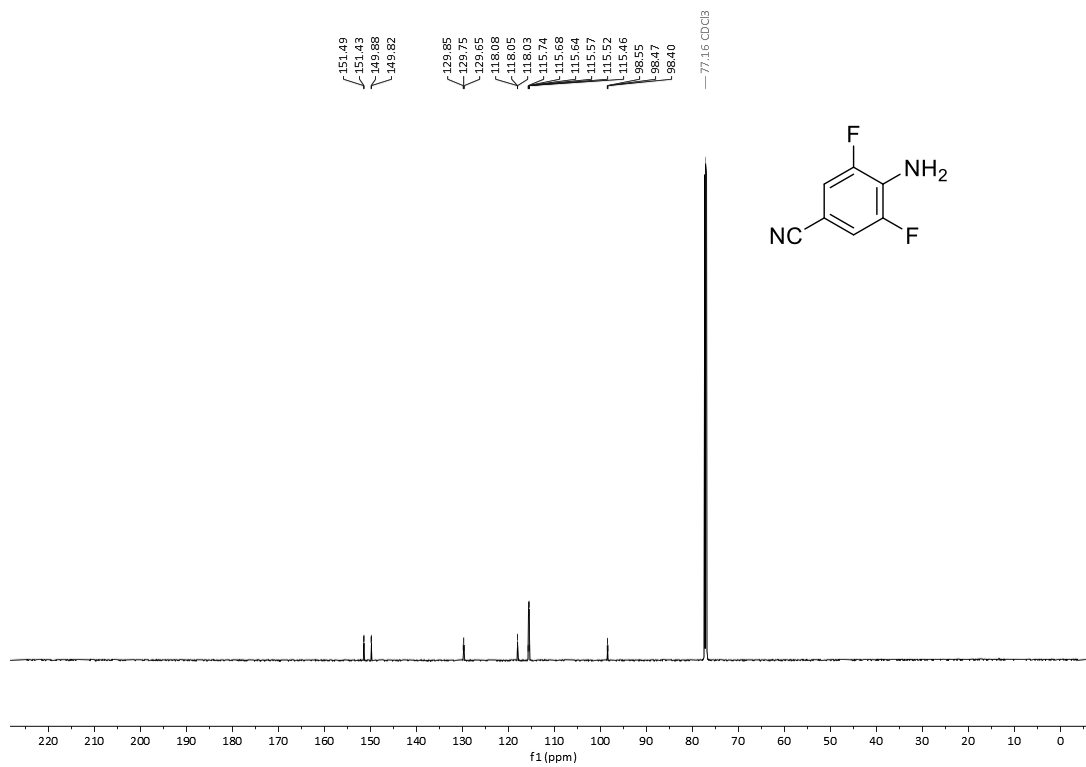
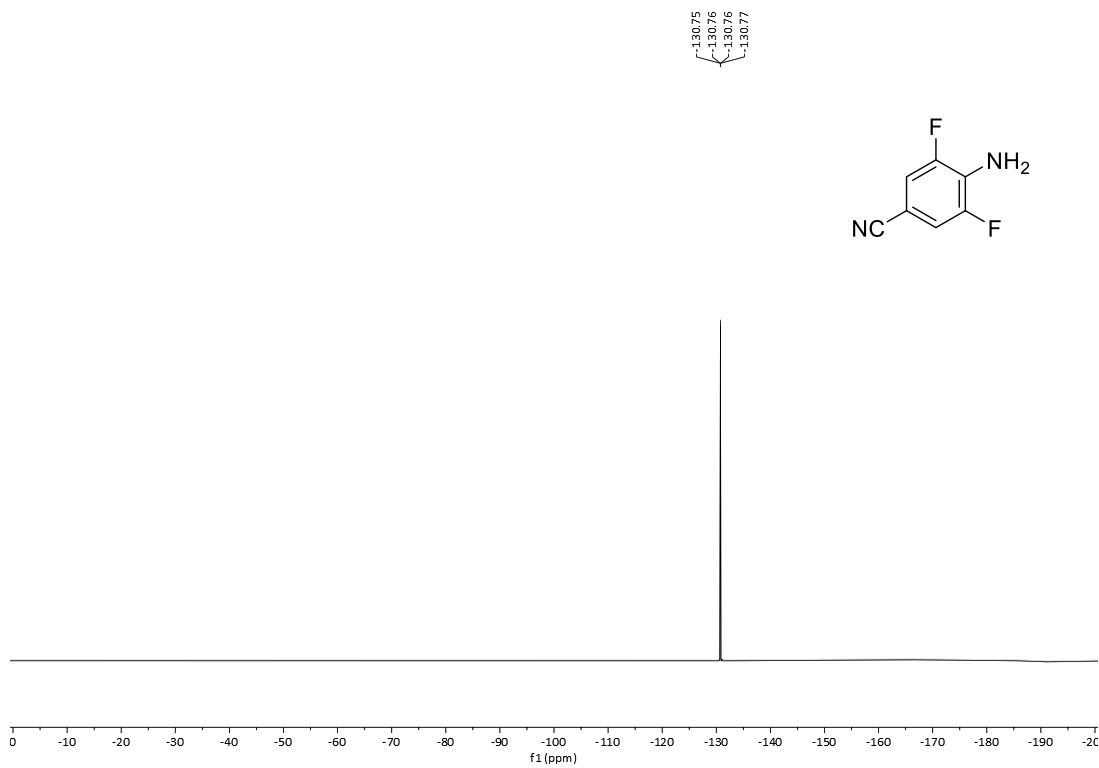
## 9-Bromononyl acrylate (S1)

Figure S26:  $^1\text{H}$  NMR spectrum of S1 in CDCl<sub>3</sub>.Figure S27:  $^{13}\text{C}\{^1\text{H}\}$  NMR spectrum of S1 in CDCl<sub>3</sub>.

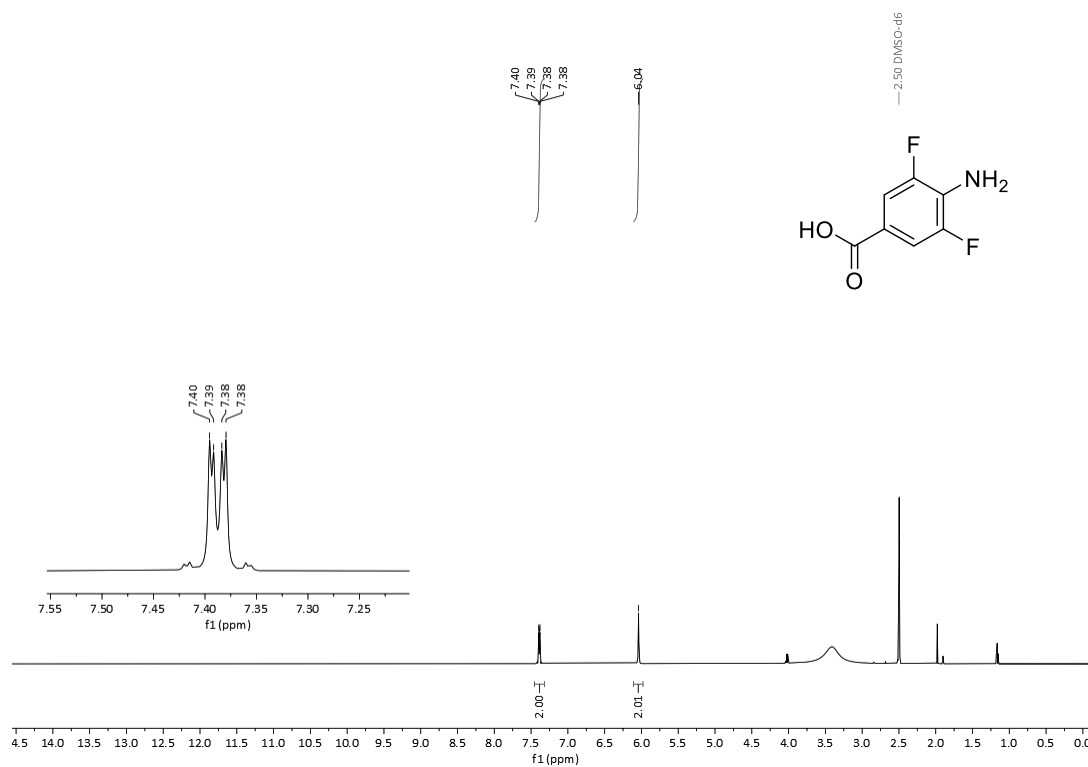
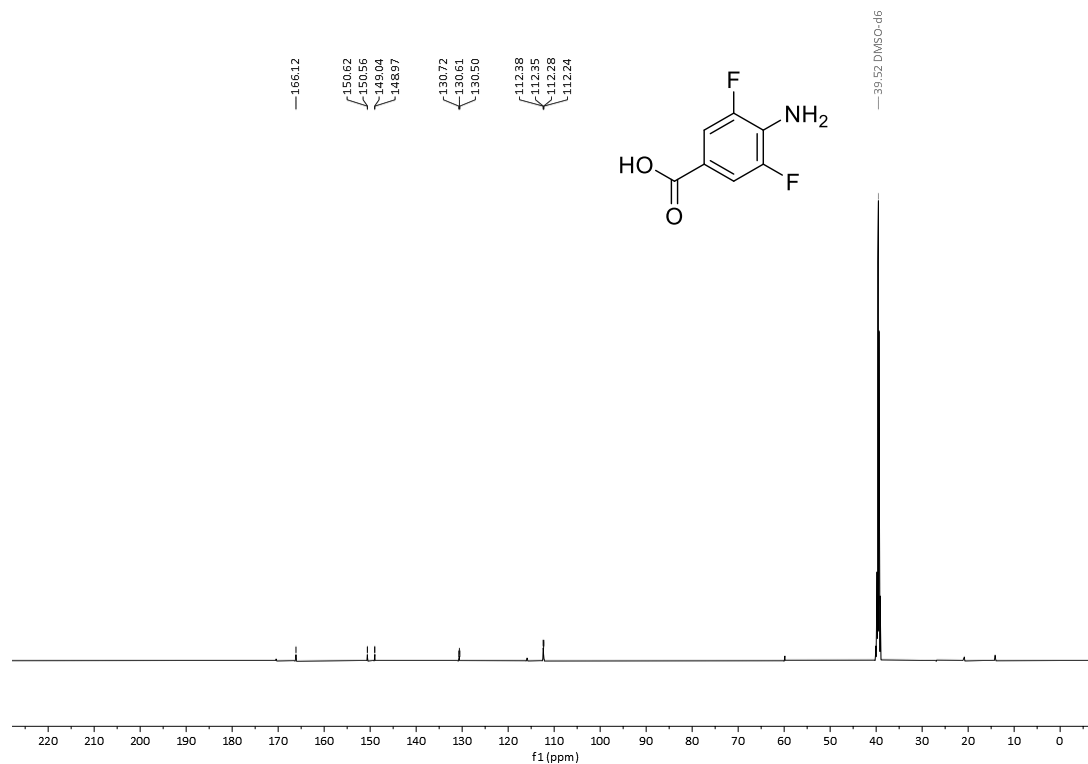
(E)-4,4'-(Diazene-1,2-diyl)bis(3,5-difluorobenzoic acid) (**2**)Figure S28: <sup>1</sup>H NMR spectrum of **2** in CDCl<sub>3</sub>.Figure S29: <sup>13</sup>C{<sup>1</sup>H} NMR spectrum of **2** in CDCl<sub>3</sub>.

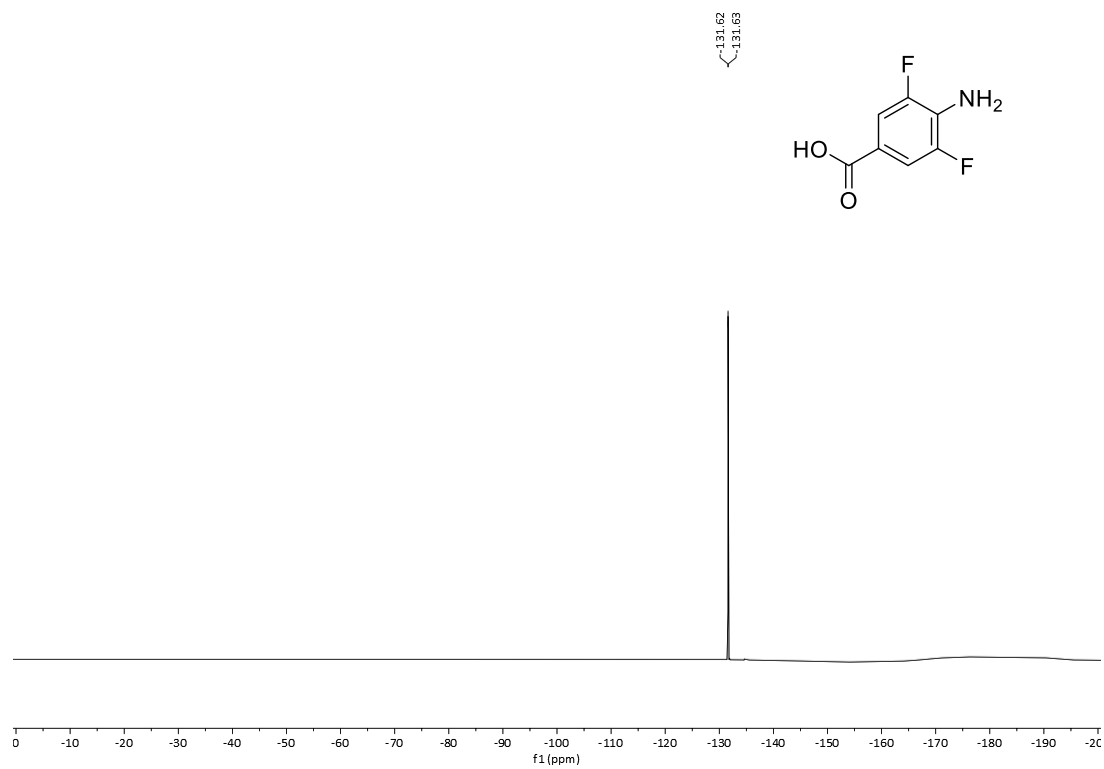
4-Bromo-2,6-difluoroaniline (**S2**)Figure S30: <sup>1</sup>H NMR spectrum of **S2** in CDCl<sub>3</sub>.Figure S31: <sup>13</sup>C{<sup>1</sup>H} NMR spectrum of **S2** in CDCl<sub>3</sub>.

Figure S32:  $^{19}\text{F}$  NMR spectrum of **S2** in  $\text{CDCl}_3$ .4-Amino-3,5-difluorobenzonitrile (**S3**)Figure S33:  $^1\text{H}$  NMR spectrum of **S3** in  $\text{CDCl}_3$ .

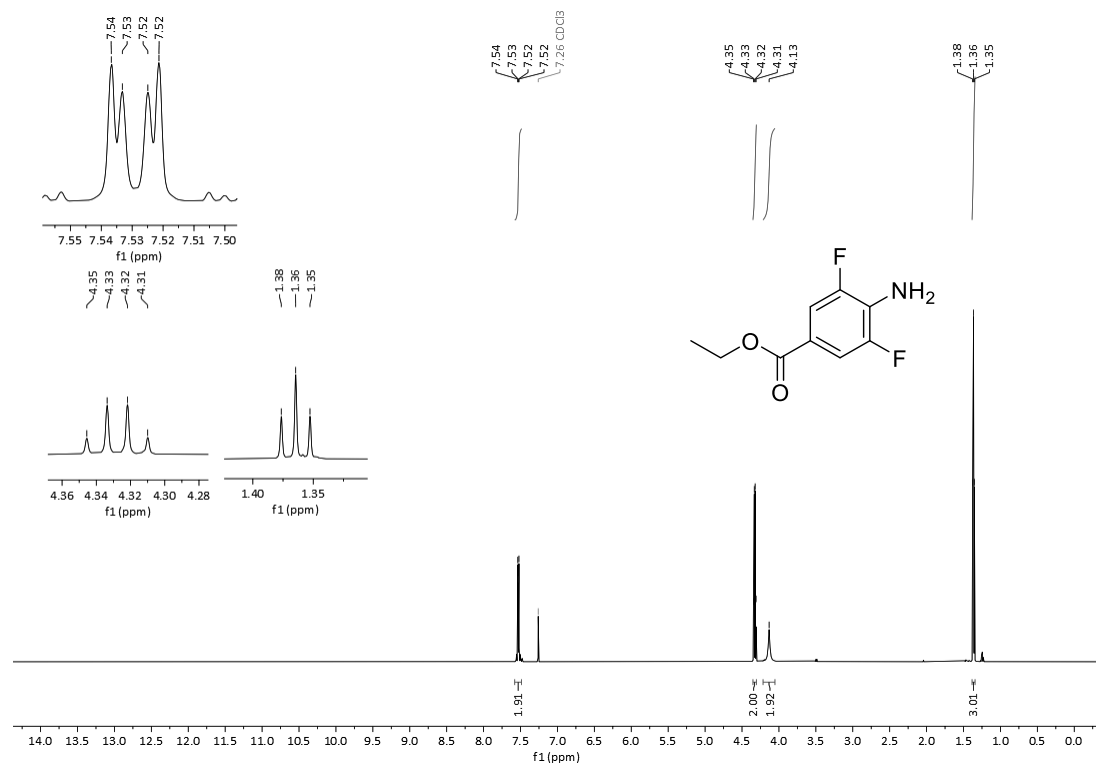
Figure S34: <sup>13</sup>C{<sup>1</sup>H} NMR spectrum of S3 in CDCl<sub>3</sub>.Figure S35: <sup>19</sup>F NMR spectrum of S3 in CDCl<sub>3</sub>.

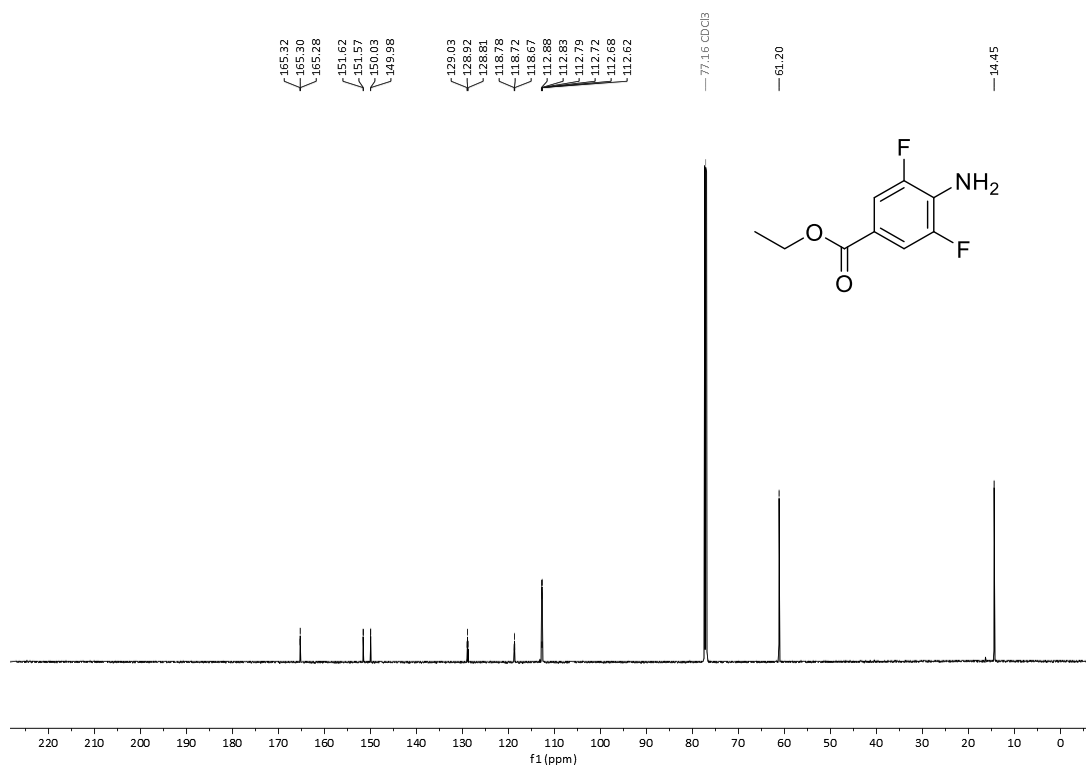
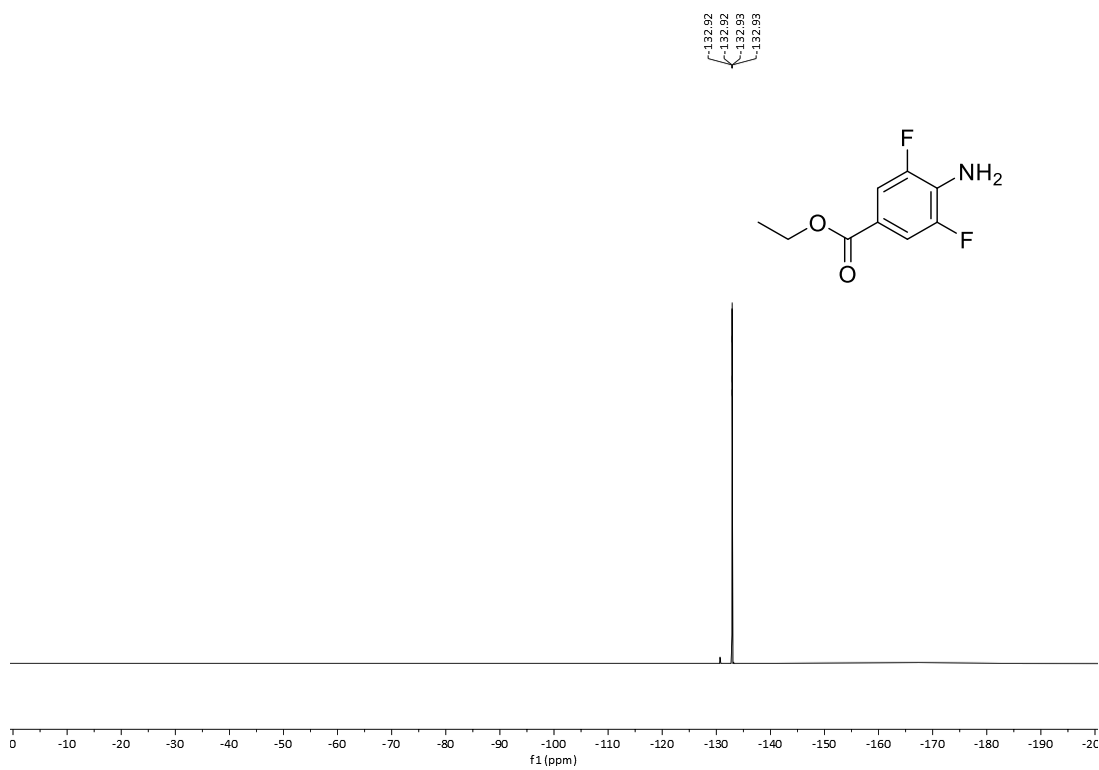


4-Amino-3,5-difluorobenzoic acid (**S4**)Figure S36:  $^1\text{H}$  NMR spectrum of **S4** in  $\text{DMSO-}d_6$ .Figure S37:  $^{13}\text{C}\{^1\text{H}\}$  NMR spectrum of **S4** in  $\text{DMSO-}d_6$ .

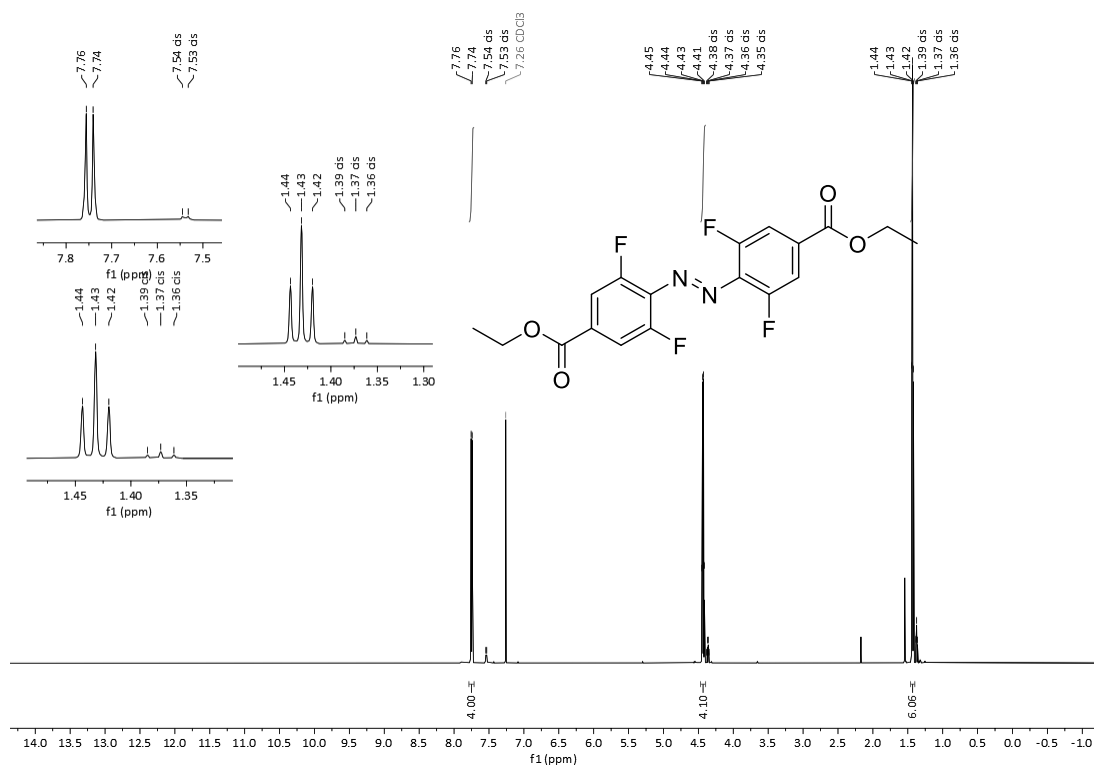
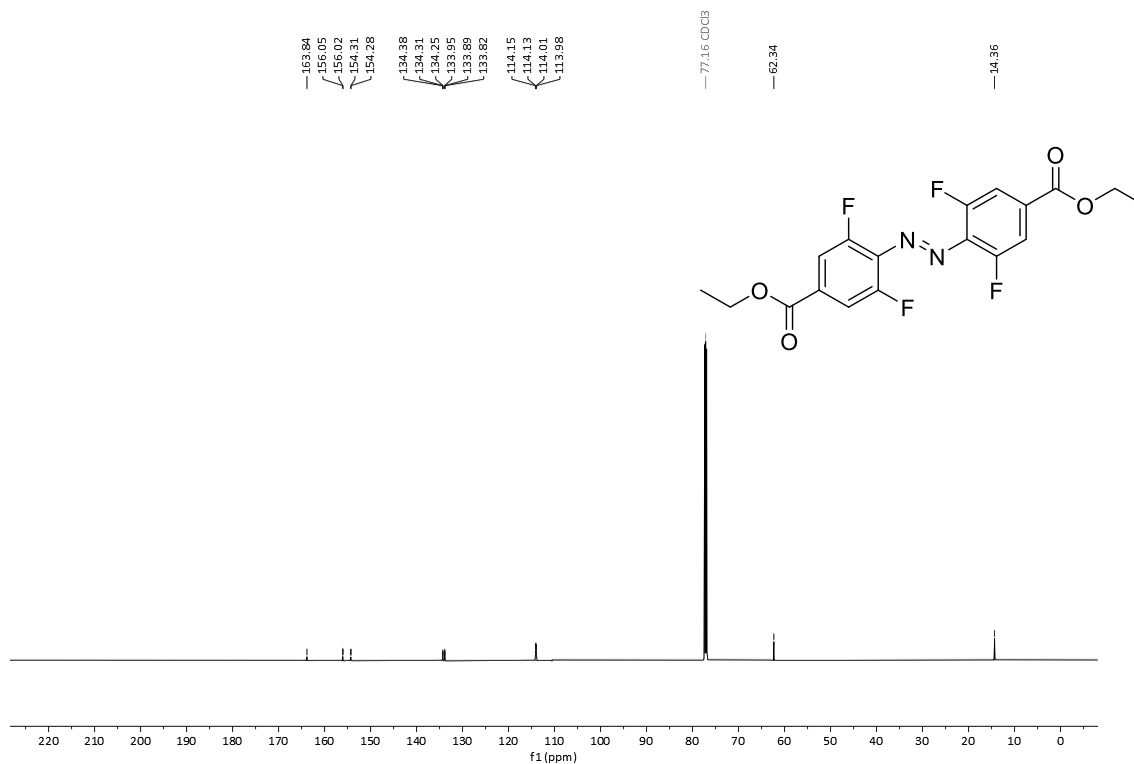
Figure S38:  $^{19}\text{F}$  NMR spectrum of S4 in  $\text{DMSO-}d_6$ .

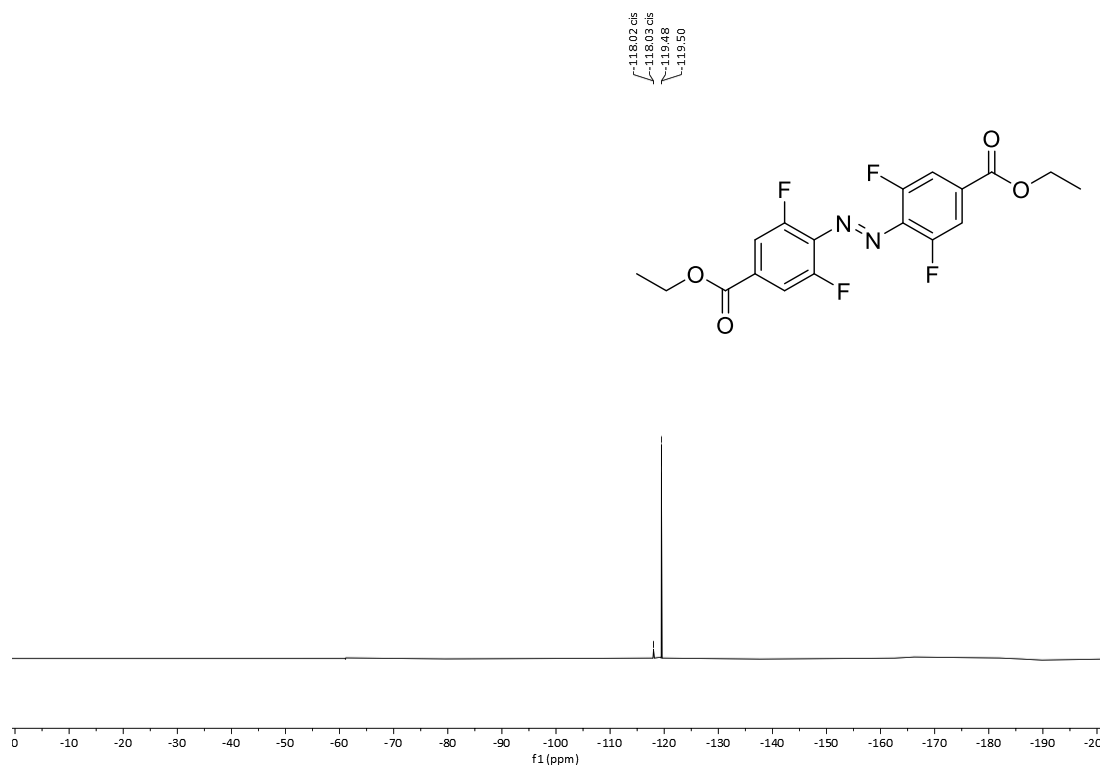
## Ethyl 4-amino-3,5-difluorobenzoate (S5)

Figure S39:  $^1\text{H}$  NMR spectrum of S5 in  $\text{CDCl}_3$ .

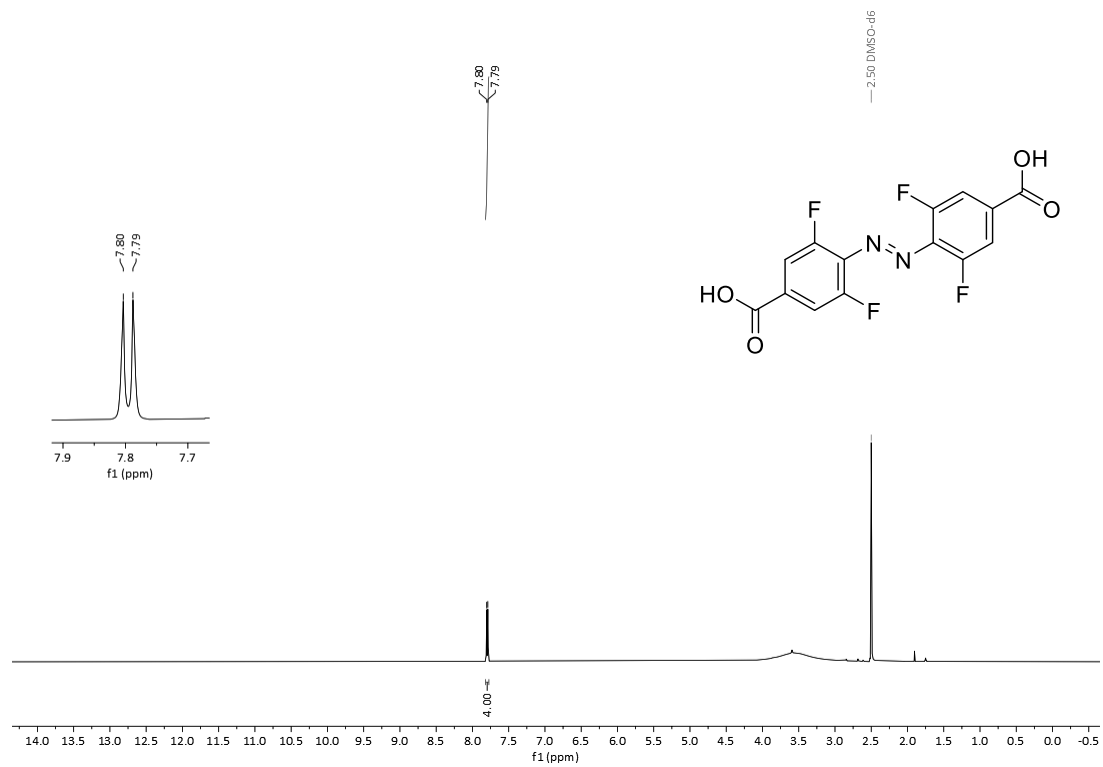
Figure S40:  $^{13}\text{C}\{^1\text{H}\}$  NMR spectrum of **55** in  $\text{CDCl}_3$ .Figure S41:  $^{19}\text{F}$  NMR spectrum of **55** in  $\text{CDCl}_3$ .

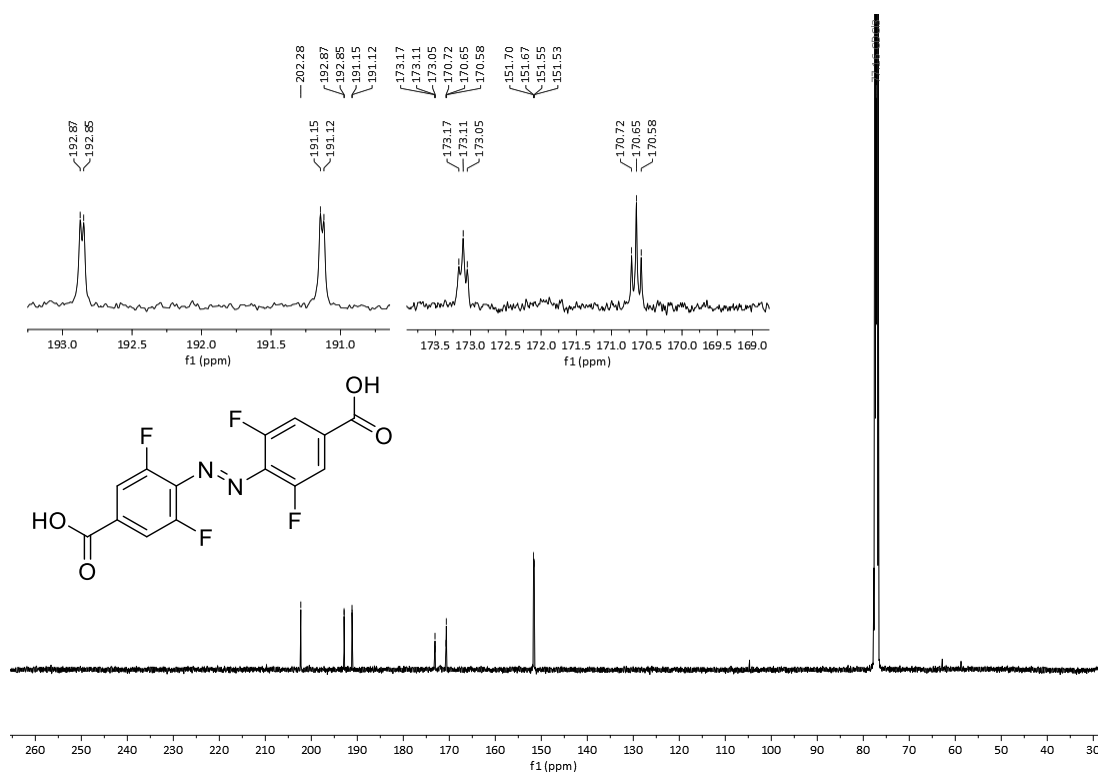
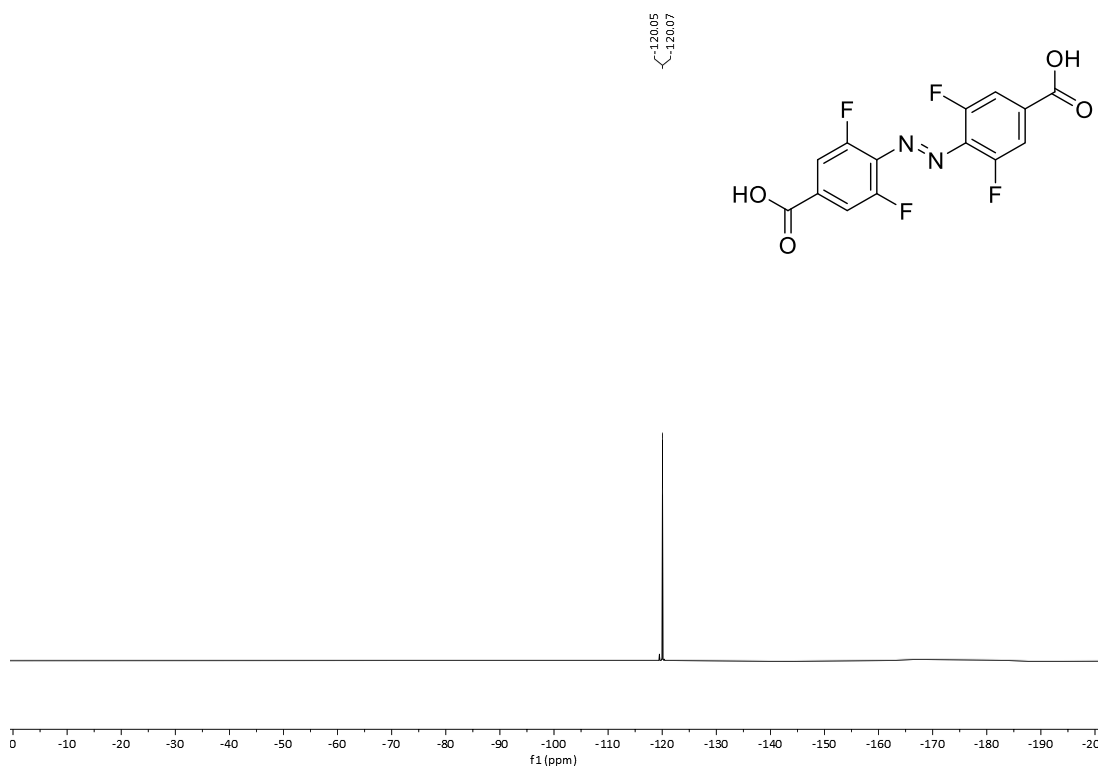
## Diethyl 4,4'-(diazene-1,2-diyl)(E)-bis(3,5-difluorobenzoate) (S6)

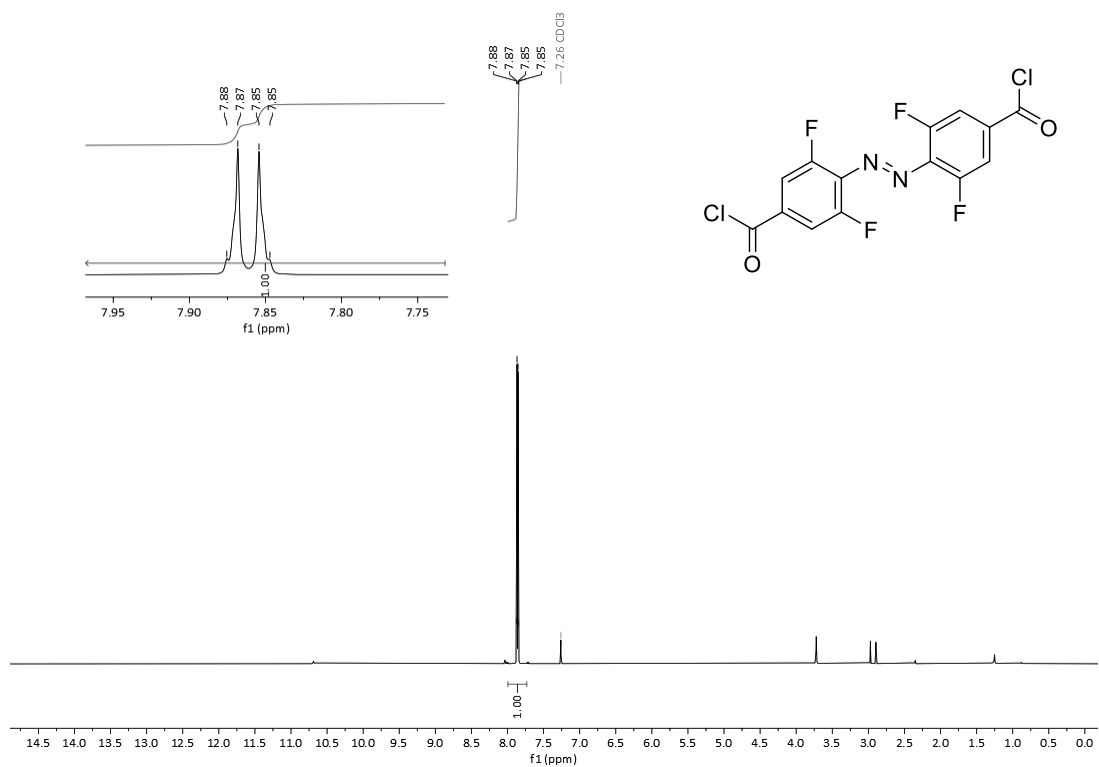
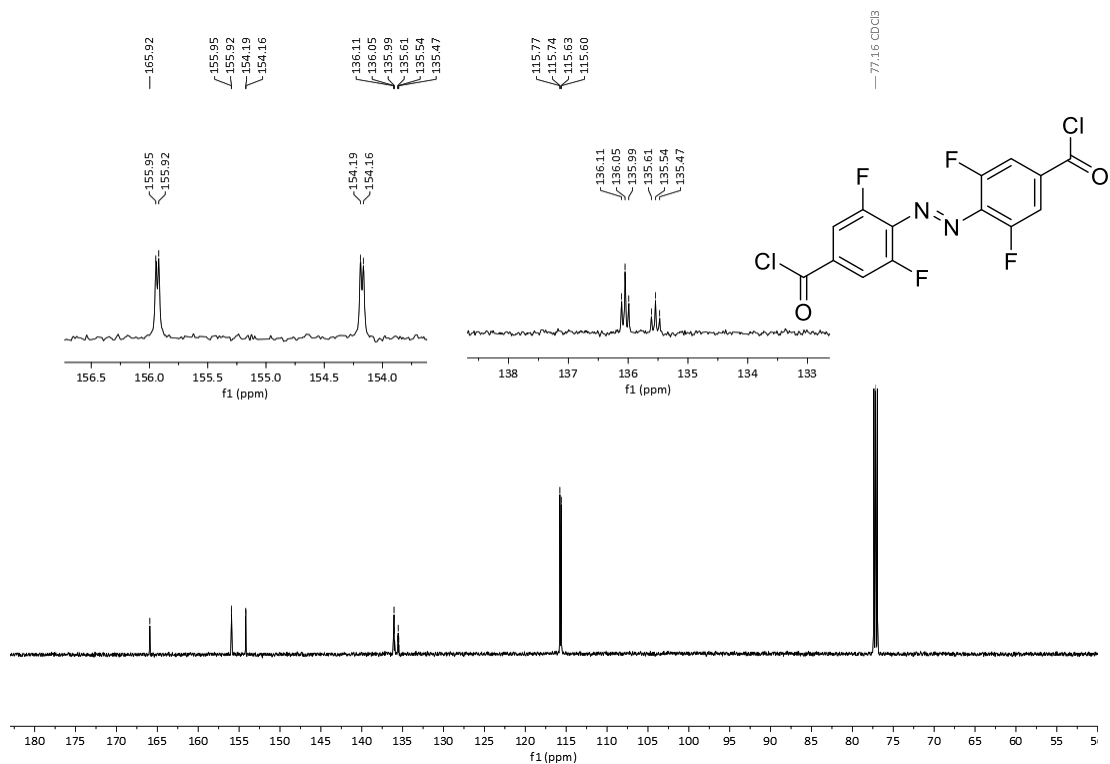
Figure S42:  $^1\text{H}$  NMR spectrum of S6 in  $\text{CDCl}_3$ .Figure S43:  $^{13}\text{C}\{^1\text{H}\}$  NMR spectrum of S6 in  $\text{CDCl}_3$ .

Figure S44:  $^{19}\text{F}$  NMR spectrum of **S6** in  $\text{CDCl}_3$ .

(*E*)-4,4'-(Diazene-1,2-diyl)bis(3,5-difluorobenzoic acid) (**S7**)

Figure S45:  $^1\text{H}$  NMR spectrum of **S7** in  $\text{DMSO}-d_6$ .

Figure S46:  $^{13}\text{C}\{^1\text{H}\}$  NMR spectrum of S7 in DMSO- $d_6$ .Figure S47:  $^{19}\text{F}$  NMR spectrum of S7 in DMSO- $d_6$ .

*(E)*-4,4'-(Diazene-1,2-diyl)bis(3,5-difluorobenzoyl chloride) (**4**)Figure S48: <sup>1</sup>H NMR spectrum of **4** in CDCl<sub>3</sub>.Figure S49: <sup>13</sup>C{<sup>1</sup>H} NMR spectrum of **4** in CDCl<sub>3</sub>.

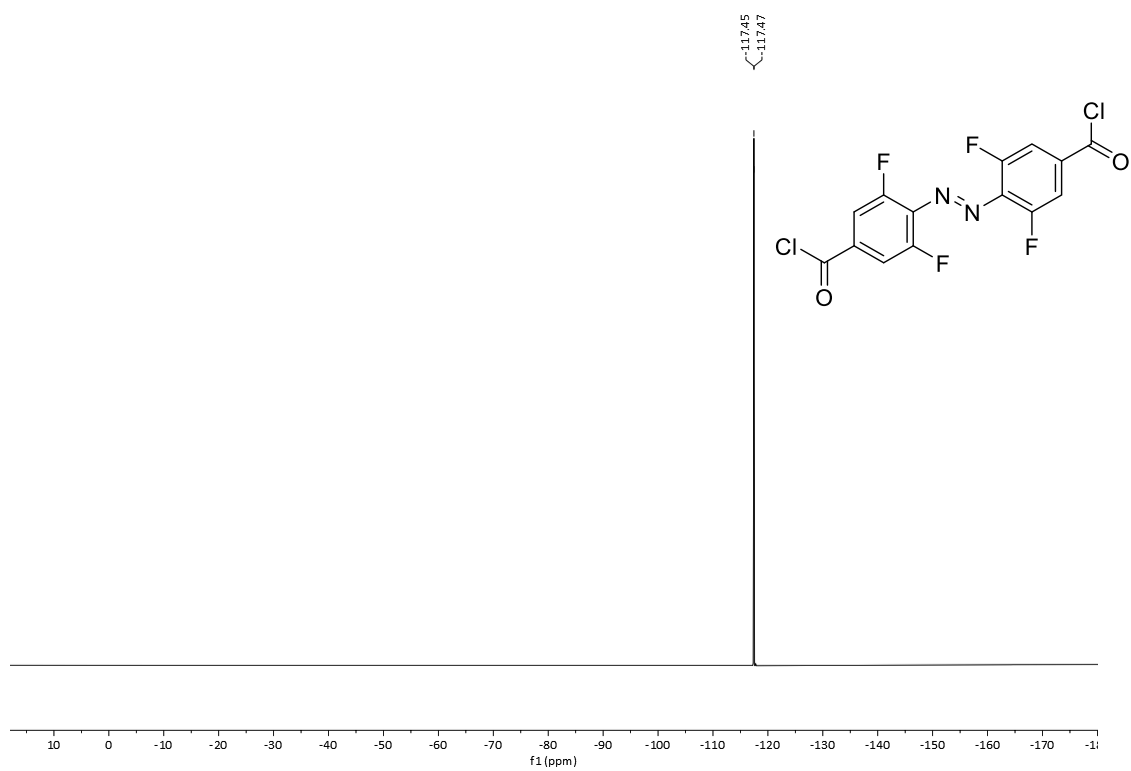
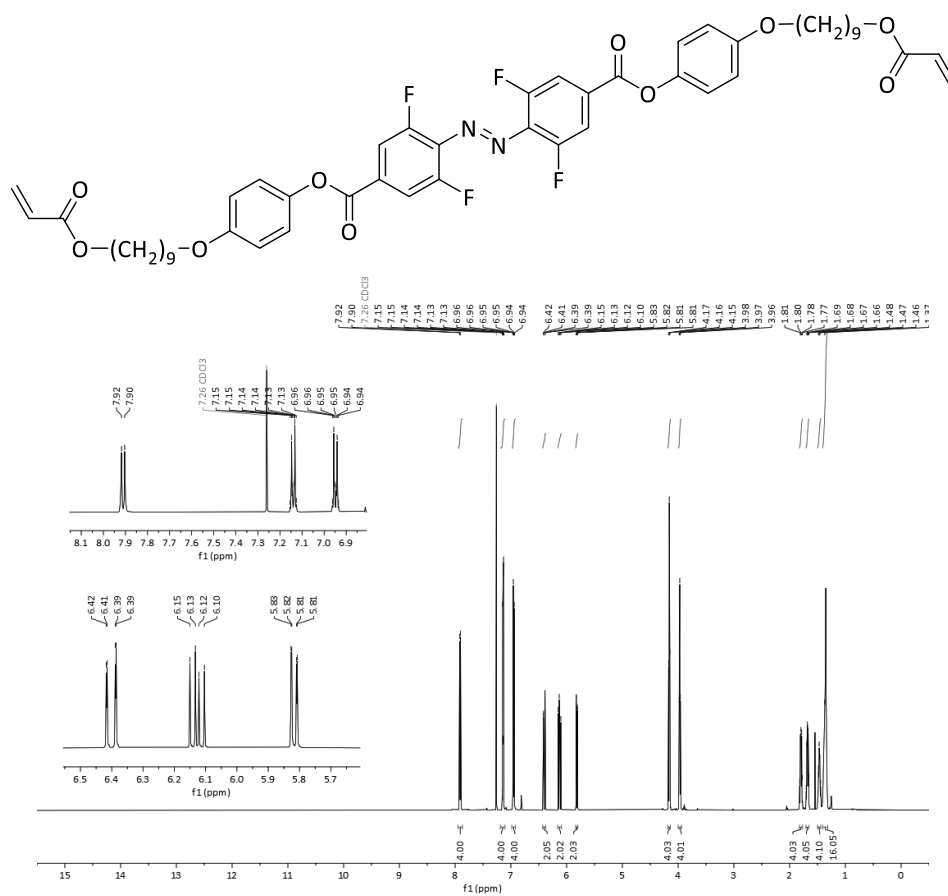
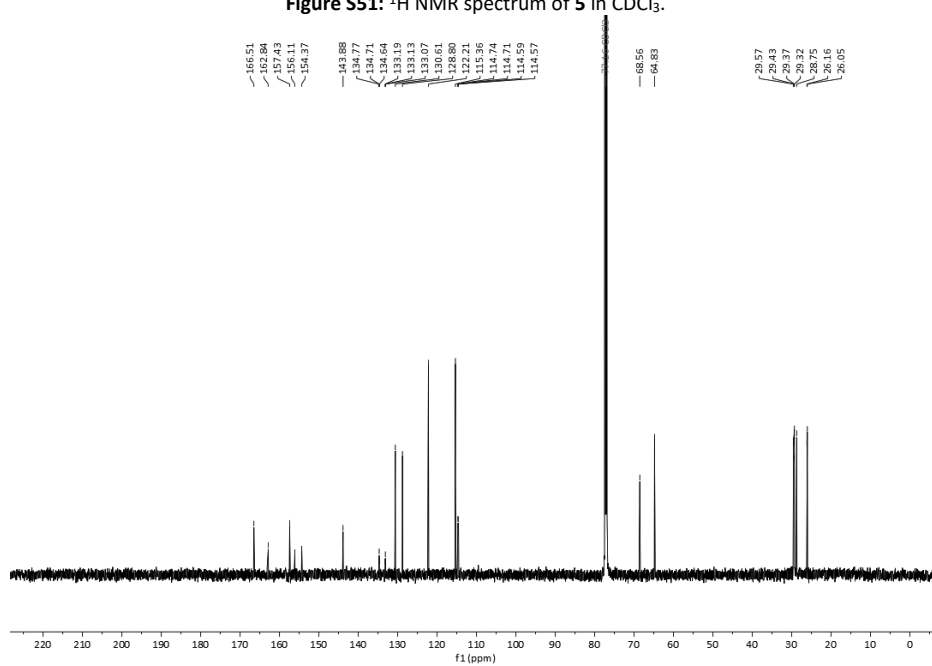
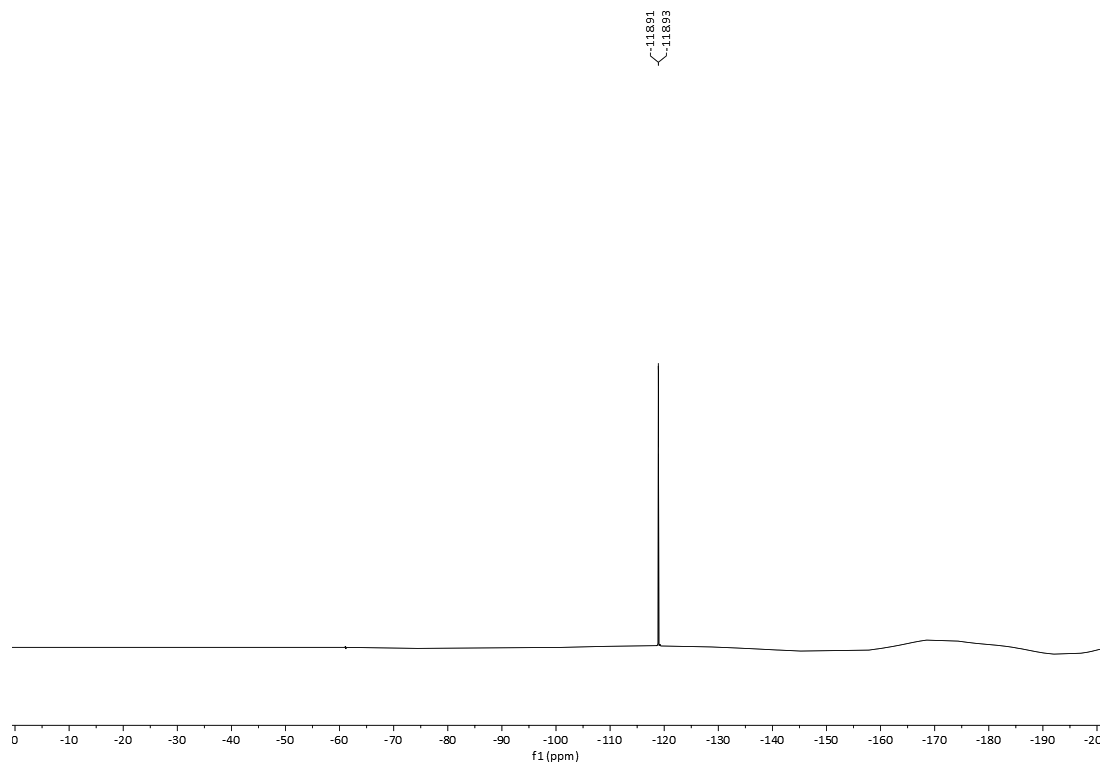
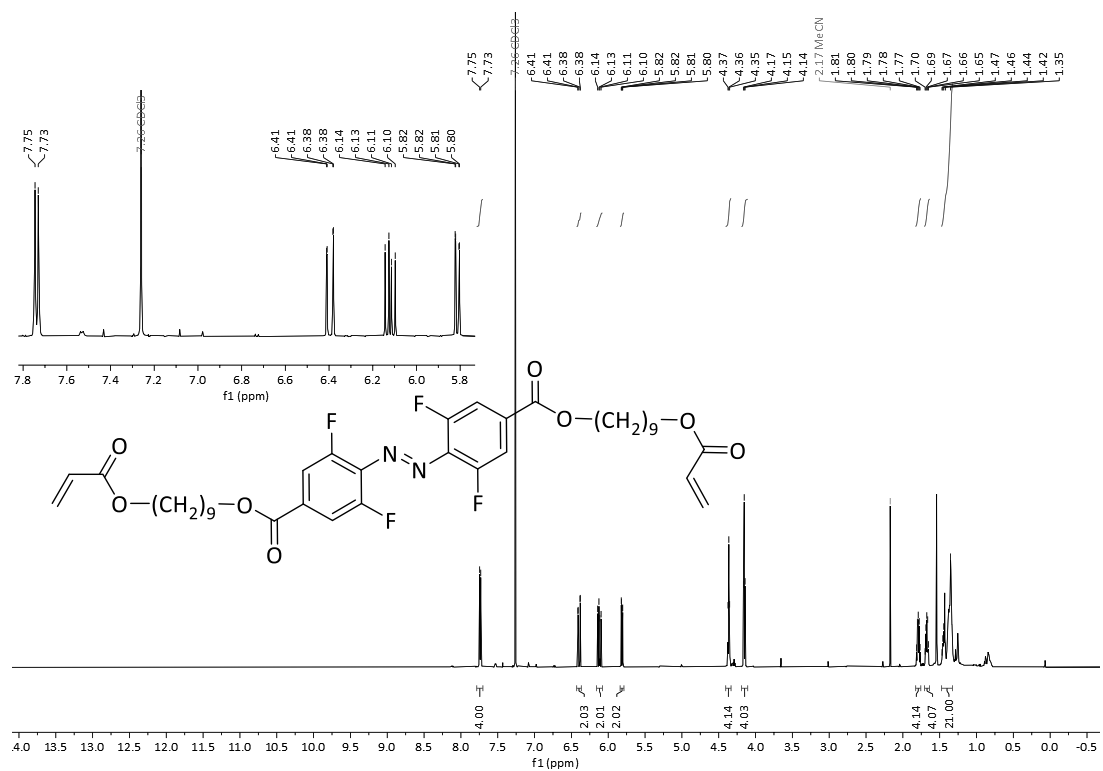
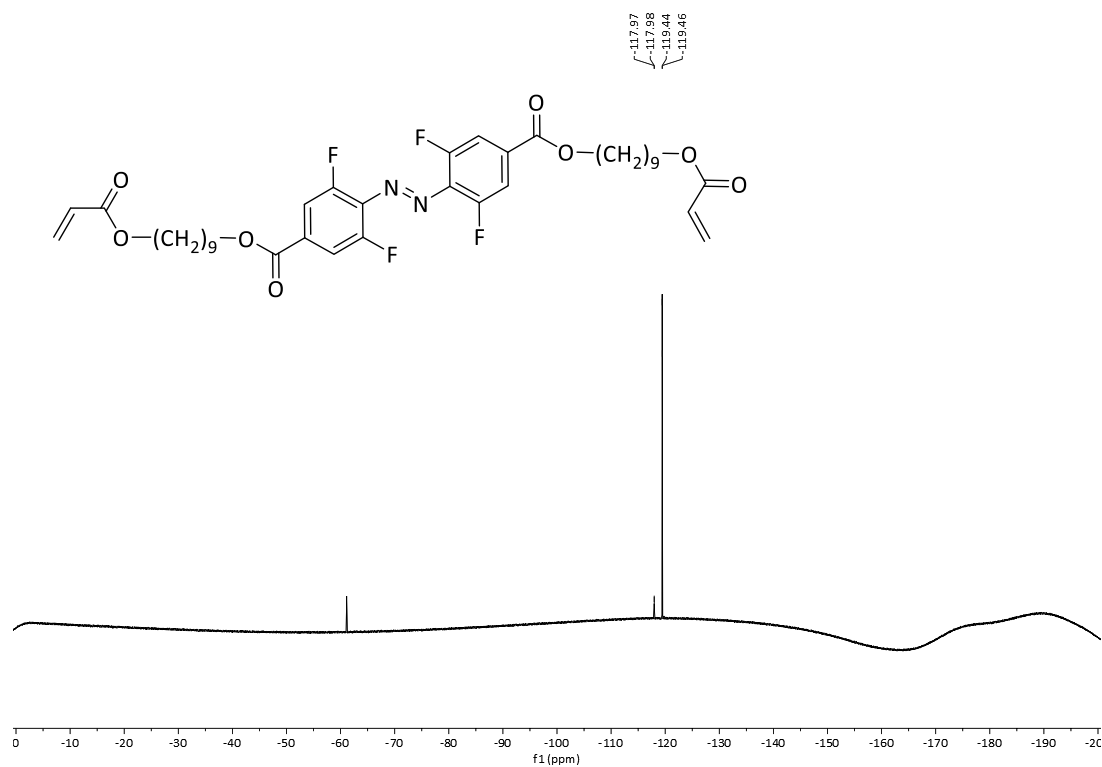
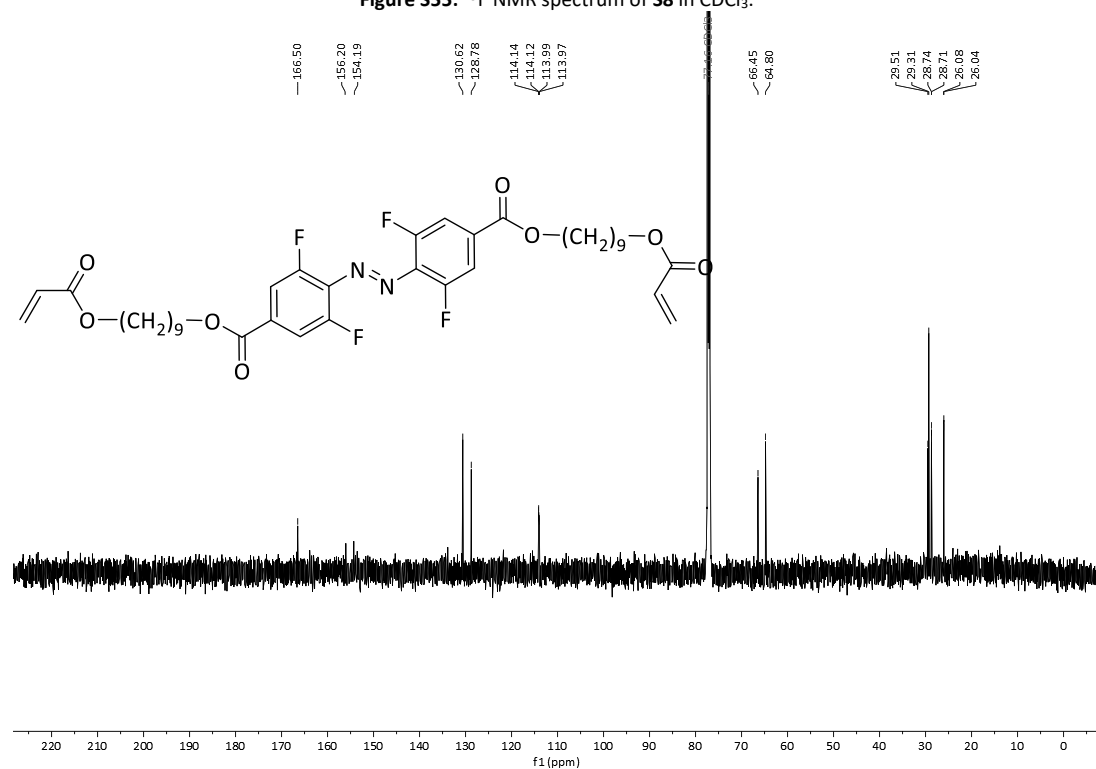


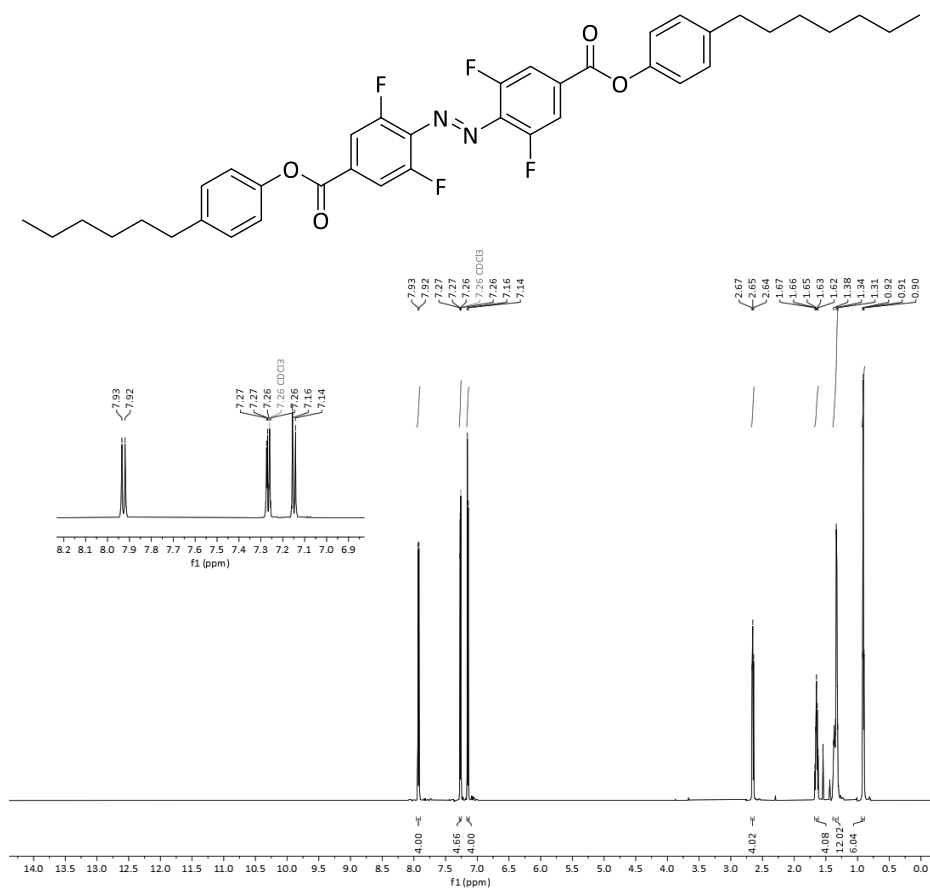
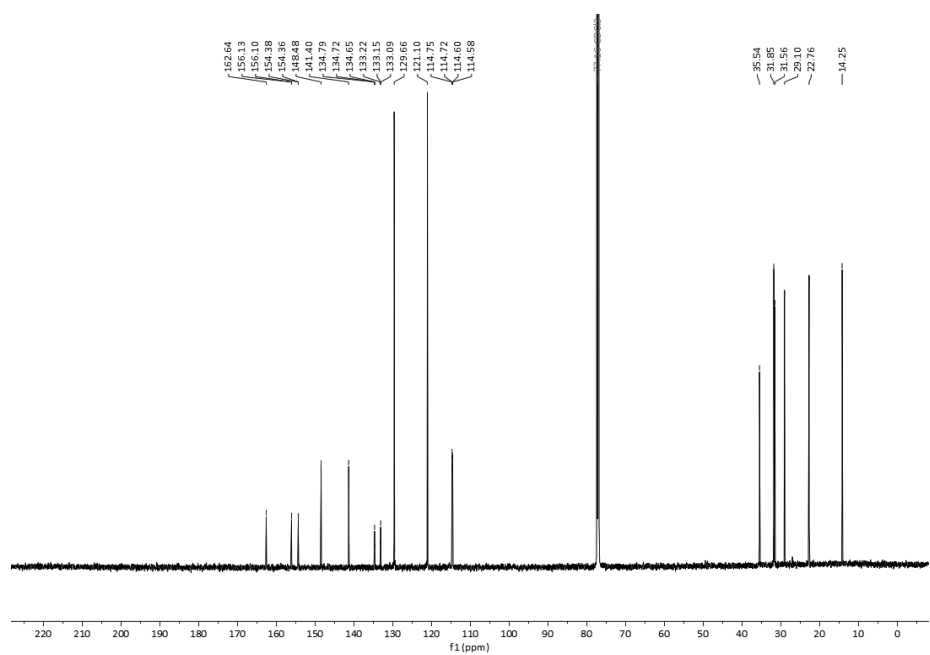
Figure S50:  $^{19}\text{F}$  NMR spectrum of **4** in  $\text{CDCl}_3$ .



*(E)*-4,4'-(Diazene-1,2-diyl)bis(3,5-difluorobenzoic acid) (5)Figure S51: <sup>1</sup>H NMR spectrum of 5 in CDCl<sub>3</sub>.Figure S52: <sup>13</sup>C{<sup>1</sup>H} NMR spectrum of 5 in CDCl<sub>3</sub>.

Figure S53:  $^{19}\text{F}$  NMR spectrum of **5** in  $\text{CDCl}_3$ .Bis(9-(acryloyloxy)nonyl 4,4'-(diazene-1,2-diyl)(E)-bis(3,5-difluorobenzoate) (**S8**)Figure S54:  $^1\text{H}$  NMR spectrum of **S8** in  $\text{CDCl}_3$ .

Figure S55:  $^{19}\text{F}$  NMR spectrum of **S8** in  $\text{CDCl}_3$ .Figure S56:  $^{13}\text{C}\{^1\text{H}\}$  NMR spectrum of **S8** in  $\text{CDCl}_3$ .

Bis(4-hexylphenyl) 4,4'-(diazene-1,2-diyl)(E)-bis(3,5-difluorobenzoate) (**6**)Figure S57:  $^1\text{H}$  NMR spectrum of **6** in  $\text{CDCl}_3$ .Figure S58:  $^{13}\text{C}\{^1\text{H}\}$  NMR spectrum of **6** in  $\text{CDCl}_3$ .

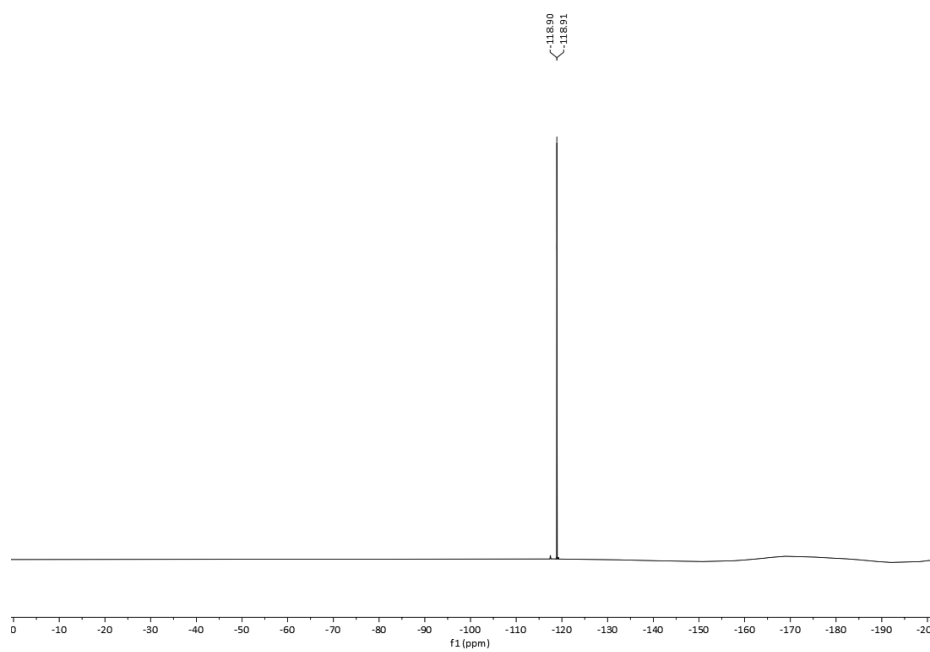
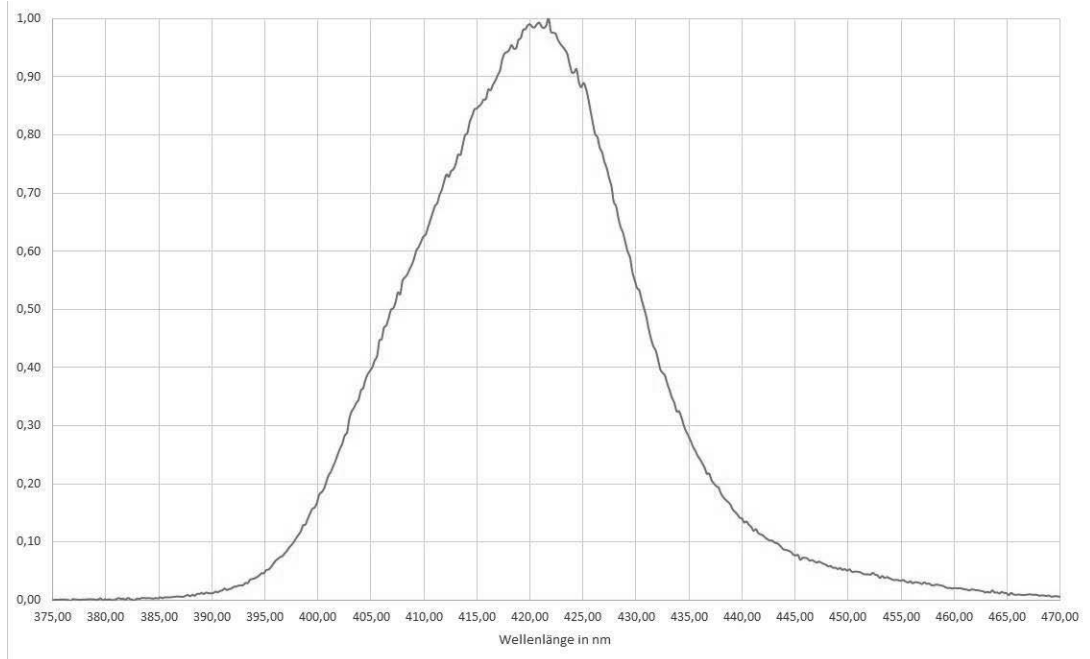
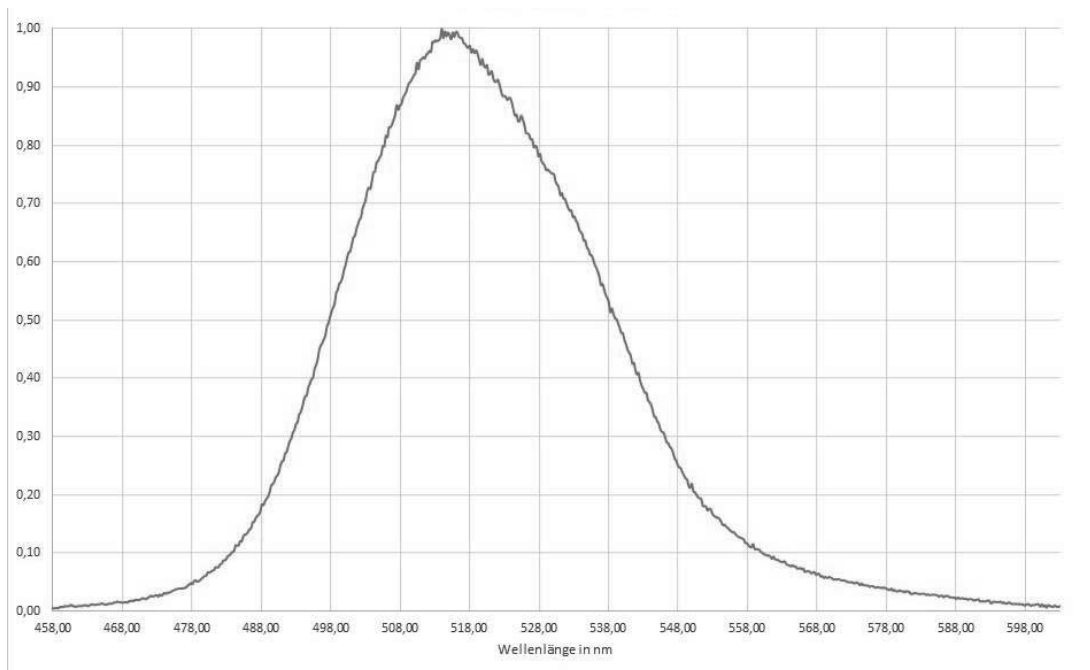


Figure S59:  $^{19}\text{F}$  NMR spectrum of **6** in  $\text{CDCl}_3$ .

### 7. Emission spectra of the LED's



**Figure S60:** Spectral measurement of the 420 nm (violet) LED measured by Avonec. Reprinted with permission from Avonec.



**Figure S61:** Spectral measurement of the 515 nm (green) LED measured by Avonec. Reprinted with permission from Avonec.

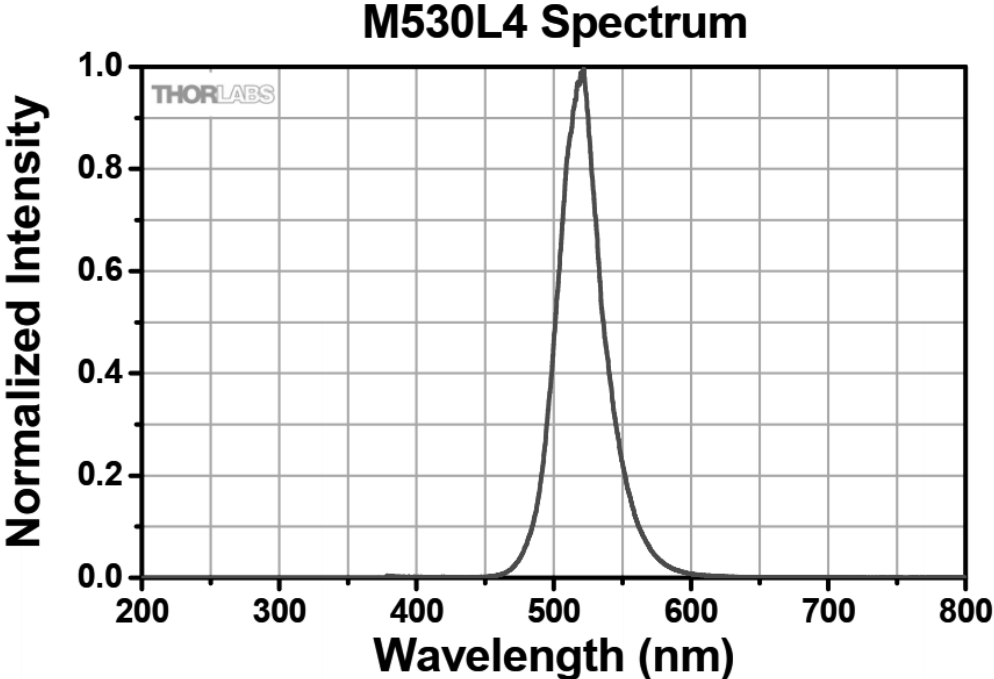


Figure S62: Spectral measurement of the 525 nm (green) LED measured by Thorlabs. Reprinted with permission from Thorlabs.

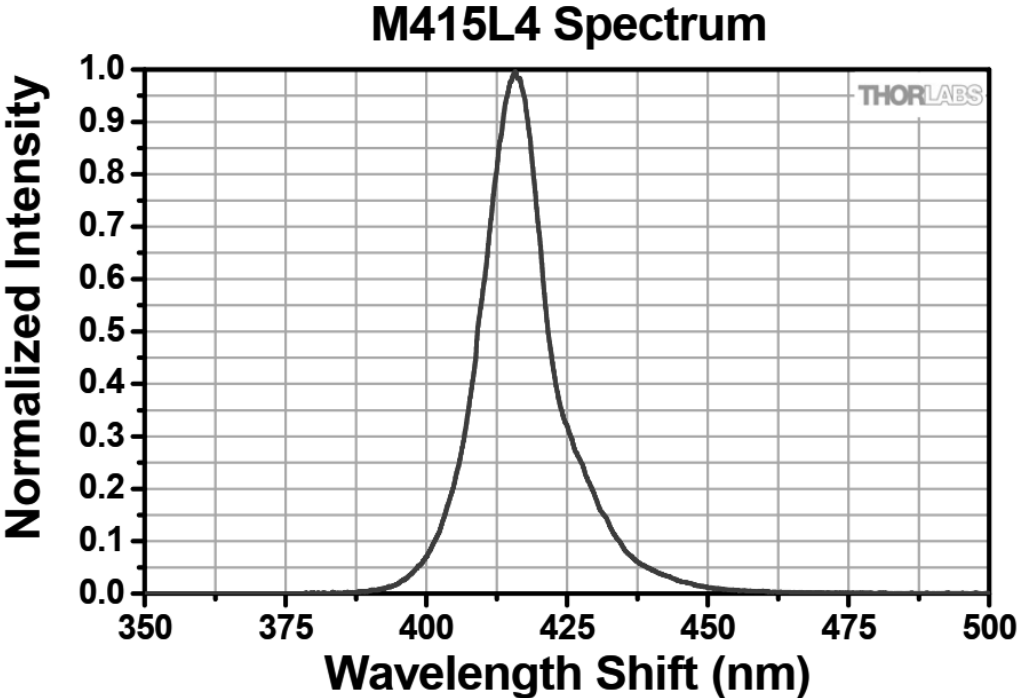


Figure S63: Spectral measurement of the 415 nm (purple) LED measured by Thorlabs. Reprinted with permission from Thorlabs.

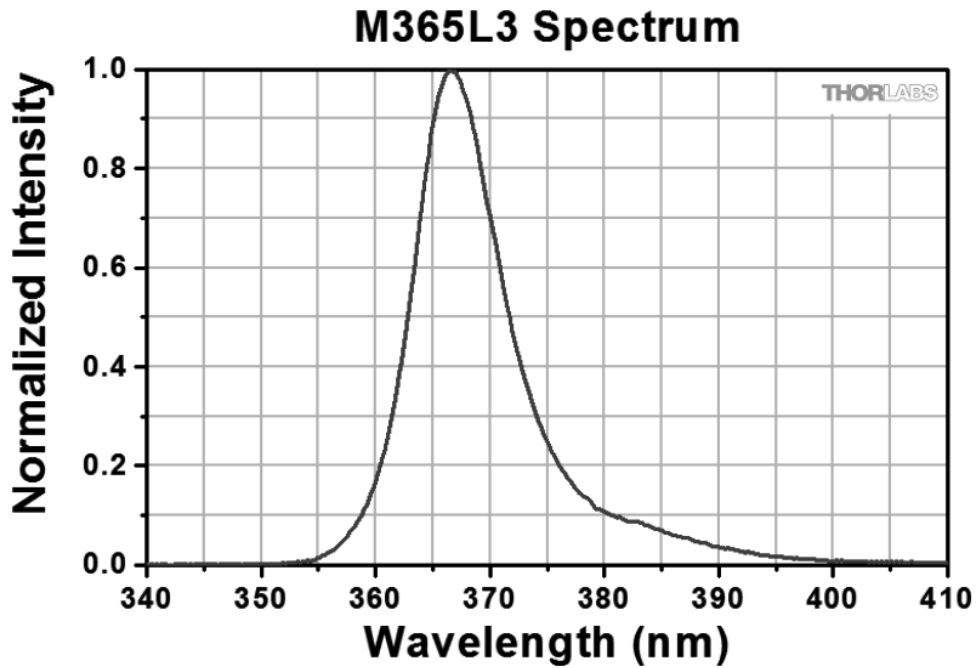


Figure S64: Spectral measurement of the 365 nm (UV) LED measured by Thorlabs. Reprinted with permission from Thorlabs.

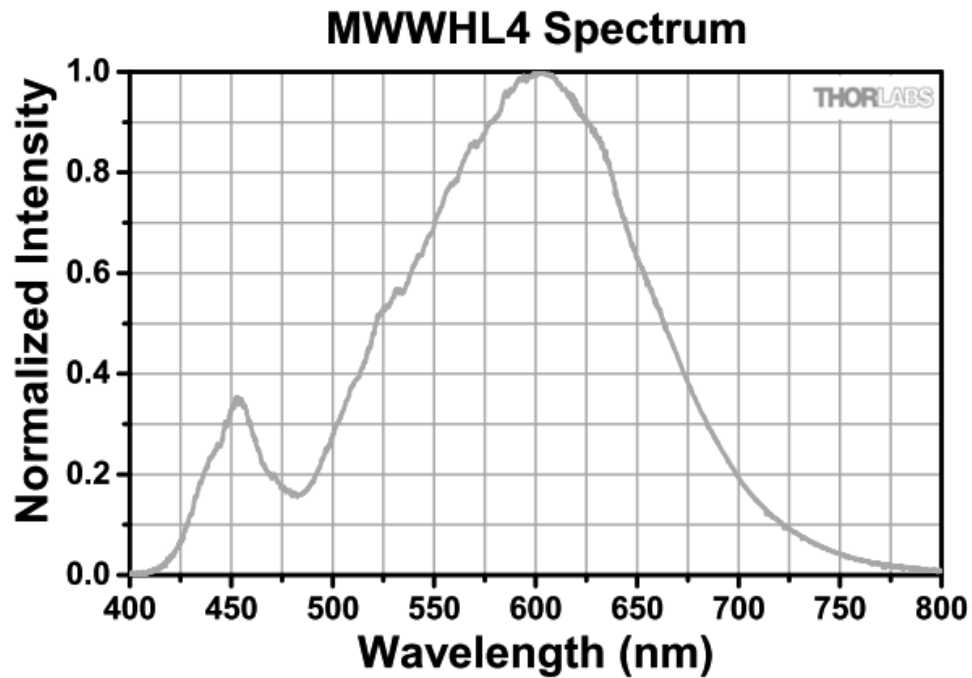


Figure S65: Spectral measurement of the 3000K LED ("warm-white") measured by Thorlabs. Reprinted with permission from Thorlabs.



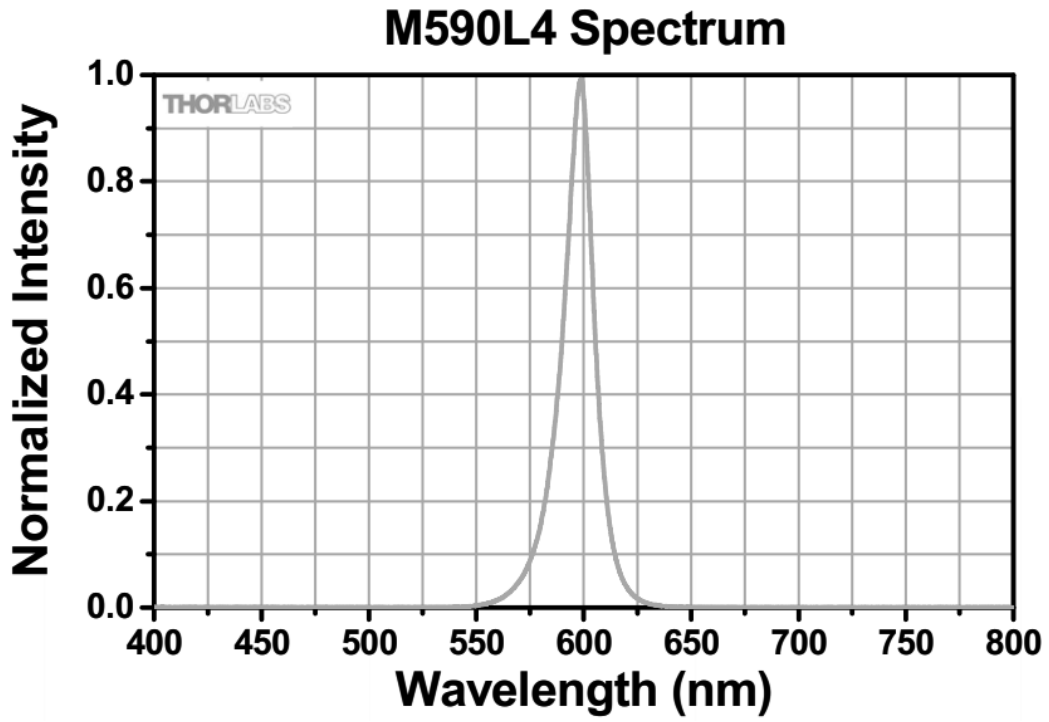


Figure S66: Spectral measurement of the 590 nm (orange) LED measured by Thorlabs. Reprinted with permission from Thorlabs.

8. Crystallographic Analysis**Table S5** : Crystal data and structure refinement for 5.

Formula	C <sub>38</sub> H <sub>38</sub> F <sub>4</sub> N <sub>2</sub> O <sub>4</sub>
Formula weight, g/mol	662.7
Temperature, K	100
Crystal system	Triclinic
Crystal size, mm <sup>3</sup>	0.57 × 0.32 × 0.25
Space group	P1
a, Å	5.4601(5)
b, Å	13.4307(12)
c, Å	22.397(2)
α, °	101.224(4)
β, °	95.268(4)
γ, °	91.462(4)
Volume, Å <sup>3</sup>	1602.6(3)
Z	2
ρ <sub>calc</sub> , g/cm <sup>3</sup>	1.373
μ (Mo; Kα), 1/mm	0.104
F(000)	696.0
θ range, deg	4.348 to 60.728
Index ranges	-7 ≤ h ≤ 7 -19 ≤ k ≤ 19 -31 ≤ l ≤ 31
No. of reflns collected	19199
Completeness to θ <sub>max</sub>	99.6%
No. indep. reflns	19199 [R <sub>int</sub> = 0.0533, R <sub>sigma</sub> = 0.0565]
Data/restraints/parameters	19199/3/870
GooF (F <sup>2</sup> )	1.023
R <sub>1</sub> (I > 2σ (I) for X-Ray)	R <sub>1</sub> = 0.0921
wR <sub>2</sub> (I > 2σ (I) for X-Ray)	wR <sub>2</sub> = 0.2510
R <sub>1</sub> (all data)	R <sub>1</sub> = 0.1282
wR <sub>2</sub> (all data)	wR <sub>2</sub> = 0.2856
Largest diff. peak/hole, e/Å <sup>3</sup>	0.68/-0.60
Flack parameter	-0.6(12)
CCDC number	2224454

## 9.4 Appendix Submitted Manuscript (V)

### *Supporting Information*

#### **Hidden Forces: Activation of Photobending in a Liquid Crystalline Elastomer by Mesogen Alignment with the Help of Thermoplastic Particles.**

Sven Schultze,<sup>1,2</sup> Philipp Schadte,<sup>3</sup> Nina Sindensberger,<sup>4</sup> Jonas Gerken,<sup>1,2</sup> Leonard Siebert,<sup>3</sup> and Anne Staubitz<sup>1,2,5\*</sup>

<sup>1</sup> University of Bremen, Institute for Organic and Analytical Chemistry,  
Leobener Straße 7, D-28359 Bremen, Germany

<sup>2</sup> University of Bremen, MAPEX Center for Materials and Processes,  
Bibliothekstraße 1, D-28359 Bremen, Germany

<sup>3</sup> Kiel University, Department of Materials Science,  
Kaiserstraße 2, D-24143 Kiel, Germany

<sup>4</sup> Technical University of Ilmenau, Faculty of Mechanical Engineering,  
Max-Planck Ring 12, D-98684 Ilmenau, Germany

<sup>5</sup> University of Kiel, Otto-Diels Institute for Organic Chemistry,  
Otto-Hahn Platz 4, D-24118 Kiel, Germany

\* Correspondence: [staubitz@uni-bremen.de](mailto:staubitz@uni-bremen.de)

## Contents

1 General Information.....	3
1.1 Reagents.....	4
1.2 Solvents.....	4
2 Analytical Data.....	5
2.1 UV-vis Analysis: Switching Behavior of <b>LC-Azo</b> .....	5
2.2 <sup>1</sup> HNMR Analysis: Quantitative Switching Behavior of <b>LC-Azo</b> .....	6
3 Syntheses.....	10
3.1 Bulk Polymerization of Polydomain-LCE.....	10
3.2 Programming of Polydomain-LCE to Monodomain-LCE.....	11
3.3 9-Bromononyl acrylate ( <b>S1</b> ).....	12
3.4 ( <i>E</i> )-4,4'-(Diazene-1,2-diyl)diphenol ( <b>S2</b> ).....	12
3.5 ( <i>E</i> )-((Diazene-1,2-diylbis(4,1-phenylene))bis(oxy))bis(nonane-9,1-diyl) diacrylate ( <b>LC-Azo</b> ).....	13
5 References.....	13
4. <sup>1</sup> H, <sup>13</sup> C{ <sup>1</sup> H} and <sup>19</sup> F NMR Spectra of the Purified Compounds.....	14

## 1 General Information

All glassware was dried in an oven at 200 °C for several hours prior to use. NMR tubes were dried in an oven at 110 °C for several hours prior to use.

NMR spectra were recorded on a Bruker Avance Neo 600 (Bruker BioSpin, Rheinstetten, Germany) (600 MHz ( $^1\text{H}$ ), 151 MHz ( $^{13}\text{C}$ ), 565 MHz ( $^{19}\text{F}$ ) at 298 K. All  $^1\text{H}$  NMR and  $^{13}\text{C}\{^1\text{H}\}$  NMR spectra were referenced to the residual proton signals of the solvent ( $^1\text{H}$ ) or the solvent itself ( $^{13}\text{C}\{^1\text{H}\}$ ).  $^{19}\text{F}$  NMR spectra were referenced internally against trichlorofluoromethane. The exact assignment of the peaks was performed by two-dimensional NMR spectroscopy such as  $^1\text{H}$  COSY,  $^{13}\text{C}\{^1\text{H}\}$  HSQC and  $^1\text{H}/^{13}\text{C}\{^1\text{H}\}$  HMBC when possible.

High resolution EI mass spectra were recorded on a MAT 95XL double-focusing mass spectrometer from Finnigan MAT (Thermo Fisher Scientific, Waltham, MA, USA) at an ionization energy of 70 eV. Samples were measured by a direct or indirect inlet method with a source temperature of 200 °C. High resolution ESI and APCI mass spectra were measured by a direct inlet method on an Impact II mass spectrometer from Bruker Daltonics (Bruker Daltonics, Bremen, Germany).

IR spectra were recorded on a Nicolet i510 FT-IR spectrometer from Thermo Fisher Scientific (Thermo Fisher Scientific, Waltham, MA, USA) with a diamond window in an area from 500 – 4 000  $\text{cm}^{-1}$  with a resolution of 4  $\text{cm}^{-1}$ . All samples were measured 16 times against a background scan.

Melting points were recorded on a Büchi Melting Point M-560 (Büchi, Essen, Germany) and are reported corrected.

For the irradiation experiments: A UPLED power supply powered the high-power LED modules: M365L3 (365 nm), M415L4 (415 nm). A collimator was used to focus the light beam. The light intensity was measured using an ILT2400 hand-held light meter manufactured by International Light Technologies, Inc., (Peabody, USA). Additionally, a 420 nm (1.0 W) and a 525 nm LED (1.0 W) from EPILED was built in our laboratories.

Thermal analyses were performed on a standalone Mettler Toledo DSC 3+ STAR (Mettler-Toledo, Columbus, OH, USA), where 40  $\mu\text{L}$  aluminum crucibles were used. In the DSC experiments, pierced lids were used. All analysis were run from -30° C up to the desired temperature. Thermo analytical data were analyzed with the STARe software (Version 16.00, Mettler-Toledo, Columbus, OH, USA) by Mettler Toledo.

Thin layer chromatography (TLC) was performed using TLC Silica gel 60 F<sub>254</sub> from Merck (Merck, Darmstadt, Germany) and the compounds were visualized by exposure to UV light at a wavelength of 254 nm. Column chromatography was performed manually using silica gel 60 (0.015-0.040 mm) from Merck (Merck, Darmstadt, Germany). The samples were applied via dry load with Celite® 503 (Macherey-Nagel, Düren, Germany) as column material. If stated, Celite® 503 was used as filtration aid.

Dynamic mechanical analysis (DMA) was conducted on a MCR 702e Multidrive (Anton Paar, Austria). A tensile test during a heating curve was run. The sample was clamped inside the oven and a force of 50 kPa or 100 kPa was applied on the sample. Upon reaching the full applied force, a temperature program (5 K/ min) was run. The elongation during the change of temperature was measured.

UV-vis spectra were recorded with a resolution of 0.5 nm on a Cary 3500 Multicell UV-Vis Spectrophotometer from Agilent (CA, USA). Chloroform (spectroscopy grade) was used as a solvent.

The use of abbreviations follows the conventions from the ACS Style guide.<sup>1</sup>

## 1.1 Reagents

All chemicals were commercially available and used without purification.

**Table S1.** List of suppliers and purity of used chemicals.

Reagent	Supplier	Purity
Acryloyl chloride	abcr	96% (stab. phenothiazoin)
4-Aminophenol	Sigma-Aldrich	>98%
4-((6-Acryloyloxy)hexyl)oxy)benzoic acid	BLD Pharm	97%
1,4-Bis-[4-(3-acryloyloxypropyloxy)benzoyloxy]-2-methylbenzene	BLD Pharm	98%
9-Bromononanol	BLD Pharm	97%
3,6-Dioxa-1,8-octanedithiol	TCI	>97%
4-Dimethylaminopyridine	TCI	99%
6-(4-Hydroxyphenoxy)hexyl acrylate	BLD Pharm	>97%
Pentaerythritol-tetrakis(3-mercaptopropionate)	Sigma-Aldrich	>95%
<i>N,N'</i> -Dicyclohexylcarbodiimide	Sigma-Aldrich	99%
Phenol	Apollo Scientific	99%
Sodium nitrite	Fisher Scientific	99%
Sodium carbonate	Chemsolute	99.8%
Sodium chloride	CarlRoth	>99.5%
Sodium hydroxide	VWR	98.6%
Triethylamine	chemPur	99% (anhydrous)

## 1.2 Solvents

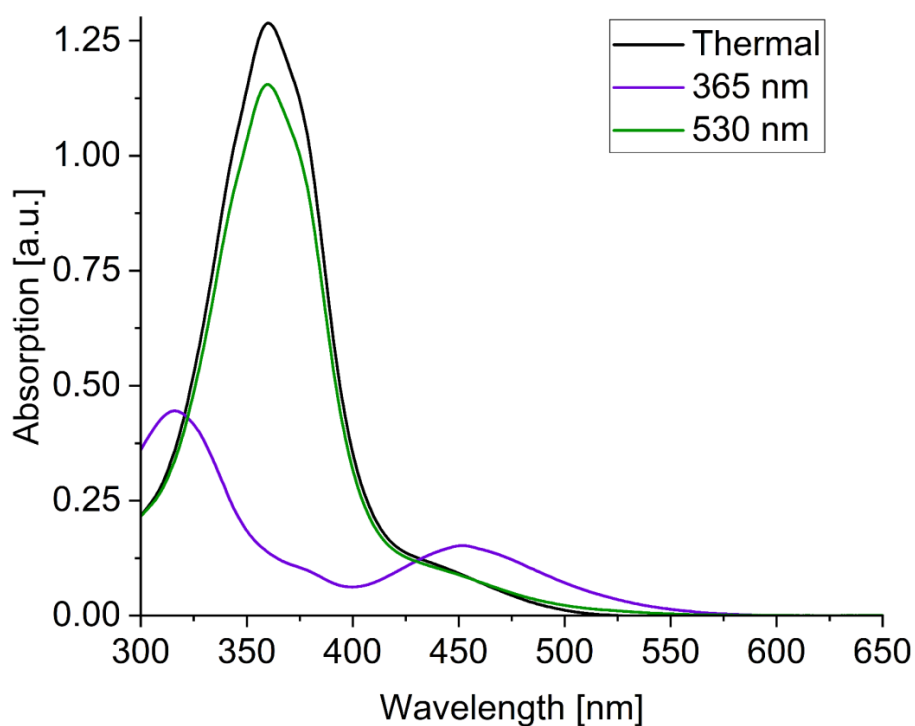
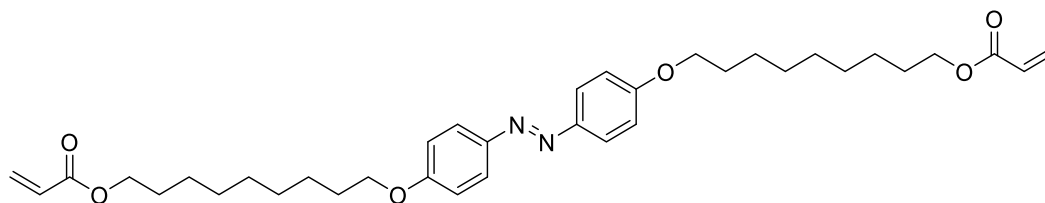
All solvents for purification and extraction were used as received. All solvents used for synthesis under inert conditions were dried by a solvent purification system (SPS) from Inert Technologies.

**Table S2.** List of supplier and purity of used solvents.

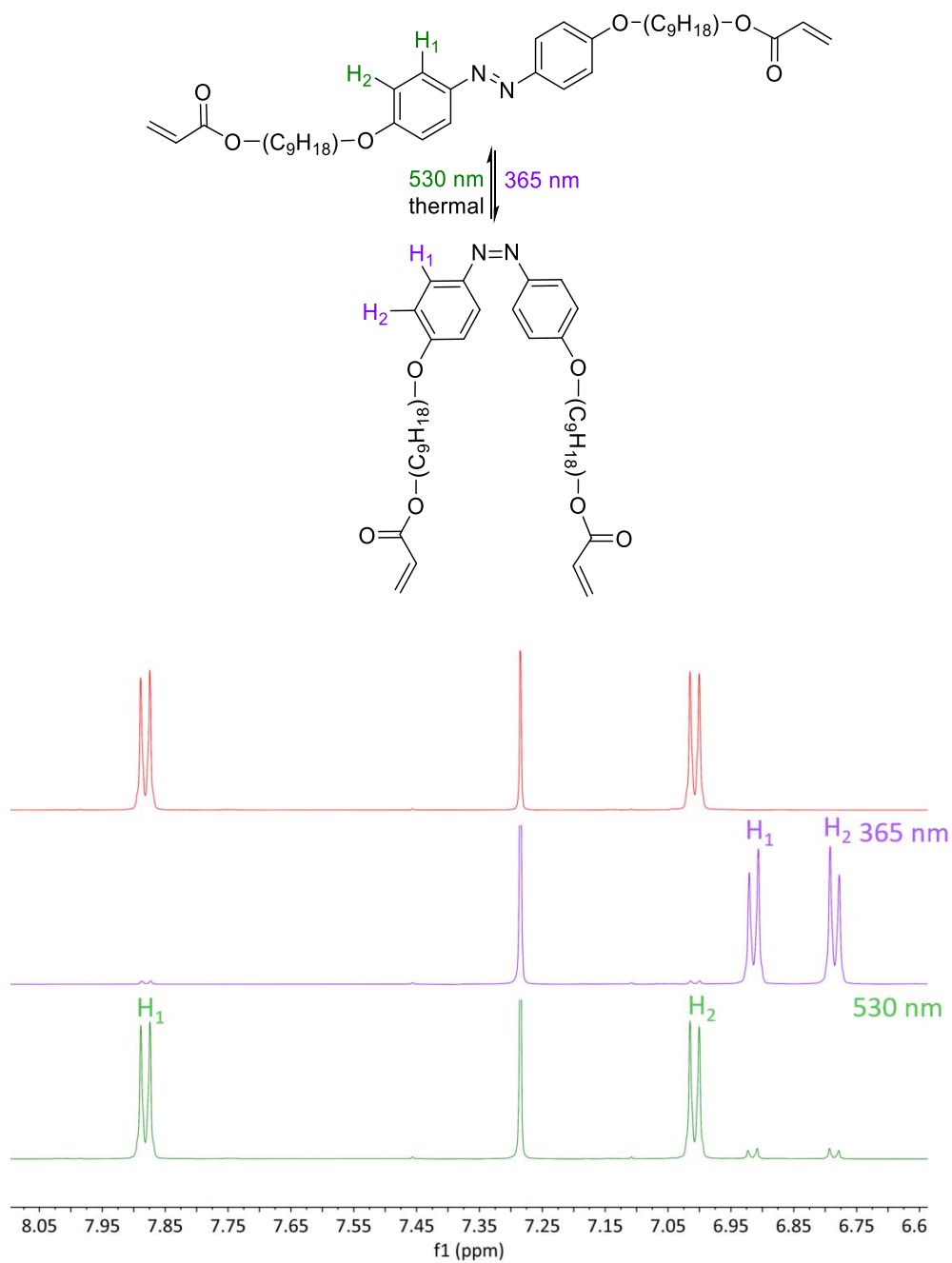
Solvent	Supplier and Purity
Acetone	Sigma Aldrich
Acetonitrile	Fisher Scientific 99.5%
Chloroform- <i>d</i> <sub>1</sub>	Euroisotop 99.8%
Cyclohexane	Merck ≥99.5% (GC)
DCM	Merck ≥99.9% (GC)
DMF	VWR, >99.5%
DMSO- <i>d</i> <sub>6</sub>	Sigma Aldrich, 99.9%
Ethanol	VWR ≥99.8%, absolute
Ethyl acetate	Merck >99.5% (GC)
Hydrochloric acid (37%)	Merck, fuming >37.0%
Methanol	VWR >99.8% (GC)
<i>n</i> -Hexane	Merck, >95%
Toluene	Merck >99.7% (GC)
Water	deionized

## 2 Analytical Data

### 2.1 UV-vis Analysis: Switching Behavior of LC-Azo



**Figure S1.** UV-vis spectra of LC-Azo in chloroform after thermal treatment of the solid before dissolution (100 °C, 12 h) and irradiation of the solution with UV-light (365 nm, 5 min, 55 mW/cm<sup>2</sup>) and green light (530 nm, 5 min, 70 mW/cm<sup>2</sup>) respectively. The PSS was reached for both isomerizations (conc = 0.052 μmol mL<sup>-1</sup>), which was indicated by no spectral change upon further irradiation.

2.2  $^1\text{H}$ NMR Analysis: Quantitative Switching Behavior of LC-Azo

**Figure S2.**  $^1\text{H}$  NMR spectroscopic study of the irradiation of LC-Azo in  $\text{CDCl}_3-d_1$  after thermal treatment (100 °C, solid state, 12 h) (red spectrum), after irradiation with UV-light (365 nm, 5 min, 55  $\text{mW}/\text{cm}^2$ ) and green light (530 nm, 5 min, 70  $\text{mW}/\text{cm}^2$ ) respectively. ( $\text{conc}_{\text{LC-Azo}} = 6.60 \mu\text{mol mL}^{-1}$ ).



**Table S3.** Summary of the NMR spectroscopic studies of the irradiation of **LC-Azo**, after irradiation with 365 nm (5 min, 55 mW/cm<sup>2</sup>) and 530 nm (5 min, 70 mW/cm<sup>2</sup>) in the solvents CDCl<sub>3</sub>-d<sub>1</sub>. The % values for the *E* and *Z* isomer were obtained by the integration of the aromatic-proton signals of the C<sub>6</sub>H<sub>4</sub> ring of the azobenzene. (conc<sub>LC-Azo</sub> = 6.60 μmol mL<sup>-1</sup>).

	LC-Azo	
	<i>E</i> -isomer	<i>Z</i> -isomer
<b>Thermal</b>	100%	0%
<b>365 nm</b>	5%	95%
<b>530 nm</b>	92%	8%

**Table S4** Overview of the effect of different polymer compositions on the final properties.

Composition	Post-Alignment	Actuation	Shape-Memory
No Particles ( <b>LCE<sub>Azo</sub></b> )	✗	✗	✗
No Crosslinking	✓	✗	✗
Dissolved PCL	✓	✓	✗
PCL-Particles ( <b>LCE<sub>Azo/PCL</sub></b> )	✓	✓	✓

Different compositions and polymerization procedures were explored to assess the impact of the particles in the system (Table 1). Without the inclusion of PCL particles, the **LCE<sub>Azo</sub>** could not be stably programmed into a monodomain shape: Although **LCE<sub>Azo</sub>** could be stretched under thermal treatment, it failed to retain the programmed shape, behaving like a typical rubber. A sample without crosslinking was produced by replacing **PETMP** with additional **EDDET**, resulting in long polymer-chains. This composite was highly flexible upon melting the particles and maintained this shape upon cooling. However, it did not exhibit a shape-memory effect or photoactuation post-stretching. This can be explained by the lack of cross-links between the polymer chains: Without covalently bonds or strong intermolecular interaction (e.g. hydrogen bonding) between the polymer chains, no actuation could be observed. There is no “restraint” to pull back to its original, pre-stretched form. A third sample was prepared by dissolving PCL particles and the monomer mixture in dichloromethane (DCM) and removing the solvent afterwards. Surprisingly, the elastomer locked the aligned state and actuation could be observed. However, reverting to the original shape beyond PCL's melting point was not observed.

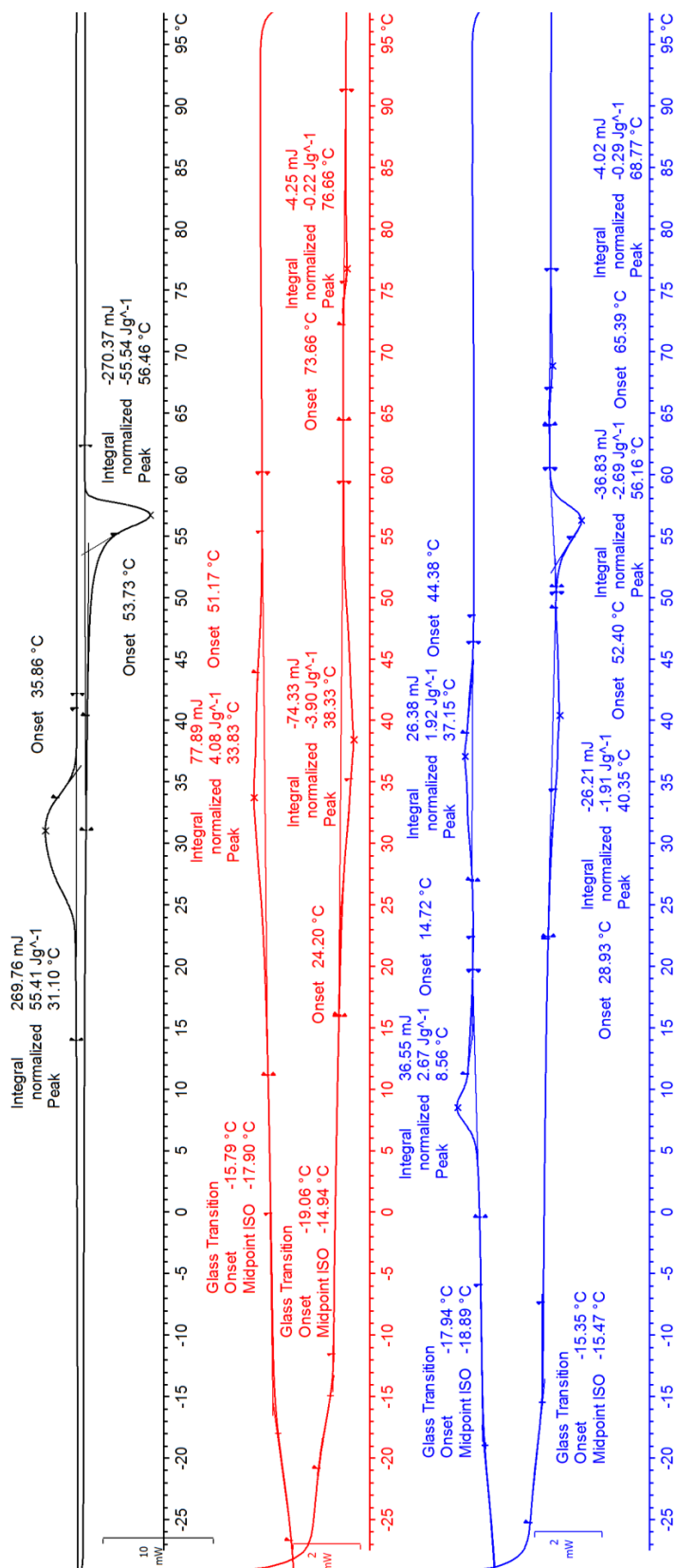


**Figure S3.** Three DSC heating (bottom curve, left to right) and cooling (top curve, right to left) curves for the PCL particles (top, black curve, 4.8681 mg), **LCE<sub>Azo</sub>** (middle, red curve, 8.7245 mg) and **LCE<sub>Azo/PCL</sub>** (bottom, blue curve, 13.7115 mg) with a heating rate of 5 K/min for the temperature range -30 °C to 100°C. Note: A sample with only 5 wt% particle inclusion for **LCE<sub>Azo/PCL</sub>** was used for clarity purpose.

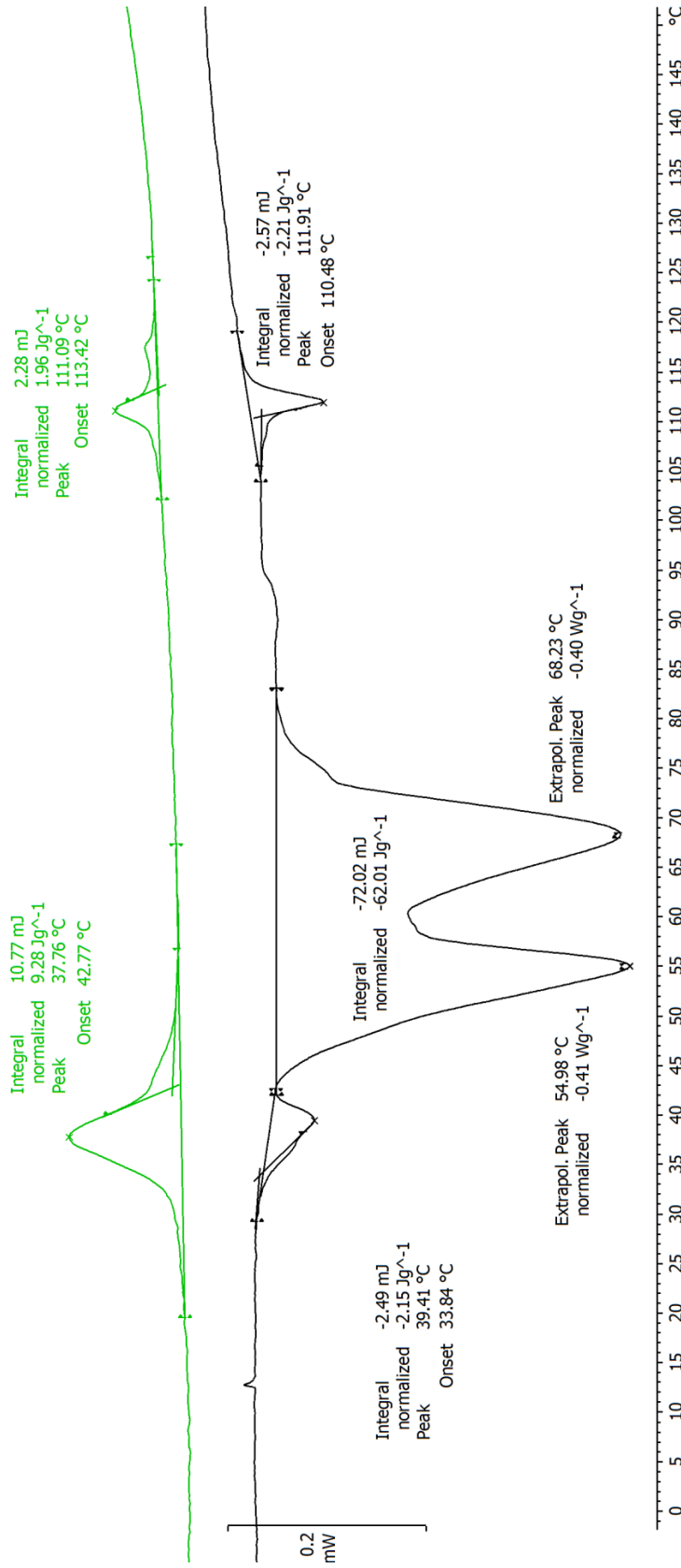
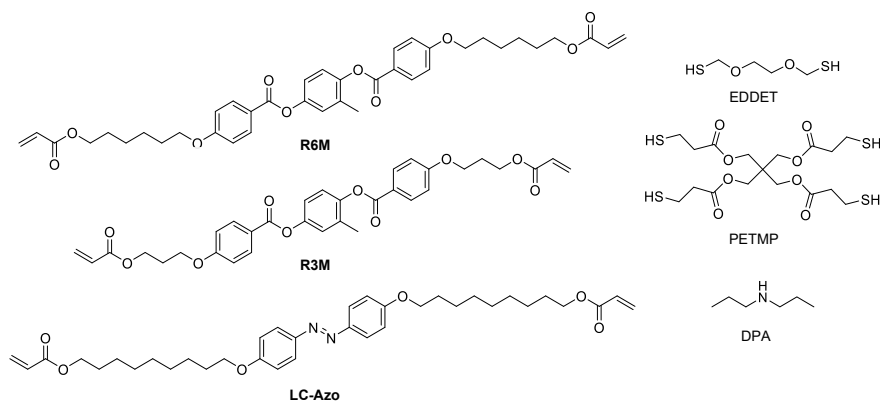


**Figure S4.** DSC heating (bottom curve, black, left to right) and cooling (top curve, green, right to left) curve for the combined mesogen monomer mixture (**R6M**, **R3M**, **LC-Azo**, 1.1615 mg) with a heating rate of 5 K/min for the temperature range 0 °C to 150°C.

### 3 Syntheses

#### 3.1 Bulk Polymerization of Polydomain-LCE

The samples were prepared by a base catalyzed thio-michael reaction with a ratio of thiols to acrylates of 1:1. The exact molecular structure of the components used is given as follows (see. Scheme 1).



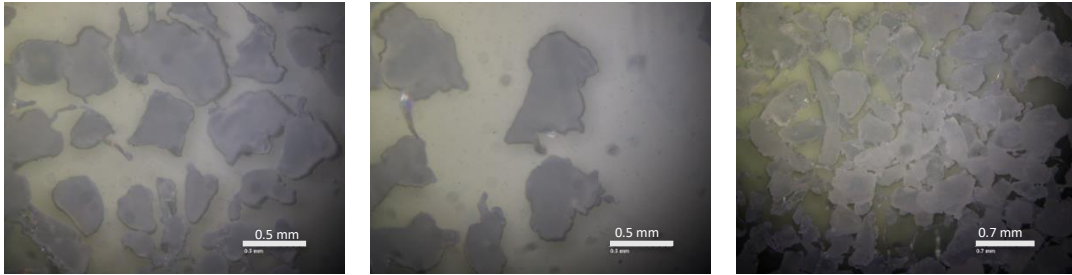
**Scheme 1:** Overview of molecules used for the preparation of LCEs.

For the preparation of the polydomain LCE, the mesogen **R6M** (303 mg, 0.450 eq., 31 wt%), **R3M** (265 mg, 0.450 eq., 27 wt%) and **LC-Azo** (60.7 mg, 0.100 eq., 6.0 wt%) were added in a vial and melt mixed. The mesogen mixture was cast in a PTFE mold and kept at 50 °C. Then, a stock solution of **EDDET** (0.800 eq.) and **PETMP** (0.100 eq.) was prepared. Via a syringe, 195 mg (**EDDET**: 146 mg, 0.800 eq., 15 wt%, **PETMP**: 49.0 mg, 0.100 eq., 5.0 wt%) of the stock solution was taken. A second freshly prepared stock solution of DME and **DPA** (20:1 wt%) was prepared and 165 mg (17 wt%, **DPA**: 8.25 mg, 0.008 eq., 0.90 wt%) taken from it. Both liquids were added to the PTFE mold (5 cm x 1 cm or “bone” type), the temperature lowered to 40 °C and the liquid manually stirred. After 1 min, polycaprolactone (PCL) particles (<400 μm, 197 mg, additional 20 wt%) were added and dispersed and well mixed in the polymer mixture. The composite was left in the oven for 2 h at 40 °C for the first curing, then 2 h at 50 °C and 16 h at 60 °C to avoid the dissolving of the particles but at the same time to ensure a complete polymerization.

For the sample without particles, the particles were not added, and the polymer directly cured at 60 °C.

For the sample without crosslinking, **PETMP** was not used and the amount of **EDDET** (182 mg, 1.00 eq.) was increased.

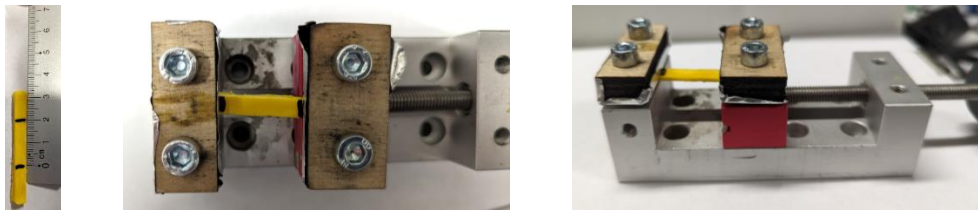
For the sample with the dissolved PCL particles, all components were dissolved in DCM and the solvent evaporated. The mixture was casted in a PTFE mold and cured at 50 °C.



**Figure S5:** Images of PCL particle under cross-polarizer under a microscope with 5x magnification (left and middle) and 3.5 magnification (right).

### 3.2 Programming of Polydomain-LCE to Monodomain-LCE

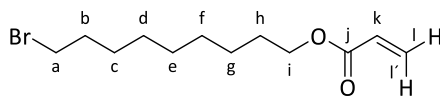
A polydomain-LCE stripe was clamped in a bench vice (Figure S6). The bench vice was placed in the oven and heated to 70 °C. The polymer was drawn to the desired length up to 190% inside the oven at 70 °C. Then the apparatus was taken out of the oven and cooled down in a stretched state.



**Figure S6 :** Images of unstretched LCE before placed in the oven.



**Figure S7:** Images of stretched LCE after taken out of the oven.

3.3 9-Bromononyl acrylate (**S1**)<sup>2</sup>

This reaction was performed under inert conditions.

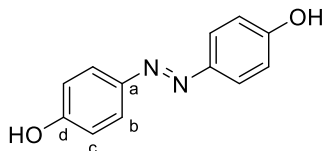
Triethylamine (9.12 g, 90.2 mmol, 1.09 eq.) and 9-bromo-nonanol (18.5 g, 82.8 mmol, 1.00 eq.) were dissolved in dry toluene (90 mL). The mixture was then cooled to  $-10\text{ }^{\circ}\text{C}$  *via* a salt and ice bath, and a solution of acryloyl chloride (8.16 g, 90.2 mmol, 1.09 eq.) in dry toluene (30 mL) was added dropwise over the course of 30 min. The reaction was warmed to  $21\text{ }^{\circ}\text{C}$  and stirred for 48 h. The organic phase was subsequently washed with sat. solution of  $\text{Na}_2\text{CO}_3$  (100 mL), an aqueous hydrochloric acid solution (1 M,  $2 \times 100\text{ mL}$ ) and with brine (50 mL). The organic phase was then dried over  $\text{MgSO}_4$ , filtered and the solvent removed *in vacuo* to obtain a slightly yellow oil. After filtration through a short plug of silica (eluent: DCM) the product **S1** was obtained as a colorless oil (17.7 g, 63.9 mmol, 77%).

<sup>1</sup>H NMR (601 MHz,  $\text{CDCl}_3$ )  $\delta$  6.40 (dd,  $^3J = 17.4$ ,  $^3J = 1.5$  Hz, 1H, H-l'), 6.12 (dd,  $^3J = 17.4$ ,  $^3J = 10.5$  Hz, 1H, H-k), 5.81 (dd,  $^3J = 10.5$ ,  $^3J = 1.5$  Hz, 1H, H-l), 4.15 (t,  $^3J = 6.8$  Hz, 2H, H-a), 3.41 (t,  $^3J = 6.8$  Hz, 2H, H-i), 1.85 (m, 2H, H-h), 1.69 – 1.64 (m, 2H, H-b), 1.31 (m, 10H, H-c,d,e,f,g).

<sup>13</sup>C{<sup>1</sup>H} NMR (151 MHz,  $\text{CDCl}_3$ )  $\delta$  = 166.48 (C-l), 130.60 (C-j), 128.78, (C-k), 64.79 (C-a), 34.14 (C-i), 32.93 (C-h), 29.43 (C-b), 29.26 (C-c,d,e,f,g), 28.80 (C-c,d,e,f,g), 28.72 (C-c,d,e,f,g), 28.26 (C-c,d,e,f,g), 26.01 (C-c,d,e,f,g) ppm.

HRMS (ESI)  $m/z$  (%):  $[\text{M}+\text{Na}]^+$  calcd for  $[\text{C}_{12}\text{H}_{21}^{79}\text{BrNaO}_2]^+$  299.06171; found 299.06185.

IR (ATR):  $\tilde{\nu}$  = 2927 (m), 2854 (m), 1721 (s), 1636 (w), 1464 (w), 1406 (m), 1294 (w), 1269 (m), 1185 (s), 1085 (m), 983 (m), 965 (m), 809 (m), 722 (w)  $\text{cm}^{-1}$ .

3.4 (*E*)-4,4'-(Diazene-1,2-diyl)diphenol (**S2**)<sup>3</sup>

The procedure was adapted from H. Qu and co-worker.<sup>3</sup>

4-Aminophenol (5.00 g, 4.60 mmol) was dissolved in HCl (6 M, 25 mL). Sodium nitrite (3.30 g, 4.78 mmol) dissolved in water (15 mL) was added dropwise over the course of 1 h. The mixture was stirred for another 30 min and the temperature kept below  $5\text{ }^{\circ}\text{C}$ . Phenol (4.35 g, 4.63 mol) and sodium hydroxide (1.85 g, 4.63 mol) were dissolved in water (50 mL) and added slowly over the course of 1 h to the diazonium salt solution. The pH value was maintained at pH = 8. The mixture was stirred for an additional 2 h at  $< 5\text{ }^{\circ}\text{C}$  and slowly warmed to  $20\text{ }^{\circ}\text{C}$  over the course of 12 h. The solution was acidified until a solid precipitated. The solid was filtrated and crystallized in a MeOH : water mixture (1 : 1) at  $-20\text{ }^{\circ}\text{C}$  to result a purple solid (5.30 g, 2.48 mmol, 54%, Lit<sup>3</sup>: 50%).

<sup>1</sup>H NMR (601 MHz,  $\text{CDCl}_3$ )  $\delta$  = 10.11 (s, 2H, C-OH), 7.71 (d,  $^3J = 8.8$  Hz, 4H, H-c), 6.90 (d,  $^3J = 8.8$  Hz, 4H, H-b) ppm.

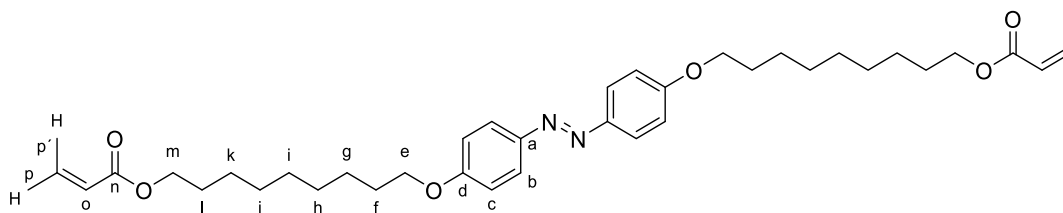
<sup>13</sup>C{<sup>1</sup>H} NMR (151 MHz,  $\text{CDCl}_3$ )  $\delta$  = 159.99 (C-d), 145.27 (C-a), 124.15 (C-c), 115.79 (C-b) ppm.

HRMS (EI, 70 eV)  $m/z$  (%):  $[\text{M}]^+$  calcd for  $[\text{C}_{12}\text{H}_{10}\text{N}_2\text{O}_2]^+$  214.07319, found 214.07368 (70), 93.0  $[\text{C}_6\text{H}_5\text{O}]^+$  (100).

IR (ATR):  $\tilde{\nu}$  = 3504 (w), 3081 (w), 1587 (s), 1500 (m), 1359 (m)  $\text{cm}^{-1}$ .

Mp:  $215\text{ }^{\circ}\text{C}$ .

### 3.5 (*E*)-((Diazene-1,2-diylbis(4,1-phenylene))bis(oxy))bis(nonane-9,1-diyl) diacrylate (**LC-Azo**)<sup>4, 5</sup>



**S2** (2.14 g, 10.0 mmol, 1.00 equiv.), **S1** (6.10 g, 22.0 mmol, 2.20 equiv.), K<sub>2</sub>CO<sub>3</sub> (2.76 g, 20.0 mmol, 2.00 equiv.), a catalytic amount KI (100 mg) was dissolved in anhydrous DMF (150 mL). The solution was stirred for 24 h at 80 °C. After cooling to 25 °C, water (500 mL) was added. The precipitate was filtered and washed with water (3 x 100 mL). Afterwards, the filter cake was dissolved in DCM (100 mL). The organic layer was washed with water (3 x 150 mL), brine (3 x 150 mL) and dried over anhydrous MgSO<sub>4</sub>. After filtration, the solvent was removed by evaporation under reduced pressure. The crude product was purified by silica gel column chromatography (eluent: DCM). The crude yellow powder was crystallized in methanol (100 mL) at -20 °C to obtain **3** as a pale-yellow solid (3.94 g, 6.50 mmol, 65%).

<sup>1</sup>H NMR (600 MHz, CDCl<sub>3</sub>) δ = 7.88 (d, <sup>3</sup>J = 8.8 Hz, 4H, *H*-b), 7.01 (d, <sup>3</sup>J = 8.8 Hz, 4H, *H*-c), 6.42 (d, <sup>3</sup>J = 17.3 Hz, 4H, *H*-p'), 6.15 (dd, <sup>3</sup>J = 17.3 Hz, <sup>3</sup>J = 10.4 Hz, 4H, *H*-o), 5.84 (d, <sup>3</sup>J = 10.4 Hz, 2H, *H*-p), 4.18 (t, <sup>3</sup>J = 6.7 Hz, 4H, *H*-m), 4.05 (t, <sup>3</sup>J = 6.5 Hz, 4H, *H*-m), 1.84 (p, <sup>3</sup>J = 6.7 Hz, 4H, *H*-f), 1.70 (s, 4H, *H*-l), 1.44-1.33 (m, 16H, *H*-g, *H*-h, *H*-i, *H*-j, *H*-k) ppm.

<sup>13</sup>C{<sup>1</sup>H} NMR (151 MHz, CDCl<sub>3</sub>) δ = 166.37 (C-n), 161.15 (C-d), 146.95 (C-a), 130.47 (C-p), 128.66 (C-o), 124.30 (C-b), 114.66 (C-c), 68.29 (C-e), 64.69 (C-m), 29.30, 29.21, 29.19, 28.61, 26.01, 25.92 ppm.

HRMS (EI, 70 eV) *m/z* (%): [M]<sup>+</sup> calcd for [C<sub>36</sub>H<sub>50</sub>N<sub>2</sub>O<sub>6</sub>]<sup>+</sup> 606.36634, found 606.36571 (100).

IR (ATR):  $\tilde{\nu}$  = 3074 (w), 2955 (w), 2930 (m), 2925 (s), 2850 (m), 1720 (s), 1608 (m), 1582 (m), 1502 (w), 1470 (m), 1410 (w), 1390 (m), 1324 (m), 1298 (m), 1243 (s), 1200 (m), 1022 (m), 840 (m) cm<sup>-1</sup>.

R<sub>f</sub>: 0.5 (DCM).

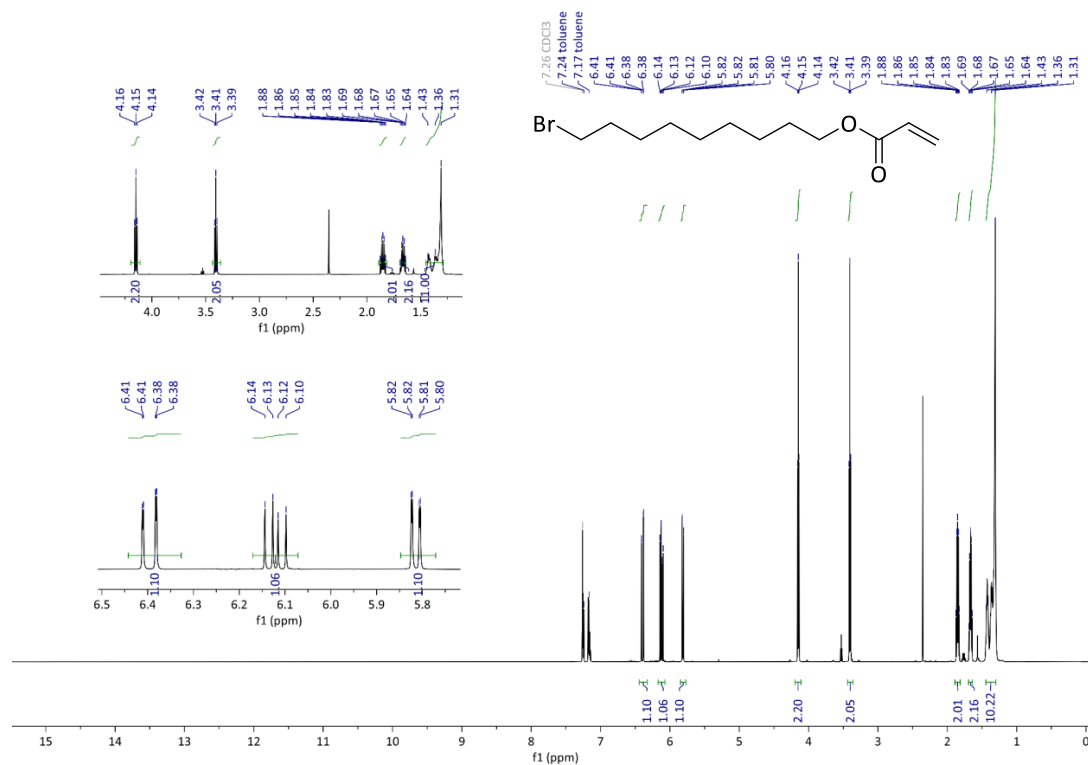
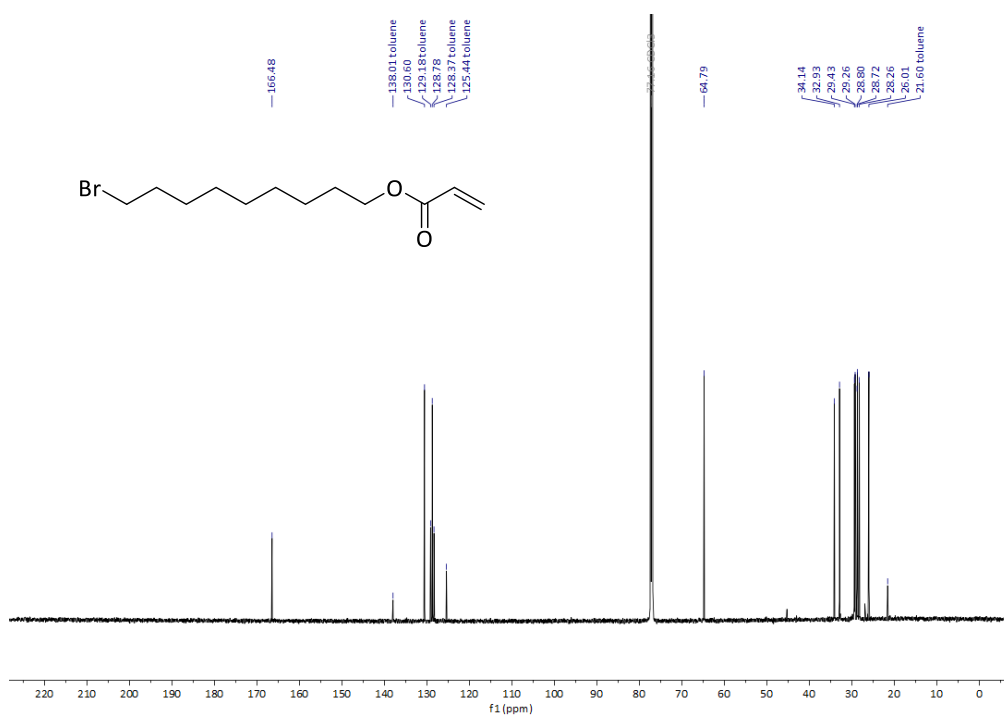
Mp: T<sub>C</sub> = 74 °C, T<sub>SMA</sub> = 91 °C.

## 5 References

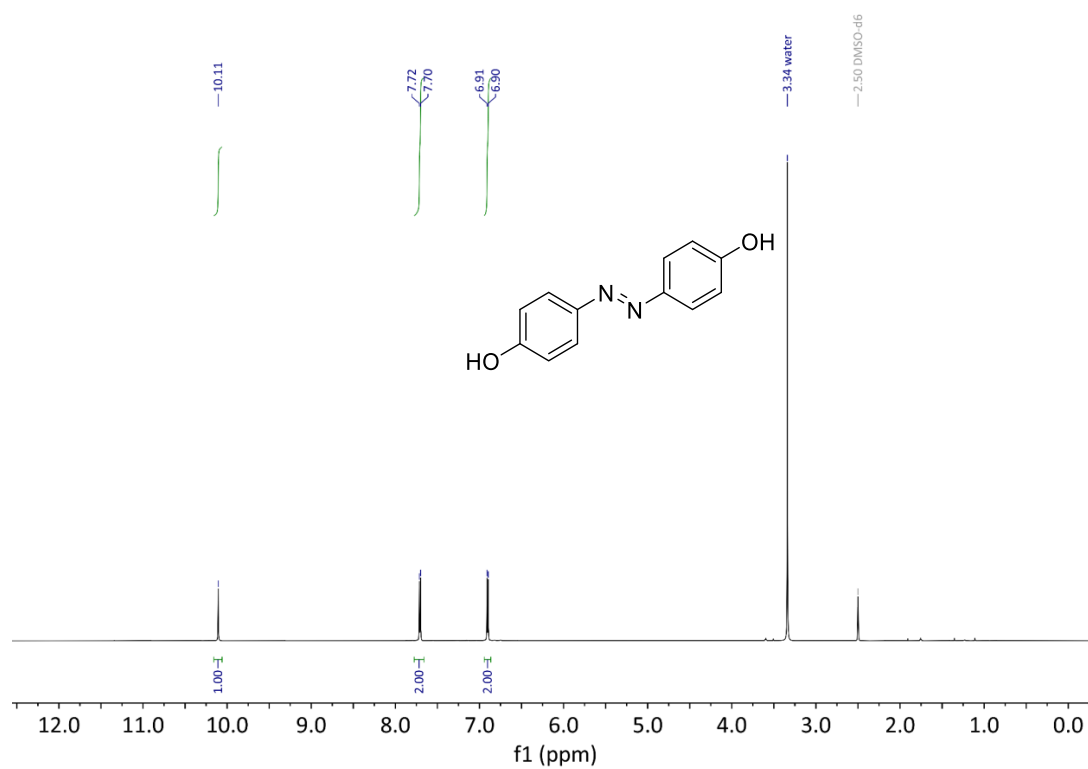
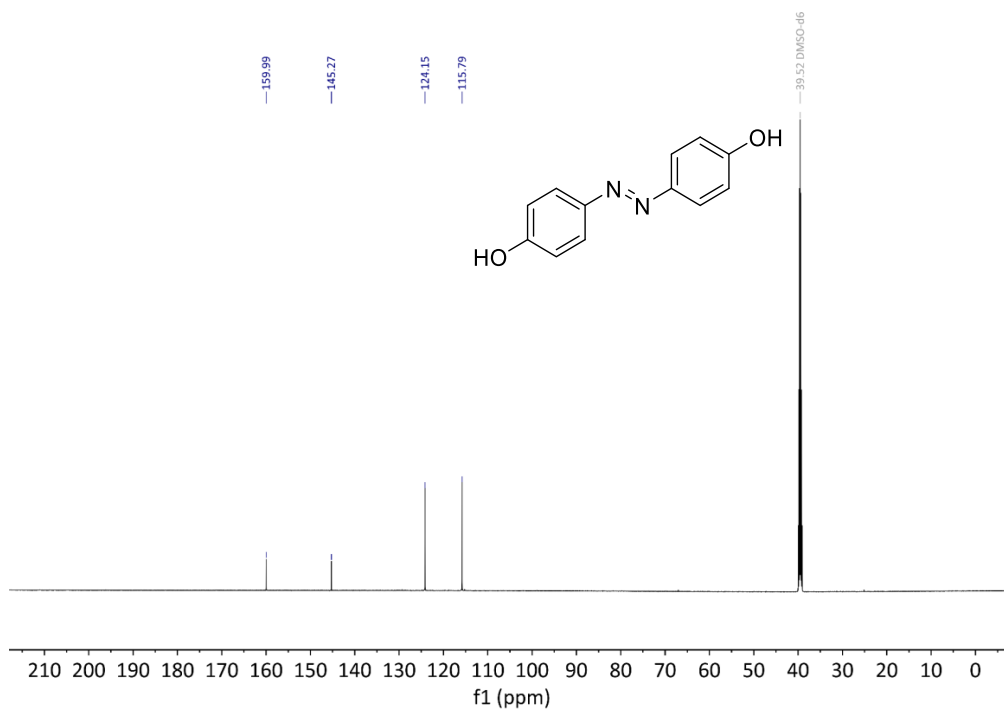
1. *The ACS Style Guide: Effective Communication of Scientific Information*, American Chemical Society, Washington, DC, 3rd edn., 2006.
2. S. Schultze, N. Scheuring, P. Puylaert, M. Lehmann and A. Staubitz, *Advanced Science*, 2023, **10**, 2302692.
3. Q. Hu, Y. Wang, J. Jia, C. Wang, L. Feng, R. Dong, X. Sun and J. Hao, *Soft Matter*, 2012, **8**, 11492-11498.
4. Y. Yu, T. Maeda, J.-i. Mamiya and T. Ikeda, *Angewandte Chemie International Edition*, 2007, **46**, 881-883.
5. E. Kizilkan, J. Strueben, X. Jin, C. F. Schaber, R. Adelung, A. Staubitz and S. N. Gorb, *Royal Society Open Science*, 2016, **3**, 150700.

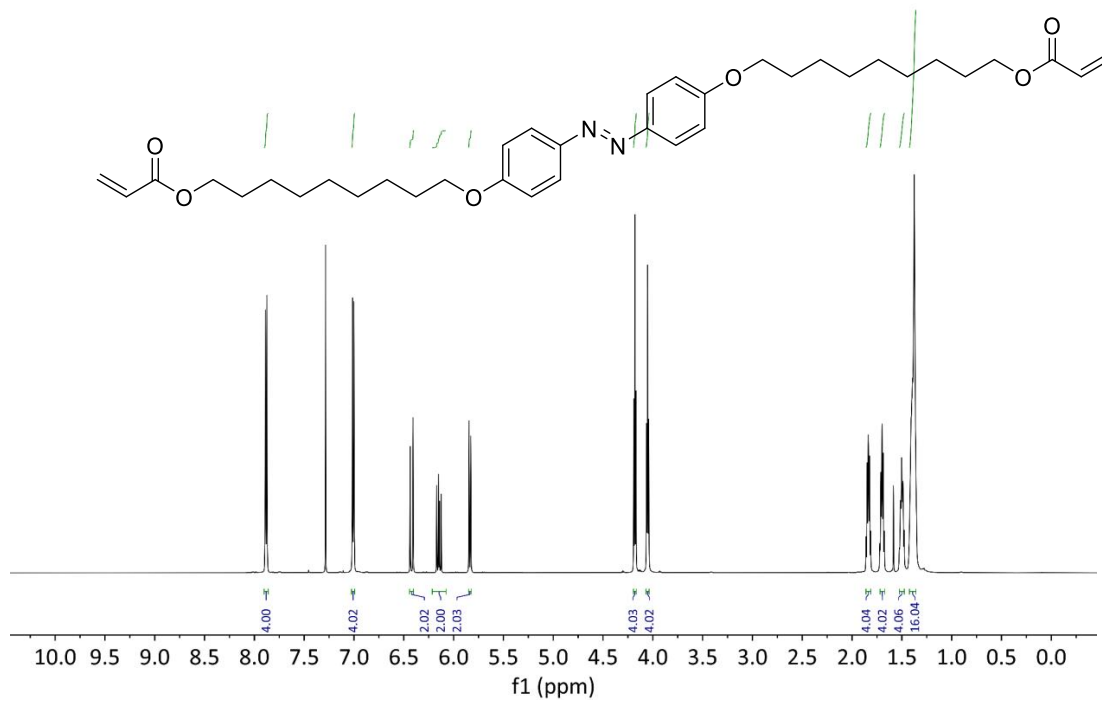
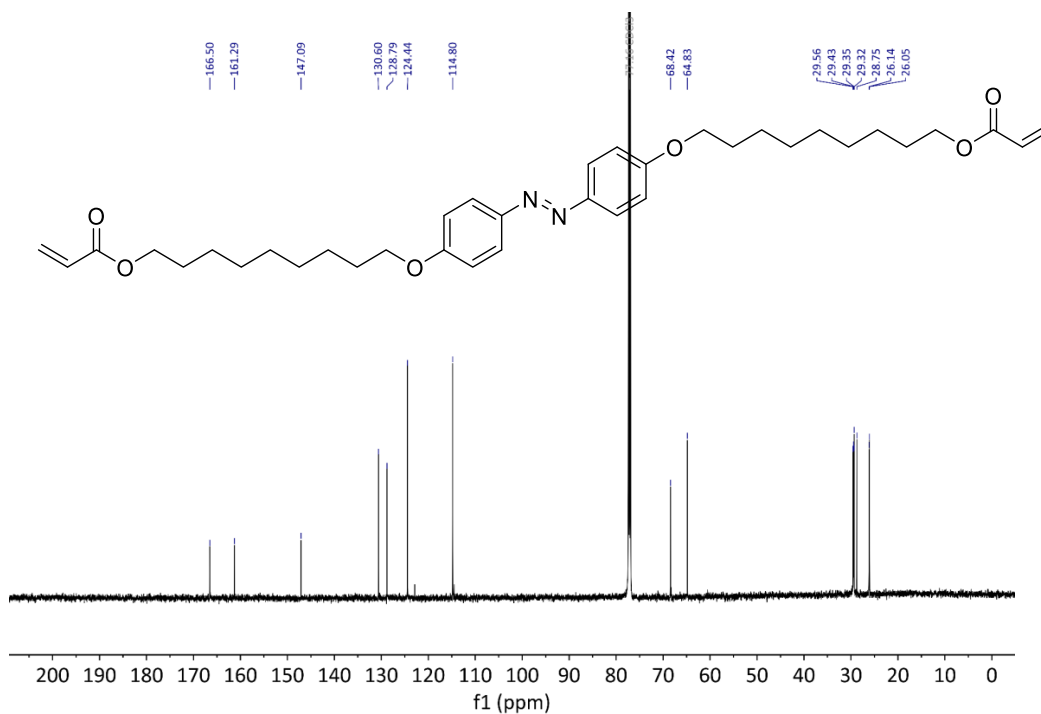
4.  $^1\text{H}$ ,  $^{13}\text{C}\{^1\text{H}\}$  and  $^{19}\text{F}$  NMR Spectra of the Purified Compounds

## 9-Bromononyl acrylate (S1)

Figure S8:  $^1\text{H}$  NMR spectrum of S1 in  $\text{CDCl}_3$ .Figure S9  $^{13}\text{C}\{^1\text{H}\}$  NMR spectrum of S1 in  $\text{CDCl}_3$ .



Figure S10:  $^1\text{H}$  NMR spectrum of **S2** in  $\text{DMSO-}d_6$ .Figure S11:  $^{13}\text{C}\{^1\text{H}\}$  NMR spectrum of **S2** in  $\text{DMSO-}d_6$ .

Figure 12:  $^1\text{H}$  NMR spectrum of LC-Azo in  $\text{CDCl}_3$ .Figure S13:  $^{13}\text{C}\{^1\text{H}\}$  NMR spectrum of LC-Azo in  $\text{CDCl}_3$ .

## 9.5 Appendix Unpublished Work

## Supporting Information

## Contents

1	General Information.....	2
1.1	Reagents.....	3
1.2	Solvents.....	3
2	Analytical Data - Part I.....	4
2.1.	UV-Vis Analysis: Switching Behavior of <b>FLOAM</b> .....	4
2.2	<sup>1</sup> H-NMR Analysis: Quantitative Switching Behavior of <b>FLOAM</b> .....	5
2.3	Half-Life Time of <b>FLOAM</b> at 100 °C.....	6
2.4	Fluorescence Emissions Spectrum of <b>E</b> - and <b>Z-FLOAM</b> .....	7
3	Crystal Structure Analysis of <b>E</b> - and <b>Z-FLOAM</b> .....	8
4	Syntheses.....	10
5.1	1,2-Dibromo-4,5-bis(bromomethyl)benzene ( <b>FI1</b> ).....	13
5.2	3,3'-(((4,5-Dibromo-1,2-phenylene)bis(methylene))bis(oxy))bis(1-fluoro-2-nitrobenzene) .... ( <b>FI2</b> ).....	13
5.3	6,6'-(((4,5-Dibromo-1,2-phenylene)bis(methylene))bis(oxy))bis(2-fluoroaniline) ( <b>FI3</b> ).....	14
5.4	( <i>E</i> )-14,15-Dibromo-4,7-difluoro-12,17-dihydrotribenzo[b,f,j][1,8]dioxo [4,5]diazacyclododecine ( <b>FI4</b> ).....	15
5.5	3,3'-Dimethoxy-1,1'-biphenyl ( <b>St2</b> ).....	16
5.6	2,2'-dibromo-5,5'-dimethoxy-1,1'-biphenyl ( <b>St3</b> ).....	16
5.7	6,6'-Dibromo-[1,1'-biphenyl]-3,3'-diol ( <b>St4</b> ).....	17
5.8	((6,6'-Dibromo-[1,1'-biphenyl]-3,3'-diyl)bis(oxy))bis( <i>tert</i> -butyldimethylsilane) ( <b>St5</b> ).....	18
5.9	2,2'-Dibromo-5,5'-bis(nonyloxy)-1,1'-biphenyl ( <b>St6</b> ).....	18
5.10	2,8-Dimethoxy-5,5-dimethyl-5H-dibenzo[b,d]stannole ( <b>St7</b> ).....	19
5.11	((5,5-Dimethyl-5H-dibenzo[b,d]stannole-2,8-diyl)bis(oxy))bis( <i>tert</i> -butyldimethylsilane) ( <b>St8</b> ) 20	
5.12	5,5-Dimethyl-2,8-bis(nonyloxy)-5H-dibenzo[b,d]stannole ( <b>St9</b> ).....	21
5.13	( <i>E</i> )-4,7-Difluoro-16,19-dimethoxy-12,23-dihydrodibenzo[b,f]triphenylene[2,3- j][1,8]dioxo[4,5]diazacyclododecine ( <b>FLOAM</b> ).....	22
5	References.....	23
4.	<sup>1</sup> H, <sup>13</sup> C{ <sup>1</sup> H}, <sup>119</sup> Sn and <sup>19</sup> F NMR Spectra of the Purified Compounds.....	24

## 1 General Information

For reactions under inert conditions, a nitrogen filled glovebox (Pure Lab<sup>HE</sup> from Inert, Amesbury, MA USA) and standard Schlenk techniques were used.

All glassware was dried in an oven at 200 °C for several hours prior to use. NMR tubes were dried in an oven at 110 °C for several hours prior to use.

NMR spectra were recorded on a Bruker Avance Neo 600 (Bruker BioSpin, Rheinstetten, Germany) (600 MHz (<sup>1</sup>H), 151 MHz (<sup>13</sup>C<sup>[1]</sup>), 565 MHz (<sup>19</sup>F) and 224 MHz (<sup>119</sup>Sn) at 298 K. All <sup>1</sup>H NMR and <sup>13</sup>C{<sup>1</sup>H} NMR spectra were referenced to the residual proton signals of the solvent (<sup>1</sup>H) or the solvent itself (<sup>13</sup>C{<sup>1</sup>H}). <sup>19</sup>F NMR spectra were referenced internally against trichlorofluoromethane. The exact assignment of the peaks was performed by two-dimensional NMR spectroscopy such as <sup>1</sup>H COSY, <sup>13</sup>C{<sup>1</sup>H} HSQC and <sup>1</sup>H/<sup>13</sup>C{<sup>1</sup>H} HMBC when possible.

High-resolution EI mass spectra were recorded on a MAT 95XL double-focusing mass spectrometer from Finnigan MAT (Thermo Fisher Scientific, Waltham, MA, USA) at an ionization energy of 70 eV. Samples were measured by a direct or indirect inlet method with a source temperature of 200 °C. High-resolution ESI and APCI mass spectra were measured by a direct inlet method on an Impact II mass spectrometer from Bruker Daltonics (Bruker Daltonics, Bremen, Germany).

IR spectra were recorded on a Nicolet i510 FT-IR spectrometer from Thermo Fisher Scientific (Thermo Fisher Scientific, Waltham, MA, USA) with a diamond window in an area from 500 – 4 000 cm<sup>-1</sup> with a resolution of 4 cm<sup>-1</sup>. All samples were measured 16 times against a background scan.

Melting points were recorded on a Büchi Melting Point M-560 (Büchi, Essen, Germany) and are reported corrected.

UV-vis spectra were recorded with a resolution of 0.5 nm with a Cary 3500 Multicell UV-Vis Spectrophotometer from Agilent (CA, USA) with a double monochromator. In all cases, DMSO (spectroscopy grade) was used as a solvent.

Emission measurements were performed using a Jasco FP-8300 spectrofluorometer and recorded from 300 to 750 nm with a resolution of 0.5 or 1 nm. The excitation wavelength was chosen to be at the respective absorption maximum of the sample or the wavelength that reached the best intensity. All measurements were performed at 23 °C in quartz cuvettes with 10 mm path length by Hellma Analytics. Absolute quantum yields were measured using an Edinburgh integrating sphere model ILF-835 100 mm. The error of the used measurement setup was estimated by repeated measurements of a reference sample (Rhodamin 6G in EtOH) over the course of 2 weeks to be around an absolute ±0.05.

For the irradiation experiments: A UPLED power supply powered the high-power LED modules: M365L3 (365 nm), M415L4 (415 nm), M530L4 (530 nm), M590L4 (590 nm). A collimator was used to focus the light beam. The light intensity was measured using an ILT2400 hand-held light meter manufactured by International Light Technologies, Inc., (Peabody, USA). Additionally, a 420 nm (1.0 W) and a 525 nm LED (1.0 W) from EPILED was built in our laboratories.

Single crystal X-ray diffraction data were collected at 100 K using an open flow nitrogen stream on a Bruker Venture D8 diffractometer (Bruker, Karlsruhe, Germany) with a Photon 100 detector in shutterless mode with Mo-K $\alpha$  (0.7107 Å) radiation. All structures were solved by intrinsic phasing and refined based on F<sup>2</sup> by use of the SHELX program package, as implemented in OLEX2<sup>[2]</sup>. All non-hydrogen atoms were refined using anisotropic displacement parameters. Hydrogen atoms attached to carbon atoms were included in geometrically calculated positions using a riding model. The crystal was obtained by slow evaporation of a concentrated solution in Et<sub>2</sub>O at 20 °C. For the Z-Isomer the solution was irradiated for 2 h with green light (525nm). The crystals were then grown by slow evaporation in the dark.

Thin layer chromatography (TLC) was performed using TLC Silica gel 60 F<sub>254</sub> from Merck (Merck, Darmstadt, Germany) and the compounds were visualized by exposure to UV light at a wavelength of 254 nm. Column chromatography was performed manually using silica gel 60 (0.015-0.040 mm) from Merck (Merck, Darmstadt, Germany). The samples were applied via dry load with Celite® 503 (Macherey-Nagel, Düren, Germany) as column material. If stated, Celite® 503 was used as filtration aid.

The use of abbreviations follows the conventions from the ACS Style guide.<sup>[3]</sup>

## 1.1 Reagents

All chemicals were commercially available and used without purification.

**Table S1.** List of suppliers and purity of used chemicals.

Reagent	Supplier	Purity
Benzoylperoxide	Sigma-Aldrich	75% (25% H <sub>2</sub> O)
1-Bromononanol	Sigma Aldrich	98%
<i>N</i> -Bromosuccinimide	TCI	>97%
Boron tribromide, 1 M in DCM	Alfa Aesar	
Cesium carbonate	TCI	>98%
1,2-Dibromo-4,5-dimethylbenzene	BLD Pharm	98%
Dichlorodimethylsilane	Sigma-Aldrich	99.5%
Hydroquinone	TCI	>99%
3-Iodoanisole	BLD Pharm	95%
Imidazole	Merck	98%
<i>n</i> -BuLi (2.5 M in hexanes)	Acros	
Sodium carbonate	Chem Solute%	99.8%
Sodium chloride	CarlRoth	>99.5%
Sodium hydroxide	VWR	98.6%
Palladium acetate	Fisher Scientific	99.9%
Bis( <i>tri-tert</i> -butylphosphine)palladium(0)	Sigma Aldrich	99%
<i>Tert</i> -butyldimethylchlorosilane	Apollo Scientific	99.6%
Tri- <i>o</i> -tolylphosphine	STREM Chemicals	99%

## 1.2 Solvents

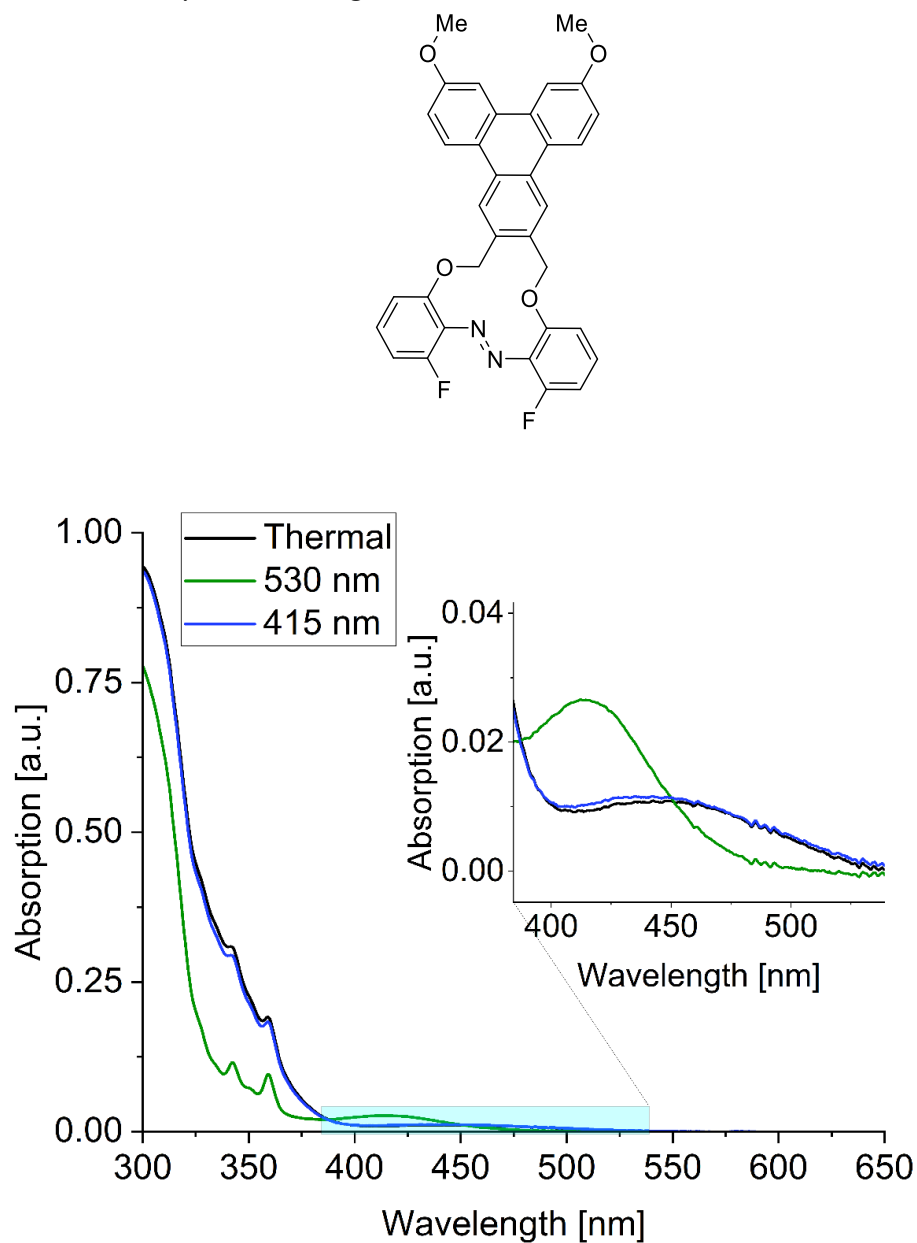
All solvents for purification and extraction were used as received. All solvents used for synthesis under inert conditions were dried by a solvent purification system (SPS) from Inert Technologies.

**Table S2.** List of supplier and purity of used solvents.

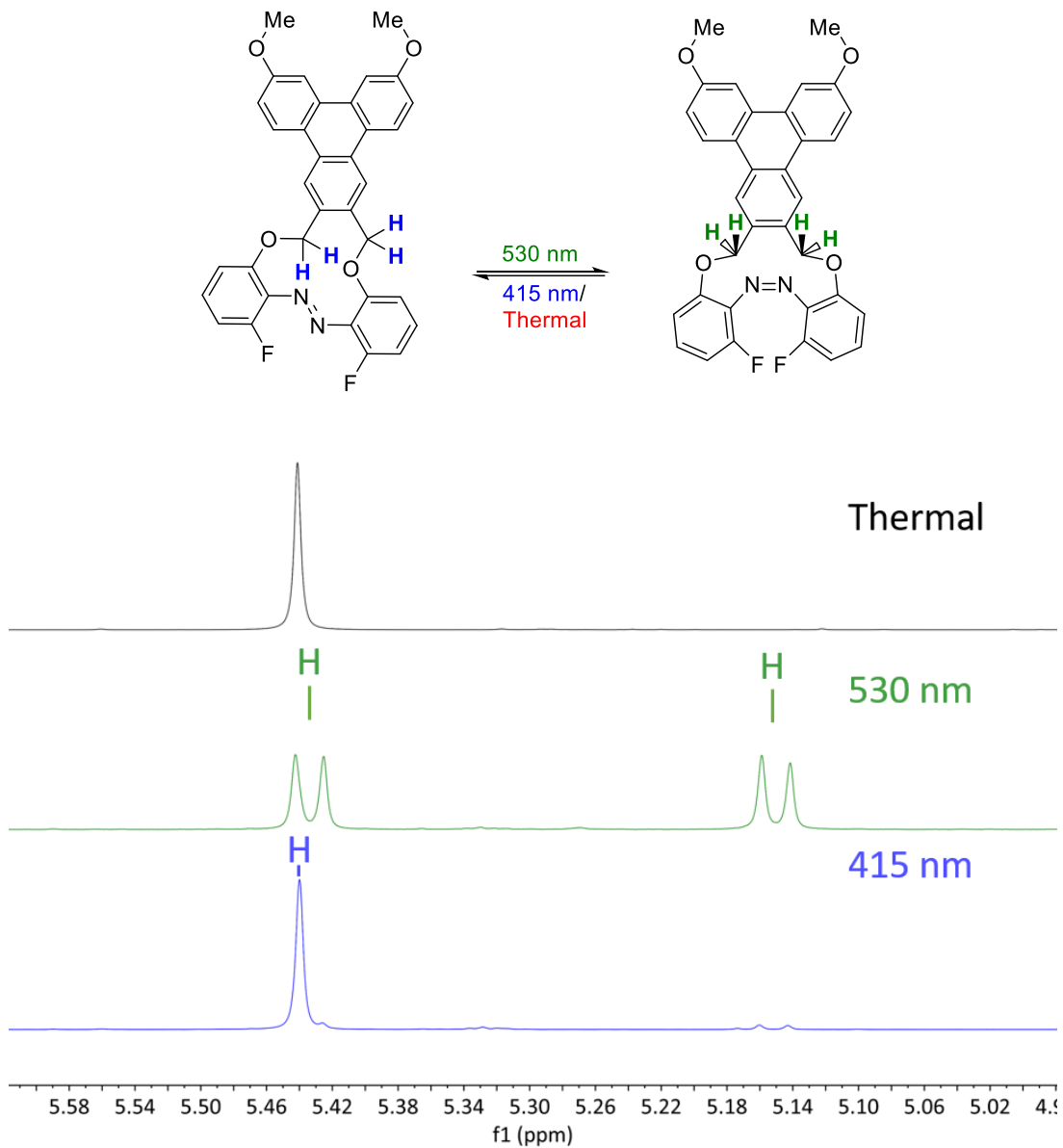
Solvent	Supplier and Purity
Acetone	Sigma Aldrich
Acetonitrile	Fisher Scientific 99.5%
Chloroform- <i>d</i> <sub>1</sub>	Euroisotop 99.8%
Cyclohexane	Merck ≥99.5% (GC)
DCM	Merck ≥99.9% (GC)
DMF	VWR, >99.5%
DMSO- <i>d</i> <sub>6</sub>	Sigma Aldrich, 99.9%
Ethanol	VWR ≥99.8%, absolute
Ethyl acetate	Merck >99.5% (GC)
Hydrochloric acid (37%)	Merck, fuming >37.0%
Methanol	VWR >99.8% (GC)
<i>n</i> -Hexane	Merck, >95%
Toluene	Merck >99.7% (GC)
Water	deionized

## 2 Analytical Data - Part I

### 2.1. UV-Vis Analysis: Switching Behavior of **FLOAM**



**Figure 1** UV-vis spectrum of **FLOAM** in DMSO after thermal treatment (black, 140 °C, 4 h) and irradiation with green (530 nm, 5min, 70 mW/cm<sup>2</sup>) and violet light (420 nm, 5min, 60 mW/cm<sup>2</sup>) respectively. The PSS was reached (conc = 0.0133 μmol mL<sup>-1</sup>).

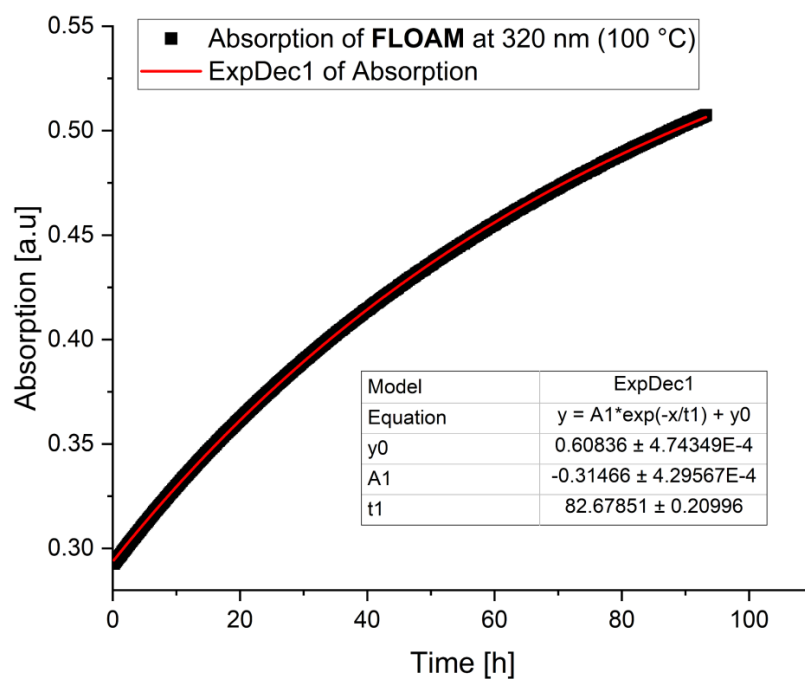
2.2  $^1\text{H-NMR}$  Analysis: Quantitative Switching Behavior of **FLOAM**

**Figure 2**  $^1\text{H-NMR}$  spectroscopic study of the irradiation of **FLOAM** in  $\text{DMSO-d}_6$  after thermal treatment (the solid was heated at  $105^\circ\text{C}$  for 72h before dissolution, black spectrum), after irradiation with green light (530 nm, 5min,  $70\text{ mW/cm}^2$ ) and violet light (420 nm, 5min,  $60\text{ mW/cm}^2$ ) ( $\text{conc}_{\text{FLOAM}} = 7.11\ \mu\text{mol mL}^{-1}$ ).

**Table S3.** Summary of  $^1\text{H-NMR}$  spectroscopic studies of the irradiation of **FLOAM**, after irradiation with 530 nm and 415 nm in the solvents  $\text{DMSO-}d_6$ . The % values for the *E* and *Z* isomer were obtained by the integration of  $\text{CH}_2$ -ethylenes bridge protons. ( $\text{conc}_{\text{FLOAM}} = 7.11 \mu\text{mol mL}^{-1}$ )

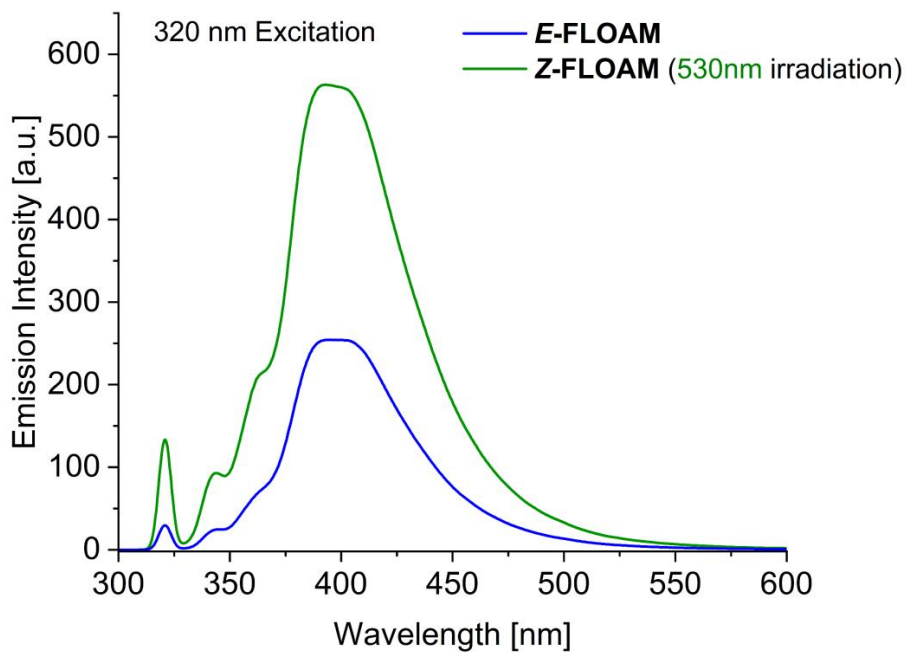
	FLOAM	
	<i>E</i> -isomer	<i>Z</i> -isomer
Thermal	100%	0%
415 nm	86%	14%
530 nm	4%	96%

### 2.3 Half-Life Time of **FLOAM** at 100 °C.



**Figure S9.** Kinetic measurements of **FLOAM** in DMSO after irradiation with green light (530 nm, 5min,  $70 \text{ mW/cm}^2$ ) at 100 °C. The first measurement points are not shown because the sample needed time to adapt to the temperature. An exponential decay fit was used to evaluate the data and determine  $t_{1/2}$  and  $k(T)$ .  $\text{conc}_{\text{FLOAM}} = 0.0133 \mu\text{mol mL}^{-1}$ .



2.4 Fluorescence Emissions Spectrum of *E*- and *Z*-FLOAM.

**Figure 3** Fluorescence spectrum of **FLOAM** after excitation with 320 nm in chloroform of *E*-FLOAM (blue) and after excitation with 320 nm of the same sample after irradiation with green light (530 nm).

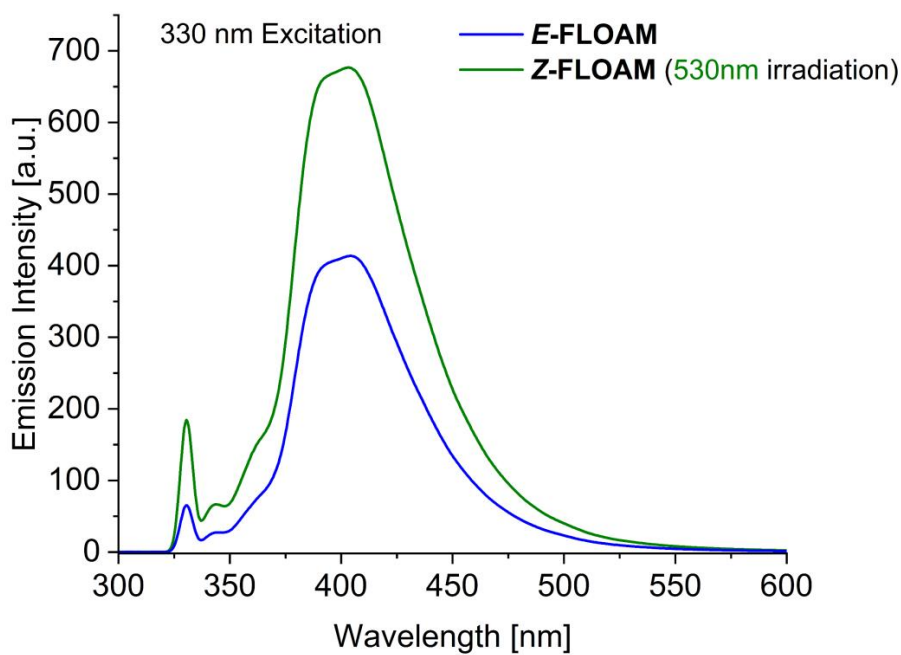


**Figure 4** Fluorescence spectrum of **FLOAM** after excitation with 330 nm in chloroform of **E-FLOAM** (blue) and after excitation with 330 nm of the same sample after irradiation with green light (530 nm).

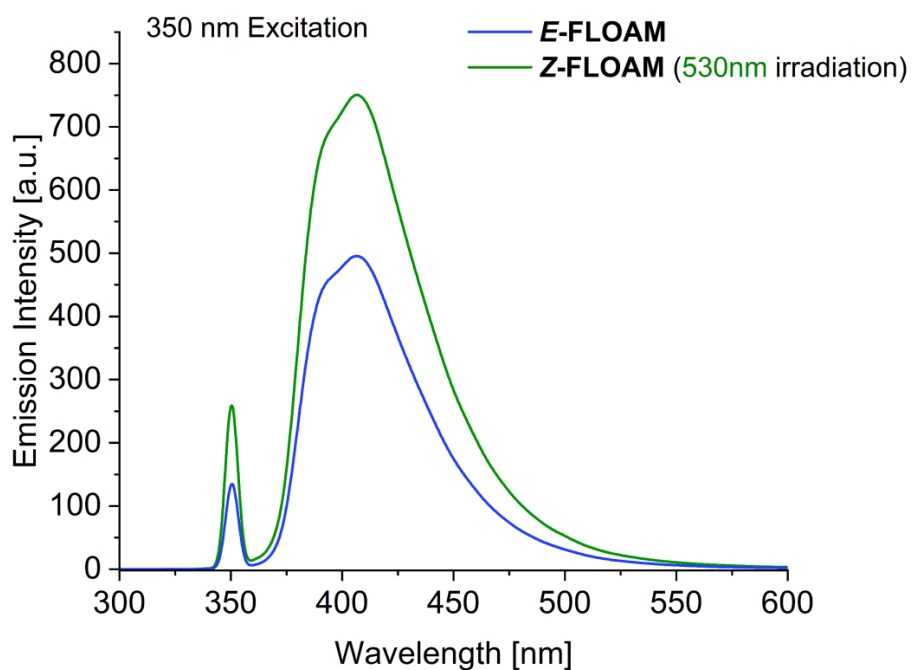


**Figure 5** Fluorescence spectrum of **FLOAM** after excitation with 350 nm in chloroform of **E-FLOAM** (blue) and after excitation with 350 nm of the same sample after irradiation with green light (530 nm).

### 3 Crystal Structure Analysis of *E*- and *Z*-FLOAM

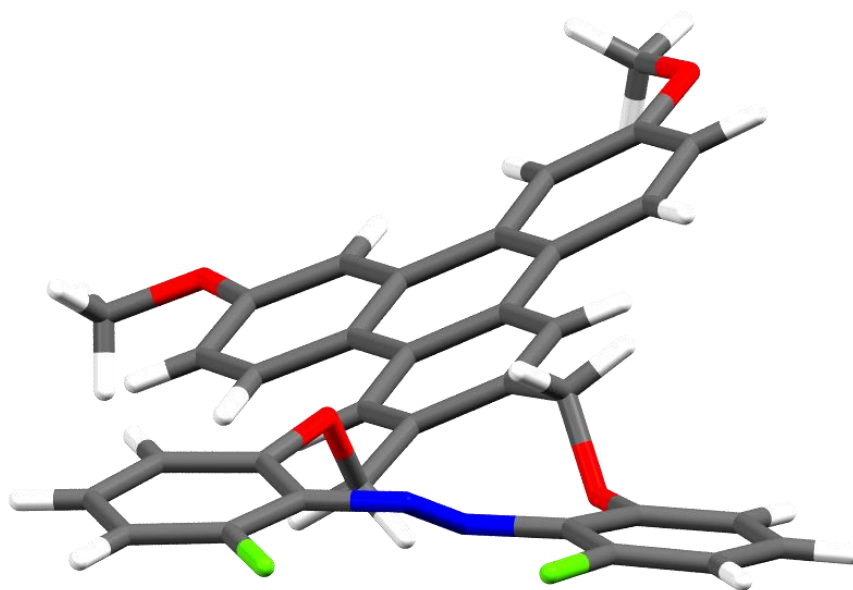


**Figure 6** Crystal structure of *E*-FLOAM.

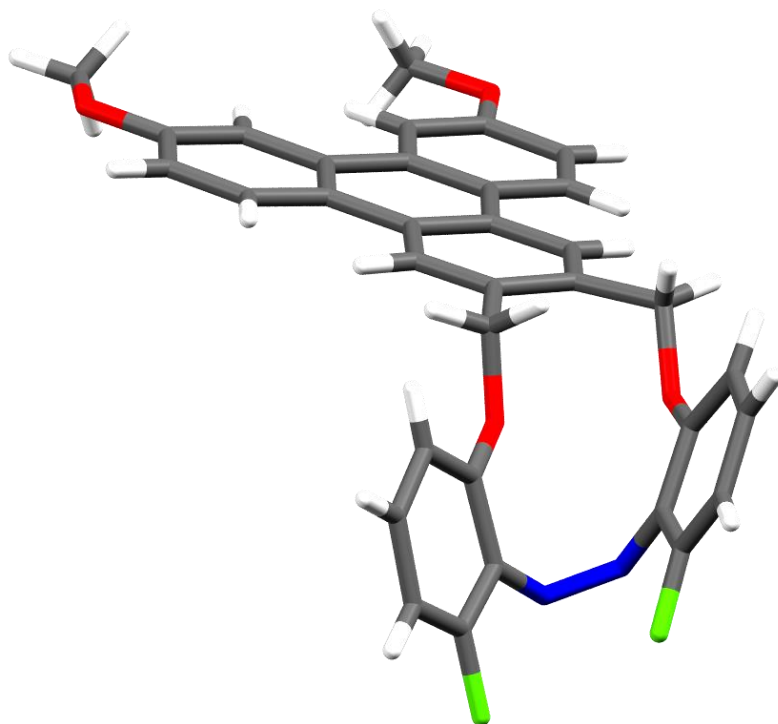
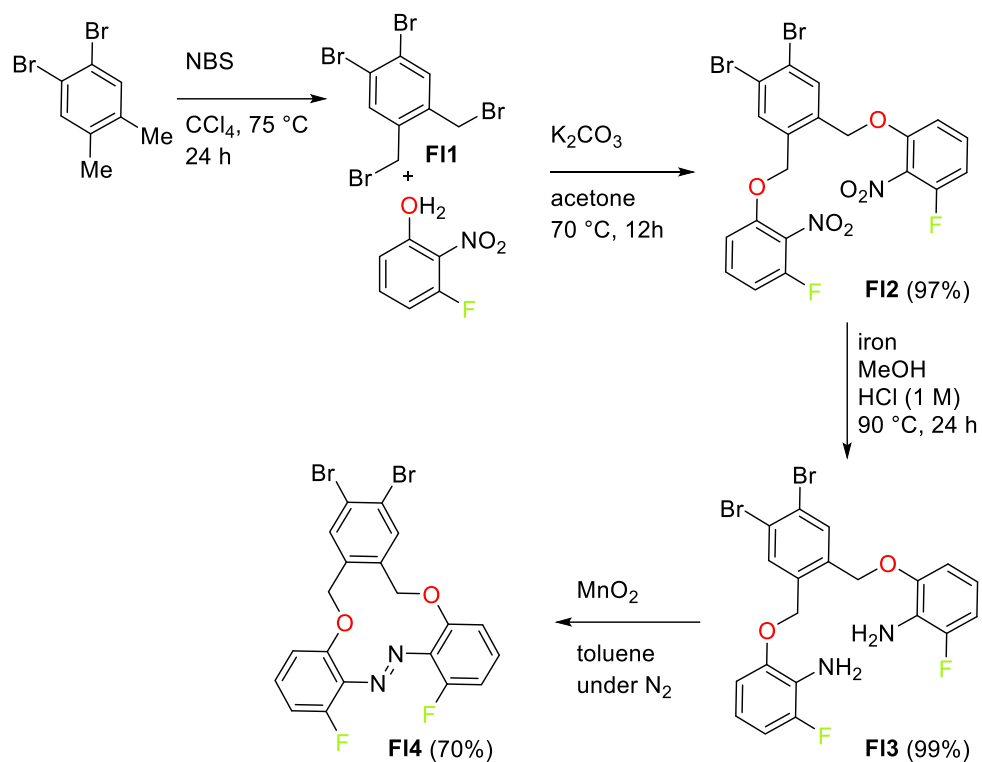
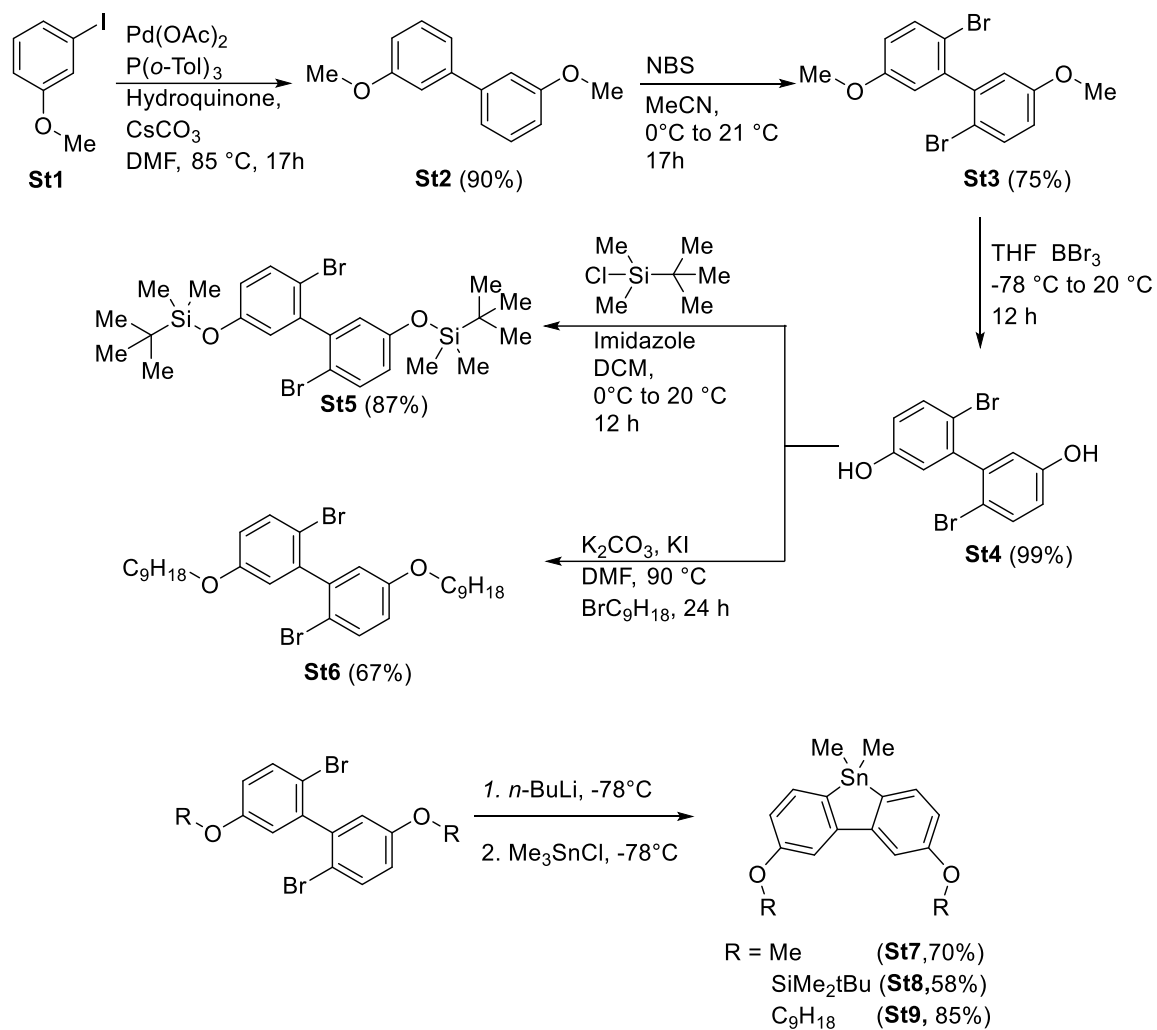


**Figure 7** Crystal structure of *Z*-FLOAM.

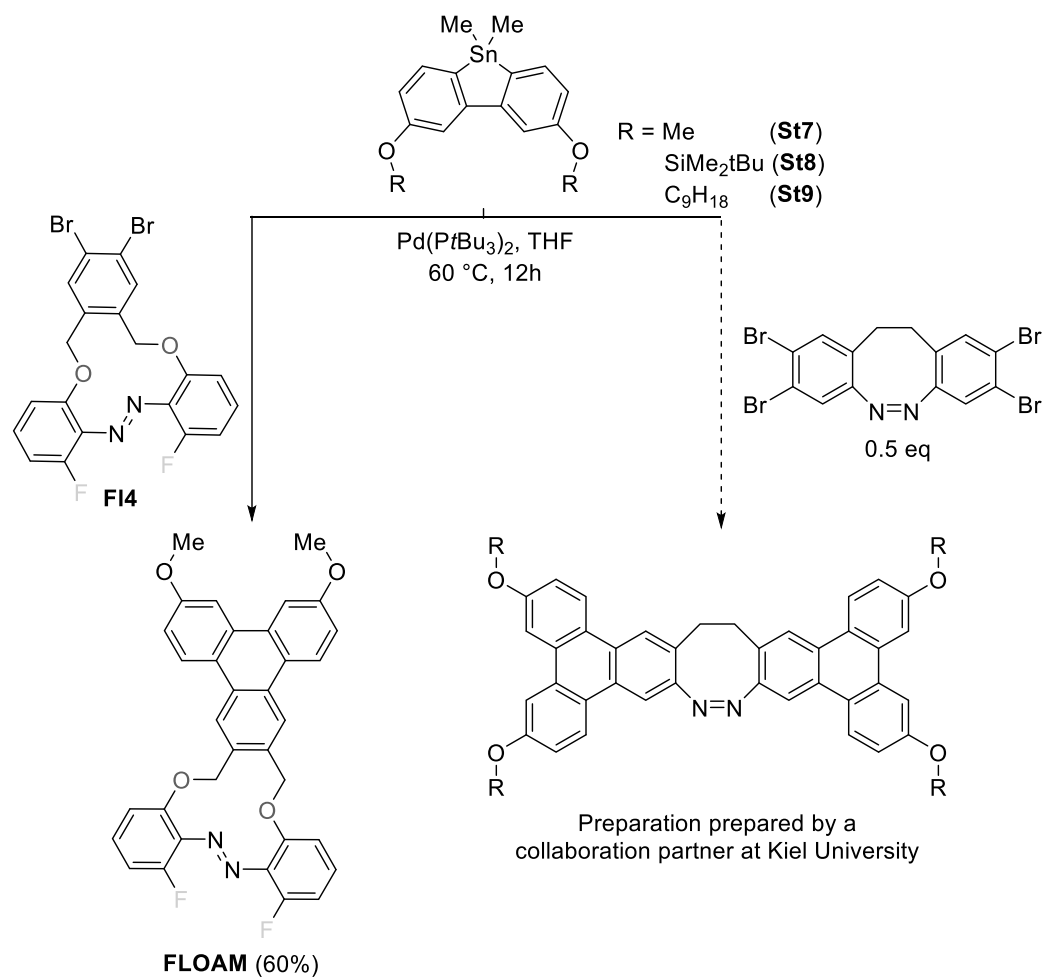
## 4 Syntheses



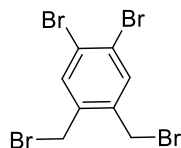
Scheme 1: General synthesis overview for the FLOAM precursor.



Scheme 2: General synthesis overview for the stannylated precursor.

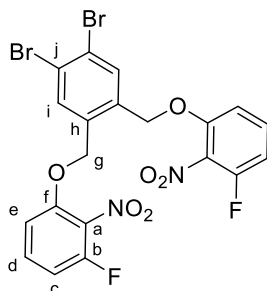


**Scheme 3:** General synthesis overview for the for **FLOAM** and a disubstituted diazocine derivate (dashed reaction path) successfully prepared by our cooperation partner AG Herges at the university of Kiel.

5.1 1,2-Dibromo-4,5-bis(bromomethyl)benzene (**FI1**)<sup>[4]</sup>

This reaction was adapted from M. Kimura and co-worker.<sup>[4]</sup>

*N*-Bromosuccinimide (NBS) (10.4 g, 58.3 mmol, 2.01 eq.), 1,2-dibromo-4,5-dimethylbenzene (7.50 g, 28.4 mmol, 1.00 eq), and benzoyl peroxide (BPO) (180 mg, 0.76 mmol, 0.03 eq.) in CCl<sub>4</sub> (200 mL) were heated to reflux while stirring for 3 h. After allowing the reaction mixture to cool and filtration to remove the by-product, the solvent was removed to yield the brominated compound (11.8 g, 98%, 70% purity) as a pale-yellow solid, which was used without further purification. The purity was analyzed by <sup>1</sup>H NMR spectra (the main-impurity was 1,2-dibromo-4,5-dimethylbenzene and 1,2-dibromo-4-bromomethylbenzene).

5.2 3,3'-(((4,5-Dibromo-1,2-phenylene)bis(methylene))bis(oxy))bis(1-fluoro-2-nitrobenzene) (**FI2**)

**FI1** (3.83 g; Note: calculated for 70% purity, 6.36 mmol, 0.50 eq.) was added over a period of 10 min to a solution of 3-fluoro-2-nitrophenol (2.00 g, 12.7 mmol, 1.00 eq.) and K<sub>2</sub>CO<sub>3</sub> (2.64 g, 69.0 mmol, 1.50 eq.) in acetone (50 mL). This mixture was heated to reflux at 70°C for 12 h. The mixture was cooled to 25°C and DCM (400 mL) was added. The organic phase was washed with water (2 x 200 mL) and brine (150 mL) and dried over MgSO<sub>4</sub>. The solvent was evaporated *in vacuo*. Purification of the residue by column chromatography (gradient: *n*-hexane → DCM), gave the product as a colorless solid (3.54 g, 6.17 mmol, 97%).

<sup>1</sup>H NMR (600 MHz, CDCl<sub>3</sub>) δ = 7.71 (s, 2H, *H*-i), 7.44 (dd, <sup>3</sup>*J* = 8.6 Hz, <sup>3</sup>*J* = 6.0 Hz, 2H, *H*-c), 6.95 (d, <sup>3</sup>*J* = 8.6 Hz, 2H, *H*-e), 6.87 (dd, <sup>3</sup>*J* = 8.6 Hz, 2H, *H*-d), 5.29 (s, 4H, *H*-g) ppm.

<sup>13</sup>C{<sup>1</sup>H} NMR (151 MHz, CDCl<sub>3</sub>) δ = 154.71 (d, <sup>1</sup>*J* = 257.8 Hz, *C*-b), 151.01 (d, <sup>3</sup>*J* = 2.4 Hz, *C*-f), 134.61 (*C*-h), 134.30 (*C*-i), 132.41 (d, <sup>2</sup>*J* = 9.7 Hz, *C*-a), 125.78 (*C*-j), 109.66 (d, <sup>2</sup>*J* = 19.2 Hz, *C*-c), 109.31 (d, <sup>4</sup>*J* = 3.2 Hz, *C*-e), 69.95 (*C*-g) ppm.

<sup>19</sup>F NMR (565 MHz, CDCl<sub>3</sub>) δ = -121.72 (m, *F*-b) ppm.

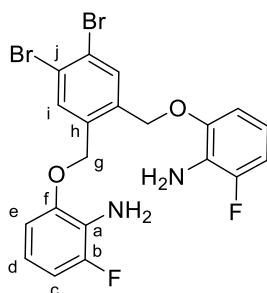
IR (ATR):  $\tilde{\nu}$  = 3119.76 (w), 2919.90 (w), 2849.28 (w), 1599.44 (m), 1524.49 (s), 1468.63 (m), 1446.64 (w), 1396.73 (w), 1360.11 (m), 1291.32 (m), 1246.86 (s), 1125.51 (w), 1086.60 (s), 1063.29 (s), 974.46 (m), 917.35 (m), 885.19 (m), 853.42 (m), 783.34 (s), 751.82 (m), 734.65 (m), 713.78 (w), 700.38 (m), 675.09 (w) cm<sup>-1</sup>.

HRMS (ESI) *m/z* (%): [M+Na]<sup>+</sup> calcd for [C<sub>20</sub>H<sub>12</sub><sup>79</sup>Br<sub>2</sub>F<sub>2</sub>N<sub>2</sub>O<sub>6</sub>+Na]<sup>+</sup> 594.89224, found 594.89154.

Mp: 202°C.

R<sub>f</sub>: 0.80 (DCM).

## 5.3 6,6'-(((4,5-Dibromo-1,2-phenylene)bis(methylene))bis(oxy))bis(2-fluoroaniline) (F13)



Iron powder (4.41 g, 78.9 mmol, 10.0 eq.) was added portion wise to a solution of **F12** (4.53 g, 7.89 mmol, 1.00 eq.) in MeOH (100 mL). Afterwards, HCl (1 M, 5 mL) was slowly added over the course of 1 min to the reaction. The reaction mixture was heated to 90°C for 70 min. After cooling down the mixture was filtered. The solid residue was washed with ethyl acetate (100 mL). The combined organic layers were washed with water (3 x 200 mL) and brine (1 x 100 mL). The organic layer was dried over MgSO<sub>4</sub> and concentrated under reduced pressure. The crude product was purified by column chromatography (ethylacetate : *n*-hexane 2:1) to obtain the product as a pink solid (4.04 g, 7.85 mmol, 99%).

<sup>1</sup>H NMR (600 MHz, CDCl<sub>3</sub>) δ = 7.77 (s, 2H, *H*-i), 6.74-6.70 (m, 2H, *H*-e), 6.62-6.60 (m, 4H, *H*-c, *H*-d), 5.09 (s, 4H, *H*-g), 3.75 (s, 4H, *NH*-a) ppm.

<sup>13</sup>C{<sup>1</sup>H} NMR (151 MHz, CDCl<sub>3</sub>) δ = 151.97 (d, <sup>1</sup>J = 237.6 Hz, *C*-b), 147.16 (d, <sup>2</sup>J = 7.2 Hz, *C*-f), 135.94 (*C*-h), 134.26 (*C*-i), 125.25 (*C*-j) (d, <sup>2</sup>J = 15.1 Hz, *C*-a), 116.72 (d, <sup>3</sup>J = 8.9 Hz, *C*-d), 109.21 (d, <sup>2</sup>J = 19.1 Hz, *C*-c), 108.00 (d, <sup>4</sup>J = 2.6 Hz, *C*-e), 67.80 (*C*-g) ppm.

IR (ATR):  $\tilde{\nu}$  = 3469.92 (w), 3374.41 (w), 2917.29 (w), 2849.32 (w), 1621.92 (w), 1599.29 (m), 1581.43 (m), 1505.78 (m), 1472.41 (s), 1448.57 (m), 1389.13 (w), 1346.07 (w), 1291.98 (m), 1256.77 (m), 1238.81 (m), 1166.90 (s), 1133.40 (m), 1061.35 (m), 1027.85 (s), 926.99 (m), 912.55 (m), 884.70 (m), 837.26 (w), 753.26 (s), 709.91 (s), 655.77 (w) cm<sup>-1</sup>.

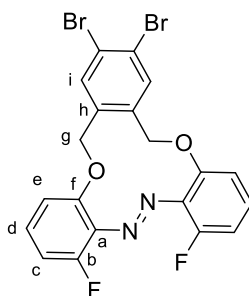
HRMS (EI, 70 eV) *m/z* (%): [M]<sup>+</sup> calcd for [C<sub>20</sub>H<sub>16</sub><sup>79</sup>Br<sub>2</sub>F<sub>2</sub>N<sub>2</sub>O<sub>2</sub>]<sup>+</sup> 511.95411, found 511.95429(10), [C<sub>6</sub>H<sub>6</sub>F<sub>2</sub>NO]<sup>+</sup> 125.8 (100).

**Mp**: 151°C.

**R<sub>f</sub>**: 0.35 (ethylacetate : *n*-hexane, 2:1).



5.4 (*E*)-14,15-Dibromo-4,7-difluoro-12,17-dihydrotribenzo[*b,f,j*][1,8]dioxo[4,5]diazacyclododecine (**FI4**)



**FI3** (961 mg, 1.87 mmol, 1.00 eq.) was dissolved in toluene (30 mL). A stream of nitrogen was passed through the solution for 1 h to degas the mixture.  $\text{MnO}_2$  (1.30 g, 15.0 mmol, 8.00 eq.) was added and the suspension was heated to 110°C for 48 h. The hot reaction mixture was filtered through celite and the celite rinsed with chloroform (2 x 30 mL). The filtrate was evaporated to dryness under reduced pressure, and the residue was purified by column chromatography (DCM : *n*-hexane 2:1) to obtain final compound (668 mg, 1.31 mmol, 70%) as a yellow solid.

$^1\text{H NMR}$  (600 MHz,  $\text{CDCl}_3$ )  $\delta$  = 7.73 (s, 2H, *H*-i), 7.41-7.37 (m, 2H, *H*-d), 7.15 (d,  $^3J$  = 8.2 Hz, 2H, *H*-e), 7.09 (dd,  $^3J$  = 8.2 Hz, 2H, *H*-c), 5.20 (s, 4H, *H*-g) ppm.

$^{13}\text{C}\{^1\text{H}\}$  NMR (151 MHz,  $\text{CDCl}_3$ )  $\delta$  = 155.60 (d,  $^1J$  = 259.9 Hz, C-b), 152.36 (d,  $^5J$  = 2.7 Hz C-f), 136.97 (C-h) 136.80 d,  $^2J$  = 8.4 Hz, C-a), 136.49 (C-i), 131.65 (C-i), 131.37 (d,  $^3J$  = 10.2 Hz, C-d), 125.34 (C-j), 118.91 (d,  $^4J$  = 3.3 Hz, C-e), 113.09 (d,  $^2J$  = 20.0 Hz, C-c), 75.39 (C-g) ppm.

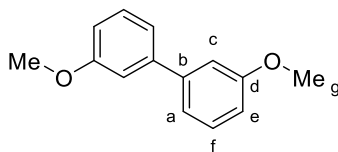
$^{19}\text{F NMR}$  (565 MHz,  $\text{CDCl}_3$ )  $\delta$  = -121.59 (dd,  $^3J$  = 10.3 Hz,  $^4J$  = 6.0 Hz, F-b) ppm.

**IR** (ATR):  $\tilde{\nu}$  = 2919.49 (w), 1600.70 (m), 1574.64 (m), 1512.31 (w), 1469.49 (s), 1405.37 (w), 1381.91 (m), 1342.81 (w), 1274.52 (m), 1240.24 (s), 1178.50 (w), 1131.42 (w), 1085.67 (w), 1059.19 (m), 1031.51 (s), 977.26 (w), 949.66 (m), 921.01 (m), 897.10 (m), 883.40 (m), 830.57 (w), 798.31 (s), 783.71 (m), 774.89 (m), 734.91 (s)  $\text{cm}^{-1}$ .

**HRMS** (ESI)  $m/z$  (%):  $[\text{M}+\text{Na}]^+$  calcd for  $[\text{C}_{20}\text{H}_{12}^{79}\text{Br}_2\text{F}_2\text{N}_2\text{O}_2+\text{Na}]^+$  530.89763, found 530.90086.

**Mp**: 209°C.

**R<sub>f</sub>**: 0.68 (DCM).

5.5 3,3'-Dimethoxy-1,1'-biphenyl (**St2**)<sup>[5]</sup>

Adapted from D. D. Hennings and co-worker.<sup>[5]</sup>

In a glovebox, 3-iodoanisole (4.68 g, 20.0 mmol, 1.00 eq.), hydroquinone (1.11 g, 10.0 mmol, 0.500 eq.), and Cs<sub>2</sub>CO<sub>3</sub> (6.52 g, 20.0 mmol, 1.00 eq.) was added a homogenous stirring solution of Pd(OAc)<sub>2</sub> (40.0 mg, 0.20 mmol) and tri-*o*-tolylphosphine (61.0 mg, 0.20 mmol) in DMF (23 mL). The reaction mixture was heated under N<sub>2</sub> at 85°C for 17 h. The reaction mixture was cooled to 20°C, quenched with HCl (2 M, 20 mL), diluted with water (20 mL), and extracted with EtOAc (3 x 30 mL). The combined organic phases were washed with 10% NaOH (4 x 40 mL), brine (40 mL), dried over MgSO<sub>4</sub>, concentrated under reduced pressure, and purified using flash column chromatography on silica gel (eluent: cyclohexane → DCM) to afford **St2** (1.93 g, 9.00 mmol, 90%, Lit<sup>[5]</sup>: 95%) as a white crystalline solid.

<sup>1</sup>H NMR (600 MHz, CDCl<sub>3</sub>) δ = 7.36 (dd, <sup>3</sup>J = 7.9 Hz, 2H, H-f), 7.18 (d, <sup>3</sup>J = 8.5 Hz, 2H, H-e), 7.13 (m, 2H, H-c), 6.91 (dd, <sup>3</sup>J = 8.5 Hz, <sup>4</sup>J = 3.1 Hz, 2H, H-a), 3.87 (s, 6H, H-g) ppm.

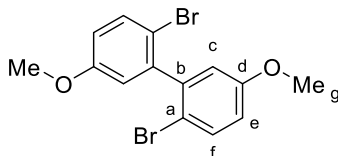
<sup>13</sup>C{<sup>1</sup>H} NMR (151 MHz, CDCl<sub>3</sub>) δ = 160.03 (C-d), 142.78 (C-b), 129.87 (C-f), 119.85 (C-e), 113.09 (C-c), 112.95 (C-a), 55.46 (C-g) ppm.

IR (ATR):  $\tilde{\nu}$  = 2998.46 (w), 2936.90 (w), 2833.13 (w), 1596.55 (s), 1573.14 (s), 1474.44 (m), 1409.69 (m), 1289.79 (w), 1277.53 (m), 1230.99 (s), 1202.35 (s), 1167.78 (s), 1090.82 (w), 1045.00 (m), 1028.53 (s), 991.82 (w), 907.94 (w), 851.18 (m), 770.82 (s), 693.23 (s) cm<sup>-1</sup>.

HRMS (EI, 70 eV) *m/z* (%): [M]<sup>+</sup> calcd for [C<sub>14</sub>H<sub>14</sub>O<sub>2</sub>]<sup>+</sup> 214.09883, found 214.09872 (100).

Mp: 37 °C.

R<sub>f</sub>: 0.50 (eluent: cyclohexane : DCM, 2:1).

5.6 2,2'-dibromo-5,5'-dimethoxy-1,1'-biphenyl (**St3**)<sup>[6]</sup>

This procedure was adapted from E. Brüllingen and co-worker.<sup>[6]</sup>

Under a N<sub>2</sub> atmosphere, **St2** (5.00 mmol, 1.07 g, 1.00 eq.) was dissolved in dry acetonitrile (15 mL). The solution was cooled by an ice bath and *N*-bromosuccinimide (NBS) (10.0 mmol, 1.78 g, 2.00 eq.) was added portion wise. The mixture was stirred for 2 h at 0°C and slowly warmed to 20°C over 17 h. The reaction was quenched with cold water (30 mL). The precipitate was filtrated and the residue purified by washing with hot water (100 mL) and hot *n*-hexane (100 mL) yielding **St3** (1.45 g, 3.90 mmol, 78% yield, Lit<sup>[6]</sup>: 75%).

<sup>1</sup>H NMR (600 MHz, CDCl<sub>3</sub>) δ = 7.53 (d, <sup>3</sup>J = 8.7 Hz, 2H, H-c), 6.83 (dd, <sup>3</sup>J = 8.7 Hz, <sup>4</sup>J = 3.1 Hz, 2H, H-e), 6.79 (d, <sup>4</sup>J = 3.1 Hz, 2H, H-f), 3.81 (s, 6H, H-g) ppm.

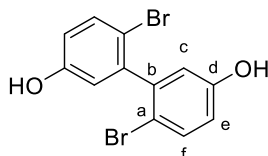
<sup>13</sup>C{<sup>1</sup>H} NMR (151 MHz, CDCl<sub>3</sub>) δ = 158.72 (C-d), 142.86 (C-b), 133.33 (C-c), 116.40 (C-f), 115.58 (C-e), 113.92 (C-a), 55.70 (C-g) ppm.

**IR** (ATR):  $\tilde{\nu}$  = 2956.39 (w), 2937.43 (w), 2832.83 (w), 1593.07 (w), 1566.97 (s), 1481.59 (w), 1459.06 (s), 1435.58 (m), 1420.20 (m), 1392.83 (w), 1298.83 (w), 1282.90 (s), 1259.21 (m), 1245.85 (s), 1224.11 (s), 1198.81 (m), 1181.96 (m), 1168.63 (s), 1138.62 (w), 1084.71 (w), 1056.96 (w), 1026.25 (s), 1010.47 (s), 937.18 (w), 905.12 (w), 887.54 (s), 870.89 (s), 805.54 (s), 713.22 (w), 702.43 (w)  $\text{cm}^{-1}$ .

**HRMS** (EI, 70 eV)  $m/z$  (%):  $[\text{M}]^+$  calcd for  $[\text{C}_{14}\text{H}_{14}^{79}\text{Br}_2\text{O}_2]^+$  369.91986, found 369.92058 (100).

**Mp**: 135°C.

### 5.7 6,6'-Dibromo-[1,1'-biphenyl]-3,3'-diol (**St4**)<sup>[7]</sup>



This procedure was adapted from I. Nagao and co-worker.<sup>[7]</sup>

A Schlenk flask was charged with **St3** (1.12 g, 3.00 mmol, 1.00 eq.) and DCM (15 mL). To the solution  $\text{BBr}_3$  (1 M in DCM, 6.50 mL, 6.50 mmol, 2.17 eq.) was added slowly at -78 °C. The resulting mixture was allowed to warm gradually to 20°C and it was stirred for 24 h before quenching it with  $\text{H}_2\text{O}$  (10 mL) at 0°C. The aqueous layer was extracted with  $\text{Et}_2\text{O}$  (4 x 20 mL). The combined organic phases were washed with sat. aq. NaCl solution (20 mL) and dried over  $\text{MgSO}_4$  to obtain **St4** (1.02 g, 2.97 mmol, 99%).

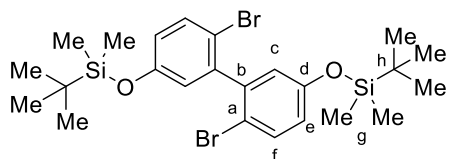
**$^1\text{H}$  NMR** (600 MHz,  $\text{DMSO}-d_6$ )  $\delta$  = 9.83 (s, 2H, OH), 7.44 (d,  $^3J$  = 8.7 Hz, 2H, H-c), 6.74 (dd,  $^3J$  = 8.7 Hz,  $^4J$  = 2.9 Hz, 2H, H-e), 6.62 (d,  $^4J$  = 2.9 Hz, 2H, H-f) ppm.

**$^{13}\text{C}\{^1\text{H}\}$  NMR** (151 MHz,  $\text{DMSO}-d_6$ )  $\delta$  = 156.61 (C-d), 142.27 (C-b), 133.00 (C-c), 117.60 (C-f), 116.97 (C-e), 110.91 (C-a) ppm.

**IR** (ATR):  $\tilde{\nu}$  = 3174.97 (m), 1587.37 (w), 1569.58 (m), 1448.20 (m), 1420.90 (s), 1368.98 (m), 1303.12 (m), 1267.47 (s), 1234.40 (s), 1219.04 (s), 1178.25 (s), 1083.78 (m), 1038.36 (m), 1013.18 (m), 942.20 (w), 856.52 (s), 833.20 (m), 807.66 (s), 720.83 (w), 712.32 (m)  $\text{cm}^{-1}$ .

**HRMS** (EI, 70 eV)  $m/z$  (%):  $[\text{M}]^+$  calcd for  $[\text{C}_{12}\text{H}_8^{79}\text{Br}_2\text{O}_2]^+$  341.88856, found 341.88910, (85),  $[\text{C}_{12}\text{H}_8\text{O}]^{2+}$  183.8 (100).

**Mp**: 212°C.

5.8 ((6,6'-Dibromo-[1,1'-biphenyl]-3,3'-diyl)bis(oxy))bis(*tert*-butyldimethylsilane) (**St5**)

Under  $N_2$  **S4** (688 mg, 2.00 mmol, 1.00 eq.) and imidazole (408 mg, 6.00 mmol, 3.00 eq.) was dissolved in dry DCM (30 mL). *Tert*-butyldimethylsilyl chloride (753 mg, 5.00 mmol, 2.50 eq.) was added portion wise and the suspension was heated to 110°C for 48 h. The hot reaction mixture was filtered through celite and the celite rinsed with chloroform (2 x 30 mL). The filtrate was evaporated to dryness under reduced pressure, and the residue was purified by column chromatography (*n*-hexane) to obtain final compound (996 mg, 1.74 mmol, 87%) as a colorless solid.

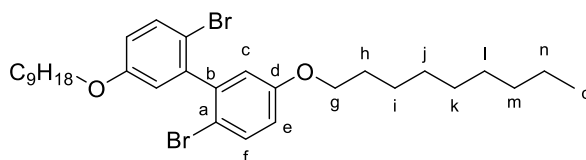
$^1H$  NMR (600 MHz,  $CDCl_3$ )  $\delta$  = 7.48 (d,  $^3J$  = 8.6 Hz, 2H, *H*-c), 6.76-6.74 (m, 2H, *H*-e), 6.73 (m, 2H, *H*-f), 0.98 (s, 18H, *H*-i), 0.20 (s, 6H, *H*-g), 0.20 (s, 6H, *H*-g) ppm.

$^{13}C\{^1H\}$  NMR (151 MHz,  $CDCl_3$ )  $\delta$  = 154.86 (*C*-d), 142.79 (*C*-b), 133.34 (*C*-c), 122.88 (*C*-f), 121.56 (*C*-e), 114.70 (*C*-a), 25.79 (*C*-i), 18.36 (*C*-h), -4.30 (d,  $^1J$  = 13.6 Hz, *C*-g) ppm.

IR (ATR):  $\tilde{\nu}$  = 2954.42 (w), 2928.69 (w), 2884.71 (w), 1583.03 (w), 1561.27 (w), 1458.01 (s), 1408.84 (m), 1362.00 (w), 1313.53 (w), 1270.91 (s), 1252.86 (s), 1229.88 (s), 1192.11 (m), 1123.36 (w), 1080.73 (w), 1040.01 (w), 1013.16 (w), 975.88 (m), 907.58 (s), 876.85 (m), 835.40 (s), 806.74 (s), 778.81 (s), 733.89 (m), 716.33 (w), 690.44 (w), 669.64 (w)  $cm^{-1}$ .

HRMS (EI, 70 eV)  $m/z$  (%):  $[M]^+$  calcd for  $[C_{24}H_{36}^{79}Br_2^{29}Si_2O_2]^+$  570.06151, found 570.06155 (85), 72.9 (100).

$R_f$ : 0.68 (*n*-hexane).

5.9 2,2'-Dibromo-5,5'-bis(nonyloxy)-1,1'-biphenyl (**St6**)

9-Bromononane (1.04 g, 5.00 mmol, 2.50 eq.) was added over a period of 10 min to a solution of **St3** (688 mg, 2.00 mmol, 1.00 eq.) and  $K_2CO_3$  (828 mg, 6.00 mmol, 3.00 eq.) in acetone (50 mL) and the mixture was heated to reflux at 70°C for 12 h. The mixture was cooled to 25°C and DCM (100 mL) was added. The organic phase was washed with water (2 x 200 mL) and brine (150 mL) and dried over  $MgSO_4$ . The solvent was evaporated *in vacuo*. Purification of the residue by column chromatography (*n*-hexane), gave the product as a colorless solid (2.00 g, 3.35 mmol, 67%).

$^1H$  NMR (600 MHz,  $CDCl_3$ )  $\delta$  = 7.51 (d,  $^3J$  = 8.6 Hz, 2H, *H*-c), 6.82-6.80 (m, 2H, *H*-e), 6.78 (m, 2H, *H*-f), 3.93 (t,  $^3J$  = 6.6 Hz, 4H, *H*-g), 1.77 (tt,  $^3J$  = 6.6 Hz, 4H, *H*-h), 1.44 (tt,  $^3J$  = 7.0 Hz, 4H, *H*-i), 1.35-1.27 (m, 20H, *H*-j, *H*-k, *H*-l, *H*-m, *H*-n), 0.88 (t,  $^3J$  = 7.0 Hz, 6H, *H*-o) ppm.

$^{13}C\{^1H\}$  NMR (151 MHz,  $CDCl_3$ )  $\delta$  = 158.26 (*C*-d), 142.87 (*C*-b), 133.23 (*C*-c), 116.90 (*C*-f), 116.15 (*C*-e), 113.63 (*C*-a), 68.51 (*C*-g), 32.02 (*C*-j, *C*-k, *C*-l, *C*-m, *C*-n), 29.66 (*C*-j, *C*-k, *C*-l, *C*-m, *C*-n), 29.52 (*C*-j, *C*-k, *C*-l, *C*-m, *C*-n), 29.39/29.31 (*C*-h), 26.13 (*C*-i), 22.82 (*C*-j, *C*-k, *C*-l, *C*-m, *C*-n), 14.26 (*C*-o) ppm.

IR (ATR):  $\tilde{\nu}$  = 3069.44 (w), 2917.54 (s), 2867.82 (w), 2852.57 (m), 1898.88 (w), 1578.16 (m), 1546.81 (w), 1484.15 (w), 1467.65 (s), 1408.74 (m), 1392.31 (w), 1328.40 (m), 1289.48 (m), 1257.83 (w), 1232.37 (s),

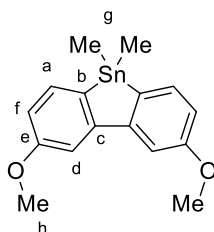
1199.11 (s), 1138.37 (m), 1125.90 (w), 1091.98 (w), 1056.70 (w), 1037.41 (m), 1012.80 (s), 974.47 (m), 939.80 (w), 905.31 (w), 875.00 (w), 851.74 (m), 834.34 (s), 822.31 (s), 776.84 (m), 746.46 (w), 719.70 (m), 708.69 (m), 668.62 (m), 653.20 (s)  $\text{cm}^{-1}$ .

**HRMS** (EI, 70 eV)  $m/z$  (%):  $[\text{M}]^+$  calcd for  $[\text{C}_{30}\text{H}_{44}^{79}\text{Br}_2\text{O}_2]^+$  594.17026, found 594.17094 (100).

**Mp**: 48.4°C.

**R<sub>f</sub>**: 0.75 (*n*-hexane).

### 5.10 2,8-Dimethoxy-5,5-dimethyl-5H-dibenzo[b,d]stannole (**St7**)<sup>[7]</sup>



The procedure was adapted from I. Nagao and co-worker.<sup>[7]</sup>

A Schlenk tube (250 mL) was charged with **St3** (1.87 g, 5.00 mmol, 1.00 eq.) and THF (50 mL). A *n*-hexane solution of *n*-BuLi (2.5 M, 4.20 mL, 10.5 mmol, 2.10 eq.) was added dropwise to the mixture at -78°C over the course of 5 min. The resulting solution was stirred for 1.5 h at -78°C before the addition of  $\text{Me}_2\text{SnCl}_2$  (1.00 g, 5.00 mmol, 1.00 eq.) in THF (10 mL) at -78°C. The mixture was allowed to warm to 20°C over 12 h. The organic solvents were removed by rotary evaporation. The residue was dissolved with *n*-hexane, filtered through a pad of celite, and concentrated *in vacuo*. The crude product was purified by crystallization from DCM / *n*-hexane at -20°C to obtain **St7** as a colorless solid (1.26 g, 3.50 mmol, 70% yield, Lit<sup>[7]</sup>: 48%).

**<sup>1</sup>H NMR** (600 MHz,  $\text{CDCl}_3$ )  $\delta$  = 7.56 (d,  $^3J$  = 7.8 Hz, 2H, *H*-a), 7.47 (d,  $^4J$  = 2.4 Hz, 2H, *H*-d), 6.88 (dd,  $^3J$  = 7.8 Hz,  $^4J$  = 2.4 Hz, 2H, *H*-f), 3.89 (s, 6H, *H*-h), 0.50 (s, 6H, *H*-g) ppm.

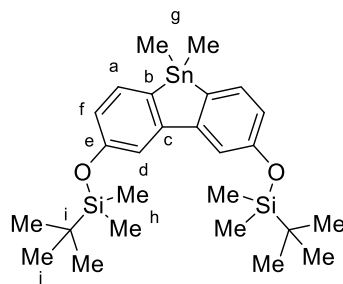
**<sup>13</sup>C{<sup>1</sup>H} NMR** (151 MHz,  $\text{CDCl}_3$ )  $\delta$  = 161.24 (*C*-e), 150.05 (*C*-c), 137.12 (*C*-g), 132.44 (*C*-d), 113.39 (*C*-b), 109.26 (*C*-a/f), 55.41 (*C*-h) ppm.

**<sup>119</sup>Sn NMR** (224 MHz,  $\text{CDCl}_3$ )  $\delta$  = -30.38 (s) ppm.

**IR** (ATR):  $\tilde{\nu}$  = 3000.57 (w), 2955.69 (w), 2932.67 (w), 2831.52 (w), 1582.22 (s), 1555.09 (s), 1472.06 (m), 1411.52 (m), 1300.31 (w), 1285.57 (s), 1258.00 (m), 1238.16 (w), 1220.66 (s), 1203.38 (s), 1176.24 (s), 1165.51 (m), 1056.11 (m), 1025.90 (s), 896.11 (m), 870.56 (w), 861.00 (m), 816.55 (m), 808.60 (s), 776.09 (m), 747.27 (m), 709.03 (m)  $\text{cm}^{-1}$ .

**HRMS** (EI, 70 eV)  $m/z$  (%):  $[\text{M}]^+$  calcd for  $[\text{C}_{16}\text{H}_{18}\text{O}_2^{120}\text{Sn}]^+$  362.03260, found 362.03298 (100).

**Mp**: 78°C.

5.11 ((5,5-Dimethyl-5H-dibenzo[b,d]stannole-2,8-diyl)bis(oxy))bis(*tert*-butyldimethylsilane) (**St8**)

The procedure was adapted from I. Nagao and co-worker.<sup>[7]</sup>

A Schlenk tube (250 mL) was charged with **St5** (2.86 g, 5.00 mmol, 1.00 eq.) and THF (50 mL). A *n*-hexane solution of *n*-BuLi (2.5 M, 4.20 mL, 10.5 mmol, 2.10 eq.) was added dropwise to the mixture at -78°C over the course of 5 min. The resulting solution was stirred for 1.5 h at -78°C before the addition of Me<sub>2</sub>SnCl<sub>2</sub> (1.00 g, 5.00 mmol, 1.00 eq.) in THF (10 mL) at -78°C. The mixture was allowed to warm to 20°C over 12 h. The organic solvents were removed by rotary evaporation. The residue was dissolved in *n*-hexane, filtered through a pad of celite, and concentrated *in vacuo*. The crude product was purified by crystallization from DCM/*n*-hexane at -20°C to obtain **St8** as a colorless solid (1.63 g, 2.90 mmol, 58% yield).

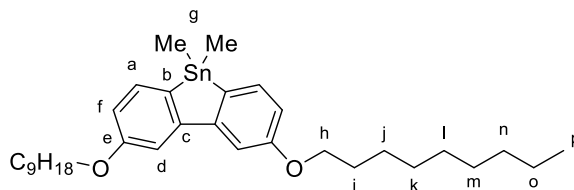
<sup>1</sup>H NMR (600 MHz, CDCl<sub>3</sub>) δ = 7.47 (d, <sup>3</sup>J = 7.6 Hz, 2H, *H*-a), 7.33 (d, <sup>4</sup>J = 2.2 Hz, 2H, *H*-d), 6.79 (dd, <sup>3</sup>J = 7.6 Hz, <sup>4</sup>J = 2.2 Hz, 2H, *H*-f), 1.02 (s, 18H, *H*-j), 0.49 (s, 6H, *H*-g), 0.26 (s, 12H, *H*-h) ppm.

<sup>13</sup>C{<sup>1</sup>H} NMR (151 MHz, CDCl<sub>3</sub>) δ = 157.25 (*C*q-e), 150.10 (*C*q-c), 137.04 (*C*-g), 132.98 (*C*-d), 119.78 (*C*-a/f), 114.70 (*C*q-b), 25.95 (*C*-j), 18.48 (*C*-i), -4.11 (*C*-h) ppm.

<sup>119</sup>Sn NMR (224 MHz, CDCl<sub>3</sub>) δ = -30.78 (s) ppm.

IR (ATR):  $\tilde{\nu}$  = 2951.24 (w), 2928.12 (m), 2855.94 (m), 1581.10 (m), 1546.88 (m), 1470.99 (m), 1400.15 (m), 1360.70 (w), 1290.38 (m), 1250.46 (m), 1222.22 (m), 1189.14 (m), 1059.68 (w), 1038.20 (w), 1010.22 (w), 974.37 (s), 939.18 (w), 905.27 (m), 875.34 (s), 835.72 (s), 776.76 (s), 700.55 (m), 668.80 (m) cm<sup>-1</sup>.

HRMS (EI, 70 eV) *m/z* (%): [M]<sup>+</sup> calcd for [C<sub>26</sub>H<sub>42</sub>O<sub>2</sub><sup>29</sup>Si<sub>2</sub><sup>120</sup>Sn]<sup>+</sup> 562.17435, found 562.17485 (100).

5.12 5,5-Dimethyl-2,8-bis(nonyloxy)-5H-dibenzo[b,d]stannole (**St9**)

The procedure was adapted from I. Nagao and co-worker.<sup>[7]</sup>

A Schlenk tube (250 mL) was charged with **St6** (2.98 g, 5.00 mmol, 1.00 eq.) and THF (50 mL). A *n*-hexane solution of *n*-BuLi (2.5 M, 4.20 mL, 10.5 mmol, 2.10 eq.) was added dropwise to the mixture at  $-78^{\circ}\text{C}$  over the course of 5 min. The resulting solution was stirred for 1.5 h at  $-78^{\circ}\text{C}$  before the addition of  $\text{Me}_2\text{SnCl}_2$  (1.00 g, 5.00 mmol, 1.00 eq.) in THF (10 mL) at  $-78^{\circ}\text{C}$ . The mixture was allowed to warm to  $20^{\circ}\text{C}$  over 12 h. The organic solvents were removed by rotary evaporation. The residue was dissolved with *n*-hexane, filtered through a pad of celite, and concentrated *in vacuo*. The crude product was purified by two times crystallization from DCM/*n*-hexane at  $-78^{\circ}\text{C}$  to obtain **St9** as a colorless liquid (2.49 g, 4.25 mmol, 85% yield).

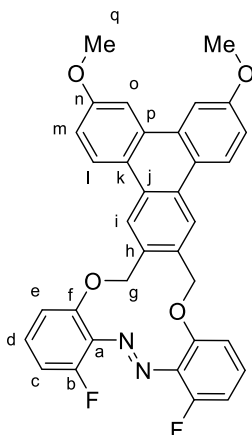
**$^1\text{H}$  NMR** (600 MHz,  $\text{CDCl}_3$ )  $\delta$  = 7.53 (d,  $^3J$  = 7.8 Hz, 2H, *H*-a), 7.46 (d,  $^4J$  = 2.3 Hz, 2H, *H*-d), 6.86 (dd,  $^3J$  = 7.8 Hz,  $^4J$  = 2.3 Hz, 2H, *H*-f), 4.03 (t,  $^3J$  = 6.6 Hz, 4H, *H*-h), 1.82 (tt,  $^3J$  = 6.6 Hz, 4H, *H*-i), 1.49 (tt,  $^3J$  = 7.2 Hz, 4H, *H*-o), 1.40-1.27 (m, 24H, *H*-j, *H*-k, *H*-l, *H*-m, *H*-n), 0.88 (t,  $^3J$  = 7.2 Hz, 6H, *H*-p), 0.49 (s, 4H, *H*-g) ppm.

**$^{13}\text{C}\{^1\text{H}\}$  NMR** (151 MHz,  $\text{CDCl}_3$ )  $\delta$  = 160.80 (*C*-e), 150.10 (*C*-c), 137.04 (*C*-g), 132.15 (*C*-d), 113.97 (*C*-b), 109.87 (*C*-a/f), 68.14 (*C*-h), 32.04 (*C*-k, *C*-l, *C*-m, *C*-n, *C*-o), 29.72 (*C*-k, *C*-l, *C*-m, *C*-n, *C*-o), 29.59 (*C*-k, *C*-l, *C*-m, *C*-n, *C*-o), 29.54/29.43 (*C*-i), 26.25 (*C*-k, *C*-l, *C*-m, *C*-n, *C*-o), 22.83 (*C*-j), 14.26 (*C*-p) ppm.

**$^{119}\text{Sn}$  NMR** (224 MHz,  $\text{CDCl}_3$ )  $\delta$  = -30.61 ppm.

**IR** (ATR):  $\tilde{\nu}$  = 2924.09 (s), 2853.58 (m), 1583.43 (s), 1553.63 (m), 1465.29 (m), 1389.03 (w), 1288.68 (s), 1250.27 (w), 1234.73 (w), 1216.61 (s), 1188.86 (s), 1038.39 (m), 1010.98 (w), 974.39 (m), 939.43 (w), 905.41 (w), 874.05 (m), 815.37 (m), 777.15 (s), 748.99 (m), 721.73 (m), 701.26 (m), 668.87 (w)  $\text{cm}^{-1}$ .

**HRMS** (EI, 70 eV)  $m/z$  (%):  $[\text{M}]^+$  calcd for  $[\text{C}_{32}\text{H}_{50}\text{O}_2^{120}\text{Sn}]^+$  586.28337, found 586.28439 (100).

5.13 (*E*)-4,7-Difluoro-16,19-dimethoxy-12,23-dihydrodibenzo[*b,f*]triphenylene[2,3-*j*][1,8]dioxo[4,5]diazacyclododecine (**FLOAM**)

The procedure was adapted from I. Nagao and co-worker.<sup>[7]</sup>

A Schlenk tube (80 mL) was charged with **F14** (266 mg, 0.500 mmol, 1.00 eq.), **St7** (199 mg, 0.550 mmol, 1.10 eq.), Pd(PtBu<sub>3</sub>)<sub>2</sub> (13.0 mg, 25.0 μmol), and THF (10 mL) in a glove box. The reaction mixture was taken outside the glove box and heated at 60°C for 12 h. The reaction mixture was filtered through a pad of celite. The filtrate was evaporated to dryness under reduced pressure, and the residue was purified by column chromatography (DCM : *n*-hexane 2:1) to obtain final compound (174 mg, 0.300 mmol, 60%) as a light yellow solid.

<sup>1</sup>H NMR (600 MHz, CDCl<sub>3</sub>) δ = 8.62 (d, <sup>3</sup>J = 9.0 Hz, 2H, *H*-l), 8.58 (s, 1H, *H*-i) 7.98 (d, <sup>4</sup>J = 2.6 Hz, 2H, *H*-o), 7.40 (dd, <sup>3</sup>J = 8.5 Hz, 5.8 Hz, 2H, *H*-d), 7.32 (d, <sup>3</sup>J = 8.5 Hz, 2H, *H*-e), 7.11-7.05 (m, 2H, *H*-m), 7.08 (d, <sup>3</sup>J = 8.5 Hz, 2H, *H*-c), 5.50 (s, 4H, *H*-g), 4.05 (s, 6H, *H*-q) ppm.

<sup>13</sup>C{<sup>1</sup>H} NMR (151 MHz, CDCl<sub>3</sub>) δ = 159.26 (*C*-o), 155.60 (d, <sup>1</sup>J = 259.6 Hz, *C*-b), 152.94 (*C*-f), 137.22 (d, <sup>2</sup>J = 8.2 Hz, *C*-a) 133.92 (*C*-k), 131.48 (*C*-j), 131.19 (d, <sup>3</sup>J = 10.4 Hz, *C*-d), 129.35 (*C*-p), 126.51 (*C*-i), 125.40 (*C*-l), 123.79 (*C*-n), 119.41 (d, <sup>4</sup>J = 3.2 Hz, *C*-e), 115.98 (*C*-m), 112.89 (d, <sup>2</sup>J = 20.0 Hz, *C*-c), 106.39 (*C*-h), 77.90 (*C*-g), 55.72 (*C*-q) ppm.

<sup>19</sup>F NMR (565 MHz, CDCl<sub>3</sub>) δ = -122.03 – -122.05 (m, *F*-b) ppm.

IR (ATR):  $\tilde{\nu}$  = 3007.58 (w), 2934.26 (w), 1604.24 (m), 1578.62 (m), 1539.48 (w), 1511.96 (w), 1499.71 (s), 1464.61 (s), 1409.38 (w), 1380.71 (m), 1367.56 (m), 1308.42 (w), 1266.68 (w), 1255.52 (w), 1238.14 (s), 1204.51 (m), 1178.91 (w), 1155.88 (w), 1114.96 (w), 1038.48 (s), 951.95 (m), 882.89 (s), 836.74 (m), 827.86 (m), 806.71 (w), 797.86 (w), 782.15 (m), 767.95 (w), 734.29 (s), 704.53 (w), 692.06 (w), 676.76 (w), 656.08 (w) cm<sup>-1</sup>.

HRMS (EI, 70 eV) *m/z* (%): [M]<sup>+</sup> calcd for [C<sub>34</sub>H<sub>24</sub>F<sub>2</sub>N<sub>2</sub>O<sub>4</sub>]<sup>+</sup> 562.16987, found 562.16951 (10), [C<sub>27</sub>H<sub>18</sub>FN<sub>2</sub>O<sub>3</sub>]<sup>3+</sup> 437.1 (100).

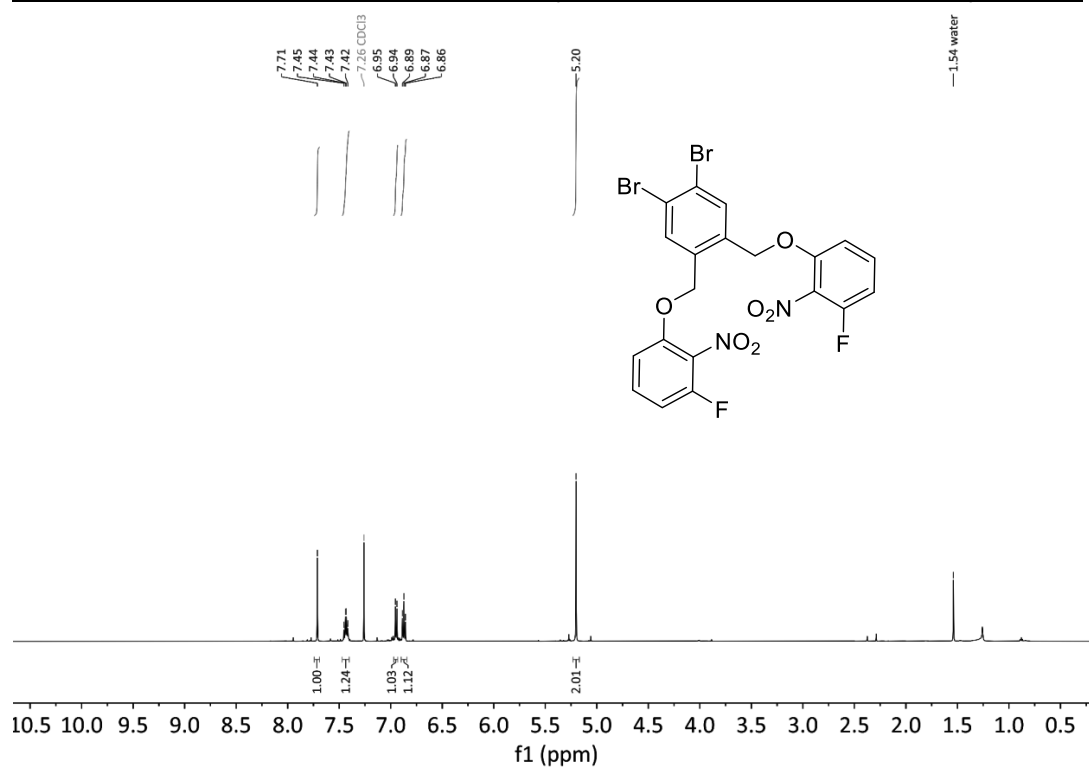
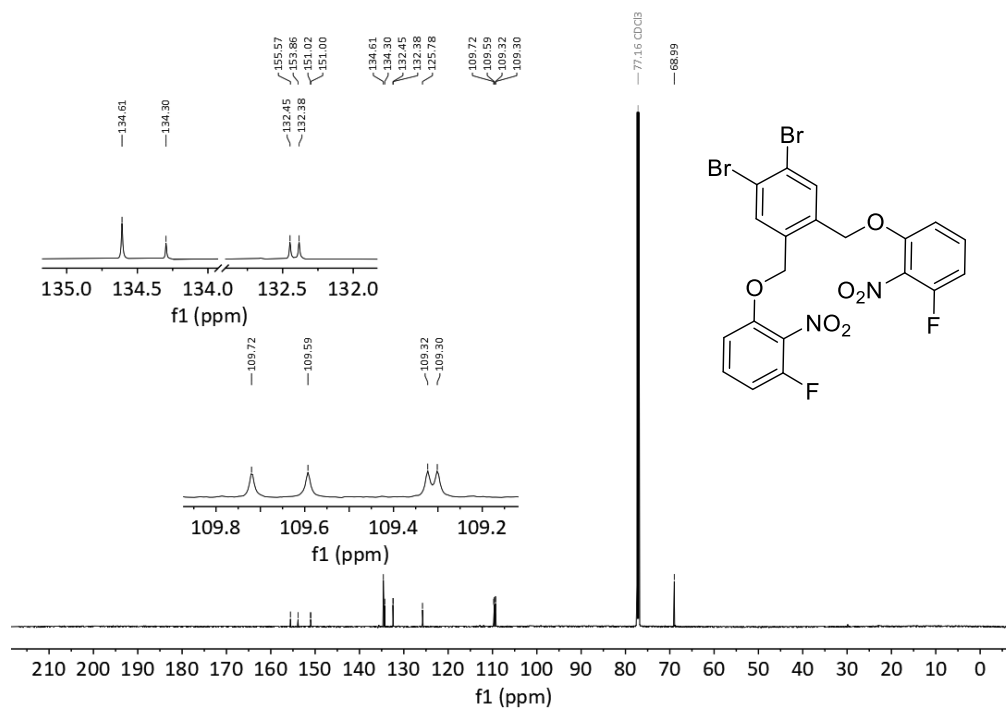
Mp: 264°C.

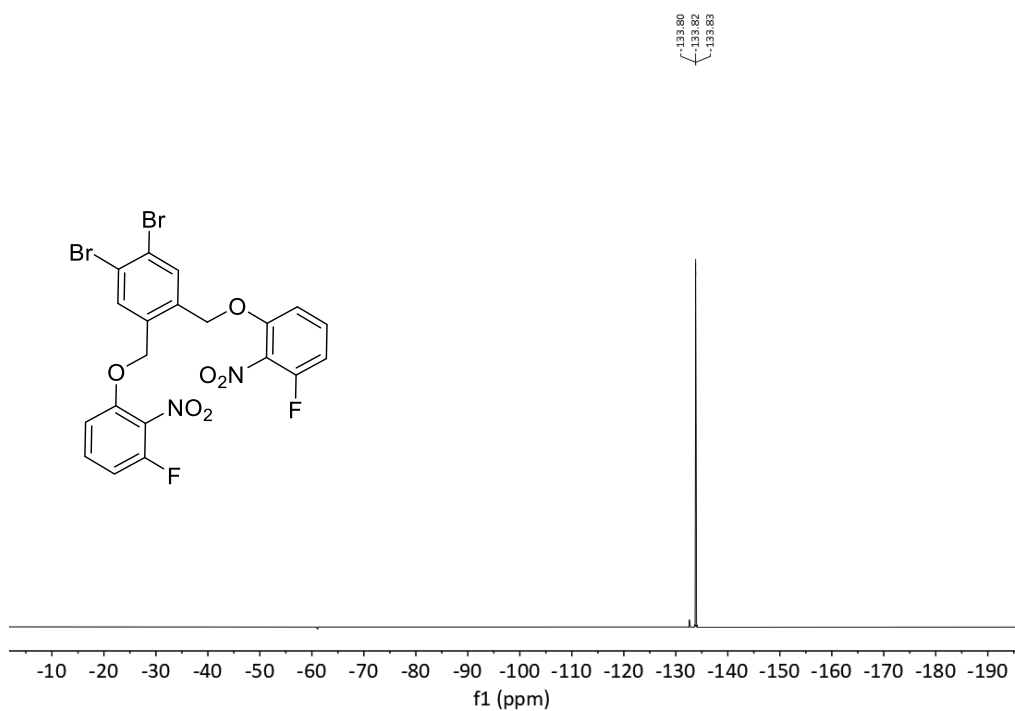
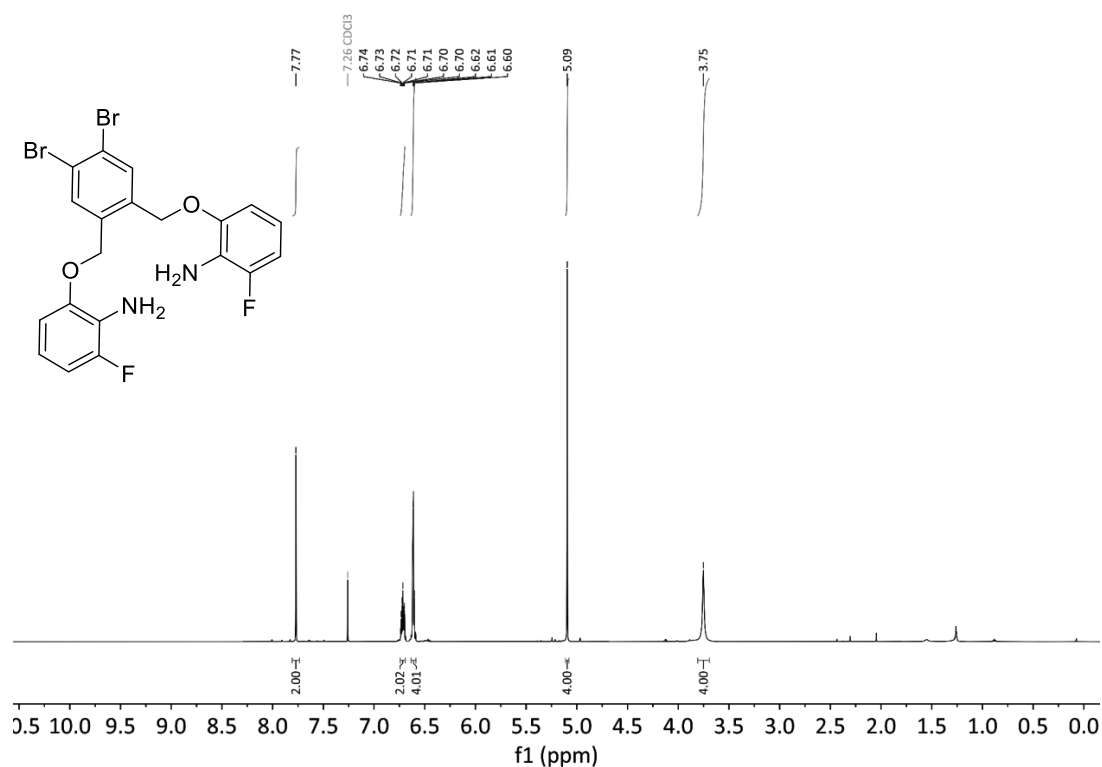
R<sub>f</sub>: 0.30 (DCM).

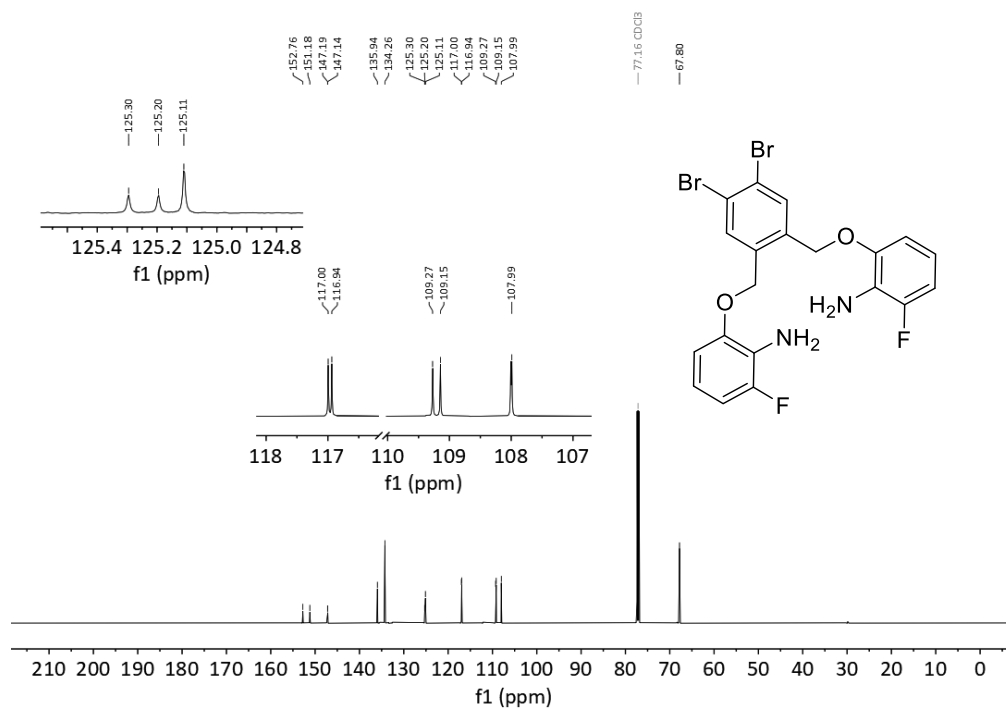
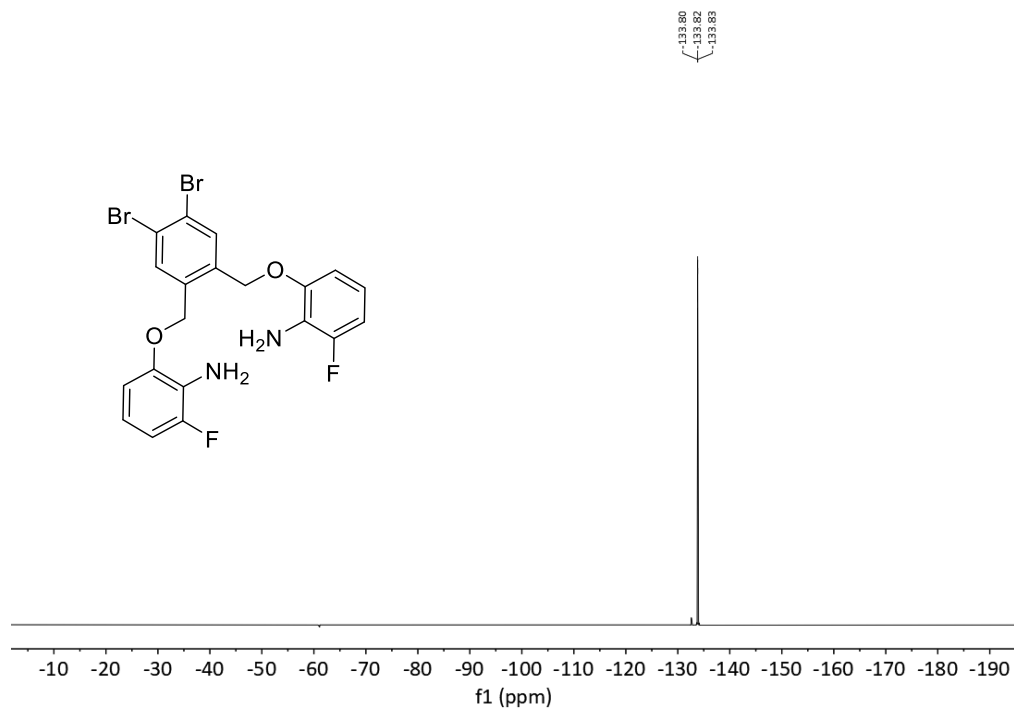


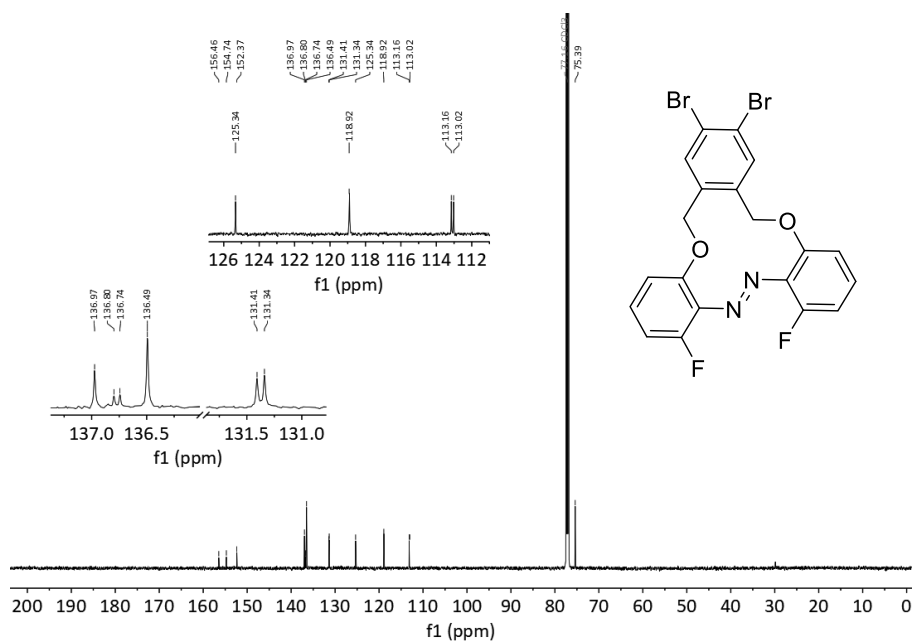
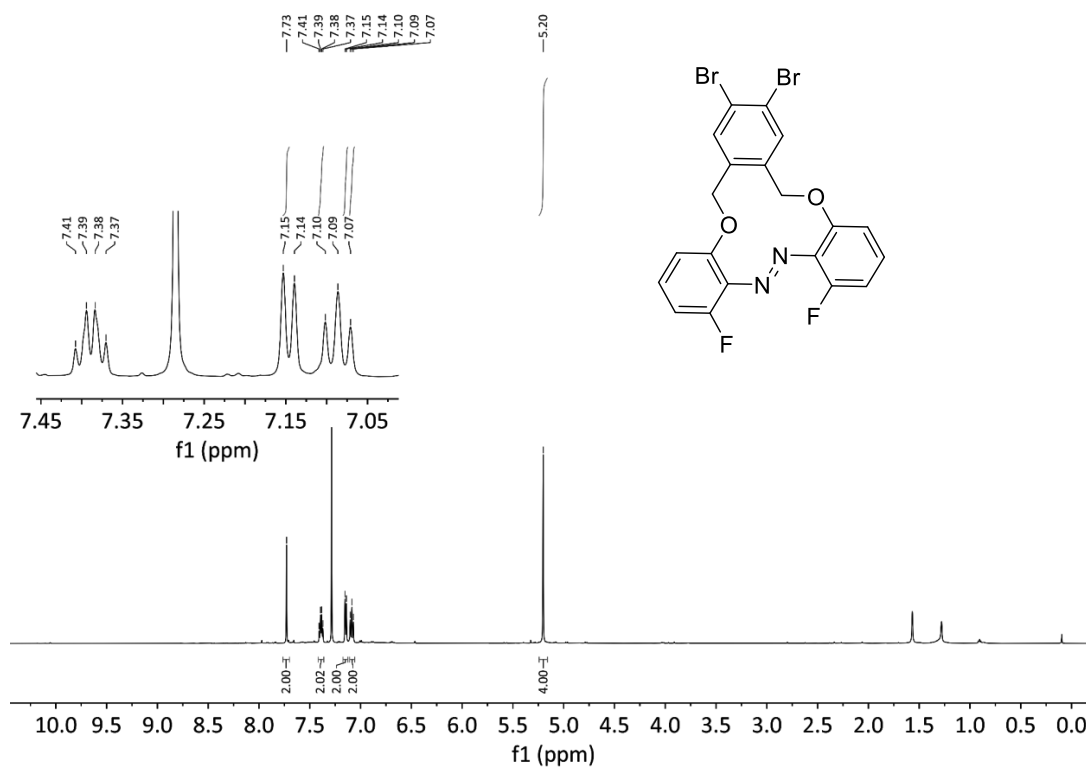
## 5 References

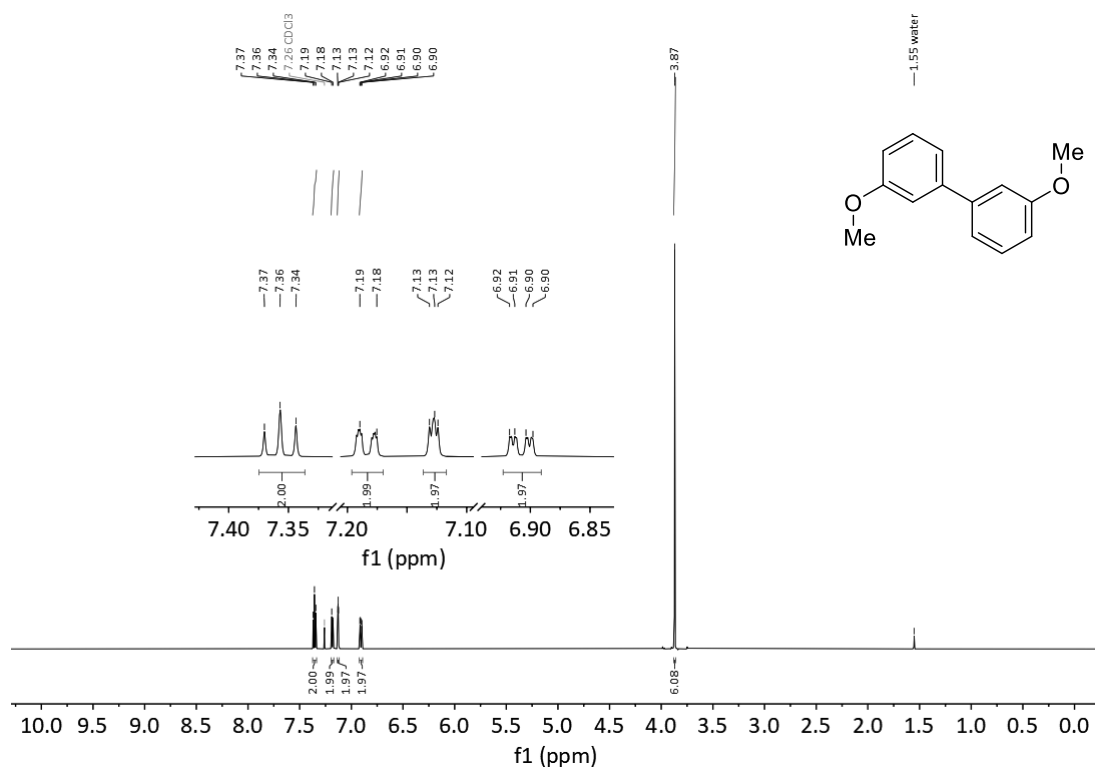
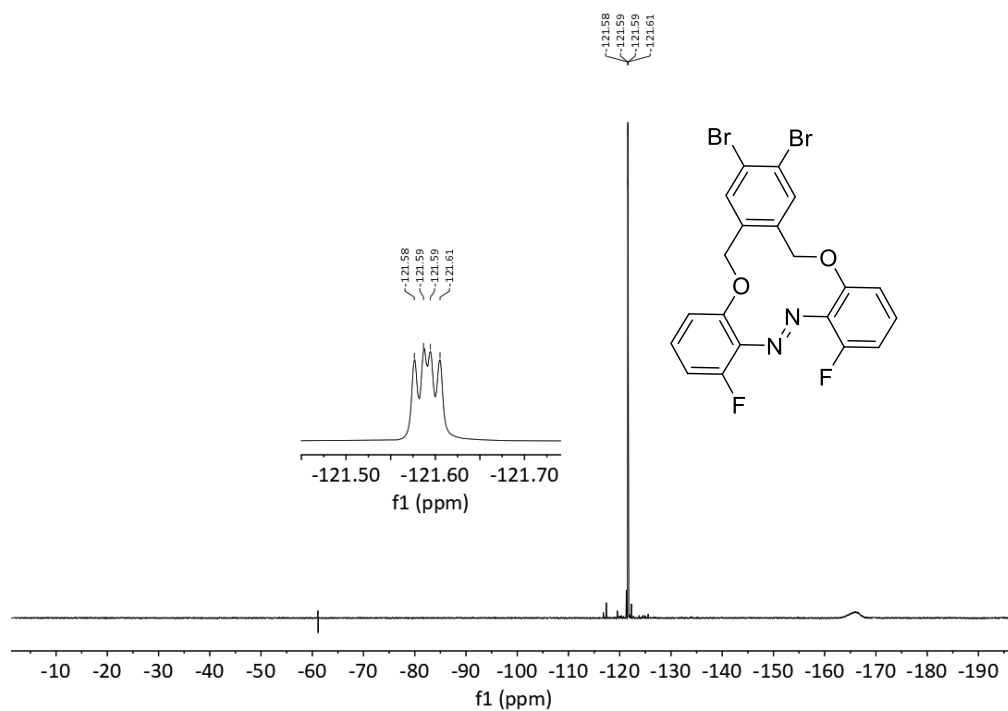
- [1] J. Bahrenburg, C. M. Sievers, J. B. Schönborn, B. Hartke, F. Renth, F. Temps, C. Näther, F. D. Sönnichsen, *Photochemical and Photobiological Sciences* **2013**, 12, 511.
- [2] O. V. Dolomanov, Bourhis, L. J., Gildea, R. J., Howard, J. A. K., Puschmann, H., *J. Appl. Crystallogr.* **2009**, 42.
- [3] *The ACS Style Guide: Effective Communication of Scientific Information*, American Chemical Society, Washington, DC **2006**.
- [4] M. Kimura, H. Narikawa, K. Ohta, K. Hanabusa, H. Shirai, N. Kobayashi, *Chemistry of Materials* **2002**, 14, 2711.
- [5] D. D. Hennings, T. Iwama, V. H. Rawal, *Organic Letters* **1999**, 1, 1205.
- [6] E. Brüllingen, J.-M. Neudörfl, B. Goldfuss, *New Journal of Chemistry* **2019**, 43, 15743.
- [7] I. Nagao, M. Shimizu, T. Hiyama, *Angewandte Chemie International Edition* **2009**, 48, 7573.

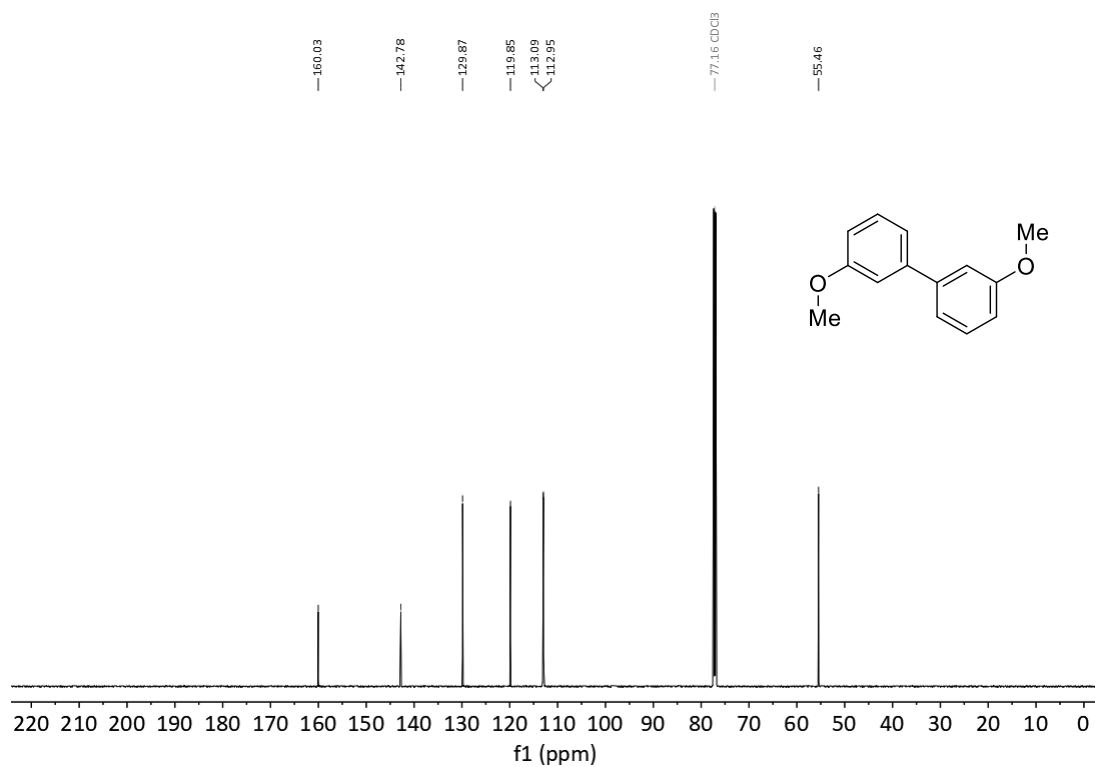
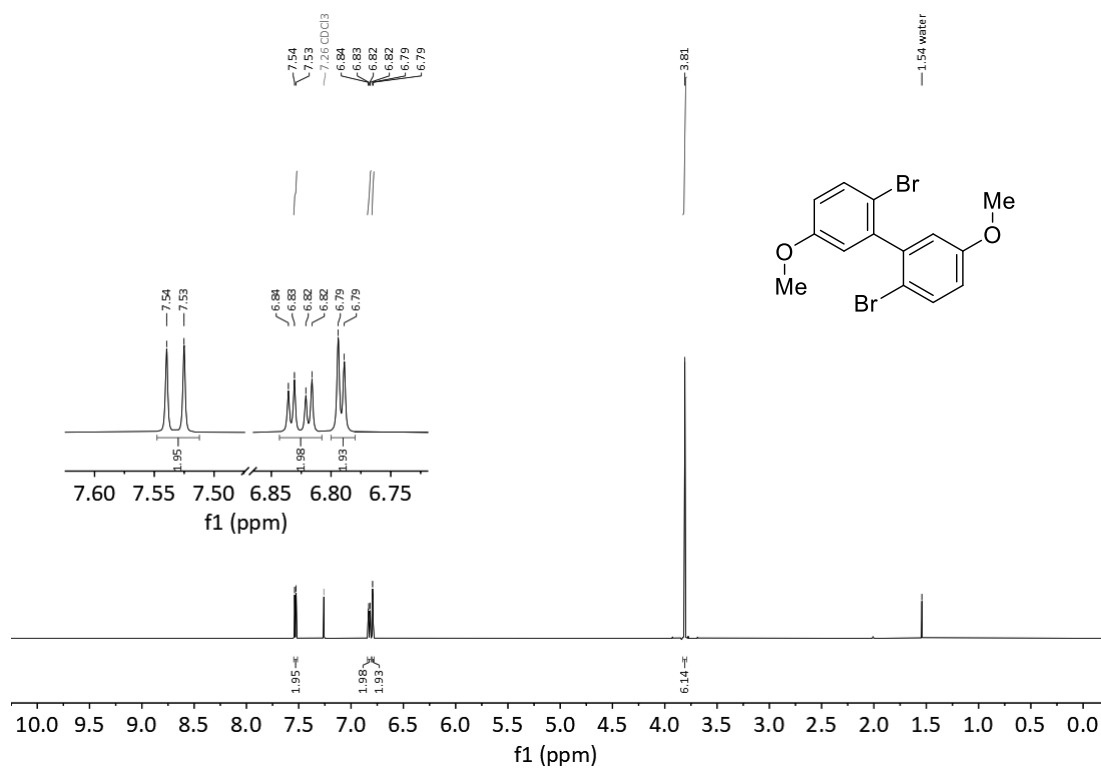
4.  $^1\text{H}$ ,  $^{13}\text{C}\{^1\text{H}\}$ ,  $^{119}\text{Sn}$  and  $^{19}\text{F}$  NMR Spectra of the Purified CompoundsFigure 8  $^1\text{H}$  NMR spectrum of FI2 in  $\text{CDCl}_3$ .Figure 9  $^{13}\text{C}\{^1\text{H}\}$  NMR spectrum of FI2 in  $\text{CDCl}_3$ .

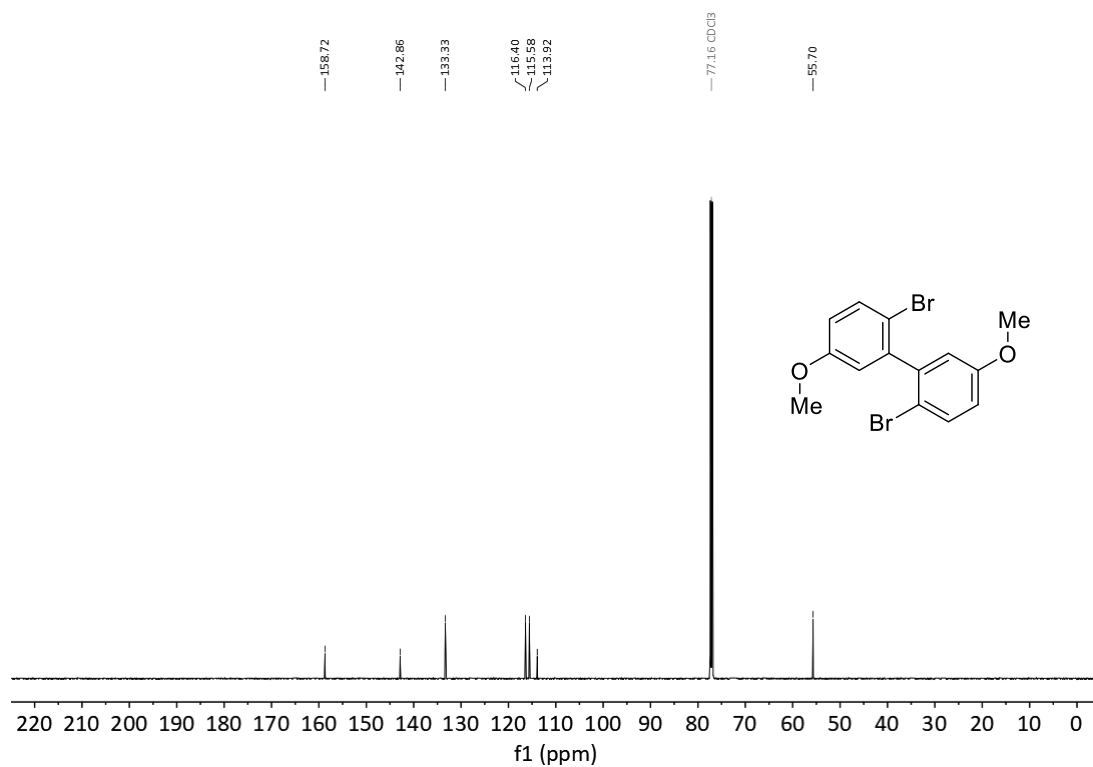
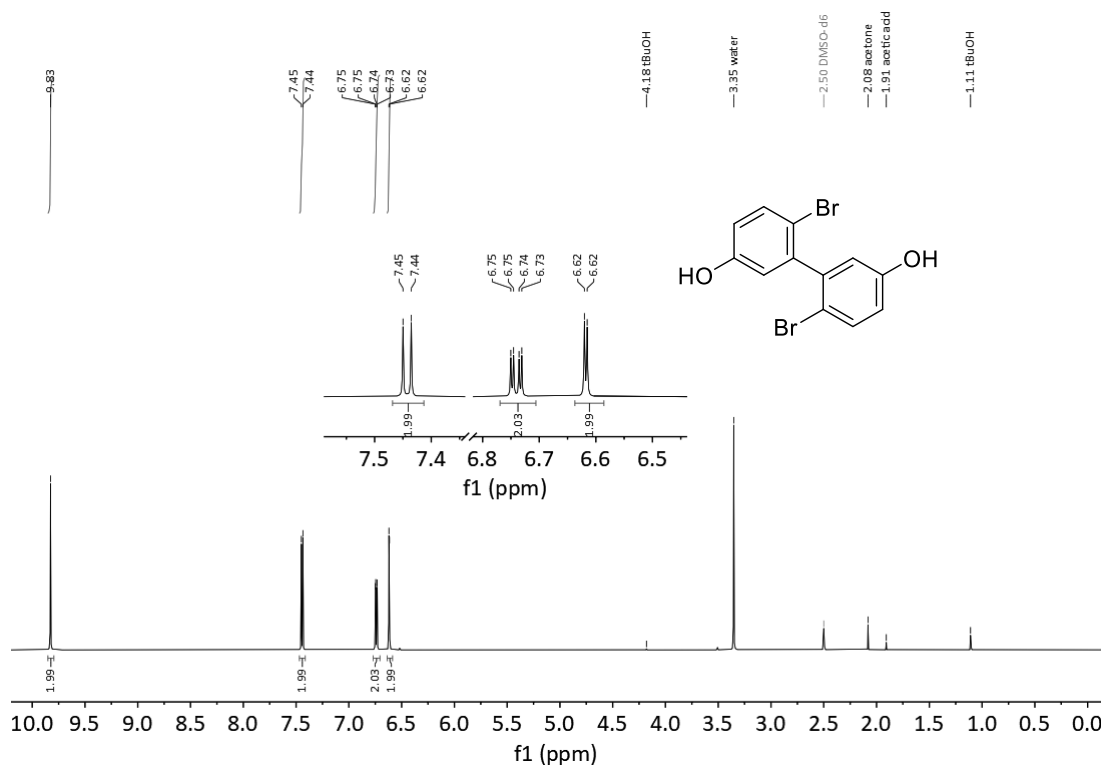
Figure 10  $^{19}\text{F}$  NMR spectrum of F12 in  $\text{CDCl}_3$ .Figure 11  $^1\text{H}$  NMR spectrum of F13 in  $\text{CDCl}_3$ .

Figure 12  $^{13}\text{C}\{^1\text{H}\}$  NMR spectrum of **F13** in  $\text{CDCl}_3$ .Figure 13  $^{19}\text{F}$  NMR spectrum of **F13** in  $\text{CDCl}_3$ .

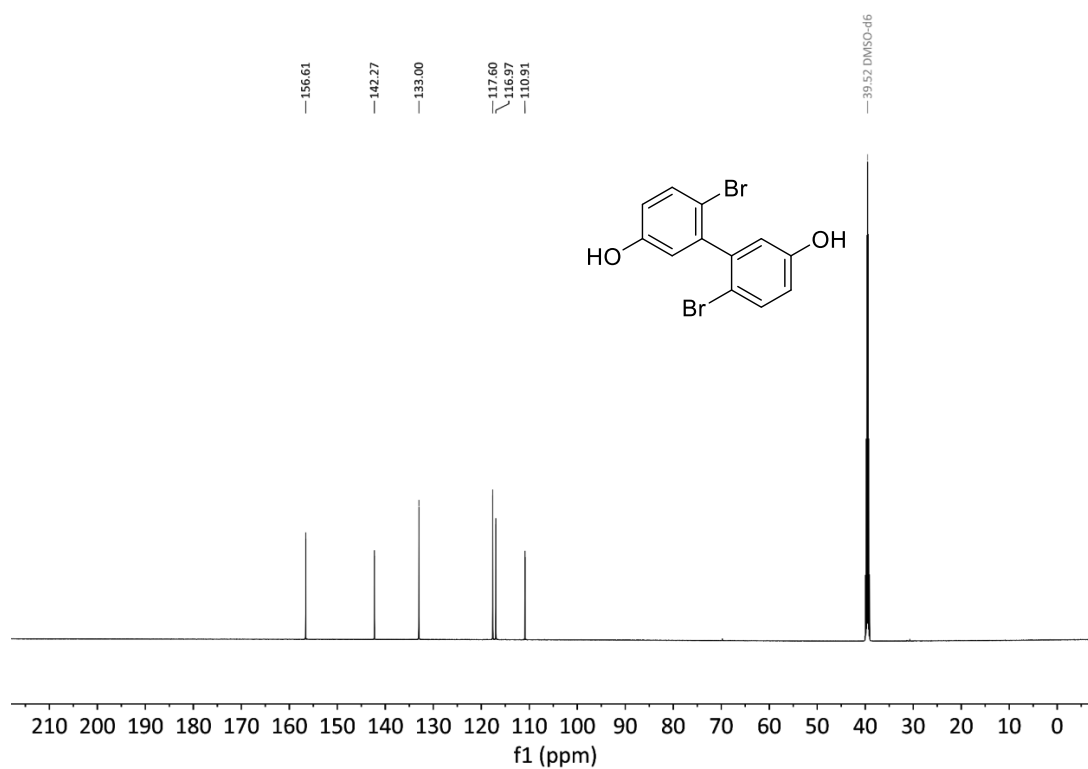
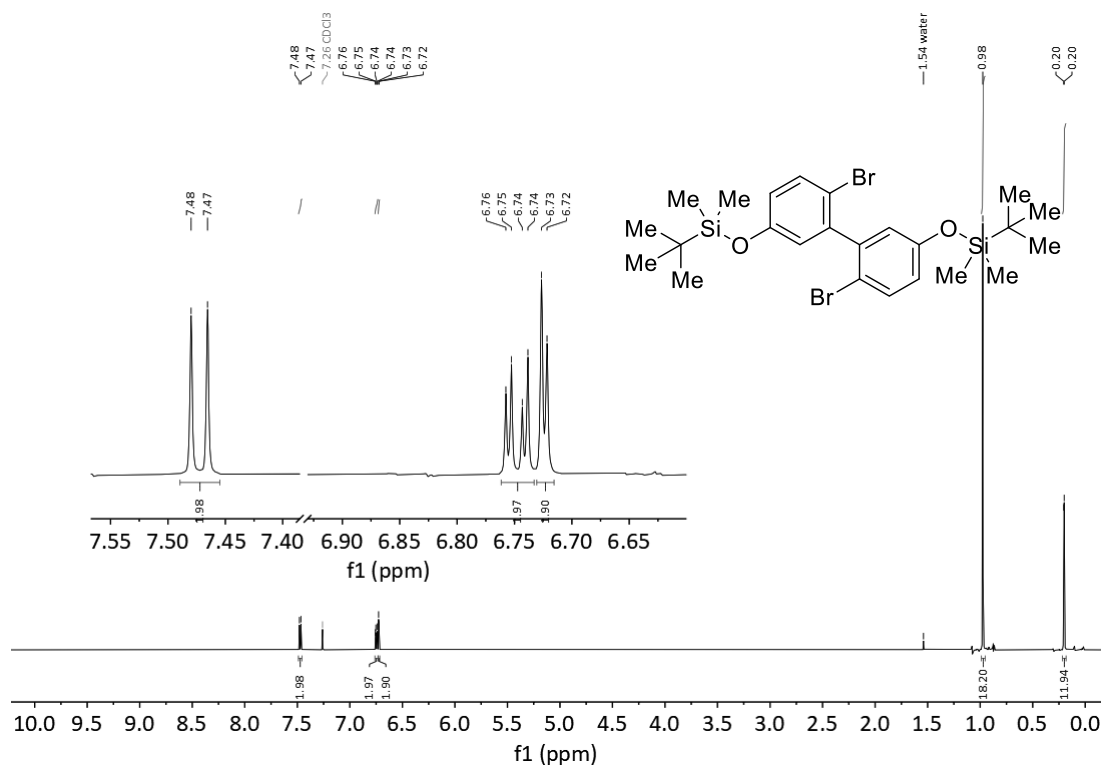


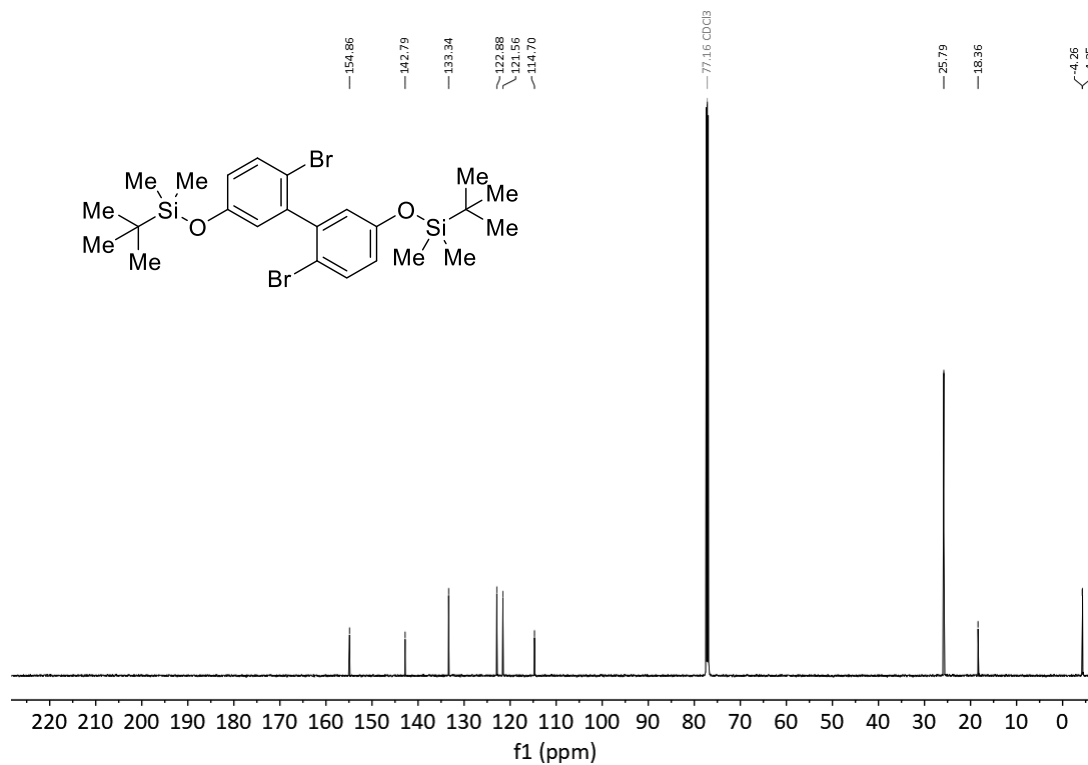
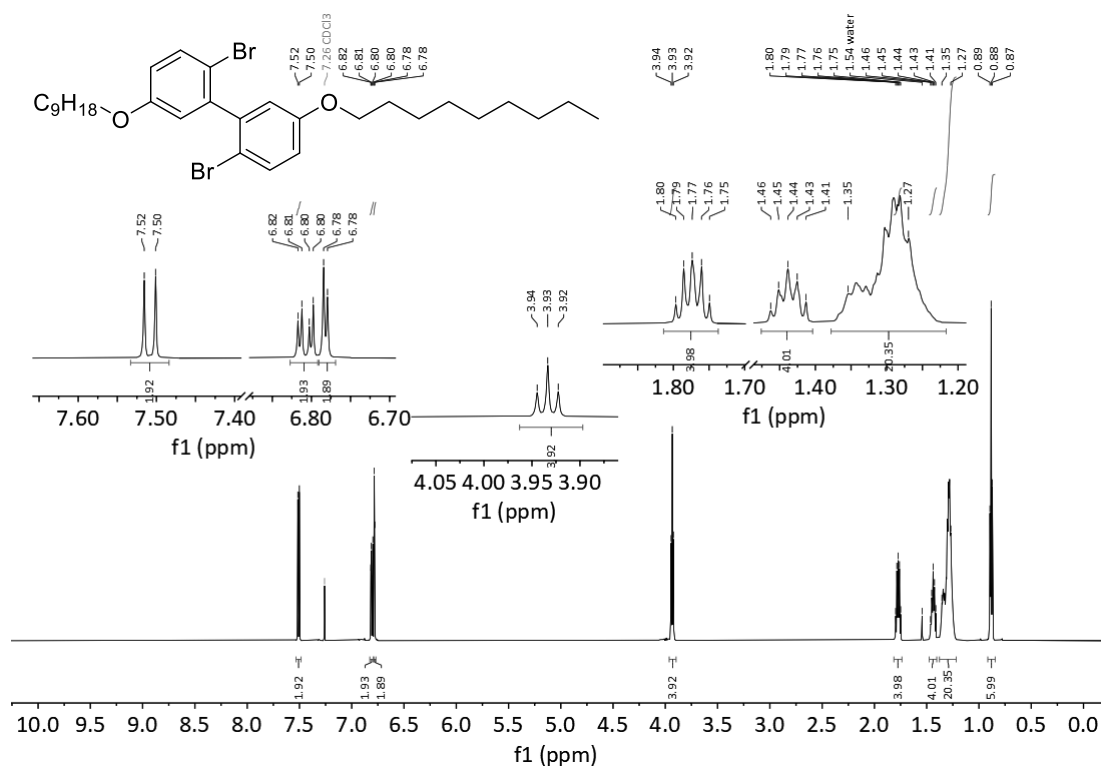


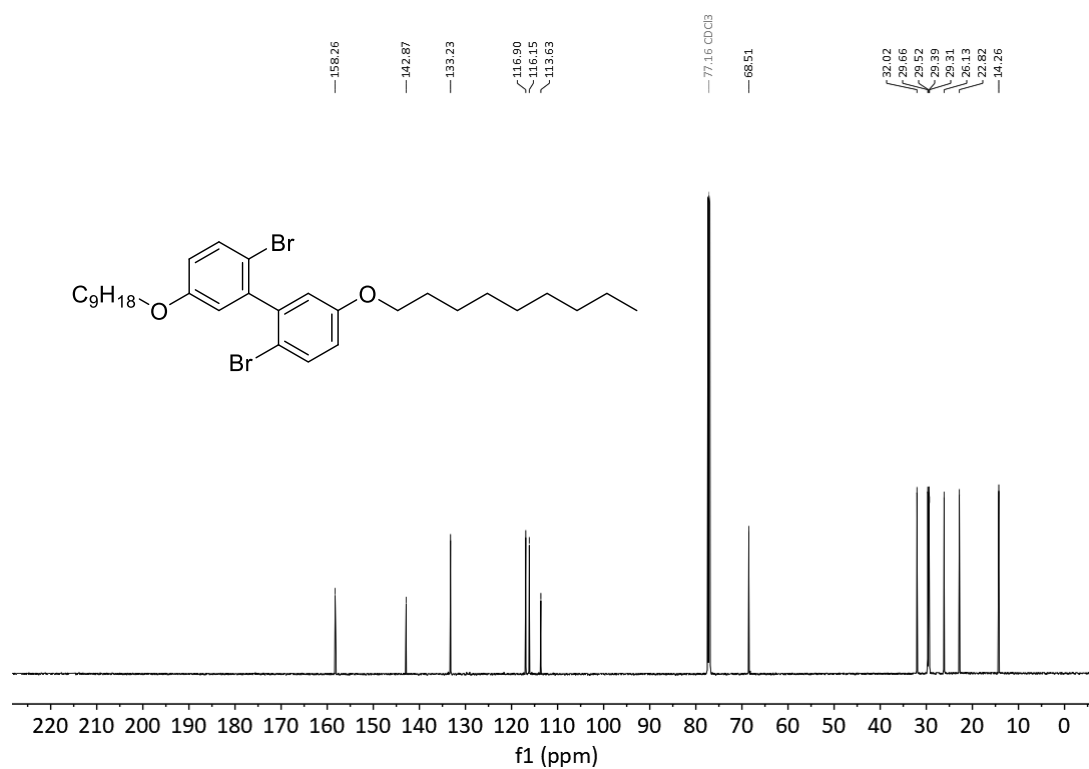
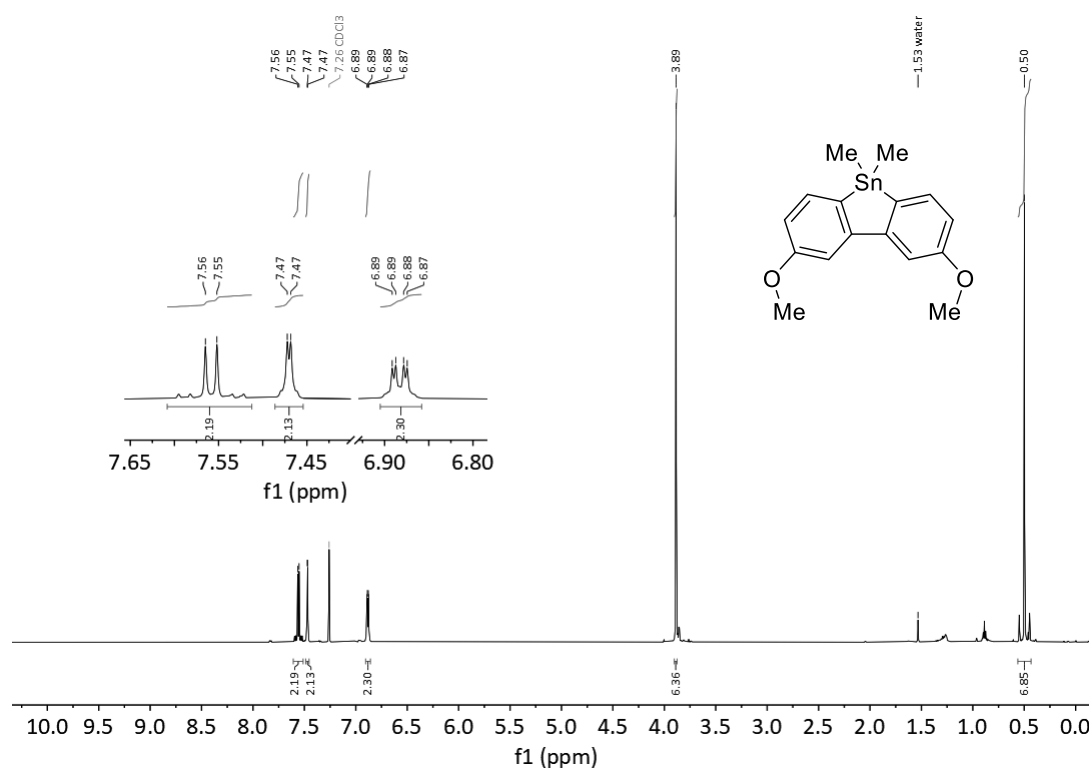
Figure 18  $^{13}\text{C}\{^1\text{H}\}$  NMR spectrum of **St2** in CDCl<sub>3</sub>.Figure 19  $^1\text{H}$  NMR spectrum of **St3** in CDCl<sub>3</sub>.

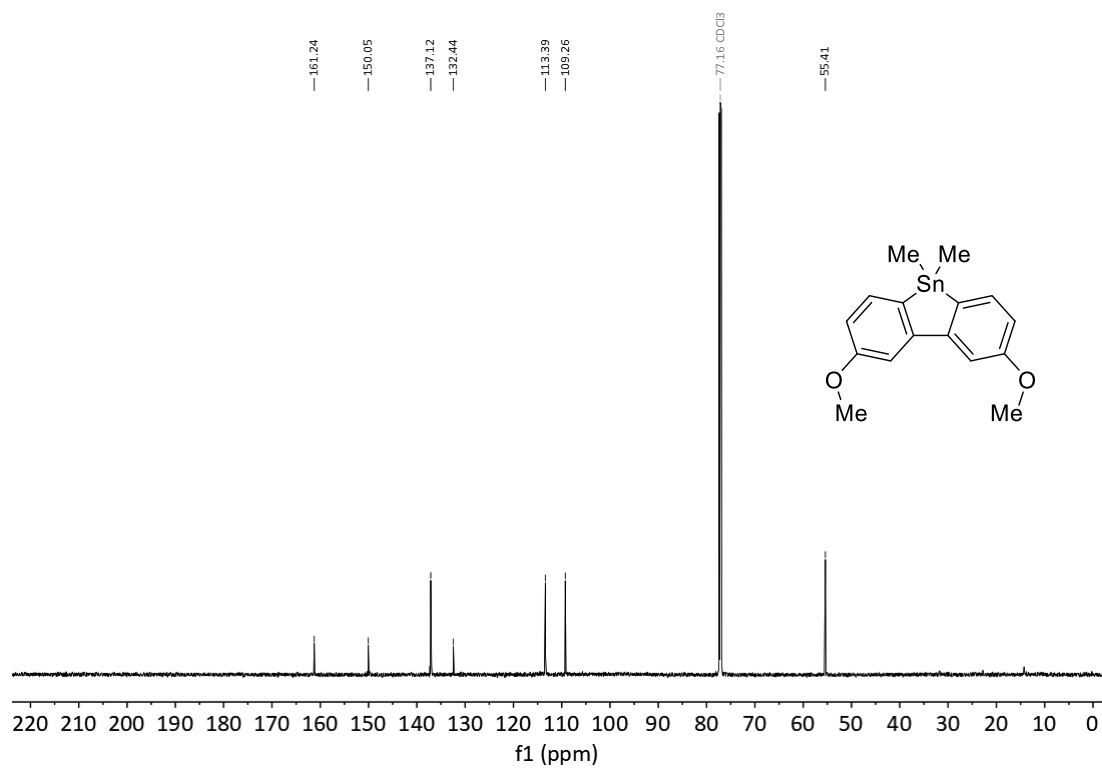
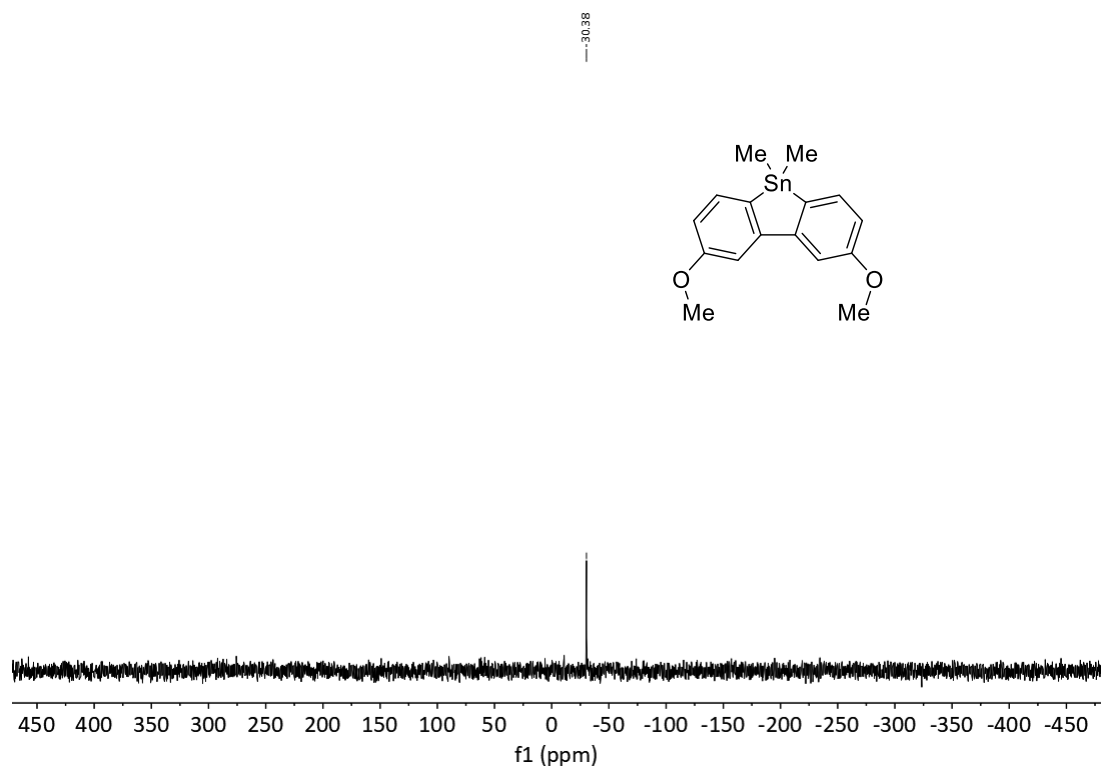
Figure 20  $^{13}\text{C}\{^1\text{H}\}$  NMR spectrum of **St3** in  $\text{CDCl}_3$ .Figure 21  $^1\text{H}$  NMR spectrum of **St4** in  $\text{DMSO-d}_6$ .

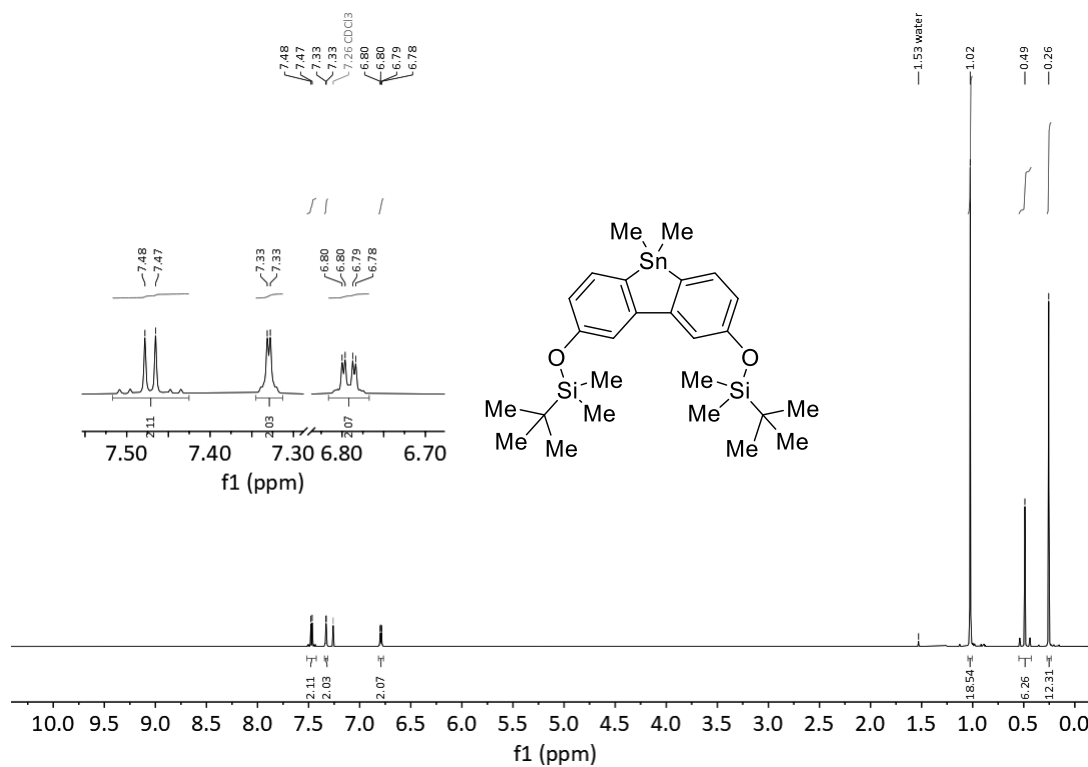


Figure 22  $^{13}\text{C}\{^1\text{H}\}$  NMR spectrum of **St3** in DMSO-d<sub>6</sub>.Figure 23  $^1\text{H}$  NMR spectrum of **St5** in CDCl<sub>3</sub>.

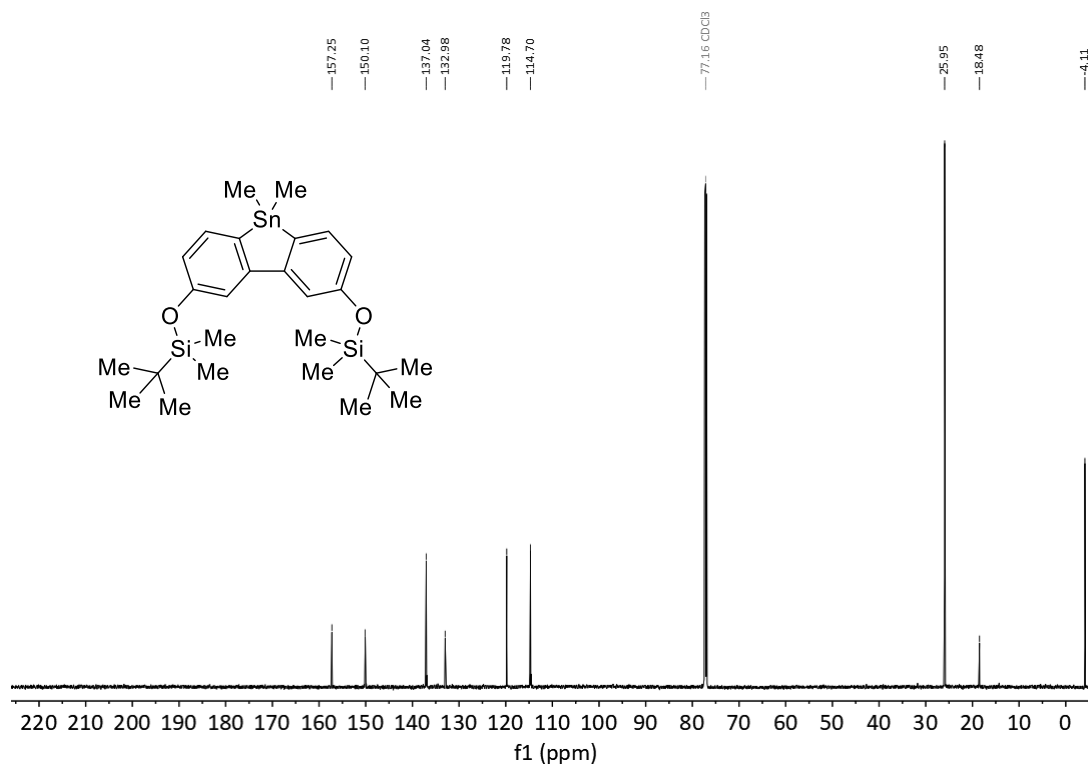
Figure 24  $^{13}\text{C}\{^1\text{H}\}$  NMR spectrum of **St5** in  $\text{CDCl}_3$ .Figure 25  $^1\text{H}$  NMR spectrum of **St6** in  $\text{CDCl}_3$ .

Figure 26  $^{13}\text{C}\{^1\text{H}\}$  NMR spectrum of **St6** in  $\text{CDCl}_3$ .Figure 27  $^1\text{H}$  NMR spectrum of **St7** in  $\text{CDCl}_3$ .

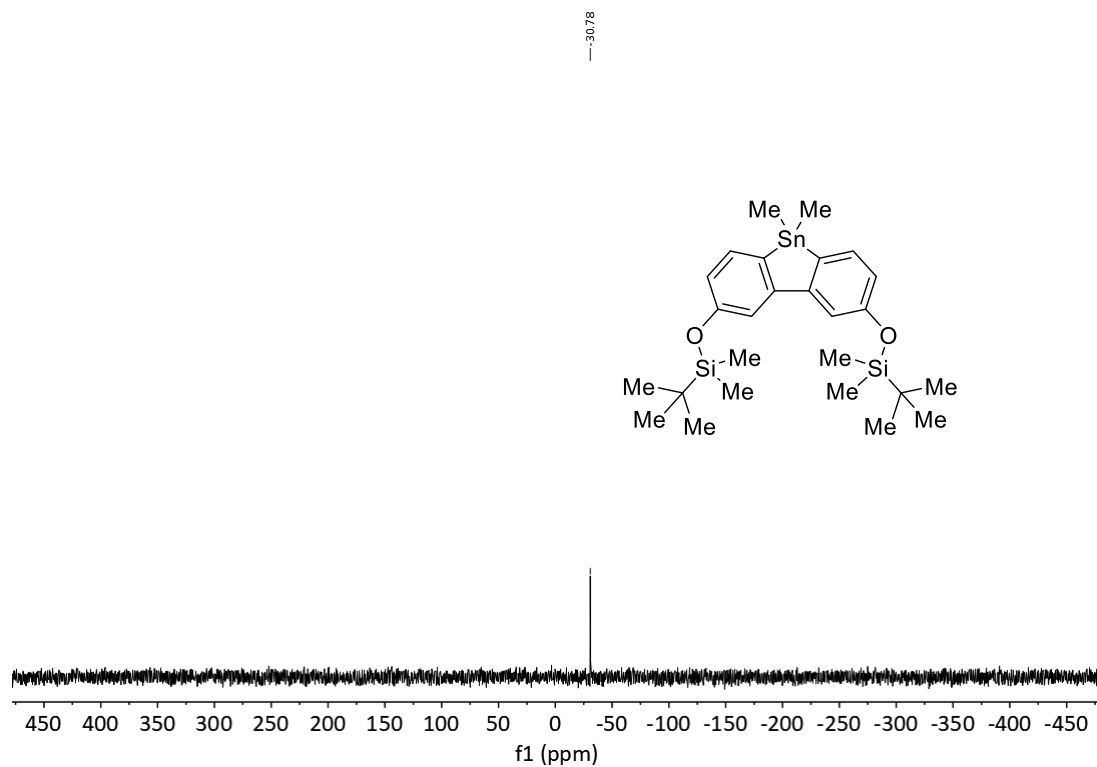
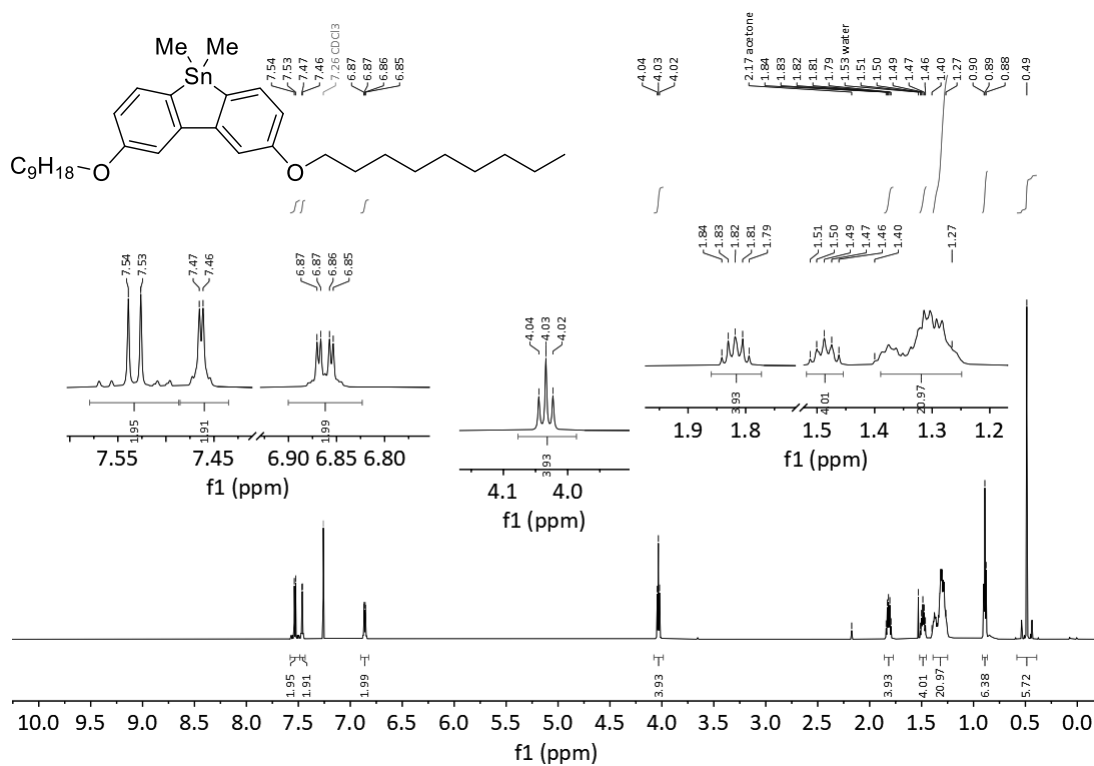
Figure 28  $^{13}\text{C}\{^1\text{H}\}$  NMR spectrum of **St7** in  $\text{CDCl}_3$ .Figure 29  $^{119}\text{Sn}$  NMR spectrum of **St7** in  $\text{CDCl}_3$ .

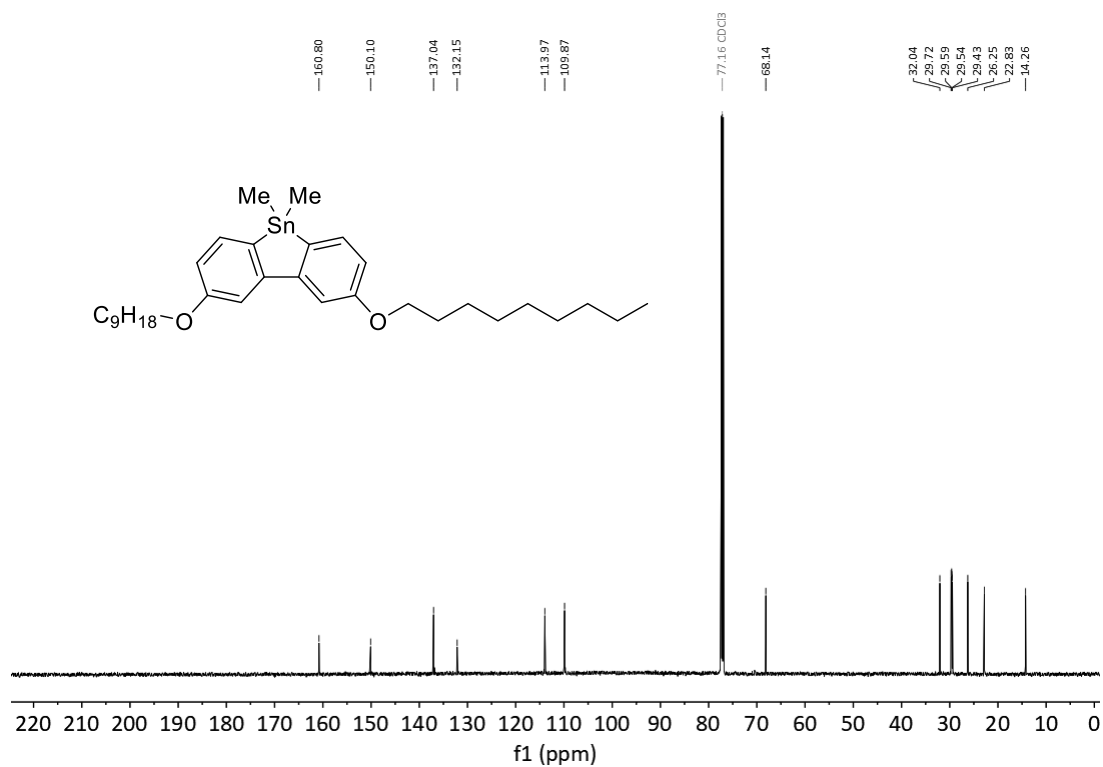
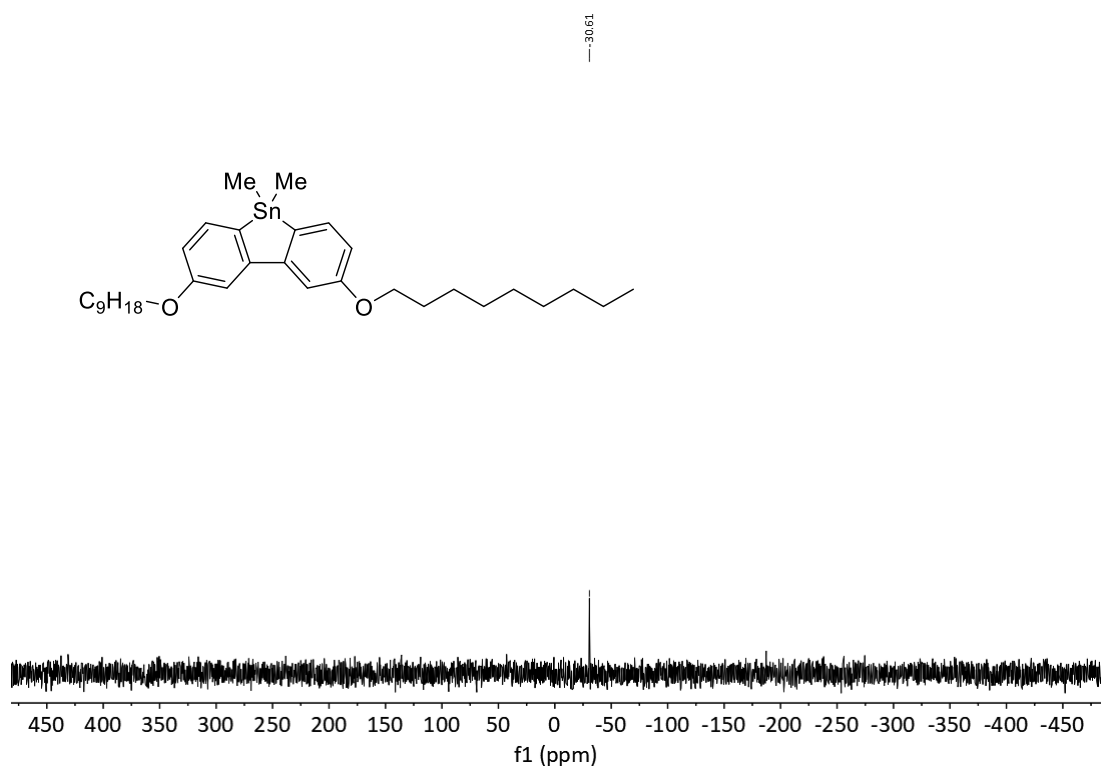


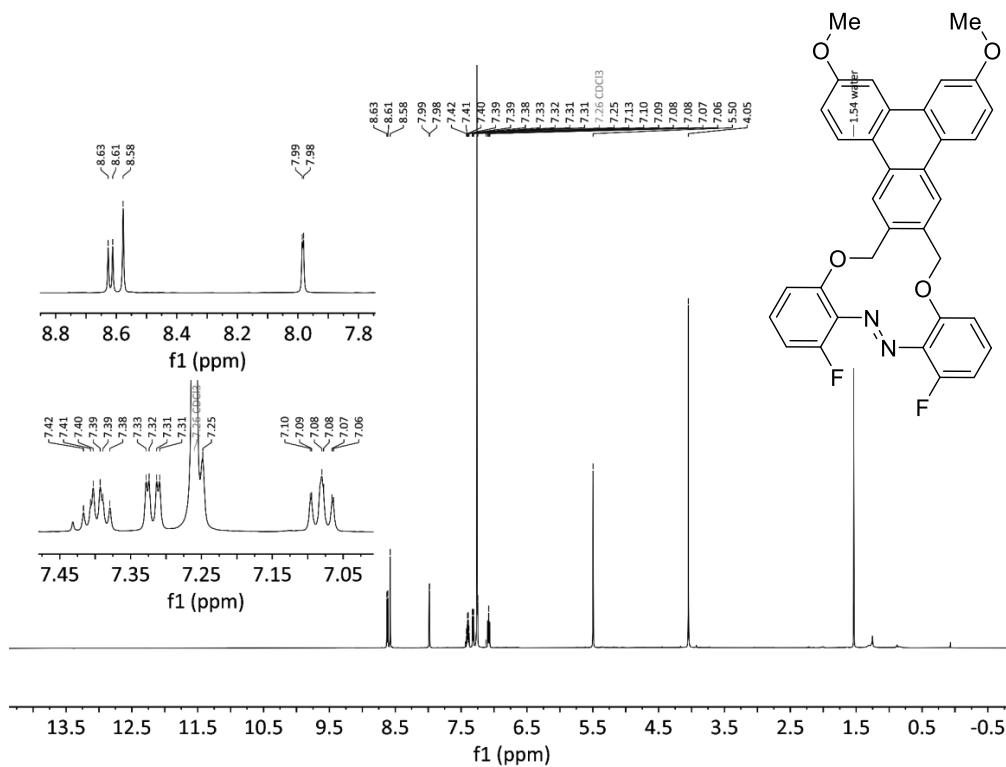
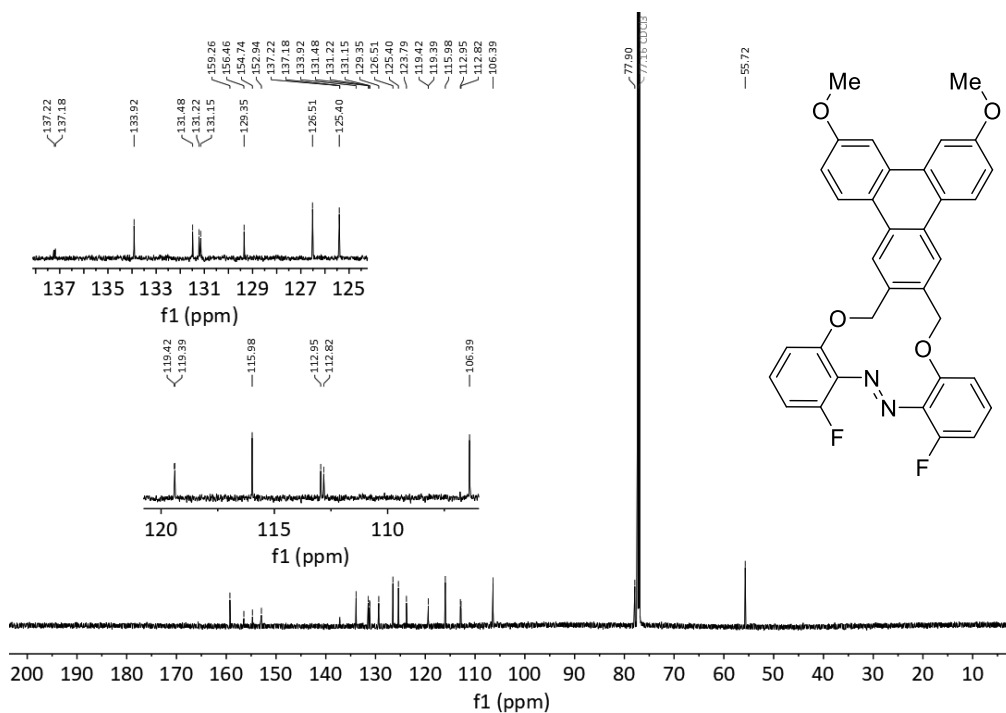
**Figure 30**  $^1\text{H}$  NMR spectrum of **St8** in  $\text{CDCl}_3$ .



**Figure 31**  $^{13}\text{C}\{^1\text{H}\}$  NMR spectrum of **St8** in  $\text{CDCl}_3$ .

Figure 32  $^{119}\text{Sn}$  NMR spectrum of **St8** in  $\text{CDCl}_3$ .Figure 33  $^1\text{H}$  NMR spectrum of **St9** in  $\text{CDCl}_3$ .

Figure 34  $^{13}\text{C}\{^1\text{H}\}$  NMR spectrum of **St9** in  $\text{CDCl}_3$ .Figure 35  $^{119}\text{Sn}$  NMR spectrum of **St9** in  $\text{CDCl}_3$ .

Figure 36  $^1\text{H}$  NMR spectrum of FLOAM in  $\text{CDCl}_3$ .Figure 37  $^{13}\text{C}\{^1\text{H}\}$  NMR spectrum of FLOAM in  $\text{CDCl}_3$ .



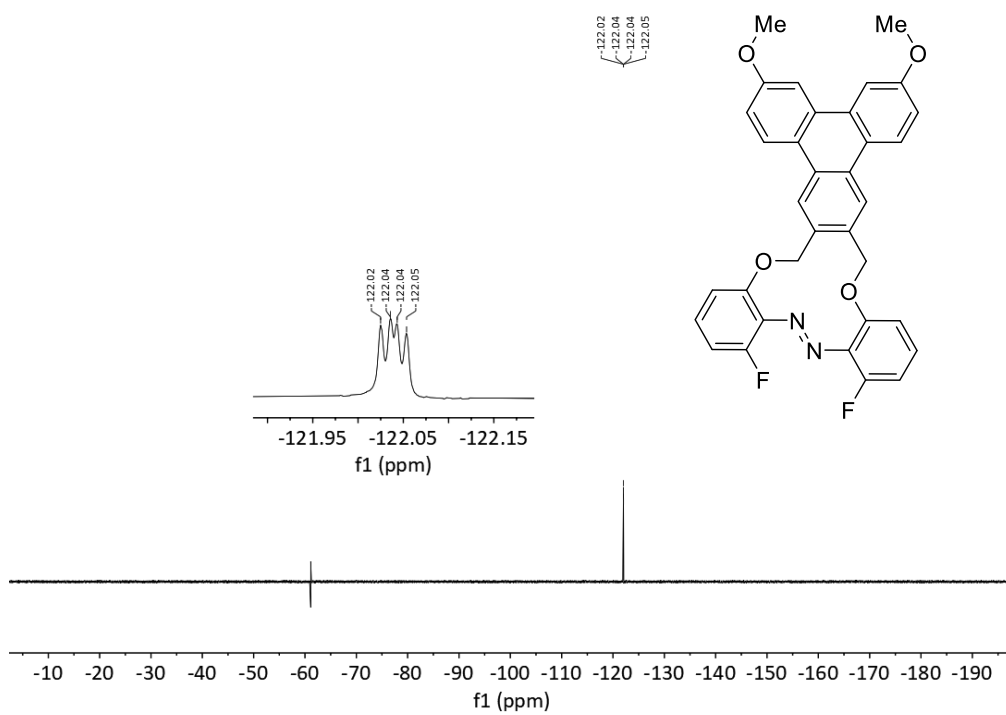


Figure 38  $^{19}\text{F}$  NMR spectrum of FLOAM in  $\text{CDCl}_3$ .

**Table S4** Crystal data and structure refinement of X-ray data for *E*- and *Z*-FLOAM.

	<b>E-FLOAM</b>	<b>Z-FLOAM</b>
Formula	C <sub>34</sub> H <sub>24</sub> F <sub>2</sub> N <sub>2</sub> O <sub>4</sub>	C <sub>34</sub> H <sub>24</sub> F <sub>2</sub> N <sub>2</sub> O <sub>4</sub>
Formula weight, g mol <sup>-1</sup>	562.55	562.55
Crystal system	monoclinic	triclinic
Crystal size, mm <sup>3</sup>	0.266 × 0.238 × 0.155	0.22 × 0.12 × 0.05
Space group	P2 <sub>1</sub> /c	P-1
a, Å	10.4687(5)	6.951(7)
b, Å	35.0333(19)	13.73(2)
c, Å	7.1437(5)	13.854(15)
α, °	90	104.14(5)
β, °	105.067(3)	97.82(4)
γ, °	90	90.90(5)
V, Å <sup>3</sup>	2529.9(3)	1269(3)
Z	4	2
Temperature, K	100.00	177.00
ρ <sub>calc</sub> , g cm <sup>-3</sup>	1.477	1.473
μ (Mo Kα), mm <sup>-1</sup>	0.107	0.107
F(000)	1168.0	584.0
2θ range for data collection, deg	5.33 to 61.098	5.924 to 54.272
Index ranges	-14 ≤ h ≤ 14 -50 ≤ k ≤ 50 -10 ≤ l ≤ 10	-8 ≤ h ≤ 8 -17 ≤ k ≤ 17 -17 ≤ l ≤ 17
No. of reflns collected	69564	56287
No. indep. Reflns	7721 [R <sub>int</sub> = 0.0485, R <sub>sigma</sub> = 0.0255]	5602 [R <sub>int</sub> = 0.0875, R <sub>sigma</sub> = 0.0415]
Data/restraints/parameters	7721/0/381	5602/0/381
Goof (F <sup>2</sup> )	1.026	1.096
R <sub>1</sub> (F) and wR <sub>2</sub> (F <sup>2</sup> ) (I > 2σ(I) for X-ray),	R <sub>1</sub> = 0.0414, wR <sub>2</sub> = 0.1172	R <sub>1</sub> = 0.1044, wR <sub>2</sub> = 0.2805
R <sub>1</sub> (F) and wR <sub>2</sub> (F <sup>2</sup> ) (all data)	R <sub>1</sub> = 0.0459, wR <sub>2</sub> = 0.1217	R <sub>1</sub> = 0.1117, wR <sub>2</sub> = 0.2847
Largest diff peak/hole, e Å <sup>-3</sup>	0.48/-0.23	0.84/-0.48
CCDC number		

# 9.6 Appendix Permissions to Reprint

**Publication I**

This article was published open access distributed under the terms of the Creative Commons CC BY license, which permits unrestricted use, distribution, and reproduction in any medium, provided the original work is properly cited (<https://creativecommons.org/licenses/by/4.0/>). The manuscript and the supporting information including detailed experimental procedures, characterization data and copies of NMR spectra are available free of charge on the journal's website.

**Publication II**

All articles published by MDPI are made immediately available worldwide under an open access license. No special permission is required to reuse all or part of the article published by MDPI, including figures and tables. For articles published under an open access Creative Common CC BY license, any part of the article may be reused without permission provided that the original article is clearly cited.

**Publication III**

This is an open access article distributed under the terms of the Creative Commons CC BY license, which permits unrestricted use, distribution, and reproduction in any medium, provided the original work is properly cited.

**Publication IV**

This article is available under the Creative Commons CC-BY-NC-ND license and permits non-commercial use of the work as published, without adaptation or alteration provided the work is fully attributed.

Universität Bremen  
Adolf-Reichwein Straße 57  
28329 Bremen  
Deutschland

Die Festo SE & Co. KG ("Festo") räumt hiermit Universität Bremen, Adolf-Reichwein Straße 57, 28329 Bremen, Deutschland – das einfache, nicht ausschließliche, nicht unternehmensbare Recht ein

[ ] Logo [ ] Film/Video Inhalte [ ] Text/Text Passagen [ ] X Bilder

mit folgendem Inhalt von Festo


**Bionic E-Trunk**  
ausschließlich für den Zweck  
des Bild in der Dissertation zur Einführung in das Thema Soft-Robotik zu verwenden. Der Titel der Arbeit lautet: **Visible Light Actuation: Von der Synthese zum Material\* und wird im Februar an der Universität Bremen veröffentlicht.**

Im Falle der Nutzung des Logo kann diese Nutzung jedernetz widerrufen werden.

Bei Film/Video, Texten/Text Passagen oder Bildern ist jeder dieser Inhalte bei jeder erlaubten Darstellung/Wiedergabe mit "©Festo SE & Co. KG, alle Rechte vorbehalten" deutlich zu kennzeichnen.

Jede weitere, andere oder abweichende Nutzung/Verwertung muss in jedem Fall vorher von Festo ausdrücklich schriftlich erlaubt werden, falls nicht hat diese Nutzung/Verwertung zu unterbleiben.

Esslingen am Neckar, 05.02.2024

I. V.  I. A.  
Festo SE & Co. KG  
Christian Osterle  
Leitung Corporate Brand Management

**JOHN WILEY AND SONS LICENSE TERMS AND CONDITIONS**  
Feb 17, 2024

This Agreement between M. Sven Schalzbe (Co) and John Wiley and Sons ("John Wiley and Sons") consists of your license details and the terms and conditions provided by John Wiley and Sons and Copyright Clearance Center.

License Number	571769824334	License Number	571693497428
License date	Feb 14, 2024	License date	Jan 27, 2024
License Content Publisher	Springer Nature	License Content Publisher	John Wiley and Sons
License Content Publication	Nature	License Content Publication	Advanced Materials
License Content Title	Directed bonding of a polymer film by light	License Content Title	Liquid Crystal Materials for Biomedical Applications
License Content Author	Yankai Yu et al	License Content Author	Luoren Shao, Fangfu Yu, Yanjun Zhao, et al
License Content Date	Sep 11, 2023	License Content Date	Jul 11, 2023
Type of Use	Thesis/Dissertation	License Content Volume	35
Requestor type	academic/university, or research institute	License Content Issue	36
Format	print and electronic	License Content Pages	29
Portion	figures/tables/illustrations	Type of use	Dissertation/Thesis
Number of figures/tables/illustrations	1	Requestor type	University/Academic
Would you like a high-resolution image with your order?	no	Format	Print and electronic
Will you be translating?	no	Portions	Figure table
Circulation distribution	1 - 29	Number of figures/tables	2
Author of this Springer Nature content		Will you be translating?	No
Title of new work	Visible Light Actuation: From Synthesis to Material	Title of new work	Visible Light Actuation: From Synthesis to Material
Institution name	University of Bremen	Institution name	University of Bremen
Expected presentation date	Feb 2024	Expected presentation date	Feb 2024
Portion	Figure 1	Portions	Figure 2 and Figure 5
Requestor Location	M. Sven Schalzbe Adolf-Reichwein Str. 27 Bremen, 28359 Germany Atl. University of Bremen	Requestor Location	M. Sven Schalzbe Adolf-Reichwein Str. 57 Bremen, 28359 Germany Atl. University of Bremen
Total	0.00 EUR	Publisher Tax ID	EU306007151
		Total	0.00 EUR

**SPRINGER NATURE LICENSE TERMS AND CONDITIONS**  
Feb 17, 2024

This Agreement between M. Sven Schalzbe ("Co") and Springer Nature ("Springer Nature") consists of your license details and the terms and conditions provided by Springer Nature and Copyright Clearance Center.

License Number	571769824334	License Number	571693497428
License date	Feb 14, 2024	License date	Jan 27, 2024
License Content Publisher	Springer Nature	License Content Publisher	John Wiley and Sons
License Content Publication	Nature	License Content Publication	Advanced Materials
License Content Title	Directed bonding of a polymer film by light	License Content Title	Liquid Crystal Materials for Biomedical Applications
License Content Author	Yankai Yu et al	License Content Author	Luoren Shao, Fangfu Yu, Yanjun Zhao, et al
License Content Date	Sep 11, 2023	License Content Date	Jul 11, 2023
Type of Use	Thesis/Dissertation	License Content Volume	35
Requestor type	academic/university, or research institute	License Content Issue	36
Format	print and electronic	License Content Pages	29
Portion	figures/tables/illustrations	Type of use	Dissertation/Thesis
Number of figures/tables/illustrations	1	Requestor type	University/Academic
Would you like a high-resolution image with your order?	no	Format	Print and electronic
Will you be translating?	no	Portions	Figure table
Circulation distribution	1 - 29	Number of figures/tables	2
Author of this Springer Nature content		Will you be translating?	No
Title of new work	Visible Light Actuation: From Synthesis to Material	Title of new work	Visible Light Actuation: From Synthesis to Material
Institution name	University of Bremen	Institution name	University of Bremen
Expected presentation date	Feb 2024	Expected presentation date	Feb 2024
Portion	Figure 1	Portions	Figure 2 and Figure 5
Requestor Location	M. Sven Schalzbe Adolf-Reichwein Str. 27 Bremen, 28359 Germany Atl. University of Bremen	Requestor Location	M. Sven Schalzbe Adolf-Reichwein Str. 57 Bremen, 28359 Germany Atl. University of Bremen
Total	0.00 EUR	Publisher Tax ID	EU306007151
		Total	0.00 EUR

JOHN WILEY AND SONS LICENSE TERMS AND CONDITIONS		JOHN WILEY AND SONS LICENSE TERMS AND CONDITIONS		JOHN WILEY AND SONS LICENSE TERMS AND CONDITIONS		JOHN WILEY AND SONS LICENSE TERMS AND CONDITIONS		JOHN WILEY AND SONS LICENSE TERMS AND CONDITIONS		JOHN WILEY AND SONS LICENSE TERMS AND CONDITIONS		JOHN WILEY AND SONS LICENSE TERMS AND CONDITIONS		JOHN WILEY AND SONS LICENSE TERMS AND CONDITIONS			
Feb 17, 2024		Feb 17, 2024		Feb 17, 2024		Feb 17, 2024		Feb 17, 2024		Feb 17, 2024		Feb 17, 2024		Feb 17, 2024			
This Agreement between Mr. Sven Schulzke ("You") and John Wiley and Sons ("John Wiley and Sons") consists of your license details and the terms and conditions provided by John Wiley and Sons and Copyright Clearance Center.		This Agreement between Mr. Sven Schulzke ("You") and John Wiley and Sons ("John Wiley and Sons") consists of your license details and the terms and conditions provided by John Wiley and Sons and Copyright Clearance Center.		This Agreement between Mr. Sven Schulzke ("You") and John Wiley and Sons ("John Wiley and Sons") consists of your license details and the terms and conditions provided by John Wiley and Sons and Copyright Clearance Center.		This Agreement between Mr. Sven Schulzke ("You") and John Wiley and Sons ("John Wiley and Sons") consists of your license details and the terms and conditions provided by John Wiley and Sons and Copyright Clearance Center.		This Agreement between Mr. Sven Schulzke ("You") and John Wiley and Sons ("John Wiley and Sons") consists of your license details and the terms and conditions provided by John Wiley and Sons and Copyright Clearance Center.		This Agreement between Mr. Sven Schulzke ("You") and John Wiley and Sons ("John Wiley and Sons") consists of your license details and the terms and conditions provided by John Wiley and Sons and Copyright Clearance Center.		This Agreement between Mr. Sven Schulzke ("You") and John Wiley and Sons ("John Wiley and Sons") consists of your license details and the terms and conditions provided by John Wiley and Sons and Copyright Clearance Center.		This Agreement between Mr. Sven Schulzke ("You") and John Wiley and Sons ("John Wiley and Sons") consists of your license details and the terms and conditions provided by John Wiley and Sons and Copyright Clearance Center.			
License Number	5718440349707	License Number	5718440349732	License Number	5727700438006	License Number	5727700438006	License Number	5727700438006	License Number	5727700438006	License Number	5727700438006	License Number	5727700438006		
License date	Jan 29, 2024	License date	Feb 14, 2024	License date	Feb 14, 2024	License date	Feb 14, 2024	License date	Feb 14, 2024	License date	Feb 14, 2024	License date	Feb 14, 2024	License date	Feb 14, 2024		
Licensed Content Publisher	John Wiley and Sons	Licensed Content Publisher	John Wiley and Sons	Licensed Content Publisher	Springer Nature	Licensed Content Publisher	Springer Nature	Licensed Content Publisher	Springer Nature	Licensed Content Publisher	Springer Nature	Licensed Content Publisher	Springer Nature	Licensed Content Publisher	John Wiley and Sons		
Licensed Content Publication	Chemistry - A European Journal	Licensed Content Publication	Advanced Materials	Licensed Content Publication	Nature	Licensed Content Publication	Nature	Licensed Content Publication	Photocrosslinkable Dynamic Networks Doped with Gold Nanorods Showing Enhanced Photocrosslinking Performance	Licensed Content Publication	Photocrosslinkable Dynamic Networks Doped with Gold Nanorods Showing Enhanced Photocrosslinking Performance	Licensed Content Publication	Photocrosslinkable Dynamic Networks Doped with Gold Nanorods Showing Enhanced Photocrosslinking Performance	Licensed Content Publication	Photocrosslinkable Dynamic Networks Doped with Gold Nanorods Showing Enhanced Photocrosslinking Performance		
Licensed Content Title	Structural Enhanced Intelligence of Liquid Crystal Elastomers	Licensed Content Title	Liquid-Crystalline Dynamic Networks Doped with Gold Nanorods Showing Enhanced Photocrosslinking Performance	Licensed Content Title	Photocrosslinkable Dynamic Networks Doped with Gold Nanorods Showing Enhanced Photocrosslinking Performance	Licensed Content Title	Photocrosslinkable Dynamic Networks Doped with Gold Nanorods Showing Enhanced Photocrosslinking Performance	Licensed Content Title	Photocrosslinkable Dynamic Networks Doped with Gold Nanorods Showing Enhanced Photocrosslinking Performance	Licensed Content Title	Photocrosslinkable Dynamic Networks Doped with Gold Nanorods Showing Enhanced Photocrosslinking Performance	Licensed Content Title	Photocrosslinkable Dynamic Networks Doped with Gold Nanorods Showing Enhanced Photocrosslinking Performance	Licensed Content Title	Photocrosslinkable Dynamic Networks Doped with Gold Nanorods Showing Enhanced Photocrosslinking Performance		
Licensed Content Author	Hong Yang, Meng Wang, Zhen-Zhou Nie	Licensed Content Author	Yue Zhao, Heikang Xia, Xia Tong, et al	Licensed Content Author	Jin-an Lv et al	Licensed Content Author	Jin-an Lv et al	Licensed Content Author	Jin-an Lv et al	Licensed Content Author	Jin-an Lv et al	Licensed Content Author	Jin-an Lv et al	Licensed Content Author	Tomoki Ikeda, Christopher J. Barrett, Motoki Kinoshita, et al		
Licensed Content Date	Jun 5, 2023	Licensed Content Date	Feb 13, 2018	Licensed Content Date	Sep 7, 2016	Licensed Content Date	Sep 7, 2016	Licensed Content Date	Sep 7, 2016	Licensed Content Date	Sep 7, 2016	Licensed Content Date	Sep 7, 2016	Licensed Content Date	Jun 16, 2008		
Licensed Content Volume	29	Licensed Content Volume	30	Type of Use	Thesis/Dissertation	Licensed Content Volume	47	Licensed Content Volume	47	Licensed Content Volume	47	Licensed Content Volume	47	Licensed Content Volume	47		
Licensed Content Issue	38	Licensed Content Issue	14	Requestor type	academic/university or research institute	Licensed Content Issue	27	Licensed Content Issue	27	Licensed Content Issue	27	Licensed Content Issue	27	Licensed Content Issue	27		
Licensed Content Pages	24	Licensed Content Pages	8	Format	print and electronic	Licensed Content Pages	3	Licensed Content Pages	3	Licensed Content Pages	3	Licensed Content Pages	3	Licensed Content Pages	3		
Type of use	Dissertation/Thesis	Type of use	Dissertation/Thesis	Portion	figures/tables/illustrations	Type of use	Dissertation/Thesis	Type of use	Dissertation/Thesis	Type of use	Dissertation/Thesis	Type of use	Dissertation/Thesis	Type of use	Dissertation/Thesis		
Requestor type	University/Academic	Requestor type	University/Academic	Number of figures/tables/illustrations	1	Requestor type	University/Academic	Requestor type	University/Academic	Requestor type	University/Academic	Requestor type	University/Academic	Requestor type	University/Academic		
Format	Print and electronic	Format	Print and electronic	Would you like a high resolution image with your order?	no	Format	Print and electronic	Format	Print and electronic	Format	Print and electronic	Format	Print and electronic	Format	Print and electronic		
Portion	Figure/table	Portion	Figure/table	Will you be translating?	no	Portion	Figure/table	Portion	Figure/table	Portion	Figure/table	Portion	Figure/table	Portion	Figure/table		
Number of figures/tables	1	Number of figures/tables	1	Circulation distribution	1 - 29	Number of figures/tables	1	Number of figures/tables	1	Number of figures/tables	1	Number of figures/tables	1	Number of figures/tables	1		
Will you be translating?	No	Will you be translating?	No	Author of this Springer Nature content	no	Will you be translating?	No	Will you be translating?	No	Will you be translating?	No	Will you be translating?	No	Will you be translating?	No		
Title of new work	Visible Light Actuation: From Synthesis to Material	Title of new work	Visible Light Actuation: From Synthesis to Material	Title of new work	Visible Light Actuation: From Synthesis to Material	Title of new work	Visible Light Actuation: From Synthesis to Material	Title of new work	Visible Light Actuation: From Synthesis to Material	Title of new work	Visible Light Actuation: From Synthesis to Material	Title of new work	Visible Light Actuation: From Synthesis to Material	Title of new work	Visible Light Actuation: From Synthesis to Material		
Institution name	University of Bremen	Institution name	University of Bremen	Institution name	University of Bremen	Institution name	University of Bremen	Institution name	University of Bremen	Institution name	University of Bremen	Institution name	University of Bremen	Institution name	University of Bremen		
Expected presentation date	Feb 2024	Expected presentation date	Feb 2024	Expected presentation date	Feb 2024	Expected presentation date	Feb 2024	Expected presentation date	Feb 2024	Expected presentation date	Feb 2024	Expected presentation date	Feb 2024	Expected presentation date	Feb 2024		
Portions	Figure 3	Portions	Figure 4	Portions	Figure 1	Portions	Figure 3	Portions	Figure 3	Portions	Figure 3	Portions	Figure 3	Portions	Figure 3		
Requestor Location	Mr. Sven Schulzke Adolf-Reichwein Str. 57 Bremen, 28359 Germany Attn: University of Bremen	Requestor Location	Mr. Sven Schulzke Adolf-Reichwein Str. 57 Bremen, 28359 Germany Attn: University of Bremen	Requestor Location	Mr. Sven Schulzke Adolf-Reichwein Str. 57 Bremen, 28359 Germany Attn: University of Bremen	Requestor Location	Mr. Sven Schulzke Adolf-Reichwein Str. 57 Bremen, 28359 Germany Attn: University of Bremen	Requestor Location	Mr. Sven Schulzke Adolf-Reichwein Str. 57 Bremen, 28359 Germany Attn: University of Bremen	Requestor Location	Mr. Sven Schulzke Adolf-Reichwein Str. 57 Bremen, 28359 Germany Attn: University of Bremen	Requestor Location	Mr. Sven Schulzke Adolf-Reichwein Str. 57 Bremen, 28359 Germany Attn: University of Bremen	Requestor Location	Mr. Sven Schulzke Adolf-Reichwein Str. 57 Bremen, 28359 Germany Attn: University of Bremen	Requestor Location	Mr. Sven Schulzke Adolf-Reichwein Str. 57 Bremen, 28359 Germany Attn: University of Bremen
Publisher Tax ID	EUR2607151	Publisher Tax ID	EUR2607151	Publisher Tax ID	EUR2607151	Publisher Tax ID	EUR2607151	Publisher Tax ID	EUR2607151	Publisher Tax ID	EUR2607151	Publisher Tax ID	EUR2607151	Publisher Tax ID	EUR2607151		
Total	0.00 EUR	Total	0.00 EUR	Total	0.00 EUR	Total	0.00 EUR	Total	0.00 EUR	Total	0.00 EUR	Total	0.00 EUR	Total	0.00 EUR		